4-30-2018

Late Quaternary East African Environmental Change based on Mineralogical and Geochemical Analysis of Outcrop and Core Material from the Southern Kenya Rift

Nathan Rabideaux

LATE QUATERNARY EAST AFRICAN ENVIRONMENTAL CHANGE BASED ON MINERALOGICAL AND GEOCHEMICAL ANALYSIS OF OUTCROP AND CORE MATERIAL FROM THE SOUTHERN KENYA RIFT

by

NATHAN M. RABIDEAUX

Under the Direction of Daniel M. Deocampo, PhD

ABSTRACT

The Olorgesailie Drilling Project (ODP) and *Hominin Sites and Paleolakes Drilling Project* (HSPDP) targeted sites in the East African Rift Valley for their archeological and geological significance. The ODP team collected cores from the Koora Graben and the HSPDP team from Lake Magadi. To compliment these projects, we collected samples throughout southern Kenya to identify weathering patterns and potential mineral reactions to trace geologic processes between geologic sources and the hydrologic sump of Lake Magadi.

Mineralogical and geochemical analyses of the ODP and HSPDP cores suggest a similar paleoclimatic history over the past ~1.0 Myr: long-term aridification and intensifying climate variability over the past ~200-350 kyr. The paleolakes that occupied the Magadi and Koora Graben basins began as freshwater lakes at ~1.0 Ma. The mineralogy and geochemistry of the

Magadi basin changed ~350 ka. The paleolake that occupied the Koora Graben experienced dessication at ~250 ka following thick volcanic ash and pumice deposition that preceded highly variable environmental conditions. Nearly all volcanic deposits recognized in the Olorgesailie cores have been zeolitized in the Magadi cores, but we assume that equivalent deposits were similar in thickness to the ODP cores. Trona deposits began to accumulate by ~100 ka, signaling intense aridification.

Mineralogical and geochemical analyses of surface and outcrop samples displayed unique characteristics associated with four distinct regions: the highlands to the north; the central area between Koora and Magadi; the greater Magadi basin in the south; and the Nguruman Escarpment to the west. Zeolitic alteration is common throughout southern Kenya. The most common zeolites in outcrop and surface samples are erionite and chabazite, which commonly occur in weathered tuffs and soils. Analcime was not present in any surface or outcrop sample, but is abundant in all cores, suggesting it forms in concentrated brines in lacustrine environments or proximal to lake basins near alkaline springs. The mineralogy and geochemistry of the ODP cores suggest the geologic source for material in the Koora Graben is primarily to the north, whereas the Magadi mineralogy suggests both western and central sources; however, much of the mineralogy reflects processes that occur within the basin itself.

INDEX WORDS: Southern Kenya Rift, Zeolites, Mineralogy, Geochemistry, Human Evolution

LATE QUATERNARY EAST AFRICAN ENVIRONMENTAL CHANGE BASED ON MINERALOGICAL AND GEOCHEMICAL ANALYSIS OF OUTCROP AND CORE MATERIAL FROM THE SOUTHERN KENYA RIFT

by

NATHAN M. RABIDEAUX

A Dissertation Submitted in Partial Fulfillment of the Requirements for the Degree of

Doctor of Philosophy

in the College of Arts and Sciences

Georgia State University

2018

LATE QUATERNARY EAST AFRICAN ENVIRONMENTAL CHANGE BASED ON MINERALOGICAL AND GEOCHEMICAL ANALYSIS OF OUTCROP AND CORE MATERIAL FROM THE SOUTHERN KENYA RIFT

by

NATHAN M. RABIDEAUX

Committee Chair: Daniel M. Deocampo

Committee: W. Crawford Elliott

Lawrence Kiage

Robin W. Renaut

Electronic Version Approved:

Office of Graduate Studies

College of Arts and Sciences

Georgia State University

May 2018

DEDICATION

I dedicate this dissertation to my wonderful and crazy mother, Yvonne (Bonnie) M. Rabideaux, for passing along her passion for life and desire to pursue knowledge in all forms. My mother had the ability to drive me completely nuts – a power most mothers have over their children, I suppose; and many have said that was because we were so much alike. No matter which level of education I obtained or however much I knew about a given subject, my mother always seemed to be convinced she knew more. She may have been on to something. Thus I thank my wonderful mom for making me who I am today and I dedicate this hellish doctoral experience to her. Love and miss you, ma!

ACKNOWLEDGEMENTS

I would like to thank my lab helpers: Thanh Vo; Michelle Watson; Lucy Mejia, M. Sanam Chaudhary; David M. Davis; Saira Hamid; and Mary Winsor, for all their assistance in processing samples. To my dissertation committee: Dr. W. Crawford Elliot; Dr. Lawrence Kiage; and Dr. Robin W. Renaut, for their feedback and assistance with completing the requirements for this doctoral degree. Of course, must thank Dr. Daniel Deocampo for his advice and support throughout this process. Thanks to the Department of Geosciences and College of Arts & Sciences for funding me throughout this doctoral program. And couldn't have done it without Basirat Lawal and Boné Drake and all their assistance along the way.

HSPDP drilling, ICD, and logistics supported by ICDP and NSF grants # 1123000, 1338553, 1241859, 1123942, and 1241595; and HKBU grant # 202213. XRD analysis supported by NSF grants # 1029020 and 1349599. Special thanks to LacCore, CSDCO, DPI, DES for providing wonderful support during drilling and ICD. Thanks to the HSPDP Scientific Teams for keeping me motivated and sharing all their wisdom. The Olorgesailie Drilling Project (ODP) is part of the Human Origins Program at the Smithsonian Institution, in collaboration with the National Museums of Kenya, and is funded by the Peter Buck Fund, the William H. Donner Foundation, the Ruth and Vernon Taylor Foundation, and Whitney and Betty MacMillan. Thanks to the ODP Scientific Team for all their work, insights, and support.

I'd also like to thank some of the wonderful people that kept me sane while completing various stages of this degree: Danny Gardner; Tom Sarvey; Keary Williams; Gabi Garcia Andreo; Rym Seoud; Aline Thomas; Marilyn Sokolovsky; Davette Gadison; Tara and Brian Mitchell; Jocelyn Ffriend; my dogs – Bear and Louie; and many more. Last, but certainly not least, I'd like to thank my family for all the crap they have had to put up with – all the

complaining, watching my dogs, et cetera, et cetera, et cetera – and for always being supportive and awesome! Thanks y'all! It's been real.

TABLE OF CONTENTS

LIST OF TABLES

LIST OF FIGURES

LIST OF ABBREVIATIONS

CSDCO	Continental Scientific Drilling Coordination Office
cm	Centimeters
EARV	East African Rift Valley
EDX	Energy Dispersive X-ray Spectrometer
FUS-ICP	Fusion ICP-MS
HMB	High Magadi Beds
HSPDP	Hominin Sites and Paleolakes Drilling Project
HSPDP-MAG14	Hominin Sites and Paleolakes Drilling Project-Lake Magadi-2014
GPS	Global Positioning System
ICD	Initial Core Description
ICP-AES	Inductively-coupled Plasma Atomic Emission Spectroscopy
ICP-MS	Inductively-coupled Plasma Mass Spectrometry
INAA	Instrumental Neutron Activation Analysis
ka	Thousand years
kg	Kilograms
kV	Kilovolts
LacCore	National Lacustrine Core Laboratory
LOI	Loss on Ignition
m	Meters
mA	Milliamps
Ma	Million years
mbs	meters below surface
mg	Milligram
ODP	Ocean Drilling Program
ODP	Olorgesailie Drilling Project
ODP-OLO12	Olorgesailie Drilling Project-Olorgesailie-2012
pH	$-\log [H^+]$
PASS	Programmable Anti-scatter Slit
PDS	Programmable Divergent Slit
PPM	Parts Per Million (mg/kg)
REE	Rare Earth Elements
SEM	Scanning Electron Microscope
TE	Trace Elements
XRD	X-ray Diffraction
XRF	X-ray Fluorescence
wt. %	Weight Percent

1 INTRODUCTION

Scientists conducting research in the Southern Kenya Rift over the past century have uncovered a wealth of information related to rift valley geology, vertebrate and hominin evolution, and prehistoric stone tool technology (e.g., Gregory, 1921; Leakey, 1952; Baker, 1958; Surdam and Eugster, 1976; Isaac, 1978; White et al., 1984; Potts, 1989; Owen et al., 2008; Potts et al., 2018; Deino et al., 2018; Behrensmeyer et al., 2018). In recent years, there has been a growing interest in the relationship between environmental change and evolutionary benchmarks (e.g., Laporte, 1990; deMenocal et al., 1995; Trauth et al., 2005, 2007, 2009). Outcrops provide limited information on paleo-environmental conditions because of weathering and erosion, and are typically discontinuous and/or altered to some degree. The desire to obtain continuous records from subaqueous environments less prone to alteration from weathering and erosion has led to a growing interest in obtaining drill cores spanning thousands to millions of years. To this end, scientists have turned to scientific drilling and coring in rift basins of eastern Africa to obtain continuous sediment cores for use in constructing long-term, high-resolution paleo-environmental records and to identify relationships between environmental change and human evolutionary benchmarks (e.g., Cohen et al., 2009, 2016).

There are competing theories on what is the primary forcing mechanism in hominin evolution and changes in stone tool technology. The most popular of these theories are 1) the savanna hypothesis, 2) the turnover-pulse hypothesis, and 3) the variability selection hypothesis. Many other possible ideas and theories explaining the mechanisms driving hominin evolution have been proposed, although few have been widely accepted as plausible. The most prominent theories are thus summarized:

1) The savanna hypothesis states that as East Africa became more arid, savannahs replaced woodland forests. This resulted in apes and other primates moving from their typical forest habitats into open grasslands on the savannas. Due to the environmental forcing, early hominin species developed adaptations better suited to these new habitat ranges (Trauth et al., 2005, 2007, 2010; Potts, 2013). With expansion of grasslands, hominins needed to see over the tall grass to hunt and avoid predation, the earliest hominins' hipbone evolved to allow for bipedalism. Soon after, the human-type foot developed, followed by the loss of body hair to allow for better cooling. These combined adaptations allowed hominins to travel further and faster than other primates or mammals (Vrba et al., 1995; Bobe et al., 2002; deMenocal, 2004; Wynn, 2004).
2) The turnover-pulse hypothesis proposed that there is no evidence of causation or close temporal relationships between aridification episodes and hominin evolution in East Africa (Vrba et al., 1985, 1995; Potts et al., 1999, 2004; Potts, 2013). This theory suggests that faunal turnover is not dependent of climate-change events, but a result of adaptations that occurred over hundreds of thousands of years. Vrba et al. (1995) suggested that faunal turnover-pulses coincided with periods of high diversity of bovids during aridification events. As is generally accepted, increased diversity levels lead to higher turnover rates, which results in increased speciation and extinction. This mechanism allowed for the adaptation of the earliest hominins and further evolution as the ecosystem heterogeneity increased (Wynn, 2004).

3) The variability selection hypothesis suggests that habitat heterogeneity within an ecosystem, similar to that of the Turkana Basin in northern Kenya, leads to episodic speciation and extinction (Potts, 1996, 1998, 2013). Evolution of flora and fauna in these ecosystems is driven by episodic flooding and aridity that occur within floodplain habitats. It has been proposed that regional climatic variability in combination with the variability of floodplain habitats creates what ecologists refer to as a waxing and waning of ecosystem entropy, which has been proposed as a control on species diversity across the East African savanna during the Plio-Pleistocene transition. These episodic events create niches that were previously non-existent, creating an opportunity for new species to fill the void. Essentially, as the savanna habitats expanded across East Africa, more opportunity existed for early hominins to exploit. The result of which was the genus *Homo* (Vrba et al., 1995; Potts, 1996, 1998; Bobe et al., 2002; deMenocal, 2004; Wynn, 2004; Maslin et al., 2014; Potts and Faith, 2015).

A more recent and less popular theory is the deep-lakes hypothesis, which is a comparative analysis of lacustrine sediments from basins throughout the East African Rift Valley (Maslin et al., 2009; Trauth et al., 2010; Potts, 2013). Initial studies found that key hominin evolution events occurred during three wet periods when deep lakes would form in the East African Rift landscape, either through periodic precessional forcing or during prolonged lake high stands. Diatomaceous sedimentary deposits provide evidence of these deep lake environments (Owen, 2002; Trauth et al., 2005, 2007, 2010; Maslin et al., 2009). Periodic development of large lakes has been proposed to drive expansion of hominin populations as well

as the possible division of a common group into separate populations. This would have aided in enhanced speciation, migration, and adaptive changes, due to dietary habits shifting and the potential for brain adaptation and growth (Maslin et al., 2009; Potts, 2013), as well as behavioral and cultural adaptations.

Figure 1.1: HSPDP and ODP drill sites in the East African Rift Valley. Northern Awash and Chew Bahir are located in Ethiopia. Lake Turkana, Lake Baringo/Tugen Hills, Lake Magadi, and Olorgesailie/Koora Graben.

The *Hominin Sites and Paleolakes Drilling Project* (HSPDP) and *Olorgesailie Drilling Project* (ODP) collected drill cores from six basins (Lake Baringo/Tugen Hills, Lake Turkana, Lake Magadi and Olorgesailie/Koora Graben in Kenya, and the Northern Awash/Afar and Chew

Bahir in Ethiopia) of the East African Rift Valley (EARV) between 2012 and 2014 (Fig. 1.1). The *Hominin Sites and Paleolakes Drilling Project* is funded mainly by the International Continental Drilling Program and National Science Foundation (USA), with contributions from European and Hong Kong funding agencies, and undertaken by an international team of scientists from more than 40 institutions in more than a dozen countries. The *Olorgesailie Drilling Project* is part of the Human Origins Program at the Smithsonian Institution, in collaboration with the National Museums of Kenya, and is funded by the Peter Buck Fund, the William H. Donner Foundation, the Ruth and Vernon Taylor Foundation, and Whitney and Betty MacMillan. Although funded and operated independently, ODP is considered part of the greater HSPDP project.

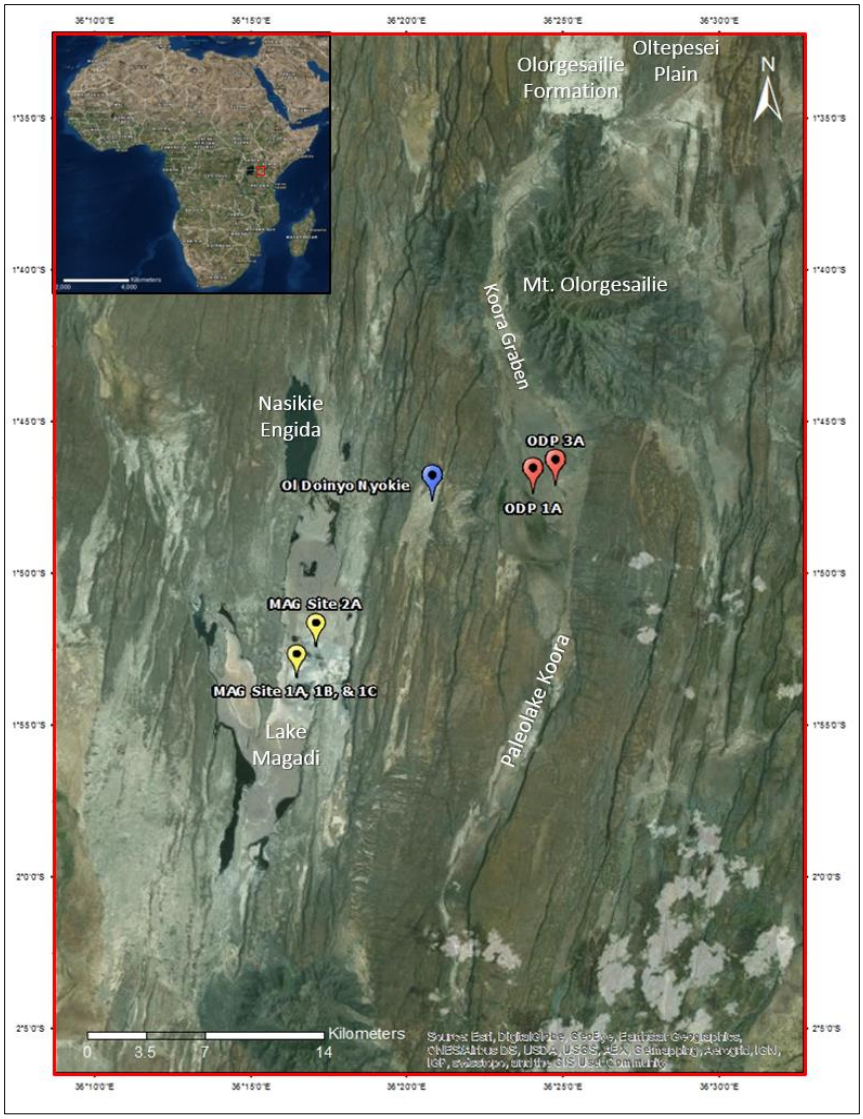

Figure 1.2: Map of the Southern Kenya Rift with important features and drilling sites labelled. Important sites labeled include: the Olorgesailie Formation and Oltepesi Plain; Mt. Olorgesailie; Koora Graben; the location of Paleolake Koora; Lake Magadi; Ol Doinyo Nyokie; HSPDP-MAG14 and ODP-OLO12 drilling sites. Inset map shows study location on inset map of African continent.

The EARV has been a setting for considerable research over the past century (e.g., Gregory, 1921; Leakey, 1952; Baker, 1958, 1963; Eugster and Jones, 1968; Isaac, 1978; Johanson and White, 1979; Yuretich, 1982; Potts, 1989; Behrensmeyer et al., 2002; Owen et al., 2008; Pottts et al., 2018). The Southern Kenya Rift is home to a number of important

archeological and paleontological sites. The most important site is Olorgesailie, where archeological excavations have uncovered extensive Acheulean handaxe, Middle Stone Age (MSA) artefacts, abundant vertebrate fossils, and *Homo erectus* specimen KNM-OG 45500 (Leakey, 1952; Isaac, 1977; Potts, 1989; Deino and Potts, 1992; Behresnmeyer et al., 2002, 2018; Potts et al., 2004, 2018; Deocampo et al., 2010). The ODP drilling sites are located in the Koora Graben, south of Mt. Olorgesailie (Figs. 1.1 & 1.2). The HSPDP drilling sites at Lake Magadi were located off causeways in the northern sub-basin, drilled in partnership with Tata Chemicals Limited (Cohen et al., 2016). The Koora Graben (site of Paleolake Koora) and Lake Magadi are adjacent basins in the Southern Kenya Rift (Figs. 1.1 & 1.2), located ~120 km southwest of Nairobi near the Tanzanian border.

East Africa has experienced long-term aridification over the past ~3 Myr, due to the cooling trend that characterizes the latter half of the Cenozoic (deMenocal, 2004). Superimposed on this trend are pulses of deep lake phases in East Africa (Trauth et al., 2005, 2007, 2009). The onset of Northern Hemisphere Glaciation, and obliquity paced glacial cycles in the northern hemisphere, began and intensified between ~3.2 and 2.6 Ma (Shackleton, 1995; Lisiecki and Raymo, 2005; deMenocal 2004; Feakins and deMenocal, 2010). The Mid-Pleistocene Climate Transition (~0.9-0.75 Ma) is marked by a shift in Earth's glacial-interglacial cycles from obliquity (~41 kyr) to eccentricity time scales (~100 kyr) (Berger and Jansen, 1994). The longer glacial cycles, which drive aridity in equatorial East Africa, are the likely cause of the sustained desiccation observed in the region over the Plio-Pleistocene (Wynn, 2004).

Throughout the Pleistocene, tropical African climate variability on time scales of tens of thousands of years (23-19 kyr) were paced by variations in Earth's orbital precession (deMenocal et al., 1993; Trauth et al, 2003, 2005, 2007). Dust and phytolith records off the coast

of West Africa, however, recorded high-latitude forcing that vary on 41 kyr and 100 kyr time scales (deMenocal et al., 1993). deMenocal et al. (1993) suggested North Atlantic sea surface temperature (SST) variability at high-latitudes and precessional monsoonal forcing at low-latitudes were influencing Pleistocene African climate. Shultz et al. (1998) identified correlations between Greenland ice cores and Arabian Sea sediment cores that reflect the role millennial-scale and centennial-scale climate fluctuations - known as the Dansgaard-Oeschgar and Heinrich Events, play in tropical climates during the Late Quaternary. This line of evidence is further supported by millennial-scale variations in SSTs and the strength of deep-water circulation during the middle Late Pleistocene, which suggests tropical processes were influencing Atlantic Meridional Overturning Circulation (Billups et al., 2011).

Modern climate variability in East Africa is primarily driven by the African-Asian monsoonal climate systems and the position of the Intertropical Convergence Zone (ITCZ), which produces two rainy seasons: one March to May and another November to December (Nicholson, 1996; McGregor and Nieuwolt, 1998; Feakins and deMenocal, 2010). The two rainy seasons are described as the south-east and north-east monsoons, respectively. The south-east monsoon is a relatively shallow air current, mostly originating in the Indian Ocean, although some of the air masses originate over continental landmasses. The north-east monsoon brings relatively dry air of mostly continental origins, passing over Somali, running parallel to the Indian Ocean coast and the Ethiopian highlands. The north-east monsoon does not bring considerable rainfall to the region until it converges with air masses in southern East Africa, where it brings considerable rainfall (McGregor and Nieuwolt, 1998).

The modern climate of the Southern Kenya Rift is characterized by low annual precipitation (< 15 cm) and high average temperature (~20-38° C) (Baker, 1958; Behr, 2002).

The Koora Graben is located on the southern flanks of Mt. Olorgesailie. Situated to the north of Mt. Olorgesailie is the well-studied Olorgesailie Formation, as well as the paleontologically and archaeologically rich Oltepesei and Oltulelei Formations (Isaac, 1977; Potts, 1989; Owen et al., 2008; Deocampo et al., 2010). The Olorgesailie Formation is comprised of lacustrine, volcaniclastic and alluvial sediments deposited between 1.2 million and 490,000 years ago (Gregory, 1921; Isaac, 1978; Potts, 1989; Deino and Potts, 1992; Behrensmeyer et al., 2002; Owen et al., 2008; Potts et al., 2018; Deino et al., 2018). The stratigraphic record from Olorgesailie indicates the area experienced variable climatic regimes, with fluctuating humid and arid conditions evidenced by paleosols, rhizoliths, wetland deposits, diatomites, and diatomaceous silts and clays (Owen et al., 2008; Deocampo et al., 2010).

The geology of the Southern Kenya Rift was first summarized during the late 1800's by early colonial explorers and geologists (e.g., Fischer, 1884; Mügge, 1885; Kaiser, 1898; Künzli, 1901). Further work in the 20th Century published the geological record of Southern Kenya in greater detail (e.g., Parkinson, 1913; Anonymous, 1923; Gregory, 1921; Leakey, 1952; Baker, 1958; Crossley, 1979; Guth, 2007). The geology is comprised of Archean basement rock overlain by Miocene to recent volcanic and sedimentary deposits. The oldest rocks of the rift floor are the gneisses, quartzites and schists that make up the Basement System of Precambrian age. There is a significant erosion surface between the metamorphic basement and Miocene-Pliocene aged Olorgesailie volcanics and the flow basalts that are associated with the Nguruman Rift faulting events. The Olorgesailie volcanics consist of augitites, trachyandesites, alkali trachytes, and nephelinites. During the late Pliocene and early Pleistocene, flow trachytes filled most of the Southern Kenya Rift floor while a second stage of faulting occurred associated with the Nguruman Rift (Crossley, 1979).

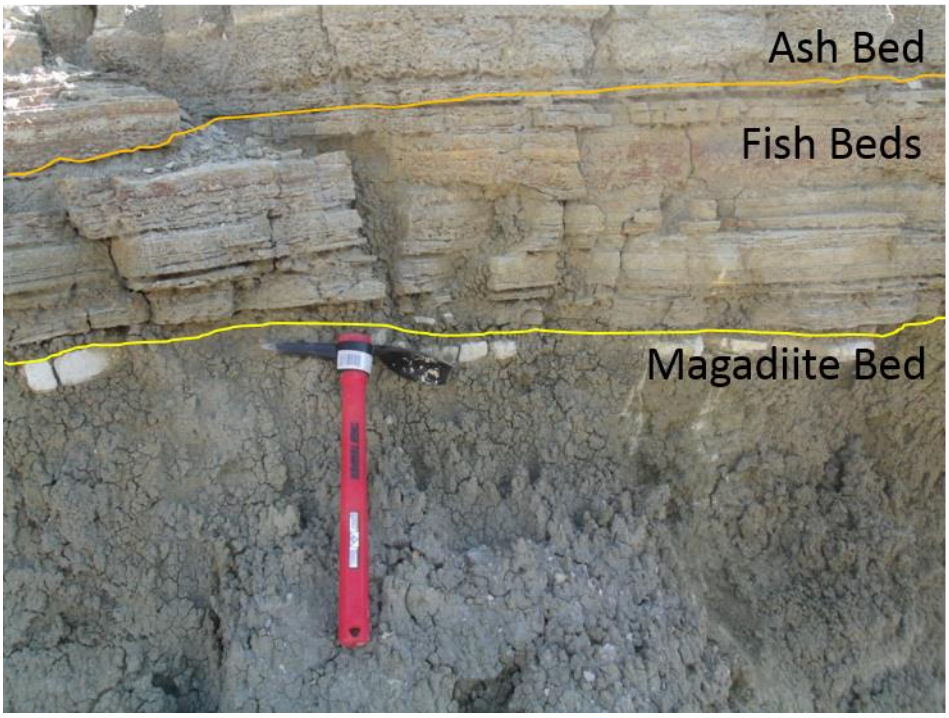

Figure 1.3: High Magadi Bed outcrop from southern lagoon at Lake Magadi, southern Kenya. Upper unit is a volcanic ash deposit. Middle unit are laminated fish fossil beds. Lower unit is this layer of magadiite.

A series of lake deposits accumulated on the rift floor during the early to Mid-Pleistocene. Grid faulting formed numerous sub-parallel faults in the rift floor, resulting in downfaulting and the formation of a series of troughs that started to accumulate sediments. The Oloronga Beds formed in the basin now occupied by Lake Magadi, and the Olorgesailie Lake Beds accumulated in an adjacent trough ~40 km to the northeast. Further faulting and erosion followed in much of the region, but further lake deposition occurred in the Magadi trough. Fine silts and clays accumulated in Lake Magadi as the High Magadi Beds during the Late Pleistocene to Holocene (Fig. 1.3). The youngest deposits in the region include thick sequences of sodium carbonate evaporites (trona and nahcolite) in the ephemeral lake basins and unconsolidated alluvium throughout much of the Southern Kenya Rift (Gregory, 1921; Baker, 1958; Herrick, 1972).

Figure 1.4: ODP-OLO12-1A Drill site, on a savanna in the Koora Plain section of the Koora Graben. Image courtesy of the Human Origins Program (http://humanorigins.si.edu) at the Smithsonian Institution National Museum of Natural History.

The drilling sites for the ODP-OLO12 cores were located in the Koora Graben, to the south of the Olorgesailie Formation (Figs. 1.2 & 1.4). Paleolake Koora was likely hydrologically open and drained into the Magadi basin through a southern spillway at different times throughout its history. During periods of hydrological closure in the Late Pleistocene to Holocene, zeolitic alteration occurred in Koora, suggesting changes in pH and salinity, due to volcanic and or hydrothermal activity and evaporative concentration, respectively. Sediments in the Koora Graben are composed of fluviolacustrine and volcaniclastic deposits overlain by alluvium. Magadi and plateau flow trachyte basement rock (~1.4-0.78 Ma) underlies the Koora Graben and Lake Magadi basins (Crossley, 1979). A series of paleolakes likely occupied the Koora Graben until the early Holocene, when the lake completely dried up. Paleoshorelines identified in outcrop at the southern end of the Koora Graben during recent field seasons confirm sustained occupation by a large lake.

Figure 1.5: HSPDP-MAG14 drill sites on Lake Magadi. (left) Site 1A on a sand and gravel drilling platform, courtesy of Tata Chemicals Magadi (image courtesy of http;//hspdp-asu.edu). (right) Site 2A drill site, located off a causeway in the northern sub-basin on a sand and gravel drilling platform.

Lake Magadi is located at the lowest point of the southern rift valley (~600 m elevation; Fig. 1.2). The sediments are fluvial and lacustrine deposits composed mostly of detrital alkali feldspars and authigenic minerals, such as zeolites and sodium silicates. The abundant authigenic mineralization is due to the extreme alkalinity and high silica activity (Surdam and Eugster, 1976). The genesis and diagenesis of these authigenic minerals are related to geochemical conditions within the basin which are driven by climatic and tectonic controls (e.g., Eugster, 1970; Jones and Eugster, 1976; Jones et al., 1977; Kaufman et al., 1990). In modern times, Lake Magadi is a saltpan with a trona crust that forms from the concentrated sodium carbonate brine in the basin (Fig. 1.5). Soda ash ($NaCO_3$) is mined for commercial value by Tata Chemicals Magadi.

1.1 Purpose of the Study

The larger goals of these projects address questions of environmentally driven cultural adaptation and hominin evolution in East Africa, and what conditions these evolutionary changes occurred under through an interdisciplinary approach, involving research in archaeology,

paleoanthropology, genetics/genomics, and earth sciences (Cohen et al., 2009). To this end, HSPDP research aims to reconstruct paleo-environmental conditions from lacustrine sediments obtained from ancient and modern lake basins in the EARV, and to identify the relationship between environmental and climate change and evolutionary benchmarks. Each site is proximal to important hominin fossil sites, which should provide insight as to how changes in climate regimes, changing environmental conditions, and tectonic activity were associated with hominin and vertebrate evolution.

This dissertation research presents new mineralogical and geochemical data of core material collected from the Koora Graben (ODP-OLO12) in 2012 and Lake Magadi (HSPDP-MAG14) in 2014 during these drilling projects, as well as a full mineralogical and geochemical characterization of outcrop and hand samples collected in the Southern Kenya Rift during the 2014 and 2015 field seasons.

1.2 Project Goals

The goals of this dissertation are to: 1) construct high-resolution Late Pleistocene records of paleoenvironmental change in the Southern Kenya Rift via X-ray diffraction (XRD), inductively-coupled plasma atomic emission spectroscopy (ICP-AES), lithium borate fusion inductively-coupled plasma mass spectrometry (ICP-MS), whole rock fusion X-ray fluorescence (XRF), and loss on ignition (LOI) analyses of core material recovered from the Koora Graben and Lake Magadi by identifying different mineralogical phases and geochemical trends and inferring associated paleoenvironmental conditions; 2) complete a detailed analysis of modern outcrop and surface samples from the Southern Kenya Rift to fully characterize the mineralogy and geochemistry of the myriad sedimentary and igneous material from the region; and 3) identify relationships between modern outcrop and core material and relate geologic materials

from source to sump. This project will further our understanding of sedimentary processes in the Southern Kenya Rift and, in concert with work being undertaken at other institutions, help develop a high-resolution record of environmental change in East Africa during the late Pleistocene epoch.

Table 1.1 Proposed Journal Submissions

Study	**Description**	**Purpose**	**Hypothesis**	**Possible Journal**
Mineralogical and Geochemical Trends of HSPDP-MAG14 Core Material	Analysis and interpretation of the Lake Magadi core material	Construct a high-resolution record of environmental change in the Magadi Basin	We hypothesize that mineralogy is associated with both tectonic and long-term climate trends in East Africa	Journal of Sedimentary Research
Mineralogical and Geochemical Insights from ODP-OLO12 Core Material	Analysis and interpretation of the Koora Graben core material	Construct a high-resolution record of environmental change in the Koora Graben	We hypothesize that mineralogical trends are primarily associated with climatic activity	Journal of Paleolimnology
Mineralogy and Geochemistry of Volcanogenic Material from the Southern Kenya Rift	Analysis and interpretation of sedimentary and igneous material from southern Kenya	Construct record of mineralogical and geochemical characterization of southern Kenya outcrop material	We hypothesize that relationships between core and outcrop material can aid in identification of sedimentary source regions	Quaternary Research

This dissertation is a compilation of three chapters (Tab. 1.1), which are based on manuscripts that will be submitted to peer-reviewed journals for publication. The first chapter consists of paleoenvironmental interpretations based on the analysis of core material from Lake Magadi obtained during the HSPDP campaign. The second chapter focuses on analysis of core material from the Koora Graben obtained by the ODP team, and the third chapter consists of mineralogical and geochemical analysis of modern surface and outcrop samples collected from the Southern Kenya Rift during the 2014 and 2015 field seasons.

2 PROJECT OBJECTIVES

We present new mineralogical and geochemical data from cores collected in adjacent half-graben rift basins in the Southern Kenya Rift that span the past ~1 Myr, as well as new mineralogical and geochemical data from outcrop and surface material collected throughout southern Kenya during the 2014 and 2015 field seasons.

Our primary research questions include: 1) What is the primary influence on environmental conditions in southern Kenya over the past ~1 Myr: climate or tectonics? 2) Can mineralogical and geochemical data from HSPDP and ODP core material provide evidence of climate cyclicity in southern Kenya? 3) What can we learn about source regions, weathering patterns, and mineral reactions across the Southern Kenya Rift and how can that inform us about what the core data is telling us? 4) Does the mineralogical and geochemical data reveal trends and rhythms in environmental and climatic conditions that correlate with hominin evolutionary benchmarks, such as species appearance-disappearance, advances in stone tool technology, and changes in culture and behavior?

We hypothesize that:

1) Authigenic sediments in the Lake Magadi basin are the product of a combination of factors, including tectonic, volcanic, and climatic events. The variable whole-rock geochemistry likely reflects evaporative concentration of lake waters due to long-term aridification in the region, as well as pulses of dilute inflow during humid phases over the past few hundred thousand years.
2) The mineralogy and geochemistry of the ODP-OLO12-1A core likely reflects a hydrologically open lake that was subject to regional desiccation over the past few hundred thousand years. Regional tectonic and volcanic activity

likely caused hydrologic closure of the Koora Graben paleolake and aided in the desiccation of the basin throughout the Mid to Late Pleistocene.

3) Modern surface and outcrop samples from southern Kenya can be used to identify weathering patterns and geologic source regions in the study area, as well as identify mineral reactions that occur in outcrop, soils, and lake basins. It is likely that zeolites form in most environments of southern Kenya, however, analcime likely requires a highly concentrated alkaline brine to precipitate. Other authigenic minerals, such as sodium carbonates (i.e. trona and nahcolite) and sodium silicates (i.e. magadiite, kenyaite and makatite) are most likely form through similar processes as analcime.
4) Hominin evolutionary events and changes in stone tool technology are related to rapid changes or increased variability in environmental conditions over the past ~1 Myr across East Africa.

We can test the first and second hypotheses through mineralogical and geochemical analysis, to identify trends and rhythms associated with global climate patterns on Milankovitch timescales (i.e. ~23, 41, and 100 kyr cycles), as well as evidence of tectonic activity or volcanic input to the basin. The third hypothesis can be tested by completing a full characterization of outcrop and surface samples and comparing the data to datasets from the HSPDP-MAG14 and ODP-OLO12 cores, as well as identifying relationships between geologic source regions and core material, presence and absence of minerals by locality, and evidence of dissolution-precipitation reactions through SEM analysis of select samples. The final hypothesis can be tested by constructing high-resolution records of environmental change from the region, interpreting the role of climate and tectonic activity in environmental variability, and working

with archeological and paleoanthropological records from nearby outcrop studies to identify relationships between paleoenvironmental change and hominin evolutionary benchmarks.

3 METHODS

Drill cores were collected in the Koora Graben (Paleolake Koora) in 2012 and from Lake Magadi in 2014, two adjacent basins in the Southern Kenya Rift during the ODP and HSPDP campaigns. Outcrop samples were collected during the 2014 and 2015 field seasons in southern Kenya. Cores were shipped to the National Lacustrine Core Facility (LacCore) and Continental Scientific Drilling Coordination Office (CSDCO) at University of Minnesota for storage and initial core descriptions, and outcrop samples were shipped through intermediaries to Georgia State University for processing and XRD and SEM analyses. Samples collected for geochemical analyses were shipped to Activation Laboratories and ALS Geochemistry.

3.1 Scientific Drilling & Coring

3.1.1 Drilling Operations

Continuous sediment cores were collected from the Koora Graben (ODP) in 2012 and Lake Magadi (HSPDP) in 2014. Summarized from Cohen et al (2016): Two holes were drilled in the Koora Graben; ODP-OLO12 Core 1A obtained ~167 m of core material and Core 3A recovered ~113 m with >90% recovery. Four holes were drilled at Lake Magadi during the HSPDP campaign. HSPDP-MAG14 Core 1A reached a depth of ~127 m and HSPDP-MAG Core 2A bottomed out at ~197 m, with ~55% average recovery. HSPDP-MAG14 Core 1B was reamed to a depth of ~122 m and ~2 m were recovered, while in HSPDP-MAG14 Core 1C the upper ~18 m and basal ~4 m were recovered - reaching a depth of ~129 m. Cores were packaged in crates and shipped to LacCore at University of Minnesota for processing and archiving. Downhole logging was undertaken at Lake Magadi in Hole 2A but not in the Koora Graben.

3.1.2 Initial Core Description & Sampling

Initial core descriptions (ICD) took place at LacCore, the National Lacustrine Core Facility – six floors underground in the Civil Engineering Building at University of Minnesota-Twin Cities, following protocol established by LacCore and CSDCO. Whole cores were logged on a Geotek Multi-Sensor Core Logger (MSCL-S) prior to the ICD. Cores were split from top down using one of three methods depending on lithology and water content: 1) a cast saw and piano wire; 2) band saw; or 3) tile saw. After cores were split and cleaned, the archive halves were imaged using high-resolution Geotek Geoscan-III, multi-scanned for magnetic susceptibility, color reflectance, grey scale, and gamma ray logging on a Geotek MSCL-XYZ, and for core description before being wrapped and placed in a D-tube for cold storage. The working halves of the cores were sampled for multi-proxy analyses. Remaining working halves were wrapped and placed in a D-tube for cold storage.

The ODP-OLO12 team collected samples for mineralogy and bulk geochemistry at 32 cm intervals, and the HSPDP-MAG14 team collected samples at 32 cm intervals for Cores 1A, 1B and 1C, but samples were taken at 16 cm intervals for HSPDP-MAG14 Core 2A. Opportunistic samples were selected from intervals where variable lithologies were observed. A total of 303 samples were obtained from ODP-OLO12 Core 1A, 202 samples from HSPDP-MAG14 Core 1A, and 716 samples from HSPDP-MAG14 Core 2A. Samples collected from HSPDP-MAG14 Cores 1B and 1C were not included in analyses for this dissertation. Samples were packaged and shipped to Georgia State University for analyses.

A second round of high-resolution sampling on ODP-OLO12 1A took place in 2015 to obtain ~100 samples from a finely laminated section of the core. Some material from HSPDP-

MAG14 1A & 2A suspected of contamination by drilling fluid were discarded and the cores were resampled throughout select intervals in 2016.

3.2 Field Sampling

We completed fieldwork during the summers of 2014 and 2015 in southern Kenya. Samples were collected from throughout the western Kajiado District, including from near Kiserian (zeolitic volcanics and vertisols), Oltepesi (weathered basalt outcrop), Olorgesailie (zeolitized tuff), Ol Doinyo Nyokie (tuffs and volcanic glass), the eastern lagoon at Lake Magadi (High Magadi Beds), Lake Magadi (trona and clays), Nasikie Engida (nahcolite and trachyte), Ewaso Ngiro (suspended sediments), and the Nguruman Escarpment (saline clay). Samples were collected with a plastic trowel, assigned a sample designation, and stored in clean plastic bags. Samples were double bagged, archived, and packaged for shipment. GPS coordinates were recorded for most sample localities but were lost or not recorded for a few sample locations.

3.3 X-ray Diffraction

Core material from ODP-OLO12 and HSPDP-MAG14 were dried in an oven for 24 to 48 hours at 40°C and powdered using a ball-and-pestle impact grinder. XRD analyses were conducted on a Panalytical X'pert Pro MPD using Cu K_{α}-radiation (λ = 1.5418 Å) operating at 45 kV and 40 mA. Randomly oriented mounts were analyzed to determine the bulk mineralogical composition using a spinning reflection sample stage. Samples were loaded in XRD sample changer mounts using Moore and Reynolds (1997) back-fill powder method. Analysis was performed with 30-minute scans from 5 to 70˚ 2θ at ~2° 2θ per minute step size with the following XRD settings: programmable divergent slit (PDS) with a fixed 1/4˚ slit, 1/2˚ fixed anti-scatter slit, a 10 mm mask, and a 0.04 rad soller slit on the incident beam; and 0.04 rad soller slits, Ni-filter, and programmable anti-scatter slit (PASS) with a fixed 1/4˚ slit on the

diffracted beam. Diffraction patterns were analyzed using Panalytical's High Score software suite with reference to PDF-2 database, Brindley and Brown (1980), and Moore and Reynolds (1997).

3.4 Geochemical Analysis

We collected samples at 32 cm intervals from ODP-OLO12 1A and HSPDP-MAG14 2A cores for bulk geochemical analysis. Samples were shipped to Activation Labs for geochemical analysis. Geochemical analysis of ODP-OLO12 and HSPDP-MAG14 samples was funded by Hong Kong Baptist University, with additional support for ODP-OLO12 analysis provided by the Smithsonian Institution's Human Origins Program. The bulk geochemical analysis utilizes a four acid digestion on Fusion ICP-MS (FUS-ICP), and trace element (TE) and rare earth element (REE) analysis on Instrumental Neutron Activation Analysis (INAA). Ten samples from the base of the ODP-OLO12 1A core - spanning the saprolitic zone to the unaltered trachytic basement, as well as 30 outcrop and surface samples from the Southern Kenya Rift were dried in an oven at 40° C for 48 hours, powdered using a ball and pestle impact grinder for 10 minutes, and sent to ALS Geochemistry for geochemical analysis via Fusion ICP-AES for bulk geochemistry and FUS-ICP for TE and REE geochemistry. Data is returned in Excel spreadsheet format, with bulk data in weight percent (wt. %) and TE and REE in parts per million (ppm) - equivalent to milligrams per kilogram (mg/kg).

3.5 Scanning Electron Microscopy & Energy Dispersive X-ray Spectrometry

We analyzed material from each sampling region for further analysis via scanning electron microscopy (SEM) and energy dispersive X-ray spectrometry (EDX) analysis. After completing XRD and geochemical analyses, materials that exhibited potential for answering questions about diagenetic reactions within the region were selected for SEM and EDX analysis

to attempt to identify which parent materials are altering to subsequent daughter products. Unprocessed samples of varying grain size were used in SEM analysis. Samples were sputter coated with carbon under vacuum to prevent “charging” due to electron accumulation on the non-charged sample surfaces. Analysis was completed at Georgia State University using a Tescan Vega 3 scanning electron microscope with an EDAX energy dispersive X-ray spectrometer.

4 MINERALOGICAL AND GEOCHEMICAL TRENDS OF THE *HOMININ SITES AND PALEOLAKES DRILLING PROJECT* IN THE LAKE MAGADI BASIN, SOUTHERN KENYA

Nathan M. Rabideaux[a], Daniel M. Deocampo[a], Tim K. Lowenstein[b], Robin W. Renaut[c], R. Bernhart Owen[d], Andrew S. Cohen[e], Chris Campisano[f]

[a] *Georgia State University, Department of Geosciences, Atlanta, GA 30302 USA*

[b] *State University of New York, Department of Geological Sciences, Binghamton, NY 13902 USA*

[c] *University of Saskatchewan, Department of Geological Sciences, Saskatoon, Saskatchewan, S7N 5E2, Canada*

[d] *Hong Kong Baptist University, Department of Geography, Kowloon Tong, Hong Kong*

[e] *University of Arizona, Department of Geosciences, Tucson, AZ 85721 USA*

[f] *Arizona State University, School of Human Evolution and Social Change, Tempe, AZ 85281 USA*

4.1 Abstract

Sediment cores were collected at Lake Magadi in southern Kenya as part of the *Hominin Sites and Paleolakes Drilling Project* to construct high-resolution paleo-environmental records of Mid to Late Pleistocene climate change. Mineralogical and geochemical analysis of core samples from Lake Magadi indicate that the lake began as a fresh to mildly saline lake at ~1.08 Ma and became more saline and alkaline over the past one million years. Carbonate grainstone at the base of the HSPDP-MAG14 cores suggests a series of shallow freshwater pools likely occupied the Magadi basin near its inception. A relatively deep lake likely occupied the basin for

~500 kyr. At ~350 ka, the mineralogical and geochemical records from Lake Magadi indicate that the geochemistry of the basin changed, with conditions becoming increasingly more saline and alkaline, which favored intensive zeolitic alteration. The alkalinity likely increased due to low-temperature surface weathering, tectonic and volcanic activity, and evaporative concentration. Abundant zeolites throughout the upper half of the cores suggest Lake Magadi experienced sustained aridification over the past ~350 kyr. Thick trona deposits began to accumulate at Lake Magadi at ~105 ka. The most common zeolites in the cores are analcime and erionite. Phillipsite, chabazite, clinoptilolite, mordenite, and natrolite are also present in varying abundance during some intervals. Analcime seems to have formed from around alkaline springs, on mudflats, or near the lake margin from Na-Al-Si gels that precipitated from concentrated brines. Erionite was formed mainly by the reaction of trachytic glass + $H_2O_{(brine)}$. Other zeolite phases formed from precursor aluminosilicate minerals reacted with concentrated brines or tuffaceous sediments reacted with dilute interstitial or surface waters. The cores contain only a few thin tephra and tuff deposits from a region known for abundant volcanism during the Pleistocene, implying that most of the volcaniclastic material was altered to zeolites. Climatic conditions trended toward increasingly arid conditions over the Late Pleistocene into the Holocene, contributing to the saline-alkaline environment of the Lake Magadi basin.

Keywords: Lake Magadi, Zeolites, Mineralogy, Geochemistry, HSPDP, Human Evolution

4.2 Introduction

The African continent has provided a robust record of hominin fossils and artifacts, which has aided scientists in understanding the origin and evolution of the human lineage. Since the Nineteenth Century, the East African Rift Valley (EARV) has drawn scientists to the region to study the rich geology, archeology, and paleontology to answer questions related to rift tectonism, volcanism, vertebrate and hominin evolution, and prehistoric stone tool technology (e.g., Gregory, 1921; Baker, 1958, 1963; Leakey, 1952; Isaac, 1978; Potts, 1996; Potts et al., 1999, 2004, 2018). Numerous sites in East Africa have produced evidence of hominin species extinction and emergence, stone tool use, control of fire, and cultural adaptations. These documented evolutionary benchmarks and adaptations have resulted in a number of theories that have attempted to explain a causal relationship between environmental change and hominin evolution (e.g., Laporte, 1990; Vrba, 1995; deMenocal, 1995, 2004; Potts, 1996, 1998; Potts et al., 1999, 2004, 2018; Trauth et al., 2005, 2007, 2009; Behrensmeyer, 2006; Cohen et al., 2009, 2016; Behrensmeyer et al., 2018; Brooks et al., 2018; Deino et al., 2018).

Perhaps the greatest challenge in developing theories concerned with the relationship between human evolution and environmental change has been the lack of continuous, unaltered environmental records that can be easily correlated with the hominin fossil and artifact records from outcrop. The most complete records of regional paleoclimatic variability have been obtained from deep-sea cores recovered in off-shore marine environments (e.g., deMenocal, 1995, 2004). Continental environments typically only provide discontinuous or altered paleo-environmental records, due to weathering and surface erosion. Additionally, there have been difficulties correlating marine and continental records due to temporal and spatial differences between the global- to regional-scale marine records and locally confined continental records

(Cohen et al., 2016). This has led to greater interest in scientific drilling and coring in continental settings, which enables the construction of long-term paleo-environmental records through multi-proxy studies. The *Hominin Sites and Paleolakes Drilling Project* (HSPDP) was established to provide high-resolution paleo-environmental records and to identify relationships between environmental change and important hominin evolutionary benchmarks (Cohen et al., 2009, 2016; Campisano et al., 2017).

HSPDP targeted six rift basins near important hominin fossil and artifact sites in Ethiopia and Kenya (Cohen et al., 2016; Campisano et al., 2017), including Lake Magadi. Lake Magadi is a modern saltpan located in the Southern Kenya Rift. The Southern Kenya Rift is an arid to semi-arid environment with low annual precipitation (<50 cm) and high daily temperatures (highs: ~35° C; lows: ~17° C). The EARV has two rainy seasons driven by the African-Asian monsoonal system (McGregor and Nieuwolt, 1998). Precessional cyclicity is thought to drive the monsoonal system, with humid periods occurring during precessional maxima and arid intervals during precessional minima on ~23 kyr timescales (deMenocal, 2004). Long-term climate cyclicity operates on eccentricity timescales, with episodes including large lakes development during 100-kyr and 400-kyr eccentricity maxima (Trauth et al., 2007).

The Magadi basin is located in an axial graben at the lowest point of the southern rift valley at an elevation of ~600 m (Fig. 4.1). The lake is primarily recharged by alkaline springs near the lake margin, with only minor input from ephemeral surface run-off that deposits material in the basin during rainy seasons (Eugster and Jones, 1968). The modern lake is characterized by concentrated alkaline brines, with ~35% salinity and pH values ranging from ~9-11. Although there are abundant detrital alkali feldspars and quartz in the basin, the vast majority of Lake Magadi sediments are comprised of authigenic minerals that formed as

chemical precipitates or through alteration of detrital material interacting with alkaline brines within the basin (Herrick, 1972; Surdam and Eugster, 1976).

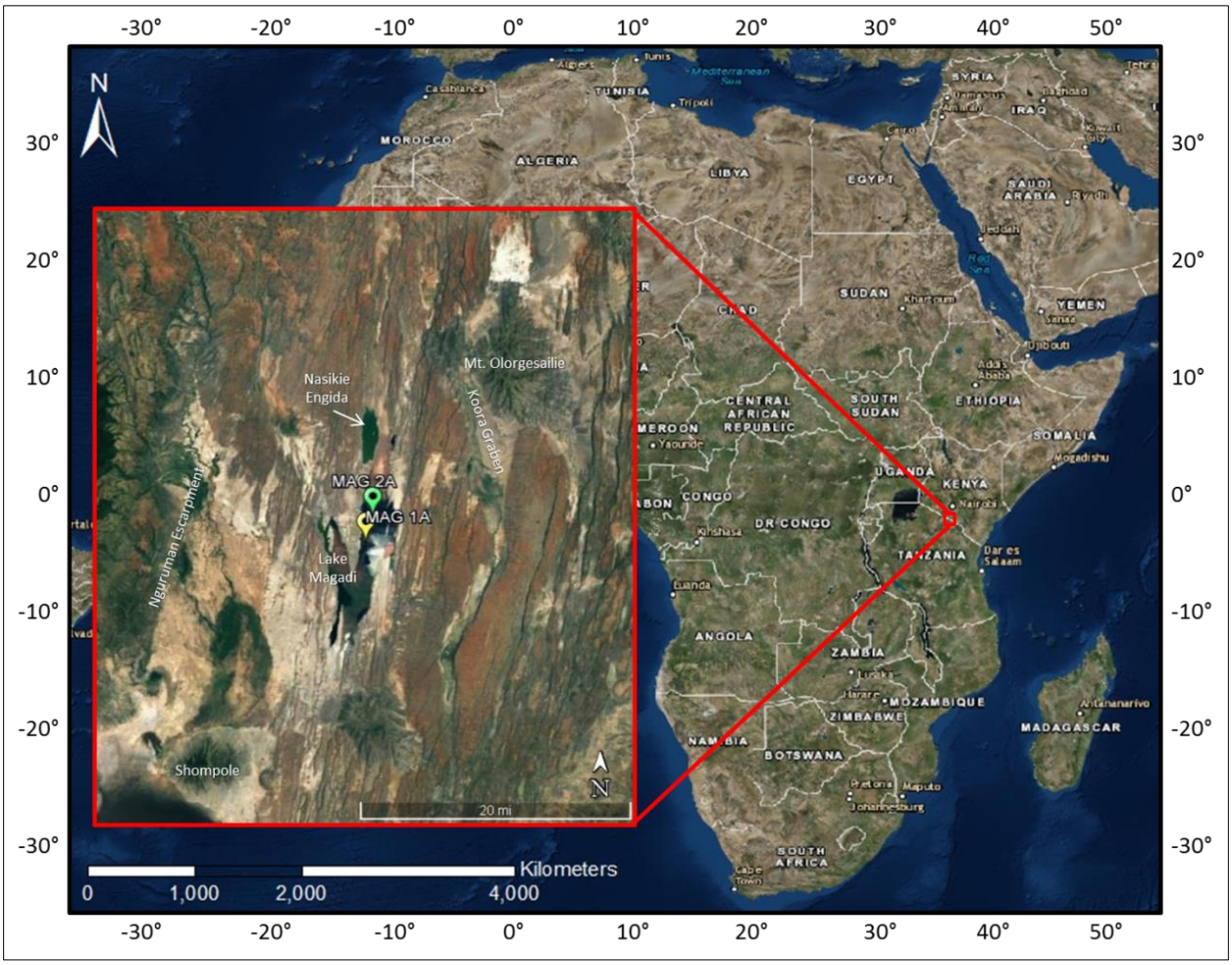

Figure 4.1: Map of African continent and zoomed inset of the Southern Kenya Rift with important features labelled.

The geology of the Southern Kenya Rift has been studied extensively over the past couple of centuries (e.g., Gregory 1921; Baker, 1958, 1963, 1987; Jones et al., 1967; Eugster, 1967, 1970, 1980; Eugster and Jones, 1968; Surdam and Eugster, 1976; Jones et al., 1977; Isaac, 1978; Owen, 1981; Owen and Renaut, 1981; Hillaire-Marcel et al., 1986; Hillaire-Marcel and Casanova, 1987; Behr and Röhricht, 2000; Behr, 2002; Owen et al., 2008, 2009, 2011; Deocampo et al., 2010). Baker (1958, 1963) provided the earliest detailed geologic study in the

region. The Precambrian basement is comprised of gneisses, quartzites, and schists. A significant hiatus marks the boundary between the metamorphic basement and the onset of Miocene volcanic rocks and ash deposits. This volcanic sequence begins with the Olorgesailie basalts, ash and pumice, which are overlain by Oltepesi basalts. Most of the rift floor in southern Kenya was blanketed by Magadi flow trachytes, which are contemporaneous in age with the Ol Doinyo Nyokie trachyte and ash deposits (~1.05 Ma; Deino et al., 1992). Carbonatite and nephelinite ash sourced from the Kerimasi and Ol Doinyo Lengai volcanoes represent some of the younger volcanic depositional episodes in the region (Hay, 1983).

Quaternary sedimentary deposits in southern Kenya are typically younger than ~1.2 Ma, when sedimentary basins began to form in the rift valley. The oldest sedimentary deposits in the Southern Kenya Rift are the Olorgesailie Formation (~1200-499 ka). The oldest sedimentary units in the Lake Magadi basin are the Oloronga Beds (~800-300 ka). The Chert Series/Green Beds (~300-80 ka) are overlain by the High Magadi Beds (~24-9 ka) in the Magadi basin. The youngest sediments are capped by the Evaporite Series (~9 ka to present), which is mostly trona and nahcolite. Abundant zeolitic alteration has been observed in sediments deposited post-Oloronga Beds in the Lake Magadi basin (Herrick, 1972; Surdam and Eugster, 1976; Crossley, 1979).

Zeolites most commonly form through the alteration of volcanic glass in saline, alkaline waters (Hay, 1963, 1966; Sheppard and Gude, 1968, 1969; Surdam and Eugster, 1976), although they have been observed in many other geologic environments. Previous studies in the Southern Kenya Rift have described the authigenic minerals of Lake Magadi and provided observations and interpretations of possible mineral reactions responsible for the formation of these assemblages in terms of glass and brine chemistry (Eugster and Jones, 1968; Surdam and

Eugster, 1976; Eugster, 1977). The importance of Na-Al-Si gels in the formation of zeolites is still a subject of some debate. Some of the proposed zeolitic reactions are as follows (Surdam and Eugster, 1976):

(1) trachytic glass + H_2O → erionite

(2) trachytic glass + Na-rich brine → Na-Al-Si gel

(3) Na-Al-Si gel → analcime + H_2O

(4) erionite + Na^+ → analcime + K^+ + SiO_2 + H_2O

Due to the low content of alkaline earths in the trachytic sediments, erionite can form from the direct alteration of trachytic glass reacting with lake waters (Surdam and Eugster, 1976). Analcime can form from Na-Al-Si gels that coalesce near alkaline springs near the lake margin and are washed into the basin by seasonal runoff or through alteration of feldspars, clay minerals, and other zeolites (Eugster and Jones, 1968). Other zeolite species (e.g., phillipsite, mordenite, clinoptilolite, chabazite) form through subsequent reactions between erionite, analcime, and volcanogenic sediments when more alkaline earths are available; Al-Si gels may act as an intermediate phase in some reactions.

This study examines the mineralogical and geochemical record from HSPDP cores collected at Lake Magadi to understand the geochemical evolution of lake waters in the basin. Additionally, we will attempt to relate these records to previous studies from the region to gain a better understanding of southern Kenya's environmental, climatic, and tectonic history. The goal of this project is to construct a high-resolution paleoenvironmental record that spans nearly one million years during the Late Quaternary in the Southern Kenya Rift.

4.3 Methods

4.3.1 Drilling and Core Recovery

Sediment cores were collected from Lake Magadi in summer 2014. Cohen et al (2016) presented the drilling outcomes for the HSPDP campaign (Fig. 3.1). Four holes were drilled at Lake Magadi. HSPDP-MAG-1A reached a depth of ~127 m and HSPDP-MAG-2A bottomed out at ~197 m, with ~55% average recovery. HSPDP-MAG14-1B was reamed to a depth of ~122 m and ~2 m were recovered, while in HSPDP-MAG-1C the upper ~18 m and basal ~4 m were recovered - reaching a depth of ~129 m. Cores were packaged in crates and shipped to LacCore at University of Minnesota for processing and archiving. Downhole logging was undertaken at Lake Magadi in Hole 2A.

4.3.2 Initial Core Description

Initial core descriptions (ICD) took place at LacCore, the National Lacustrine Core Facility – six floors underground in the Civil Engineering Building at University of Minnesota-Twin Cities, following protocol established by LacCore and CSDCO. Samples for mineralogy were taken at 32 cm intervals HSPDP-MAG14 Cores 1A, 1B and 1C, whereas samples were taken at 16 cm intervals for HSPDP-MAG14 Core 2A. Samples for geochemical analysis were collected at 32 cm intervals from HSPDP-MAG14 Core 2A. Opportunistic samples were taken from intervals where variable lithologies were observed. A total of 202 samples were obtained from HSPDP-MAG14-1A and 716 samples from HSPDP-MAG14-2A. Samples collected from HSPDP-MAG14 Cores 1B and 1C were not included in this study.

4.3.3 XRD Analysis

Samples from HSPDP-MAG14 were dried in an oven for 24 to 48 hours at 40°C and powdered using a ball-and-pestle impact grinder to remove residual moisture. XRD analyses

were conducted on a PANalytical X'pert Pro MPD using Cu K_α-radiation (λ = 1.5418 Å) operating at 45 kV and 40 mA. Randomly oriented mounts were analyzed to determine the bulk mineralogical composition using a spinning reflection sample stage. Samples were loaded in XRD sample changer mounts using Moore and Reynolds (1997) back-fill powder method. Analyses were performed with 30-minute scans from 5 to 70˚ 2θ at ~2° 2θ per minute step. Diffraction patterns were analyzed using PANalytical's High Score software suite with reference to PDF-2 database, Brindley and Brown (1980), and Moore and Reynolds (1997).

4.3.4 Geochemical Analysis

Geochemical analysis was funded by Hong Kong Baptist University grant #202213. We collected samples at 32 cm intervals from HSPDP-MAG14-2A cores for bulk geochemical analysis. Samples for geochemical analysis were shipped to Activation Labs. Bulk geochemical analysis was completed using a four acid digestion on Fusion ICP-MS (FUS-ICP), and trace element (TE) and rare earth element (REE) analysis on Instrumental Neutron Activation Analysis (INAA).

4.3.5 Age Model

The age model for the HSPDP-MAG14 cores was constructed using a variety of absolute and relative dating techniques that included: $^{40}Ar/^{39}Ar$ dating of single-crystal feldspars collected from volcanic tuffs, pumices, and tephras (Deino); radiocarbon dating of organic matter and microcharcoal in the upper portion of the cores (Cohen); disequilibrium Th/U-dating of cherts (Lowenstein et al., 2017, 2018); and paleomagnetic dating through identification of the Brunhes-Matuyama magnetic reversal (Sier). The age model for HSPDP-MAG14-2A is complete, but the age model for HSPDP-MAG14-1A is still in the preliminary stages. The age model was run compiled through Bacon for R.

4.4 Results

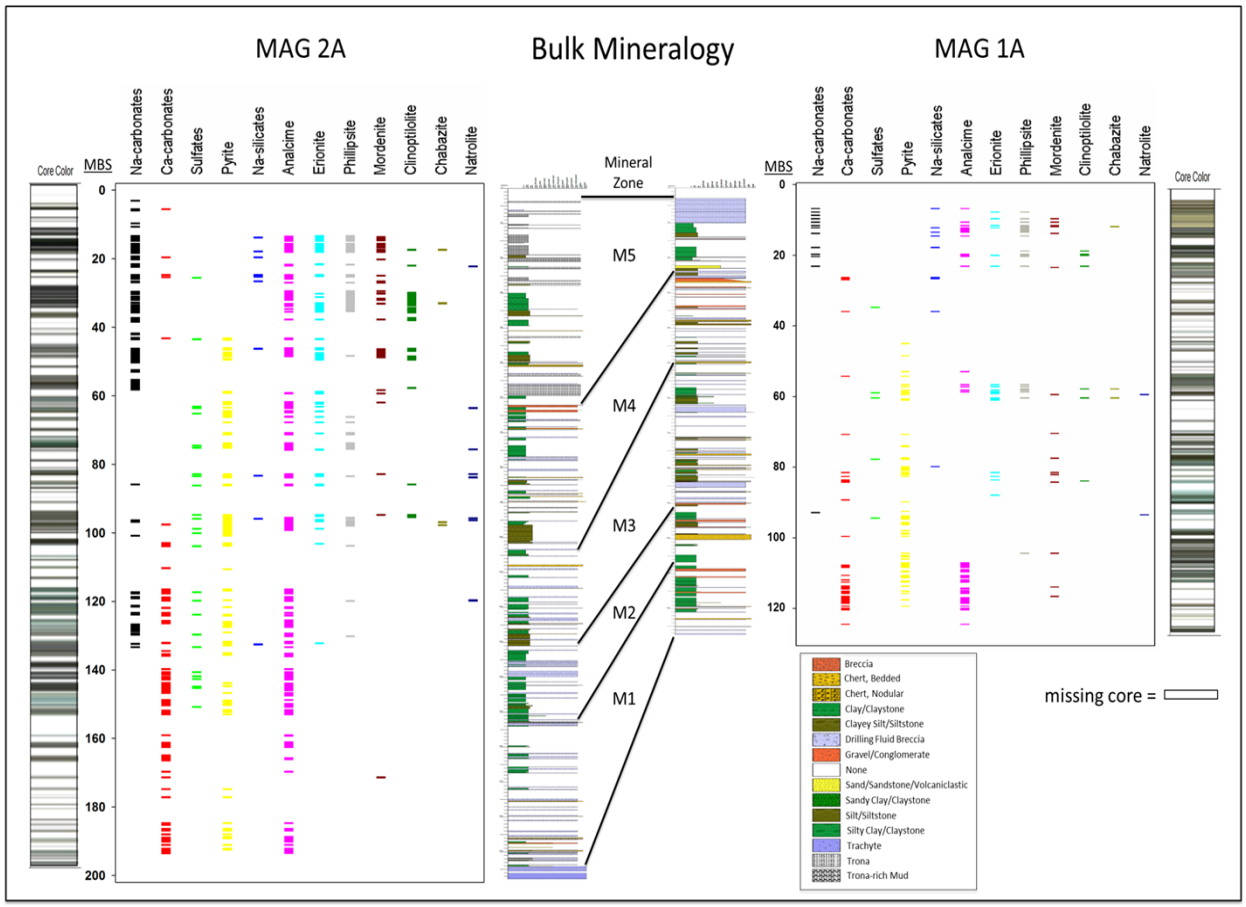

Figure 4.2: Composite figure of HSPDP-MAG14 core material, including mineralogy and mineral zones (this study), core color, lithologies, an stratigraphic columns (Cohen et al., 2016).

4.4.1 Mineralogy

The HSPDP-MAG14 cores are comprised of mostly authigenic minerals, although there are abundant detrital alkali feldspars (sanidine and anorthoclase) throughout the cores (Fig. 4.2). HSPDP-MAG14-1A exhibits a similar overall pattern of mineralogy to HSPDP-MAG14-2A, although there are significant gaps in the 1A record due to drilling mud contamination, lower resolution sampling intervals, and zeolite assemblages that differ from that of HSPDP-MAG14-2A (Figs. 4.2 & 4.3). We present the results of HSPDP-MAG14-2A here with some reference to HSPDP-MAG14-1A.

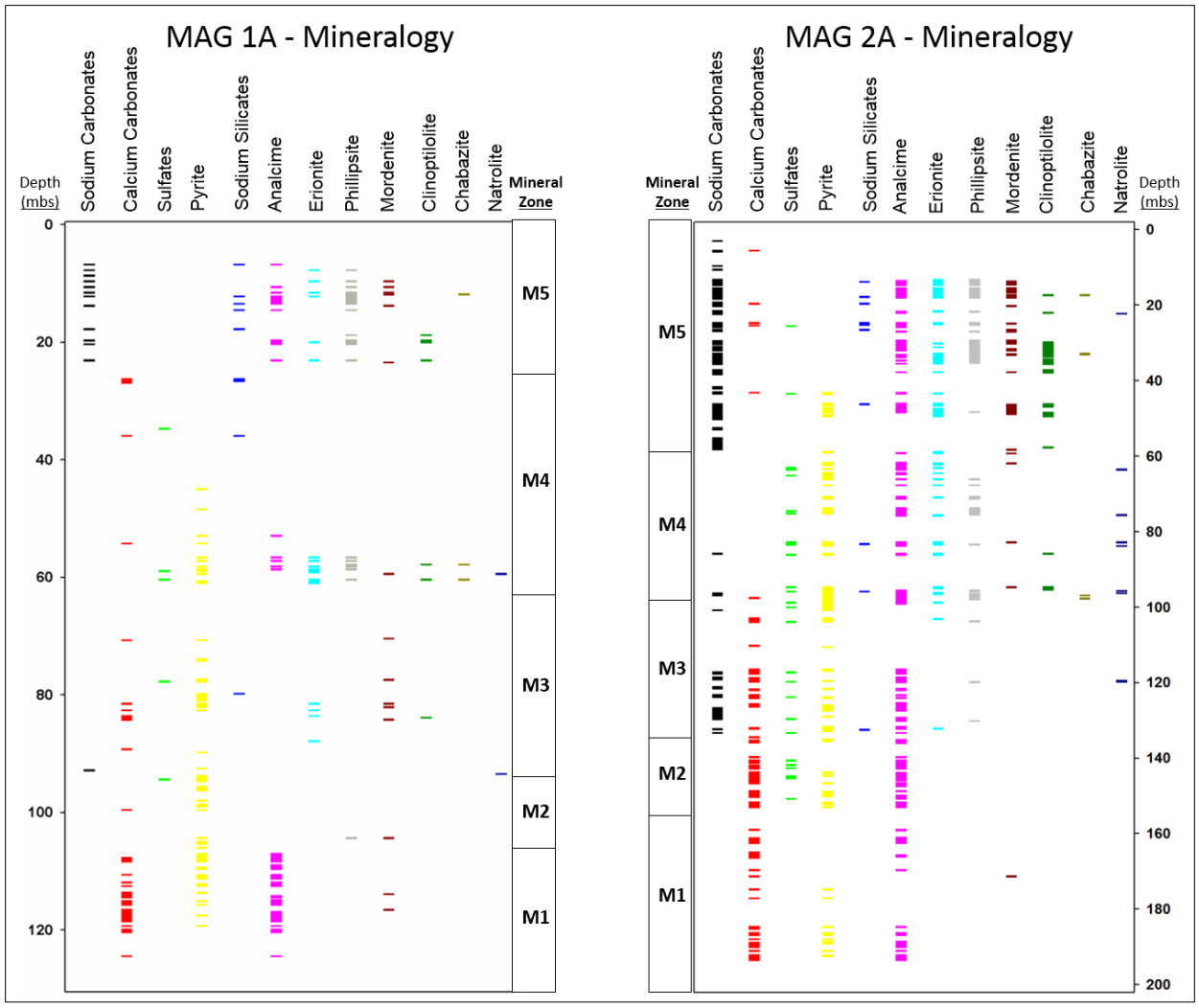

Figure 4.3: Mineralogy of HSPDP-MAG14 Cores 1A and 2A plotted versus depth, with correlating mineral zones.

We divided the HSPDP-MAG14 Core 2A into five distinct mineral zones based on primary mineral assemblages (Fig. 4.3). Bulk mineralogy in Zone M1 (from the base of the core to ~158 mbs) of the HSPDP-MAG14-2A core hosts mostly calcium carbonates, pyrite, and analcime. Zone M2 (~158 to 138 mbs) contains, calcium carbonates, pyrite, sulfates, and analcime. There are abundant calcium carbonates, as well as significant sodium carbonates, sulfates, pyrite, and analcime in Zone M3 (~138 to 100 mbs). Abundant zeolites, as well as pyrite and sulfates constitute the bulk of authigenic minerals in Zone M4 (~100 to 60 mbs). The

uppermost Zone M5 (~60 mbs to top of core) contains mostly sodium carbonates and zeolites. From ~60 to 45 mbs, sodium carbonates are the main mineral components. In the ~45 to 25 mbs interval, the mineralogy contains abundant zeolites, sodium carbonates, and pyrite. The uppermost ~25 m contains a mix of mostly trona and a diverse assemblage of zeolites, as well as minor calcium carbonates and sodium silicates (Fig. 4.3). Detrital feldspars and quartz are present throughout the cores, as well as abundant authigenic chert and opal-A.

4.4.2 Geochemistry

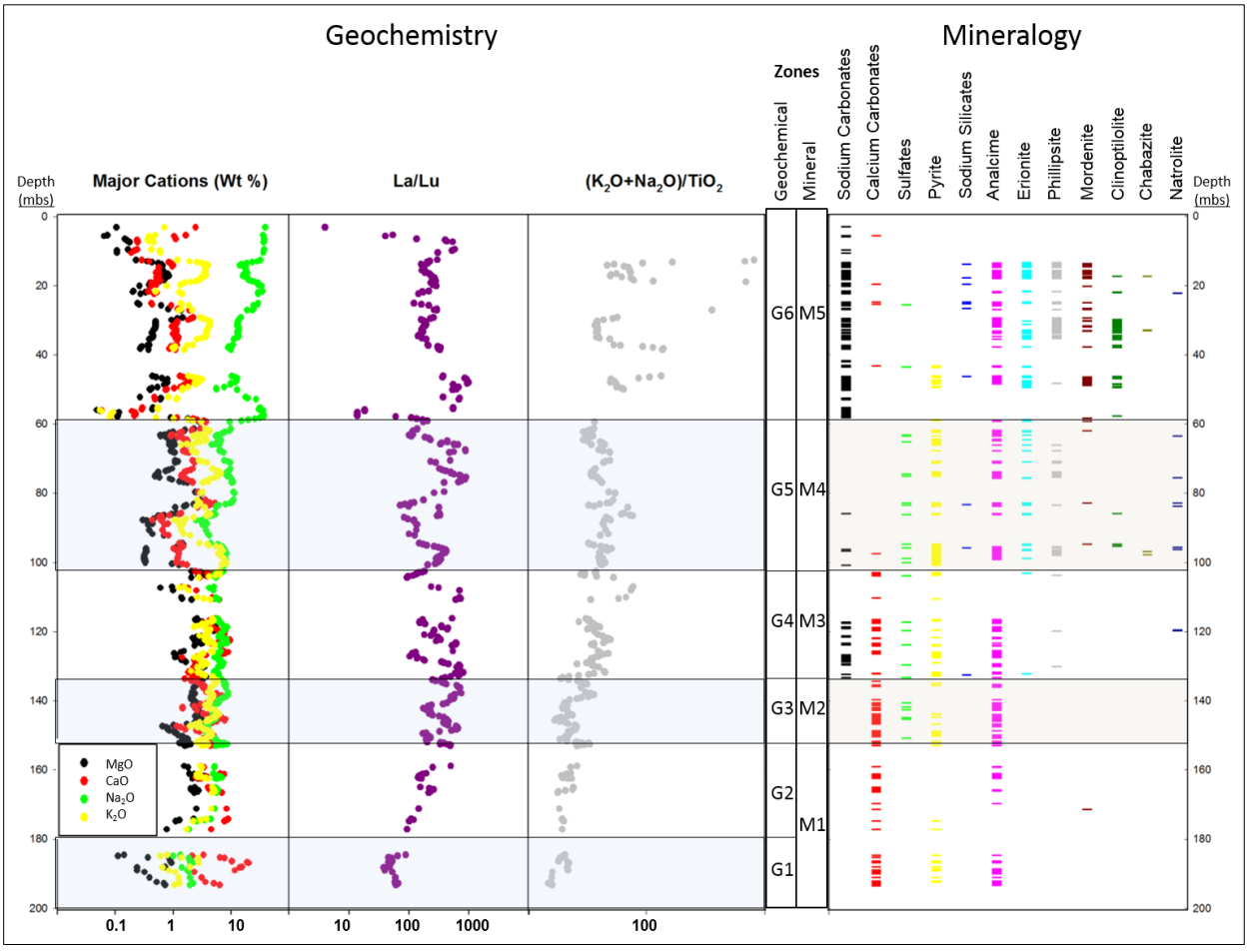

Figure 4.4: Composite analytical plot for HSPDP-MAG14-2A. Geochemistry plots for (L to R) major cations, indicator of light versus heavy rare earth elements, and salinity indicator, with geochemical zones. Mineralogy and corresponding mineral zones on the right. All plotted against depth.

All geochemical data are plotted on logarithmic scales with five-point running averages. Six distinct geochemical zones are identifiable in HSPDP-MAG14-2A (Fig. 4.4). Geochemical Zone G1 (from the base of the core to ~180 mbs) is represented by high Ca/Na ratios, and low Zirconium-Titanium (Zr/Ti) and Strontium-Calcium (Sr/Ca) ratios, high La/Lu ratios, and low $(K_2O + Na_2O)/TiO_2$ values. Zone G2 (~180 to 152 mbs) is represented by increasing $(K_2O + Na_2O)/TiO_2$ values and higher Sr/Ca ratios, as well as increasing Mg^+ concentrations, low Ca/Na ratios, and lighter REE enrichment. Mineralogical Zone M1 correlates well with both Zones G1 and G2. Geochemical Zone G3 (~152 to 105 mbs) is marked by higher Zr/Ti ratios, lower Sr/Ca ratios, enrichment of lighter REE, and increasing $(K_2O + Na_2O)/TiO_2$ values. Geochemical Zone G3 correlates with Zone M2. Zone G4 (~105 to 58 mbs) contains a pronounced increase in $(K_2O + Na_2O)/TiO_2$ values and enrichment of light REE, as well as intervals of increased Zr/Ti and Sr/Ca ratios, increasing Mg^+ concentration, and a pronounced decrease in Ca^{2+}. Geochemical Zone G4 correlates with mineralogical Zone M3. Geochemical Zone G5 (~60 to 40 mbs) is marked by higher Zr/Ti and Sr/Ca ratios and significantly higher $(K_2O + Na_2O)/TiO_2$ values, as well as a pronounced decrease in major cations (Ca^{2+}, K^+, and Mg^{2+}) relative to Na^+. Geochemical Zone G5 correlates well with mineralogical Zone M4 (Fig. 4.4).

4.5 Discussion

Mineralogical analysis indicated the sedimentary deposits at Lake Magadi are dominated by authigenic minerals (Herrick, 1972; Surdam and Eugster, 1976), with the exception of abundant detrital alkali feldspars and quartz that are washed into the basin by seasonal runoff and eolian dust transported by wind. Geochemical analysis indicates the lake was relatively fresh during the Lake Oloronga phase (~800 to 300 ka), and became progressively more saline throughout the Pleistocene (Figs. 4.4 & 4.5). There is also some variation between Sites 1A and

2A, with less analcime and more Ca/Mg-zeolites (i.e. mordenite, chabazite) forming in the lower portion of the core in HSPDP-MAG14-1A (Figs. 4.2 & 4.3). This type of mineral variation in a basin is likely reflecting evaporative concentration displaying zeolitic zonation, with HSPDP-MAG14-1A being closer to the lake margin and receiving more input of alkaline earths from dilute surface inflow and HSPDP-MAG14-2A reflecting more concentrated waters in the deeper part of the basin.

Our data suggest Lake Magadi was a fresh to mildly saline environment during its inception and became more saline with increased alkalinity prior to ~320 ka (Fig. 4.4), and eventually became a hypersaline ephemeral lake by ~70 ka. Zeolitic alteration in HSPDP-MAG14 core material varied significantly between sites, as did the abundance of sulfur-bearing minerals (Figs. 4.2 & 4.3). The transition from calcium carbonate precipitation to zeolitic alteration at ~320 ka (~100 mbs) suggests lake waters became increasingly more saline, and the precipitation of sodium carbonates ~70 ka (~60 mbs) indicates conditions became much more alkaline (pH > 9). Progressive zeolitic alteration in the upper ~100 meters of HSPDP-MAG14-2A suggests the lake waters became more concentrated and more saline through the Pleistocene and early Holocene. Variability in zeolite assemblages may reflect lake level fluctuations, with alkaline zeolites forming when dilute waters interact with concentrated brines. Alternatively, percolating brines could become depleted in Na^+ when sodium carbonates are precipitating at the lake surface, promoting the formation of alkaline earth-hosting zeolites in the shallow lake beds.

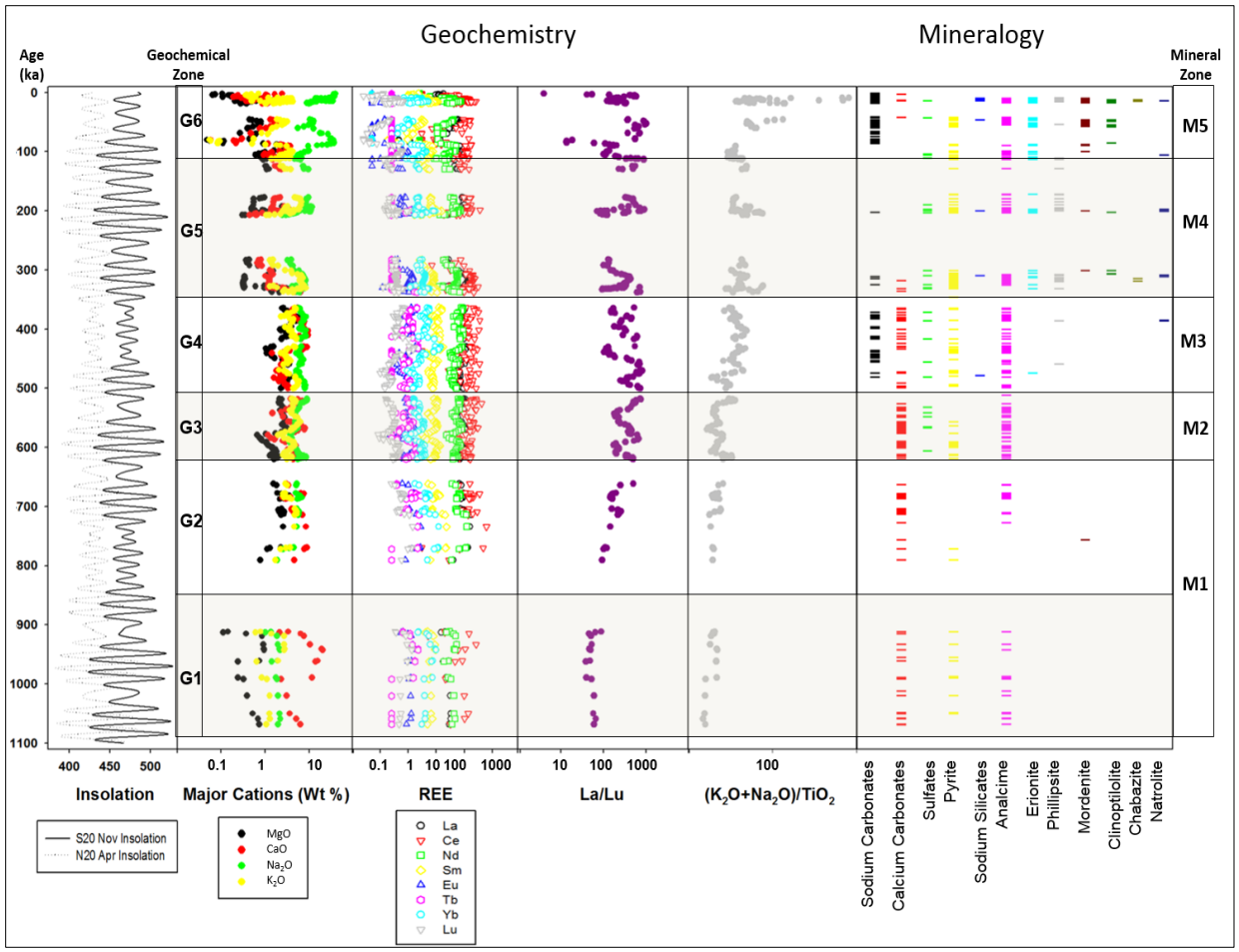

Figure 4.5: Composite analytical plot for HSPDP-MAG14-2A. Geochemistry plots for (L to R) spring and fall insolation in equatorial East Africa, major cations, indicator of light versus heavy rare earth elements, and salinity indicator, with geochemical zones. Mineralogy and corresponding mineral zones on the right. All are plotted against age. Geochemistry data plotted on logarithmic scales with five-point running averages..

4.5.1 Mineralogical Zone M1 and Geochemical Zones G1 & G2 (~197-153 mbs; ~1.1 Ma-620 ka)

Mineral Zone M1 consists of primarily low Mg-calcite and analcime, as well as intervals of calcite, chert, and pyrite appear in the record from ~1,100-620 ka (~150 to 135 mbs). Major element geochemistry indicates Ca^{2+} was the dominant major cation from the base of the core to ~110 mbs (Figs. 4.5). The basal sedimentary unit in both cores is a carbonate grainstone, which sits on the Magadi Trachyte (~1.4-0.7 Ma) and contains some gastropods and ostracodes in the

HSPDP-MAG14-1A core. This suggests sedimentation in the Magadi basin likely originated on a relatively flat surface of trachyte in a series of shallow freshwater pools or wetlands. Interbedded black and green muds and chert lay upon the carbonate grainstone, with some muds containing euhedral pyrite and chert intervals with preserved diatoms. Analcime is a common constituent of the muds in HSPDP-MAG14-2A, whereas mordenite is more common in the lower portion of HSPDP-MAG14-1A (Fig. 4.2 & 4.3). The interbedded mud and chert sequence may be indicative of fluctuating lake levels, with the muds accumulating during highstands and the chert precipitating during lowstands. Alternatively, this sequence may suggest a deep stratified lake with a chemocline.

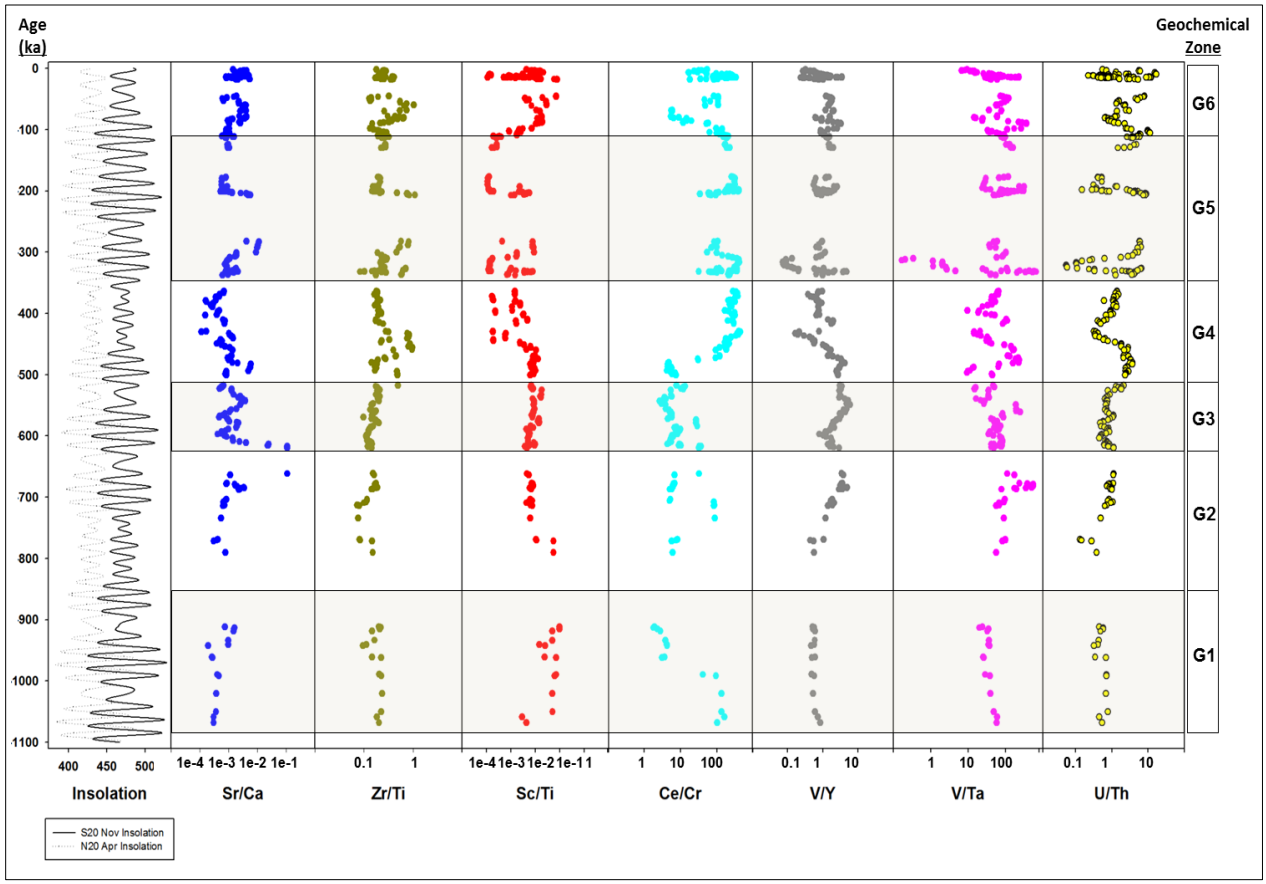

Figure 4.6: Geochemical source indicators for HSPDP-MAG14-2A. Plotted on logarithmic scales with five-point running averages.

The zeolite assemblages we see in the HSPDP-MAG14-2A core suggest analcime has likely been forming from Na-Al-Si gels since the onset of sedimentation just after basin formation, while the lake was still relatively fresh. There is a similar pattern of authigenic quartz (chert) in the HSPDP-MAG14-2A core (Figs. 4.2 & 4.3), which may indicate similar processes are involved in the formation of the aluminosilicate gels and sodium silicates (precursors to inorganic chert).

Subsequent studies on the origin of cherts at Lake Magadi proposed another method of formation for sodium silicates and cherts (Behr and Röhricht, 2000; Behr, 2002). Behr (2002) suggested that sodium silicates were formed partially through early diagenesis on mudflats, and were subsequently silicified into chert through interaction with silica-rich surface brines. This model did not necessitate a deep lake or a chemocline, which were included as necessary features in the formation of sodium silicates and chert in previous models (Eugster, 1967, 1969; Hay, 1968; Behr, 2002). This may provide sufficient explanation as to why there are abundant chert intervals in the HSPDP-MAG14 cores, but only a few intervals with significant sodium silicates (Figs. 4.2 & 4.3).

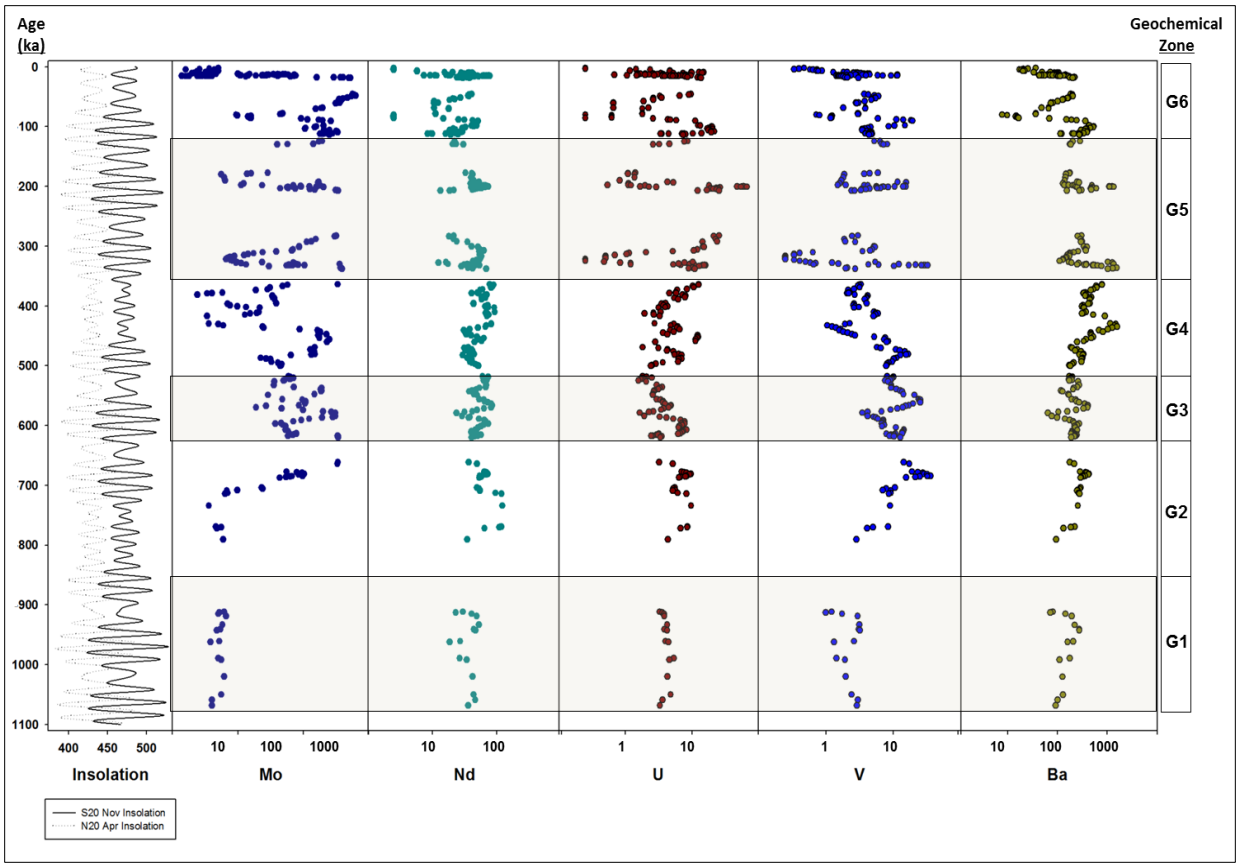

Figure 4.7: Geochemical single-element source indicators from HSPDP-MAG14-2A. All plotted on logarithmic scales with five-point running averages.

4.5.2 Mineralogical Zone M2 and Geochemical Zone G3 (~153-135 mbs; ~620-510 ka))

Zone M2 is mostly comprised of analcime and low Mg-calcite, in addition to calcite, pyrite, sulfates (bloedite and thenardite), sodium carbonates (trona and nahcolite), and minor amounts of erionite, phillipsite, and sodium silicates (magadiite and makatite) (Figs. 4.2 & 4.3). Zirconium-titanium ratios indicate changes in source material in Zone G3 (Figs. 4.6 & 4.7). Salinity indicators and major cation ratios suggest the lake waters became more saline.

Alternatively, changes in the water chemistry may have been the result of a local volcanic event, which may have deposited nepheline and or alkali carbonate-rich material erupted from the Kerimasi volcano into the basin resulting in more saline alkaline conditions in the lake. The

earliest interval of Zone G3 is marked by an increase in Zr/Ti ratios, which is indicative of changing source material (Fig. 4.6). In this case, it is most likely due to volcanic ash deposited in the basin and not a change in hydrologic source region. The Kerimasi and Ol Doinyo Lengai strato-volcanoes are a probable source of nephelinite and carbonatite ash in this interval, and Kerimasi may have deposited material in the basin during pulses of active volcanism in the late Pleistocene, followed by later eruptions from Ol Doinyo Lengai during the late Pleistocene through early Holocene (Dawson, 1962, 2008; Hay, 1983). The presence of dawsonite and minor natrolite in Zone M2 may further support this interpretation (Figs. 4.2 & 4.3). Although Di Piazza et al. (1959) experimentally showed that zeolites do not form from nepheline, Hay (1963) presented evidence that tuffs from Bed V at Olduvai Gorge exhibited zeolitic alteration of nepheline-rich tuffs. Hay suggested hydration and carbonation as the principal chemical changes in the zeolitic alteration of nepheline according to the following reaction:

$$3H_2O + CO_2 + 3NaAlSiO_{4(\text{nepheline})} = NaAl(OH)_2CO_{3(\text{dawsonite})} + Na_2Al_2Si_3O_{10} \cdot 2H_2O_{(\text{natrolite})}.$$

4.5.3 Mineralogical Zone M3 and Geochemical Zones G4 (~135-105 mbs; ~510-350 Ka)

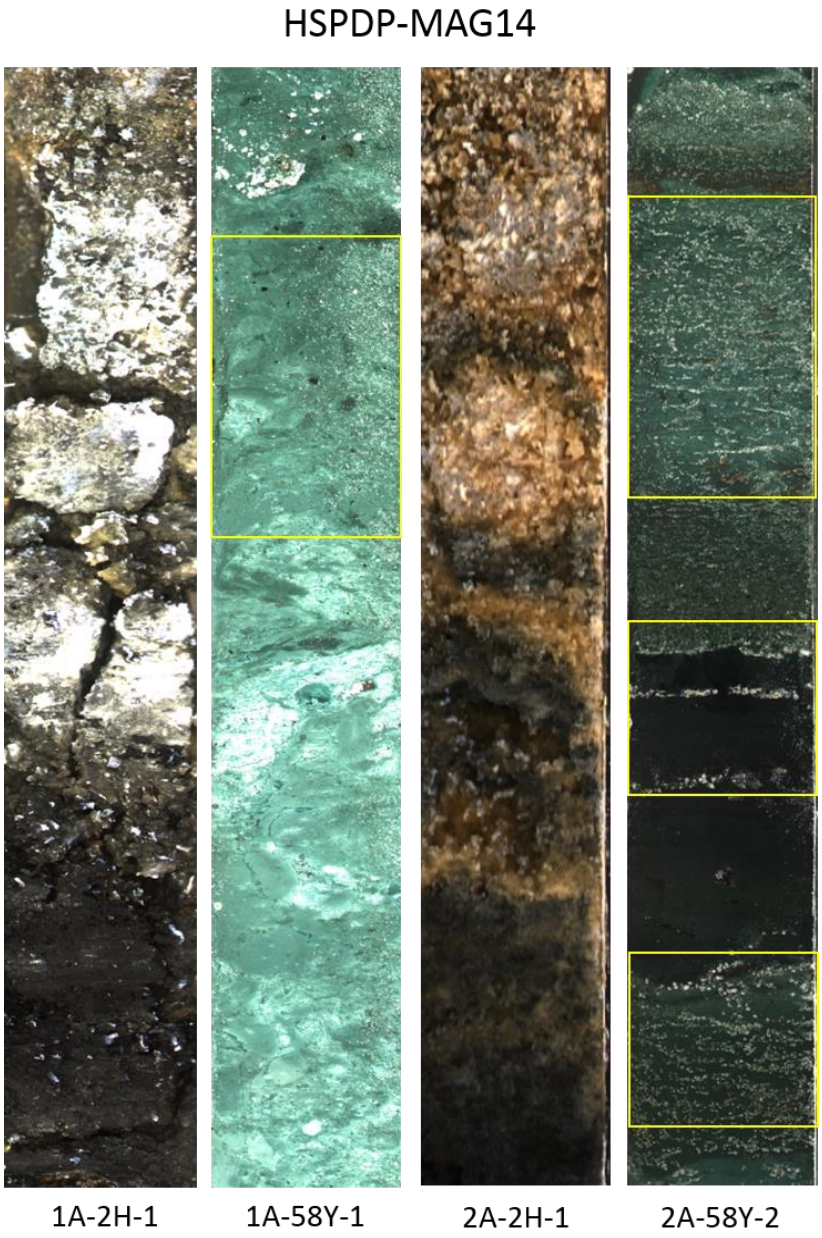

Figure 4.8: Core images from HSPDP-MAG14 showing primary versus diagenetic trona. (far left) Bedded trona transitioning into trona-rich mud. (middle-left) Diagenetic trona infilling pores [yellow box]. (middle-right) Primary bedded trona transitioning into trona-rich mud. (far right) Diagenetic trona infilling porespaces in black mud [yellow boxes].

This mineral zone is likely the result of early-stage diagenesis, evidenced by the euhedral trona and nahcolite crystals that appear to have infilled porous sediment from ~480-340 ka (~135

to 115 mbs) (Figs. 4.2, 4.3 & 4.8). This diagenetic episode may have been the result of a regional tectonic event which introduced hydrothermal fluids into the basin, subsequently altering groundwater chemistry. Studies from the Olorgesailie Basin, ~40 km northeast of Lake Magadi, suggest the region experienced active rift-related faulting ~490-360 ka (Behrensmeyer et al., 2002, 2007).

The mineralogy of Zone M3 is characterized by abundant analcime, erionite, phillipsite, and pyrite, as well as minor sulfates, sodium silicates, natrolite, mordenite, clinoptilolite, and chabazite. Salinity indicators (Sr/Ca and $(K_2O + Na_2O)/TiO_2$) from Core 2A suggest that the region experienced a long-term drying trend throughout the Pleistocene, with pulses of wetter conditions (Figs. 4.5, 4.6 & 4.7). HSPDP-MAG14-2A is dominated by zeolites, pyrite, and sulfates in this zone. One possible explanation for the abundant pyrite and sulfates would be the presence of sulfur fumaroles near Lake Magadi, which could have contributed to sulfate precipitation and the occurrence of hydrothermal pyrite. The more likely scenario is that pyrite was formed under reducing conditions in poorly oxygenated waters, whereas sulfates would have likely formed by subsequent oxidation of pyrite in a well oxygenated shallow lacustrine environment or in shallow pools in wetlands. The shallowing of waters at Lake Magadi may be the result of significant volcaniclastic material deposited in the basin around that time, which could have simulated a desiccation event, or “mock aridity” (Harris and Van Couvering, 1995), and may have caused oxygen depletion in the lake system.

4.5.4 Mineralogical Zone M4 and Geochemical Zone G5 (~105-58 mbs; ~350-105 Ka)

Zone M4 consists of mostly analcime, erionite, phillipsite, sulfates, and pyrite, as well as minor sodium silicates and natrolite. Zone G5 is characterized by increasing salinity with low Ca/Na ratios. The mineralogy is indicative of an altered ash deposit that produced mostly Na-

zeolites, which suggests relatively concentrated waters. However, the pyrite indicates a reducing environment that subsequently oxidized to produce sulfates. The pyrite could have formed in marshlands, which subsequently dried up and subaerially exposed pyrite oxidizing to form sulfates.

The onset of intensive zeolitic alteration at ~350 ka (~105 mbs) may have been enhanced by a significant input of volcanic ash and pumice, as well as supports further concentration of lake waters. As lake waters become more concentrated and saline, volcanic ash deposits will typically reflect zeolitic zonation in the lake sediments, with K- and Ca-zeolites grading laterally basinward into Na-zeolites, and authigenic K-feldspar at the center of the basin in the most extreme settings (Hay, 1966; Sheppard and Gude, 1968, 1969; Langella et al., 2001). However, zeolite deposits in *Playa-lake systems* display a concentric zonation pattern (Surdam, 1977; Langella et al, 2001), but due to basin morphology *Rift-type systems* may not display the same concentric zeolitic zonation. This is because rift areas lack the broad, flat areas necessary for that kind of lateral variation (Langella et al., 2001). The Lake Magadi basin morphology is typical of the constrained *Rift-type systems* described by Surdam (1977), and thus may not exhibit the concentric zonation of *Playa-lake systems*. However, the zeolite assemblages observed at Site 1A versus Site 2A vary throughout the cores, with Site 1A forming more Ca- and K-bearing zeolites and Site 2A favoring more Na-bearing zeolites. This may suggest that the Magadi Basin does display some degree of zeolitic zonation, with the deeper part of the basin reflecting more concentrated waters.

Stromatolite records from southern Kenya and northern Tanzania have been dated by a combination of Th/U and ^{14}C techniques (Hillaire-Marcel et al., 1986; Hillaire-Marcel and Casanova, 1987; Casanova and Hillaire-Marcel, 1992). Three generations of stromatolites were

observed in the Magadi-Natron Basin. These were dated to ≥240 ka, 135 ka ± 10 ka, and ~12-10 ka. Interestingly, these highstands coincide with the last three glacial terminations and the last stromatolite record would correlate temporally with the onset of the African Humid Period (e.g., Trauth et al., 2005, 2007).

4.5.5 Mineralogical Zone M5 and Geochemical Zone G6 (~58 mbs to top; ~105 Ka to recent)

The uppermost Zone M5 is dominated by sodium carbonates and a diverse assemblage of zeolites (analcime, erionite, phillipsite, mordenite, clinoptilolite, and chabazite), as well as rare calcium carbonates, sodium silicates, and pyrite. While bedded trona and zeolites dominate the upper ~60 meters of HSPDP-MAG 2A, that sequence is limited to the upper ~25 meters in HSPDP-MAG 1A. Zone G7 represents higher strontium-calcium ratios and higher $(K_2O+Na_2O)/TiO_2$ values, suggesting the basin experienced a sustained desiccation event, with warmer temperatures and increased salinity during the Holocene.

Figure 4.9: Sodium carbonate and sodium silicate minerals precipitating at the margin of Nasikie Engida.

Abundant sodium silicate minerals present in Zone M5 suggest variable lake levels, with precursor Na-Al-Si gels forming during lowstands in concentrated brines at the lake margins or on mudflats. Such aluminosilicate gels precipitate near alkaline springs and at the lake margin in both Nasikie Engida and Lake Magadi (Fig. 4.8). If one assumes that these gels are semi-annually washed into the basin and accumulate, a significant deposit could form in lake beds and crystallize into zeolites and or chert (Eugster and Jones, 1968; Eugster, 1969). This would explain the presence of analcime in Lake Magadi sediments since the earliest lake stages in the basin (Figs. 4.2, 4.3, 4.4 & 4.5).

Lake Magadi became a hypersaline ephemeral lake ~100 ka and sodium silicate minerals such as makatite and magadiite have been forming from the lake's concentrated brines at various times during the late Pleistocene and Holocene. Eugster (1967) suggested that sodium silicates

would have likely formed from gels that precipitated from alkaline brines near hot springs. Percolating brines could have removed Na^+, and this process would have continued until all sodium was removed and chert was formed from sodium silicate precursors (Eugster, 1967, 1969). Cherts throughout the HSPDP-MAG14 cores likely formed through the Eugster model and silicification of a wide variety of precursor material, including gastropods, calcium carbonate minerals, and plant detritus (Leet et al., 2016). Behr's model (2002) did not necessitate a lacustrine environment with a chemocline; rather he suggested that chert precursors form from gels which accumulate on mudflats from the interaction of volcaniclastic material and concentrated alkaline brines.

Records from Lake Malawi indicate a series of megadroughts between ~135 and 75 kyr ago and enhanced precessional variability (Scholtz et al., 2007, 2011; Konecky et al., 2011), which coincides with the onset of hypersaline conditions at Lake Magadi at ~100 ka. Foraminiferal oxygen isotope records from Ocean Drilling Project (ODP) Sites 967 and 969 indicate warm surface waters were influenced by precession cycles, but the mixed-layer signal modulated on obliquity timescales (Joannin et al., 2007). The pollen data from those sites indicates there are two kinds of vegetation successions: short-term successions controlled by precessional forcing and long-term coinciding with decreases in precessional amplitude during the Pleistocene. Mineralogical records from Lake Magadi do not reflect orbital forcing, but rather a long-term drying trend over the past ~350 kyr. The geochemistry records display some cyclicity, however, these cycles do not appear to be on Milankovitch timescales.

4.6 Conclusion

Table 4.1: Paleoenvironmental interpretations for the HSPDP-MAG14-2A core based on inferences from mineralogical and geochemical data.

Mineral Zone	Age	Mineralogy	Paleoenvironment
M5	~105 ka to present	Low Mg-calcite, Sodium carbonates, Zeolites, Halite, Diatom-rich	Ephemeral Hypersaline Saline Lake/Salt Pan
M4	~350 to 105 ka	Zeolites, Pyrite, Sulfates, Sodium silicates	Shallow Hypersaline Lake/ Marshlands & Mudflats
M3	~500 to 350 ka	Analcime, Pyrite, Sulfates, diagenetic Sodium carbonates	Shallow Saline Lake/ Diagenetic Zone
M2	~610 to 500 ka	Analcime, Pyrite, Sulfates, Calcium carbonates	Deep Stratified Saline Lake
M1	~1,080 to 610 ka	Analcime, Pyrite, Calcium carbonates	Shallow Freshwater Pools transitioning to Deep Mildly Saline Lake

The paleoenvironmental history of Lake Magadi reveals a long-term drying trend spanning the past ~1,080 ka, with intensified aridification and intermittent pulses of humid periods over the past ~320 ka (Tab. 4.1). Mineralogical and geochemical evidence indicates a shallow freshwater inception ~1,080 ka, followed by a deep mildly saline lake for ~300 kyr. A volcanic ash deposited in the Lake Magadi basin altered basin hydrochemistry ~320 ka, simulating a significant desiccation event in the basin. Highly variable environmental conditions

followed for ~200 kyr. After ~100 ka, Lake Magadi became a hypersaline ephemeral lake, with pulses of lake highstand during humid phases.

5 MINERALOGICAL AND GEOCHEMICAL INSIGHTS FROM THE *OLORGESAILIE DRILLING PROJECT* IN THE KOORA GRABEN OF THE SOUTHERN KENYA RIFT

Nathan M. Rabideaux[1], Daniel M. Deocampo[1], R. Potts[2], A. Kay Behrensmeyer[2], R. Bernhart Owen[3], Robin W. Renaut[4]

[1]Georgia State University, Department of Geosciences, Atlanta, GA 30302 USA

[2]Smithsonian Institution, Natural History Museum, Human Origins Program, Washington D.C.

[3]Hong Kong Baptist University, Kowloon, Hong Kong

[4]University of Saskatchewan, Saskatoon, Saskatchewan, CA

5.1 Abstract

Mt. Olorgesailie and its surrounding area in the southern Kenya Rift host a robust collection of archeological and paleontological findings dating back to the Miocene (Deino and Ambrose, 2007). Field studies of the southern Kenya Rift led to the *Olorgesailie Drilling Project* in the Koora Graben, on the southern flanks of Mt. Olorgesailie. Sediment cores collected from two sites in the Koora Graben span the past ~1.0 Myr. The southern Koora Graben is a half-graben rift basin adjacent to Lake Magadi.

Bulk mineralogical and geochemical analyses of the ODP-OLO12-1A core material suggests the Koora Graben was occupied by a series of paleolakes throughout the Mid Pleistocene to early Holocene (~1.0 Ma to 80 ka), with a long-term aridification trend in the region leading the termination of lacustrine phases in the southern Koora Graben by ~8 ka. The presence of only detrital and diatom-rich sediments in the lower ~25 m of core indicates that a

large hydrologically open freshwater lake likely occupied the basin from at least ~1.0 Ma until ~700 ka. The Southern Kenya Rift became increasingly more arid at ~700 ka, with significant low Mg-calcite precipitation and accumulation of diatom-rich sediments from ~145 to 125 mbs suggesting the lake became more saline until ~370 ka. A significant volume of volcanic ash and pumice was deposited in the basin at ~250 ka. Intensive zeolitic alteration of the ash and pumice deposit dominates the core from ~100 to 45 mbs. Following the input of volcanic ash and pumice, the lake level fluctuated between a shallow saline lake and subaerially exposed surfaces with paleosols overprinting on lacustrine sediments from ~250-80 ka. Remnants of Paleolake Koora occupied the Koora Graben until the early Holocene, at which time the lake completely dried up.

Keywords: Olorgesailie, Koora Graben, Mineralogy, Geochemistry, Zeolites

5.2 Introduction

The Southern Kenya Rift is home to a number of important archeological and paleontological sites (e.g., Gregory, 1921; Leakey, 1952; Isaac, 1978; Potts, 1989). The most important site being near Mt. Olorgesailie, where archeological excavations have uncovered extensive Acheulean handaxe deposits, Middle Stone Age tools, abundant vertebrate fossils, and hominin specimen KNM-OG 45500 (Leakey, 1952; Potts, 1989; Deino and Potts, 1992; Potts et al., 2004). The East African Rift Valley was a draw for colonial explorers and geologists during the late Nineteenth Century (e.g., Fischer, 1884; Mügge, 1885; Kaiser, 1898), with comprehensive geologic records of the southern Kenya Rift produced during the early to mid-Twentieth Century (e.g., Gregory, 1921; Leakey, 1952; Baker, 1958, 1963; Crossley, 1979; Guth, 2007).

The geology is comprised of Archean basement rock overlain by Miocene to recent volcanic and sedimentary deposits. The oldest rocks of the rift floor are gneisses, quartzites and schists that make up the Basement System of Precambrian age. A significant erosional surface marks the boundary between the Archean basement and Miocene-Pliocene aged Olorgesailie volcanics and the flow basalts that are associated with the Nguruman Rift faulting events. The Olorgesailie volcanics consisted of augites, trachyandesites, alkali trachytes, and nephelinites. During the late Pliocene and early Pleistocene, flow trachytes filled most of the Southern Kenya Rift floor while a second stage of faulting occurred associated with the Nguruman Rift (Baker, 1958, 1963; Crossley, 1979; Guth, 2007).

The modern configuration of the Southern Kenya Rift was established by ~1.0 Ma. A series of small lake deposits began to accumulate in troughs on the rift floor during the Pleistocene. The Olorgesailie Lake Beds accumulated to the northwest of Mt. Olorgesailie, and

the Oloronga Beds formed in the basin now occupied by Lake Magadi. Further faulting and erosion followed in much of the region and lake deposition continued in Olorgesailie until ~320 ka (Behrensmeyer et al., 2002). The sediments of the Olorgesailie Formation have been studied extensively over the past couple of decades (Potts, 1989; Owen et al., 2008, 2011; Behrensmeyer et al., 2002, 2007; Deocampo et al., 2010), and provide a great deal of insight into paleoenvironmental conditions from ~1.0 to 0.3 Ma. The youngest deposits in the region include thick sequences of sodium carbonate evaporites (trona and nahcolite) in the ephemeral lake basins (Magadi) and unconsolidated alluvium throughout much of the Southern Kenya Rift (Gregory, 1921; Baker, 1958).

The most abundant authigenic minerals found in many sedimentary environments include silica, zeolites, carbonates, and clay minerals. Authigenic minerals in lacustrine sediments provide information about paleoenvironmental conditions and the evolution of basin geochemistry over time (Hay, 1976; Hay and Kyser, 1996; 2001; Deocampo et al., 2010; Deocampo and Jones, 2014). In environments with extreme alkalinity and high silica activity authigenic silicate minerals dominate the sedimentary record (Herrick, 1972; Surdam and Eugster, 1976). Authigenic aluminosilicates form as chemical precipitates, through diagenesis of precursor minerals, or through biogenic activity (Eugster, 1967; Surdam and Eugster, 1976; Behr, 2002). Some of the most common authigenic aluminosilicate minerals are zeolites. Zeolites are tectosilicate minerals that commonly form through alteration of volcanic glass in saline, alkaline waters (Hay, 1963, 1976).

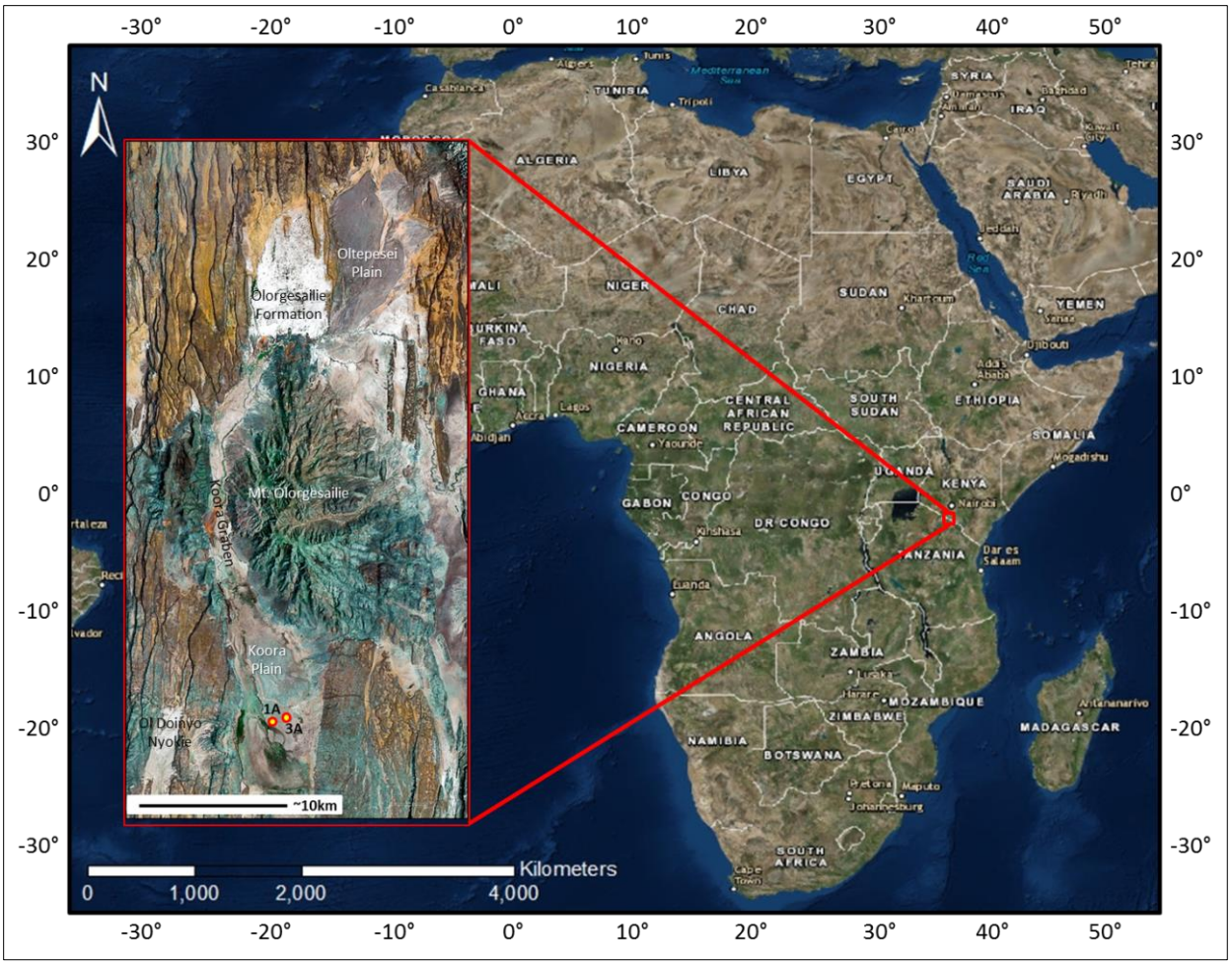

Figure 5.1: Map of the African continent and zoomed inset map of the Olorgesailie Archeological Site and surrounding area in the Southern Kenya Rift, with important features and drilling sites labelled.

We present new mineralogical and geochemical data from the ODP-OLO12-1A core collected in the Koora Graben to gain an understanding of the environmental history of the paleolakes that occupied the basin over the past ~1.0 Ma (Fig. 5.1). Additionally, we will attempt to relate these records to other studies from the region to gain a better understanding of Southern Kenya's climatic and tectonic history. The goal of this project is to construct a high-resolution paleo-environmental record that spans the Middle and Late Pleistocene in the Southern Kenya Rift.

5.3 Drilling Project & Site Location

The Koora Graben is located on the southern flanks of Mt. Olorgesailie. Situated to the north of Mt. Olorgesailie is the well-studied Olorgesailie Formation (Fig. 5.1), as well as the paleontologically and archaeologically rich Oltepesei and Oltulelei Formations (Potts, 1989; Behrensmeyer et al., 2002, 2018; Owen et al., 2008; Deocampo et al., 2010). The Olorgesailie Formation is comprised of lacustrine, volcaniclastic and alluvial sediments that were deposited between 1.2 million and 490,000 years ago (Gregory, 1921; Isaac, 1978; Potts, 1989; Behrensmeyer et al., 2002; Owen et al., 2008). The stratigraphic record from Olorgesailie indicates the area experienced variable climatic regimes, with fluctuating humid and arid conditions evidenced by paleosols, rhizoliths, wetland deposits, diatomites, and diatomaceous silts and clays (Owen et al., 2008; Deocampo et al., 2010).

The Olorgesailie Drilling Project (ODP) collected sediment cores in the Koora Plain, south of Mt. Olorgesailie, in 2012. The Koora Plain is located in the central portion of the Koora Graben in the southern Kenya Rift, around 100 km (~60 miles) southwest of Nairobi (Fig. 5.1). The southern Kenya Rift Valley is a semi-arid to arid environment that receives an average of <44 cm annual precipitation (Baker, 1958; Behr, 2002).

The geology of the Mt. Olorgesailie-Koora Graben-Lake Magadi area has been described in a number of previous studies (*e.g.*, Gregory, 1921; Baker, 1958; Isaac, 1978; Baker, 1987; Behrensmeyer et al., 2002; Owen et al., 2008). An updated map of the area has been generated by Guth (2007). We will briefly summarize the main geologic units here (according to Baker, 1958): the basement rocks are metamorphic gneisses, quartzites, and schists of Precambrian age; there is a significant erosion surface that spans the Precambrian to mid-Cenozoic; the Nguruman escarpment began to fault in the Miocene, followed by deposition of the Olorgesailie volcanics,

Ol Keju Nyiro Basalts, and Lengitoto Trachytes in the Pliocene; during the early Pleistocene, trachyte flows and Ol Doinyo Nyegi volcanics were deposited prior to the Oloronga Beds; in the mid-Pleistocene the Olorgesailie Formation was deposited and the Chert Series (Green Beds) formed near Lake Magadi; the High Magadi Beds were deposited in the late Pleistocene; and Holocene to modern deposits are dominated by evaporates and boulder-rich alluvium.

The Koora Plain is an open savanna environment adjacent to the southern flanks of Mt. Olorgesailie in the Koora Graben of the Southern Kenya Rift. The Koora Graben is a half-graben fault block typical of extensional rift valley settings (Gregory, 1921; Baker, 1958), and was at times occupied by Paleolake Koora during the late Pleistocene to Holocene. Paleoshorelines were identified in the southern Koora Graben during the 2015 field season, confirming prolonged occupation of the basin by Paleolake Koora.

5.4 Methods

Sediment cores were drilled and collected from the Koora Graben in the summer of 2012. A complete summary of the drilling outcomes has been provided by Cohen et al (2016). Two holes were drilled in the Koora Graben. ODP-OLO Core 1A obtained ~167 m of core material and Core 3A recovered ~113 m with >90% recovery. Cores were shipped to LacCore, the National Lacustrine Core Facility, at University of Minnesota for initial core description (ICD), sampling, and storage at their repository. Sub-samples for multi-proxy analysis were collected after the splitting, imaging, logging, and description of cores. Samples for X-ray diffraction (XRD) analysis were collected at 32 cm intervals and at higher resolution within sections of laminated lacustrine muds. Each of the ~400 samples were dried at 40° C for 48 hours and powdered using a ball-and-pestle impact grinder.

XRD analysis was conducted on a PANalytical X'pert Pro MPD using Cu K_α-radiation (λ = 1.5418 Å) operating at 45 kV and 40 mA. Bulk analysis measured 5 to 70° 2θ with 30-minute scan times. Powder diffraction patterns were analyzed using PANalytical High Score software suite with reference to PDF-2 database, Moore and Reynolds (1997), and Brindley and Brown (1980). Samples collected for geochemical analysis were shipped to Activation Laboratories in Ancaster, Canada.

The age model for the ODP-OLO 1A core was derived primarily by the single-crystal, incremental heating $^{40}Ar/^{39}Ar$ dating approach on more than 20 volcanic tephra and trachytic basement lavas, with a precision of ±0.3 to 10% which varies with grain size, feldspar chemistry and the number of crystals available for analysis (Deino et al., 2016). The ODP-OLO team held a meeting in 2015 to determine the best method for determining a "Z-prime" depth for Core 1A. A "Z-prime" depth correction is applied once event deposits and hiatuses have been accounted for, resulting in an adjusted depth scale. The criteria considered included presence or absence of bedding, grain size, composition, and evidence to warrant compression. Compression criteria were considered on the basis of volcanic event deposits, zeolitic alteration, and intrusion of drilling mud causing expansion. Some sections were expanded to compensate for non-deposition during paleosol development in subaerial exposed environments. Ages for ODP-OLO 1A ranged from ~1.1 Ma for the Magadi Trachyte at the base of the core to ~90 ka for a tephra near the top (Deino et al., 2016).

5.5 Results

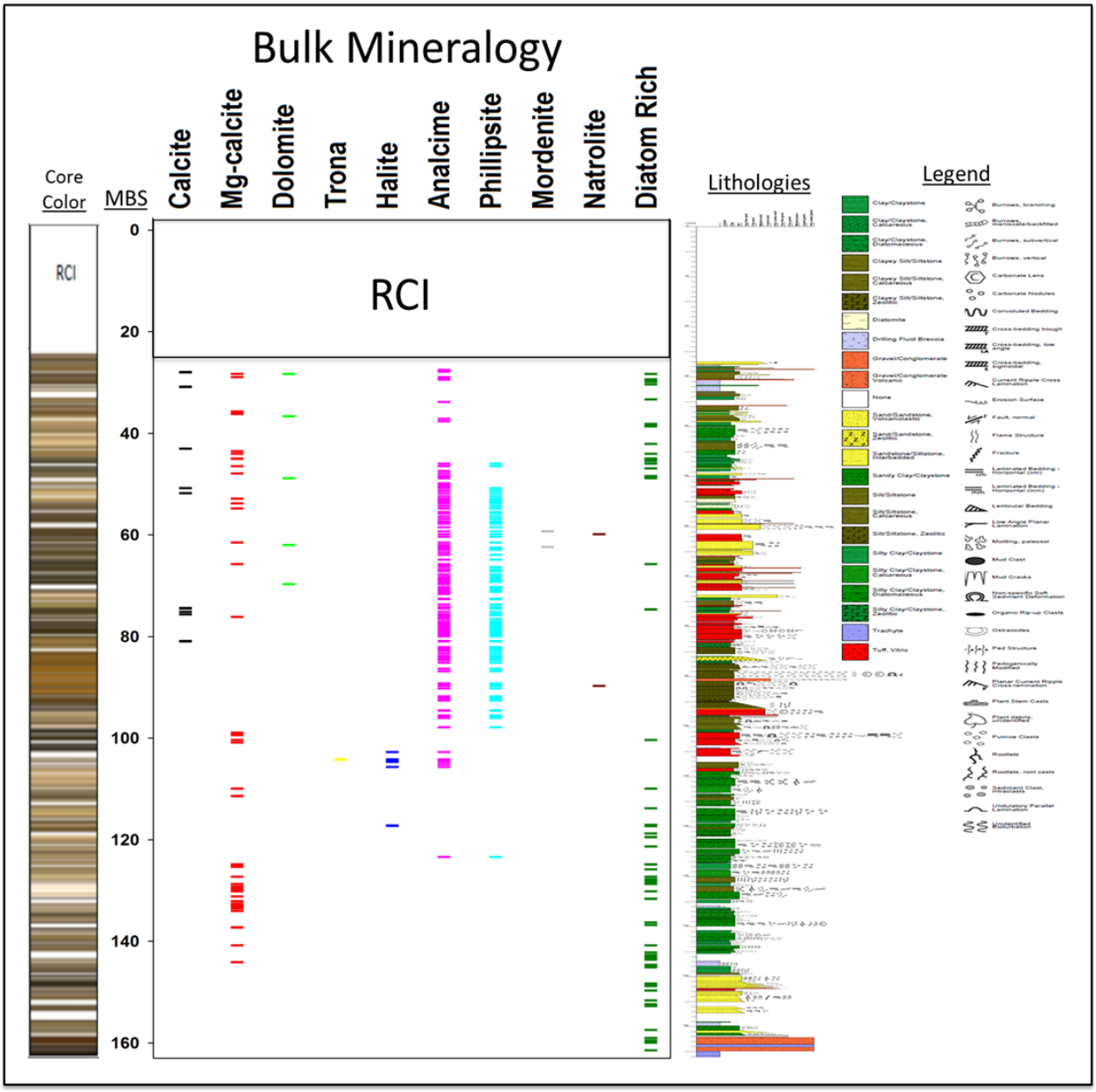

Figure 5.2: Composite figure of ODP-OLO12 Core 1A, including mineralogy and corresponding mineral zones (this study), core color (Cohen et al., 2016), stratigraphic columns, lithologies, sediment characteristics, and fossils (Behrensmeyer et al., in prep).

5.5.1 Mineralogy

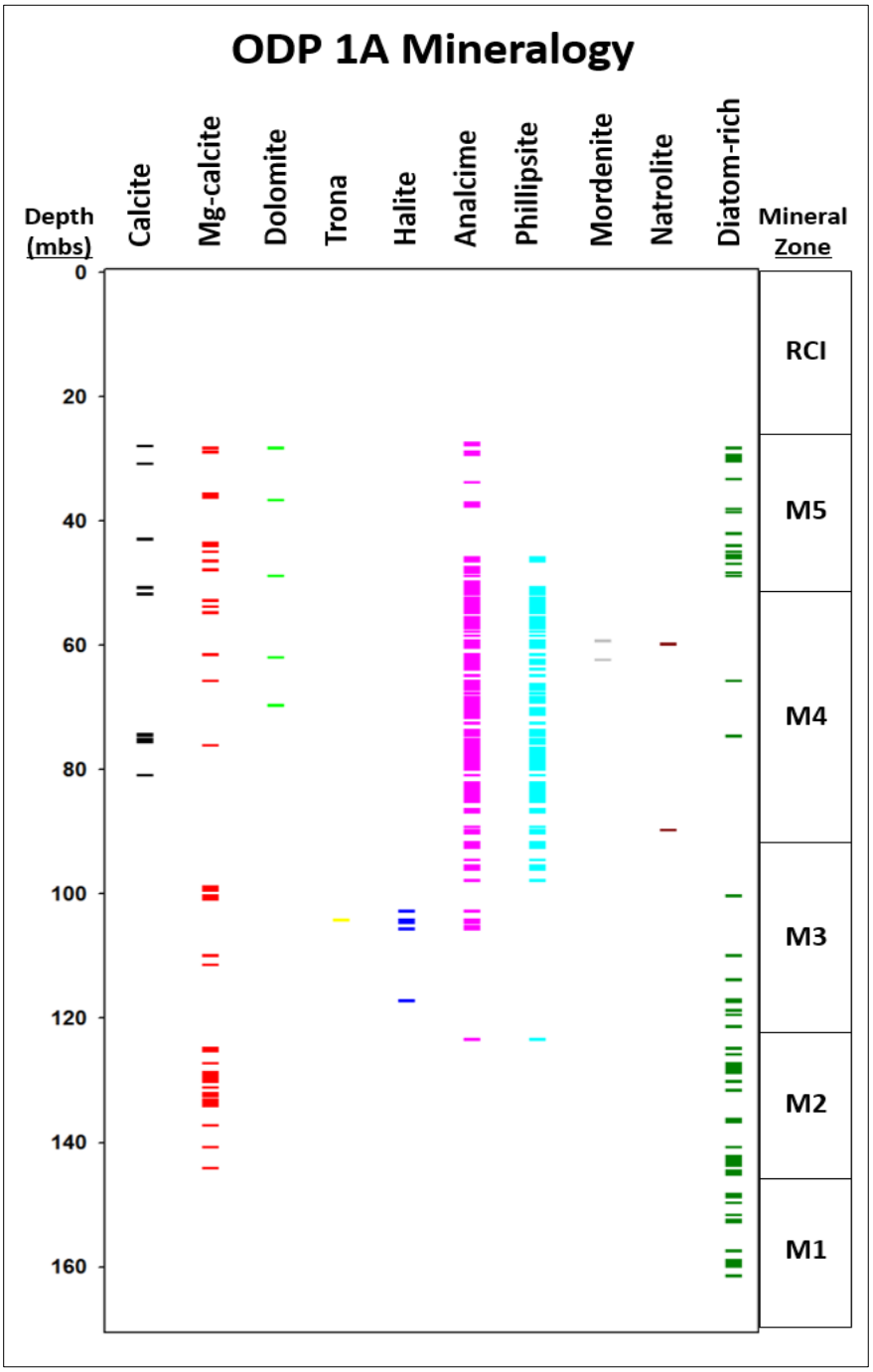

Figure 5.3: Mineralogy of ODP-OLO12 Core 1A plotted against depth (mbs), and corresponding mineral zones. The upper ~27 m were bored and bagged in one meter intervals using reverse circulation with the drill bit.

Detrital feldspars are present throughout the ODP-OLO12 cores (Fig. 5.2). The bulk mineralogy of ODP-OLO 1A core can be divided into five distinct mineral zones from the base of the core to ~27 meters below surface (mbs); the upper ~27 m is mostly detrital alluvium (Figs. 5.2 & 5.3). Mineralogical Zone M1 (base of the core to ~145 mbs) is dominated by silica polymorphs and detrital minerals. Mineralogical Zone M2 (~145 to 125 mbs) is comprised of silica polymorphs, low Mg-calcite, and clay minerals. Mineralogical Zone M3 (~125 to 90 mbs) contains zeolites, particularly phillipsite and analcime, low Mg-calcite, and silica polymorphs. From ~120 to 100 mbs, a few samples contained diagenetic trona and or halite. Zeolites are the most abundant mineral group in Mineralogical Zone M4 (~90 to 45 mbs), along with intervals of pedogenic carbonates. Mineralogical Zone M5 (~45 to 27 mbs) contains carbonates, silica polymorphs, and zeolites. Diatom-rich sediments are abundant below ~110 mbs and above ~45 mbs, but mostly absent in the most zeolitized interval from ~100 to 45 mbs. The uppermost ~25 meters were unconsolidated alluvium, which was dominated by a detrital mix of quartz, analcime, and feldspars.

5.5.2 Geochemistry

All geochemical data are plotted on logarithmic scales with five-point running averages. Bulk geochemical analysis indicated that there were five distinct geochemical zones. Geochemical Zone G1 (base of core to ~150 mbs) is characterized by low Ca/Na ratios, low Mg, light REE become increasingly enriched, and $(K_2O+Na_2O)/TiO_2$ ratios are slightly variable. Geochemical Zone G1 correlates mostly with Mineralogical Zone M1. Geochemical Zone G2 (~150 to 127 mbs) displays increasing Ca/Na ratios and decreasing heavy REE concentrations, but low $(K_2O+Na_2O)/TiO_2$ ratios. Ce/Cr and U/Th ratios become much more variable in Zone G2. Geochemical Zone G2 is slightly offset from Mineralogical Zone M2 and precedes it by ~5

m. Geochemical Zone G3 (~127 to 110 mbs) is characterized by high but variable Ca/Na ratios, increasing $(K_2O+Na_2O)/TiO_2$ ratios, and heavy REE concentrations decrease until ~115 mbs and then decline significantly while U/Th and Ce/Cr ratios increase at ~115 mbs. Geochemical Zone G3 has an offset from Mineralogical Zone M3 as Zone G2 has from M2. Geochemical Zone G4 (~110 to 50 mbs) is characterized by significant variability in REE values, Ca/Na ratios, and $(K_2O+Na_2O)/TiO_2$ values. Geochemical Zone G4 precedes the onset of Mineralogical Zone M4 by ~5 m but correlates well following that initial offset. Geochemical Zone G5 (~50 to 27 mbs) has high Ca/Na ratios until ~45 mbs and low Ca/Na from ~45 to 27 mbs, variable REE concentrations, and increasing $(K_2O+Na_2O)/TiO_2$ values. Geochemical Zone G5 correlates well with Mineralogical Zone M5.

5.6 Discussion

The two cores collected during the ODP campaign consisted of interbedded muds, diatomites, fine to coarse grained sands, some pumice-rich gravel and conglomerate intervals, as well as some carbonate marls (Cohen et al., 2016). Analysis of bulk mineralogy from the Koora Plain indicated that Paleolake Koora experienced alternating stages of fresh and saline water, which was also found to be the case in Members 1 through 7 in the Olorgesailie Formation (Owen et al., 2008; Deocampo et al., 2010). In the lacustrine sedimentary sequence, freshwater stages are suggestive of an open basin, when diatomaceous silts and diatomites accumulated, whereas closed basin intervals are indicated by saline diatoms and zeolitic facies (Owen et al., 2008). Diatomaceous silts and diatomites are abundant throughout the lower portion of the ODP-OLO12-1A core, which correlates temporally with the Olorgesailie Formation (Deino and Potts, 1990). Sedimentation ceased in the Olorgesailie Basin by ~320 ka (Behrensmeyer et al., 2002,

2007, 2018; Owen et al., 2008), which correlates with the onset of pronounced environmental variability in the ODP-OLO12-1A core ~320 ka.

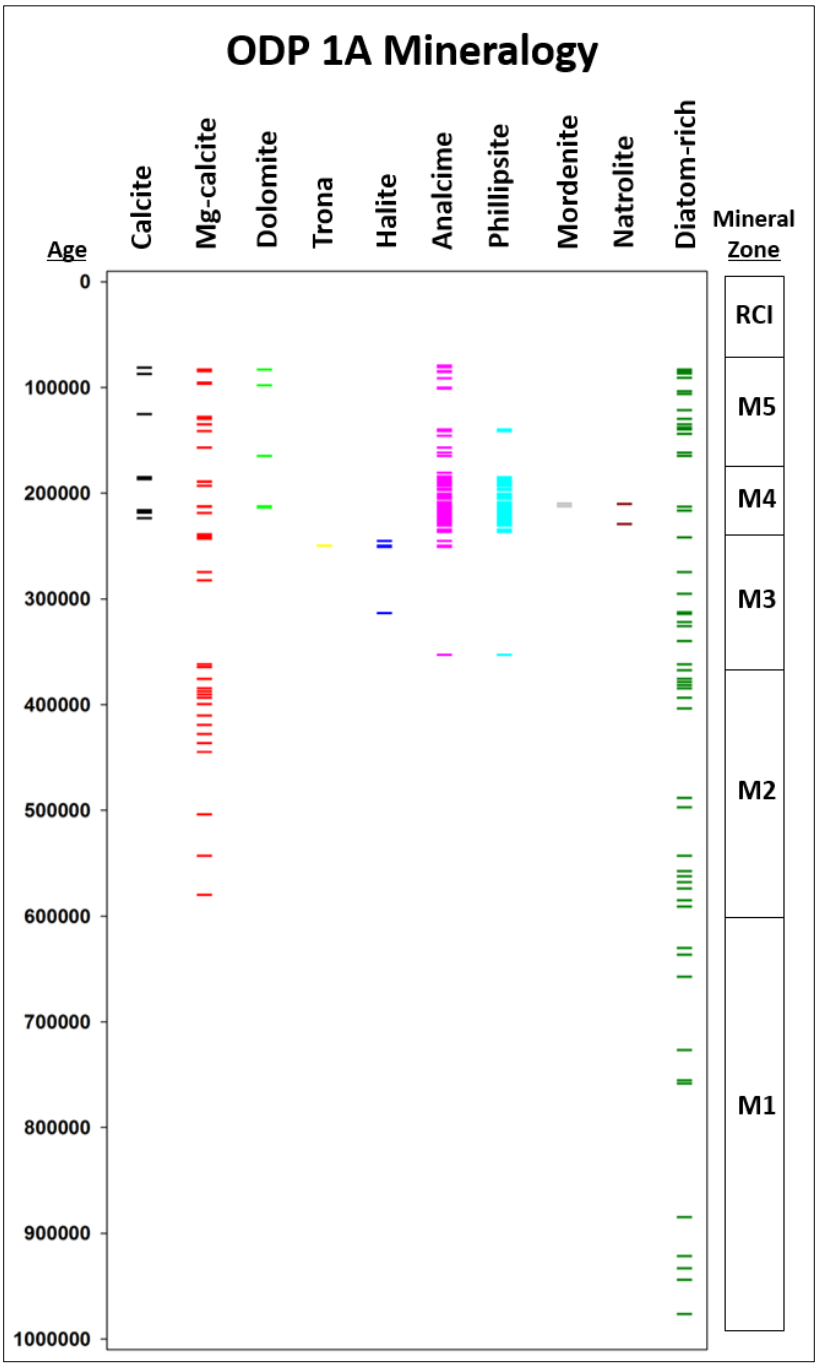

Figure 5.4: Mineralogy of ODP-OLO12 Core 1A plotted against the Bayesian Age Model developed for this drilling project by Deino et al. (in prep.).

The dominant zeolites in the ODP core from the Koora Plain are analcime and phillipsite, with pronounced zeolitic zones alternating with zones of other authigenic minerals such as low Mg-calcite (Fig. 5.4). In contrast to Lake Magadi, where erionite is the primary zeolite species, the zeolite assemblage from Koora suggests the geochemistry of the two adjacent basins may have differed significantly. The preservation of tuffs in the ODP core is further evidence of intervals of freshwater paleolake conditions, whereas nearly all volcanic material has been altered in the Lake Magadi cores.

5.6.1 Mineralogical Zone M1 and Geochemical Zone G1 (~167-145 mbs; ~1.0-0.68 Ma)

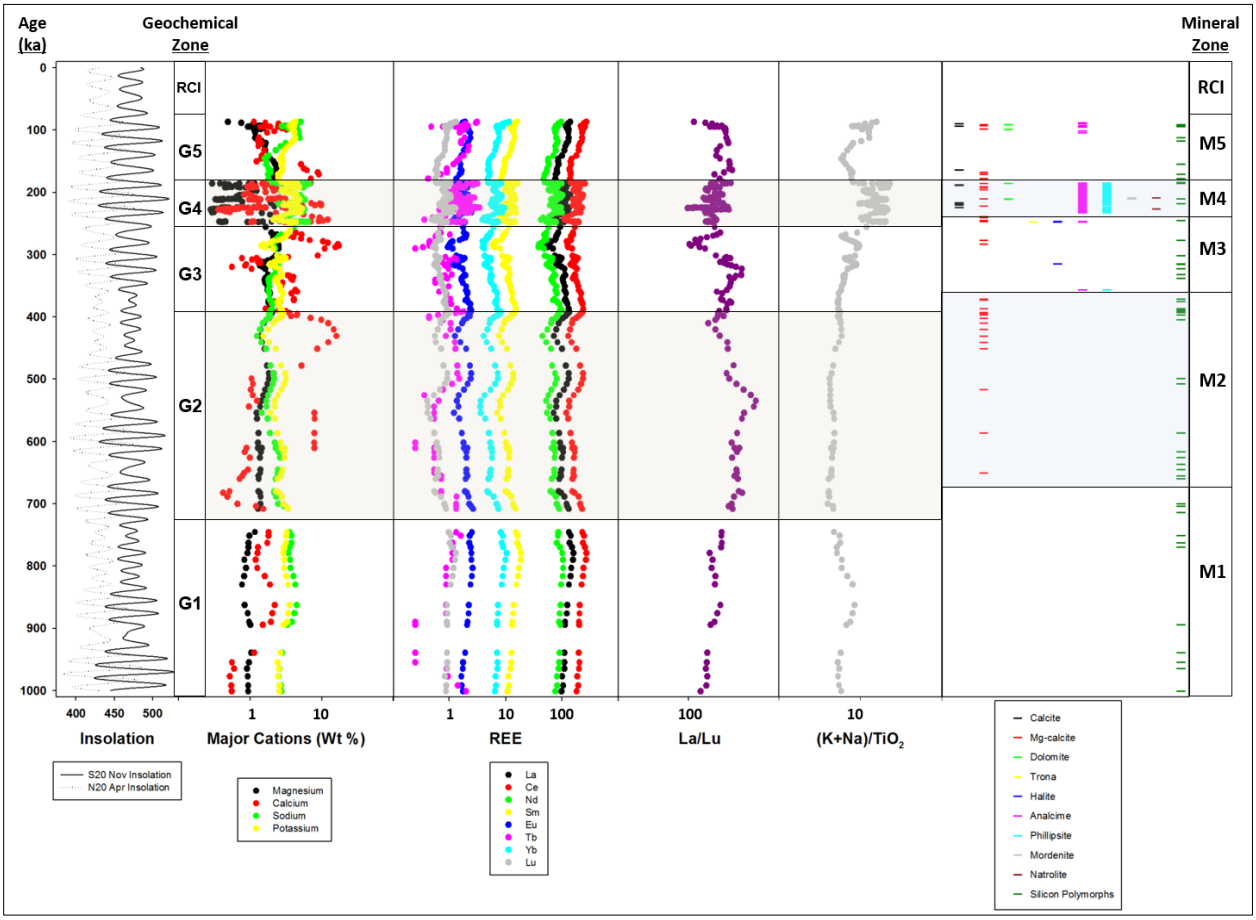

Figure 5.5: Composite figure for ODP-OLO12-1A with (L to R) spring and fall insolation in equatorial East Africa, geochemical zones, major cations, rare earth elements, light versus heavy rare earth elements, salinity indicator, mineralogy, and mineral zones. All are plotted against Bayesian age model.

Mineralogical Zone M1 consists of mostly detrital quartz and feldspars, as well as silica polymorphs and diatomaceous silts and clays, which suggests a hydrologically open, relatively freshwater lake began to occupy the basin ~1.0 Ma. Geochemical Zone G1 displays low Ca/Na ratios from ~1.0-0.95 Ma, after which there is a pronounced shift to higher values. There is a significant decrease in Tb from ~0.95-0.9 Ma that precedes a steady increase in light REE enrichment relative to heavy REE and a brief increase in $(K_2O + Na_2O)/TiO_2$ values (Fig. 5.5). The increase in Ca^{2+} at ~0.95 Ma may be indicative of an increase in ostracod abundance. Members 1-9 of the Olorgesailie Formation correlate temporally with Zones M1 and G1 of the ODP-OLO12-1A core (Deino and Potts, 1990; Behrensmeyer et al., 2002; Owen et al., 2008) (Fig. 5.5).

Owen et al. (2008, 2009, 2011) described the sequence of the Olorgesailie Formation in great detail as a variety of lacustrine, wetland, and terrestrial facies. Owen (2002) developed a classification system for sediments and diatom facies of the East African Rift System. Diatom data indicates highly variable environmental conditions during the deposition of Member 1 and lower Member 2, with an extensive paleosol in upper Member 1 (UM1p: Upper Member 1 paleosol) and evidence for myriad environmental conditions in the basin between ~1.0 to 0.9 Ma.

Weathering and interstitial waters in soils can play a significant role in Mg-enrichment. Deocampo et al. (2010) suggested that Mg-rich clays in UM1p of the Olorgesailie Formation were from Mg-rich paleo-waters discharged from a volcanic aquifer into a siliceous and alkaline paleolake, whereas UM7p (Upper Member 7 paleosol) contains smectite that was deposited in a saline lake but subsequently lost some Mg^{2+} due to weathering upon subaerial exposure. UM7p is a waxy green claystone with pedogenic overprinting that is capped with an unconformity, suggesting an extended interval of non-deposition and perhaps landscape stability that lasted an

estimated ~190 kyr (Potts et al., 1999; Owen et al., 2008). This level of variability was not identified in the ODP-OLO12-1A core; rather the sediments in the southern Koora Graben suggest sustained occupation by a fresh to mildly saline lake during this time interval.

5.6.2 Mineralogical Zone M2 and Geochemical Zone G2 (~145-125 mbs; ~0.68-0.38 Ma)

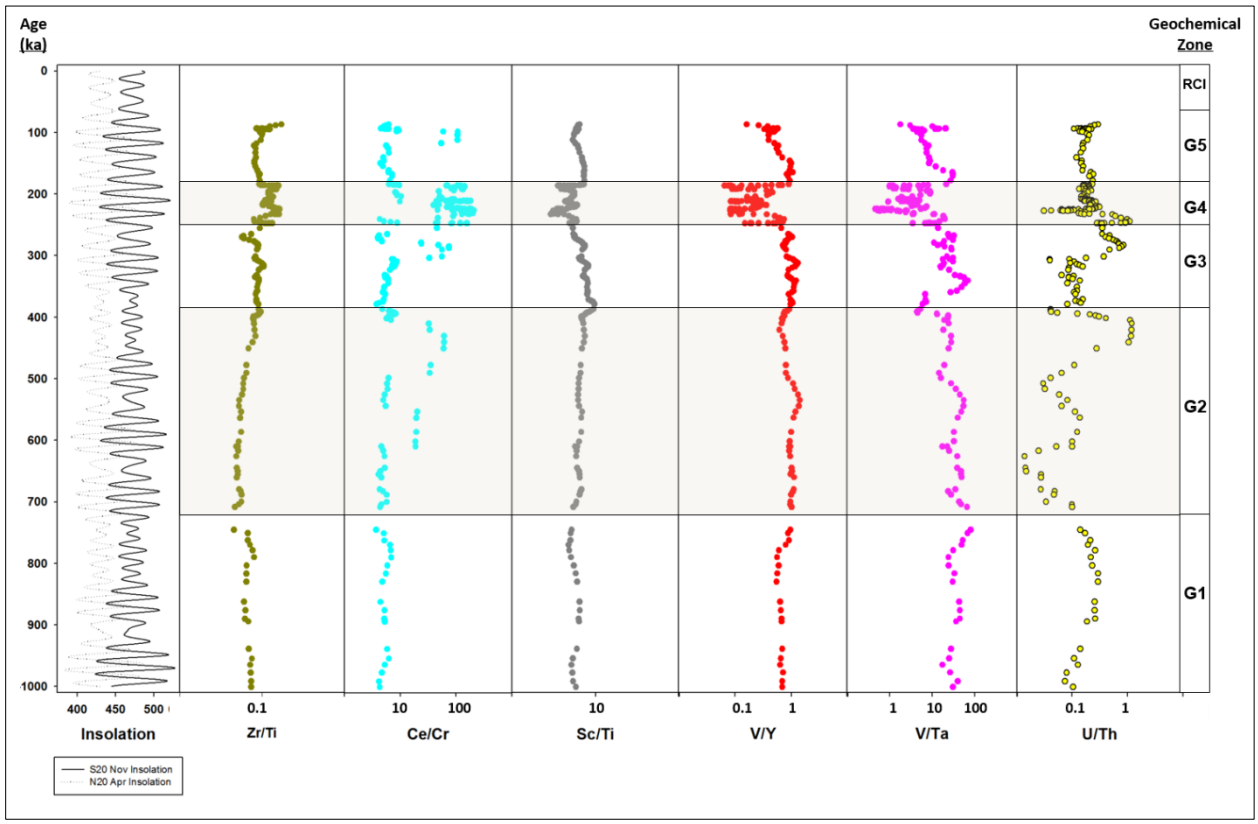

Figure 5.6: Geochemical plot for ODP-OLO12 Core 1A of source indicators. All plotted on logarithmic scales with five-point running averages.

Mineralogical Zone M2 is marked by the onset of carbonate mineral accumulation and more abundant diatom-bearing intervals, which may indicate an increase in biogenic activity in the paleolake. Geochemical Zone G2 displays highly variable Ca/Na ratios and REE concentrations, which may indicate volcanic input or changes in hydrology. Following a steady increase in La/Lu values, they decrease rapidly ~550 ka. Geochemical source indicators Ce/Cr and U/Th suggest variable geologic source regions, likely due to the active volcanism in the East

African Rift system (Figs. 5.5, 5.6 and 5.7). Mineralogical Zone M2 and Geochemical Zone G2 of the ODP-OLO12-1A core correlate with Members 9-14 of the Olorgesailie Formation (Deino and Potts, 1990; Behrensmeyer et al., 2002; Owen et al., 2008). Behrensmeyer et al. (2002) concluded that there were two main intervals in the Olorgesailie Basin: 1) a relatively stable, subsiding, hydrologically closed basin (~1.0-0.5 Ma); and 2) a tectonically active and unstable basin with alternating erosional and depositional phases (~0.5 Ma-recent).

The uppermost portion of Zones M2 and G2 capture the transition from stable to unstable basin, with higher Ca/Na ratios and increasing low Mg-calcite precipitation (Fig. 5.5). During the later interval (~0.5 Ma-recent), faulting and subsidence in the Koora Graben and Olorgesailie Basin resulted in a new depositional regime of cut-and-fill cycles that is consistent with other observations in the Southern Kenya Rift, which observed an increase in tectonic and volcanic activity around this time (Behrensmeyer et al., 2002; Baker, 1958). The Oltulelei Formation was deposited in this later interval (Behrensmeyer et al., 2018).

5.6.3 Mineralogical Zone M3 and Geochemical Zone G3 (~125-90 mbs; ~0.38-0.24 Ma)

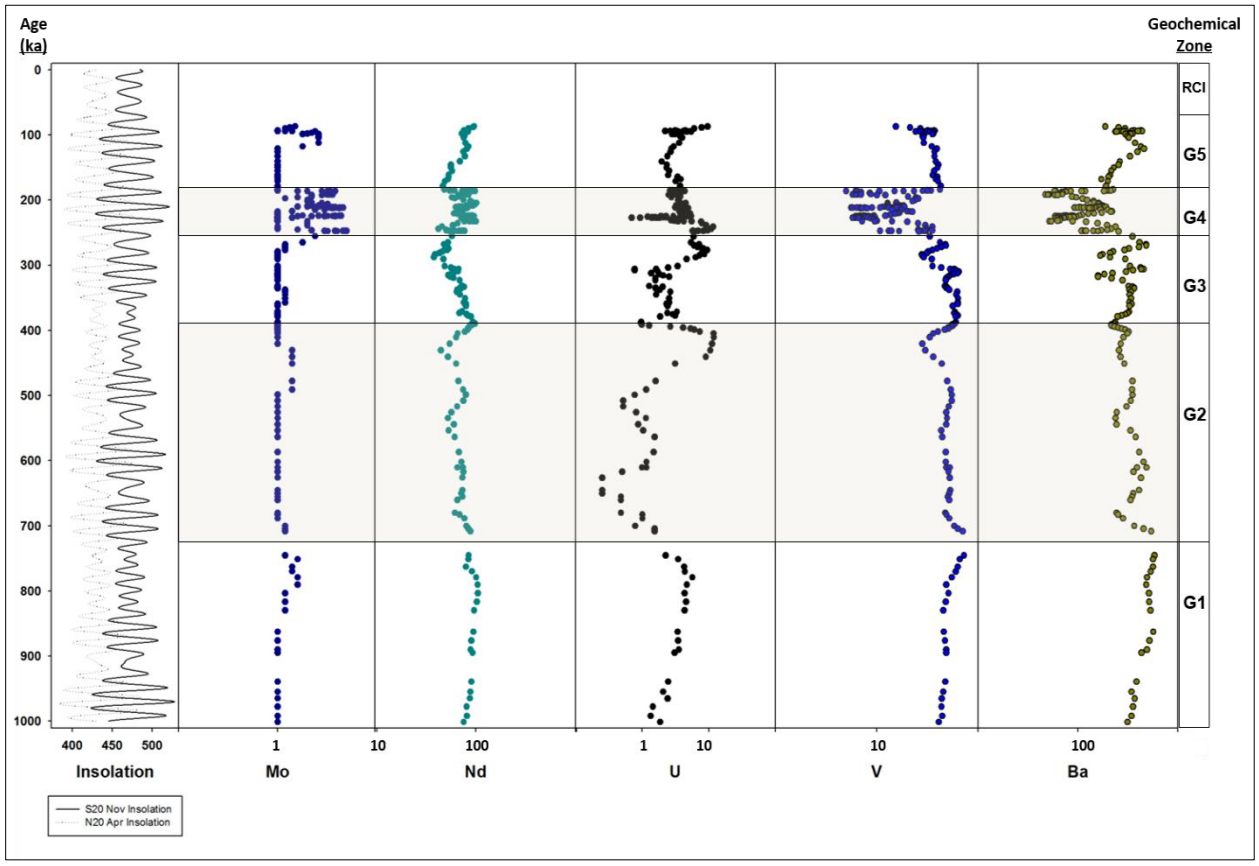

Figure 5.7: Geochemical indicators from ODP-OLO12 Core 1A of single-element source indicators. All plotted on logarithmic scales with five-point running averages.

Mineralogical Zone M3 can best be described as a diagenetic mineral zone, and consists primarily of detrital quartz and feldspars as well as silicon polymorphs. However, there are intervals of trona, halite, and zeolites that likely result from early diagenesis in interstitial waters that were altered due to tectonic activity in the Southern Kenya Rift (Fig. 5.5). Geochemical Zone G3 displays greater variability in Ca/Na ratios and REE concentrations. Geochemical indicators suggest the lake began to see increased salinity ~320 ka, which coincided with a pronounced decrease in light REE relative to heavy REE and significant increase in Ca/Na ratios. There is a positive correlation between Ce/Cr and U/Th in Geochemical Zone G3, suggesting geologic materials are derived from a similar source (Figs. 5.6, 5.7 and 5.8).

Zones M3 and G3 correlate with the lower Oltulelei Formation (Isaac, 1978; Behrensmeyer et al., 2002, 2018). The Oltulelei Formation is comprised of the "post-Olorgesailie deposits" and "Oltepesi Beds" as described by Shackleton (1944, 1978) and Isaac (1978), respectively (Behrensmeyer et al., 2002, 2018). The "post-Olorgesailie deposits" were attributed to the development of the Ol Keju Nyiro River, which would have down-cut and deposited volcanogenic sediments following faulting and tilting of the northern basin to the south (Isaac, 1978; Behrensmeyer et al., 2018). The increase in tectonic and volcanic activity during this interval is consistent with our interpretation that tectonic activity likely led to changes in groundwater chemistry and more saline, alkaline conditions in the basin. A similar environmental regime was likely influencing the wet-dry cyclicity we observe in the ODP-OLO12-1A core, with relatively rapid transitions between fresher lacustrine conditions and terrestrial exposure evidenced by ichnofacies and pedogenic surfaces.

Previous studies have placed the age of the Olorgesailie and Oltulelei Formations at ~1.0 Ma to 49 ka (Deino and Potts, 1990; Deino and Potts, 1992). More recent studies have produced better age controls on sediments from the Olorgesailie and Oltulelei Formations, dating the Olorgesailie Formation to ~1.2-0.499 Ma and allowed division of the Oltulelei Formation (~320-36 ka) into three distinct members: Olkesiteti Member (~320-190 ka), Oltepesi Member (~190-50 ka), and Tinga Member (~50-36 ka). The Oltepesi Beds are characterized by an orange-brown color and contains higher carbonate rhizoliths concentrations (Behrensmeyer et al., 2018), and likely relate to the zeolitically altered interval in the ODP-OLO12-1A core.

5.6.4 Mineralogical Zone M4 and Geochemical Zone G4 (~90-50 mbs; ~0.24-0.18 Ma)

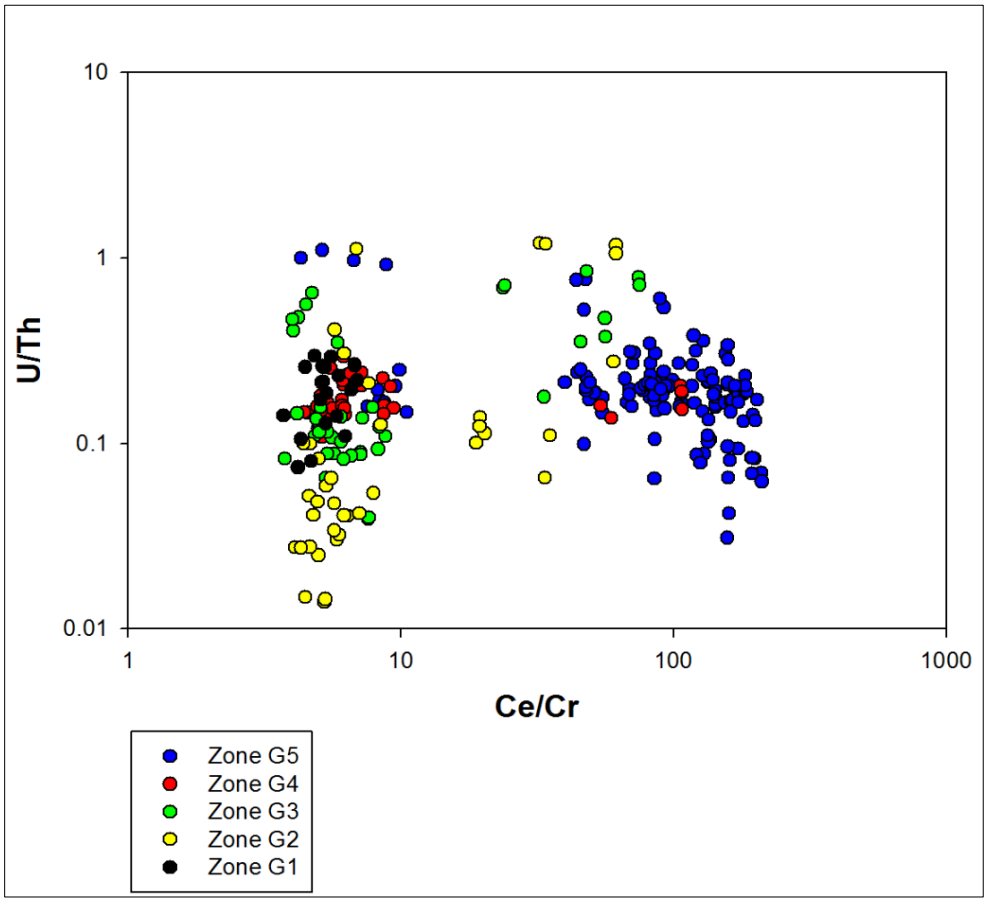

Figure 5.8: Geochemical X-Y plot of U/Th-Ce/Cr ratios. G1 has a tight correlation that is slightly positive. G2 and G3 display a weak positive correlation. G4 displays a constant U/Th with variable Ce/Cr ratios. G5 has a weak negative correlation.

Mineralogical Zone M4 contains large volcanic ash and pumice deposits that have been heavily altered to the zeolites analcime and phillipsite from ~240-180 ka (Fig. 5.5). Intense zeolitic alteration is indicative of extreme alkalinity and high silica activity (Hay, 1986). During this interval, paleolake conditions must have fluctuated between slightly fresher paleo-waters to saline, alkaline conditions, as calcite, Mg-calcite, and dolomite precipitation alternated with zeolitic alteration throughout this section of the core. All geochemical data indicate that paleoenvironmental conditions were highly variable from ~250-180 ka (Figs. 5.5, 5.6 and 5.7). Mineralogical Zone M4 and Geochemical Zone G4 coincide with the more cut-and-fill cycles

that occurred post-Oltulelei Formation (Behrensmeyer et al., 2018). There is no correlative surface to the north, only sedimentary deposits of the Ol Keju Nyiro River and unconsolidated alluvium.

5.6.5 Mineralogical Zone M5 and Geochemical Zone G5 (~50-27 mbs; ~0.18-0.08 Ma)

Mineralogical Zone M5 consists of lacustrine sediments overprinted with paleosols. The mineralogy consists of carbonate minerals and silicon polymorphs, as well as intervals of analcime, which is consistent with a fluctuating lake margin that alternates between shallow lacustrine and subaerial exposed surface environments. From ~108-150 ka, Ca/Na ratios are high and $(K_2O + Na_2O)/TiO_2$ values are decreasing, after which Ca/Na ratios decrease and $(K_2O + Na_2O)/TiO_2$ values increase indicating increased salinity. REE concentrations increase throughout Zone G5 with the exception of Tb, which decreases significantly at ~100 ka. Source indicators U/Th and Ce/Cr have a relatively strong negative correlation, indicating that uranium enrichment may be influenced by pedogenic carbonate precipitation and not directly related to geologic source. Zones M5 and G5 represents the final sedimentary sequence of the ODP-OLO12-1A core. During this interval, the mineralogy and geochemistry indicate a terminal lake facies systems tract, with a lacustrine facies transitioning to fluvial-deltaic facies and then terrestrial facies, which are overlain by unconsolidated alluvium.

East Africa has experienced long-term desiccation over the past ~3 Myr, primarily due to the sustained cooling trend that characterizes the latter half of the Cenozoic (deMenocal, 2004). Pulses of deep lake phases in East Africa are superimposed on this record (Trauth et al., 2005, 2007, 2009, 2010; Maslin et al., 2009; Potts, 2013). The onset of Northern Hemisphere Glaciation began and intensified between ~3.2 and 2.6 Ma, ushering in obliquity paced glacial cycles in the northern hemisphere (Shackleton, 1995; Lisiecki and Raymo, 2005; deMenocal

2004; Feakins and deMenocal, 2010). The Mid-Pleistocene Climate Transition (~0.9-0.75 Ma) is characterized by a shift in Earth's glacial-interglacial cycles from obliquity pacing (~41 kyr) to eccentricity time scales (~100 kyr) (Berger and Jansen, 1994). The longer glacial cycles, which drive aridity in equatorial East Africa, are the likely cause of the sustained desiccation observed in the region throughout the Plio-Pleistocene (Wynn, 2004). Our records from ODP-OLO12 core material suggest southern Kenya has experienced a long-term desiccation of the environment over the past ~1 myr. However, there is no apparent orbital control on the climate in this region over that time.

5.7 Conclusion

Table 5.1: Paleoenvironmental interpretations of Paleolake Koora based on inferences from mineralogical and geochemical data.

ODP 1A

Mineral Zone	Age	Mineralogy	Paleoenvironment
RCI	~85 ka to present	Unconsolidated Alluvium	Fluvial-deltaic/ Alluvial Fan/ Savanna
M5	~180 to 85 ka	Carbonates, Zeolites, Diatom-rich	Shallow Saline Lake/ Subaerial Exposed Surface
M4	~250 to 180 ka	Carbonates, Zeolites	Shallow Saline Lake/ Zeolite Facies
M3	~390 to 250 ka	Low Mg-calcite, Sodium carbonates, Zeolites, Halite, Diatom-rich	Shallow Saline Lake/ Diagenetic Zone
M2	~0.710 to 390 ka	Low Mg-calcite, Diatom-rich	Hydrologically Closed Saline Lake
M1	~1.0 Ma to 710 ka	Diatom-rich Sediments	Hydrologically Open Freshwater Lake

Paleolake Koora began as a shallow saline lake that quickly developed into a freshwater hydrologically open basin for a sustained period of time. The lake likely began to transition from a hydrologically open to a closed basin ~710 ka. Volcanic deposits and tectonic activity altered

the hydrochemistry of the basin ~390-250 ka. A significant desiccation event is marked by intensive zeolitic alteration ~250 ka. Variable environmental conditions, fluctuating between shallow lake and paleosol development, followed the ash deposition and zeolitic alteration. No lacustrine sediments accumulated over the past ~80 ka. The series of paleolakes that occupied the Koora Graben reached a terminal phase by the early Holocene (Tab. 5.1).

6 FROM TRACHYTE TO TRONA: EVIDENCE OF WEATHERING PATTERNS AND MINERAL REACTIONS FROM THE SOUTHERN KENYA RIFT

Nathan M. Rabideaux, Daniel M. Deocampo

Georgia State University, Department of Geosciences, Atlanta, GA 30302

6.1 Abstract

The southern Kenya Rift is dominated by volcanogenic material, including trachytic and basaltic tuffs and flow deposits, volcanic soils, and volcaniclastic sediments. A suite of 41 samples were collected from modern surface and outcrop localities throughout the southern Kenya Rift to characterize the parent material and weathering patterns of fluviolacustrine and volcanogenic sediments located within the Lake Magadi and Olorgesailie/Koora Graben watersheds via X-ray diffraction, petrographic and scanning electron microscopy, and bulk geochemical analyses. Principle component analysis of X-ray diffraction data revealed four clusters, each primarily sourced from a distinct area of the southern Kenya Rift. Principal Component 1 is composed of trachytic material with minor zeolitic alteration; this largely originates in the western part of the region near the Nguruman Escarpment and Nasikie Engida (Little Magadi). Principal Component 2 is comprised of abundant authigenic silicate minerals and carbonates, as well as detrital feldspathic material and pyroxene, mostly contained in samples from the Magadi Basin. Principal Component 3 contains authigenic and detrital silicate minerals, mostly from the Olorgesailie Basin, Ol Kejo Nyiro, and Ol Doinyo Nyokie. Principal Component 4 is mostly pedogenic material from the Kiserian region – in the highlands to the north of Lake Magadi and Mt. Olorgesailie. Geochemical analyses indicate that there is a strong

positive correlation between Fe, Al, Ti, and P (detrital); Si and K (sanidine); and Na vs. LOI (trona). There is a strong negative correlation between Na, Al, Fe, and Mn (basalt vs. trachyte source); and Si, Mn vs. LOI (perhaps chert?). These data suggest that the fluviolacustrine sediments in the Koora Graben are likely sourced from the Kiserian region of the northern parts of the area, whereas parent material for Lake Magadi sediments is primarily sourced in the west near the Nguruman Escarpment and to a lesser extent from the east near Ol Doinyo Nyokie. The fluviolacustrine and volcanogenic sediments found in the Olorgesailie and Magadi basins and the mineral reactions observed in the southern Kenya Rift provide a framework for tracing material from geologic source to hydrologic sump.

Keywords: Zeolites, Weathering, Authigenic Minerals, Lake Magadi, Olorgesailie

6.2 Introduction

The authigenic mineralogy and bulk geochemistry of lacustrine sediments can provide valuable information in regards to weathering patterns, regional climate history, and watershed hydrochemistry (Bradley and Eugster, 1969; Surdam and Parker, 1972; Eugster and Hardie, 1975; Surdam and Eugster, 1976; Hay and Kyser, 2001; Owen et al., 2018*). Alteration of volcanic glass in saline alkaline waters commonly produces authigenic aluminosilicate minerals, such as authigenic clay minerals and zeolites (e.g., Hay, 1963; Surdam and Parker, 1972; Surdam and Eugster, 1976). Authigenic minerals from lacustrine sediments have been studied extensively in sites such as the Green River Formation in the western United States, Olduvai Gorge in northern Tanzania, and Lake Magadi in the Southern Kenya Rift.

The geology of the Southern Kenya Rift was first described by colonialists in the late Nineteenth Century (e.g., Fischer, 1884; Mügge, 1885; Kaiser, 1898). Further work in the Twentieth Century published a more detailed geological record of southern Kenya (e.g., Künzli, 1901; Parkinson, 1913; Anonymous, 1923; Gregory, 1921; Leakey, 1952; Baker, 1958; Crossley, 1979). The geology is comprised of Precambrian basement rock overlain by Miocene to recent volcanic and sedimentary deposits. The oldest rocks of the rift floor are the gneisses, quartzites and schists that make up the Basement System. There is a significant erosion surface between the metamorphic basement and Miocene-Pliocene aged Olorgesailie volcanics and the flow basalts that are associated with the Nguruman Rift faulting events. The Olorgesailie volcanics consist of augitites, trachyandesites, alkali trachytes, and nephelinites. During the late Pliocene and early Pleistocene, flow trachytes filled most of the Southern Kenya Rift floor while a second stage of faulting occurred associated with the Nguruman Rift (Baker, 1958, 1963; Crossley, 1979).

Lacustrine sediments began to accumulate on the rift floor during the early to middle Pleistocene. The Oloronga Beds formed in the basin now occupied by Lake Magadi, and the lake beds of the Olorgesailie Formation accumulated in an adjacent trough to the northeast near Mt. Olorgesailie. Further faulting and erosion followed in much of the region, but further lake deposition occurred in the Magadi trough during the Late Pleistocene to Holocene. The Green Beds, which are younger that the Oloronga Beds, were overlain by fine tuffaceous silts and clays that accumulated during a humid phase in Lake Magadi, known as the High Magadi Beds. The youngest deposits in the region include thick sequences of sodium carbonate evaporites (trona and nahcolite) in saltpans and unconsolidated alluvium throughout much of the Southern Kenya Rift (Gregory, 1921; Baker, 1958; Crossley, 1979).

The Southern Kenya Rift extends from Lake Naivasha at the north end to Lake Magadi at the southern extent, encompassing diverse landscapes and is home to the famous Olorgesailie Prehistorical Site, the Koora Graben, and the Lake Magadi basin. The climate of the Southern Kenya Rift is arid to semi-arid, with low average annual precipitation (< 50 cm) and high average daily temperatures (~20-38° C) (Baker, 1958; Behr, 2002). The study area covers localities throughout the Southern Kenya Rift, ranging from the relatively humid Kiserian region of the highlands (~2000 m elevation) in the northeastern part of the region to the semi-arid savannas to the arid to semi-arid region surrounding Lake Magadi near the southernmost end of the Kenya Rift. Recent investigations of the Southern Kenya Rift have produced robust records of environmental change that span roughly the past one million years (Cohen et al., 2016; Campisano et al., 2017).

Situated to the north of Mt. Olorgesailie is the well-studied Olorgesailie Formation, as well as the paleontologically and archaeologically rich Oltepesi and Oltulelei Formations (Owen

et al., 2008; Potts, 1989; Deocampo et al., 2010). The Olorgesailie Formation is comprised of lacustrine, volcaniclastic and alluvial sediments that were deposited between ~1.2 and 0.49 Ma (Gregory, 1921; Isaac, 1978; Potts, 1989; Deino and Potts, 1990, 1992; Behrensmeyer et al., 2002; Owen et al., 2008). The stratigraphic record from Olorgesailie shows that the area experienced variable climatic regimes, with fluctuating humid and arid conditions evidenced by paleosols, rhizoliths, wetland deposits, diatomites, and diatomaceous silts and clays (Owen et al., 2008; Deocampo et al., 2010; Behrensmeyer et al., 2018). The Koora Graben is located on the southern flanks of Mt. Olorgesailie. Recent fieldwork and core analysis have found evidence that indicates the Koora Graben was occupied by a series of paleolakes from ~1.0 Ma to the early Holocene (see Chapter 4).

This study examines the mineralogy and geochemistry of sedimentary and volcanic material collected throughout the Southern Kenya Rift to understand weathering patterns and mineral reactions of geologic material from different source regions and to determine their relationships to sediments deposited in the Koora Graben and Lake Magadi over the past ~ 1.0 Ma. We then relate these data to records from the *Olorgesailie Drilling Project* in the Koora Graben and the *Hominin Sites and Paleolakes Drilling Project* at Lake Magadi. The goal of this study is to trace sediments from geologic source to the hydrologic sump in the Southern Kenya Rift.

6.3 Methods

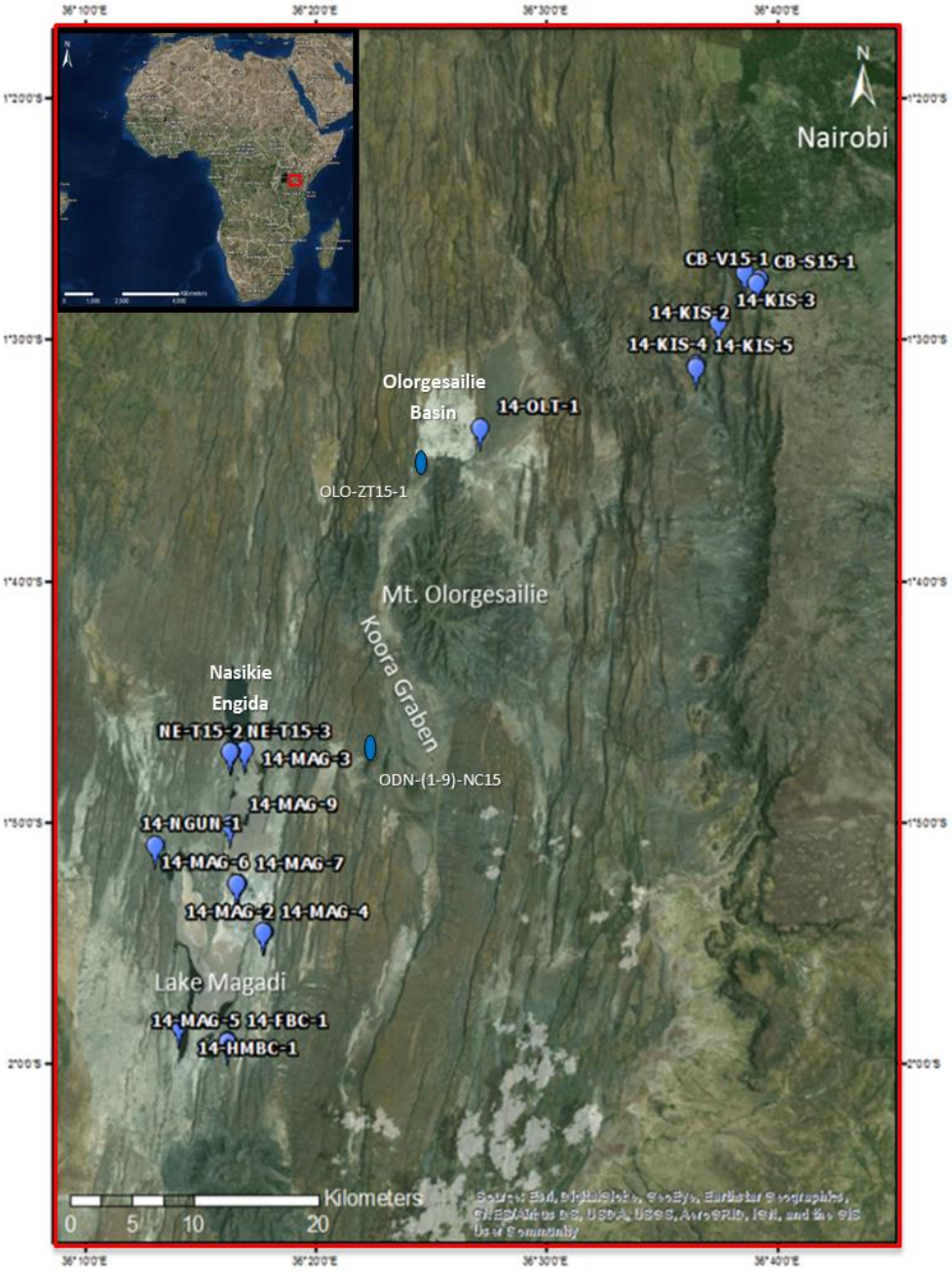

Figure 6.1: Map of the Southern Kenya Rift with sample locations and important features labelled. Inset map of African continent with study region outlined.

A suite of 41 samples were collected during the 2014 and 2015 fields season from modern surface and outcrop locations throughout the Southern Kenya Rift (Fig. 6.1). Sample material collected included soils, volcanic material, chemical sediments, altered tuffaceous

material, and unconsolidated volcanogenic sediment. Samples were collected from throughout the western Kajiado District, including from near Kiserian (zeolitic volcanics and paleosols), Oltepesi (weathered basalt outcrop), Olorgesailie (zeolitized tuff), Ol Doinyo Nyokie (tuffs and volcanic glass), the eastern lagoon at Lake Magadi (High Magadi Beds), Lake Magadi (trona and clays), Nasikie Engida (nahcolite and trachyte), Ewaso Ngiro (suspended sediments), and the Nguruman Escarpment (saline clay) (Fig. 6.1). We collected modern surface samples by hand from randomly selected fresh outcrop localities with a plastic trowel, assigned a sample designation, and stored them in clean plastic bags. Samples were then double bagged, archived, and packaged for shipment. GPS coordinates were recorded for most sample localities, although a few sample locations were lost or not recorded (Tab. 6.1).

Table 6.1: Sample list with GPS coordinates and description for select samples.

Latitude	Longitude	Sample Identifier	Sample ID
		Suspended sediment collected from Ewaso Ngiro	14-Ewaso-1
			14-Nguru-2
S 01 51.177	E 36 12.996		14-NGUN-1
			14-NGUN-2
			14-NGUN-3
S 01 51.177	E 36 12.996		14-NGUN-4
		Trachyte sample collected from shore of Nasikie Engida	NE-T15-1
		Trachyte sample collected from shore of Nasikie Engida	NE-T15-2
		Trachyte sample collected from shore of Nasikie Engida	NE-T15-3
S 1˚ 54’ 45.46”	E 36˚ 17’41.56”		14-MAG-2
S 01 47.215	E 36 16.854		14-MAG-3
S 01 54’ 47.76”	E 36˚ 17’38.53”		14-MAG-4
S 1˚ 59’ 18.63”	E 36˚ 16’09.20”		14-MAG-5
S 1˚ 52’ 45.87”	E 36˚ 16’ 33.63”		14-MAG-6
S 1˚ 52’ 47.85”	E 36˚ 16’ 32.88”		14-MAG-7
S 1˚ 50’ 21.93”	E 36˚ 16’ 15.91”		14-MAG-9

S 1˚ 58’ 35.34”	E 36˚ 14’ 2.85”		14-HMBC-1
S 1˚ 59’ 19.04”	E 36˚ 16’ 9.30”	Fish bed clay	14-FBC-1
		Saline clay	14-SCM-1
S 1˚ 59’ 19.04”	E 36˚ 16’ 9.30”	High Magadi Ash Bed	15-HMAB-1
S01.77935	E036.34886	Tuff collected near Ol Doinyo Nyokie camp	ODN-1-NC15
S01.77961	E036.34880	Tuff collected near Ol Doinyo Nyokie camp	ODN-2-NC15
S01.77973	E036.34861	Tuff collected near Ol Doinyo Nyokie camp	ODN-3-NC15
S01.77975	E036.34853	Tuff collected near Ol Doinyo Nyokie camp	ODN-4-NC15
S01.77985	E036.34846	Tuff collected near Ol Doinyo Nyokie camp	ODN-5-NC15
S01.77983	E036.34861	Tuff collected near Ol Doinyo Nyokie camp	ODN-6-NC15
S01.77960	E036.34870	Tuff collected near Ol Doinyo Nyokie camp	ODN-7-NC15
S01.77999	E036.34837	Tuff collected near Ol Doinyo Nyokie camp	ODN-8-NC15
S01.77947	E036.34882	Tuff collected near Ol Doinyo Nyokie camp	ODN-9-NC15
		Obsidian collected near Ol Doinyo Nyokie camp	15-ODN-3
		Zeolitized tuff from southern outcrop of Olorgesailie Formation	OLO-ZT15-1
S 01 33.914	E 36 27.068	Weathered basalt clay	14-OLT-1
			14-TLB-1
S 01 27.810	E 36 39.153		14-KIS-1
S 1˚ 27’ 28.46”	E 36˚ 38’32.95”		14-KIS-2
S 01 29.536	E 36 37.375		14-KIS-3
S 01 31.310	E 36 36.400		14-KIS-4
S 01 31.398	E 36 36.440		14-KIS-5
		Vesicular volcanic rock collected from Kona Baridi, on Magadi Road	CB-V15-1
		Vesicular volcanic rock collected from Kona Baridi, on Magadi Road	CB-V15-2
		Vesicular volcanic rock collected from Kona Baridi, on Magadi Road	CB-S15-1

Sample material was dried in an oven at 40° C for 48 hours to remove excess moisture. Sample material for scanning electron microscopy (SEM) was extracted and the remainder of the sample was powdered using a ball-and-pestle impact grinder for 10 minutes. Aliquots of each sample were designated for powder X-ray diffraction (XRD) and bulk geochemical analysis.

We completed XRD powder analysis on all 41 samples using a Panalytical X'pert Pro MPD diffractometer running at 45 kV and 40 mA. Scans were performed on each sample from 5 to 70° 2Θ for 30 minutes. Pattern analysis was completed using Panalytical High Score software with reference to the PDF-2 mineral database to determine bulk mineralogy.

A total of 41 outcrop and surface samples from the Southern Kenya Rift were sent to ALS Geochemistry for geochemical analysis via fusion inductively-coupled plasma atomic emission spectroscopy (ICP-AES) for bulk geochemistry and fusion inductively-coupled plasma mass spectrometry (FUS-ICP) for trace element (TE) and rare earth element (REE) geochemistry. Data were returned in Excel spreadsheet format, with bulk data in weight percent (wt %) and TE and REE in parts per million (ppm) or milligrams per kilogram (mg/kg).

We completed SEM analysis on 15 samples from the Southern Kenya Rift. We selected samples from each source region based on mineralogy and geochemistry. Analysis was completed at Georgia State University using a Tescan Vega 3 scanning electron microscope with an EDAX energy dispersive X-ray spectrometer.

6.4 Results

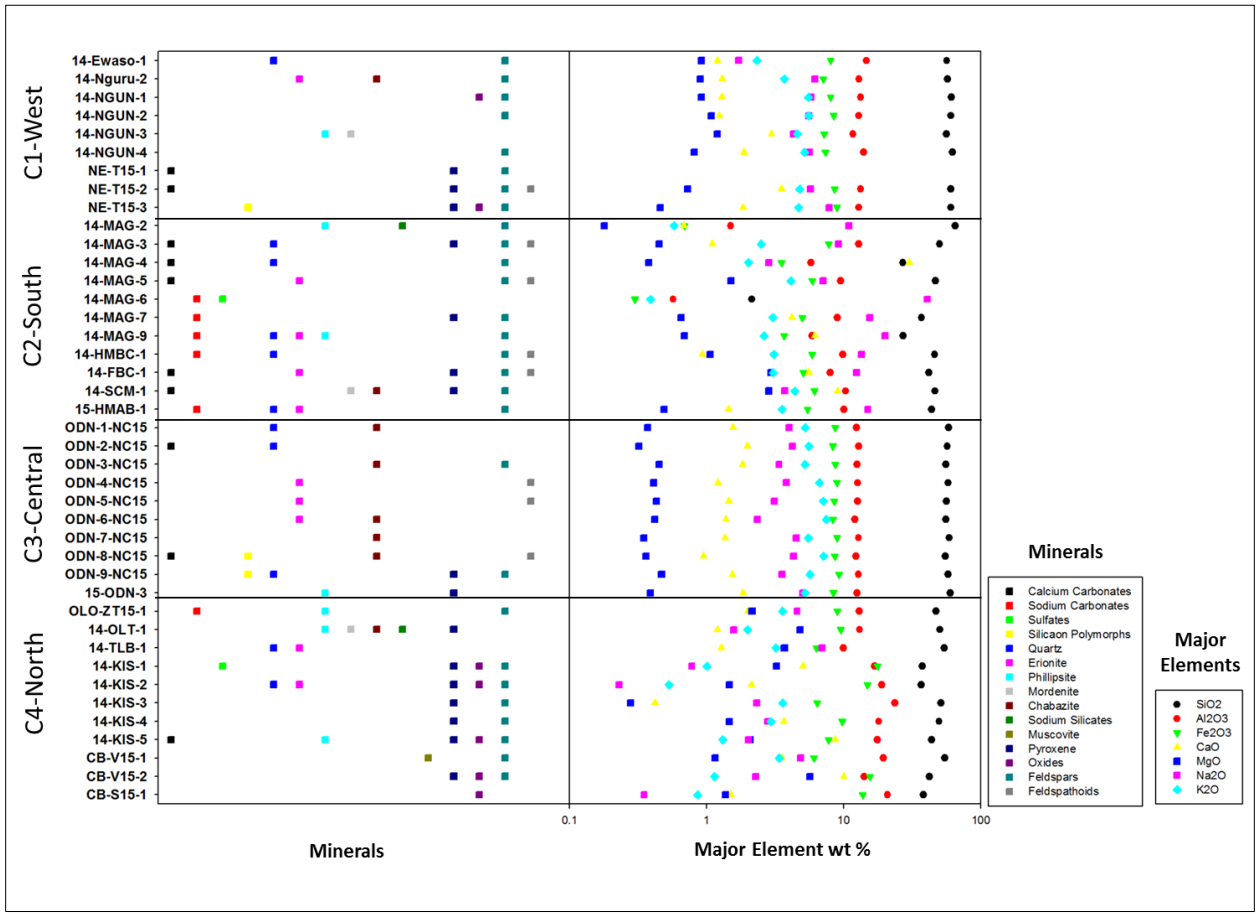

Figure 6.2: Mineralogy and major element geochemistry of rock outcrop and surface samples from the Southern Kenya Rift. There are four distinct clusters based off principal component analysis: Cluster 1 is to the west near the Nguruman Escarpment; Cluster 2 is the Lake Magadi basin to the south; Cluster 3 is centrally located proximal to Ol Doinyo Nyokie Group Ranch; and Cluster 4 is located in the northern section of the region in the Kiserian region of Kenya.

6.4.1 Mineralogy

Principal component analysis (PCA) of bulk mineralogical data revealed four distinct mineral clusters by principal mineral components: 1) the western area near the Nguruman Escarpment; 2) the southern end of the rift in the Lake Magadi basin; 3) in the central area on the Ol Doinyo Nyokie Group Ranch; and 4) the highlands of the northeastern area of the Kiserian region (Fig. 6.2). The mineralogy of the western area (Cluster 1) is comprised of mostly detrital

feldspars and pyroxene, in addition to some erionite, mordenite, phillipsite, and chabazite. The Lake Magadi basin in the southernmost area (Cluster 2) contained calcium carbonates, sodium carbonates, erionite, phillipsite, chabazite, sodium silicates, and quartz, as well as detrital feldspars and pyroxene. The central area near Ol Doinyo Nyokie (Cluster 3) contained quartz and silicon polymorphs, calcium carbonates, erionite, and chabazite. In the Kiserian highlands in the northeastern area of the Southern Kenya Rift, the mineralogy consisted mostly of volcanic feldspathic and pyroxene minerals, as well as quartz, erionite, phillipsite, mordenite, chabazite, sodium silicates, and muscovite (Fig. 6.2).

6.4.2 Geochemistry

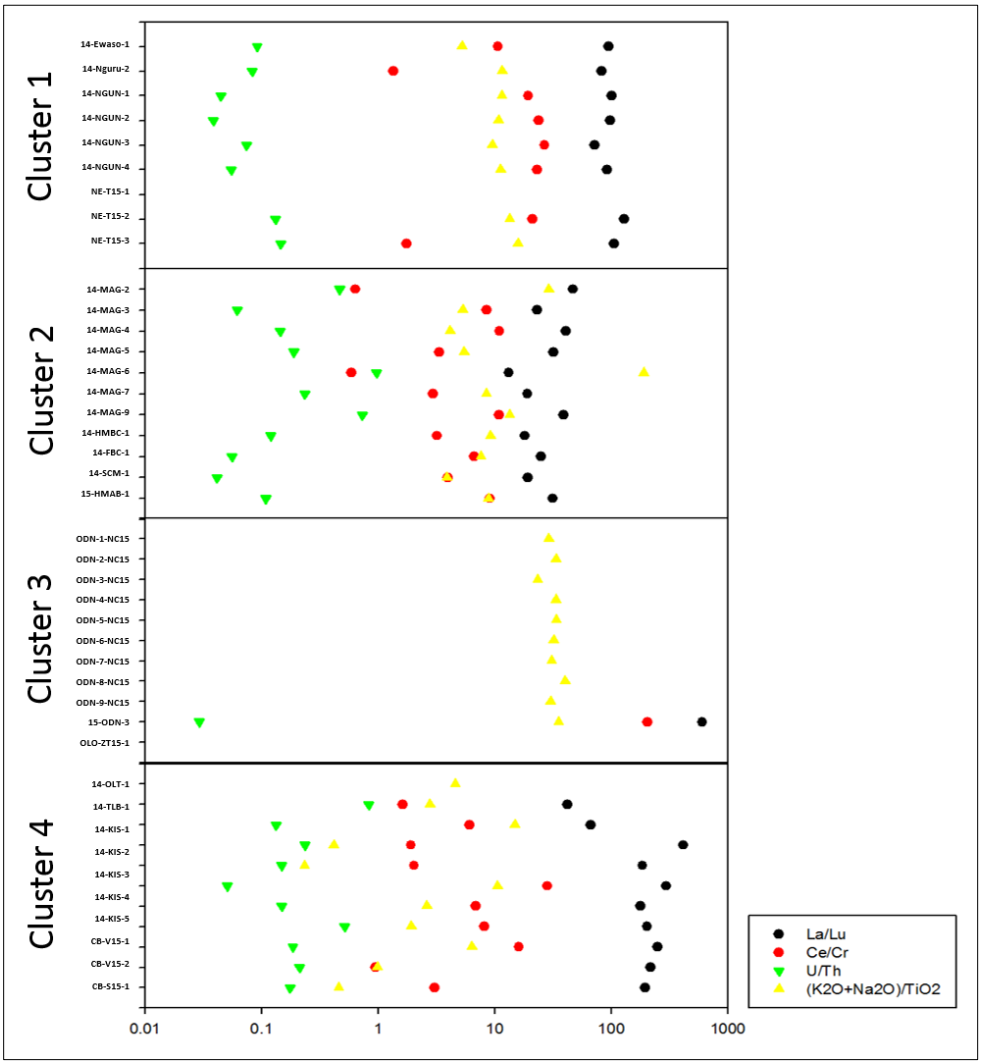

Figure 6.3: Geochemical indicators for Southern Kenya Rift outcrop and surface samples. La/Lu indicates light versus heavy REE. Ce/Cr and U/Th are source indicators. ($K_2O+Na_2O)/TiO_2$ is a salinity indicator. The geochemical dataset for Cluster 3 is incomplete.

Major element geochemistry for these samples displays similar variations to the mineral clusters, with four distinct regions (Figs. 6.2 and 6.3). Cluster 1 is characterized by relatively low Na_2O concentrations, high K_2O, SiO_2 and TiO_2 concentrations, enrichment in light REE relative to heavy REE, and relatively high $(K_2O + Na_2O)/TiO_2$ values. There are strong correlations between SiO_2 and TiO_2, as well as K_2O and SiO_2. Cluster 2 is enriched in heavy REE relative to light REE, high CaO and Na_2O concentrations, and variable $(K_2O + Na_2O)/TiO_2$ values. There

are strong positive correlations between SiO_2-TiO_2 K_2O-SiO_2 and K_2O-TiO_2, and strong negative correlations between Na_2O and TiO_2. Cluster 3 has similar geochemical correlations to Cluster 1, with strong correlations between SiO_2-TiO_2 and K_2O-SiO_2. However, Cluster 3 is also characterized by low MgO values and high $(K_2O + Na_2O)/TiO_2$ values. Cluster 4 is characterized by depletion of heavy REE relative to light REE, low $(K_2O + Na_2O)/TiO_2$ values, relatively high Al_2O_3, MgO, and CaO concentrations, and low K_2O concentrations. There is a strong positive correlation between K_2O and SiO_2, and strong negative correlations between SiO_2-TiO_2, K_2O-TiO_2, Na_2O-TiO_2, and Na_2O-SiO_2. Geochemical source indicators U/Th and Ce/Cr suggest Cluster 1 has a different geologic source than Clusters 2 and 4. A complete geochemical dataset was not obtained for most samples in Cluster 3 (Fig. 6.3).

6.4.3 Scanning Electron Microscopy

SEM analysis revealed a wide variety of materials. Minerals identified included detrital anorthoclase and sanidine, as well as authigenic minerals such as phillipsite, analcime, and chabazite. No identifiable mineral relationships (e.g., visual evidence for dissolution and re-precipitation) were seen in the selected samples.

6.5 Discussion

The bedrock and sediments of the Magadi area were first described by early colonial explorers and geologists, but the first detailed geologic surveys were carried out by Gregory (1921), Baker (1958, 1963), and Eugster (1969). Nearly all the sediments in the Magadi basin are comprised of authigenic minerals, with the exception of detrital sanidine and anorthoclase. Surdam and Eugster (1976) described the authigenic minerals of Lake Magadi and interpretations of the mineral reactions responsible for the formation of these assemblages in terms of glass and brine chemistry.

6.5.1 Mineralogy

Principal component analysis of bulk mineralogical data indicates there are four distinct mineral clusters, each associated with a different area of the Southern Kenya Rift (Fig. 6.2). These mineral clusters suggest parent material may be less important than aqueous processes in regards to what is the more important influence on zeolite assemblages. We identified diverse zeolite assemblages of erionite, phillipsite, mordenite and chabazite in Clusters 1, 2 and 4, whereas Cluster 3 from Ol Doinyo Nyokie contained only erionite and chabazite (Fig. 6.2). Calcium carbonates are most abundant in the south around Lake Magadi, forming through pedogenesis in soils, but also formed in the lake basins from dilute waters near the lake margin.

Zeolites form as diagenetic products of a large variety of aluminosilicate geologic material including volcanic glass, aluminosilicate gels, some phyllosilicate minerals (i.e., smectite and kaolinite), feldspars, and feldspathoids (Sheppard and Hay, 2001). Zeolites most commonly form through alteration of volcanic glass in saline, alkaline waters (Hay, 1963, 1966; Sheppard and Gude, 1968, 1969). There are two main influences on zeolite assemblages: parent material and water chemistry.

The Southern Kenya Rift floor is composed of mostly trachytic volcaniclastic material (Baker, 1958, 1963; Crossley, 1979), although Kerimasi and Ol Doinyo Lengai have likely contributed nephelinite and carbonatite volcaniclastic deposits to the region during the late Pleistocene to Holocene (Hay, 1983). The diversity of zeolite assemblages we observed across different areas of the Southern Kenya Rift implies that geochemical variability of parent material may have some influence on zeolite formation, however it seems that water chemistry is the more important factor. For example, analcime was not present in any of the modern surface and outcrop samples, whereas analcime is the most abundant zeolite in the HSPDP-MAG14 and

ODP-OLO12 cores (see Chapters 3 and 4 of this dissertation). This suggests analcime formation requires an evaporatively concentrated sodium-rich brine, whereas other zeolite species – particularly erionite and chabazite, can form through interaction with dilute surface waters (Fig. 6.4).

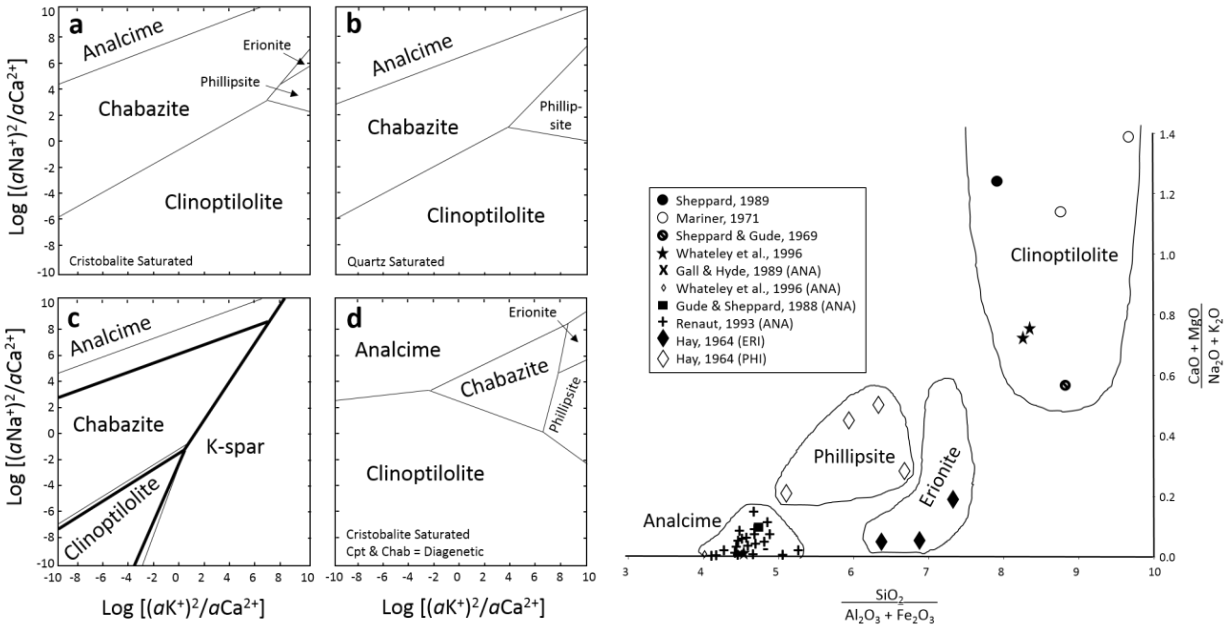

Figure 6.4: Zeolite phase diagram and X-Y plot for silica concentration versus cation concentration. (left) Log[(αK⁺)²/αCa²⁺] vs. log[(αNa⁺)²/αCa²⁺] diagrams for the zeolite species occurring in saline, alkaline lake. All are calculated assuming 35° C and (a) An aqueous silica activity in equilibrium with cristobalite; (b) An aqueous silica activity in equilibrium with quartz; (c) Same as (a) & (b) with the addition of K-feldspar included in the calculation, thin lines = cristobalite & thick lines = quartz; and (d) Same as (a) except diagenetic compositions for chabazite and clinoptilolite were included in the calculations. (Adapted from Chipera and Apps, 2001). (right) $SiO_2/(Al_2O_3+Fe_2O_3)$ vs. $(CaO+MgO)/(Na_2O+K_2O)$ molar diagram compilation for select zeolite species in closed hydrologic systems. (From Langella et al., 2001).

The brines of Lake Magadi are hypersaline and alkaline, which favors the formation of Na-bearing zeolites such as analcime. Previous studies have shown that as a lake becomes more concentrated and saline, a volcanic ash deposit will reflect zeolitic zonation, with K- and Ca-zeolites progressing inward towards Na-zeolites at the center of most concentrated saline alkaline water (Hay, 1966; Sheppard and Gude, 1968, 1969; Langella et al., 2001). In certain lake basins

this process can progress to form authigenic K-feldspar in the most concentrated waters at the center of the basin. This type of zeolitic zonation was not present in the ODP-OLO12-1A core, however some zeolitic zonation is identifiable in HSPDP-MAG14 cores 1A and 2A. HSPDP-MAG14-1A is proximal to the lake margin whereas HSPDP-MAG14-2A is located near the deepest part of the basin, and analcime is the most dominant zeolite species in both HSPDP-MAG14 cores 1A and 2A. However, HSPDP-MAG14-1A contains more alkaline earth-bearing zeolite species than HSPDP-MAG14-2A, in particular mordenite. The most common zeolites present in the modern surface and outcrop samples were erionite and chabazite (Fig. 6.2), which were most common in the ODN tuff samples. Other factors influencing zeolite speciation include cation activity and silica activity in the lake waters (Fig. 6.4).

Studies on the origin of sodium-aluminum-silicate gels at Lake Magadi suggest they are related to the formation of authigenic zeolites, and perhaps chert deposits (Eugster and Jones, 1968; Eugster, 1969). Eugster and Jones (1968) observed these gels precipitating primarily in two locations of the greater Magadi Basin: proximal to hot springs that feed the northeastern lagoon at the northern end of Lake Magadi; and at the north end of Nasikie Engida (aka Little Magadi) near the confluence of hot springs and a river of hot water enter the lake. However, we have only observed gels accumulating at the lake margin of both Lake Magadi and Nasikie Engida. If one were to assume that these gels are washed into the basin and accumulate on the lake bottom, a significant deposit could form in lake beds and crystallize into zeolites or chert (Eugster and Jones, 1968; Eugster, 1969).

Clusters 2 and 4 also contain sodium silicate minerals (Fig. 6.2), which form in concentrated alkaline brines. Two hydrous sodium-silicate minerals – magadiite and kenyaite, are well known from Lake Magadi, and are precursors for inorganic bedded chert (Eugster,

1967). Eugster (1967) suggested that magadiite would have likely formed from alkaline brines, and kenyaite would have formed as sodium was leached from magadiite by percolating brines. This process would have continued until all sodium was removed and chert was formed (Eugster, 1967, 1969). Hay (1968) suggested two mechanisms for the magadiite deposits: 1) thin, widespread layers precipitated by mixing of freshwater with silica-rich brine in a chemically stratified lake; and 2) localized masses formed by the infiltrating freshwater interacting with dense brine. However, Eugster (1980) acknowledged that magadiite could form from volcanogenic sediments interacting with alkaline brines, which is commonplace at Lake Magadi. This model, with a deep lake and a chemocline, may also explain abundant analcime deposits in the HSPDP-MAG14 and ODP-OLO12 cores. If lake levels fluctuated rapidly and significantly, surface waters could become highly concentrated during lake lowstands and form dense sinking brines during highstands. The dense brine interacting with freshwater and sediments may allow for the dissolution and precipitation of mineral species (i.e. analcime and magadiite) at the sediment-water interface in a chemically stratified lake.

Later studies by Behr and Röhricht (2000) and Behr (2002) further examined the origin of cherts at Lake Magadi, and Behr (2002) suggested another model for the formation of sodium silicates and cherts of the High Magadi Beds. He suggested that sodium silicates were formed partially through early diagenesis in lake muds, and the sodium silicates were silicified into chert mainly by silica-rich surface brines. This model does not necessitate a deep lake or a chemocline, which were included as necessary features in the formation of magadiite in previous models (Eugster, 1967, 1969; Hay, 1968). This supports our hypothesis that analcime and sodium silicate minerals form from precursor Na-Al-Si gels on mud flats and proximal to alkaline hot springs and the margins of Lake Magadi and Nasikie Engida.

Lake Magadi contains abundant pyrite and sulfates throughout the HSPDP-MAG14 cores, whereas the ODP-OLO12-1A core contains no pyrite or sulfates. Lakes in the East African Rift Valley typically host sodium-carbonate brines, indicating any sulfate mineral in lacustrine sediments is a diagenetic product formed by oxidation of pyrite. However, it is possible that sulfur fumaroles related to tectonic fissures were present in the Magadi basin at times during more tectonically active intervals, providing sufficient sulfur-rich hydrothermal fluids to precipitate pyrite and/or sulfates. As there is no pyrite in the modern surface and outcrop samples, it must have formed *in situ* in a wetland or lacustrine environment. Pyrite most likely formed in shallow anoxic waters (i.e. wetlands) or a deep stratified lake through microbial reduction or in hydrothermal veins, and sulfates formed through oxidation of pyrite in well-oxygenated lake waters or upon subaerial exposure during a desiccation event. This most likely reflects fluctuating lake levels, which would have also facilitated the formation of Na-Al-Si gels on mud flats aiding in the formation of zeolites, sodium silicates, and chert.

6.5.2 Geochemistry

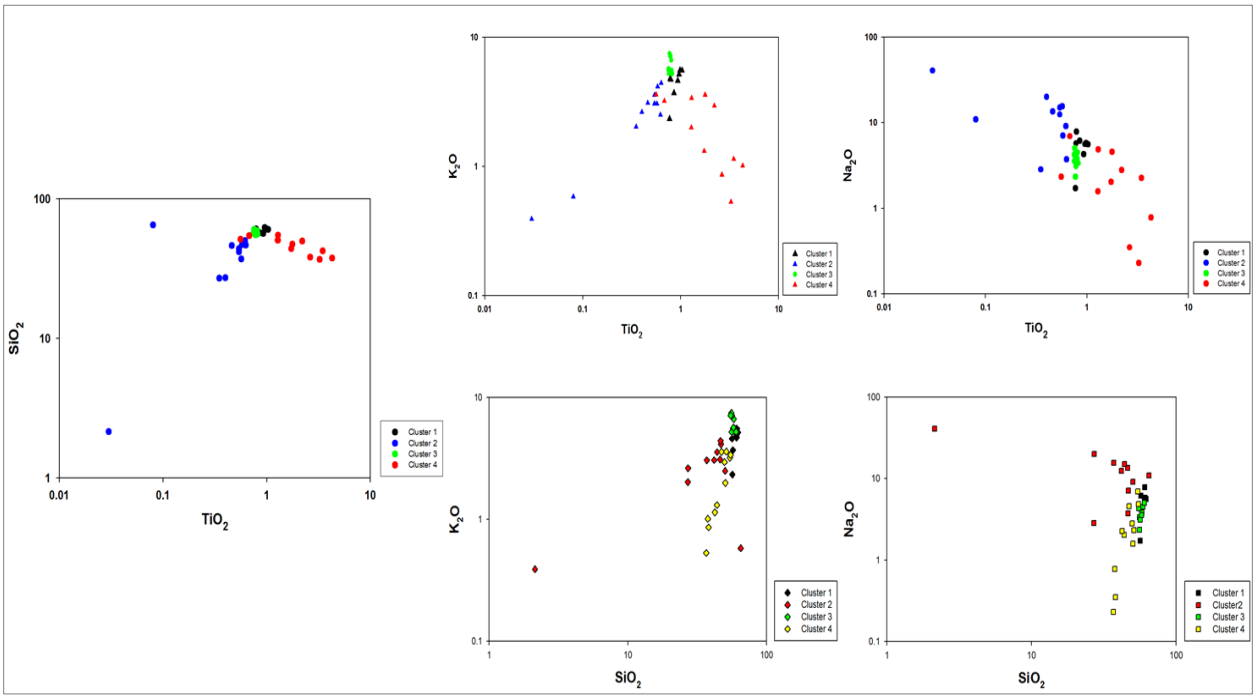

Figure 6.5: Geochemical plots of samples displayed by clusters based on principal component analysis. (Left) SiO_2 vs. TiO_2. (Center top) K_2O vs. TiO_2. (Center bottom) Na_2O vs. SiO_2. (Right top) K_2O vs. TiO_2. (Right bottom) Na_2O vs. SiO_2.

Comparing the geochemistry of the distinct mineral clusters revealed considerable variation between sample localities. Cluster 2 has a strong positive correlation between SiO_2-TiO_2 whereas Cluster 4 has a strong negative correlation (Fig. 6.4), suggesting a significant difference in either parent material or hydrochemistry between the two source regions. However, both Clusters 2 and 4 have negative correlations between Na_2O-TiO_2 salinity indicator and U/Th-Ce/Cr source indicators (Figs. 6.4 and 6.5).

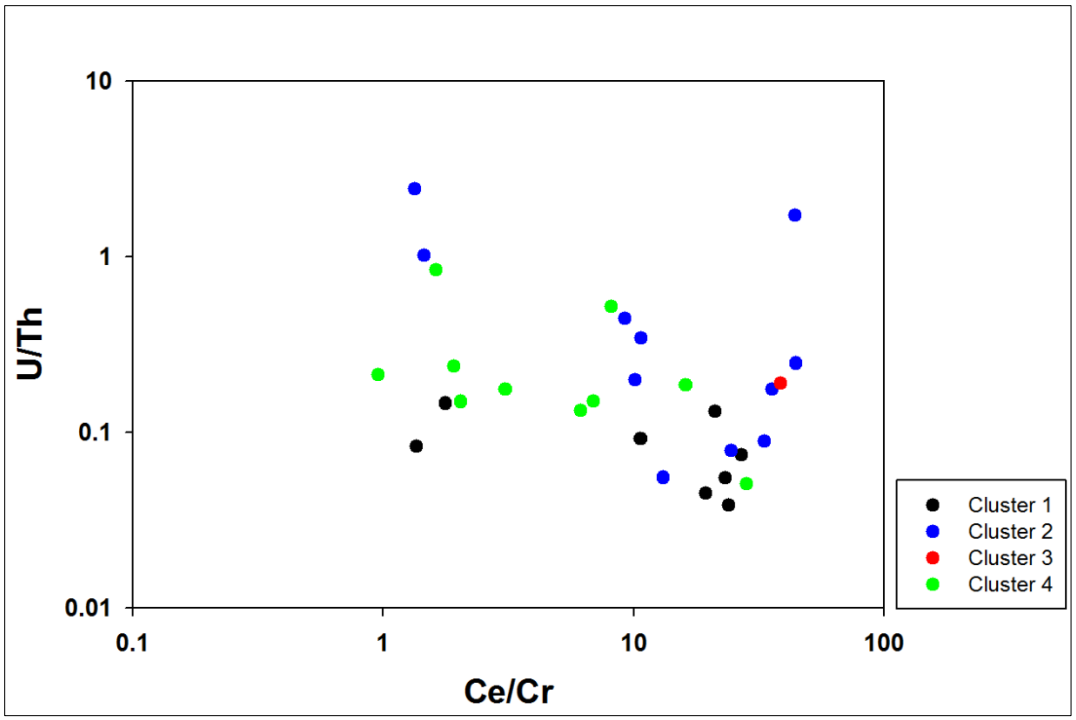

Figure 6.6: Geochemical X-Y plot comparing different source indicators separated by geographic region: Cluster 1 is to the West; Cluster 2 to the South; Cluster 3 is Central; and Cluster 4 is in the North.

The geochemistry of the Southern Kenya Rift indicates there is significant variation between source regions. Comparison of Ce/Cr and U/Th ratios indicate there is a negative correlation between each source region (Fig. 6.6), which suggests uranium enrichment is mostly associated with inorganic chert and soil carbonate precipitation and not influenced by source region. When compared with geochemical data from HSPDP-MAG14 and ODP-OLO12 cores (Fig. 6.7), it seems Lake Magadi sediments are more associated with surface and outcrop samples from the south and west, whereas sediments in the ODP core are derived from the north and central regions of the rift. Samples from the Lake Magadi basin in the south produced the most unique mineralogical dataset and the most diverse assemblage of authigenic minerals.

Southern Kenya Outcrop and Surface Samples Matrix of Intercorrelations

	SiO2	Al2O3	Fe2O3	MnO	MgO	CaO	Na2O	K2O	TiO2	P2O5	LOI	S	Fe-Al-Ti-P	Parent Material
SiO2	1	0.343	0.162	0.423	-0.001	-0.323	-0.582	0.613	-0.062	0.051	-0.823		Si-K	Detrital
Al2O3	0.343	1	0.732	0.631	0.217	-0.132	-0.737	0.186	0.61	0.374	-0.661		Na-LOI	Evaporite
Fe2O3	0.162	0.732	1	0.588	0.533	-0.029	-0.678	-0.032	0.914	0.681	-0.566		Al-Mn	
MnO	0.423	0.631	0.588	1	0.096	0.107	-0.669	0.462	0.302	0.204	-0.669			
MgO	-0.001	0.217	0.533	0.096	1	0.133	-0.383	-0.166	0.552	0.556	-0.259		Si vs (LOI/Na)	
CaO	-0.323	-0.132	-0.029	0.107	0.133	1	-0.208	-0.107	0.048	0.106	0.061			
Na2O	-0.582	-0.737	-0.678	-0.669	-0.383	-0.208	1	-0.225	-0.537	-0.391	0.786			
K2O	0.613	0.186	-0.032	0.462	-0.166	-0.107	-0.225	1	-0.308	-0.098	-0.628			
TiO2	-0.062	0.61	0.914	0.302	0.552	0.048	-0.537	-0.308	1	0.737	-0.342			
P2O5	0.051	0.374	0.681	0.204	0.556	0.106	-0.391	-0.098	0.737	1	-0.393			
LOI	-0.823	-0.661	-0.566	-0.669	-0.259	0.061	0.786	-0.628	-0.342	-0.393	1			
S												1		

HSPDP-MAG 2A Matrix of Intercorrelations

	SiO2	Al2O3	Fe2O3	MnO	MgO	CaO	Na2O	K2O	TiO2	P2O5	LOI	S	Fe-Al-Mn-Ti-K	Detrital
SiO2	1	-0.003	0.015	-0.067	-0.029	-0.106	-0.84	0.031	0.032	0.035	-0.911	0.011	Na-LOI	Evaporite
Al2O3	-0.003	1	0.695	0.68	0.186	0.056	-0.317	0.877	0.793	0.053	-0.378	0.283	Fe-S	Pyrite
Fe2O3	0.015	0.695	1	0.654	0.12	-0.014	-0.304	0.631	0.523	0.01	-0.326	0.835		
MnO	-0.067	0.68	0.654	1	0.232	0.364	-0.315	0.644	0.581	0.062	-0.249	0.456	Si vs (LOI/Na)	
MgO	-0.029	0.186	0.12	0.232	1	0.289	-0.306	0.335	0.515	0.056	-0.077	-0.039		
CaO	-0.106	0.056	-0.014	0.364	0.289	1	-0.276	0.109	0.15	0.219	-0.017	-0.027		
Na2O	-0.84	-0.317	-0.304	-0.315	-0.306	-0.276	1	-0.375	-0.404	-0.122	0.921	-0.178		
K2O	0.031	0.877	0.631	0.644	0.335	0.109	-0.375	1	0.759	0.06	-0.393	0.281		
TiO2	0.032	0.793	0.523	0.581	0.515	0.15	-0.404	0.759	1	0.128	-0.333	0.104		
P2O5	0.035	0.053	0.01	0.062	0.056	0.219	-0.122	0.06	0.128	1	-0.081	-0.007		
LOI	-0.911	-0.378	-0.326	-0.249	-0.077	-0.017	0.921	-0.393	-0.333	-0.081	1	-0.181		
S	0.011	0.283	0.835	0.456	-0.039	-0.027	-0.178	0.281	0.104	-0.007	-0.181	1		

ODP-OLO 1A Matrix of Intercorrelations

	SiO2	Al2O3	Fe2O3	MnO	MgO	CaO	Na2O	K2O	TiO2	P2O5	LOI	S	Fe-Al-Na-K	Detrital
SiO2	1	0.283	0.191	-0.477	-0.26	-0.765	0.087	0.086	0.172	-0.241	-0.678	0.066	P-Ti	Detrital
Al2O3	0.283	1	0.789	0.039	-0.5	-0.703	0.555	0.678	0.43	-0.061	-0.768	0.186	Ca-Mg-LOI	Carbonates
Fe2O3	0.191	0.789	1	0.236	-0.57	-0.711	0.573	0.71	0.229	-0.114	-0.597	0.23	Na-S	??
MnO	-0.477	0.039	0.236	1	-0.423	0.245	0.404	0.392	-0.376	-0.101	0.067	0.27		
MgO	-0.26	-0.5	-0.57	-0.423	1	0.463	-0.73	-0.686	0.213	0.381	0.566	-0.323	Detrital vs Carbonates	
CaO	-0.765	-0.703	-0.711	0.245	0.463	1	-0.403	-0.54	-0.283	0.24	0.761	-0.098		
Na2O	0.087	0.555	0.573	0.404	-0.73	-0.403	1	0.875	-0.366	-0.536	-0.606	0.562		
K2O	0.086	0.678	0.71	0.392	-0.686	-0.54	0.875	1	-0.237	-0.445	-0.586	0.449		
TiO2	0.172	0.43	0.229	-0.376	0.213	-0.283	-0.366	-0.237	1	0.51	-0.165	-0.435		
P2O5	-0.241	-0.061	-0.114	-0.101	0.381	0.24	-0.536	-0.445	0.51	1	0.292	-0.373		
LOI	-0.678	-0.768	-0.597	0.067	0.566	0.761	-0.606	-0.586	-0.165	0.292	1	-0.399		
S	0.066	0.186	0.23	0.27	-0.323	-0.098	0.562	0.449	-0.435	-0.373	-0.399	1		

Figure 6.7: Matrices of Intercorrelations for (top) modern surface and outcrop samples from the Southern Kenya Rift (this study), (middle) core material from HSPDP-MAG14-2A (Chapter 3 of this dissertation), and (bottom) core material from ODP-OLO12-1A (Chapter 4 of this dissertation).

Analysis of geochemical data suggests there is a strong positive correlation between iron, aluminum, titanium, and phosphorus, which indicates a strong detrital influence. There is also a strong positive correlation between silica and potassium – likely indicating detrital sanidine, and sodium versus loss on ignition, which indicates evaporate minerals (i.e. trona and nahcolite). There is a strong negative correlation between silica, manganese and loss-on-ignition. There is

also a strong negative correlation between sodium, aluminum, iron, and manganese, which likely indicates variation in volcanic parent material (basalt versus trachyte) (Fig. 6.7).

6.6 Conclusions

Four distinct mineral clusters are associated with four distinct regions of the rift, suggesting parent material is an important influence on the mineralogy of sediments in the Lake Magadi and Olorgesailie basins. Lake Magadi (HSPDP-MAG14) sediments are mostly sourced from the west and south, where carbonates, silica polymorphs, and zeolites are the dominant authigenic mineral groups. Olorgesailie and Koora (ODP-OLO12) sediments are mostly sourced from the northern area, in the relatively more humid highlands, where oxides and clay minerals dominate the mineralogy, although some zeolites are present. Analcime is not present in any of the outcrop and surface samples, suggesting its formation is mostly associated with aqueous processes and is not a direct product of the parent material; rather it likely forms from Na-Al-Si gels or precursor aluminosilicates; an intermediary gel phase may be necessitated in forming analcime under any conditions.

7 SUMMARY

Temperature is the most important climate variable at high latitudes, but precipitation is main climatic control in the tropics (deMenocal and Bloemendal, 1995; McGregor and Nieuwolt, 1998; deMenocal, 2004; Wynn, 2004; Feakins and deMenocal, 2010). Low-latitude precipitation is primarily the product of the monsoonal circulation system. The position of the Congo Air Boundary is associated with the Atlantic and Indian Ocean monsoons (Nicholson, 1996). Possible factors influencing migrations of the Congo Air Boundary include high-latitude cooling, the position and migration pattern of the ITCZ, and moisture gradients associated with the El Niño-Southern Oscillation (Russell and Johnson, 2007). Seasonal migrations of the ITCZ strongly influence seasonal rainfall patterns across much of Africa (Feakins and DeMenocal, 2010).

Organic-rich sapropels form in the Eastern Mediterranean in response to eustatic sea level changes (e.g., Mangini and Schlosser, 1985), due to increased precipitation in tropical Africa. Eleven sapropel horizons were deposited over the past ~465 ka, and dated using oxygen isotopic chronostratigraphy (Rossignol-Strick, 1984). The African monsoonal system is strongly related to the formation of Mediterranean sapropels during high precession insolation of northern hemisphere summer (Rossignol-Strick, 1984). Sapropels are organic-rich sediments associated with fluxes of freshwater input. Sapropel formation in the Eastern Mediterranean are associated with humid phases in northern and eastern Africa, when the monsoonal system strengthens due to enhanced precessional amplitude. Precessional forcing acts as a “pacemaker” for wet-dry cycles in Sub-Saharan Africa. Continental landmasses heat up at a more rapid pace than the ocean, which creates high-pressure systems that continue to grow, resulting in moisture-rich air masses circulating over the land creating the monsoons (McGregor and Nieuwolt, 1998). In

contrast, when land is cooled more rapidly than the ocean mixed-layer, it creates a low-pressure system that results in a cool and dry regional climate in continental environments (deMenocal and Bloemendal, 1995; deMenocal, 2004).

Climate change on the African continent during the past 5 million years is marked by two separate processes: 1) orbital precession forcing controlled the wet-dry cycles, acting as a "monsoonal pacemaker" and 2) a long-term drying trend toward more variable conditions superimposed on these wet and dry conditions, beginning ~3 Ma and reaching peak intensity near 1.8 to 1.6 Ma (deMenocal 2004, 2011). Localized cooling in the Mediterranean (~1.77 Ma; Raffi et al., 1993), as well as increased dust flux off the African coast (~2-1.7 Ma; Wagner, 2002) indicate increased aridity in North Africa, and suggests a major reorganization of the tropical Pacific Ocean-atmosphere system to a mean La Niña-like mean state (Feakins and deMenocal, 2010).

The Late Pliocene is marked by a pronounced transition from a warm and wet global climate to a colder and drier one. During the Late Pliocene, the East Antarctic ice sheet reestablished itself, in addition to the development of the Greenland and the West Antarctic ice sheets (Vrba et al., 1985; deMenocal and Bloemendal, 1995; Wynn, 2004). It is generally agreed that the West Antarctic ice sheet began to develop in the Early Pliocene, but it was during the Late Pliocene that the major ice shelves of the West Antarctic ice sheet developed (Ruddiman, 2001). The formation of the Greenland ice sheet was a significant development in global climate, as it was the first appearance of a Northern Hemisphere terrestrial ice sheet during the Cenozoic (deMenocal and Bloemendal, 1995).

During the Plio-Pleistocene transition, the prevailing East African paleoclimate cycles resulted in a cool and dry climate during glacial stages, and a warm and humid climate during

interglacials. The evidence for these paleoclimate shifts, and the resulting environmental changes in East Africa were obtained from the analyses of sea floor sediments and paleosol samples (deMenocal, 2004; Trauth et al., 2005, 2007; Lisiecki and Raymo, 2005). Sea floor sediment samples collected off the east coast of Africa in the Indian Ocean and off the west coast in the equatorial and sub-tropical North Atlantic contained increased levels of dust particles (Fig. 11), suggesting increased aridification across the Northern part of the African continent (deMenocal, 2004). Marine sediments also showed that Indian Ocean sea surface temperatures (SSTs), and not North Atlantic thermohaline circulation, was the prevailing mechanism influencing the climate regime in East Africa (deMenocal and Bloemendal, 1995; deMenocal, 2004; Wynn, 2004).

The Pleistocene is generally considered an epoch of prolonged cooling, but it is marked by some warmer-than-present interglacial stages (Imbrie et al., 1984; Vrba et al., 1995; Wynn, 2004; Trauth et al., 2005, 2007, 2009). Wynn (2004) argued that the West Antarctic ice sheet may have collapsed during one or more of the warm interglacial stages of the Pleistocene. The expansion of ice sheets on Antarctica and Greenland were characteristic of Pleistocene glacial stages, and created a cooler and drier global climate (Imbrie et al., 1984; deMenocal and Bloemendal, 1995; Shultz, 1998; Trauth et al., 2005, 2007; Lisiecki and Raymo, 2005; Maslin and Christensen, 2007; Filippelli and Flores, 2009; Cartmill and Smith, 2009).

The Early Pleistocene was characterized by ~41 kyr glacial, cold and dry, and interglacial, hot and humid cycles, due to orbital periodicities. The Mid-Pleistocene (~0.9 myr) is marked by a transition in global climate, when the orbital periodicity of the shifted to ~100 kyr glacial-interglacial cycles (Trauth et al., 2005, 2007; Lisiecki and Raymo, 2005; Campisano, 2012), amplifying the cooling trend of global climate (deMenocal and Bloemendal, 1995;

deMenocal, 2004; Wynn, 2004). Our mineralogical records from the Koora Graben and Lake Magadi do display the long-term drying trend that is commonly observed over the past ~1 Myr, but no climate cycles were observed in mineralogical records that correlate with orbital periodicities.

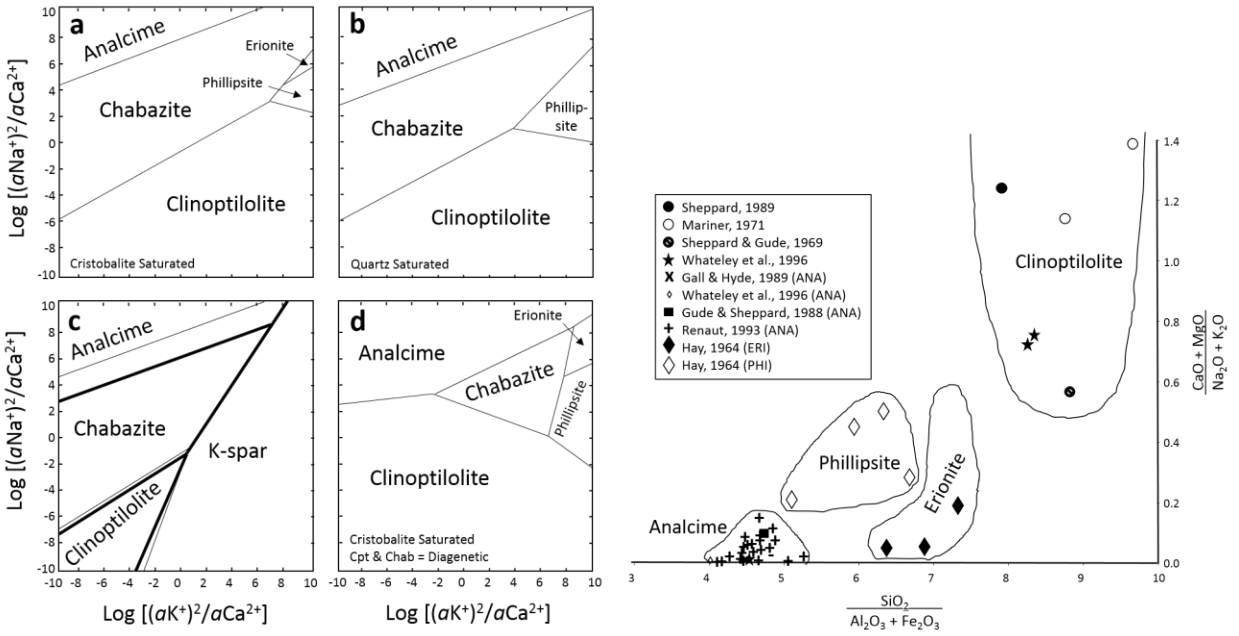

Figure 7.1: Zeolite phase diagram and X-Y plot for silica concentration versus cation concentration. (left) Log[(αK⁺)²/αCa²⁺] vs. log[(αNa⁺)²/αCa²⁺] diagrams for the zeolite species occurring in saline, alkaline lake. All calculated assuming 35° C and (a) An aqueous silica activity in equilibrium with cristobalite; (b) An aqueous silica activity in equilibrium with quartz; (c) Same as (a) & (b) with the addition of K-feldspar included in the calculation, thin lines = cristobalite & thick lines = quartz; and (d) Same as (a) except diagenetic compositions for chabazite and clinoptilolite were included in the calculations. (Adapted from Chipera and Apps, 2001). (right) $SiO_2/(Al_2O_3+Fe_2O_3)$ vs. $(CaO+MgO)/(Na_2O+K_2O)$ molar diagram compilation for select zeolite species in closed hydrologic systems. (From Langella et al., 2001).

Early studies of zeolites from East Africa suggested that zeolitic alteration occurred at the same rate (~20 kyr) as the weathering of clay minerals in the tropics (Hay, 1960, 1963). Zeolites of the central basin and eastern lake margin at Olduvai Gorge formed primarily through reaction of pore fluids with detrital clays and volcanic glass (Hay, 1970; Hay and Kyser, 2001). Analysis of the Loboi Silts of the Sandai Plain (Renaut, 1993) was in agreement with the interpretation by

Hay (1970, 1976) that zeolitic alteration occurred at and/or close to the land surface primarily by evaporation in shallow, marginal lake groundwaters. Surdam and Eugster (1976) determined that erionite could form directly from trachytic glass in water; and analcime could form from Na-Al-Si gels or precursor zeolites.

Zeolites are hydrated aluminosilicate minerals with a tectosilicate framework (e.g., Passaglia and Sheppard, 2001), in which the primary building blocks are tetrahedral with 1:2 cation to oxygen ratios (Armbruster and Gunter, 2001; Passaglia and Sheppard, 2001). These minerals can potentially form in most environments, but most commonly form from the alteration of volcanic glass in saline, alkaline waters (Hay, 1963, 1966, 1970; Sheppard and Gude, 1968, 1969; Surdam and Eugster, 1976; Surdam, 1977). Ca/K-zeolites, such as clinoptilolite or phillipsite would form in lesser saline waters, but would alter to the Na-zeolite analcime as the lake became more progressively saline (Fig. 7.1), and under certain conditions the alteration would progress to form K-feldspar in the most concentrated brines (Hay, 1966; Sheppard and Gude, 1968, 1969; Langella et al., 2001).

The zeolite assemblages we see in the HSPDP-MAG14 cores suggest analcime has likely been forming from Na-Al-Si gels since the earliest Oloronga Lake stages. There is a similar pattern of authigenic quartz in the cores, which support the hypothesis that similar processes are involved in the formation of the aluminosilicate gels (analcime precursor) and Na-silicates. The onset of intensive zeolitic alteration likely occurred due to large inputs of volcanic ash, which would have shallowed the lake and simulated aridity in the basin (Harris and Van Couvering, 1995). Variability in zeolite assemblages between HSPDP-MAG14-1A and Core 2A may reflect lake level fluctuations, with Ca/Mg-bearing zeolites forming when dilute waters interact with brines closer to the lake margin. Na-bearing zeolites continually formed in the deeper portions of

the lake, where surface brines could become concentrated through intensive evaporation and sink, interacting with freshwater and minerals at the sediment-water interface. Diverse zeolite assemblages in HSPDP-MAG14-2A during the latest Pleistocene and Holocene, which may suggest that percolating brines may be depleted in Na^+ when Na-carbonates are precipitating at the lake surface, promoting the formation of alkaline earth hosting zeolites in the lake beds.

The zeolite assemblages we observed in the ODP-OLO12-1A core indicates the lake waters became highly saline and alkaline after deposition of thick volcanic ash and pumice ~250 ka. However, the lack of erionite in the ODP-OLO12 core is interesting, as erionite is the second most abundant zeolite species in the HSPDP-MAG14 cores. Surdam and Eugster (1976) suggested that erionite formed from direct alteration of volcanic glass in H_2O. Phase diagrams on zeolite minerals indicate that erionite requires high Na^+ and K^+ activity and relatively high SiO_2 activity, whereas phillipsite forms with lower SiO_2 activity and with higher concentrations of alkaline earths (Fig. 7.1). Phillipsite formed in combination with analcime throughout the ODP-OLO12 record, which may indicate that analcime was incorporating all the Na^+ into its structure and the lake was depleted in SiO_2, which resulted in conditions that favored phillipsite precipitation over erionite.

We addressed our primary research questions as follows:

1) What is the primary influence on environmental conditions in southern Kenya over the past ~1 Myr: climate or tectonics?

   The primary control on environmental conditions seems to be long-term global cooling due to Northern Hemisphere Glaciations. However, tectonic and volcanic activity exerted considerable influence on environmental conditions over the past

~350 ka. Enhanced aridification occurred in southern Kenya beginning ~100 ka and the climate may have become much more variable at that time, as well.

2) Can mineralogical and geochemical data from HSPDP and ODP core material provide evidence of climate cyclicity in southern Kenya?

   Mineralogical data from both drill sites did not present evidence of cyclical environmental change associated with insolation, or Milankovitch cyclicity. Our geochemical records exhibit some cyclicity, but not on Milankovitch timescales.

3) What can we learn about source regions, weathering patterns, and mineral reactions across the Southern Kenya Rift and how can that inform us about what the core data is telling us?

   Mineralogical and geochemical data from the region indicated four distinct regions for source material, however the authigenic minerals in both cores suggest that parent material is less important than basin hydrochemistry. Geochemical correlations provide evidence of potential source regions for the Magadi and Koora Graben basins. We did not observe evidence of specific mineral reactions or weathering patterns indicative of climatic variability.

4) Does the mineralogical and geochemical data reveal trends and rhythms in environmental and climatic conditions that correlate with hominin evolutionary benchmarks, such as species appearance-disappearance, advances in stone tool technology, and changes in culture and behavior?

   Recent studies from southern Kenya have produced robust records of hominin behavior and changes in stone tool technology (Potts et al., 2018; Deino et al., 2018; Behrensmeyer et al., 2018; Brooks et al., 2018). These studies have placed a date of

first appearance of Middle Stone Age tools at ~248 ka. The earliest *Homo sapiens* emerged between ~300 and 200 ka. Our records indicate a significant change in environmental conditions occurred between ~350 and 250 ka, which correlates temporally with these two significant benchmarks in the human lineage. These data seem to support the link between environmental variability and hominin evolution, although it is difficult to assert causality.

The most commonly supported theories on human evolution are the savanna hypothesis, the turnover-pulse hypothesis, and the variability selection hypothesis. The significant change in environmental conditions that occurred in southern Kenya between ~350 and 250 ka and the subsequent environmental variability do coincide with the emergence of *Homo sapiens* and the appearance of Middle Stone Age tools, as well as changes in hominin behavior. Our data support the variability selection hypothesis, due to these temporal relationships between our paleoenvironemntal records and recent evidence on hominin evolution and stone tool technology from southern Kenya.

These studies have raised the question of whether there was a paleohydrologic connection between paleolakes in the Magadi and Koora Graben basins. If so, the timing and duration of these connections should be a subject of future studies in southern Kenya. Questions regarding multiple lake highstands over the past ~250 kyr in the Natron-Magadi basin, and whether there was a mega-paleolake connecting the Magadi-Natron-Manyara basins, will be a focal point of future drilling projects in northern Tanzania.

8 FUTURE WORK

Future work includes continuing fieldwork in southern Kenya working on the possible paleohydrologic connection between the Koora Graben paleolake and the Magadi basin. In

addition, continued work on the outcrops and stromatolites in the Magadi-Natron basin to reconstruct paleolake levels would aid in our understanding of paleoenvironmental conditions and how lake levels and salinity would have impacted hominin behavior during the Mid to Late Pleistocene. This is work to be completed in concert with initial fieldwork in northern Tanzania around the Natron, Manyara, and Eyasi basins. We have also proposed the scientific drilling of the Natron, Manyara, and Eyasi basins in northern Tanzania to obtain long-term paleoenvironmental records spanning at least the past ~1.7 Myr. Lakes Natron, Manyara, and Eyasi are located in the eastern arm of the greater East African Rift System. These lakes span a region stretching southward and westward, respectively, from the southern border of Kenya near Lake Magadi.

Stromatolites and lacustrine sediments from northern Tanzania and southern Kenya indicate the presence of a Natron-Magadi mega-paleolake during the late Pleistocene and Holocene. To combine these adjacent basins, lake levels must have been 20 to 60 m higher than those of the modern lakes (Hillaire-Marcel and Casanova, 1987). Stromatolite records from southern Kenya and northern Tanzania have been dated by a combination of Th/U and ^{14}C techniques (Hillaire-Marcel et al., 1986; Hillaire-Marcel and Casanova, 1987; Casanova and Hillaire-Marcel, 1992). Three generations of stromatolites were observed in the Magadi-Natron Basin dated at ≥240 ka, 135 ka ± 10 ka, and ~12-10 ka. The use of $\delta^{18}O$ and $\delta^{13}C$ isotopic analysis to stromatolites, when compared to the values for water and carbonates, may provide paleohydrological information (Hillaire-Marcel et al., 1986; Hillaire-Marcel and Casanova, 1987). Five lake highstands were also recorded at Lake Naivasha over the last ~175 kyr (Trauth et al., 2001, 2002). The highest lake level recorded at Naivasha was dated to ~139-133 kyr (Trauth et al., 2002), which correlates well with one of the Magadi-Natron highstands recorded

by the stromatolites. Two generations of stromatolites were documented at Lake Manyara. These two generations of stromatolites have been dated to ~90 ka and between ~27-23 ka (Casanova and Hillaire-Marcel, 1992). The timing of the highstands at Lake Manyara do not correlate temporally with those from the Magadi-Natron basin.

The timing of these stromatolite-inferred highstands of a megalake in the Natron basin coincides with the last three deglaciations, but the nature of these highstand occurrences is still poorly understood. Similarly, the Manyara basin is thought to have been occupied during the Pleistocene by a mega-paleolake (e.g., Bachofer et al., 2014), although there is disagreement regarding whether the Manyara and Natron basin could have coalesced under one lake. Adding complexity to the interpretation, the timing of stromatolite-inferred mega-lake highstands in the Manyara lake basin do not appear to correlate with highstands from the Natron lake basin. The sensitivity of these basins to different pacing is intriguing considering their geographic proximity and similar climatic settings.

The drilling project would provide the first continuous high resolution paleoenvironmental records encompassing the past ~1.7 Ma from this region, when sedimentation in the Manyara basin is thought to begin (e.g., Ring et al., 2005; Frost et al., 2012)). Lacustrine deposits of similar age (~1.7 to 1.5 Ma) are present at the Peninj Site at West Natron (e.g., Dominguez-Rodriguez et al., 2002), and while the onset of sedimentation at Lake Eyasi has not been sufficiently studied to date, it likely slightly precedes or began around the same time as Natron and Manyara. The modern rift configuration of northern Tanzania was established by ~1.2 Ma (Ebinger et al., 1997), although this does not rule out tectonic influences on basin morphology after that date. Fluviolacustrine strata known as the Manyara Beds are located in the west of the Lake Manyara basin and are ~100m above modern lake levels. The

Manyara Beds are subdivided into a lower lacustrine member and an upper fluvial member. The lower lacustrine member includes dolomites, mudstones, marls, and diatomites, with a total thickness of ~15 m. The upper fluvial member is comprised of mostly breccias, sandstones, and siltstones that total ~13 m in thickness (Ring et al., 2005). The lacustrine sedimentary sequence at Lake Natron is estimated to exceed ~500 m in total thickness (Ebinger et al., 1997). While outcrop studies from each of these basins has produced rich archeological and paleontological records, their findings are limited to discreet site localities and only produced discontinuous stratigraphic information. The multi-proxy records obtained from scientific drilling would allow us to infer basin-wide paleoenvironmental and regional paleoclimatic trends via geochemical records, sedimentological records, and diatom assemblages.

The anticipated results of this drilling campaign will further our understanding of paleoenvironmental and paleoclimatic changes in northern Tanzania during the Quaternary, how these changes impacted hominin behavior and culture during the Plio-Pleistocene, and potentially how future environmental change may impact hominin evolution under variable climatic and environmental regimes. This combined with field studies and research carried out by others in the region will provide a much more detailed record of environmental change over the past ~1.7 Myr in northern Tanzania and southern Kenya.

9 CONCLUSIONS

Cores from the Koora Graben and Lake Magadi suggest a long-term aridification spanning the past ~0.8 Myr in the Southern Kenya Rift, with intensified drying beginning at ~350 ka and increasing climate variability over the past ~200 ka. Lake Magadi originated as a shallow freshwater lake that quickly became a deep mildly saline lake until ~350 ka. Nearly all volcaniclastic deposits in the Magadi cores altered to zeolites, but we assume the ash deposits

were similar in thickness to those in the Olorgesailie cores. Trona deposits began to accumulate by ~200 ka, suggesting intense aridification with pulses of humid periods over the past two hundred thousand years resulting in the modern ephemeral lake/salt pan.

The paleolake that occupied the Koora Graben began as a deep freshwater lake that became mildly saline by ~800 ka. The region experienced volcanic eruptions that blanketed the basin in thick volcanic ash and pumice deposits. The ash deposit created a desiccation event in the paleolake, which preceded highly variable environmental conditions until the terminal lake phase at ~10 ka.

Analysis of the mineralogy and geochemistry of surface and outcrop samples from the Southern Kenya Rift indicate that there are four distinct regions: the highlands to the northeast in the Kiserian region; the central area near Ol Doinyo Nyokie; the greater Lake Magadi basin in the southern area; and the Nguruman Escarpment area to the west. The mineralogy and geochemistry of the ODP-OLO12 core suggests a north-northeastern source region for deposits in the Koora Graben, whereas the Lake Magadi mineralogy suggests both western and central sources for parent material. The mineralogy of Lake Magadi sediments implies that most of the minerals formed in the basin through diagenetic processes.

Zeolites can form in variety of environments, including soils, weathered tuffaceous outcrops, and lacustrine sediments. Erionite and chabazite are most commonly associated with trachytic parent material, suggesting an origin in dilute water from low-temperature surface weathering of volcaniclastic material. Analcime was not found in any surface or outcrop sample, which indicates that it likely forms in concentrated brines in lacustrine settings or around alkaline springs; a Na-Al-Si gel precursor or intermediary phase is highly likely.

REFERENCES

Anonymous, 1923. The Soda Deposits of Lake Magadi in Kenya. *Bulletin Imp. Institution*. v. 21. p. 431-444.

Armbuster, T., Gunter, M.E. 2002. "Crystal Structures of Natural Zeolites." *In* D.L. Bish & D.W. Ming (eds.), *Reviews in Mineralogy & Geochemistry. Volume 45: Natural Zeolites: Occurrence, Properties, Applications*. Washington D.C. Mineralogical Society of America. p. 1-67.

Bachofer, F., Quénéhervé, G., Märker, M. 2013. The Delineation of paleo-Shorelines in the Lake Manyara Basin Using TerraSAR-X Data. *Remote Sensing*. v. 6. n. 3. p. 2195-2212.

Baker, B.H. 1958. Geology of the Magadi Area: Degree Sheet 51, SW Quarter. *Geological Survey of Kenya*. Report n. 42.

Baker, B.H. 1963. Geology of the Area South of Magadi. Degree Sheet 58. N.W. Quarter. Ministry of Commerce and Industry, Geological Survey of Kenya. 33 pp.

Baker, B.H. 1987. Outline of the petrology of the Kenya rift alkaline province. *in* Fitton, J.G. & Upton, B.G.J. (*eds*.), Alkaline Igneous Rocks, *Geological Society Special Publications*. n. 30. p. 293-311.

Behr, H.-J. 2002, Magadiite and Magadi Chert: A Critical Analysis of the Silica Sediments in the Lake Magadi Basin, Kenya. *in* Renaut, R.W. and Ashley, G.A. (eds.) Sedimentation in Continental Rifts. *SEPM Special Publication*, n. 73, p. 257-273.

Behr, H.-J., Röhricht, C. 2000. "Record of seismotectonic events in siliceous cyanobacterial sediments (Magadi cherts), Lake Magadi, Kenya." *International Journal of Earth Science*. v. 89. p. 268-283.

Behrensmeyer, A.K. 2006. Climate change and human evolution. *Science*. v. 311. p. 476-478.

Behrensmeyer, A.K., Potts, R., Deino, A., Ditchfield, P. 2002. Olorgesailie, Kenya: A Million Years in the Life of a Rift Basin. *in* Renaut, R.W. & Ashley, G.M. (*eds.*), Sedimentation in Continental Rifts, *SEPM Special Publications*. n. 73. p. 97-106.

Behrensmeyer, A.K., Potts, R. Deino, A. 2007. Cycles of erosion and deposition in the Pleistocene Olorgesailie Basin of southern Kenya and their impact on the paleoanthropological record. *GSA Annual Meeting: Abstracts with Programs*. v. 125-2. p. 343.

Behrensmeyer, A.K., Potts, R., Deino, A. 2018. The Oltulelei Formation of the southern Kenya Rift Valley: A chronical of rapid landscape transformation over the last 500 k.y. *GSA Bulletin*. DOI: https://doi.org/10.1130/B31853.1

Berger, W.H., Jansen, E. 1994. Mid-Pleistocene Climate Shift – The Nansen Connection. *In* O.M. Johannessen, R.D. Muench & J.E. Overland (eds.), *The Polar Oceans and Their Role in Shaping the Global Environment*. Washington D.C. American Geophysical Union. p. 295-311.

Billups, K., Rabideaux, N., Stoffel, J. 2011. Suborbital-scale surface and deep water records in the subtropical North Atlantic: implications on thermohaline overturn. *Quaternary Science Reviews*. v. 30. n. 21-22. p. 2976-2987.

Bradley, W.H., Eugster, H.P. 1969. Geochemistry and paleolimnology of the trona deposits and associated authigenic minerals of the Green River Formation of Wyoming. U.S. Geological Survey Professional Paper 496-B. 71 pp.

Bobe, R., Behrensmeyer, A.K., Chapman, R.E. "Faunal change, environmental variability and late Pliocene hominin evolution." *Journal of Human Evolution*. 2002. v. 42, p. 475-497.

Brindley, G.W., Brown, G. (Eds.). *Crystal Structures of Clay Minerals and their X-ray Identification*. Mineralogical Society, London. 1980. 495 pp.

Brooks, A.S., Yellen, J.E., Potts, R., Behrensmeyer, A.K., Deino, A.L., Leslie, D.E., Ambrose, S.H., Ferguson, J.R., d'Errico, F., Zipkin, A.M., Whittaker, S., Post, J., Veatch, E.G., Foecke, K., Clark, J.B. 2018. Long-distance stone transport and pgment use in the earliest Middle Stone Age. *Science*. v. 360. p. 90-94.

Campisano, C. J. 2012. "Milankovitch Cycles, Paleoclimatic Change, and Hominin Evolution." *Nature Education Knowledge.* v. 4. n. 3. p. 5.

Campisano, C., Cohen A.S., Arrowsmith, J.R., Asrat, A., Behrensmeyer, A.K., Borwn, E.T., Deino, A.L., Deocampo, D.M., Feibel, C.S., Kingston, J.D., Lamb, H.F., Lowenstein, T.K., Noren, A., Olago, D.O., Owen, R.B., Pelletier, J.D., Potts, R., Reed, K.E., Renaut, R.W., Russell, J.M., Russell, J.L., Schäbitz, F., Trauth, M.H., Wynn, J.G. 2017. The Hominin Sites and Paleolakes Drilling Project: High-Resolution Paleoclimate Records from the East African Rift System and Their Implications for Understanding the Environmental Context of Hominin Evolution. *Paleoanthropology 2017*. p. 1-43.

Cartmill, M., Smith, M.H. *The Human Lineage*. Wiley-Blackwell Publishing (NJ). ISBN: 978-0-471-21491-5.

Casanova, J., Hillaire-Marcel, C. 1992. "Chronology and Paleohydrology of Late Quaternary High Lake Levels in the Manyara Basin (Tanzania) from Isotopic Data (^{18}O, ^{13}C, ^{14}C, Th/U) on Fossil Stromatolites." *Quaternary Research*. v. 38. p. 205-226.

Chipera, S.J., Apps, J.A. 2002. "Geochemical Stability of Natural Zeolites" *In* D.L. Bish & D.W. Ming (eds.), *Reviews in Mineralogy & Geochemistry. Volume 45: Natural Zeolites:*

Occurrence, Properties, Applications. Washington D.C. Mineralogical Society of America. p. 117-161.

Cohen, A., Arrowsmith, R., Behrensmeyer, A.K., Campisano, C., Feibel, C., Fisseha, S., Johnson, R., Bedaso, Z.K., Lockwood, C., Mbua, E., Olago, D., Potts, R., Reed, K., Renaut, R., Tiercelin, J.-J., Umer, M. 2009, Understanding Paleoclimate and Human Evolution Through the Hominin Sites and Paleolakes Drilling Project. *Scientific Drilling*, n. 8, p. 60-65.

Cohen, A., Campisano, C., Arrowsmith, R., Asrat, A., Behrensmeyer, A. K., Deino, A., Feibel, C., Hill, A., Johnson, R., Kingston, J., Lamb, H., Lowenstein, T., Noren, A., Olago, D., Owen, R. B., Potts, R., Reed, K., Renaut, R., Schäbitz, F., Tiercelin, J.-J., Trauth, M. H., Wynn, J., Ivory, S., Brady, K., O'Grady, R., Rodysill, J., Githiri, J., Russell, J., Foerster, V., Dommain, R., Rucina, S., Deocampo, D., Russell, J., Billingsley, A., Beck, C., Dorenbeck, G., Dullo, L., Feary, D., Garello, D., Gromig, R., Johnson, T., Junginger, A., Karanja, M., Kimburi, E., Mbuthia, A., McCartney, T., McNulty, E., Muiruri, V., Nambiro, E., Negash, E. W., Njagi, D., Wilson, J. N., Rabideaux, N., Raub, T., Sier, M. J., Smith, P., Urban, J., Warren, M., Yadeta, M., Yost, C., and Zinaye, B. 2016, The Hominin Sites and Paleolakes Drilling Project: inferring the environmental context of human evolution from eastern African rift lake deposits. *Scientific Drilling*, n. 21, p. 1-16, doi:10.5194/sd-21-1-2016.

Crossley, R. 1979. The Cenozoic stratigraphy and structure of the western part of the Rift Valley in southern Kenya. *Journal of Geological Society*. v. 136. p. 393-405.

Dawson, J.B. 1962. Sodium carbonate lavas from Oldoinyo Lengai, Tanganyika. *Nature*. V. 195. n. 4846. p. 1075.

Dawson, J.B. 2008. Carbonatitic volcanic ashes in Northern Tanganyika. *Bulletin Volcanologique*. v. 27. p. 81-91.

deMenocal, P. 1995. Plio-Pleistocene African Climate. *Science*. v. 270. p. 53-59.

deMenocal, P. 2004. African climate change and faunal evolution during the Pliocene-Pleistocene. *Earth and Planetary Science Letters*. v. 220. i. 1-2. p. 3-24.

deMenocal, P.B., Bloemendal, J. 1995. Plio-Pleistocene climatic variability in subtropical Africa and the paleoenvironment of hominid evolution: A combined data-model approach. *In* E.S. Vrba, G.H. Denton, T.C. Partridge & L.H. Burckle (eds.), *Paleoclimate and Evolution, with Emphasis on Human Origins*. New Haven. Yale University Press. p. 262-288.

deMenocal, P., Ruddiman, W.F. 1993. Influences of high- and low-latitude processes on African terrestrial climate Pleistocene eolian records from equatorial Atlantic Ocean Drilling Program site 663. *Paleoceanography*. v. 8. n. 2. p. 209-242.

Deino, A., Potts, R. 1990. Single-crystal $^{40}Ar/^{39}Ar$ dating of the Olorgesailie Formation, southern Kenya Rift. *Journal of Geophysical Research*. v. 95. p. 8453-8470.

Deino, A., Potts, R. 1992. Age-probability spectra for examination of single-crystal $^{40}Ar/^{39}Ar$ dating results: Examples from Olorgesailie, southern Kenya Rift. *Quaternary International*. v. 13-14. p. 47-53.

Deino, A., Potts, R., Dommain, R., Behrensmeyer, A.K., ODP Research Group. 2016. The Olorgesailie Drilling Project (ODP): Understanding the Last 1 Ma of Palaeoclimate and Human Evolution in East Africa. *Quaternary International*. v. 404. p. 199.

Deino, A., King, J., Heil, C., Potts, R., Behrensmeyer, A.K., Dommain, R. Poster presentation: "Chronology of the Olorgesailie Drilling Project Core 1a, Koora Graben, southern Kenya Rift." *Geo. Soc. Amer. Ann. Mtg*., 2016, Denver.

Deino, A., Behrensmeyer, A.K., Brooks, A.S., Yellen, J.E., Sharp, W.D., Potts, R. 2018. Chronology of the Acheulean to Middle Stone Age transition in eastern Africa. *Science*. v. 360. p. 95-98.

Deocampo, D.M., Jones, B.F. 2014. Geochemistry of Saline Lakes. *in* Drever, J.J. (ed.), *Surface and Groundwater, Weathering and Soils: Treatise of Geochemistry*. Amsterdam. Elsevier. v. 7. p. 437-469.

Deocampo, D.M., Behrensmeyer, A.K., Potts, R. 2010. Ultrafine clay minerals of the Pleistocene Olorgesailie Formation, Southern Kenya Rift: Diagenesis and paleoenvironments of early hominins. *Clays and Clay Minerals*. v. 58. n. 3. p. 294-310.

Di Piazza, J.J., Regis, A.J., Sand, L.B., 1959. Formation of zeolites by the alteration of glass by alkaline solution. *GSA Bulletin*. v. 70. p. 1589-1590.

Dominguez-Rodriguez, M., Díez-Martin, F., Mabulla, A., Luque, L., Alcalá, L., Tarriño, A., López-Sáez, J.A., Barba, R., Bushozi, P. The Archaeology of the Middle Pleistocene Deposits of Lake Eyasi, Tanzania. *Journal of African Anthropology*. v. 5. n. 1. p. 47-78.

Ebinger, C., Djomani, Y.P., Mbede, E., Foster, A., Dawson, J.B. 1997. Rifting Archaean lithosphere: the Eyasi-Manyara-Natron rifts, East Africa. *Journal of Goelogical Society*. v. 154. n. 6. p. 947-960.

Eugster, H.P. 1967, Hydrous Sodium Silicates from Lake Magadi, Kenya: Precursors of Bedded Chert. *Science*, v. 157, p. 1177-180.

Eugster, H.P. 1969. Inorganic Bedded Chert from the Magadi area, Kenya. *Contr. Mineral. and Petrol*. v. 22. p. 1-31.

Eugster, H.P. 1970, Chemistry and Origin of the Brines of Lake Magadi, Kenya. *Mineralogical Society of America Special Papers*, v. 3, p. 213-235.

Eugster, H.P. 1980. Lake Magadi, Kenya, and its Precursors. Ch. 15. *in* A. Nissenbaum (ed.), *Hypersaline Brines and Evaporitic Environments*. Amsterdam. Developments in Sedimentology. n. 28. p. 195-232.

Eugster, H.P., Hardie, L.A. 1975. Sedimentation in an Ancient Playa-lake Complex: The Wilkins Peak Member of the Green River Formation of Wyoming. *GSA Bulletin*. v. 86. p. 319-334.

Eugster, H.P., Jones, B.F. 1968, Gels Composed of Sodium-Aluminum Silicate, Lake Magadi, Kenya. *Science*, v. 161, p. 160-163.

Feakins, S.J., deMenocal, P.B. 2008. Global and African Regional Climate during the Cenozoic. *In* L. Werdelin & B. Sanders (eds.), *Cenozoic Mammals of Africa*. Oakland. UC Press. p. 45-55.

Filippelli, G.M., Flores, J-A. 2009. "From the warm Pliocene to the cold Pleistocene: A tale of two oceans." *Geology*. v. 37. p. 959-960.

Fischer, G.A. 1884. Bericht über die im Auftrage der Geographischen Gesellschaft in Hamburg unternommene Reise in das Masai-Land. *Mitt. Geogr. Ges.* Hamburg, 1882-1883, Pt. I Allgemeiner Bericht, p. 36-99.

Frost, S.R., Schwartz, H.L., Giemsch, L., Morgan, L.E., Renne, P.R., Wildgoose, M., Saanane, C., Schrenk, F., Harvati, K. 2012. Refined age estimates and Paleoanthropological

investigation of the Manyara Beds, Tanzania. *Journal of Anthropological Sciences*. v. 90. p. 1-12.

Gregory, J.W. 1921. The Rift Valleys and Geology of East Africa. *Seeley Service*, London.

Guth, A.L. 2007. Evolution of S. Kenya Rift from Miocene to Present with a Focus on the Magadi Area. College of Engineering at Michigan Technological University, *Master's Thesis*, Houghton, MI USA.

Harris, J., Van Couvering, J. 1995, Mock aridity and the paleoecology of volcanicity influenced ecosystems. *Geology*, v. 23, n. 7, p. 593-596.

Hay, R.L. 1963. Zeolitic Weathering in Olduvai Gorge, Tanganyika. *Geological Society of America bulletin*. v. 74. p. 1281-1286.

Hay, R.L. 1966. Zeolites and zeolitic reactions in sedimentary rocks. *GSA Special Papers*. v. 85. p. 130.

Hay, R.L. 1976. *Geology of the Olduvai Gorge*. University of California Press, Berkeley.

Hay, R.L. 1983. Natrocarbonatite tephra of Kerimasi volcano, Tanzania. *Geology*. v. 11. p. 599-602.

Hay, R.L. 1986. Geologic occurrence of zeolites and some associated minerals. *Pure & Applied Chemistry*. v. 58. i. 10. p. 1339-1342.

Hay, R.L. Kyser, T.K., 1996. Hominid-bearing deposits of Bed I and Bed II, Olduvai Gorge: A clay mineral and isotopic contribution. *Geological Society of America Abstracts with Programs*. v. 28. n. 6. p. 44.

Hay, R.L., Kyser, T.K. 2001. Chemical sedimentology and paleoenvironmental history of Lake Olduvai, a Pliocene Lake in northern Tanzania. *Geological Society of America Bulletin*. v. 113. n. 12. p. 1505-1521.

Hay, R.L., Sheppard, R.A. 2002. Occurrence of Zeolites in Sedimentary Rocks. *In* D.L. Bish & D.W. Ming (eds.), *Reviews in Mineralogy & Geochemistry. Volume 45: Natural Zeolites: Occurrence, Properties, Applications*. Washington D.C. Mineralogical Society of America. p. 217-234.

Herrick, R., 1972. Authigenic minerals in the Pleistocene and recent sediments of Lake Magadi, Kenya. MSc thesis, University of Wyoming.

Hillaire-Marcel, C., Casanova, J. 1986. ^{14}C and Th/U Dating of Pleistocene and Holocene Stromatolites from East African Paleolakes. *Quaternary Research*. v. 25. p. 312-329.

Hillaire-Marcel, C., Casanova, J. 1987. Isotopic Hydrology and Paleohydrology of the Magadi (Kenya)-Natron (Tanzania) Basin During the Late Quaternary. *Palaeogeography, Palaeoclimatology, Palaeoecology*. v. 58. p. 155-181.

Imbrie, J., Hays, J.D., Martinson, D.G., McIntyre, A., Mix, A.C., Morley, J.J., Pisas, N.G., Prell, W.L., Shackleton, N.J. 1984. "The Orbital Theory of Pleistocene Climate: Support from a Revised Chronology of the Marine $\delta^{18}O$ Record." A.L. Berger et al. (eds.) *Milankovitch and Climate, Part I*. Dordrecht. D. Reidel Publishing. p. 269-305.

Isaac, G.L., Isaac, B. 1977. Olorgesailie: Archeological Studies of a Middle Pleistocene Lake Basin in Kenya. University of Chicago Press, Chicago.

Isaac, G.L. 1978. The Olorgesailie Formation: stratigraphy, tectonics, and the paleogeographic context of the Middle Pleistocene archaeological sites. *In* Bishop, W.W. (*ed.*), Geological Background to Fossil Man. *Scottish Academic Press*, Edinburgh. p. 173-206.

Joannin, S., Quillévéré, F., Suc, J.-P., Lécuyer, C., Martineau, F. 2007. Early Pleistocene climate changes in the central Mediterranean region as inferred from integrated pollen and planktonic foraminiferal stable isotope analyses. *Quaternary Research*. v. 67. p. 264-274.

Johanson, D.C., White, T.D. 1979. A systematic assessment of early African hominids. *Science*. v. 203. p. 321-330.

Jones, B.F., Rettig, S.L., Eugster, H. 1967. Silica in Alkaline Brines. *Science*. v. 158. p. 1310-1314.

Jones, B.F., Eugster, H.P., Rettig, S.L. 1977. "Hydrochemistry of the Lake Magadi basin, Kenya." *Geochemica et Cosmochemica Acta*. v. 41. p. 53-72.

Kaiser, A. 1898. Die Schöllersche Expedition in Aequatorial-Ost-afrika. *Bericht. St. Gall. Naturwiss Ges.*, 1896-1897. p. 314-342.

Kaufman, A., Margaritz, M., Paul, M., Hillaire-Marcel, C., Hollos, G., Boaretto, E., Taieb, M. 1990, The ^{36}Cl ages of brines in the Magadi-Natron basin, East Africa. *Geochimica et Cosmochimica Acta*, v. 54, p. 2827-2833.

Konecky, B.L., Russell, J.M., Johnson, T.C., Brown, E.T., Berke, M.A., Werne, J.P., Yongsong, H. 2011. Atmospheric circulation patterns during late Pleistocene climate changes at Lake Malawi, Africa. *Earth and Planetary Letters*. v. 312. p. 318-326.

Künzli, E. 1901. Die petrographische Ausbeute der Schöller'-schen Expedition in Aequatorial-Ostafrica (Massailand). *Viertel jahr. Naturf. Ges. Zurich*, XLVI. p. 128-172.

Langella, A., Cappelletti, P., de' Gennaro, M. 2002. Zeolites in Closed Hydrologic Systems. *In* D.L. Bish & D.W. Ming (eds.), *Reviews in Mineralogy & Geochemistry. Volume 45: Natural Zeolites: Occurrence, Properties, Applications*. Washington D.C. Mineralogical Society of America. p. 233-260.

Laporte, L.F. 1990, Establishment of a Geologic Framework for Paleoanthropology. *Geological Society of America Special Papers*, n. 242, 74 pp.

Leakey, L.S.B. 1952, The Olorgesailie Prehistoric Site. in Leakey, L.S.B. and Cole, S. (eds.) Proceedings of the First Pan-African Congress on Prehistory, 1947, p. 209.

Leet, K., Lowenstein, T.K., Owen, R.B., Renaut, R.W., Deocampo, D.M., Cohen, A.S., McNulty, E.P., Muiruri, V.M., Rabideaux, N.M., Billingsley, A.L., Mbuthia, A. Oral presentation: "Origins of Magadi-type Chert: New Clues from the HSPDP Lake Magadi Drill Cores." *Geo. Soc. Amer. Ann. Mtg*., 2016, Denver.

Lisiecki, L.E., Raymo, M.E. 2007. Plio-Pleistocene climate evolution: trends and transitions in glacial cycle dynamics. *Quaternary Science Reviews*. v. 26. p. 56-69.

Mangini, A., Schlosser, P. 1986. "The Formation of Eastern Mediterranean Sapropels." *Marine Geology*. V. 72. P. 115-124.

Maslin, M.A., Christensen, B. "Tectonics, orbital forcing, global climate change, and human evolution in Africa: introduction to the African paleoclimate special volume." *Journal of Human Evolution*. 2007. v. 53. p. 443-464.

Maslin, M.A., Trauth, M.H. 2009. Plio-Pleistocene East African Pulsed Climate Variability and Its Influence on Early Human Evolution. *In* Grine F.E et al. (eds.), *The First Humans: Origin and Early Evolution of the Genus Homo*. Berlin. Springer Science and Business Media p. 151-158.

McGregor, G.R., Nieuwolt, S. 1998. *Tropical Climatology, Second Edition*. New York. John Wiley & Sons. 339 pp.

Moore, D.M., Reynolds, R.C. *X-ray Diffraction and the Identification and Analysis of Clay Minerals*. 2nd Edition. Oxford University Press. New York. 1997. 378 pp.

Mügge, O. 1885. Untersuchung der von Dr. G. A. Fischer gesammelten Gesteine. *Mitt. Geogr. Ges. Hamburg*. 1882-1883. p. 238-264.

Nicholson, S.E. 1996. A review of climate dynamics and climate variability in eastern Africa. *In* T.C. Johnson & E. Olada (eds.), *The limnology, climatology, and paleoclimatology of East African lakes*. Amsterdam. Gordon and Breach. p. 25-56.

Owen, R.B. 1981.Quaternary diatomaceous sediments and the geological evolution of Lakes Turkana, Baringo and Bogoria, Kenya Rift Valley. Ph.D. Thesis, University of London. 465 pp.

Owen, R.B., Renaut, R.W. 1981. Paleoenvironments and sedimentology of the Middle Pleistocene Olorgesailie Formation, southern Kenya Rift Valley. *Paleoecology of Africa*. v. 13. p. 147-174.

Owen, R.B. 2002. Sedimentological Characteristics and Origins of Diatomaceous Deposits in the East African Rift System. *In* R.W. Renaut & G.M. Ashley (eds.) *Sedimentation in Continental Rifts*. Tulsa. SEPM Special Publications. n. 73. p. 233-246.

Owen, R.B., Potts, R., Behrensmeyer, A.K., Ditchfield, P. 2008. Diatomaceous sediments and environmental change in the Pleistocene Olorgesailie Formation, southern Kenya Rift Valley. *Palaeogeography, Palaeoclimatology, Palaeoecology*. v. 269. p. 17-37.

Owen, R.B., Renaut, R.W., Scott, J.J., Potts, R., Behrensmeyer, A.K. 2009. Wetland sedimentation and associated diatoms in the Pleistocene Olorgesailie Basin, southern Kenya Rift Valley. *Sedimentary Geology*. v. 222. i. 1-2. p. 124-137.

Owen R.B., Renaut, R.W., Potts, R., Behrensmeyer, A.K. 2011. Geochemical trends through time and lateral variability of diatom floras in the Pleistocene Olorgesailie Formation, southern Kenya Rift Valley. *Quaternary Research*. v. 76. i. 1. p. 167-179.

Parkinson, J. 1914. The East African trough in the neighbourhood of the Soda lakes. *Geog. Journ*. Vol. XLIV. p. 33-49.

Passaglia, E., Sheppard, R.A. “The Crystal Chemistry of Zeolites.” *In* D.L. Bish & D.W. Ming (eds.), *Reviews in Mineralogy & Geochemistry*. *Volume 45: Natural Zeolites: Occurrence, Properties, Applications*. Washington D.C. Mineralogical Society of America. p. 69-116.

Potts, R. 1989. Olorgesailie: New Excavations and Findings in Early and Middle Pleistocene contexts, Southern Kenya Rift Valley. Journal of Human Evolution, v. 18, p. 477-484.

Potts, R. 1996. Evolution and climate variability. *Science*. v. 273. p. 922-923.

Potts, R. 1998. Variability selection hypothesis in hominid evolution. *Evolutionary Anthropology*. v. 7. p. 81-96.

Potts, R. “Hominin evolution in settings of strong environmental variability.” *Quaternary Science Reviews*. 2013. v. 73. p. 1-13.

Potts, R., Behrensmeyer, A.K., Ditchfield, P. 1999. Paleolandscape variation and Early Pleistocene hominid activities: Members 1 and 7, Olorgesailie Formation, Kenya. *Journal of Human Evolution*. v. 37. p. 747-788.

Potts, R., Behrensmeyer, A.K., Deino, A., Ditchfield, P., Clark, J. 2004. Small Mid-Pleistocene Hominin Associated with East African Acheulean Technology. *Science*. v. 305. p. 75-78.

Potts, R., Faith, J.T. 2015. Alternating high and low climate variability: The context of natural selection and speciation in Plio-Pleistocene hominin evolution. *Journal of Human Evolution*. v. 87. p. 5-20.

Potts, R., Behrensmeyer, A.K., Faith, j.T., Tryon, C.A., Brooks, A.S., Yellen, J.E., Deino, A.L., Kinyanjui, R., Clark, J.B., Haradon, C.M., Levin, N.E., Meijer, H.J.M., Veatch, E.G., Owen, R.B., Renaut, R.W. 2018. Enviornmental dynamics during the onset of the Middle Stone Age in eastern Africa. *Science*. v. 360. p. 86-90.

Raffi, I., Backman, J., Rio, D., Shackleton, N.J. 1993. "Plio-Pleistocene Nannofossil Biostratigraphy and Calibration to Oxygen Isotope Stratigraphies from DeepSea Drilling Project Site 607 and Ocean Drilling Program Site 677." *Paleoceanography*. V. 8. I. 3. P. 387-408.

Renaut, R.W. 1993. Eolitic diagenesis of the late Quaternary fluviolacustrine sediments and associated calcrete formation in the Lake Bogoria Basin, Kenya Rift Valley." *Seidmentology*. V. 40. P. 271-301.

Ring, U., Schwartz, H.L., Bromage, T.G., Sanaane, C. 2005. Kinematic and sedimentological evolution of the Manyara Rift in northern Tanzania, East Africa. *Geol. Mag.* v. 142. n. 4. p. 355-368.

Rossignol-Strick, M. 1984. "Mediterranean Quaternary Sapropels, an Immediate Response of the African Monsoon to Variation of iInsolation." *Palaeogeography, Palaeoclimatology, Palaeoecology*. v. 49. p. 237-263.

Russell, J.M., Johnson, T.C. 2007. Little Ice Age drought in equatorial Africa: Intertropical Convergence migrations and El Niño-Southern Oscillation variability. *Geology*. v. 35. n. 1. p. 21-24.

Scholz, C. 2007. East African megadroughts between 135 and 75 thousand years ago and bearing on early-modern human origins. *PNAS*. v. 104. n. 42. p. 16416-16421.

Scholz, C.A., Cohen, A.S., Johnson, T.C., King, J., Talbot, M.R., Brown, E.T. 2011. Scientific drilling in the Great Rift Valley: The 2005 Lake Malawi Scientific Drilling Project – An overview of the past 145,000 years of climate variability in Southern Hemisphere East Africa. *Palaeogeography, Palaeoclimatology, Palaeoecology*. v. 303. p. 3-19.

Schulz, H., von Rad, U., Erlenkeuser, H. 1998. Correlation between Arabian Sea and Grenland climate oscillations of the past 110,000 years. *Nature*. v. 393. p. 54-57.

Shackleton, R.M. 1944. Preliminary Report on the Olorgesailie Prehistoric Site: Nairobi, Kenya, Mines and Geological Department.

Shackleton, R.M. 1978. Geological map of Olorgesailie area. *In* Bishop, W.W. (ed.). *Geologic Background to Fossil Man*. Edinburgh, UK. Scottish Academic Press. p. 171-172 and map insert.

Shackleton, N.J. 1995. New data on the evolutions of Pliocene climate variability."*In* E.S. Vrba, G.H. Denton, T.C. Partridge & L.H. Burckle (eds.), *Paleoclimate and Evolution, with Emphasis on Human Origins*. New Haven. Yale University Press. p. 242-248.

Sheppard, R.A., Gude, A.J. 1968. Distribution and genesis of authigenic silicate minerals in tuffs of Pleistocene Lake Tecopa, Inyo County, California. USGS Professional Paper. n. 597. 38 pp.

Sheppard, R.A., Gude, A.J. 1969. Diagenesis of tuffs in the Barstow Formation, Mud Hills, San Bernadino County, California. USGS Professional Paper. n. 634. 35 pp.

Surdam, R.C. 1977. Zeolites in closed hydrologic systems. *Reviews in Mineralogy*. n. 4. p. 65-91.

Surdam, R.C., Eugster, H.P. 1976, Mineral Reactions in the Sedimentary Deposits of the Lake Magadi Region, Kenya. Geological Society of America Bulletin, v. 87, p. 1739-1752.

Surdam, R.C., Parker, R.D. 1972. Authigenic aluminosilicate minerals in the tuffaceous rocks of the Green River Formation, Wyoming. *GSA Bulletin*. v. 83. p. 689-700.

Trauth, M.H., Deino, A., Strecker, M.R. 2001. Response of the East African climate to orbital forcing during the last interglacial (130-117 ka) and the early last glacial (117-60 ka). *Geology*. v. 29. n. 6. p. 499-502.

Trauth, M.H., Maslin, M.A., Deino, A.L., Strecker, M.R., Bergner, A.G.N., Dühnforth, M. 2002. High- and low-latitude forcing of Plio-Pleistocene East African climate and human evolution. *Journal of Human Evolution*. v. 53. i. 5. p. 475-486.

Trauth, M.H., Deino, A.L., Bergner, A.G.N., Strecker, M.R. 2003. East African climate change and orbital forcing during the last 175 kyr BP. *Earth and Planetary Letters*. v. 206. i. 3-4. p. 297-313.

Trauth, M.H., Maslin, M.A., Deino, A., Strecker, M.R. 2005. Late Cenozoic Moisture history of East Africa. *Science*. v. 309. p. 2051-2053.

Trauth, M.H., Maslin, M.A., Deino, A.L., Strecker, M.R., Bergner, A.G.N., Duhnforth, M. 2007. High- and low-latitude forcing of Plio-Pleistocene East African climate and human evolution. *Journal of human Evolution*. v. 53. p. 475-486.

Trauth, M.H., Larrasoaña, J.C., Mudelsee, M. 2009. Trends, rhythms, and events in Plio-Pleistocene African climate. *Quaternary Science Reviews*. v. 28, p. 399-411.

Trauth, M.H., Maslin, M.A., Deino, A.L., Junginger, A., Lesoloyia, M., Odada, E., Olago, D.A., Olaka, L.A., Strecker, M.R., Tiedemann, R. 2010. Human evolution in a variable environment: The amplifier lakes of Eastern Africa. *Quaternary Science Reviews.* v. 29. p. 2981–2988.

Vrba, E.S., Denton, G.H., Partridge, T.C., Burckle, L.H. 1995. Paleoclimate and Evolution: with Emphasis on Human Origins. Yale University. Bookcrafters Inc. Chelsea, MI.

White, T.D., Moore, R.V., Suwa, G. 1984. Hadar Biostratigraphy and Hominid Evolution. *Journal of Vertebrate Paleontology*. v. 4. n. 4. p. 575-583.

Wynn, J.G. 2004. Influence of Plio-Pleistocene Aridification on Human Evolution: Evidence from Paleosols of the Turkana Basin, Kenya. *American Journal of Physical Anthropology*. v. 123, p. 106-118.

Yuretich, R.F. 1982, Possible Influences Upon Lake Development in the East African Rift Valley. *Journal of Geology*, v. 90, p. 329-337.

APPENDICES

Appendix A: Select X-ray Diffraction Patterns with d-Spacing Labeled

Appendix A.1: Labeled XRD Patterns for HSPDP-MAG-1A

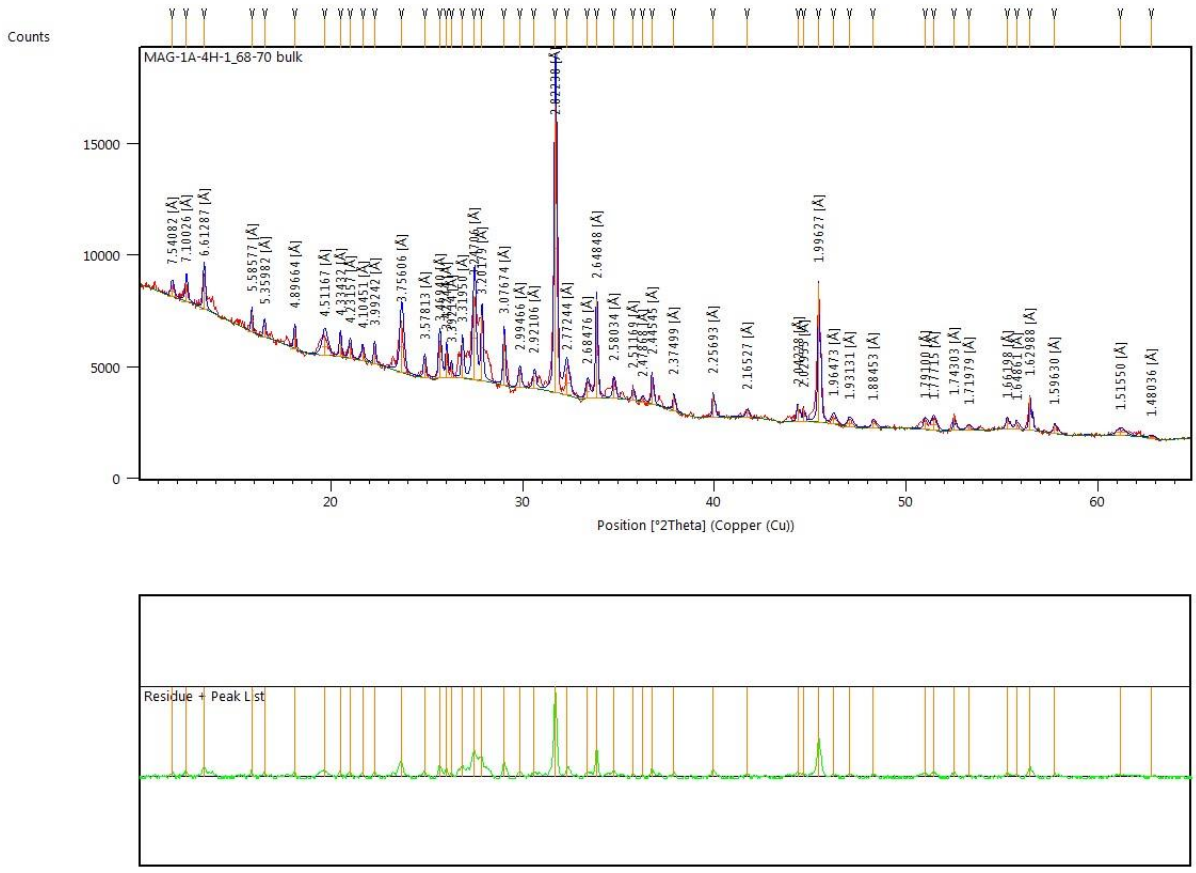

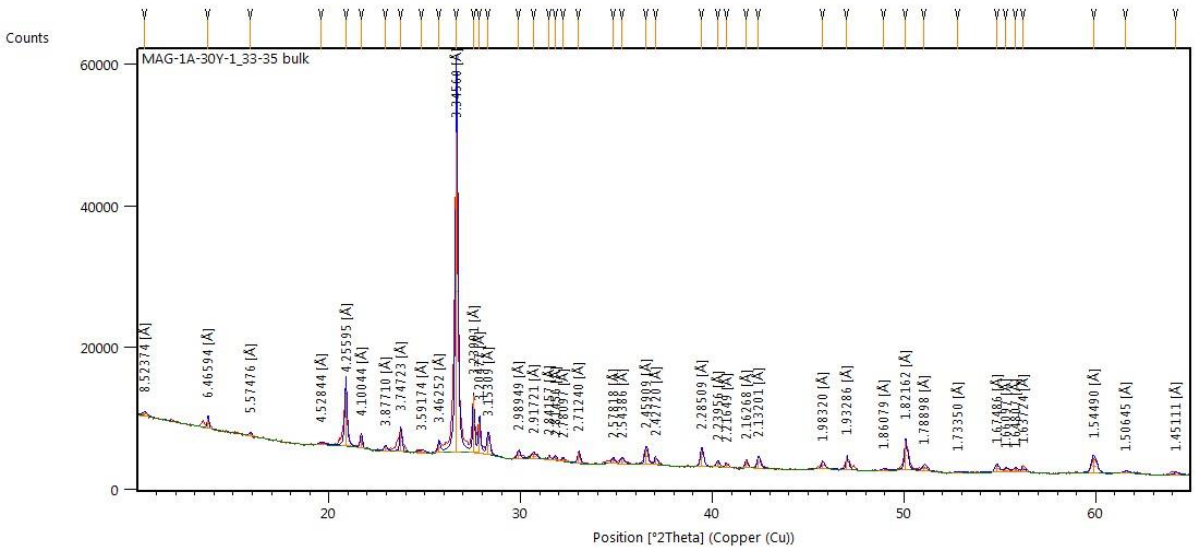
Counts
MAG-1A-30Y-1_33-35 bulk
60000
40000
20000
0
20
30
40
50
60
Position [°2Theta] (Copper (Cu))

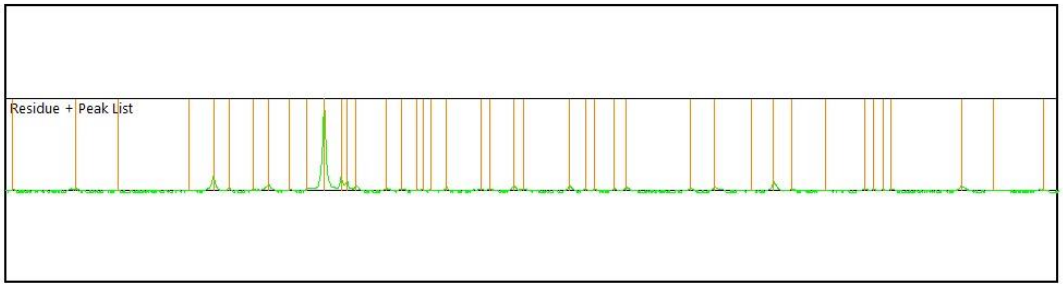
Residue + Peak List

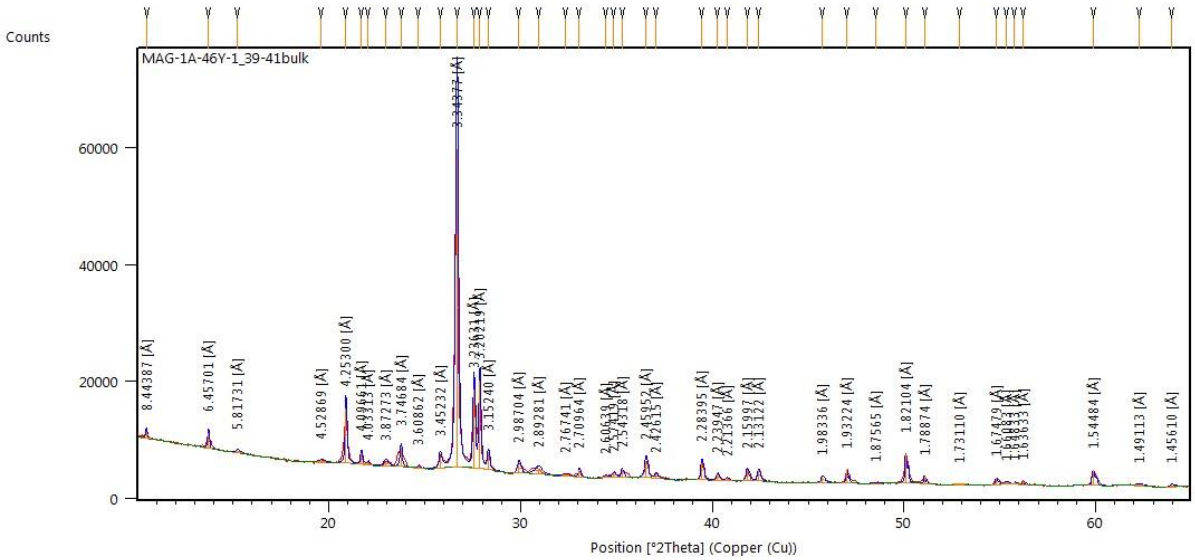
Counts
MAG-1A-46Y-1_39-41bulk
60000
40000
20000
0
20
30
40
50
60
Position [°2Theta] (Copper (Cu))

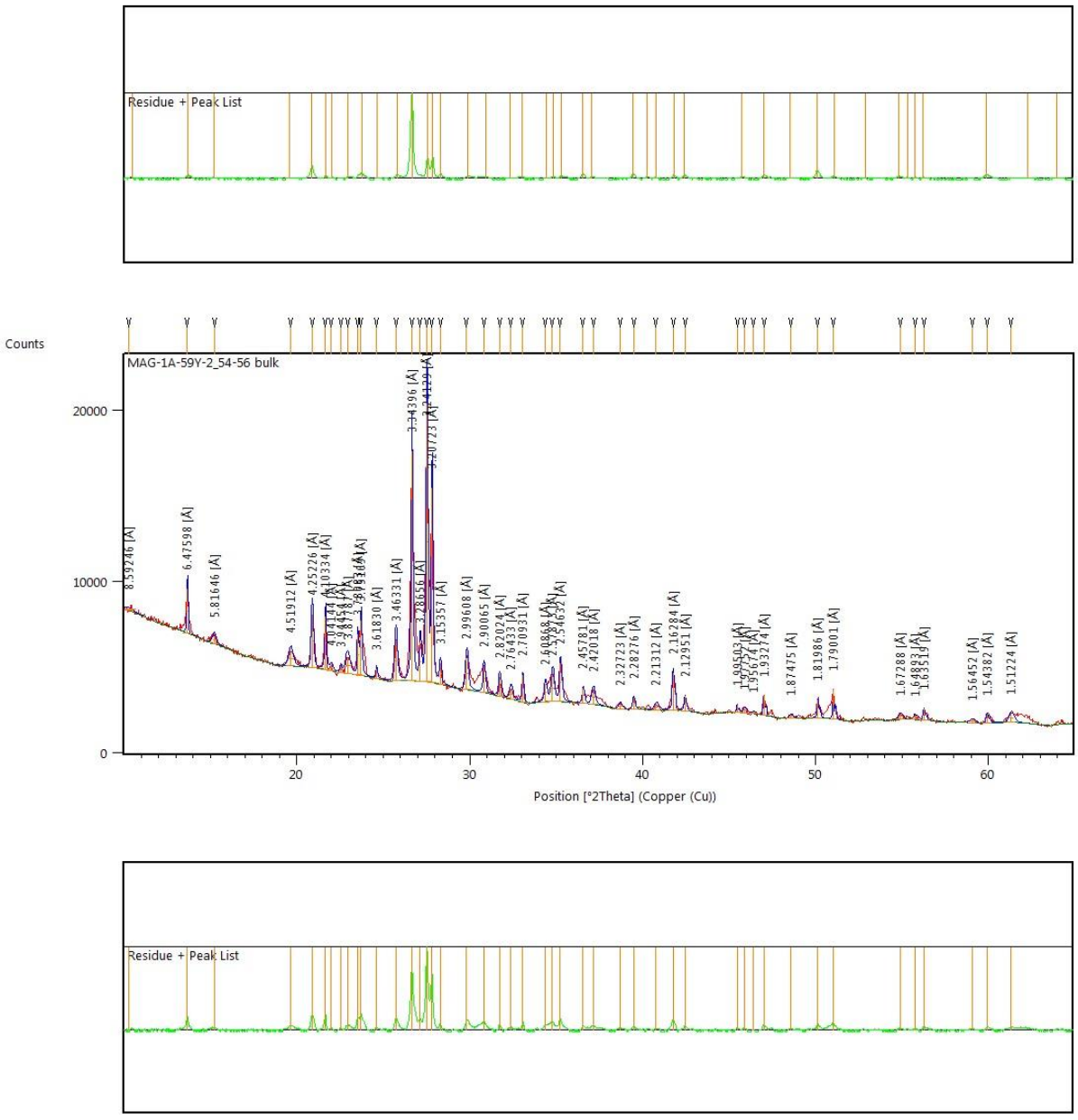
Residue + Peak List
Counts
MAG-1A-59Y-2_54-56 bulk
20000
10000
0
8.59246 [Å]
6.47598 [Å]
5.81646 [Å]
4.51912 [Å]
4.25226 [Å]
4.10334 [Å]
3.61830 [Å]
3.46331 [Å]
3.34396 [Å]
3.15357 [Å]
2.99608 [Å]
2.90065 [Å]
2.82024 [Å]
2.76433 [Å]
2.70931 [Å]
2.54632 [Å]
2.45781 [Å]
2.42018 [Å]
2.32723 [Å]
2.28276 [Å]
2.21312 [Å]
2.16284 [Å]
2.12951 [Å]
1.93274 [Å]
1.87475 [Å]
1.81986 [Å]
1.79001 [Å]
1.67288 [Å]
1.56452 [Å]
1.54382 [Å]
1.51224 [Å]
20
30
40
50
60
Position [°2Theta] (Copper (Cu))
Residue + Peak List

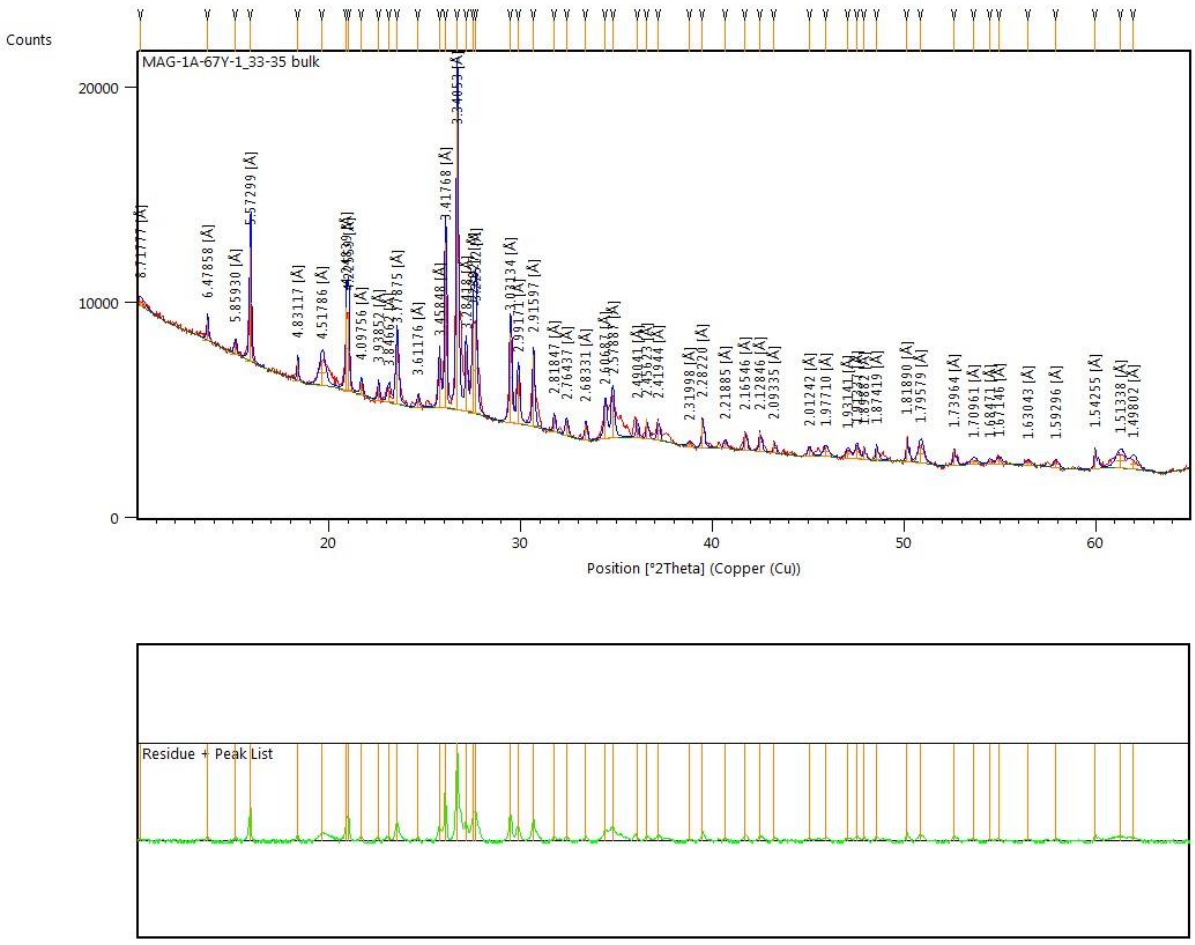
Counts
MAG-1A-67Y-1_33-35 bulk
20000
10000
0
20
30
40
50
60
Position [°2Theta] (Copper (Cu))
8.71777 [Å]
6.47858 [Å]
5.85930 [Å]
5.57299 [Å]
4.83117 [Å]
4.51786 [Å]
4.09756 [Å]
3.93852 [Å]
3.84662 [Å]
3.77875 [Å]
3.61176 [Å]
3.45848 [Å]
3.41768 [Å]
3.34053 [Å]
3.02134 [Å]
2.91597 [Å]
2.81847 [Å]
2.76437 [Å]
2.68331 [Å]
2.60683 [Å]
2.55788 [Å]
2.49043 [Å]
2.45313 [Å]
2.41944 [Å]
2.31998 [Å]
2.28220 [Å]
2.21885 [Å]
2.16546 [Å]
2.12846 [Å]
2.09335 [Å]
2.01242 [Å]
1.97710 [Å]
1.93141 [Å]
1.89882 [Å]
1.87419 [Å]
1.81890 [Å]
1.79579 [Å]
1.73964 [Å]
1.70961 [Å]
1.68471 [Å]
1.67146 [Å]
1.63043 [Å]
1.59296 [Å]
1.54255 [Å]
1.51338 [Å]
1.49802 [Å]
Residue + Peak List

Appendix A.2: Labeled XRD Patterns for HSPDP-MAG14-2A

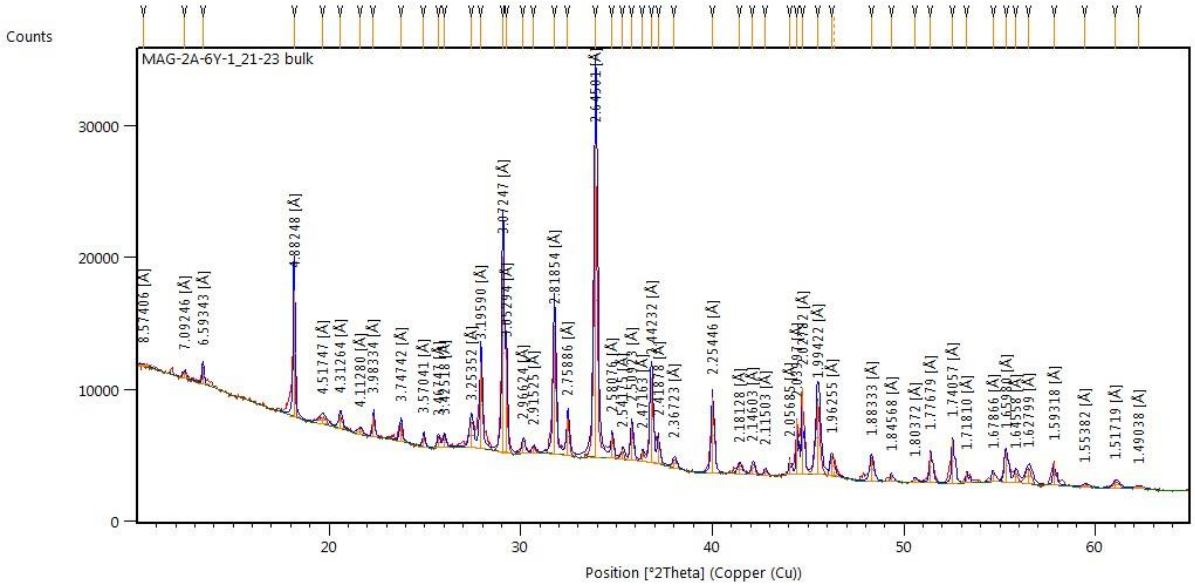

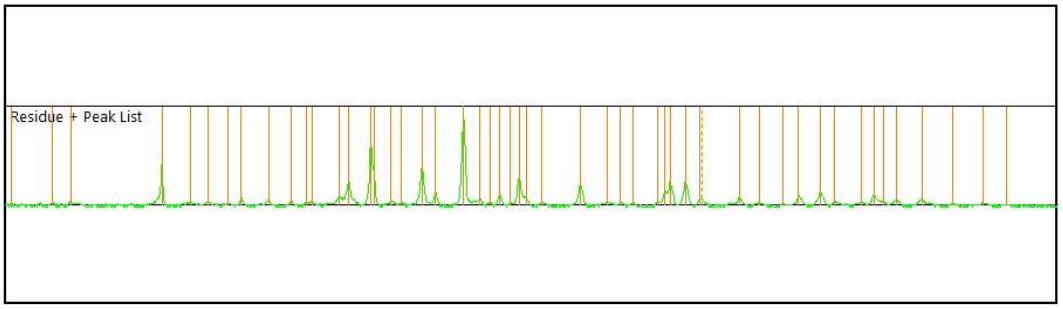

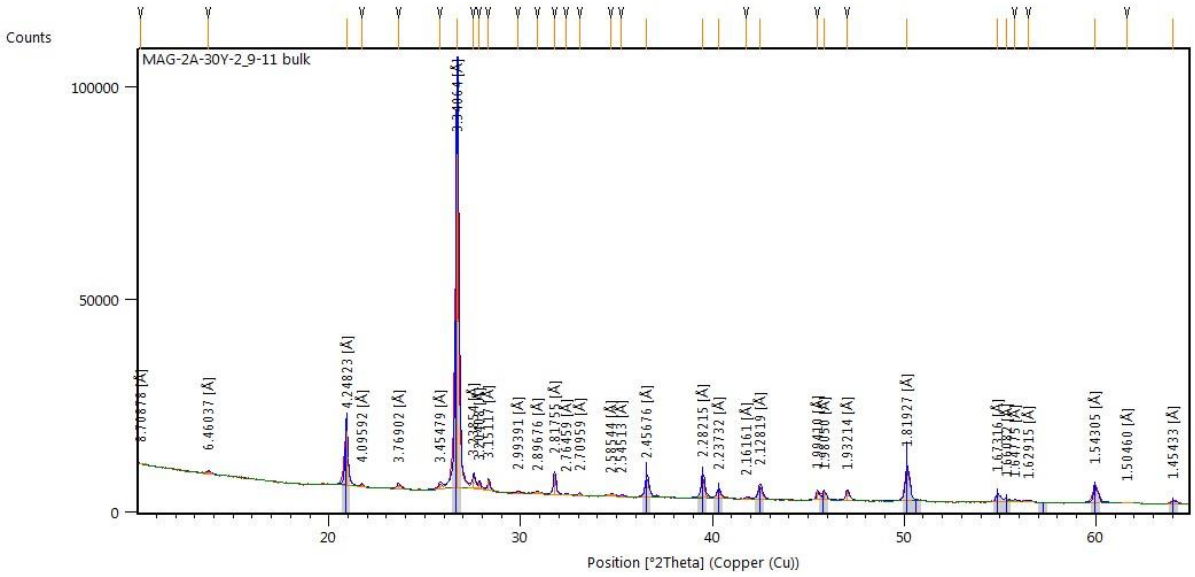

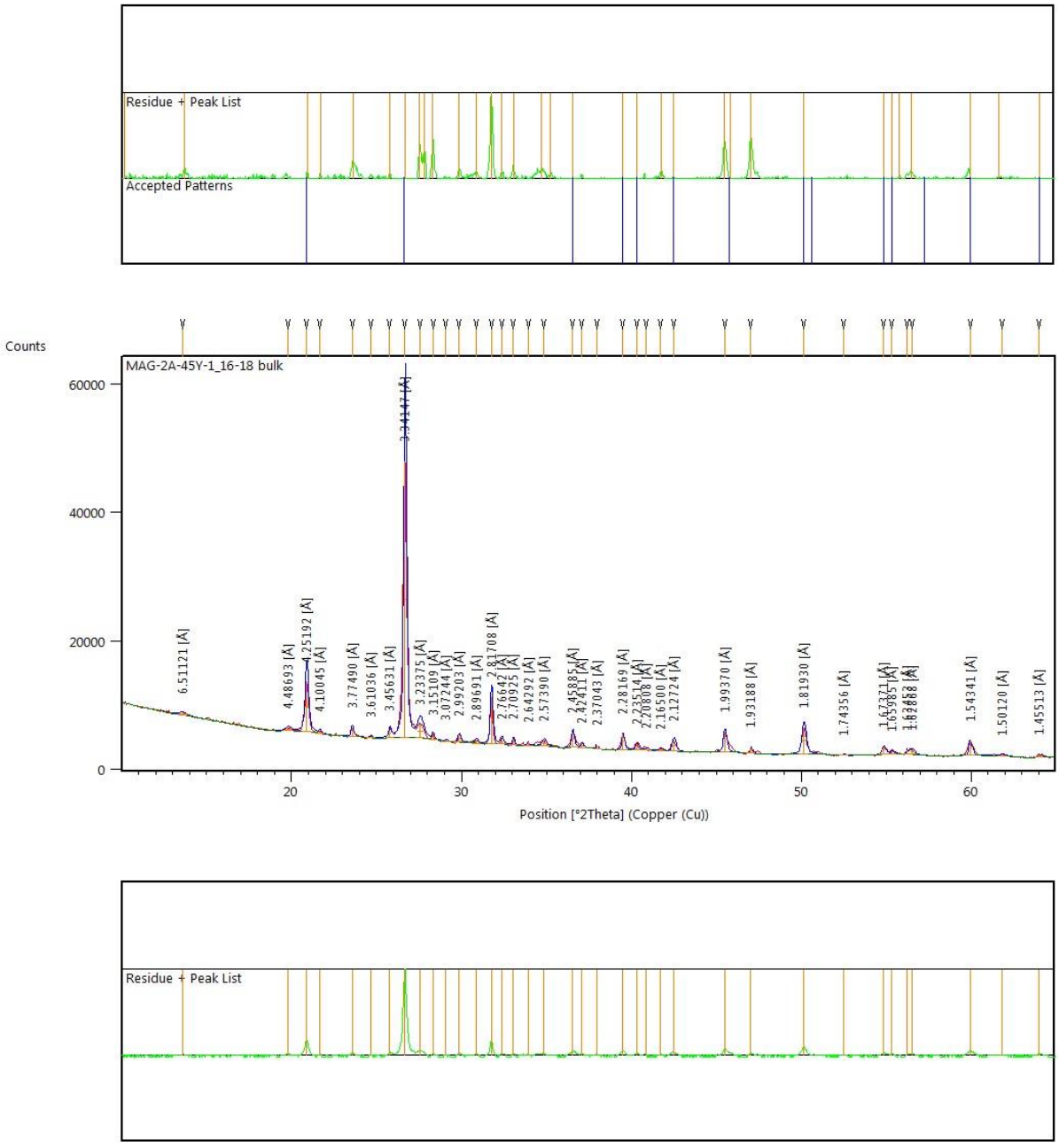
Residue + Peak List
Accepted Patterns
Counts
MAG-2A-45Y-1_16-18 bulk
60000
40000
20000
0
6.51121 [Å]
4.48693 [Å]
4.25192 [Å]
4.10045 [Å]
3.77490 [Å]
3.61036 [Å]
3.45631 [Å]
3.23375 [Å]
3.15109 [Å]
3.07244 [Å]
2.99203 [Å]
2.89691 [Å]
2.81708 [Å]
2.76842 [Å]
2.70925 [Å]
2.64292 [Å]
2.57390 [Å]
2.45885 [Å]
2.42411 [Å]
2.37043 [Å]
2.28169 [Å]
2.21514 [Å]
2.20808 [Å]
2.16500 [Å]
2.12724 [Å]
1.99370 [Å]
1.93188 [Å]
1.81930 [Å]
1.74356 [Å]
1.54341 [Å]
1.50120 [Å]
1.45513 [Å]
20
30
40
50
60
Position [°2Theta] (Copper (Cu))
Residue + Peak List

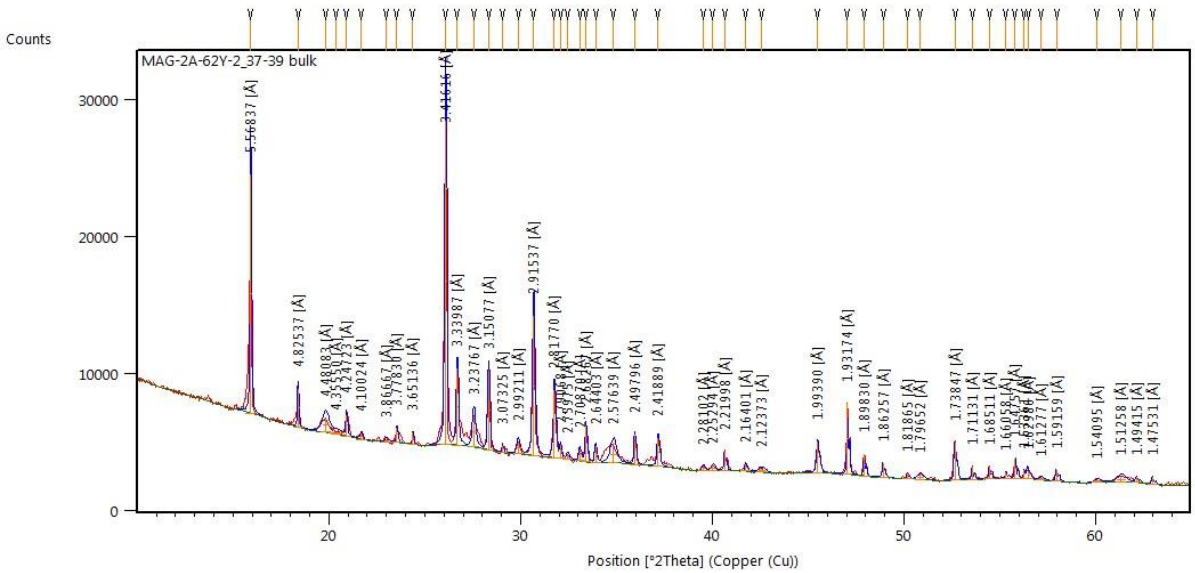
Counts
MAG-2A-62Y-2_37-39 bulk
Position [°2Theta] (Copper (Cu))

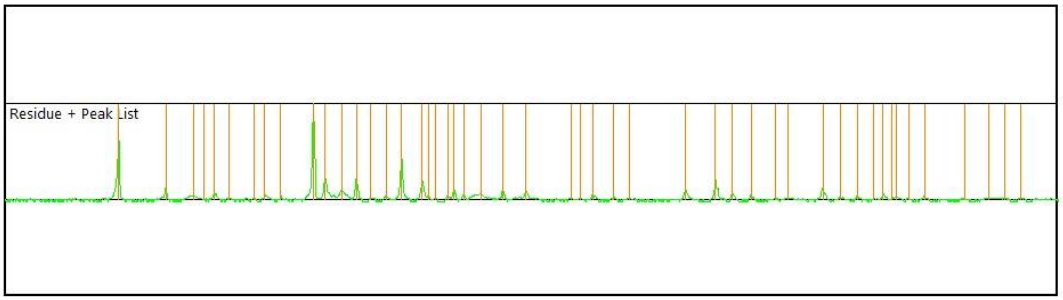
Residue + Peak List

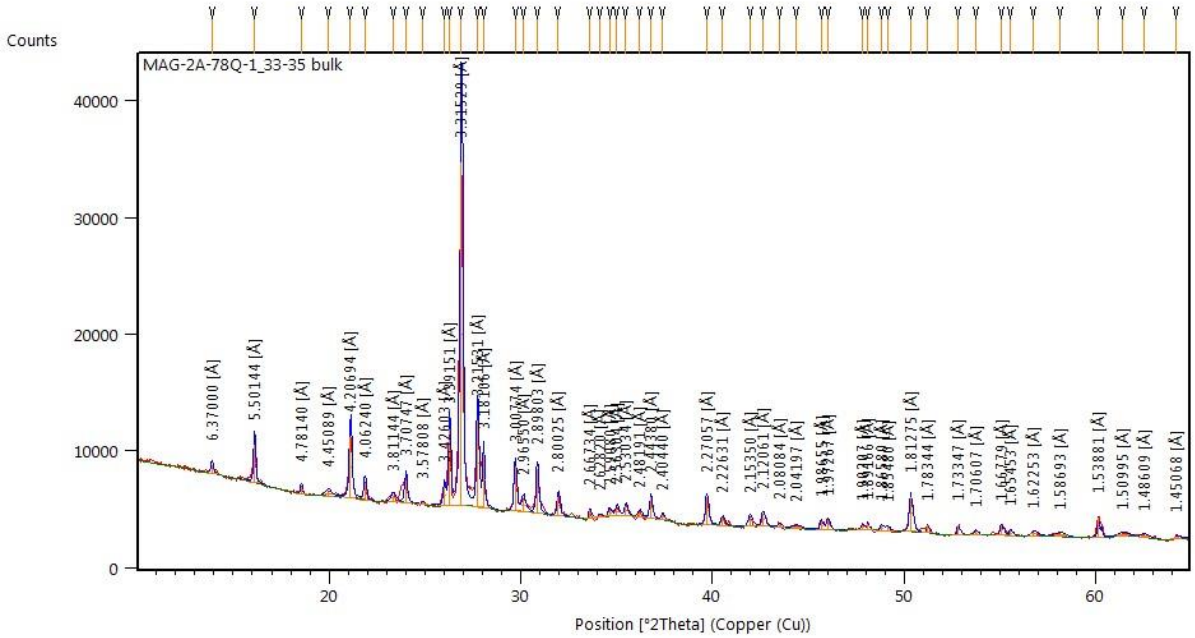
Counts
MAG-2A-78Q-1_33-35 bulk
Position [°2Theta] (Copper (Cu))

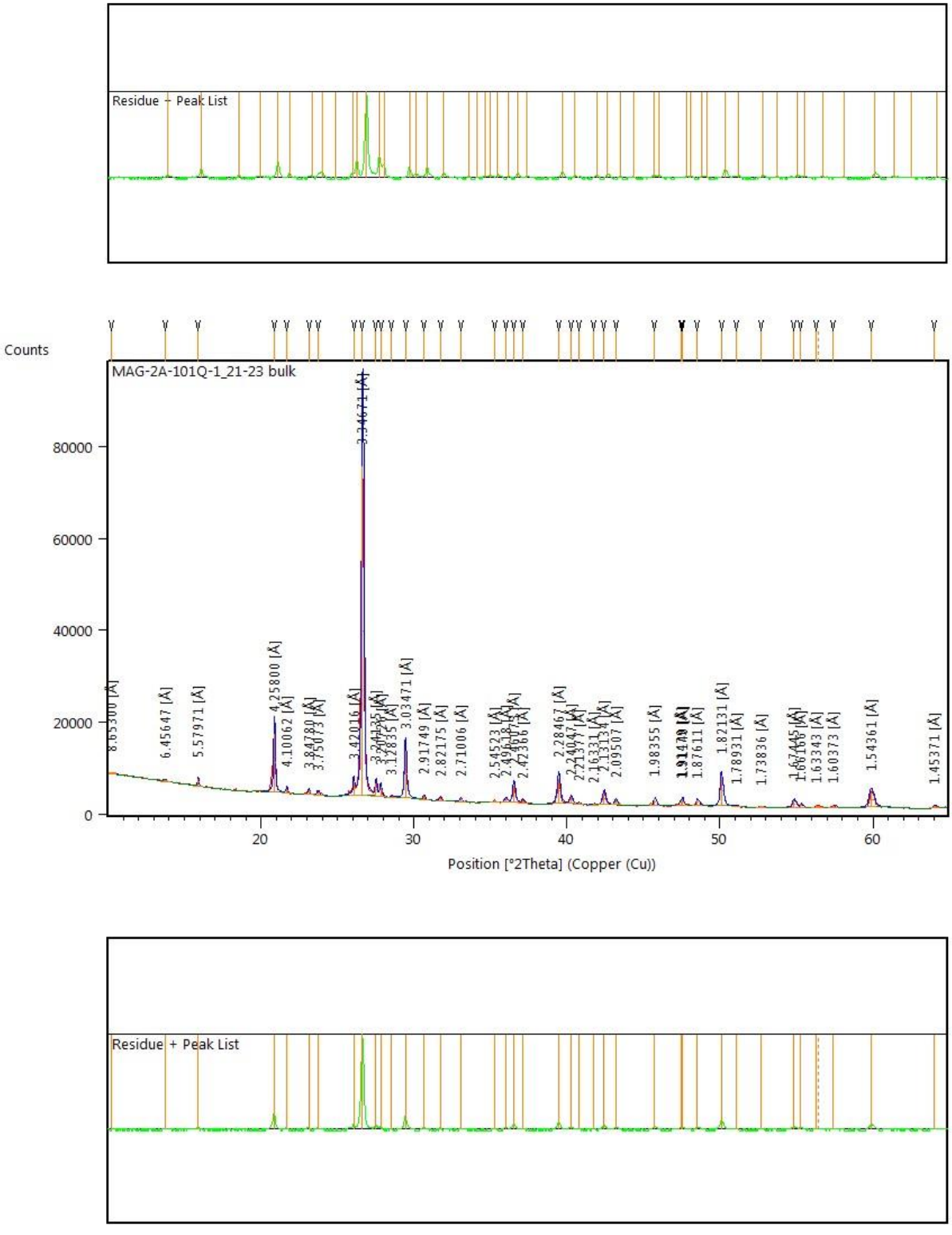
Residue + Peak List
Counts
MAG-2A-101Q-1_21-23 bulk
80000
60000
40000
20000
0
20
30
40
50
60
Position [°2Theta] (Copper (Cu))
Residue + Peak List

Appendix A.3: Labeled XRD Patterns for ODP-OLO12-1A

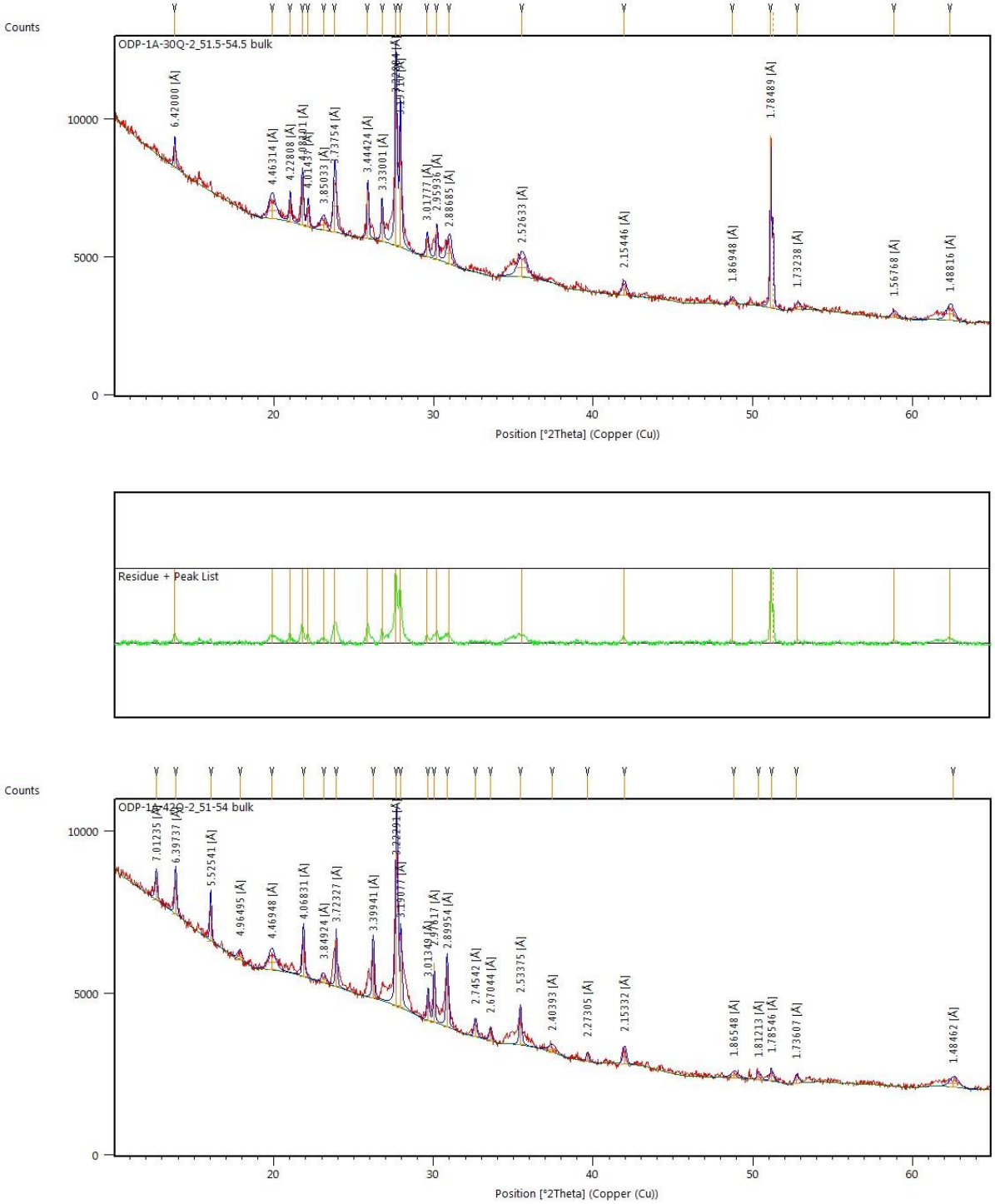

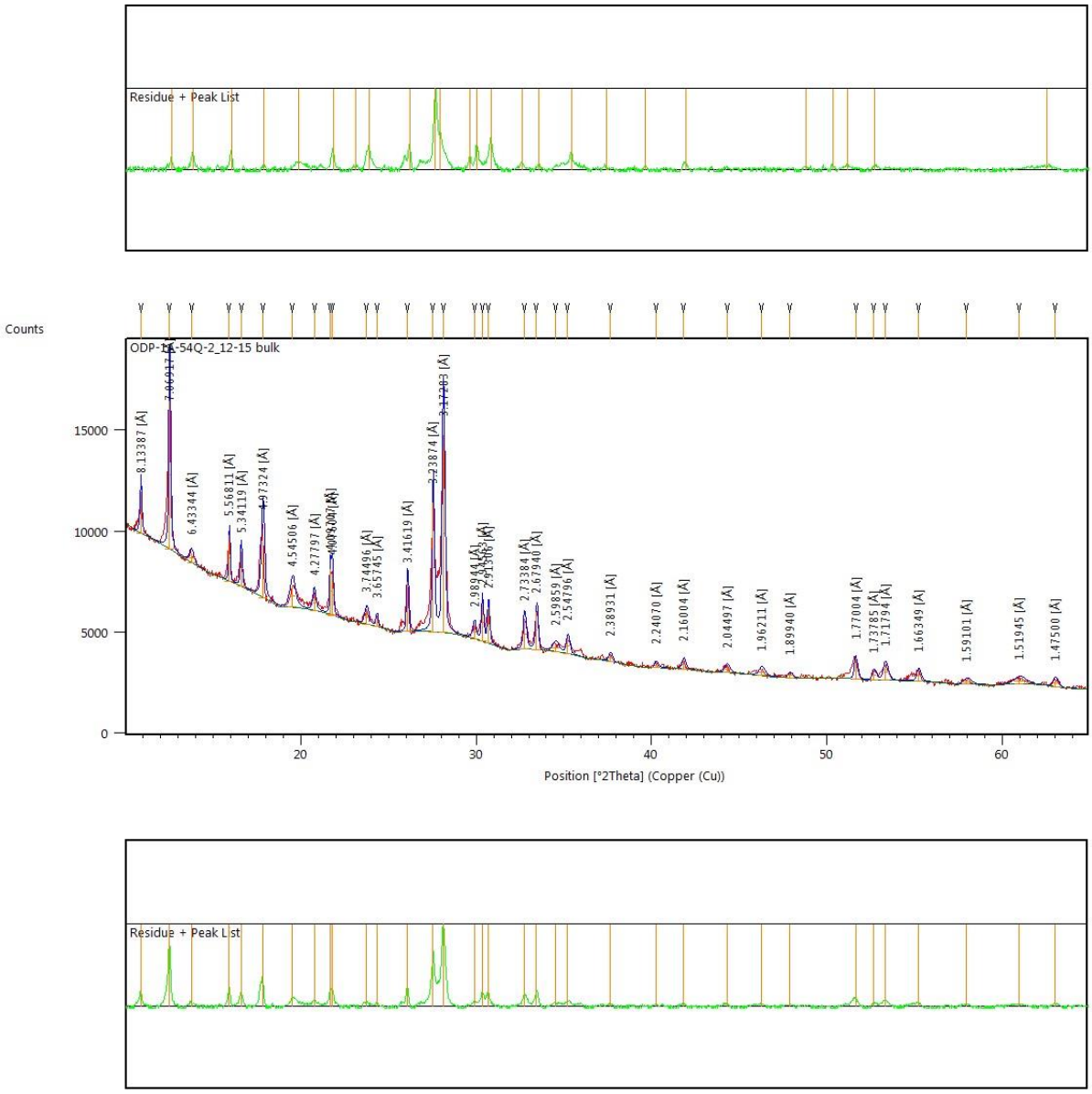
Residue + Peak List
Counts
ODP-1...54Q-2_12-15 bulk
15000
10000
5000
0
8.13387 [Å]
7.06117 [Å]
6.43344 [Å]
5.56811 [Å]
5.34119 [Å]
4.97324 [Å]
4.54506 [Å]
4.27797 [Å]
3.74496 [Å]
3.65745 [Å]
3.41619 [Å]
3.23874 [Å]
3.17283 [Å]
2.98944 [Å]
2.91506 [Å]
2.73384 [Å]
2.67940 [Å]
2.59859 [Å]
2.54796 [Å]
2.38931 [Å]
2.24070 [Å]
2.16004 [Å]
2.04497 [Å]
1.96211 [Å]
1.89940 [Å]
1.77004 [Å]
1.73785 [Å]
1.71794 [Å]
1.66349 [Å]
1.59101 [Å]
1.51945 [Å]
1.47500 [Å]
20
30
40
50
60
Position [°2Theta] (Copper (Cu))
Residue + Peak List

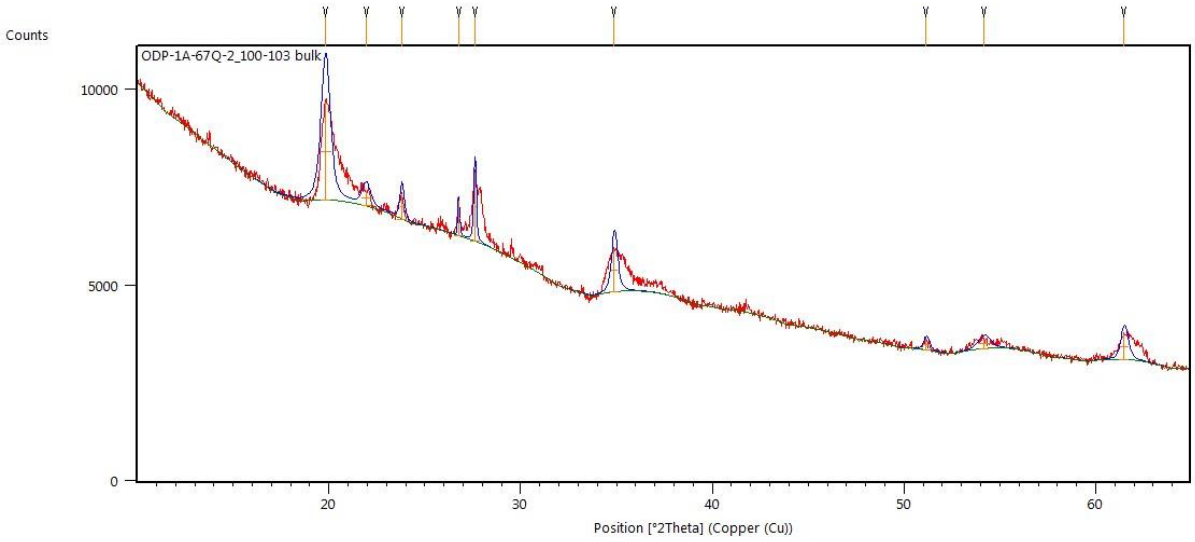
Counts
ODP-1A-67Q-2_100-103 bulk
10000
5000
0
20
30
40
50
60
Position [°2Theta] (Copper (Cu))

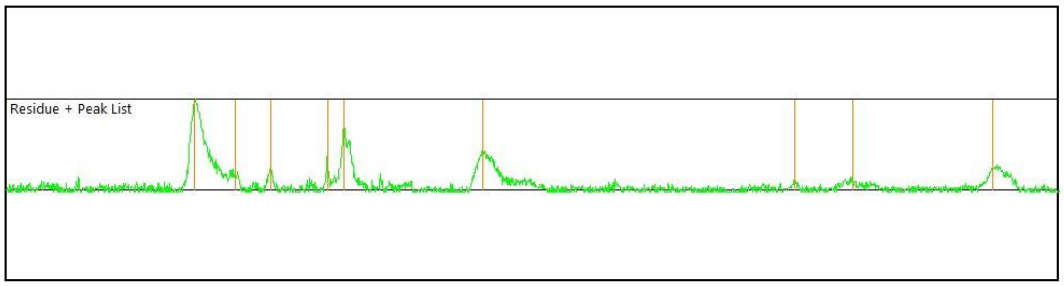
Residue + Peak List

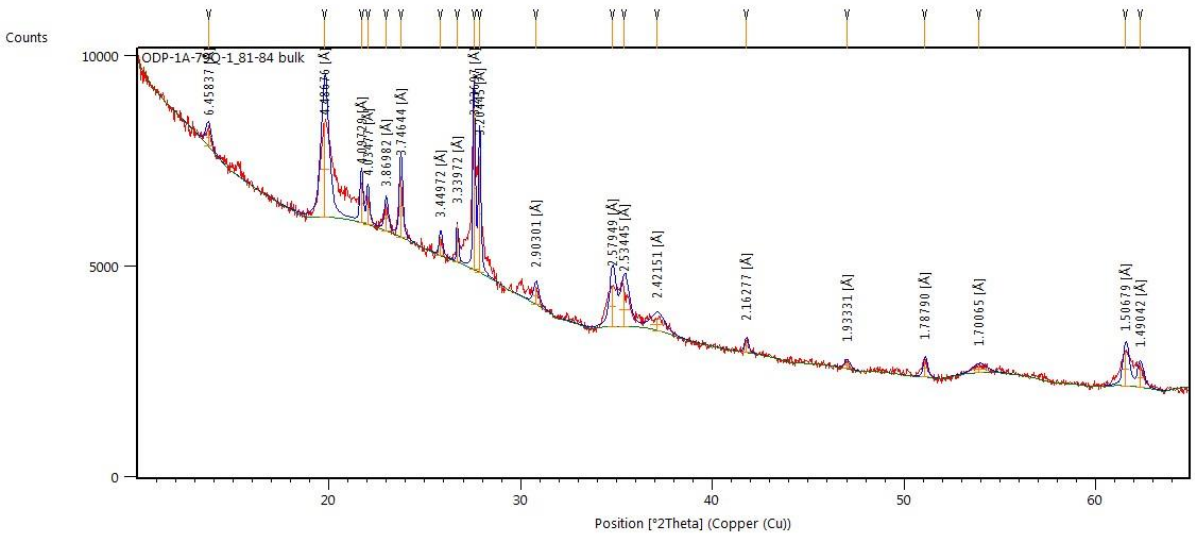
Counts
ODP-1A-7
10000
5000
0
6.45837 [Å]
4.09477 [Å]
3.86982 [Å]
3.74644 [Å]
3.44972 [Å]
3.33972 [Å]
2.90301 [Å]
2.57949 [Å]
2.53445 [Å]
2.42151 [Å]
2.16277 [Å]
1.93331 [Å]
1.78790 [Å]
1.70065 [Å]
1.50679 [Å]
1.49042 [Å]
20
30
40
50
60
Position [°2Theta] (Copper (Cu))

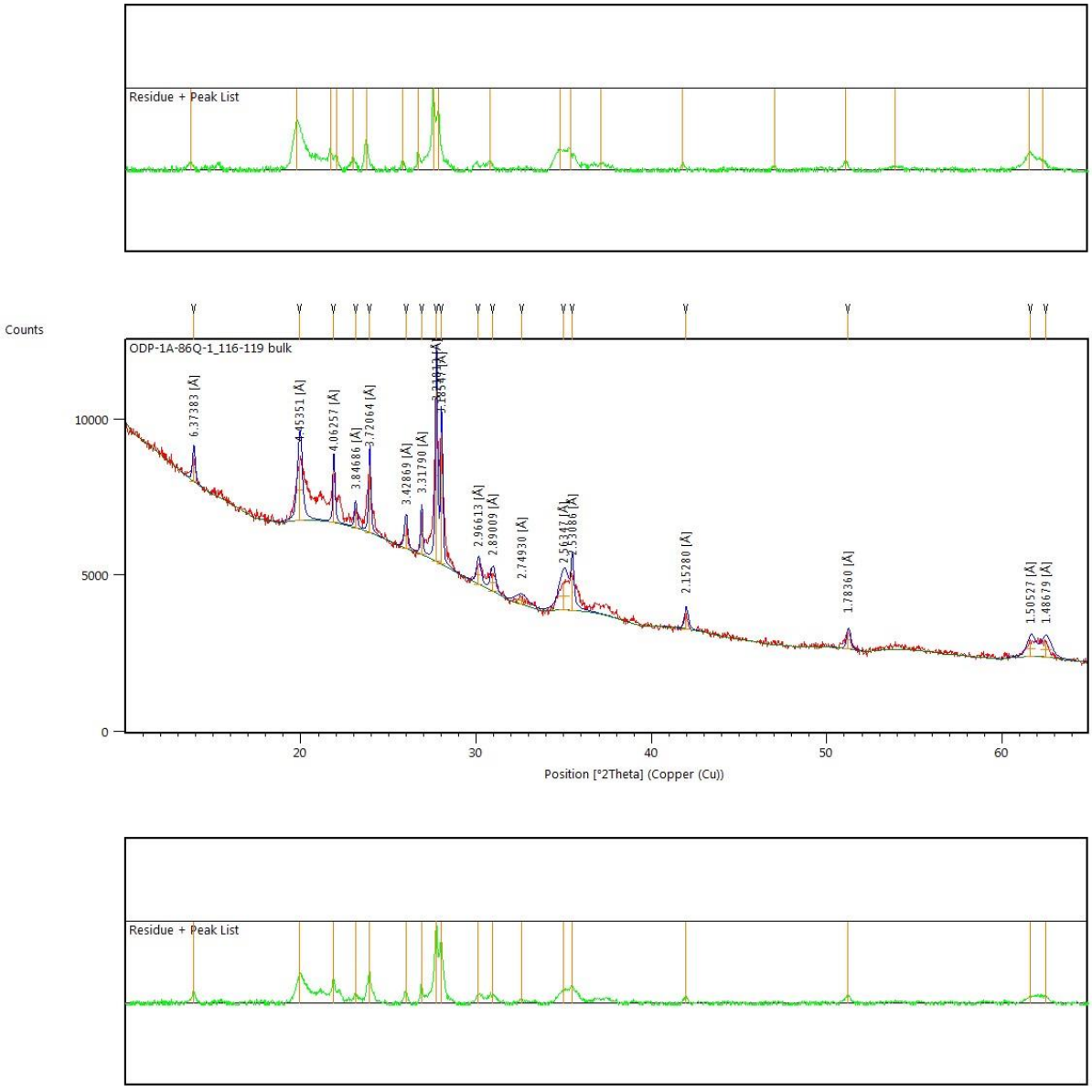
Residue + Peak List
Counts
ODP-1A-86Q-1_116-119 bulk
6.37383 [Å]
4.45351 [Å]
4.06257 [Å]
3.84686 [Å]
3.72064 [Å]
3.42869 [Å]
3.31790 [Å]
3.23111 [Å]
3.18547 [Å]
2.96613 [Å]
2.89009 [Å]
2.74930 [Å]
2.56347 [Å]
2.53086 [Å]
2.15280 [Å]
1.78360 [Å]
1.50527 [Å]
1.48679 [Å]
10000
5000
0
20
30
40
50
60
Position [°2Theta] (Copper (Cu))
Residue + Peak List

Appendix A.4: Labeled XRD Patterns for Modern Surface and Outcrop Samples

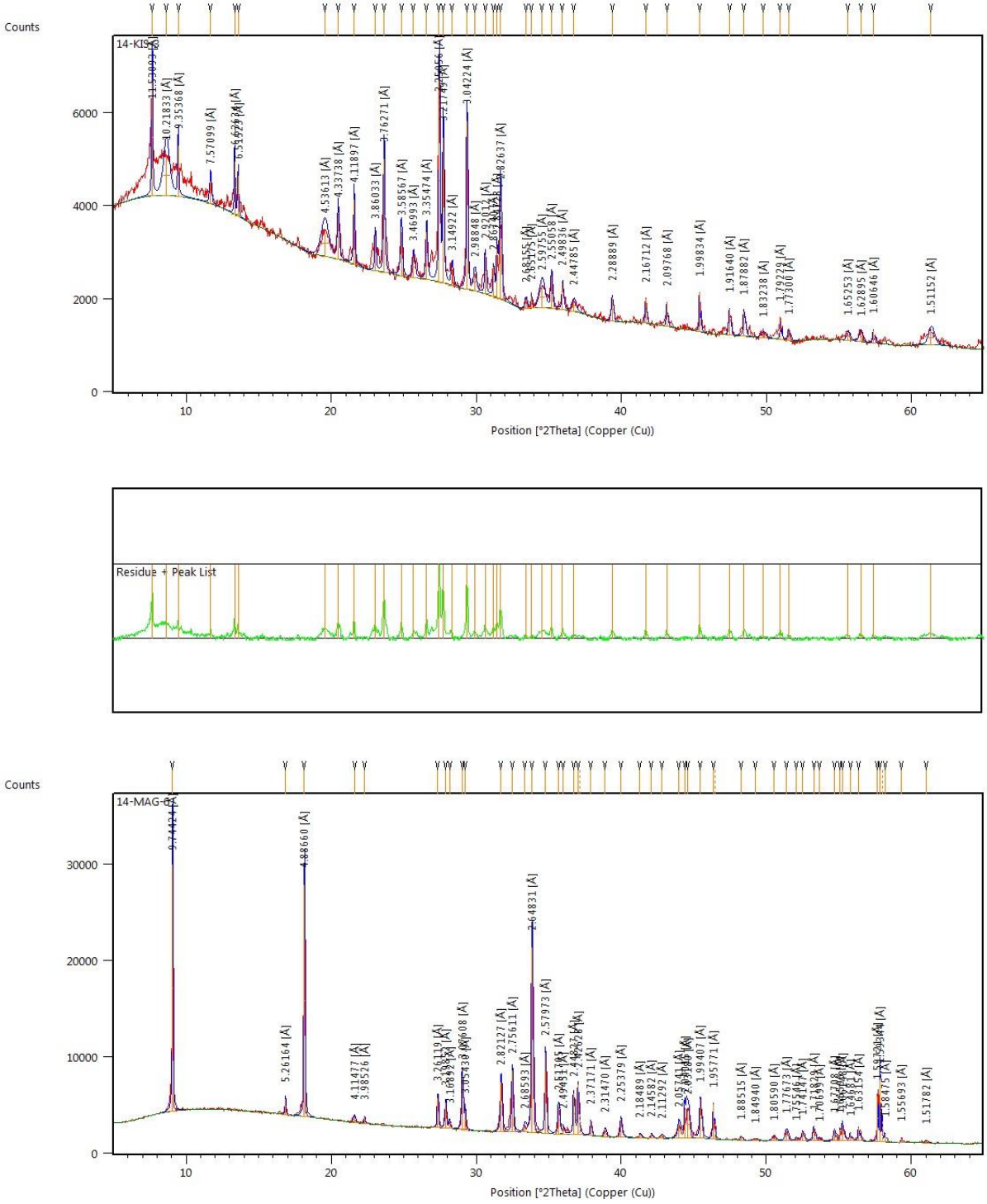

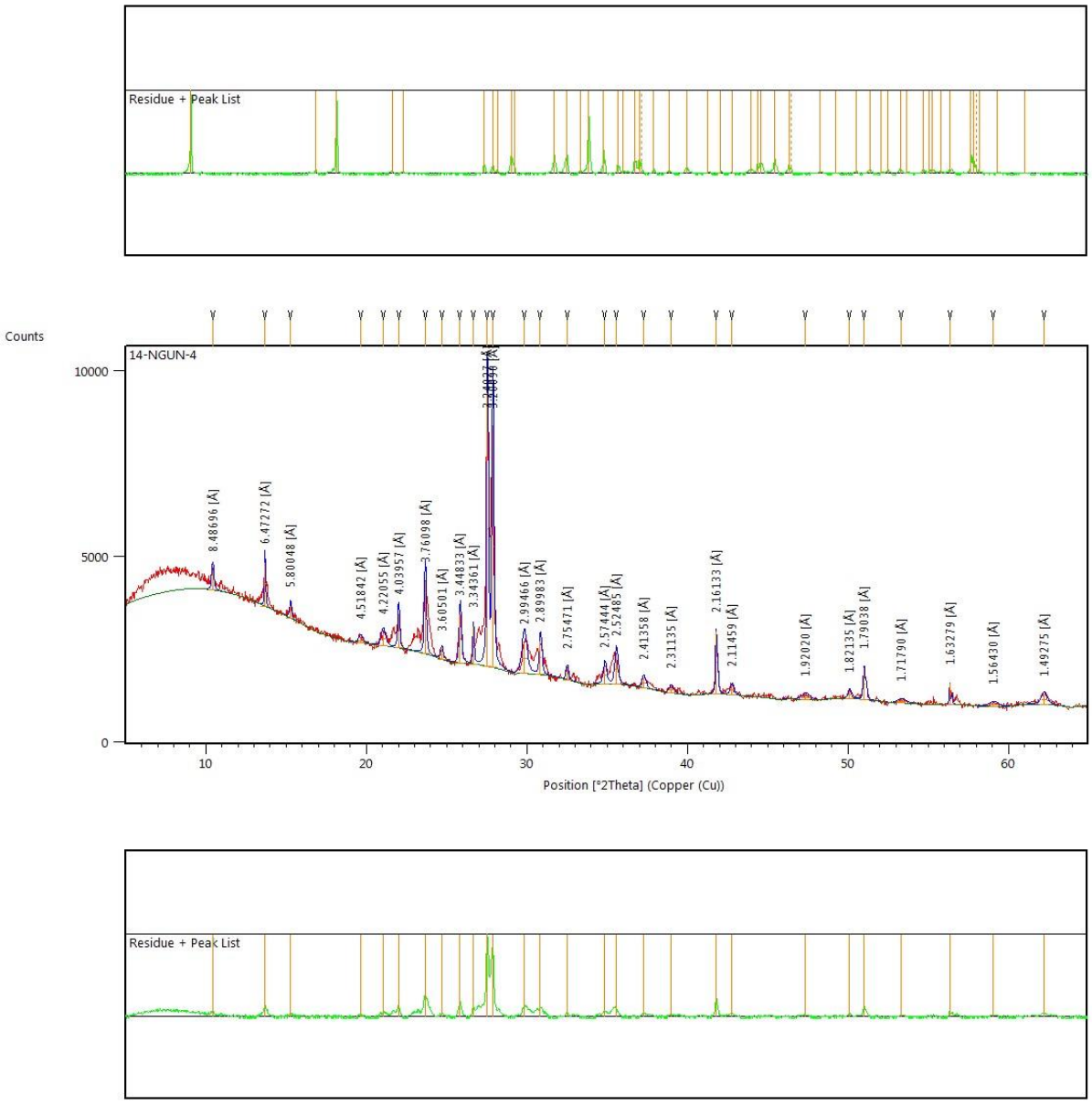
Residue + Peak List
Counts
14-NGUN-4
10000
5000
0
8.48696 [Å]
6.47272 [Å]
5.80048 [Å]
4.51842 [Å]
4.22055 [Å]
4.03957 [Å]
3.76098 [Å]
3.60501 [Å]
3.44833 [Å]
3.34361 [Å]
2.99466 [Å]
2.89983 [Å]
2.75471 [Å]
2.57444 [Å]
2.52485 [Å]
2.41358 [Å]
2.31135 [Å]
2.16133 [Å]
2.11459 [Å]
1.92020 [Å]
1.82135 [Å]
1.79038 [Å]
1.71790 [Å]
1.63279 [Å]
1.56430 [Å]
1.49275 [Å]
10
20
30
40
50
60
Position [°2Theta] (Copper (Cu))
Residue + Peak List

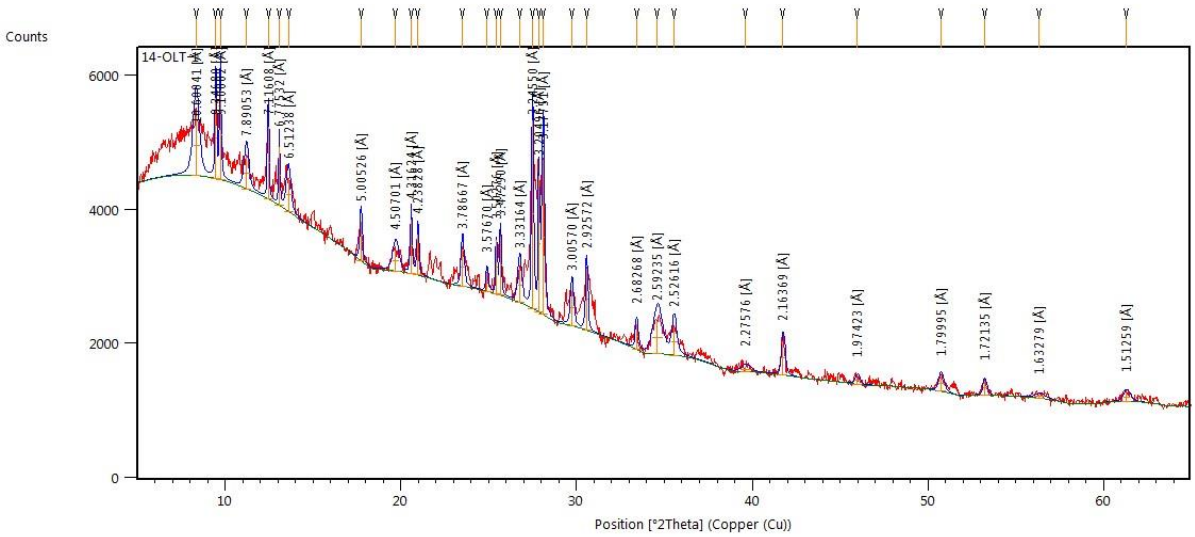
Counts
14-OLT-1
7.89053 [Å]
6.51238 [Å]
5.00526 [Å]
4.50701 [Å]
3.78667 [Å]
3.33164 [Å]
3.00570 [Å]
2.92572 [Å]
2.68268 [Å]
2.59235 [Å]
2.52616 [Å]
2.27576 [Å]
2.16369 [Å]
1.97423 [Å]
1.79995 [Å]
1.72135 [Å]
1.63279 [Å]
1.51259 [Å]
6000
4000
2000
0
10
20
30
40
50
60
Position [°2Theta] (Copper (Cu))

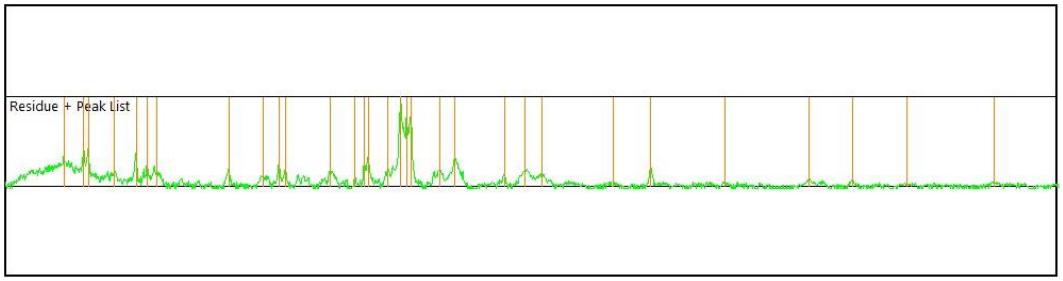
Residue + Peak List

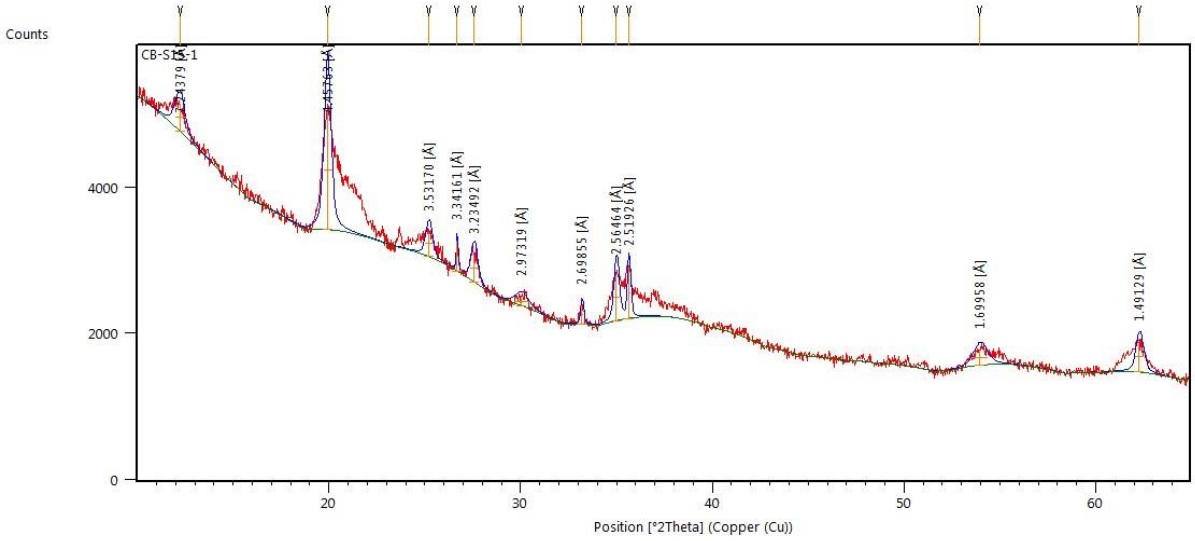
Counts
CB-STD-1
3.53170 [Å]
3.34161 [Å]
3.23492 [Å]
2.97319 [Å]
2.69855 [Å]
2.56464 [Å]
2.51926 [Å]
1.69958 [Å]
1.49129 [Å]
4000
2000
0
20
30
40
50
60
Position [°2Theta] (Copper (Cu))

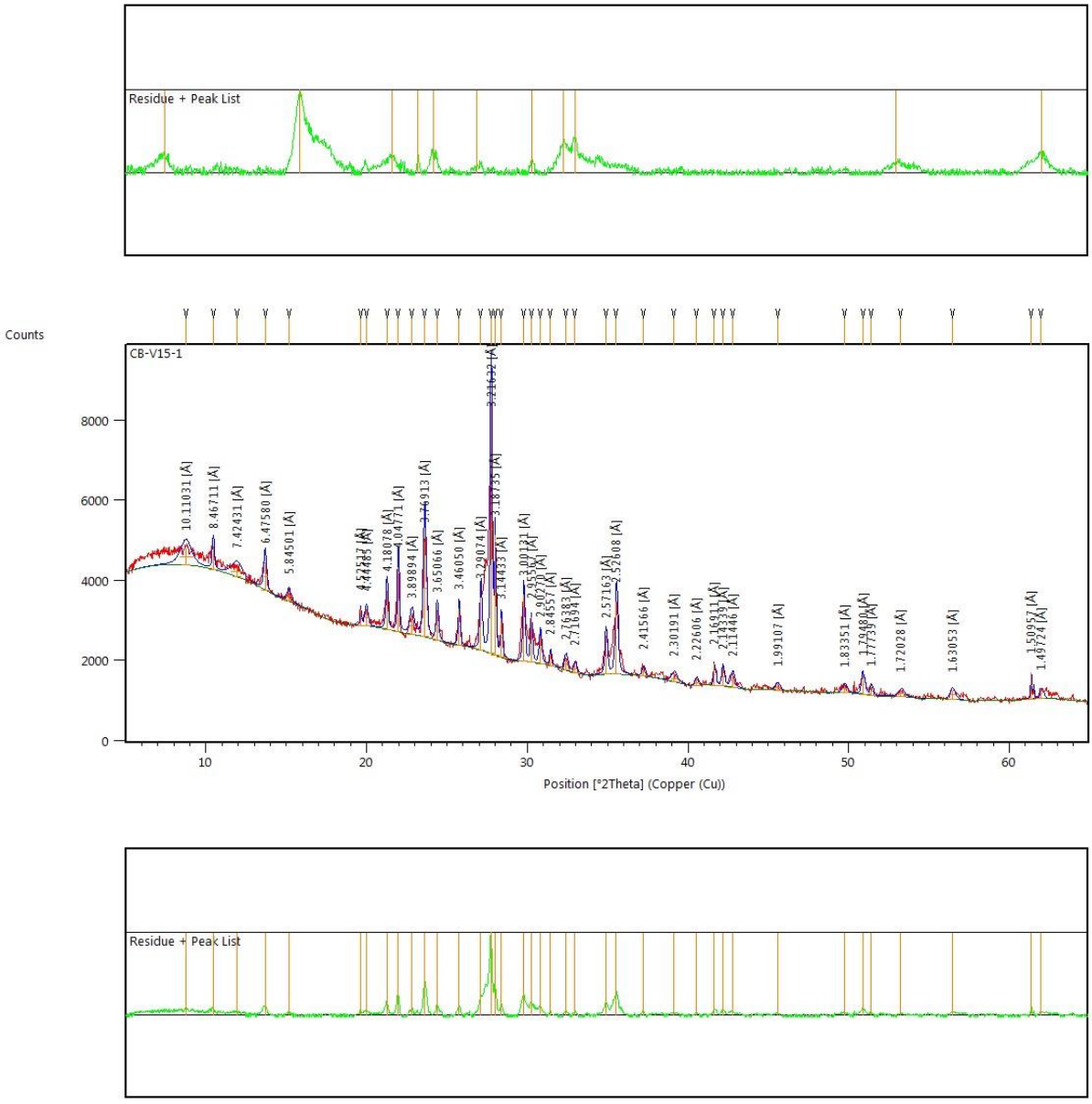
Residue + Peak List
Counts
CB-V15-1
8000
6000
4000
2000
0
10.11031 [Å]
8.46711 [Å]
7.42431 [Å]
6.47580 [Å]
5.84501 [Å]
4.18078 [Å]
4.04771 [Å]
3.89894 [Å]
3.76913 [Å]
3.65066 [Å]
3.46050 [Å]
3.20074 [Å]
3.18735 [Å]
3.14433 [Å]
2.84557 [Å]
2.76383 [Å]
2.71694 [Å]
2.57163 [Å]
2.52608 [Å]
2.41566 [Å]
2.30191 [Å]
2.22606 [Å]
1.99107 [Å]
1.83351 [Å]
1.72028 [Å]
1.63053 [Å]
10
20
30
40
50
60
Position [°2Theta] (Copper (Cu))
Residue + Peak List

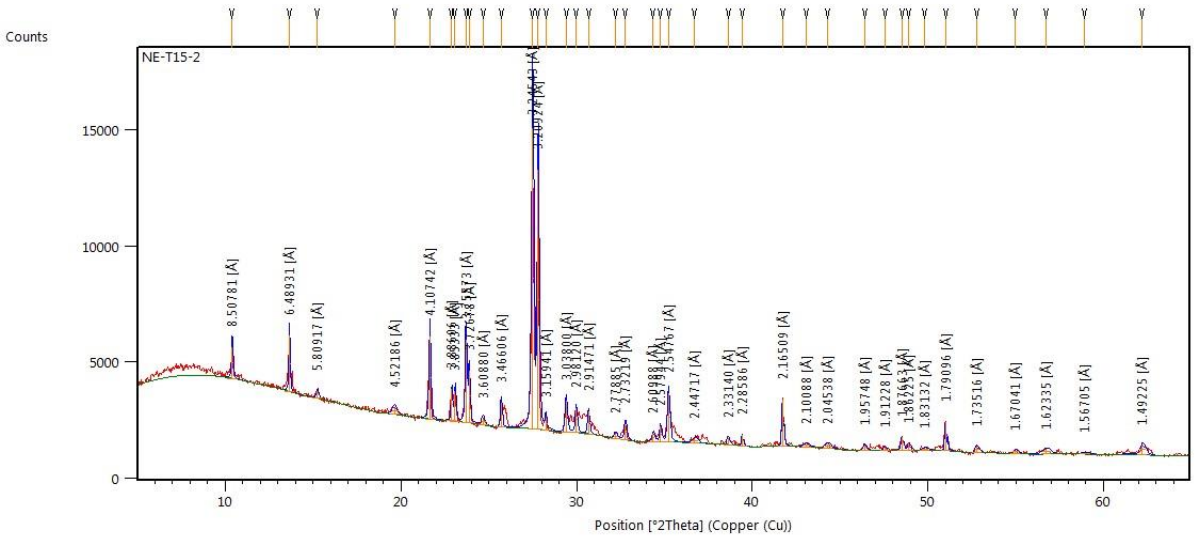
Counts
NE-T15-2
15000
10000
5000
0
8.50781 [Å]
6.48931 [Å]
5.80917 [Å]
4.52186 [Å]
4.10742 [Å]
3.60880 [Å]
3.46606 [Å]
3.15941 [Å]
2.91471 [Å]
2.73219 [Å]
2.54767 [Å]
2.44717 [Å]
2.33140 [Å]
2.28586 [Å]
2.16509 [Å]
2.10088 [Å]
2.04538 [Å]
1.95748 [Å]
1.91228 [Å]
1.83132 [Å]
1.79096 [Å]
1.73516 [Å]
1.67041 [Å]
1.62335 [Å]
1.56705 [Å]
1.49225 [Å]
10
20
30
40
50
60
Position [°2Theta] (Copper (Cu))

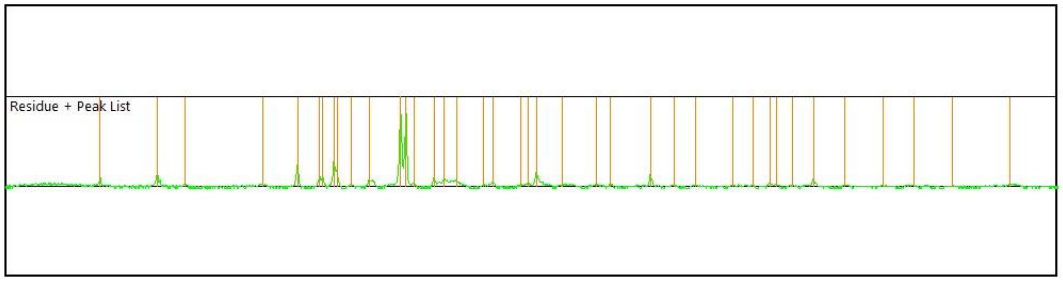
Residue + Peak List

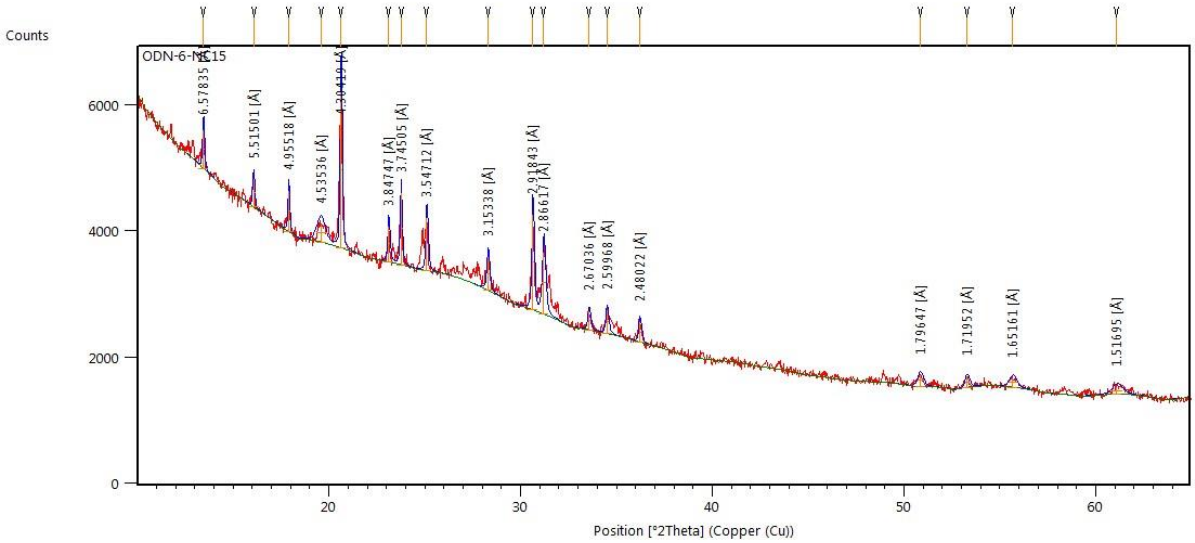
Counts
ODN-6-NE15
6000
4000
2000
0
6.57835 [Å]
5.51501 [Å]
4.95518 [Å]
4.53536 [Å]
3.84747 [Å]
3.74505 [Å]
3.54712 [Å]
3.15338 [Å]
2.91843 [Å]
2.86617 [Å]
2.67036 [Å]
2.59968 [Å]
2.48022 [Å]
1.79647 [Å]
1.71952 [Å]
1.65161 [Å]
1.51695 [Å]
20
30
40
50
60
Position [°2Theta] (Copper (Cu))

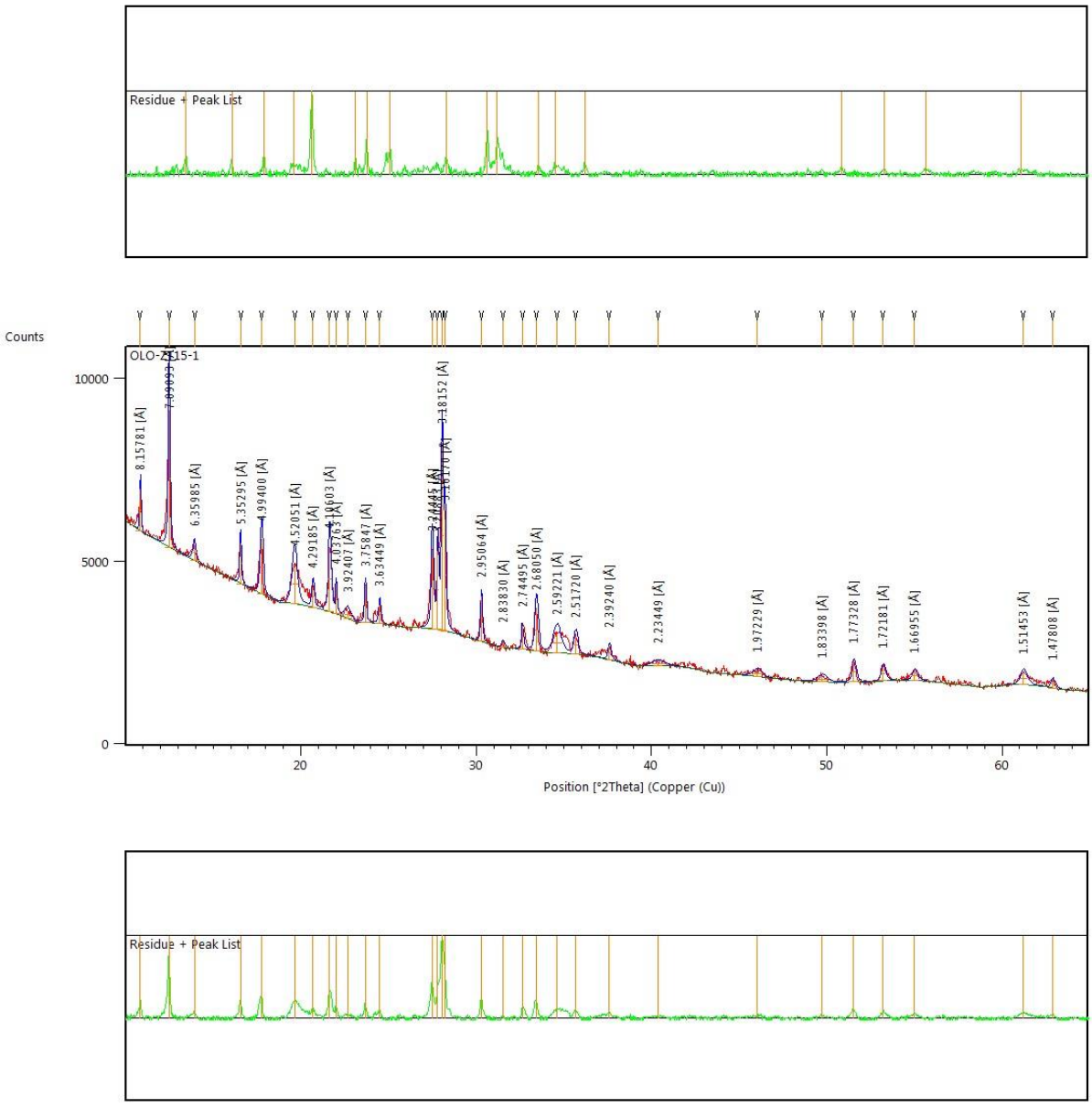
Residue + Peak List
Counts
OLO-Z115-1
10000
5000
0
8.15781 [Å]
7.09033 [Å]
6.35985 [Å]
5.35295 [Å]
4.99400 [Å]
4.52051 [Å]
4.29185 [Å]
4.07613 [Å]
3.92407 [Å]
3.75847 [Å]
3.63449 [Å]
3.18152 [Å]
2.95064 [Å]
2.83830 [Å]
2.74495 [Å]
2.68050 [Å]
2.59221 [Å]
2.51720 [Å]
2.39240 [Å]
2.23449 [Å]
1.97229 [Å]
1.83398 [Å]
1.77328 [Å]
1.72181 [Å]
1.66955 [Å]
1.51453 [Å]
1.47808 [Å]
20
30
40
50
60
Position [°2Theta] (Copper (Cu))
Residue + Peak List

Appendix B: HSPDP-MAG14 - Lake Magadi

Appendix B.1: X-ray Diffraction Patterns

Appendix B.1.1: HSPDP-MAG14-1A

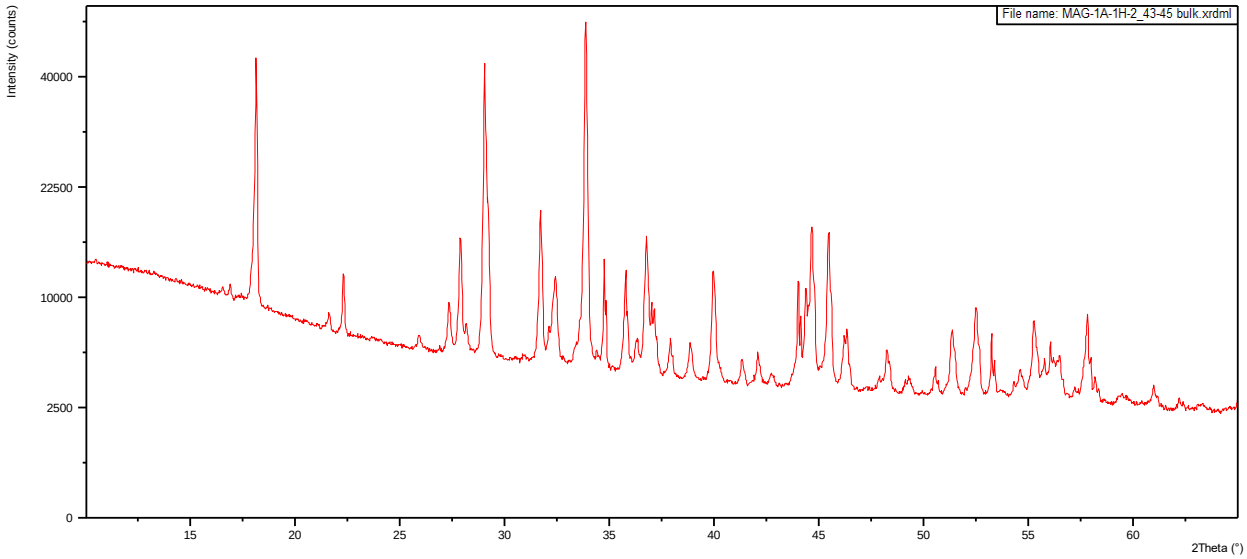

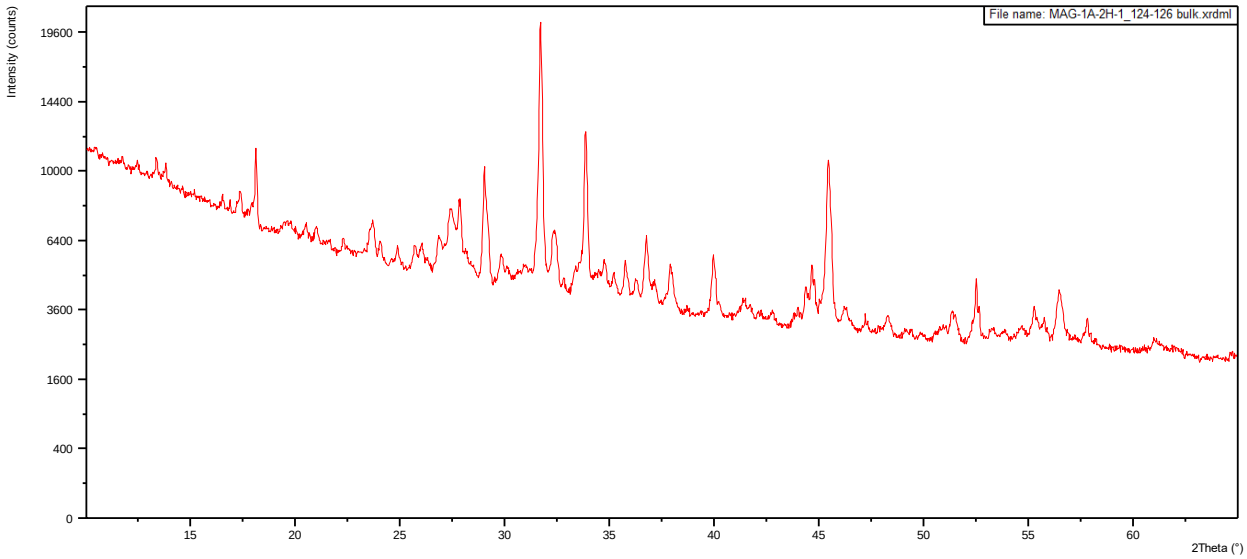

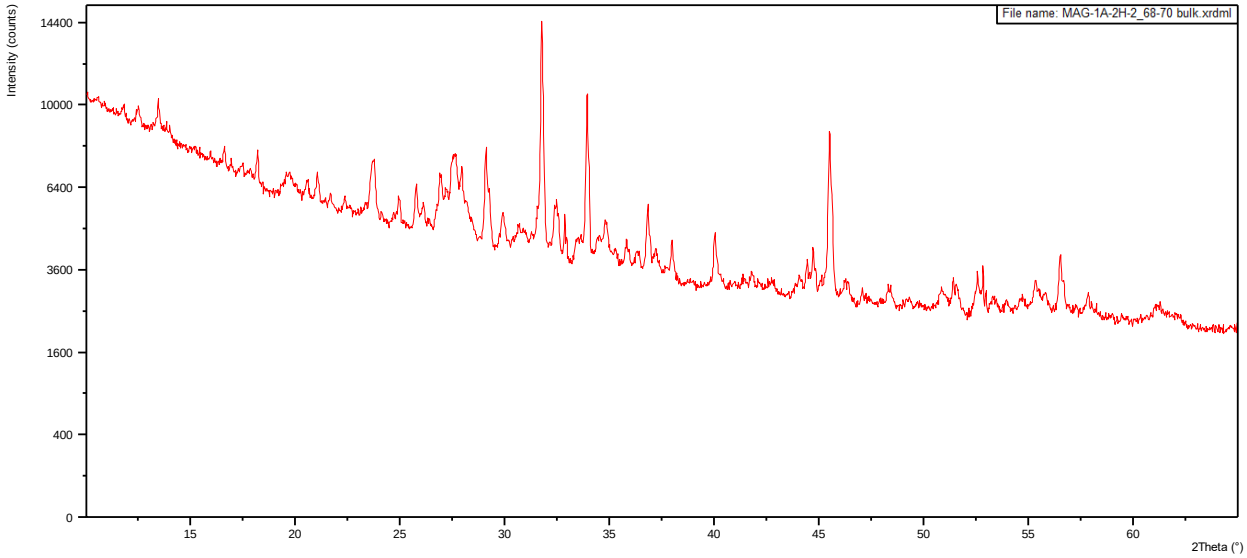
File name: MAG-1A-2H-2_68-70 bulk.xrdml
Intensity (counts)
14400
10000
6400
3600
1600
400
0
15
20
25
30
35
40
45
50
55
60
2Theta (°)

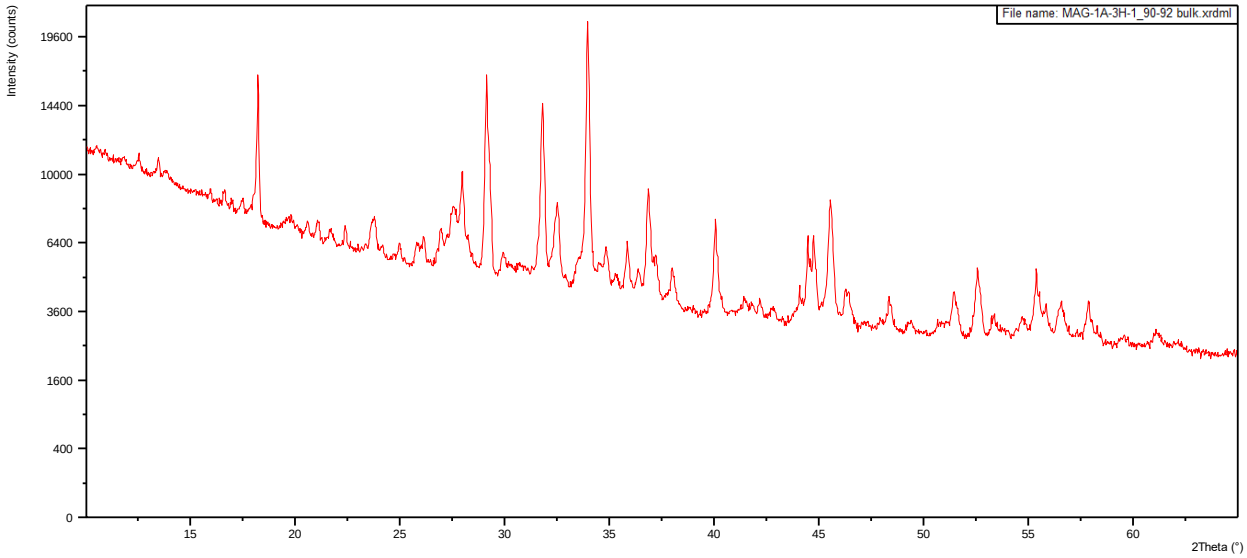
File name: MAG-1A-3H-1_90-92 bulk.xrdml
Intensity (counts)
19600
14400
10000
6400
3600
1600
400
0
15
20
25
30
35
40
45
50
55
60
2Theta (°)

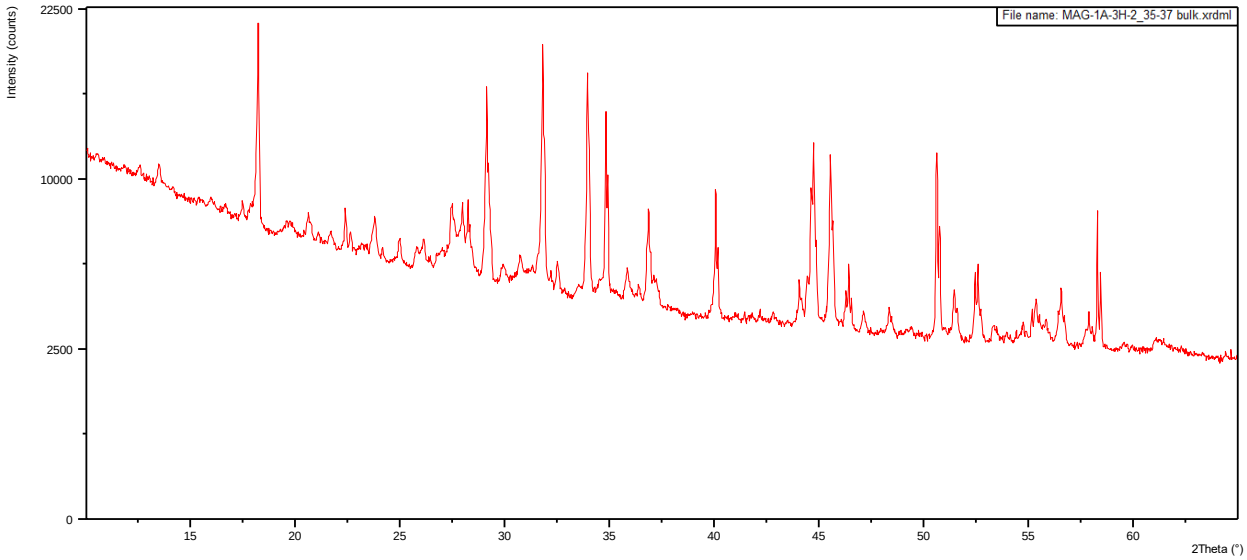
File name: MAG-1A-3H-2_35-37 bulk.xrdml
Intensity (counts)
22500
10000
2500
0
15
20
25
30
35
40
45
50
55
60
2Theta (°)

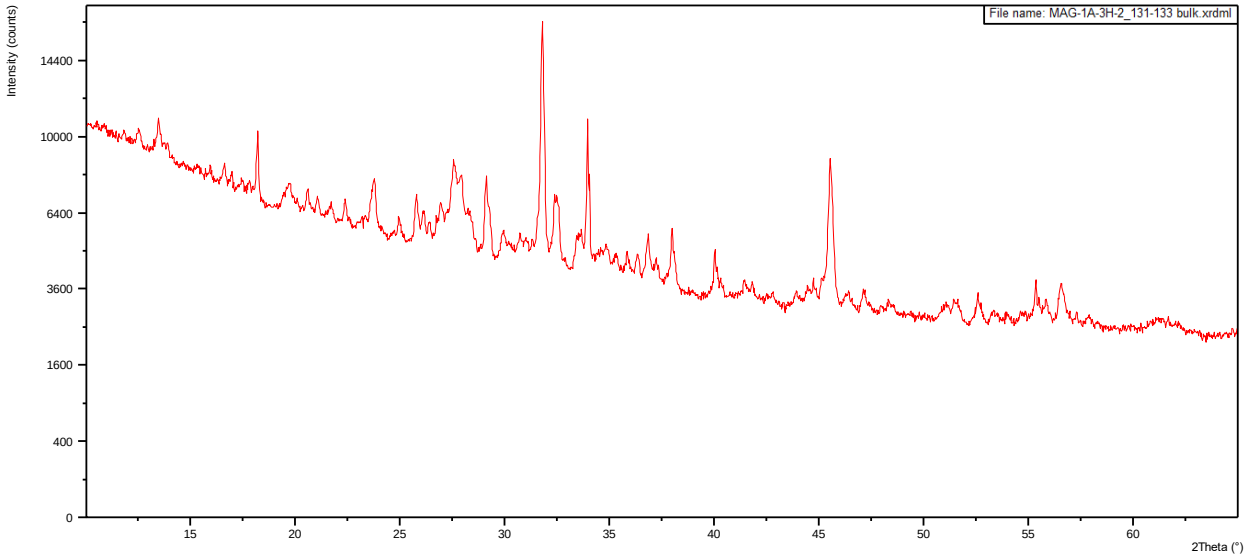
File name: MAG-1A-3H-2_131-133 bulk.xrdml
Intensity (counts)
14400
10000
6400
3600
1600
400
0
15
20
25
30
35
40
45
50
55
60
2Theta (°)

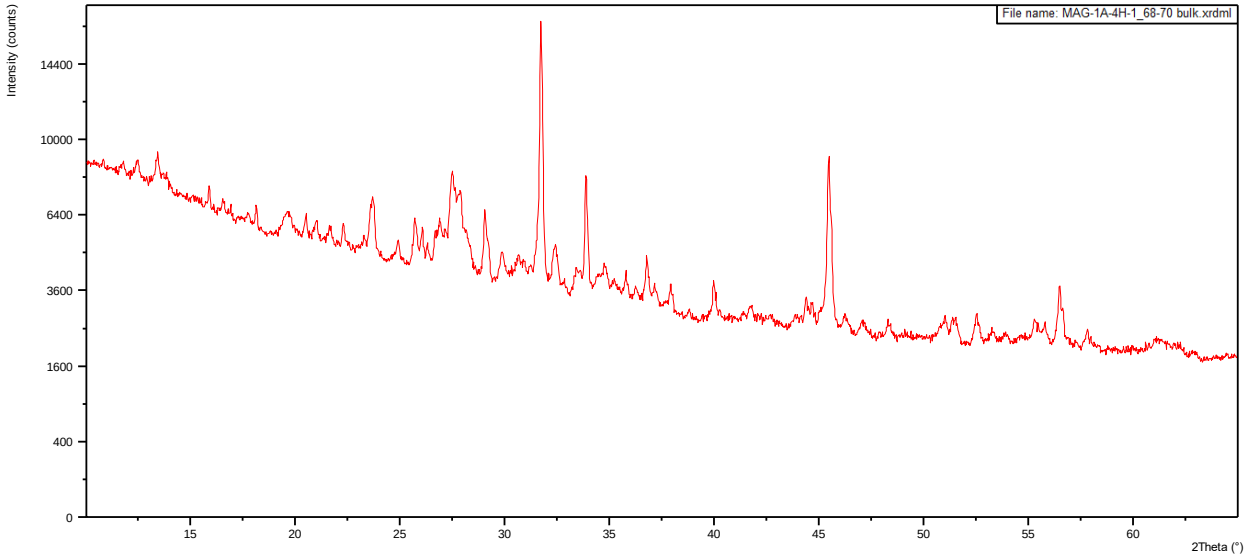
File name: MAG-1A-4H-1_68-70 bulk.xrdml
Intensity (counts)
14400
10000
6400
3600
1600
400
0
15
20
25
30
35
40
45
50
55
60
2Theta (°)

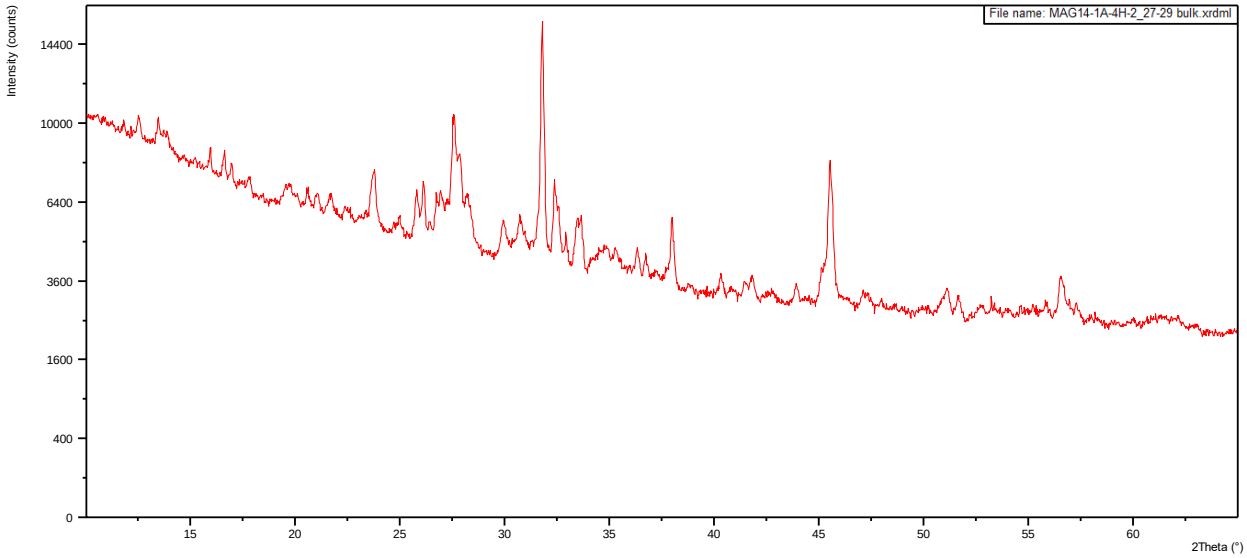
File name: MAG14-1A-4H-2_27-29 bulk.xrdml
Intensity (counts)
14400
10000
6400
3600
1600
400
0
15
20
25
30
35
40
45
50
55
60
2Theta (°)

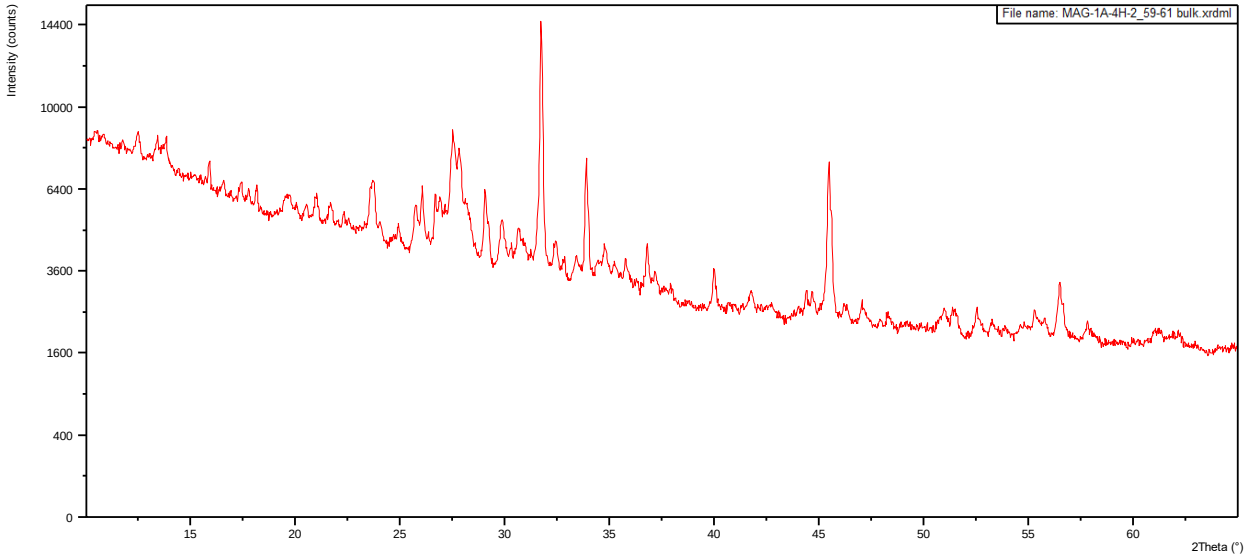
File name: MAG-1A-4H-2_59-61 bulk.xrdml
Intensity (counts)
14400
10000
6400
3600
1600
400
0
15
20
25
30
35
40
45
50
55
60
2Theta (°)

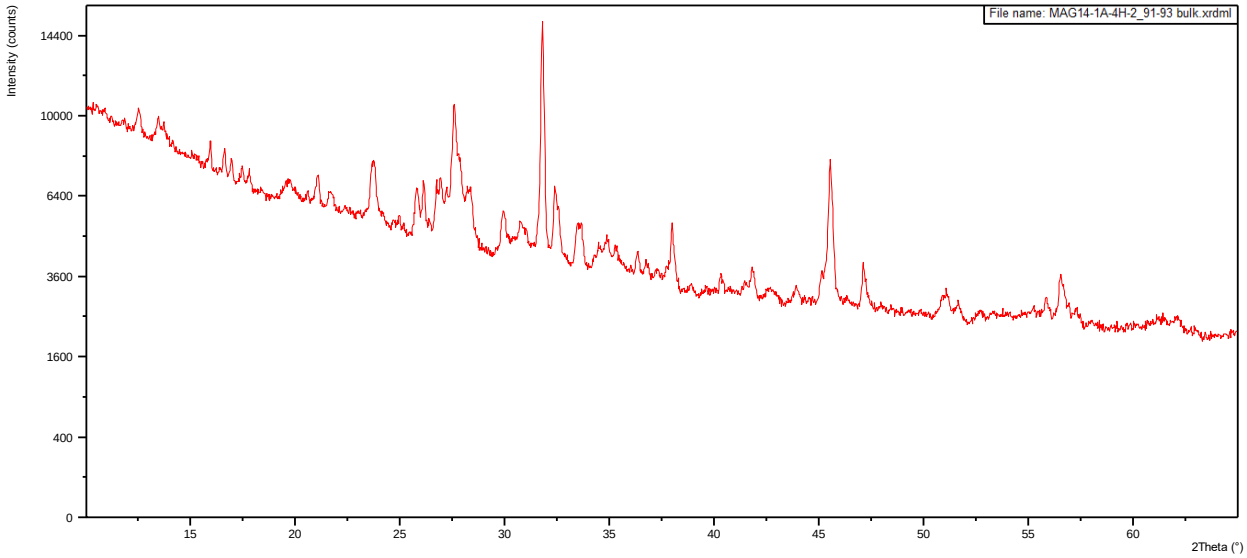
File name: MAG14-1A-4H-2_91-93 bulk.xrdml
Intensity (counts)
14400
10000
6400
3600
1600
400
0
15
20
25
30
35
40
45
50
55
60
2Theta (°)

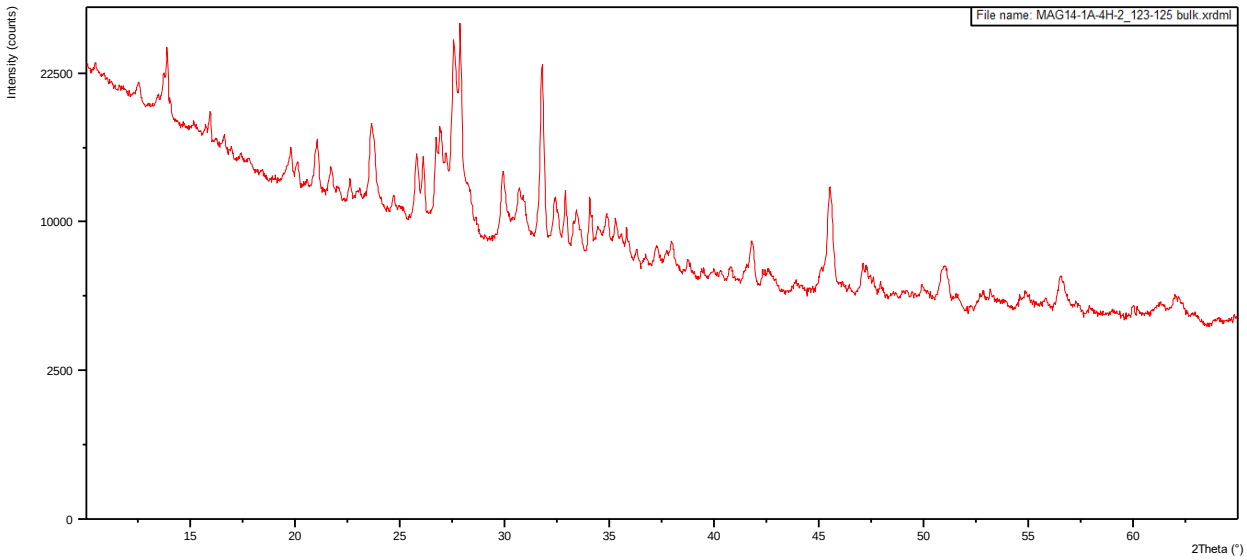
File name: MAG14-1A-4H-2_123-125 bulk.xrdml
Intensity (counts)
22500
10000
2500
0
15
20
25
30
35
40
45
50
55
60
2Theta (°)

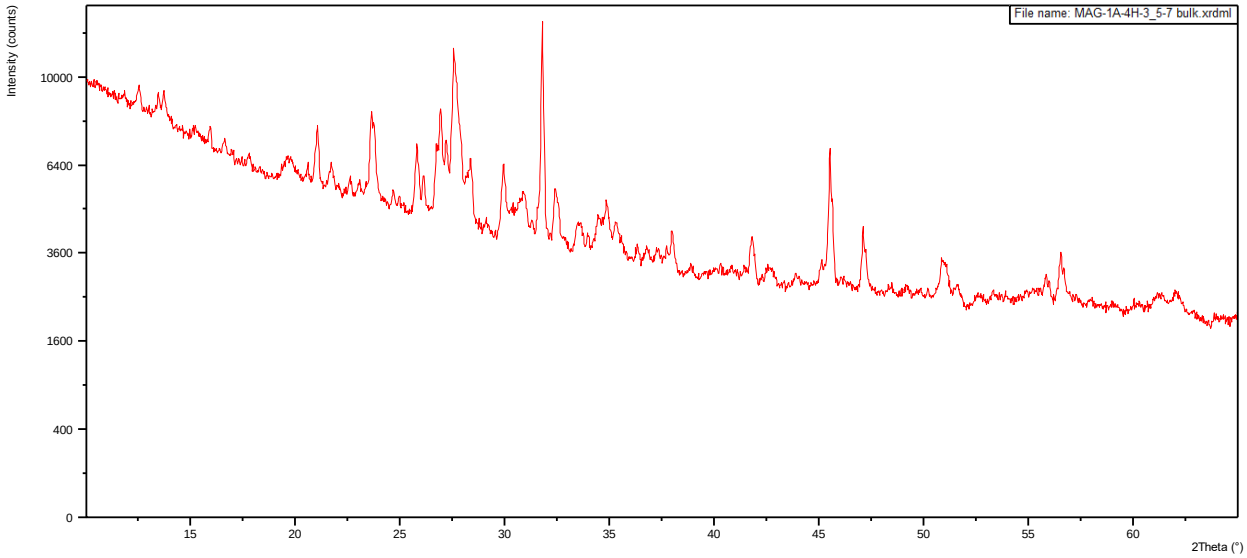
File name: MAG-1A-4H-3_5-7 bulk.xrdml
Intensity (counts)
10000
6400
3600
1600
400
0
15
20
25
30
35
40
45
50
55
60
2Theta (°)

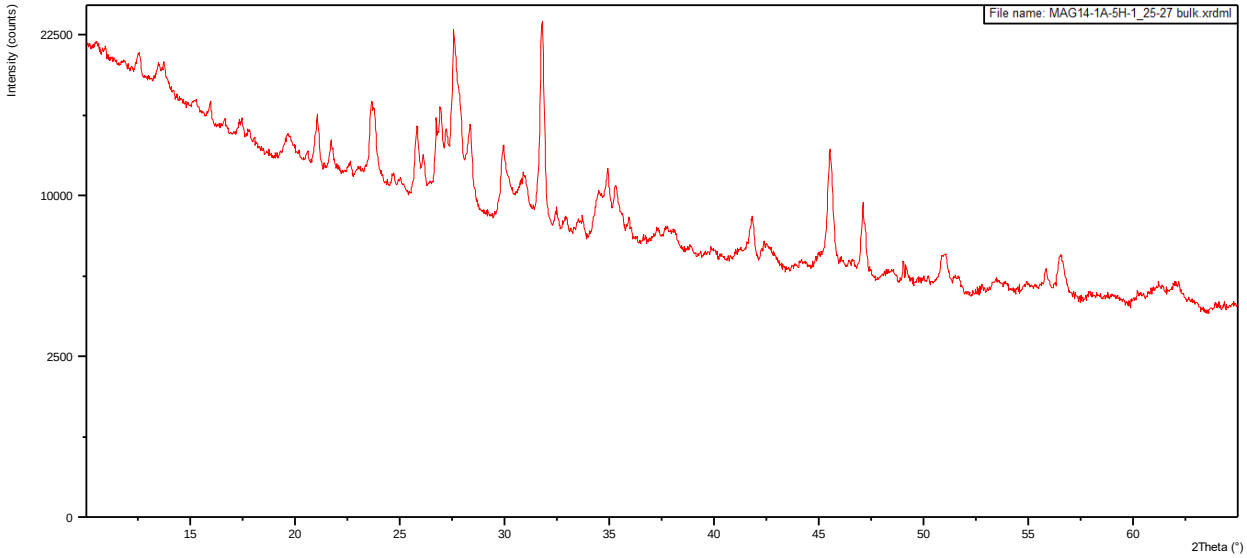
File name: MAG14-1A-5H-1_25-27 bulk.xrdml
Intensity (counts)
22500
10000
2500
0
15
20
25
30
35
40
45
50
55
60
2Theta (°)

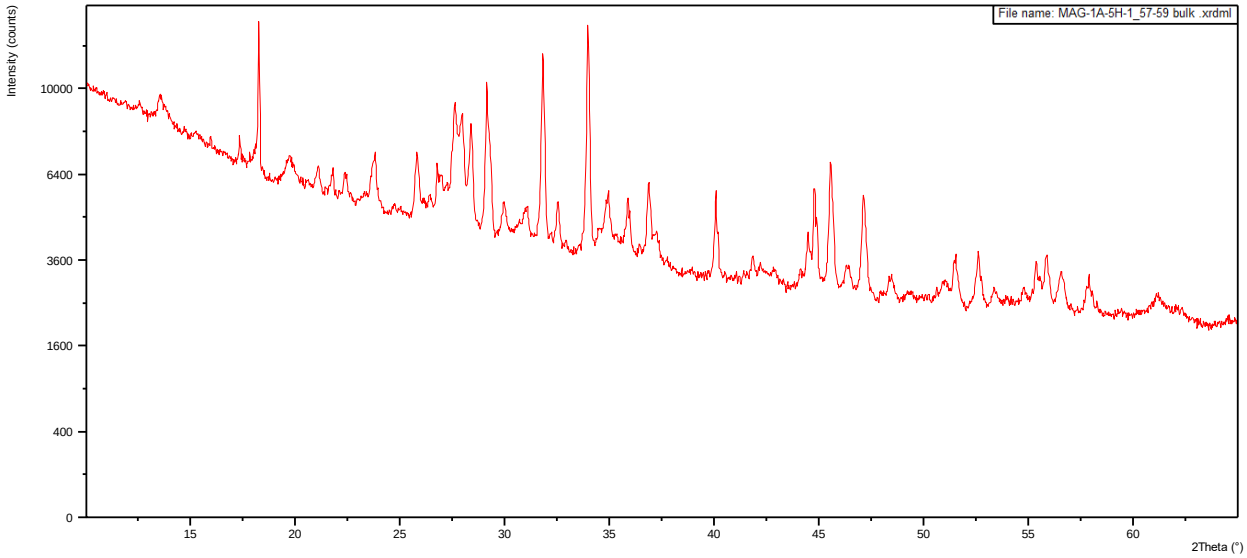
File name: MAG-1A-5H-1_57-59 bulk .xrdml
Intensity (counts)
10000
6400
3600
1600
400
0
15
20
25
30
35
40
45
50
55
60
2Theta (°)

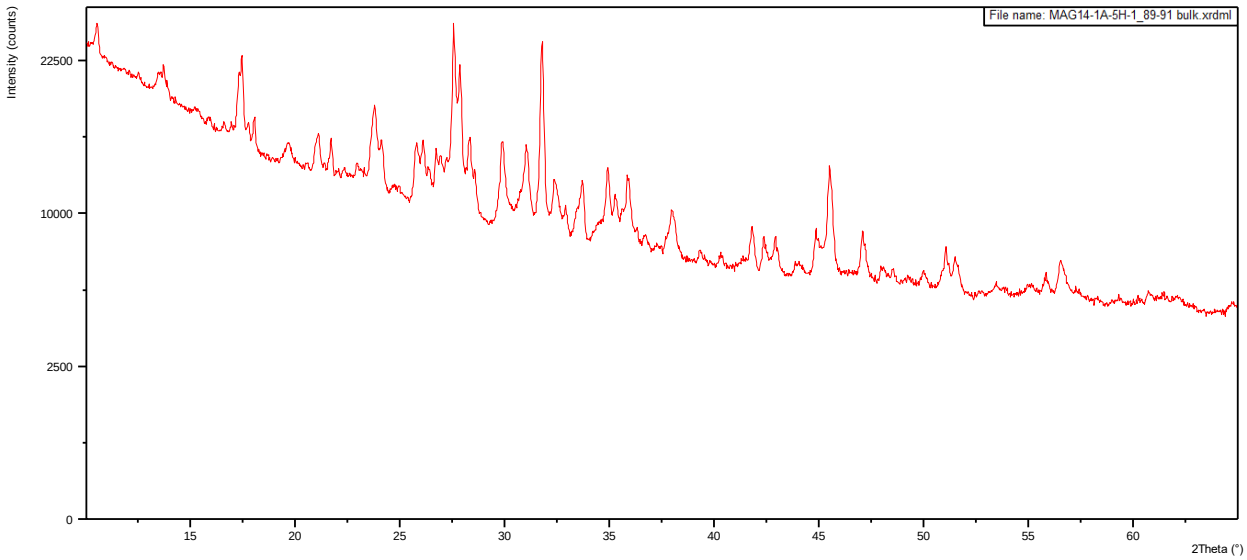
File name: MAG14-1A-5H-1_89-91 bulk.xrdml
Intensity (counts)
22500
10000
2500
0
15
20
25
30
35
40
45
50
55
60
2Theta (°)

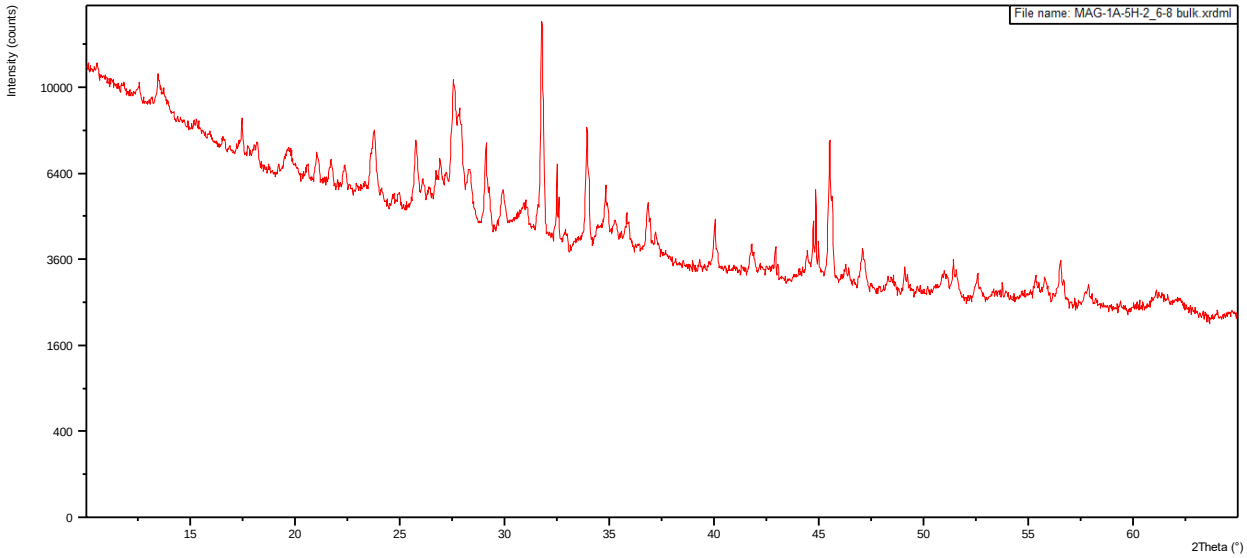
File name: MAG-1A-5H-2_6-8 bulk.xrdml
Intensity (counts)
10000
6400
3600
1600
400
0
15
20
25
30
35
40
45
50
55
60
2Theta (°)

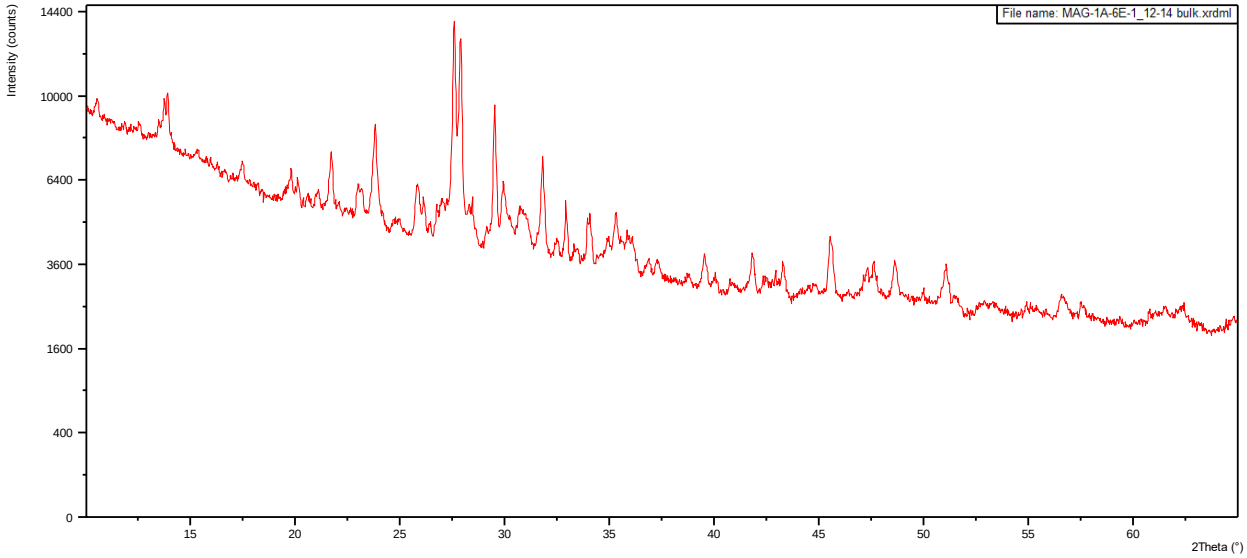
File name: MAG-1A-6E-1_12-14 bulk.xrdml
Intensity (counts)
14400
10000
6400
3600
1600
400
0
15
20
25
30
35
40
45
50
55
60
2Theta (°)

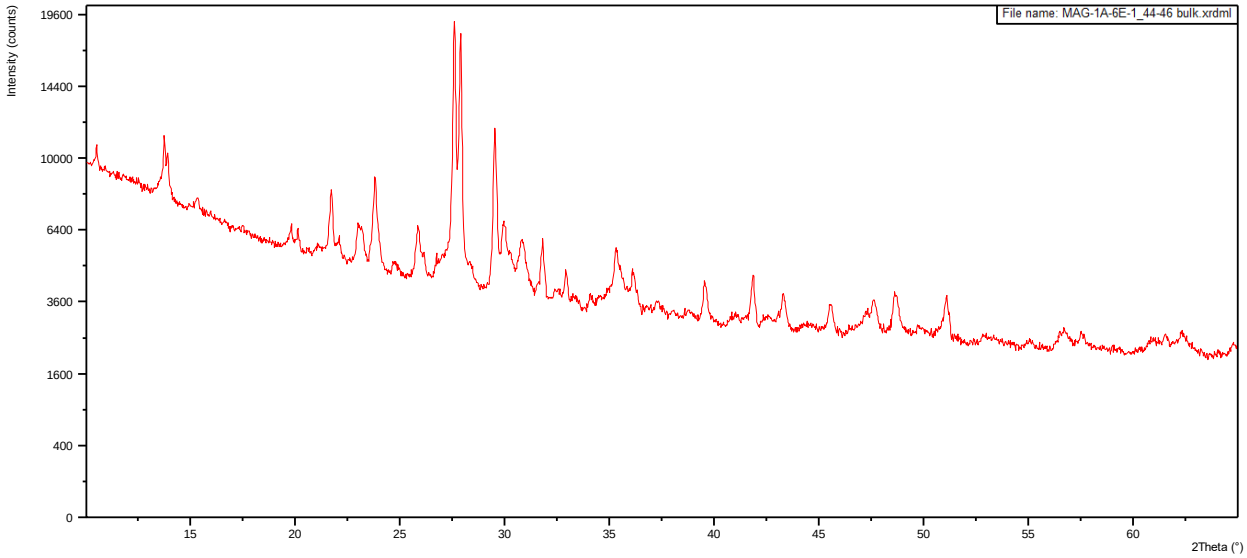
File name: MAG-1A-6E-1_44-46 bulk.xrdml
Intensity (counts)
19600
14400
10000
6400
3600
1600
400
0
15
20
25
30
35
40
45
50
55
60
2Theta (°)

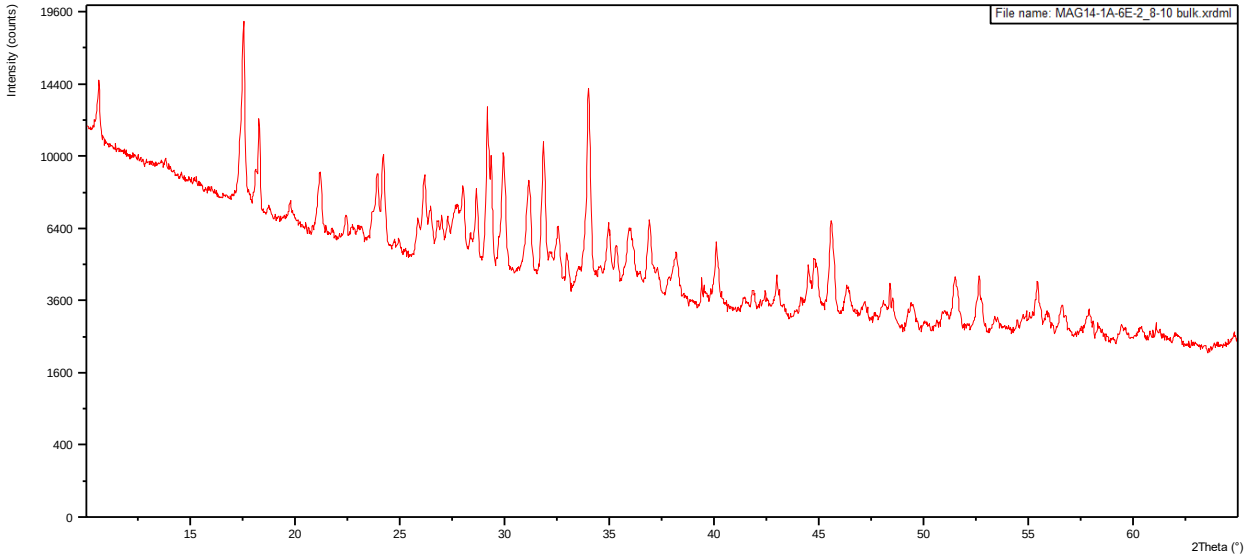
File name: MAG14-1A-6E-2_8-10 bulk.xrdml
Intensity (counts)
19600
14400
10000
6400
3600
1600
400
0
15
20
25
30
35
40
45
50
55
60
2Theta (°)

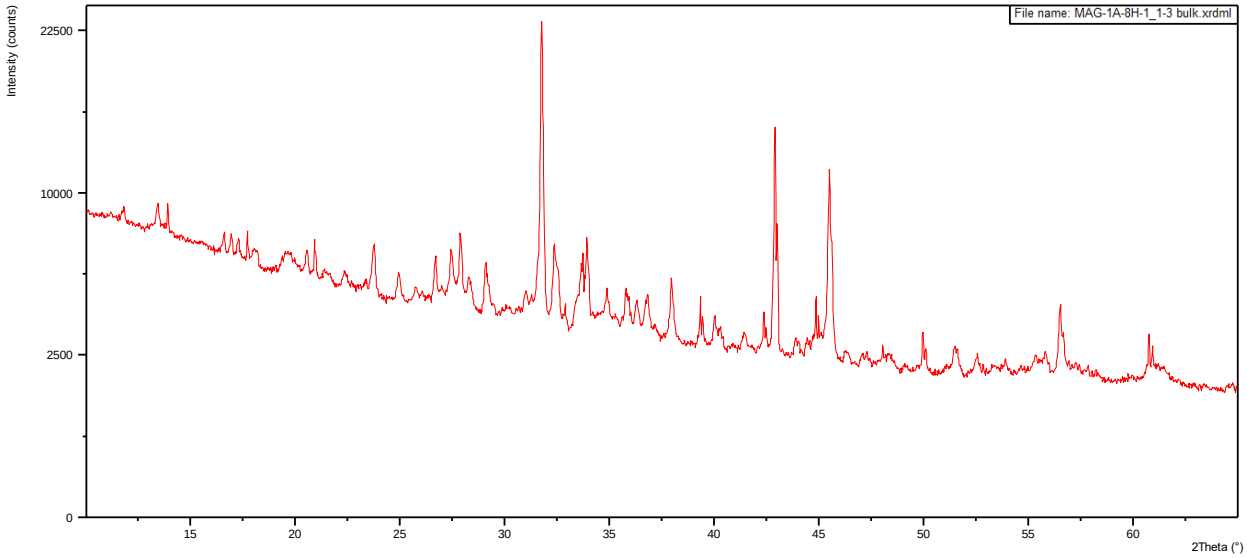
File name: MAG-1A-8H-1_1-3 bulk.xrdml
Intensity (counts)
22500
10000
2500
0
15
20
25
30
35
40
45
50
55
60
2Theta (°)

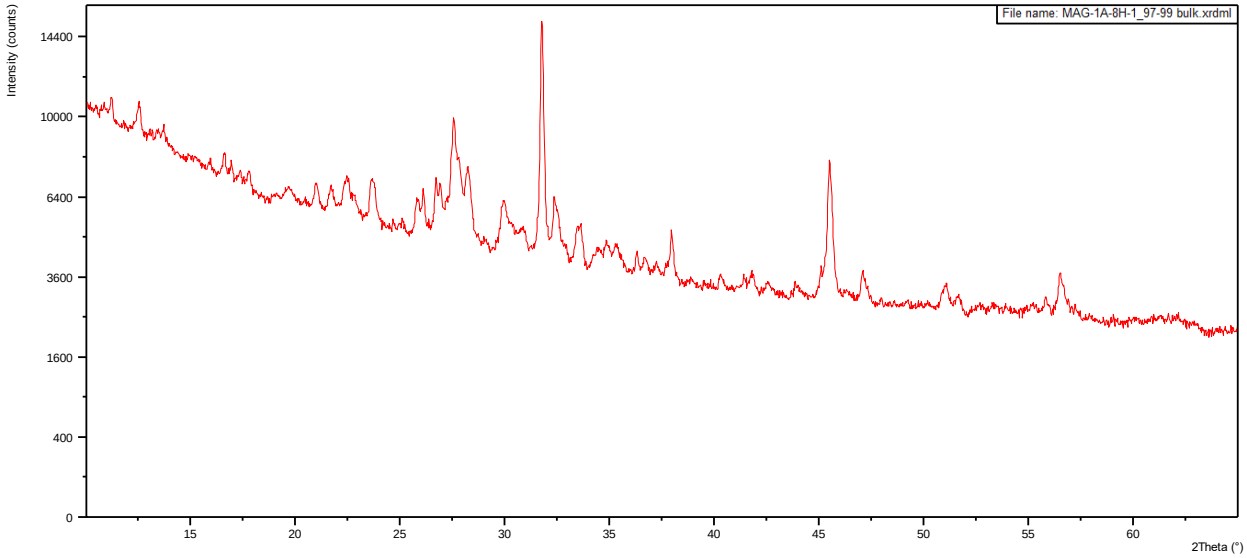
File name: MAG-1A-8H-1_97-99 bulk.xrdml
Intensity (counts)
14400
10000
6400
3600
1600
400
0
15
20
25
30
35
40
45
50
55
60
2Theta (°)

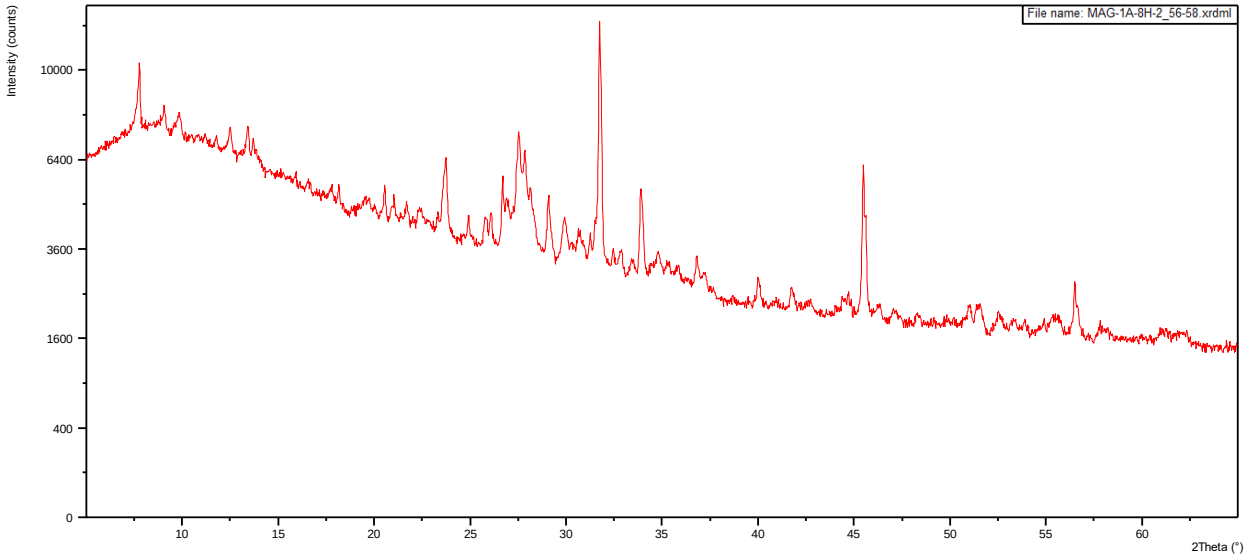
File name: MAG-1A-8H-2_56-58.xrdml
Intensity (counts)
10000
6400
3600
1600
400
0
10
15
20
25
30
35
40
45
50
55
60
2Theta (°)

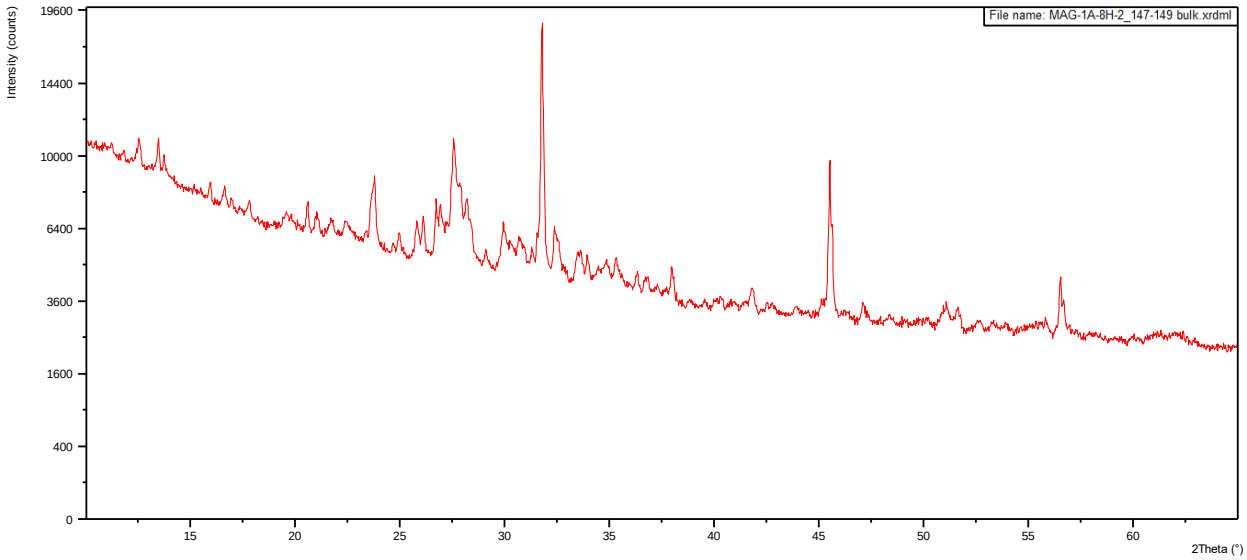
File name: MAG-1A-8H-2_147-149 bulk.xrdml
Intensity (counts)
19600
14400
10000
6400
3600
1600
400
0
15
20
25
30
35
40
45
50
55
60
2Theta (°)

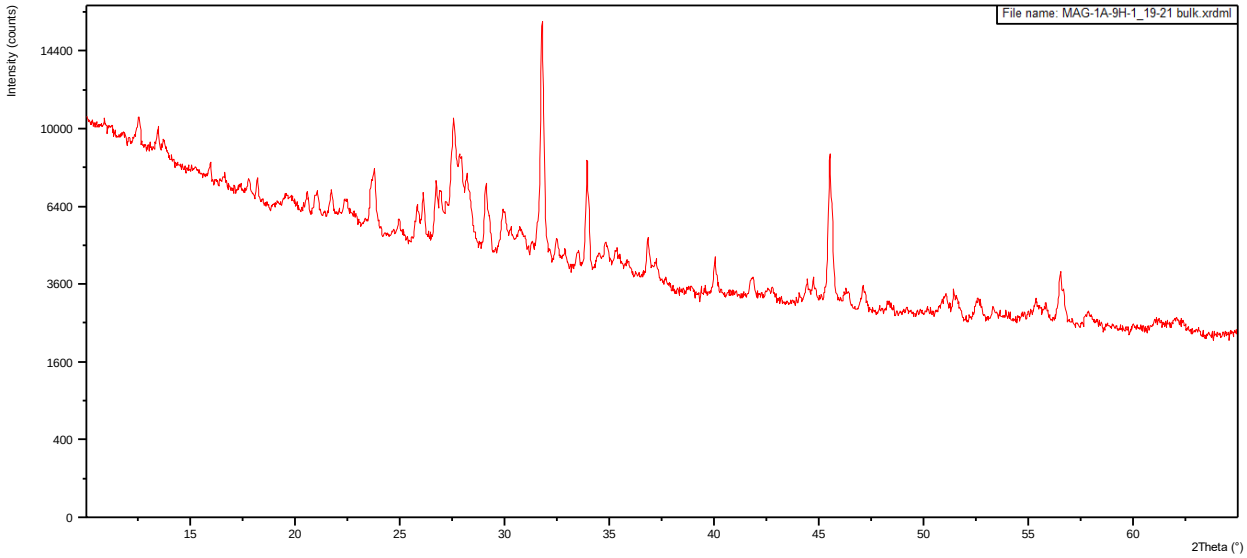
File name: MAG-1A-9H-1_19-21 bulk.xrdml
Intensity (counts)
14400
10000
6400
3600
1600
400
0
15
20
25
30
35
40
45
50
55
60
2Theta (°)

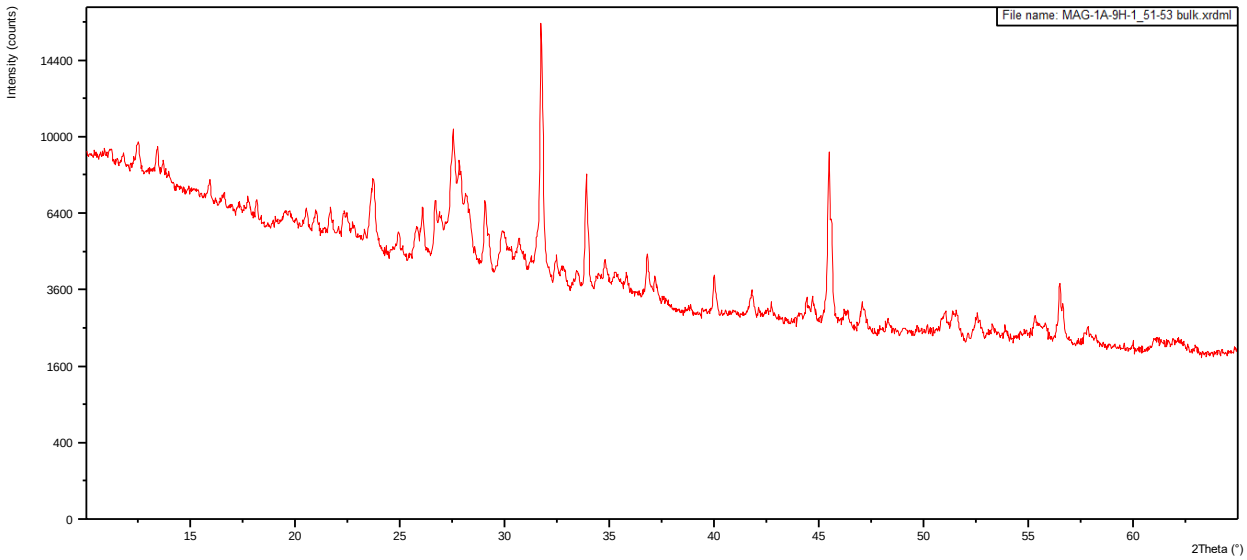
File name: MAG-1A-9H-1_51-53 bulk.xrdml
Intensity (counts)
14400
10000
6400
3600
1600
400
0
15
20
25
30
35
40
45
50
55
60
2Theta (°)

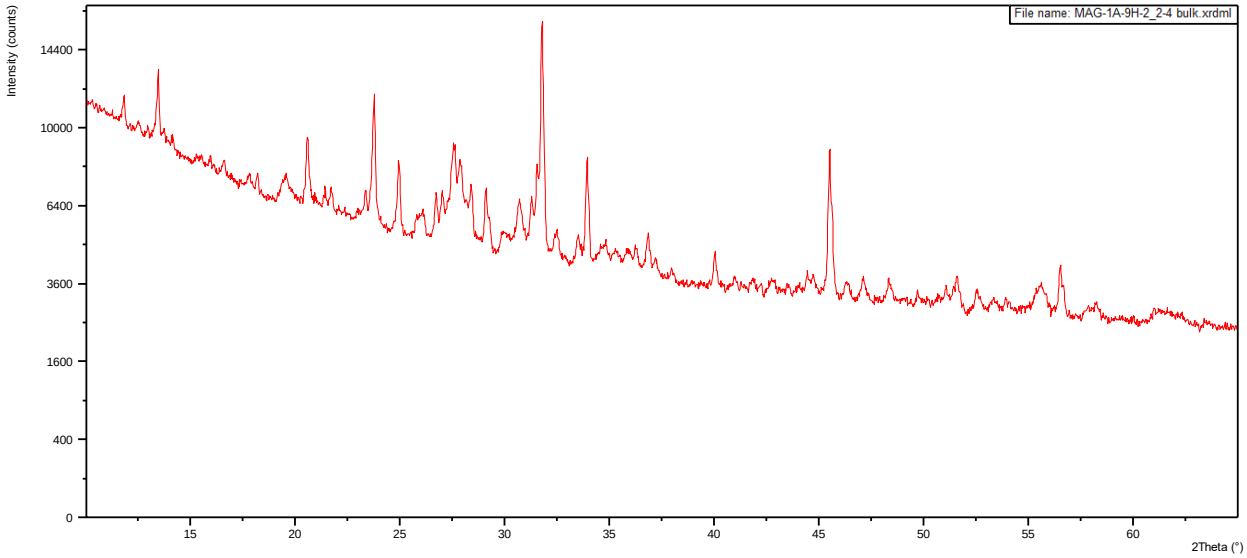
File name: MAG-1A-9H-2_2-4 bulk.xrdml
Intensity (counts)
14400
10000
6400
3600
1600
400
0
15
20
25
30
35
40
45
50
55
60
2Theta (°)

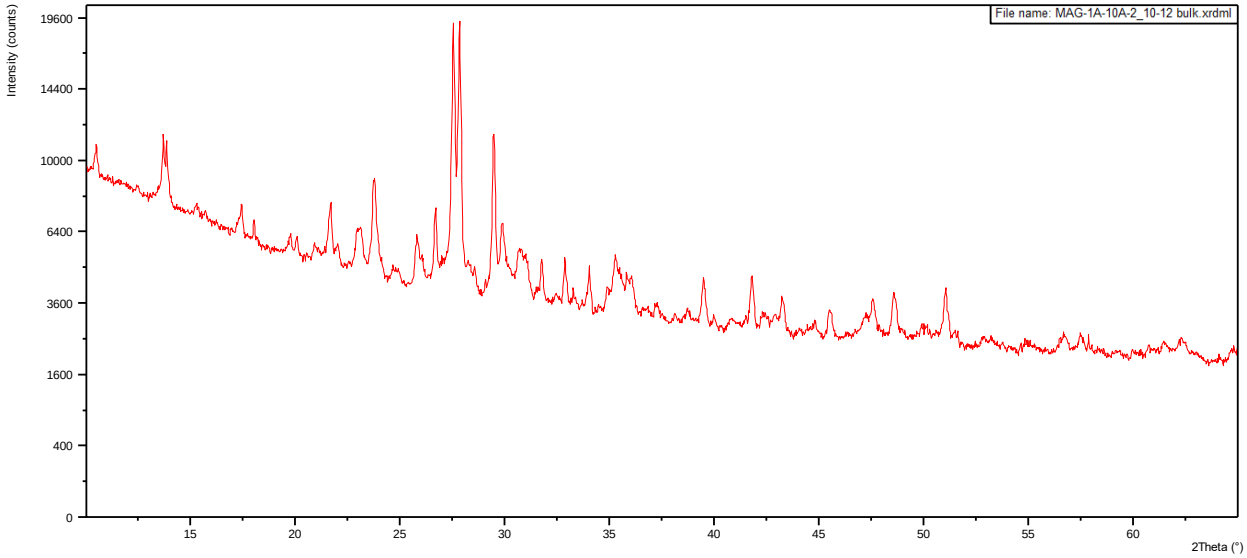
File name: MAG-1A-10A-2_10-12 bulk.xrdml
Intensity (counts)
19600
14400
10000
6400
3600
1600
400
0
15
20
25
30
35
40
45
50
55
60
2Theta (°)

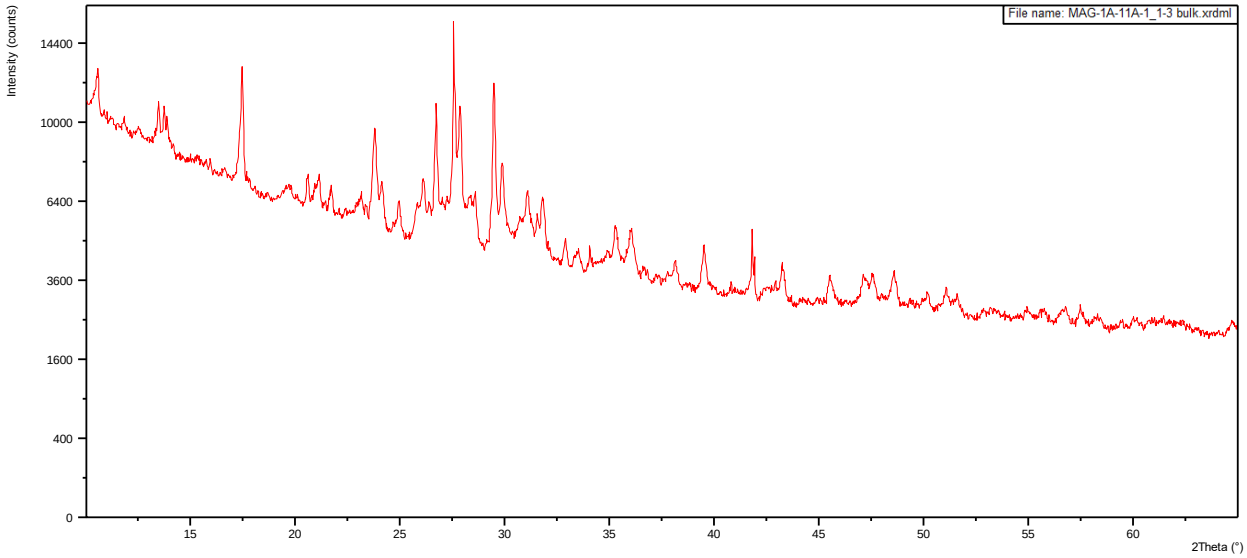
File name: MAG-1A-11A-1_1-3 bulk.xrdml
Intensity (counts)
14400
10000
6400
3600
1600
400
0
15
20
25
30
35
40
45
50
55
60
2Theta (°)

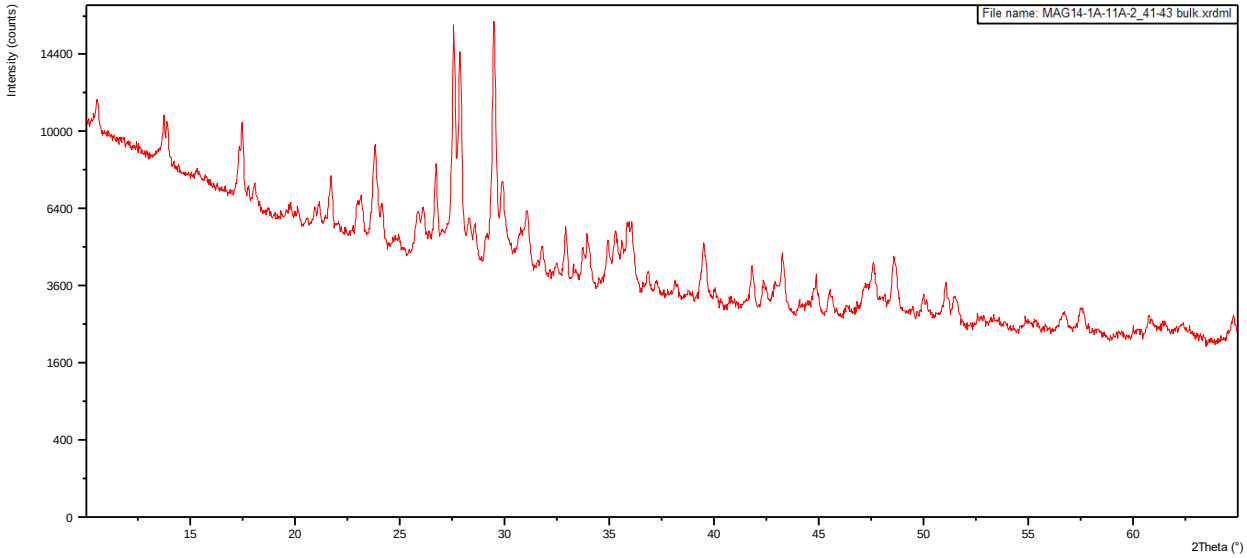
File name: MAG14-1A-11A-2_41-43 bulk.xrdml
Intensity (counts)
14400
10000
6400
3600
1600
400
0
15
20
25
30
35
40
45
50
55
60
2Theta (°)

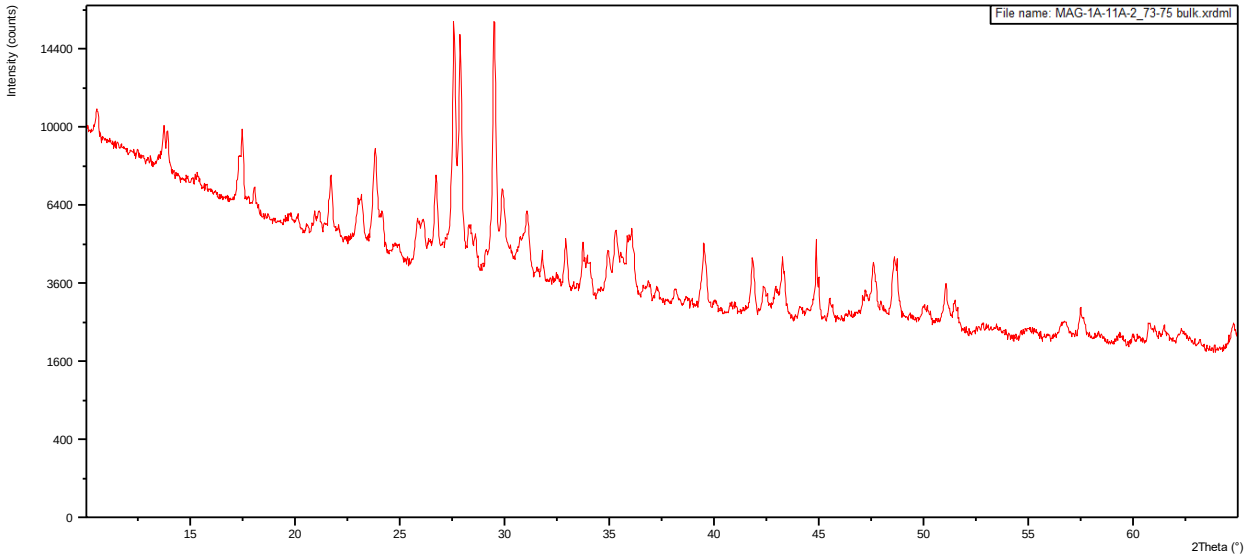
File name: MAG-1A-11A-2_73-75 bulk.xrdml
Intensity (counts)
14400
10000
6400
3600
1600
400
0
15
20
25
30
35
40
45
50
55
60
2Theta (°)

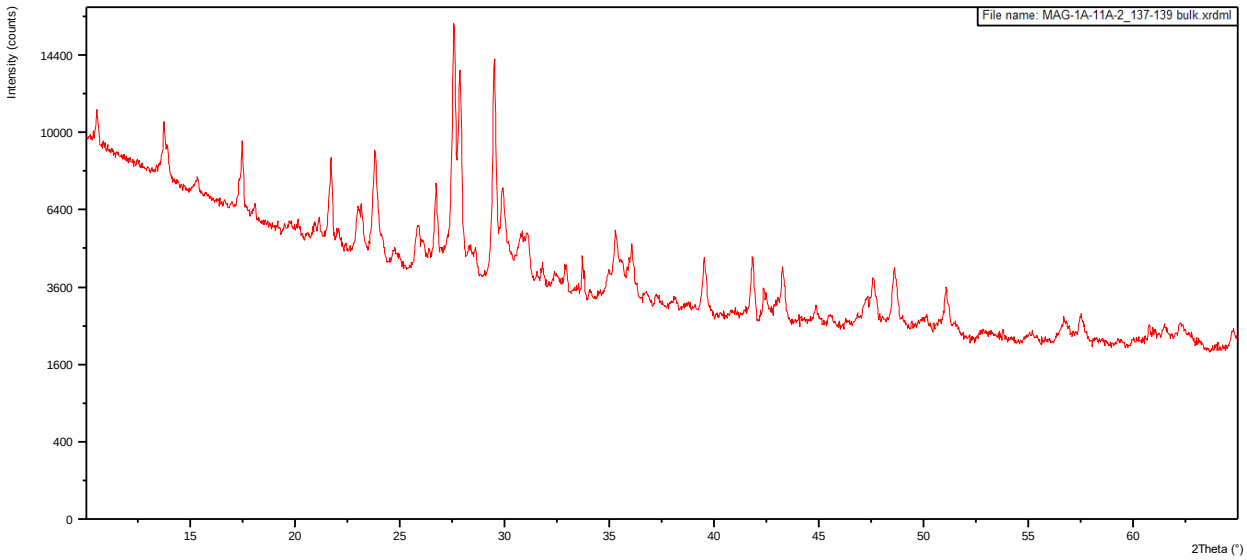
File name: MAG-1A-11A-2_137-139 bulk.xrdml
Intensity (counts)
14400
10000
6400
3600
1600
400
0
15
20
25
30
35
40
45
50
55
60
2Theta (°)

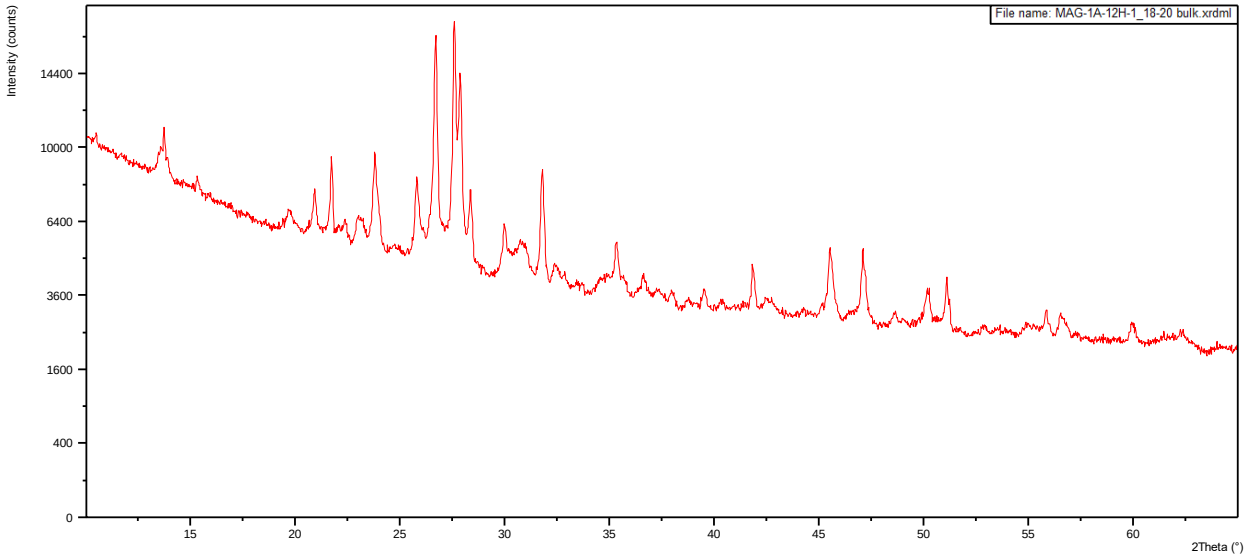
File name: MAG-1A-12H-1_18-20 bulk.xrdml
Intensity (counts)
14400
10000
6400
3600
1600
400
0
15
20
25
30
35
40
45
50
55
60
2Theta (°)

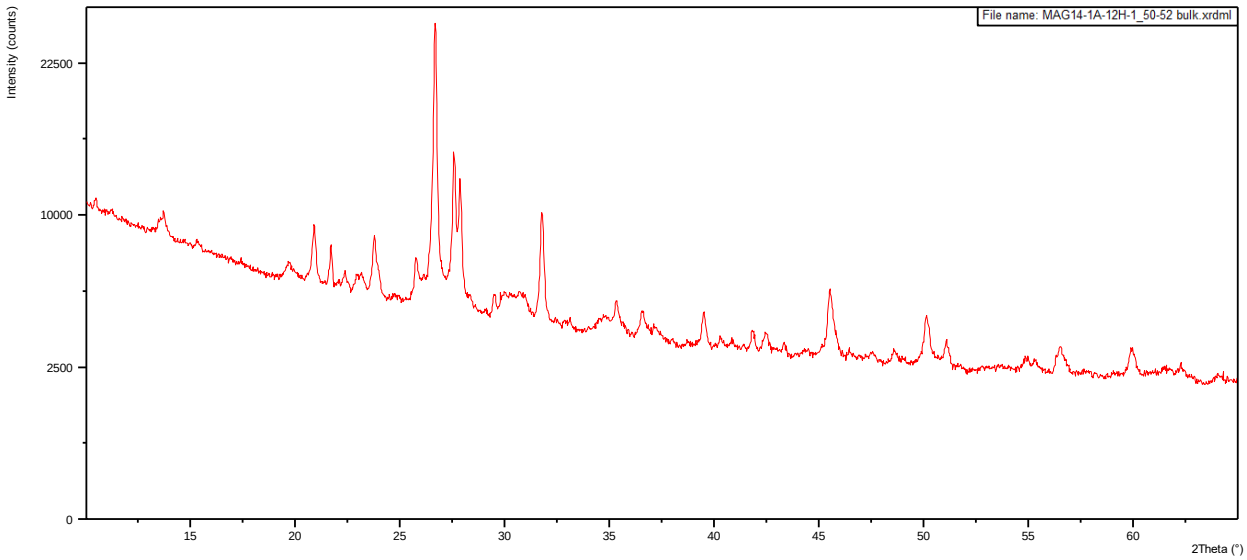
File name: MAG14-1A-12H-1_50-52 bulk.xrdml
Intensity (counts)
22500
10000
2500
0
15
20
25
30
35
40
45
50
55
60
2Theta (°)

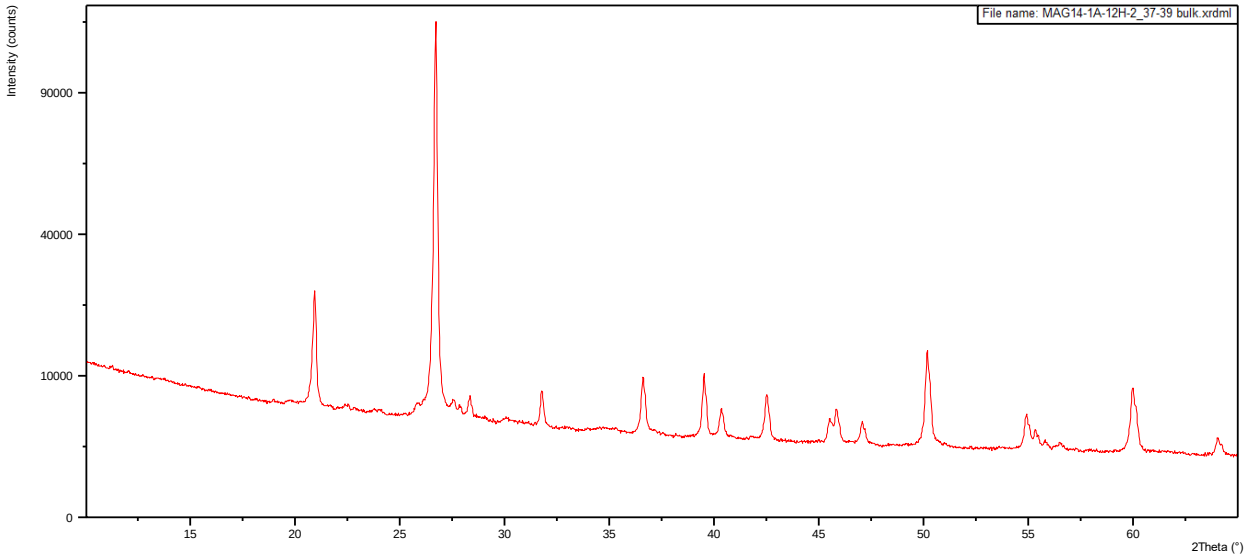
File name: MAG14-1A-12H-2_37-39 bulk.xrdml
Intensity (counts)
90000
40000
10000
0
15
20
25
30
35
40
45
50
55
60
2Theta (°)

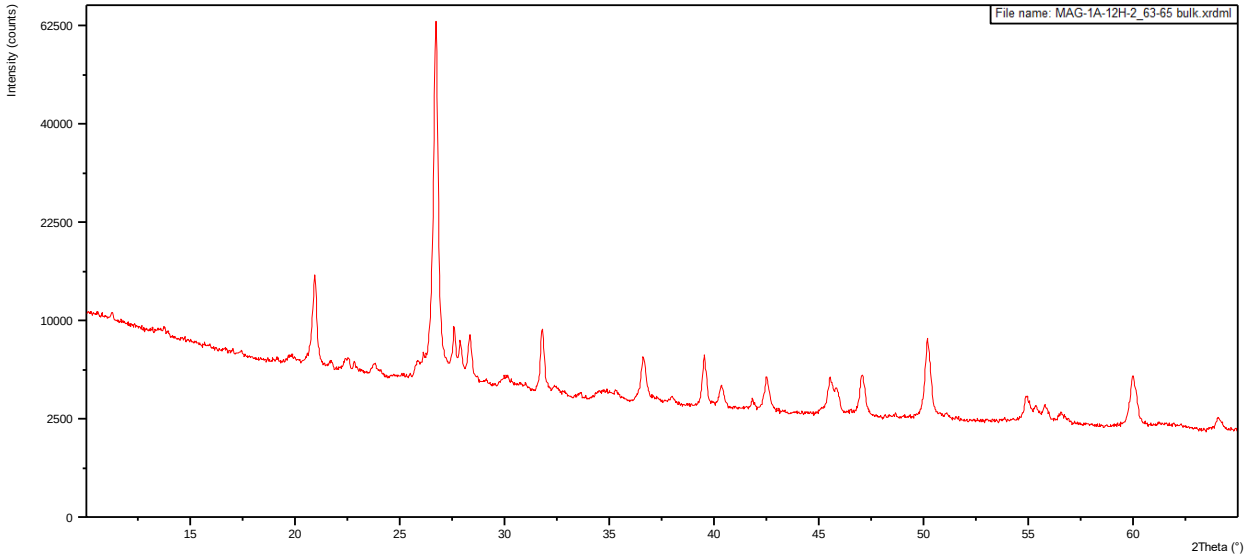
File name: MAG-1A-12H-2_63-65 bulk.xrdml
Intensity (counts)
62500
40000
22500
10000
2500
0
15
20
25
30
35
40
45
50
55
60
2Theta (°)

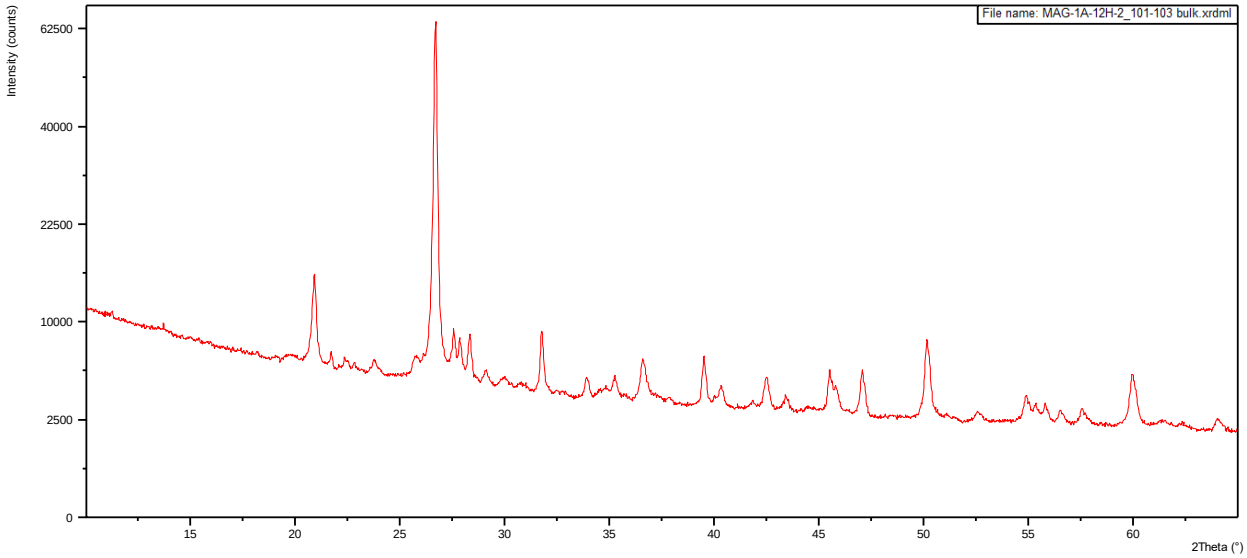
File name: MAG-1A-12H-2_101-103 bulk.xrdml
Intensity (counts)
62500
40000
22500
10000
2500
0
15
20
25
30
35
40
45
50
55
60
2Theta (°)

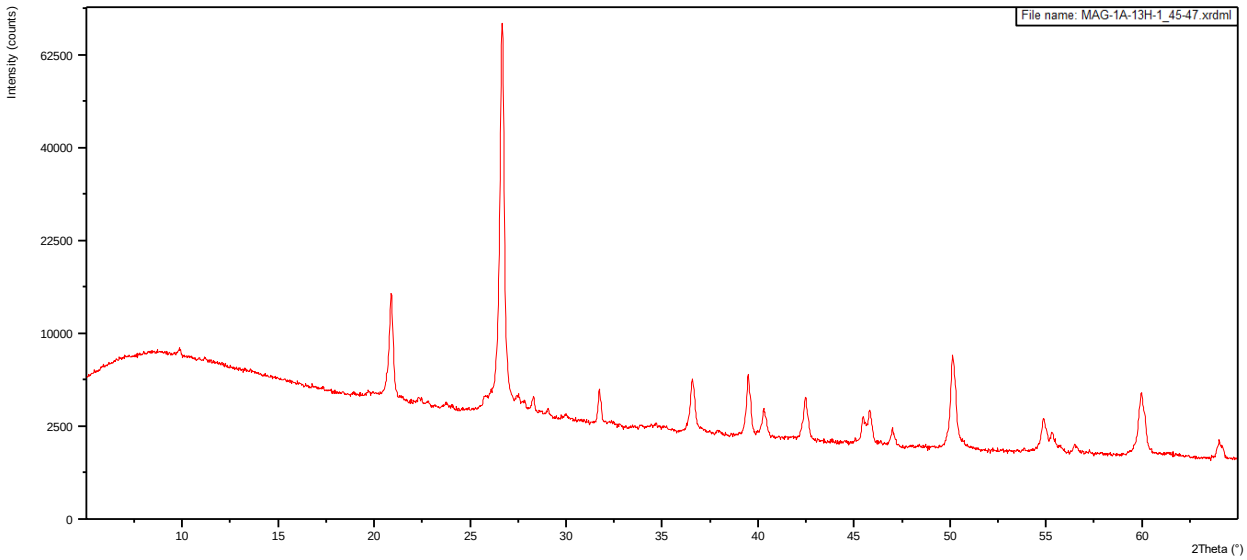
File name: MAG-1A-13H-1_45-47.xrdml
Intensity (counts)
62500
40000
22500
10000
2500
0
10
15
20
25
30
35
40
45
50
55
60
2Theta (°)

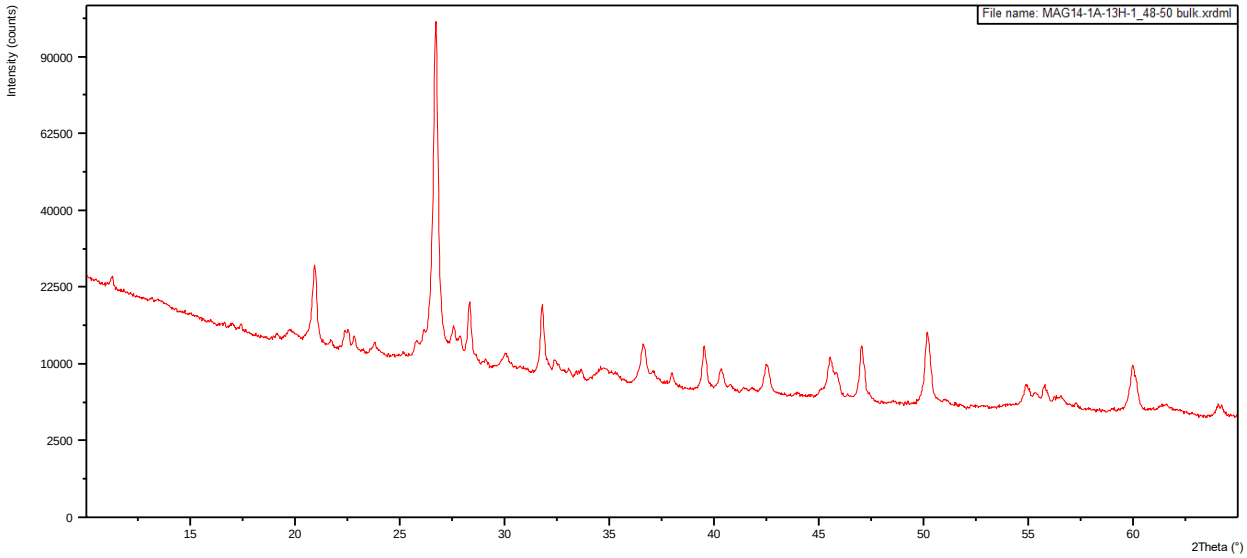
File name: MAG14-1A-13H-1_48-50 bulk.xrdml
Intensity (counts)
90000
62500
40000
22500
10000
2500
0
15
20
25
30
35
40
45
50
55
60
2Theta (°)

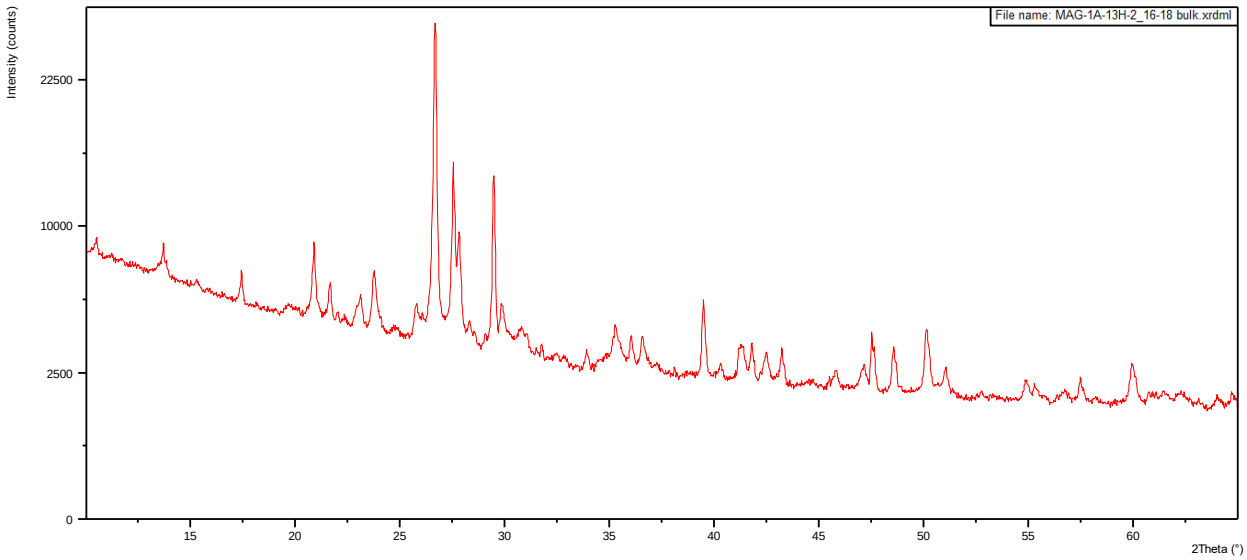
File name: MAG-1A-13H-2_16-18 bulk.xrdml
Intensity (counts)
22500
10000
2500
0
15
20
25
30
35
40
45
50
55
60
2Theta (°)

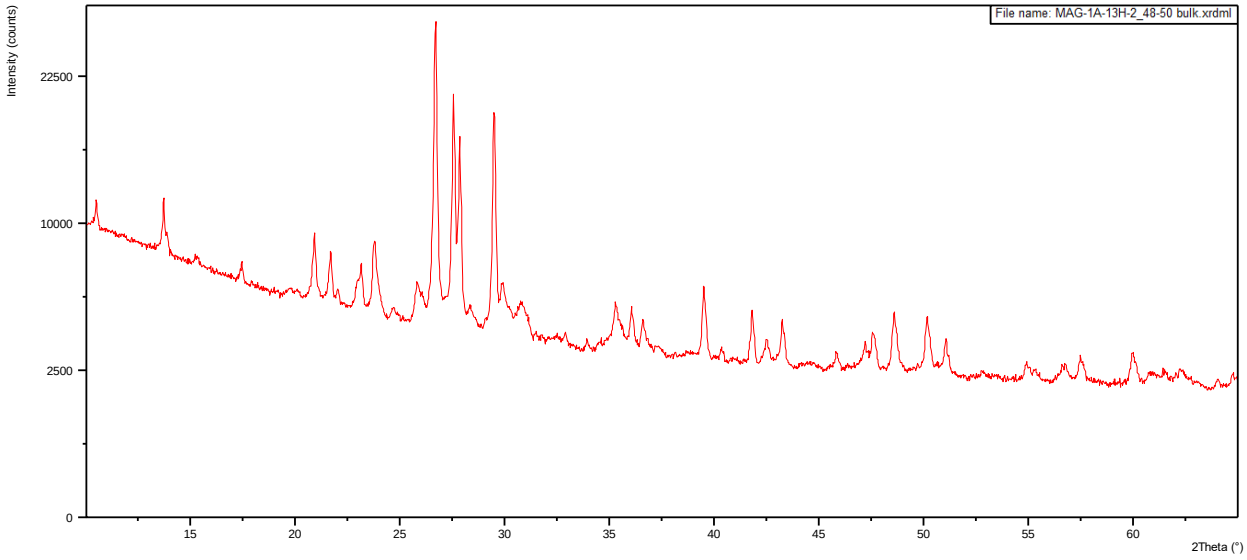
File name: MAG-1A-13H-2_48-50 bulk.xrdml
Intensity (counts)
22500
10000
2500
0
15
20
25
30
35
40
45
50
55
60
2Theta (°)

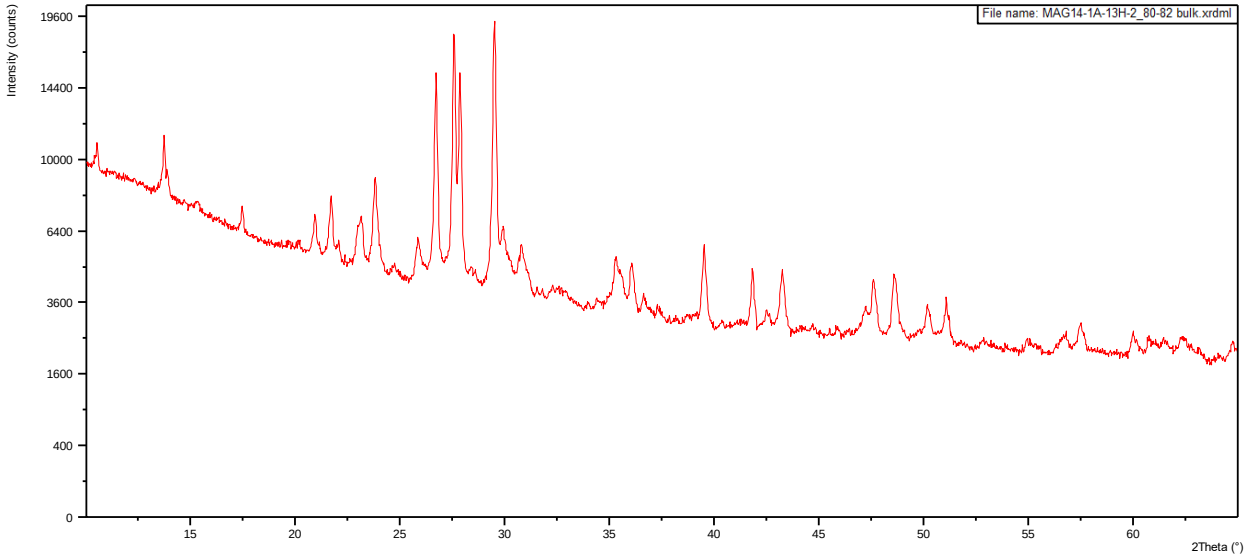
File name: MAG14-1A-13H-2_80-82 bulk.xrdml
Intensity (counts)
19600
14400
10000
6400
3600
1600
400
0
15
20
25
30
35
40
45
50
55
60
2Theta (°)

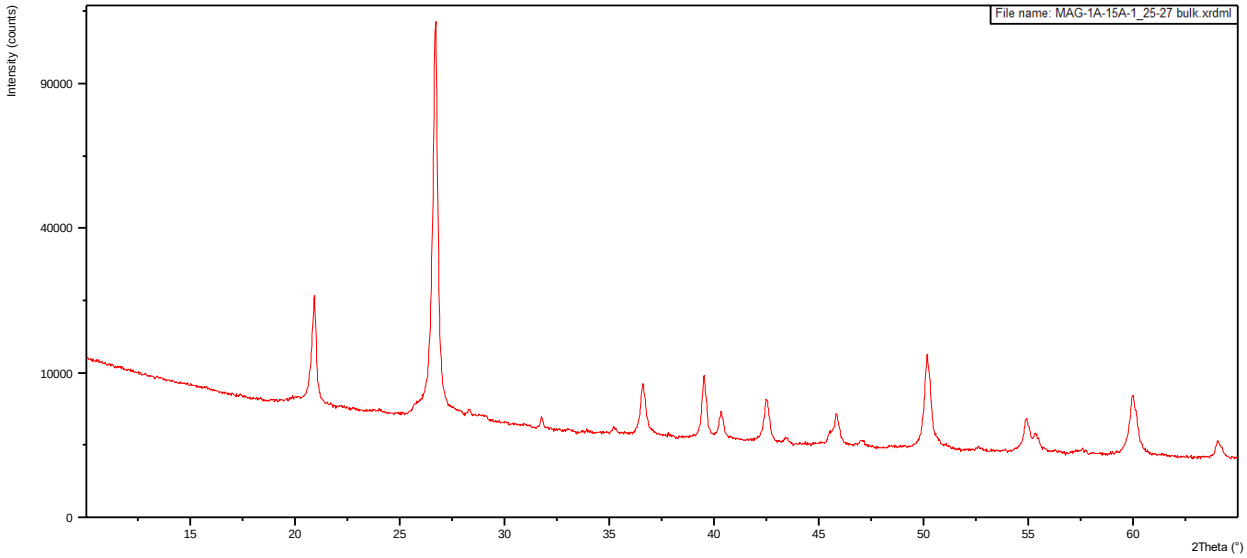
File name: MAG-1A-15A-1_25-27 bulk.xrdml
Intensity (counts)
90000
40000
10000
0
15
20
25
30
35
40
45
50
55
60
2Theta (°)

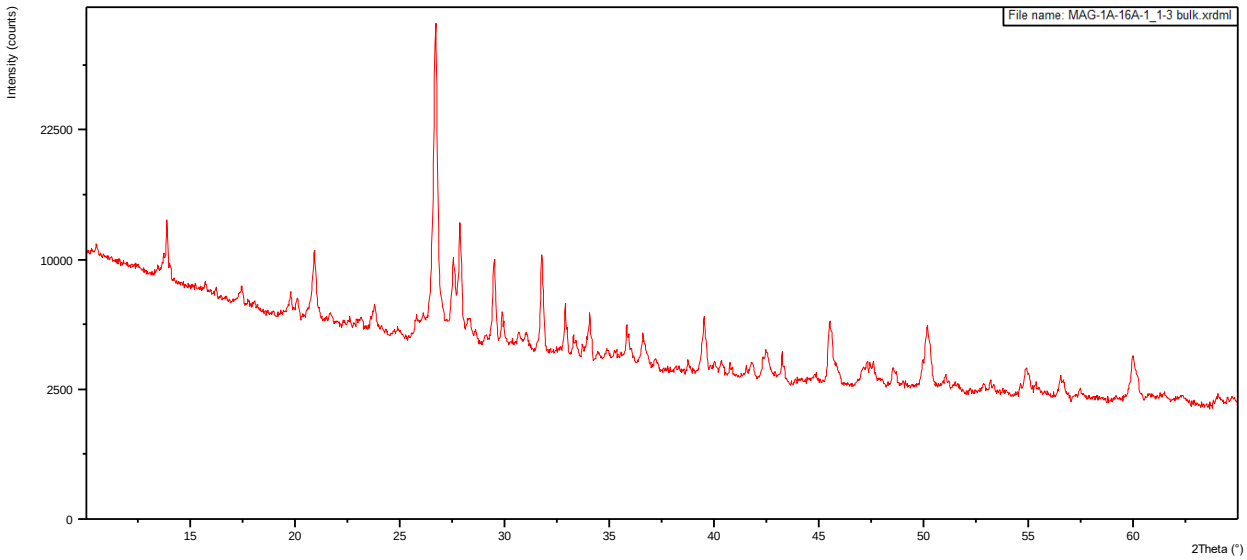
File name: MAG-1A-16A-1_1-3 bulk.xrdml
Intensity (counts)
22500
10000
2500
0
15
20
25
30
35
40
45
50
55
60
2Theta (°)

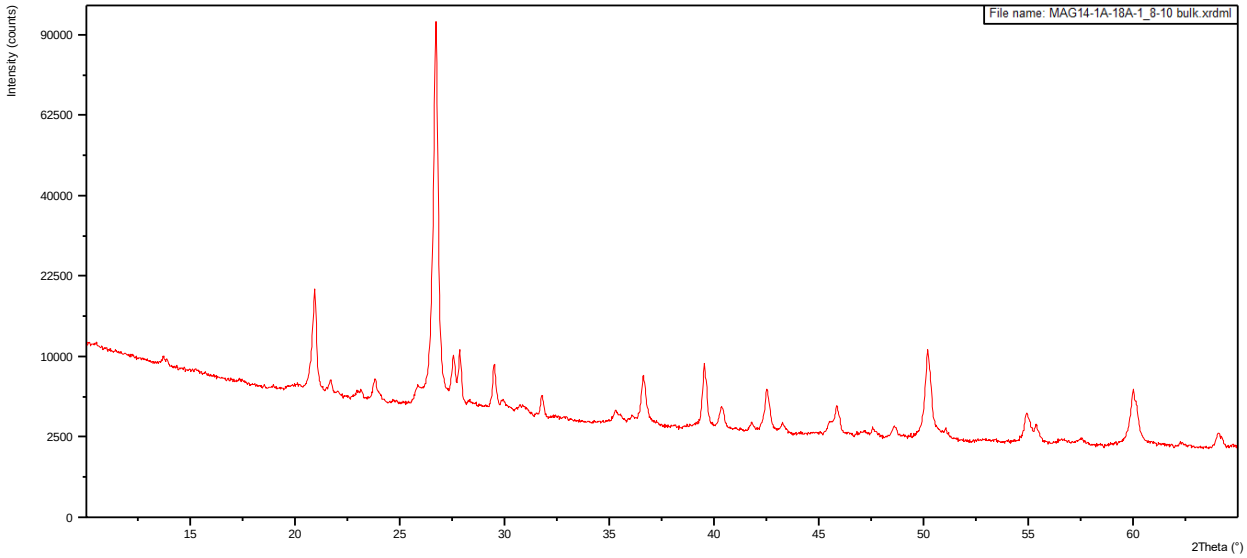
File name: MAG14-1A-18A-1_8-10 bulk.xrdml
Intensity (counts)
90000
62500
40000
22500
10000
2500
0
15
20
25
30
35
40
45
50
55
60
2Theta (°)

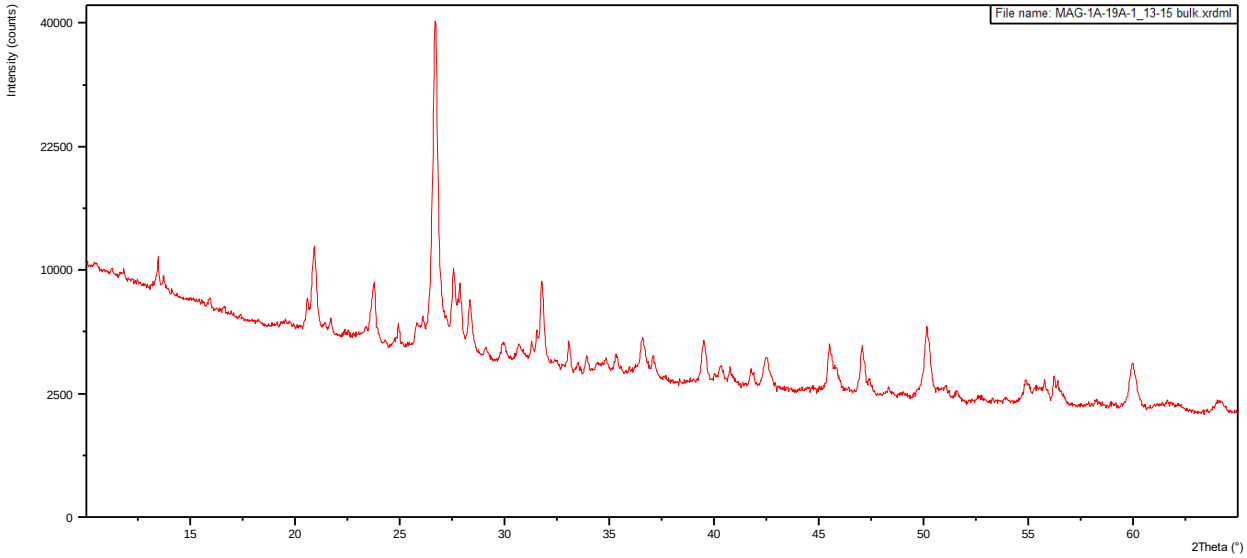
File name: MAG-1A-19A-1_13-15 bulk.xrdml
Intensity (counts)
40000
22500
10000
2500
0
15
20
25
30
35
40
45
50
55
60
2Theta (°)

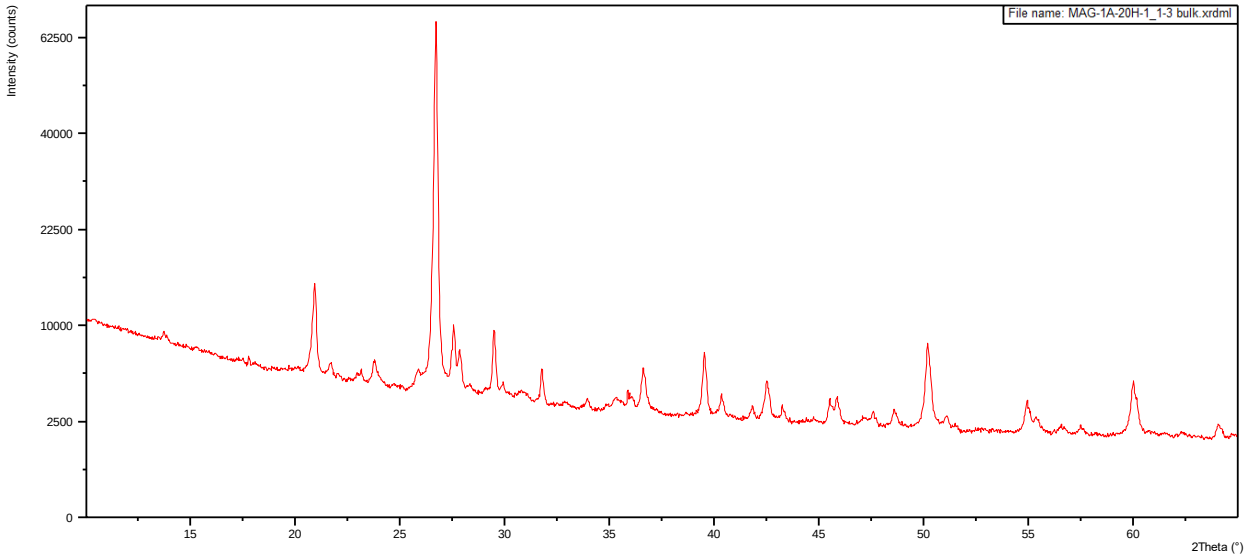
File name: MAG-1A-20H-1_1-3 bulk.xrdml
Intensity (counts)
62500
40000
22500
10000
2500
0
15
20
25
30
35
40
45
50
55
60
2Theta (°)

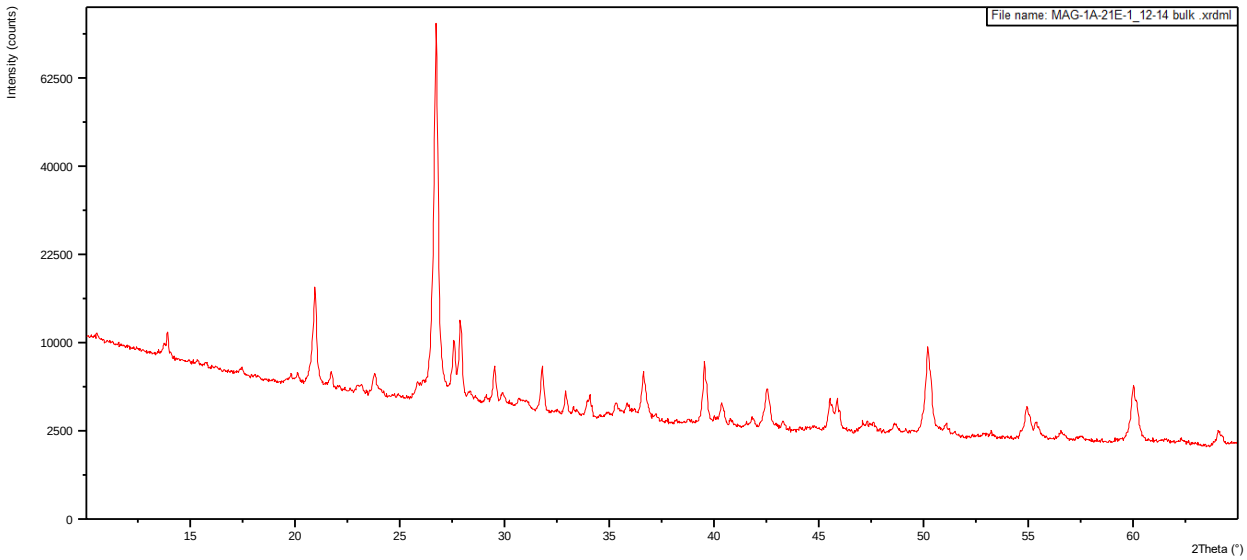
File name: MAG-1A-21E-1_12-14 bulk .xrdml
Intensity (counts)
62500
40000
22500
10000
2500
0
15
20
25
30
35
40
45
50
55
60
2Theta (°)

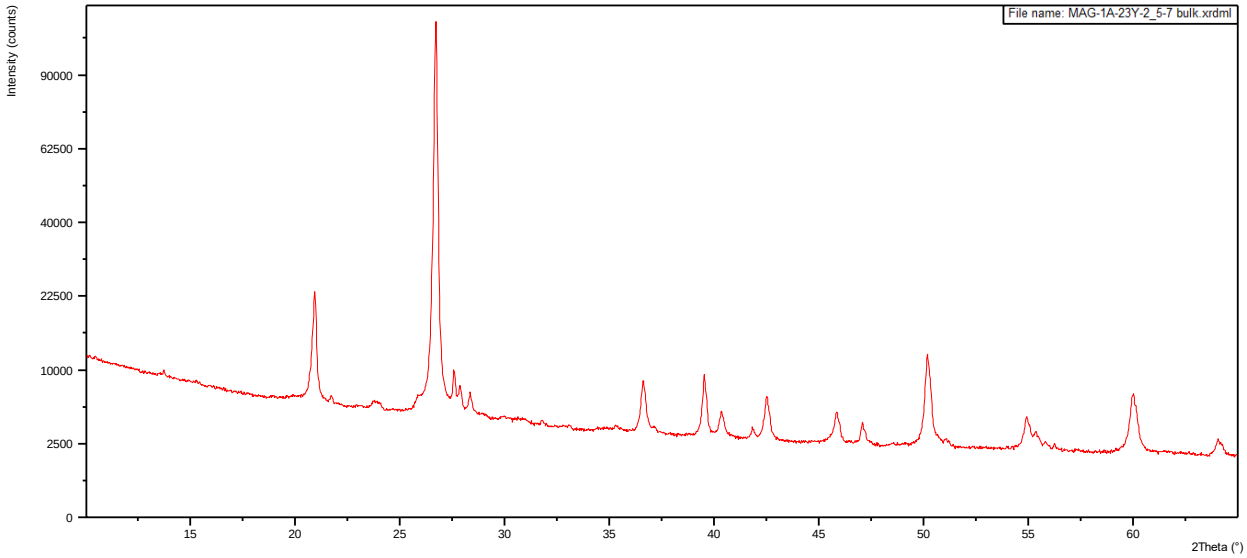
File name: MAG-1A-23Y-2_5-7 bulk.xrdml
Intensity (counts)
90000
62500
40000
22500
10000
2500
0
15
20
25
30
35
40
45
50
55
60
2Theta (°)

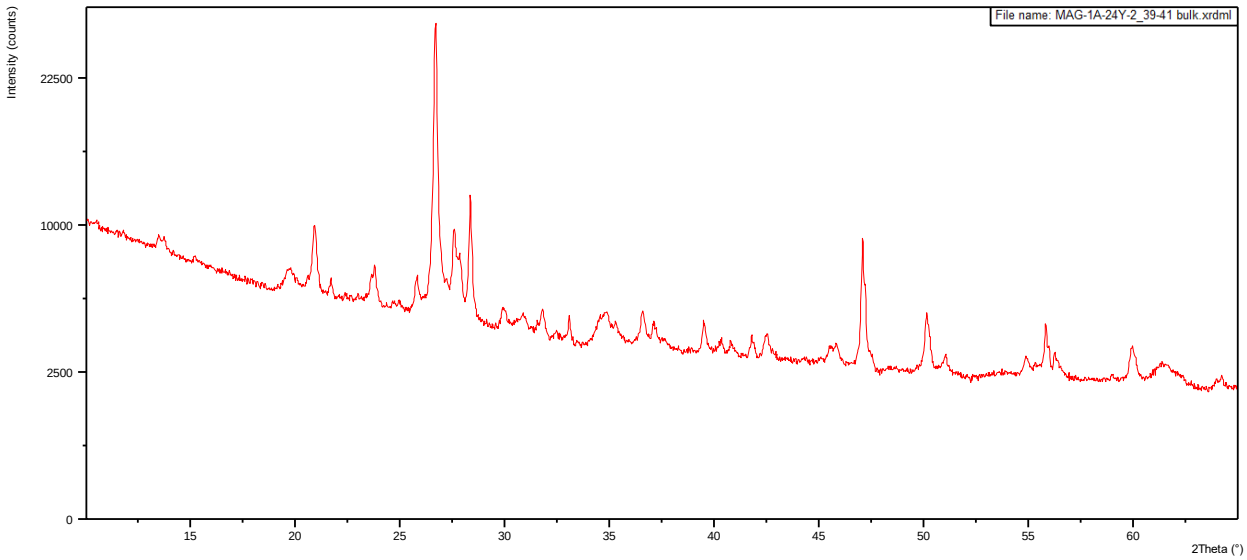
File name: MAG-1A-24Y-2_39-41 bulk.xrdml
Intensity (counts)
22500
10000
2500
0
15
20
25
30
35
40
45
50
55
60
2Theta (°)

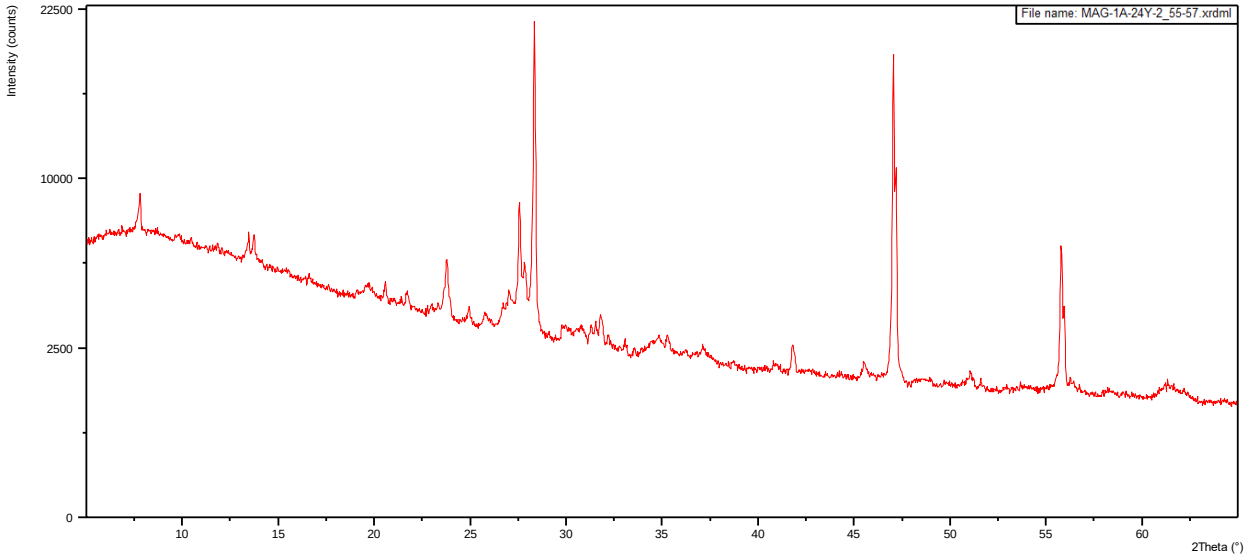
File name: MAG-1A-24Y-2_55-57.xrdml
Intensity (counts)
22500
10000
2500
0
10
15
20
25
30
35
40
45
50
55
60
2Theta (°)

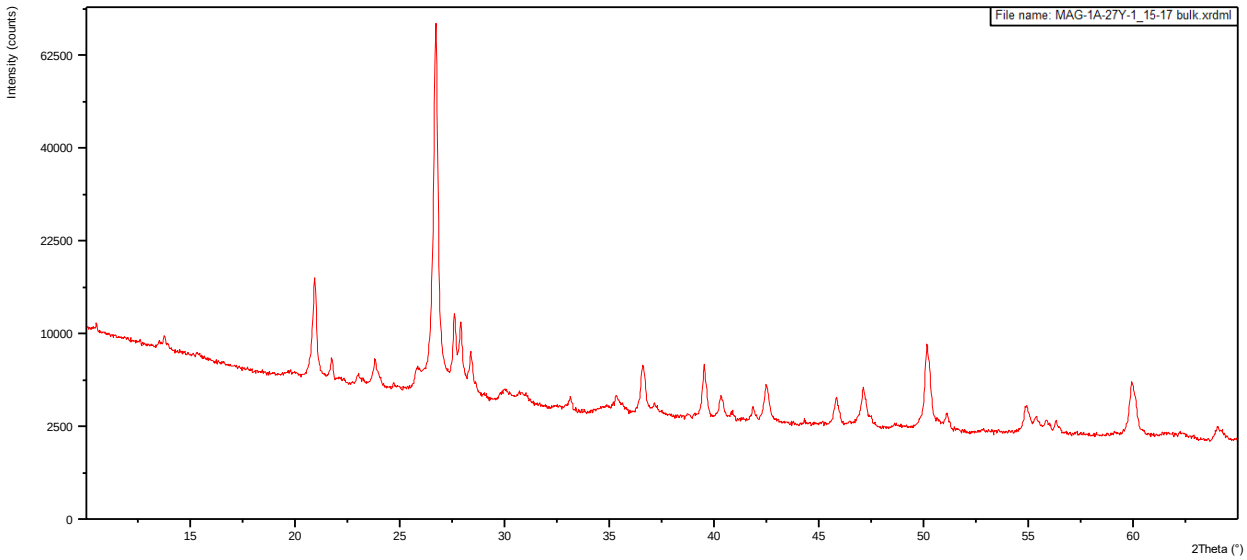
File name: MAG-1A-27Y-1_15-17 bulk.xrdml
Intensity (counts)
62500
40000
22500
10000
2500
0
15
20
25
30
35
40
45
50
55
60
2Theta (°)

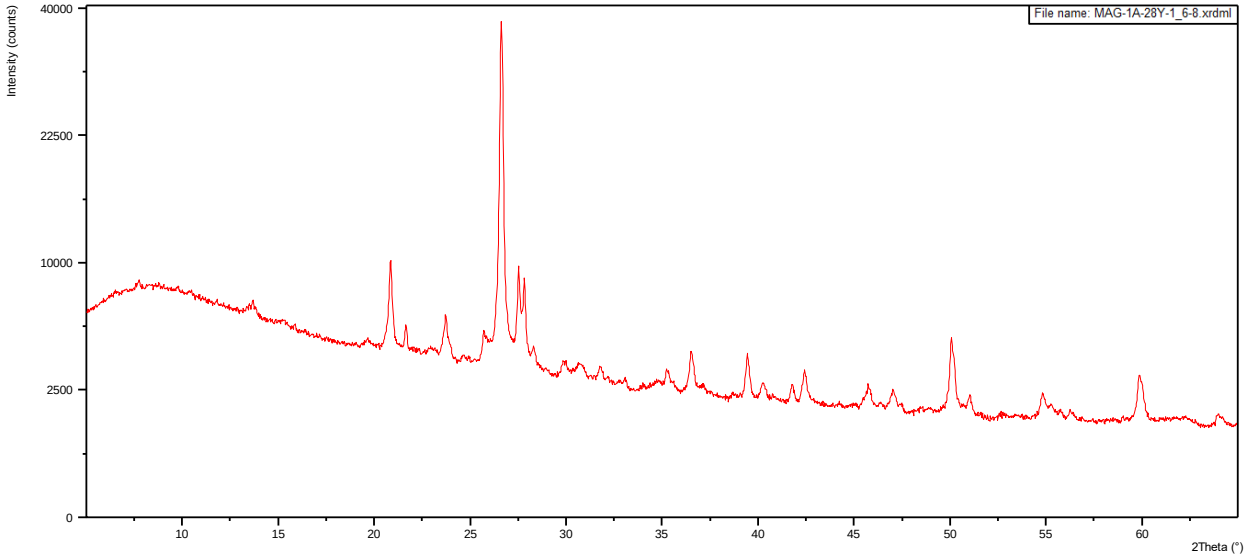
File name: MAG-1A-28Y-1_6-8.xrdml
Intensity (counts)
40000
22500
10000
2500
0
10
15
20
25
30
35
40
45
50
55
60
2Theta (°)

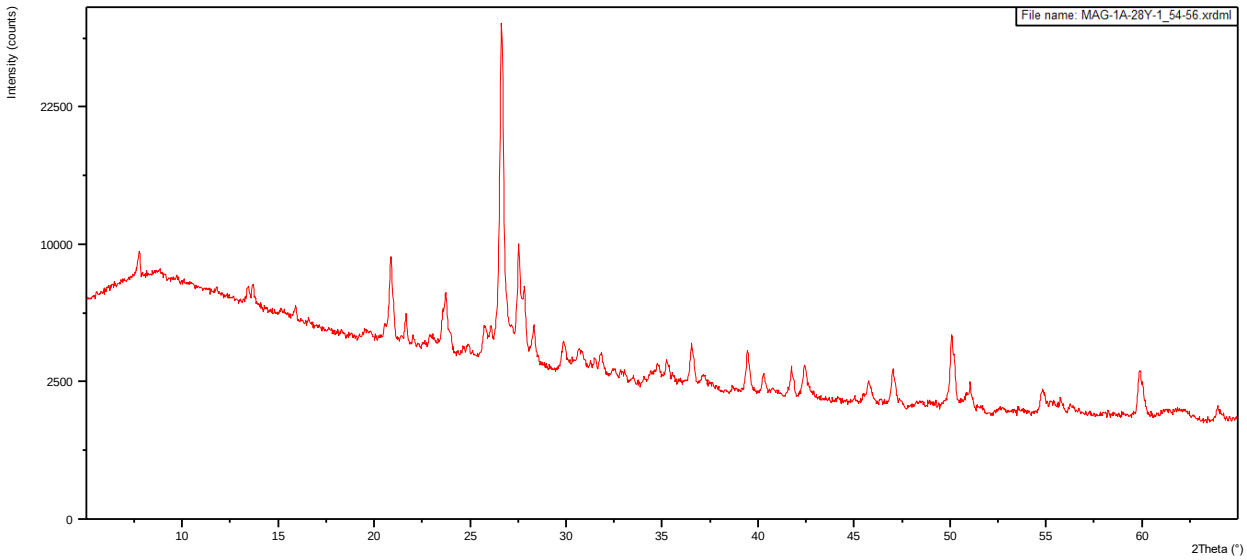
File name: MAG-1A-28Y-1_54-56.xrdml
Intensity (counts)
22500
10000
2500
0
10
15
20
25
30
35
40
45
50
55
60
2Theta (°)

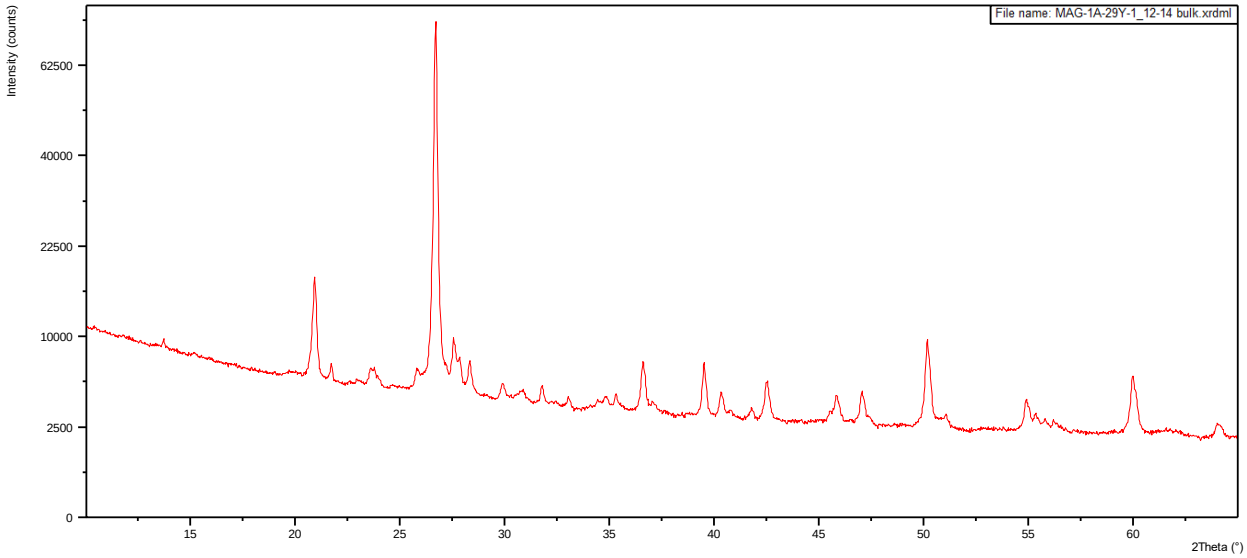
File name: MAG-1A-29Y-1_12-14 bulk.xrdml
Intensity (counts)
62500
40000
22500
10000
2500
0
15
20
25
30
35
40
45
50
55
60
2Theta (°)

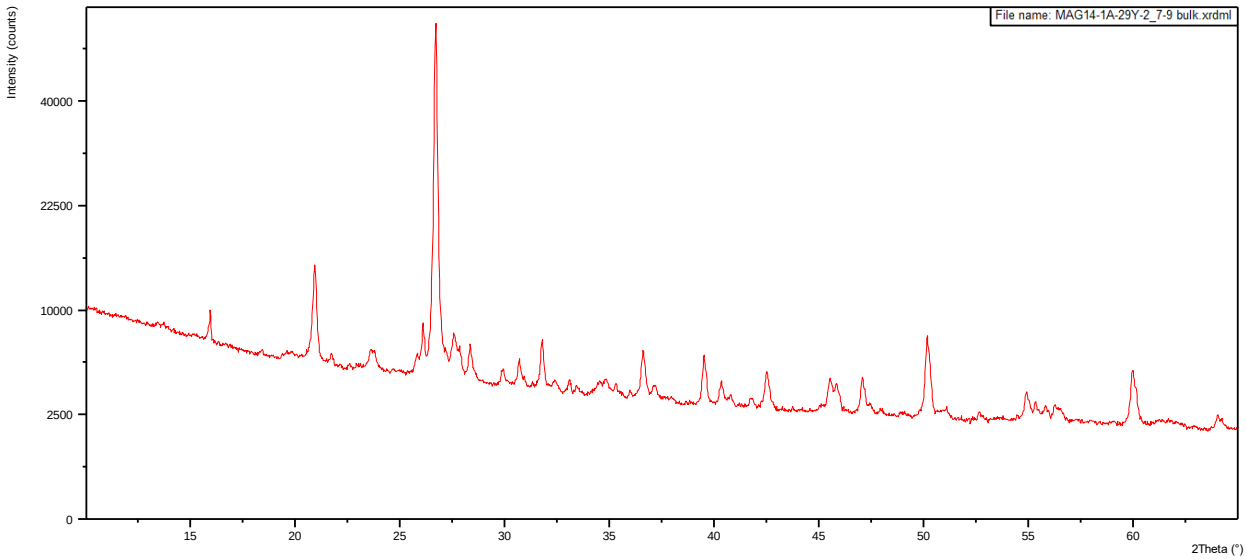
File name: MAG14-1A-29Y-2_7-9 bulk.xrdml
Intensity (counts)
40000
22500
10000
2500
0
15
20
25
30
35
40
45
50
55
60
2Theta (°)

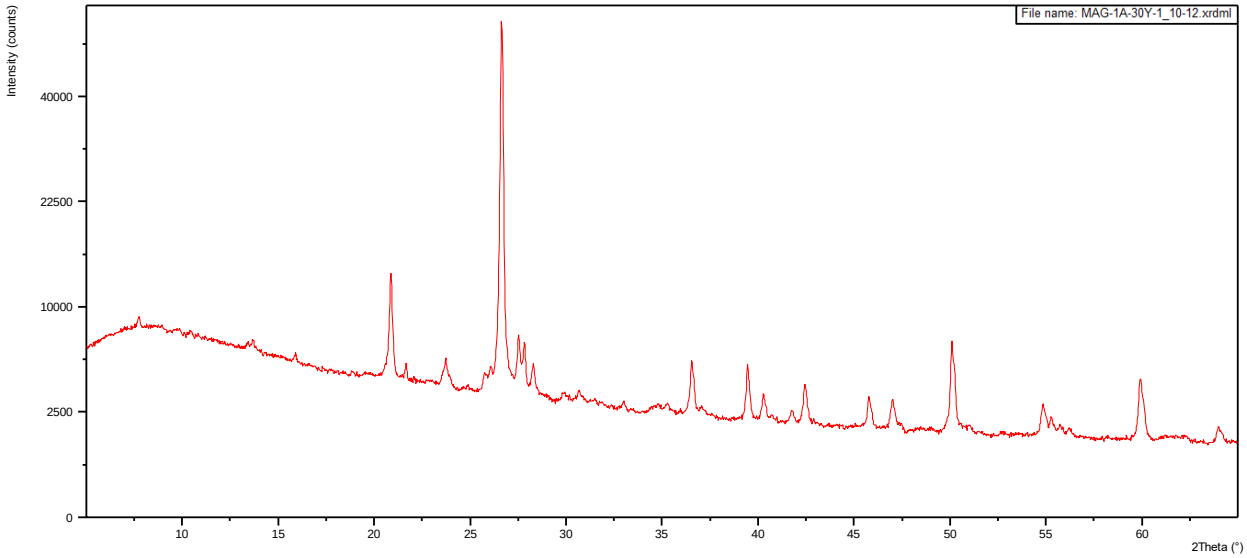
File name: MAG-1A-30Y-1_10-12.xrdml
Intensity (counts)
40000
22500
10000
2500
0
10
15
20
25
30
35
40
45
50
55
60
2Theta (°)

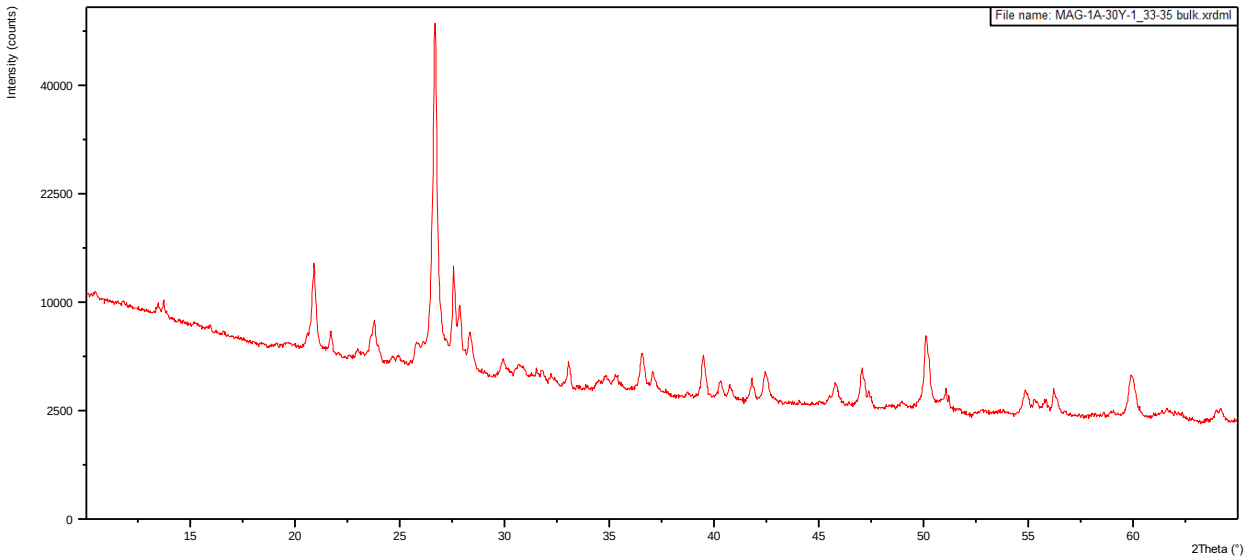
File name: MAG-1A-30Y-1_33-35 bulk.xrdml
Intensity (counts)
40000
22500
10000
2500
0
15
20
25
30
35
40
45
50
55
60
2Theta (°)

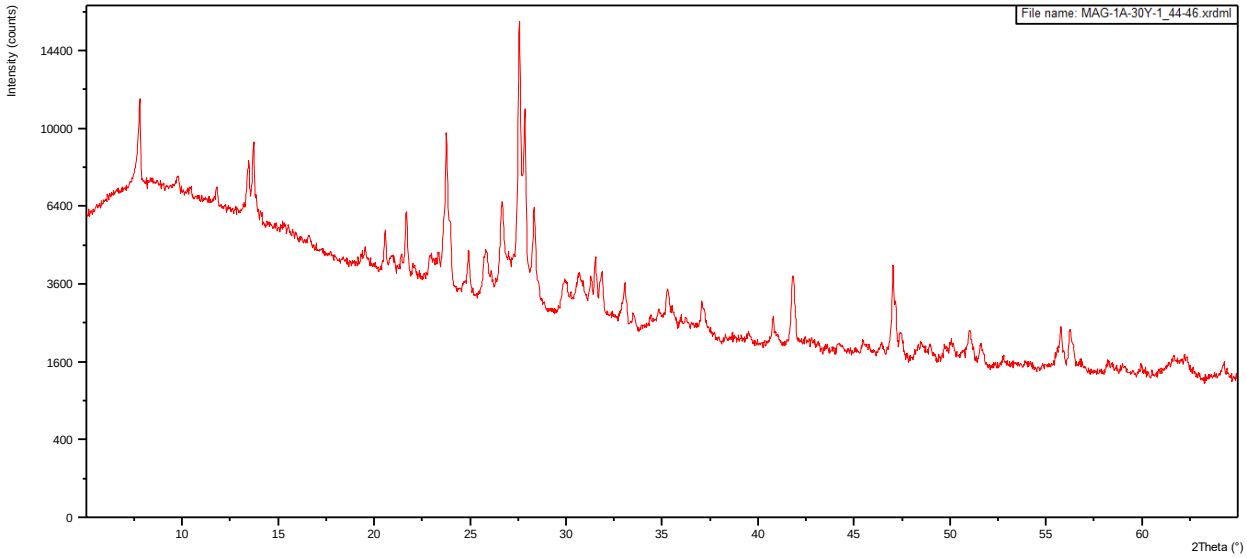
File name: MAG-1A-30Y-1_44-46.xrdml
Intensity (counts)
14400
10000
6400
3600
1600
400
0
10
15
20
25
30
35
40
45
50
55
60
2Theta (°)

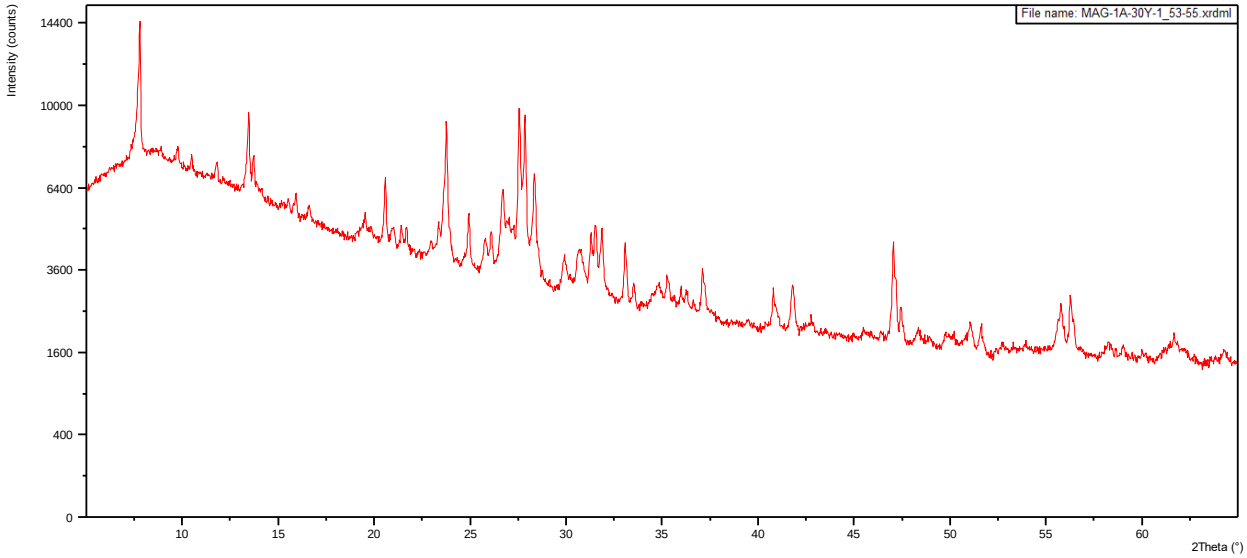
File name: MAG-1A-30Y-1_53-55.xrdml
Intensity (counts)
14400
10000
6400
3600
1600
400
0
10
15
20
25
30
35
40
45
50
55
60
2Theta (°)

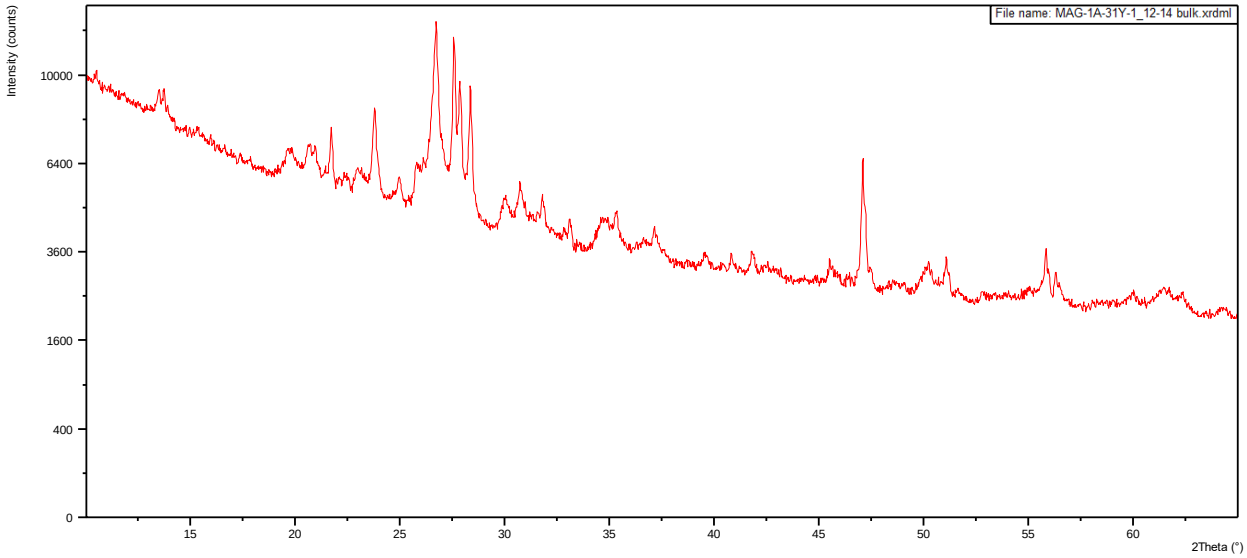
File name: MAG-1A-31Y-1_12-14 bulk.xrdml
Intensity (counts)
10000
6400
3600
1600
400
0
15
20
25
30
35
40
45
50
55
60
2Theta (°)

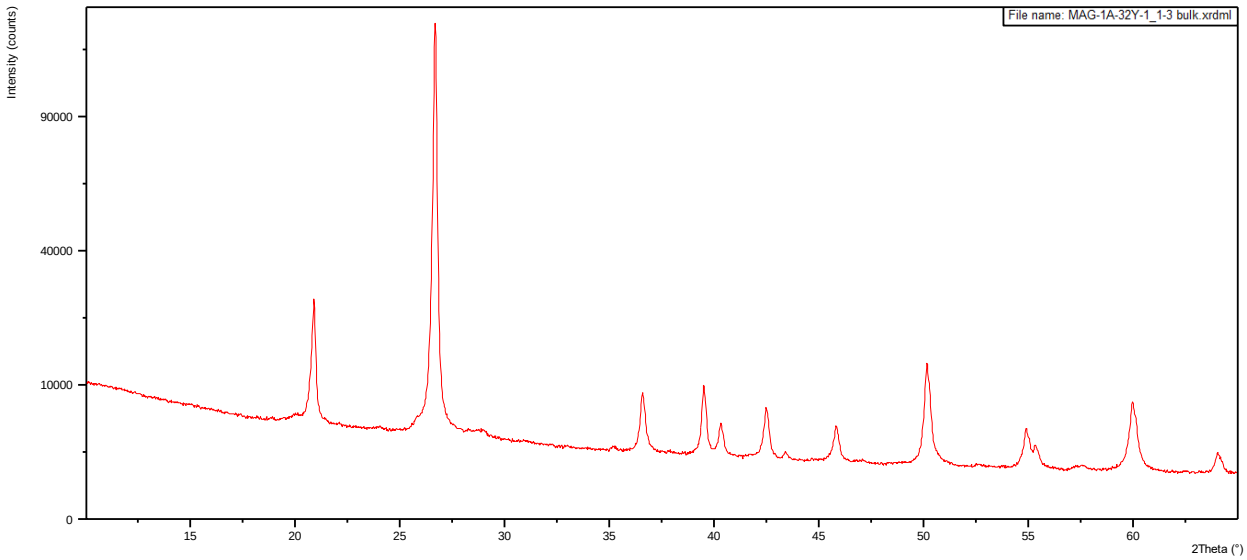
File name: MAG-1A-32Y-1_1-3 bulk.xrdml
Intensity (counts)
90000
40000
10000
0
15
20
25
30
35
40
45
50
55
60
2Theta (°)

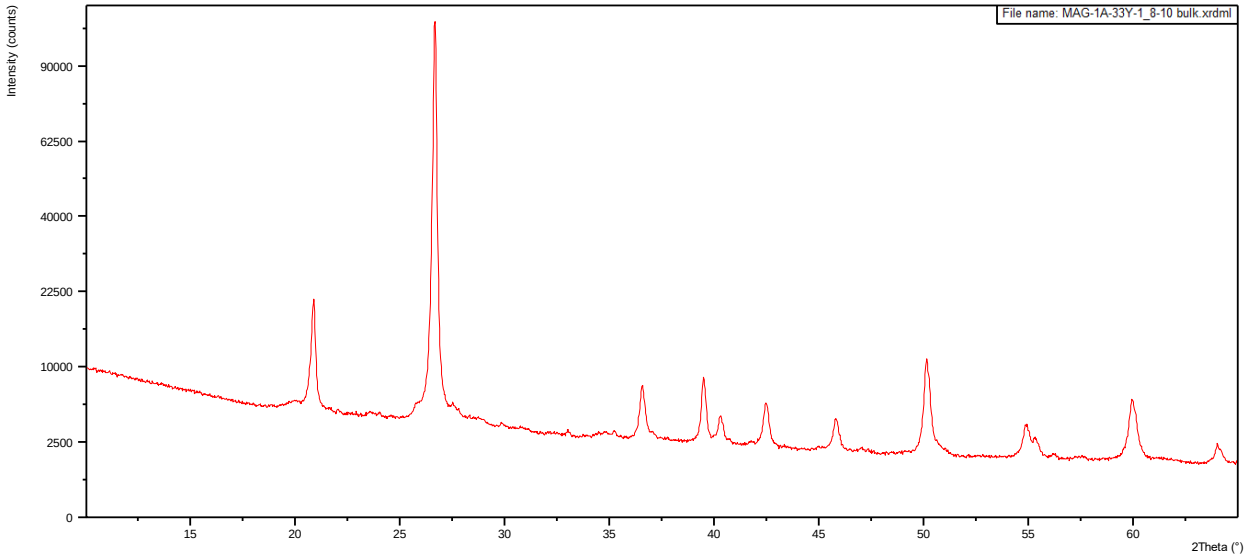
File name: MAG-1A-33Y-1_8-10 bulk.xrdml
Intensity (counts)
90000
62500
40000
22500
10000
2500
0
15
20
25
30
35
40
45
50
55
60
2Theta (°)

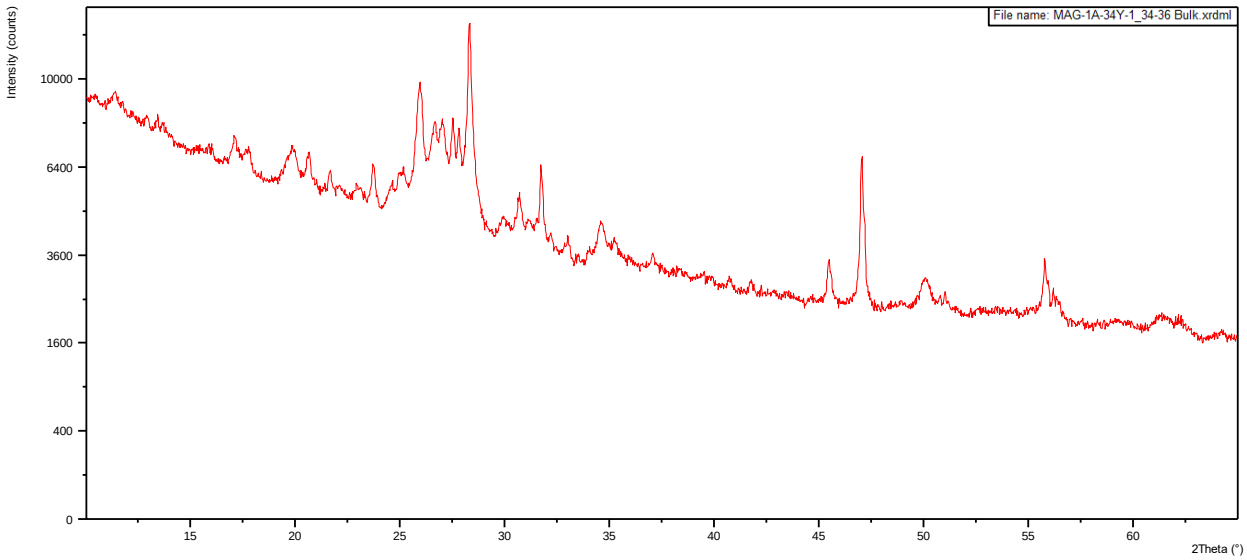
File name: MAG-1A-34Y-1_34-36 Bulk.xrdml
Intensity (counts)
10000
6400
3600
1600
400
0
15
20
25
30
35
40
45
50
55
60
2Theta (°)

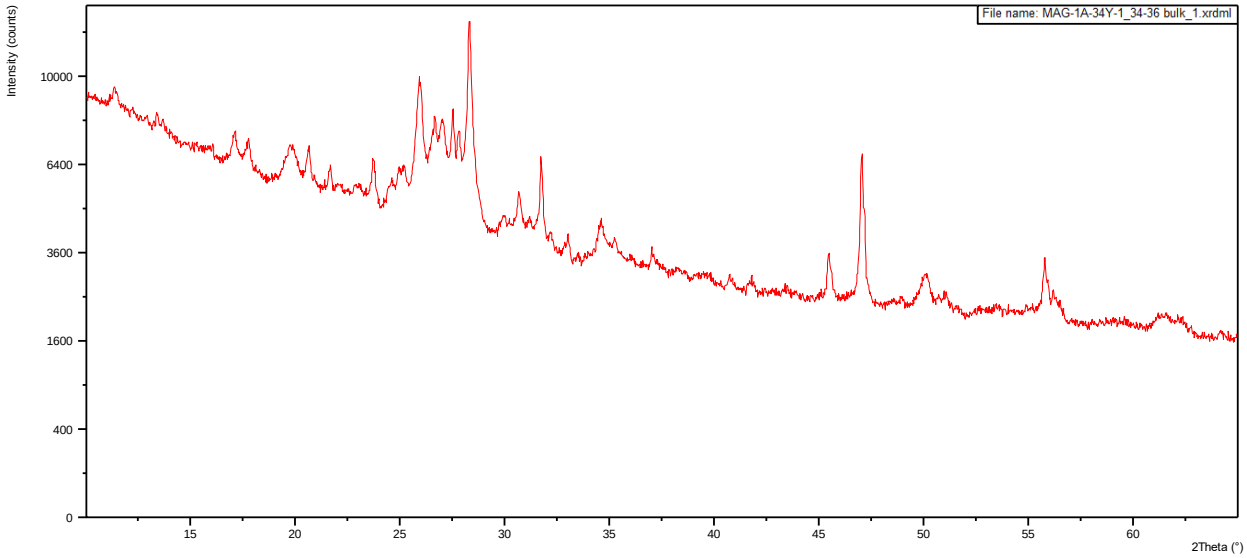
File name: MAG-1A-34Y-1_34-36 bulk_1.xrdml
Intensity (counts)
10000
6400
3600
1600
400
0
15
20
25
30
35
40
45
50
55
60
2Theta (°)

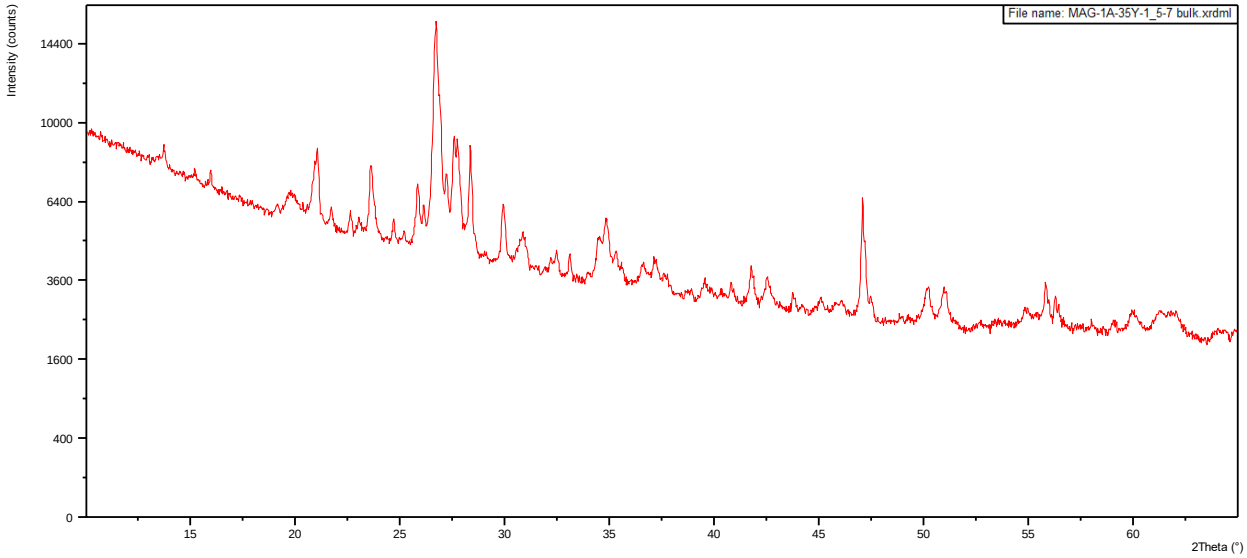
File name: MAG-1A-35Y-1_5-7 bulk.xrdml
Intensity (counts)
14400
10000
6400
3600
1600
400
0
15
20
25
30
35
40
45
50
55
60
2Theta (°)

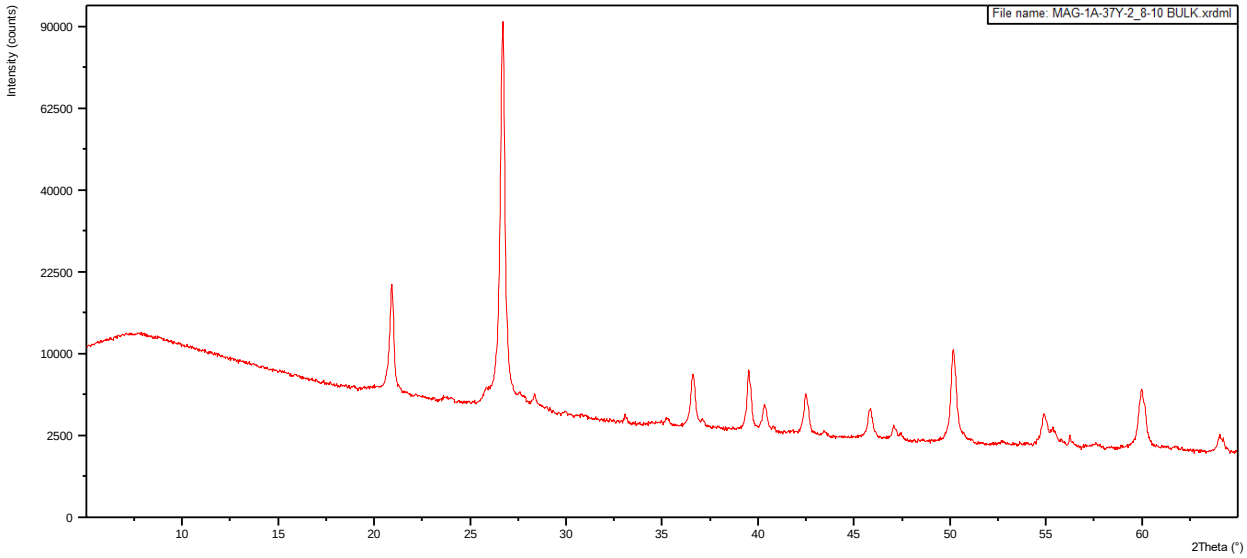
File name: MAG-1A-37Y-2_8-10 BULK.xrdml
Intensity (counts)
90000
62500
40000
22500
10000
2500
0
10
15
20
25
30
35
40
45
50
55
60
2Theta (°)

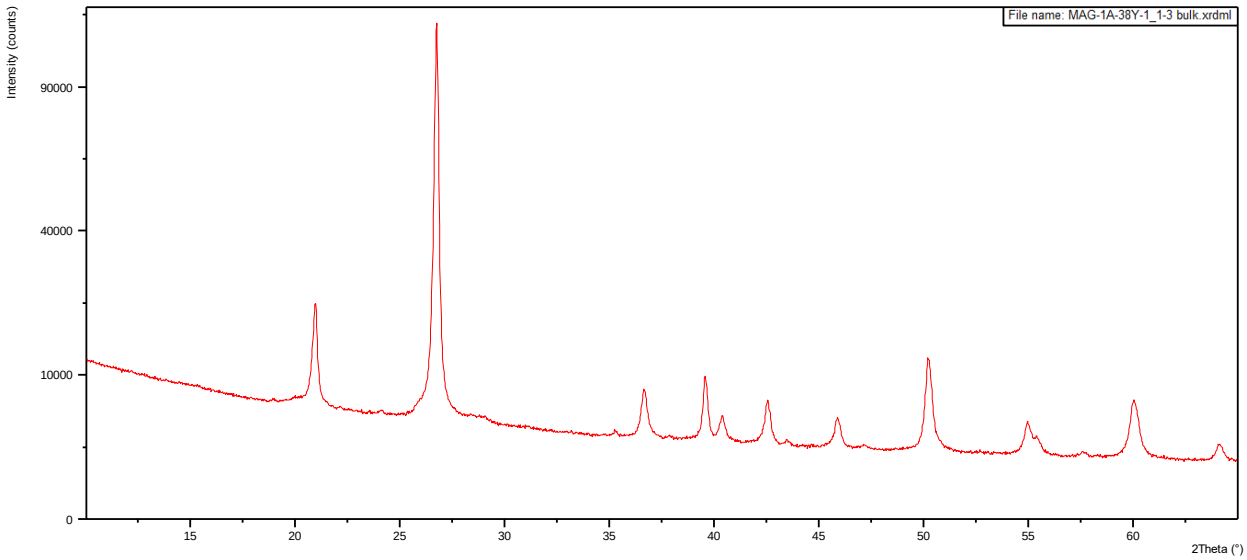
File name: MAG-1A-38Y-1_1-3 bulk.xrdml
Intensity (counts)
90000
40000
10000
0
15
20
25
30
35
40
45
50
55
60
2Theta (°)

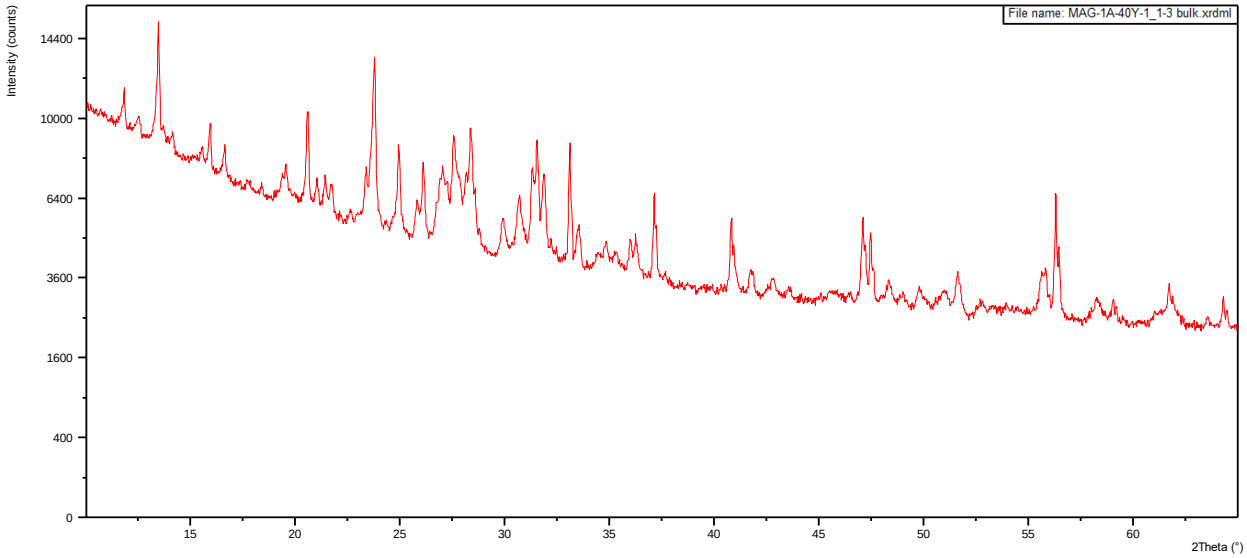
File name: MAG-1A-40Y-1_1-3 bulk.xrdml
Intensity (counts)
14400
10000
6400
3600
1600
400
0
15
20
25
30
35
40
45
50
55
60
2Theta (°)

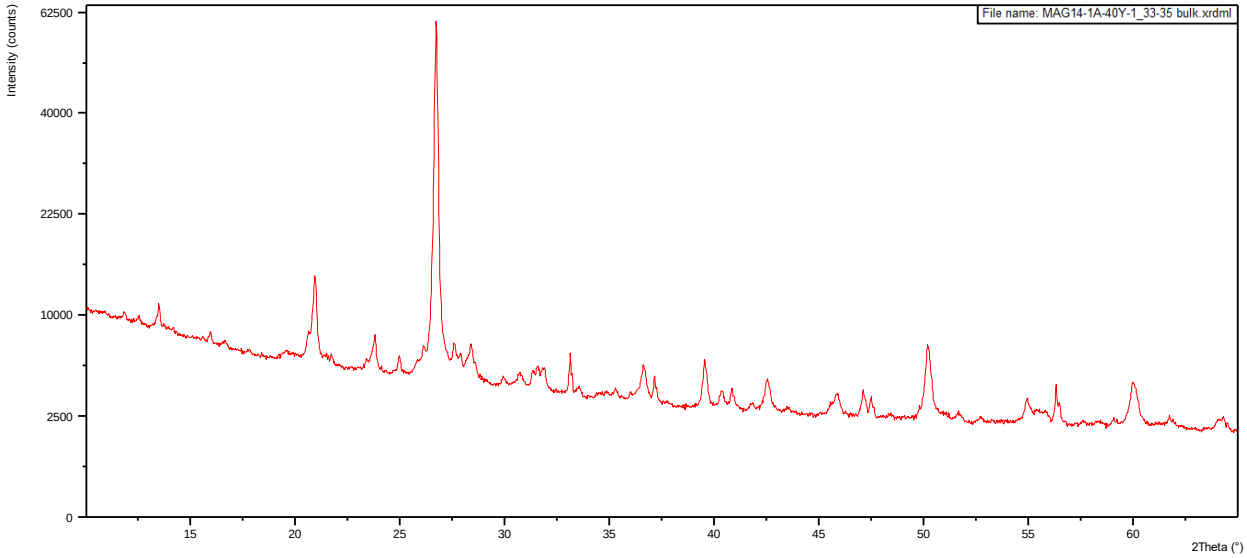
File name: MAG14-1A-40Y-1_33-35 bulk.xrdml
Intensity (counts)
62500
40000
22500
10000
2500
0
15
20
25
30
35
40
45
50
55
60
2Theta (°)

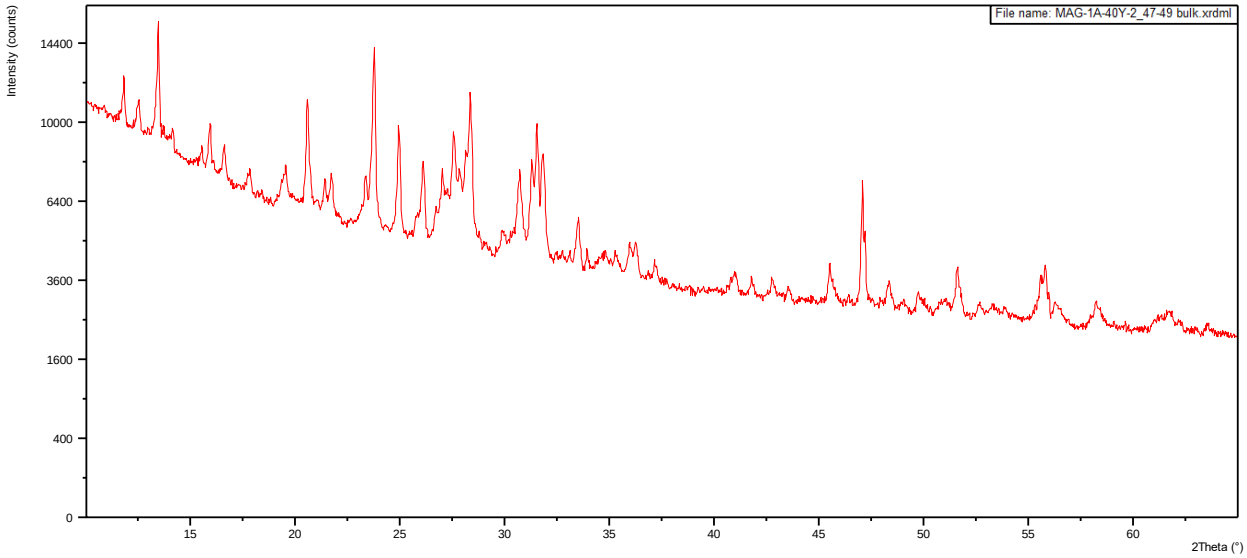
File name: MAG-1A-40Y-2_47-49 bulk.xrdml
Intensity (counts)
14400
10000
6400
3600
1600
400
0
15
20
25
30
35
40
45
50
55
60
2Theta (°)

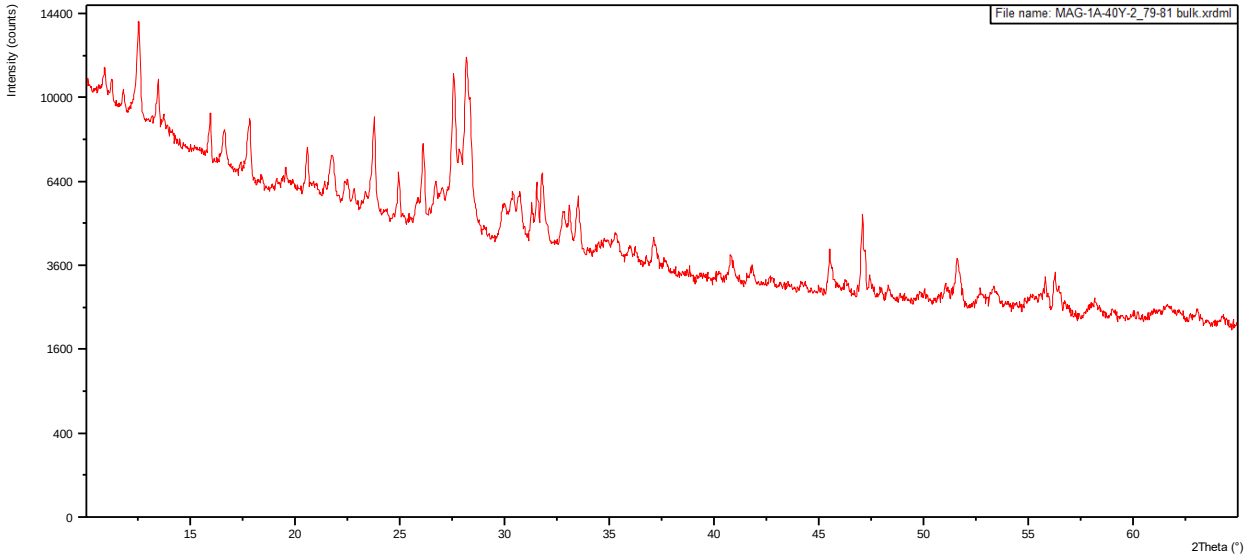
File name: MAG-1A-40Y-2_79-81 bulk.xrdml
Intensity (counts)
14400
10000
6400
3600
1600
400
0
15
20
25
30
35
40
45
50
55
60
2Theta (°)

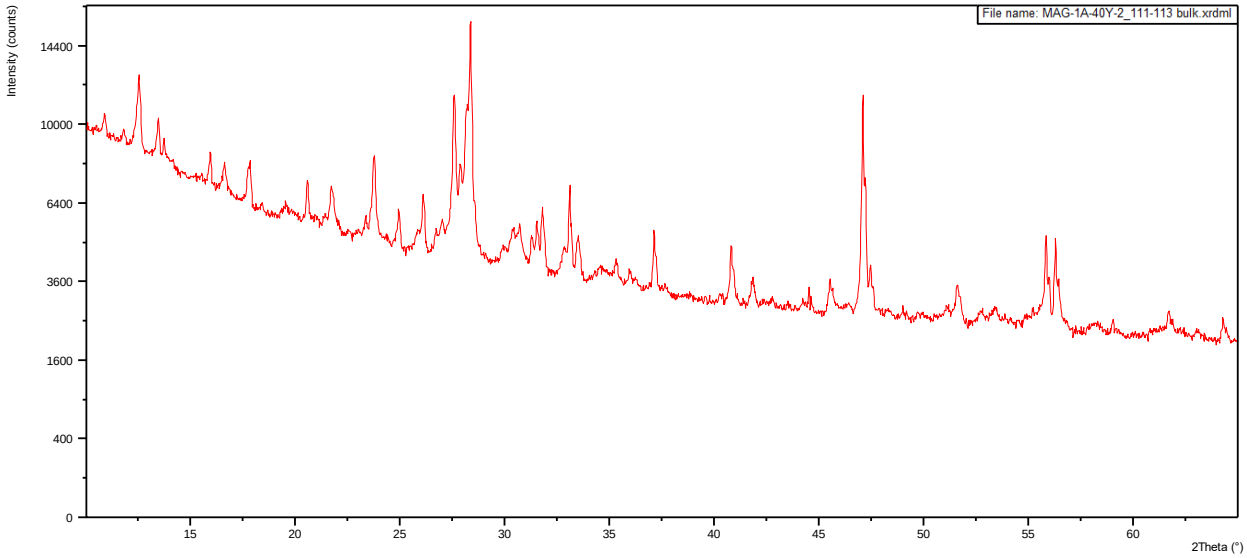
File name: MAG-1A-40Y-2_111-113 bulk.xrdml
Intensity (counts)
14400
10000
6400
3600
1600
400
0
15
20
25
30
35
40
45
50
55
60
2Theta (°)

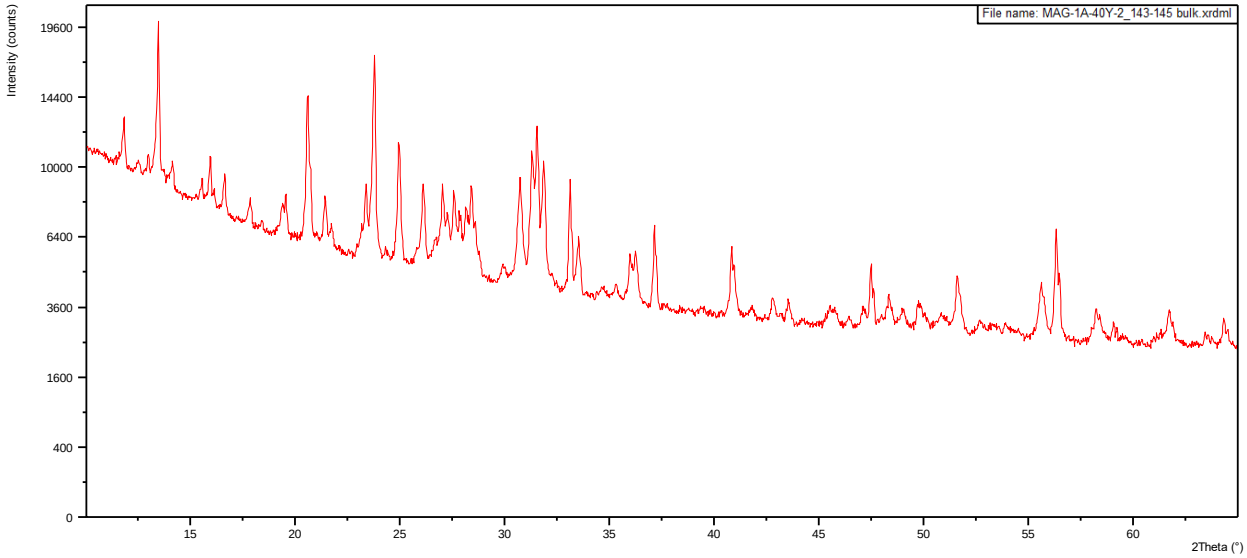
File name: MAG-1A-40Y-2_143-145 bulk.xrdml
Intensity (counts)
19600
14400
10000
6400
3600
1600
400
0
15
20
25
30
35
40
45
50
55
60
2Theta (°)

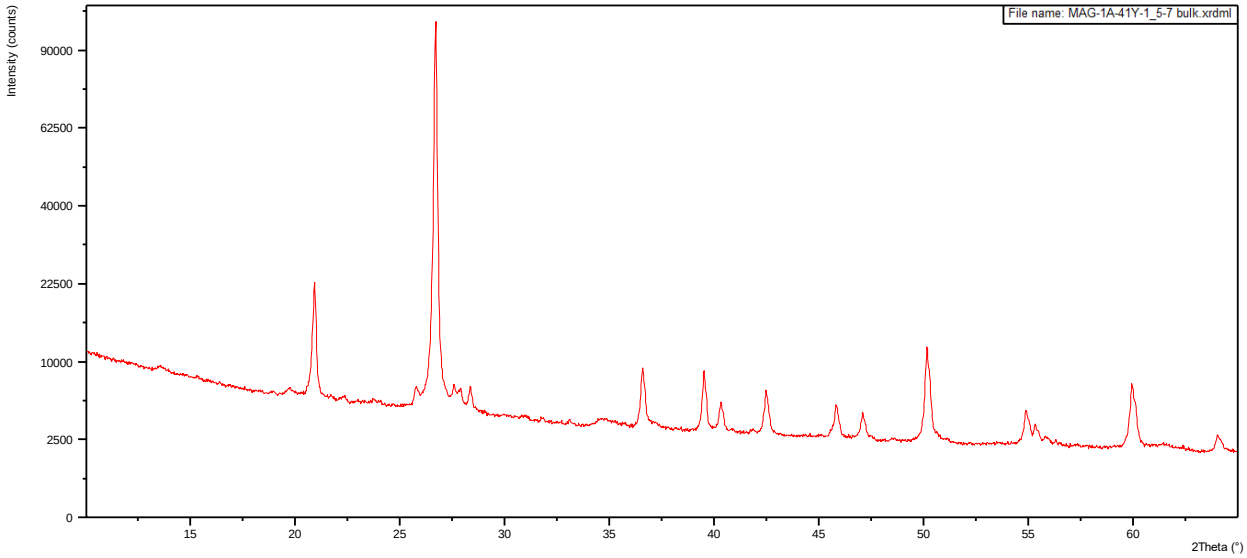
File name: MAG-1A-41Y-1_5-7 bulk.xrdml
Intensity (counts)
90000
62500
40000
22500
10000
2500
0
15
20
25
30
35
40
45
50
55
60
2Theta (°)

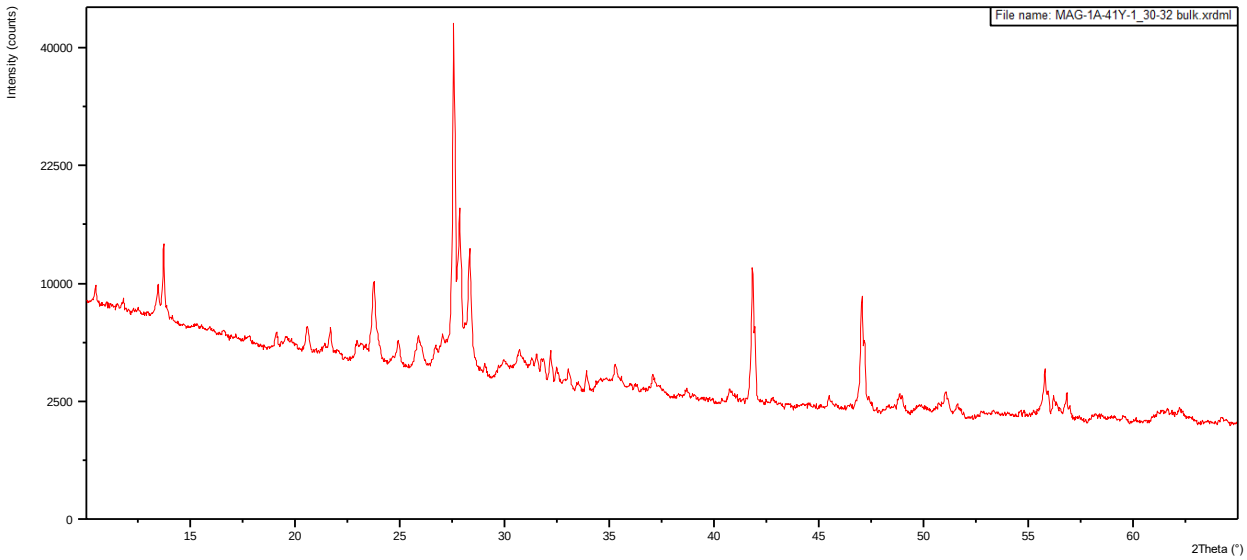
File name: MAG-1A-41Y-1_30-32 bulk.xrdml
Intensity (counts)
40000
22500
10000
2500
0
15
20
25
30
35
40
45
50
55
60
2Theta (°)

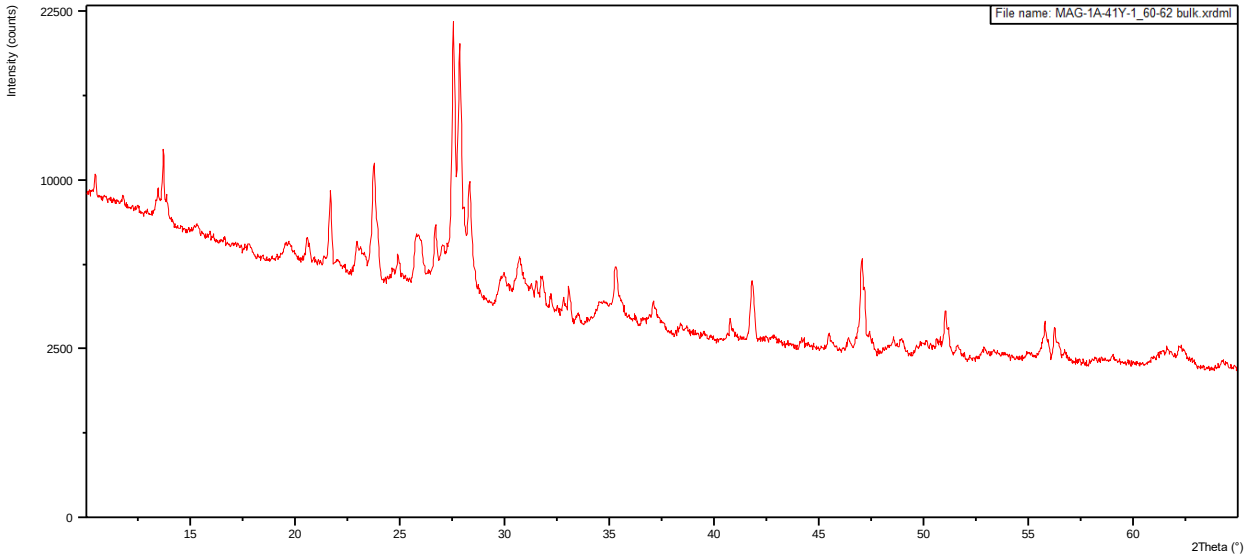
File name: MAG-1A-41Y-1_60-62 bulk.xrdml
Intensity (counts)
22500
10000
2500
0
15
20
25
30
35
40
45
50
55
60
2Theta (°)

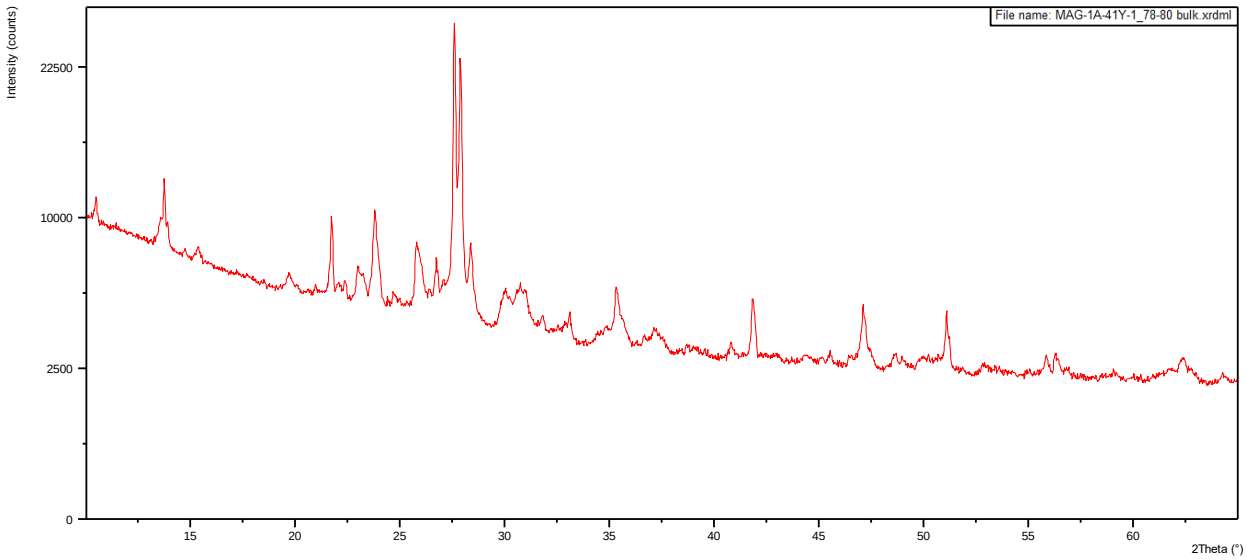
File name: MAG-1A-41Y-1_78-80 bulk.xrdml
Intensity (counts)
22500
10000
2500
0
15
20
25
30
35
40
45
50
55
60
2Theta (°)

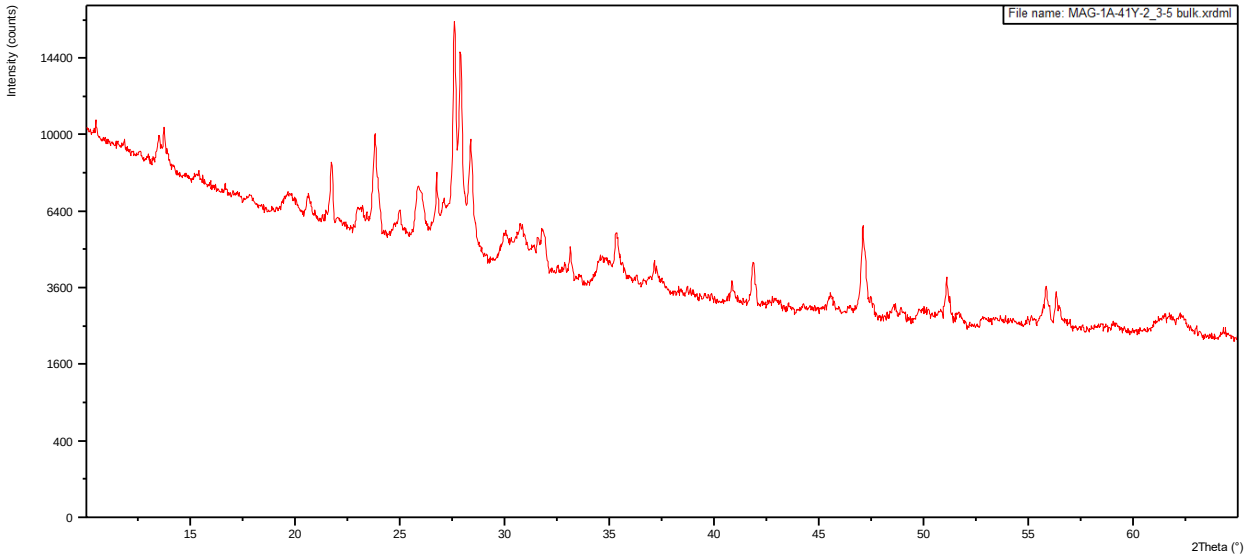
File name: MAG-1A-41Y-2_3-5 bulk.xrdml
Intensity (counts)
14400
10000
6400
3600
1600
400
0
15
20
25
30
35
40
45
50
55
60
2Theta (°)

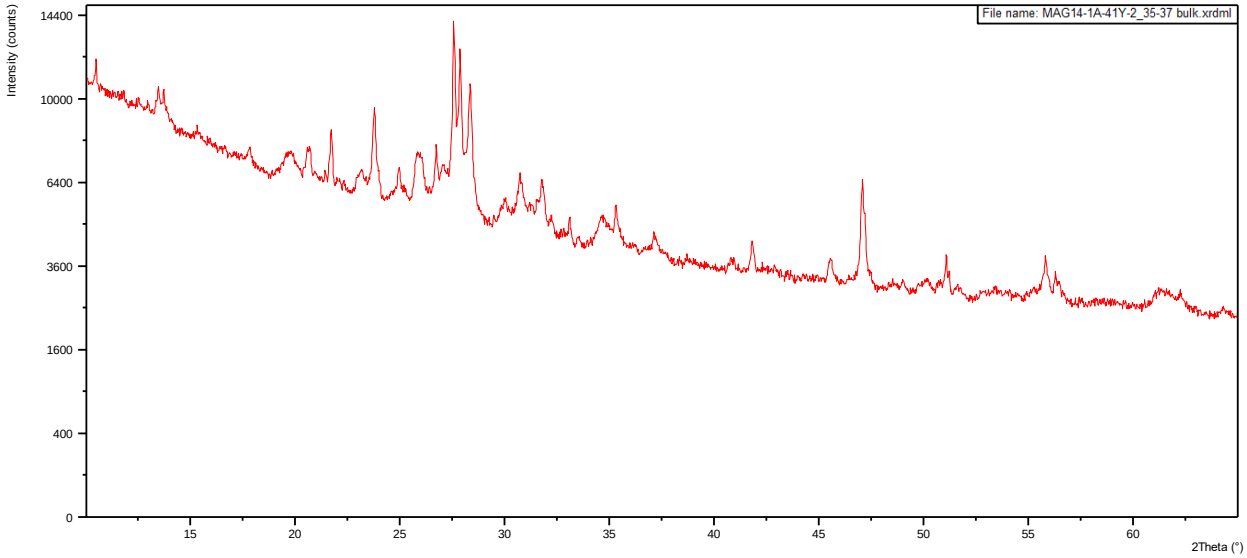
File name: MAG14-1A-41Y-2_35-37 bulk.xrdml
Intensity (counts)
14400
10000
6400
3600
1600
400
0
15
20
25
30
35
40
45
50
55
60
2Theta (°)

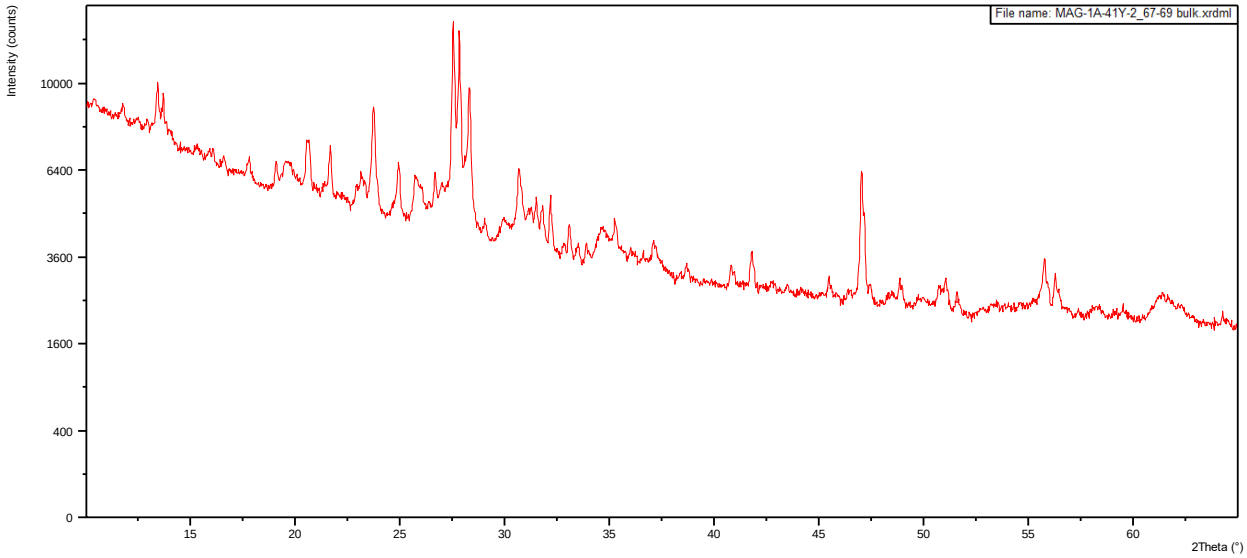
File name: MAG-1A-41Y-2_67-69 bulk.xrdml
Intensity (counts)
10000
6400
3600
1600
400
0
15
20
25
30
35
40
45
50
55
60
2Theta (°)

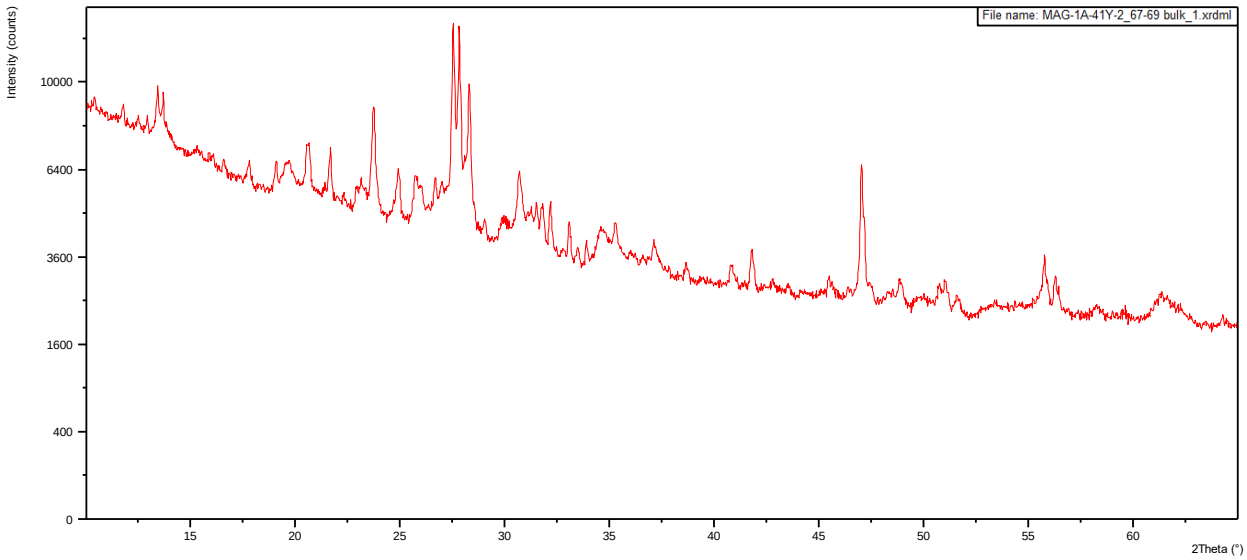
File name: MAG-1A-41Y-2_67-69 bulk_1.xrdml
Intensity (counts)
10000
6400
3600
1600
400
0
15
20
25
30
35
40
45
50
55
60
2Theta (°)

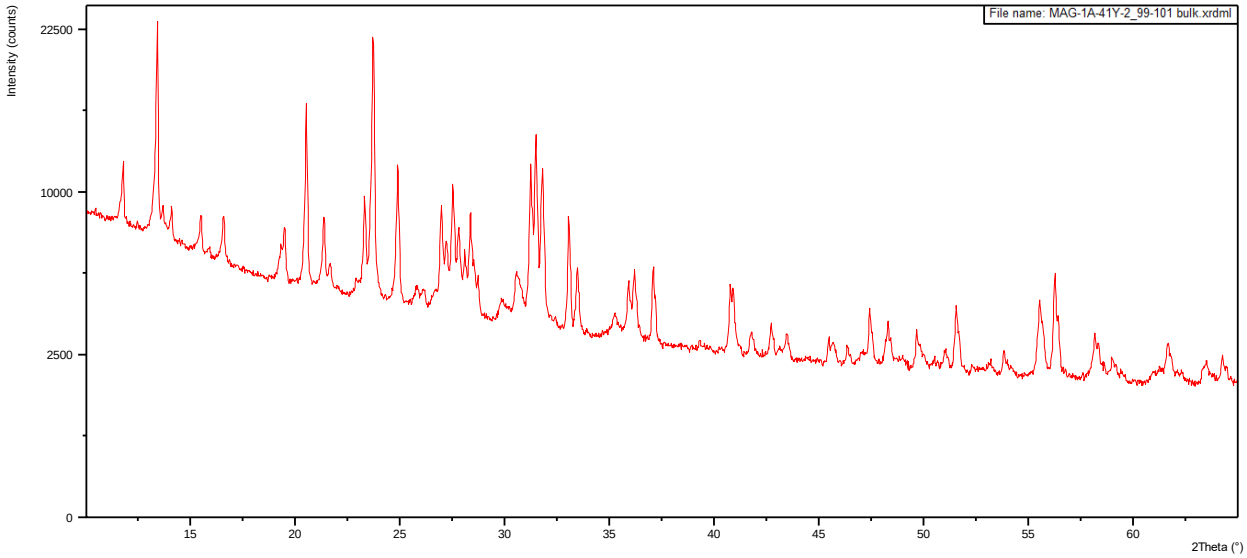
File name: MAG-1A-41Y-2_99-101 bulk.xrdml
Intensity (counts)
22500
10000
2500
0
15
20
25
30
35
40
45
50
55
60
2Theta (°)

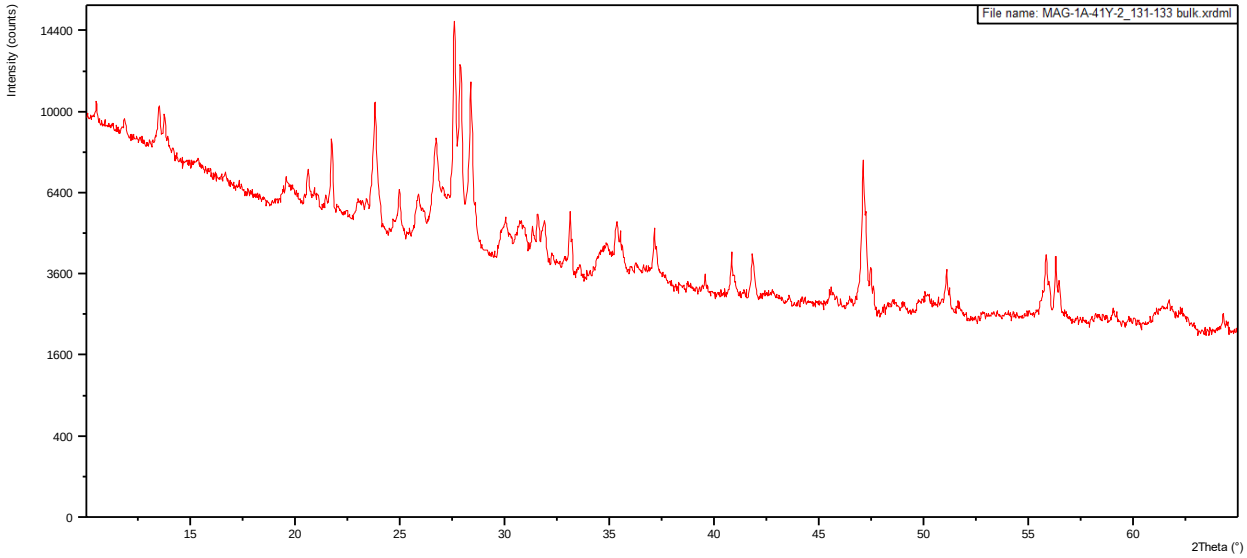
File name: MAG-1A-41Y-2_131-133 bulk.xrdml
Intensity (counts)
14400
10000
6400
3600
1600
400
0
15
20
25
30
35
40
45
50
55
60
2Theta (°)

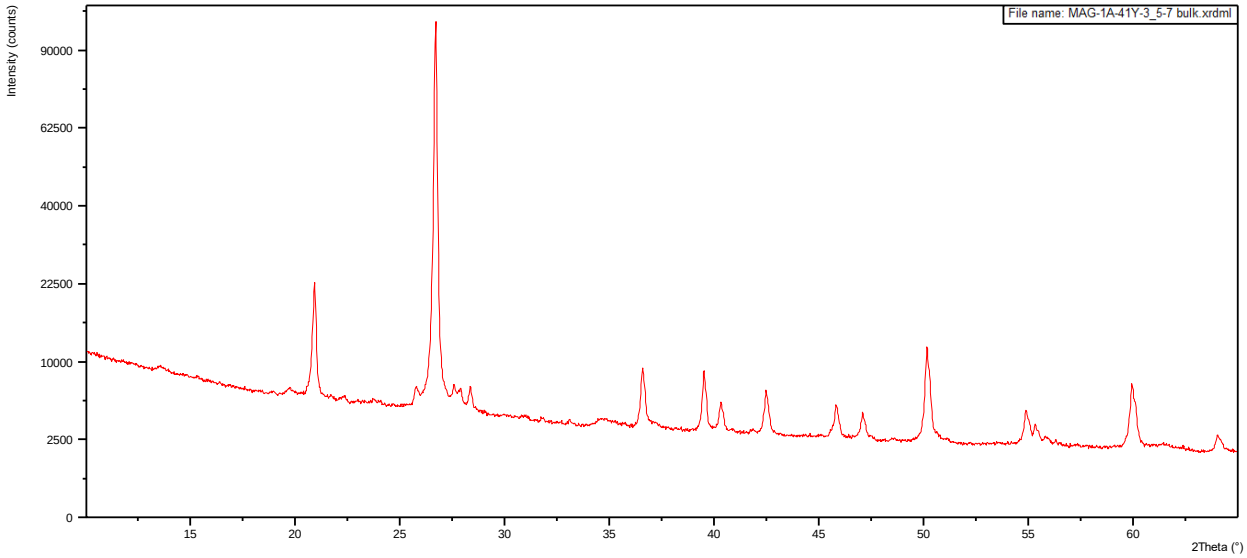
File name: MAG-1A-41Y-3_5-7 bulk.xrdml
Intensity (counts)
90000
62500
40000
22500
10000
2500
0
15
20
25
30
35
40
45
50
55
60
2Theta (°)

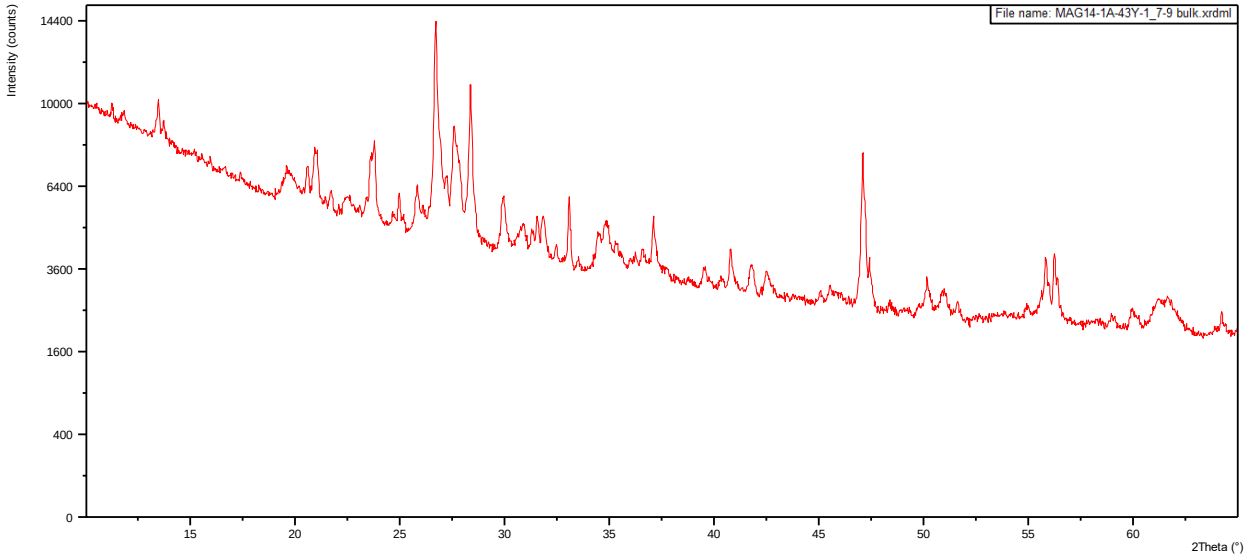
File name: MAG14-1A-43Y-1_7-9 bulk.xrdml
Intensity (counts)
14400
10000
6400
3600
1600
400
0
15
20
25
30
35
40
45
50
55
60
2Theta (°)

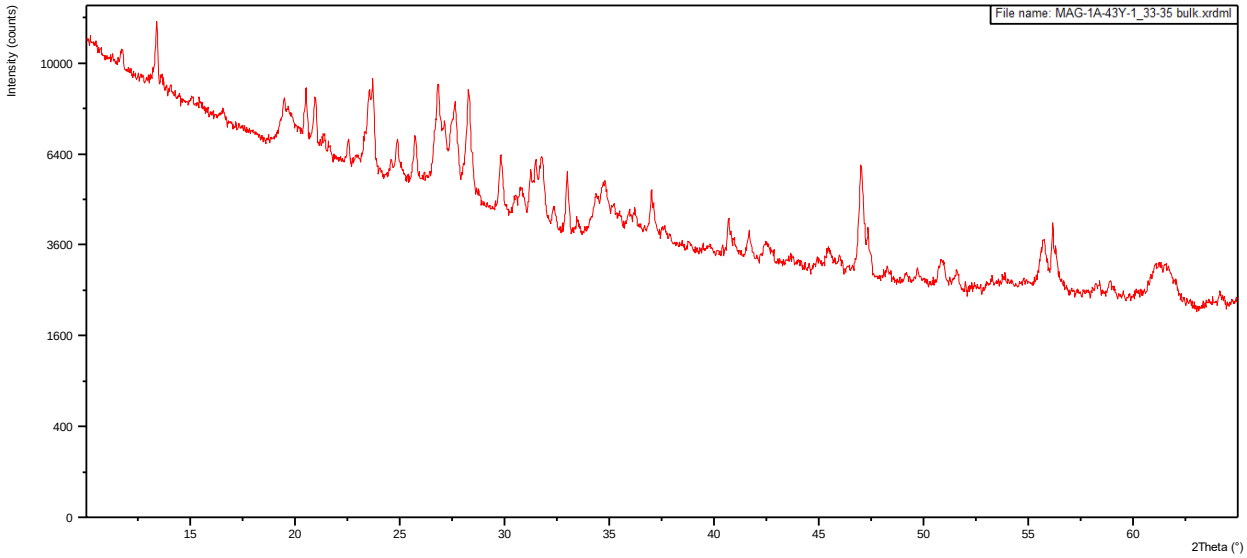
File name: MAG-1A-43Y-1_33-35 bulk.xrdml
Intensity (counts)
10000
6400
3600
1600
400
0
15
20
25
30
35
40
45
50
55
60
2Theta (°)

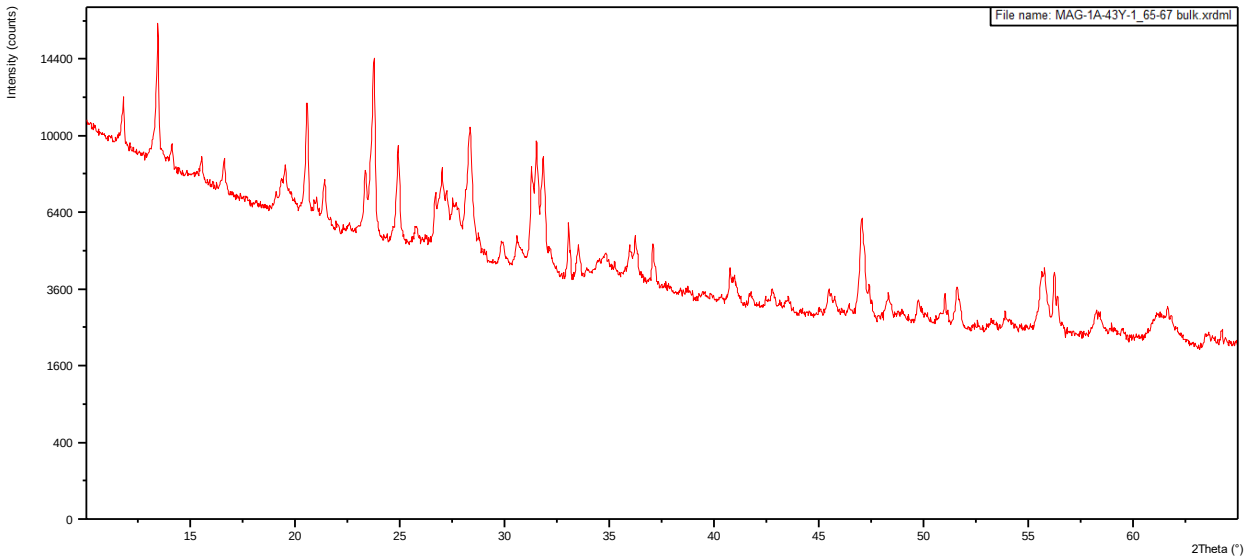
File name: MAG-1A-43Y-1_65-67 bulk.xrdml
Intensity (counts)
14400
10000
6400
3600
1600
400
0
15
20
25
30
35
40
45
50
55
60
2Theta (°)

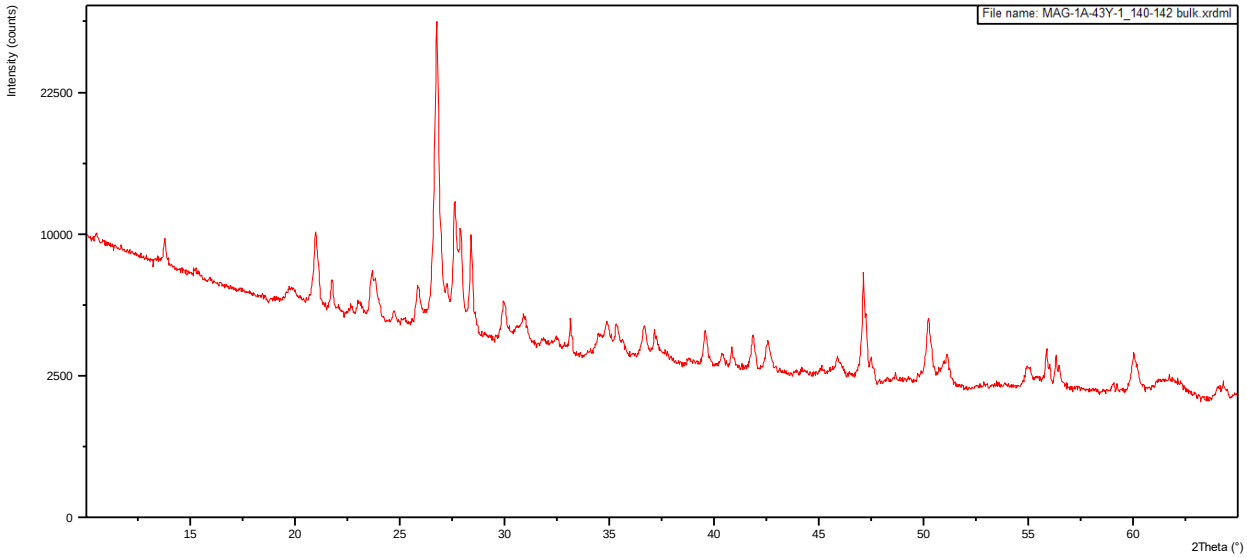
File name: MAG-1A-43Y-1_140-142 bulk.xrdml
Intensity (counts)
22500
10000
2500
0
15
20
25
30
35
40
45
50
55
60
2Theta (°)

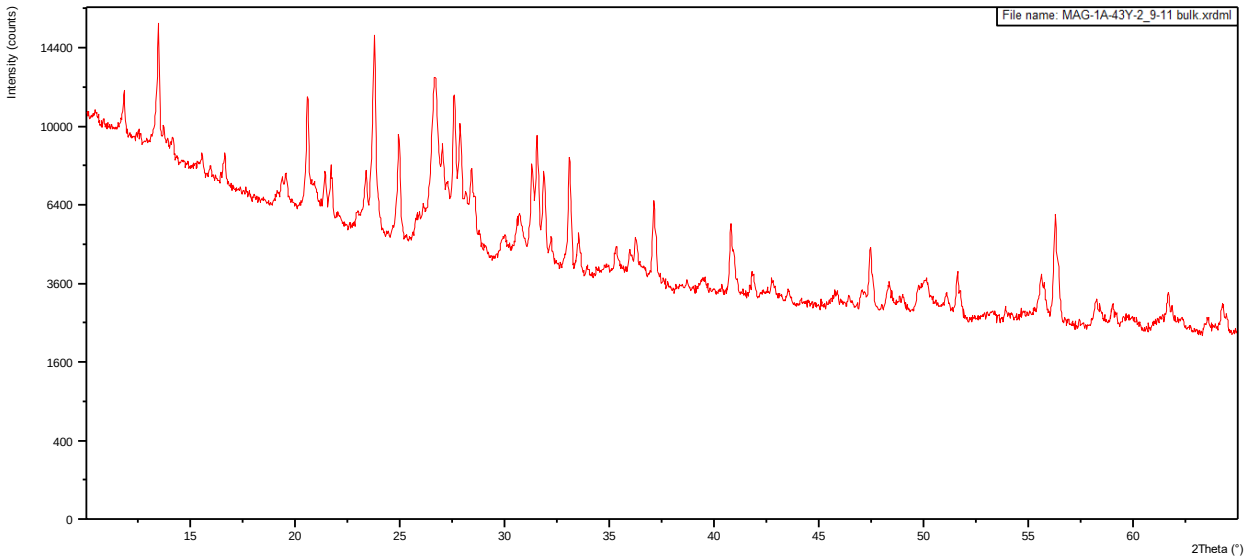
File name: MAG-1A-43Y-2_9-11 bulk.xrdml
Intensity (counts)
14400
10000
6400
3600
1600
400
0
15
20
25
30
35
40
45
50
55
60
2Theta (°)

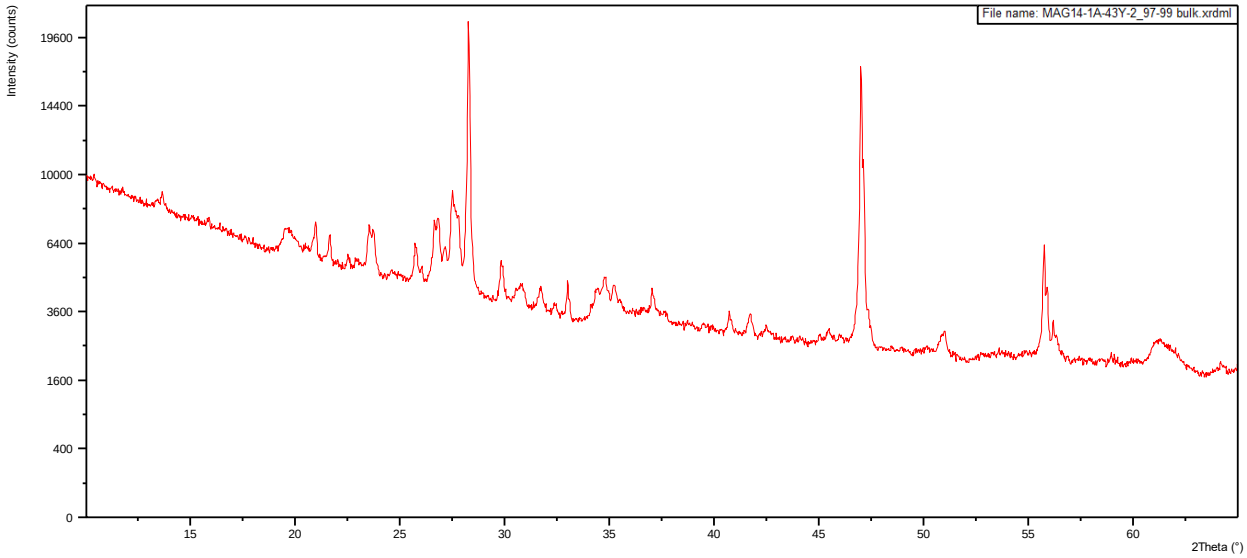
File name: MAG14-1A-43Y-2_97-99 bulk.xrdml
Intensity (counts)
19600
14400
10000
6400
3600
1600
400
0
15
20
25
30
35
40
45
50
55
60
2Theta (°)

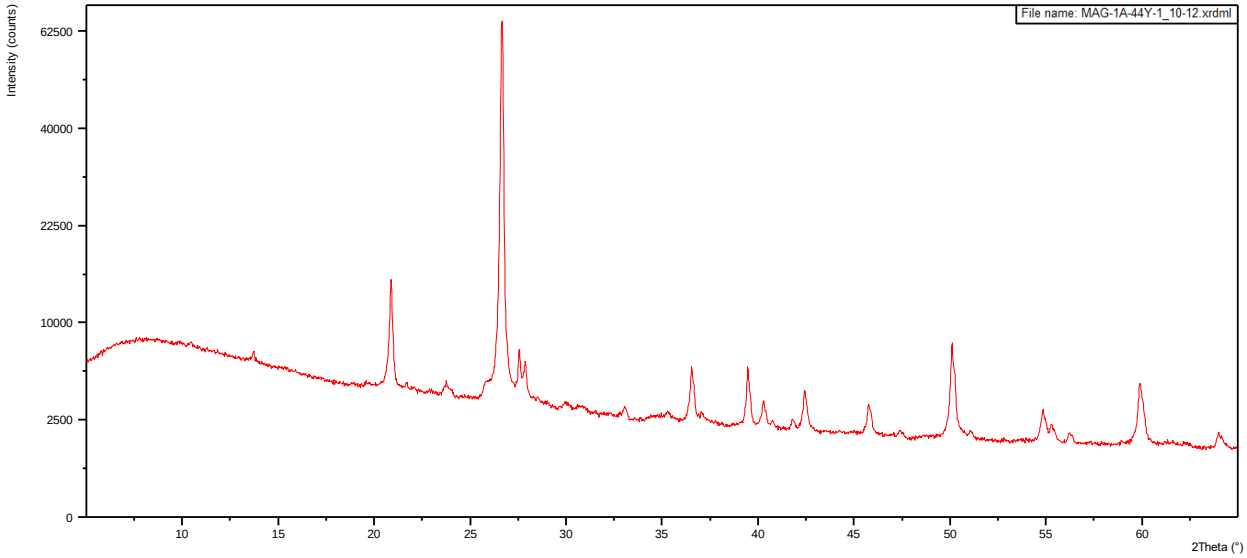
File name: MAG-1A-44Y-1_10-12.xrdml
Intensity (counts)
62500
40000
22500
10000
2500
0
10
15
20
25
30
35
40
45
50
55
60
2Theta (°)

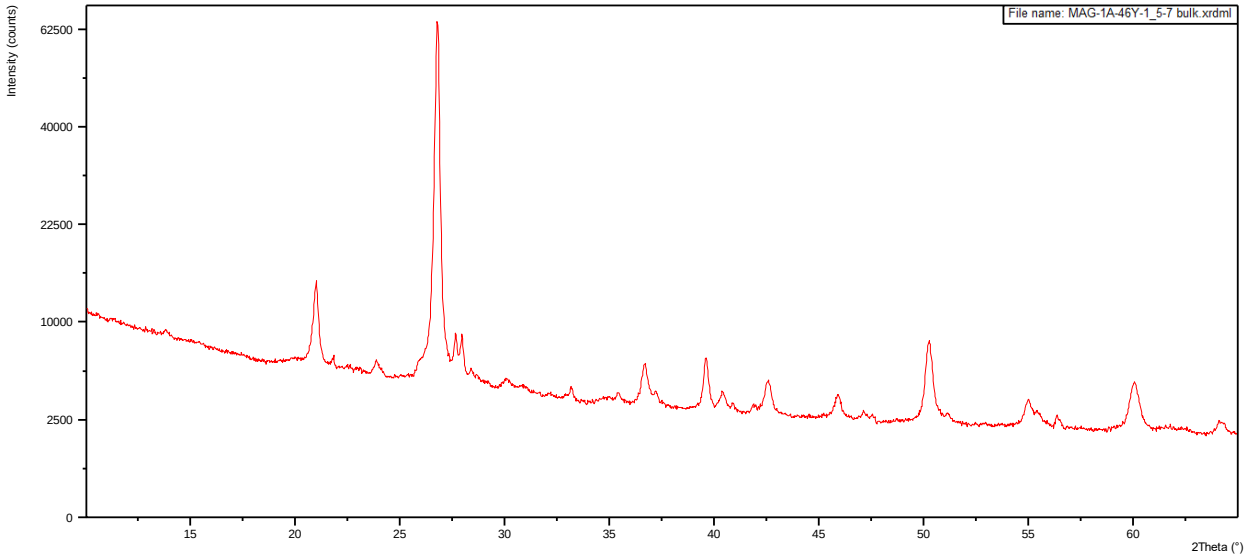
File name: MAG-1A-46Y-1_5-7 bulk.xrdml
Intensity (counts)
62500
40000
22500
10000
2500
0
15
20
25
30
35
40
45
50
55
60
2Theta (°)

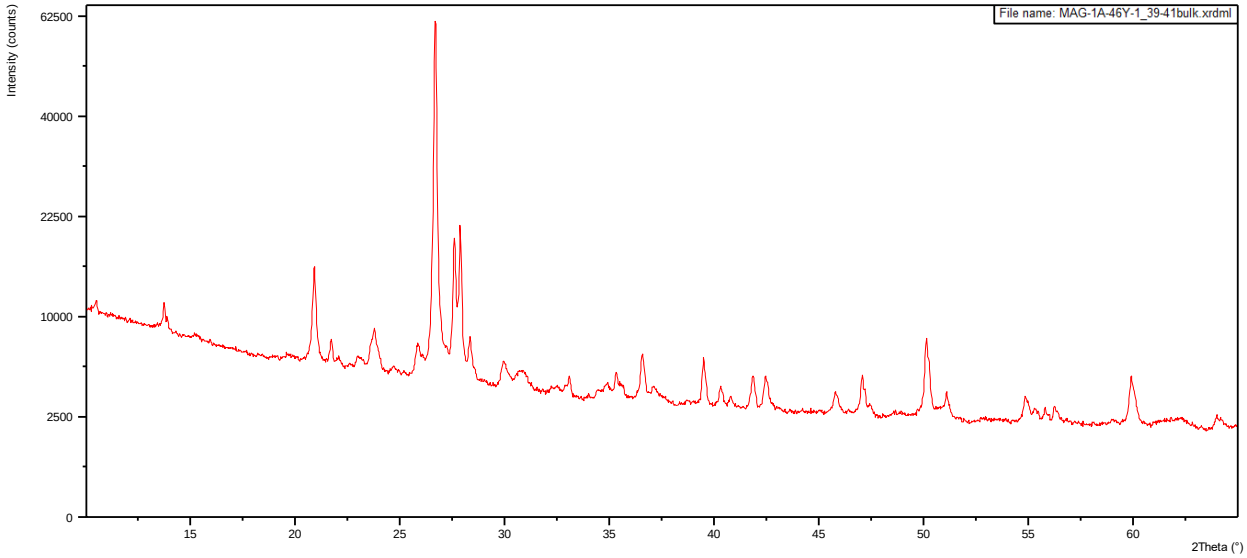
File name: MAG-1A-46Y-1_39-41bulk.xrdml
Intensity (counts)
62500
40000
22500
10000
2500
0
15
20
25
30
35
40
45
50
55
60
2Theta (°)

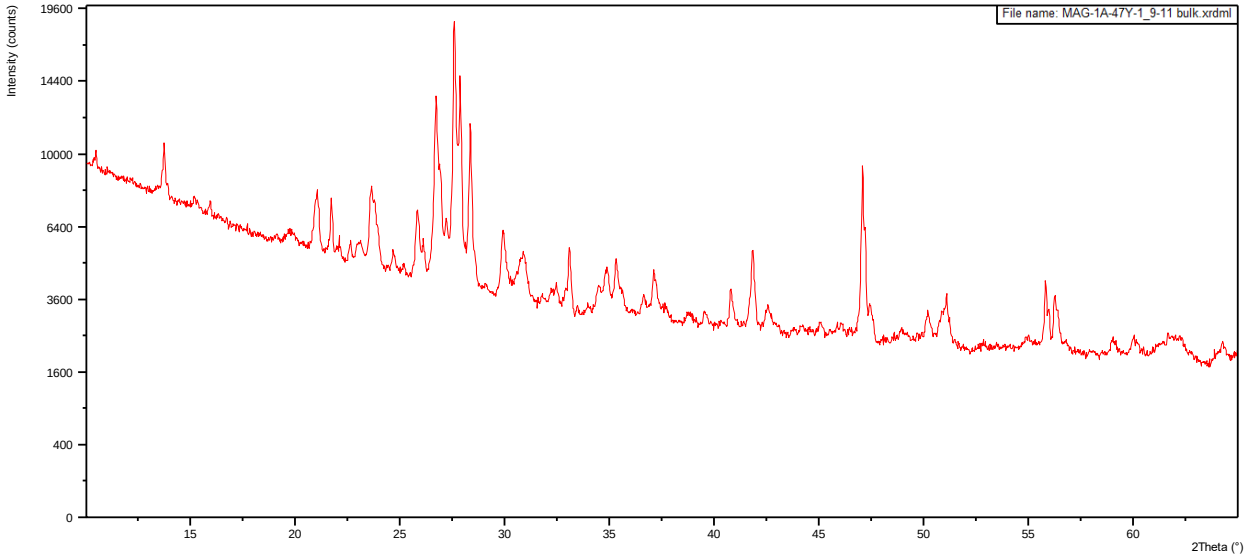
File name: MAG-1A-47Y-1_9-11 bulk.xrdml
Intensity (counts)
19600
14400
10000
6400
3600
1600
400
0
15
20
25
30
35
40
45
50
55
60
2Theta (°)

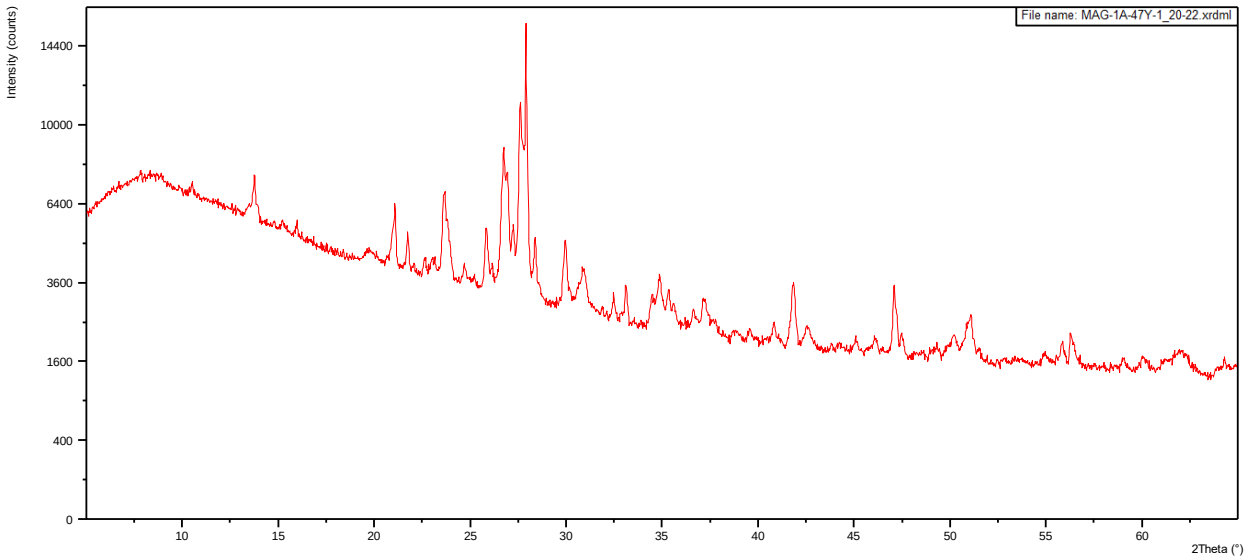
File name: MAG-1A-47Y-1_20-22.xrdml
Intensity (counts)
14400
10000
6400
3600
1600
400
0
10
15
20
25
30
35
40
45
50
55
60
2Theta (°)

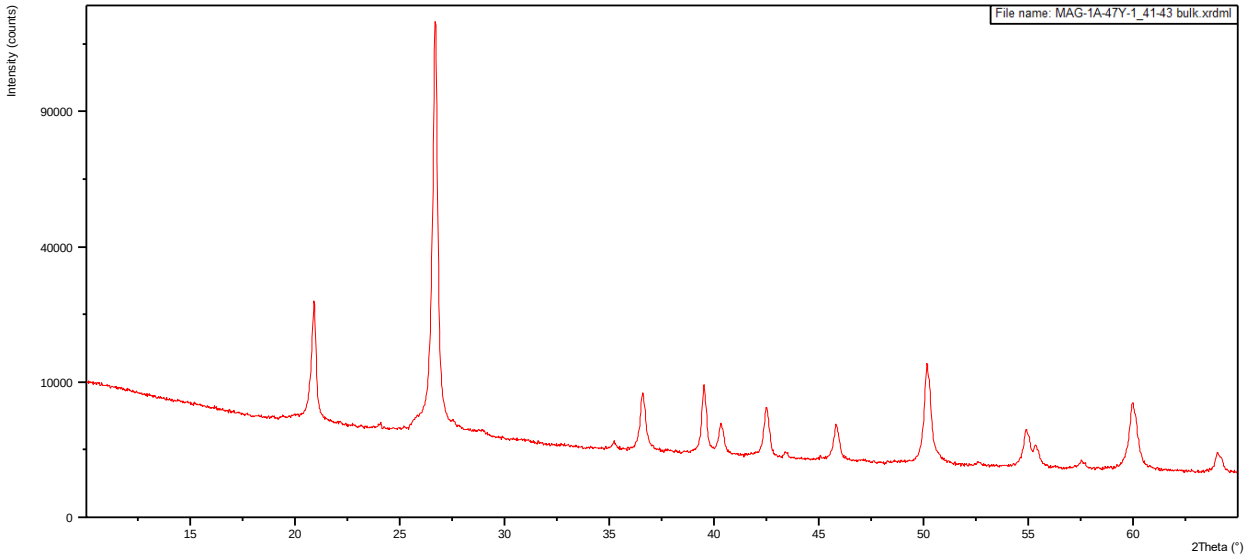
File name: MAG-1A-47Y-1_41-43 bulk.xrdml
Intensity (counts)
90000
40000
10000
0
15
20
25
30
35
40
45
50
55
60
2Theta (°)

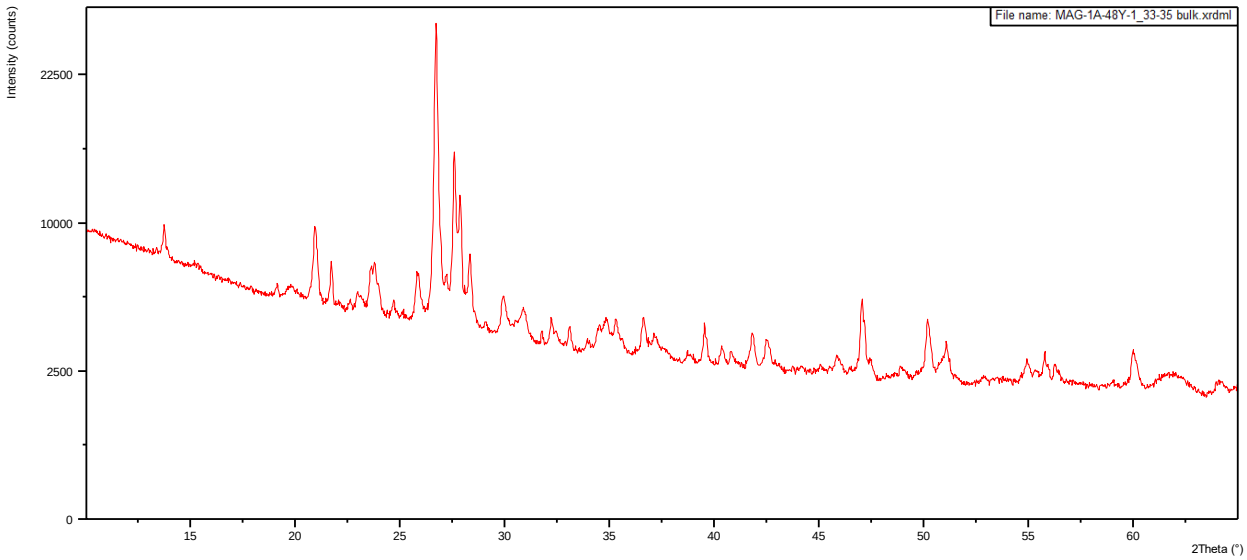
File name: MAG-1A-48Y-1_33-35 bulk.xrdml
Intensity (counts)
22500
10000
2500
0
15
20
25
30
35
40
45
50
55
60
2Theta (°)

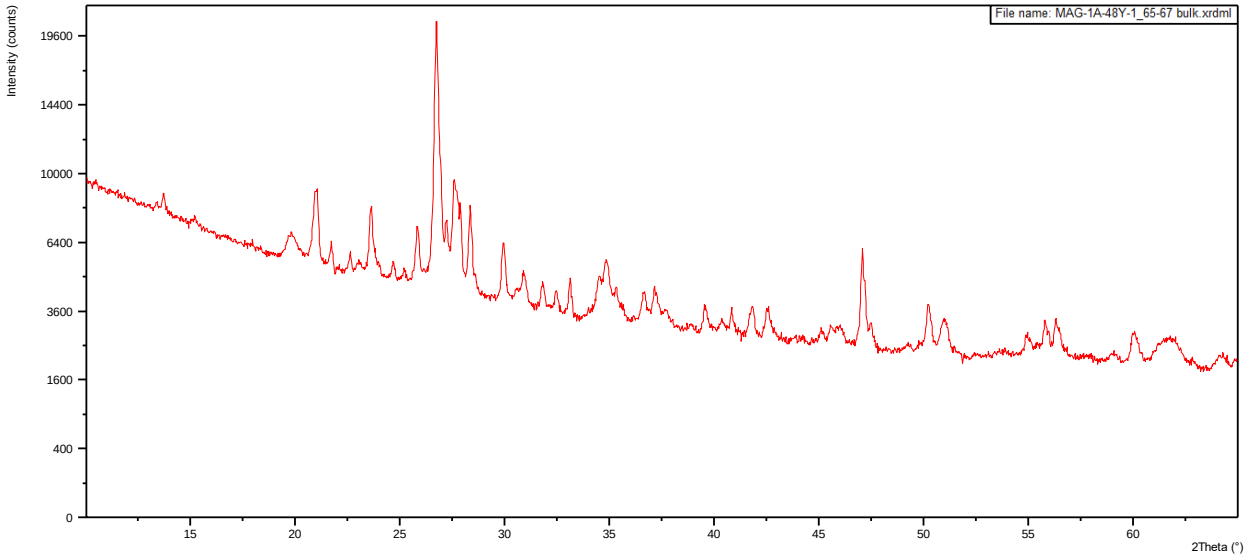
File name: MAG-1A-48Y-1_65-67 bulk.xrdml
Intensity (counts)
19600
14400
10000
6400
3600
1600
400
0
15
20
25
30
35
40
45
50
55
60
2Theta (°)

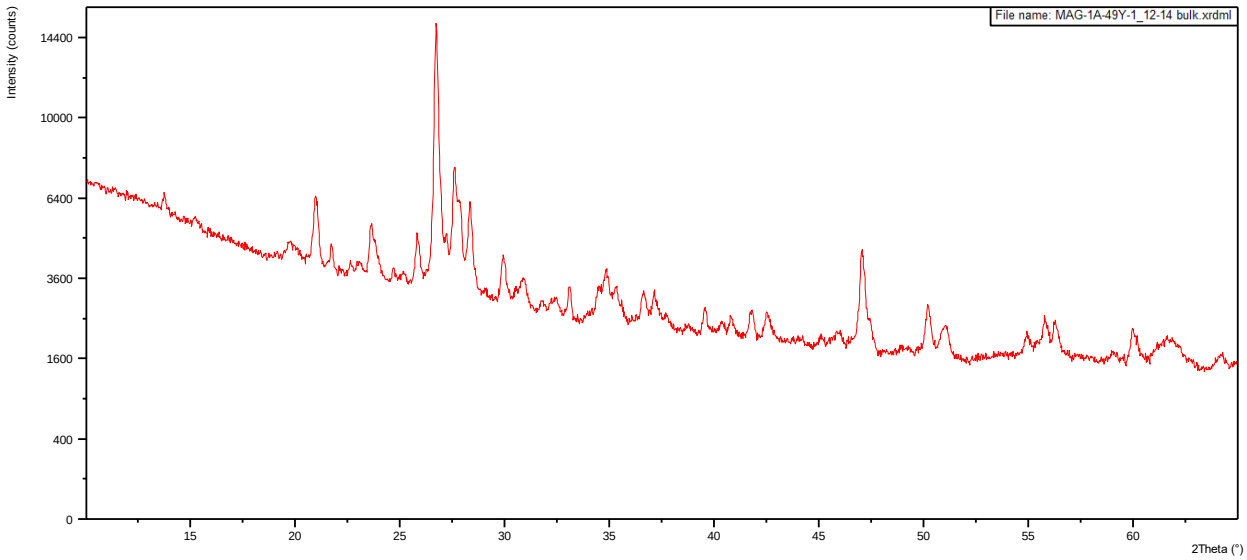
File name: MAG-1A-49Y-1_12-14 bulk.xrdml
Intensity (counts)
14400
10000
6400
3600
1600
400
0
15
20
25
30
35
40
45
50
55
60
2Theta (°)

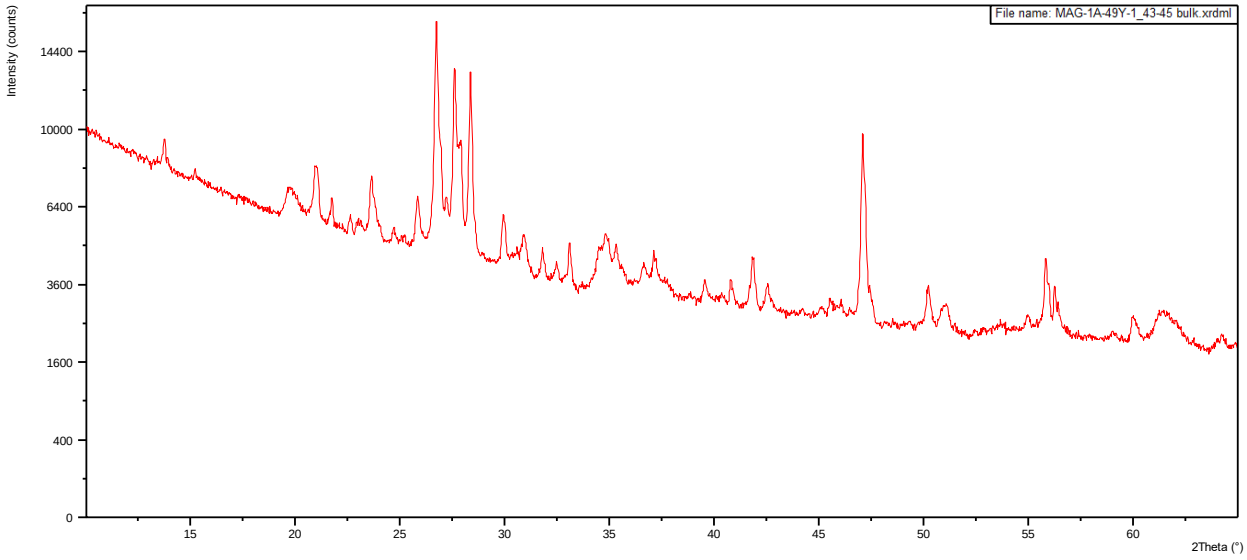
File name: MAG-1A-49Y-1_43-45 bulk.xrdml
Intensity (counts)
14400
10000
6400
3600
1600
400
0
15
20
25
30
35
40
45
50
55
60
2Theta (°)

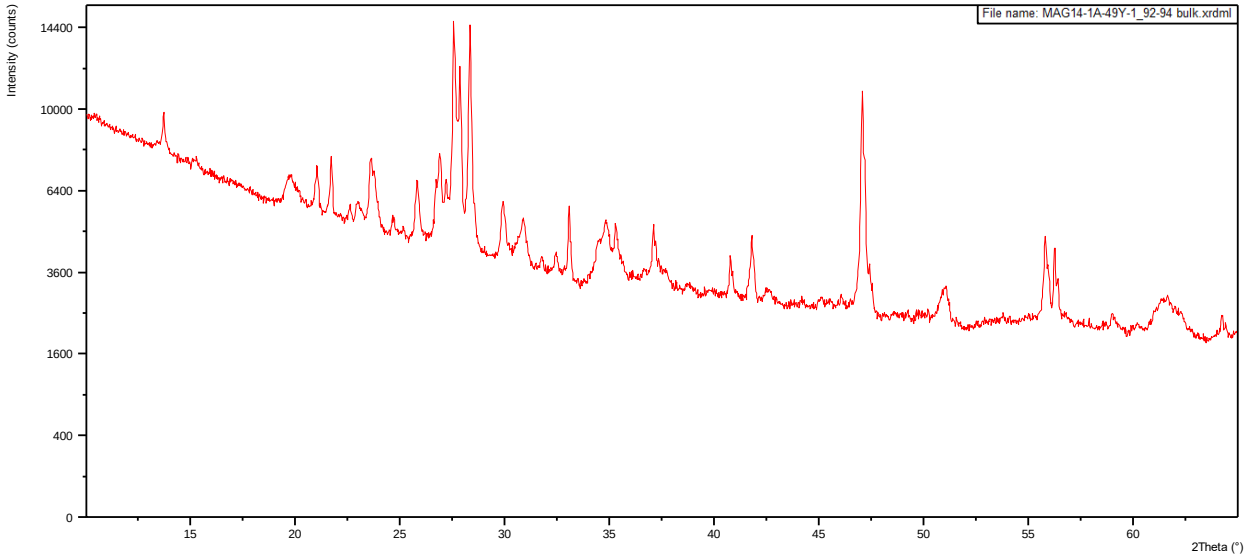
File name: MAG14-1A-49Y-1_92-94 bulk.xrdml
Intensity (counts)
14400
10000
6400
3600
1600
400
0
15
20
25
30
35
40
45
50
55
60
2Theta (°)

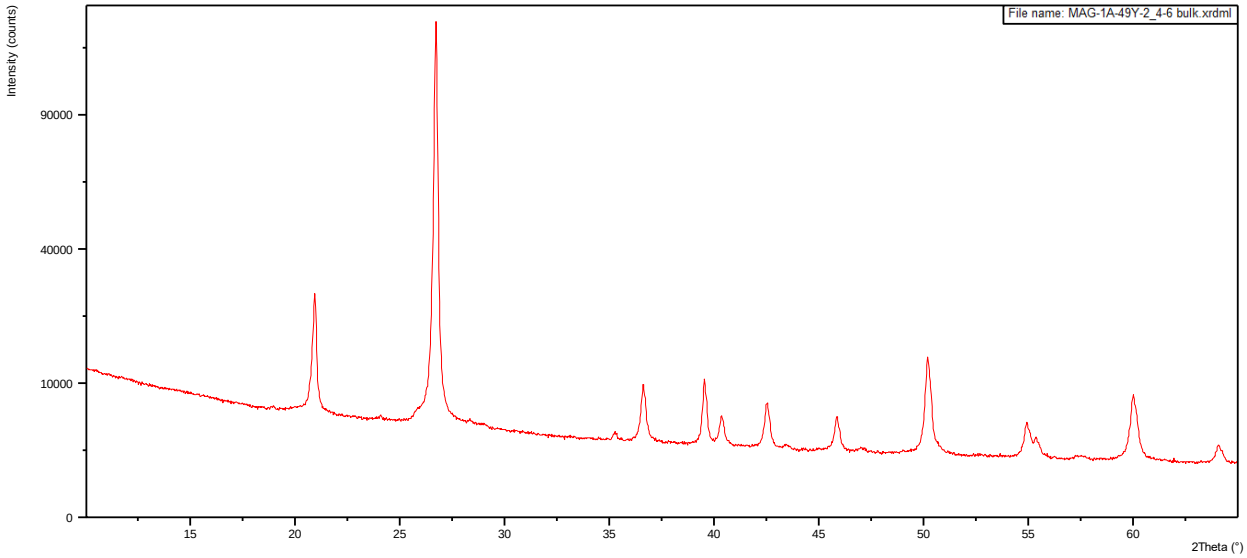
File name: MAG-1A-49Y-2_4-6 bulk.xrdml
Intensity (counts)
90000
40000
10000
0
15
20
25
30
35
40
45
50
55
60
2Theta (°)

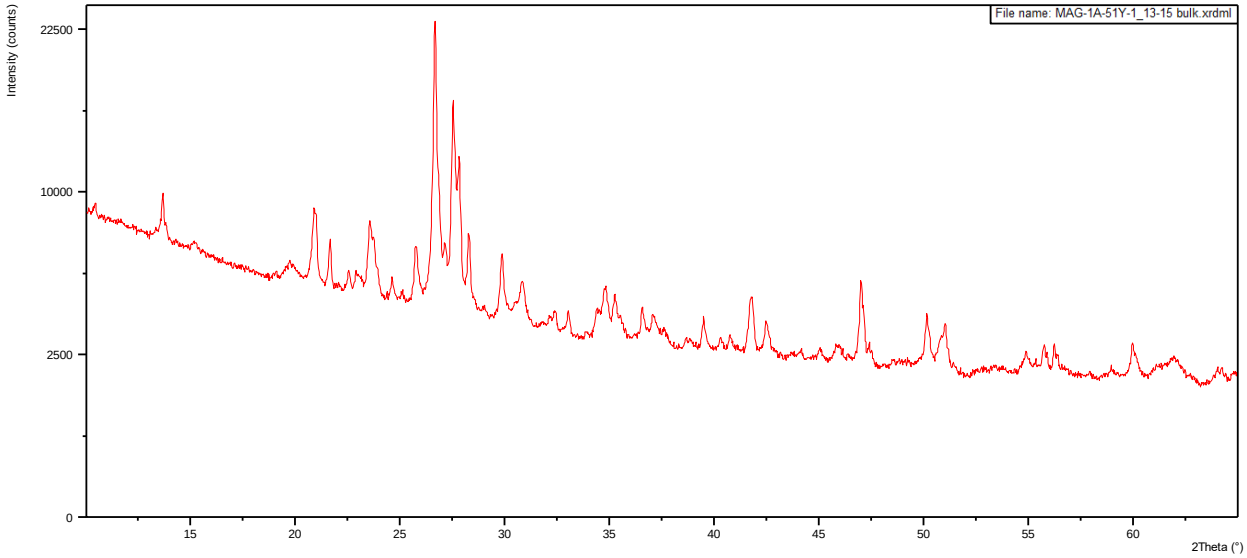
File name: MAG-1A-51Y-1_13-15 bulk.xrdml
Intensity (counts)
22500
10000
2500
0
15
20
25
30
35
40
45
50
55
60
2Theta (°)

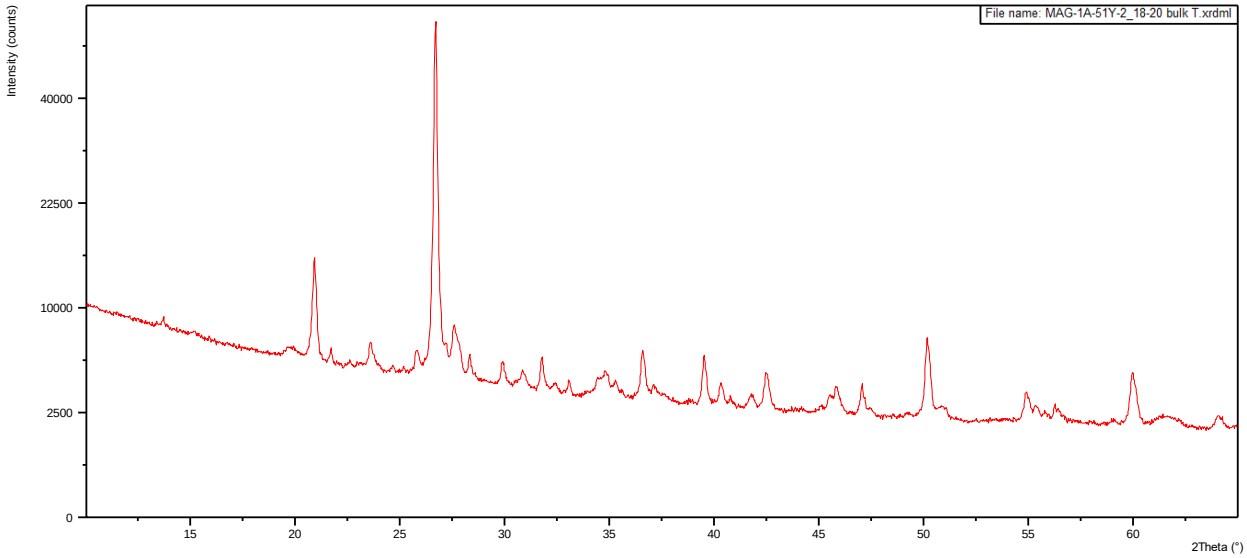
File name: MAG-1A-51Y-2_18-20 bulk T.xrdml
Intensity (counts)
40000
22500
10000
2500
0
15
20
25
30
35
40
45
50
55
60
2Theta (°)

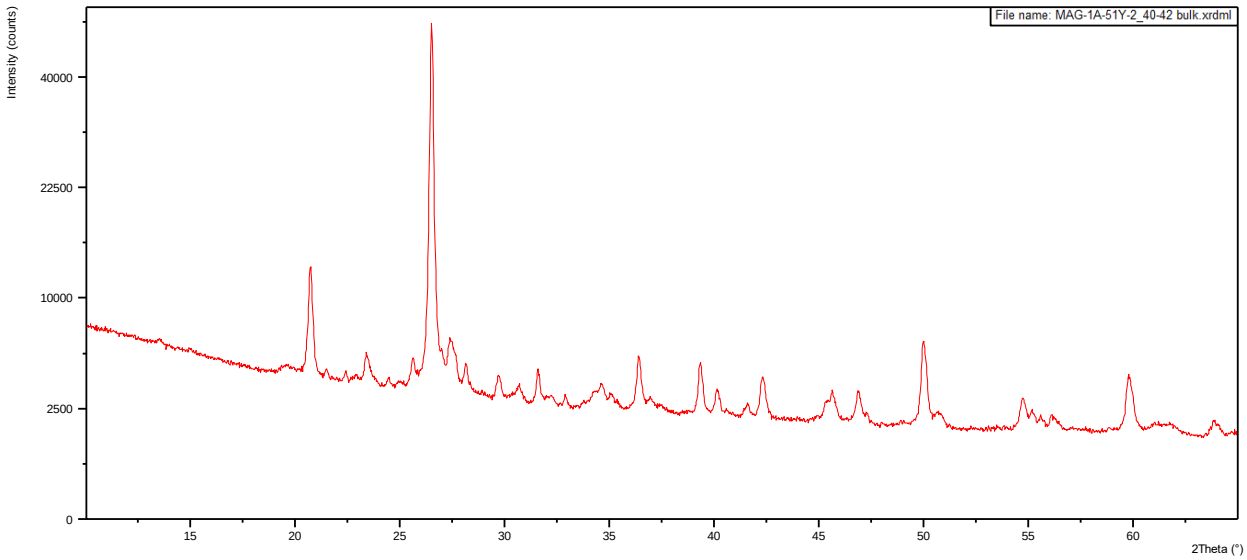
File name: MAG-1A-51Y-2_40-42 bulk.xrdml
Intensity (counts)
40000
22500
10000
2500
0
15
20
25
30
35
40
45
50
55
60
2Theta (°)

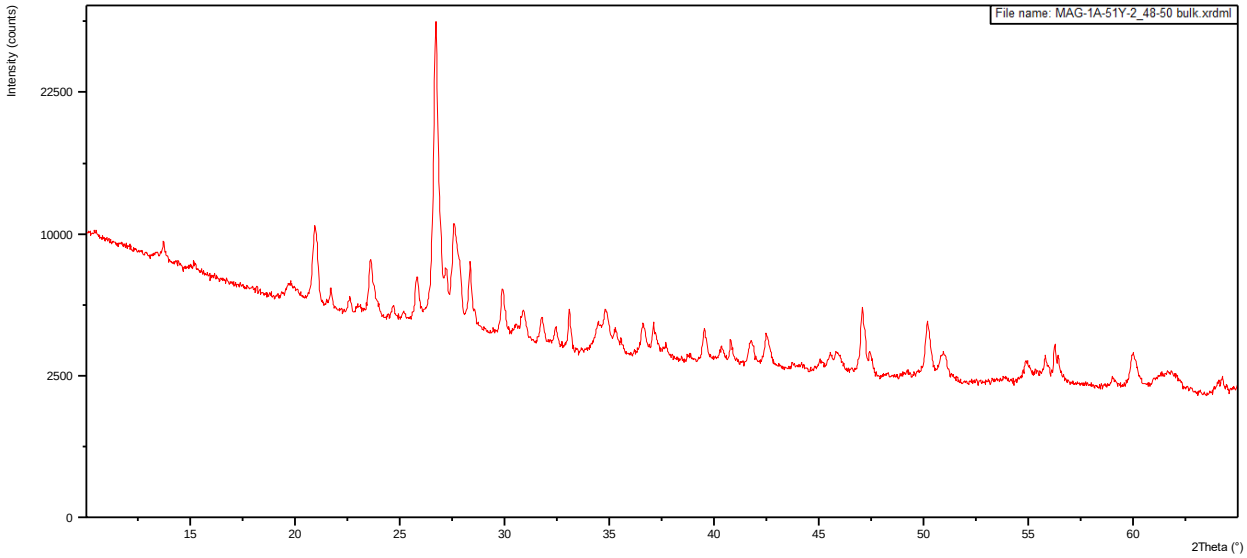
File name: MAG-1A-51Y-2_48-50 bulk.xrdml
Intensity (counts)
22500
10000
2500
0
15
20
25
30
35
40
45
50
55
60
2Theta (°)

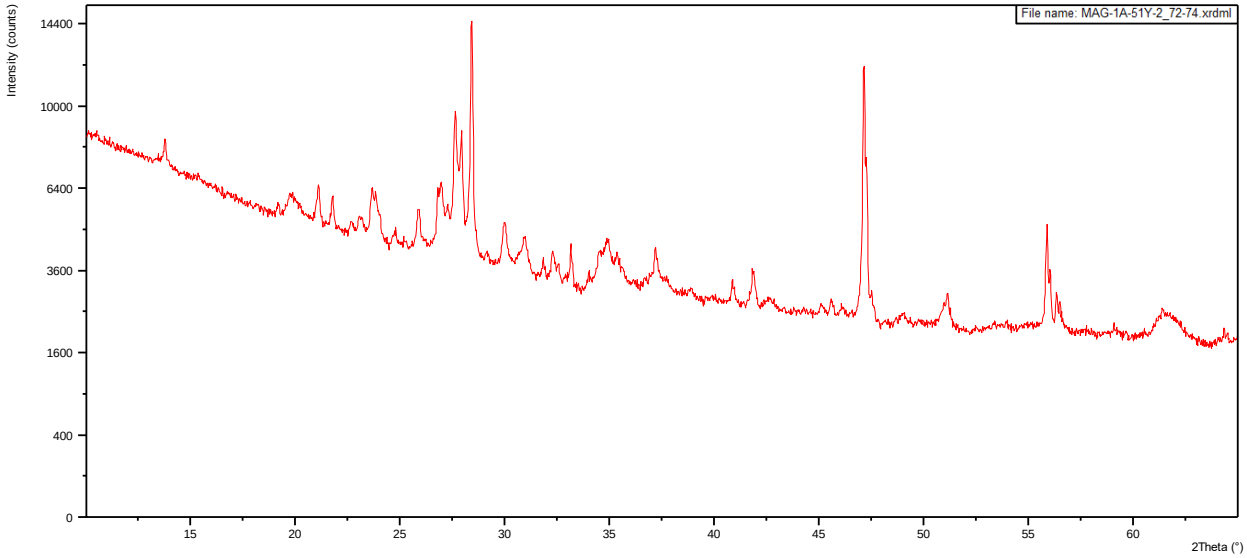
File name: MAG-1A-51Y-2_72-74.xrdml
Intensity (counts)
14400
10000
6400
3600
1600
400
0
15
20
25
30
35
40
45
50
55
60
2Theta (°)

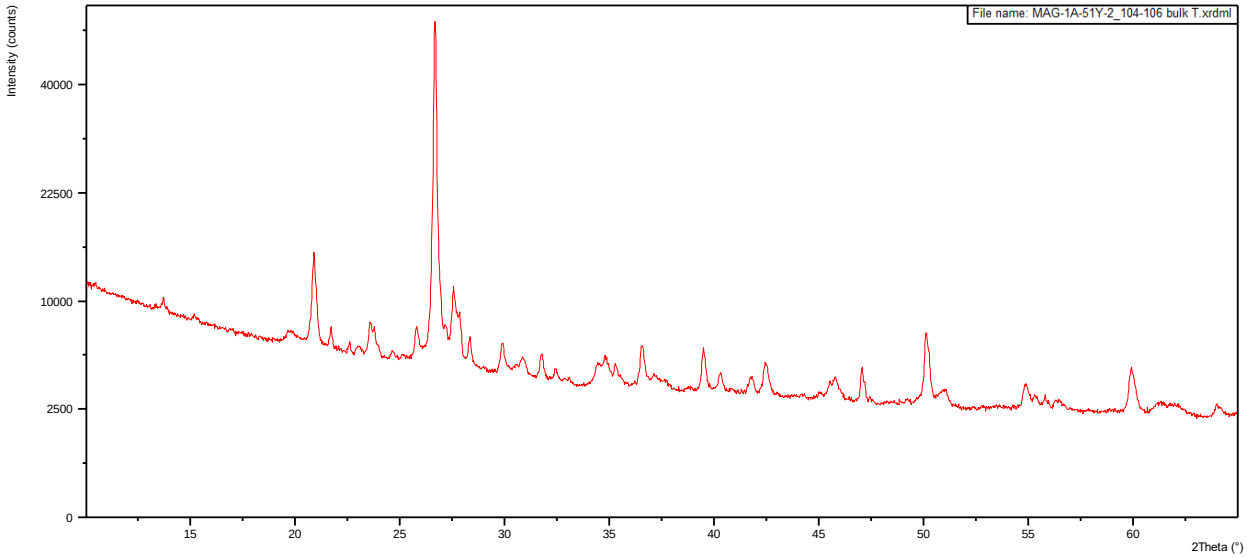
File name: MAG-1A-51Y-2_104-106 bulk T.xrdml
Intensity (counts)
40000
22500
10000
2500
0
15
20
25
30
35
40
45
50
55
60
2Theta (°)

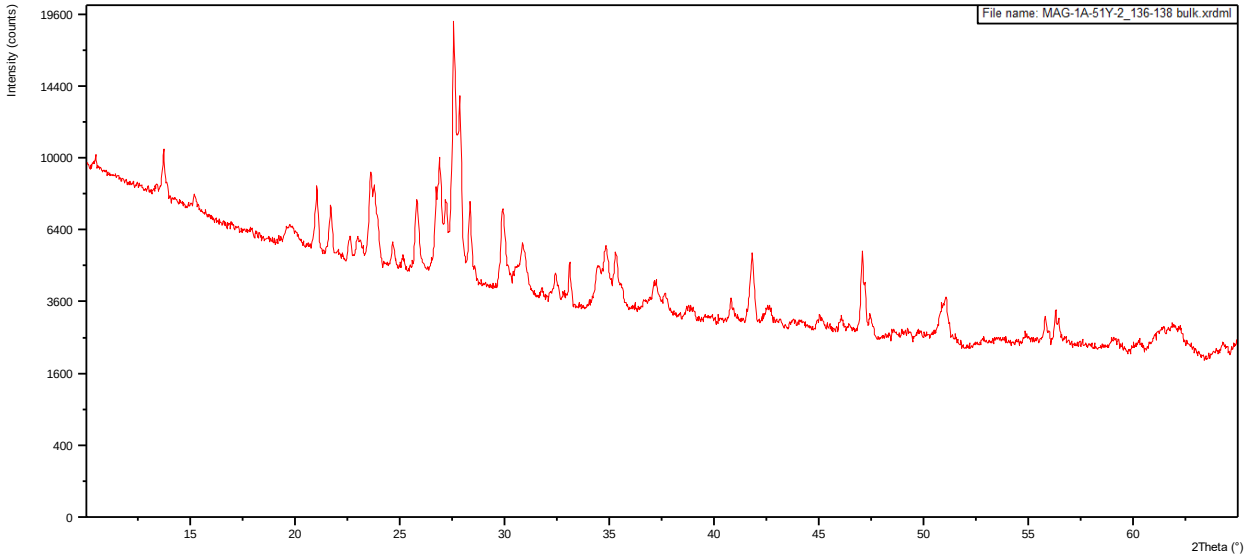
File name: MAG-1A-51Y-2_136-138 bulk.xrdml
Intensity (counts)
19600
14400
10000
6400
3600
1600
400
0
15
20
25
30
35
40
45
50
55
60
2Theta (°)

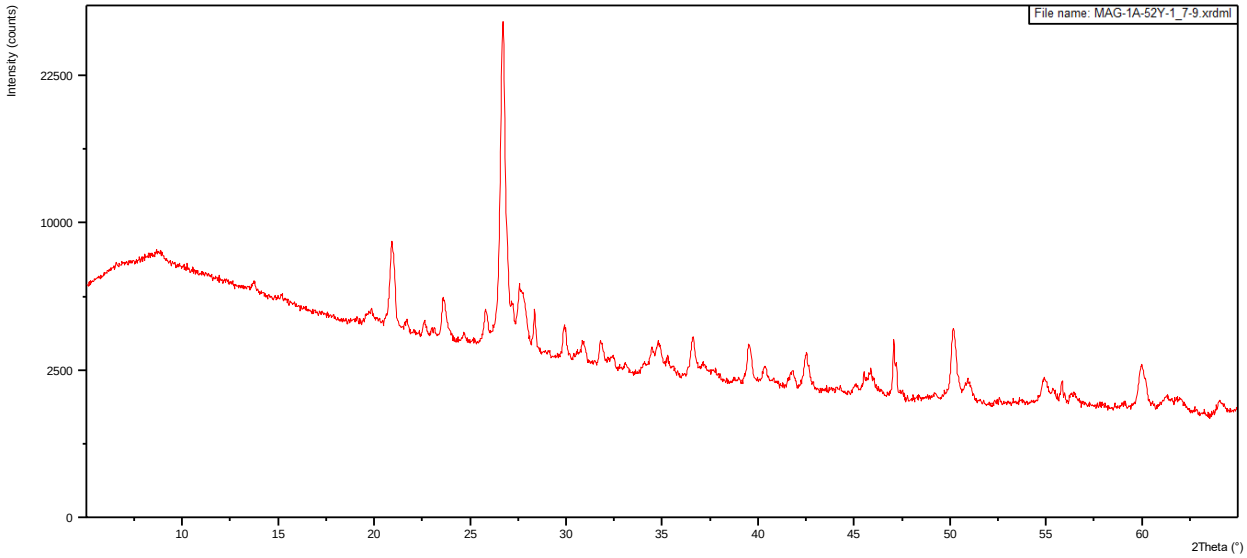
File name: MAG-1A-52Y-1_7-9.xrdml
Intensity (counts)
22500
10000
2500
0
10
15
20
25
30
35
40
45
50
55
60
2Theta (°)

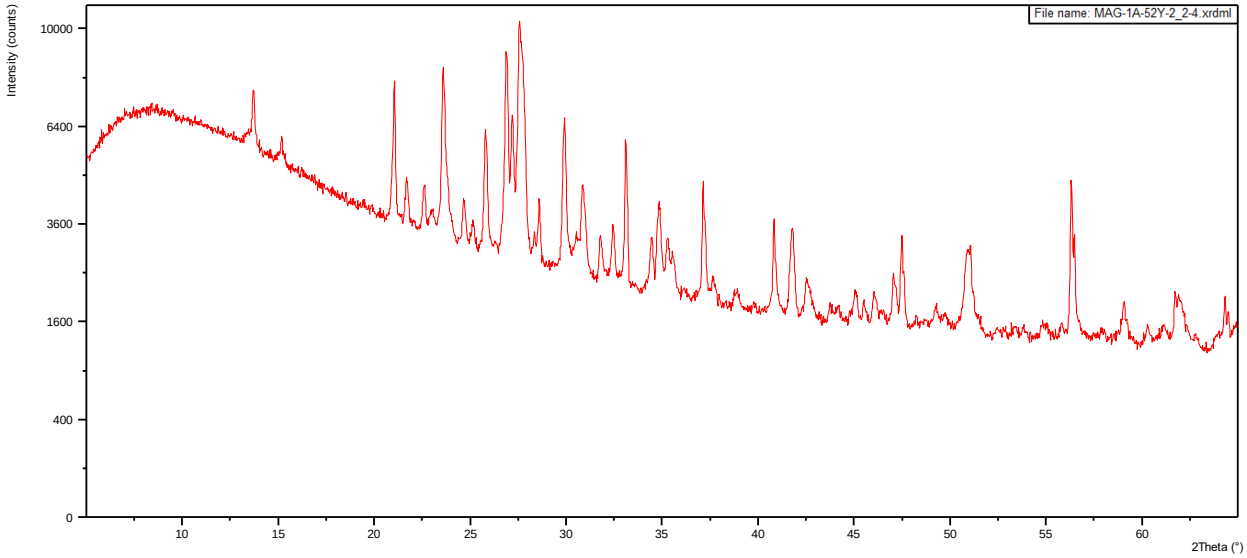
File name: MAG-1A-52Y-2_2-4.xrdml
Intensity (counts)
10000
6400
3600
1600
400
0
10
15
20
25
30
35
40
45
50
55
60
2Theta (°)

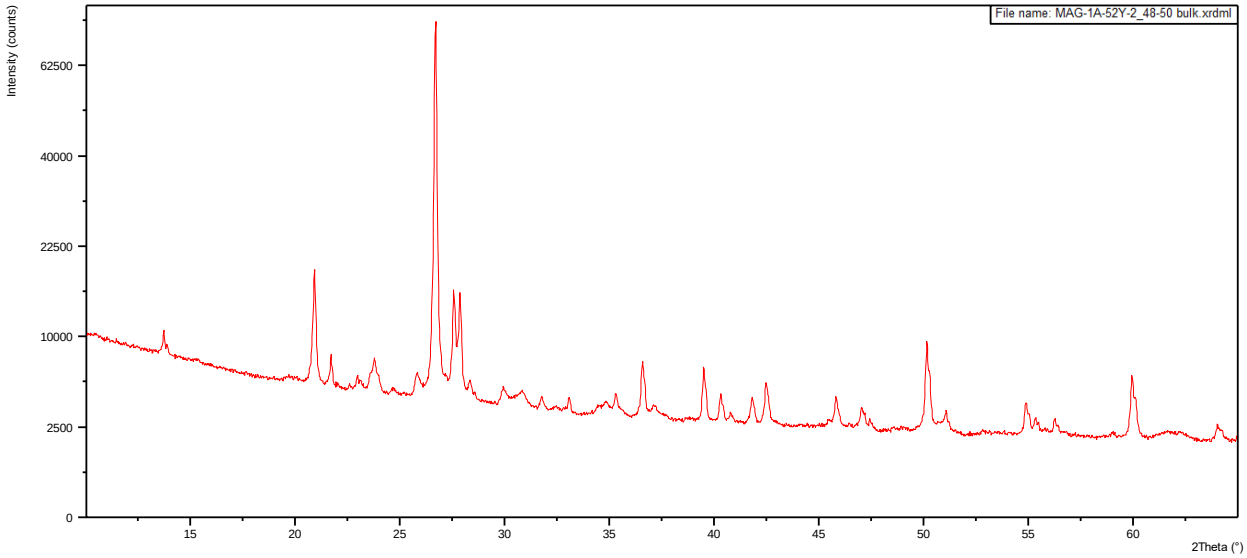
File name: MAG-1A-52Y-2_48-50 bulk.xrdml
Intensity (counts)
62500
40000
22500
10000
2500
0
15
20
25
30
35
40
45
50
55
60
2Theta (°)

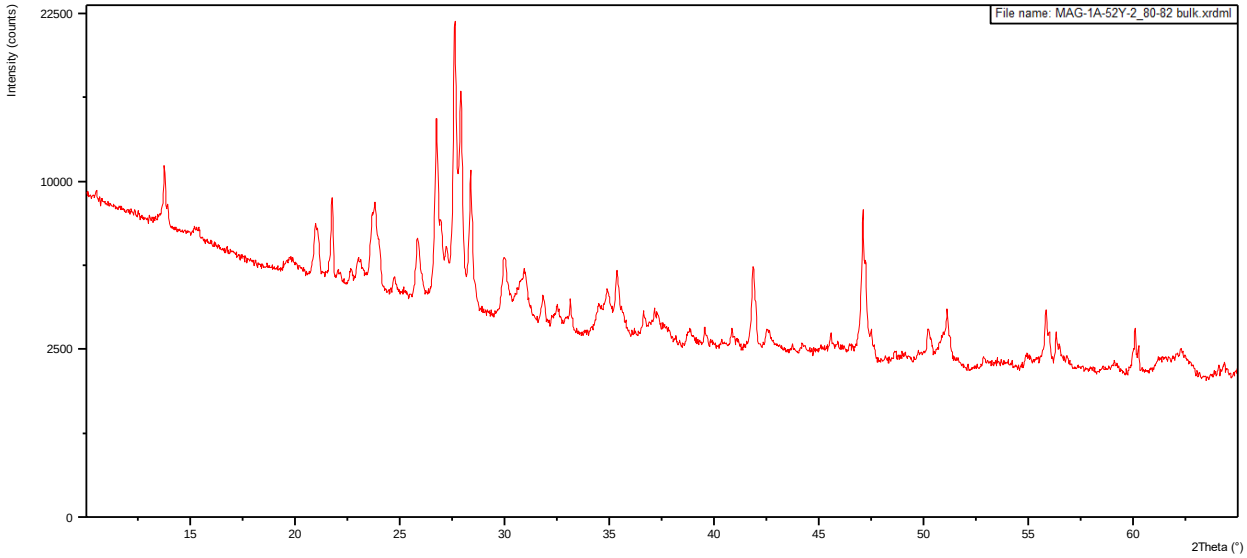
File name: MAG-1A-52Y-2_80-82 bulk.xrdml
Intensity (counts)
22500
10000
2500
0
15
20
25
30
35
40
45
50
55
60
2Theta (°)

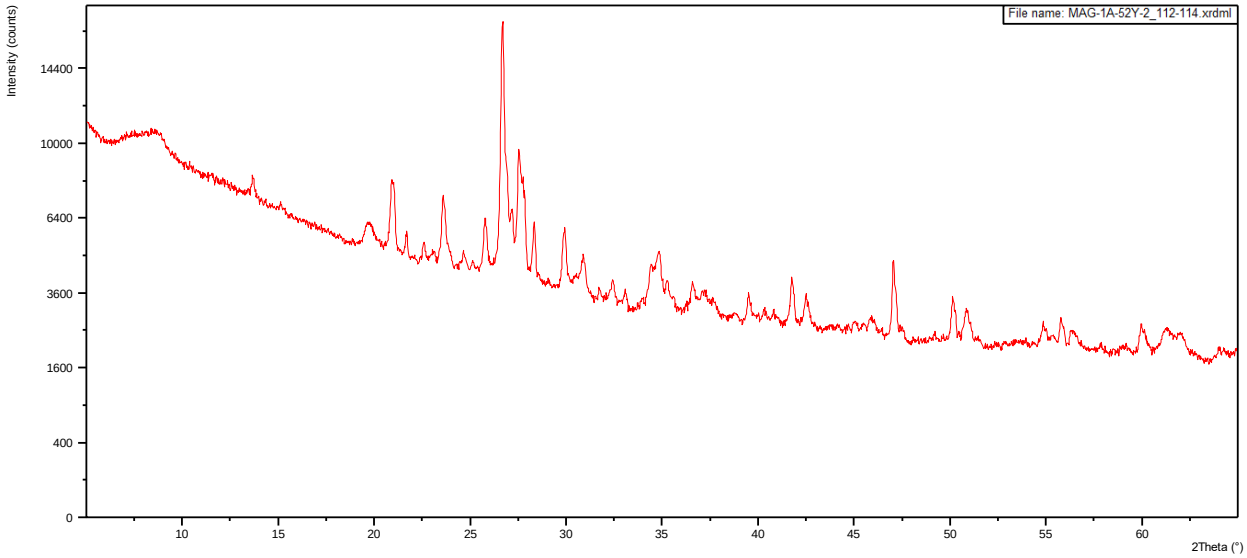
File name: MAG-1A-52Y-2_112-114.xrdml
Intensity (counts)
14400
10000
6400
3600
1600
400
0
10
15
20
25
30
35
40
45
50
55
60
2Theta (°)

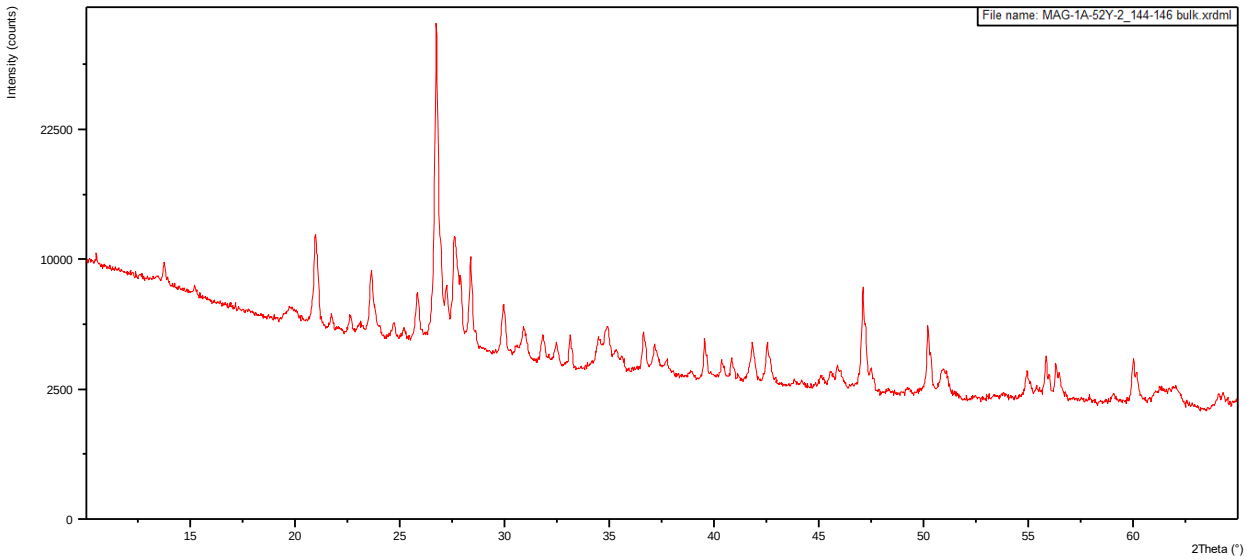
File name: MAG-1A-52Y-2_144-146 bulk.xrdml
Intensity (counts)
22500
10000
2500
0
15
20
25
30
35
40
45
50
55
60
2Theta (°)

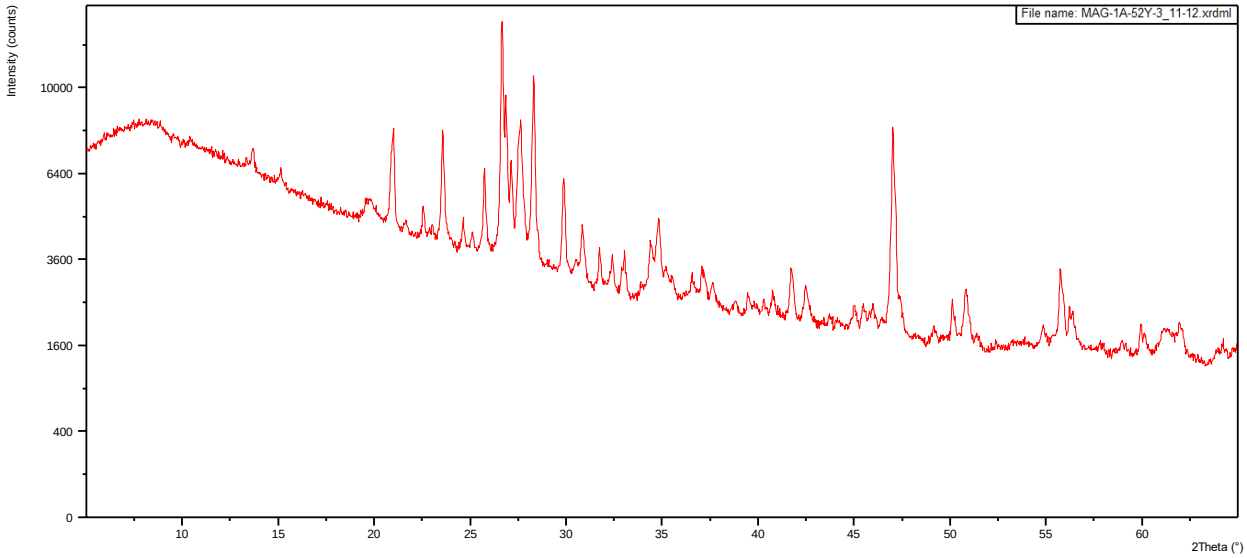
File name: MAG-1A-52Y-3_11-12.xrdml
Intensity (counts)
10000
6400
3600
1600
400
0
10
15
20
25
30
35
40
45
50
55
60
2Theta (°)

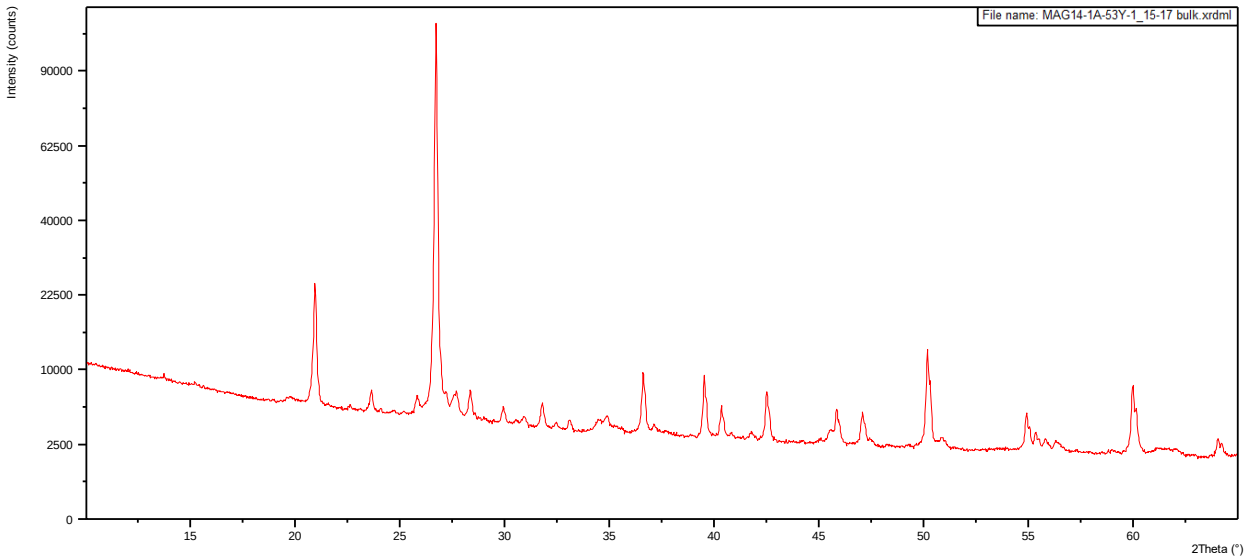
File name: MAG14-1A-53Y-1_15-17 bulk.xrdml
Intensity (counts)
90000
62500
40000
22500
10000
2500
0
15
20
25
30
35
40
45
50
55
60
2Theta (°)

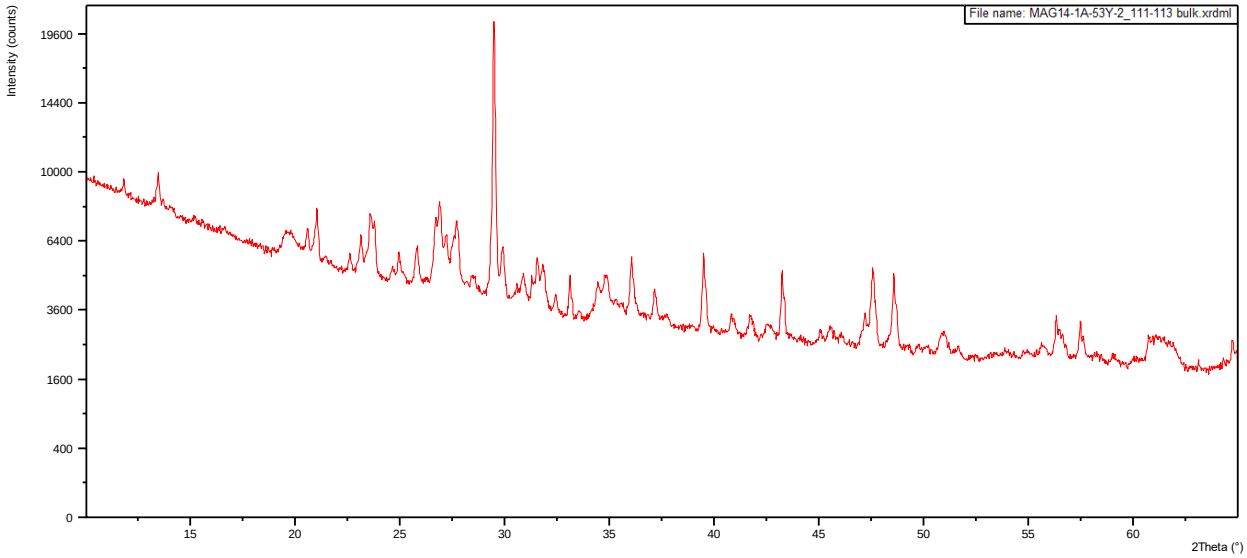
File name: MAG14-1A-53Y-2_111-113 bulk.xrdml
Intensity (counts)
19600
14400
10000
6400
3600
1600
400
0
15
20
25
30
35
40
45
50
55
60
2Theta (°)

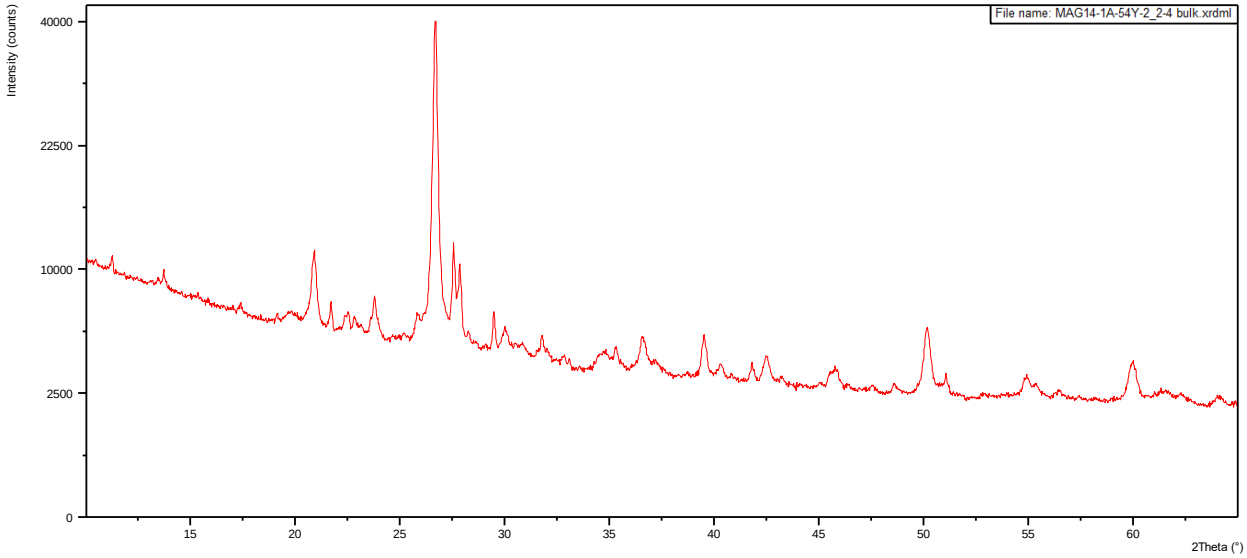
File name: MAG14-1A-54Y-2_2-4 bulk.xrdml
Intensity (counts)
40000
22500
10000
2500
0
15
20
25
30
35
40
45
50
55
60
2Theta (°)

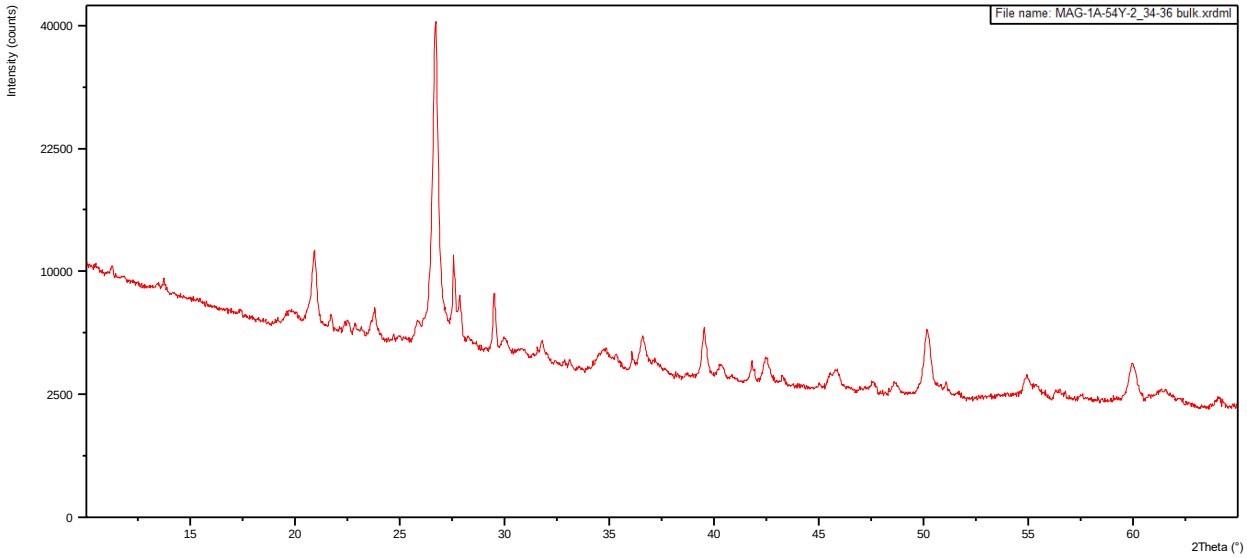
File name: MAG-1A-54Y-2_34-36 bulk.xrdml
Intensity (counts)
40000
22500
10000
2500
0
15
20
25
30
35
40
45
50
55
60
2Theta (°)

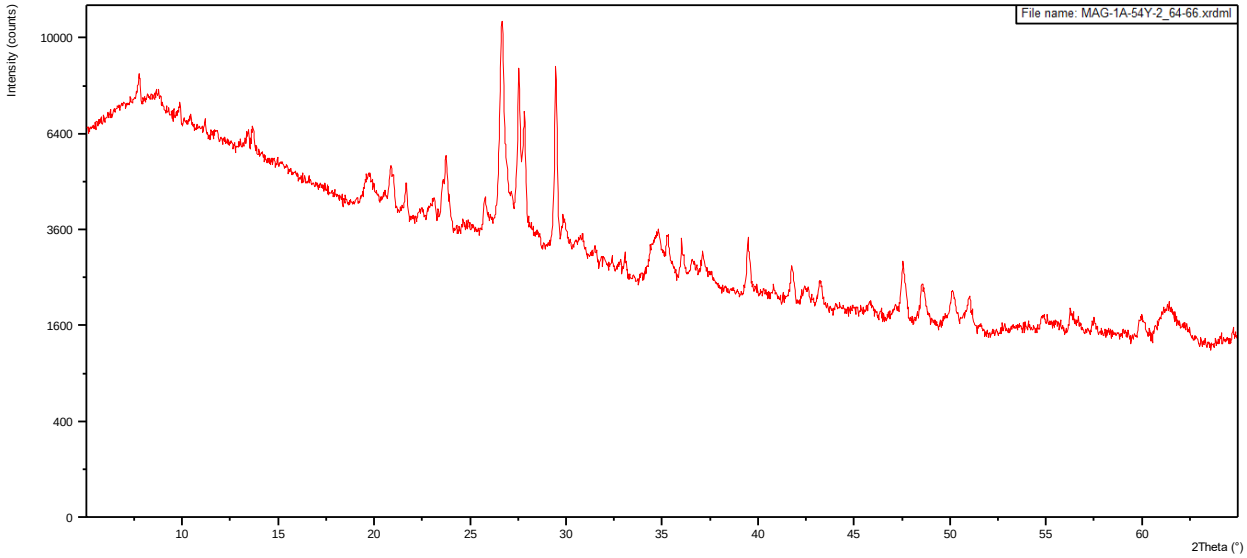
File name: MAG-1A-54Y-2_64-66.xrdml
Intensity (counts)
10000
6400
3600
1600
400
0
10
15
20
25
30
35
40
45
50
55
60
2Theta (°)

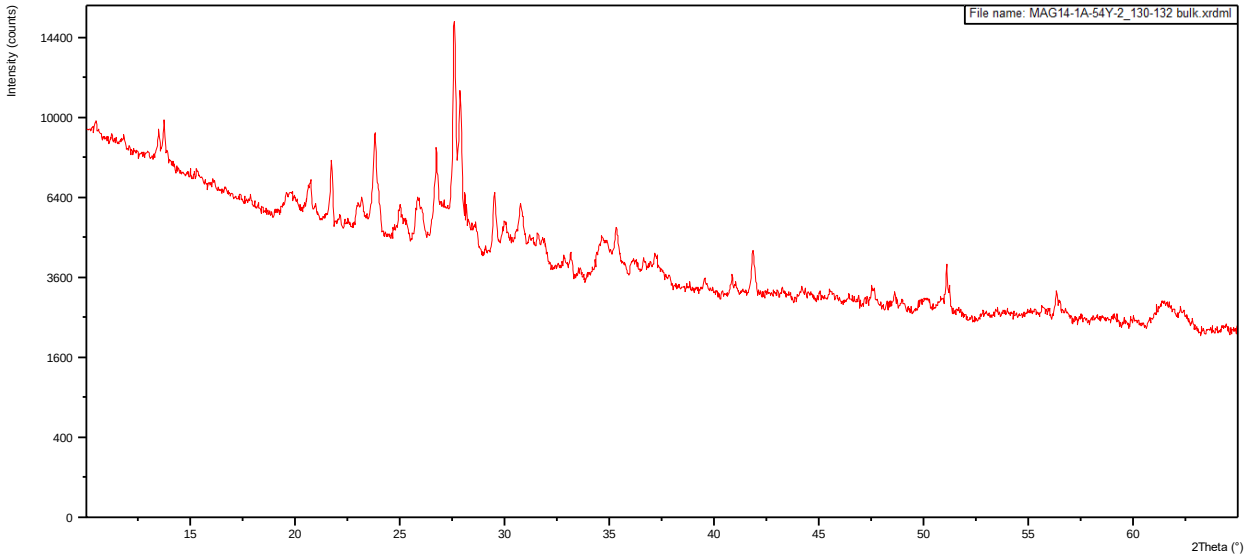
File name: MAG14-1A-54Y-2_130-132 bulk.xrdml
Intensity (counts)
14400
10000
6400
3600
1600
400
0
15
20
25
30
35
40
45
50
55
60
2Theta (°)

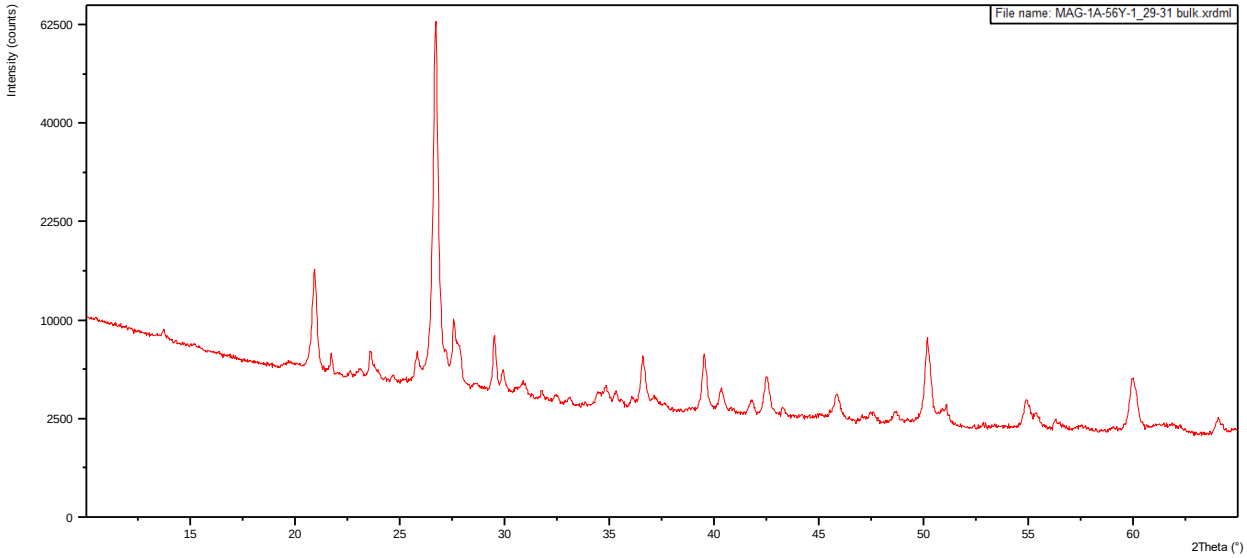
File name: MAG-1A-56Y-1_29-31 bulk.xrdml
Intensity (counts)
62500
40000
22500
10000
2500
0
15
20
25
30
35
40
45
50
55
60
2Theta (°)

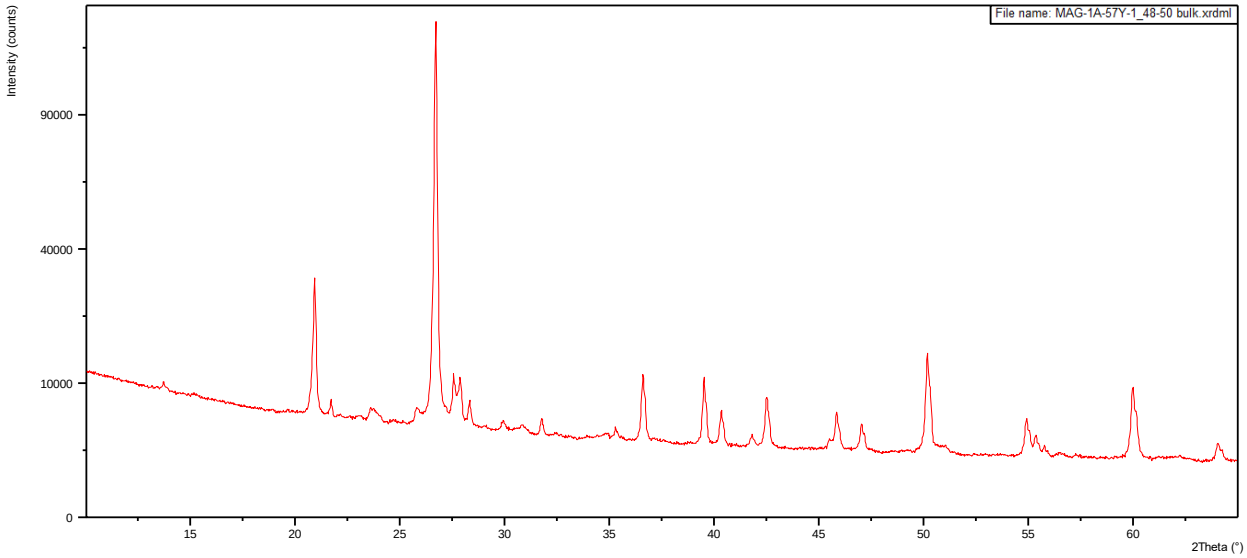
File name: MAG-1A-57Y-1_48-50 bulk.xrdml
Intensity (counts)
90000
40000
10000
0
15
20
25
30
35
40
45
50
55
60
2Theta (°)

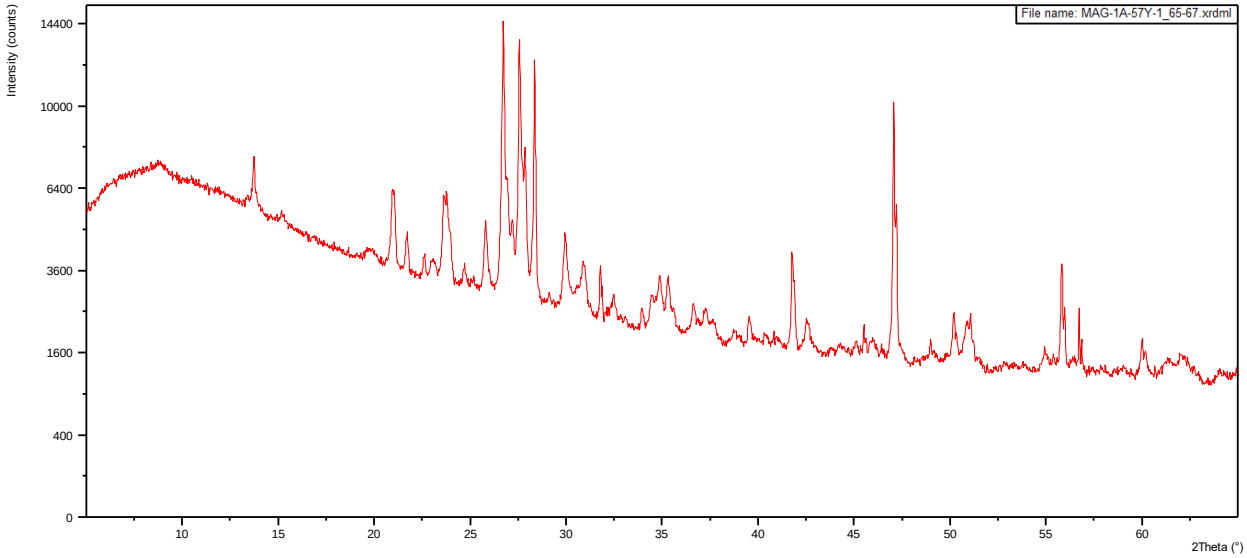
File name: MAG-1A-57Y-1_65-67.xrdml
Intensity (counts)
14400
10000
6400
3600
1600
400
0
10
15
20
25
30
35
40
45
50
55
60
2Theta (°)

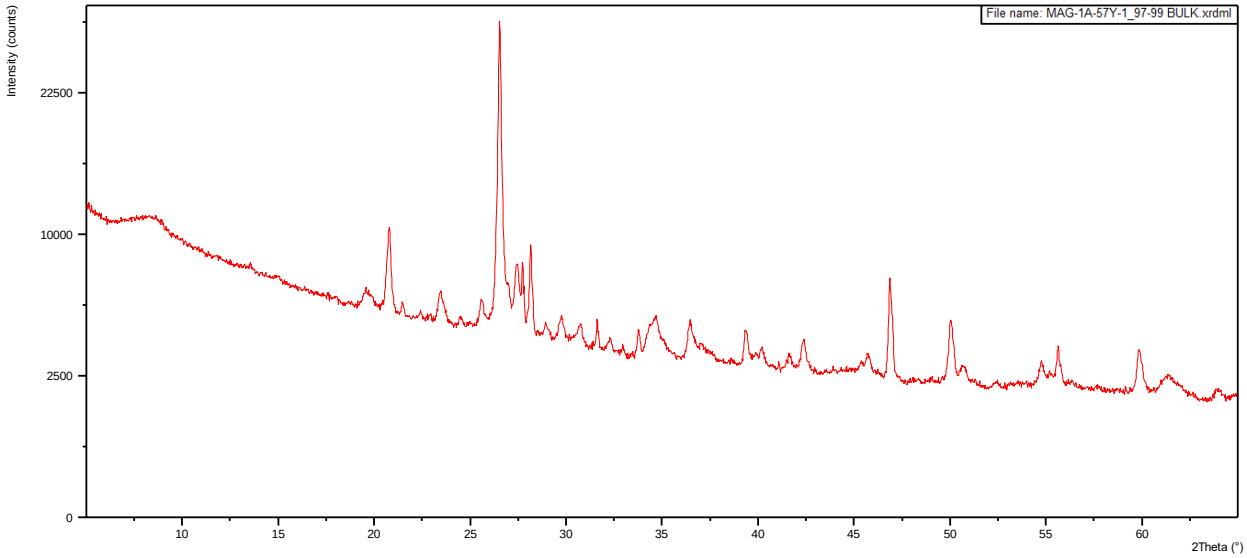
File name: MAG-1A-57Y-1_97-99 BULK.xrdml
Intensity (counts)
22500
10000
2500
0
10
15
20
25
30
35
40
45
50
55
60
2Theta (°)

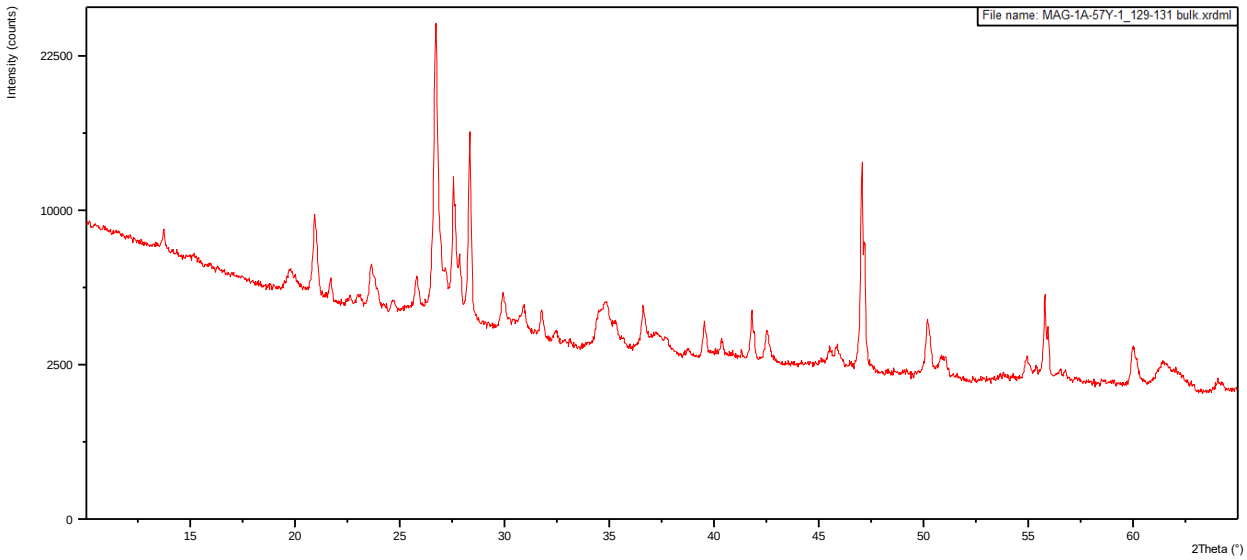
File name: MAG-1A-57Y-1_129-131 bulk.xrdml
Intensity (counts)
22500
10000
2500
0
15
20
25
30
35
40
45
50
55
60
2Theta (°)

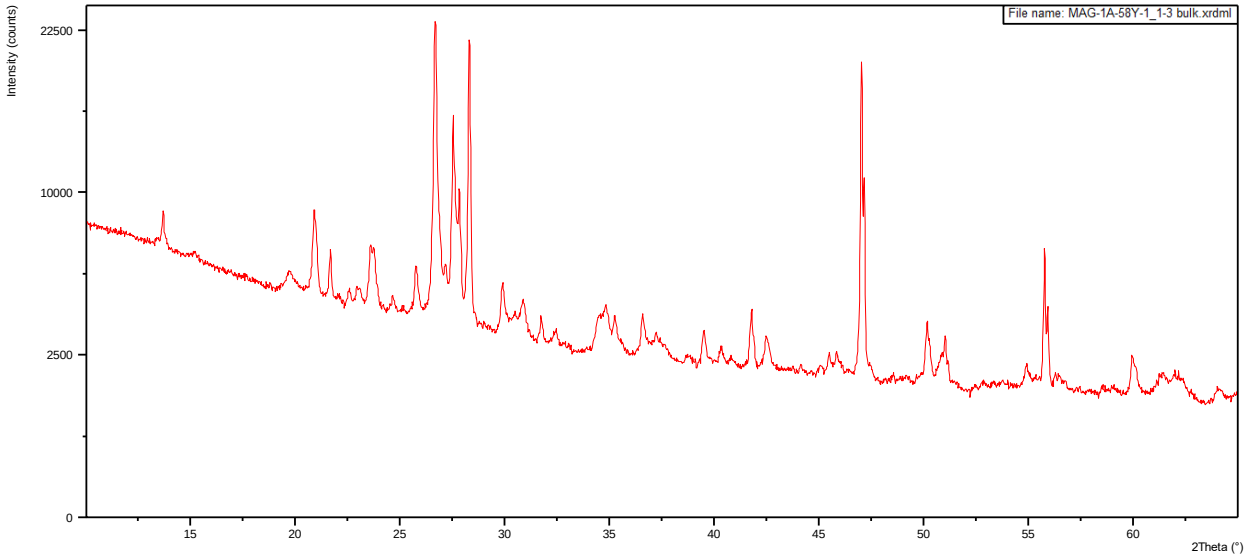
File name: MAG-1A-58Y-1_1-3 bulk.xrdml
Intensity (counts)
22500
10000
2500
0
15
20
25
30
35
40
45
50
55
60
2Theta (°)

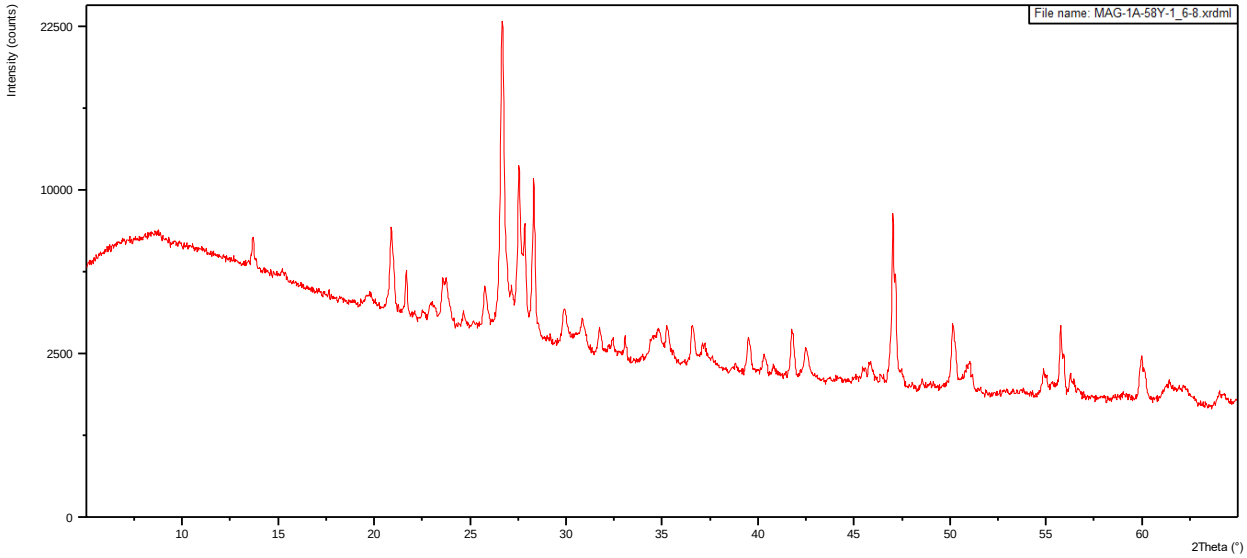
File name: MAG-1A-58Y-1_6-8.xrdml
Intensity (counts)
22500
10000
2500
0
10
15
20
25
30
35
40
45
50
55
60
2Theta (°)

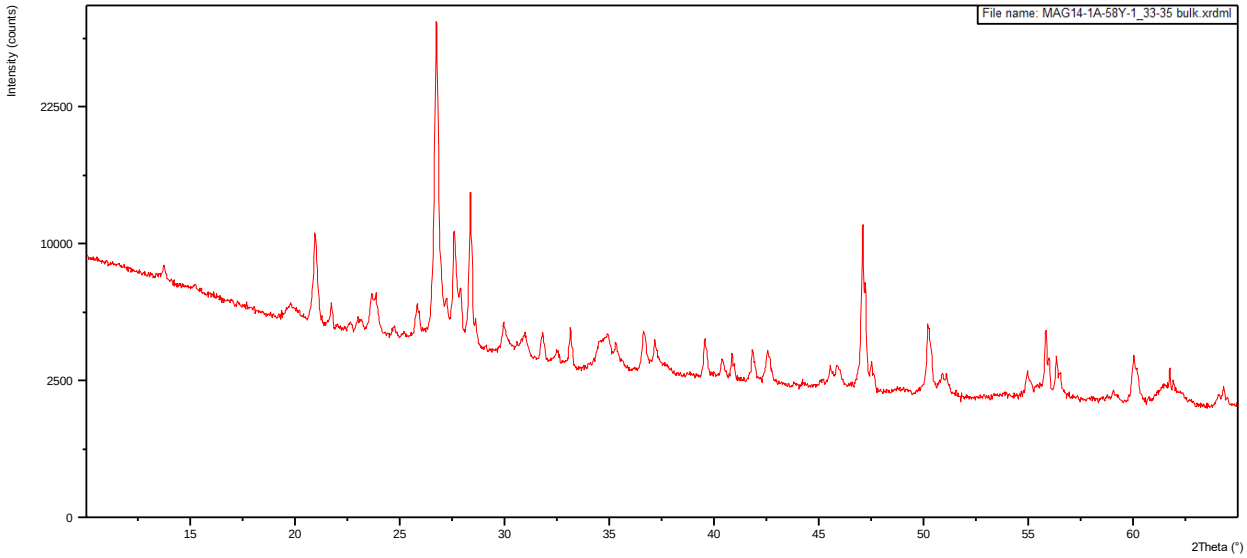
File name: MAG14-1A-58Y-1_33-35 bulk.xrdml
Intensity (counts)
22500
10000
2500
0
15
20
25
30
35
40
45
50
55
60
2Theta (°)

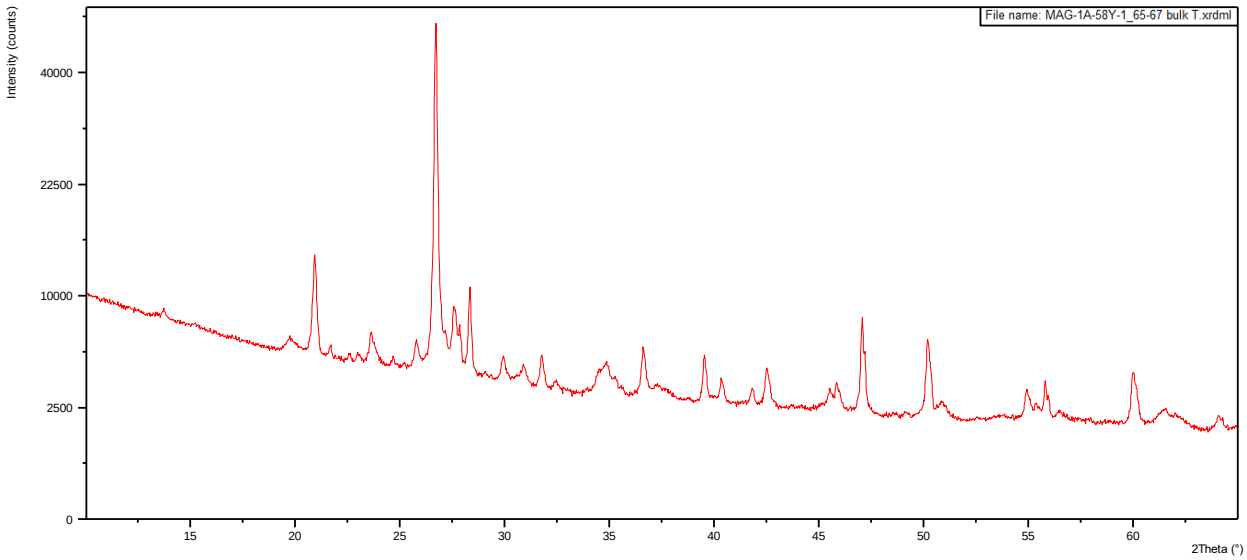
File name: MAG-1A-58Y-1_65-67 bulk T.xrdml
Intensity (counts)
40000
22500
10000
2500
0
15
20
25
30
35
40
45
50
55
60
2Theta (°)

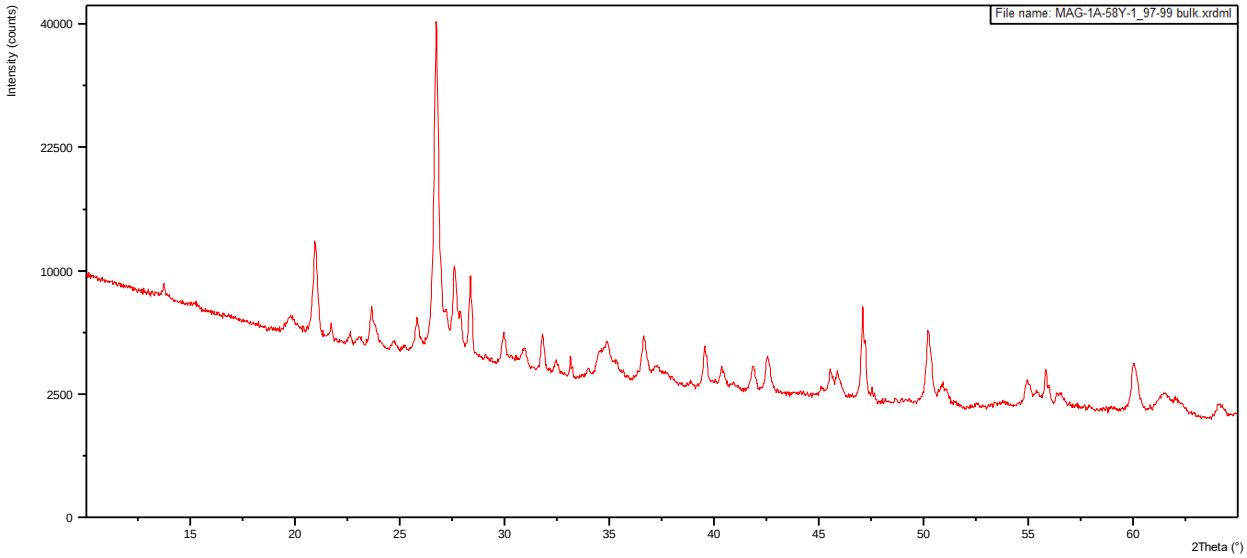
File name: MAG-1A-58Y-1_97-99 bulk.xrdml
Intensity (counts)
40000
22500
10000
2500
0
15
20
25
30
35
40
45
50
55
60
2Theta (°)

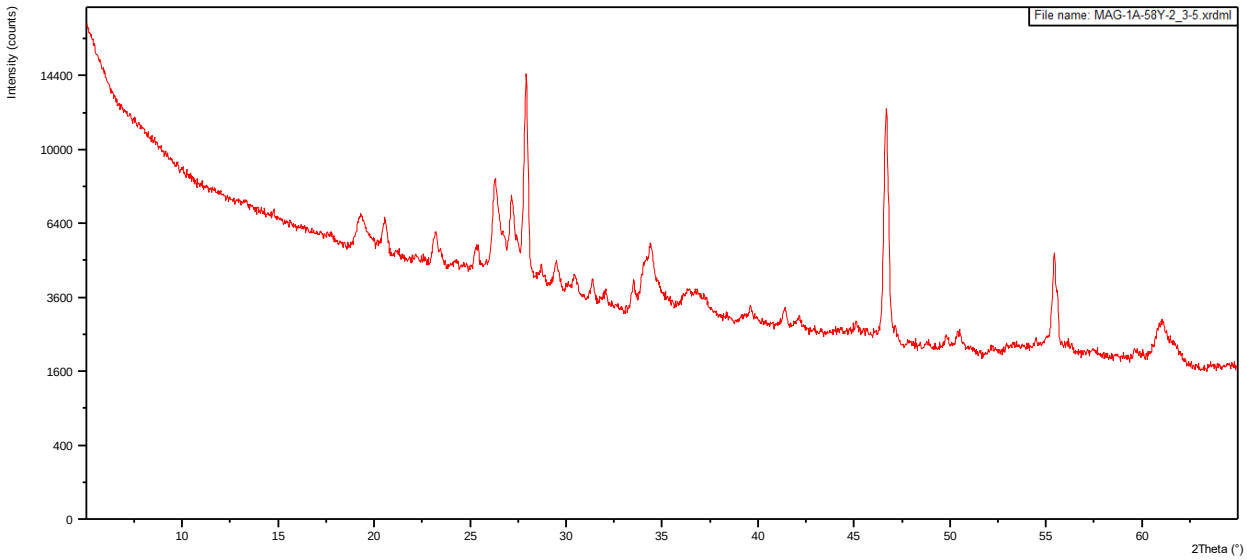
File name: MAG-1A-58Y-2_3-5.xrdml
Intensity (counts)
14400
10000
6400
3600
1600
400
0
10
15
20
25
30
35
40
45
50
55
60
2Theta (°)

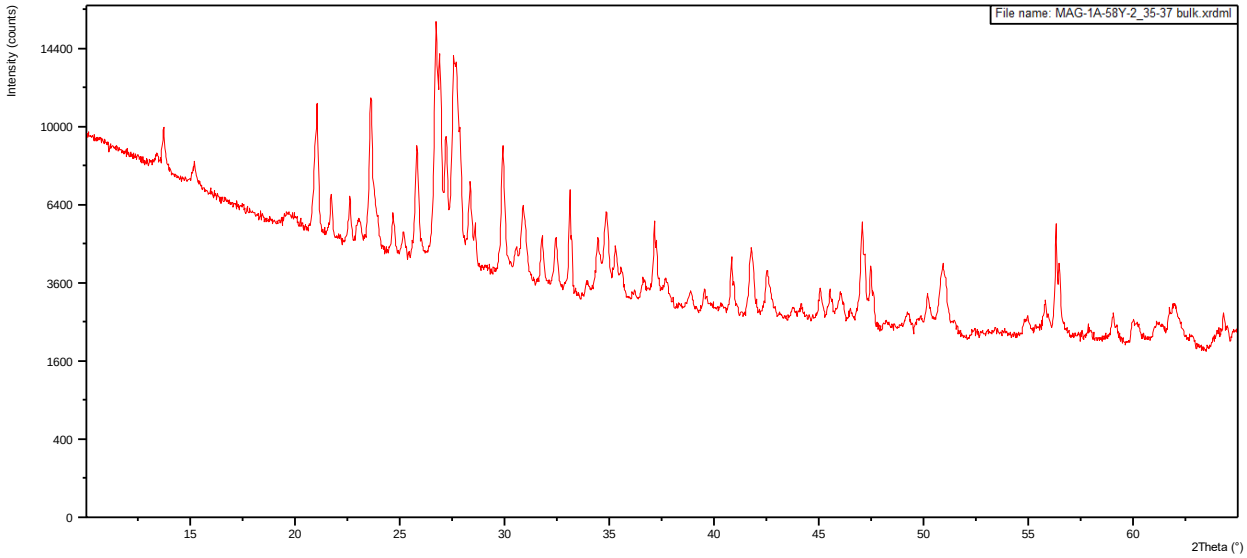
File name: MAG-1A-58Y-2_35-37 bulk.xrdml
Intensity (counts)
14400
10000
6400
3600
1600
400
0
15
20
25
30
35
40
45
50
55
60
2Theta (°)

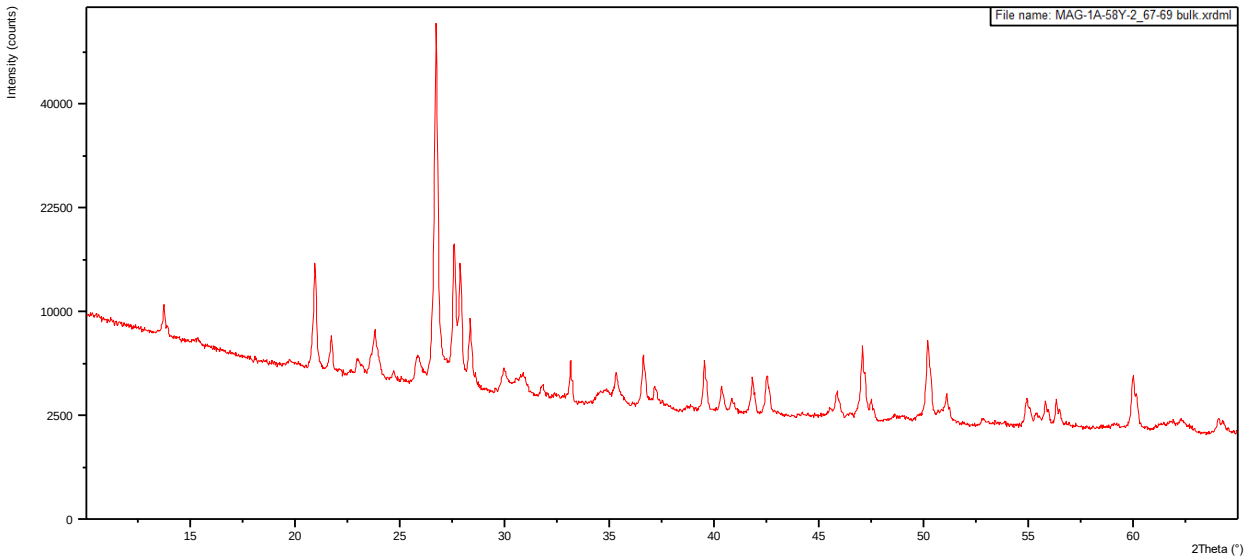
File name: MAG-1A-58Y-2_67-69 bulk.xrdml
Intensity (counts)
40000
22500
10000
2500
0
15
20
25
30
35
40
45
50
55
60
2Theta (°)

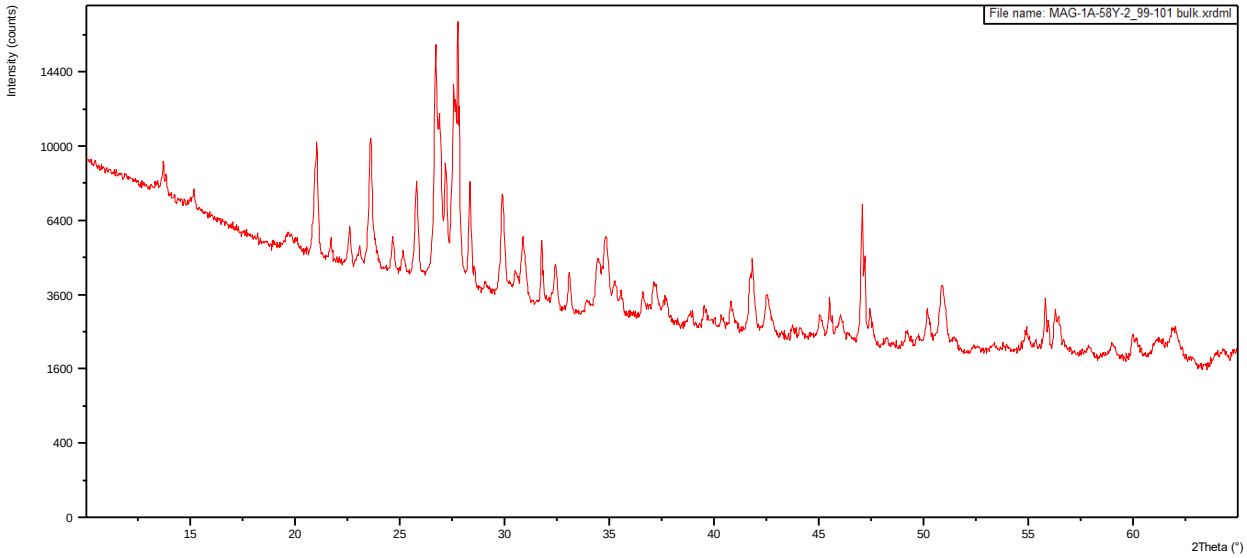
File name: MAG-1A-58Y-2_99-101 bulk.xrdml
Intensity (counts)
14400
10000
6400
3600
1600
400
0
15
20
25
30
35
40
45
50
55
60
2Theta (°)

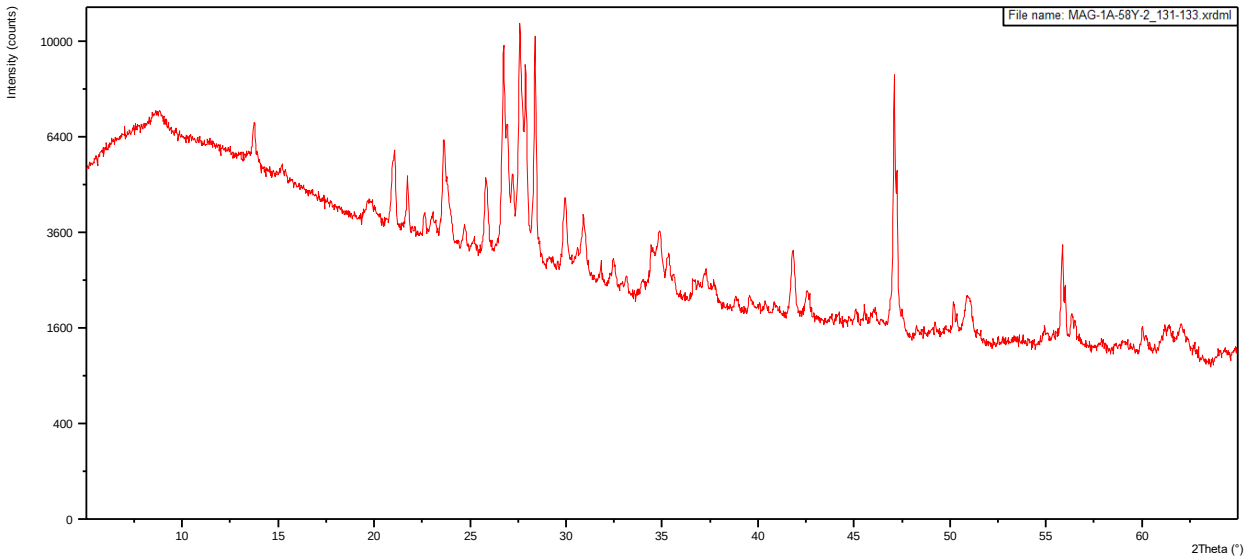
File name: MAG-1A-58Y-2_131-133.xrdml
Intensity (counts)
10000
6400
3600
1600
400
0
10
15
20
25
30
35
40
45
50
55
60
2Theta (°)

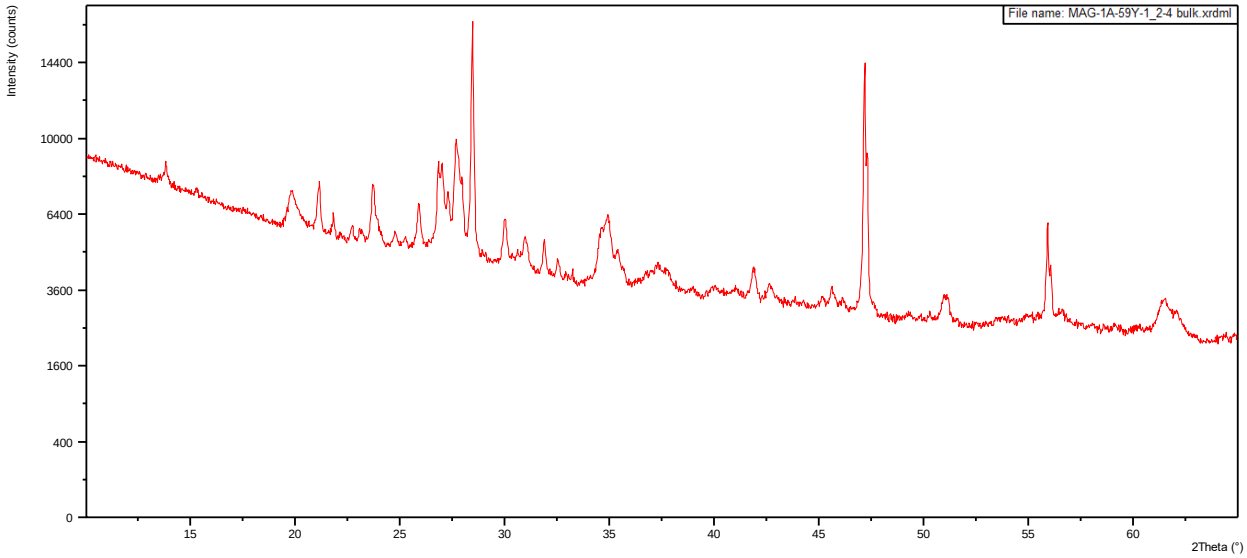
File name: MAG-1A-59Y-1_2-4 bulk.xrdml
Intensity (counts)
14400
10000
6400
3600
1600
400
0
15
20
25
30
35
40
45
50
55
60
2Theta (°)

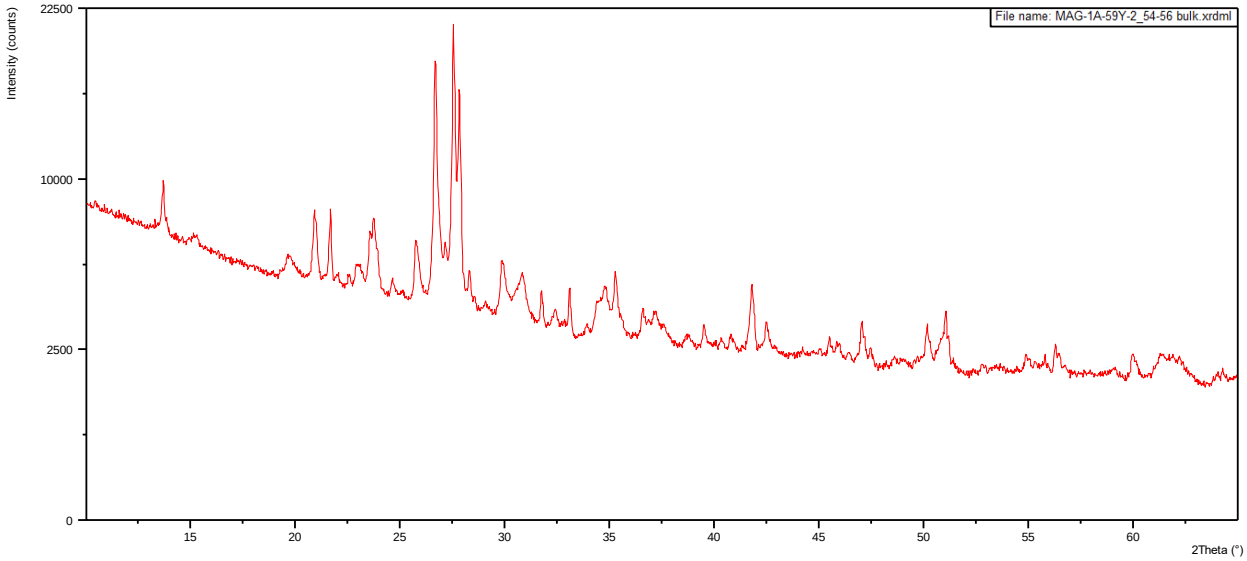
File name: MAG-1A-59Y-2_54-56 bulk.xrdml
Intensity (counts)
22500
10000
2500
0
15
20
25
30
35
40
45
50
55
60
2Theta (°)

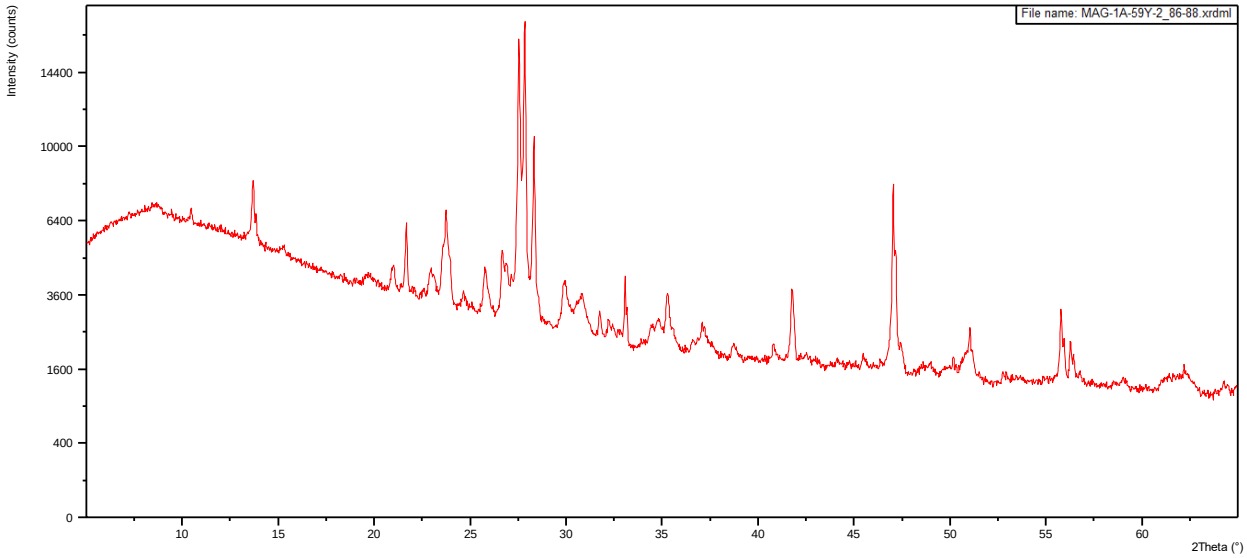
File name: MAG-1A-59Y-2_86-88.xrdml
Intensity (counts)
14400
10000
6400
3600
1600
400
0
10
15
20
25
30
35
40
45
50
55
60
2Theta (°)

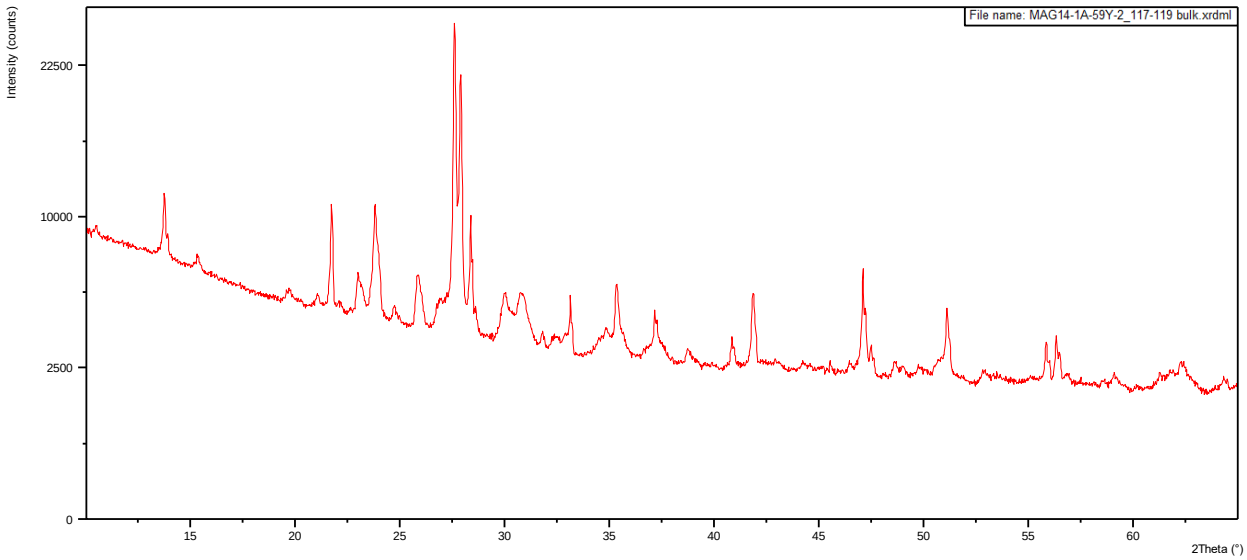
File name: MAG14-1A-59Y-2_117-119 bulk.xrdml
Intensity (counts)
22500
10000
2500
0
15
20
25
30
35
40
45
50
55
60
2Theta (°)

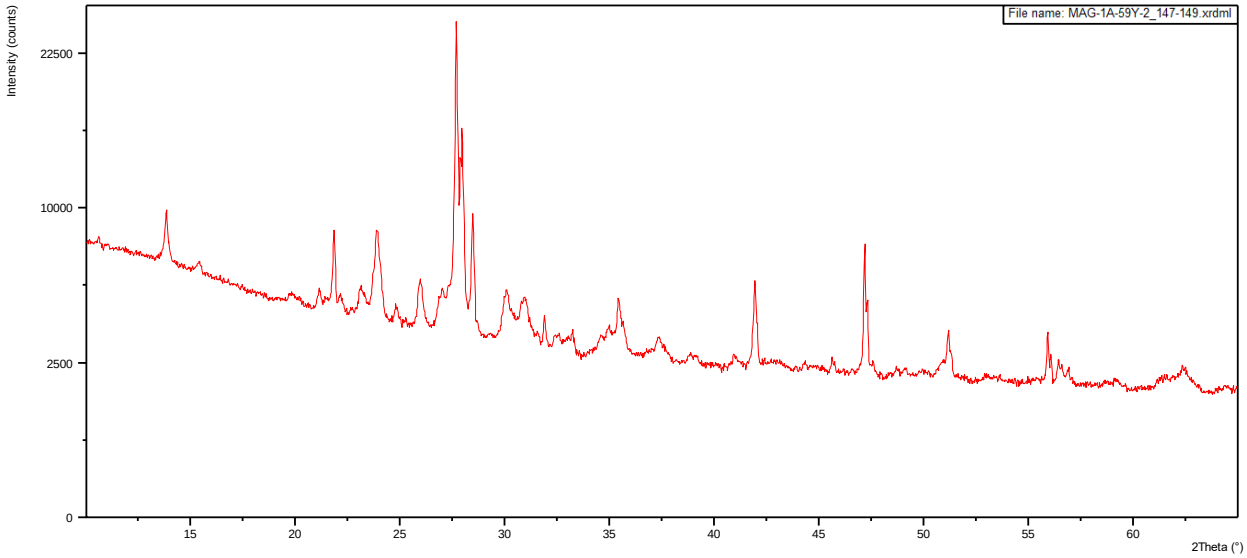
File name: MAG-1A-59Y-2_147-149.xrdml
Intensity (counts)
22500
10000
2500
0
15
20
25
30
35
40
45
50
55
60
2Theta (°)

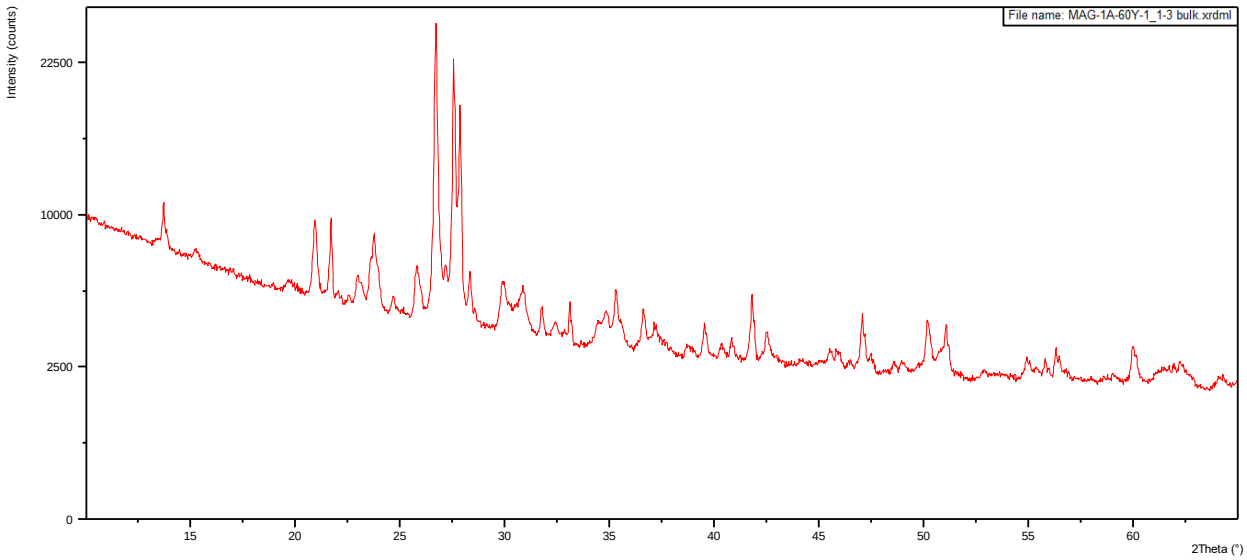
File name: MAG-1A-60Y-1_1-3 bulk.xrdml
Intensity (counts)
22500
10000
2500
0
15
20
25
30
35
40
45
50
55
60
2Theta (°)

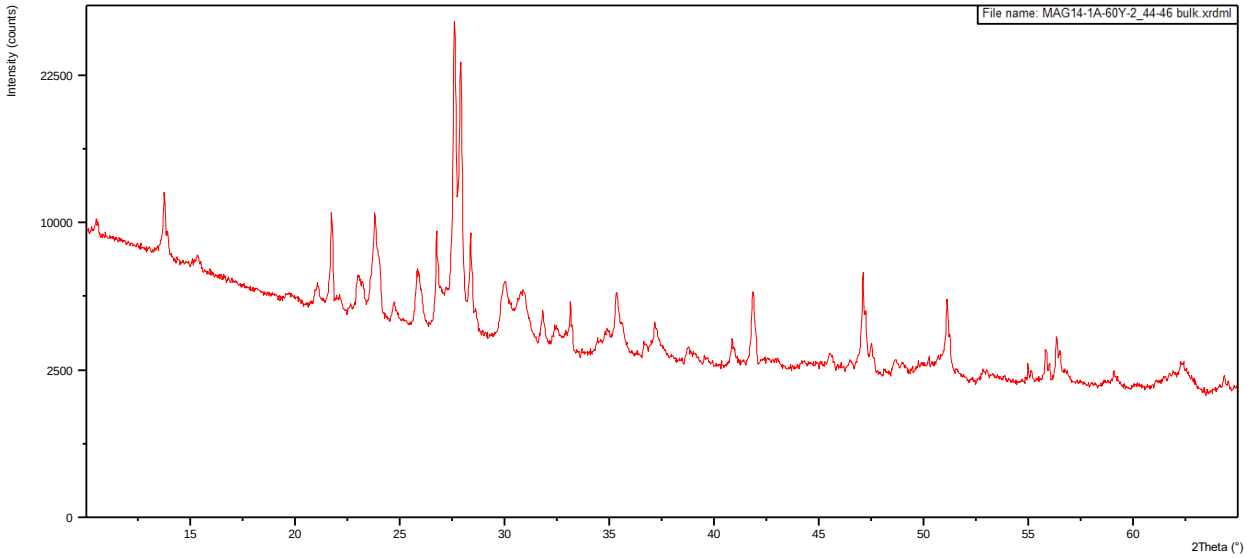
File name: MAG14-1A-60Y-2_44-46 bulk.xrdml
Intensity (counts)
22500
10000
2500
0
15
20
25
30
35
40
45
50
55
60
2Theta (°)

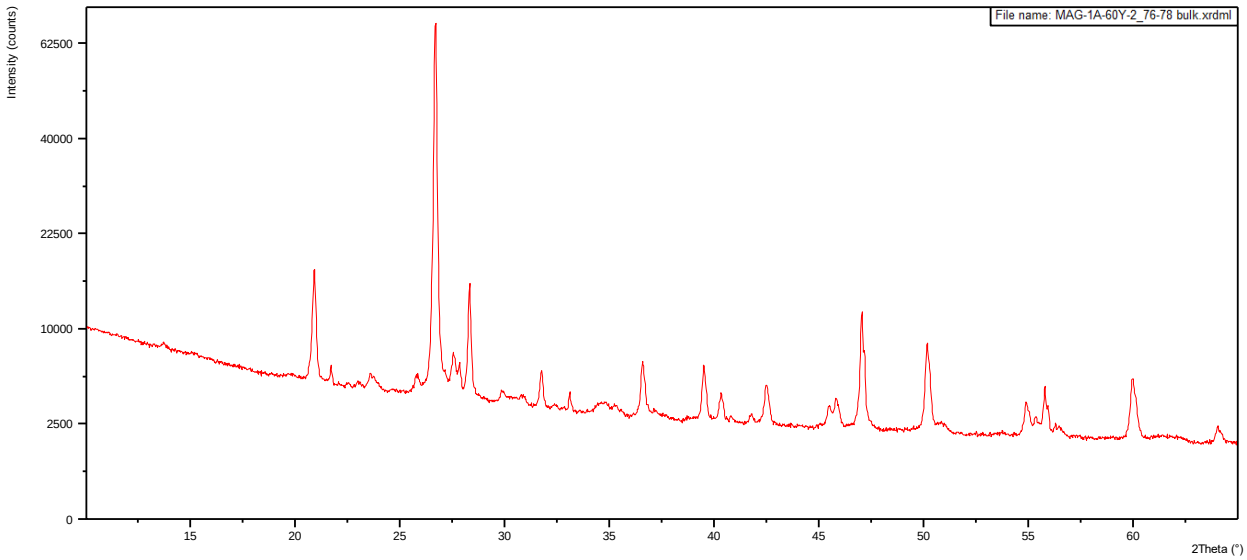
File name: MAG-1A-60Y-2_76-78 bulk.xrdml
Intensity (counts)
62500
40000
22500
10000
2500
0
15
20
25
30
35
40
45
50
55
60
2Theta (°)

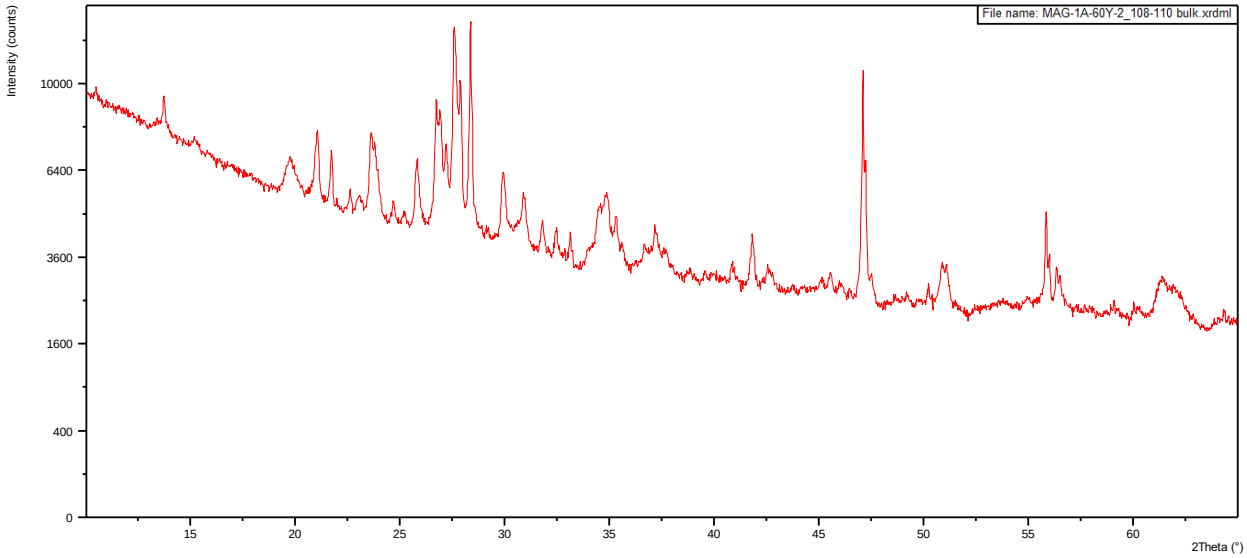
File name: MAG-1A-60Y-2_108-110 bulk.xrdml
Intensity (counts)
10000
6400
3600
1600
400
0
15
20
25
30
35
40
45
50
55
60
2Theta (°)

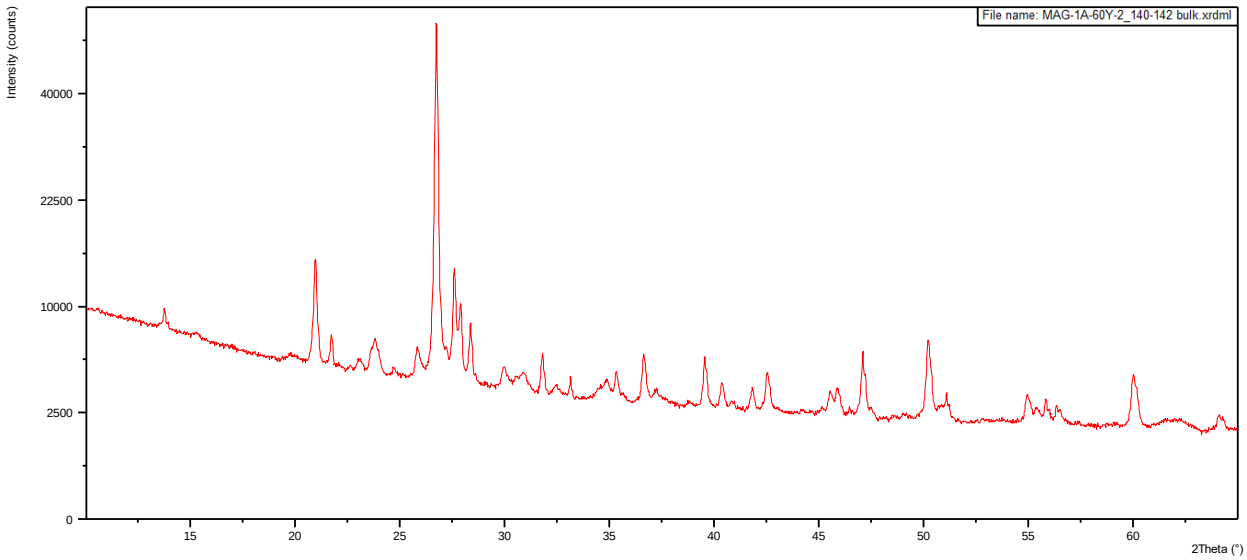
File name: MAG-1A-60Y-2_140-142 bulk.xrdml
Intensity (counts)
40000
22500
10000
2500
0
15
20
25
30
35
40
45
50
55
60
2Theta (°)

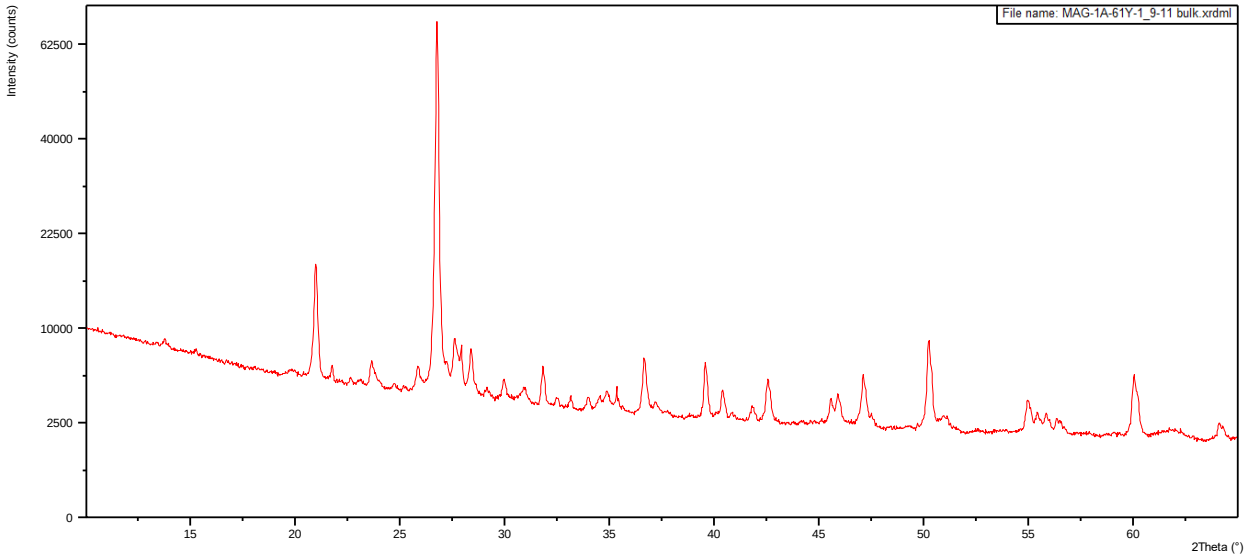
File name: MAG-1A-61Y-1_9-11 bulk.xrdml
Intensity (counts)
62500
40000
22500
10000
2500
0
15
20
25
30
35
40
45
50
55
60
2Theta (°)

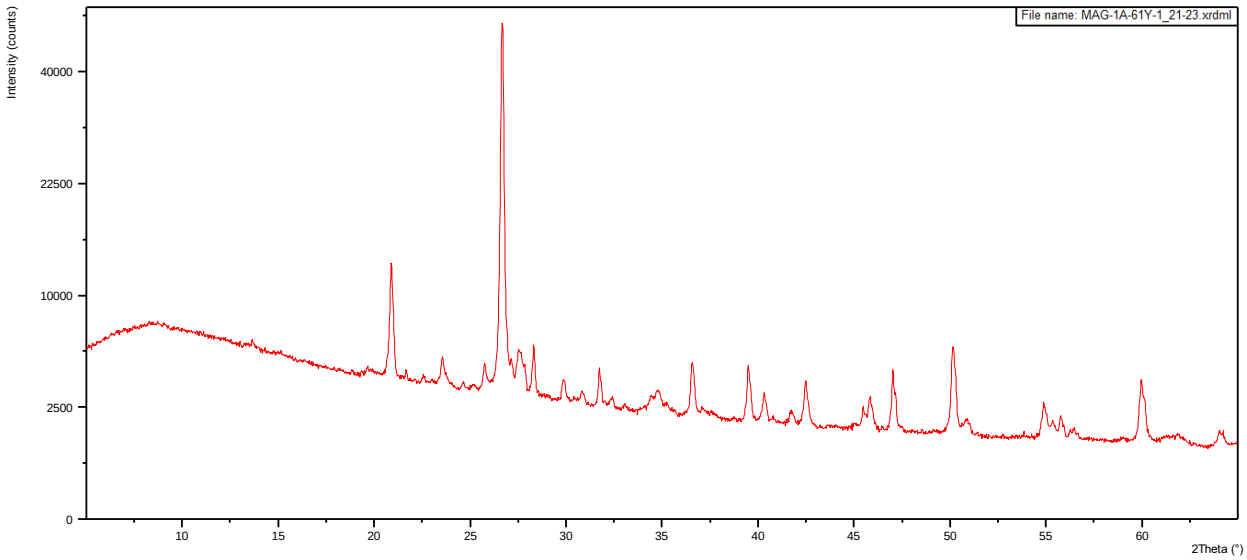
File name: MAG-1A-61Y-1_21-23.xrdml
Intensity (counts)
40000
22500
10000
2500
0
10
15
20
25
30
35
40
45
50
55
60
2Theta (°)

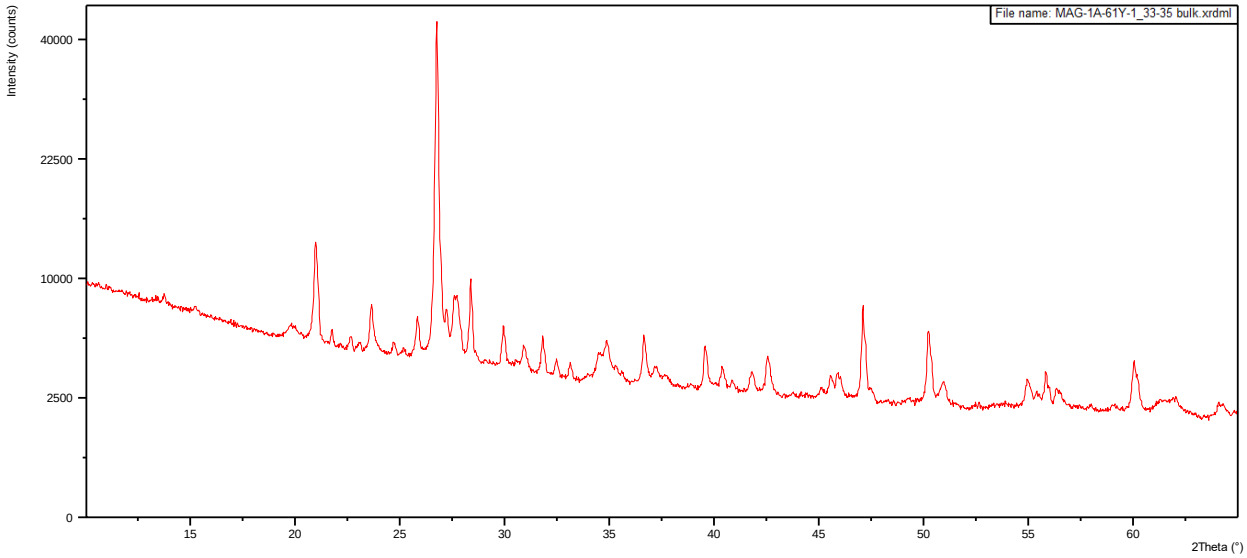
File name: MAG-1A-61Y-1_33-35 bulk.xrdml
Intensity (counts)
40000
22500
10000
2500
0
15
20
25
30
35
40
45
50
55
60
2Theta (°)

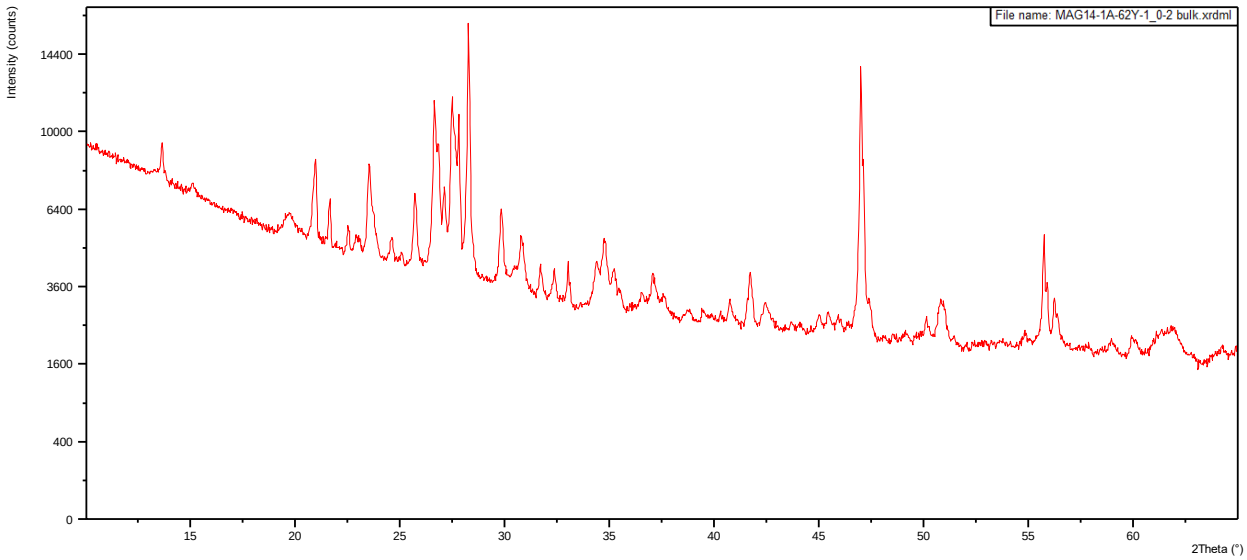
File name: MAG14-1A-62Y-1_0-2 bulk.xrdml
Intensity (counts)
14400
10000
6400
3600
1600
400
0
15
20
25
30
35
40
45
50
55
60
2Theta (°)

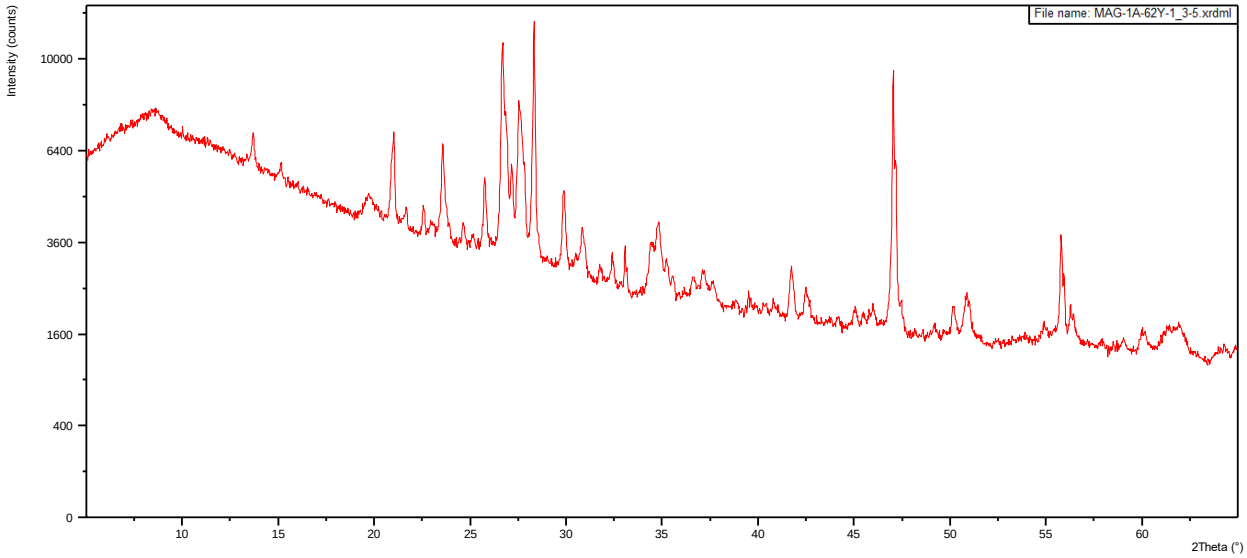
File name: MAG-1A-62Y-1_3-5.xrdml
Intensity (counts)
10000
6400
3600
1600
400
0
10
15
20
25
30
35
40
45
50
55
60
2Theta (°)

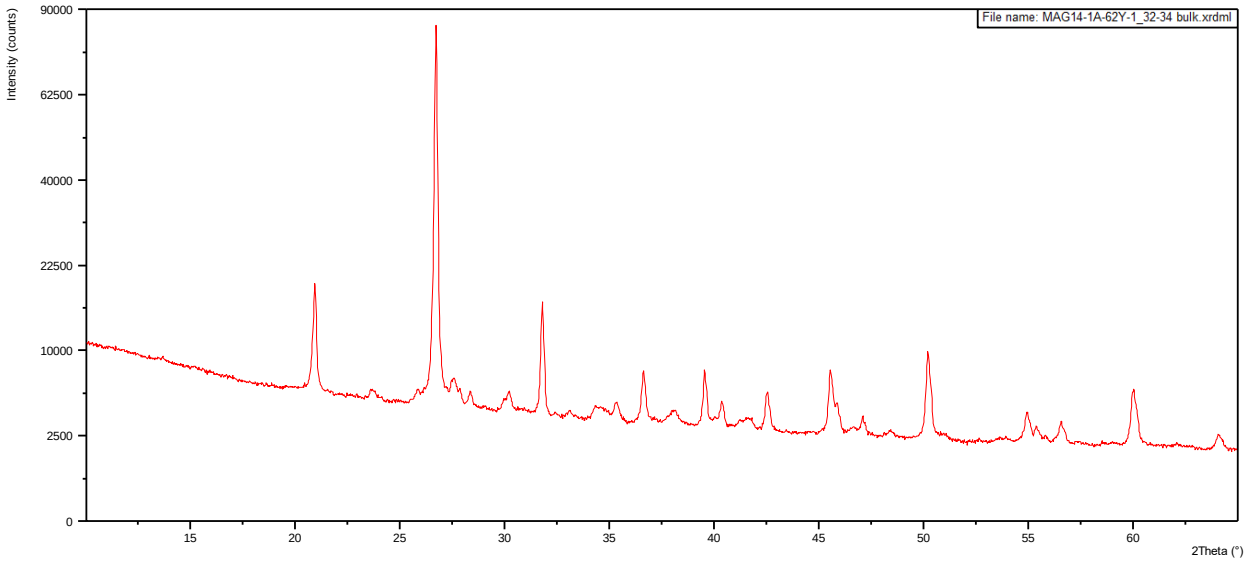
File name: MAG14-1A-62Y-1_32-34 bulk.xrdml
Intensity (counts)
90000
62500
40000
22500
10000
2500
0
15
20
25
30
35
40
45
50
55
60
2Theta (°)

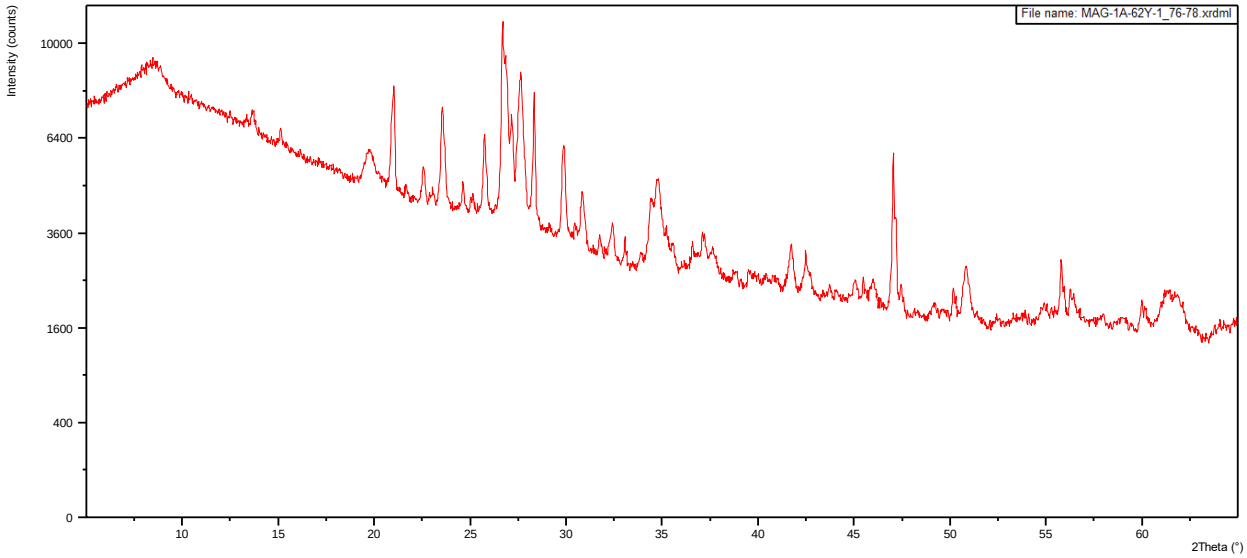
File name: MAG-1A-62Y-1_76-78.xrdml
Intensity (counts)
10000
6400
3600
1600
400
0
10
15
20
25
30
35
40
45
50
55
60
2Theta (°)

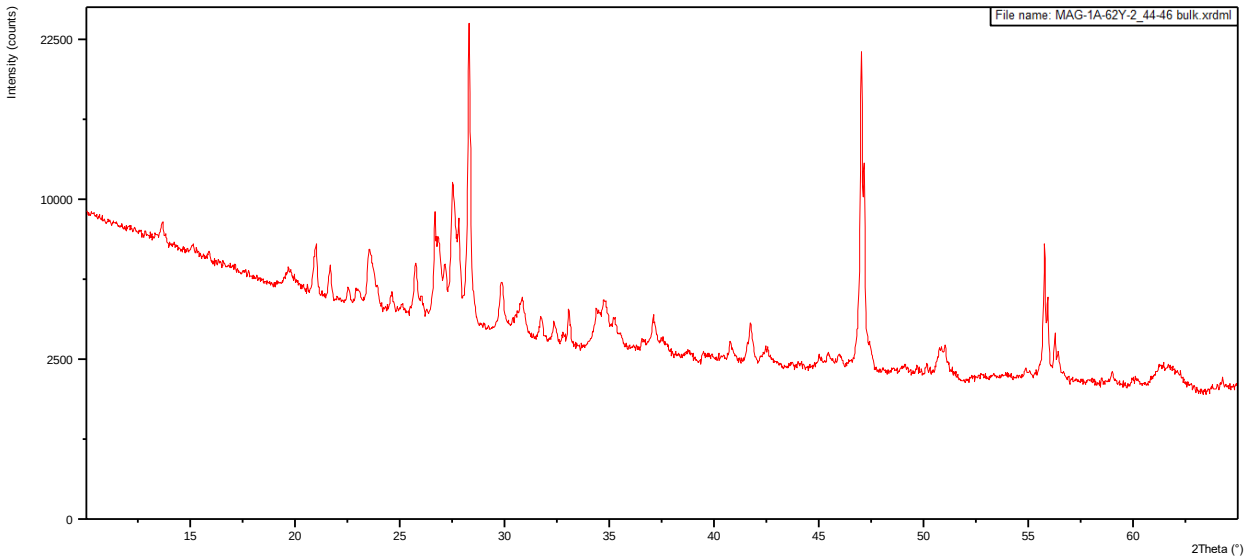
File name: MAG-1A-62Y-2_44-46 bulk.xrdml
Intensity (counts)
22500
10000
2500
0
15
20
25
30
35
40
45
50
55
60
2Theta (°)

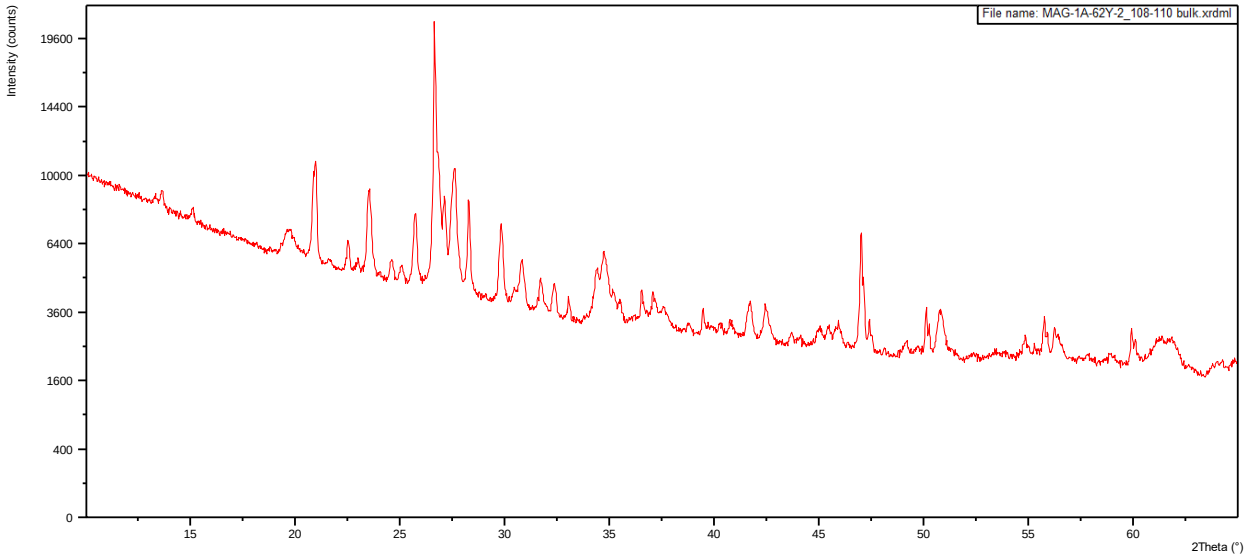
File name: MAG-1A-62Y-2_108-110 bulk.xrdml
Intensity (counts)
19600
14400
10000
6400
3600
1600
400
0
15
20
25
30
35
40
45
50
55
60
2Theta (°)

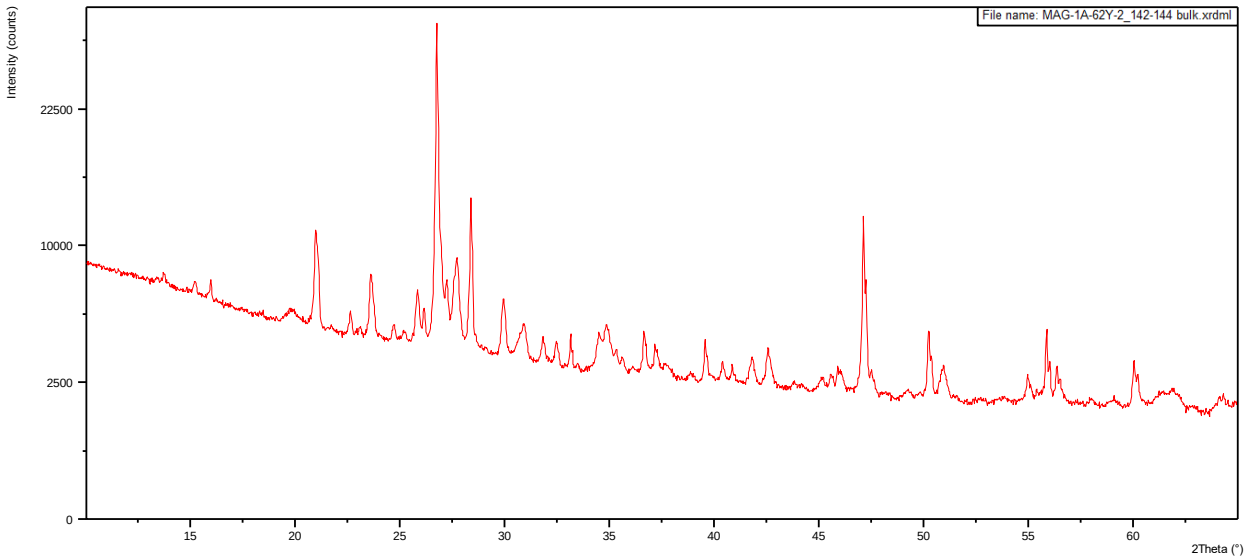
File name: MAG-1A-62Y-2_142-144 bulk.xrdml
Intensity (counts)
22500
10000
2500
0
15
20
25
30
35
40
45
50
55
60
2Theta (°)

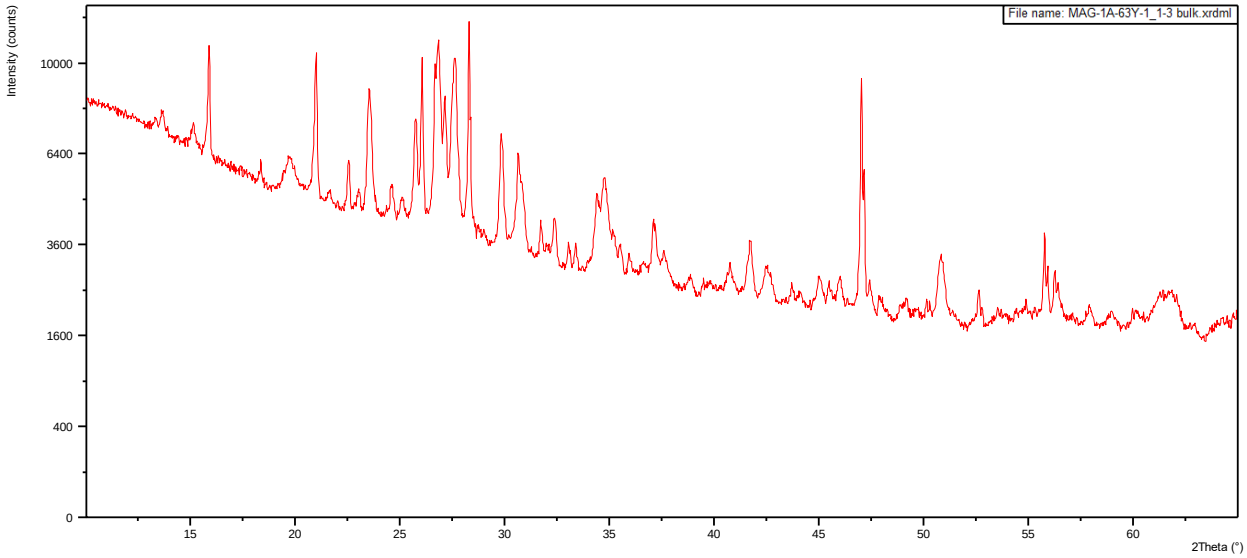
File name: MAG-1A-63Y-1_1-3 bulk.xrdml
Intensity (counts)
10000
6400
3600
1600
400
0
15
20
25
30
35
40
45
50
55
60
2Theta (°)

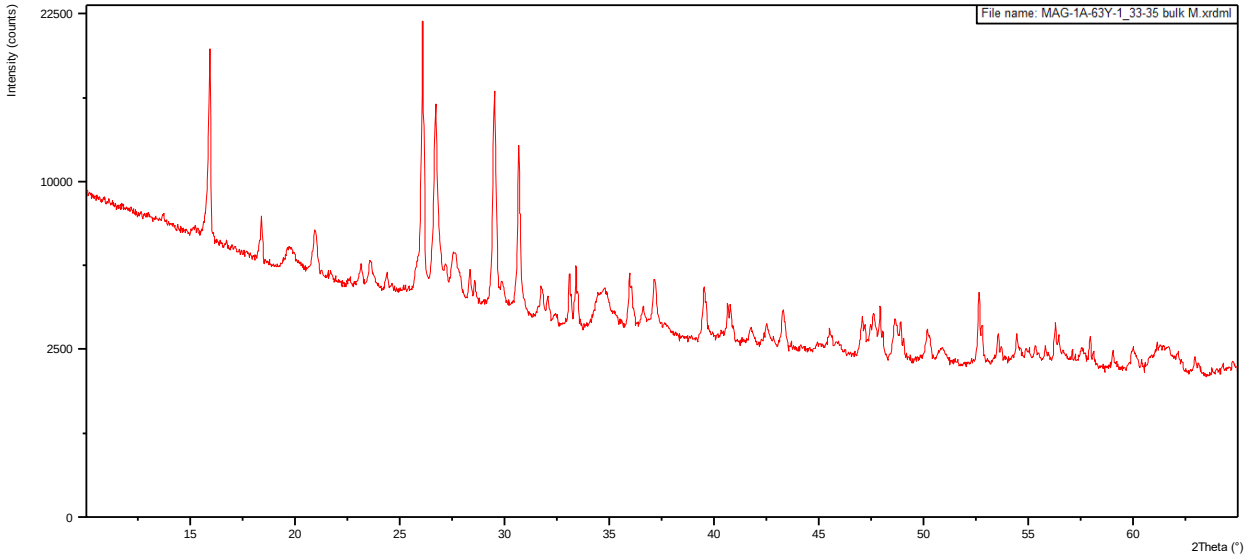
File name: MAG-1A-63Y-1_33-35 bulk M.xrdml
Intensity (counts)
22500
10000
2500
0
15
20
25
30
35
40
45
50
55
60
2Theta (°)

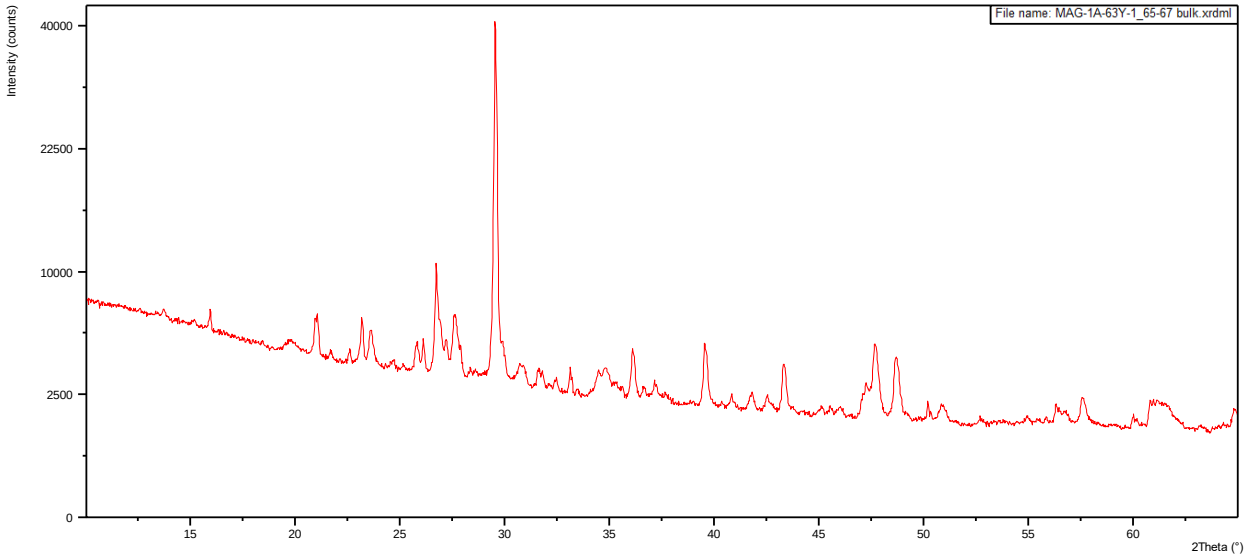
File name: MAG-1A-63Y-1_65-67 bulk.xrdml
Intensity (counts)
40000
22500
10000
2500
0
15
20
25
30
35
40
45
50
55
60
2Theta (°)

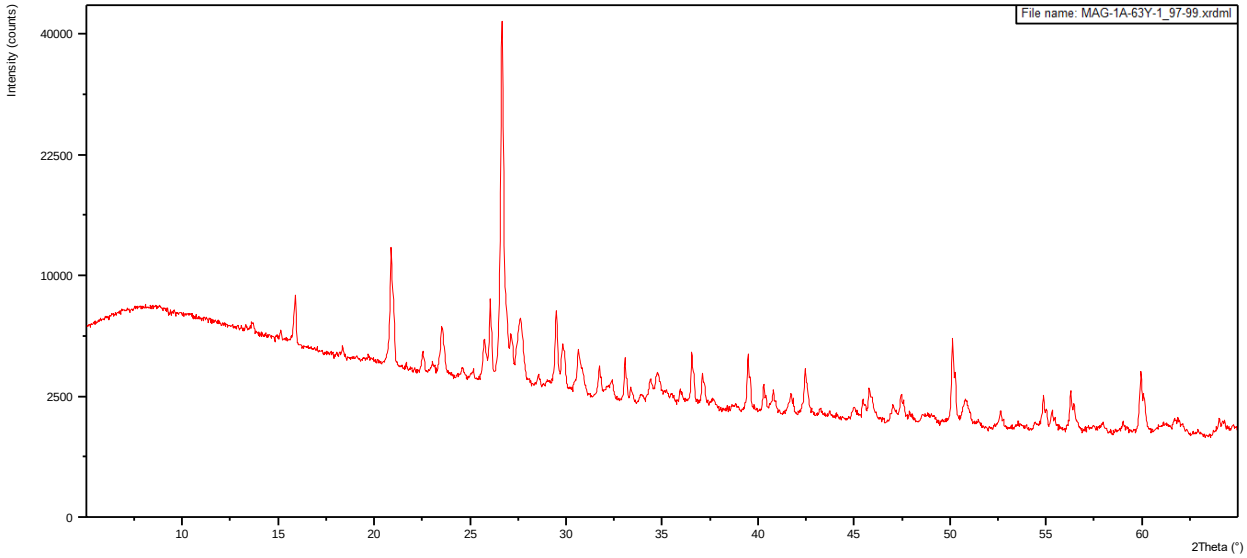
File name: MAG-1A-63Y-1_97-99.xrdml
Intensity (counts)
40000
22500
10000
2500
0
10
15
20
25
30
35
40
45
50
55
60
2Theta (°)

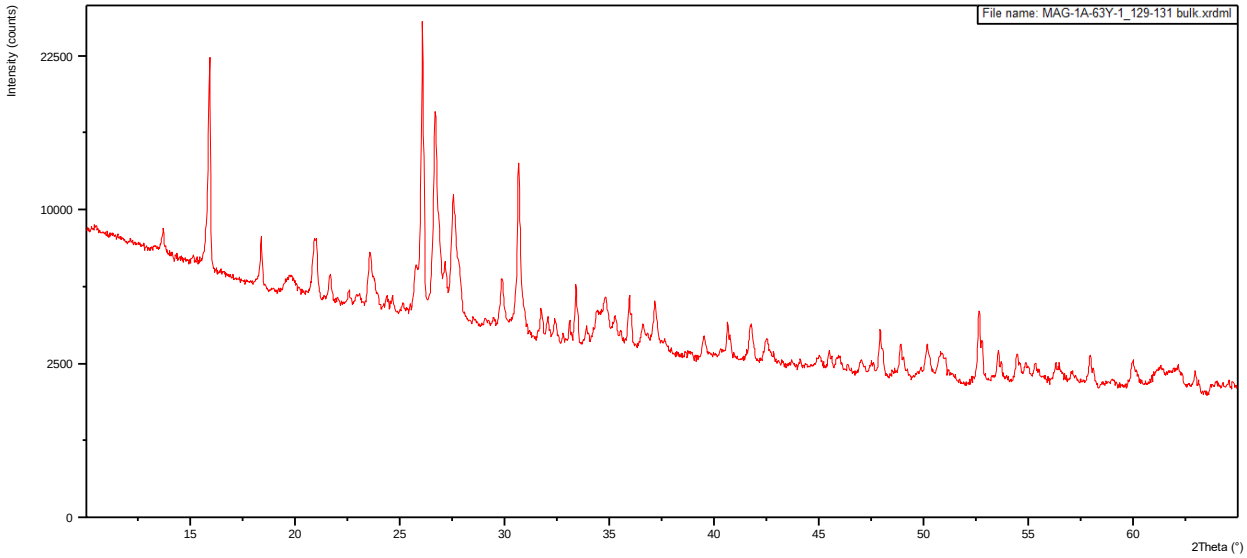
File name: MAG-1A-63Y-1_129-131 bulk.xrdml
Intensity (counts)
22500
10000
2500
0
15
20
25
30
35
40
45
50
55
60
2Theta (°)

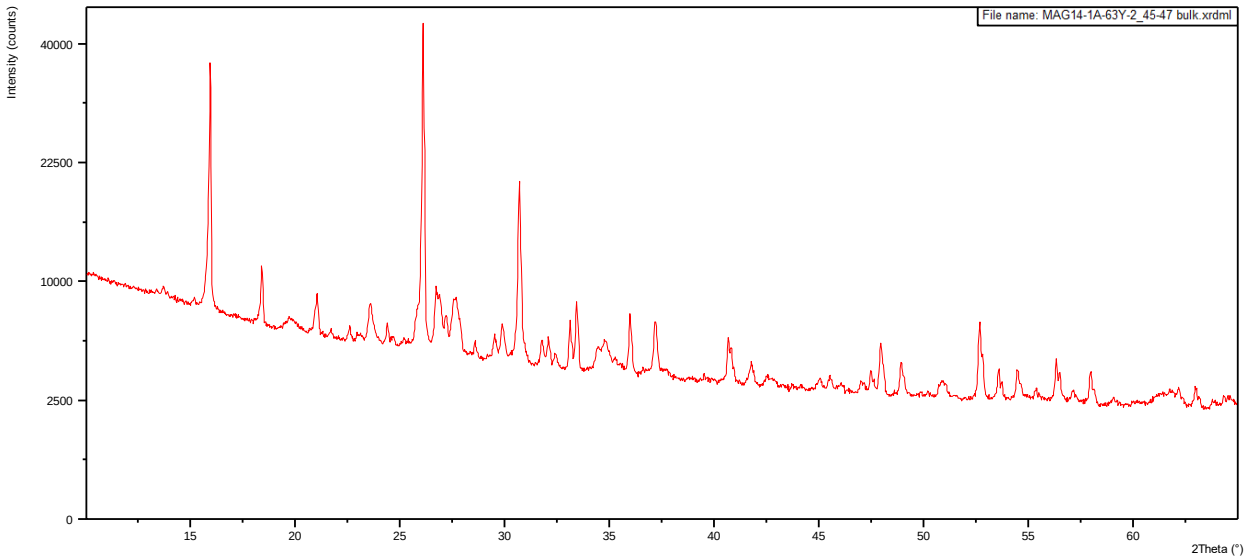
File name: MAG14-1A-63Y-2_45-47 bulk.xrdml
Intensity (counts)
40000
22500
10000
2500
0
15
20
25
30
35
40
45
50
55
60
2Theta (°)

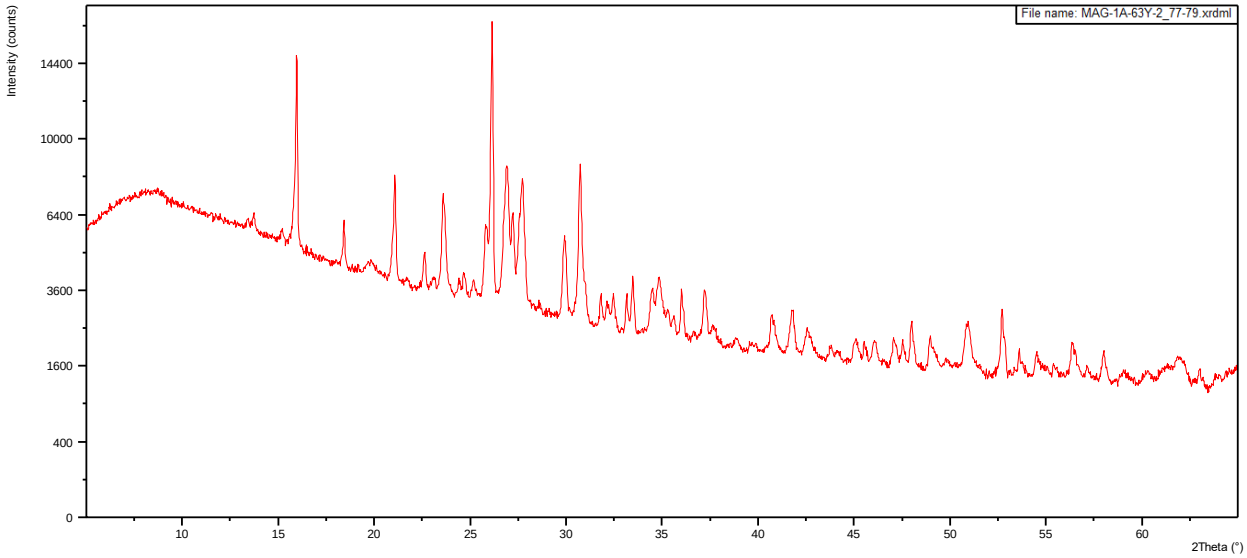
File name: MAG-1A-63Y-2_77-79.xrdml
Intensity (counts)
14400
10000
6400
3600
1600
400
0
10
15
20
25
30
35
40
45
50
55
60
2Theta (°)

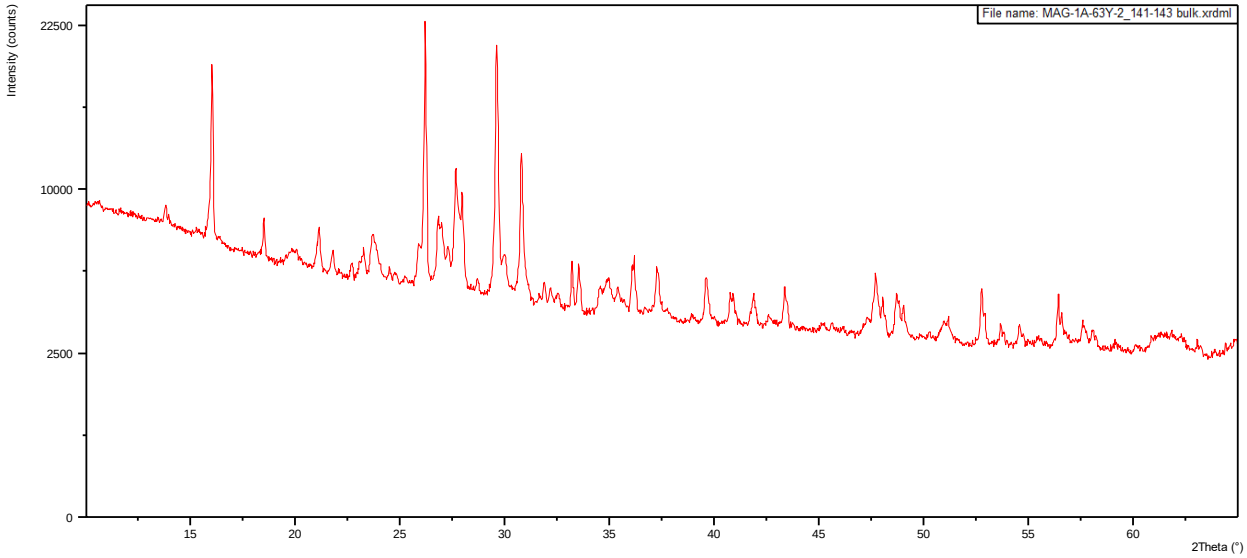
File name: MAG-1A-63Y-2_141-143 bulk.xrdml
Intensity (counts)
22500
10000
2500
0
15
20
25
30
35
40
45
50
55
60
2Theta (°)

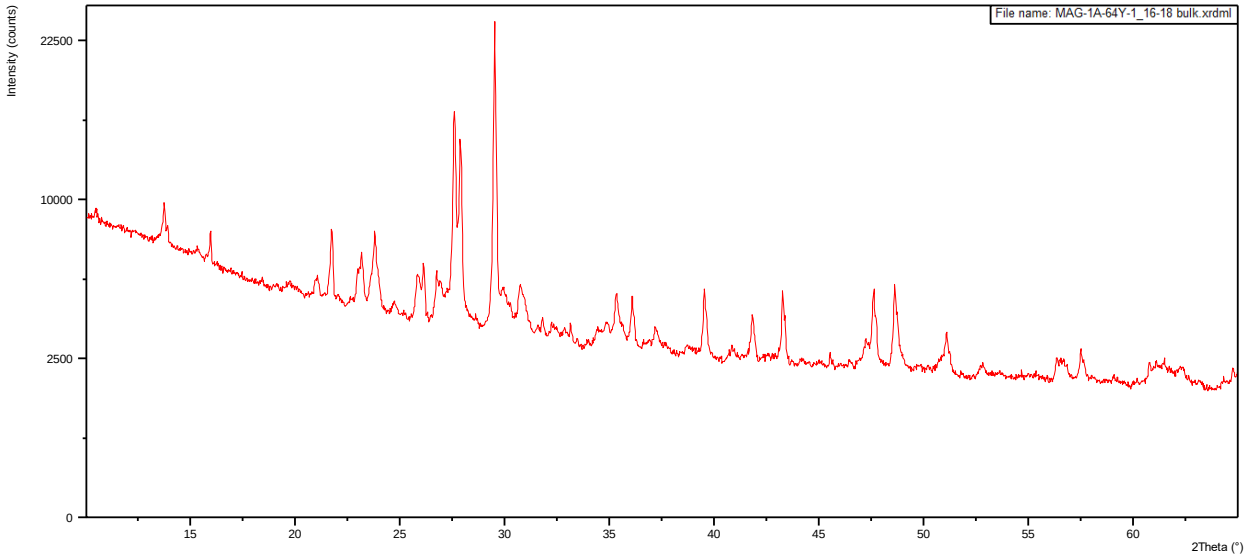
File name: MAG-1A-64Y-1_16-18 bulk.xrdml
Intensity (counts)
22500
10000
2500
0
15
20
25
30
35
40
45
50
55
60
2Theta (°)

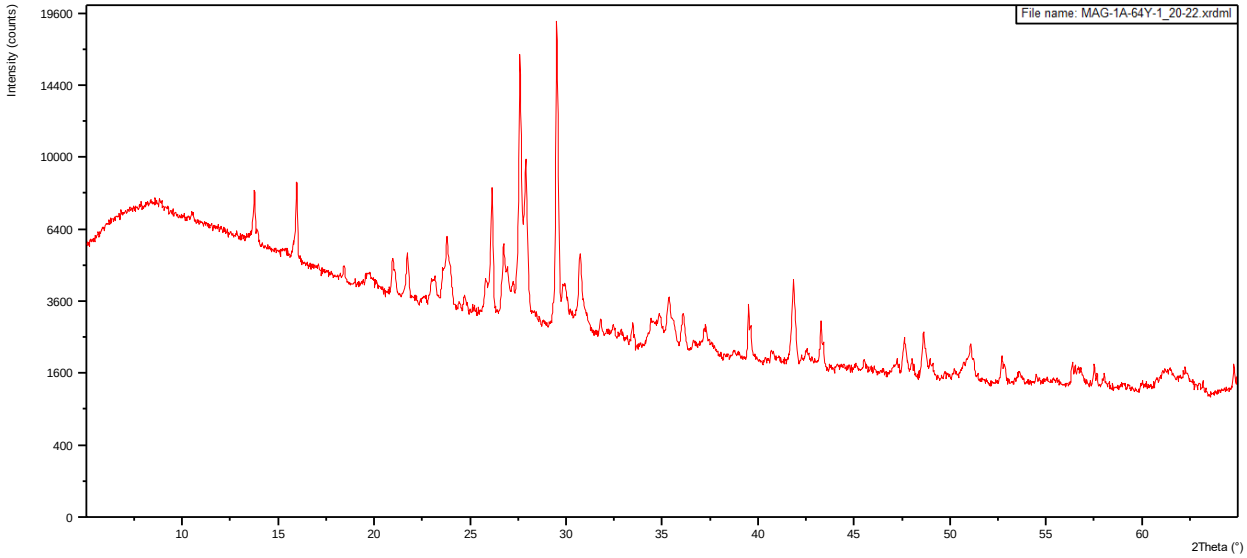
File name: MAG-1A-64Y-1_20-22.xrdml
Intensity (counts)
19600
14400
10000
6400
3600
1600
400
0
10
15
20
25
30
35
40
45
50
55
60
2Theta (°)

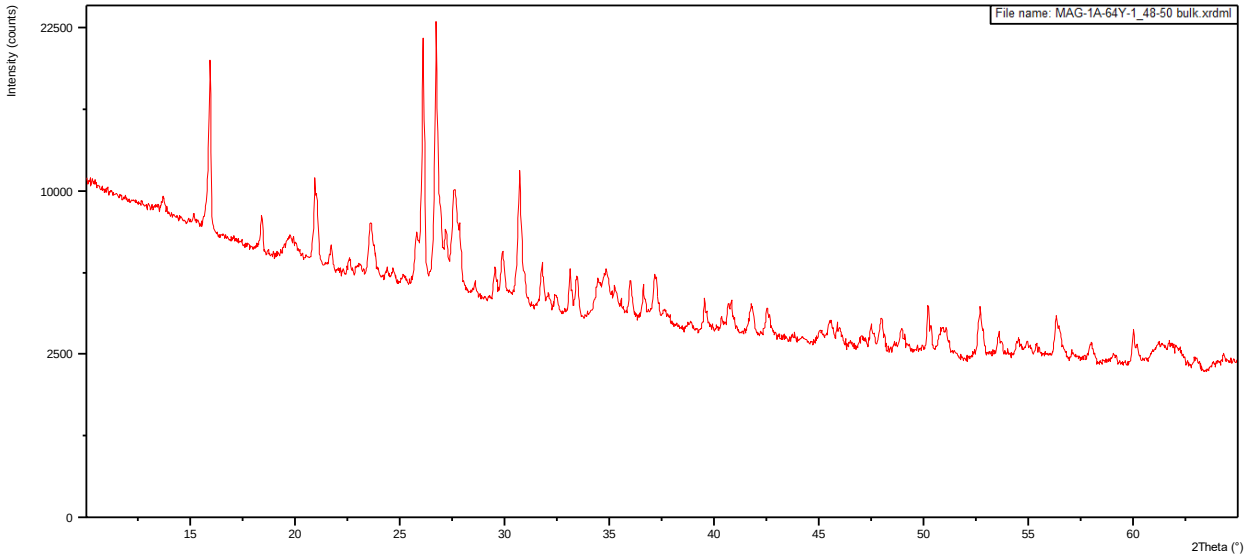
File name: MAG-1A-64Y-1_48-50 bulk.xrdml
Intensity (counts)
22500
10000
2500
0
15
20
25
30
35
40
45
50
55
60
2Theta (°)

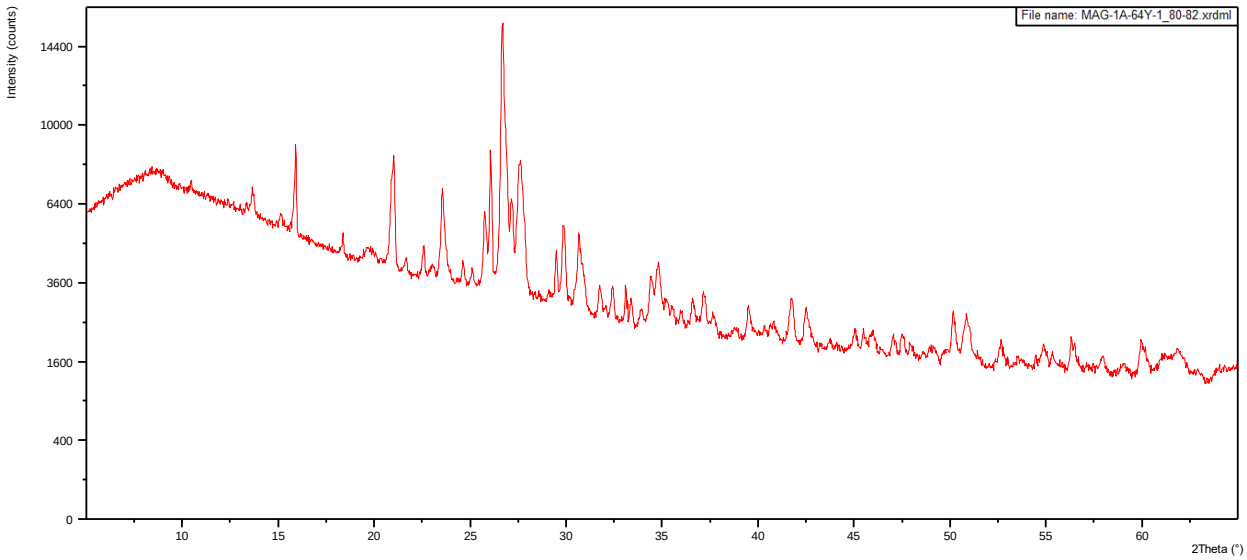
File name: MAG-1A-64Y-1_80-82.xrdml
Intensity (counts)
14400
10000
6400
3600
1600
400
0
10
15
20
25
30
35
40
45
50
55
60
2Theta (°)

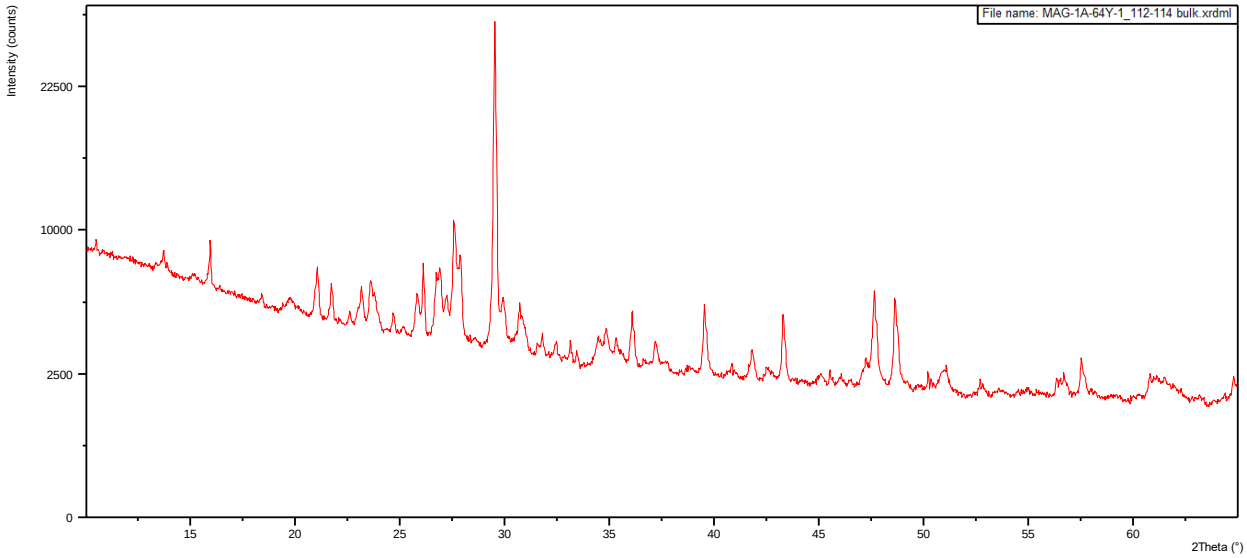
File name: MAG-1A-64Y-1_112-114 bulk.xrdml
Intensity (counts)
22500
10000
2500
0
15
20
25
30
35
40
45
50
55
60
2Theta (°)

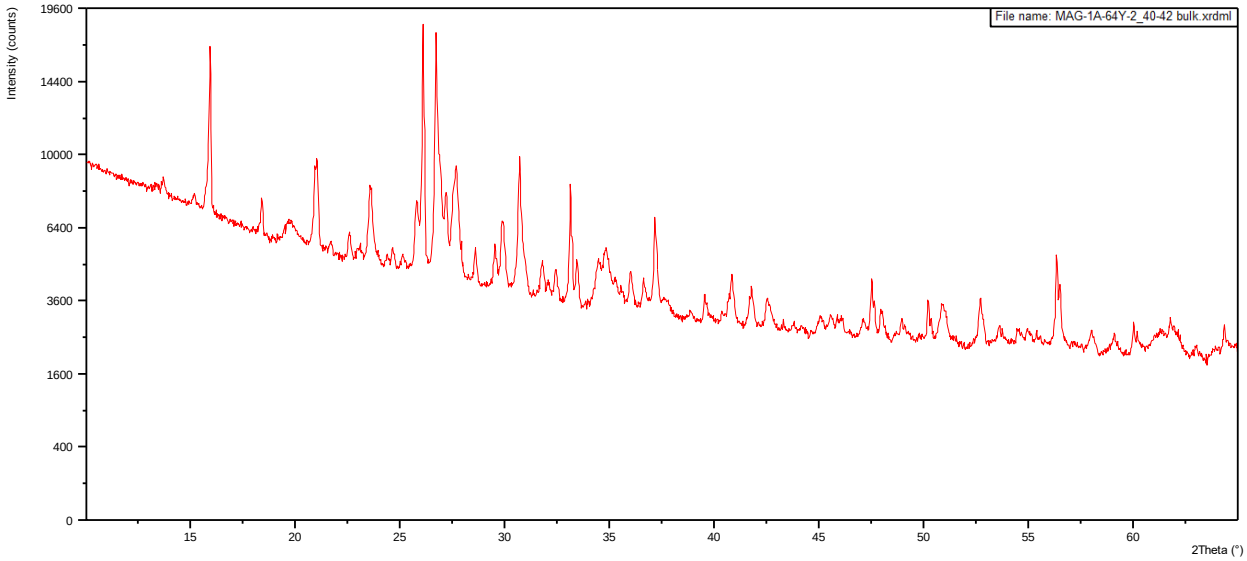
File name: MAG-1A-64Y-2_40-42 bulk.xrdml
Intensity (counts)
19600
14400
10000
6400
3600
1600
400
0
15
20
25
30
35
40
45
50
55
60
2Theta (°)

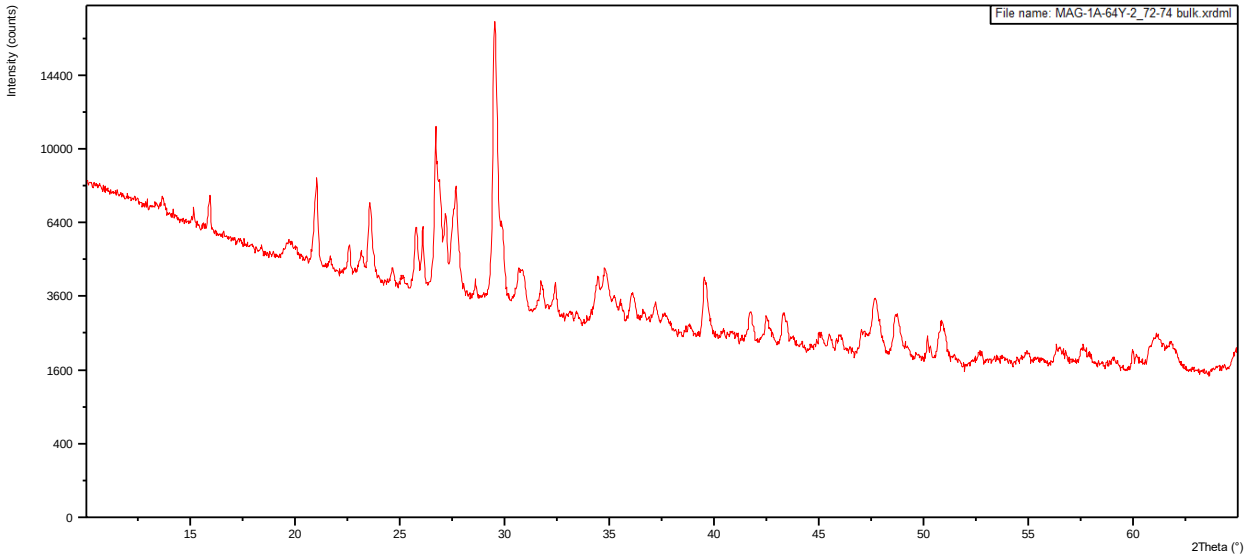
File name: MAG-1A-64Y-2_72-74 bulk.xrdml
Intensity (counts)
14400
10000
6400
3600
1600
400
0
15
20
25
30
35
40
45
50
55
60
2Theta (°)

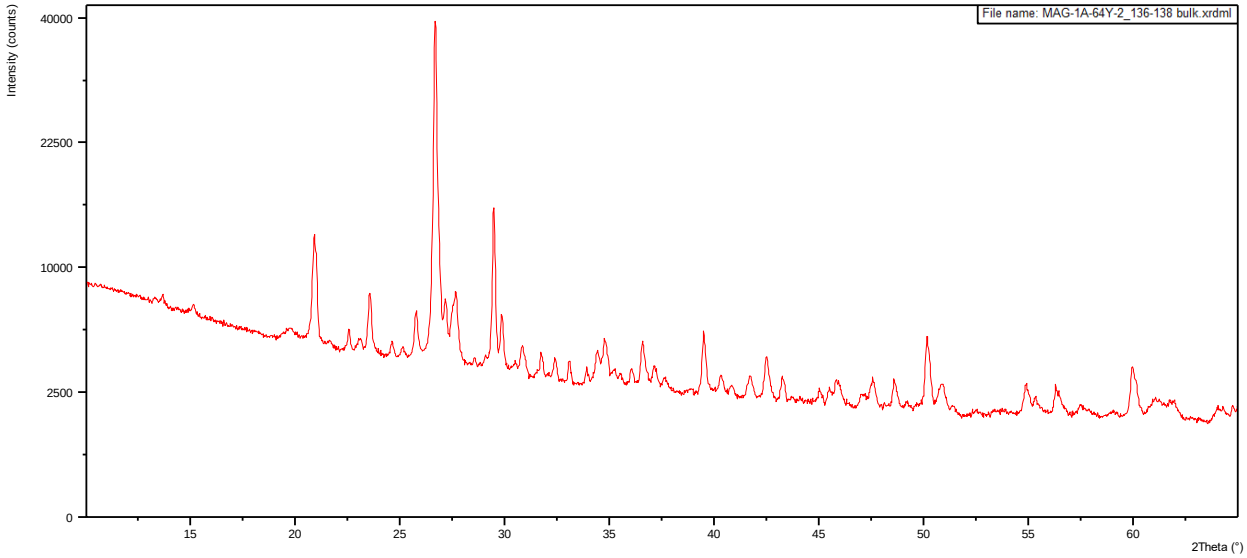
File name: MAG-1A-64Y-2_136-138 bulk.xrdml
Intensity (counts)
40000
22500
10000
2500
0
15
20
25
30
35
40
45
50
55
60
2Theta (°)

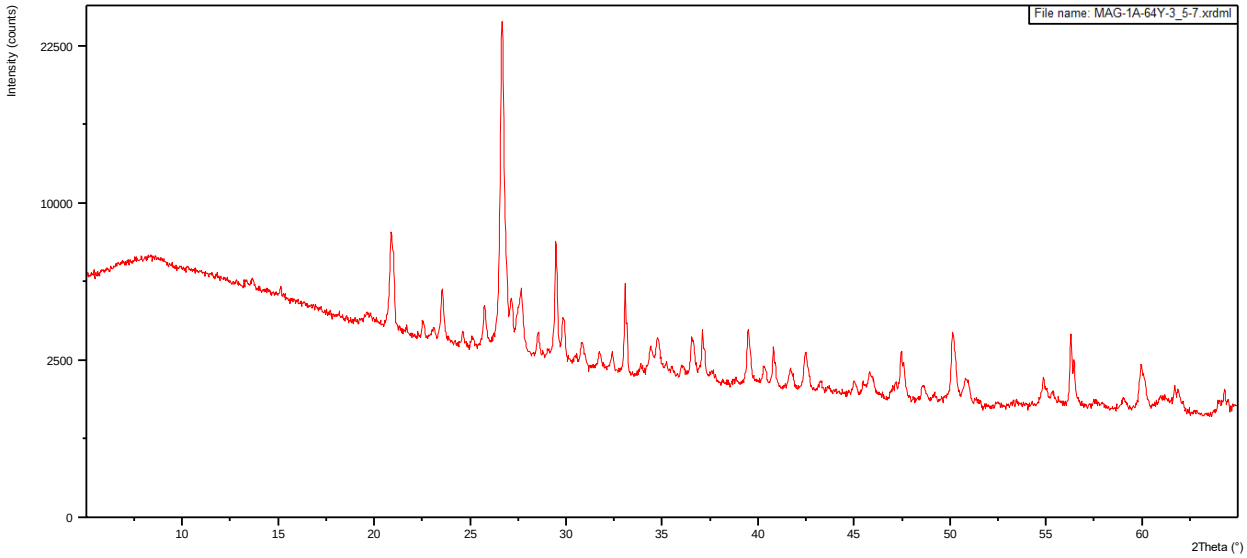
File name: MAG-1A-64Y-3_5-7.xrdml
Intensity (counts)
22500
10000
2500
0
10
15
20
25
30
35
40
45
50
55
60
2Theta (°)

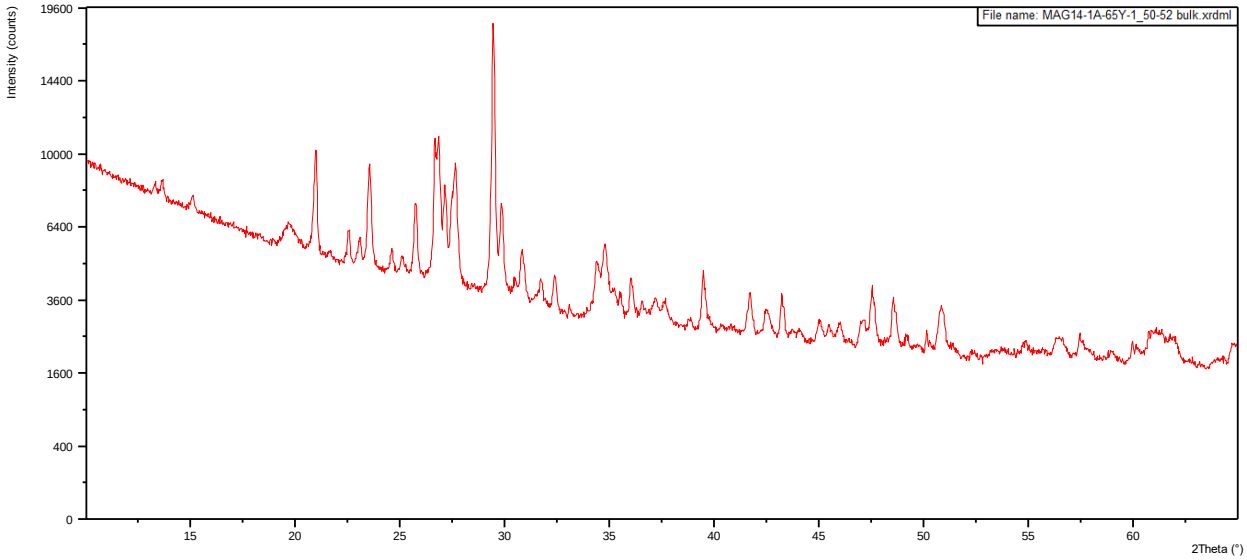
File name: MAG14-1A-65Y-1_50-52 bulk.xrdml
Intensity (counts)
19600
14400
10000
6400
3600
1600
400
0
15
20
25
30
35
40
45
50
55
60
2Theta (°)

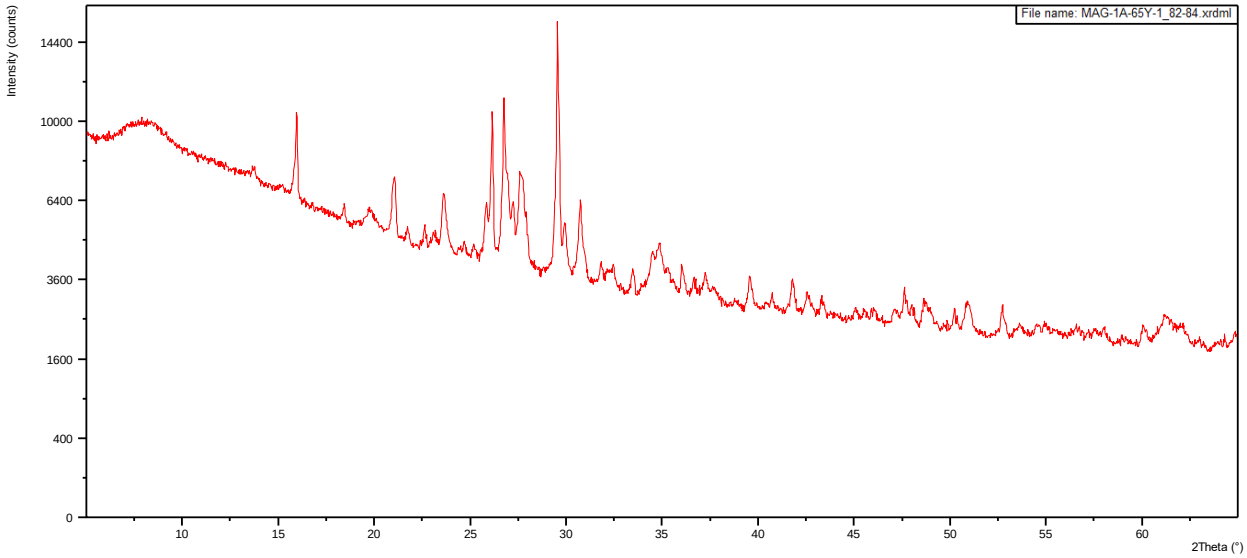
File name: MAG-1A-65Y-1_82-84.xrdml
Intensity (counts)
14400
10000
6400
3600
1600
400
0
10
15
20
25
30
35
40
45
50
55
60
2Theta (°)

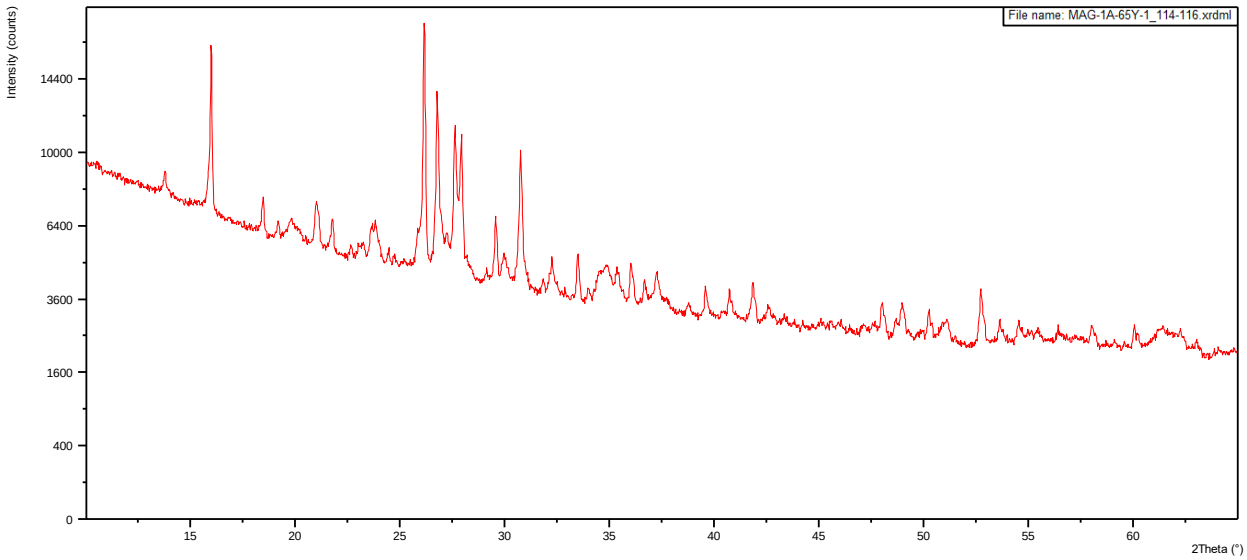
File name: MAG-1A-65Y-1_114-116.xrdml
Intensity (counts)
14400
10000
6400
3600
1600
400
0
15
20
25
30
35
40
45
50
55
60
2Theta (°)

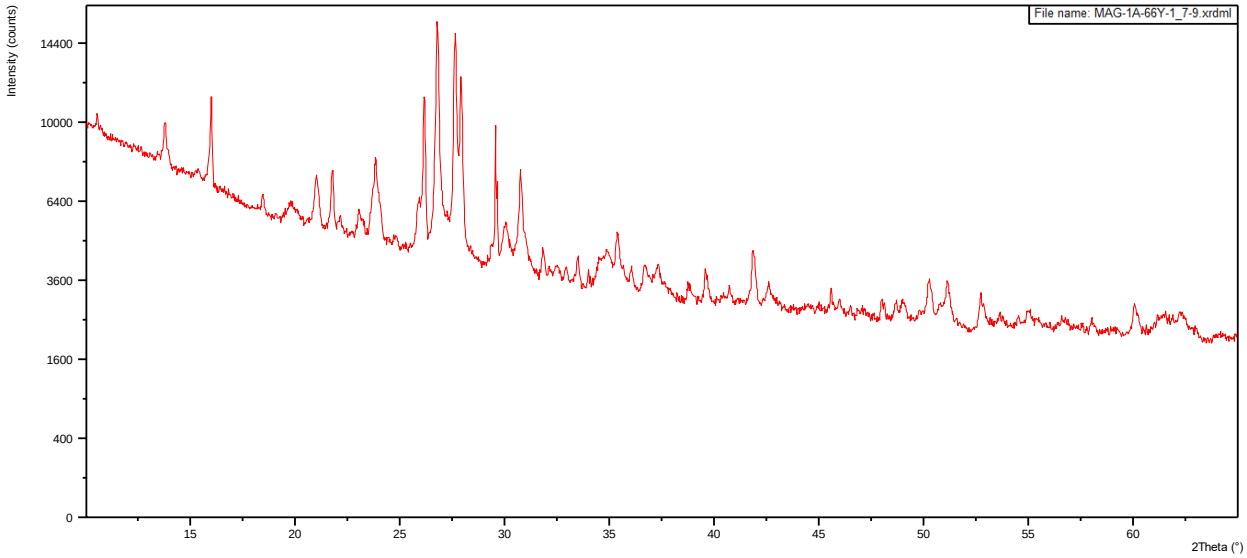
File name: MAG-1A-66Y-1_7-9.xrdml
Intensity (counts)
14400
10000
6400
3600
1600
400
0
15
20
25
30
35
40
45
50
55
60
2Theta (°)

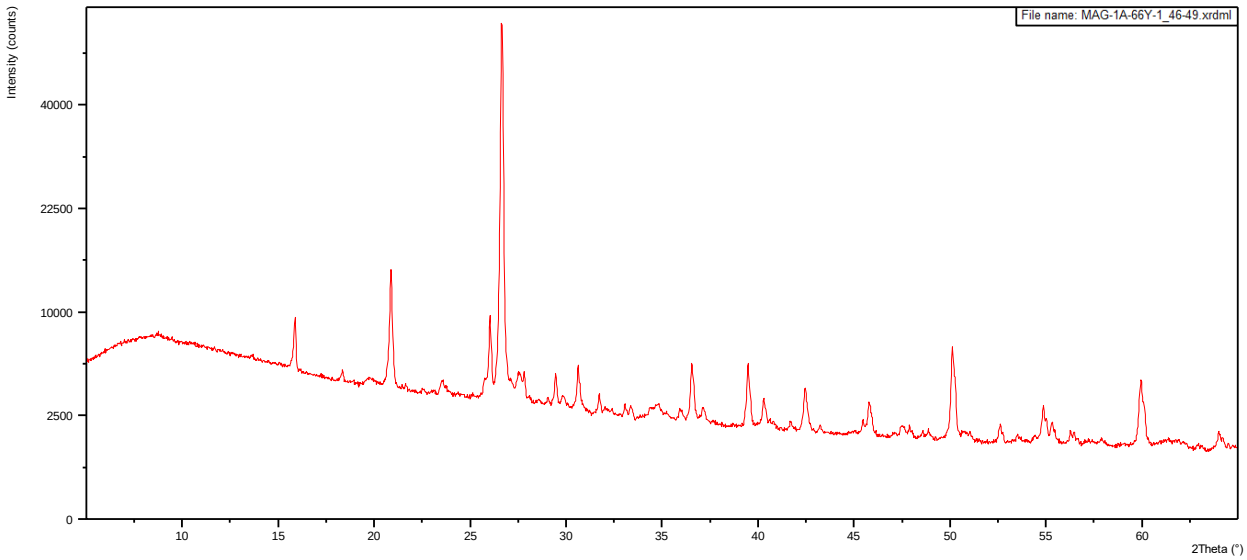
File name: MAG-1A-66Y-1_46-49.xrdml
Intensity (counts)
40000
22500
10000
2500
0
10
15
20
25
30
35
40
45
50
55
60
2Theta (°)

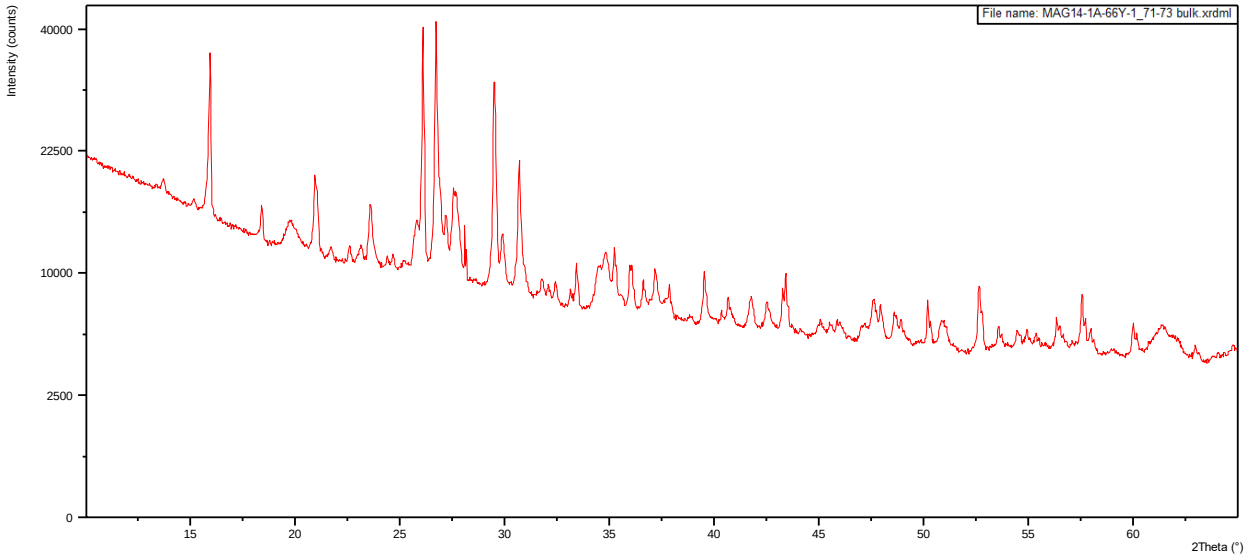
File name: MAG14-1A-66Y-1_71-73 bulk.xrdml
Intensity (counts)
40000
22500
10000
2500
0
15
20
25
30
35
40
45
50
55
60
2Theta (°)

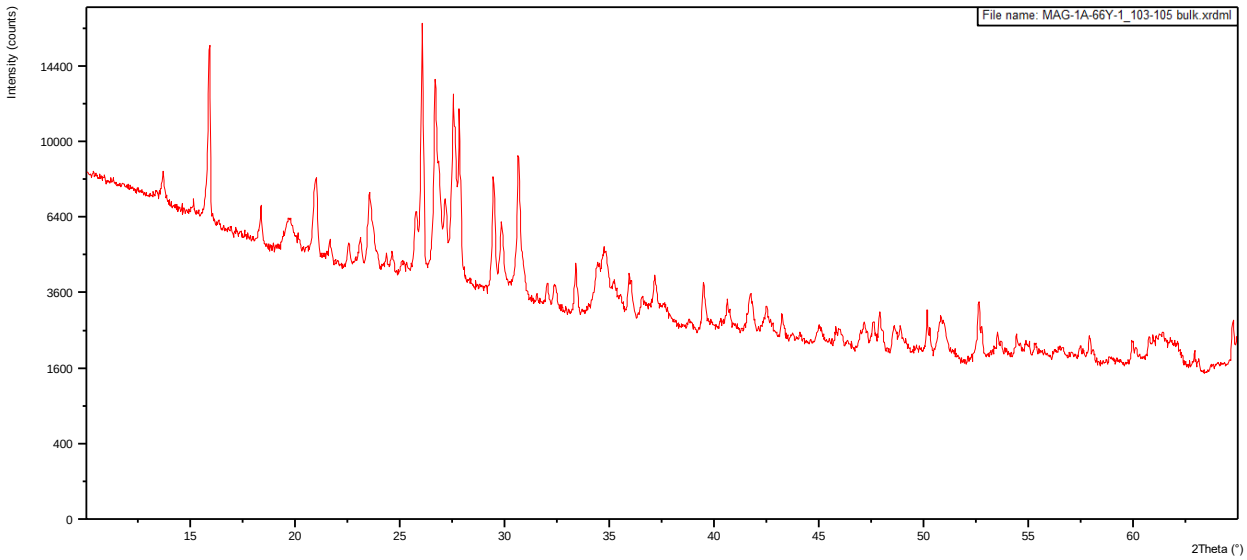
File name: MAG-1A-66Y-1_103-105 bulk.xrdml
Intensity (counts)
14400
10000
6400
3600
1600
400
0
15
20
25
30
35
40
45
50
55
60
2Theta (°)

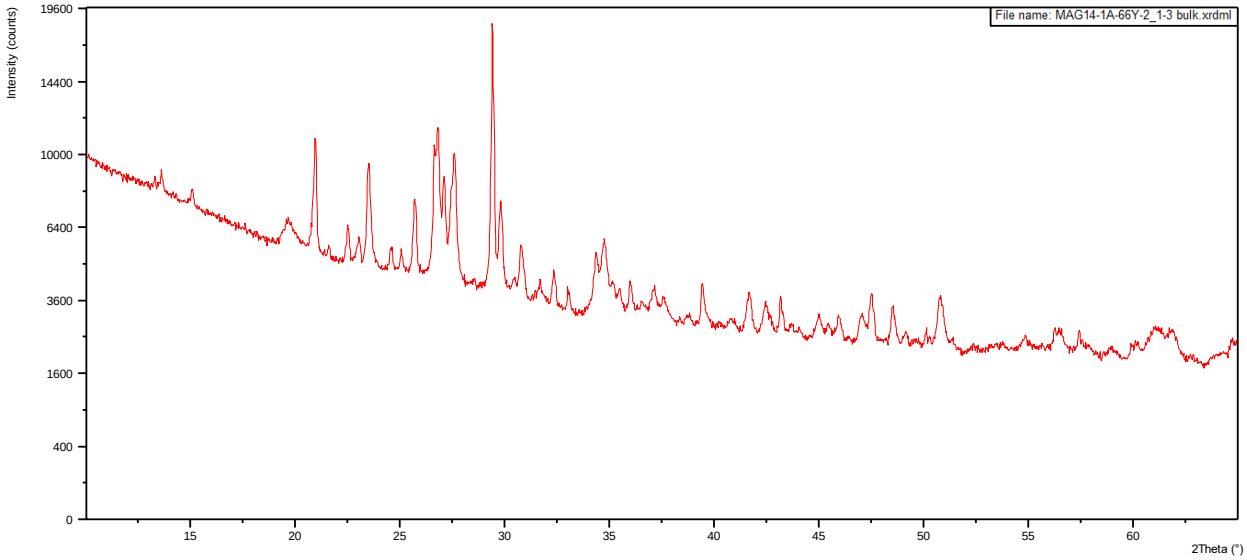
File name: MAG14-1A-66Y-2_1-3 bulk.xrdml
Intensity (counts)
19600
14400
10000
6400
3600
1600
400
0
15
20
25
30
35
40
45
50
55
60
2Theta (°)

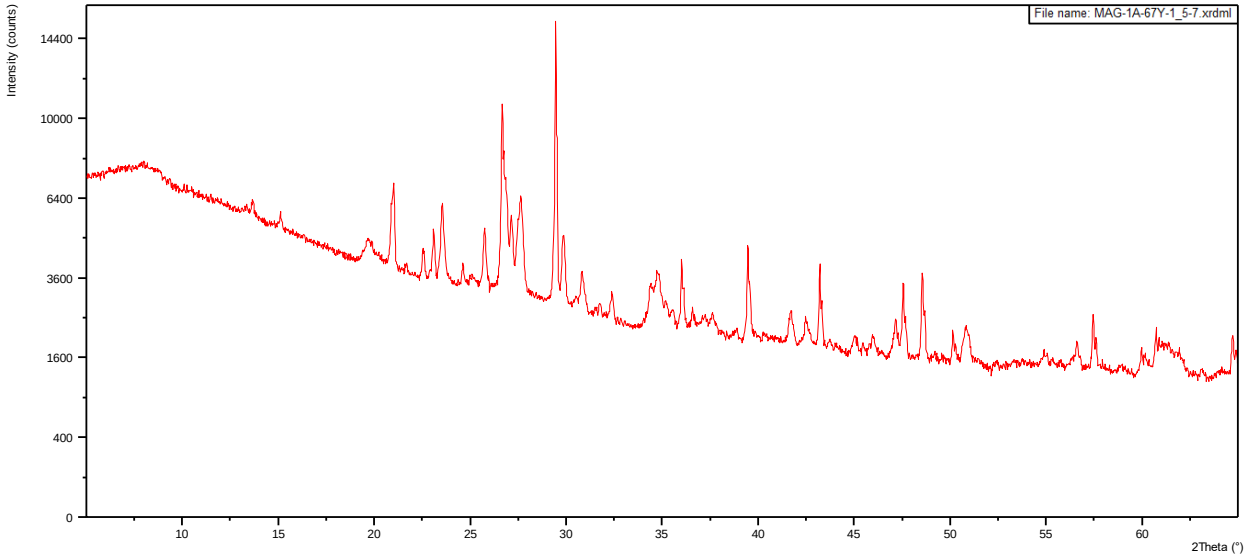
File name: MAG-1A-67Y-1_5-7.xrdml
Intensity (counts)
14400
10000
6400
3600
1600
400
0
10
15
20
25
30
35
40
45
50
55
60
2Theta (°)

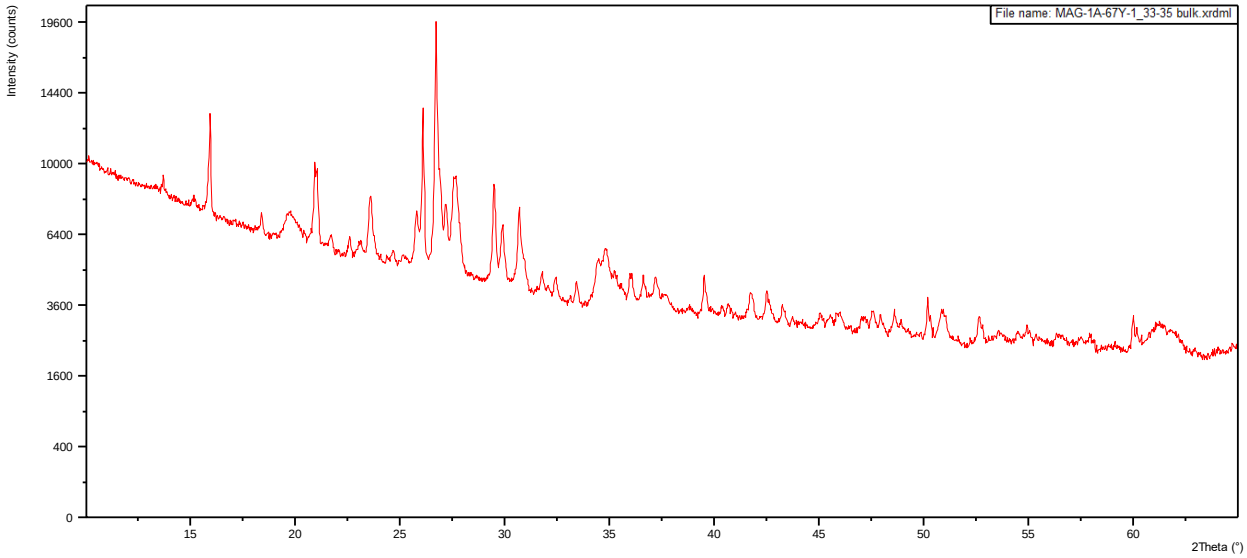
File name: MAG-1A-67Y-1_33-35 bulk.xrdml
Intensity (counts)
19600
14400
10000
6400
3600
1600
400
0
15
20
25
30
35
40
45
50
55
60
2Theta (°)

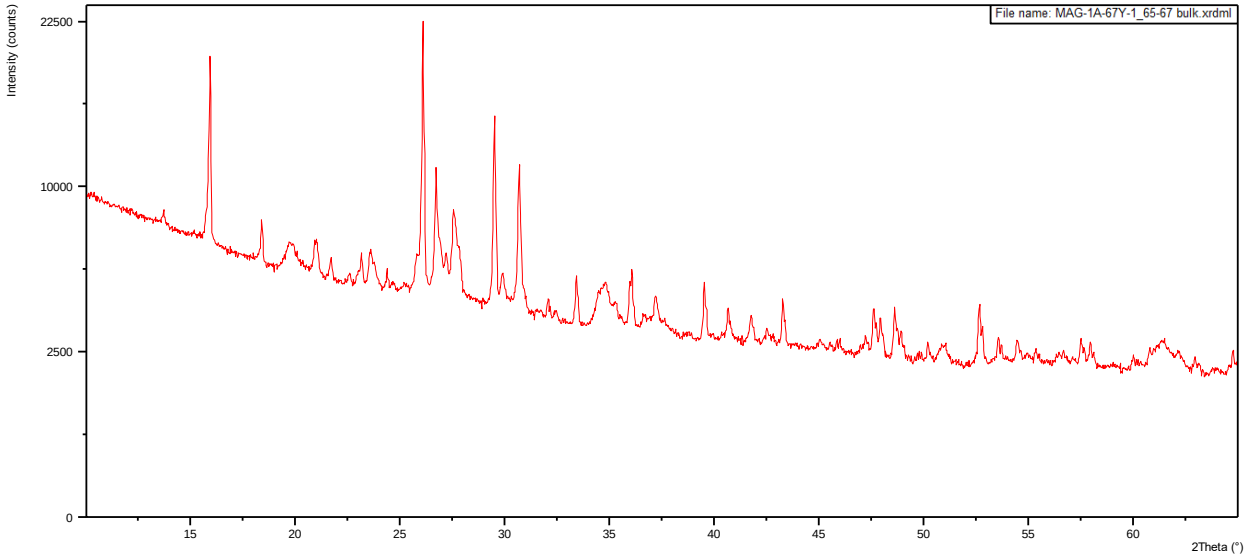
File name: MAG-1A-67Y-1_65-67 bulk.xrdml
Intensity (counts)
22500
10000
2500
0
15
20
25
30
35
40
45
50
55
60
2Theta (°)

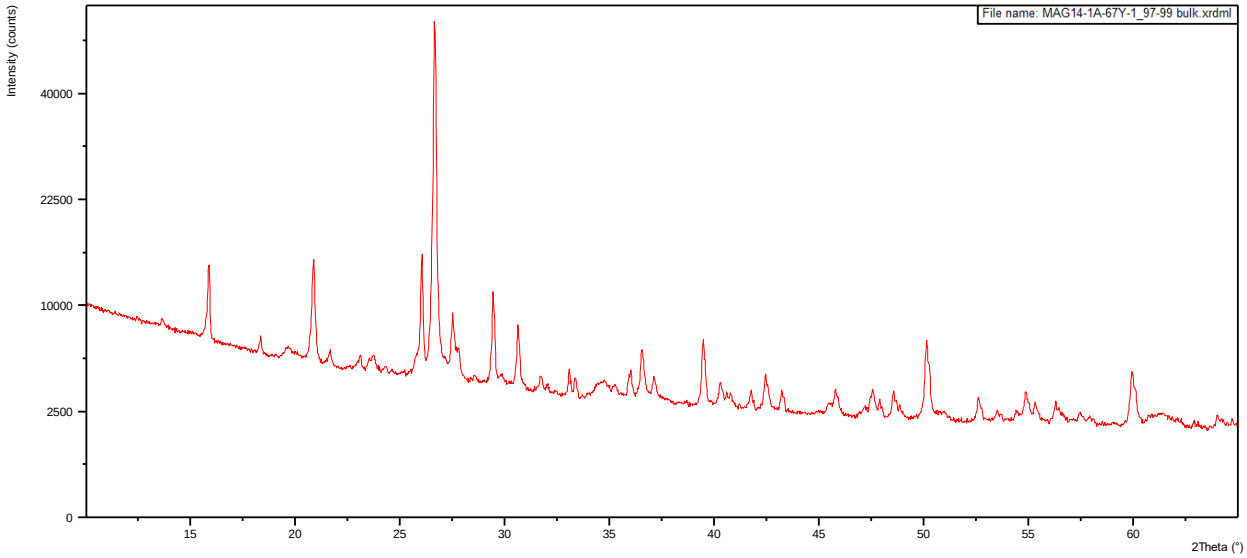
File name: MAG14-1A-67Y-1_97-99 bulk.xrdml
Intensity (counts)
40000
22500
10000
2500
0
15
20
25
30
35
40
45
50
55
60
2Theta (°)

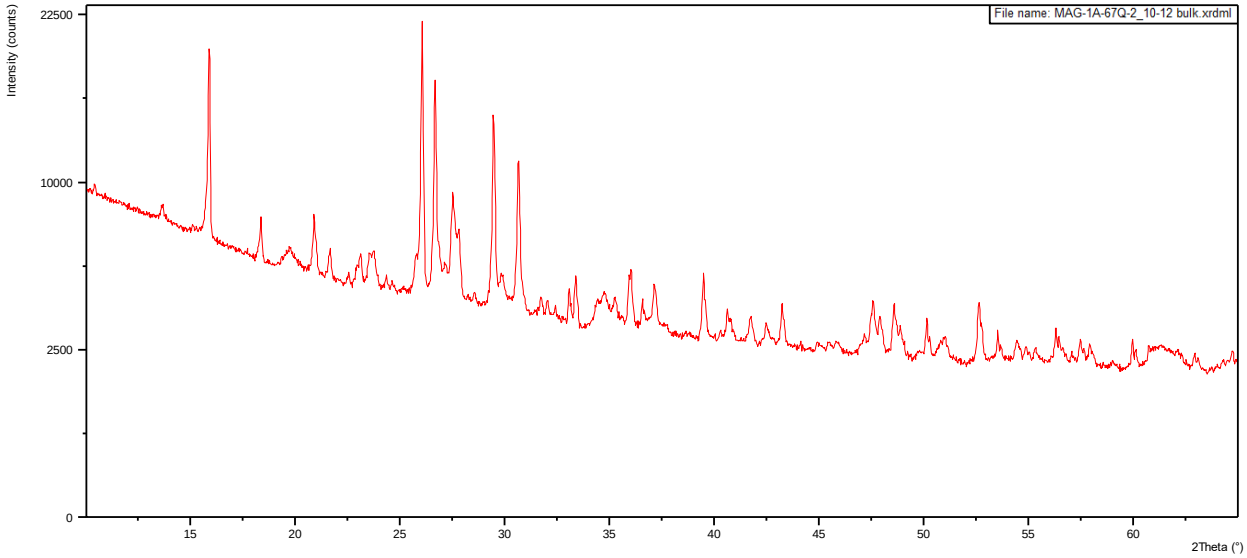
File name: MAG-1A-67Q-2_10-12 bulk.xrdml
Intensity (counts)
22500
10000
2500
0
15
20
25
30
35
40
45
50
55
60
2Theta (°)

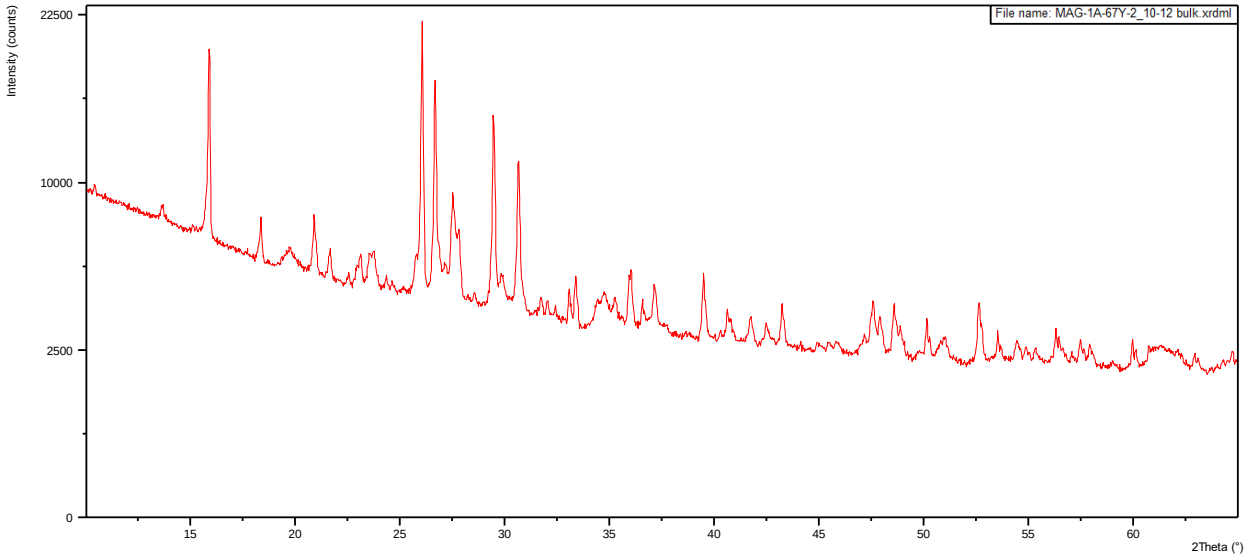
File name: MAG-1A-67Y-2_10-12 bulk.xrdml
Intensity (counts)
22500
10000
2500
0
15
20
25
30
35
40
45
50
55
60
2Theta (°)

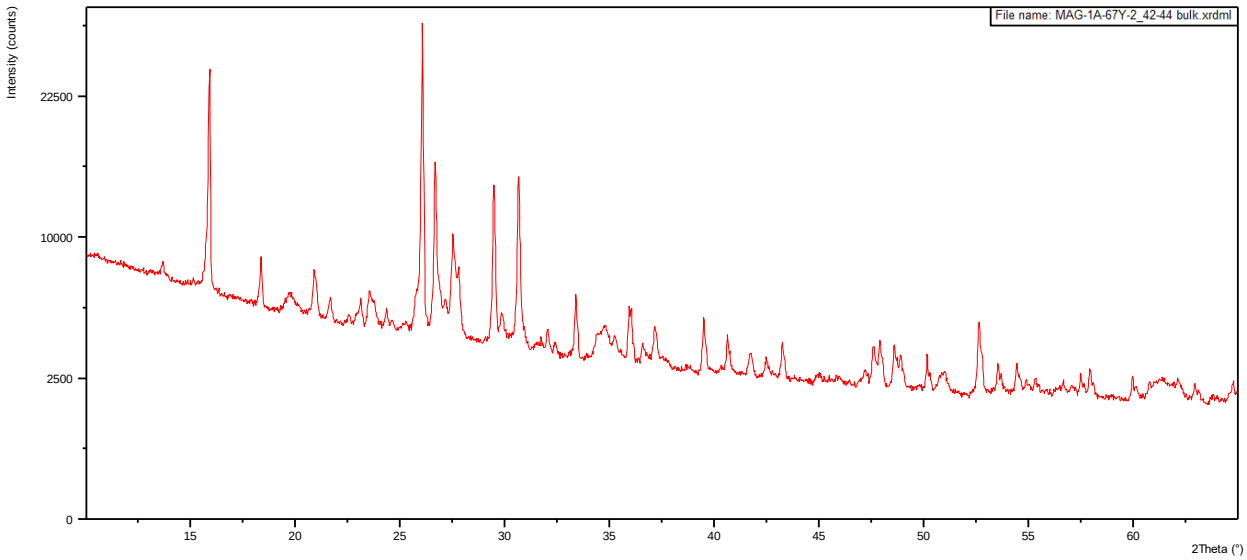
File name: MAG-1A-67Y-2_42-44 bulk.xrdml
Intensity (counts)
22500
10000
2500
0
15
20
25
30
35
40
45
50
55
60
2Theta (°)

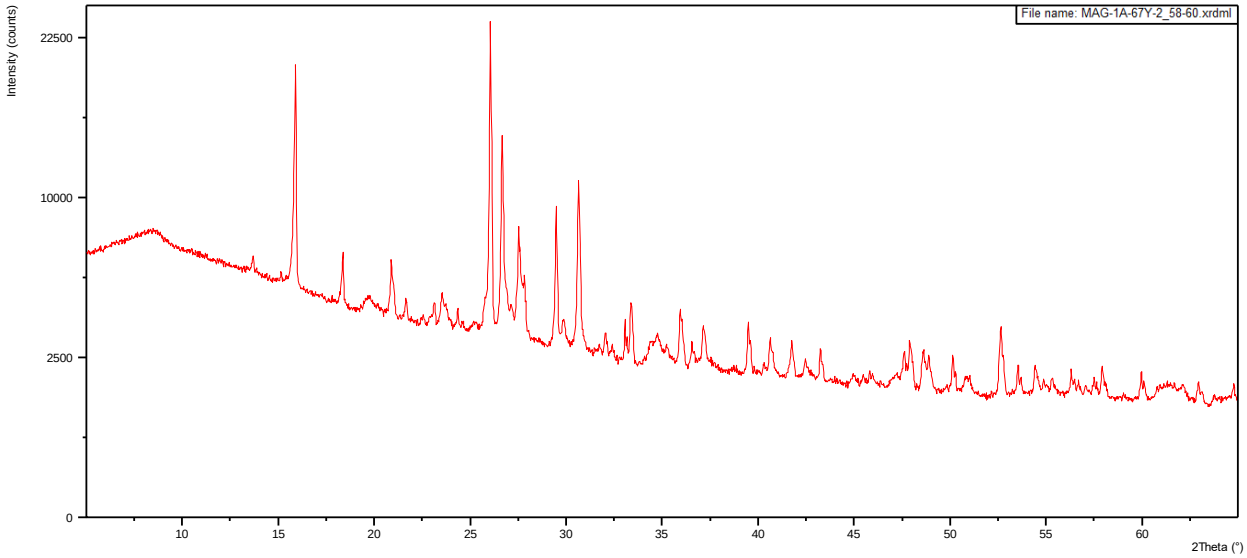
File name: MAG-1A-67Y-2_58-60.xrdml
Intensity (counts)
22500
10000
2500
0
10
15
20
25
30
35
40
45
50
55
60
2Theta (°)

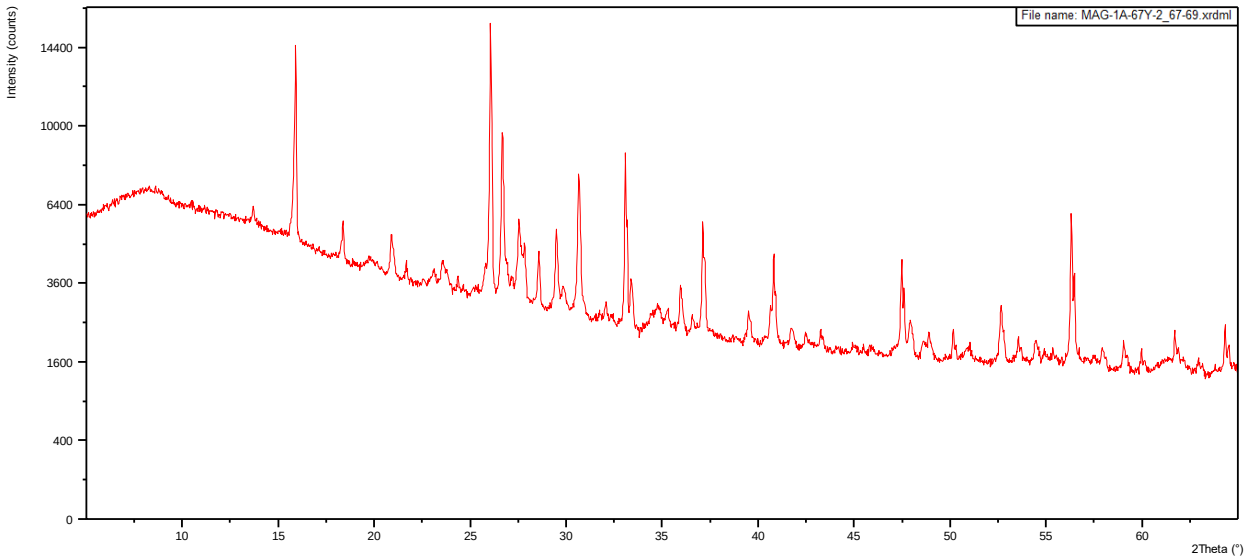
File name: MAG-1A-67Y-2_67-69.xrdml
Intensity (counts)
14400
10000
6400
3600
1600
400
0
10
15
20
25
30
35
40
45
50
55
60
2Theta (°)

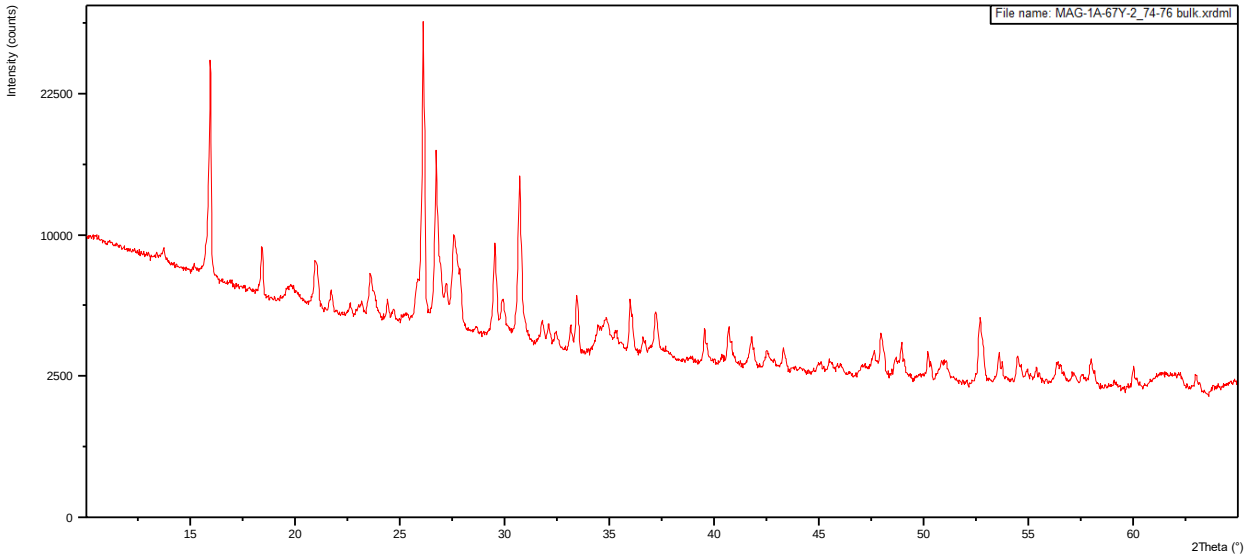
File name: MAG-1A-67Y-2_74-76 bulk.xrdml
Intensity (counts)
22500
10000
2500
0
15
20
25
30
35
40
45
50
55
60
2Theta (°)

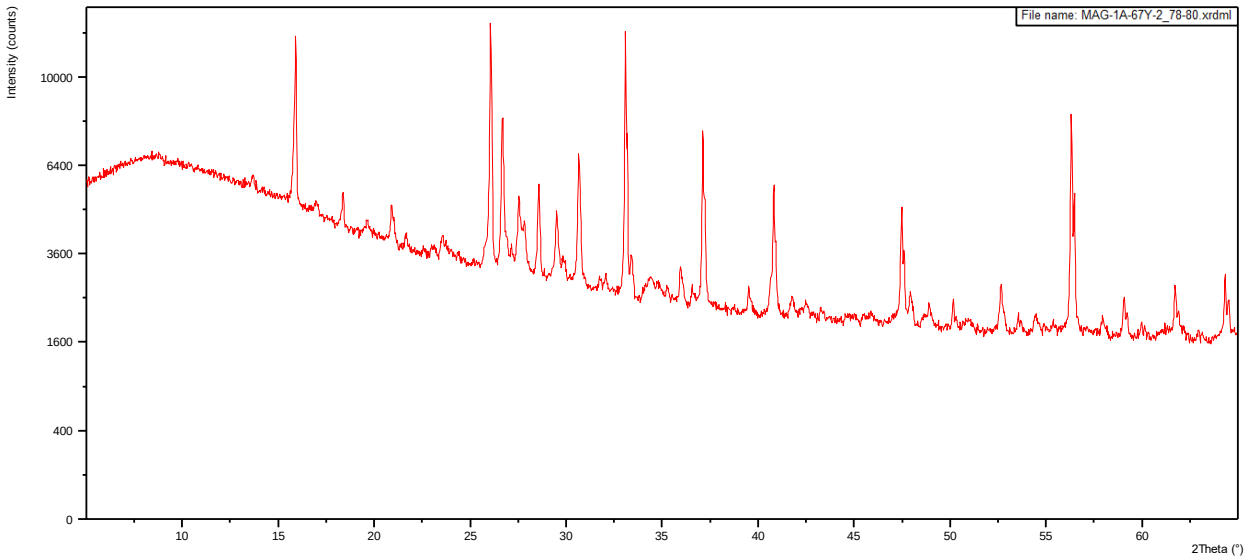
File name: MAG-1A-67Y-2_78-80.xrdml
Intensity (counts)
10000
6400
3600
1600
400
0
10
15
20
25
30
35
40
45
50
55
60
2Theta (°)

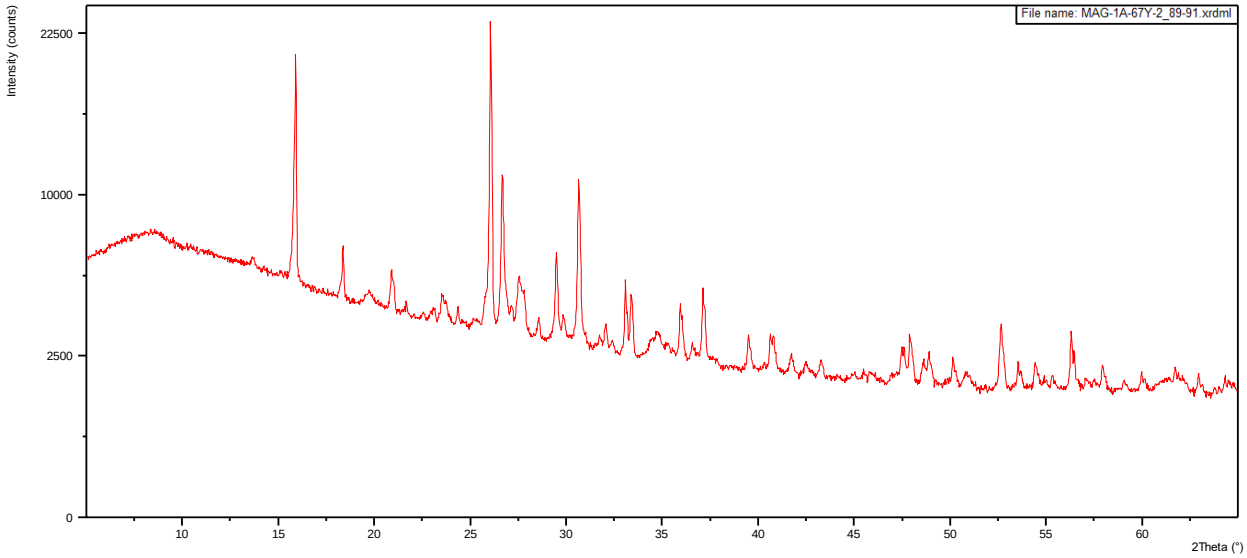
File name: MAG-1A-67Y-2_89-91.xrdml
Intensity (counts)
22500
10000
2500
0
10
15
20
25
30
35
40
45
50
55
60
2Theta (°)

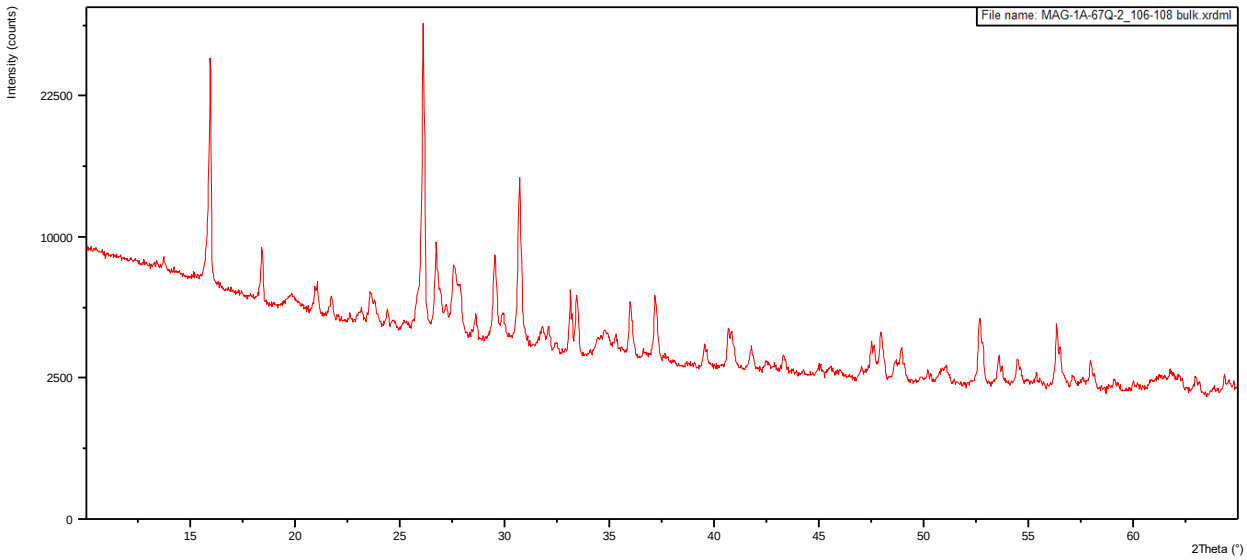
File name: MAG-1A-67Q-2_106-108 bulk.xrdml
Intensity (counts)
22500
10000
2500
0
15
20
25
30
35
40
45
50
55
60
2Theta (°)

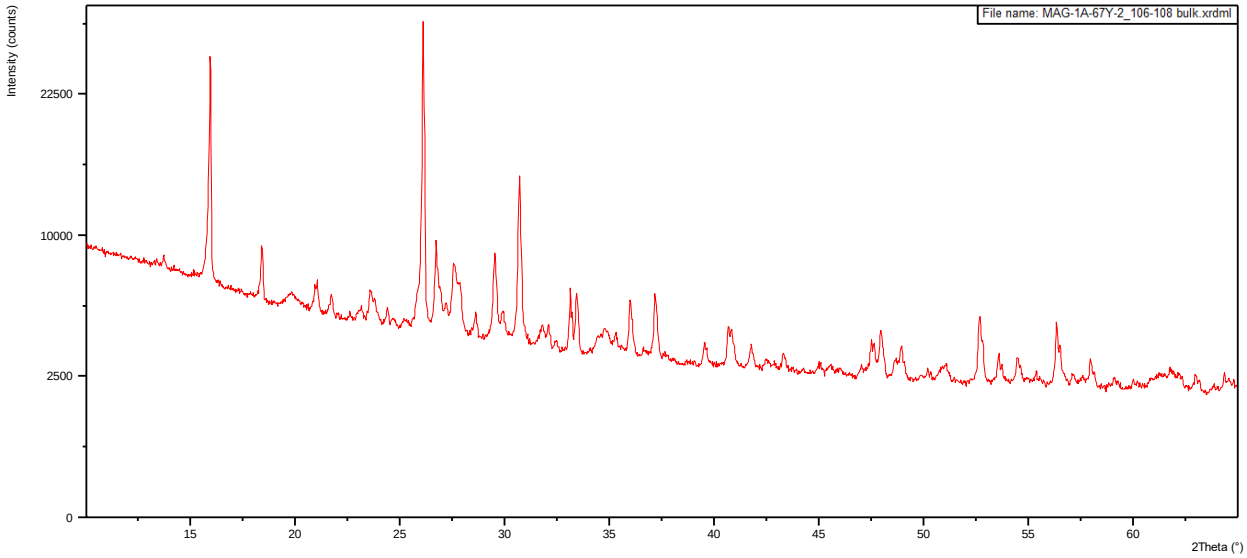
File name: MAG-1A-67Y-2_106-108 bulk.xrdml
Intensity (counts)
22500
10000
2500
0
15
20
25
30
35
40
45
50
55
60
2Theta (°)

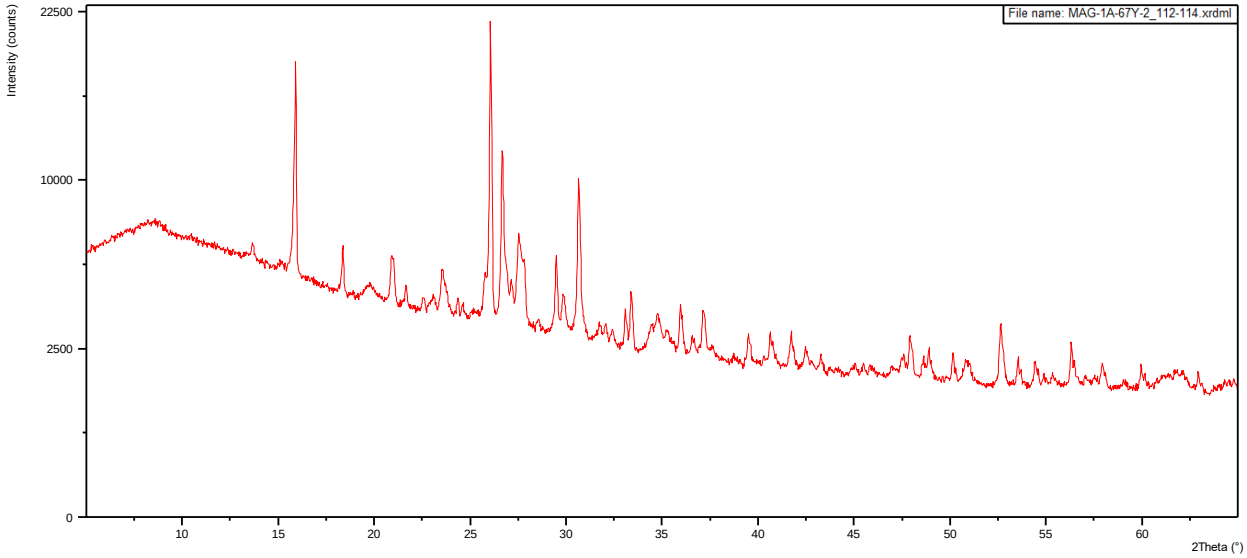
File name: MAG-1A-67Y-2_112-114.xrdml
Intensity (counts)
22500
10000
2500
0
10
15
20
25
30
35
40
45
50
55
60
2Theta (°)

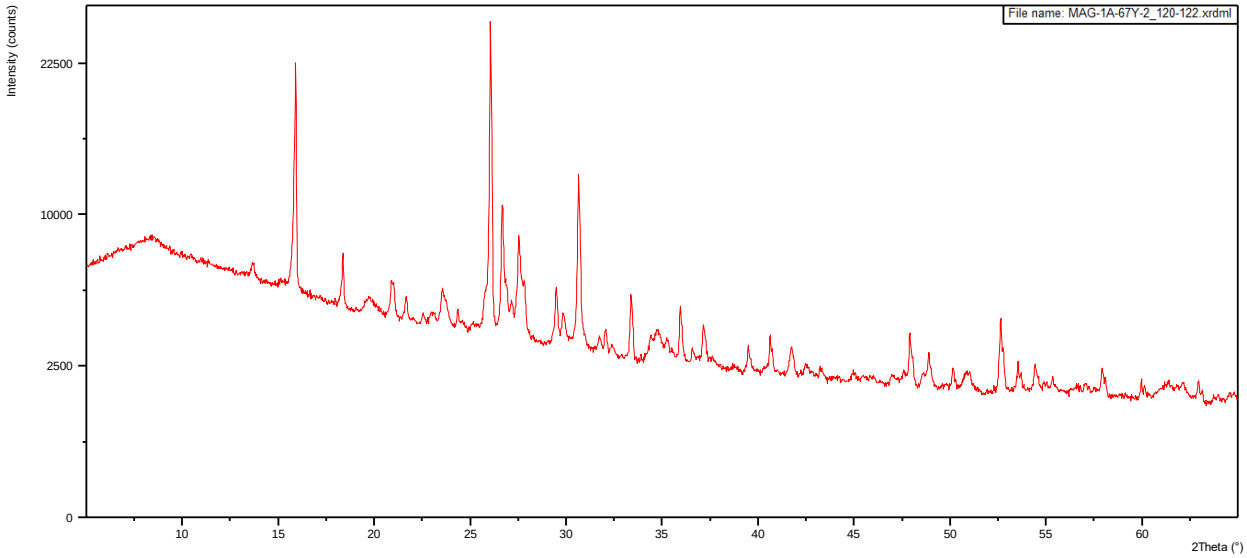
File name: MAG-1A-67Y-2_120-122.xrdml
Intensity (counts)
22500
10000
2500
0
10
15
20
25
30
35
40
45
50
55
60
2Theta (°)

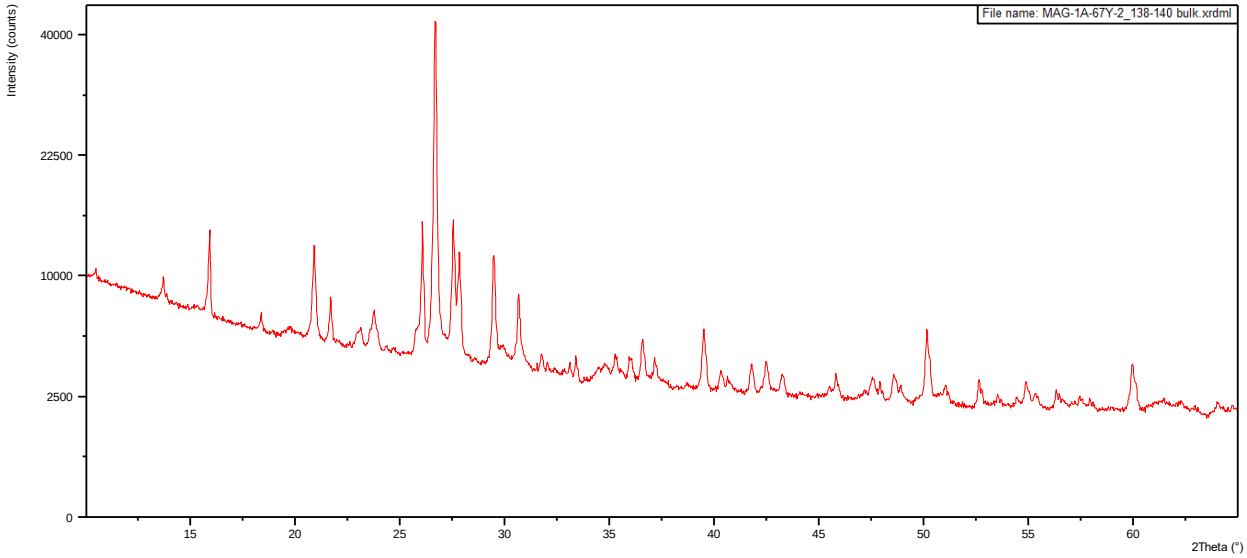
File name: MAG-1A-67Y-2_138-140 bulk.xrdml
Intensity (counts)
40000
22500
10000
2500
0
15
20
25
30
35
40
45
50
55
60
2Theta (°)

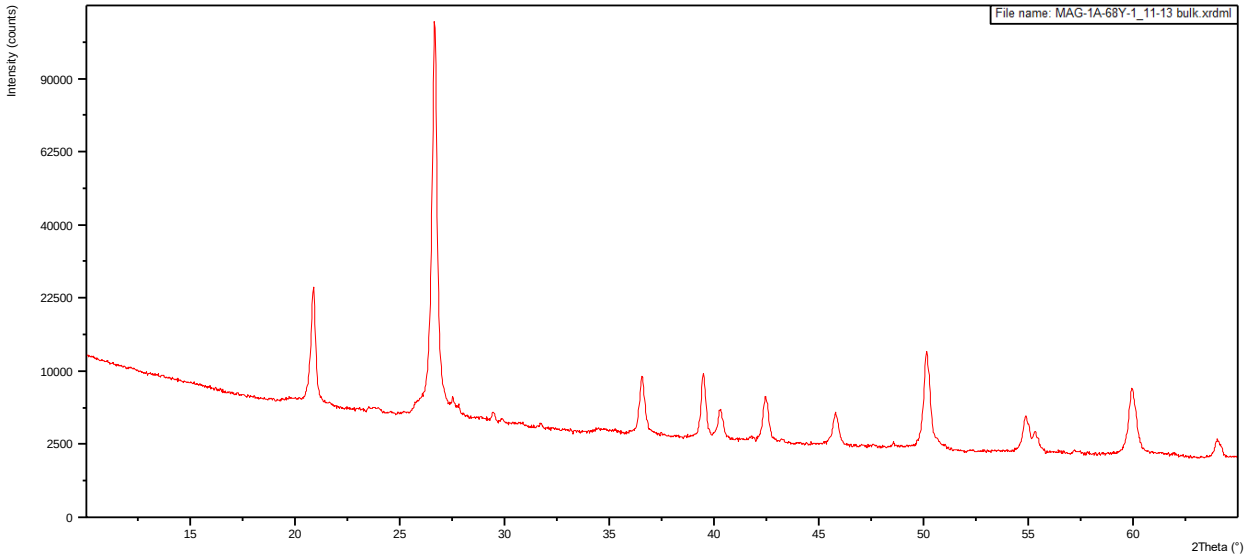
File name: MAG-1A-68Y-1_11-13 bulk.xrdml
Intensity (counts)
90000
62500
40000
22500
10000
2500
0
15
20
25
30
35
40
45
50
55
60
2Theta (°)

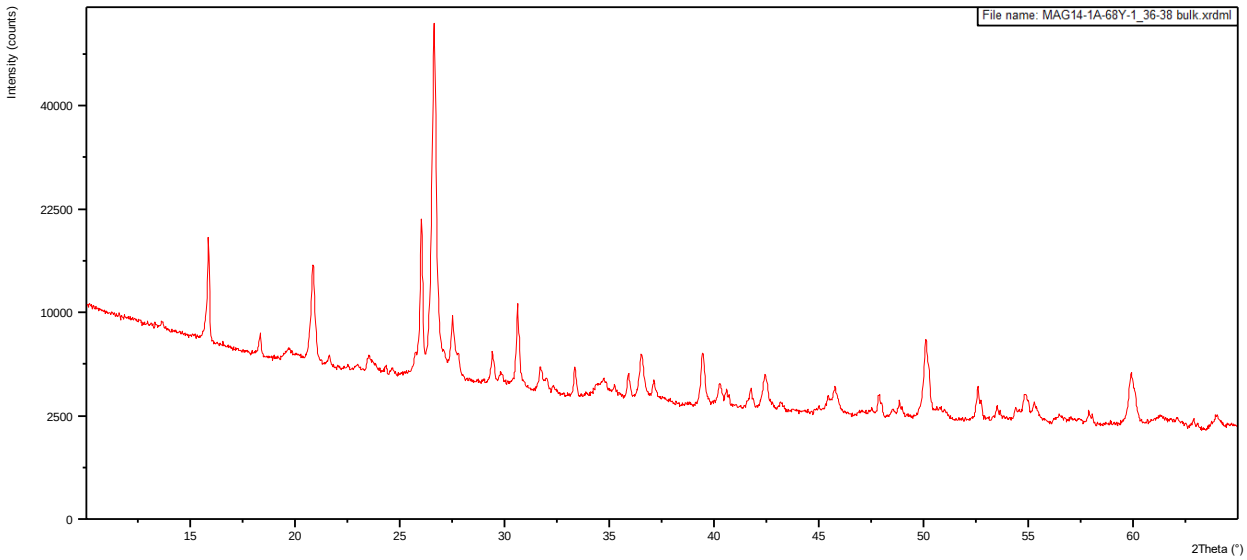
File name: MAG14-1A-68Y-1_36-38 bulk.xrdml
Intensity (counts)
40000
22500
10000
2500
0
15
20
25
30
35
40
45
50
55
60
2Theta (°)

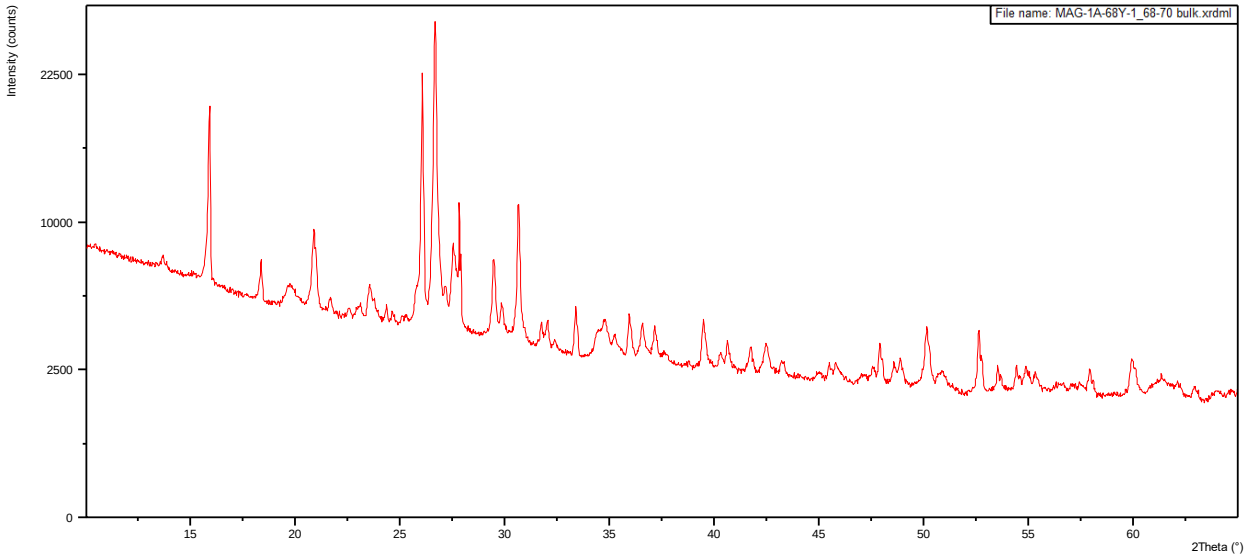
File name: MAG-1A-68Y-1_68-70 bulk.xrdml
Intensity (counts)
22500
10000
2500
0
15
20
25
30
35
40
45
50
55
60
2Theta (°)

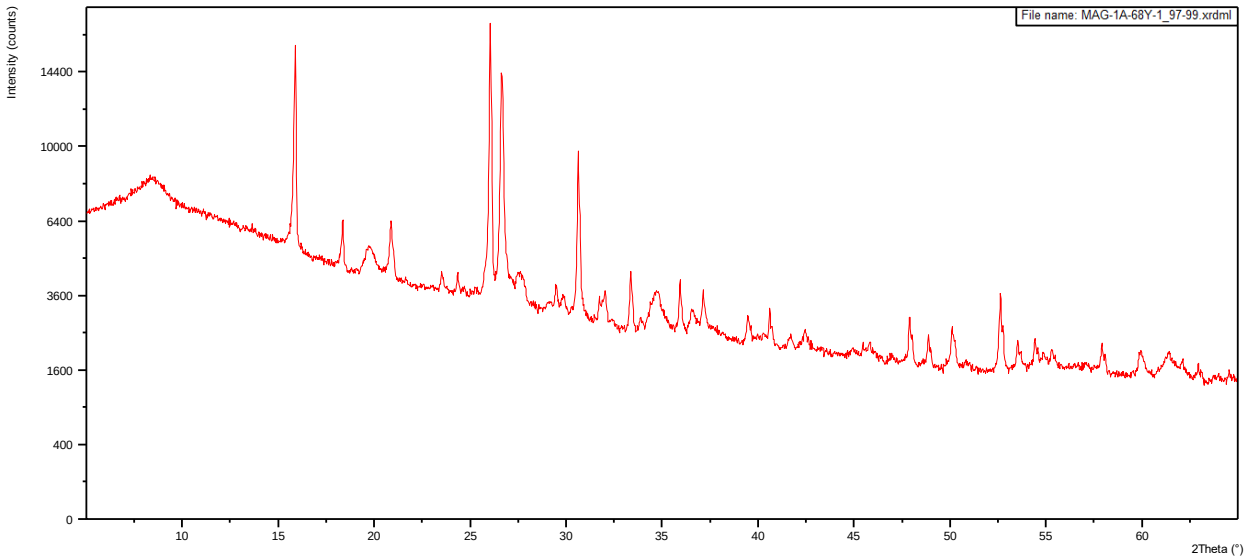
File name: MAG-1A-68Y-1_97-99.xrdml
Intensity (counts)
14400
10000
6400
3600
1600
400
0
10
15
20
25
30
35
40
45
50
55
60
2Theta (°)

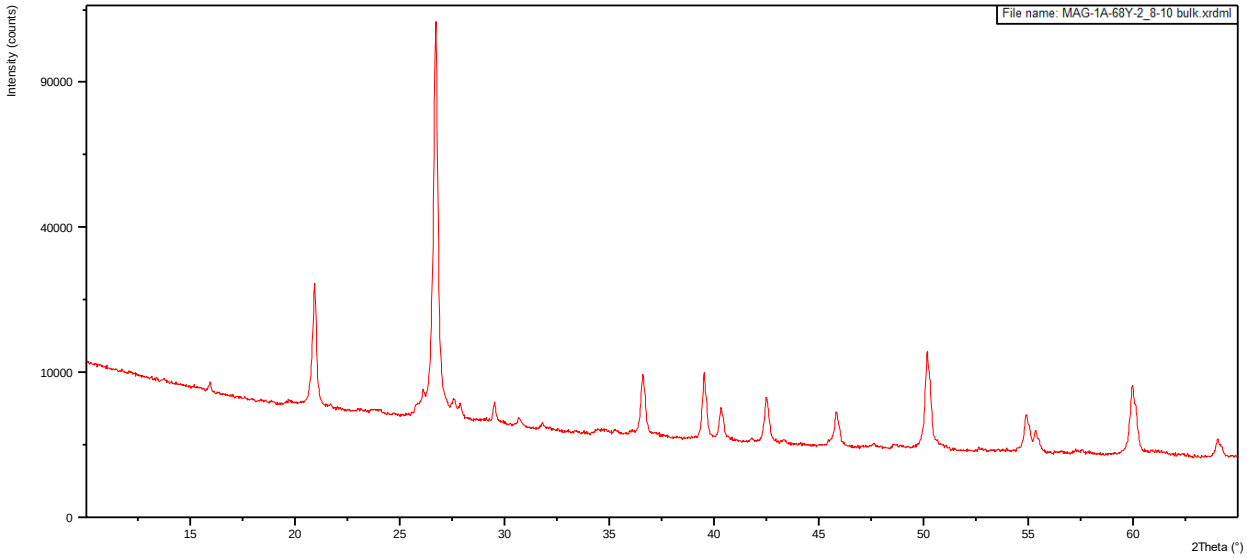
File name: MAG-1A-68Y-2_8-10 bulk.xrdml
Intensity (counts)
90000
40000
10000
0
15
20
25
30
35
40
45
50
55
60
2Theta (°)

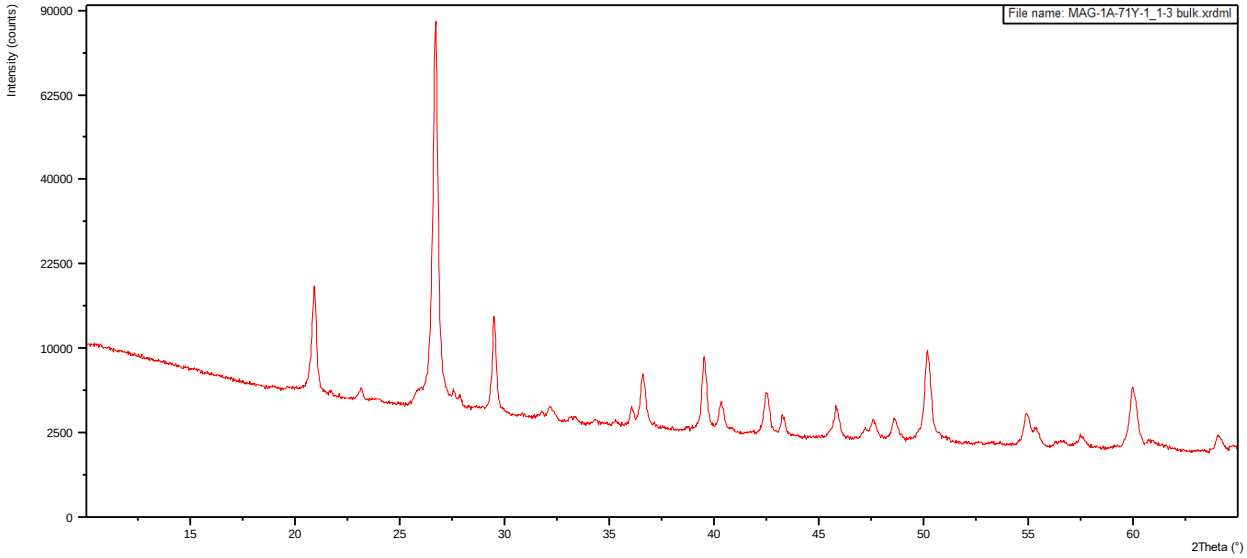
File name: MAG-1A-71Y-1_1-3 bulk.xrdml
Intensity (counts)
90000
62500
40000
22500
10000
2500
0
15
20
25
30
35
40
45
50
55
60
2Theta (°)

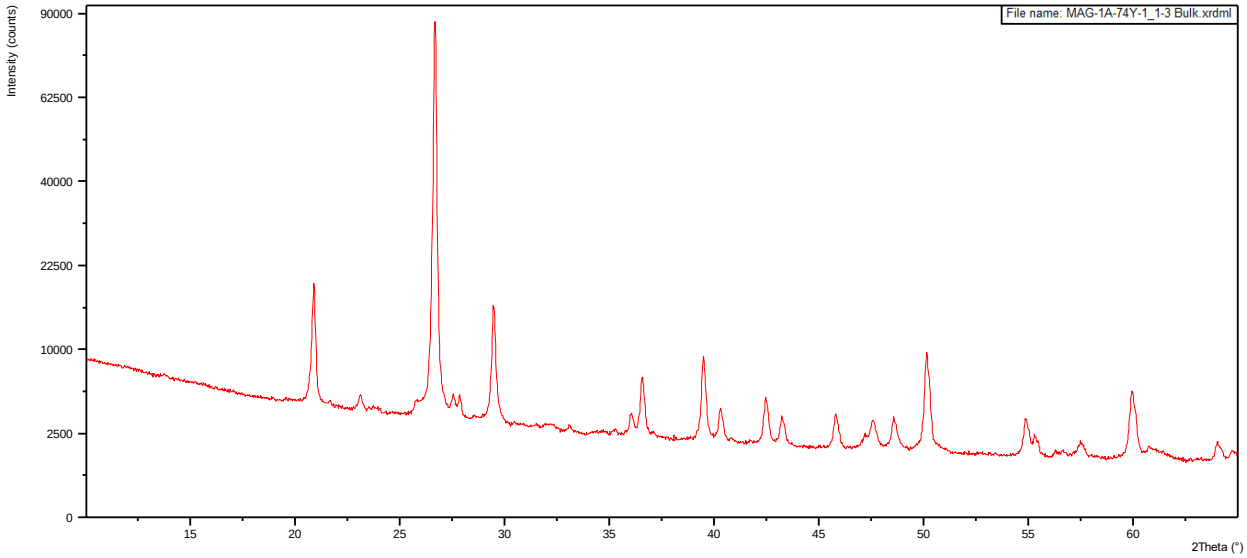
File name: MAG-1A-74Y-1_1-3 Bulk.xrdml
Intensity (counts)
90000
62500
40000
22500
10000
2500
0
15
20
25
30
35
40
45
50
55
60
2Theta (°)

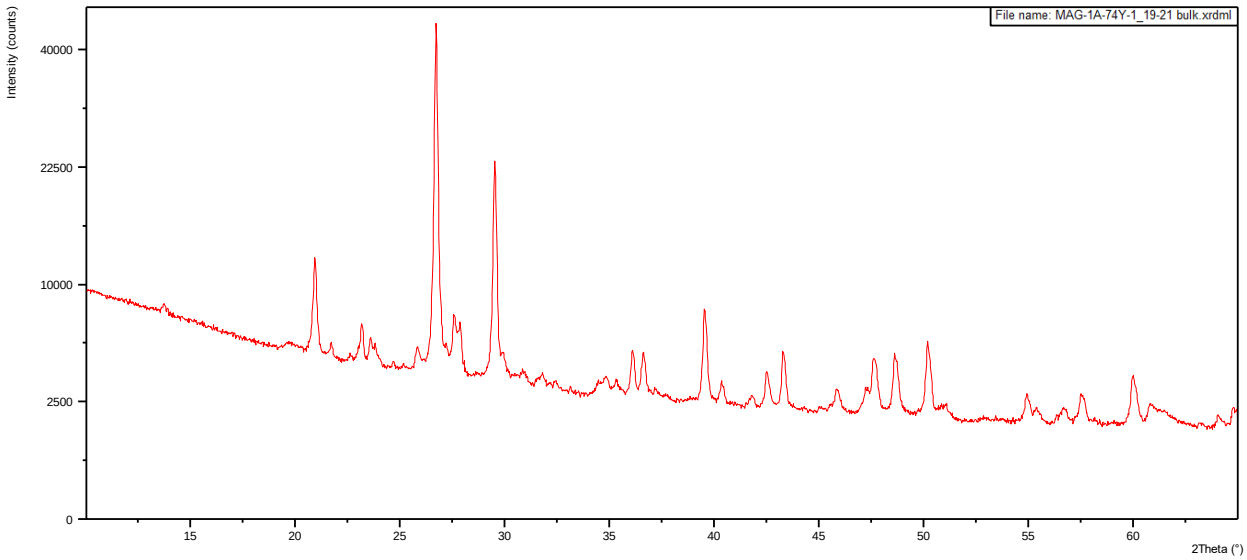

Appendix B.1.2: HSPDP-MAG14-2A

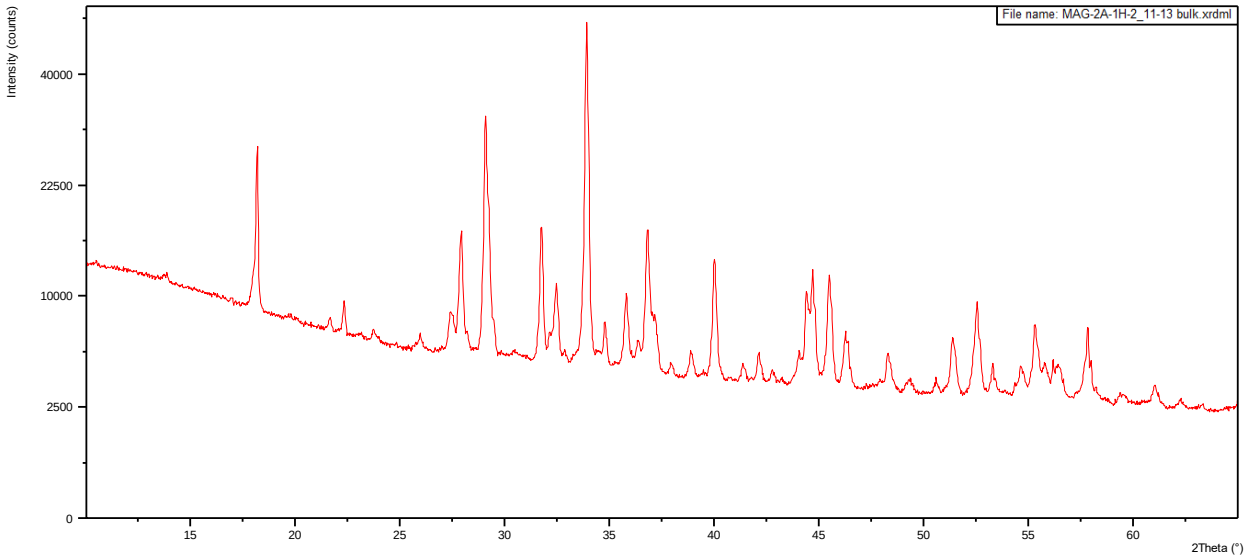

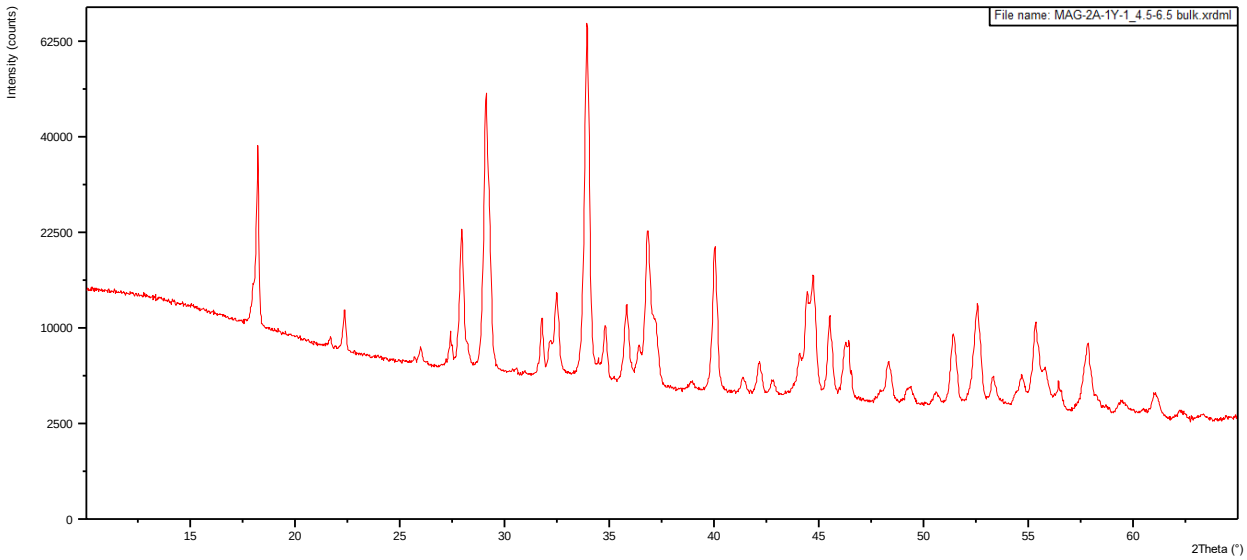
File name: MAG-2A-1Y-1_4.5-6.5 bulk.xrdml
Intensity (counts)
62500
40000
22500
10000
2500
0
15
20
25
30
35
40
45
50
55
60
2Theta (°)

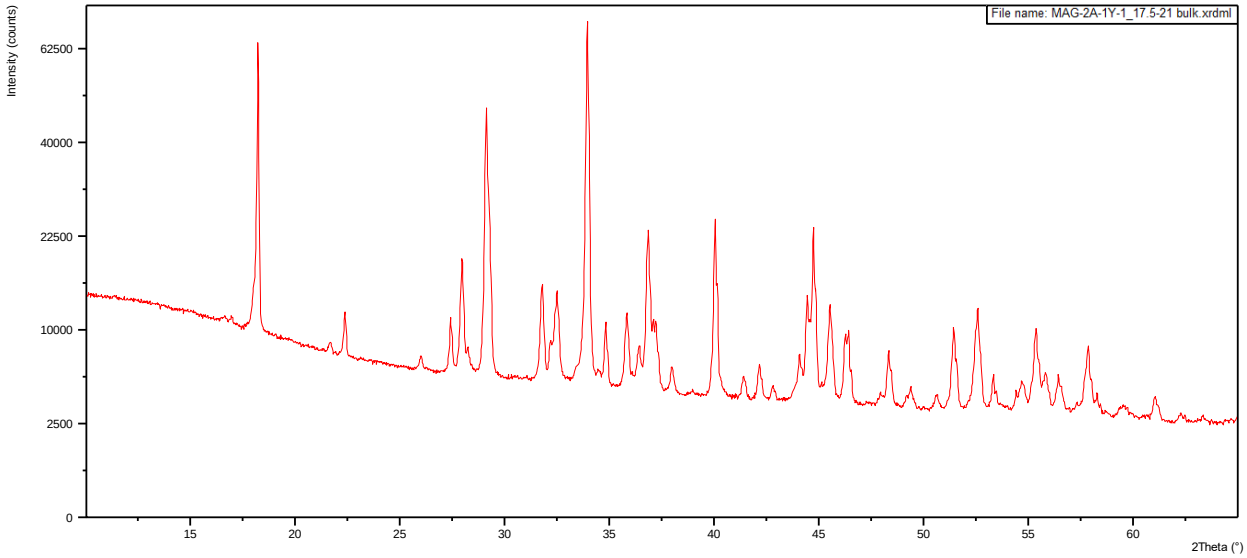
File name: MAG-2A-1Y-1_17.5-21 bulk.xrdml
Intensity (counts)
62500
40000
22500
10000
2500
0
15
20
25
30
35
40
45
50
55
60
2Theta (°)

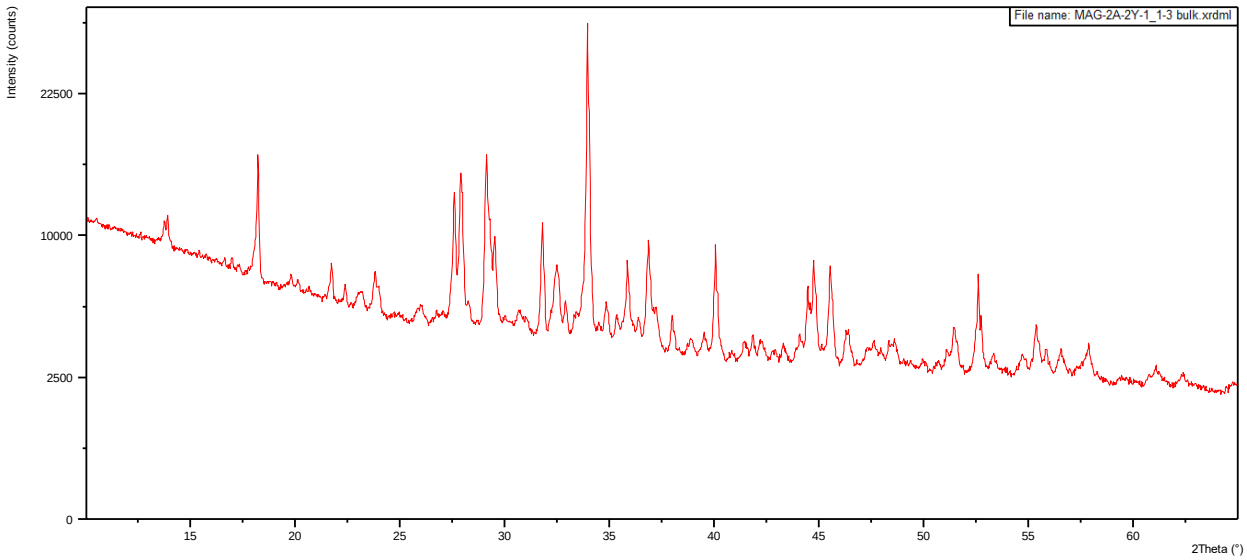
File name: MAG-2A-2Y-1_1-3 bulk.xrdml
Intensity (counts)
22500
10000
2500
0
15
20
25
30
35
40
45
50
55
60
2Theta (°)

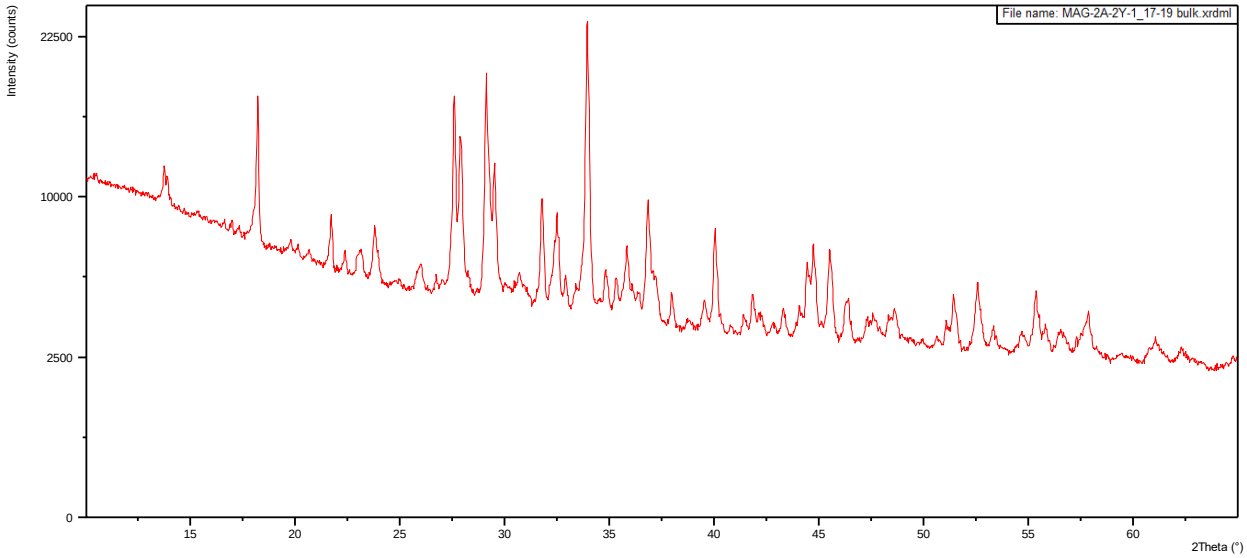
File name: MAG-2A-2Y-1_17-19 bulk.xrdml
Intensity (counts)
22500
10000
2500
0
15
20
25
30
35
40
45
50
55
60
2Theta (°)

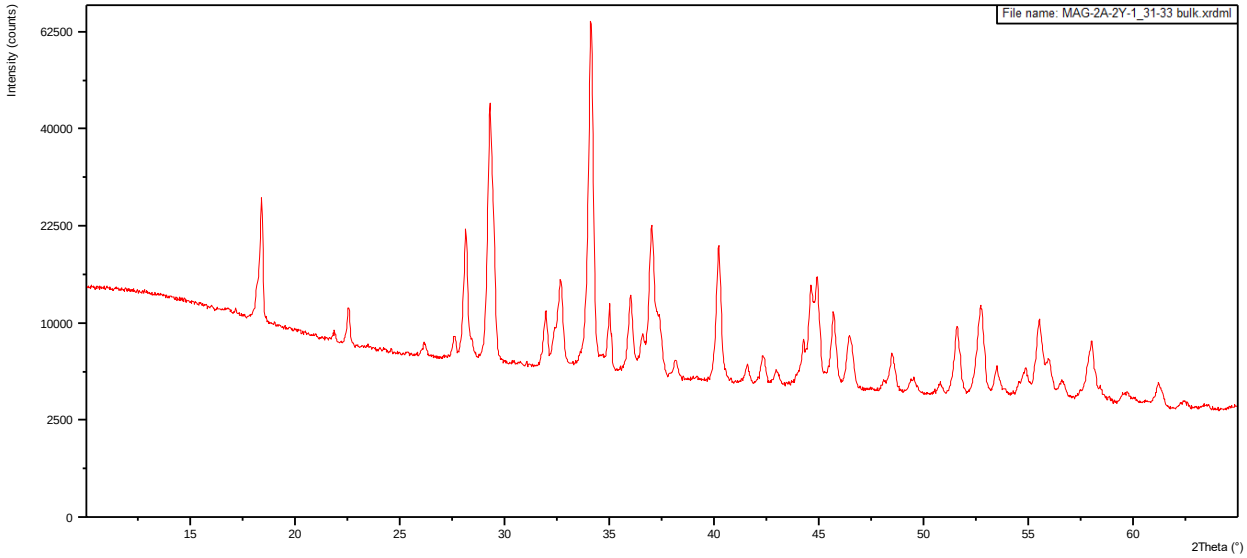
File name: MAG-2A-2Y-1_31-33 bulk.xrdml
Intensity (counts)
62500
40000
22500
10000
2500
0
15
20
25
30
35
40
45
50
55
60
2Theta (°)

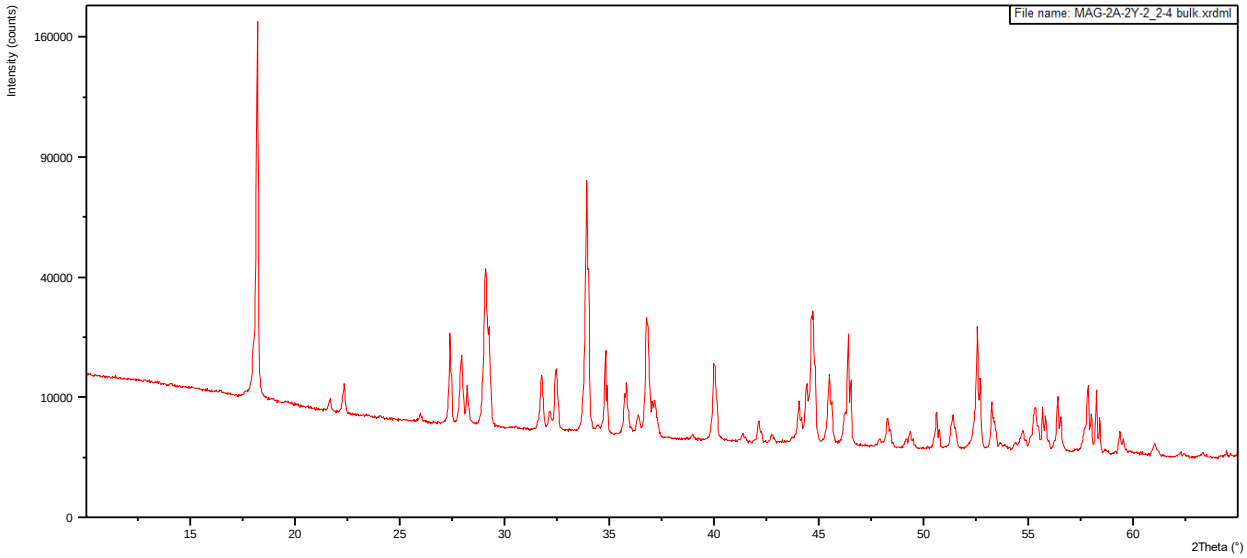
File name: MAG-2A-2Y-2_2-4 bulk.xrdml
Intensity (counts)
160000
90000
40000
10000
0
15
20
25
30
35
40
45
50
55
60
2Theta (°)

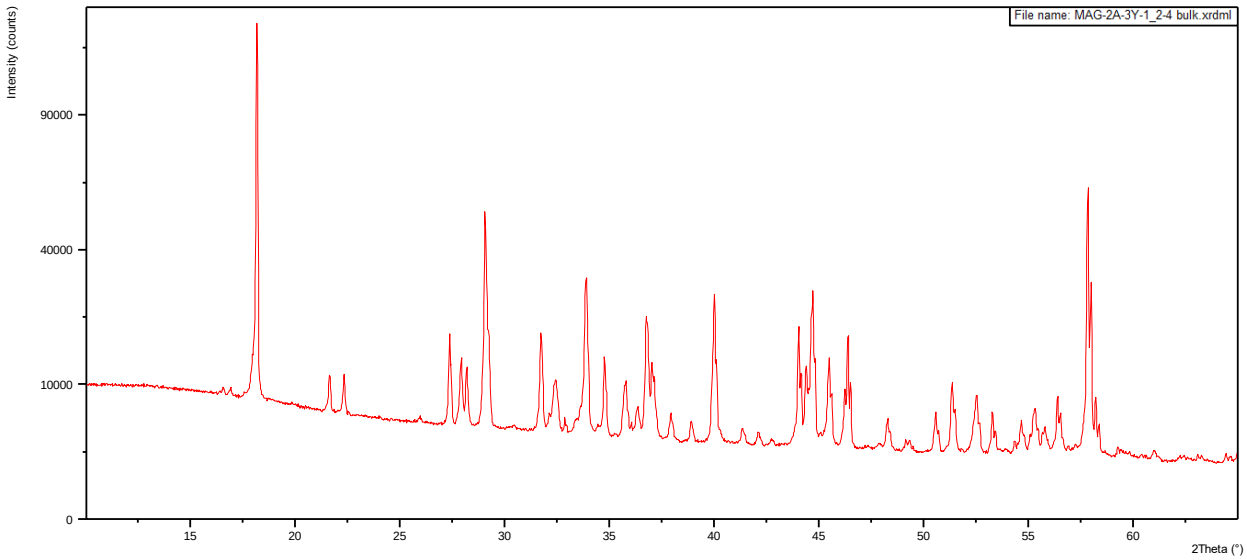
File name: MAG-2A-3Y-1_2-4 bulk.xrdml
Intensity (counts)
90000
40000
10000
0
15
20
25
30
35
40
45
50
55
60
2Theta (°)

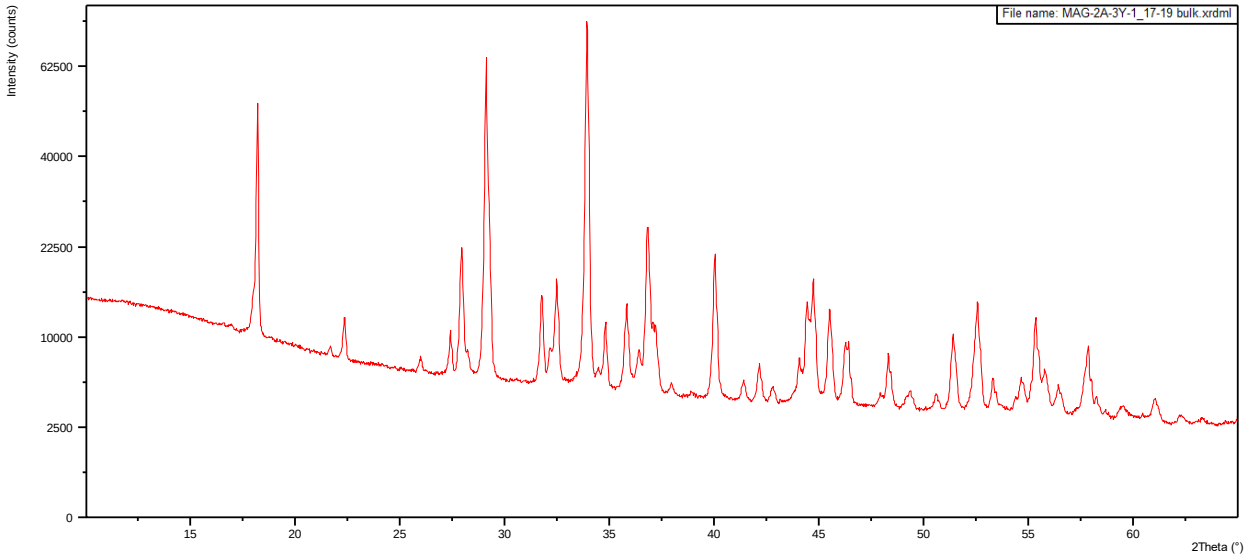
File name: MAG-2A-3Y-1_17-19 bulk.xrdml
Intensity (counts)
62500
40000
22500
10000
2500
0
15
20
25
30
35
40
45
50
55
60
2Theta (°)

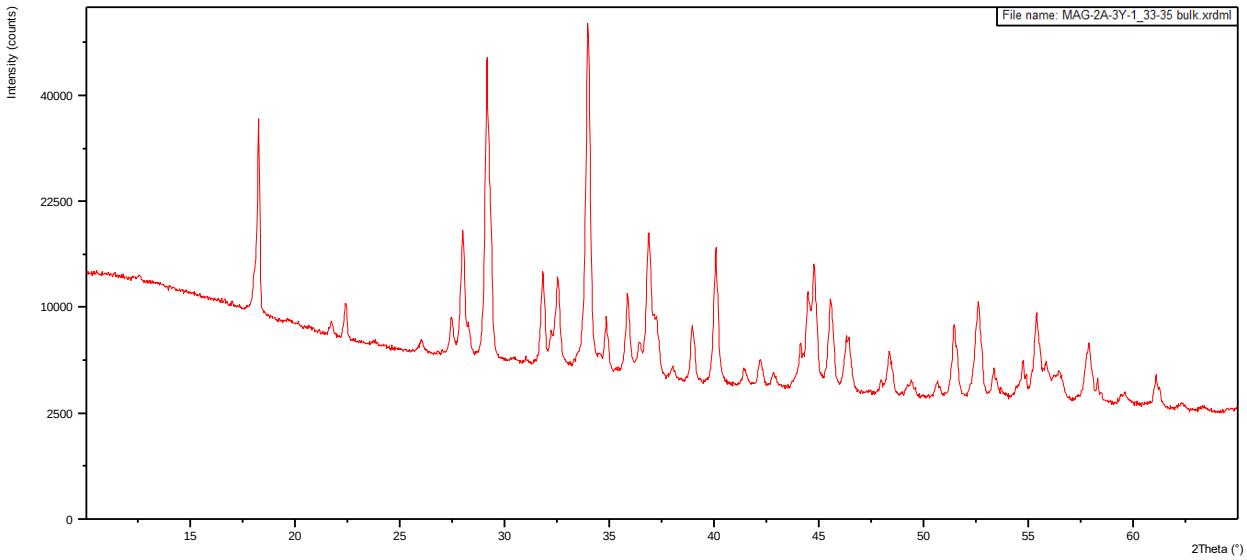
File name: MAG-2A-3Y-1_33-35 bulk.xrdml
Intensity (counts)
0
2500
10000
22500
40000
15
20
25
30
35
40
45
50
55
60
2Theta (°)

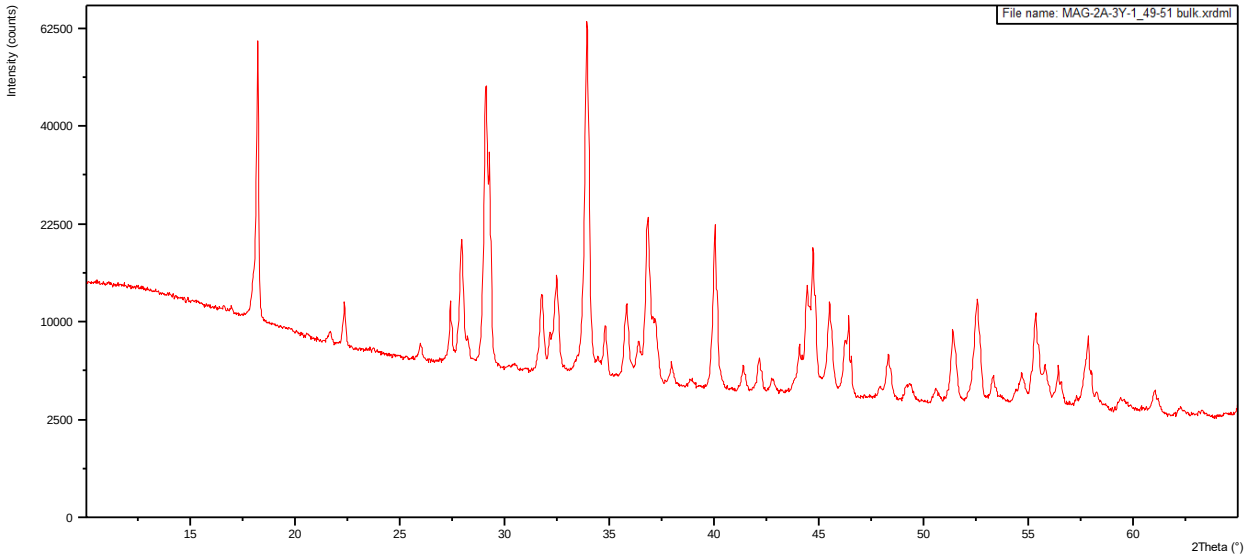
File name: MAG-2A-3Y-1_49-51 bulk.xrdml
Intensity (counts)
0
2500
10000
22500
40000
62500
15
20
25
30
35
40
45
50
55
60
2Theta (°)

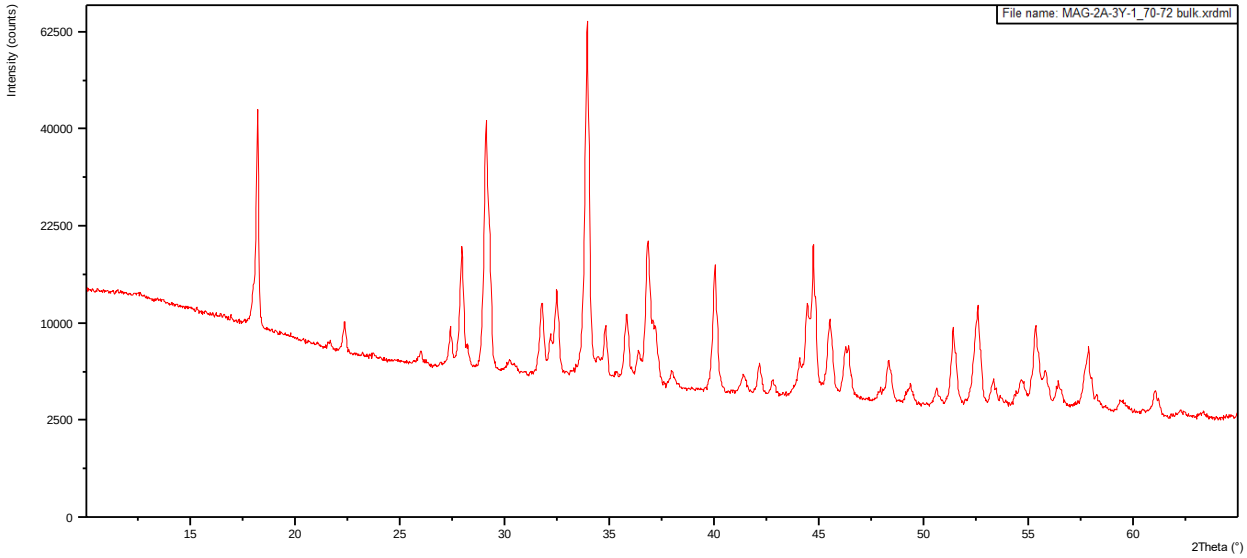
File name: MAG-2A-3Y-1_70-72 bulk.xrdml
Intensity (counts)
62500
40000
22500
10000
2500
0
15
20
25
30
35
40
45
50
55
60
2Theta (°)

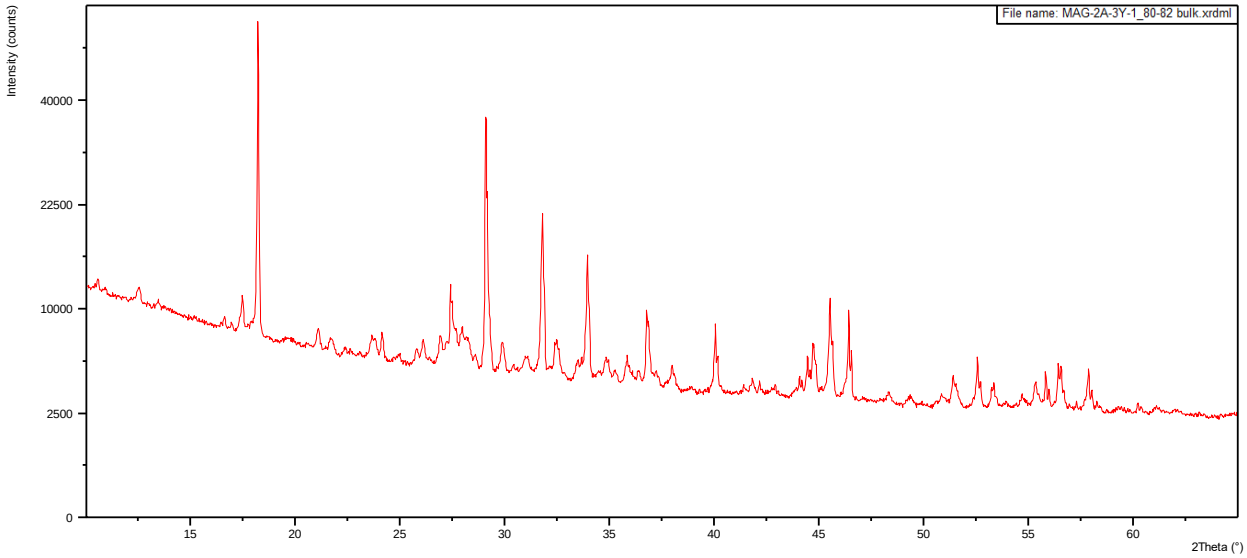
File name: MAG-2A-3Y-1_80-82 bulk.xrdml
Intensity (counts)
40000
22500
10000
2500
0
15
20
25
30
35
40
45
50
55
60
2Theta (°)

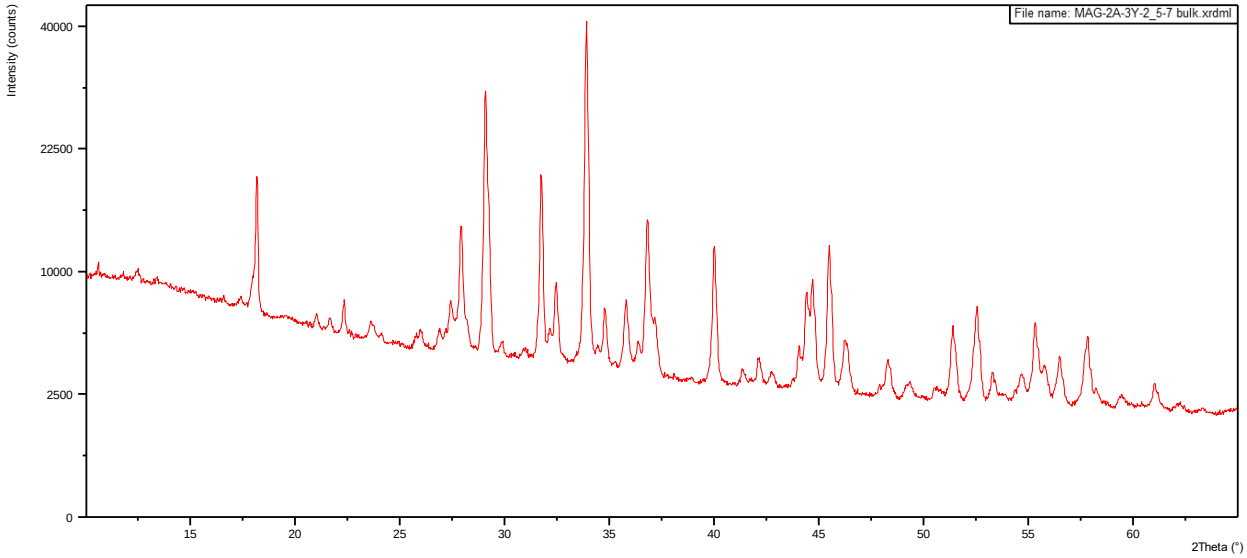
File name: MAG-2A-3Y-2_5-7 bulk.xrdml
Intensity (counts)
40000
22500
10000
2500
0
15
20
25
30
35
40
45
50
55
60
2Theta (°)

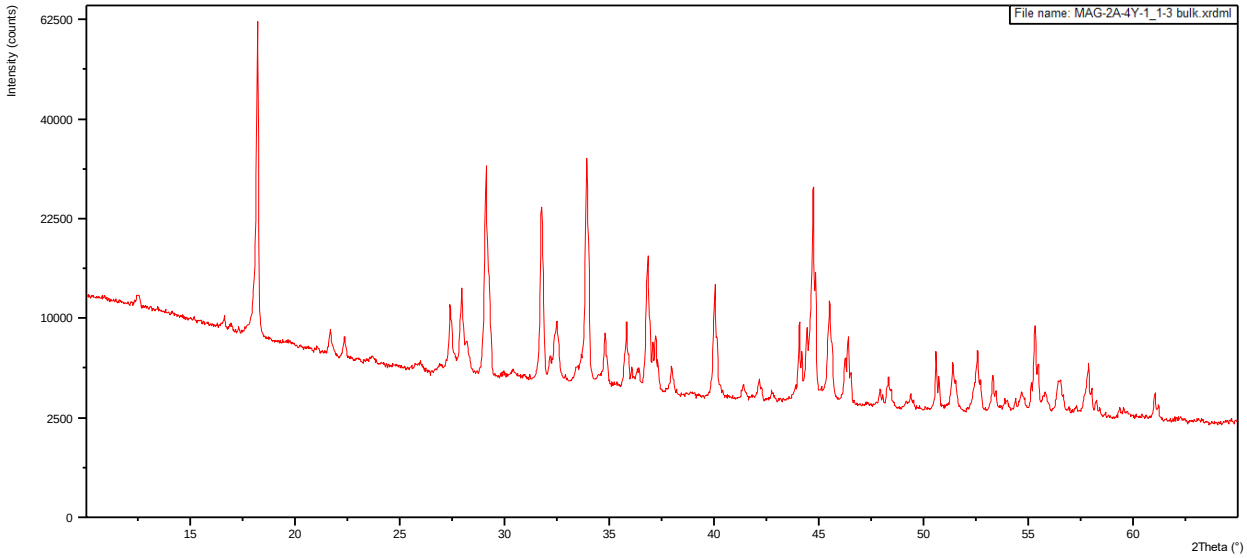
File name: MAG-2A-4Y-1_1-3 bulk.xrdml
Intensity (counts)
62500
40000
22500
10000
2500
0
15
20
25
30
35
40
45
50
55
60
2Theta (°)

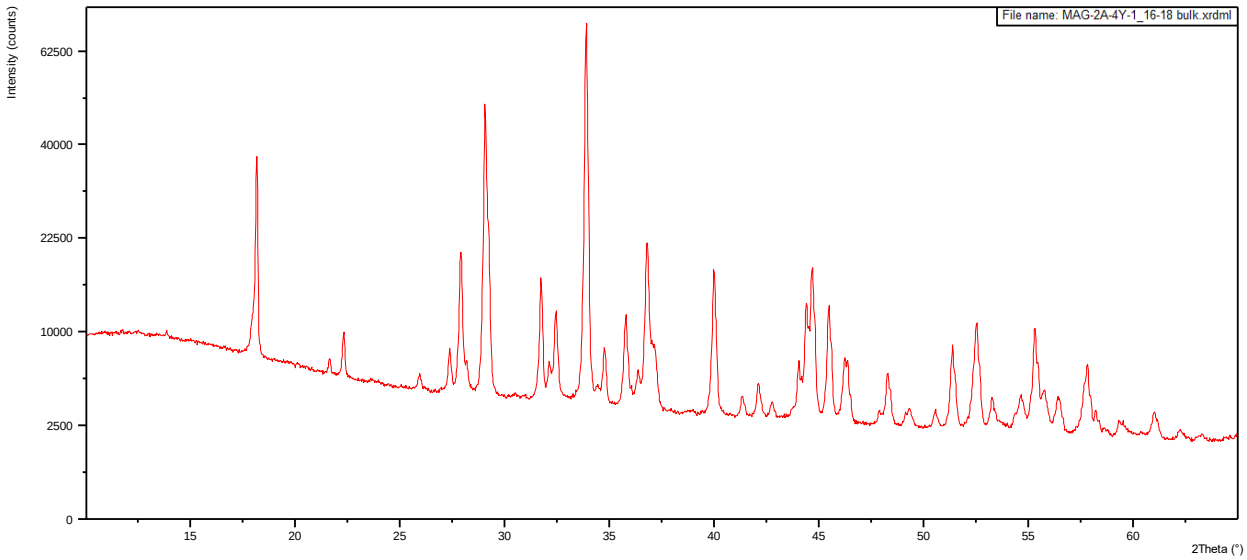
File name: MAG-2A-4Y-1_16-18 bulk.xrdml
Intensity (counts)
62500
40000
22500
10000
2500
0
15
20
25
30
35
40
45
50
55
60
2Theta (°)

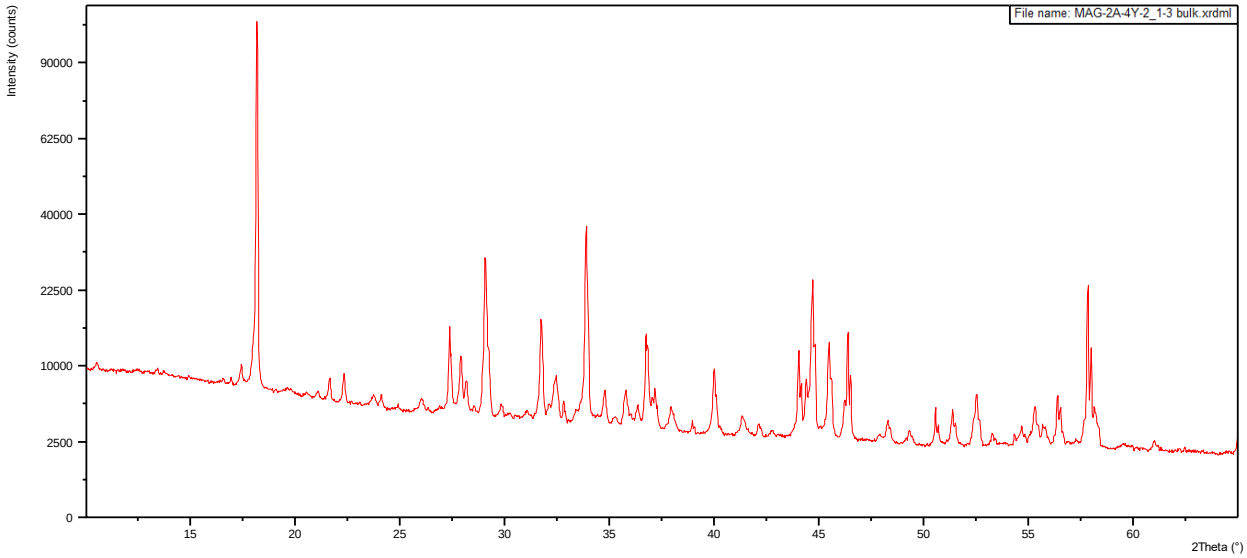
File name: MAG-2A-4Y-2_1-3 bulk.xrdml
Intensity (counts)
90000
62500
40000
22500
10000
2500
0
15
20
25
30
35
40
45
50
55
60
2Theta (°)

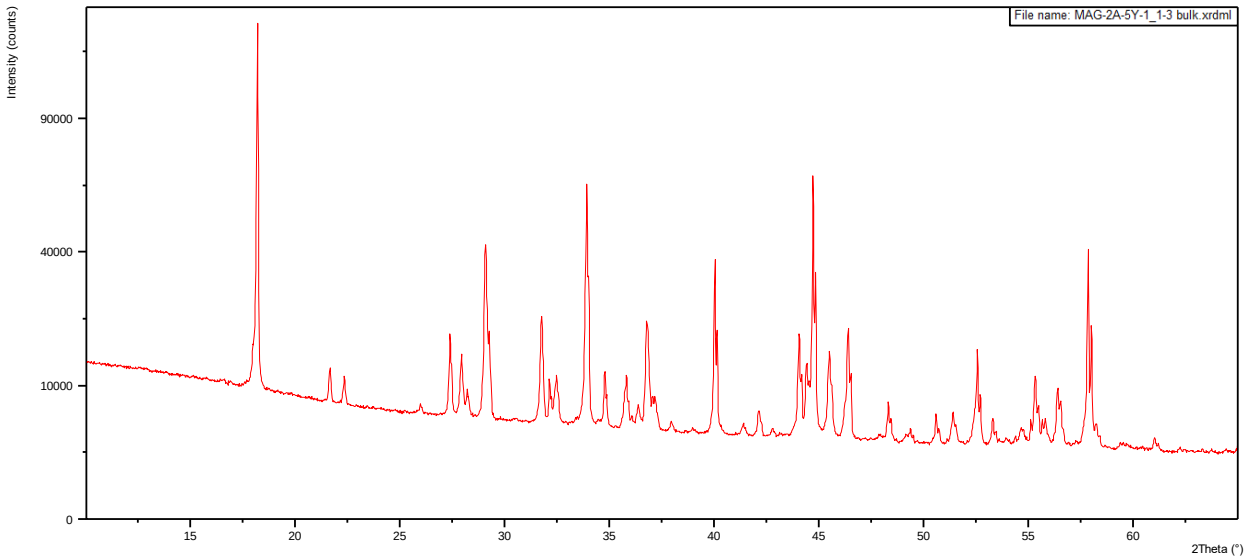
File name: MAG-2A-5Y-1_1-3 bulk.xrdml
Intensity (counts)
90000
40000
10000
0
15
20
25
30
35
40
45
50
55
60
2Theta (°)

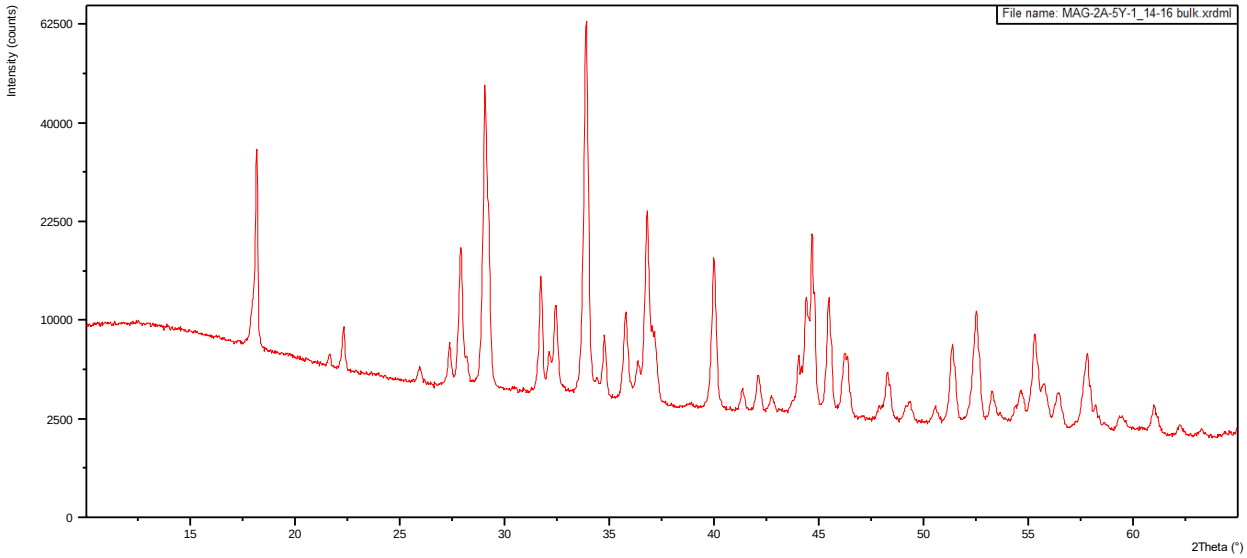
File name: MAG-2A-5Y-1_14-16 bulk.xrdml
Intensity (counts)
62500
40000
22500
10000
2500
0
15
20
25
30
35
40
45
50
55
60
2Theta (°)

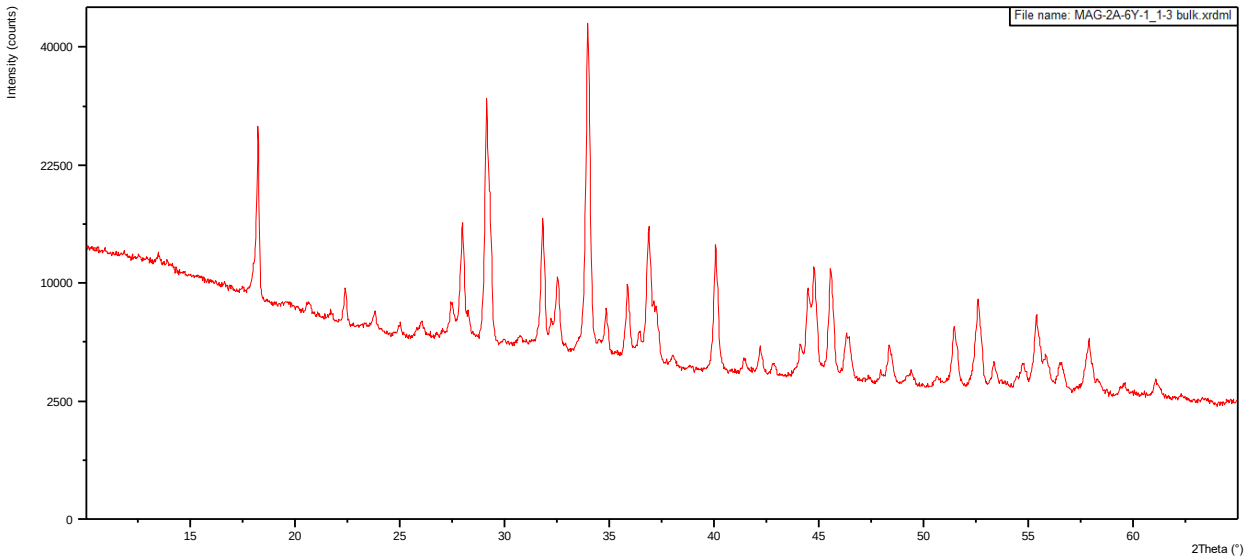
File name: MAG-2A-6Y-1_1-3 bulk.xrdml
Intensity (counts)
40000
22500
10000
2500
0
15
20
25
30
35
40
45
50
55
60
2Theta (°)

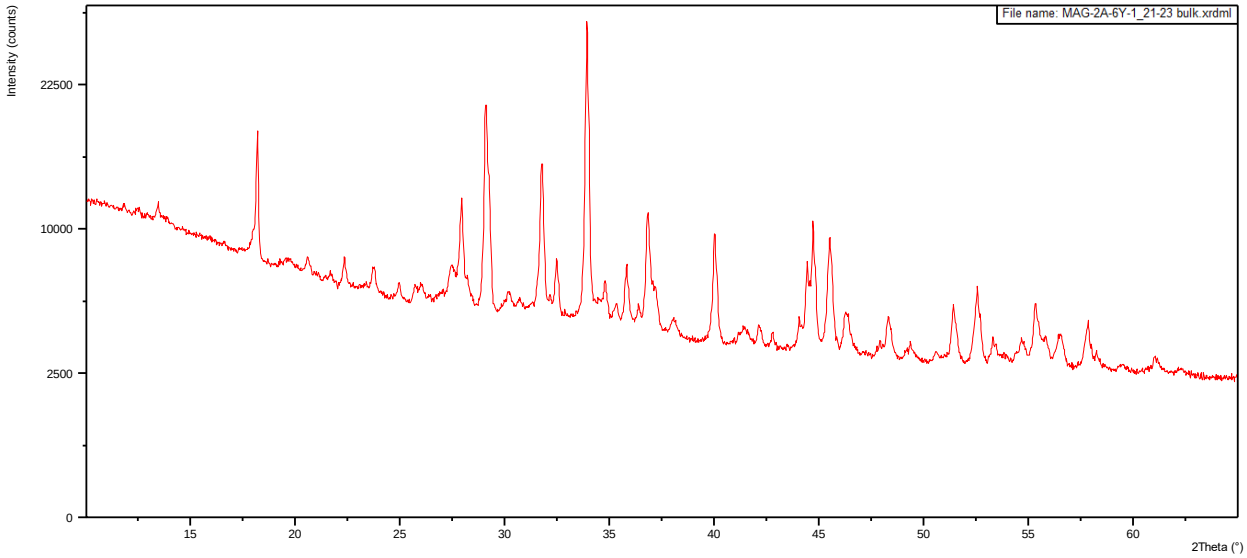
File name: MAG-2A-6Y-1_21-23 bulk.xrdml
Intensity (counts)
22500
10000
2500
0
15
20
25
30
35
40
45
50
55
60
2Theta (°)

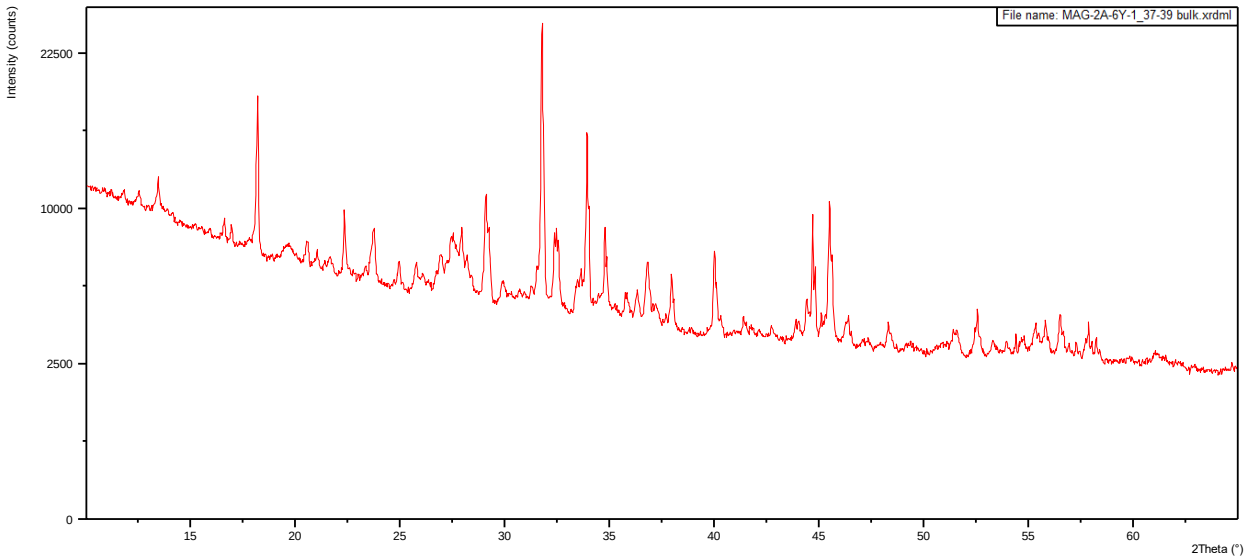
File name: MAG-2A-6Y-1_37-39 bulk.xrdml
Intensity (counts)
22500
10000
2500
0
15
20
25
30
35
40
45
50
55
60
2Theta (°)

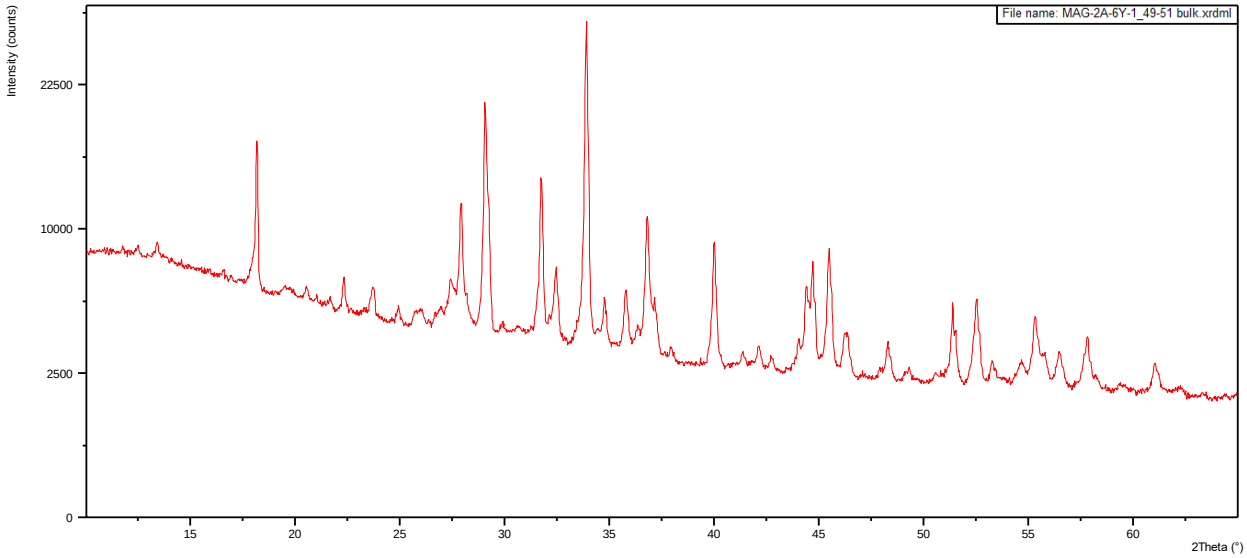
File name: MAG-2A-6Y-1_49-51 bulk.xrdml
Intensity (counts)
22500
10000
2500
0
15
20
25
30
35
40
45
50
55
60
2Theta (°)

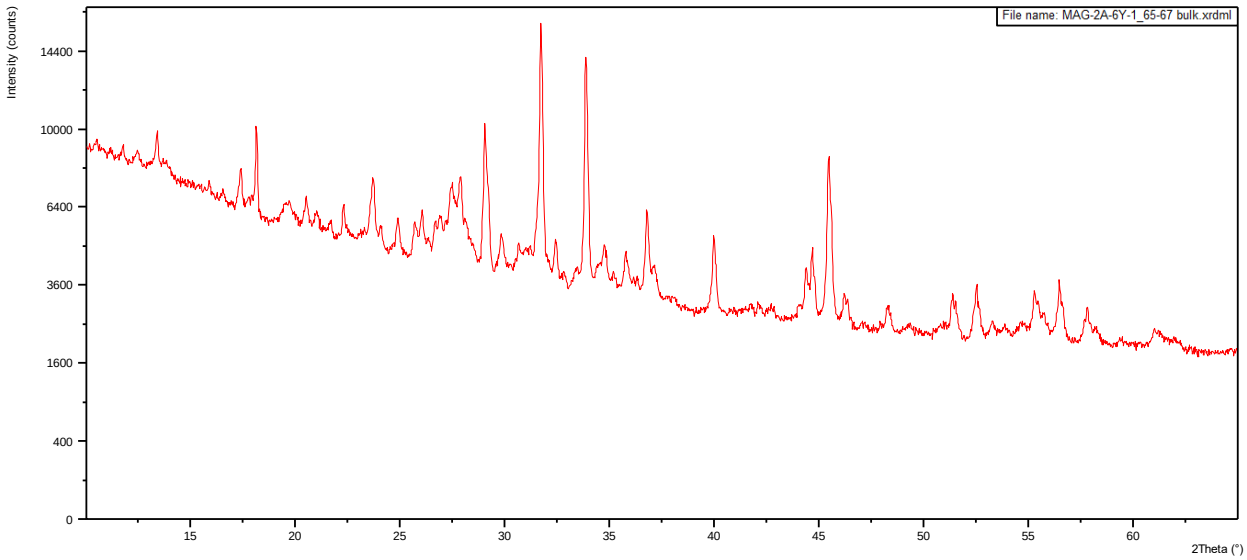
File name: MAG-2A-6Y-1_65-67 bulk.xrdml
Intensity (counts)
14400
10000
6400
3600
1600
400
0
15
20
25
30
35
40
45
50
55
60
2Theta (°)

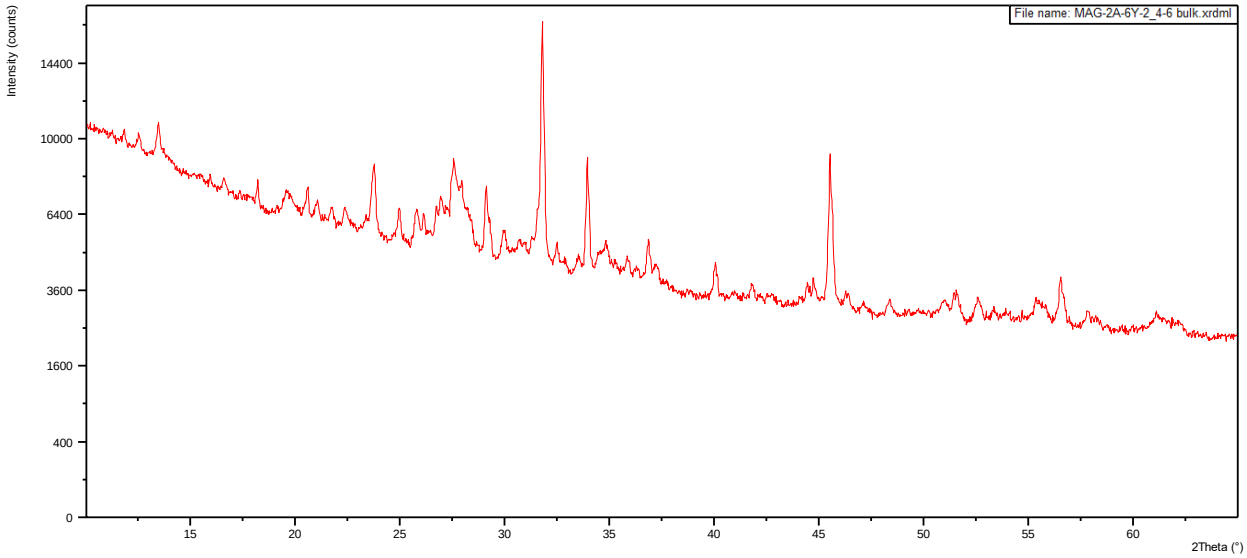
File name: MAG-2A-6Y-2_4-6 bulk.xrdml
Intensity (counts)
14400
10000
6400
3600
1600
400
0
15
20
25
30
35
40
45
50
55
60
2Theta (°)

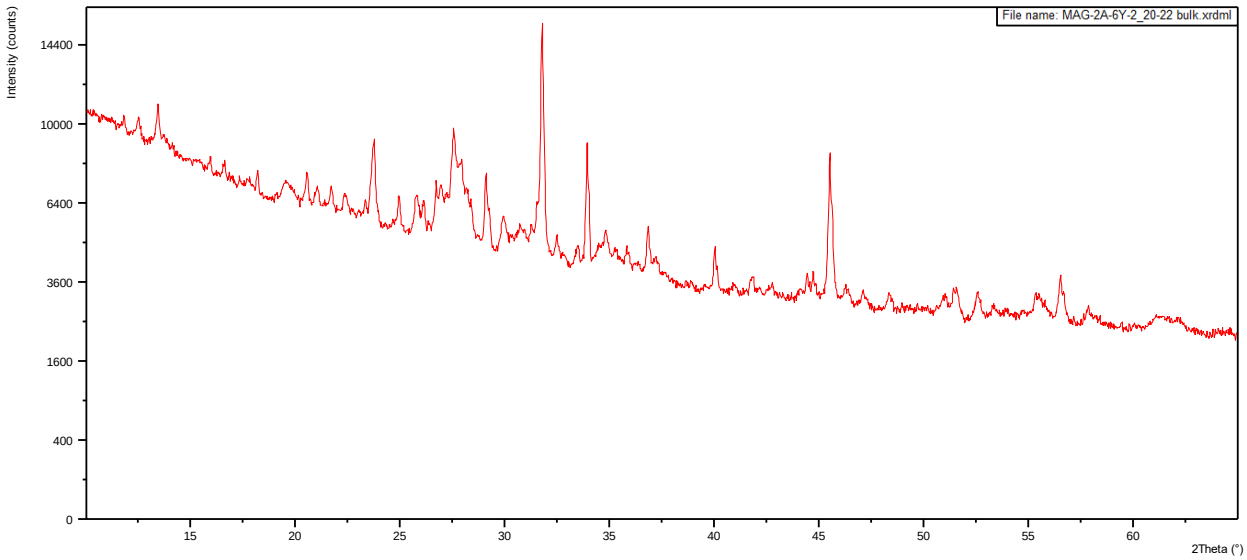
File name: MAG-2A-6Y-2_20-22 bulk.xrdml
Intensity (counts)
14400
10000
6400
3600
1600
400
0
15
20
25
30
35
40
45
50
55
60
2Theta (°)

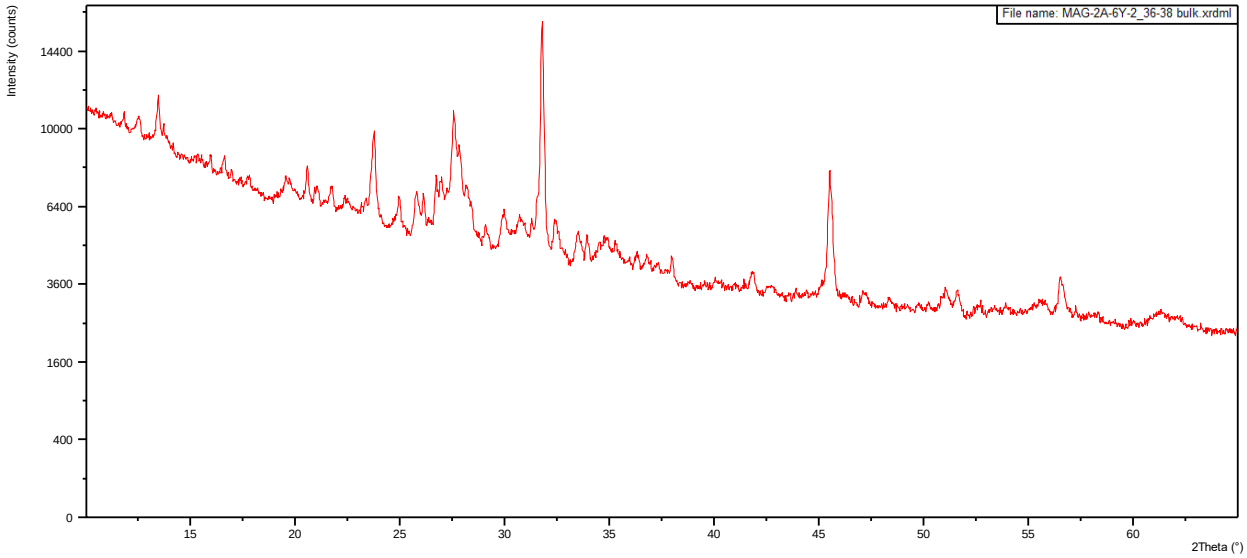
File name: MAG-2A-6Y-2_36-38 bulk.xrdml
Intensity (counts)
14400
10000
6400
3600
1600
400
0
15
20
25
30
35
40
45
50
55
60
2Theta (°)

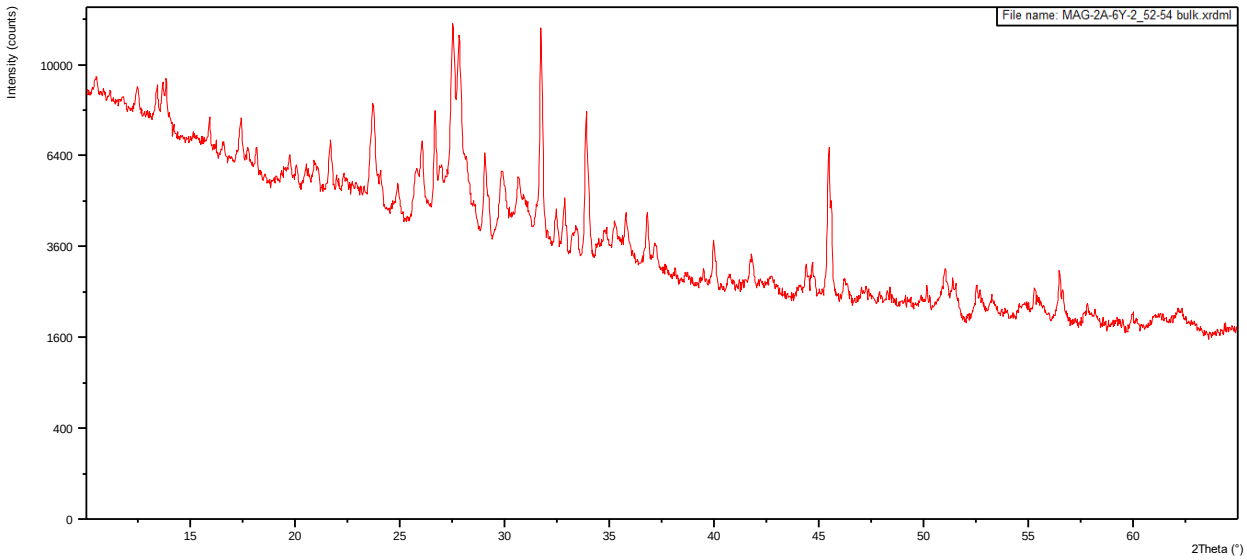
File name: MAG-2A-6Y-2_52-54 bulk.xrdml
Intensity (counts)
10000
6400
3600
1600
400
0
15
20
25
30
35
40
45
50
55
60
2Theta (°)

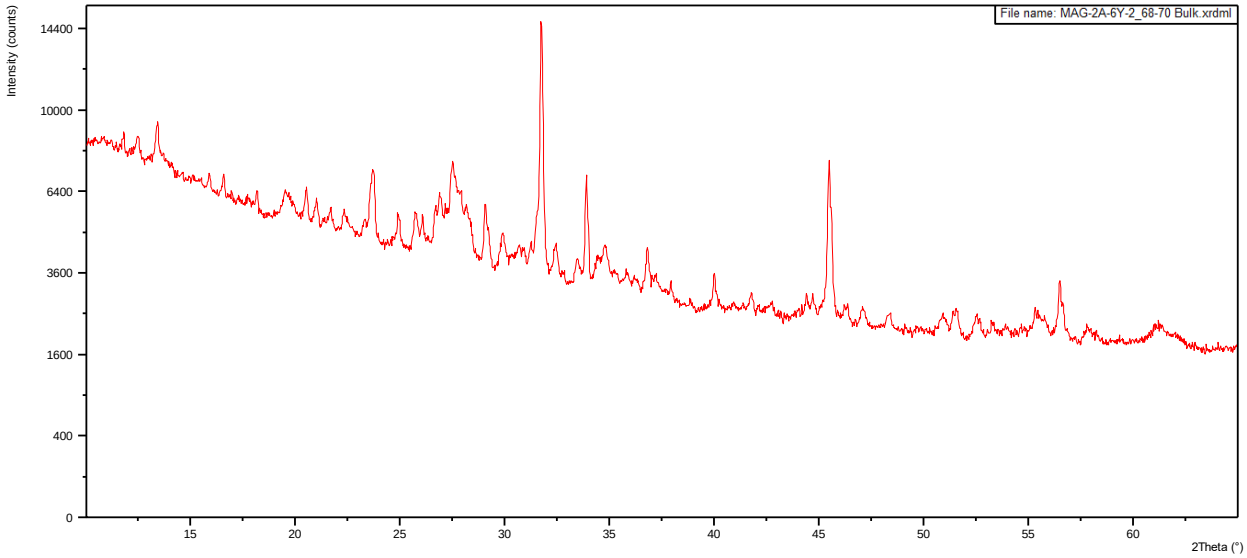
File name: MAG-2A-6Y-2_68-70 Bulk.xrdml
Intensity (counts)
14400
10000
6400
3600
1600
400
0
15
20
25
30
35
40
45
50
55
60
2Theta (°)

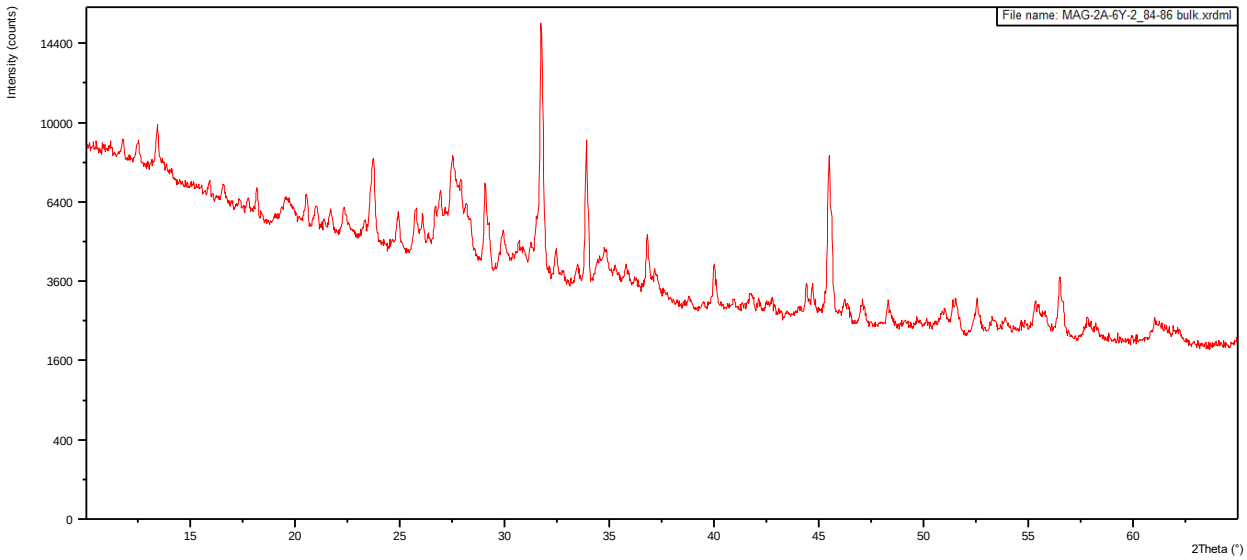
File name: MAG-2A-6Y-2_84-86 bulk.xrdml
Intensity (counts)
14400
10000
6400
3600
1600
400
0
15
20
25
30
35
40
45
50
55
60
2Theta (°)

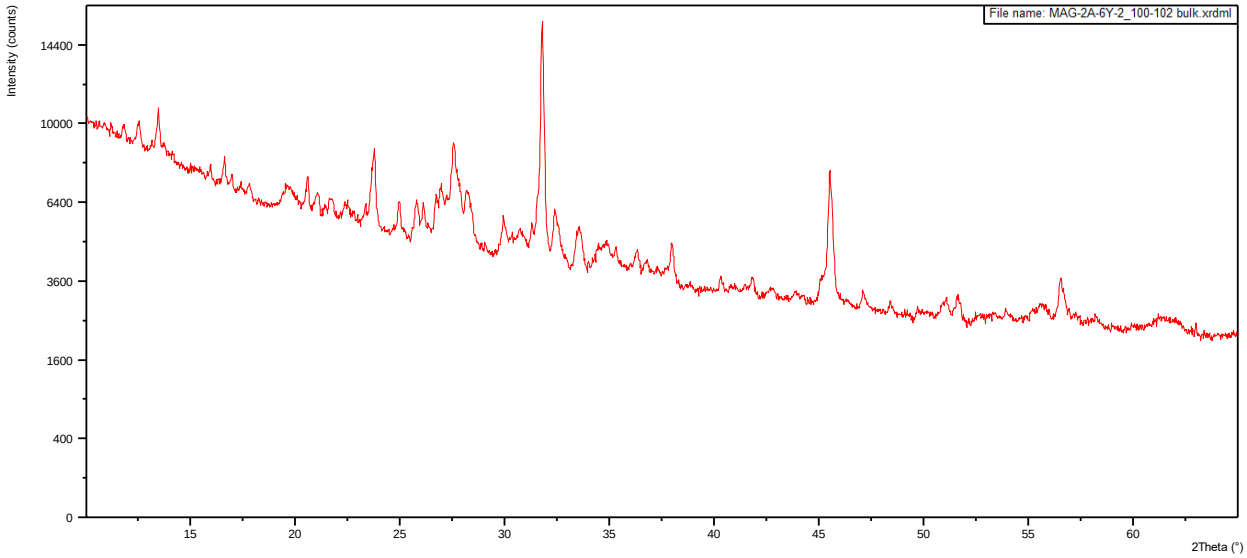
File name: MAG-2A-6Y-2_100-102 bulk.xrdml
Intensity (counts)
14400
10000
6400
3600
1600
400
0
15
20
25
30
35
40
45
50
55
60
2Theta (°)

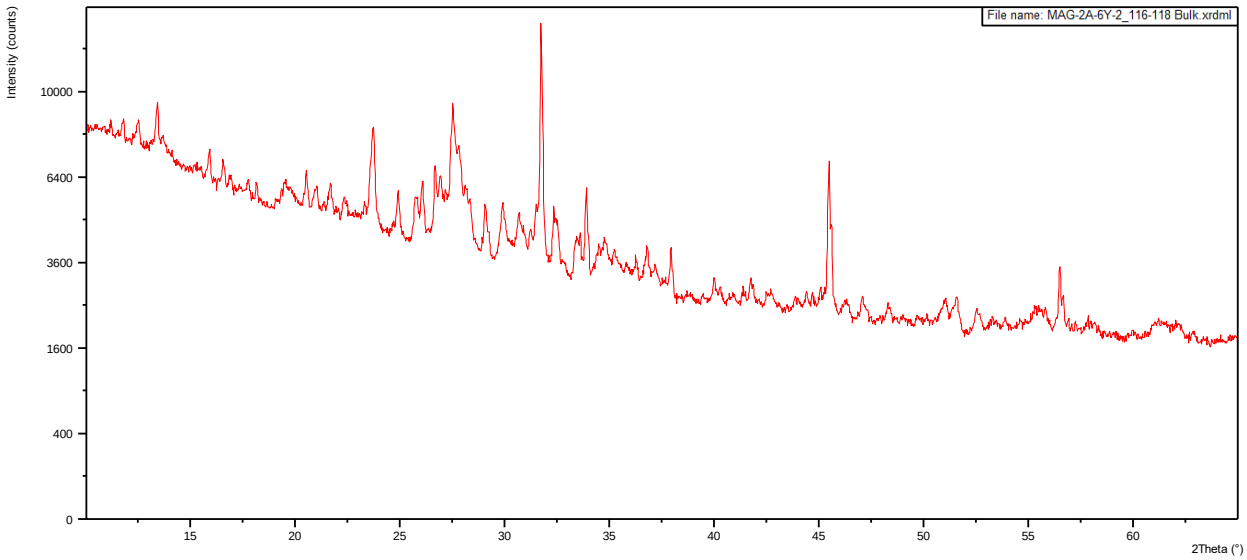
File name: MAG-2A-6Y-2_116-118 Bulk.xrdml
Intensity (counts)
10000
6400
3600
1600
400
0
15
20
25
30
35
40
45
50
55
60
2Theta (°)

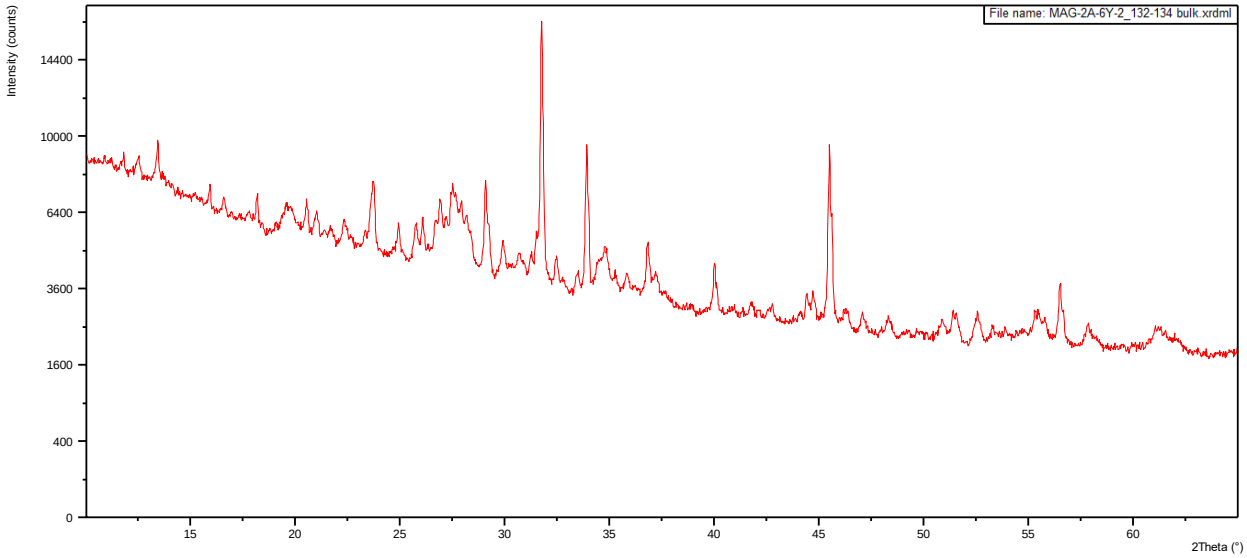
File name: MAG-2A-6Y-2_132-134 bulk.xrdml
Intensity (counts)
14400
10000
6400
3600
1600
400
0
15
20
25
30
35
40
45
50
55
60
2Theta (°)

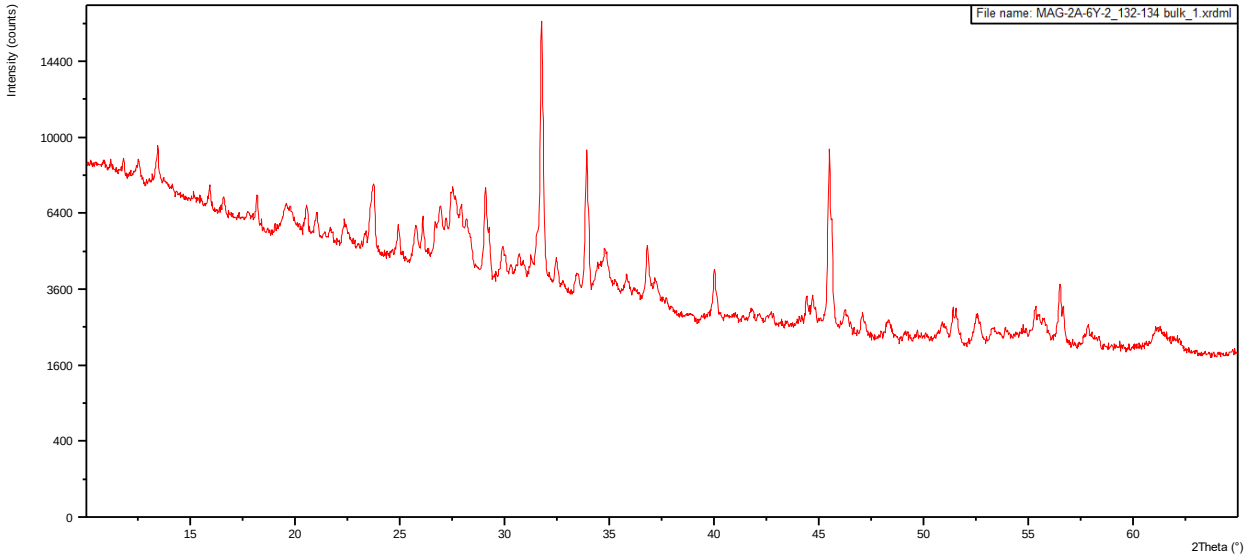
File name: MAG-2A-6Y-2_132-134 bulk_1.xrdml
Intensity (counts)
14400
10000
6400
3600
1600
400
0
15
20
25
30
35
40
45
50
55
60
2Theta (°)

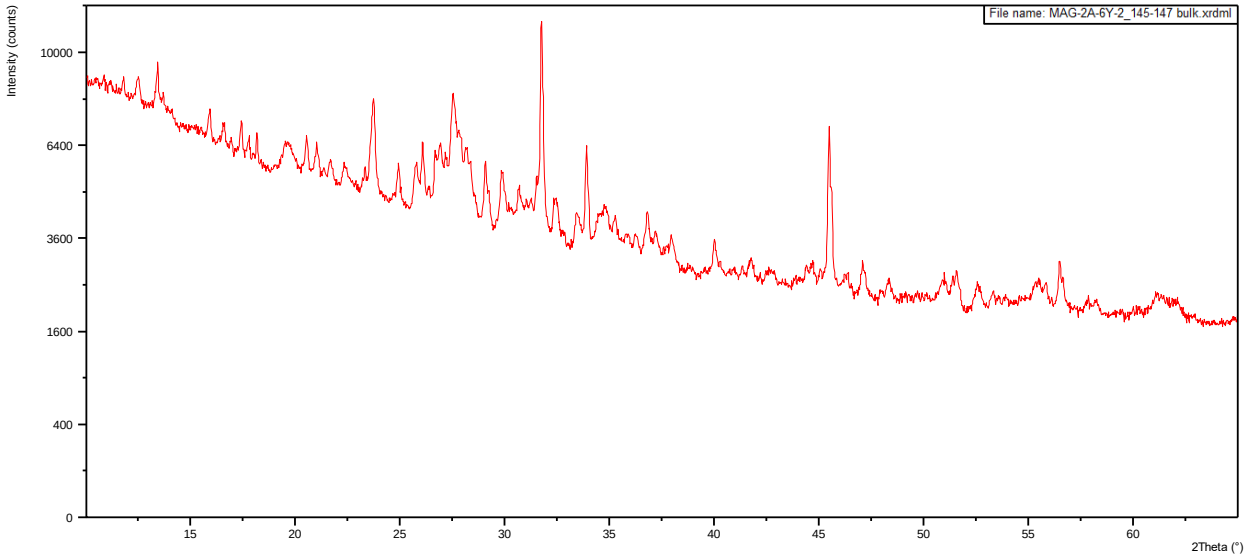
File name: MAG-2A-6Y-2_145-147 bulk.xrdml
Intensity (counts)
10000
6400
3600
1600
400
0
15
20
25
30
35
40
45
50
55
60
2Theta (°)

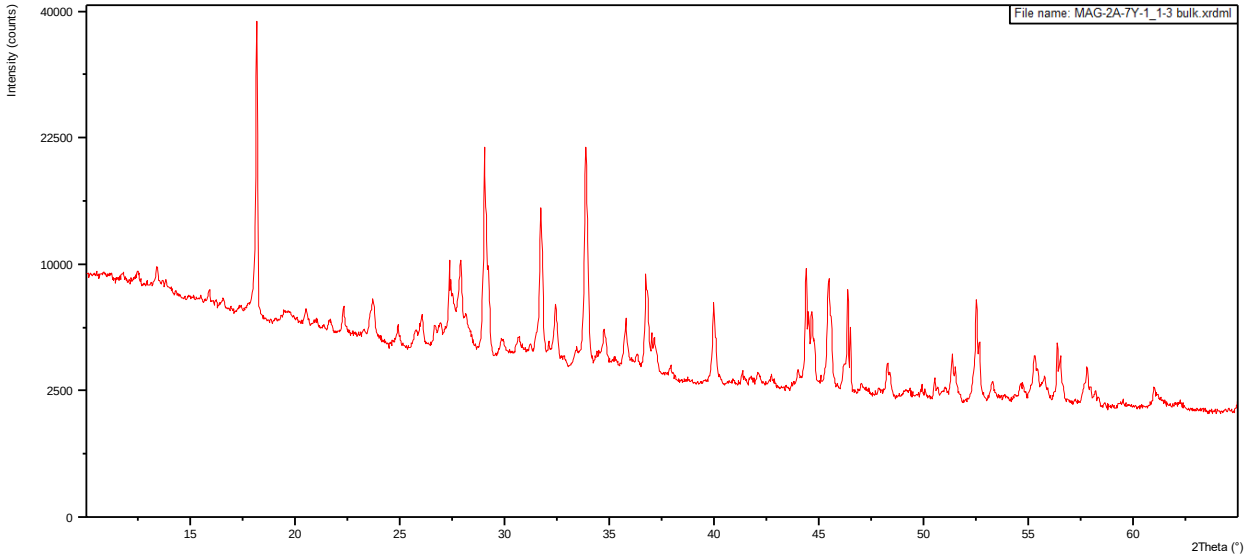
File name: MAG-2A-7Y-1_1-3 bulk.xrdml
Intensity (counts)
40000
22500
10000
2500
0
15
20
25
30
35
40
45
50
55
60
2Theta (°)

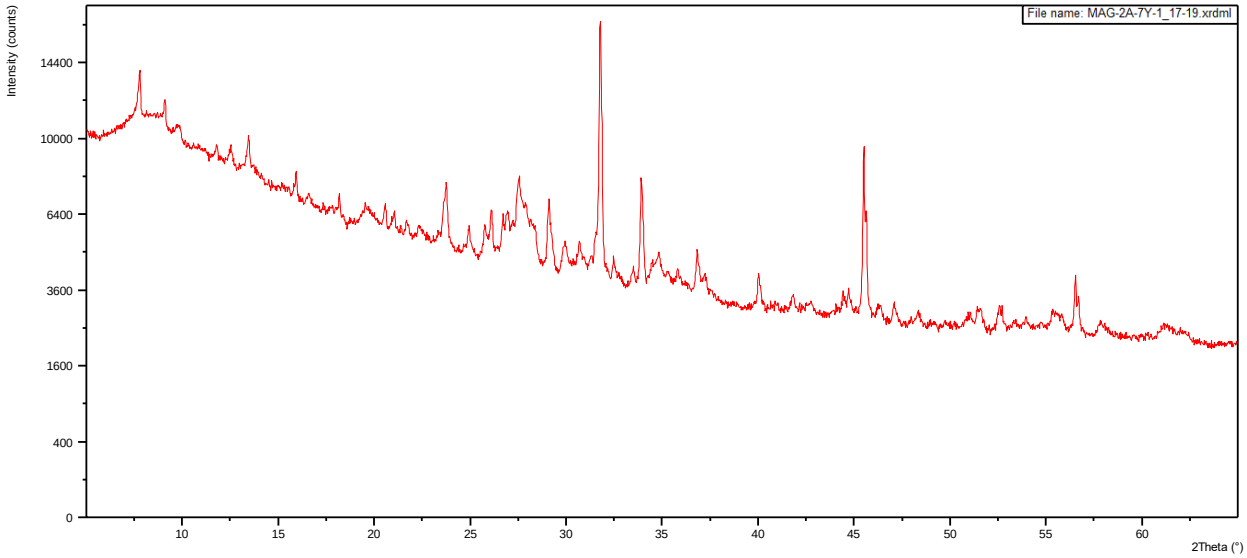
File name: MAG-2A-7Y-1_17-19.xrdml
Intensity (counts)
14400
10000
6400
3600
1600
400
0
10
15
20
25
30
35
40
45
50
55
60
2Theta (°)

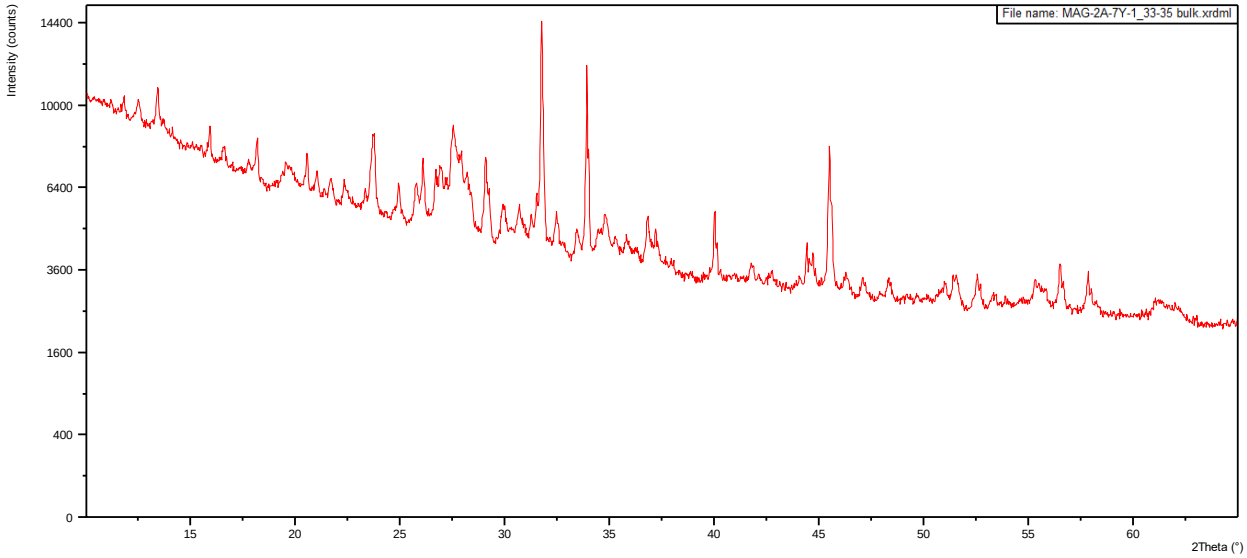
File name: MAG-2A-7Y-1_33-35 bulk.xrdml
Intensity (counts)
14400
10000
6400
3600
1600
400
0
15
20
25
30
35
40
45
50
55
60
2Theta (°)

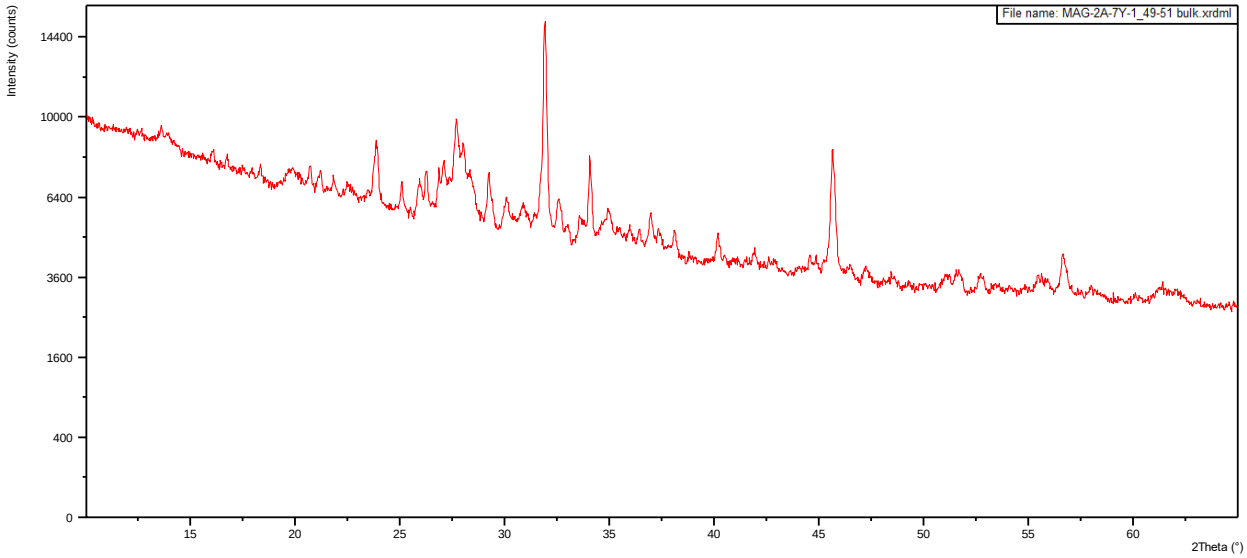
File name: MAG-2A-7Y-1_49-51 bulk.xrdml
Intensity (counts)
14400
10000
6400
3600
1600
400
0
15
20
25
30
35
40
45
50
55
60
2Theta (°)

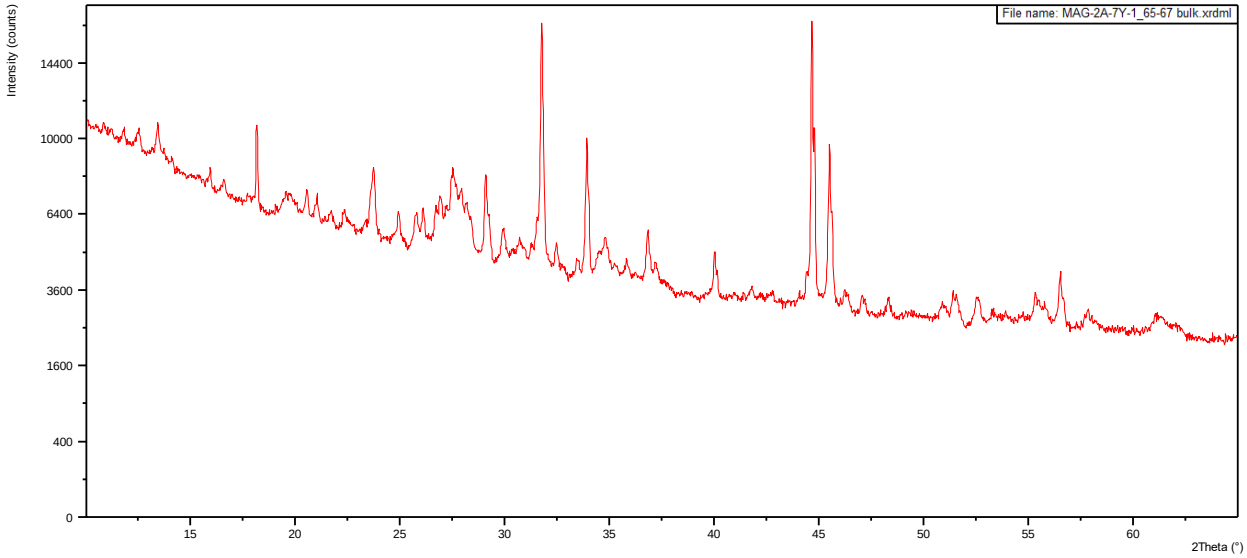
File name: MAG-2A-7Y-1_65-67 bulk.xrdml
Intensity (counts)
14400
10000
6400
3600
1600
400
0
15
20
25
30
35
40
45
50
55
60
2Theta (°)

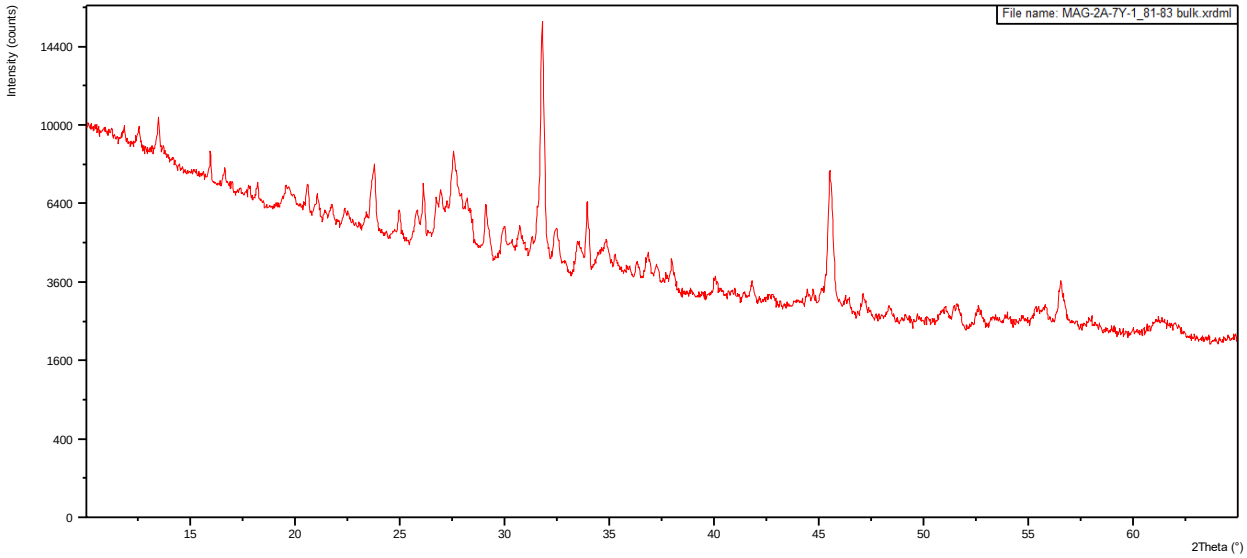
File name: MAG-2A-7Y-1_81-83 bulk.xrdml
Intensity (counts)
14400
10000
6400
3600
1600
400
0
15
20
25
30
35
40
45
50
55
60
2Theta (°)

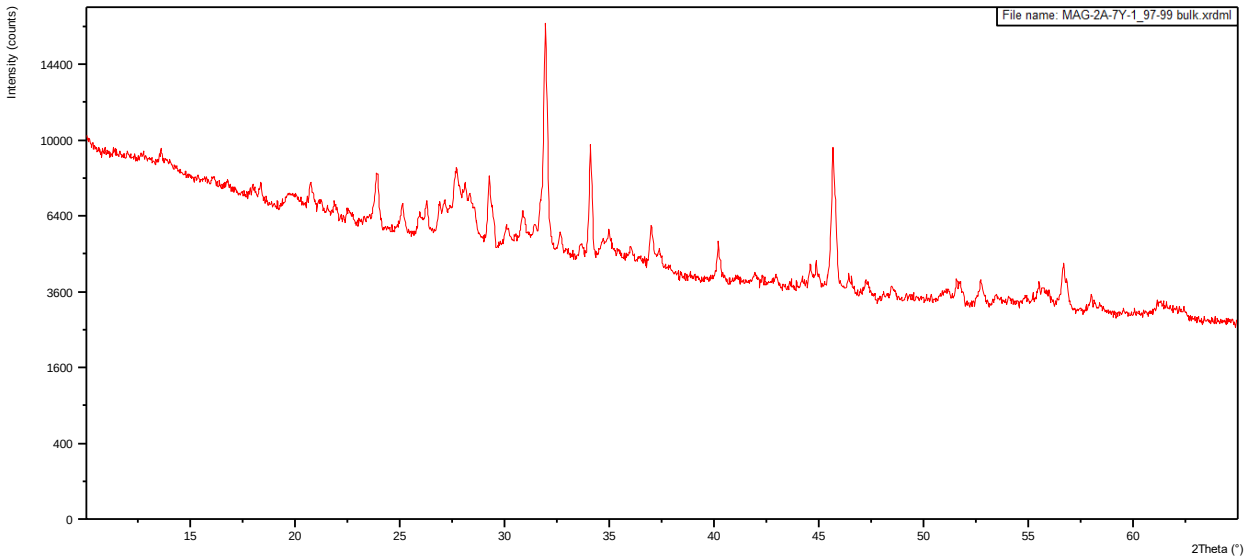
File name: MAG-2A-7Y-1_97-99 bulk.xrdml
Intensity (counts)
14400
10000
6400
3600
1600
400
0
15
20
25
30
35
40
45
50
55
60
2Theta (°)

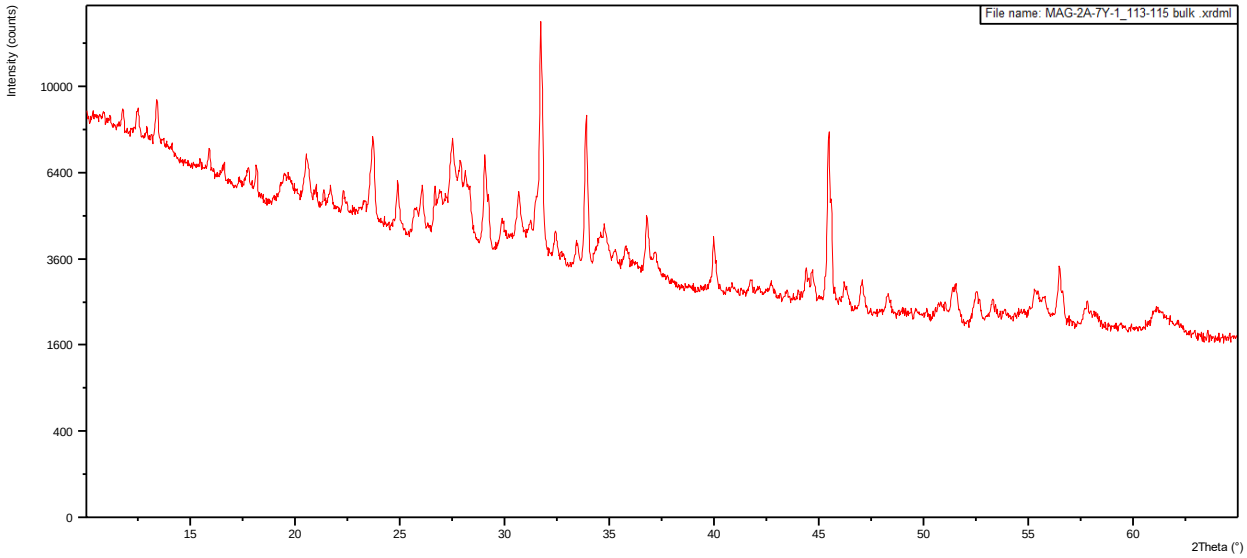
File name: MAG-2A-7Y-1_113-115 bulk .xrdml
Intensity (counts)
10000
6400
3600
1600
400
0
15
20
25
30
35
40
45
50
55
60
2Theta (°)

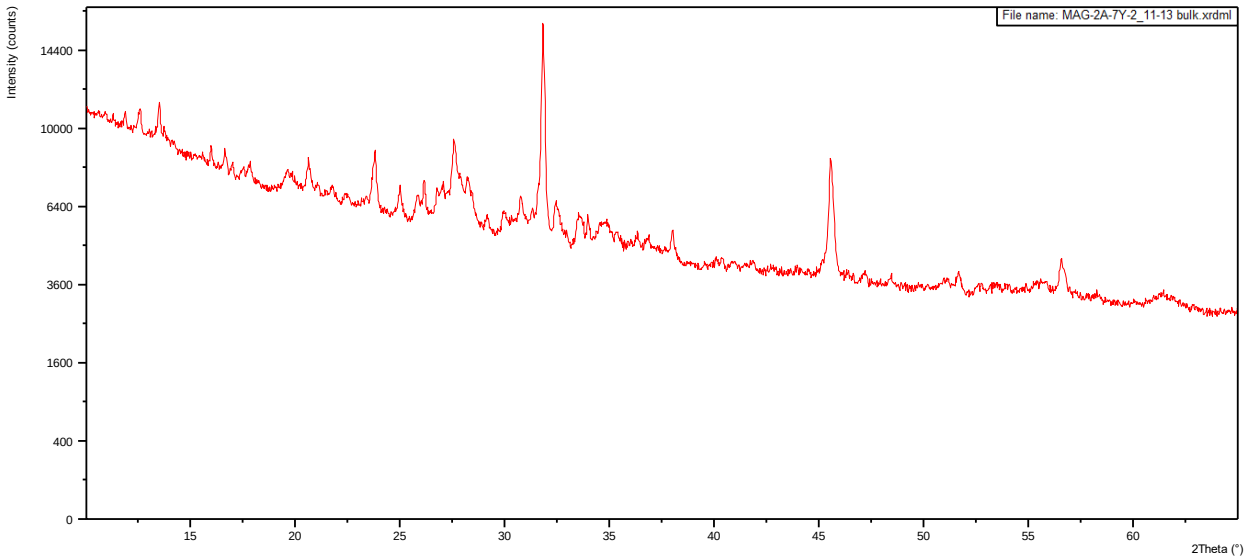
File name: MAG-2A-7Y-2_11-13 bulk.xrdml
Intensity (counts)
14400
10000
6400
3600
1600
400
0
15
20
25
30
35
40
45
50
55
60
2Theta (°)

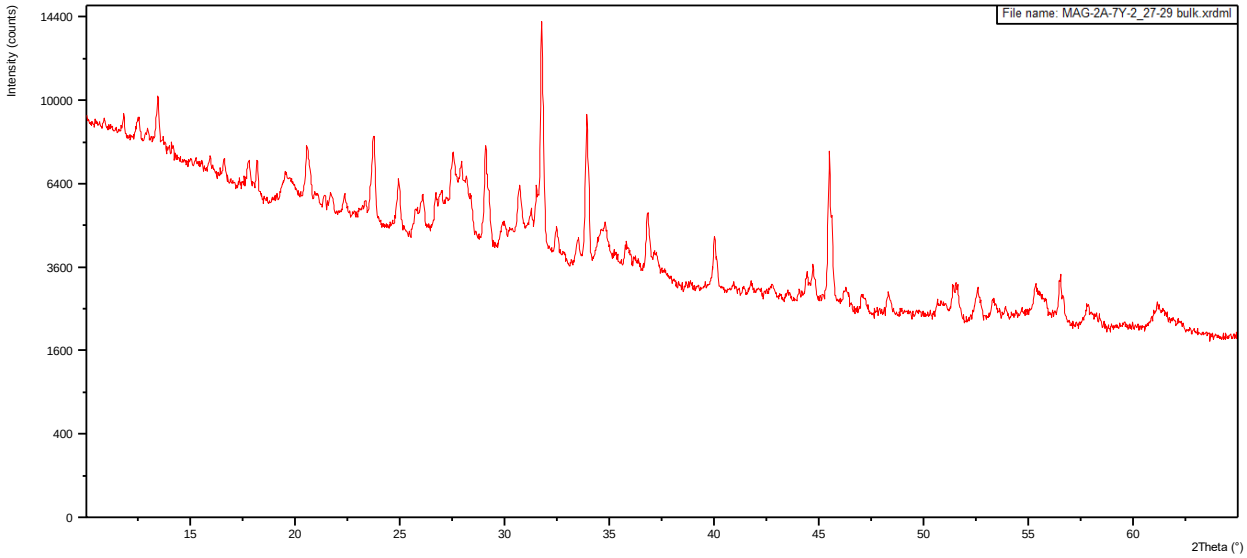
File name: MAG-2A-7Y-2_27-29 bulk.xrdml
Intensity (counts)
14400
10000
6400
3600
1600
400
0
15
20
25
30
35
40
45
50
55
60
2Theta (°)

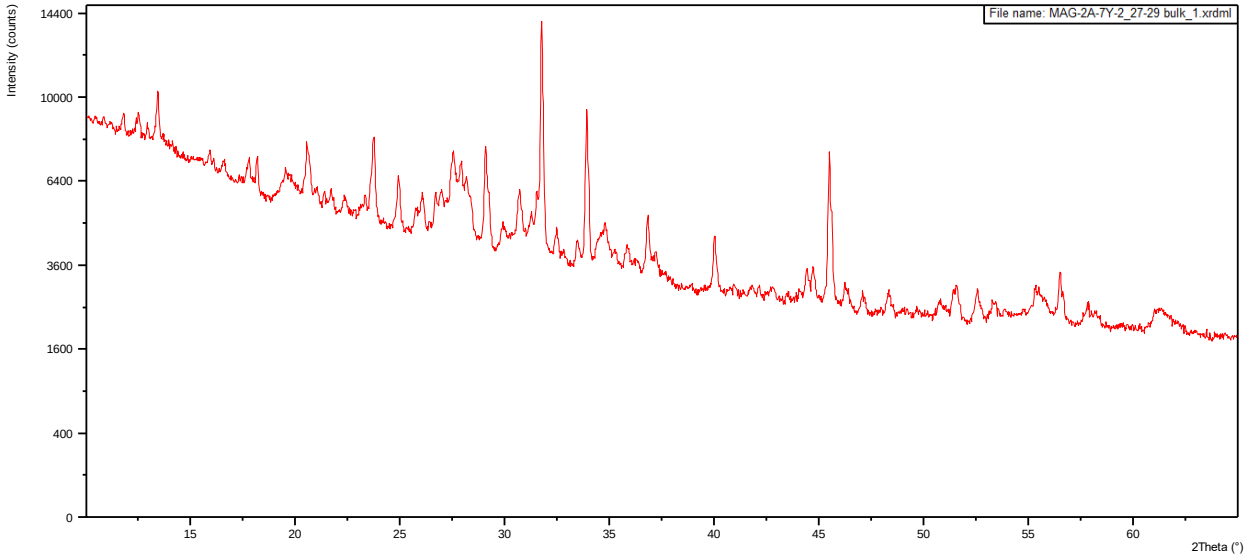
File name: MAG-2A-7Y-2_27-29 bulk_1.xrdml
Intensity (counts)
14400
10000
6400
3600
1600
400
0
15
20
25
30
35
40
45
50
55
60
2Theta (°)

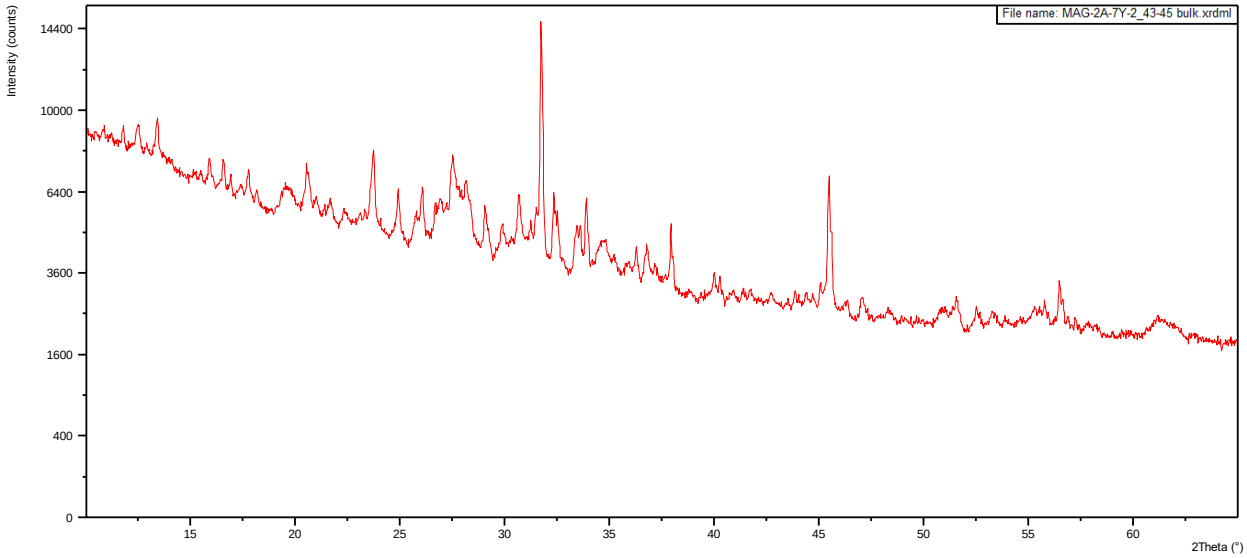
File name: MAG-2A-7Y-2_43-45 bulk.xrdml
Intensity (counts)
14400
10000
6400
3600
1600
400
0
15
20
25
30
35
40
45
50
55
60
2Theta (°)

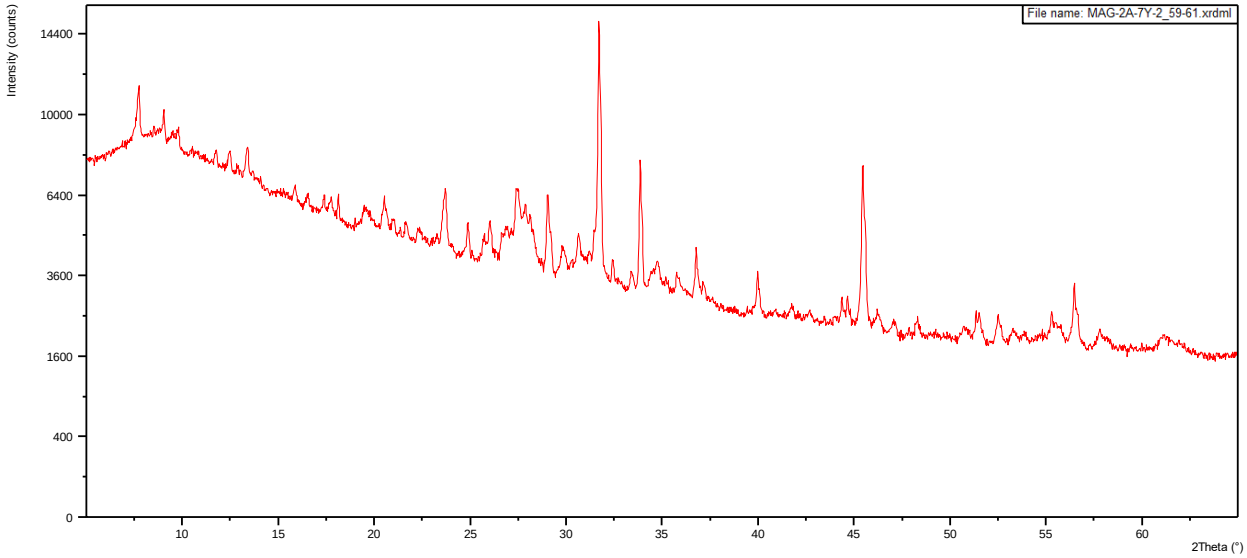
File name: MAG-2A-7Y-2_59-61.xrdml
Intensity (counts)
14400
10000
6400
3600
1600
400
0
10
15
20
25
30
35
40
45
50
55
60
2Theta (°)

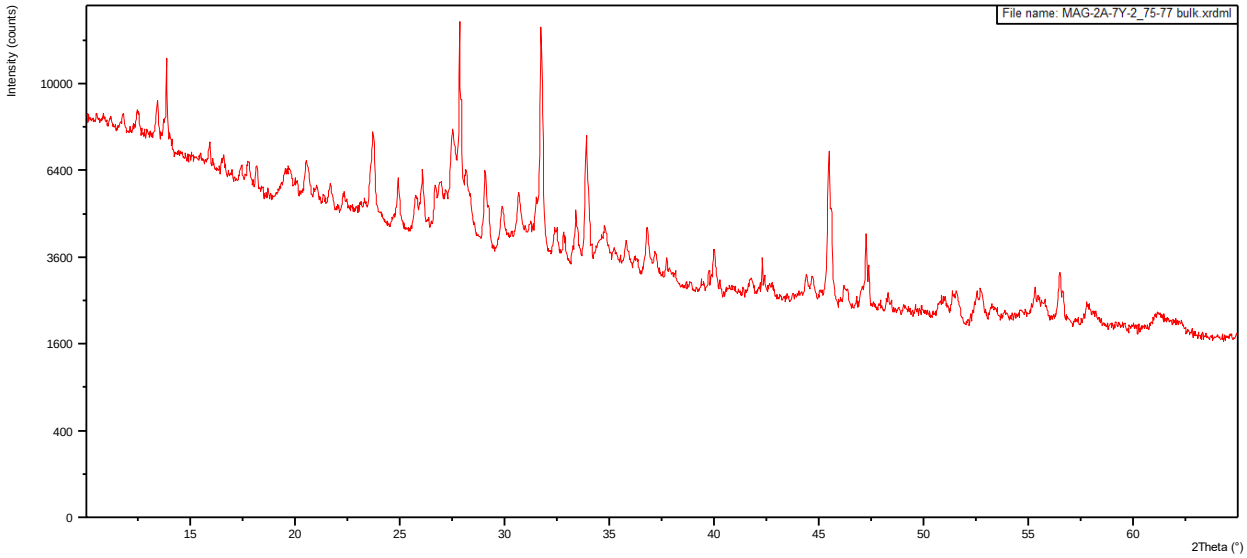
File name: MAG-2A-7Y-2_75-77 bulk.xrdml
Intensity (counts)
10000
6400
3600
1600
400
0
15
20
25
30
35
40
45
50
55
60
2Theta (°)

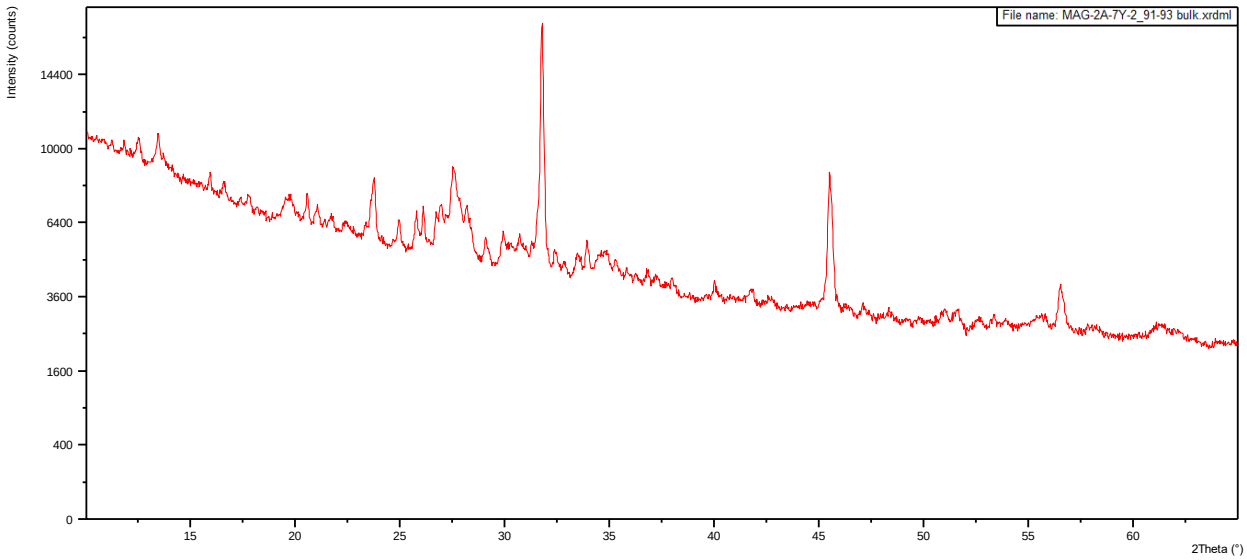
File name: MAG-2A-7Y-2_91-93 bulk.xrdml
Intensity (counts)
14400
10000
6400
3600
1600
400
0
15
20
25
30
35
40
45
50
55
60
2Theta (°)

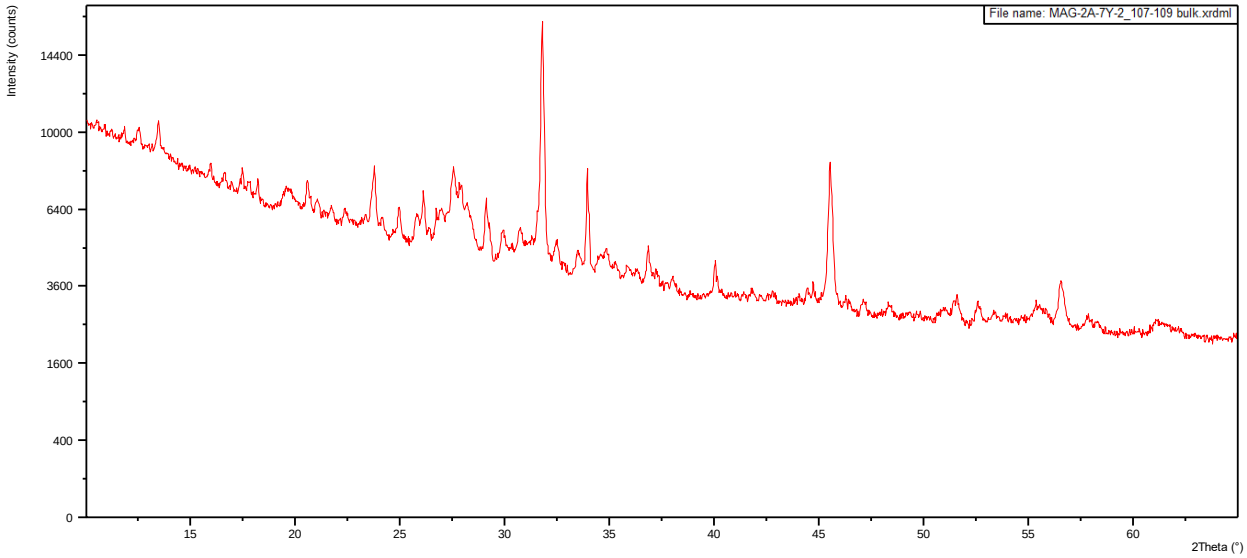
File name: MAG-2A-7Y-2_107-109 bulk.xrdml
Intensity (counts)
14400
10000
6400
3600
1600
400
0
15
20
25
30
35
40
45
50
55
60
2Theta (°)

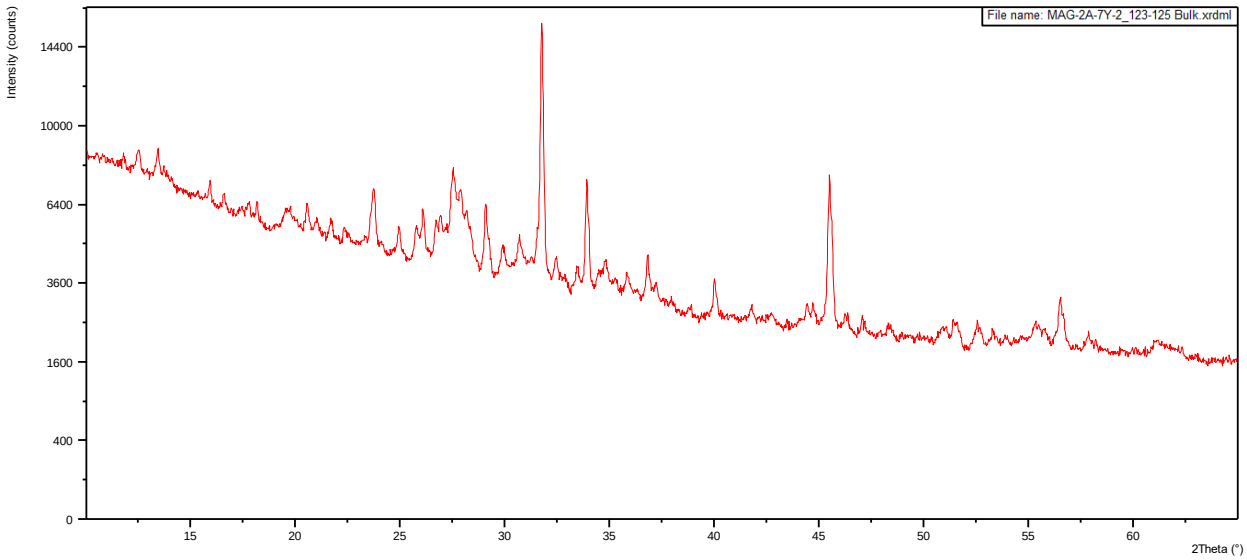
File name: MAG-2A-7Y-2_123-125 Bulk.xrdml
Intensity (counts)
14400
10000
6400
3600
1600
400
0
15
20
25
30
35
40
45
50
55
60
2Theta (°)

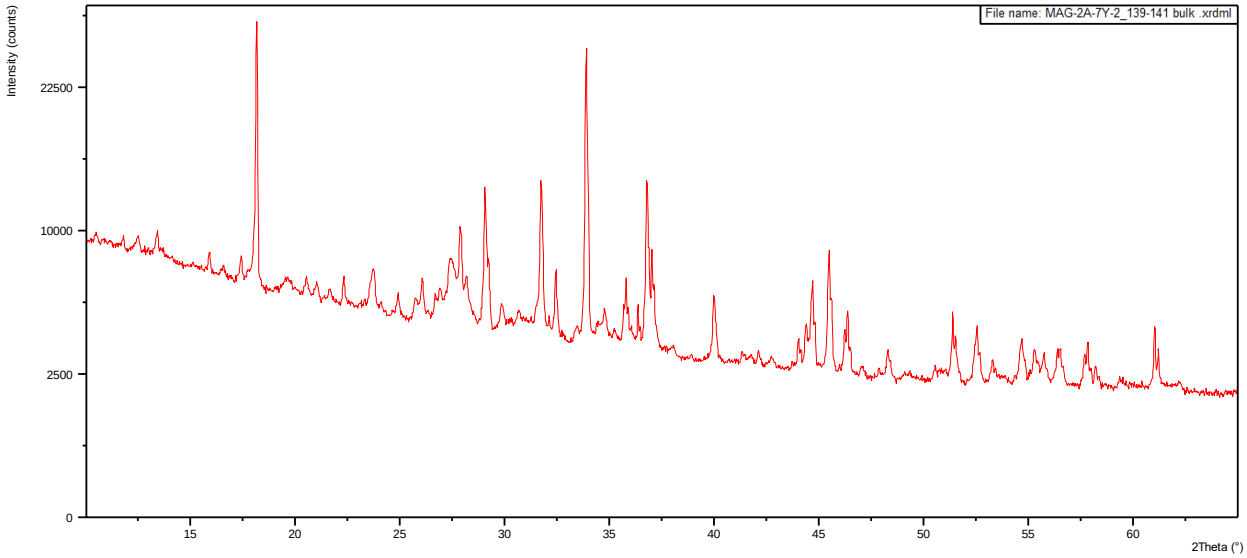
File name: MAG-2A-7Y-2_139-141 bulk .xrdml
Intensity (counts)
22500
10000
2500
0
15
20
25
30
35
40
45
50
55
60
2Theta (°)

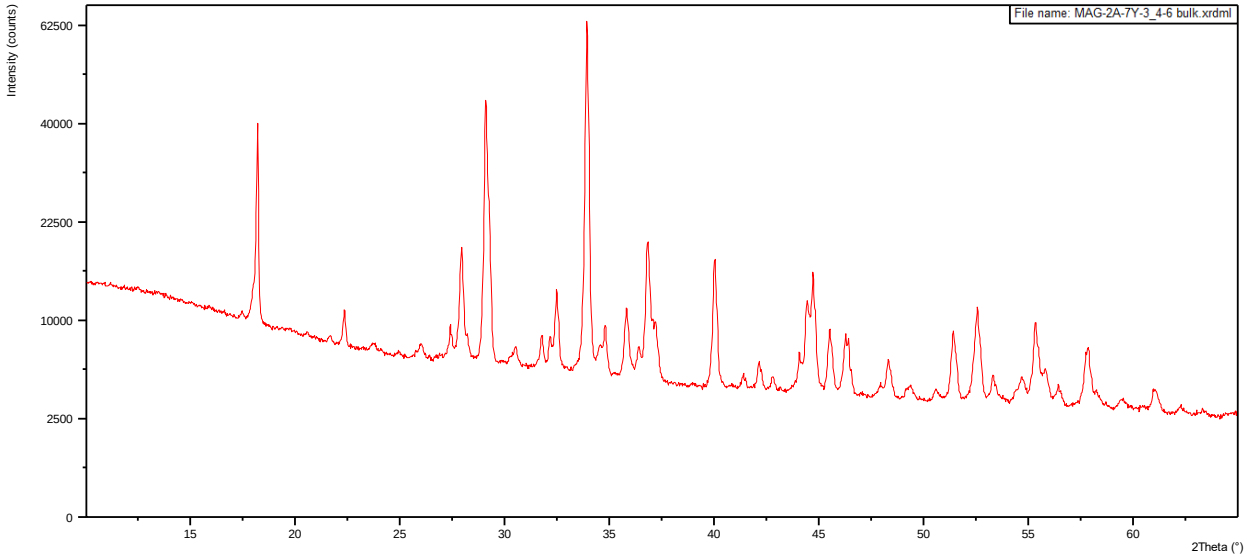
File name: MAG-2A-7Y-3_4-6 bulk.xrdml
Intensity (counts)
62500
40000
22500
10000
2500
0
15
20
25
30
35
40
45
50
55
60
2Theta (°)

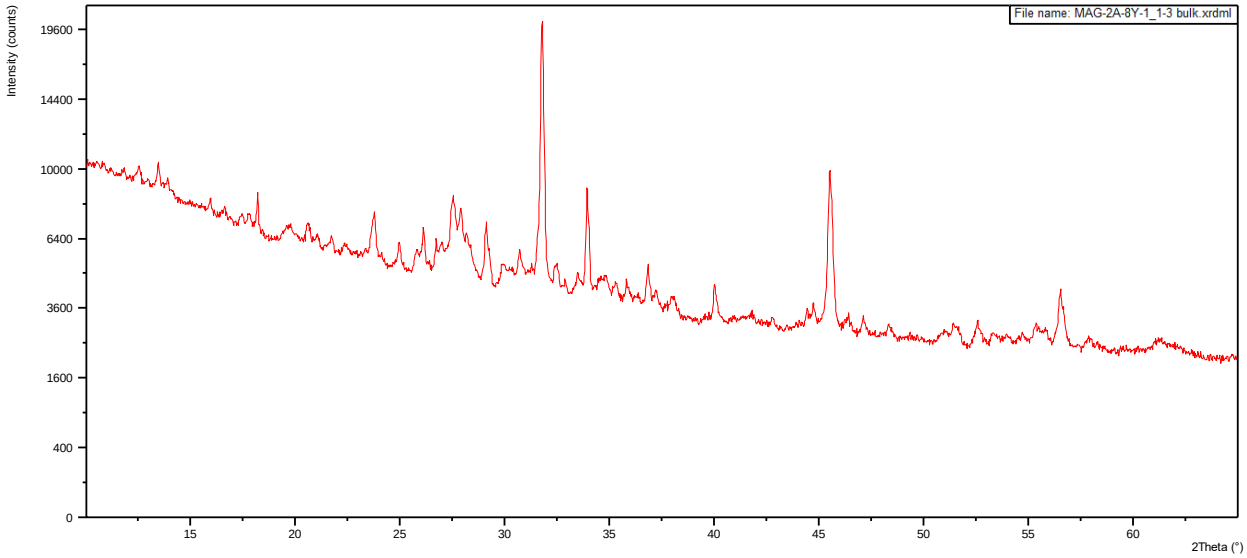
File name: MAG-2A-8Y-1_1-3 bulk.xrdml
Intensity (counts)
19600
14400
10000
6400
3600
1600
400
0
15
20
25
30
35
40
45
50
55
60
2Theta (°)

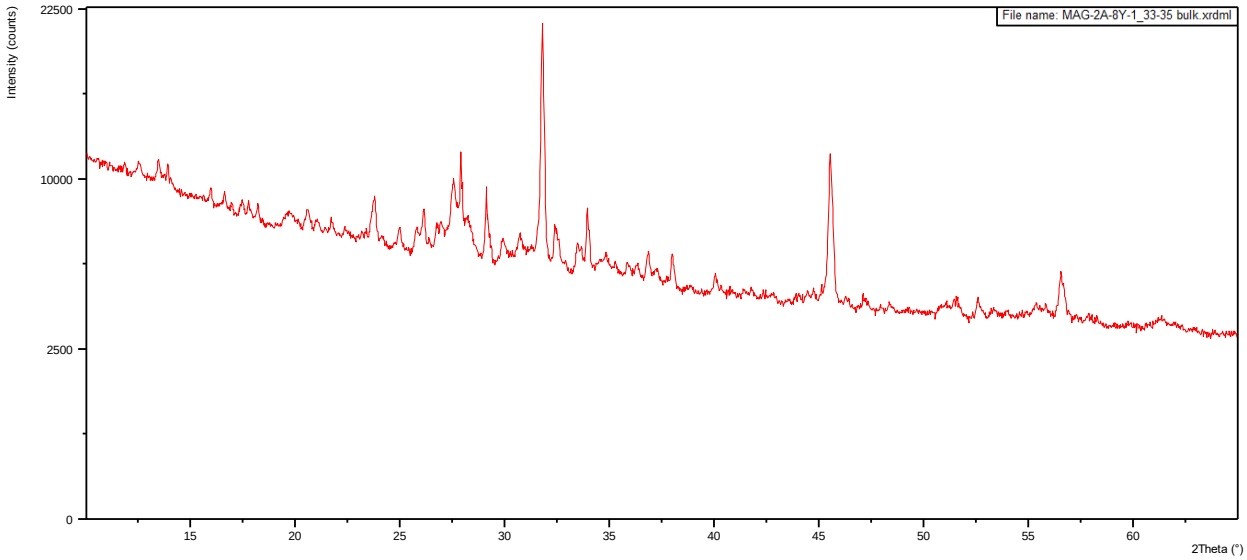
File name: MAG-2A-8Y-1_33-35 bulk.xrdml
Intensity (counts)
22500
10000
2500
0
15
20
25
30
35
40
45
50
55
60
2Theta (°)

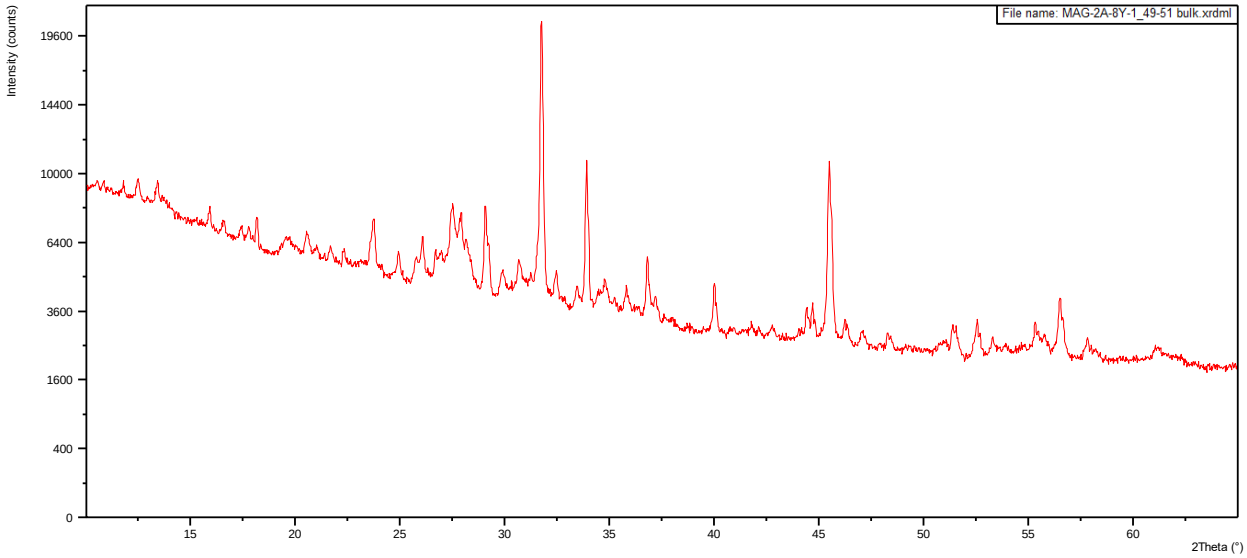
File name: MAG-2A-8Y-1_49-51 bulk.xrdml
Intensity (counts)
19600
14400
10000
6400
3600
1600
400
0
15
20
25
30
35
40
45
50
55
60
2Theta (°)

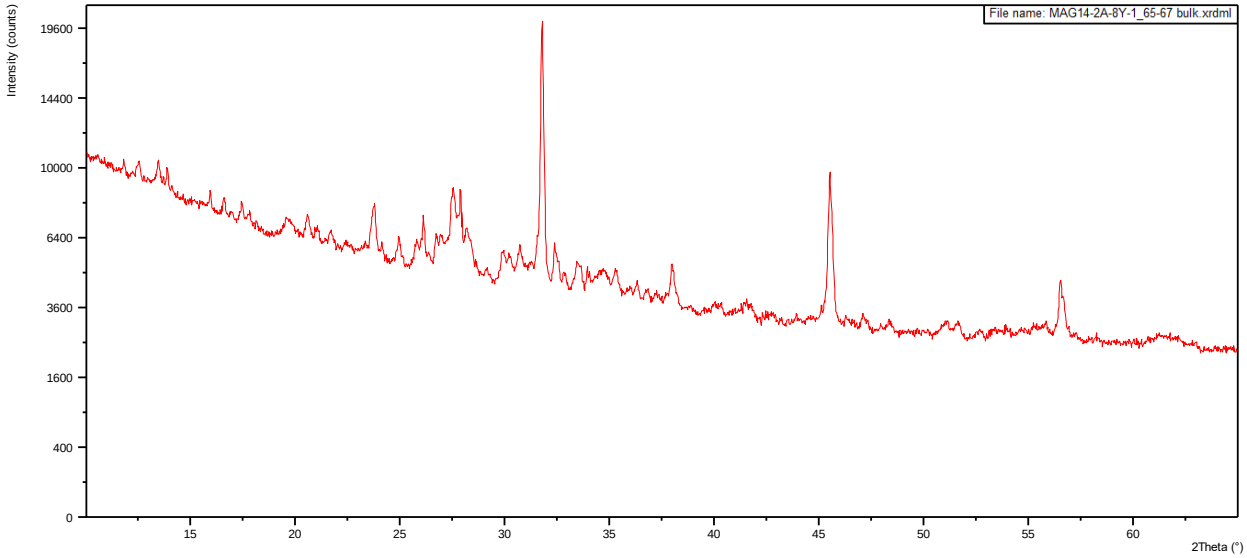
File name: MAG14-2A-8Y-1_65-67 bulk.xrdml
Intensity (counts)
19600
14400
10000
6400
3600
1600
400
0
15
20
25
30
35
40
45
50
55
60
2Theta (°)

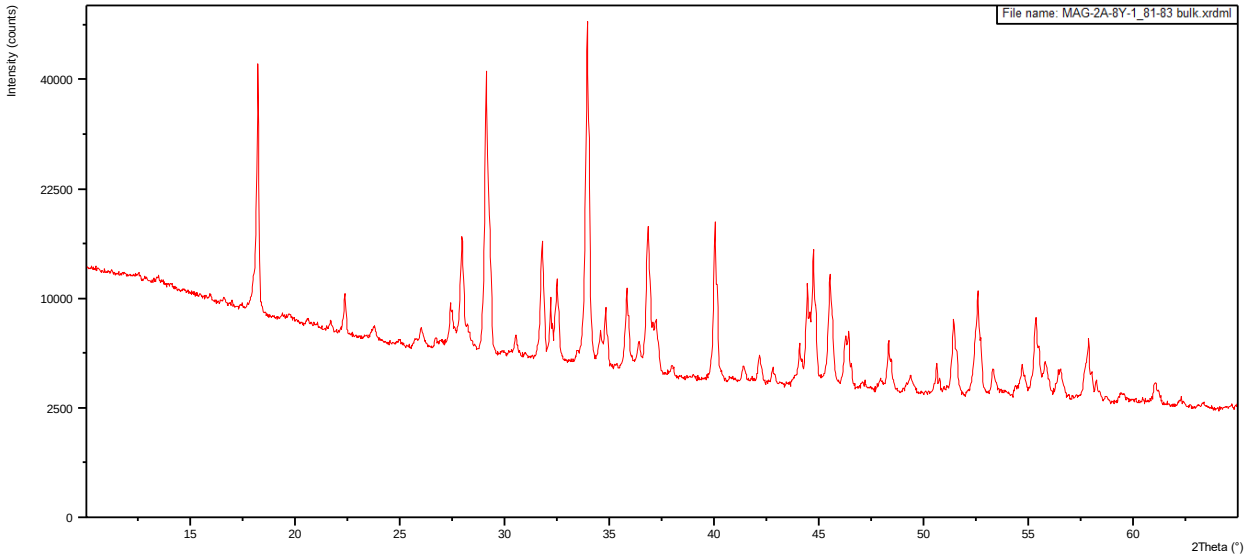
File name: MAG-2A-8Y-1_81-83 bulk.xrdml
Intensity (counts)
40000
22500
10000
2500
0
15
20
25
30
35
40
45
50
55
60
2Theta (°)

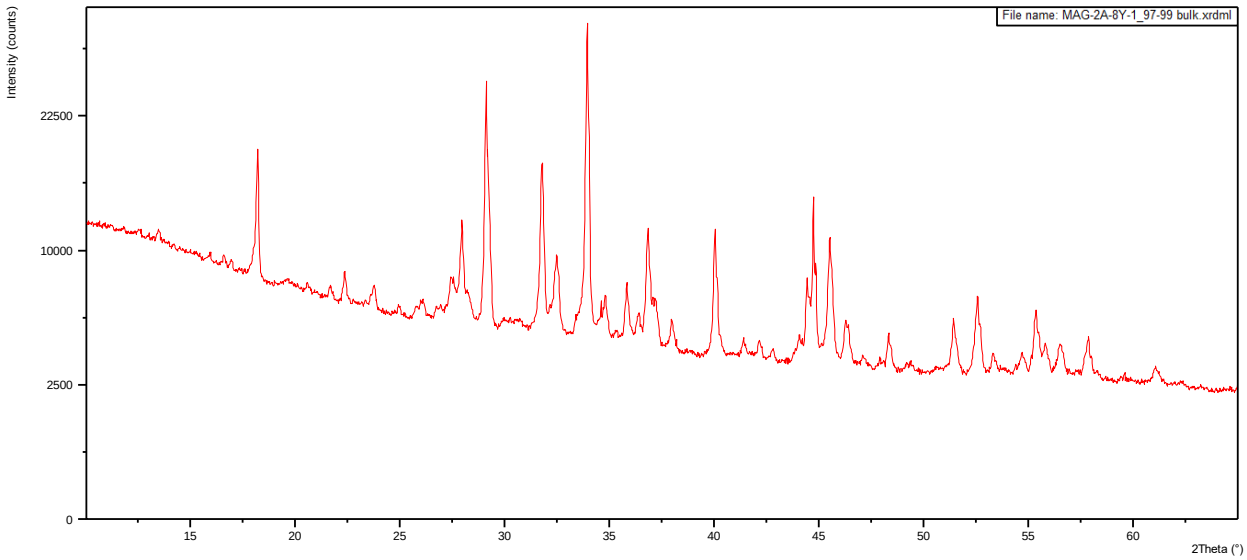
File name: MAG-2A-8Y-1_97-99 bulk.xrdml
Intensity (counts)
22500
10000
2500
0
15
20
25
30
35
40
45
50
55
60
2Theta (°)

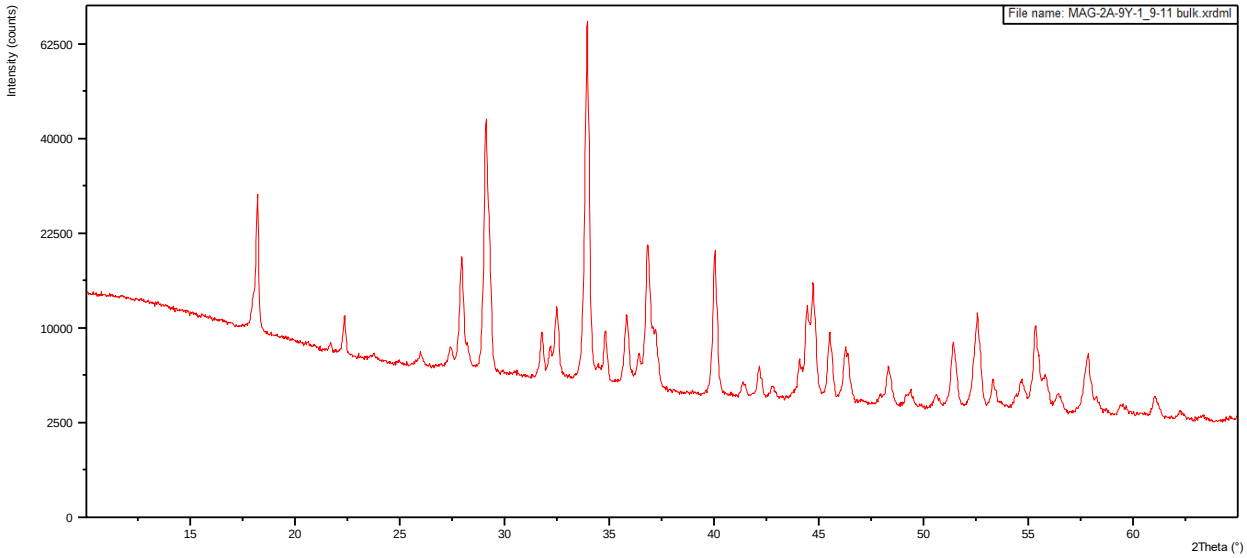
File name: MAG-2A-9Y-1_9-11 bulk.xrdml
Intensity (counts)
62500
40000
22500
10000
2500
0
15
20
25
30
35
40
45
50
55
60
2Theta (°)

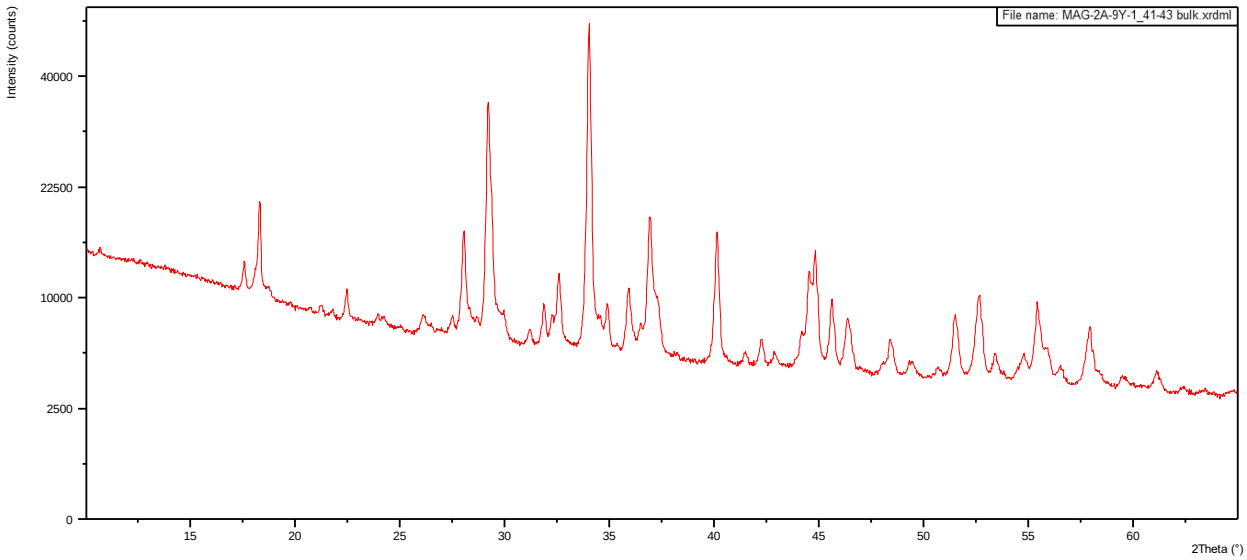
File name: MAG-2A-9Y-1_41-43 bulk.xrdml
Intensity (counts)
0
2500
10000
22500
40000
15
20
25
30
35
40
45
50
55
60
2Theta (°)

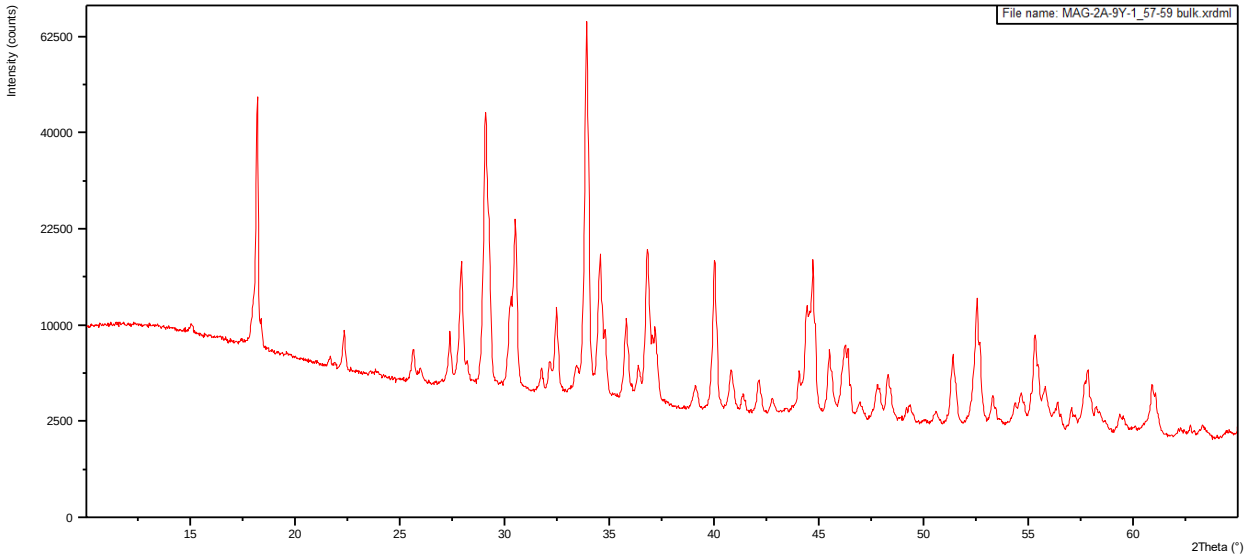
File name: MAG-2A-9Y-1_57-59 bulk.xrdml
Intensity (counts)
0
2500
10000
22500
40000
62500
15
20
25
30
35
40
45
50
55
60
2Theta (°)

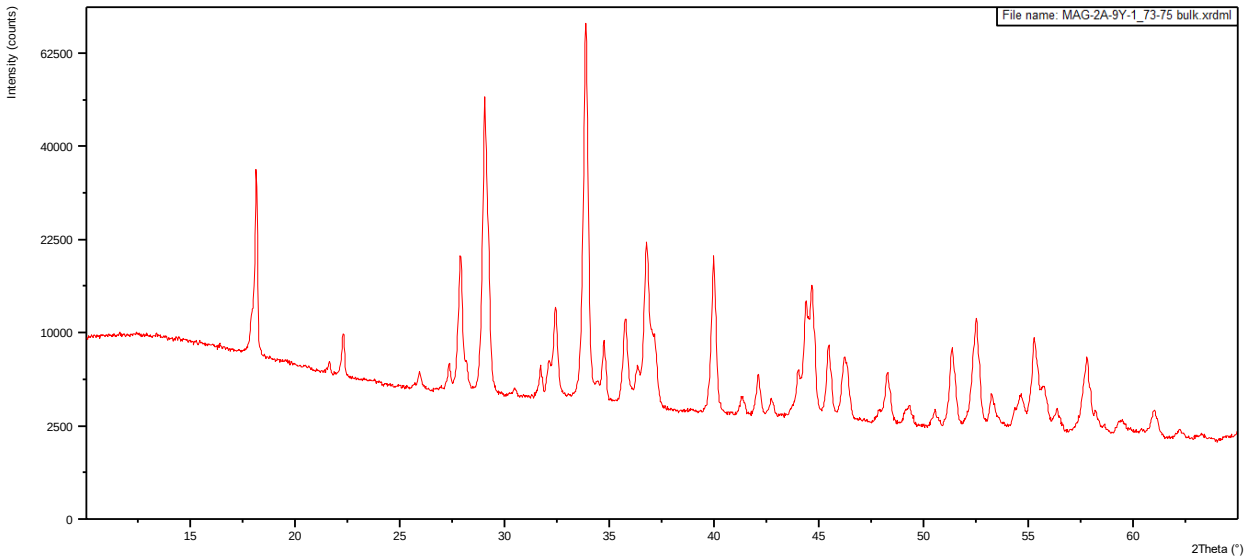
File name: MAG-2A-9Y-1_73-75 bulk.xrdml
Intensity (counts)
62500
40000
22500
10000
2500
0
15
20
25
30
35
40
45
50
55
60
2Theta (°)

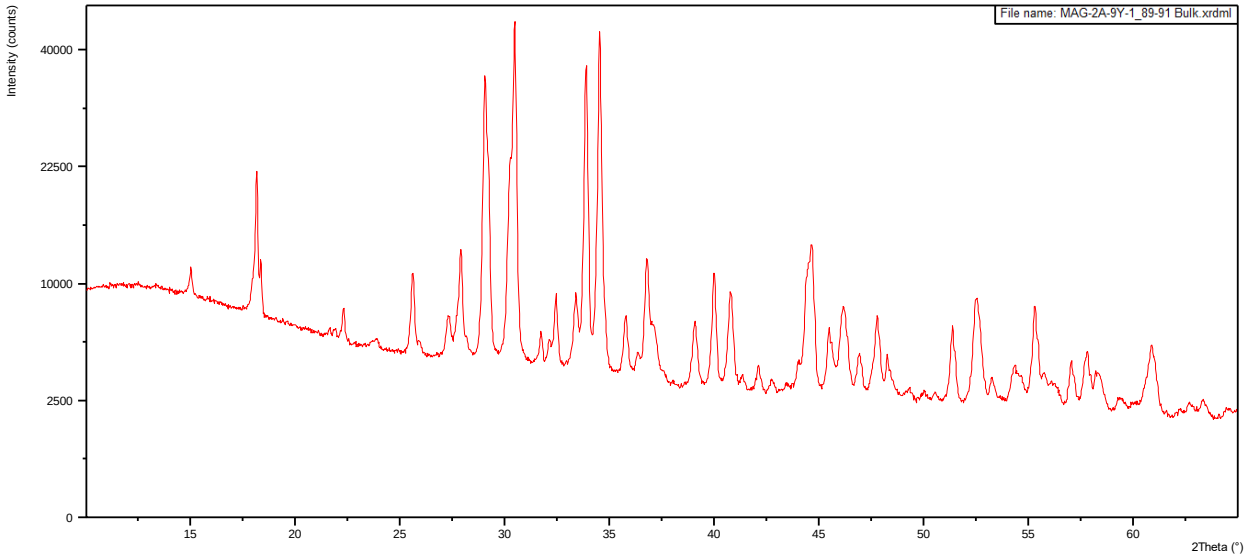
File name: MAG-2A-9Y-1_89-91 Bulk.xrdml
Intensity (counts)
40000
22500
10000
2500
0
15
20
25
30
35
40
45
50
55
60
2Theta (°)

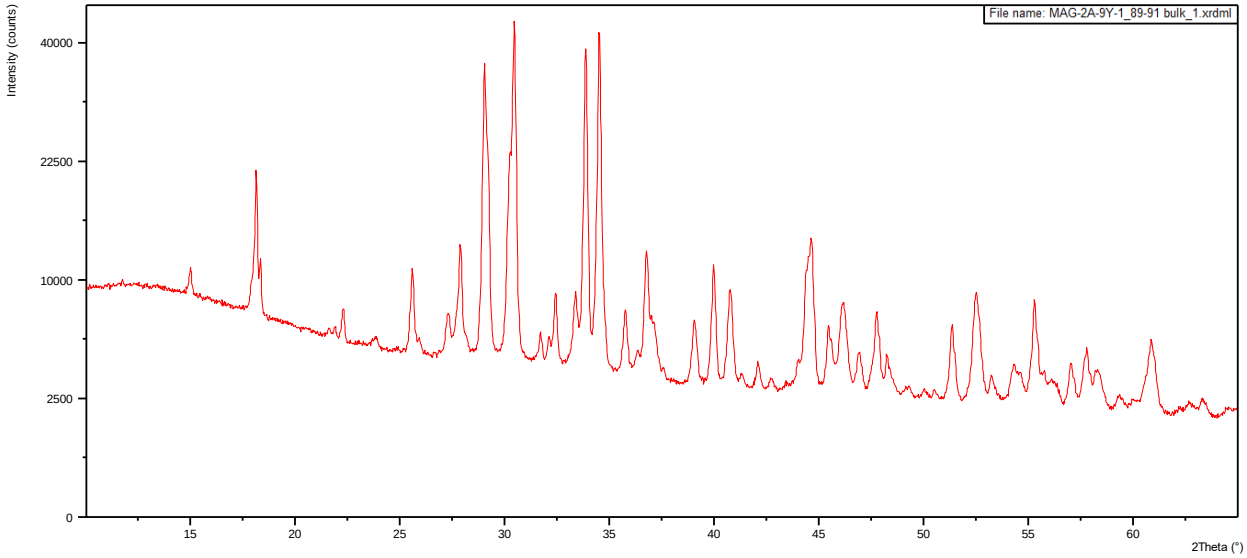
File name: MAG-2A-9Y-1_89-91 bulk_1.xrdml
Intensity (counts)
40000
22500
10000
2500
0
15
20
25
30
35
40
45
50
55
60
2Theta (°)

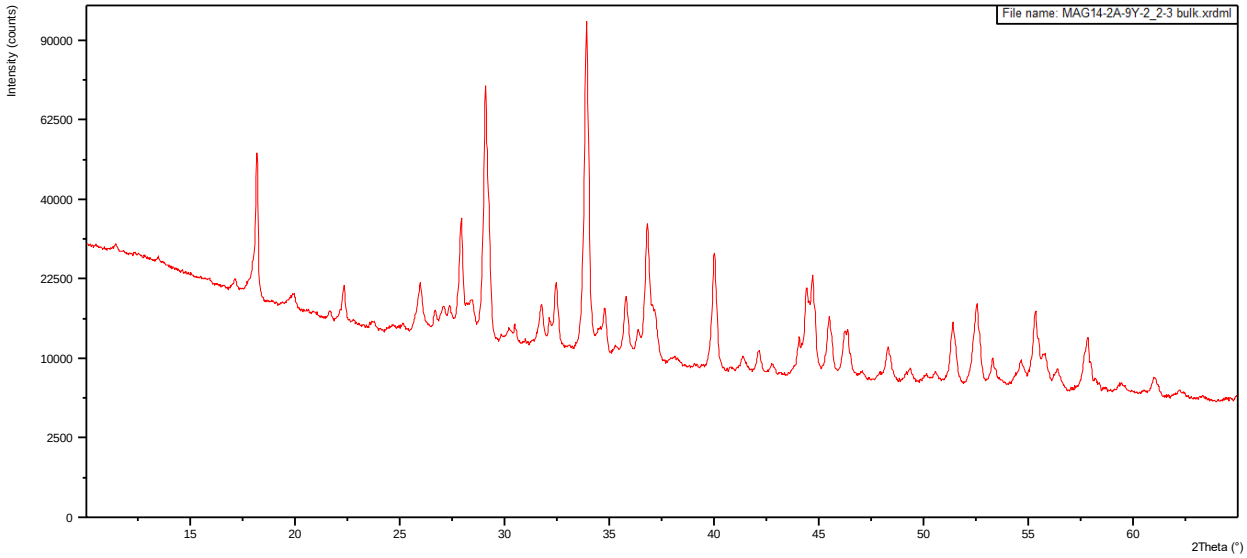
File name: MAG14-2A-9Y-2_2-3 bulk.xrdml
Intensity (counts)
90000
62500
40000
22500
10000
2500
0
15
20
25
30
35
40
45
50
55
60
2Theta (°)

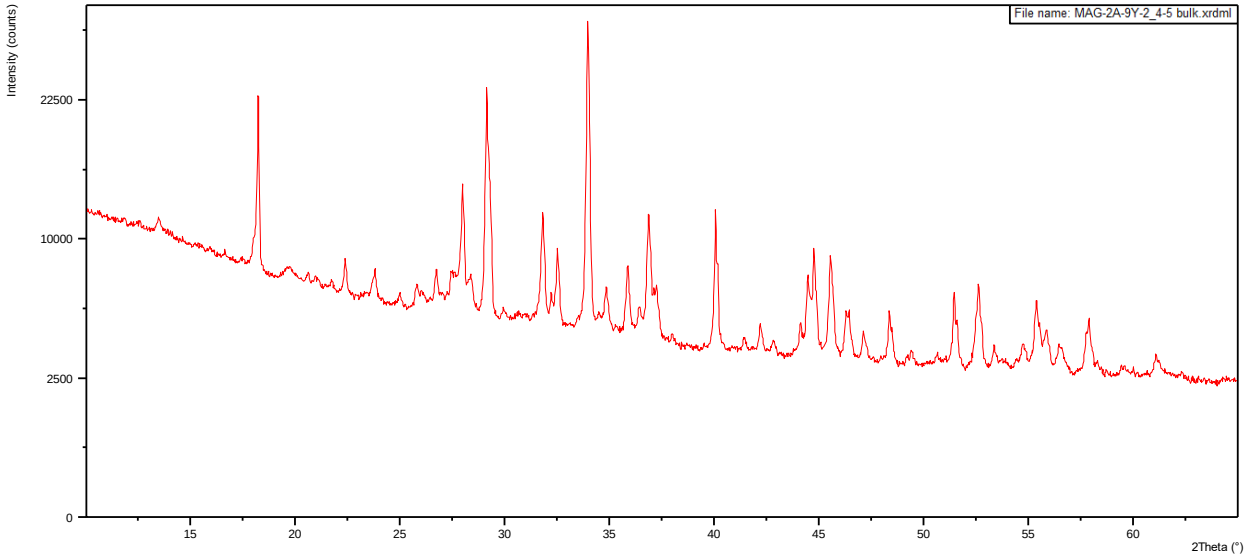
File name: MAG-2A-9Y-2_4-5 bulk.xrdml
Intensity (counts)
22500
10000
2500
0
15
20
25
30
35
40
45
50
55
60
2Theta (°)

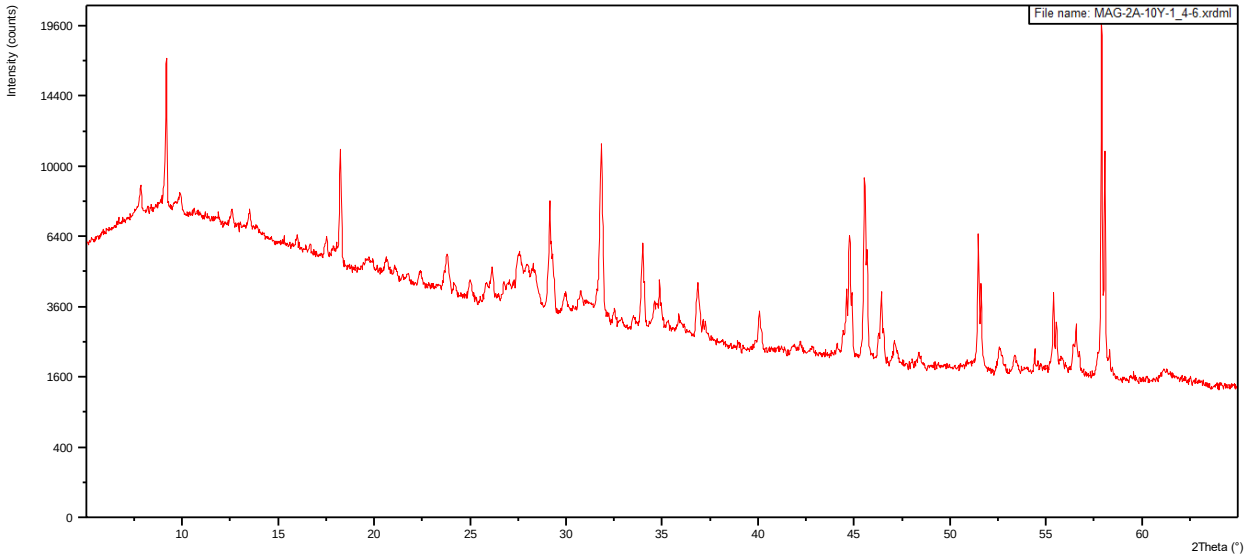
File name: MAG-2A-10Y-1_4-6.xrdml
Intensity (counts)
19600
14400
10000
6400
3600
1600
400
0
10
15
20
25
30
35
40
45
50
55
60
2Theta (°)

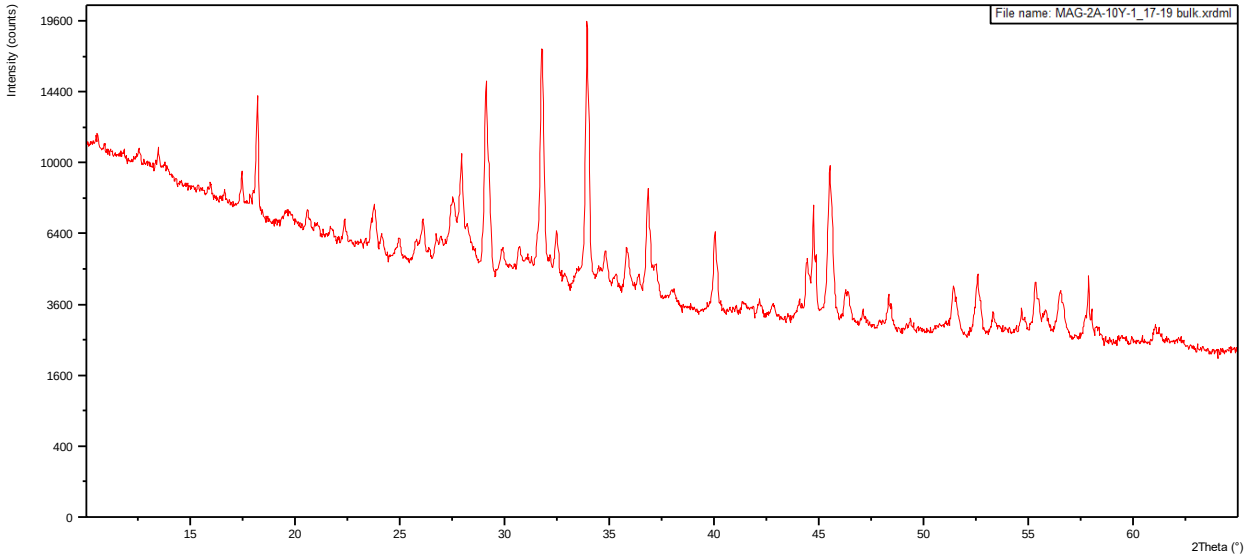
File name: MAG-2A-10Y-1_17-19 bulk.xrdml
Intensity (counts)
19600
14400
10000
6400
3600
1600
400
0
15
20
25
30
35
40
45
50
55
60
2Theta (°)

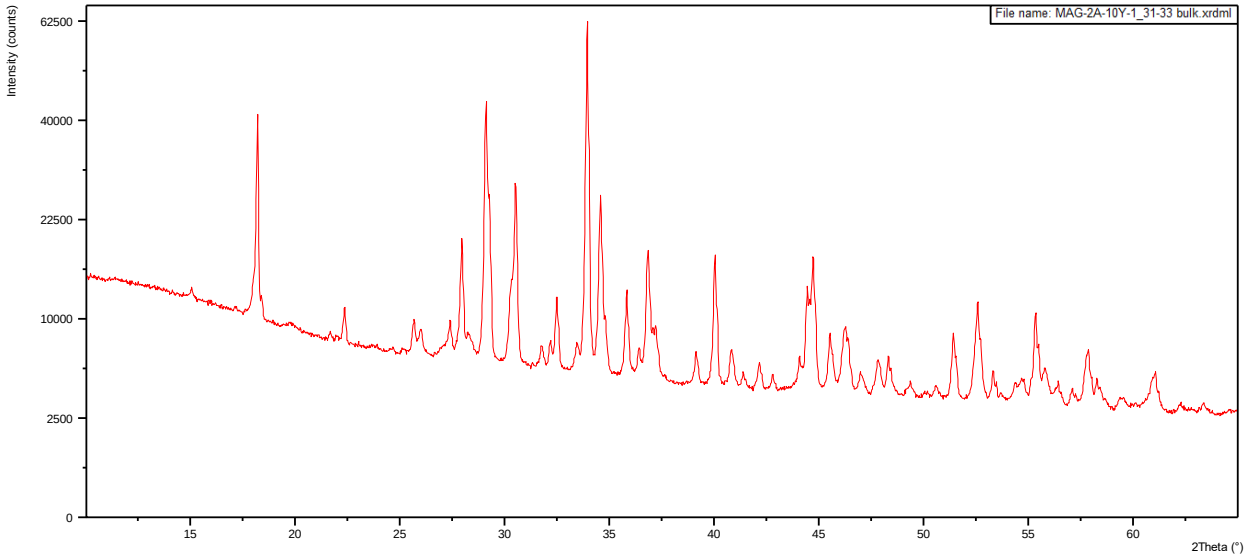
File name: MAG-2A-10Y-1_31-33 bulk.xrdml
Intensity (counts)
62500
40000
22500
10000
2500
0
15
20
25
30
35
40
45
50
55
60
2Theta (°)

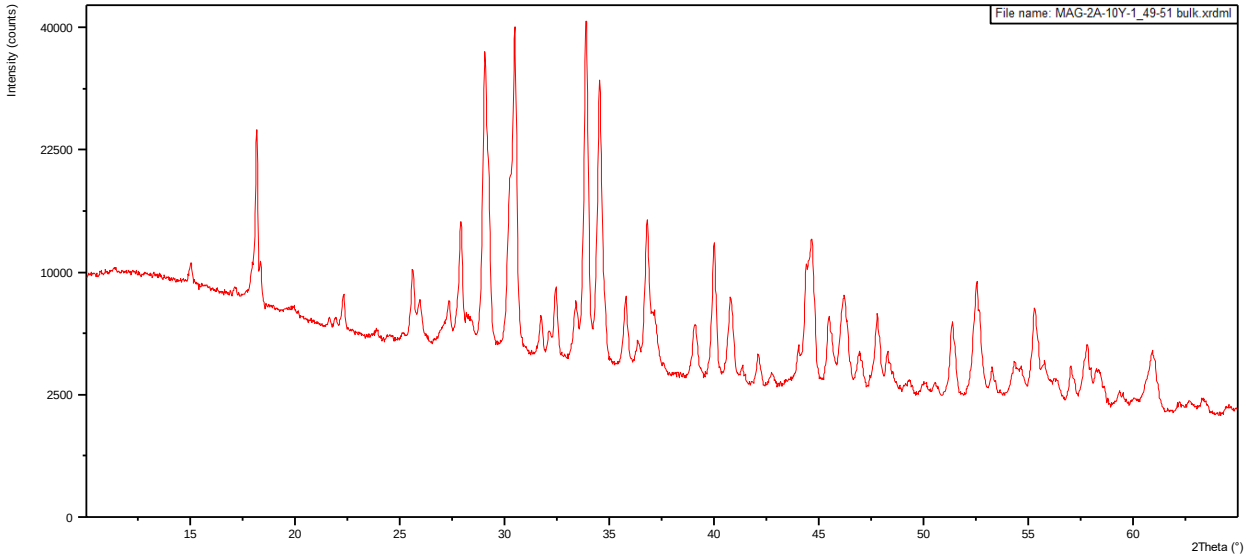
File name: MAG-2A-10Y-1_49-51 bulk.xrdml
Intensity (counts)
40000
22500
10000
2500
0
15
20
25
30
35
40
45
50
55
60
2Theta (°)

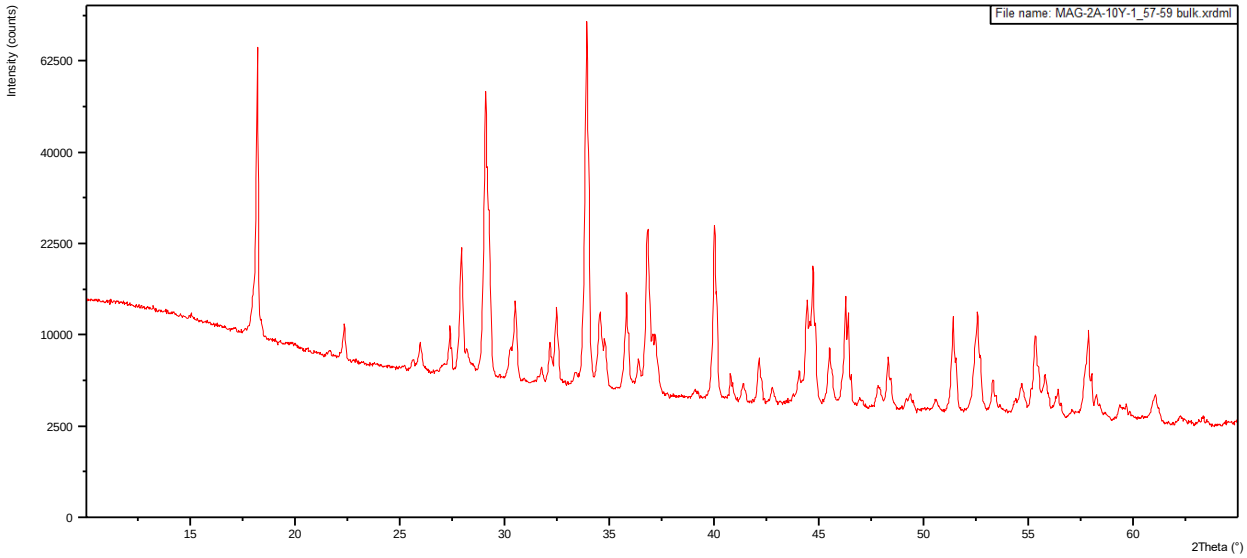
File name: MAG-2A-10Y-1_57-59 bulk.xrdml
Intensity (counts)
62500
40000
22500
10000
2500
0
15
20
25
30
35
40
45
50
55
60
2Theta (°)

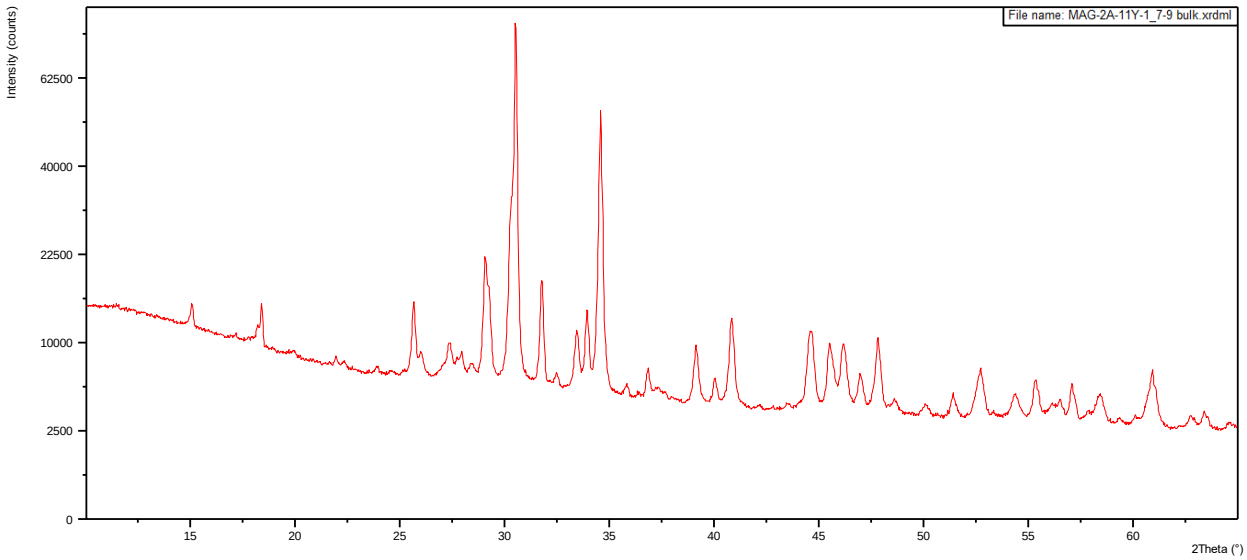
File name: MAG-2A-11Y-1_7-9 bulk.xrdml
Intensity (counts)
62500
40000
22500
10000
2500
0
15
20
25
30
35
40
45
50
55
60
2Theta (°)

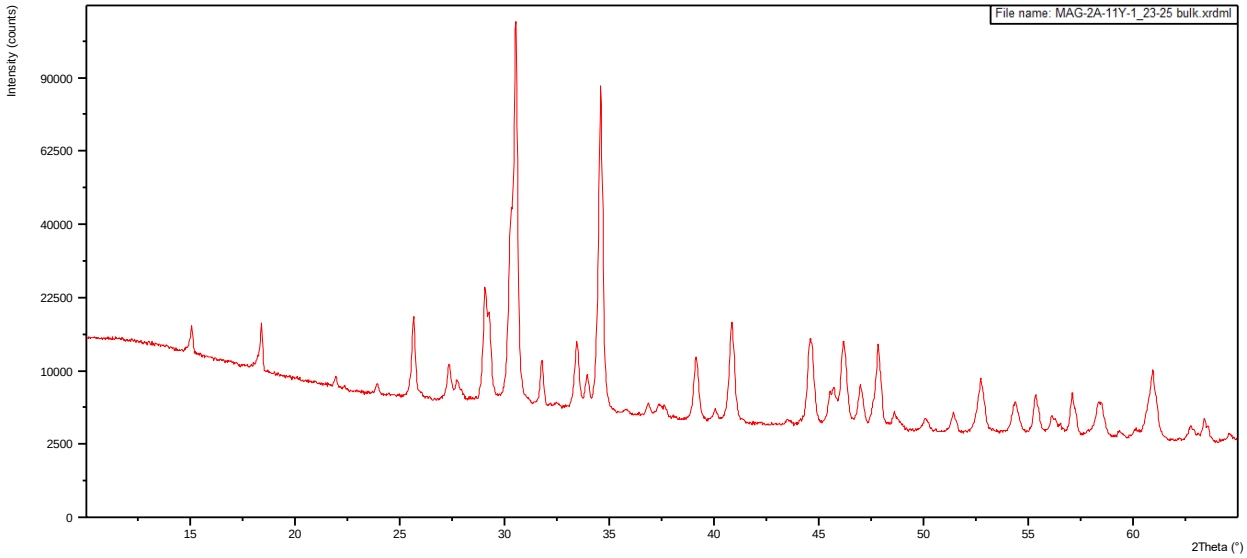
File name: MAG-2A-11Y-1_23-25 bulk.xrdml
Intensity (counts)
90000
62500
40000
22500
10000
2500
0
15
20
25
30
35
40
45
50
55
60
2Theta (°)

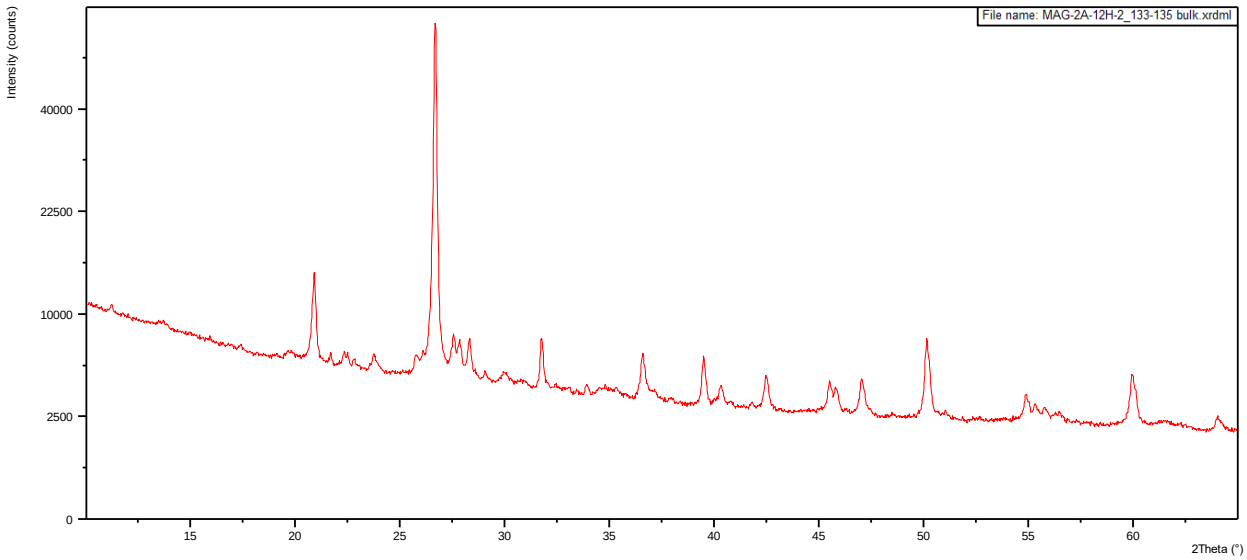
File name: MAG-2A-12H-2_133-135 bulk.xrdml
Intensity (counts)
40000
22500
10000
2500
0
15
20
25
30
35
40
45
50
55
60
2Theta (°)

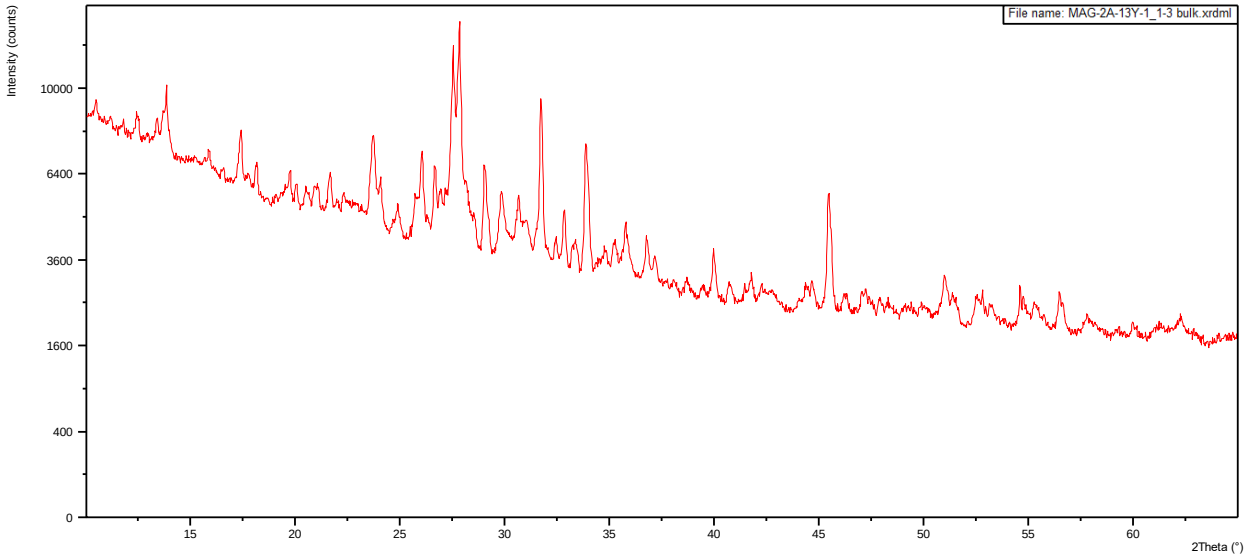
File name: MAG-2A-13Y-1_1-3 bulk.xrdml
Intensity (counts)
10000
6400
3600
1600
400
0
15
20
25
30
35
40
45
50
55
60
2Theta (°)

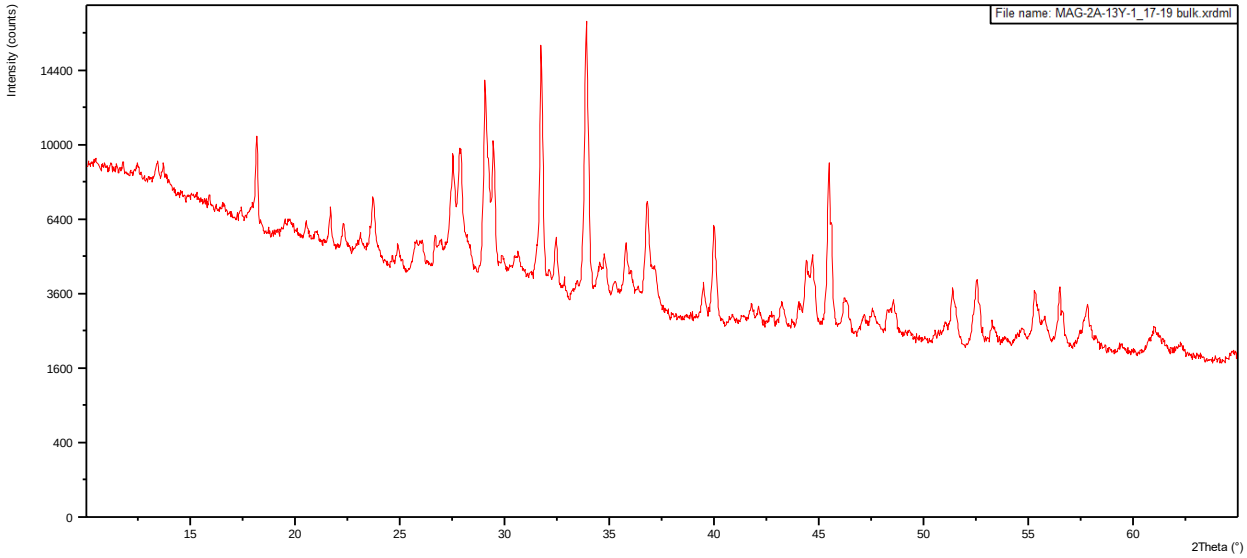
File name: MAG-2A-13Y-1_17-19 bulk.xrdml
Intensity (counts)
14400
10000
6400
3600
1600
400
0
15
20
25
30
35
40
45
50
55
60
2Theta (°)

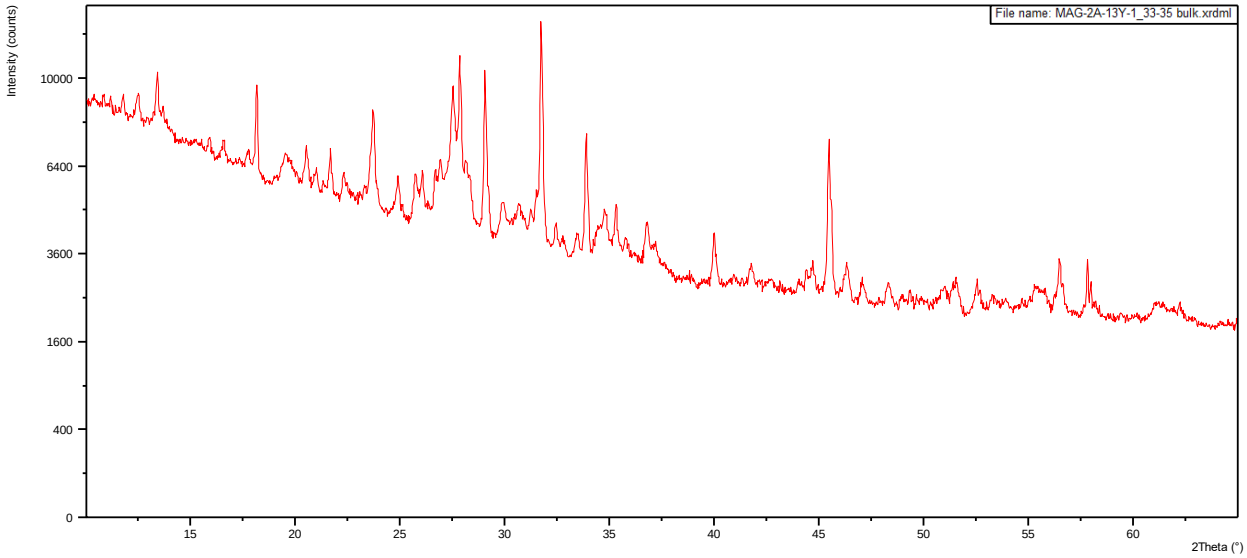
File name: MAG-2A-13Y-1_33-35 bulk.xrdml
Intensity (counts)
10000
6400
3600
1600
400
0
15
20
25
30
35
40
45
50
55
60
2Theta (°)

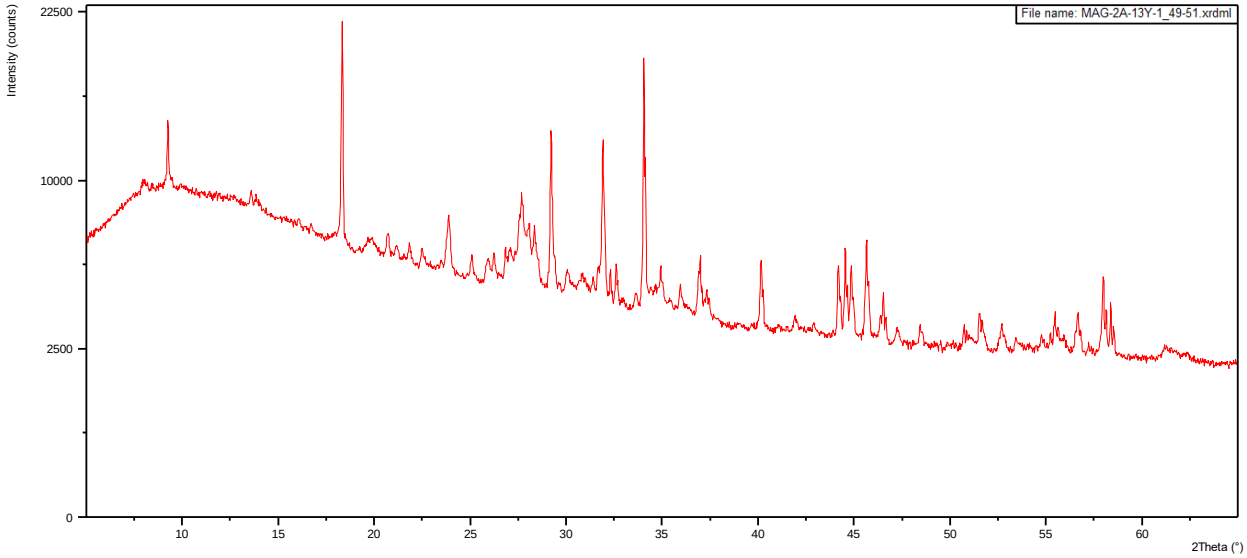
File name: MAG-2A-13Y-1_49-51.xrdml
Intensity (counts)
22500
10000
2500
0
10
15
20
25
30
35
40
45
50
55
60
2Theta (°)

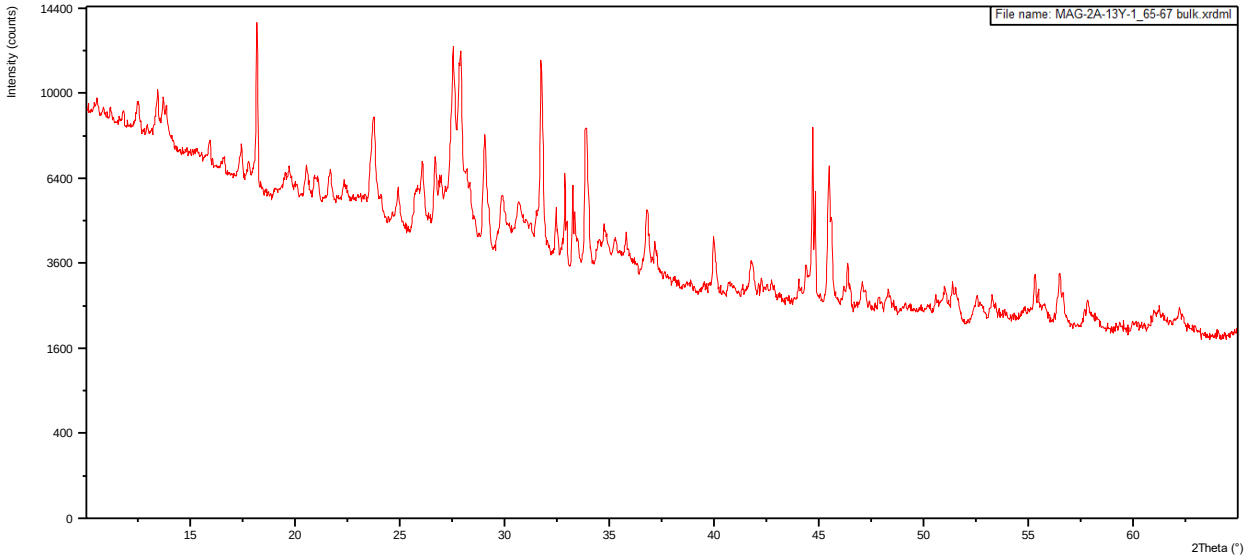
File name: MAG-2A-13Y-1_65-67 bulk.xrdml
Intensity (counts)
14400
10000
6400
3600
1600
400
0
15
20
25
30
35
40
45
50
55
60
2Theta (°)

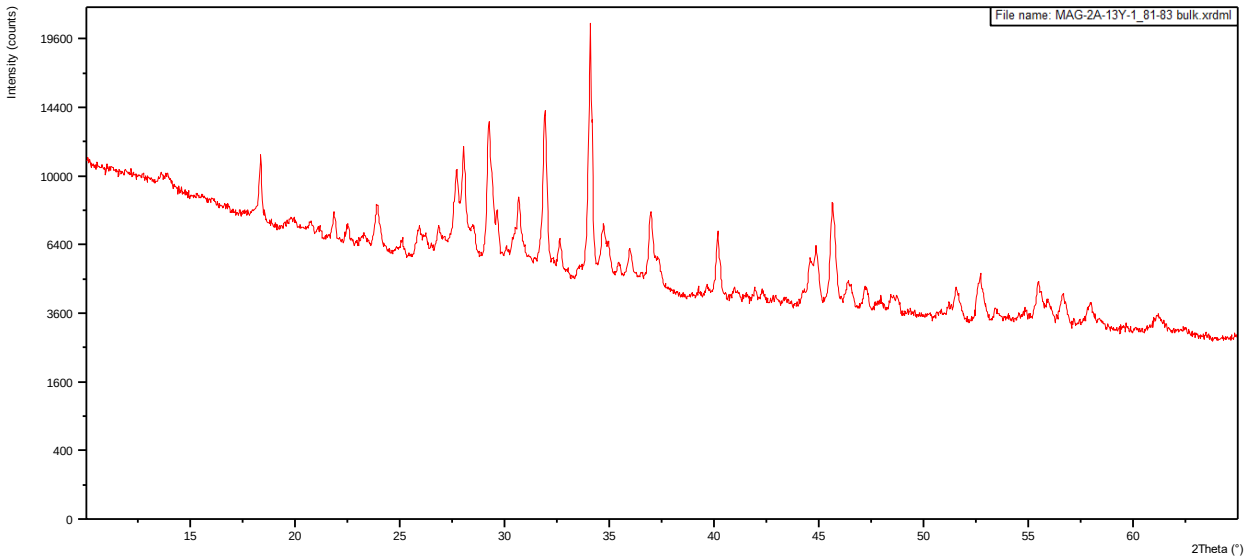
File name: MAG-2A-13Y-1_81-83 bulk.xrdml
Intensity (counts)
19600
14400
10000
6400
3600
1600
400
0
15
20
25
30
35
40
45
50
55
60
2Theta (°)

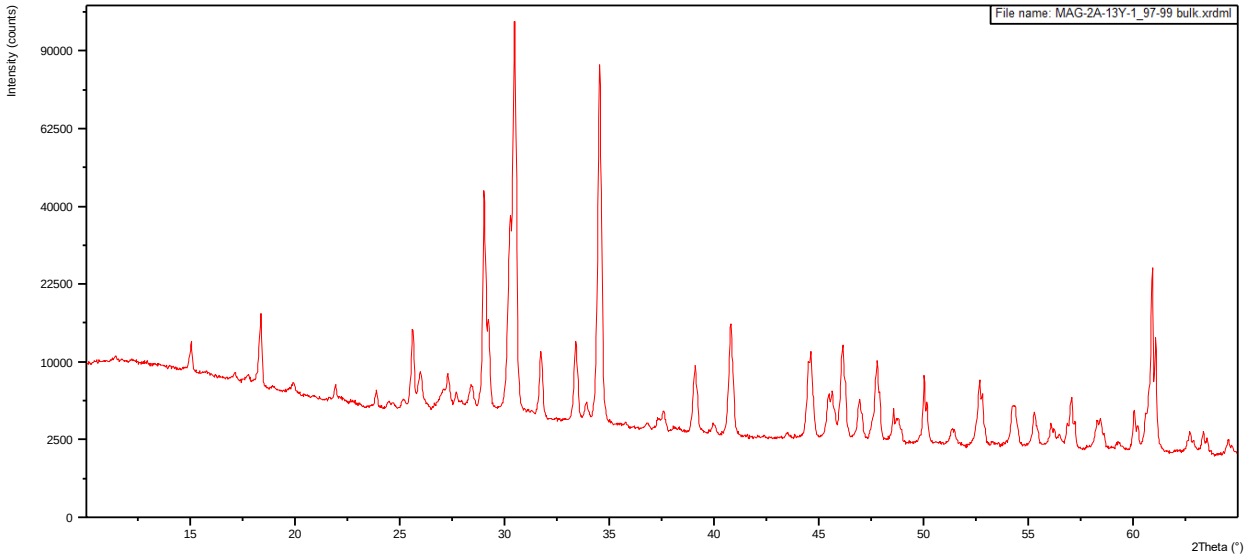
File name: MAG-2A-13Y-1_97-99 bulk.xrdml
Intensity (counts)
90000
62500
40000
22500
10000
2500
0
15
20
25
30
35
40
45
50
55
60
2Theta (°)

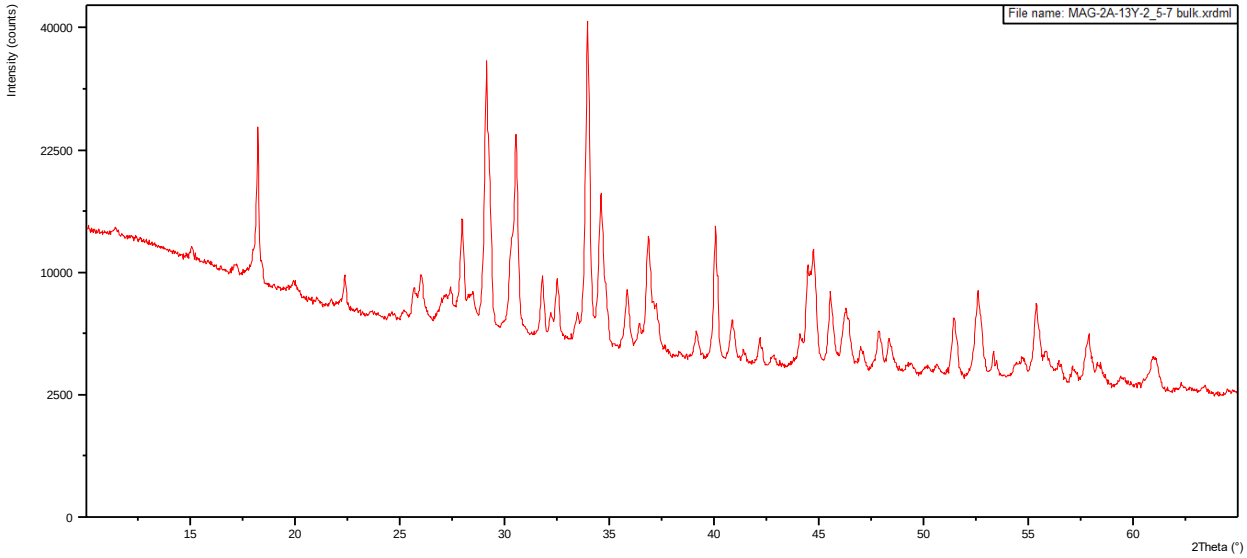
File name: MAG-2A-13Y-2_5-7 bulk.xrdml
Intensity (counts)
40000
22500
10000
2500
0
15
20
25
30
35
40
45
50
55
60
2Theta (°)

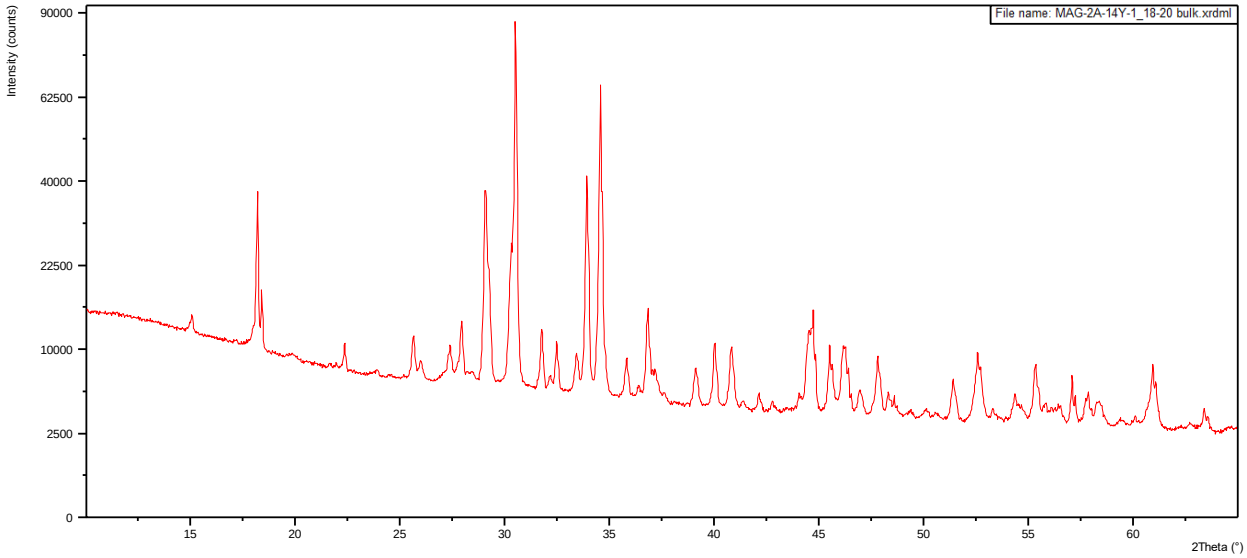
File name: MAG-2A-14Y-1_18-20 bulk.xrdml
Intensity (counts)
90000
62500
40000
22500
10000
2500
0
15
20
25
30
35
40
45
50
55
60
2Theta (°)

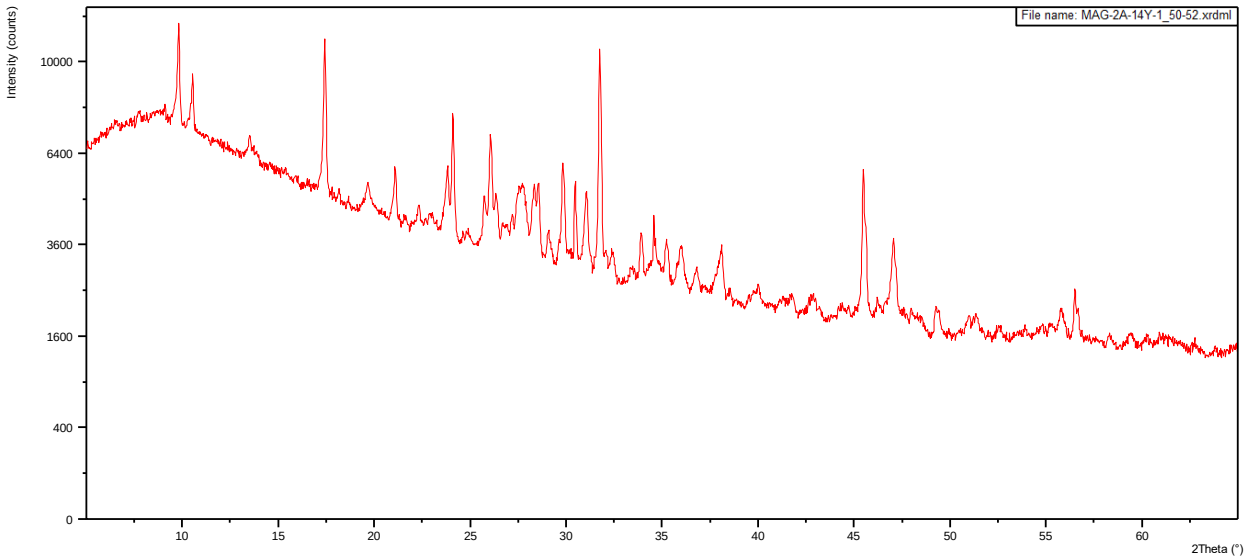
File name: MAG-2A-14Y-1_50-52.xrdml
Intensity (counts)
0
400
1600
3600
6400
10000
10
15
20
25
30
35
40
45
50
55
60
2Theta (°)

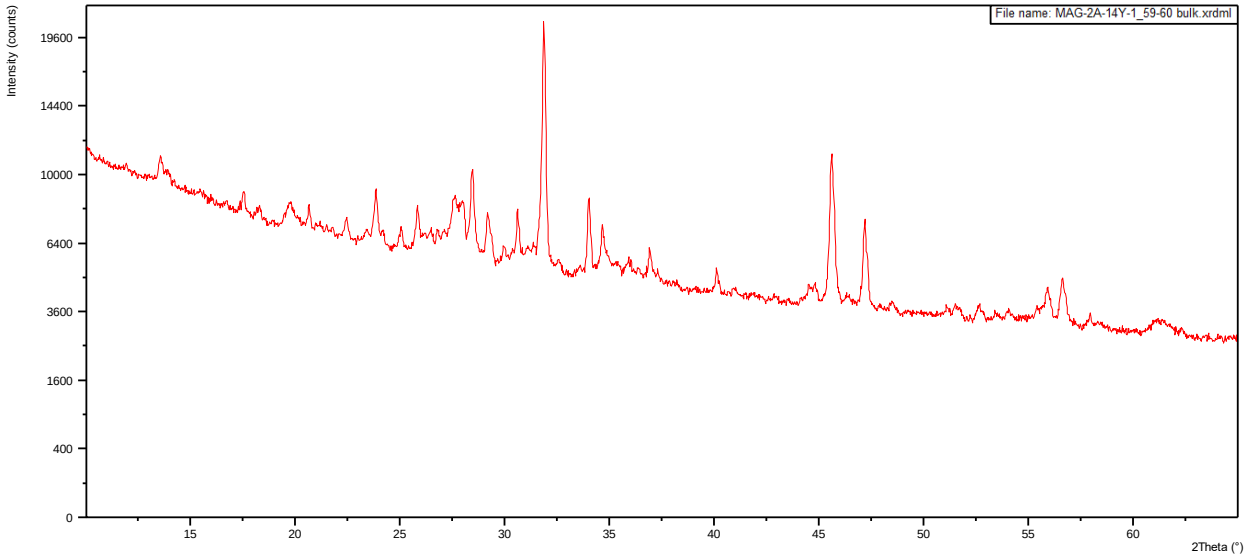
File name: MAG-2A-14Y-1_59-60 bulk.xrdml
Intensity (counts)
0
400
1600
3600
6400
10000
14400
19600
15
20
25
30
35
40
45
50
55
60
2Theta (°)

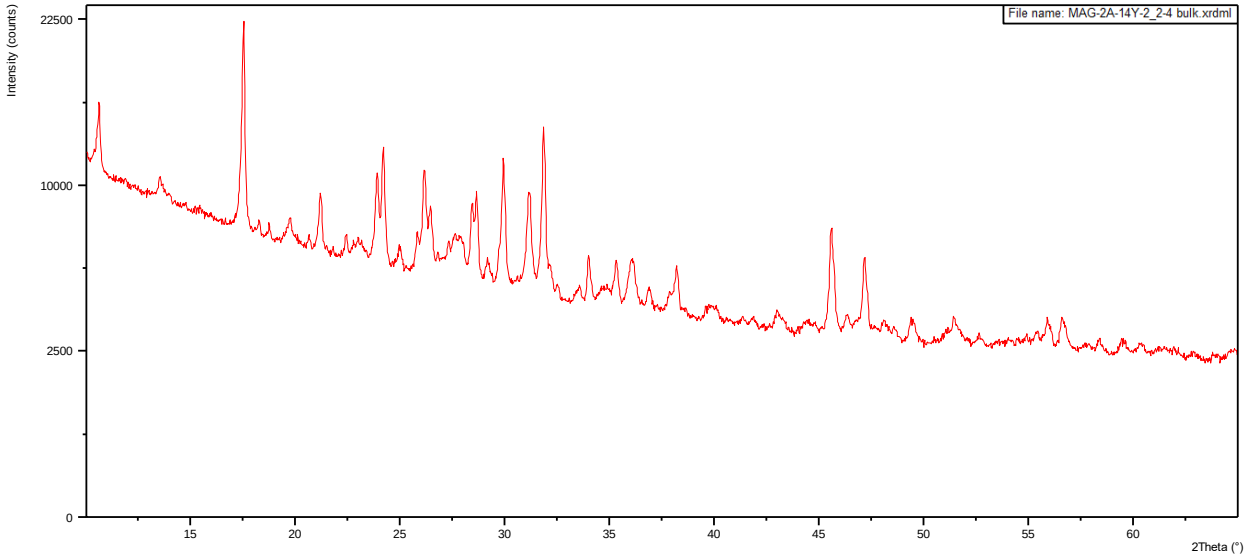
File name: MAG-2A-14Y-2_2-4 bulk.xrdml
Intensity (counts)
22500
10000
2500
0
15
20
25
30
35
40
45
50
55
60
2Theta (°)

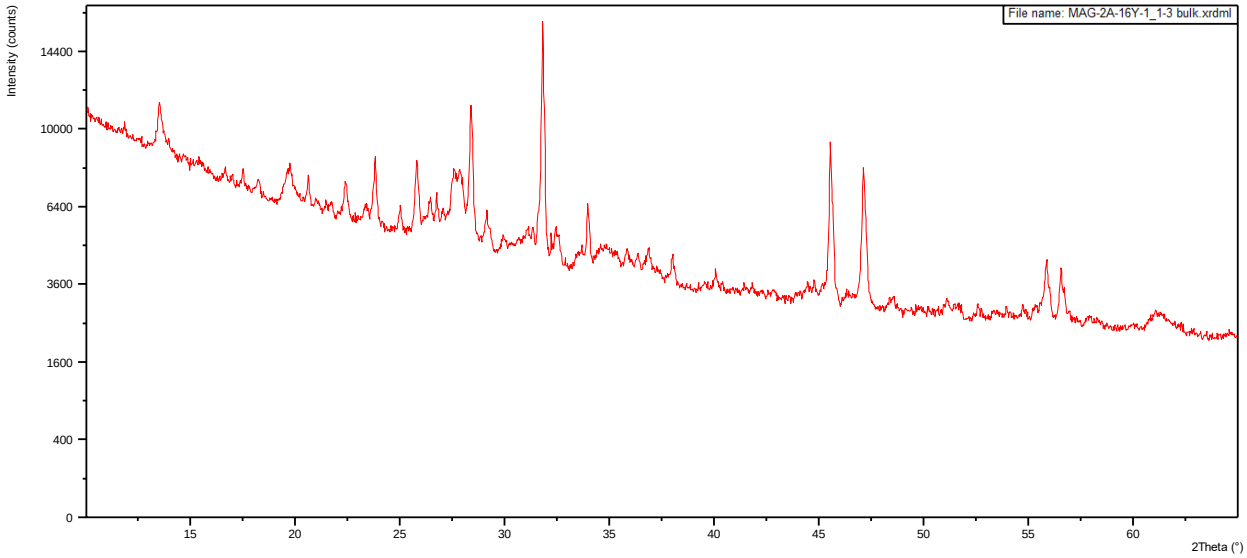
File name: MAG-2A-16Y-1_1-3 bulk.xrdml
Intensity (counts)
14400
10000
6400
3600
1600
400
0
15
20
25
30
35
40
45
50
55
60
2Theta (°)

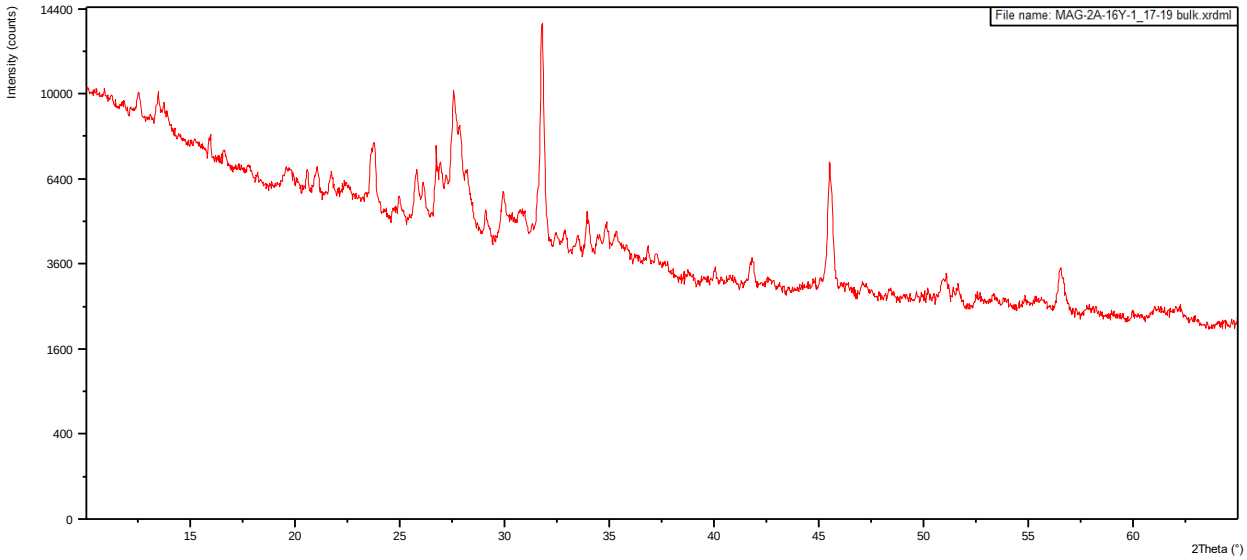
File name: MAG-2A-16Y-1_17-19 bulk.xrdml
Intensity (counts)
14400
10000
6400
3600
1600
400
0
15
20
25
30
35
40
45
50
55
60
2Theta (°)

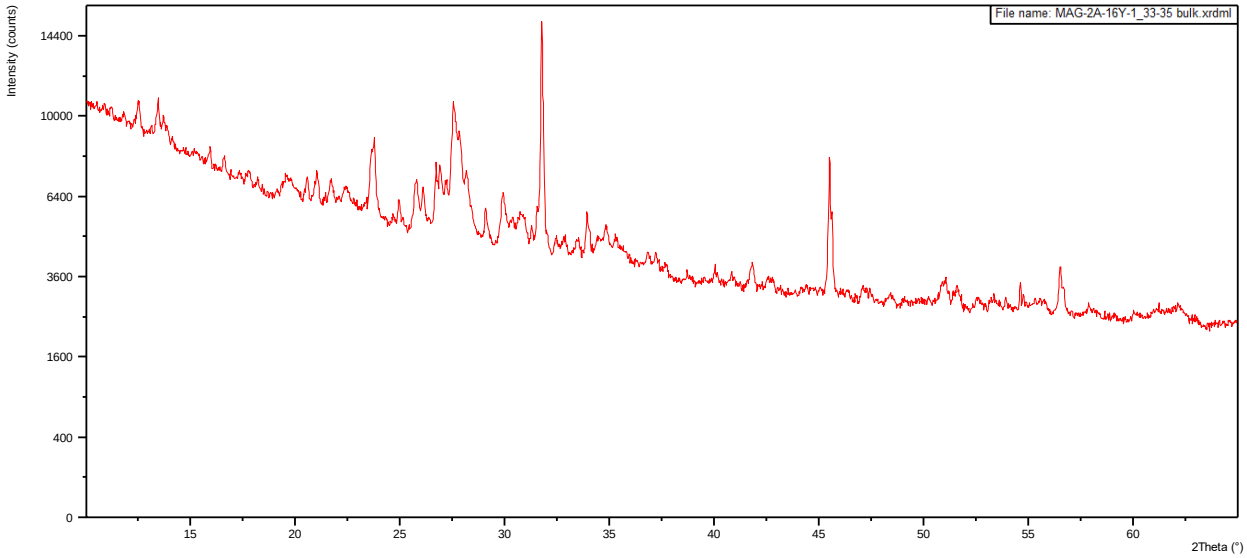
File name: MAG-2A-16Y-1_33-35 bulk.xrdml
Intensity (counts)
14400
10000
6400
3600
1600
400
0
15
20
25
30
35
40
45
50
55
60
2Theta (°)

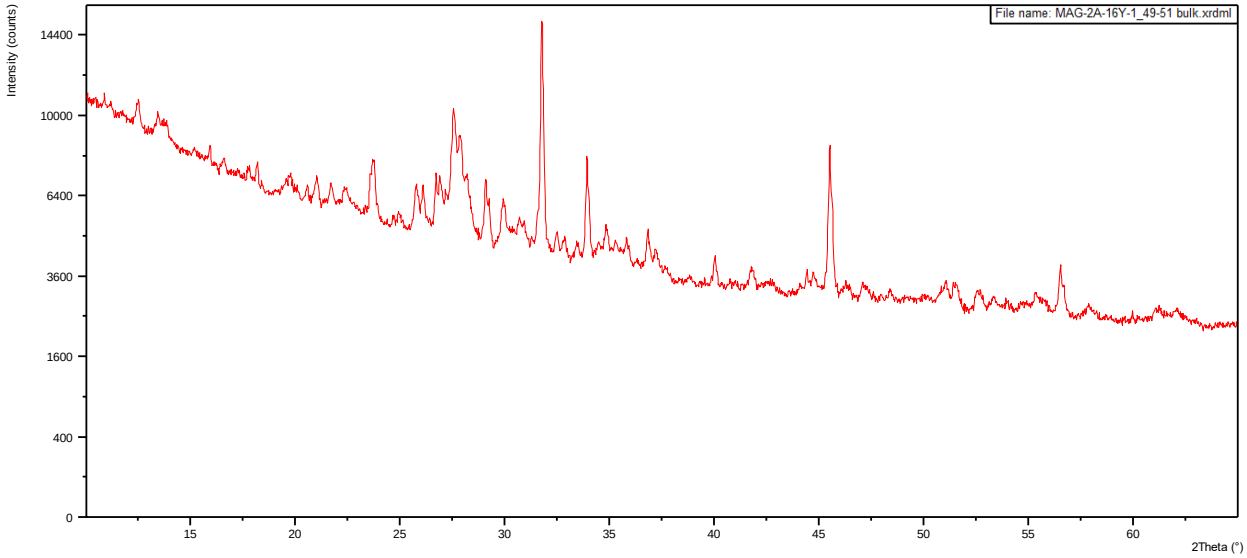
File name: MAG-2A-16Y-1_49-51 bulk.xrdml
Intensity (counts)
14400
10000
6400
3600
1600
400
0
15
20
25
30
35
40
45
50
55
60
2Theta (°)

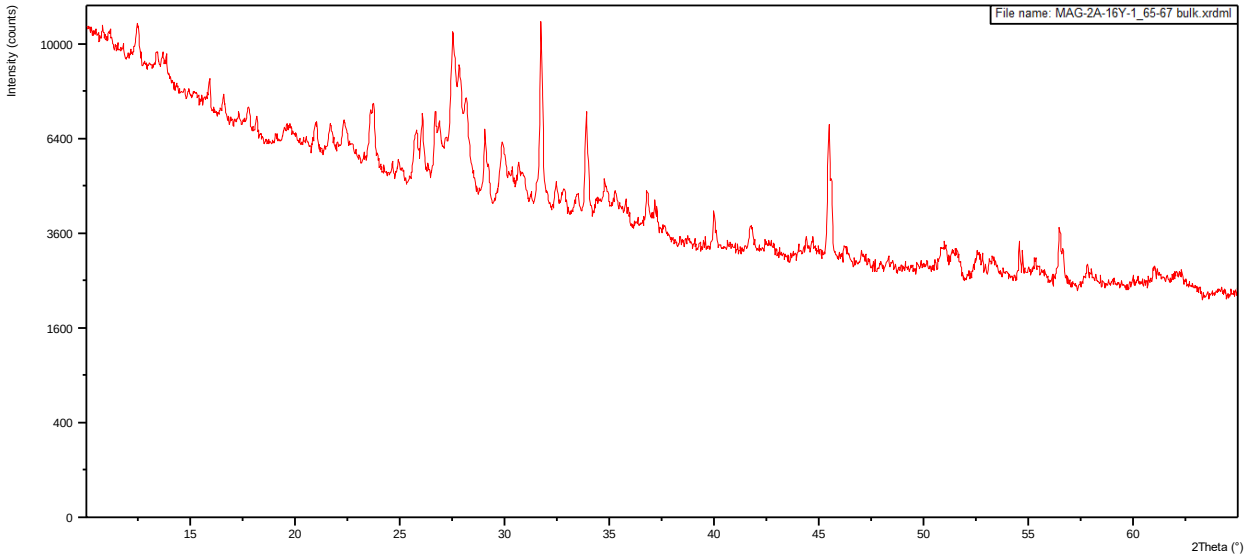
File name: MAG-2A-16Y-1_65-67 bulk.xrdml
Intensity (counts)
10000
6400
3600
1600
400
0
15
20
25
30
35
40
45
50
55
60
2Theta (°)

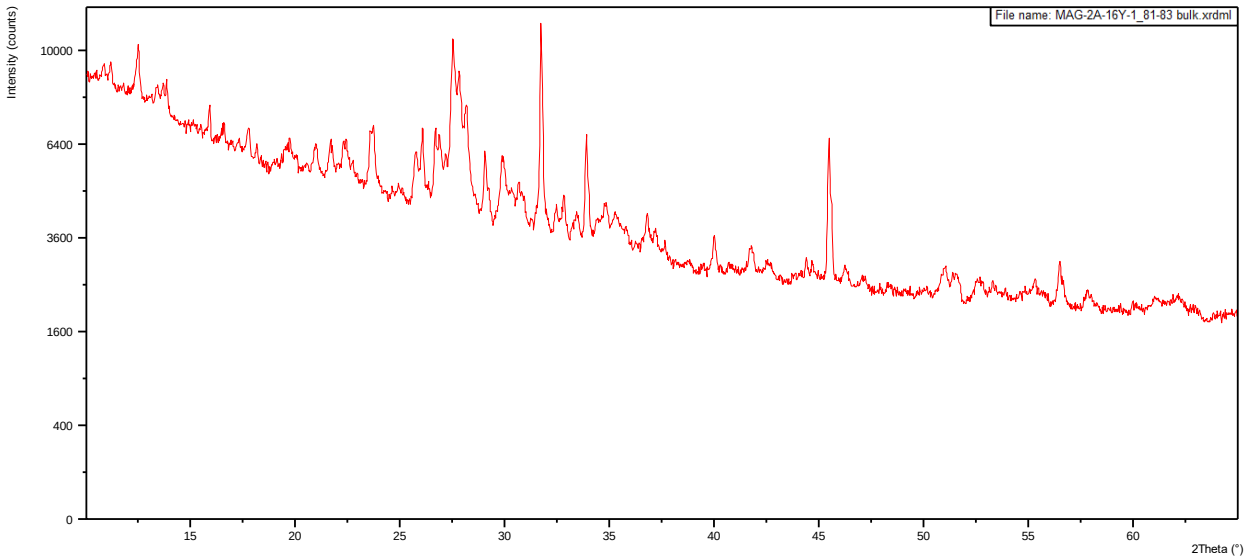
File name: MAG-2A-16Y-1_81-83 bulk.xrdml
Intensity (counts)
10000
6400
3600
1600
400
0
15
20
25
30
35
40
45
50
55
60
2Theta (°)

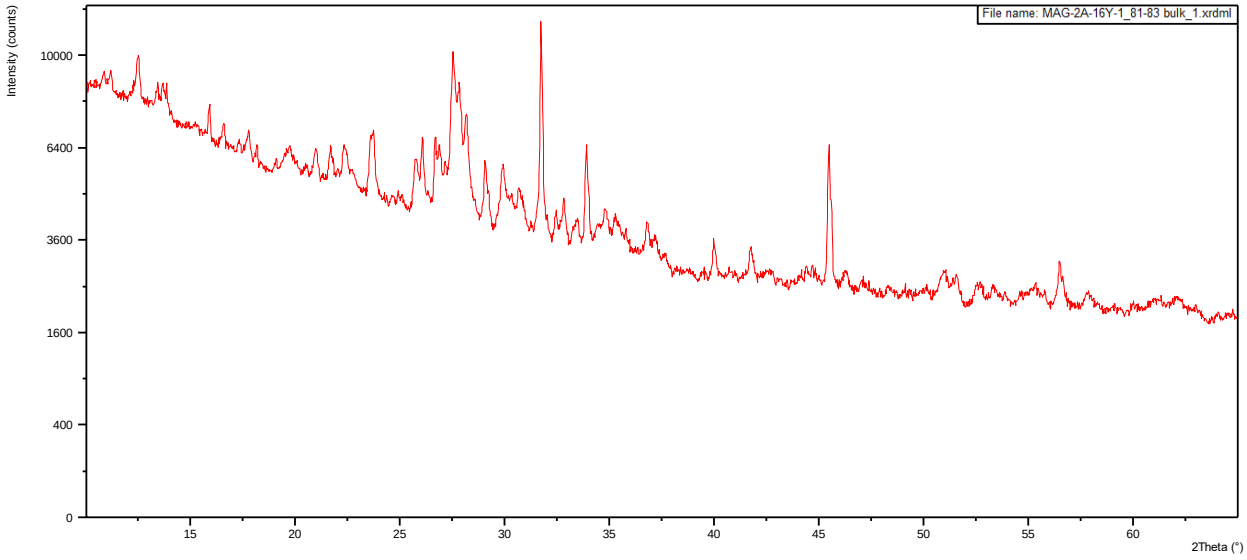
File name: MAG-2A-16Y-1_81-83 bulk_1.xrdml
Intensity (counts)
10000
6400
3600
1600
400
0
15
20
25
30
35
40
45
50
55
60
2Theta (°)

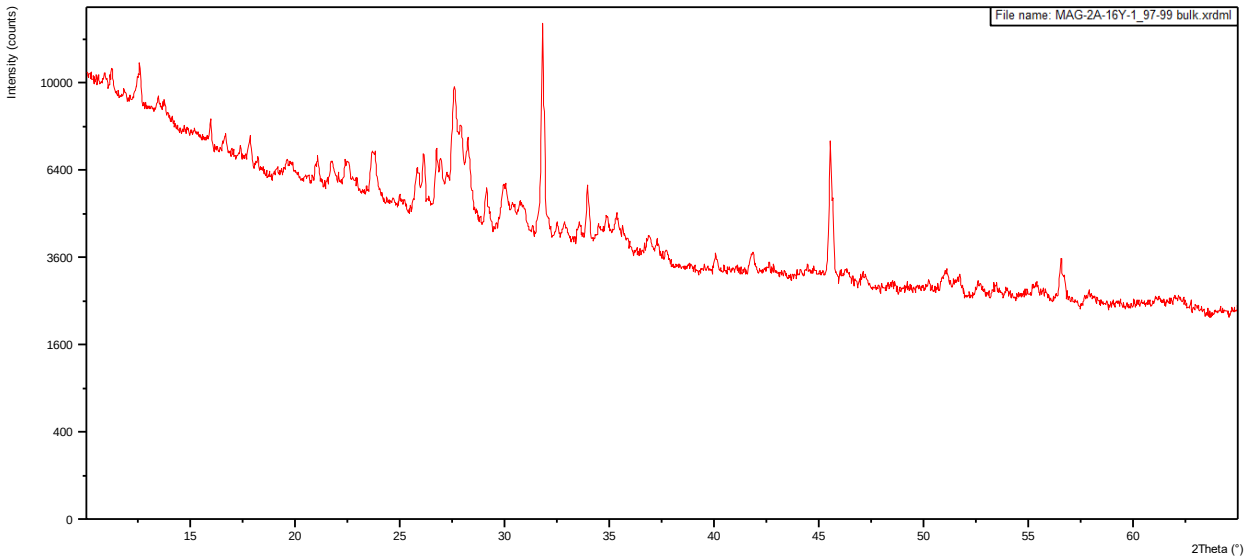
File name: MAG-2A-16Y-1_97-99 bulk.xrdml
Intensity (counts)
10000
6400
3600
1600
400
0
15
20
25
30
35
40
45
50
55
60
2Theta (°)

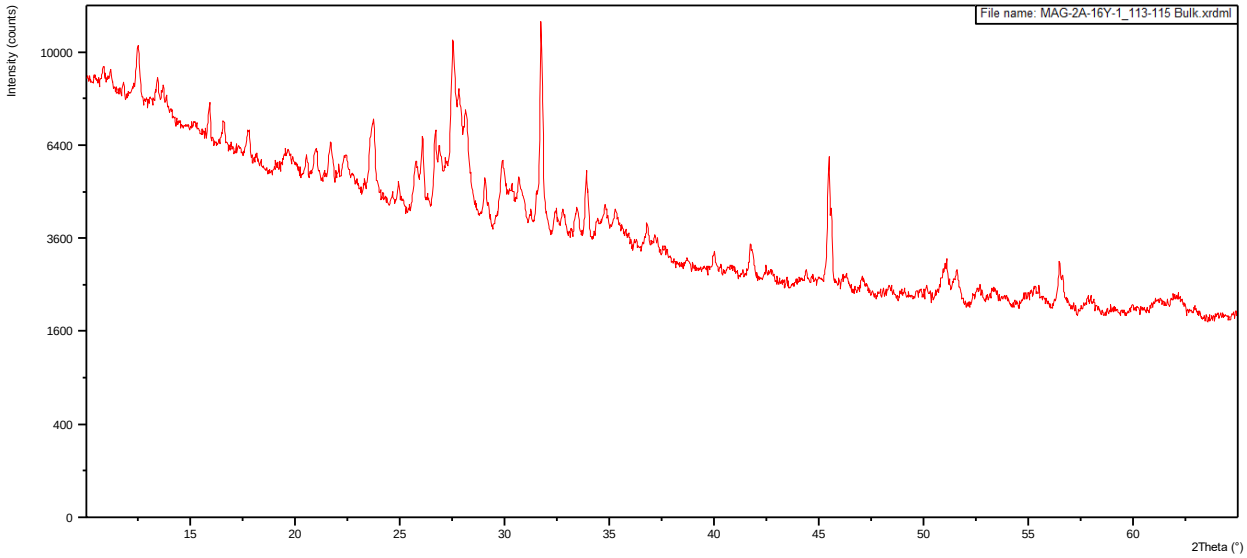
File name: MAG-2A-16Y-1_113-115 Bulk.xrdml
Intensity (counts)
10000
6400
3600
1600
400
0
15
20
25
30
35
40
45
50
55
60
2Theta (°)

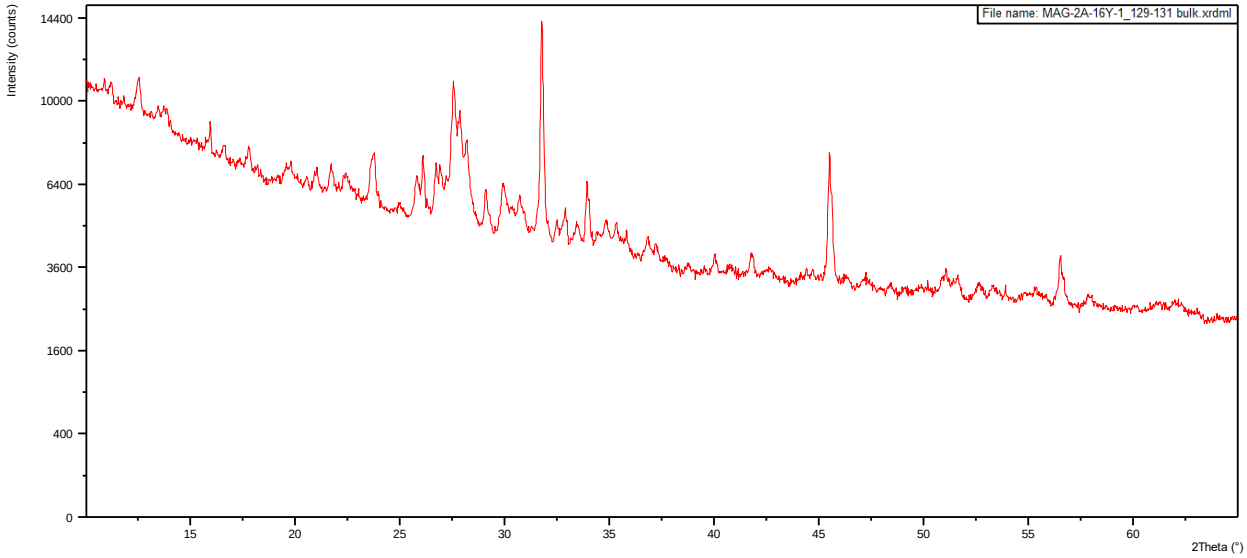
File name: MAG-2A-16Y-1_129-131 bulk.xrdml
Intensity (counts)
14400
10000
6400
3600
1600
400
0
15
20
25
30
35
40
45
50
55
60
2Theta (°)

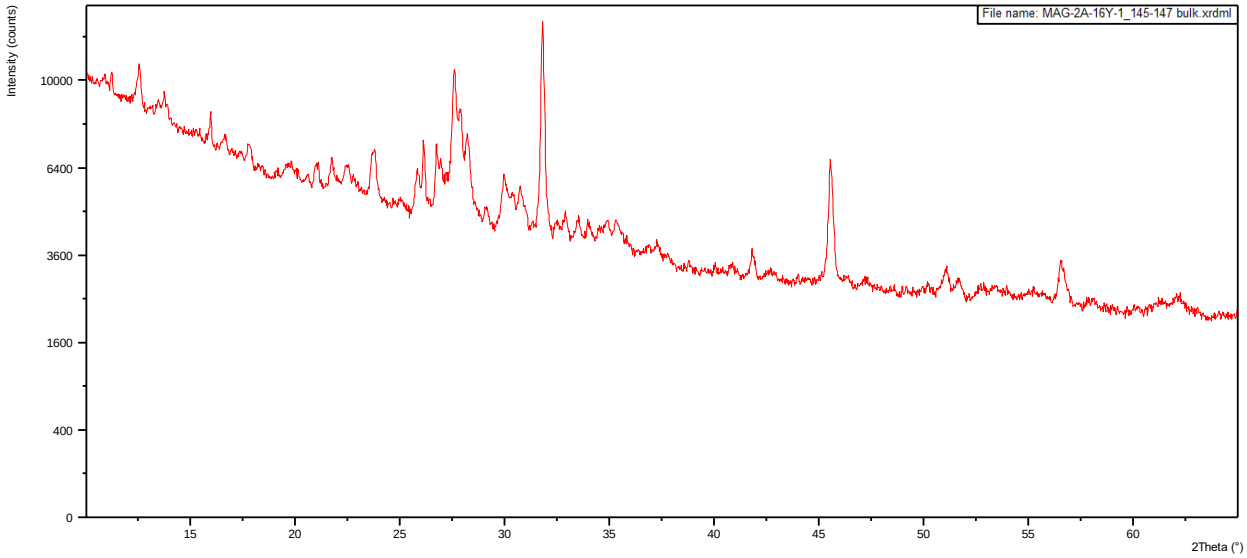
File name: MAG-2A-16Y-1_145-147 bulk.xrdml
Intensity (counts)
10000
6400
3600
1600
400
0
15
20
25
30
35
40
45
50
55
60
2Theta (°)

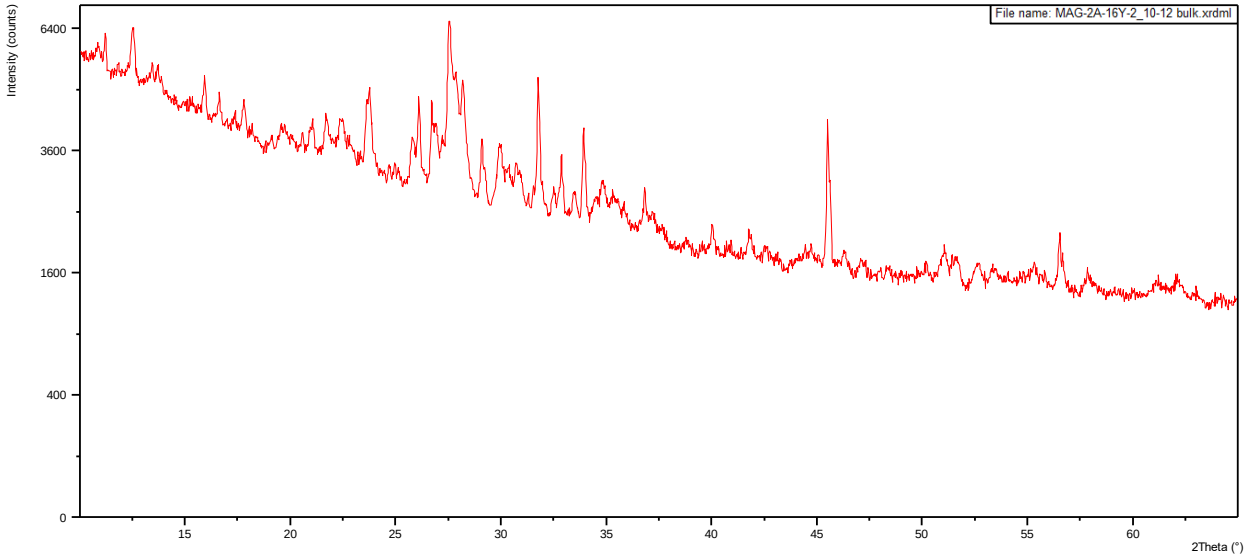
File name: MAG-2A-16Y-2_10-12 bulk.xrdml
Intensity (counts)
6400
3600
1600
400
0
15
20
25
30
35
40
45
50
55
60
2Theta (°)

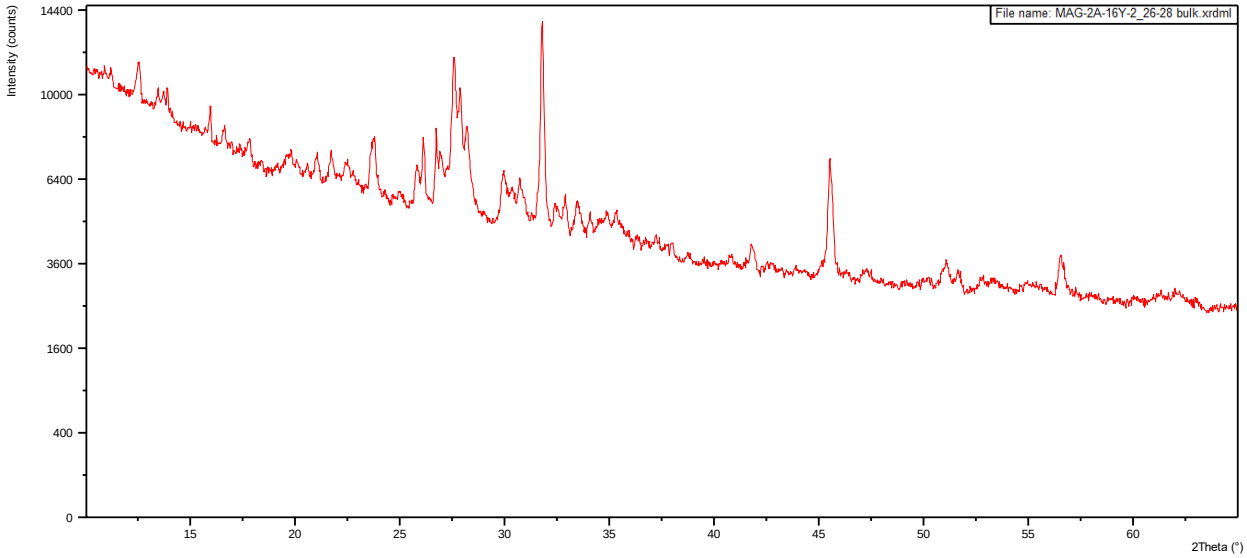
File name: MAG-2A-16Y-2_26-28 bulk.xrdml
Intensity (counts)
14400
10000
6400
3600
1600
400
0
15
20
25
30
35
40
45
50
55
60
2Theta (°)

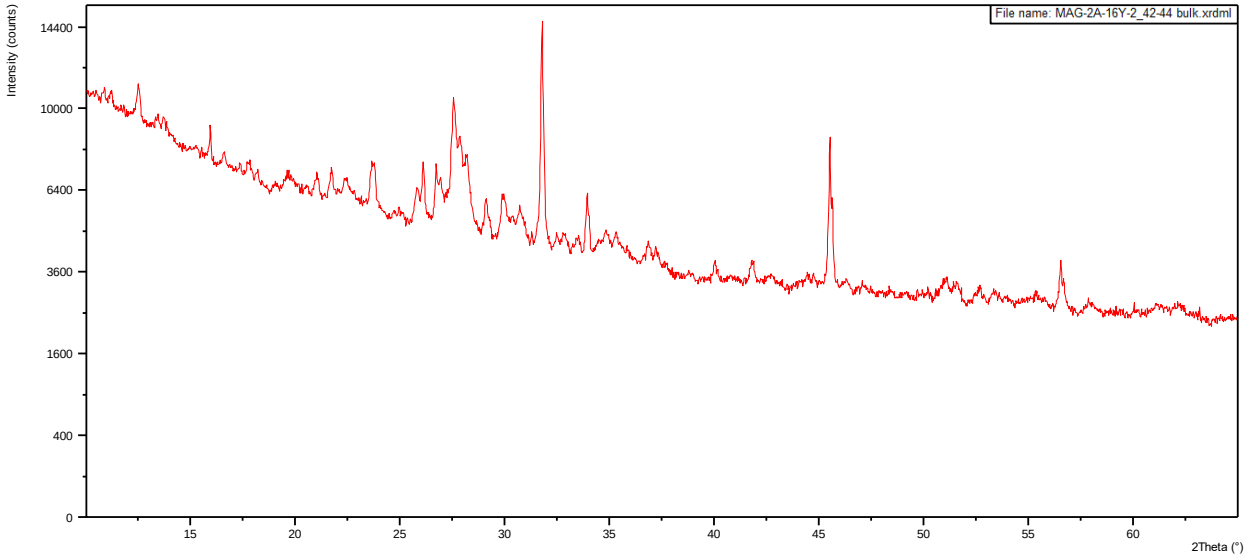
File name: MAG-2A-16Y-2_42-44 bulk.xrdml
Intensity (counts)
14400
10000
6400
3600
1600
400
0
15
20
25
30
35
40
45
50
55
60
2Theta (°)

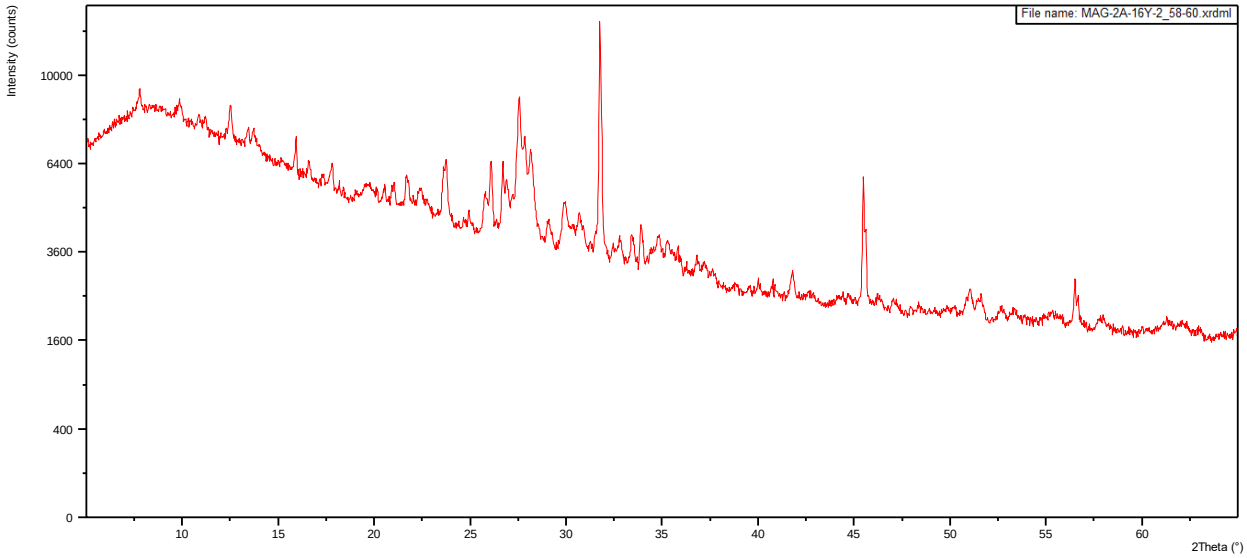
File name: MAG-2A-16Y-2_58-60.xrdml
Intensity (counts)
10000
6400
3600
1600
400
0
10
15
20
25
30
35
40
45
50
55
60
2Theta (°)

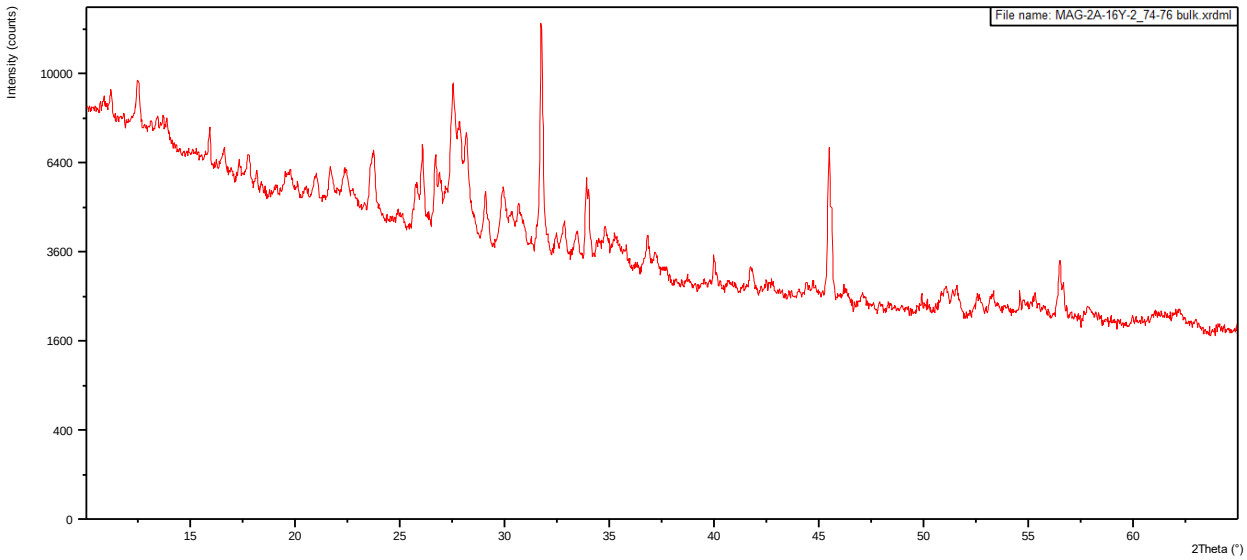
File name: MAG-2A-16Y-2_74-76 bulk.xrdml
Intensity (counts)
10000
6400
3600
1600
400
0
15
20
25
30
35
40
45
50
55
60
2Theta (°)

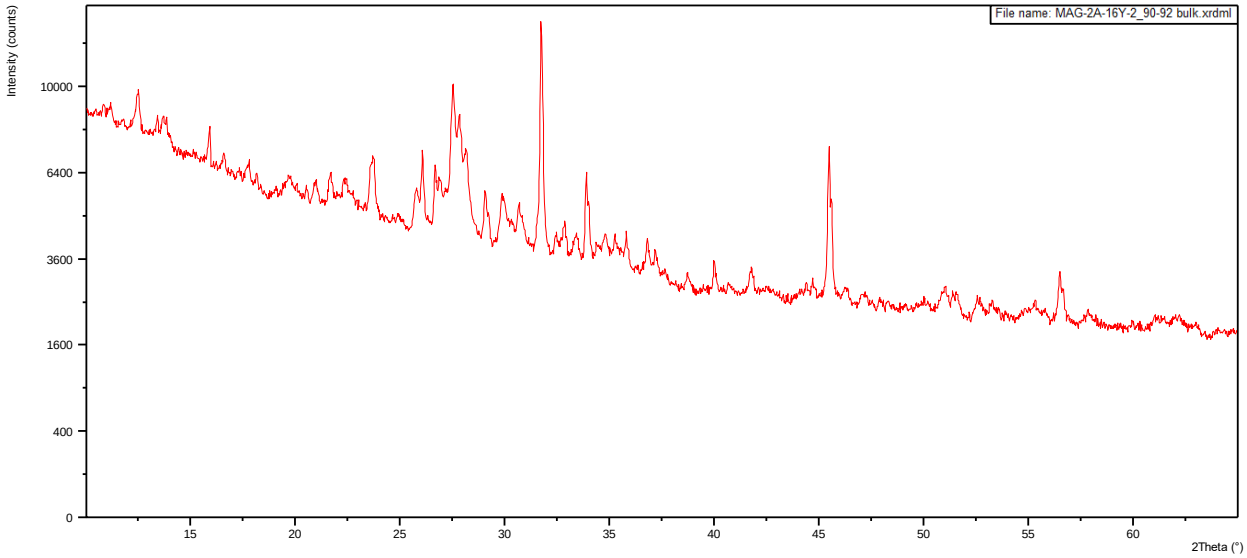
File name: MAG-2A-16Y-2_90-92 bulk.xrdml
Intensity (counts)
10000
6400
3600
1600
400
0
15
20
25
30
35
40
45
50
55
60
2Theta (°)

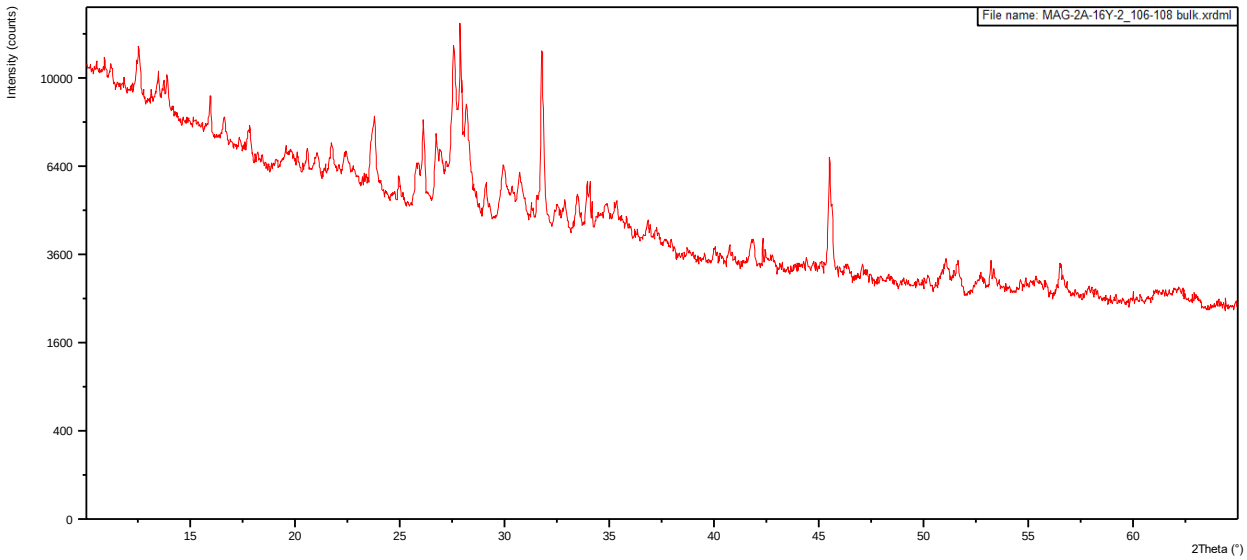
File name: MAG-2A-16Y-2_106-108 bulk.xrdml
Intensity (counts)
10000
6400
3600
1600
400
0
15
20
25
30
35
40
45
50
55
60
2Theta (°)

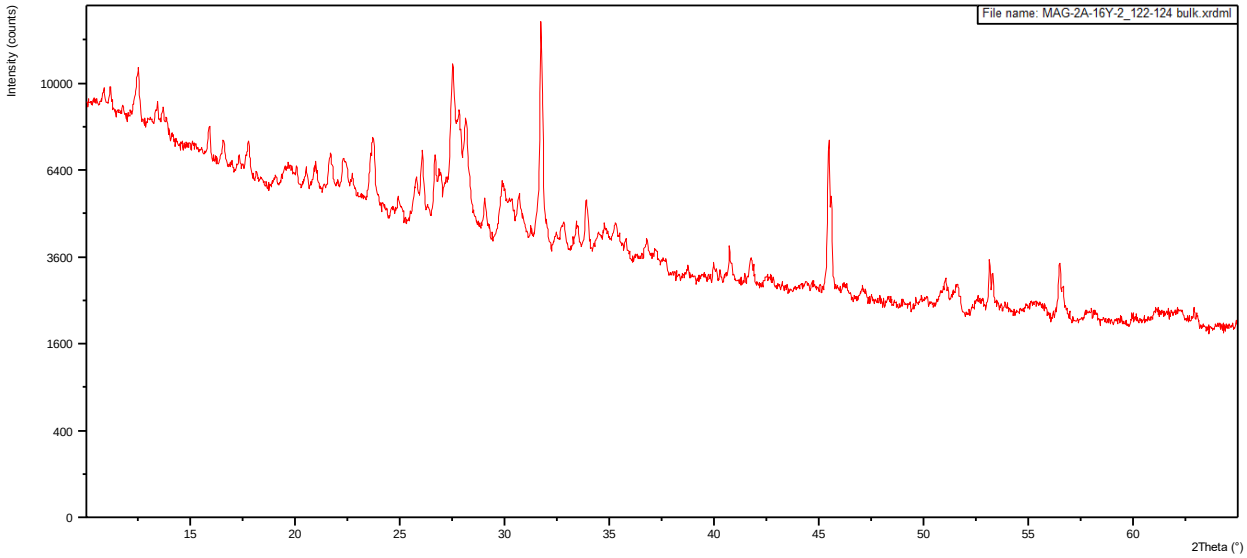
File name: MAG-2A-16Y-2_122-124 bulk.xrdml
Intensity (counts)
10000
6400
3600
1600
400
0
15
20
25
30
35
40
45
50
55
60
2Theta (°)

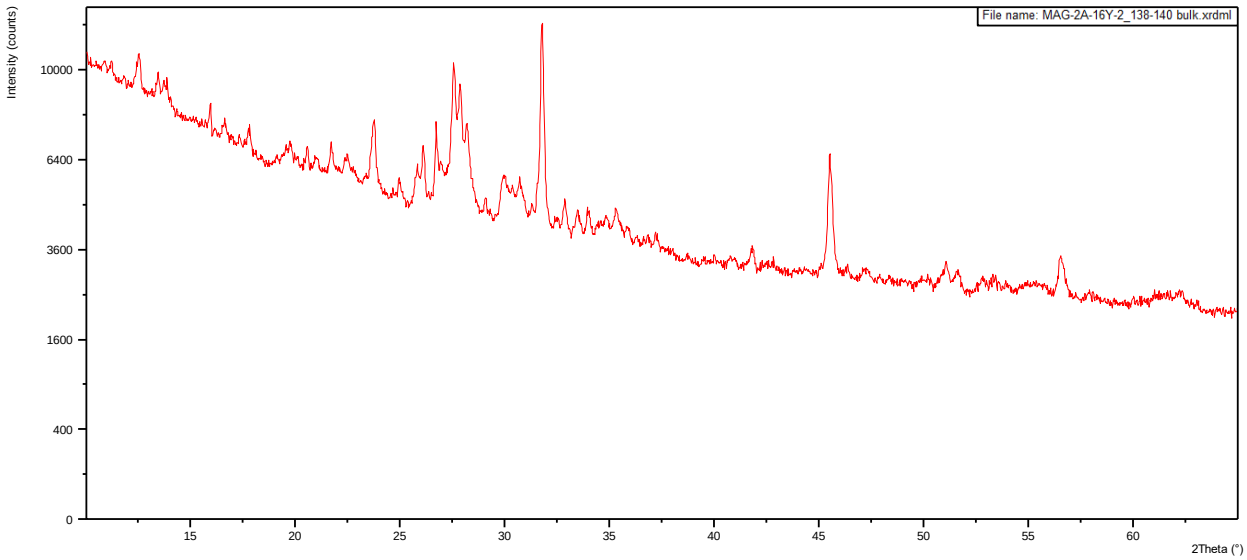
File name: MAG-2A-16Y-2_138-140 bulk.xrdml
Intensity (counts)
10000
6400
3600
1600
400
0
15
20
25
30
35
40
45
50
55
60
2Theta (°)

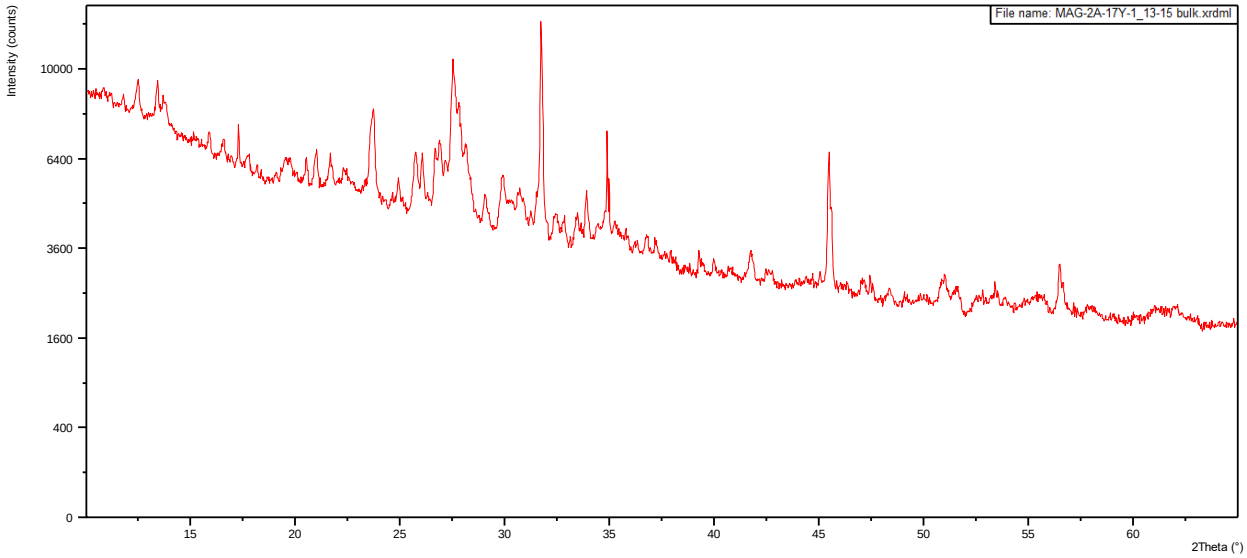
File name: MAG-2A-17Y-1_13-15 bulk.xrdml
Intensity (counts)
10000
6400
3600
1600
400
0
15
20
25
30
35
40
45
50
55
60
2Theta (°)

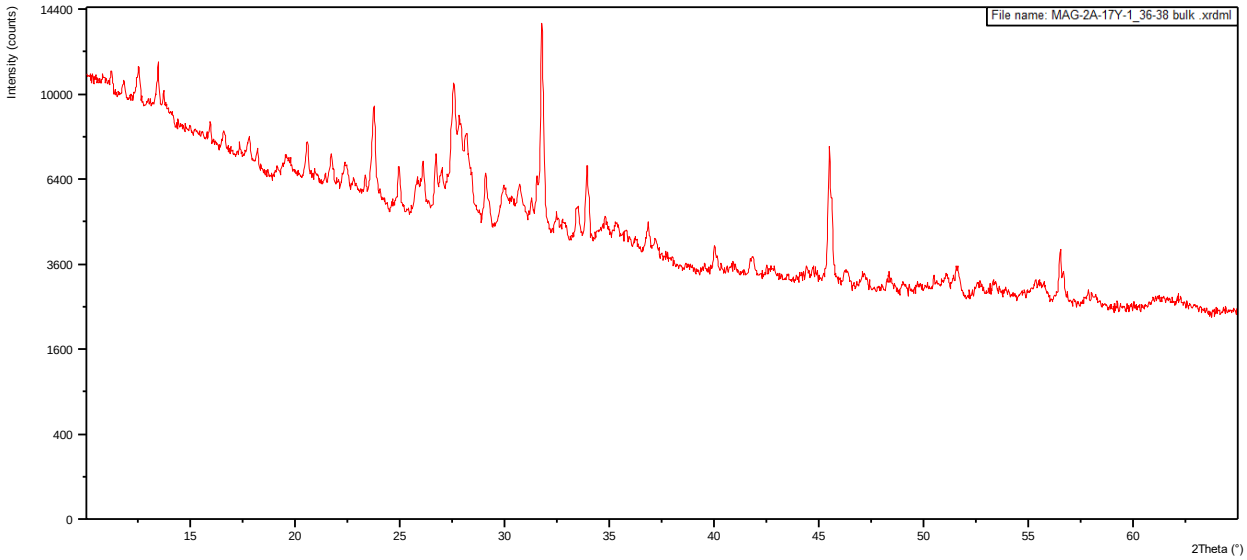
File name: MAG-2A-17Y-1_36-38 bulk .xrdml
Intensity (counts)
14400
10000
6400
3600
1600
400
0
15
20
25
30
35
40
45
50
55
60
2Theta (°)

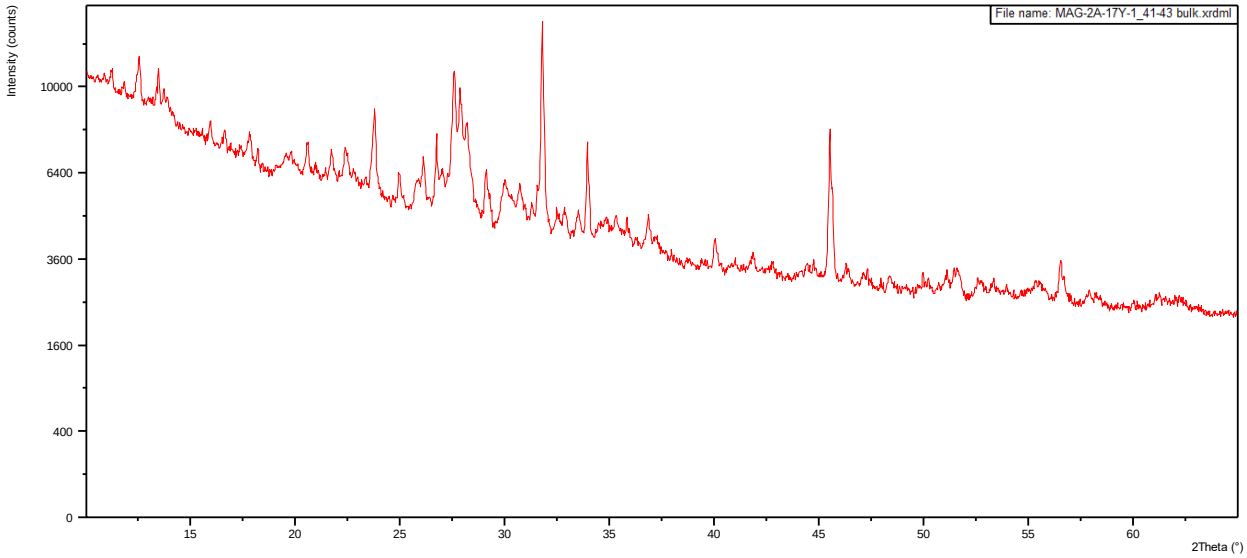
File name: MAG-2A-17Y-1_41-43 bulk.xrdml
Intensity (counts)
10000
6400
3600
1600
400
0
15
20
25
30
35
40
45
50
55
60
2Theta (°)

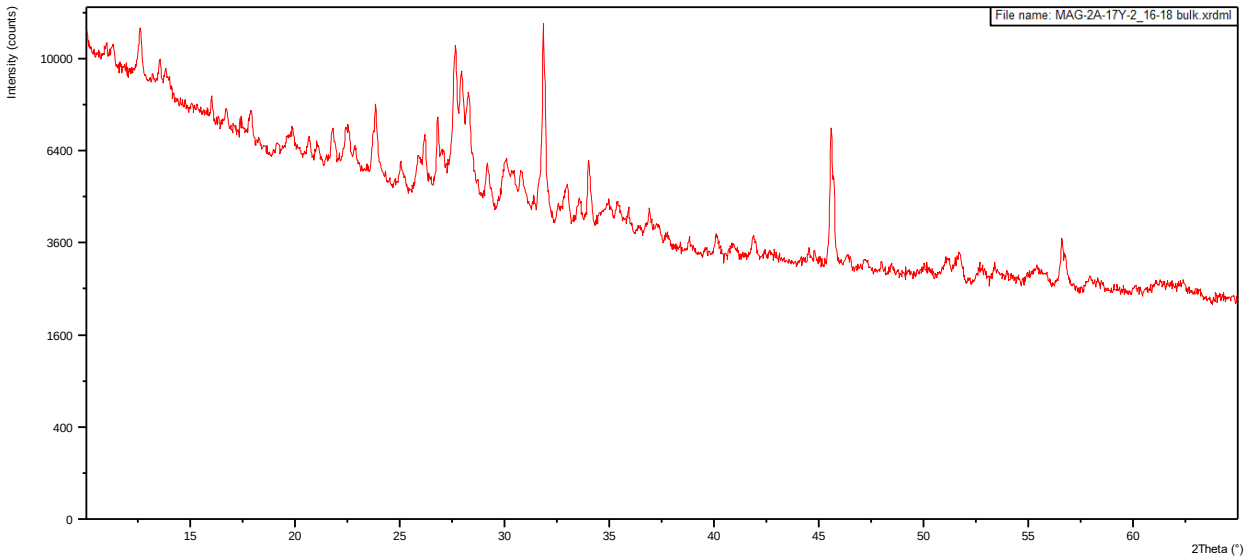
File name: MAG-2A-17Y-2_16-18 bulk.xrdml
Intensity (counts)
10000
6400
3600
1600
400
0
15
20
25
30
35
40
45
50
55
60
2Theta (°)

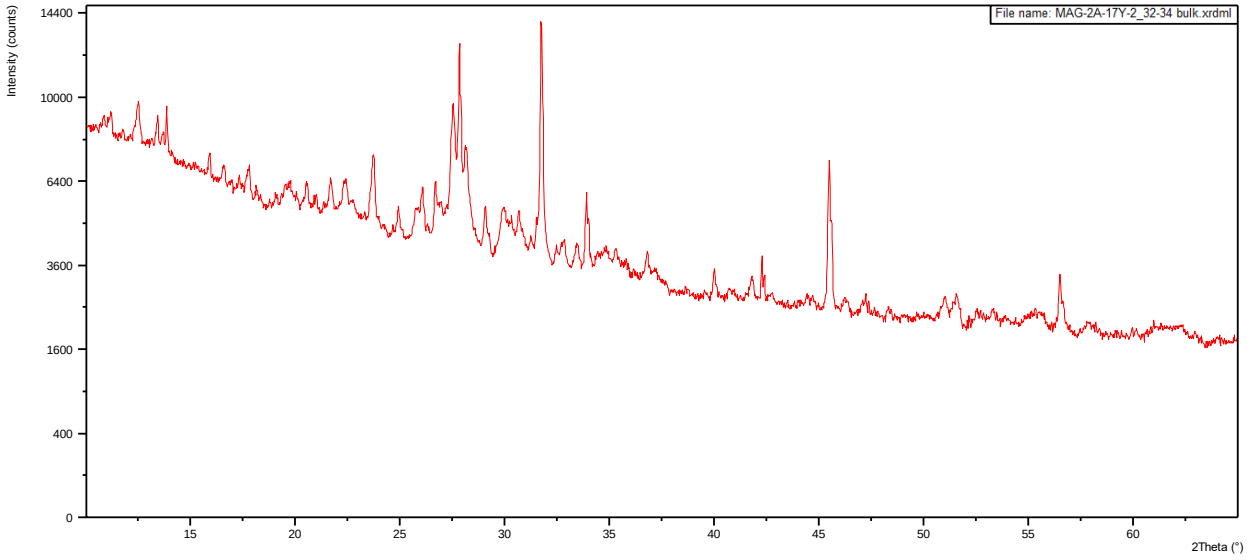
File name: MAG-2A-17Y-2_32-34 bulk.xrdml
Intensity (counts)
14400
10000
6400
3600
1600
400
0
15
20
25
30
35
40
45
50
55
60
2Theta (°)

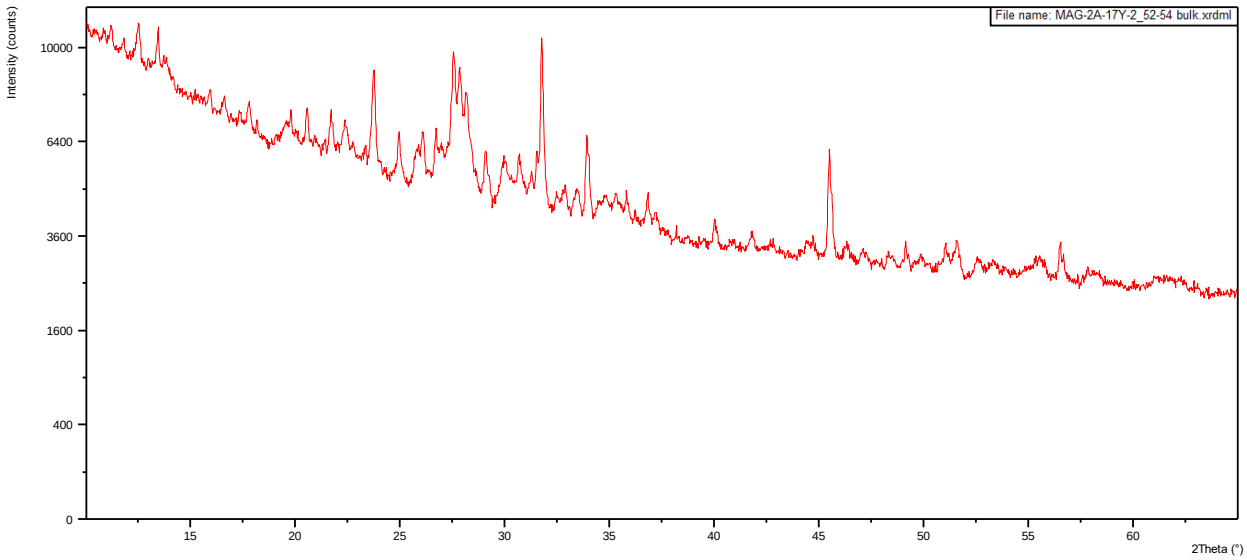
File name: MAG-2A-17Y-2_52-54 bulk.xrdml
Intensity (counts)
10000
6400
3600
1600
400
0
15
20
25
30
35
40
45
50
55
60
2Theta (°)

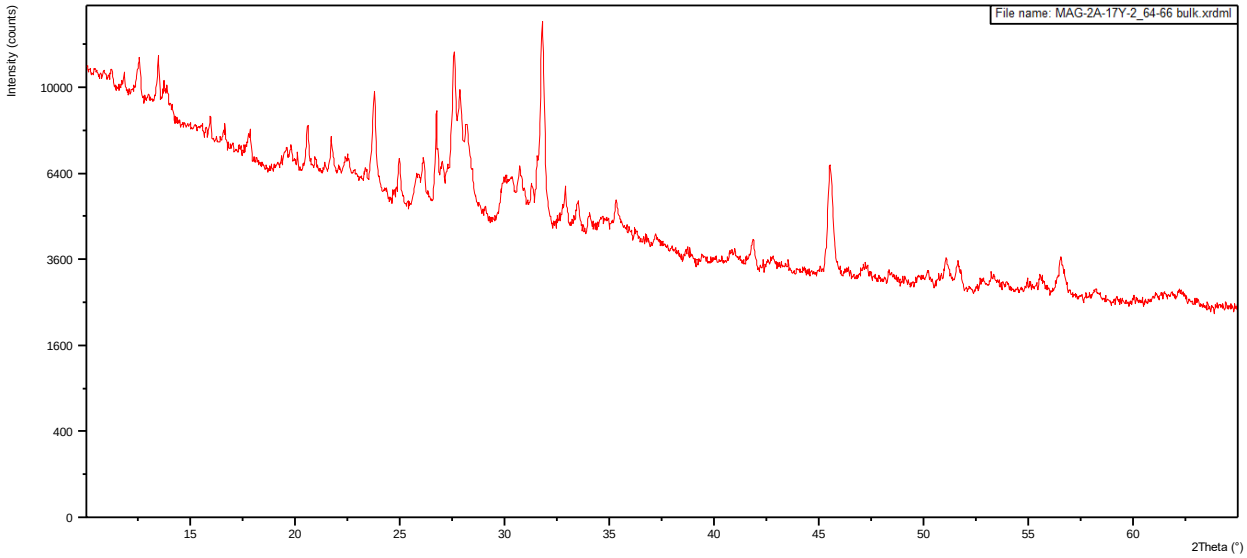
File name: MAG-2A-17Y-2_64-66 bulk.xrdml
Intensity (counts)
10000
6400
3600
1600
400
0
15
20
25
30
35
40
45
50
55
60
2Theta (°)

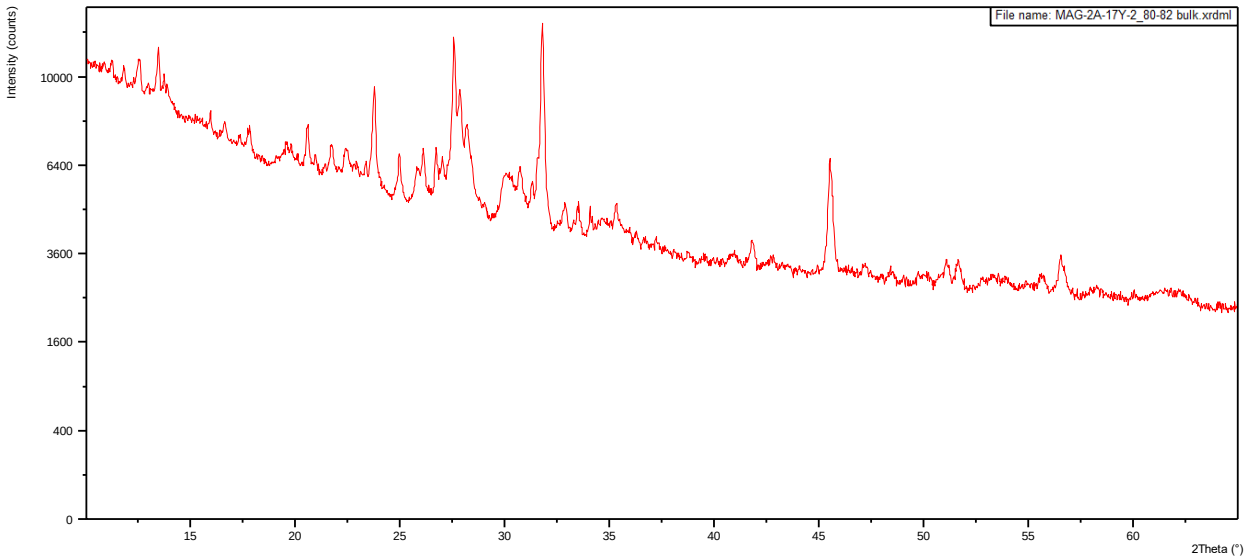
File name: MAG-2A-17Y-2_80-82 bulk.xrdml
Intensity (counts)
10000
6400
3600
1600
400
0
15
20
25
30
35
40
45
50
55
60
2Theta (°)

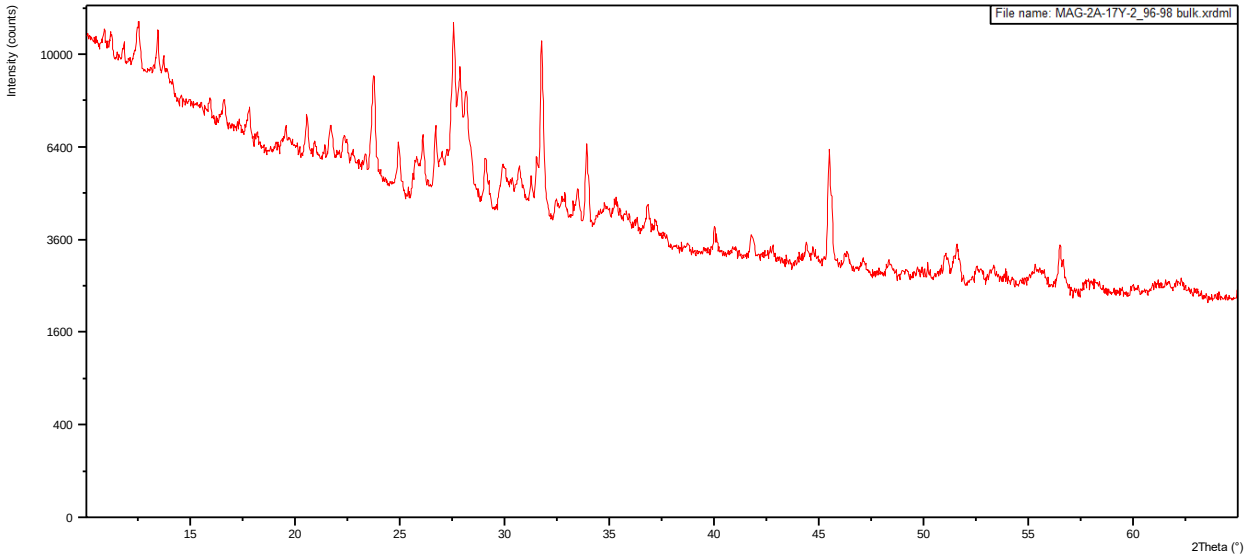
File name: MAG-2A-17Y-2_96-98 bulk.xrdml
Intensity (counts)
10000
6400
3600
1600
400
0
15
20
25
30
35
40
45
50
55
60
2Theta (°)

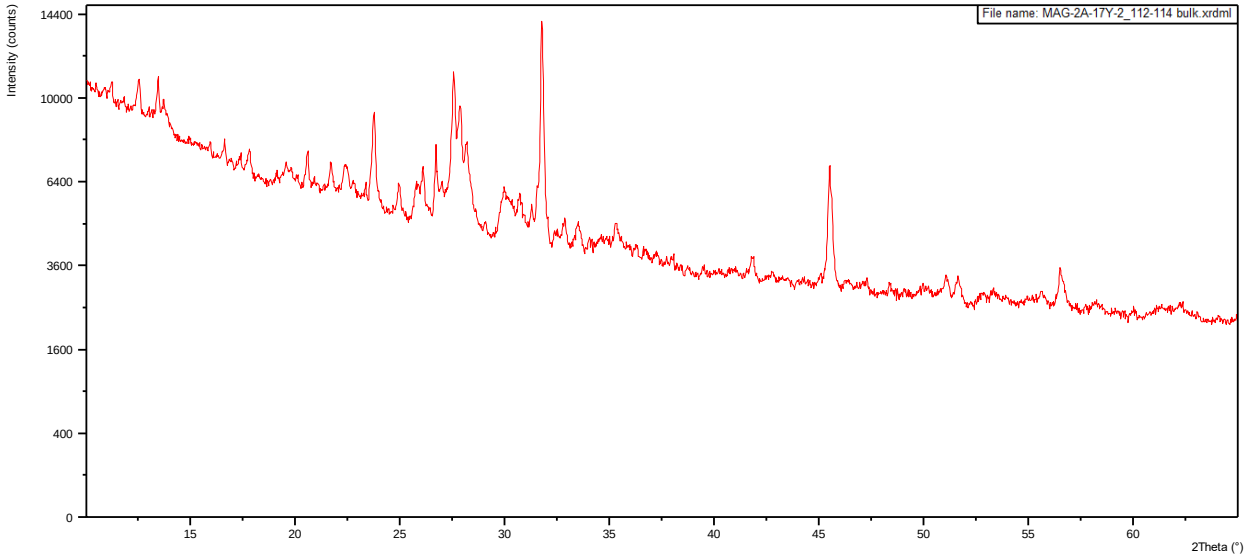
File name: MAG-2A-17Y-2_112-114 bulk.xrdml
Intensity (counts)
14400
10000
6400
3600
1600
400
0
15
20
25
30
35
40
45
50
55
60
2Theta (°)

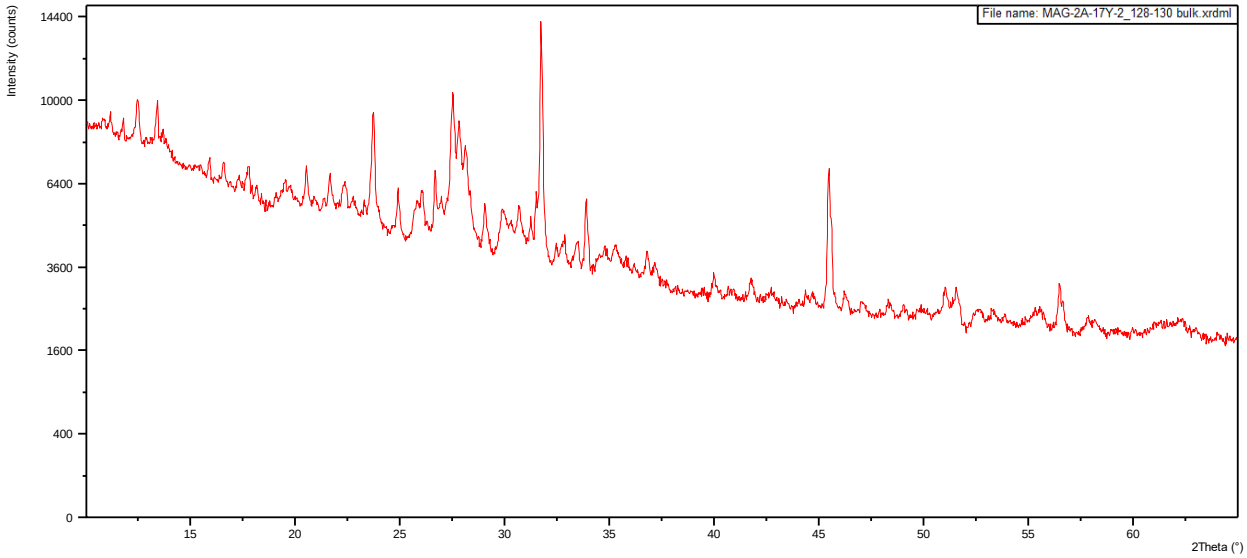
File name: MAG-2A-17Y-2_128-130 bulk.xrdml
Intensity (counts)
14400
10000
6400
3600
1600
400
0
15
20
25
30
35
40
45
50
55
60
2Theta (°)

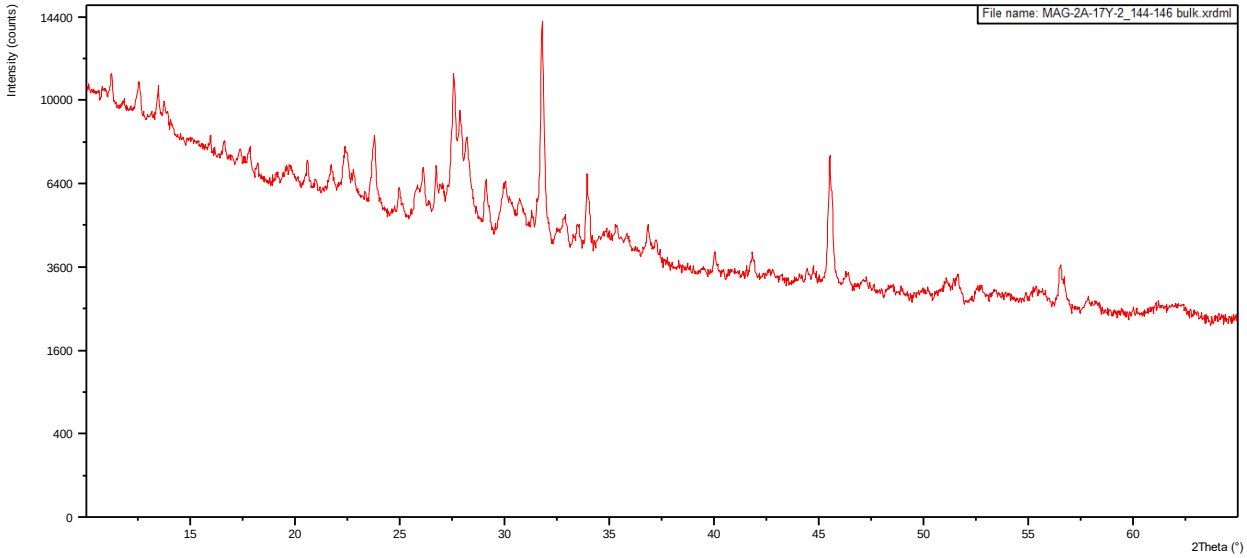
File name: MAG-2A-17Y-2_144-146 bulk.xrdml
Intensity (counts)
14400
10000
6400
3600
1600
400
0
15
20
25
30
35
40
45
50
55
60
2Theta (°)

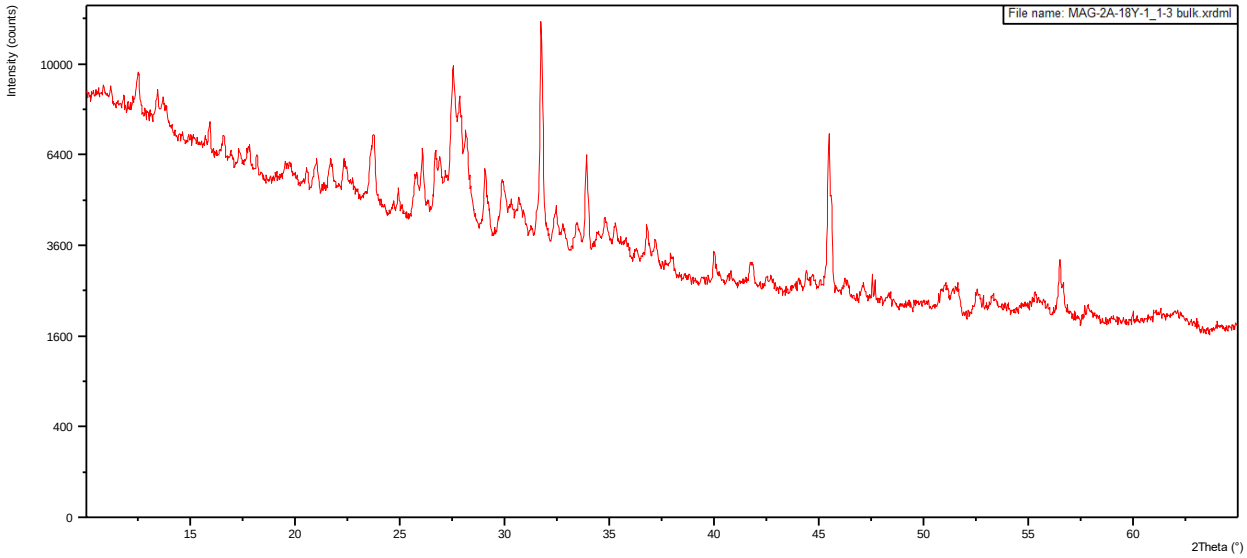
File name: MAG-2A-18Y-1_1-3 bulk.xrdml
Intensity (counts)
10000
6400
3600
1600
400
0
15
20
25
30
35
40
45
50
55
60
2Theta (°)

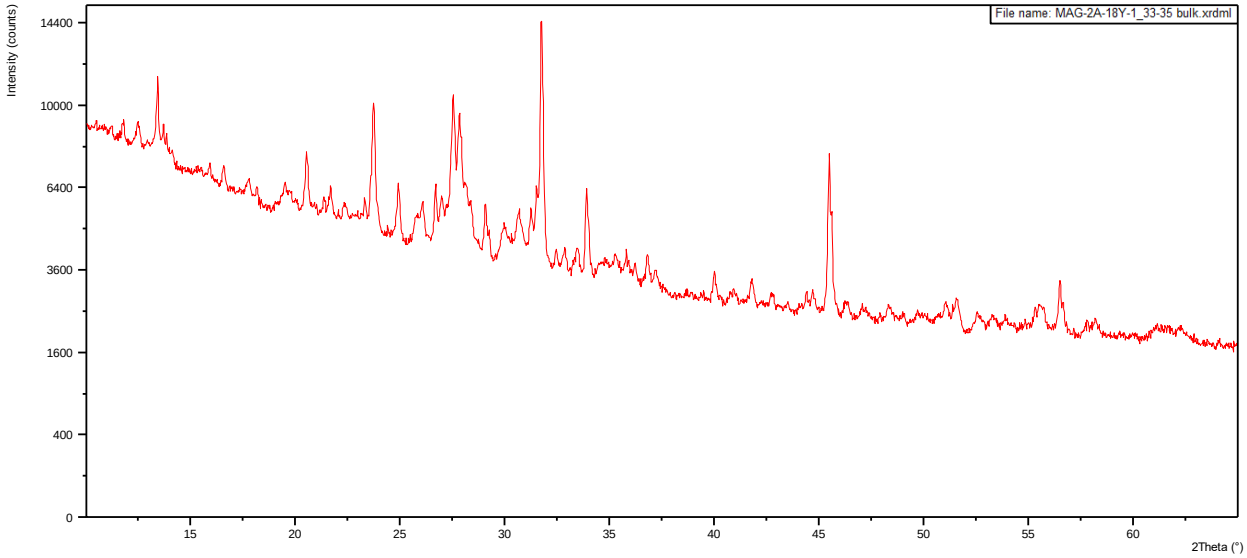
File name: MAG-2A-18Y-1_33-35 bulk.xrdml
Intensity (counts)
14400
10000
6400
3600
1600
400
0
15
20
25
30
35
40
45
50
55
60
2Theta (°)

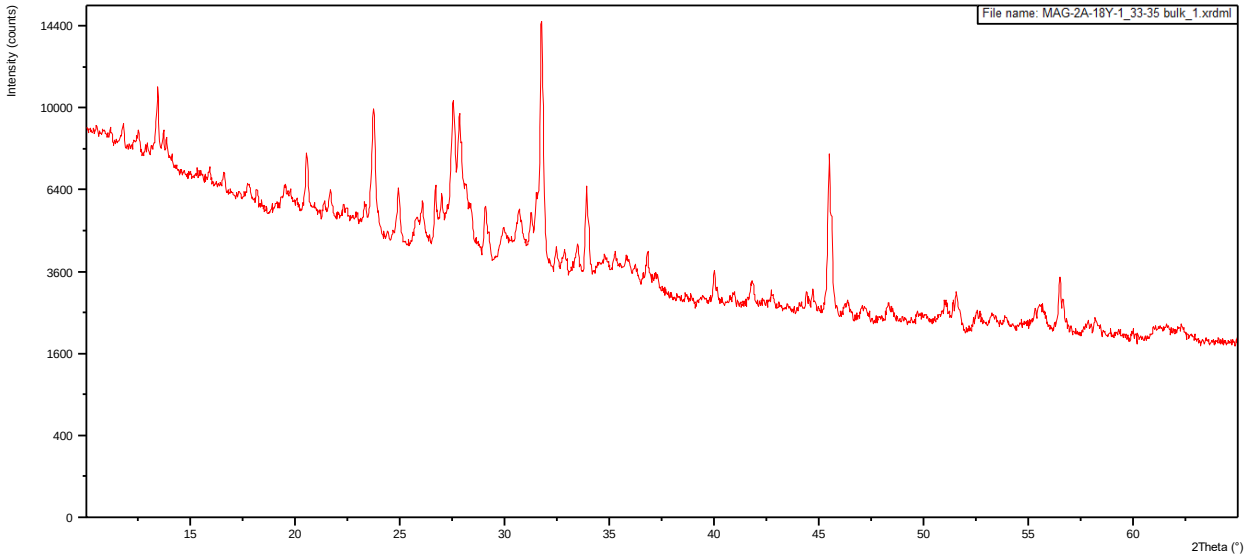
File name: MAG-2A-18Y-1_33-35 bulk_1.xrdml
Intensity (counts)
14400
10000
6400
3600
1600
400
0
15
20
25
30
35
40
45
50
55
60
2Theta (°)

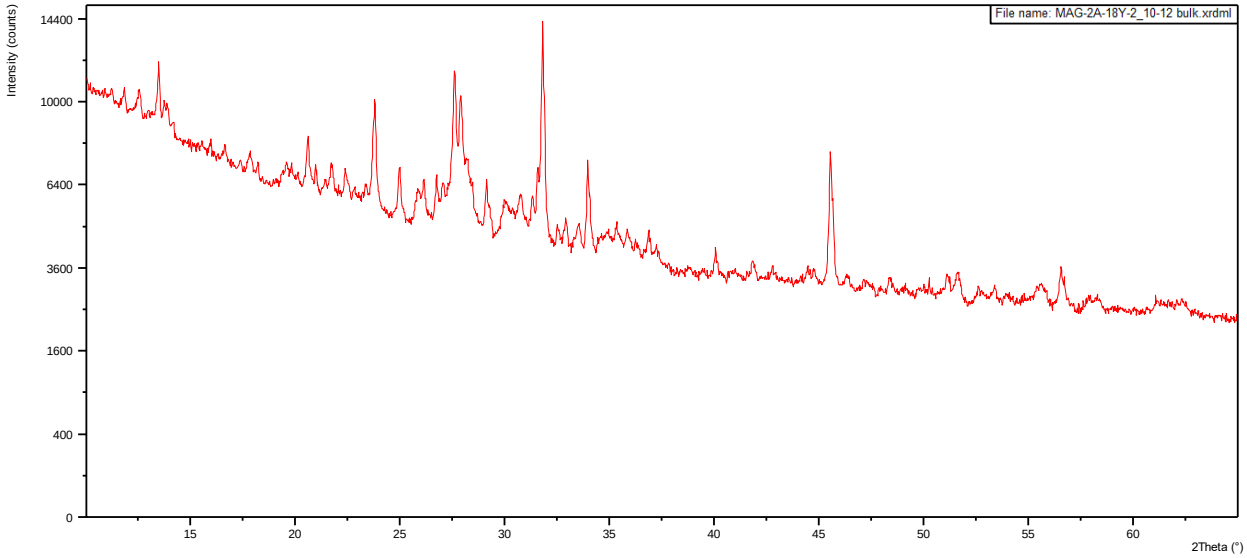
File name: MAG-2A-18Y-2_10-12 bulk.xrdml
Intensity (counts)
14400
10000
6400
3600
1600
400
0
15
20
25
30
35
40
45
50
55
60
2Theta (°)

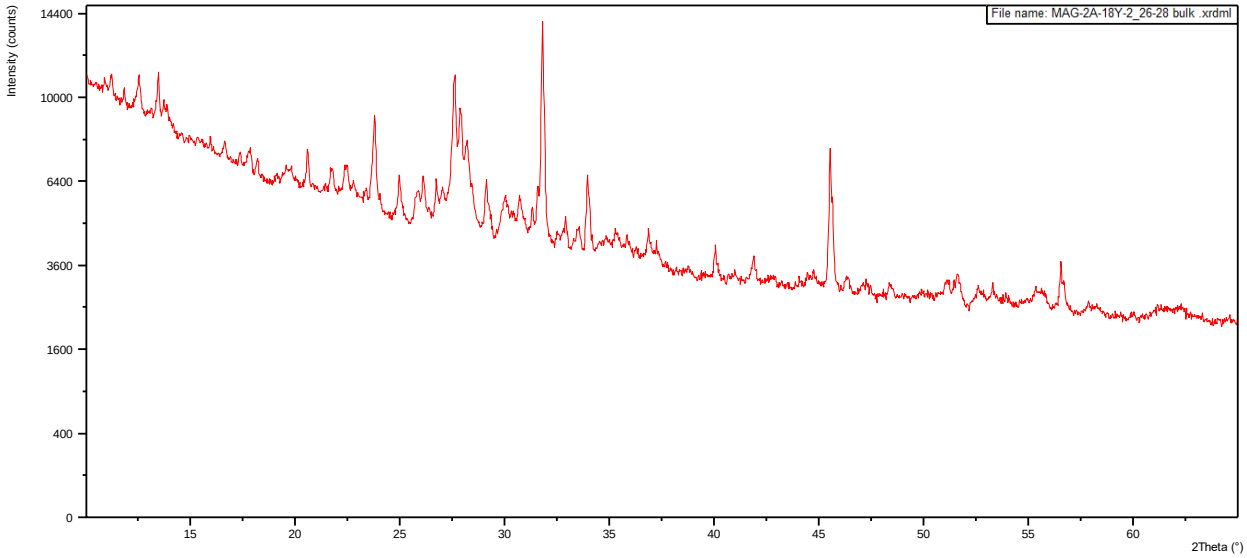
File name: MAG-2A-18Y-2_26-28 bulk .xrdml
Intensity (counts)
14400
10000
6400
3600
1600
400
0
15
20
25
30
35
40
45
50
55
60
2Theta (°)

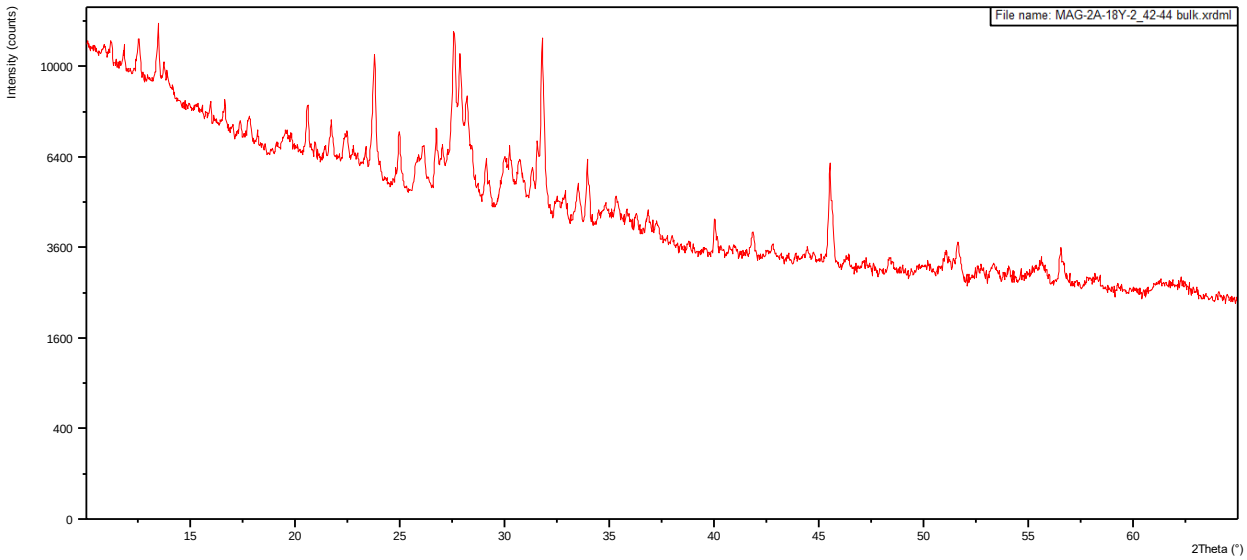
File name: MAG-2A-18Y-2_42-44 bulk.xrdml
Intensity (counts)
10000
6400
3600
1600
400
0
15
20
25
30
35
40
45
50
55
60
2Theta (°)

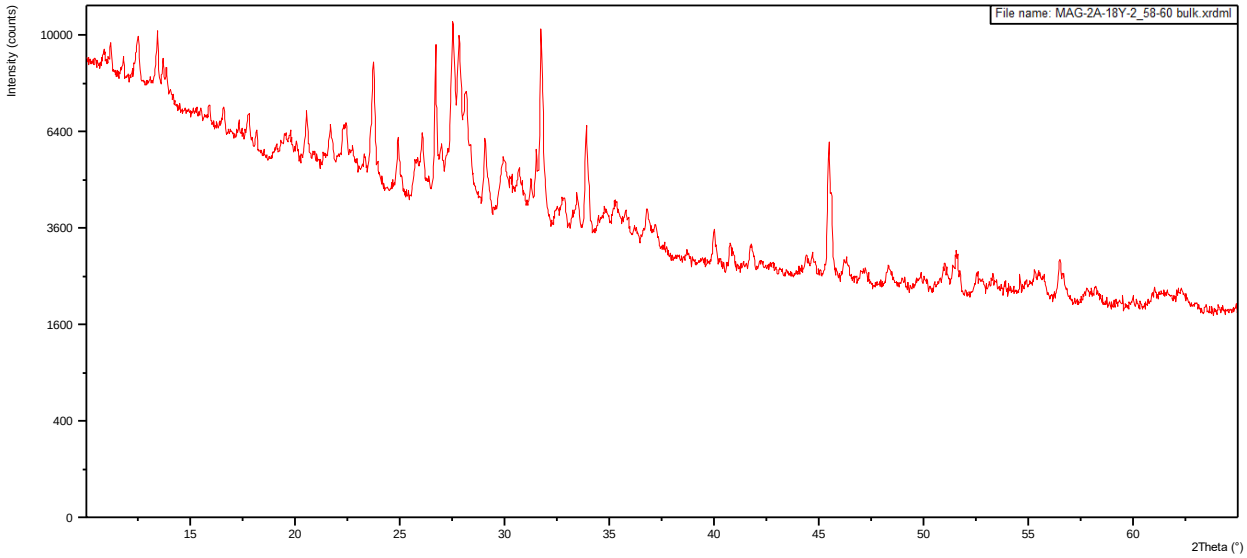
File name: MAG-2A-18Y-2_58-60 bulk.xrdml
Intensity (counts)
10000
6400
3600
1600
400
0
15
20
25
30
35
40
45
50
55
60
2Theta (°)

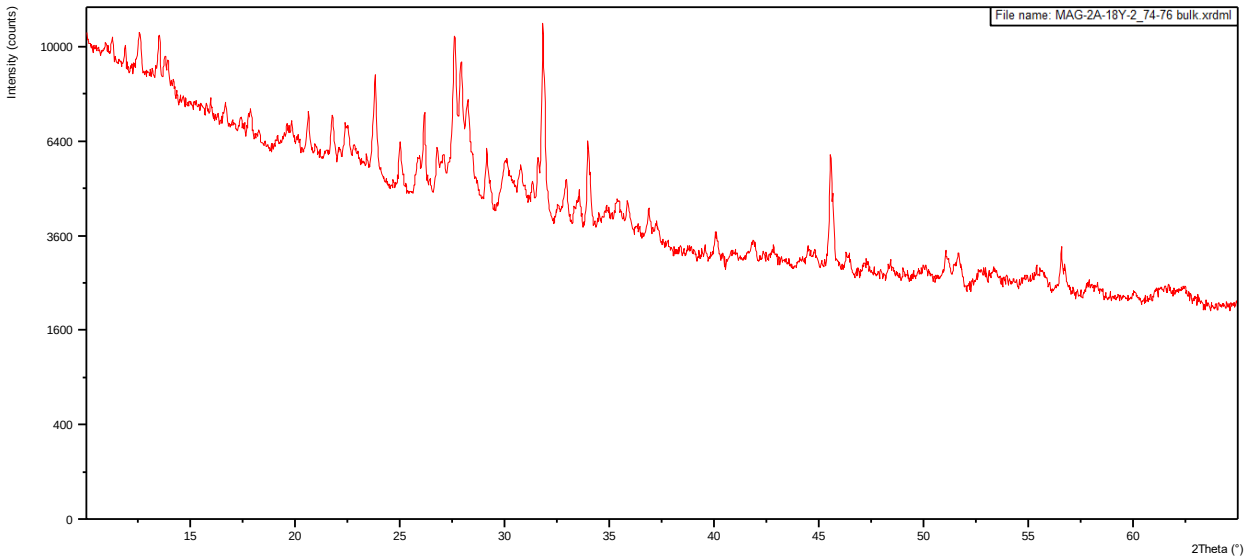
File name: MAG-2A-18Y-2_74-76 bulk.xrdml
Intensity (counts)
10000
6400
3600
1600
400
0
15
20
25
30
35
40
45
50
55
60
2Theta (°)

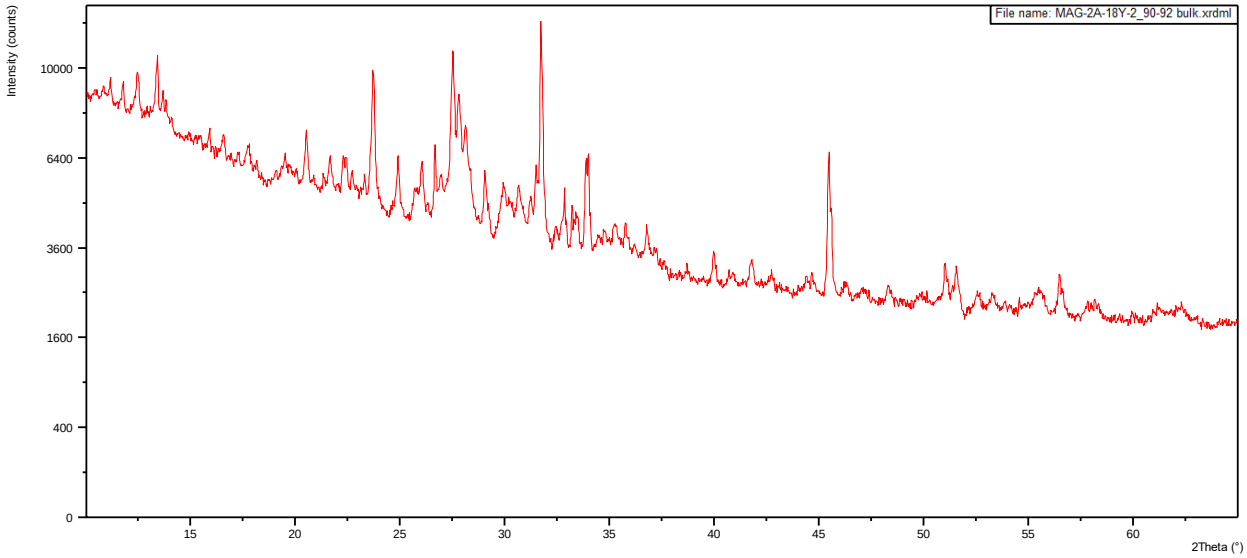
File name: MAG-2A-18Y-2_90-92 bulk.xrdml
Intensity (counts)
10000
6400
3600
1600
400
0
15
20
25
30
35
40
45
50
55
60
2Theta (°)

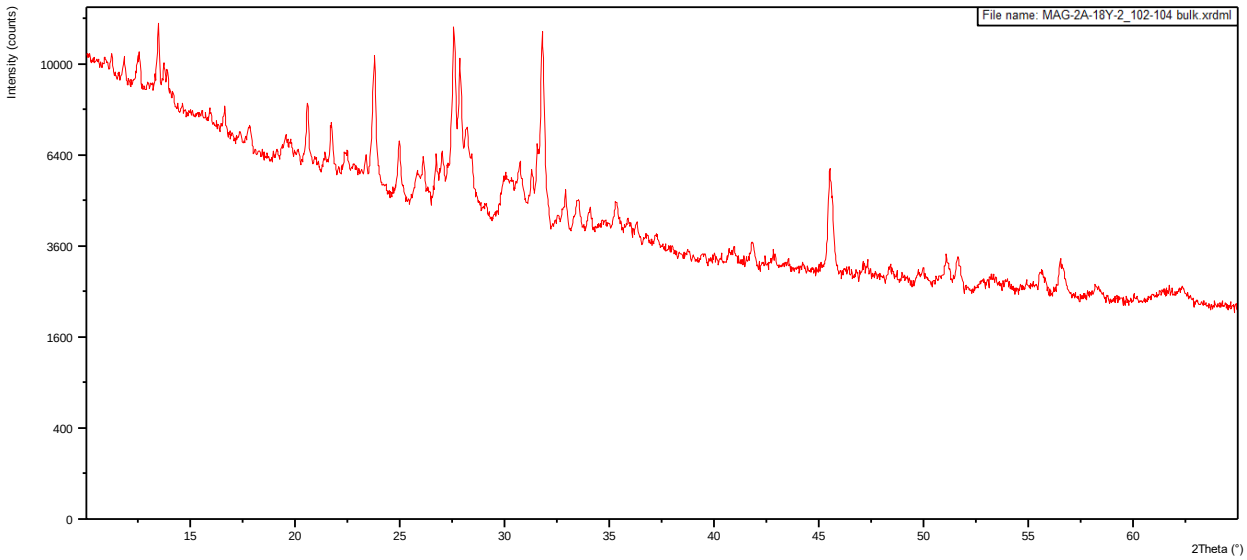
File name: MAG-2A-18Y-2_102-104 bulk.xrdml
Intensity (counts)
10000
6400
3600
1600
400
0
15
20
25
30
35
40
45
50
55
60
2Theta (°)

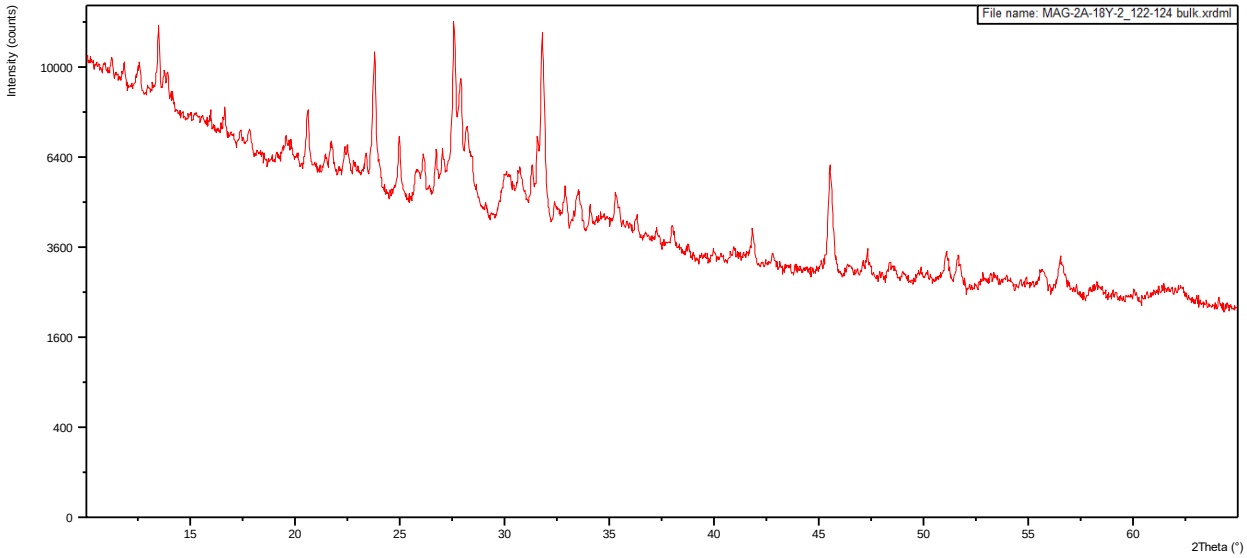
File name: MAG-2A-18Y-2_122-124 bulk.xrdml
Intensity (counts)
10000
6400
3600
1600
400
0
15
20
25
30
35
40
45
50
55
60
2Theta (°)

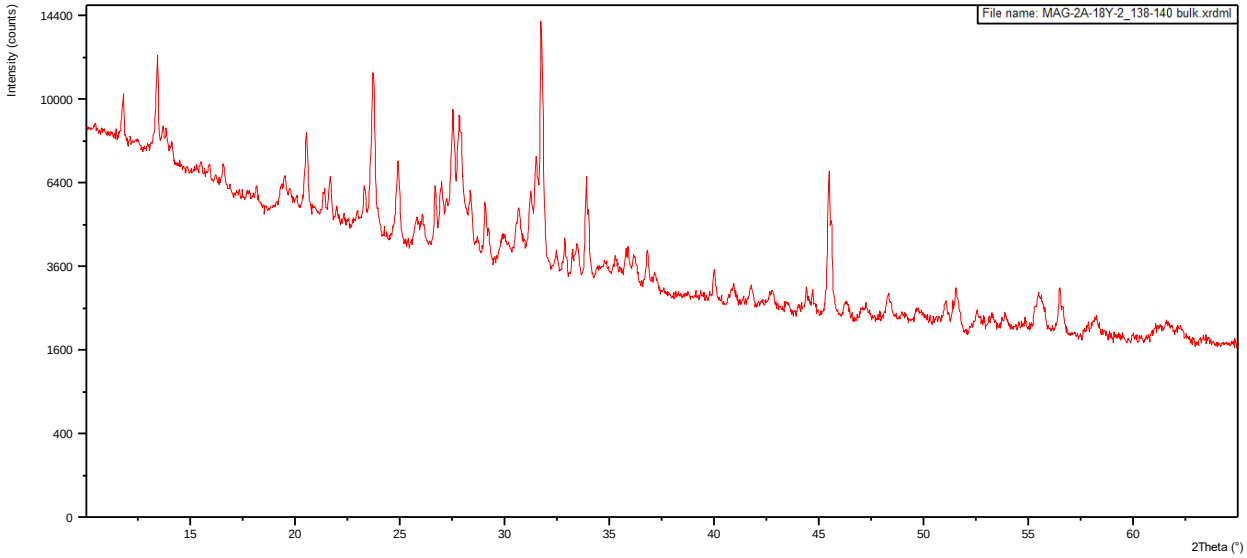
File name: MAG-2A-18Y-2_138-140 bulk.xrdml
Intensity (counts)
14400
10000
6400
3600
1600
400
0
15
20
25
30
35
40
45
50
55
60
2Theta (°)

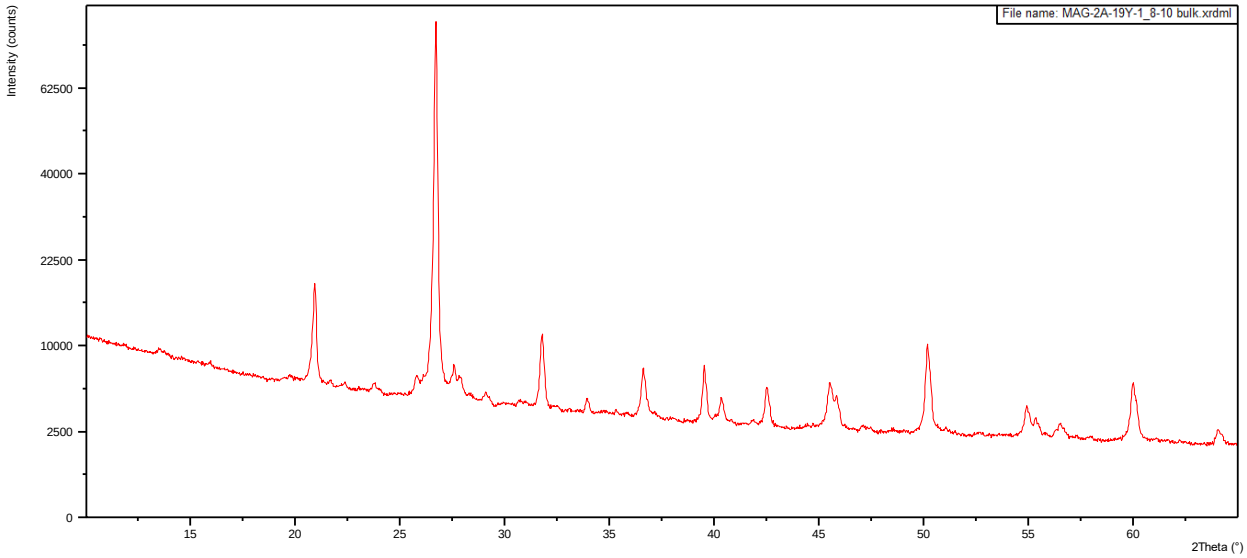
File name: MAG-2A-19Y-1_8-10 bulk.xrdml
Intensity (counts)
62500
40000
22500
10000
2500
0
15
20
25
30
35
40
45
50
55
60
2Theta (°)

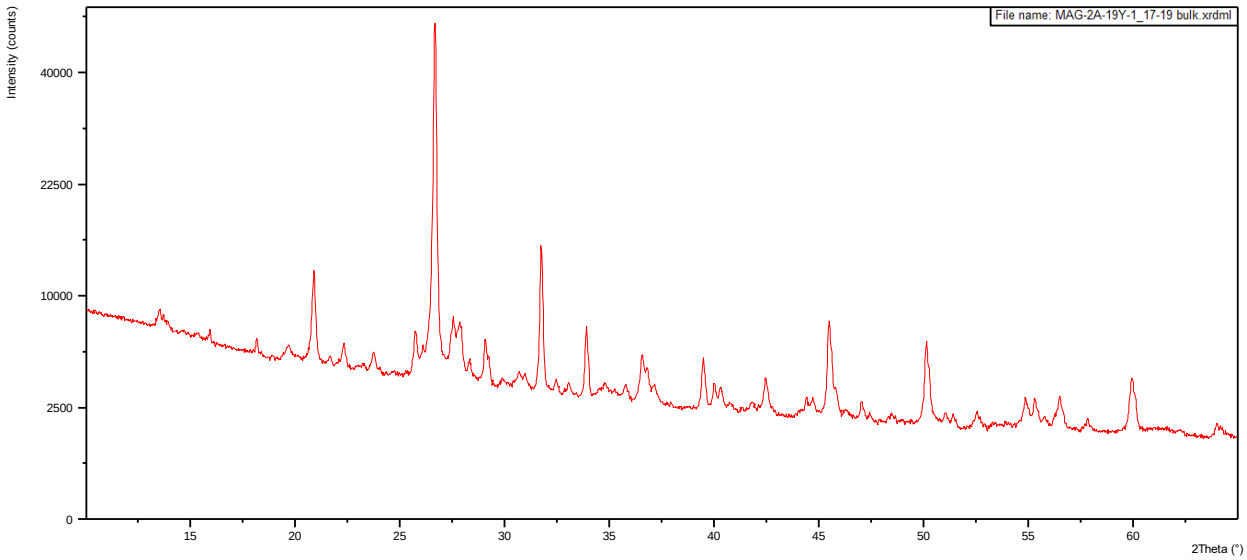
File name: MAG-2A-19Y-1_17-19 bulk.xrdml
Intensity (counts)
40000
22500
10000
2500
0
15
20
25
30
35
40
45
50
55
60
2Theta (°)

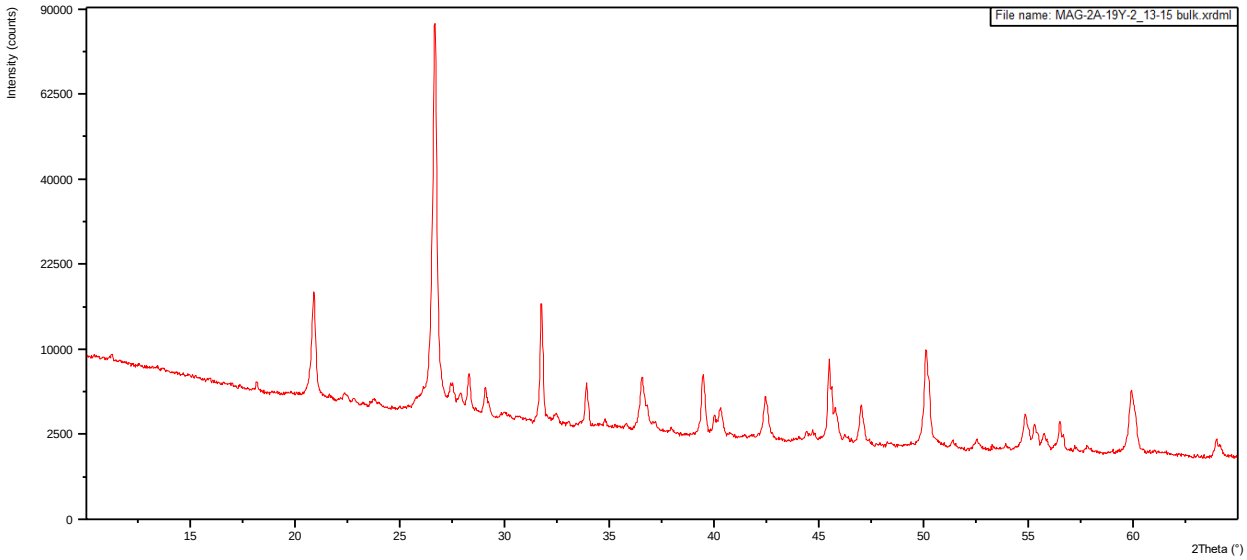
File name: MAG-2A-19Y-2_13-15 bulk.xrdml
Intensity (counts)
90000
62500
40000
22500
10000
2500
0
15
20
25
30
35
40
45
50
55
60
2Theta (°)

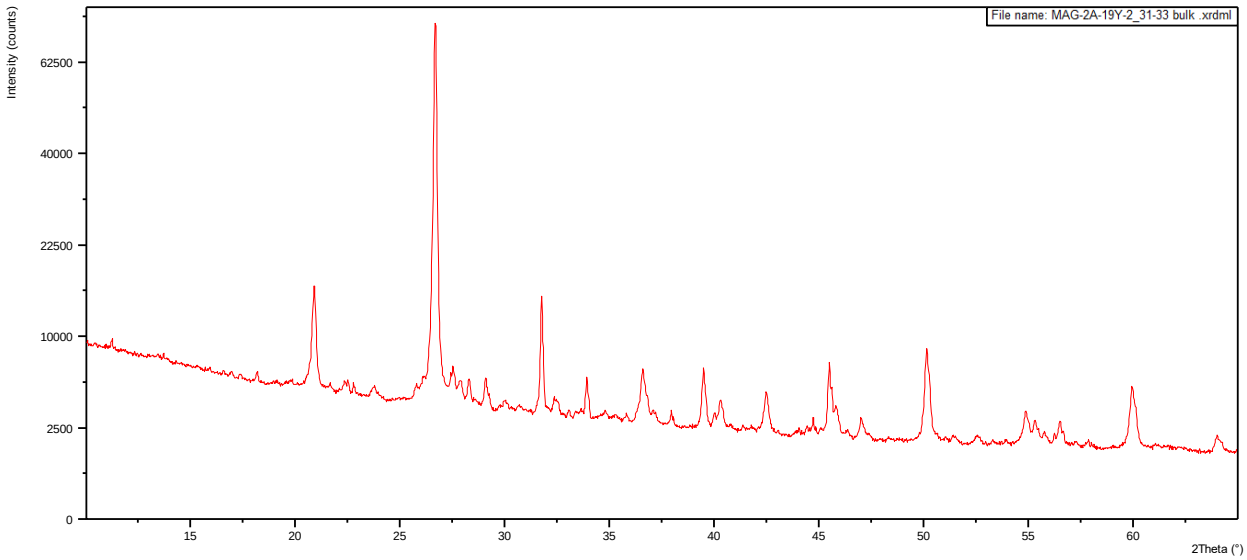
File name: MAG-2A-19Y-2_31-33 bulk .xrdml
Intensity (counts)
62500
40000
22500
10000
2500
0
15
20
25
30
35
40
45
50
55
60
2Theta (°)

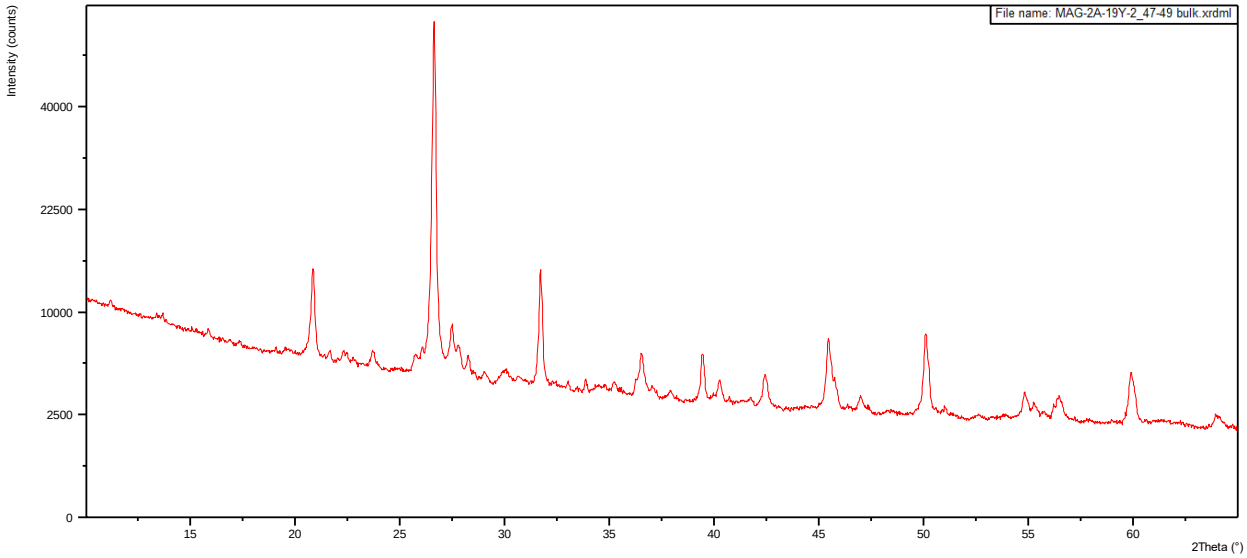
File name: MAG-2A-19Y-2_47-49 bulk.xrdml
Intensity (counts)
40000
22500
10000
2500
0
15
20
25
30
35
40
45
50
55
60
2Theta (°)

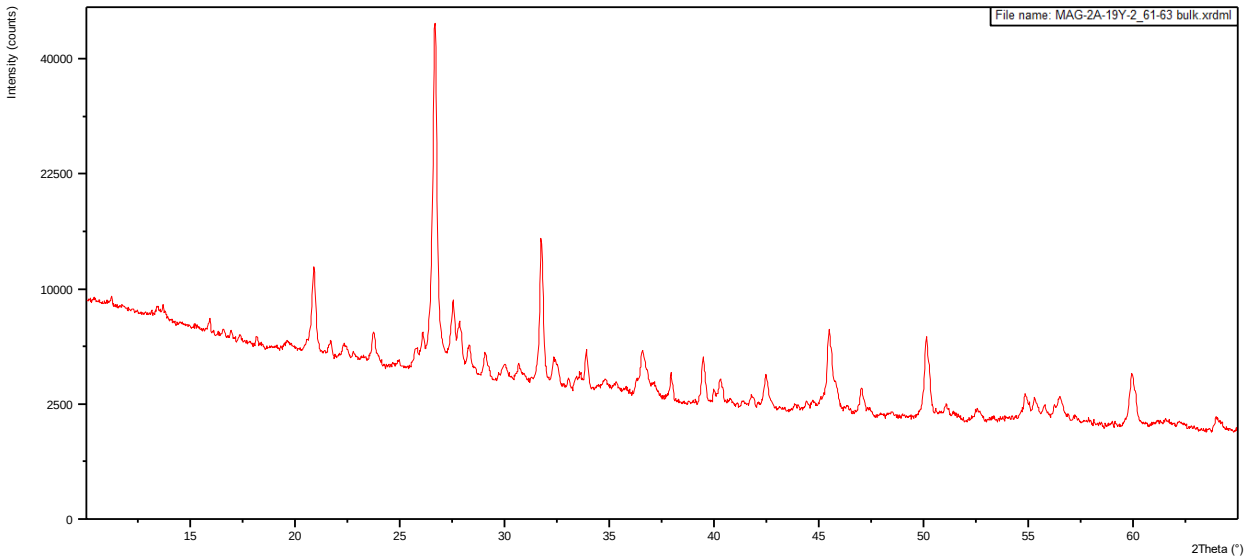
File name: MAG-2A-19Y-2_61-63 bulk.xrdml
Intensity (counts)
40000
22500
10000
2500
0
15
20
25
30
35
40
45
50
55
60
2Theta (°)

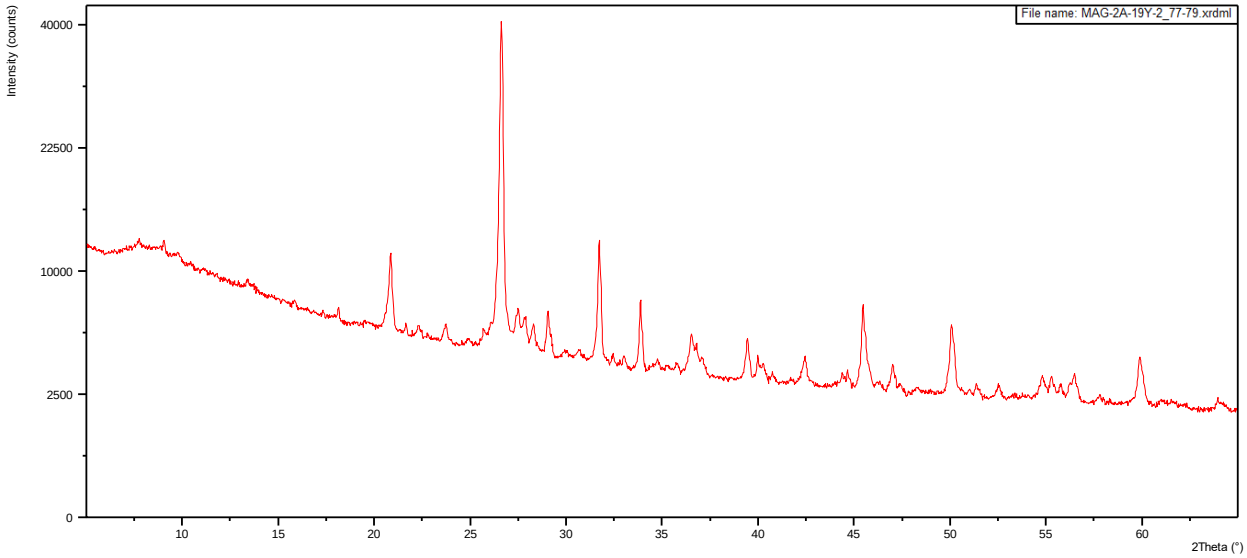
File name: MAG-2A-19Y-2_77-79.xrdml
Intensity (counts)
40000
22500
10000
2500
0
10
15
20
25
30
35
40
45
50
55
60
2Theta (°)

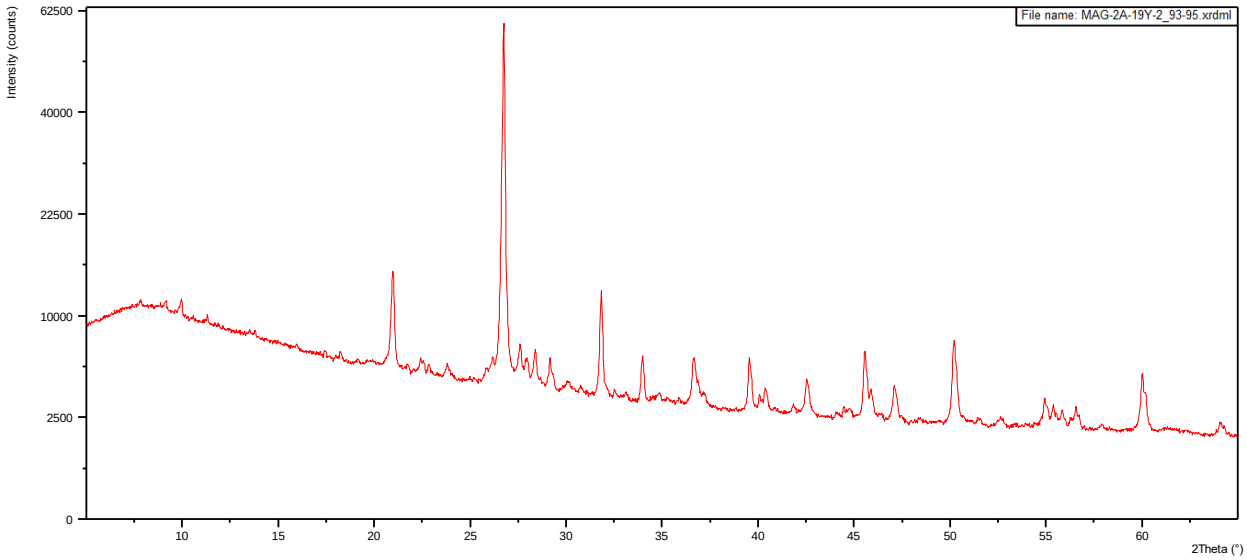
File name: MAG-2A-19Y-2_93-95.xrdml
Intensity (counts)
62500
40000
22500
10000
2500
0
10
15
20
25
30
35
40
45
50
55
60
2Theta (°)

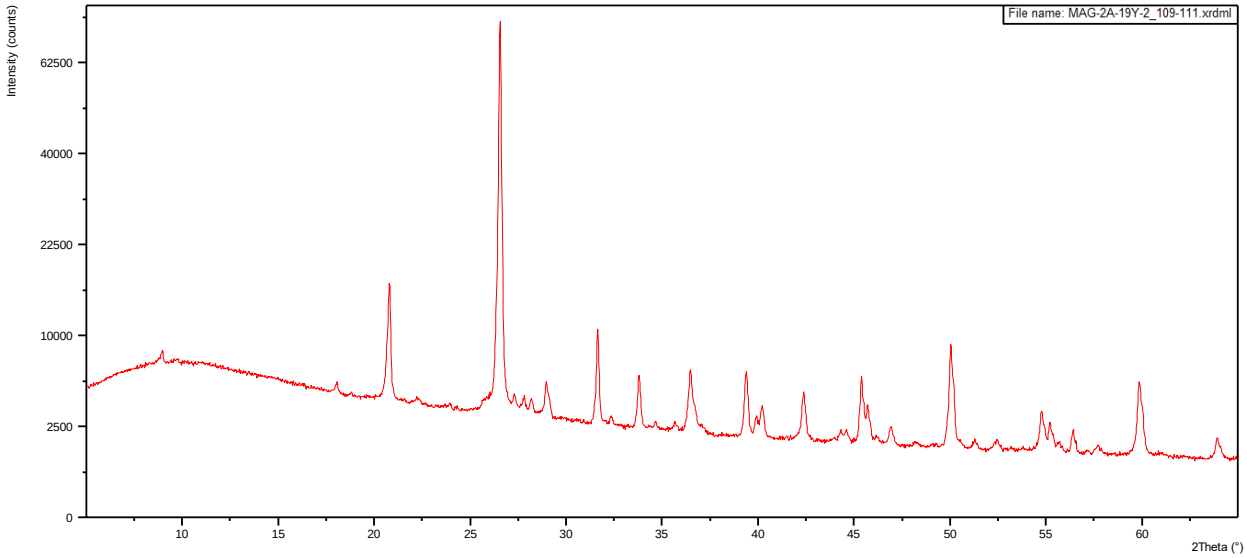
File name: MAG-2A-19Y-2_109-111.xrdml
Intensity (counts)
62500
40000
22500
10000
2500
0
10
15
20
25
30
35
40
45
50
55
60
2Theta (°)

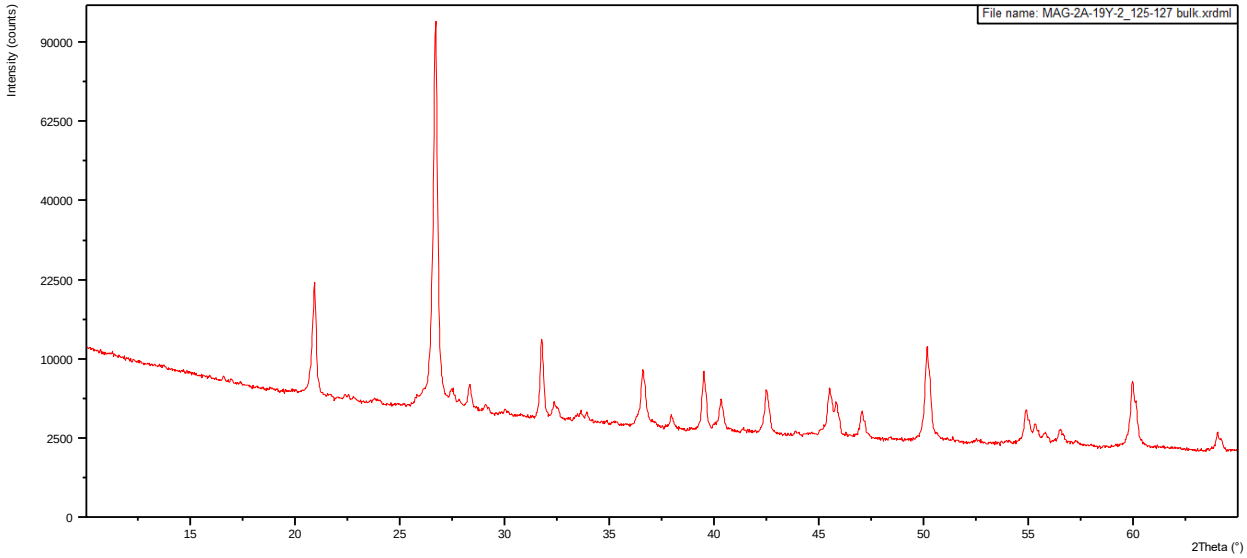
File name: MAG-2A-19Y-2_125-127 bulk.xrdml
Intensity (counts)
90000
62500
40000
22500
10000
2500
0
15
20
25
30
35
40
45
50
55
60
2Theta (°)

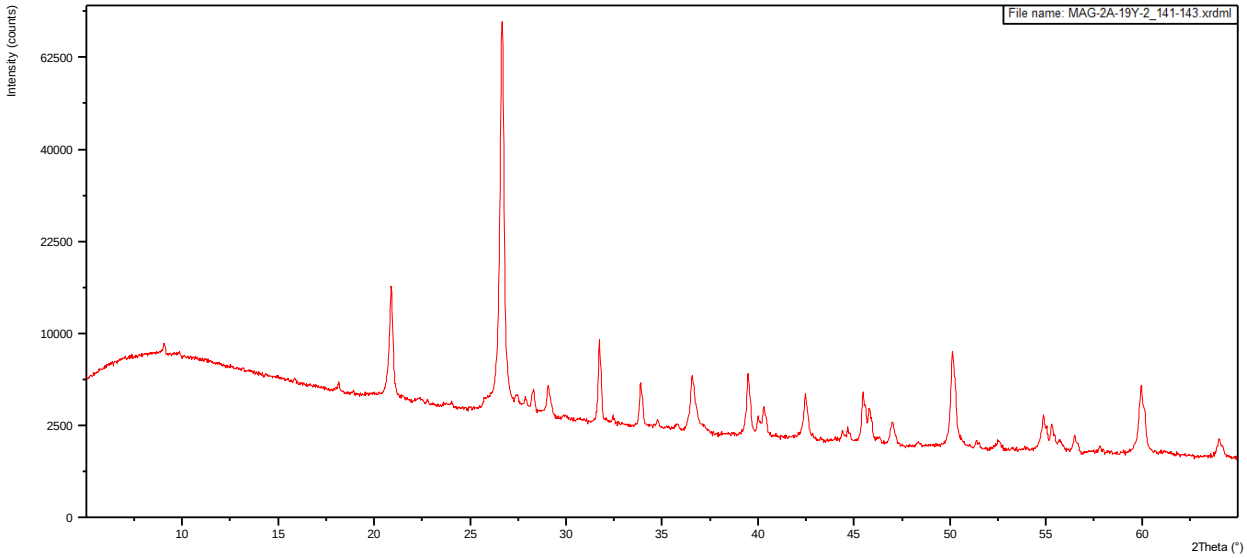
File name: MAG-2A-19Y-2_141-143.xrdml
Intensity (counts)
62500
40000
22500
10000
2500
0
10
15
20
25
30
35
40
45
50
55
60
2Theta (°)

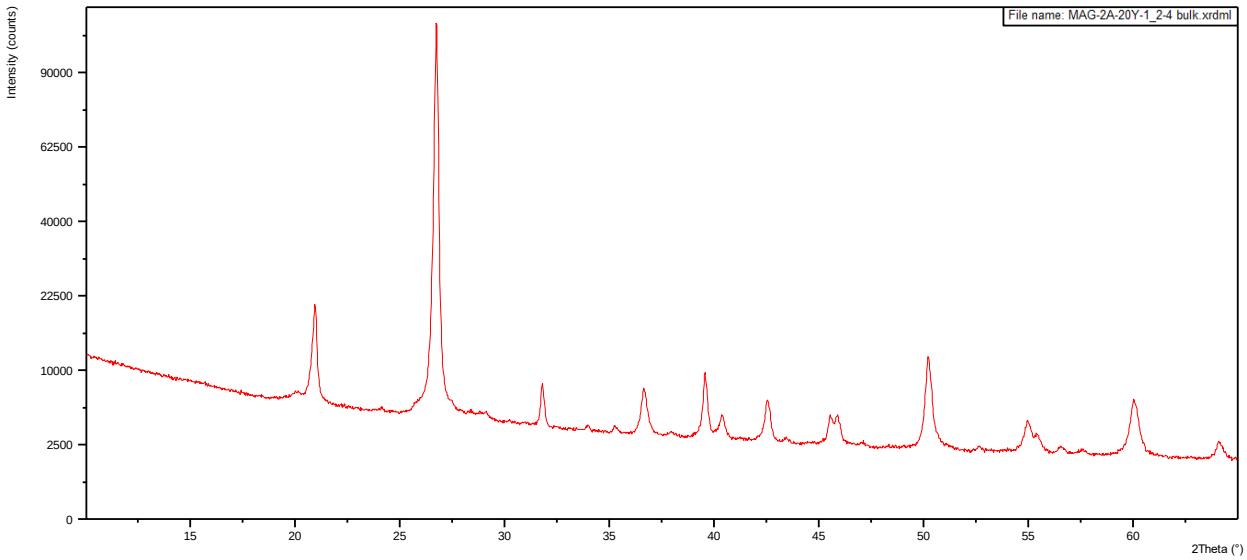
File name: MAG-2A-20Y-1_2-4 bulk.xrdml
Intensity (counts)
90000
62500
40000
22500
10000
2500
0
15
20
25
30
35
40
45
50
55
60
2Theta (°)

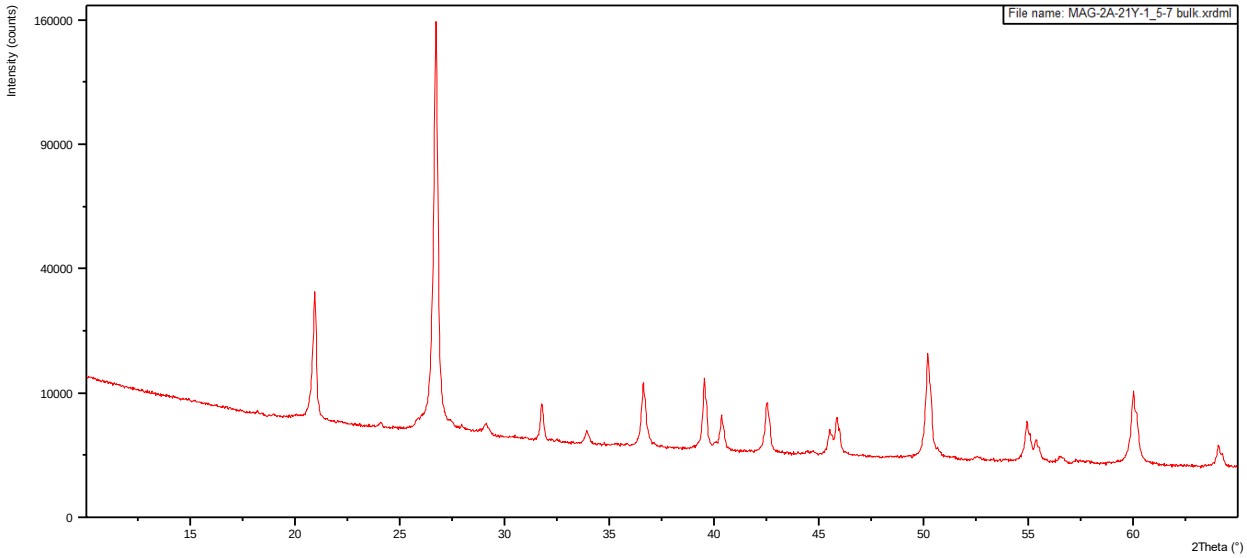
File name: MAG-2A-21Y-1_5-7 bulk.xrdml
Intensity (counts)
160000
90000
40000
10000
0
15
20
25
30
35
40
45
50
55
60
2Theta (°)

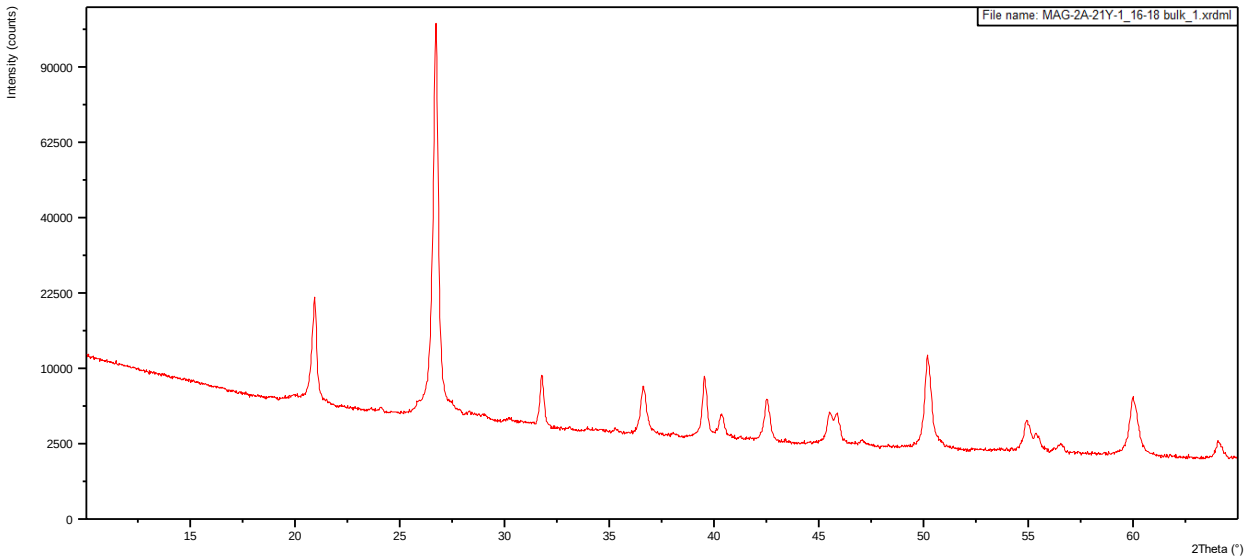
File name: MAG-2A-21Y-1_16-18 bulk_1.xrdml
Intensity (counts)
90000
62500
40000
22500
10000
2500
0
15
20
25
30
35
40
45
50
55
60
2Theta (°)

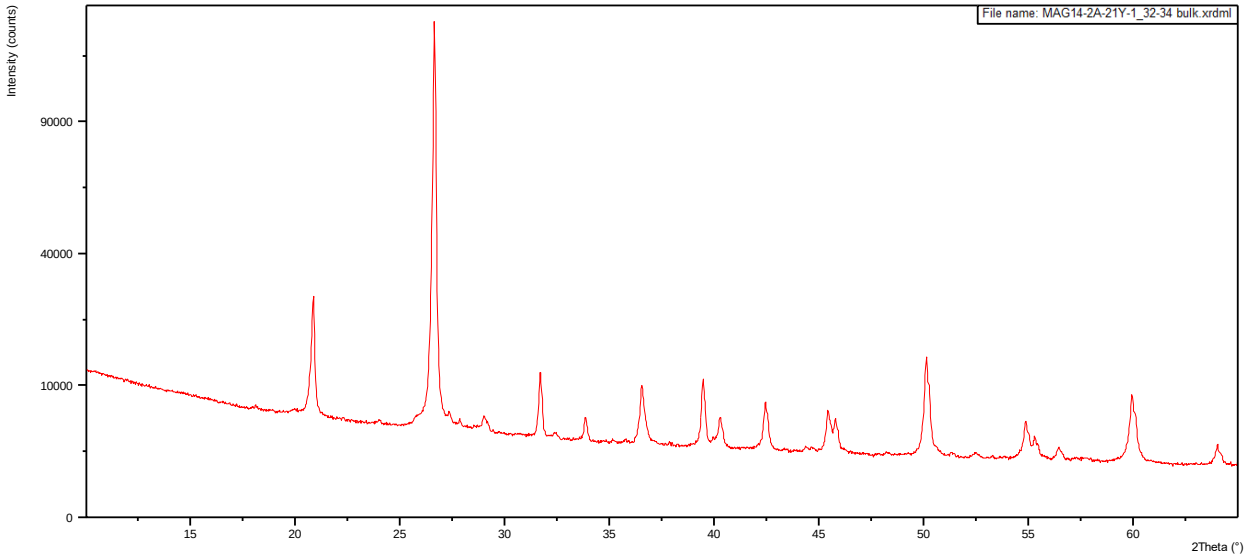
File name: MAG14-2A-21Y-1_32-34 bulk.xrdml
Intensity (counts)
90000
40000
10000
0
15
20
25
30
35
40
45
50
55
60
2Theta (°)

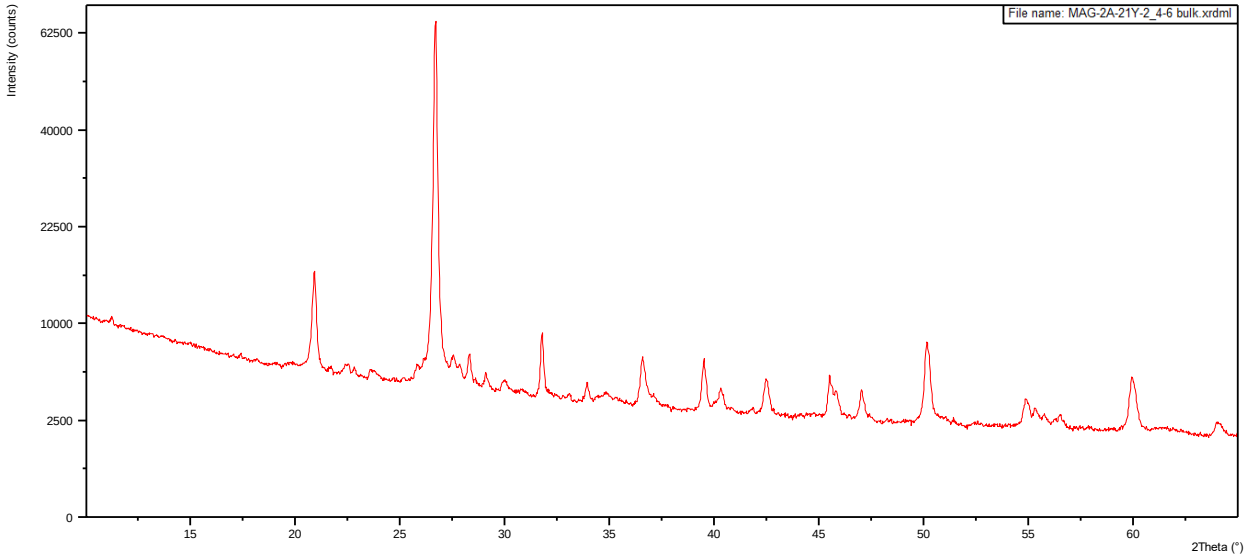
File name: MAG-2A-21Y-2_4-6 bulk.xrdml
Intensity (counts)
62500
40000
22500
10000
2500
0
15
20
25
30
35
40
45
50
55
60
2Theta (°)

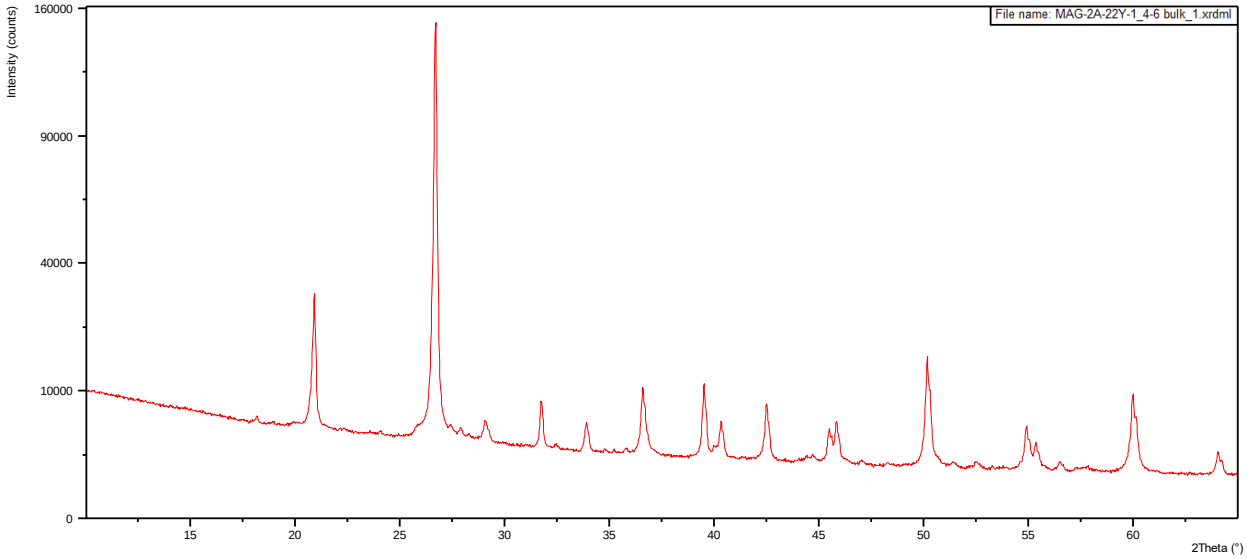
File name: MAG-2A-22Y-1_4-6 bulk_1.xrdml
Intensity (counts)
160000
90000
40000
10000
0
15
20
25
30
35
40
45
50
55
60
2Theta (°)

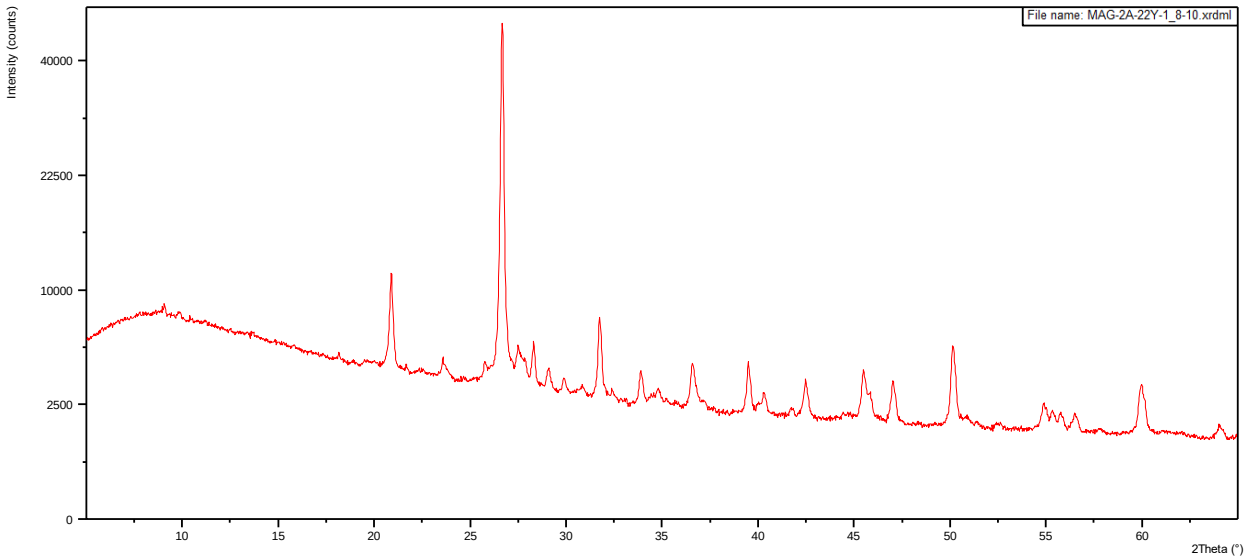
File name: MAG-2A-22Y-1_8-10.xrdml
Intensity (counts)
40000
22500
10000
2500
0
10
15
20
25
30
35
40
45
50
55
60
2Theta (°)

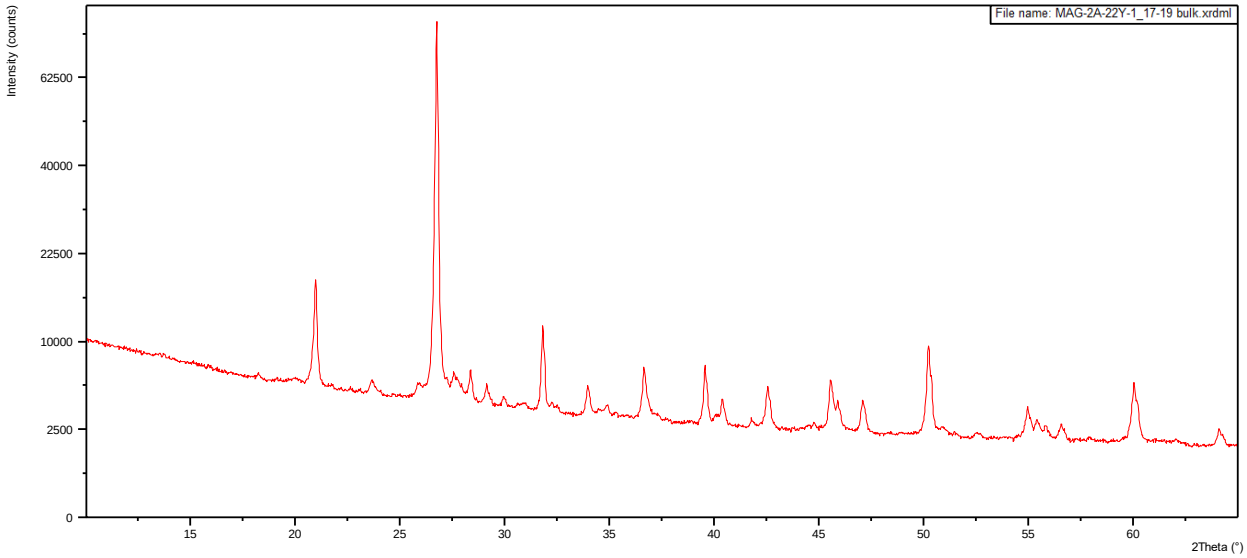
File name: MAG-2A-22Y-1_17-19 bulk.xrdml
Intensity (counts)
62500
40000
22500
10000
2500
0
15
20
25
30
35
40
45
50
55
60
2Theta (°)

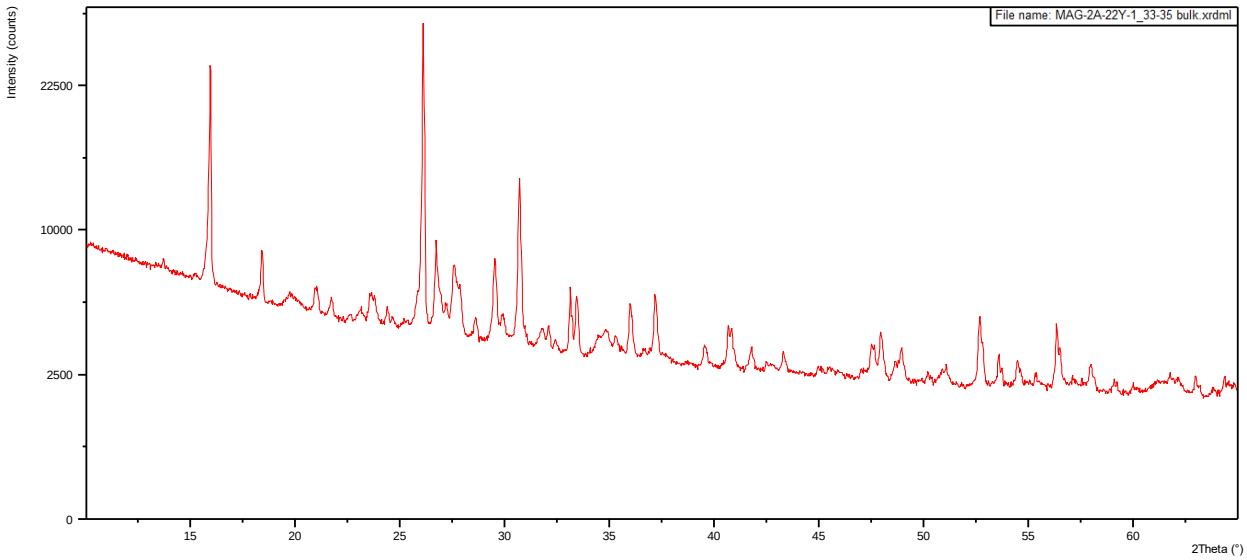
File name: MAG-2A-22Y-1_33-35 bulk.xrdml
Intensity (counts)
22500
10000
2500
0
15
20
25
30
35
40
45
50
55
60
2Theta (°)

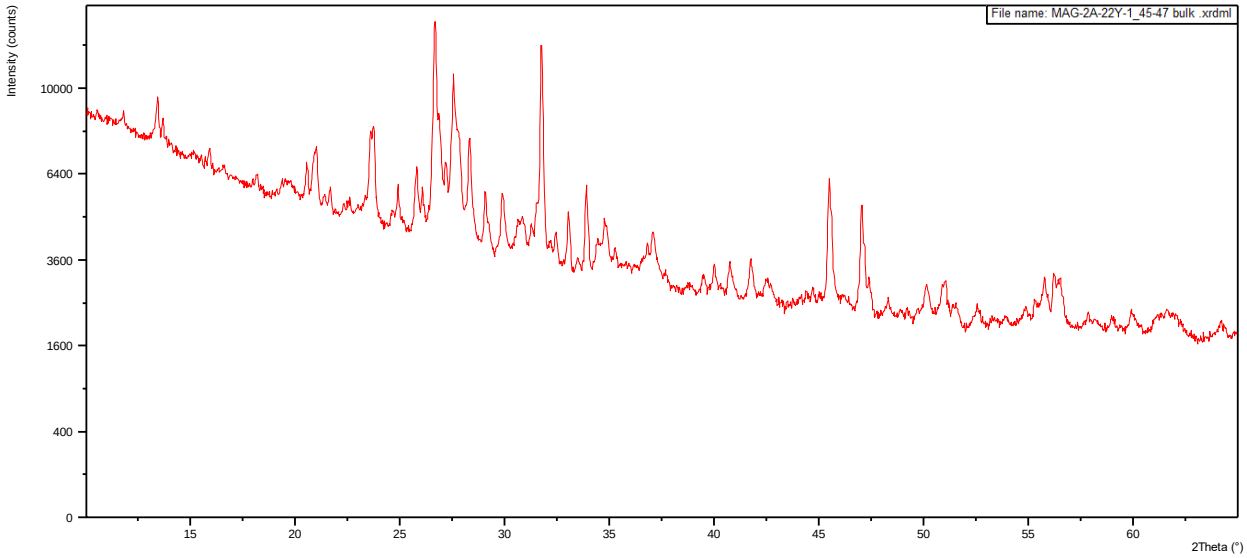
File name: MAG-2A-22Y-1_45-47 bulk .xrdml
Intensity (counts)
10000
6400
3600
1600
400
0
15
20
25
30
35
40
45
50
55
60
2Theta (°)

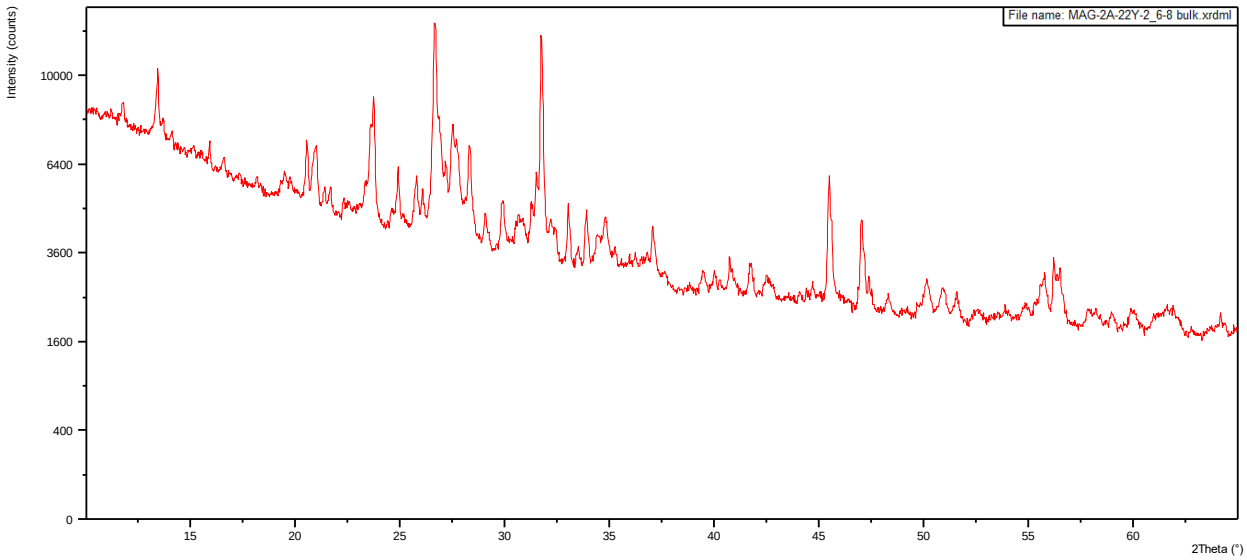
File name: MAG-2A-22Y-2_6-8 bulk.xrdml
Intensity (counts)
10000
6400
3600
1600
400
0
15
20
25
30
35
40
45
50
55
60
2Theta (°)

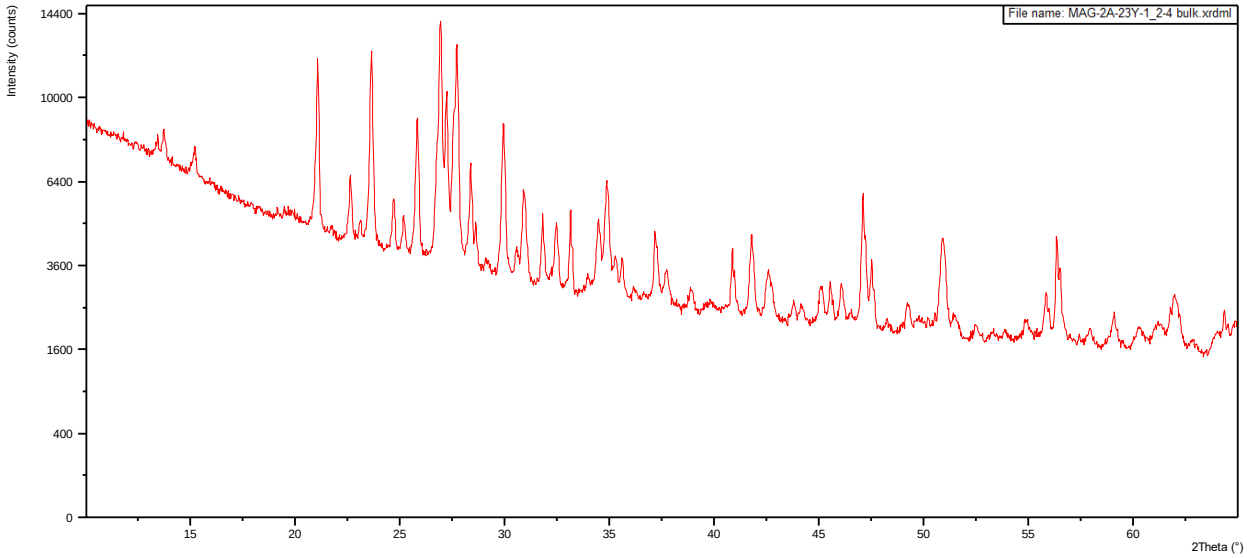
File name: MAG-2A-23Y-1_2-4 bulk.xrdml
Intensity (counts)
14400
10000
6400
3600
1600
400
0
15
20
25
30
35
40
45
50
55
60
2Theta (°)

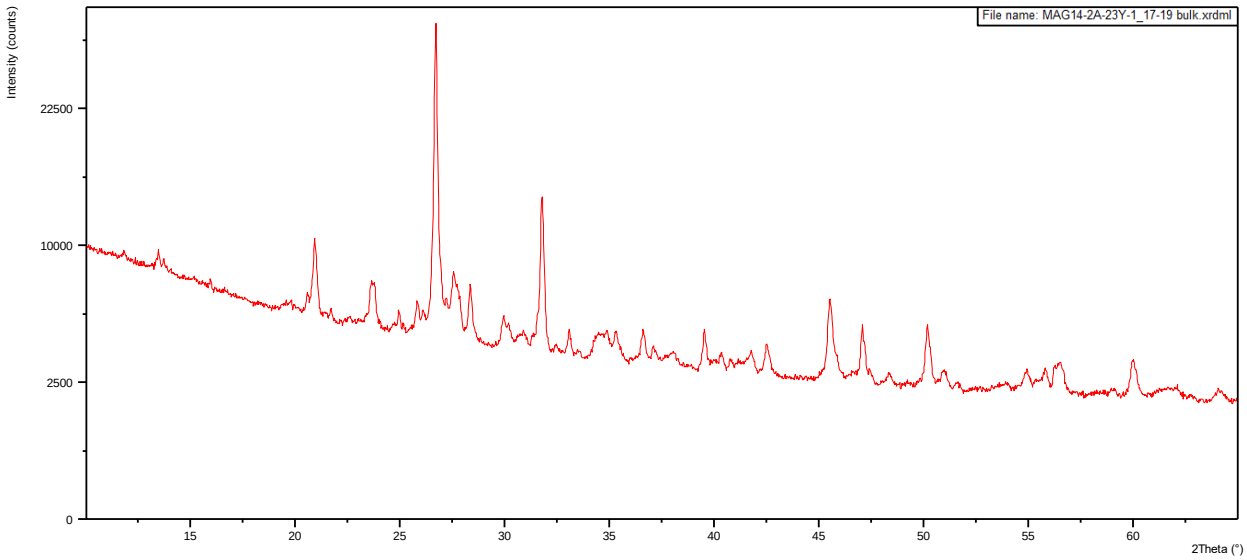
File name: MAG14-2A-23Y-1_17-19 bulk.xrdml
Intensity (counts)
22500
10000
2500
0
15
20
25
30
35
40
45
50
55
60
2Theta (°)

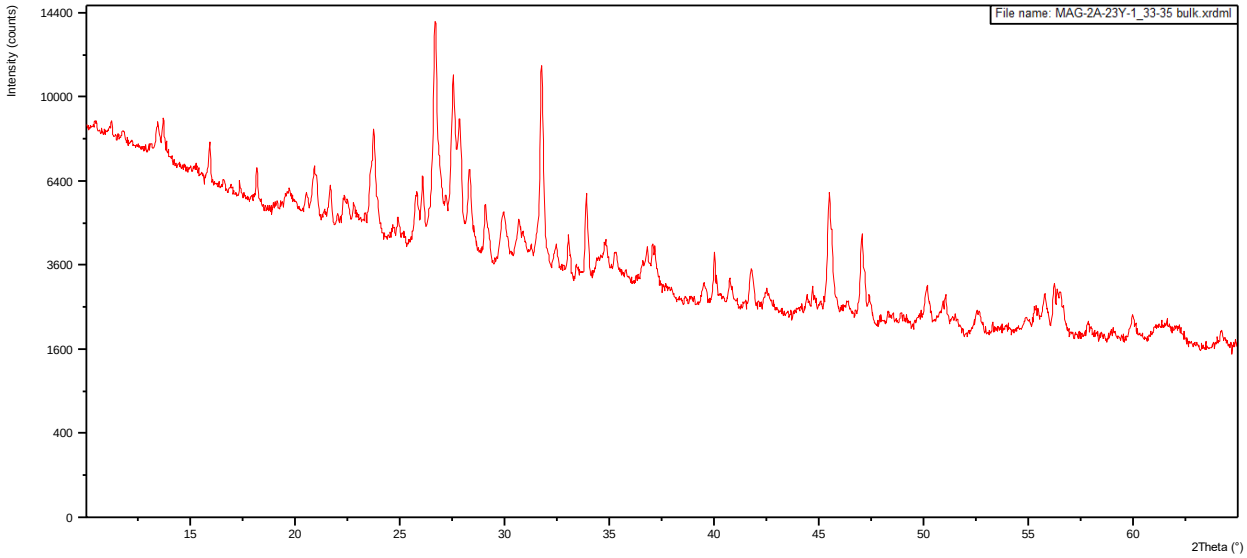
File name: MAG-2A-23Y-1_33-35 bulk.xrdml
Intensity (counts)
14400
10000
6400
3600
1600
400
0
15
20
25
30
35
40
45
50
55
60
2Theta (°)

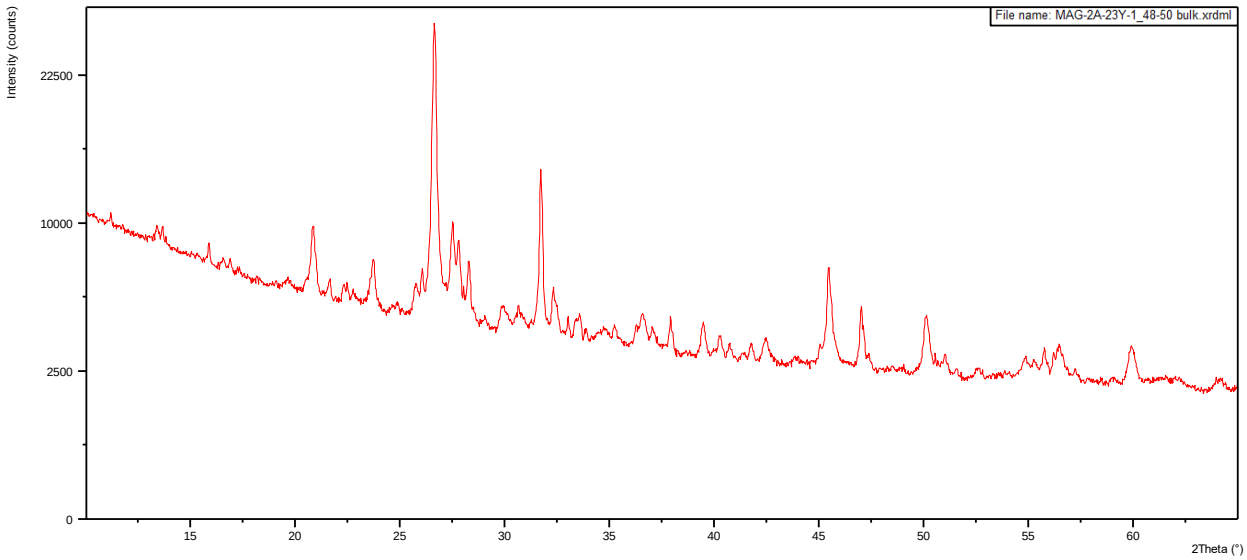
File name: MAG-2A-23Y-1_48-50 bulk.xrdml
Intensity (counts)
22500
10000
2500
0
15
20
25
30
35
40
45
50
55
60
2Theta (°)

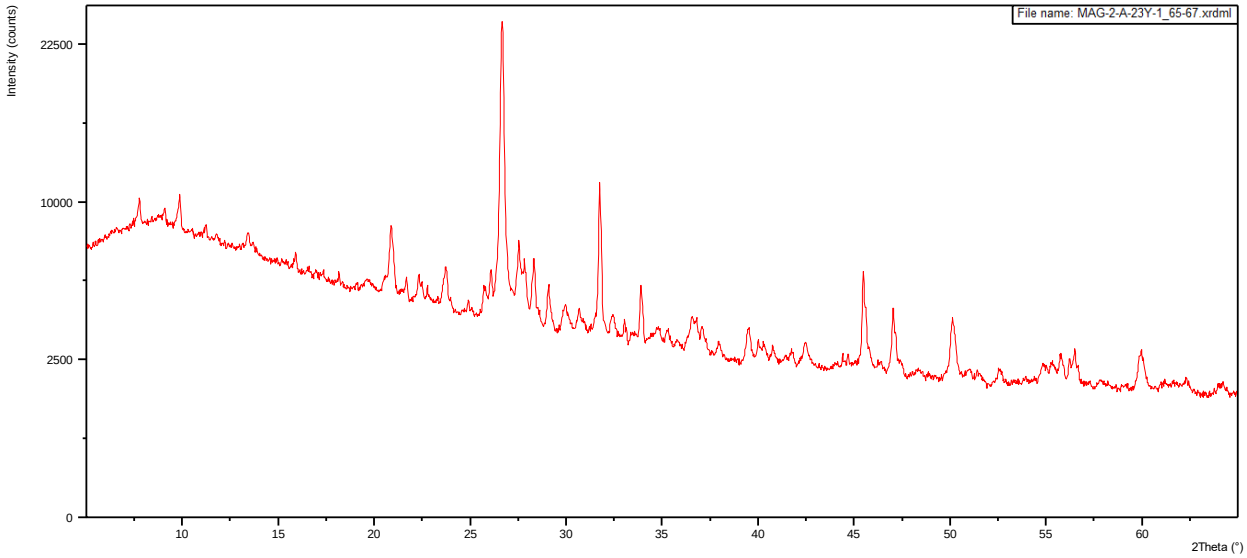
File name: MAG-2-A-23Y-1_65-67.xrdml
Intensity (counts)
22500
10000
2500
0
10
15
20
25
30
35
40
45
50
55
60
2Theta (°)

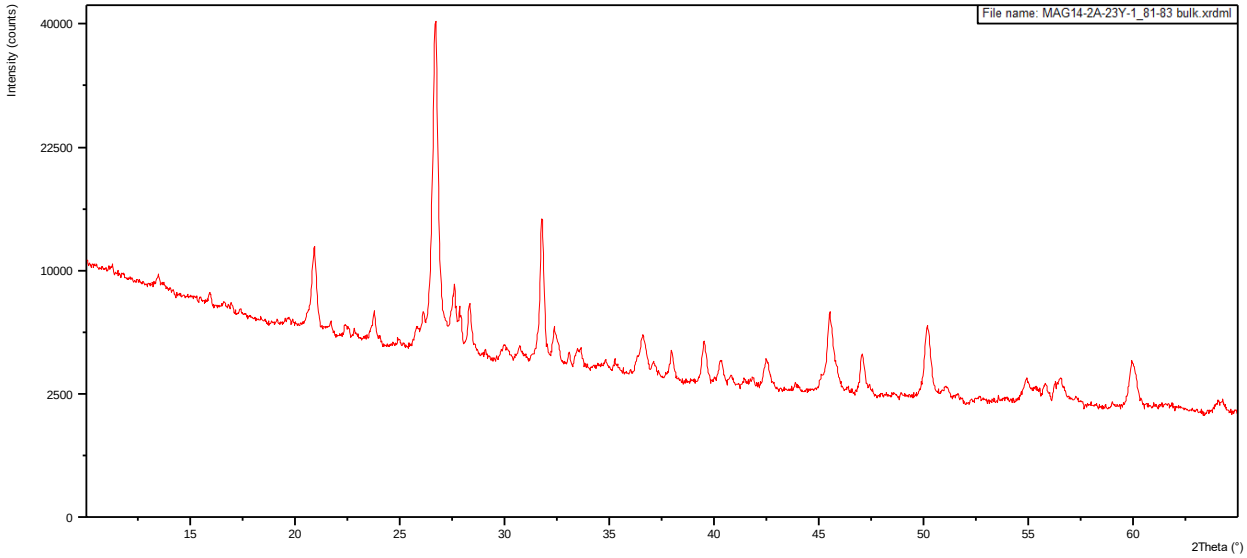
File name: MAG14-2A-23Y-1_81-83 bulk.xrdml
Intensity (counts)
40000
22500
10000
2500
0
15
20
25
30
35
40
45
50
55
60
2Theta (°)

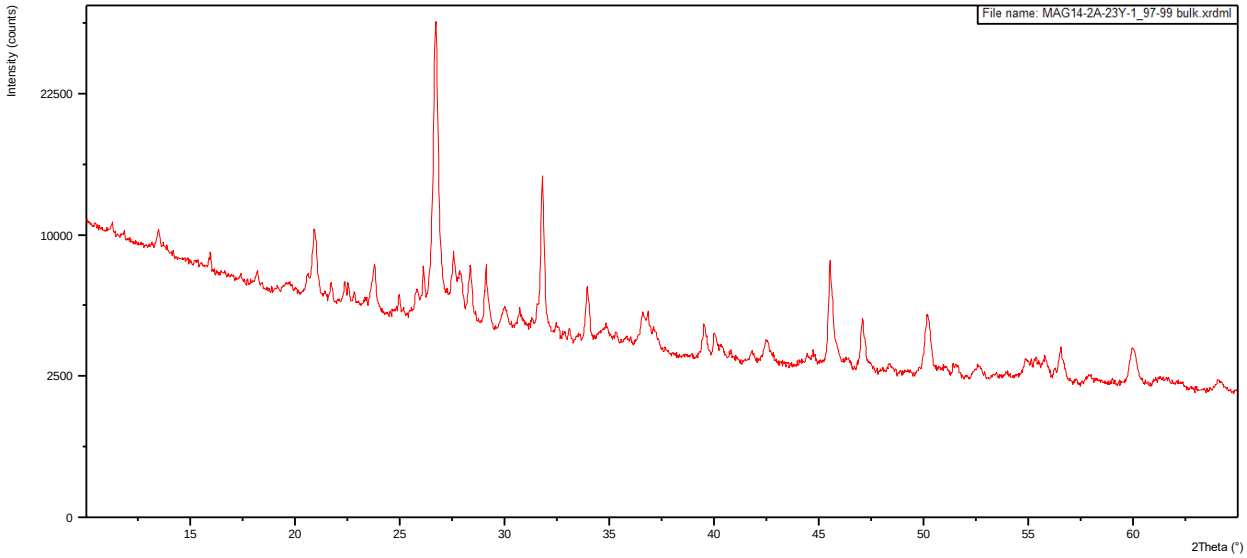
File name: MAG14-2A-23Y-1_97-99 bulk.xrdml
Intensity (counts)
22500
10000
2500
0
15
20
25
30
35
40
45
50
55
60
2Theta (°)

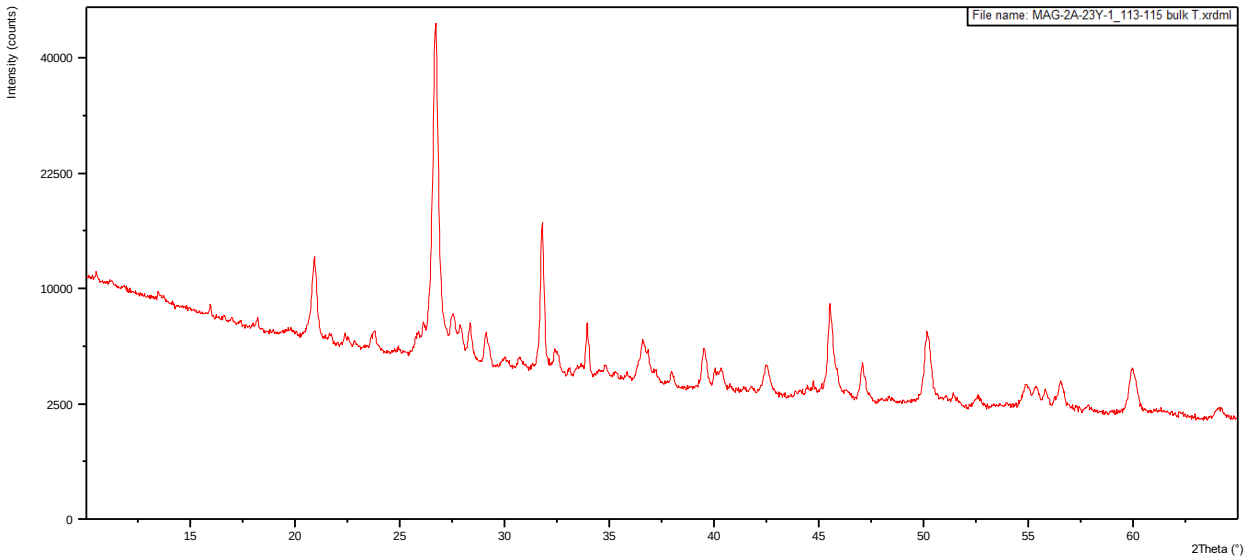
File name: MAG-2A-23Y-1_113-115 bulk T.xrdml
Intensity (counts)
40000
22500
10000
2500
0
15
20
25
30
35
40
45
50
55
60
2Theta (°)

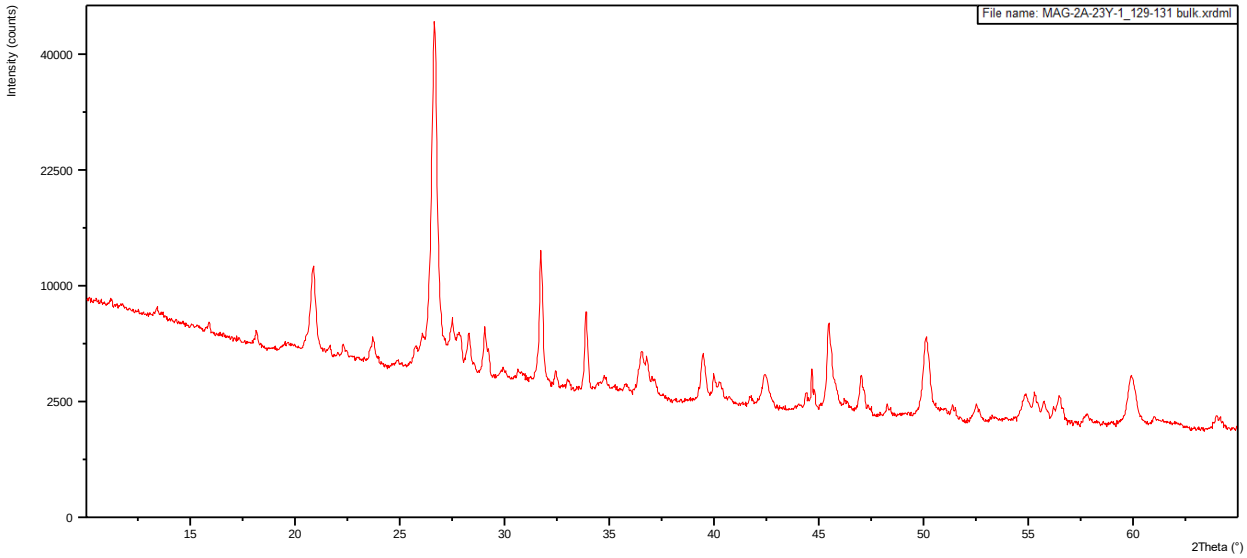
File name: MAG-2A-23Y-1_129-131 bulk.xrdml
Intensity (counts)
40000
22500
10000
2500
0
15
20
25
30
35
40
45
50
55
60
2Theta (°)

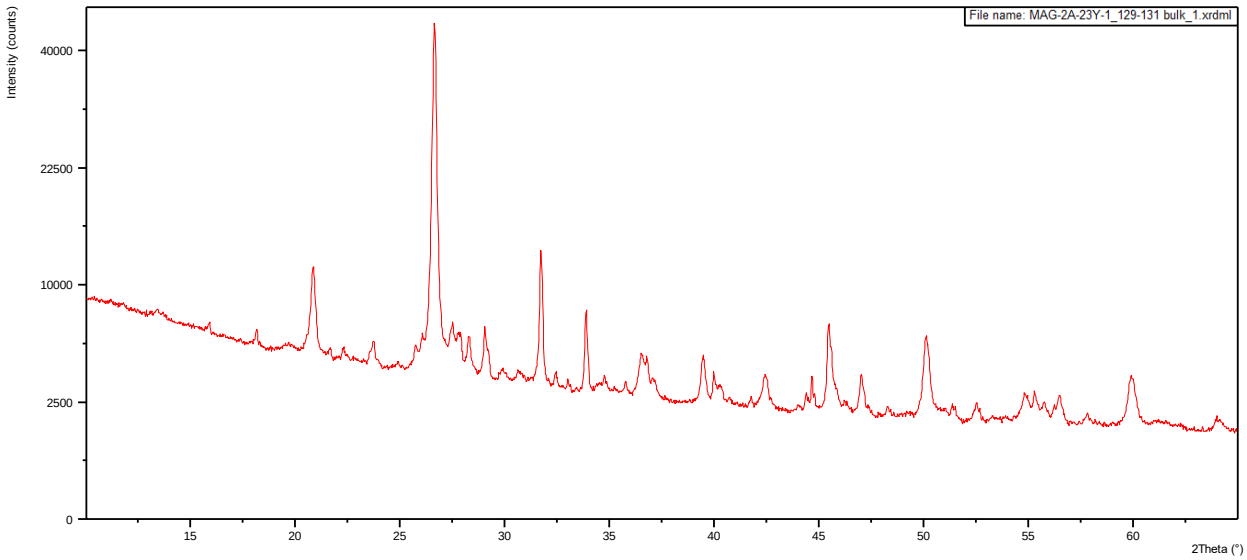
File name: MAG-2A-23Y-1_129-131 bulk_1.xrdml
Intensity (counts)
40000
22500
10000
2500
0
15
20
25
30
35
40
45
50
55
60
2Theta (°)

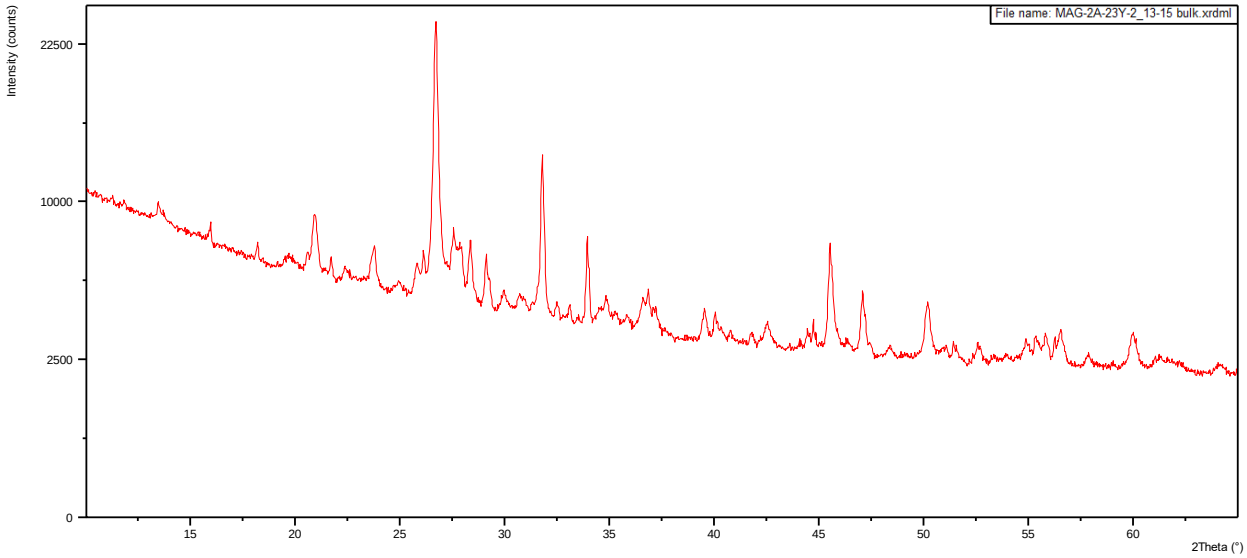
File name: MAG-2A-23Y-2_13-15 bulk.xrdml
Intensity (counts)
22500
10000
2500
0
15
20
25
30
35
40
45
50
55
60
2Theta (°)

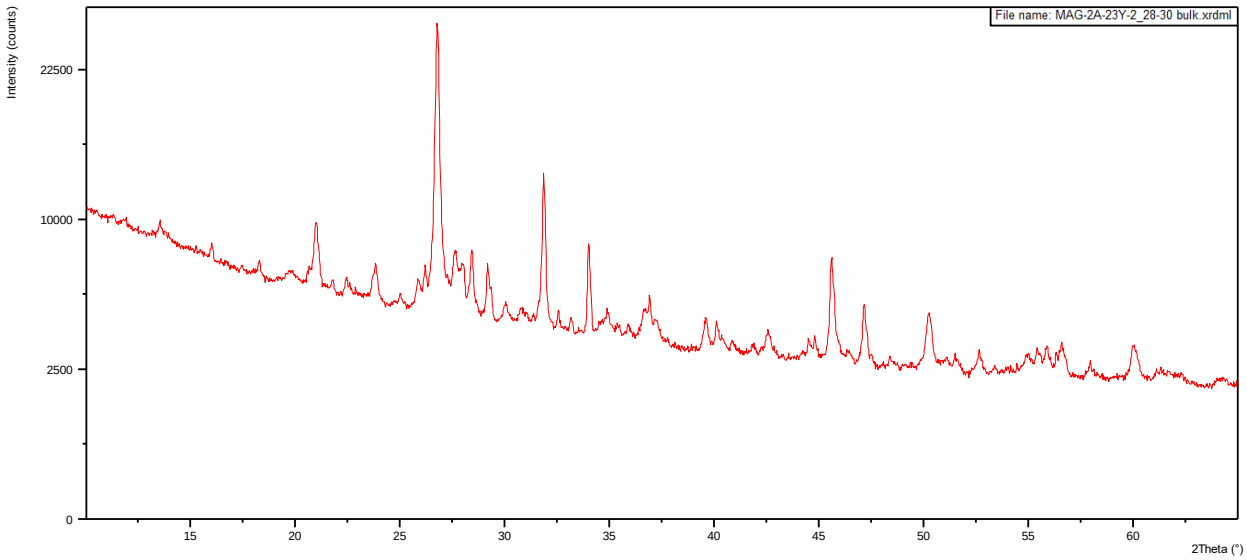
File name: MAG-2A-23Y-2_28-30 bulk.xrdml
Intensity (counts)
22500
10000
2500
0
15
20
25
30
35
40
45
50
55
60
2Theta (°)

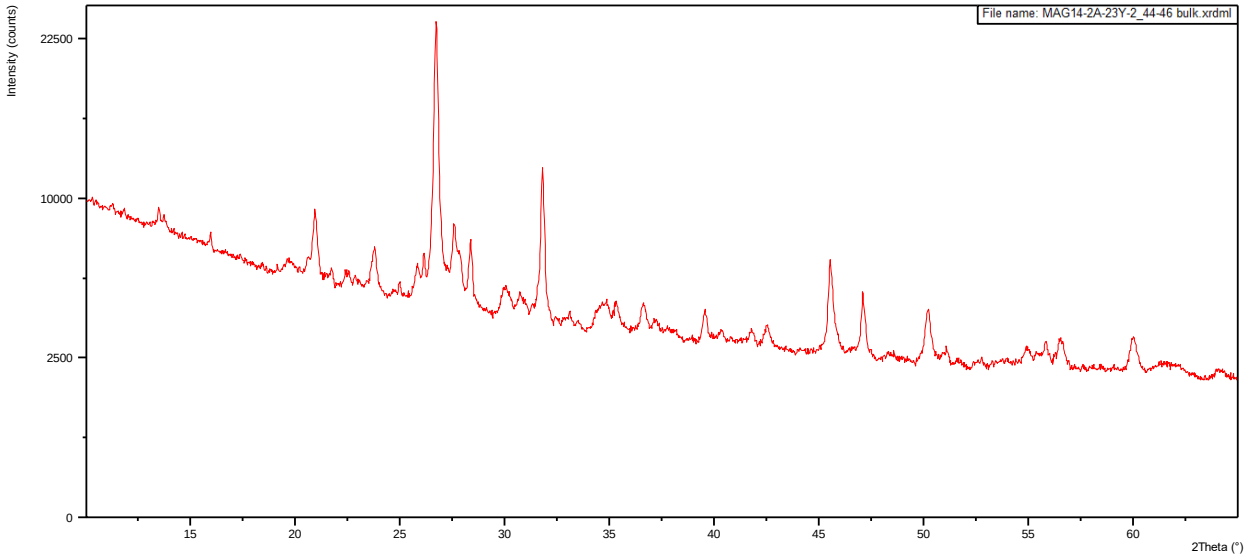
File name: MAG14-2A-23Y-2_44-46 bulk.xrdml
Intensity (counts)
22500
10000
2500
0
15
20
25
30
35
40
45
50
55
60
2Theta (°)

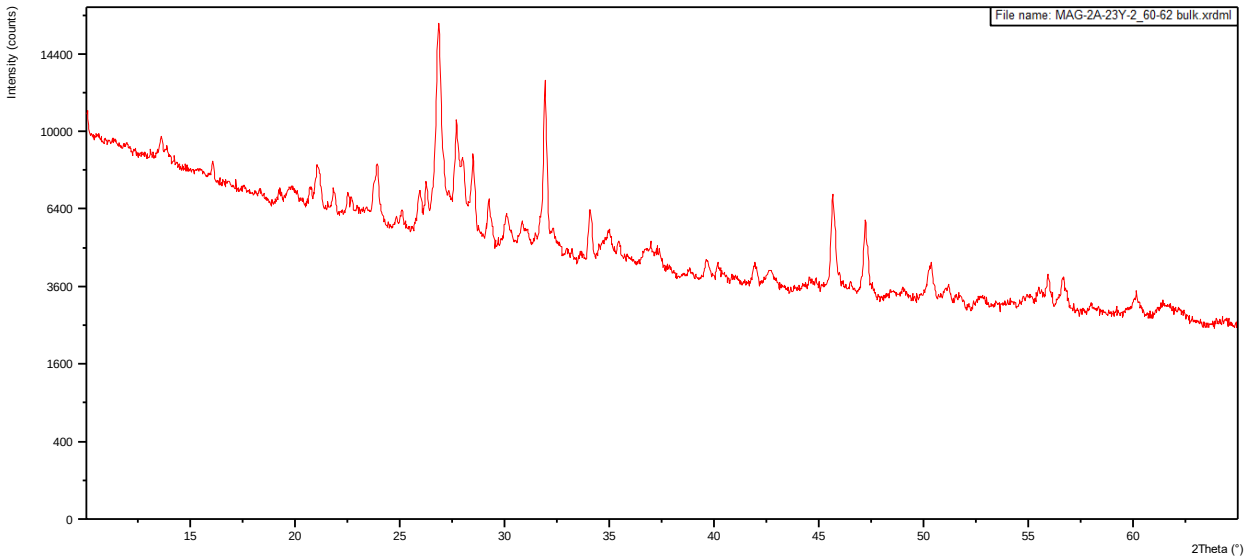
File name: MAG-2A-23Y-2_60-62 bulk.xrdml
Intensity (counts)
14400
10000
6400
3600
1600
400
0
15
20
25
30
35
40
45
50
55
60
2Theta (°)

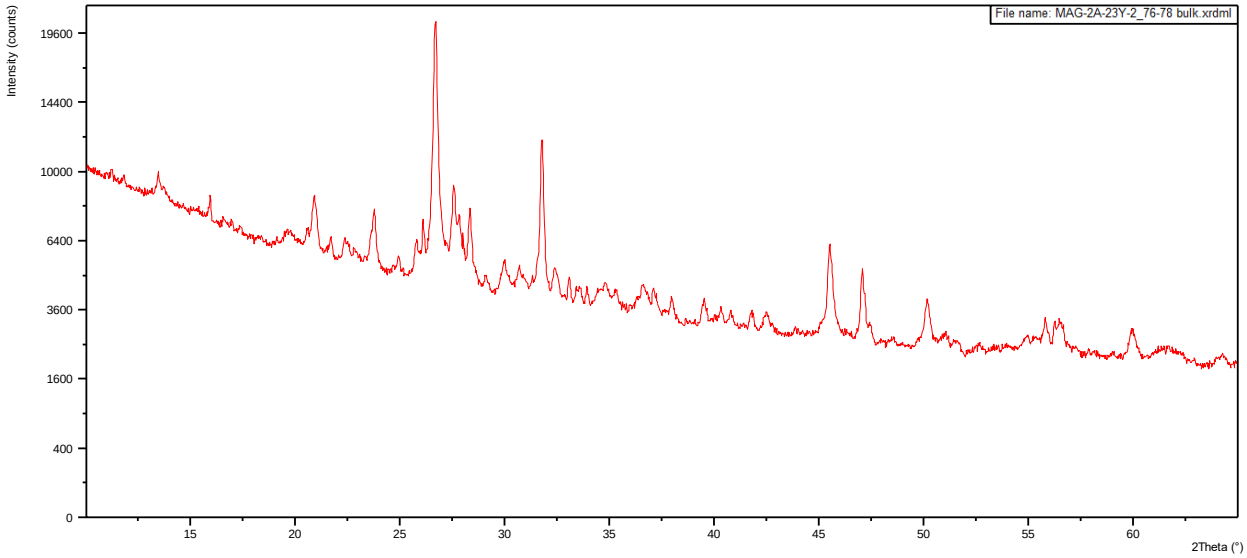
File name: MAG-2A-23Y-2_76-78 bulk.xrdml
Intensity (counts)
19600
14400
10000
6400
3600
1600
400
0
15
20
25
30
35
40
45
50
55
60
2Theta (°)

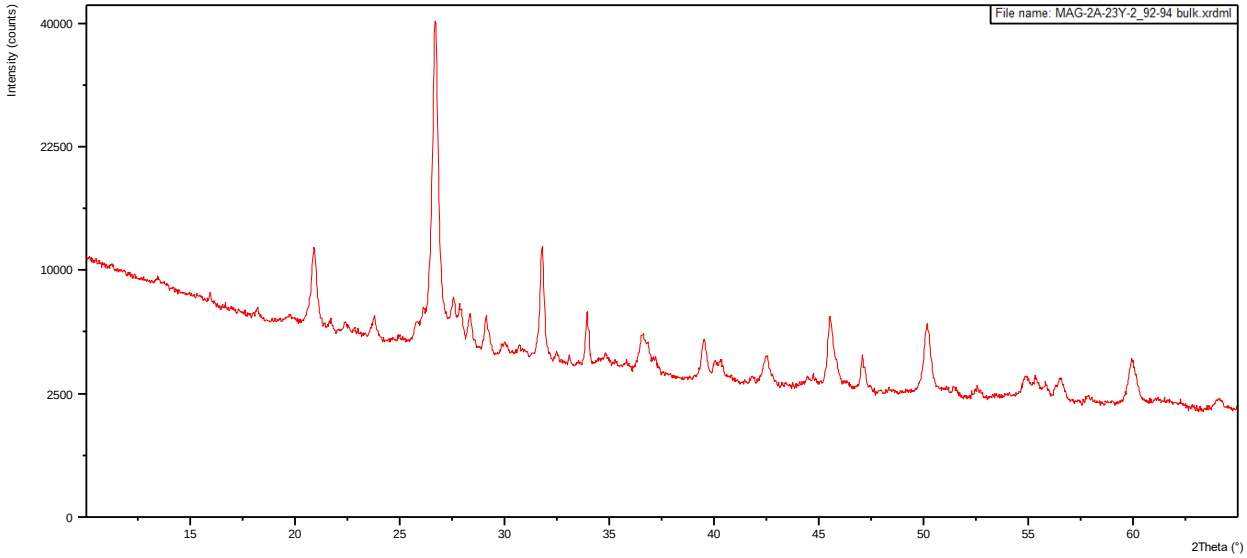
File name: MAG-2A-23Y-2_92-94 bulk.xrdml
Intensity (counts)
40000
22500
10000
2500
0
15
20
25
30
35
40
45
50
55
60
2Theta (°)

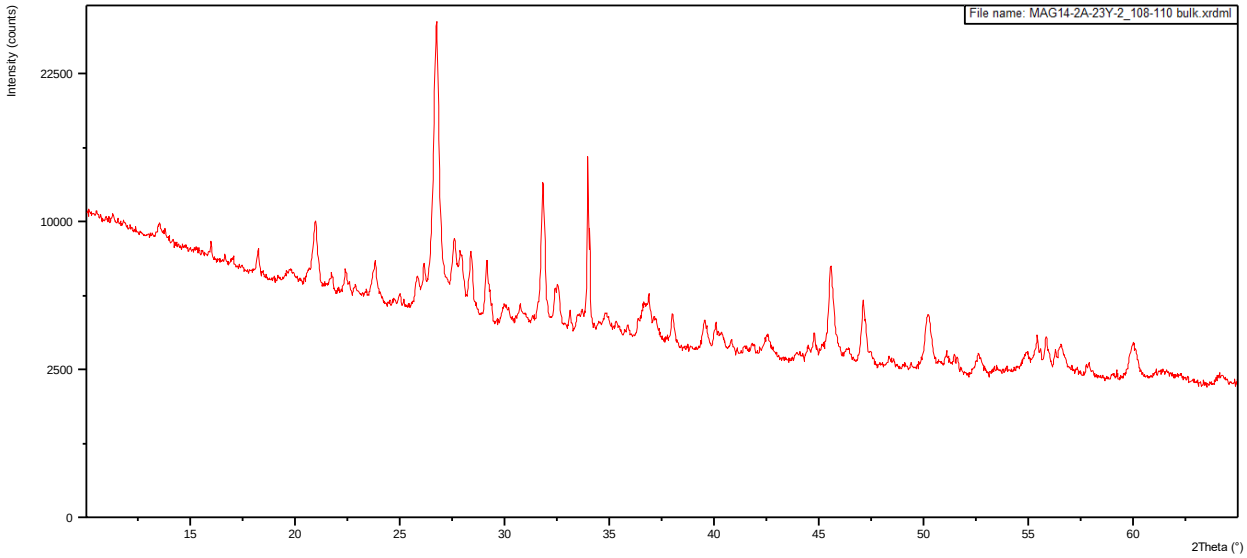
File name: MAG14-2A-23Y-2_108-110 bulk.xrdml
Intensity (counts)
22500
10000
2500
0
15
20
25
30
35
40
45
50
55
60
2Theta (°)

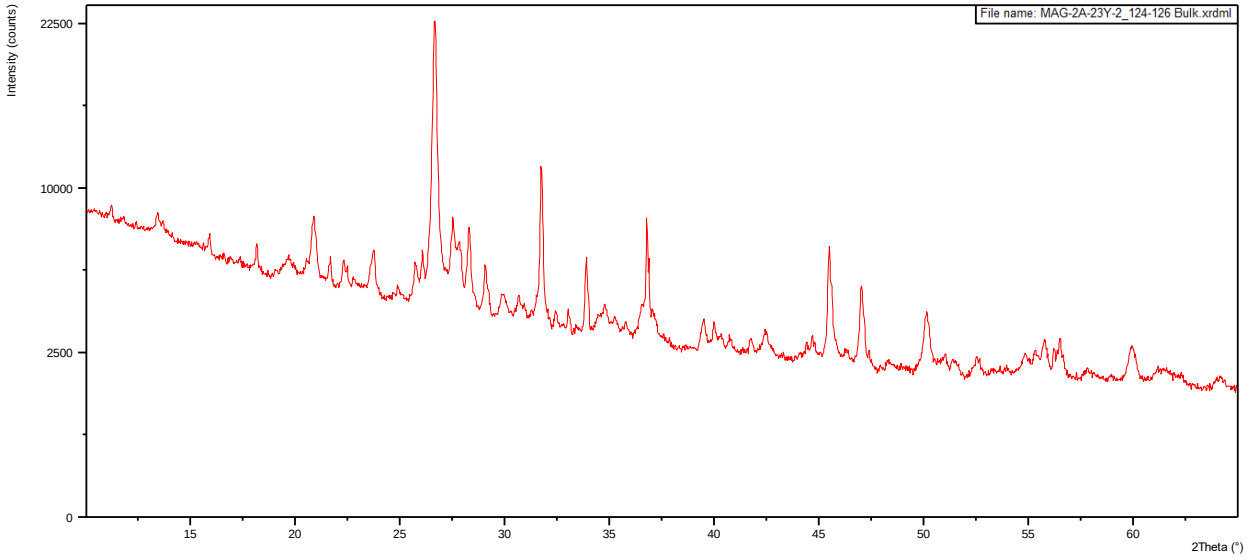
File name: MAG-2A-23Y-2_124-126 Bulk.xrdml
Intensity (counts)
22500
10000
2500
0
15
20
25
30
35
40
45
50
55
60
2Theta (°)

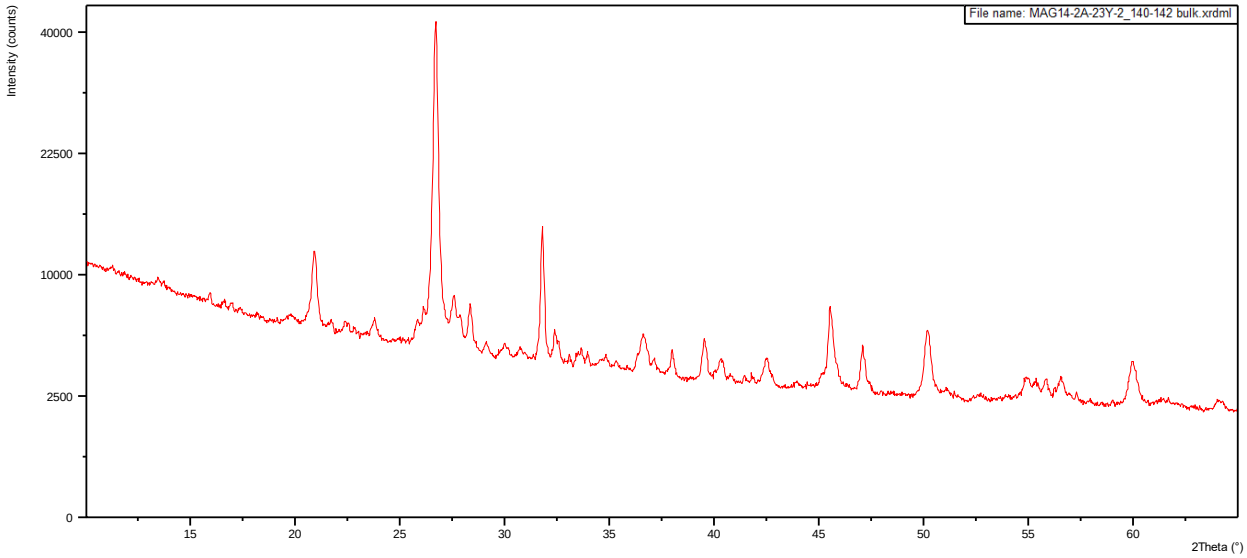
File name: MAG14-2A-23Y-2_140-142 bulk.xrdml
Intensity (counts)
40000
22500
10000
2500
0
15
20
25
30
35
40
45
50
55
60
2Theta (°)

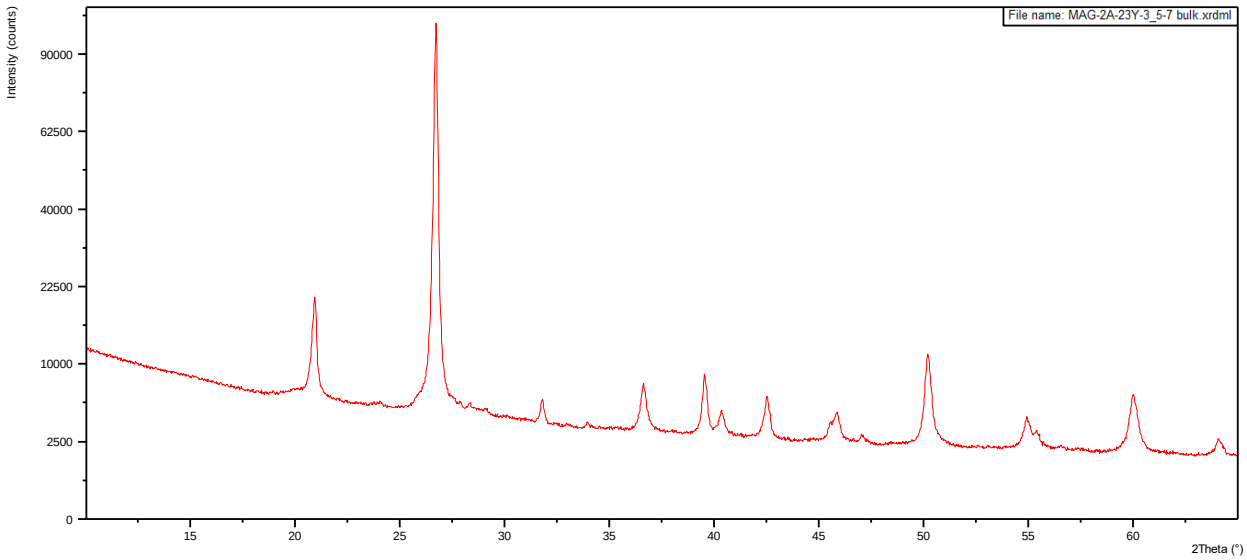
File name: MAG-2A-23Y-3_5-7 bulk.xrdml
Intensity (counts)
90000
62500
40000
22500
10000
2500
0
15
20
25
30
35
40
45
50
55
60
2Theta (°)

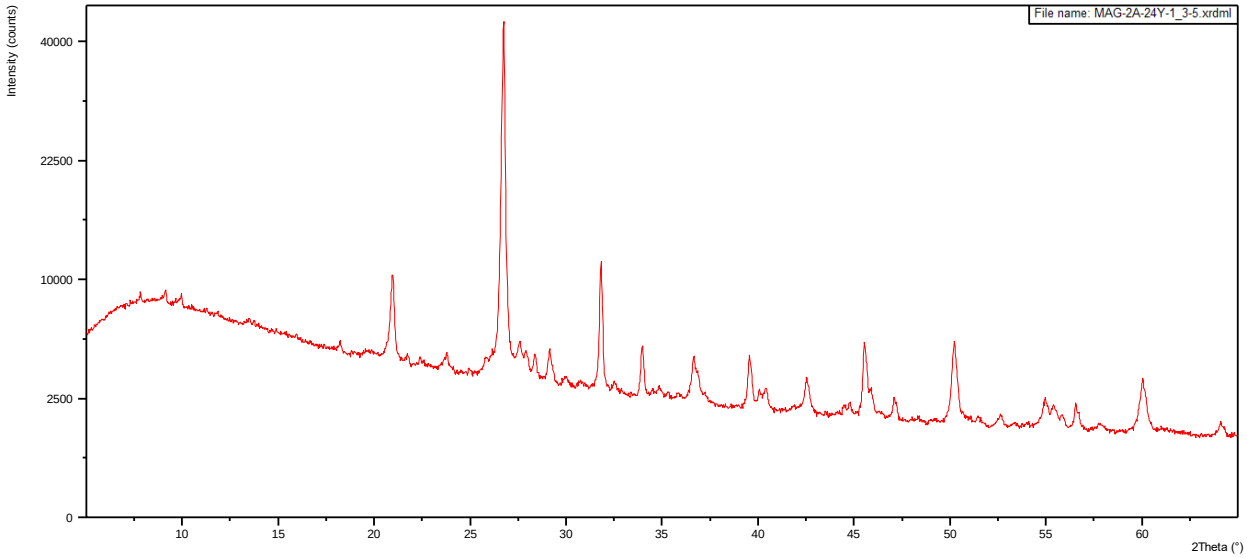
File name: MAG-2A-24Y-1_3-5.xrdml
Intensity (counts)
40000
22500
10000
2500
0
10
15
20
25
30
35
40
45
50
55
60
2Theta (°)

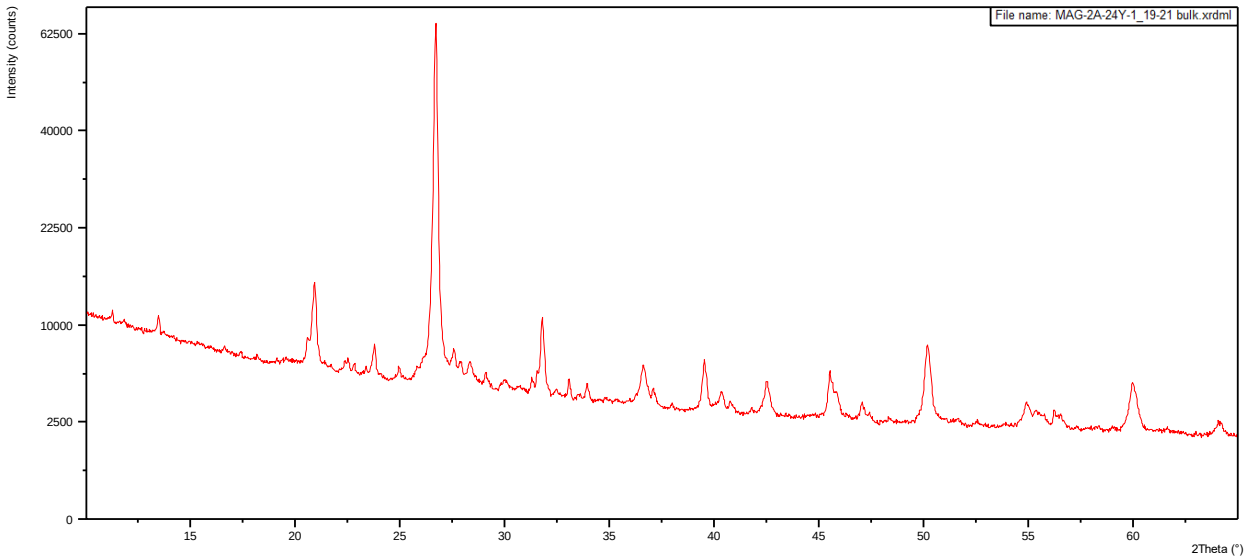
File name: MAG-2A-24Y-1_19-21 bulk.xrdml
Intensity (counts)
62500
40000
22500
10000
2500
0
15
20
25
30
35
40
45
50
55
60
2Theta (°)

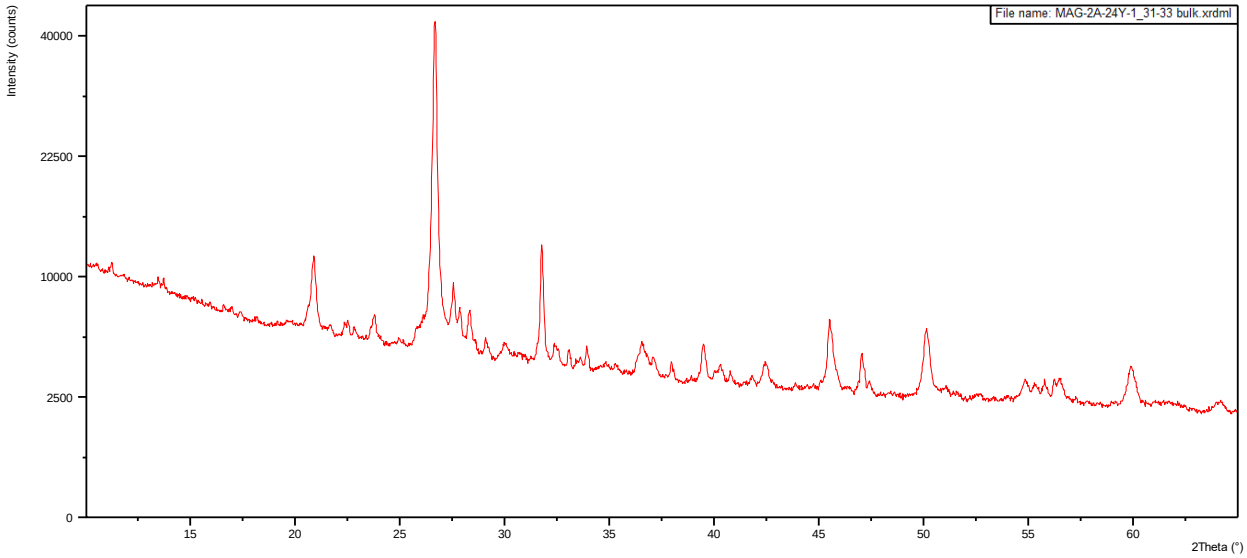
File name: MAG-2A-24Y-1_31-33 bulk.xrdml
Intensity (counts)
40000
22500
10000
2500
0
15
20
25
30
35
40
45
50
55
60
2Theta (°)

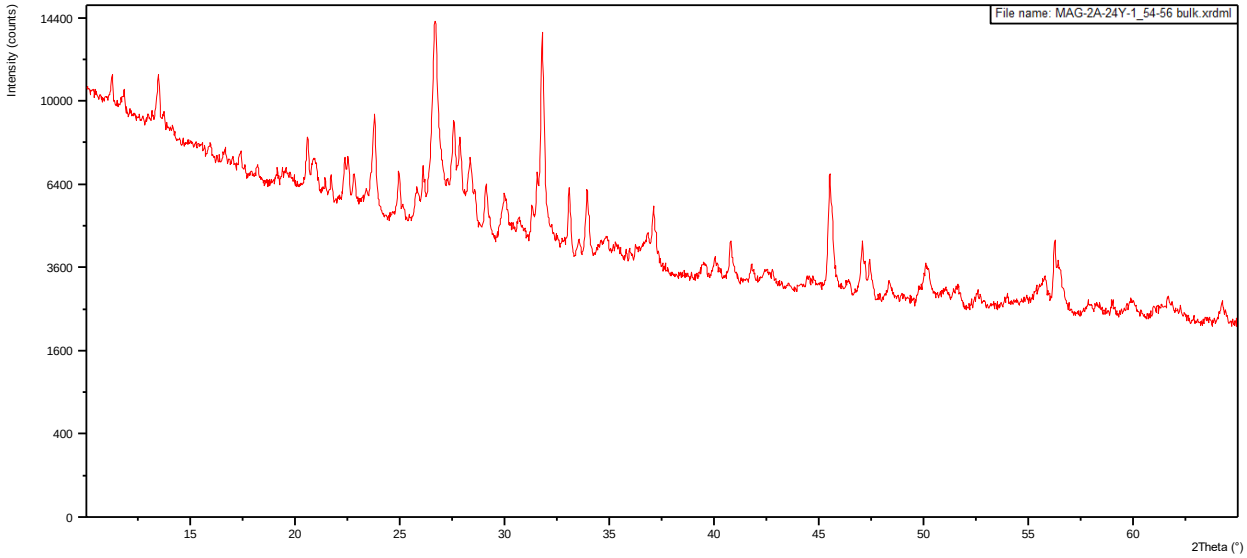
File name: MAG-2A-24Y-1_54-56 bulk.xrdml
Intensity (counts)
14400
10000
6400
3600
1600
400
0
15
20
25
30
35
40
45
50
55
60
2Theta (°)

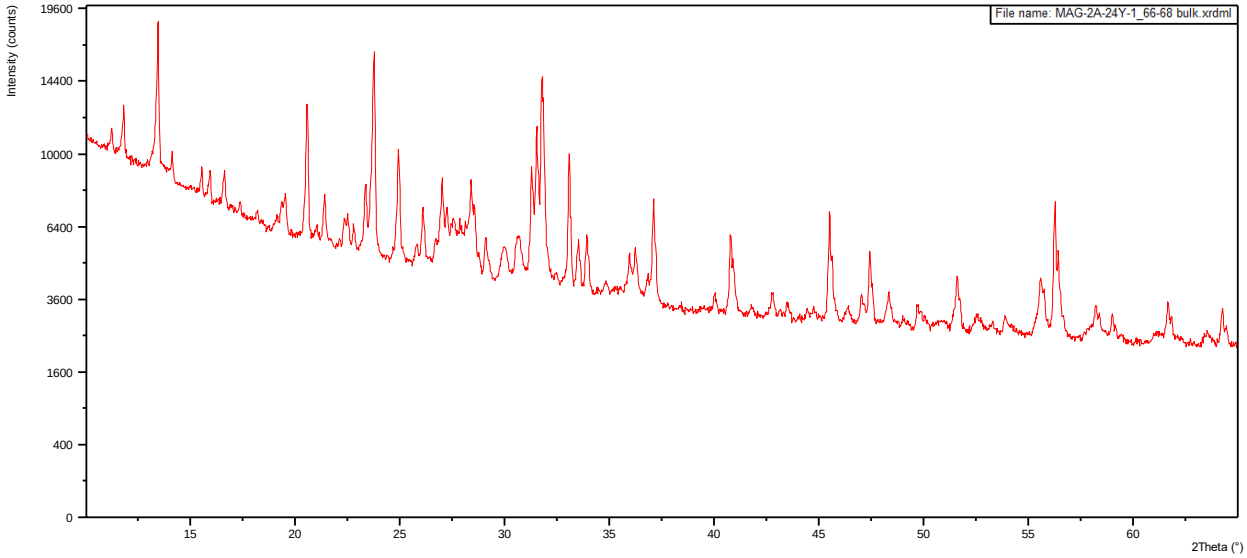
File name: MAG-2A-24Y-1_66-68 bulk.xrdml
Intensity (counts)
19600
14400
10000
6400
3600
1600
400
0
15
20
25
30
35
40
45
50
55
60
2Theta (°)

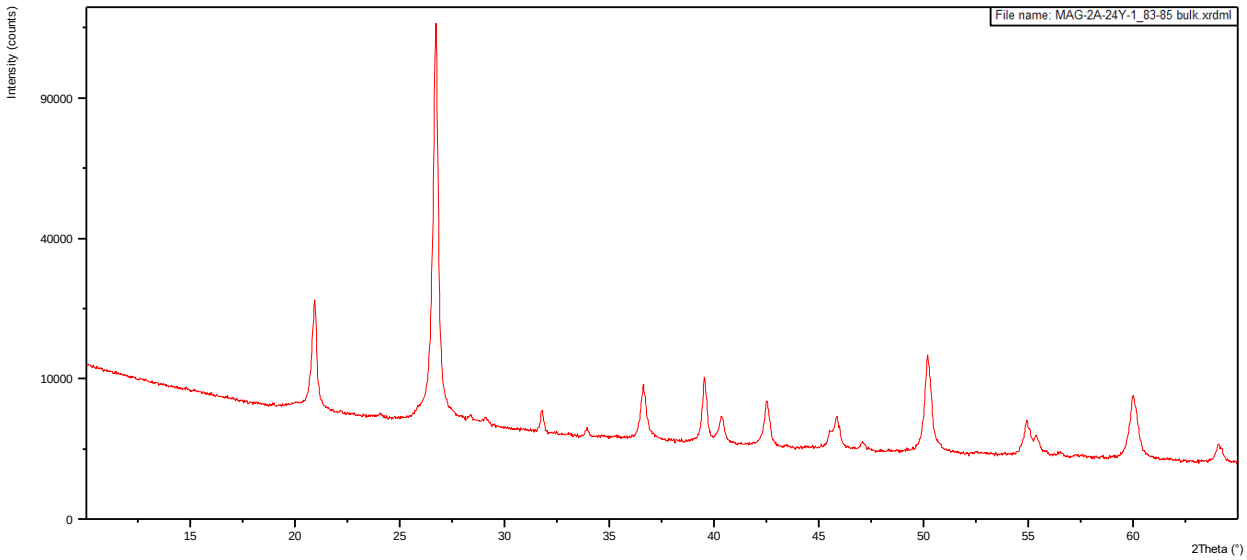
File name: MAG-2A-24Y-1_83-85 bulk.xrdml
Intensity (counts)
90000
40000
10000
0
15
20
25
30
35
40
45
50
55
60
2Theta (°)

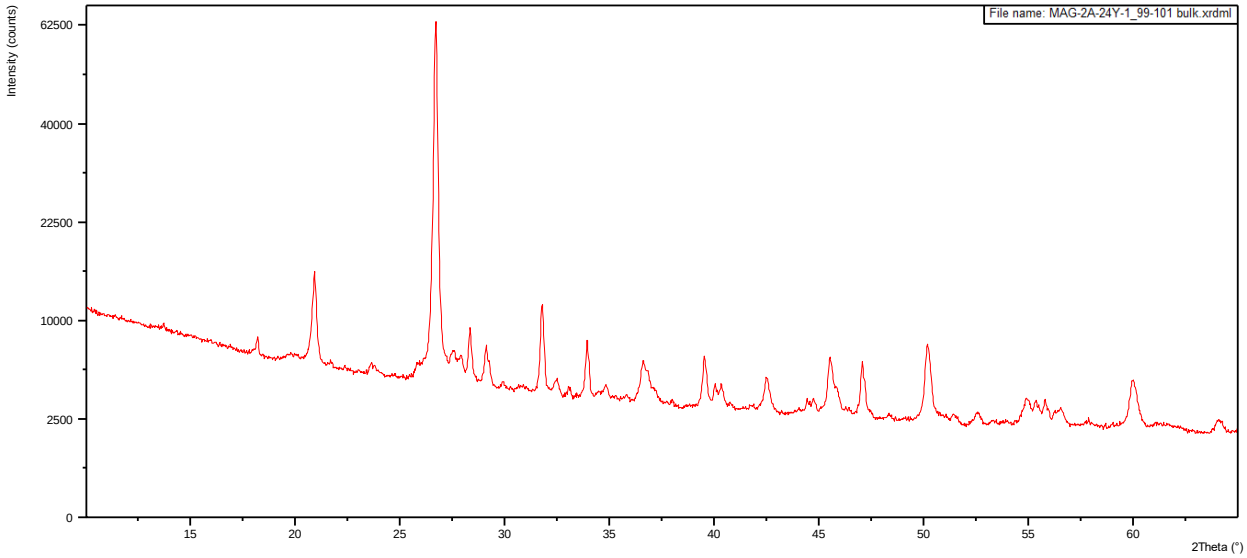
File name: MAG-2A-24Y-1_99-101 bulk.xrdml
Intensity (counts)
62500
40000
22500
10000
2500
0
15
20
25
30
35
40
45
50
55
60
2Theta (°)

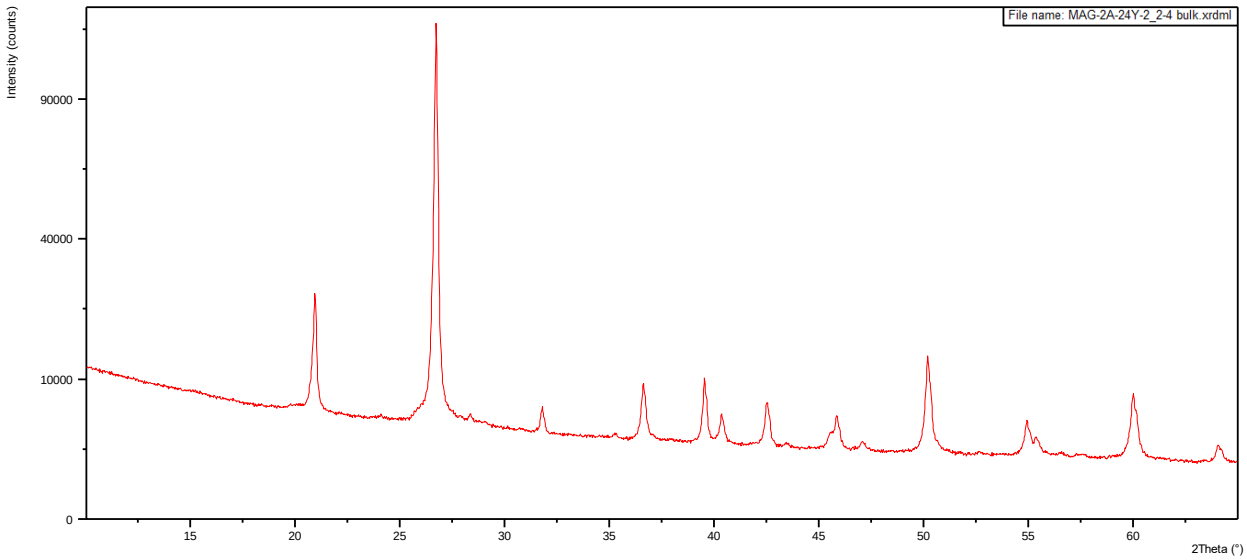
File name: MAG-2A-24Y-2_2-4 bulk.xrdml
Intensity (counts)
90000
40000
10000
0
15
20
25
30
35
40
45
50
55
60
2Theta (°)

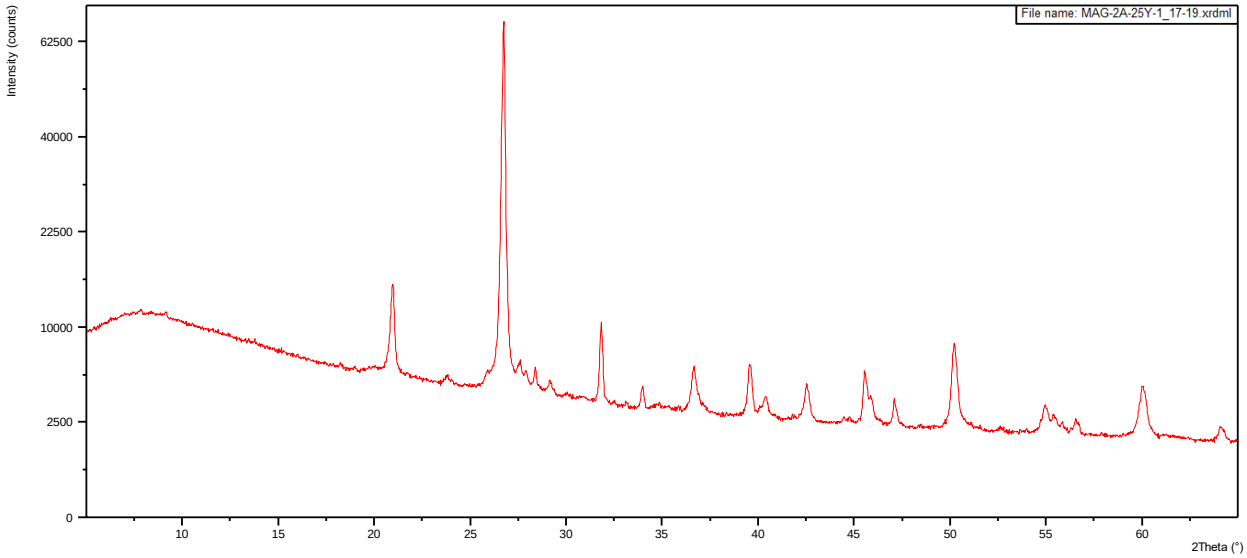
File name: MAG-2A-25Y-1_17-19.xrdml
Intensity (counts)
62500
40000
22500
10000
2500
0
10
15
20
25
30
35
40
45
50
55
60
2Theta (°)

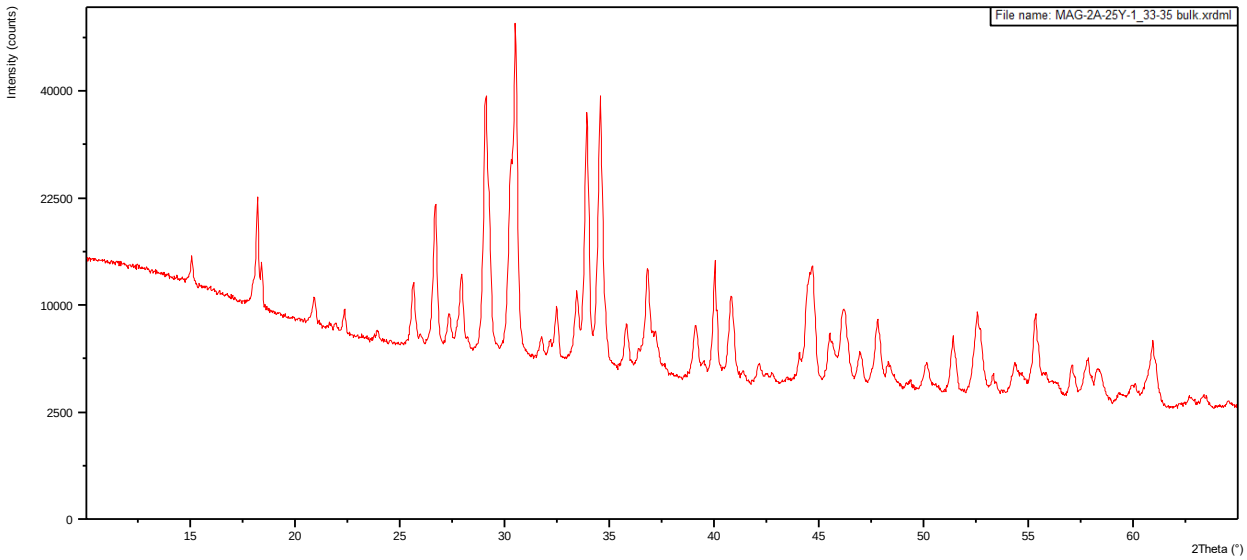
File name: MAG-2A-25Y-1_33-35 bulk.xrdml
Intensity (counts)
40000
22500
10000
2500
0
15
20
25
30
35
40
45
50
55
60
2Theta (°)

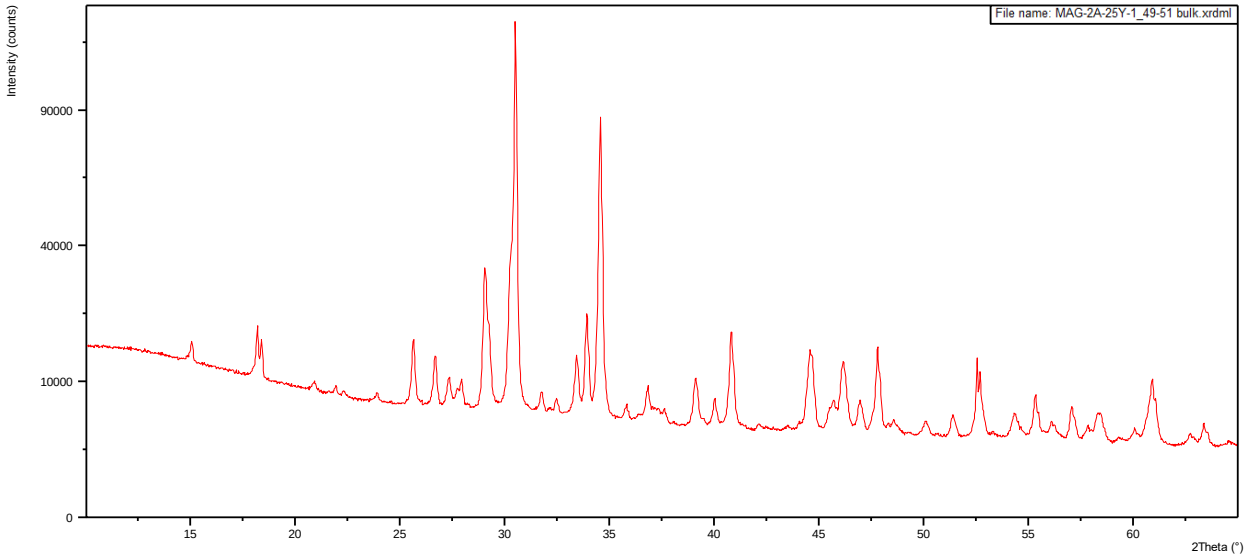
File name: MAG-2A-25Y-1_49-51 bulk.xrdml
Intensity (counts)
90000
40000
10000
0
15
20
25
30
35
40
45
50
55
60
2Theta (°)

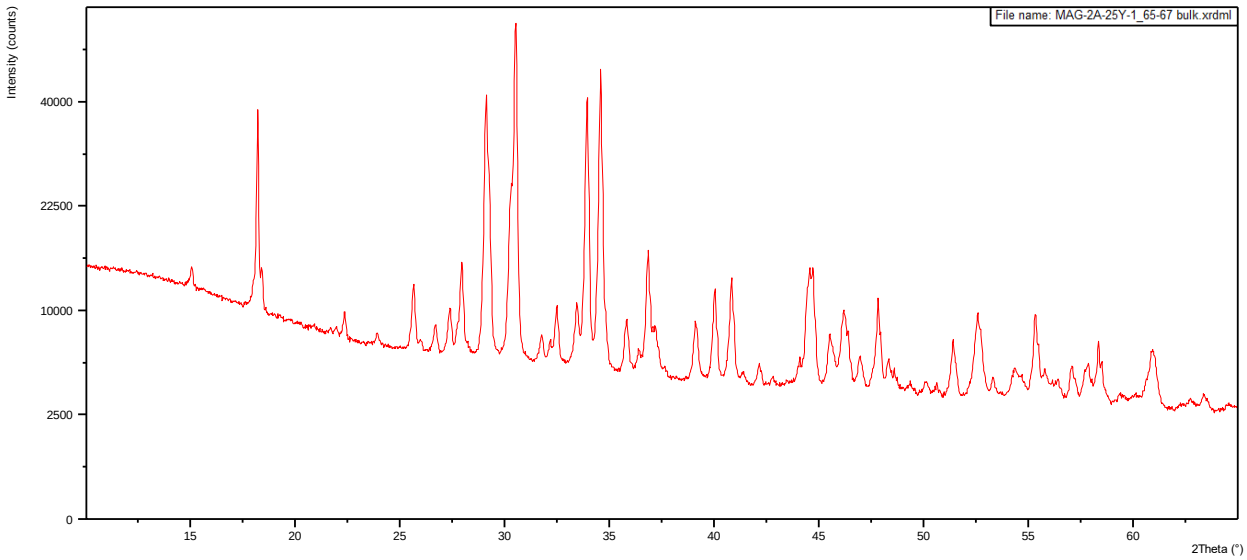
File name: MAG-2A-25Y-1_65-67 bulk.xrdml
Intensity (counts)
40000
22500
10000
2500
0
15
20
25
30
35
40
45
50
55
60
2Theta (°)

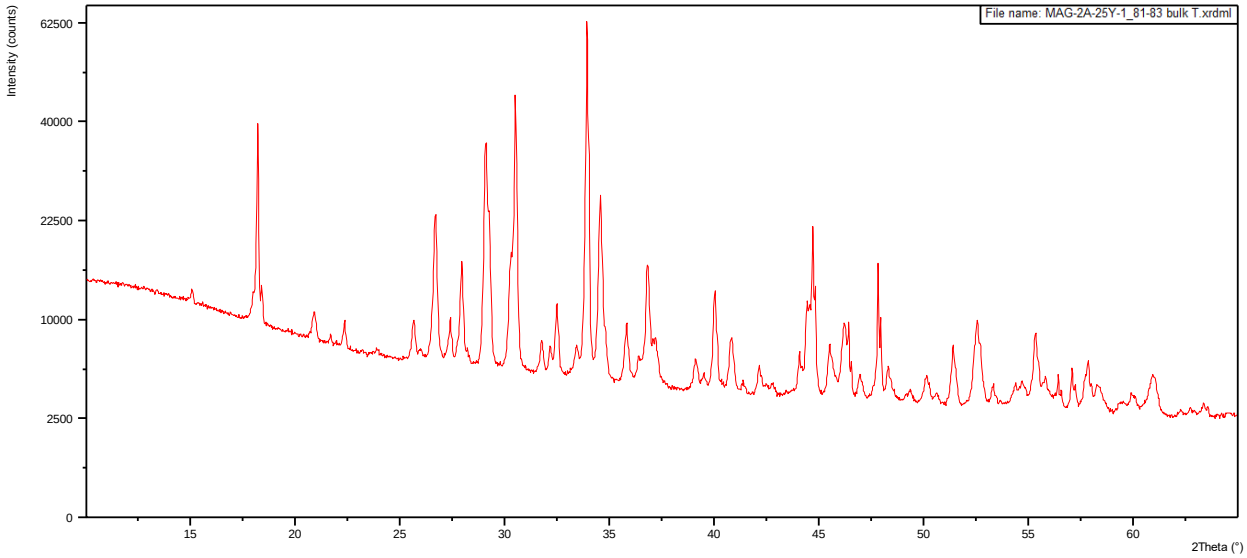
File name: MAG-2A-25Y-1_81-83 bulk T.xrdml
Intensity (counts)
62500
40000
22500
10000
2500
0
15
20
25
30
35
40
45
50
55
60
2Theta (°)

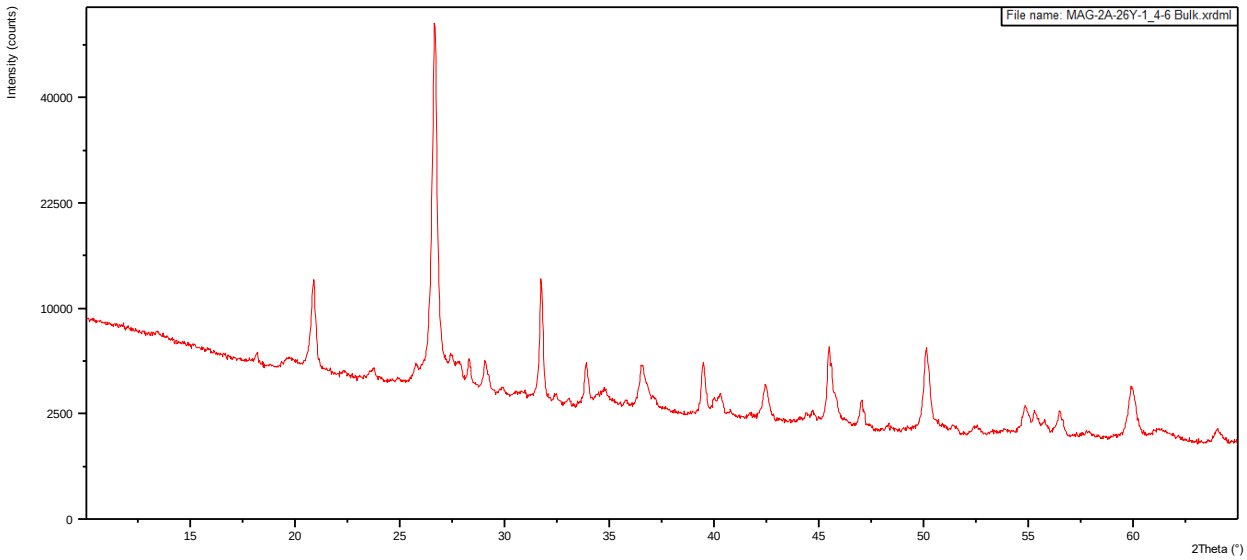
File name: MAG-2A-26Y-1_4-6 Bulk.xrdml
Intensity (counts)
40000
22500
10000
2500
0
15
20
25
30
35
40
45
50
55
60
2Theta (°)

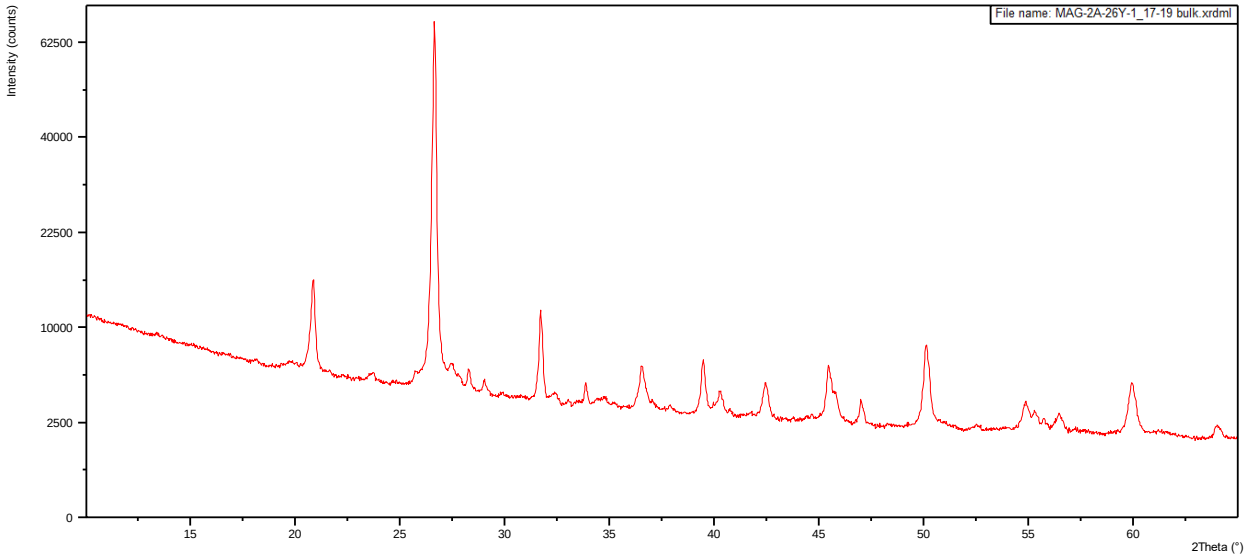
File name: MAG-2A-26Y-1_17-19 bulk.xrdml
Intensity (counts)
62500
40000
22500
10000
2500
0
15
20
25
30
35
40
45
50
55
60
2Theta (°)

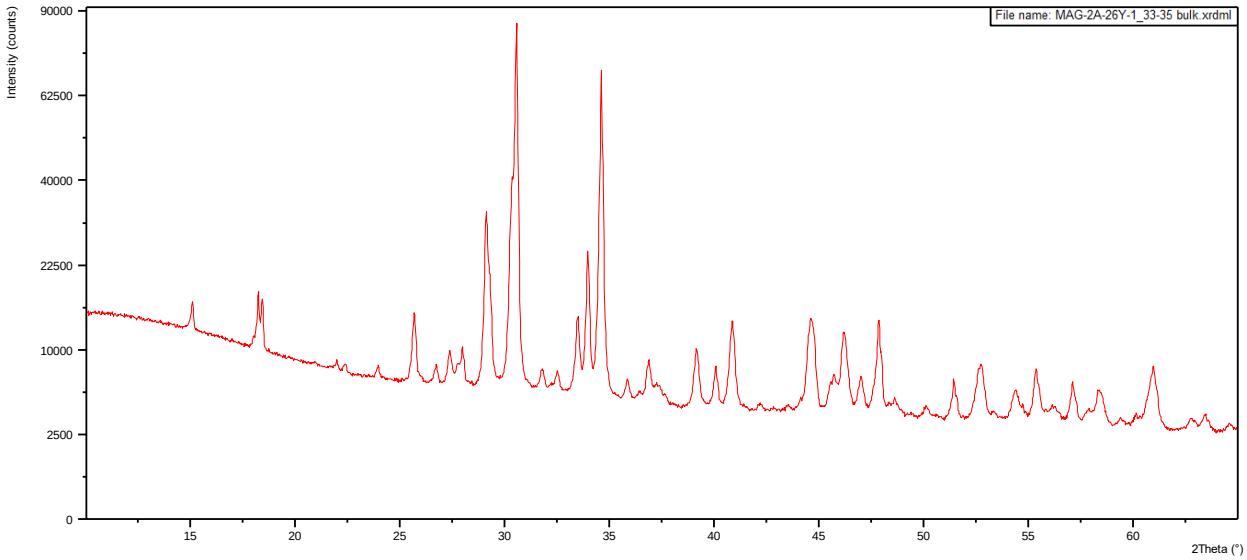
File name: MAG-2A-26Y-1_33-35 bulk.xrdml
Intensity (counts)
90000
62500
40000
22500
10000
2500
0
15
20
25
30
35
40
45
50
55
60
2Theta (°)

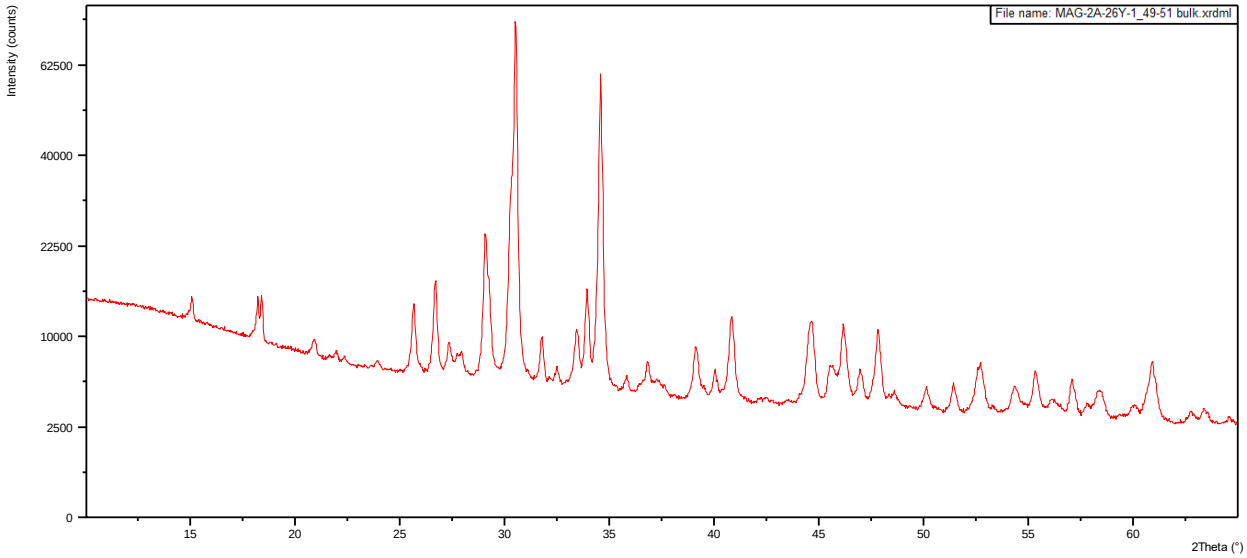
File name: MAG-2A-26Y-1_49-51 bulk.xrdml
Intensity (counts)
62500
40000
22500
10000
2500
0
15
20
25
30
35
40
45
50
55
60
2Theta (°)

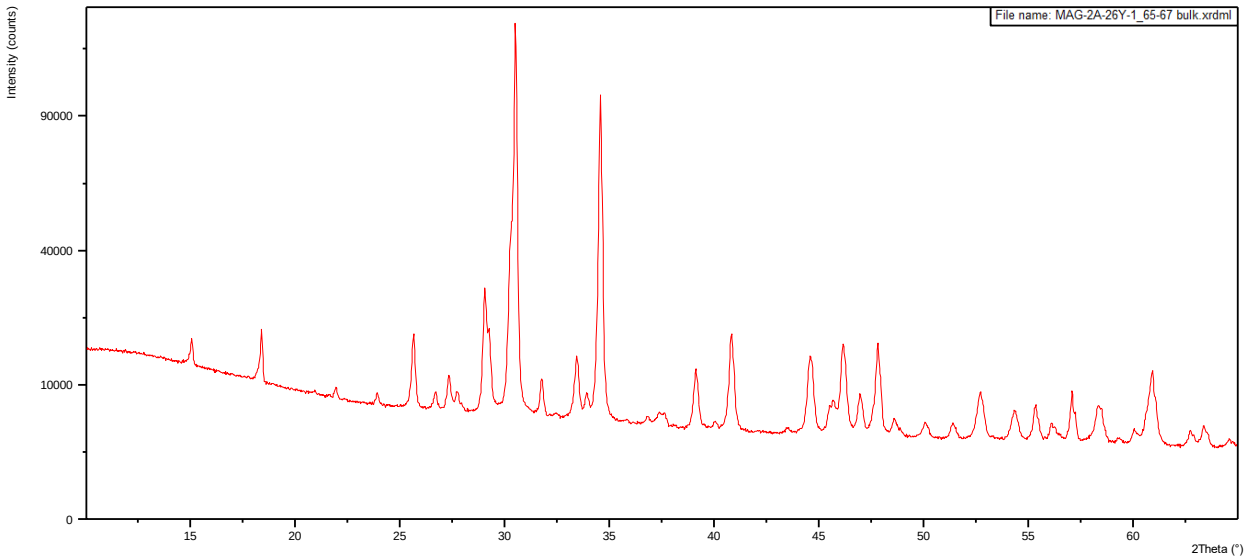
File name: MAG-2A-26Y-1_65-67 bulk.xrdml
Intensity (counts)
90000
40000
10000
0
15
20
25
30
35
40
45
50
55
60
2Theta (°)

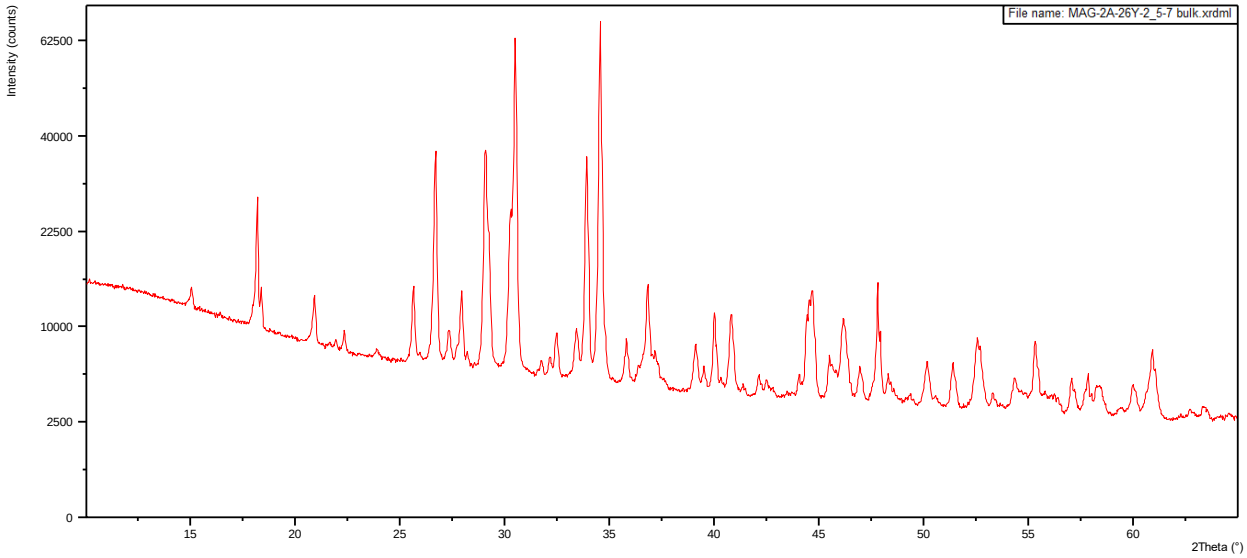
File name: MAG-2A-26Y-2_5-7 bulk.xrdml
Intensity (counts)
62500
40000
22500
10000
2500
0
15
20
25
30
35
40
45
50
55
60
2Theta (°)

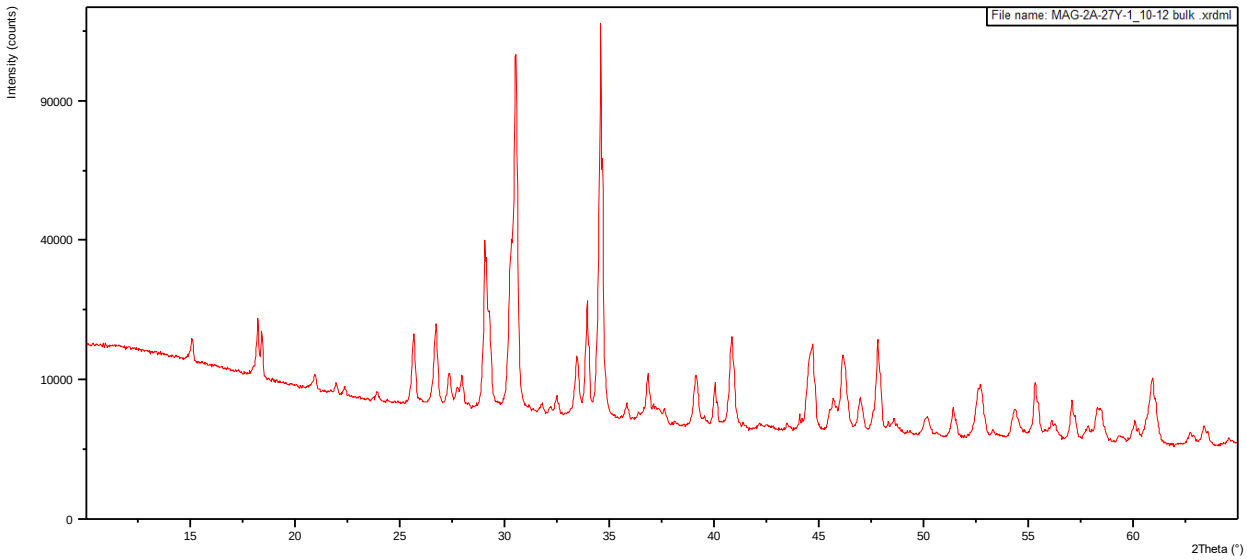
File name: MAG-2A-27Y-1_10-12 bulk .xrdml
Intensity (counts)
90000
40000
10000
0
15
20
25
30
35
40
45
50
55
60
2Theta (°)

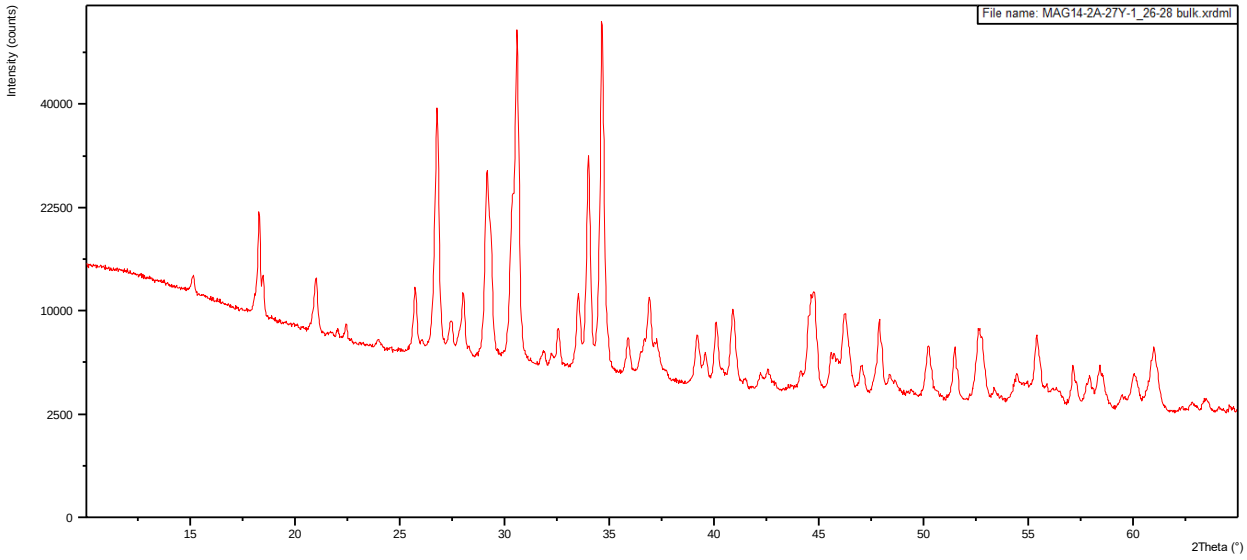
File name: MAG14-2A-27Y-1_26-28 bulk.xrdml
Intensity (counts)
40000
22500
10000
2500
0
15
20
25
30
35
40
45
50
55
60
2Theta (°)

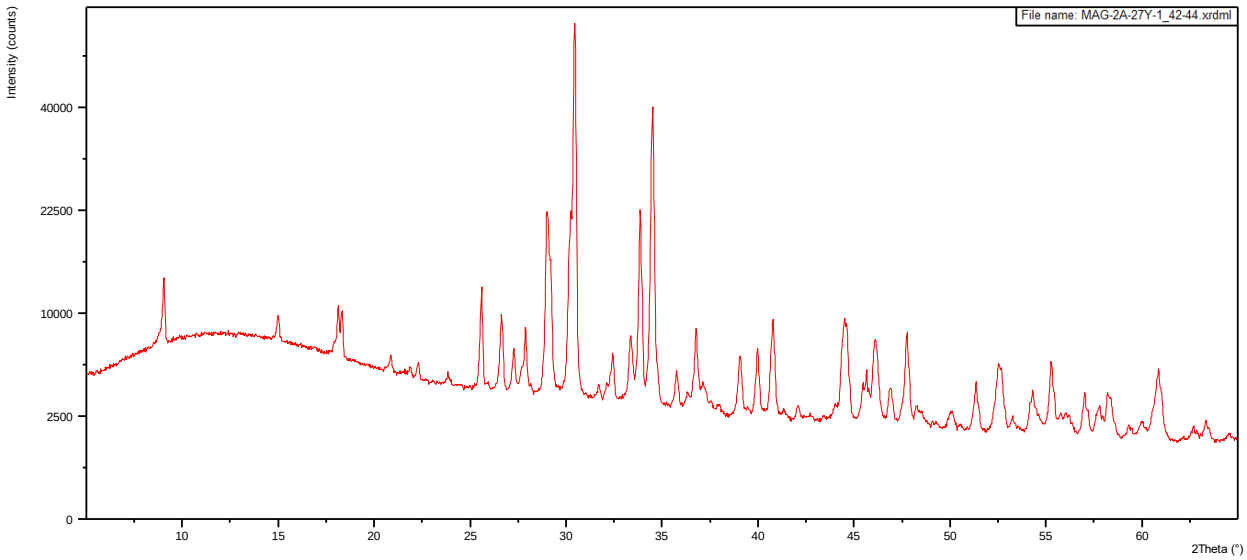
File name: MAG-2A-27Y-1_42-44.xrdml
Intensity (counts)
40000
22500
10000
2500
0
10
15
20
25
30
35
40
45
50
55
60
2Theta (°)

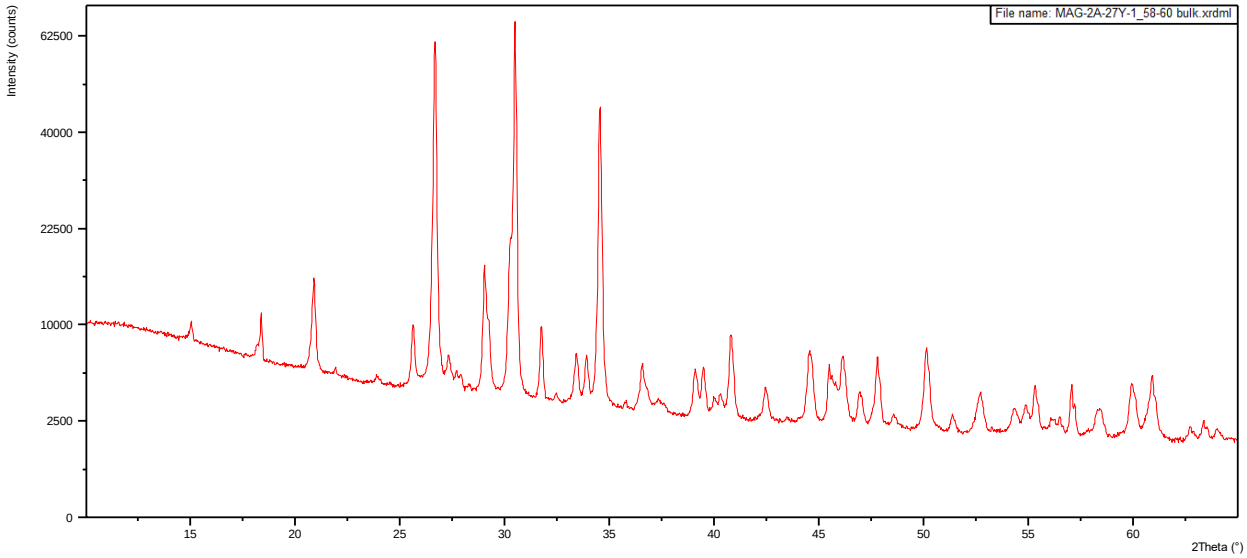
File name: MAG-2A-27Y-1_58-60 bulk.xrdml
Intensity (counts)
62500
40000
22500
10000
2500
0
15
20
25
30
35
40
45
50
55
60
2Theta (°)

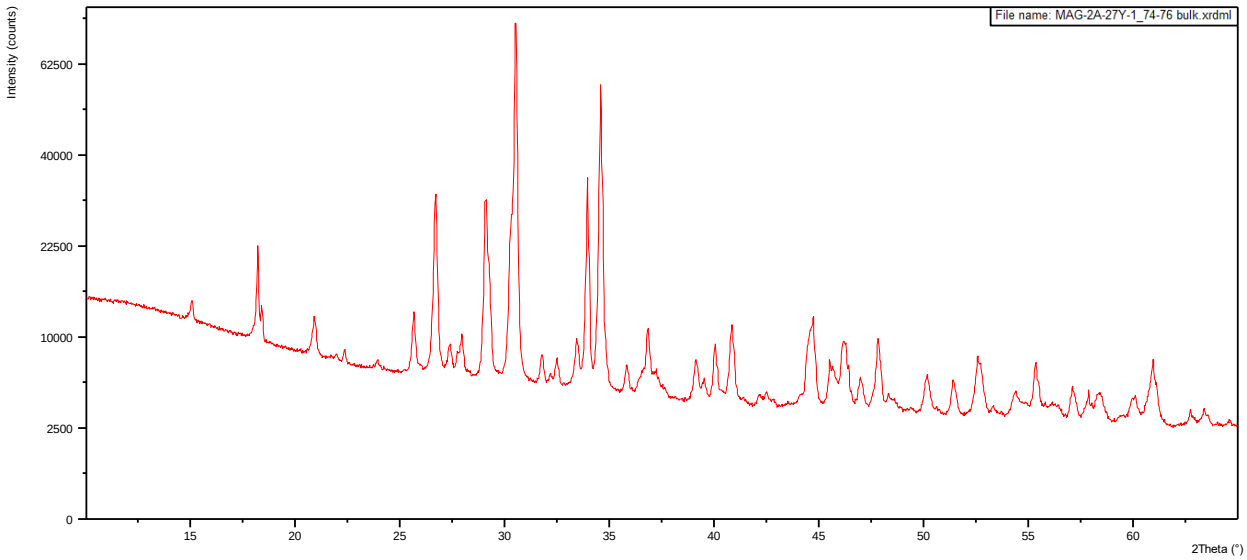
File name: MAG-2A-27Y-1_74-76 bulk.xrdml
Intensity (counts)
62500
40000
22500
10000
2500
0
15
20
25
30
35
40
45
50
55
60
2Theta (°)

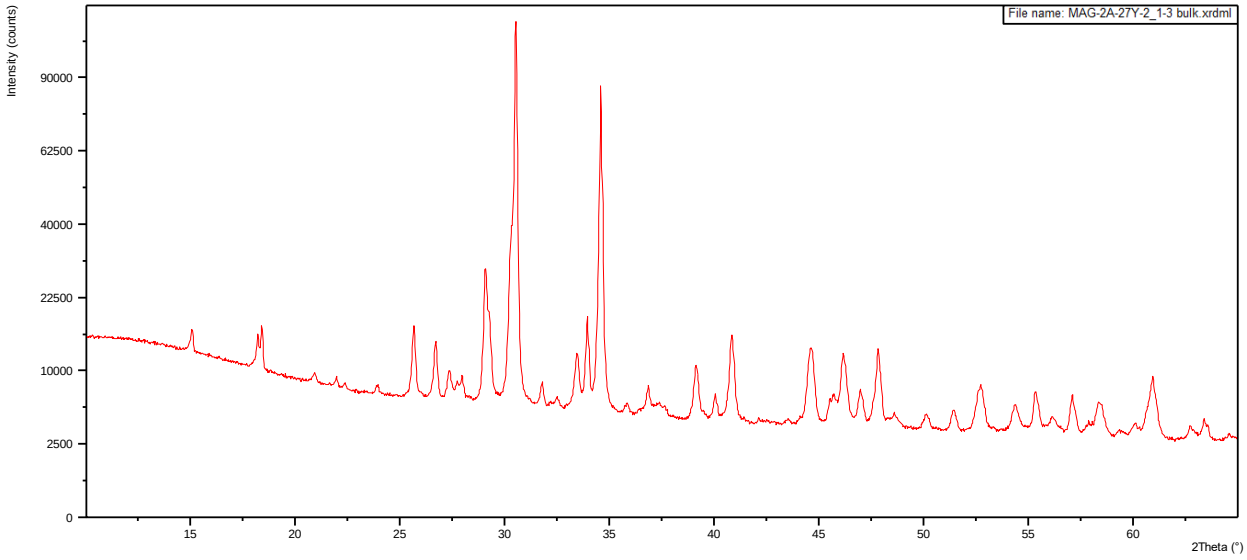
File name: MAG-2A-27Y-2_1-3 bulk.xrdml
Intensity (counts)
90000
62500
40000
22500
10000
2500
0
15
20
25
30
35
40
45
50
55
60
2Theta (°)

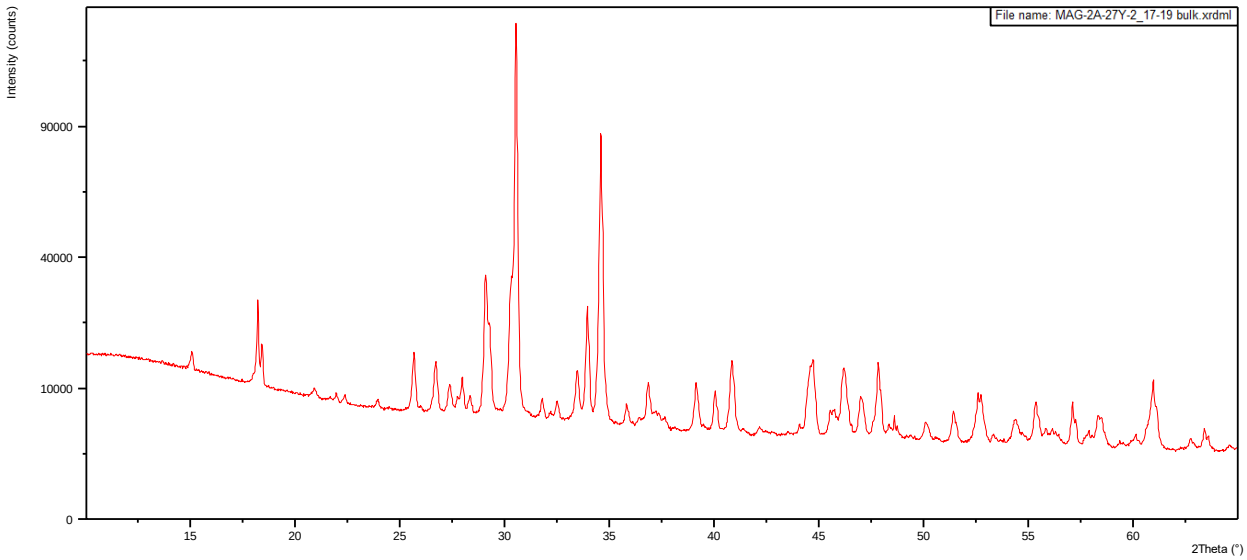
File name: MAG-2A-27Y-2_17-19 bulk.xrdml
Intensity (counts)
90000
40000
10000
0
15
20
25
30
35
40
45
50
55
60
2Theta (°)

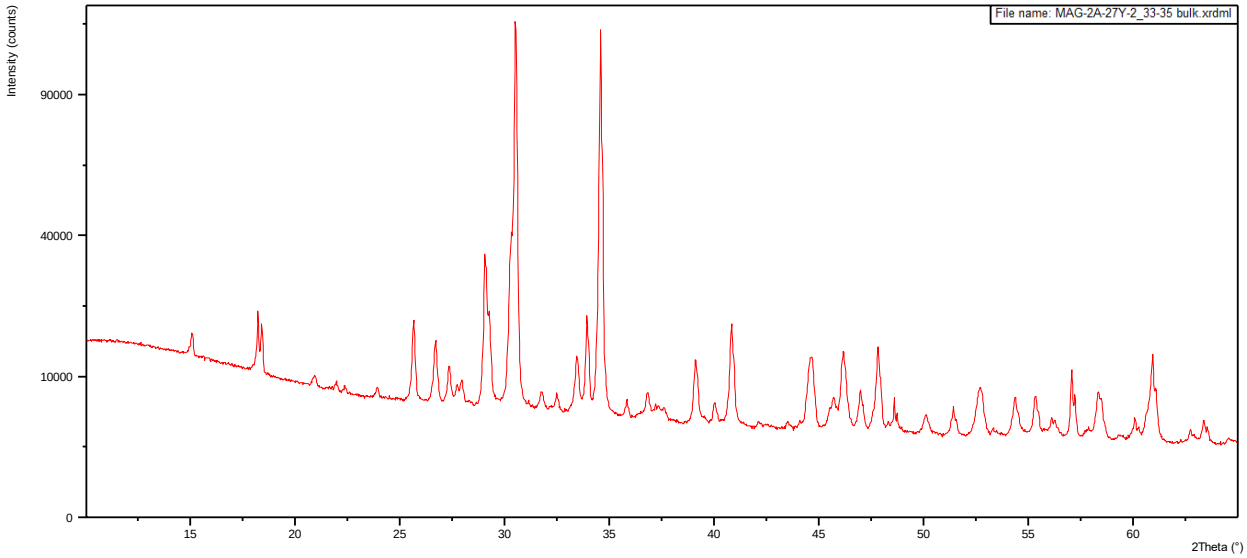
File name: MAG-2A-27Y-2_33-35 bulk.xrdml
Intensity (counts)
90000
40000
10000
0
15
20
25
30
35
40
45
50
55
60
2Theta (°)

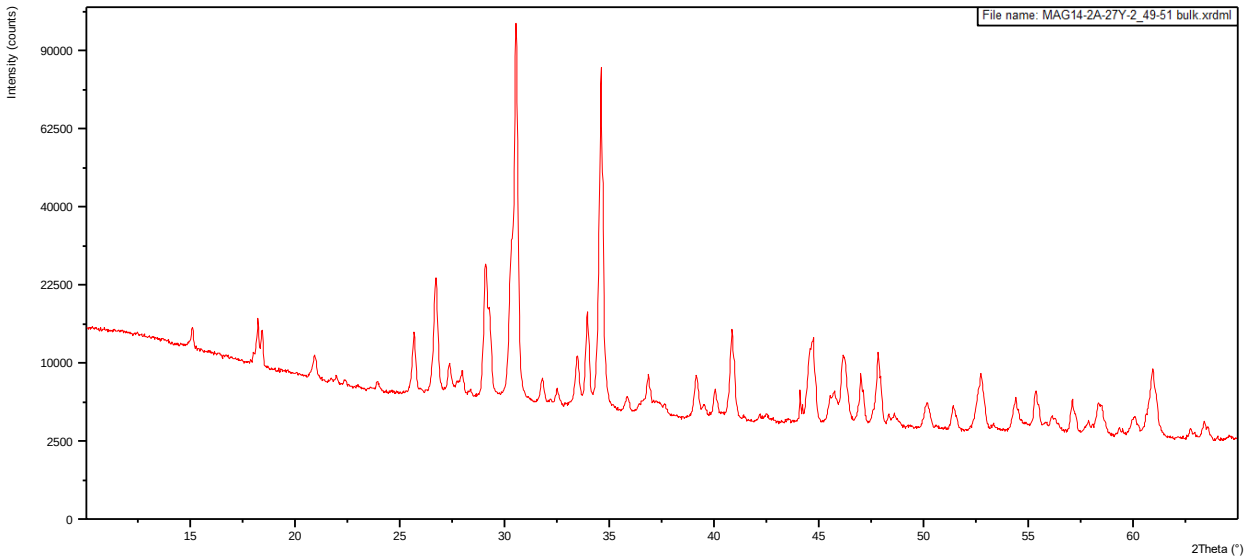
File name: MAG14-2A-27Y-2_49-51 bulk.xrdml
Intensity (counts)
90000
62500
40000
22500
10000
2500
0
15
20
25
30
35
40
45
50
55
60
2Theta (°)

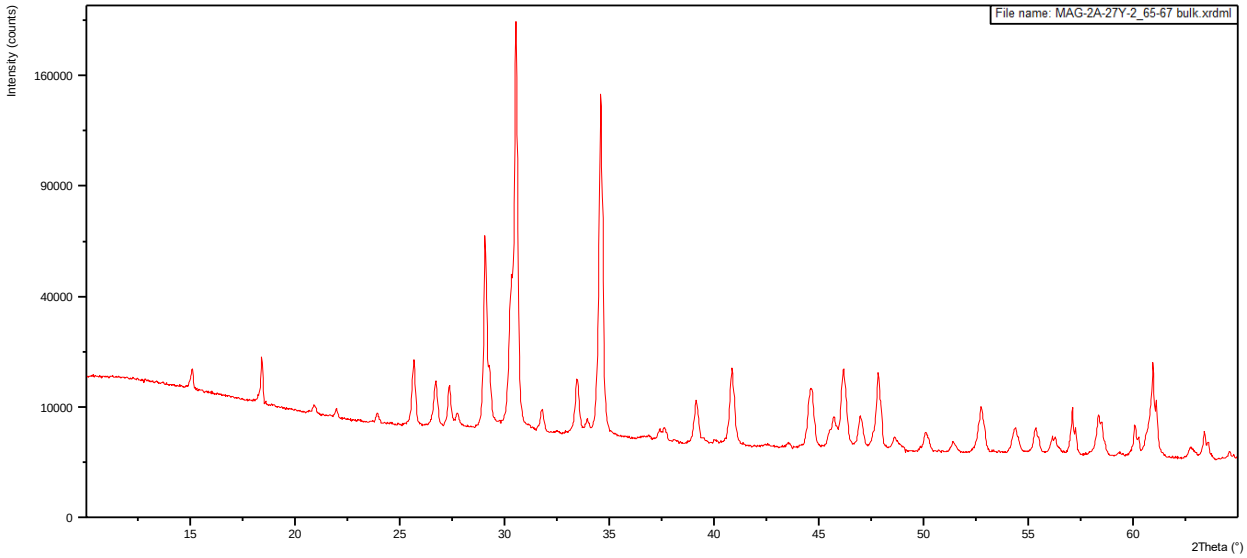
File name: MAG-2A-27Y-2_65-67 bulk.xrdml
Intensity (counts)
160000
90000
40000
10000
0
15
20
25
30
35
40
45
50
55
60
2Theta (°)

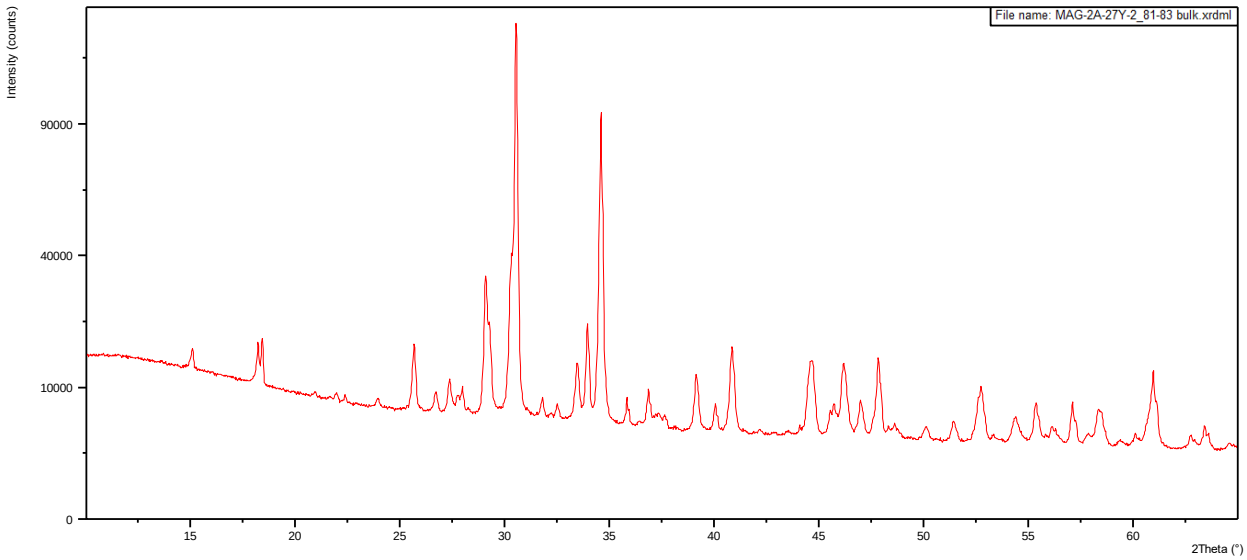
File name: MAG-2A-27Y-2_81-83 bulk.xrdml
Intensity (counts)
90000
40000
10000
0
15
20
25
30
35
40
45
50
55
60
2Theta (°)

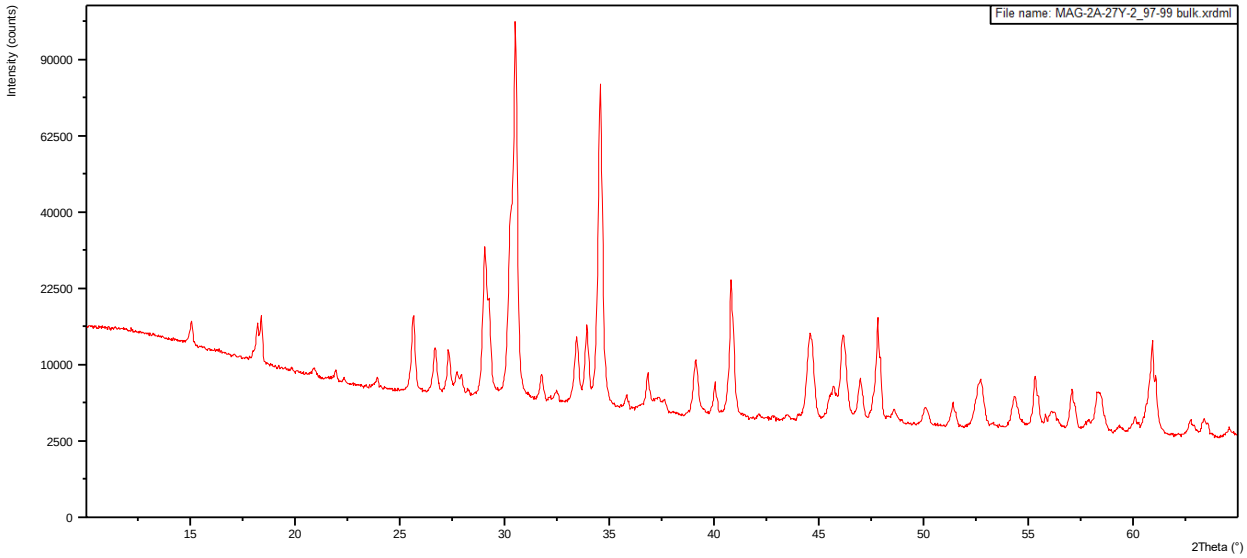
File name: MAG-2A-27Y-2_97-99 bulk.xrdml
Intensity (counts)
90000
62500
40000
22500
10000
2500
0
15
20
25
30
35
40
45
50
55
60
2Theta (°)

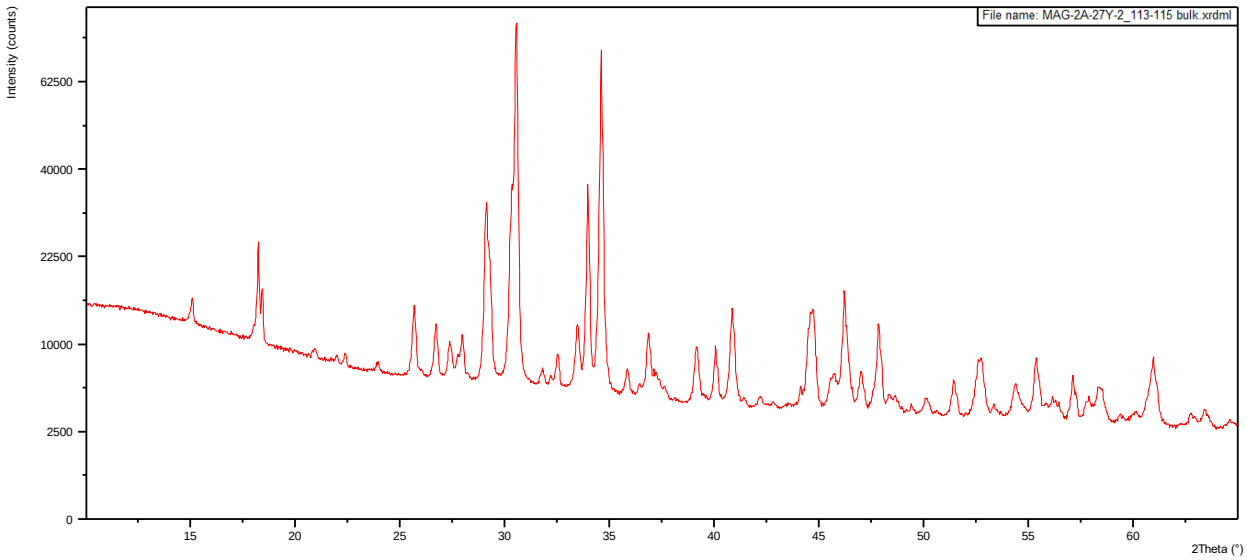
File name: MAG-2A-27Y-2_113-115 bulk.xrdml
Intensity (counts)
62500
40000
22500
10000
2500
0
15
20
25
30
35
40
45
50
55
60
2Theta (°)

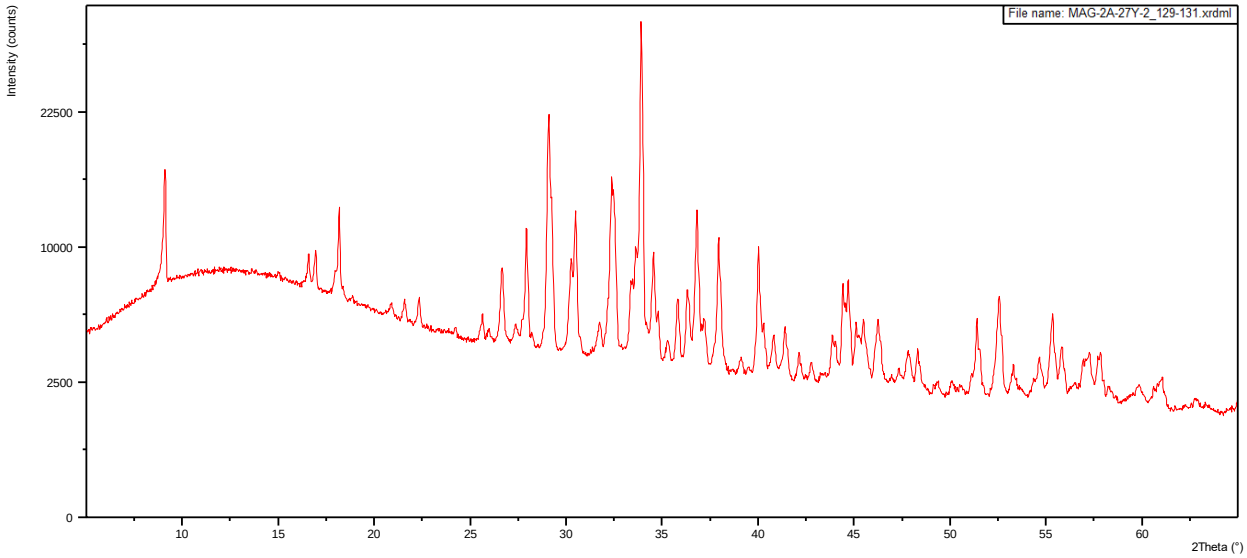
File name: MAG-2A-27Y-2_129-131.xrdml
Intensity (counts)
22500
10000
2500
0
10
15
20
25
30
35
40
45
50
55
60
2Theta (°)

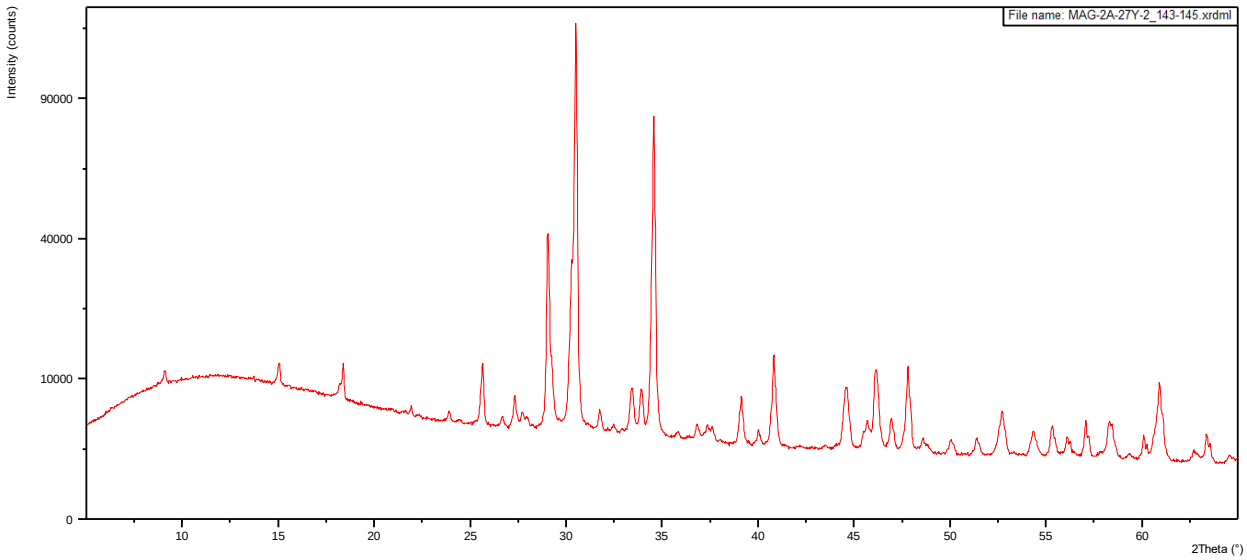
File name: MAG-2A-27Y-2_143-145.xrdml
Intensity (counts)
90000
40000
10000
0
10
15
20
25
30
35
40
45
50
55
60
2Theta (°)

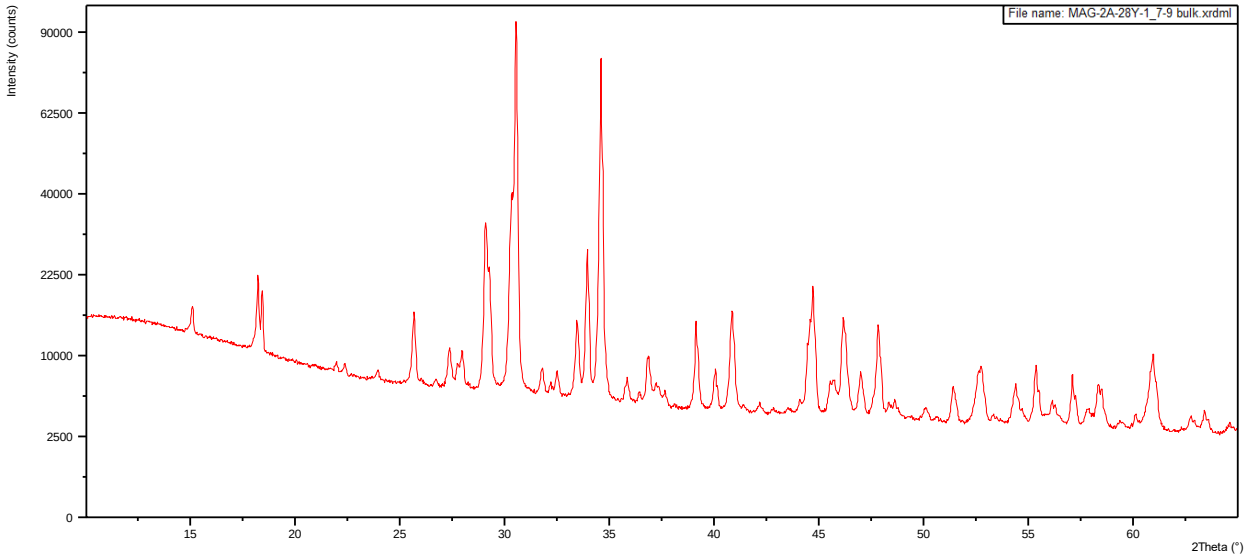
File name: MAG-2A-28Y-1_7-9 bulk.xrdml
Intensity (counts)
90000
62500
40000
22500
10000
2500
0
15
20
25
30
35
40
45
50
55
60
2Theta (°)

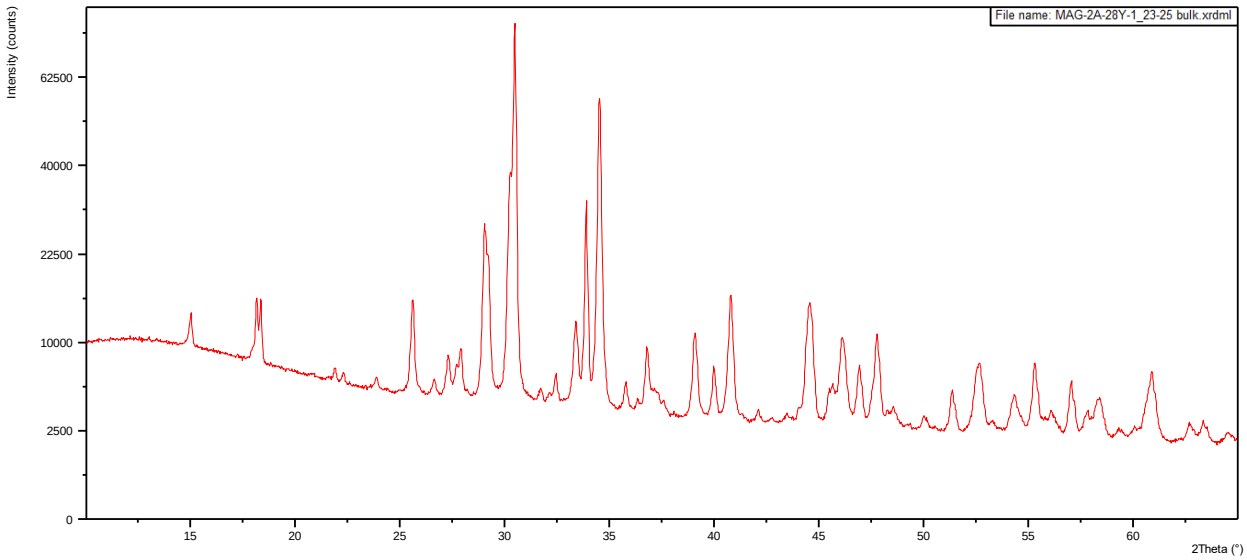
File name: MAG-2A-28Y-1_23-25 bulk.xrdml
Intensity (counts)
62500
40000
22500
10000
2500
0
15
20
25
30
35
40
45
50
55
60
2Theta (°)

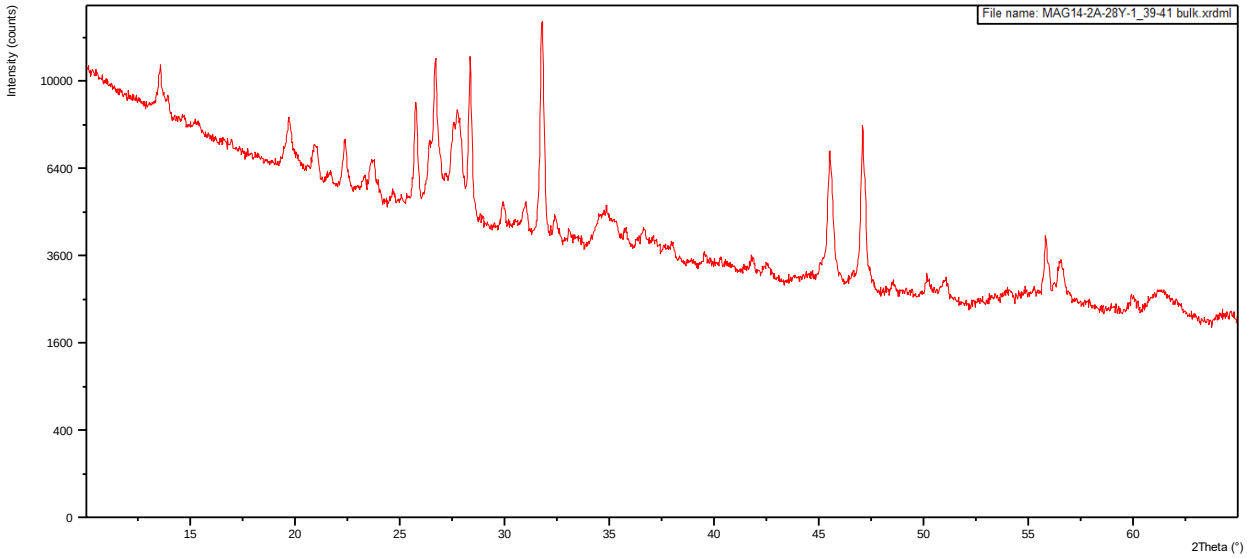
File name: MAG14-2A-28Y-1_39-41 bulk.xrdml
Intensity (counts)
10000
6400
3600
1600
400
0
15
20
25
30
35
40
45
50
55
60
2Theta (°)

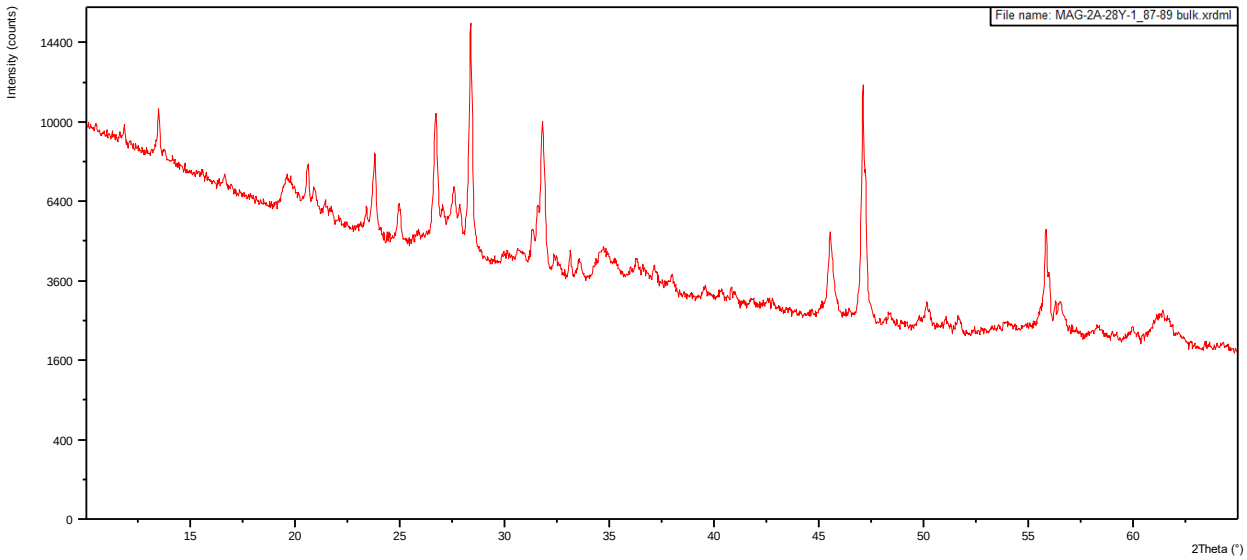
File name: MAG-2A-28Y-1_87-89 bulk.xrdml
Intensity (counts)
14400
10000
6400
3600
1600
400
0
15
20
25
30
35
40
45
50
55
60
2Theta (°)

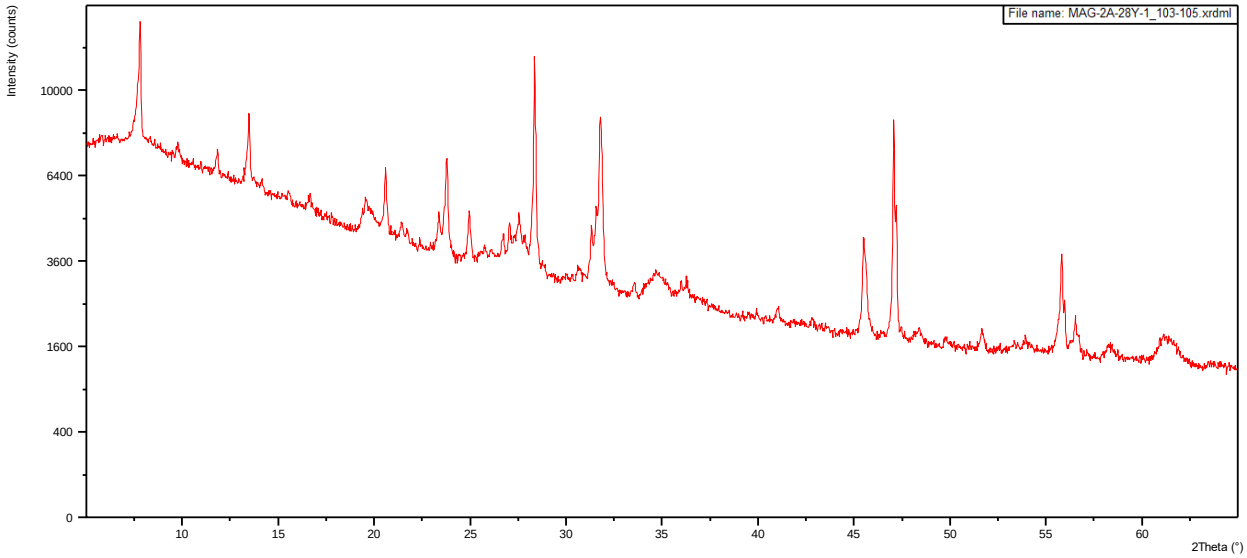
File name: MAG-2A-28Y-1_103-105.xrdml
Intensity (counts)
10000
6400
3600
1600
400
0
10
15
20
25
30
35
40
45
50
55
60
2Theta (°)

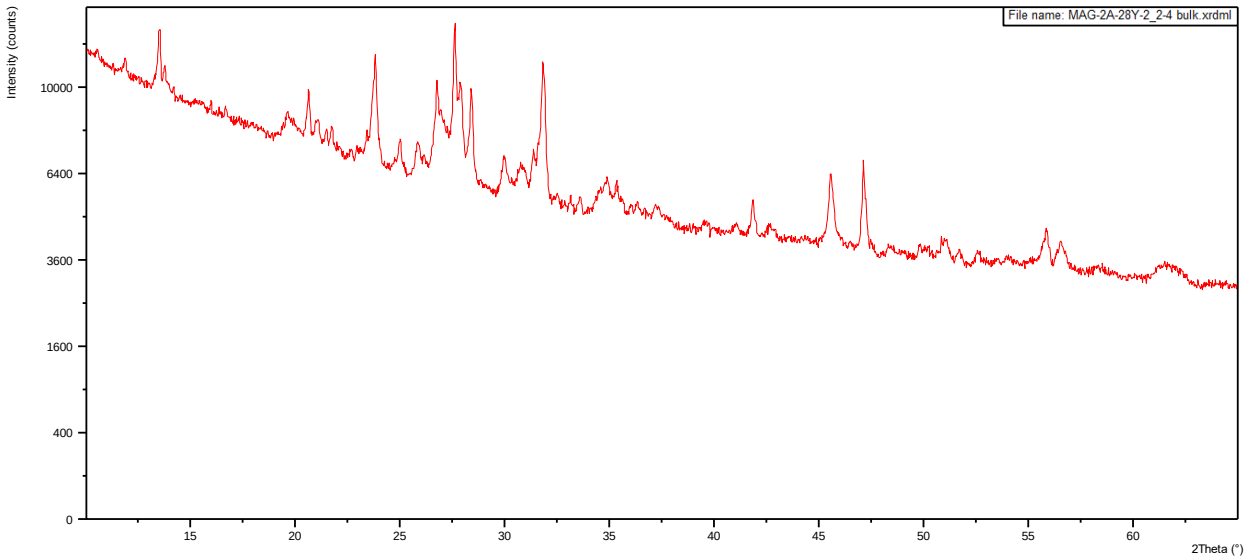
File name: MAG-2A-28Y-2_2-4 bulk.xrdml
Intensity (counts)
10000
6400
3600
1600
400
0
15
20
25
30
35
40
45
50
55
60
2Theta (°)

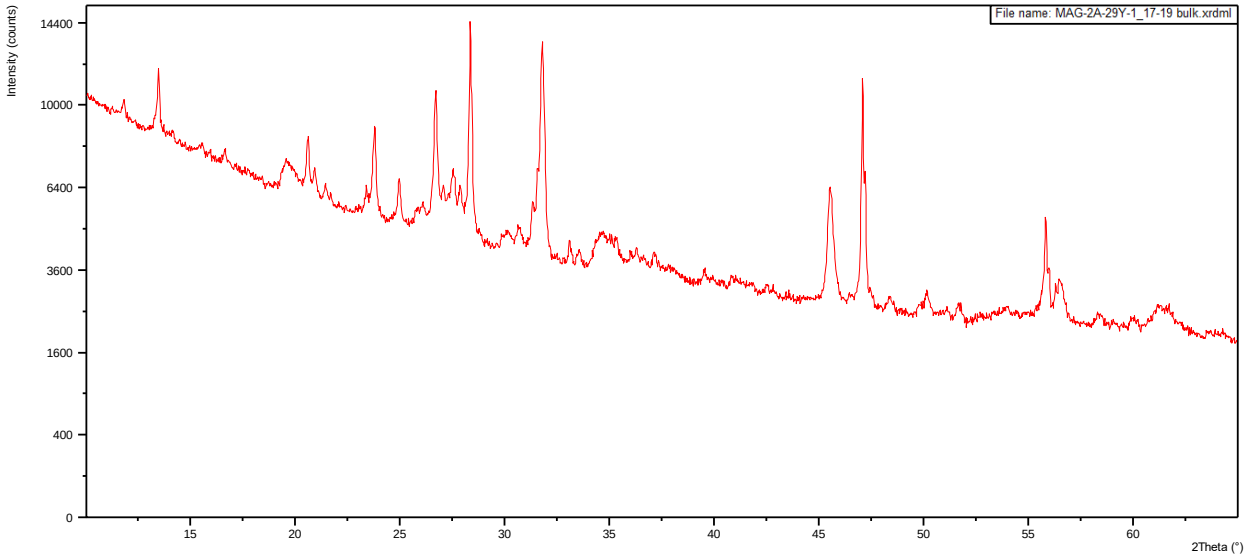
File name: MAG-2A-29Y-1_17-19 bulk.xrdml
Intensity (counts)
14400
10000
6400
3600
1600
400
0
15
20
25
30
35
40
45
50
55
60
2Theta (°)

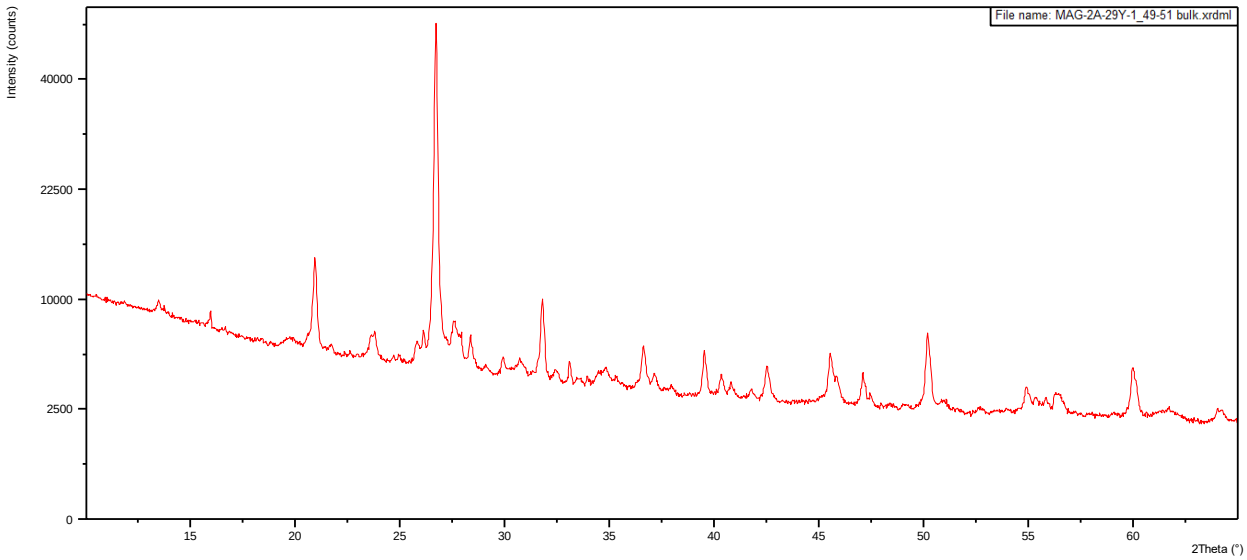
File name: MAG-2A-29Y-1_49-51 bulk.xrdml
Intensity (counts)
40000
22500
10000
2500
0
15
20
25
30
35
40
45
50
55
60
2Theta (°)

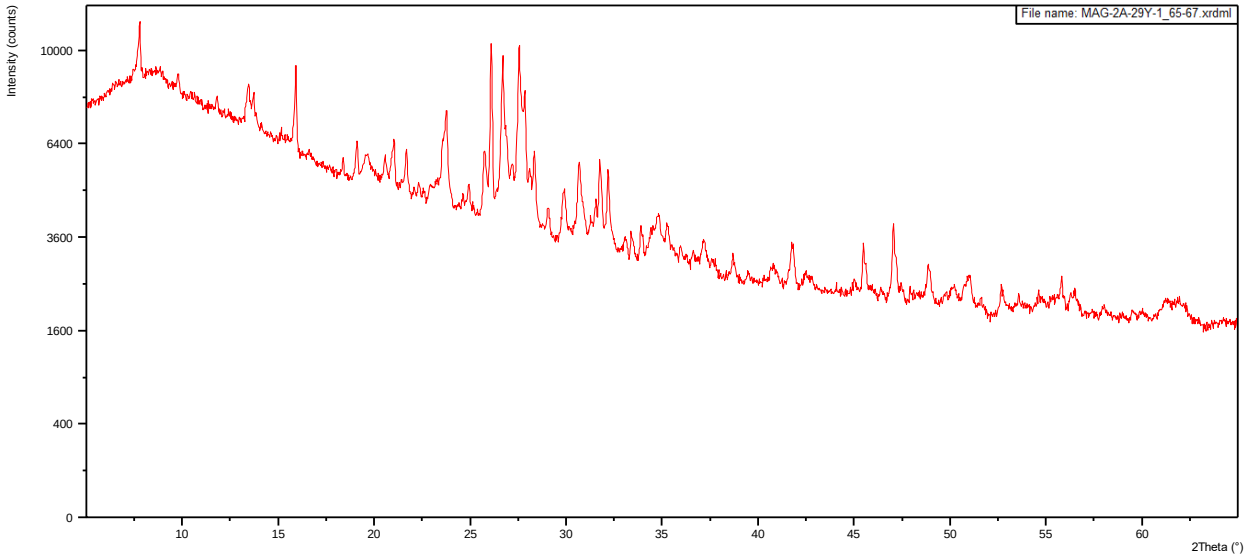
File name: MAG-2A-29Y-1_65-67.xrdml
Intensity (counts)
10000
6400
3600
1600
400
0
10
15
20
25
30
35
40
45
50
55
60
2Theta (°)

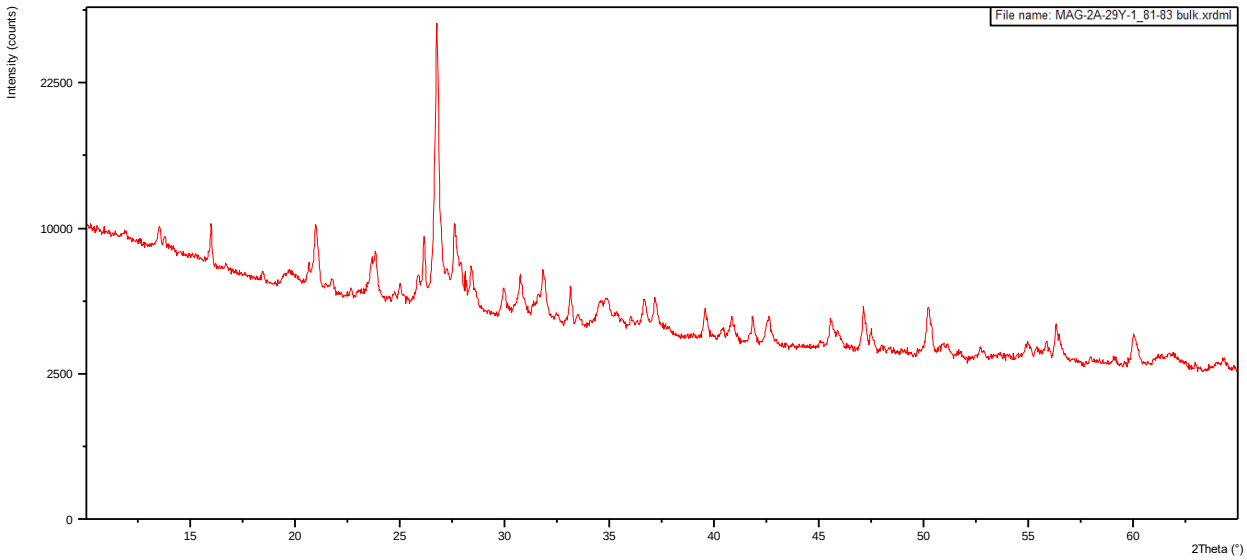
File name: MAG-2A-29Y-1_81-83 bulk.xrdml
Intensity (counts)
22500
10000
2500
0
15
20
25
30
35
40
45
50
55
60
2Theta (°)

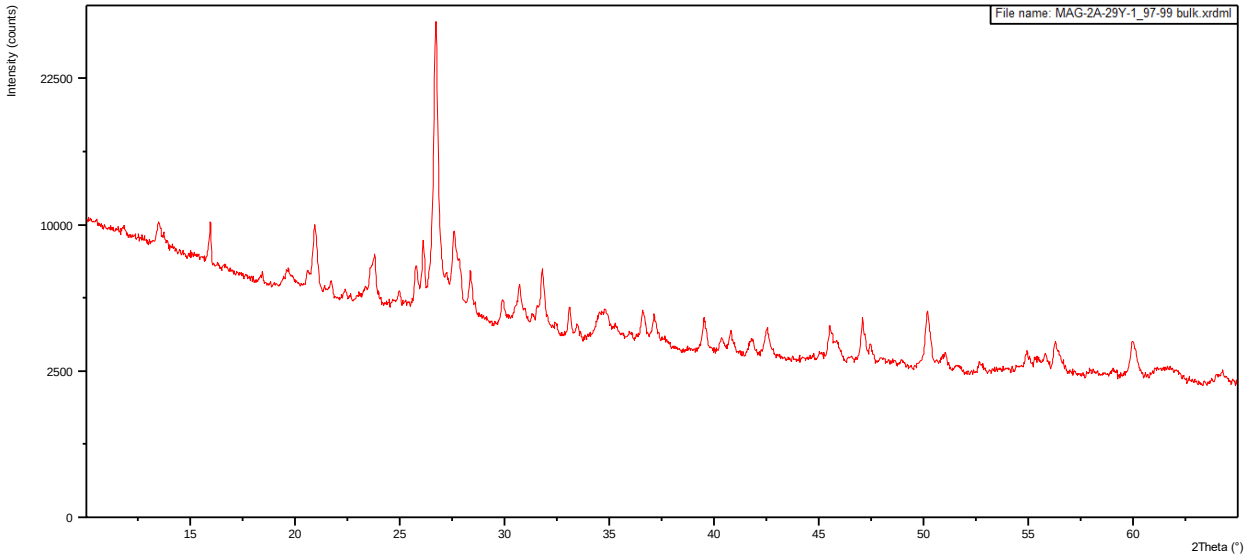
File name: MAG-2A-29Y-1_97-99 bulk.xrdml
Intensity (counts)
22500
10000
2500
0
15
20
25
30
35
40
45
50
55
60
2Theta (°)

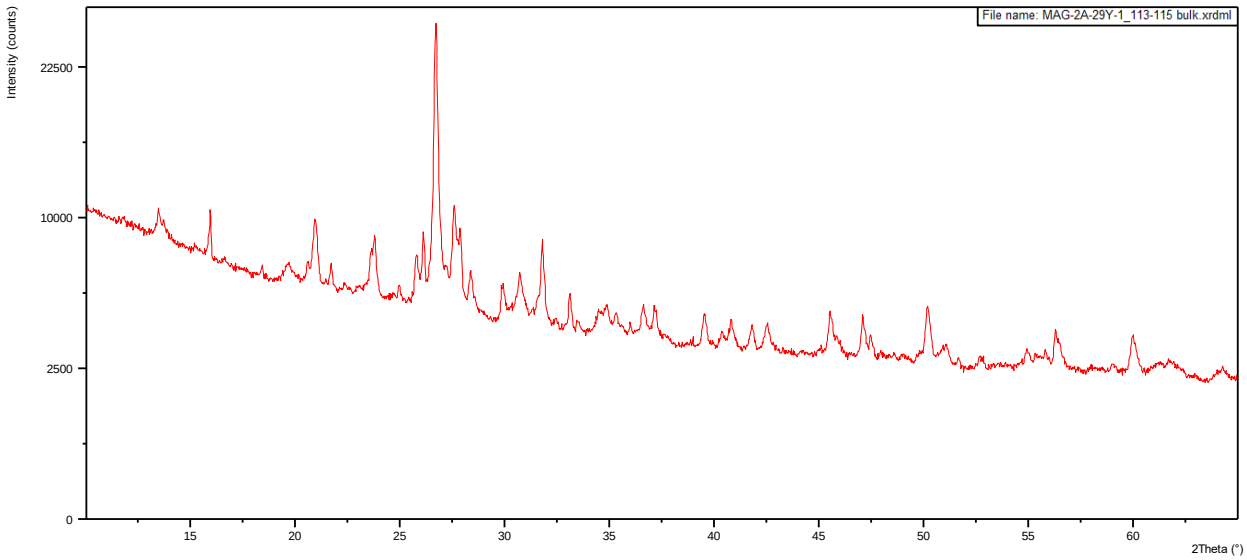
File name: MAG-2A-29Y-1_113-115 bulk.xrdml
Intensity (counts)
22500
10000
2500
0
15
20
25
30
35
40
45
50
55
60
2Theta (°)

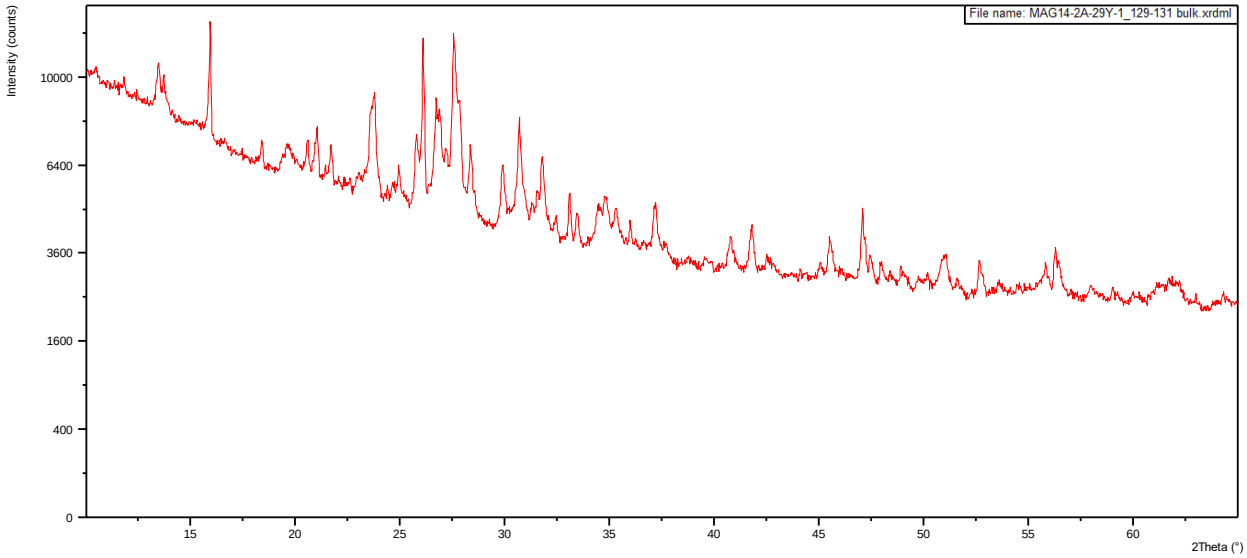
File name: MAG14-2A-29Y-1_129-131 bulk.xrdml
Intensity (counts)
10000
6400
3600
1600
400
0
15
20
25
30
35
40
45
50
55
60
2Theta (°)

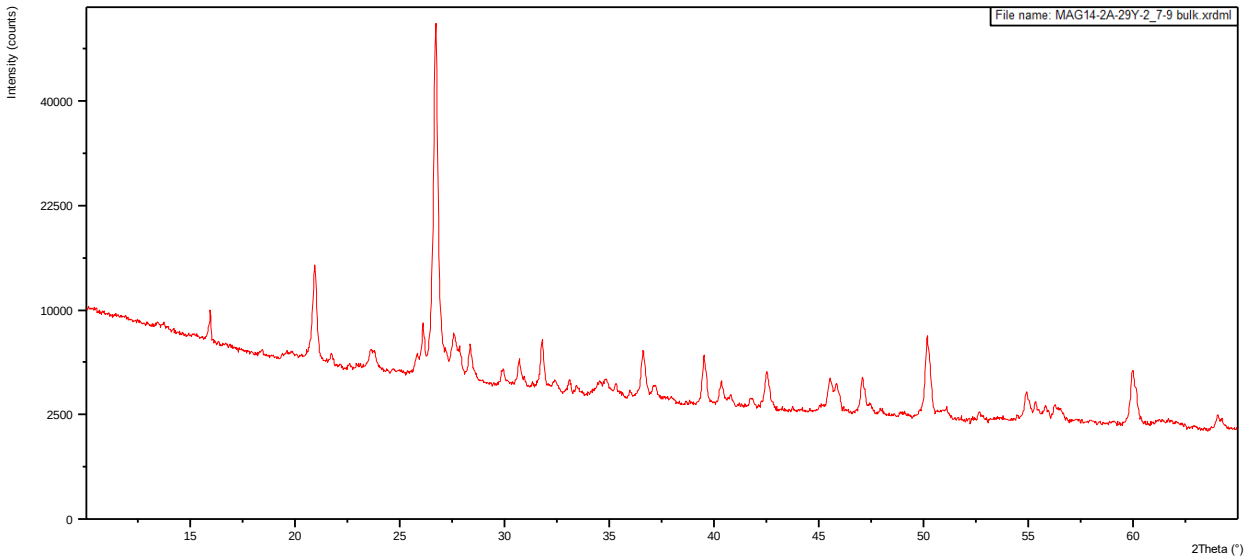
File name: MAG14-2A-29Y-2_7-9 bulk.xrdml
Intensity (counts)
40000
22500
10000
2500
0
15
20
25
30
35
40
45
50
55
60
2Theta (°)

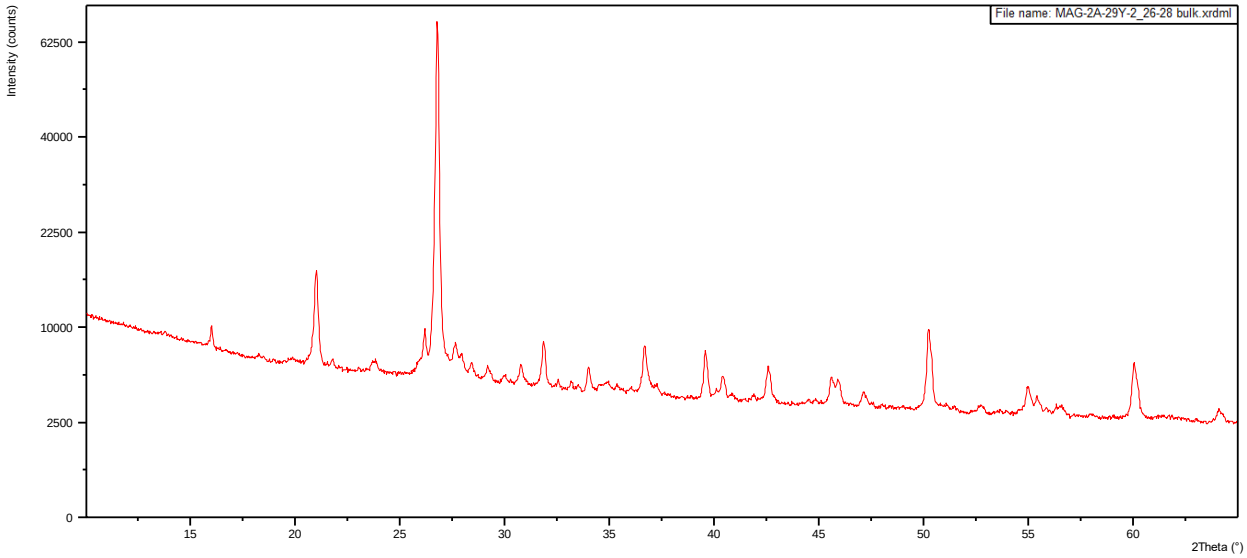
File name: MAG-2A-29Y-2_26-28 bulk.xrdml
Intensity (counts)
62500
40000
22500
10000
2500
0
15
20
25
30
35
40
45
50
55
60
2Theta (°)

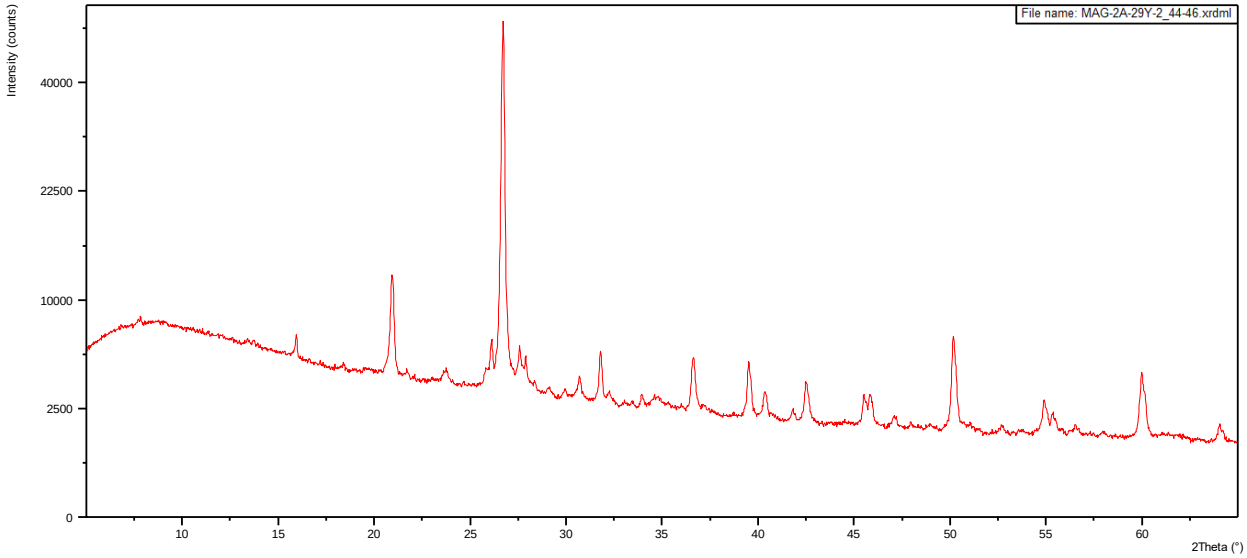
File name: MAG-2A-29Y-2_44-46.xrdml
Intensity (counts)
0
2500
10000
22500
40000
10
15
20
25
30
35
40
45
50
55
60
2Theta (°)

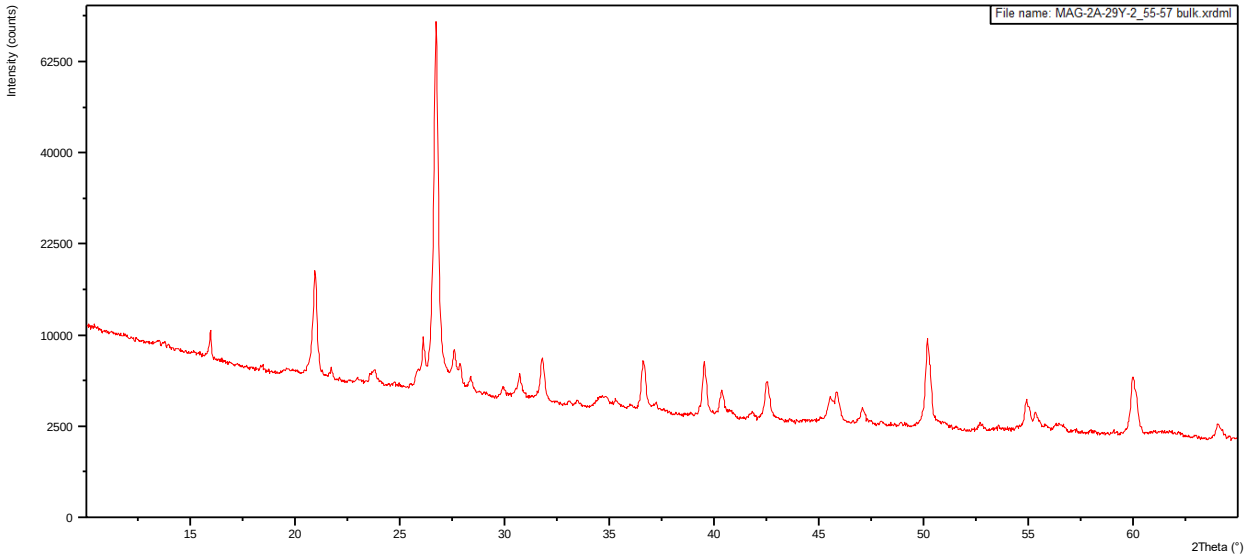
File name: MAG-2A-29Y-2_55-57 bulk.xrdml
Intensity (counts)
0
2500
10000
22500
40000
62500
15
20
25
30
35
40
45
50
55
60
2Theta (°)

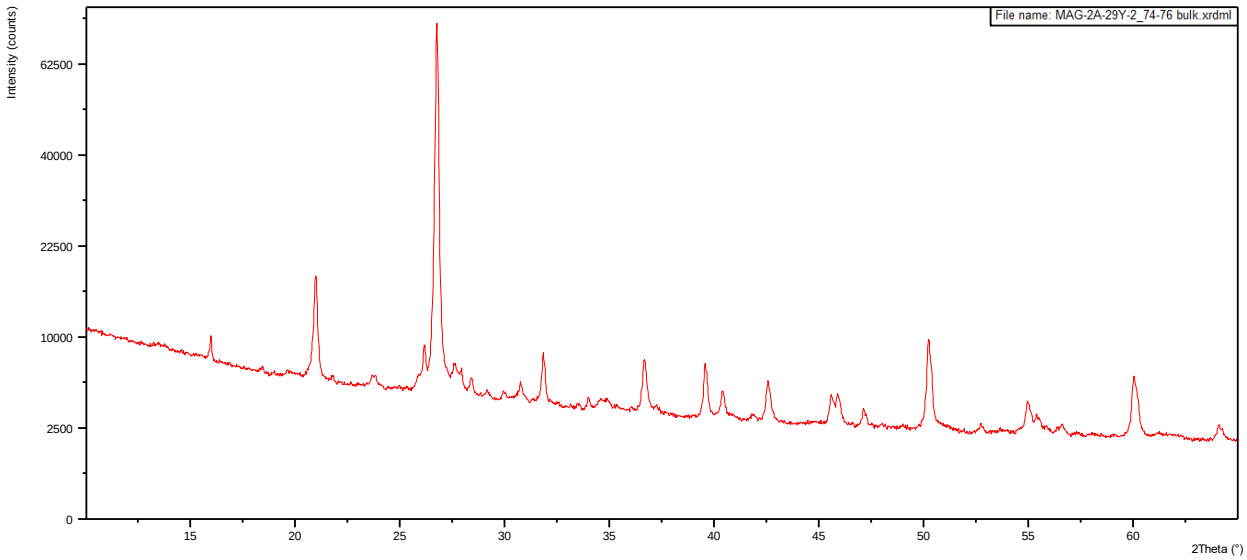
File name: MAG-2A-29Y-2_74-76 bulk.xrdml
Intensity (counts)
62500
40000
22500
10000
2500
0
15
20
25
30
35
40
45
50
55
60
2Theta (°)

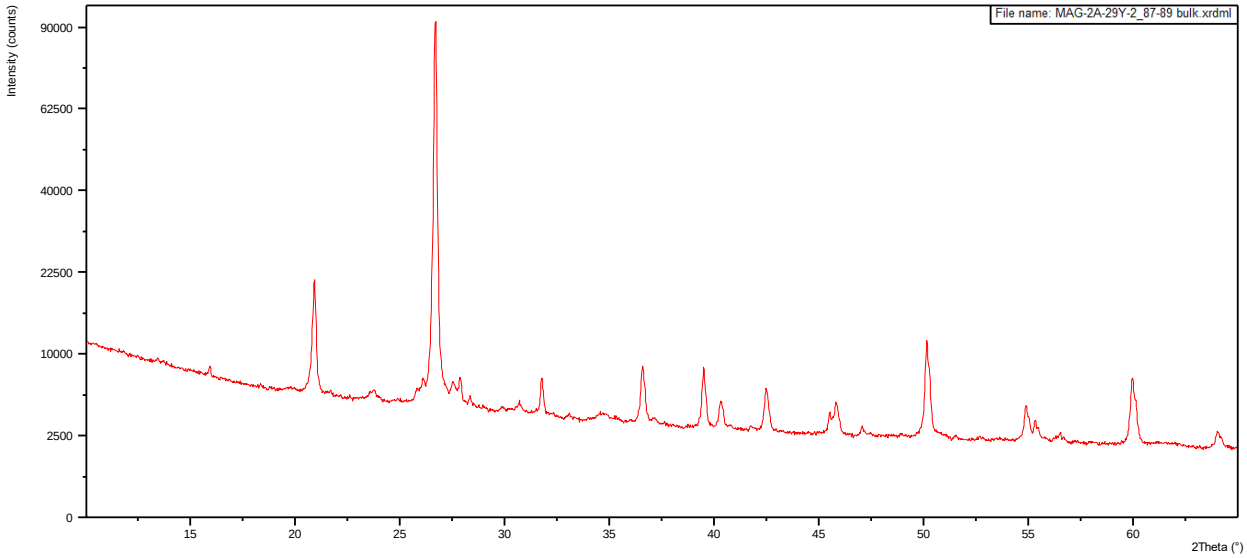
File name: MAG-2A-29Y-2_87-89 bulk.xrdml
Intensity (counts)
90000
62500
40000
22500
10000
2500
0
15
20
25
30
35
40
45
50
55
60
2Theta (°)

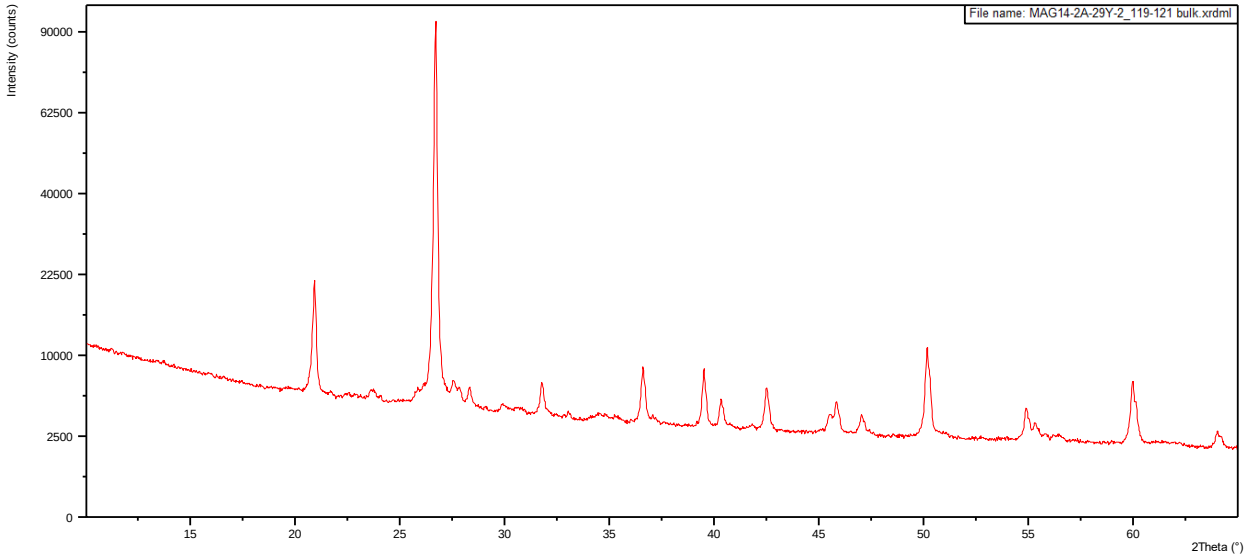
File name: MAG14-2A-29Y-2_119-121 bulk.xrdml
Intensity (counts)
90000
62500
40000
22500
10000
2500
0
15
20
25
30
35
40
45
50
55
60
2Theta (°)

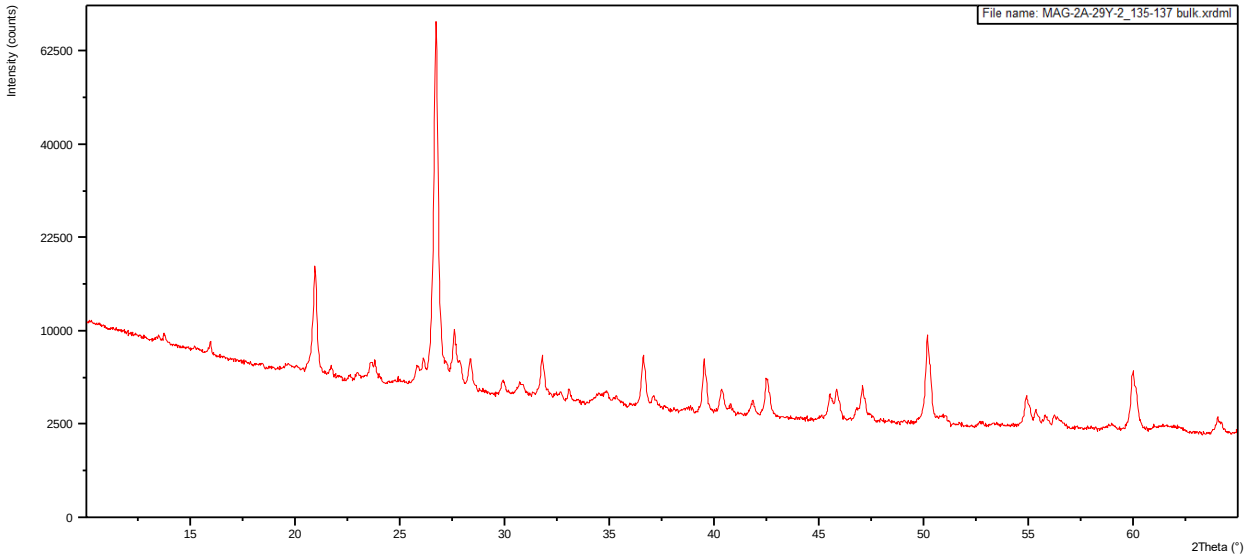
File name: MAG-2A-29Y-2_135-137 bulk.xrdml
Intensity (counts)
62500
40000
22500
10000
2500
0
15
20
25
30
35
40
45
50
55
60
2Theta (°)

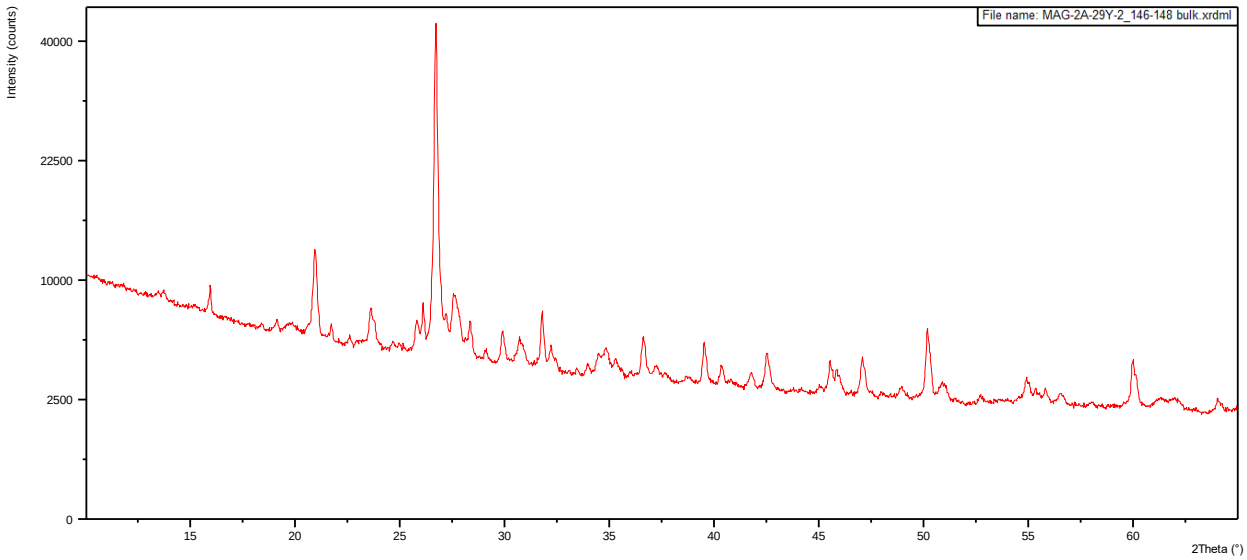
File name: MAG-2A-29Y-2_146-148 bulk.xrdml
Intensity (counts)
40000
22500
10000
2500
0
15
20
25
30
35
40
45
50
55
60
2Theta (°)

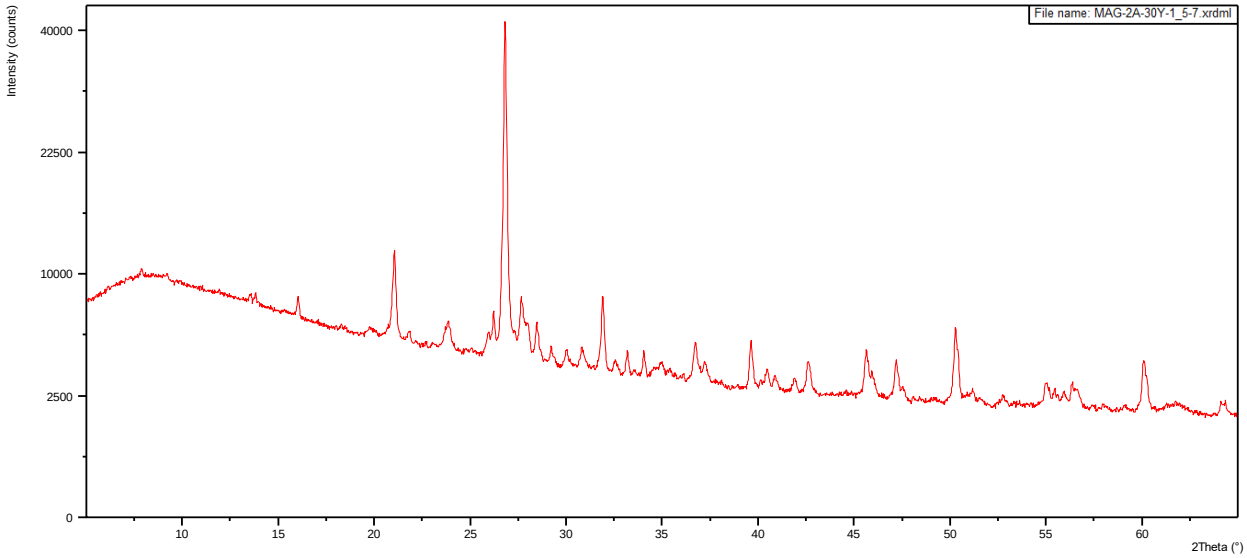
File name: MAG-2A-30Y-1_5-7.xrdml
Intensity (counts)
40000
22500
10000
2500
0
10
15
20
25
30
35
40
45
50
55
60
2Theta (°)

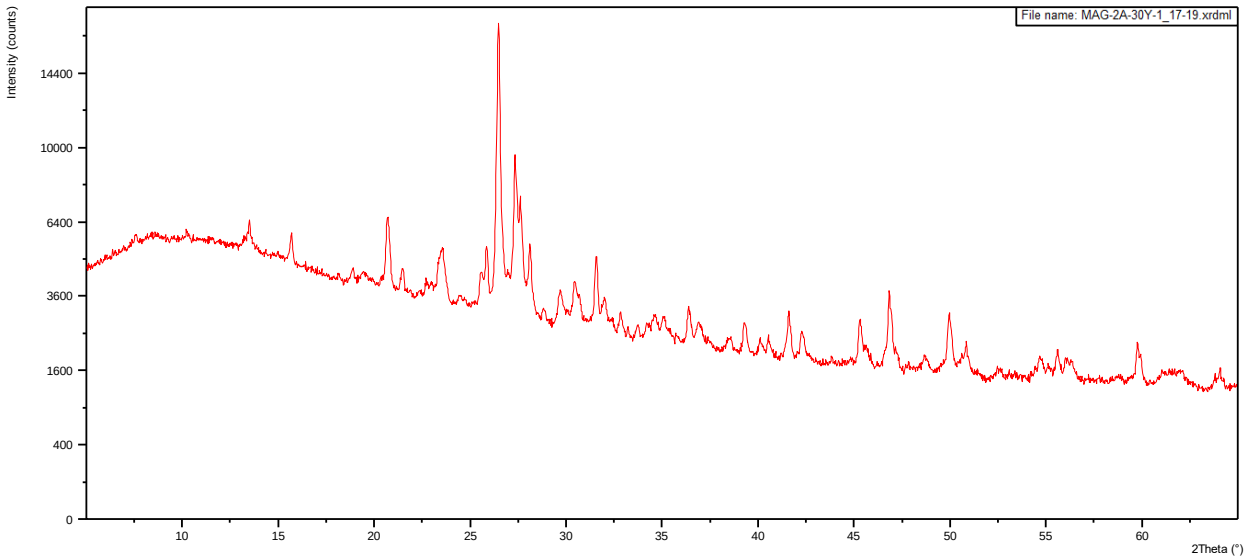
File name: MAG-2A-30Y-1_17-19.xrdml
Intensity (counts)
14400
10000
6400
3600
1600
400
0
10
15
20
25
30
35
40
45
50
55
60
2Theta (°)

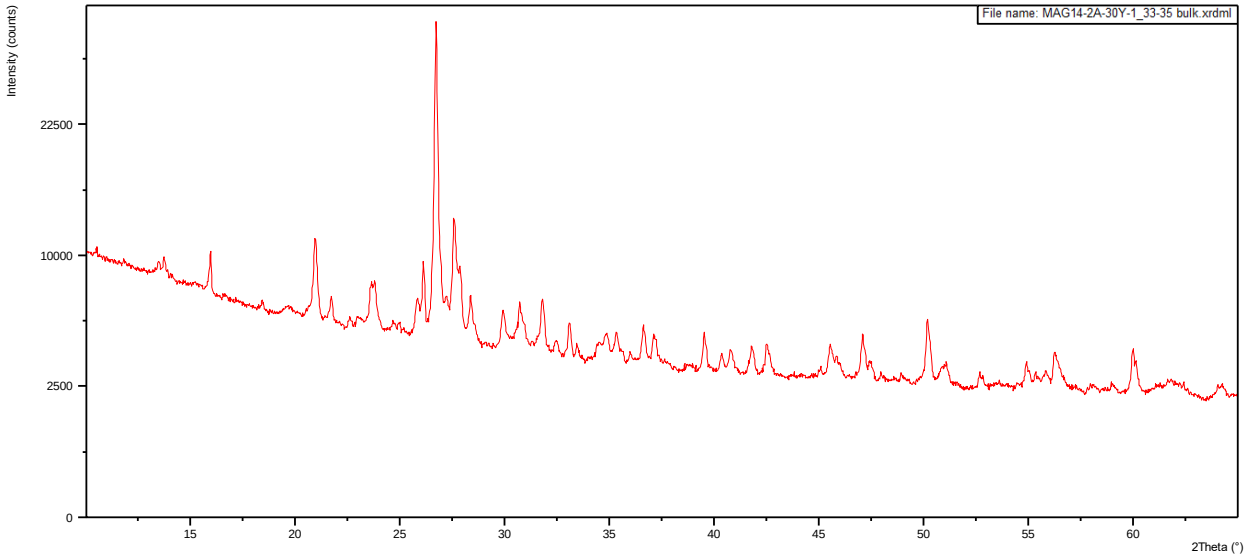
File name: MAG14-2A-30Y-1_33-35 bulk.xrdml
Intensity (counts)
22500
10000
2500
0
15
20
25
30
35
40
45
50
55
60
2Theta (°)

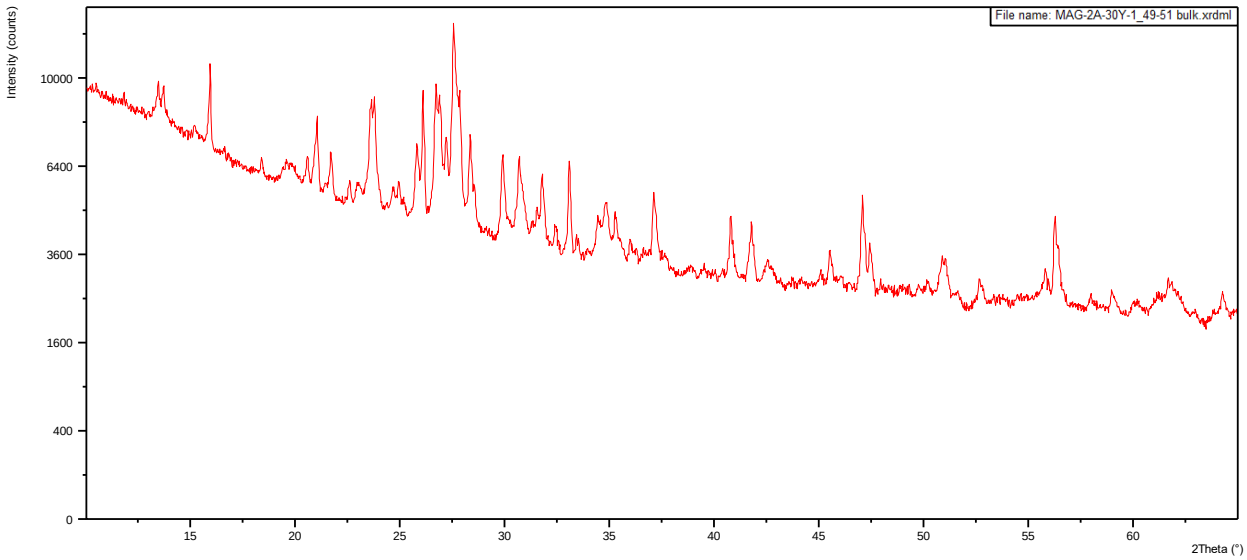
File name: MAG-2A-30Y-1_49-51 bulk.xrdml
Intensity (counts)
10000
6400
3600
1600
400
0
15
20
25
30
35
40
45
50
55
60
2Theta (°)

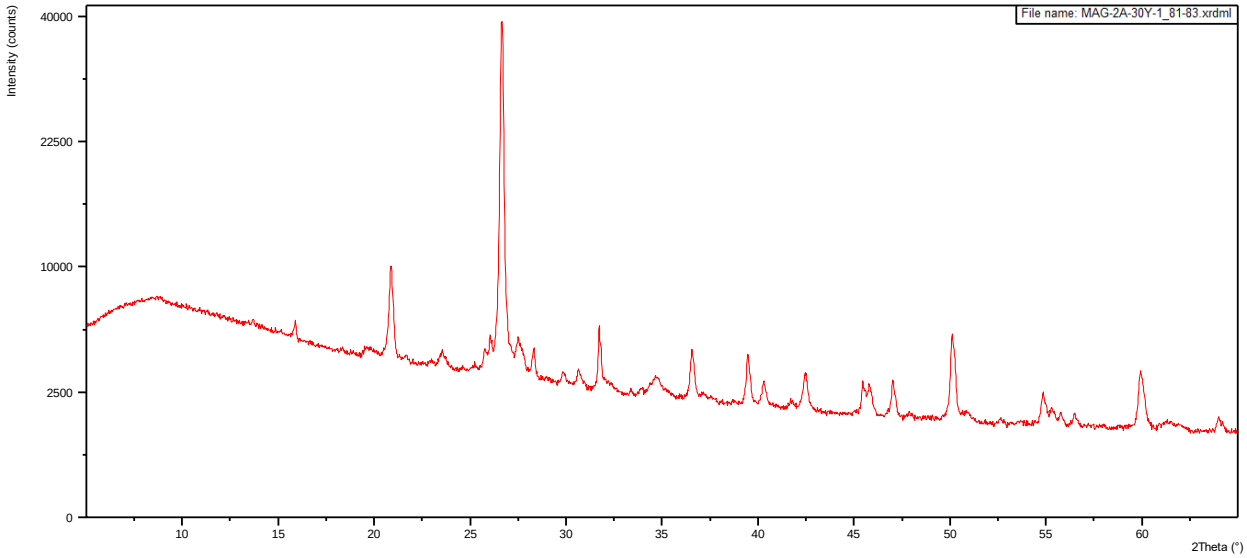
File name: MAG-2A-30Y-1_81-83.xrdml
Intensity (counts)
40000
22500
10000
2500
0
10
15
20
25
30
35
40
45
50
55
60
2Theta (°)

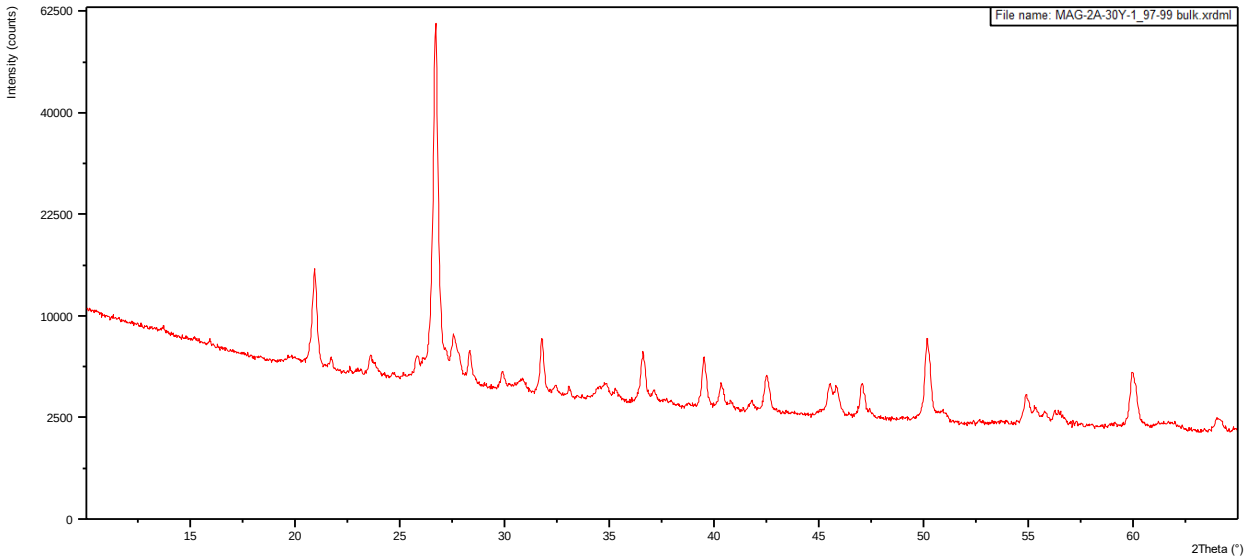
File name: MAG-2A-30Y-1_97-99 bulk.xrdml
Intensity (counts)
62500
40000
22500
10000
2500
0
15
20
25
30
35
40
45
50
55
60
2Theta (°)

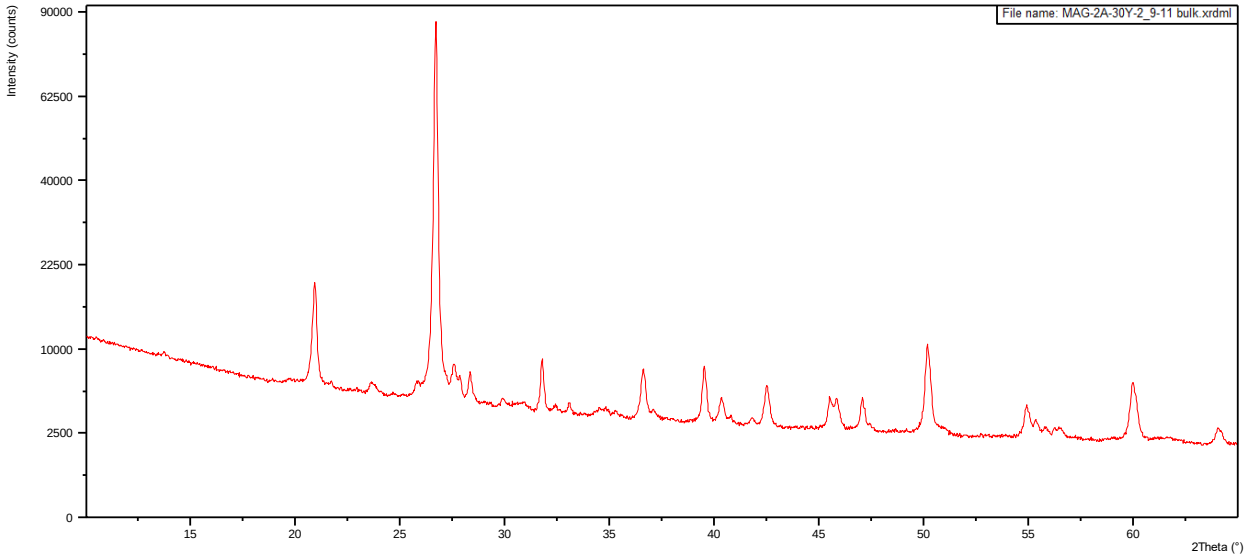
File name: MAG-2A-30Y-2_9-11 bulk.xrdml
Intensity (counts)
90000
62500
40000
22500
10000
2500
0
15
20
25
30
35
40
45
50
55
60
2Theta (°)

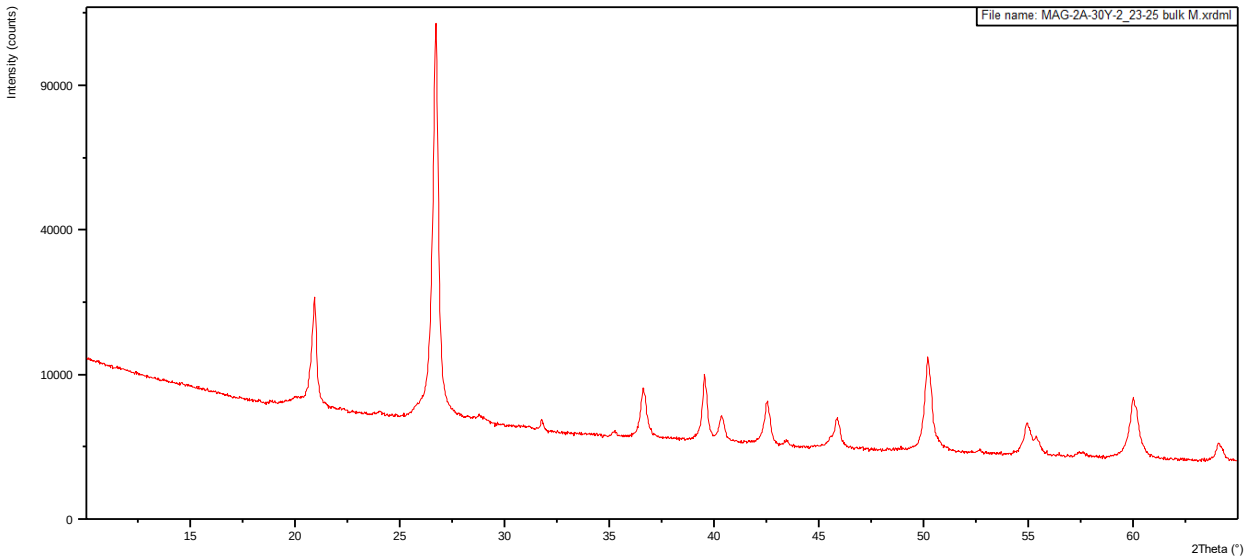
File name: MAG-2A-30Y-2_23-25 bulk M.xrdml
Intensity (counts)
90000
40000
10000
0
15
20
25
30
35
40
45
50
55
60
2Theta (°)

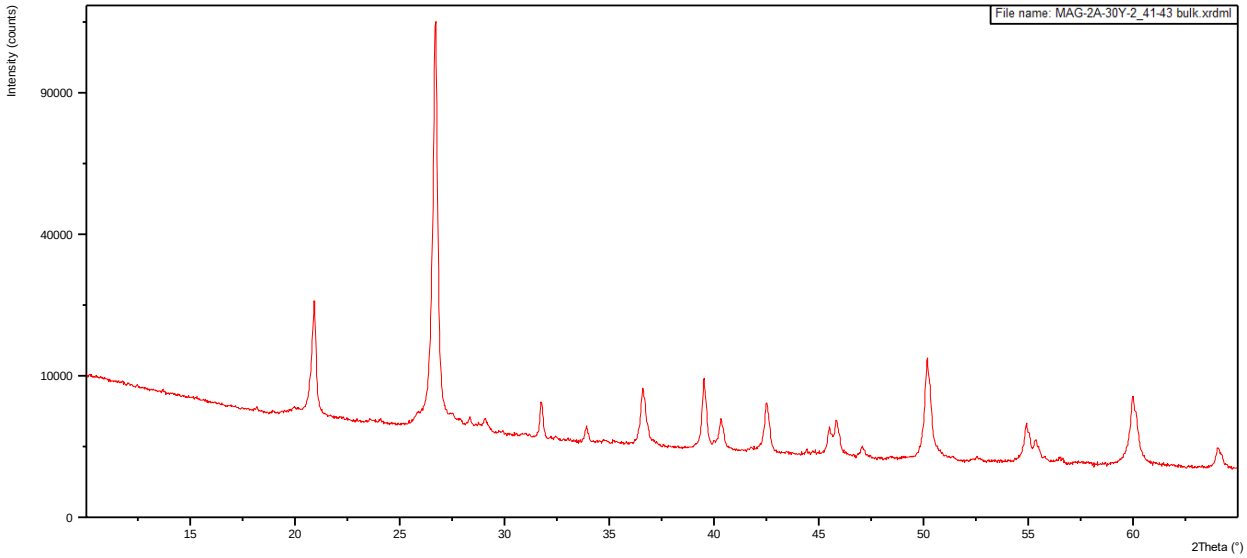
File name: MAG-2A-30Y-2_41-43 bulk.xrdml
Intensity (counts)
90000
40000
10000
0
15
20
25
30
35
40
45
50
55
60
2Theta (°)

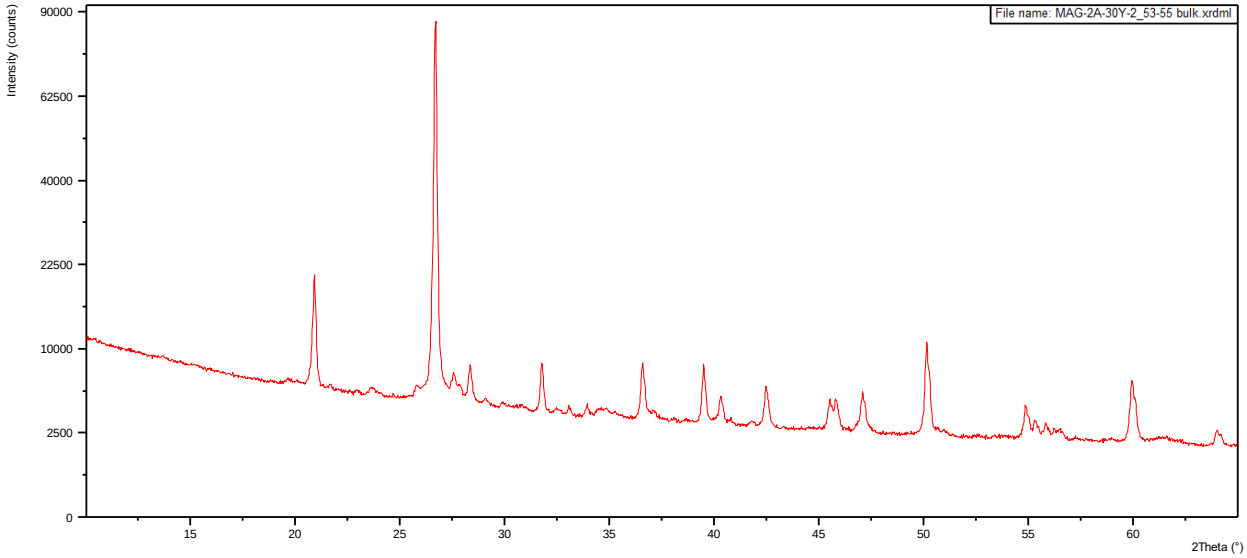
File name: MAG-2A-30Y-2_53-55 bulk.xrdml
Intensity (counts)
90000
62500
40000
22500
10000
2500
0
15
20
25
30
35
40
45
50
55
60
2Theta (°)

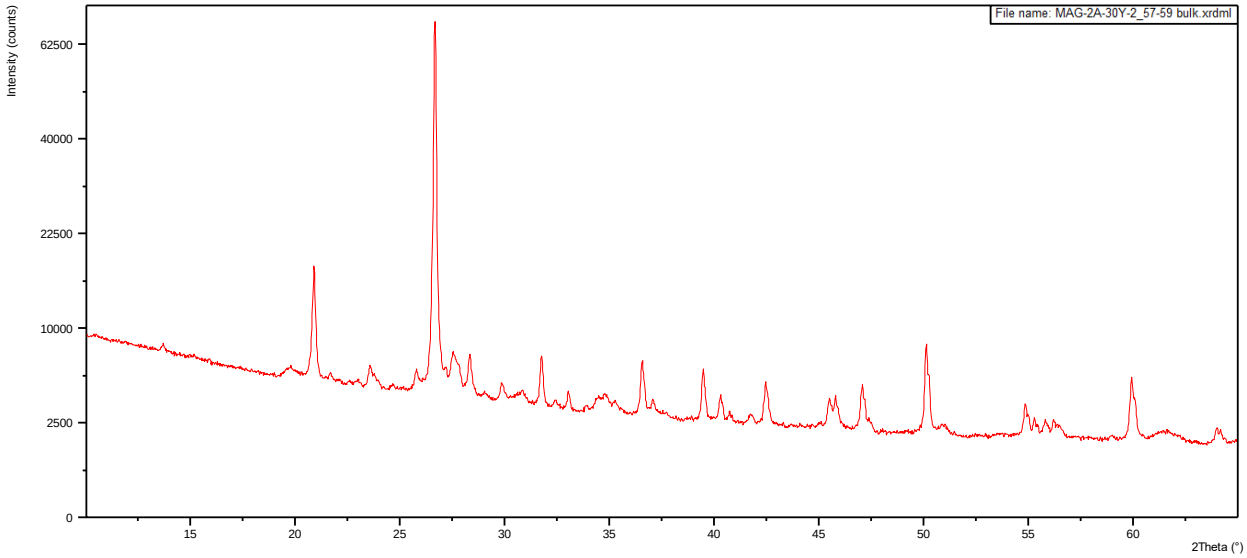
File name: MAG-2A-30Y-2_57-59 bulk.xrdml
Intensity (counts)
62500
40000
22500
10000
2500
0
15
20
25
30
35
40
45
50
55
60
2Theta (°)

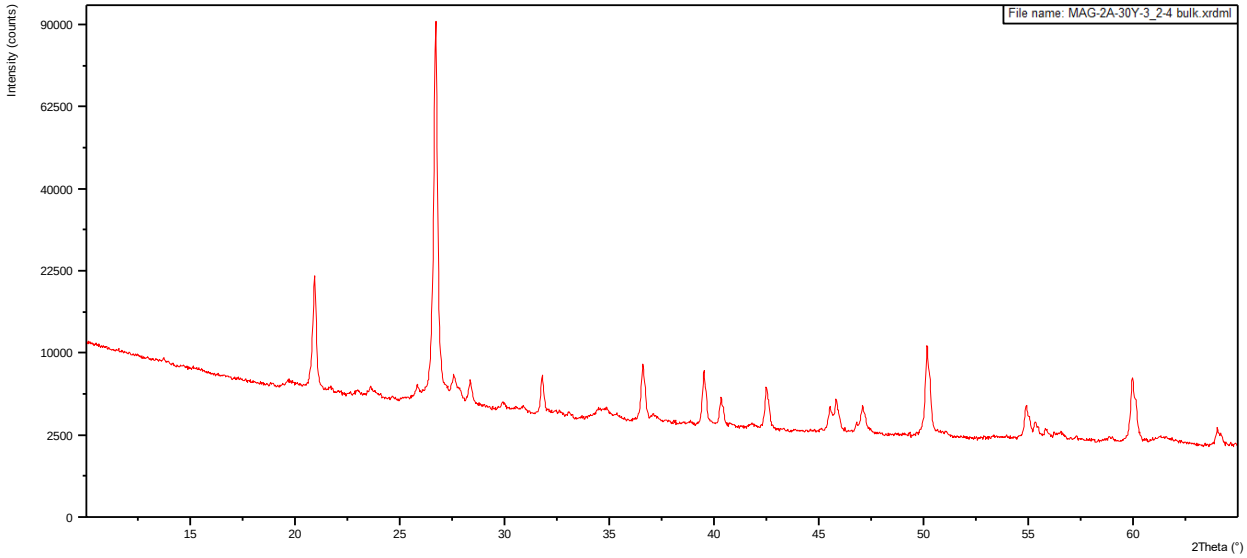
File name: MAG-2A-30Y-3_2-4 bulk.xrdml
Intensity (counts)
90000
62500
40000
22500
10000
2500
0
15
20
25
30
35
40
45
50
55
60
2Theta (°)

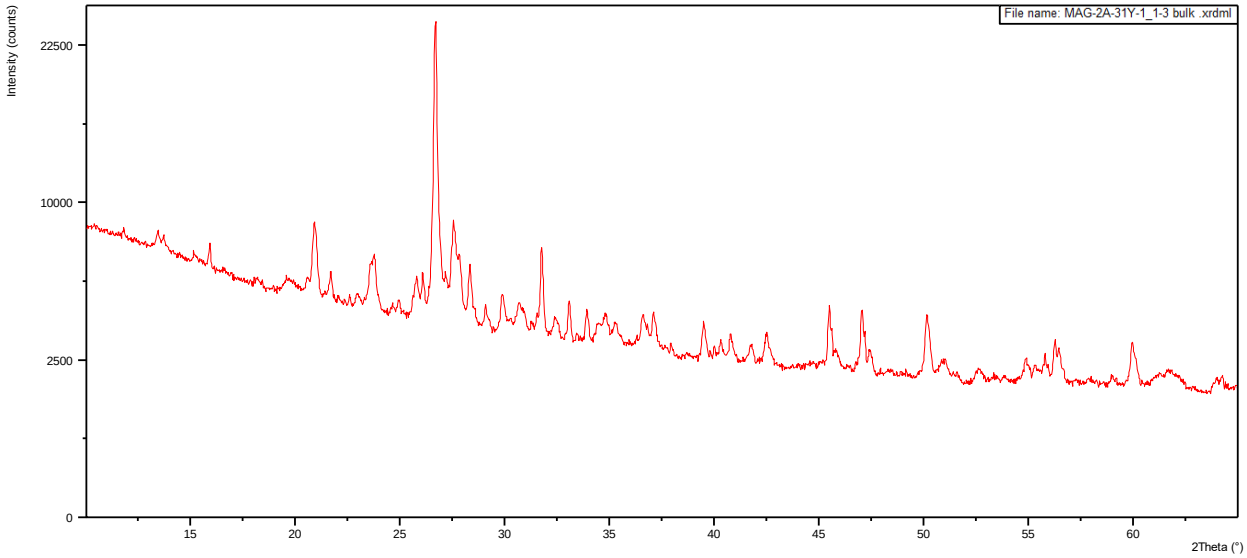
File name: MAG-2A-31Y-1_1-3 bulk .xrdml
Intensity (counts)
22500
10000
2500
0
15
20
25
30
35
40
45
50
55
60
2Theta (°)

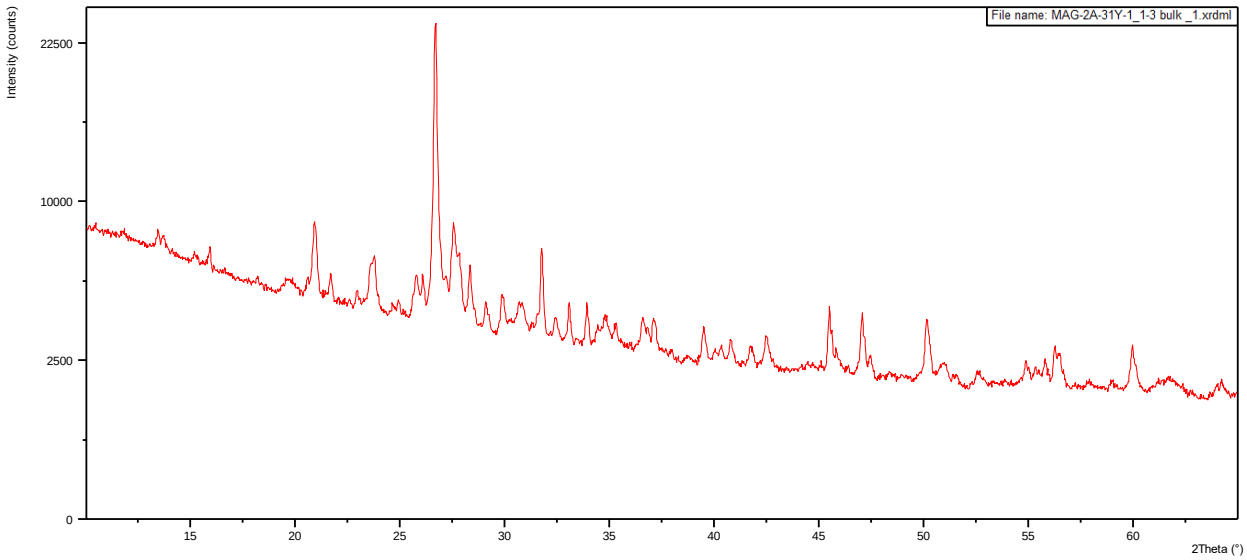
File name: MAG-2A-31Y-1_1-3 bulk _1.xrdml
Intensity (counts)
22500
10000
2500
0
15
20
25
30
35
40
45
50
55
60
2Theta (°)

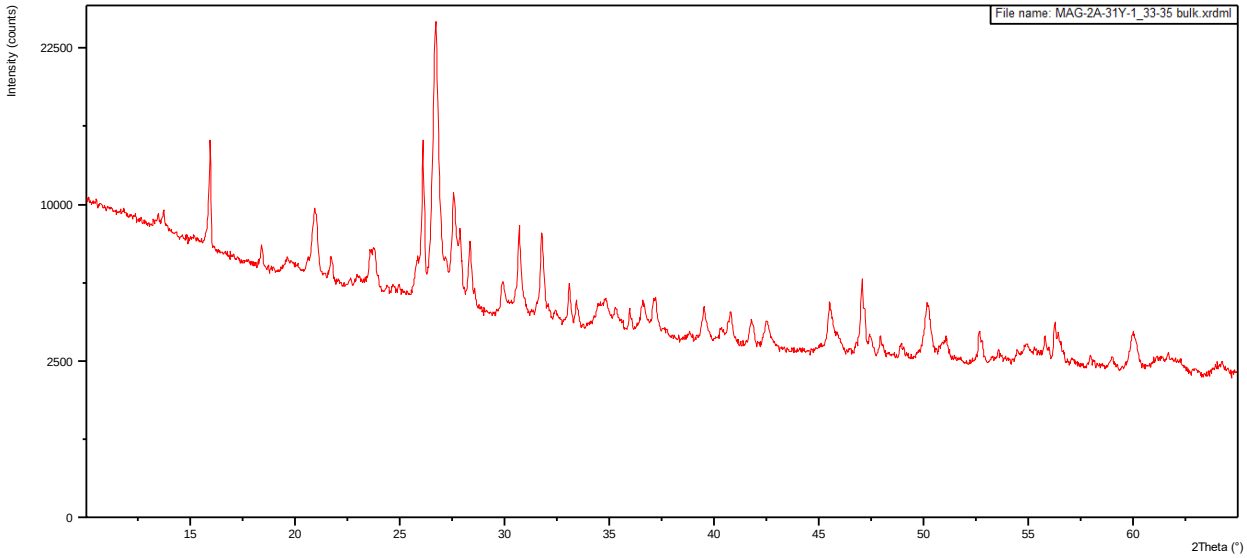
File name: MAG-2A-31Y-1_33-35 bulk.xrdml
Intensity (counts)
22500
10000
2500
0
15
20
25
30
35
40
45
50
55
60
2Theta (°)

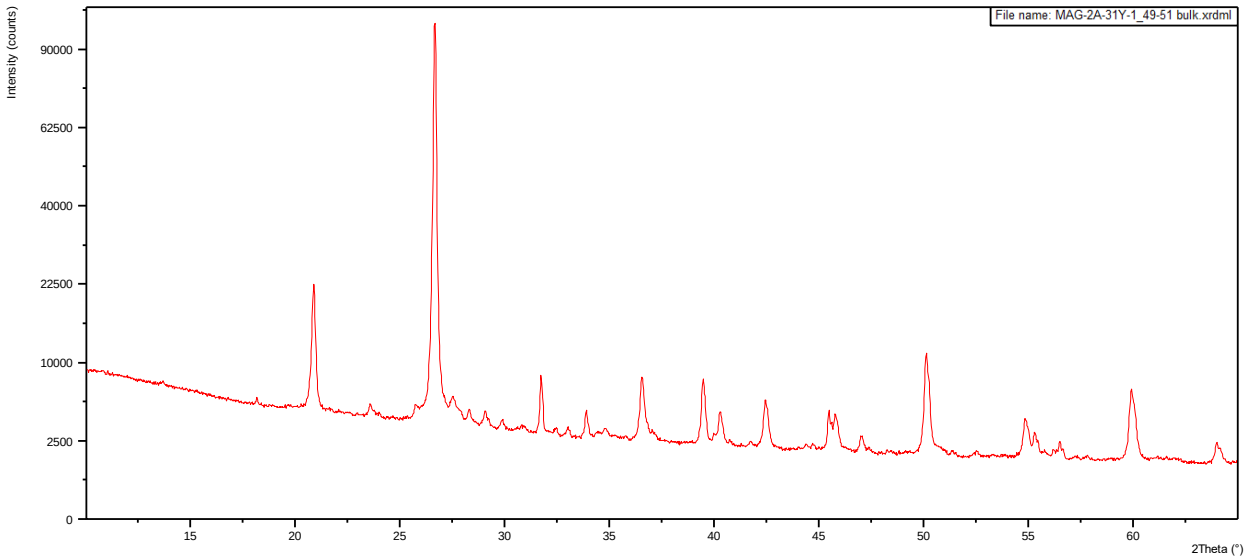
File name: MAG-2A-31Y-1_49-51 bulk.xrdml
Intensity (counts)
90000
62500
40000
22500
10000
2500
0
15
20
25
30
35
40
45
50
55
60
2Theta (°)

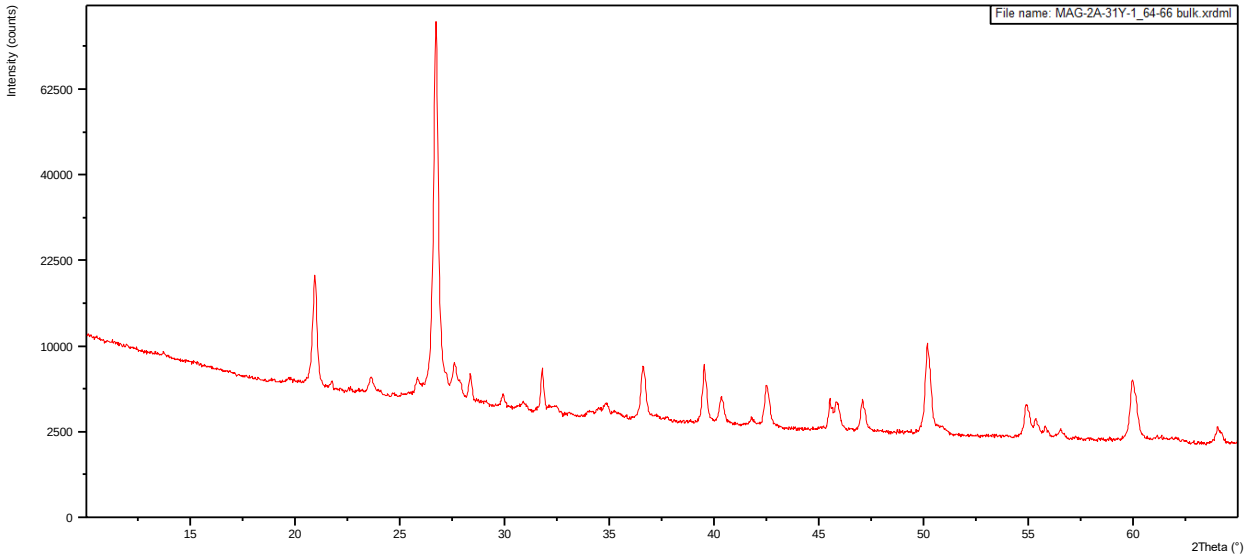
File name: MAG-2A-31Y-1_64-66 bulk.xrdml
Intensity (counts)
62500
40000
22500
10000
2500
0
15
20
25
30
35
40
45
50
55
60
2Theta (°)

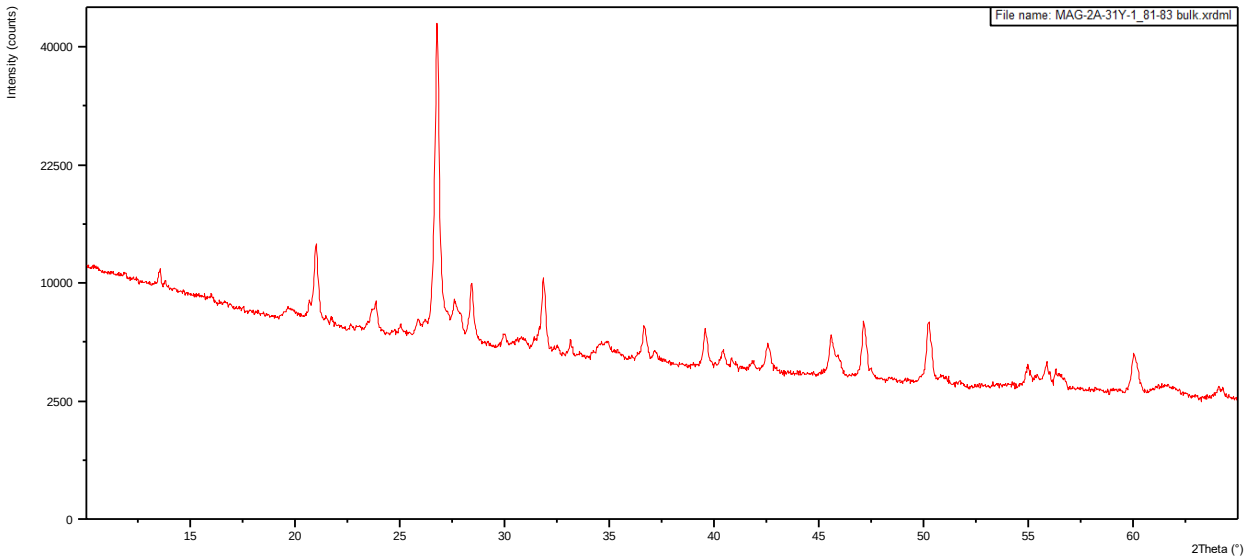
File name: MAG-2A-31Y-1_81-83 bulk.xrdml
Intensity (counts)
40000
22500
10000
2500
0
15
20
25
30
35
40
45
50
55
60
2Theta (°)

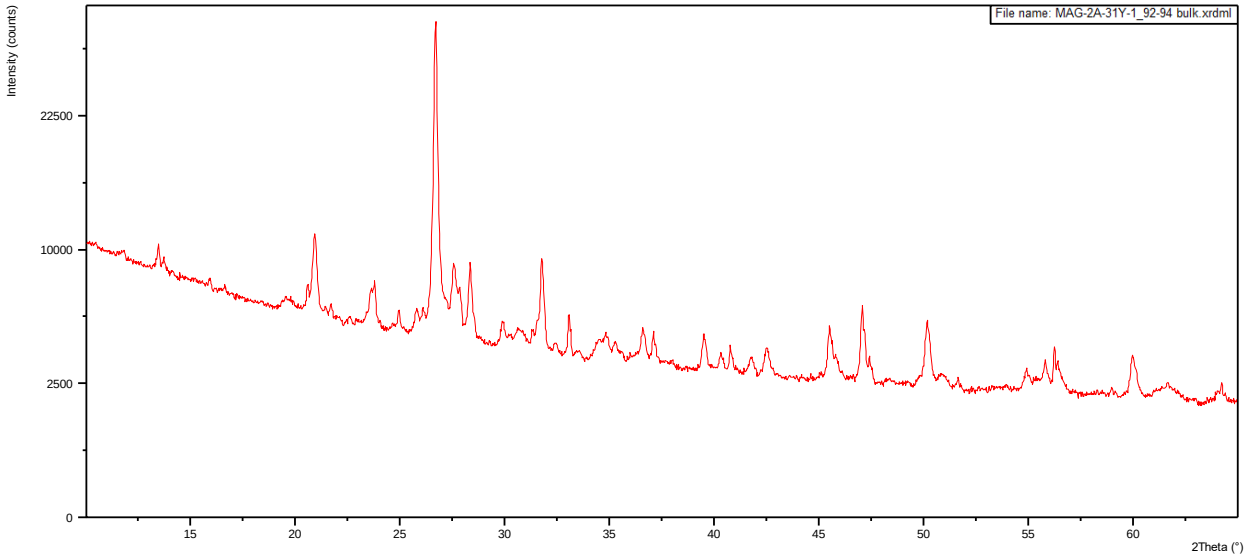
File name: MAG-2A-31Y-1_92-94 bulk.xrdml
Intensity (counts)
22500
10000
2500
0
15
20
25
30
35
40
45
50
55
60
2Theta (°)

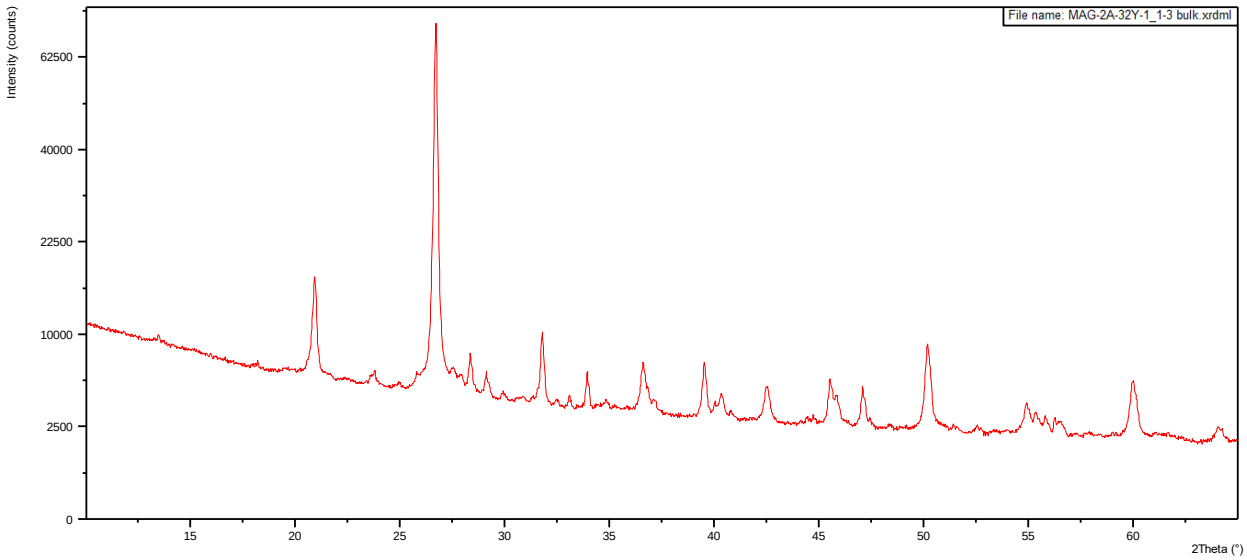
File name: MAG-2A-32Y-1_1-3 bulk.xrdml
Intensity (counts)
62500
40000
22500
10000
2500
0
15
20
25
30
35
40
45
50
55
60
2Theta (°)

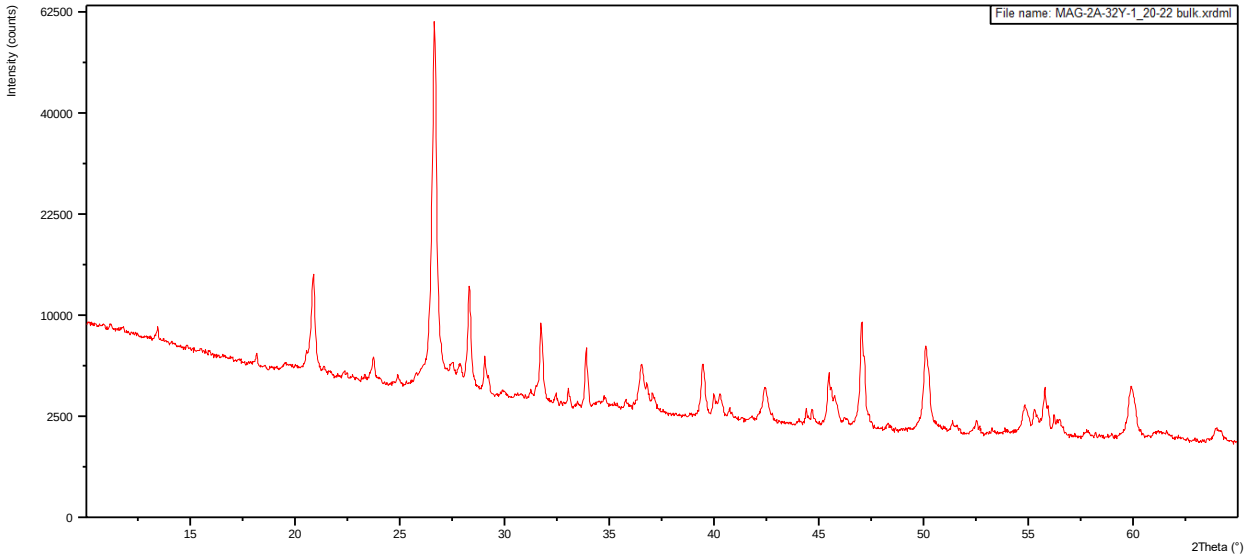
File name: MAG-2A-32Y-1_20-22 bulk.xrdml
Intensity (counts)
62500
40000
22500
10000
2500
0
15
20
25
30
35
40
45
50
55
60
2Theta (°)

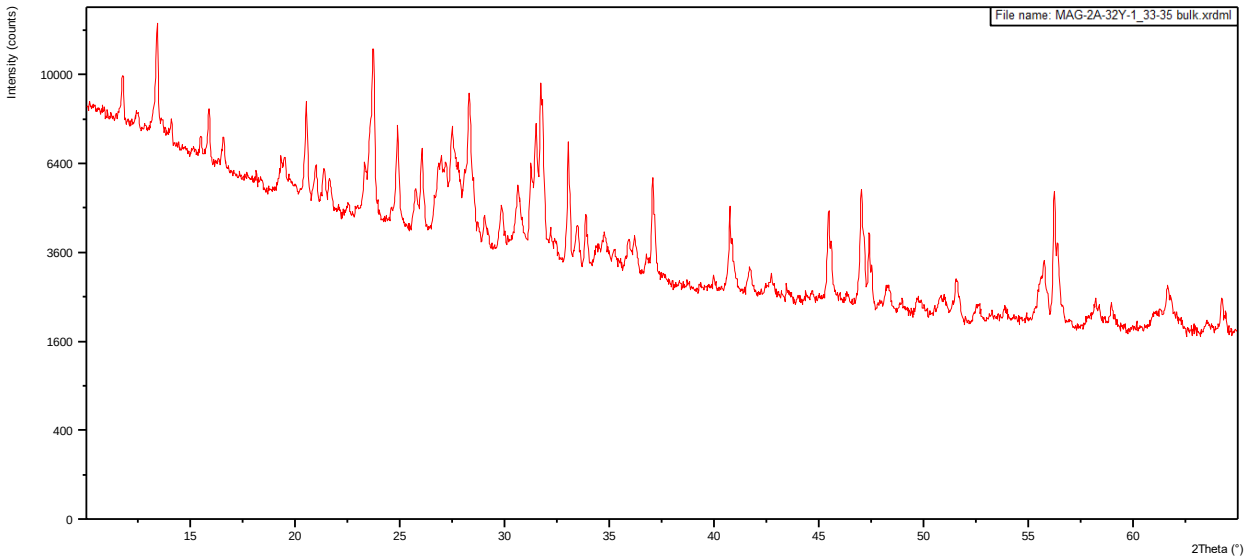
File name: MAG-2A-32Y-1_33-35 bulk.xrdml
Intensity (counts)
10000
6400
3600
1600
400
0
15
20
25
30
35
40
45
50
55
60
2Theta (°)

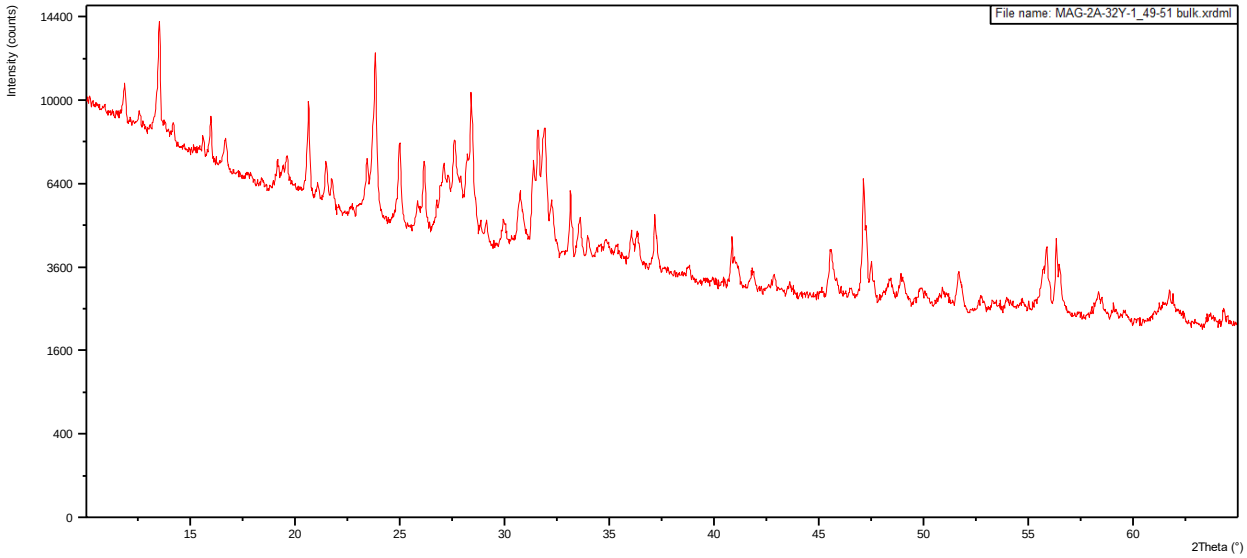
File name: MAG-2A-32Y-1_49-51 bulk.xrdml
Intensity (counts)
14400
10000
6400
3600
1600
400
0
15
20
25
30
35
40
45
50
55
60
2Theta (°)

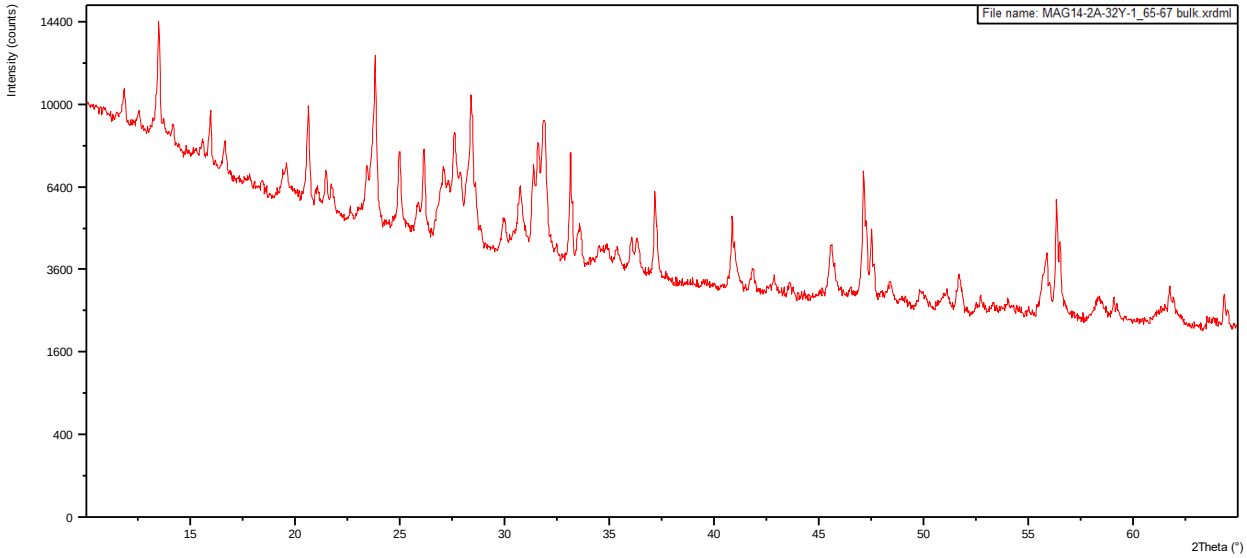
File name: MAG14-2A-32Y-1_65-67 bulk.xrdml
Intensity (counts)
14400
10000
6400
3600
1600
400
0
15
20
25
30
35
40
45
50
55
60
2Theta (°)

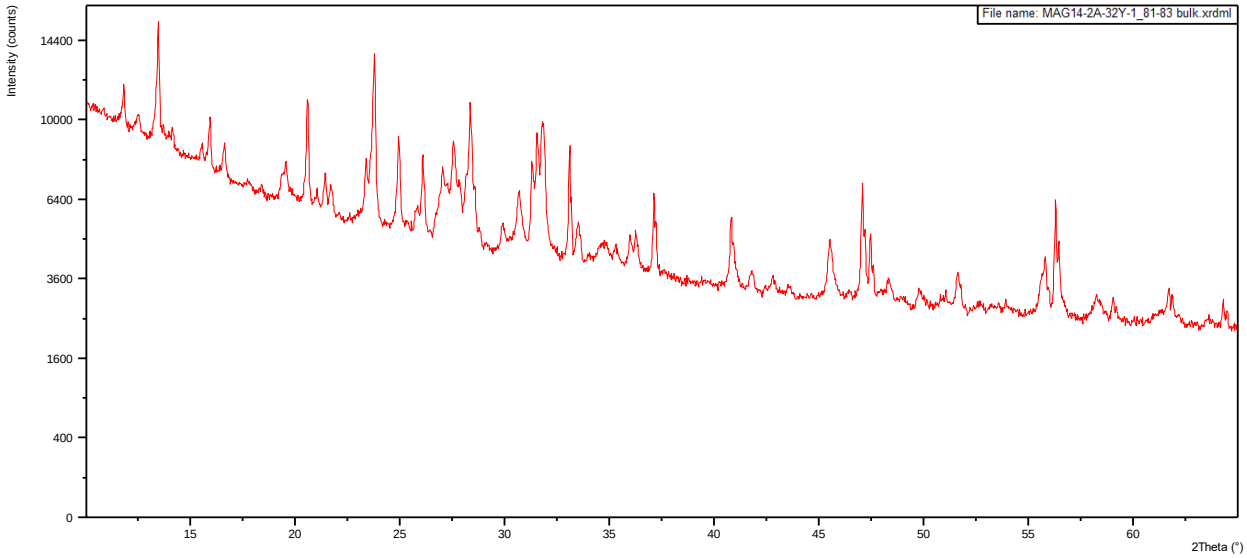
File name: MAG14-2A-32Y-1_81-83 bulk.xrdml
Intensity (counts)
14400
10000
6400
3600
1600
400
0
15
20
25
30
35
40
45
50
55
60
2Theta (°)

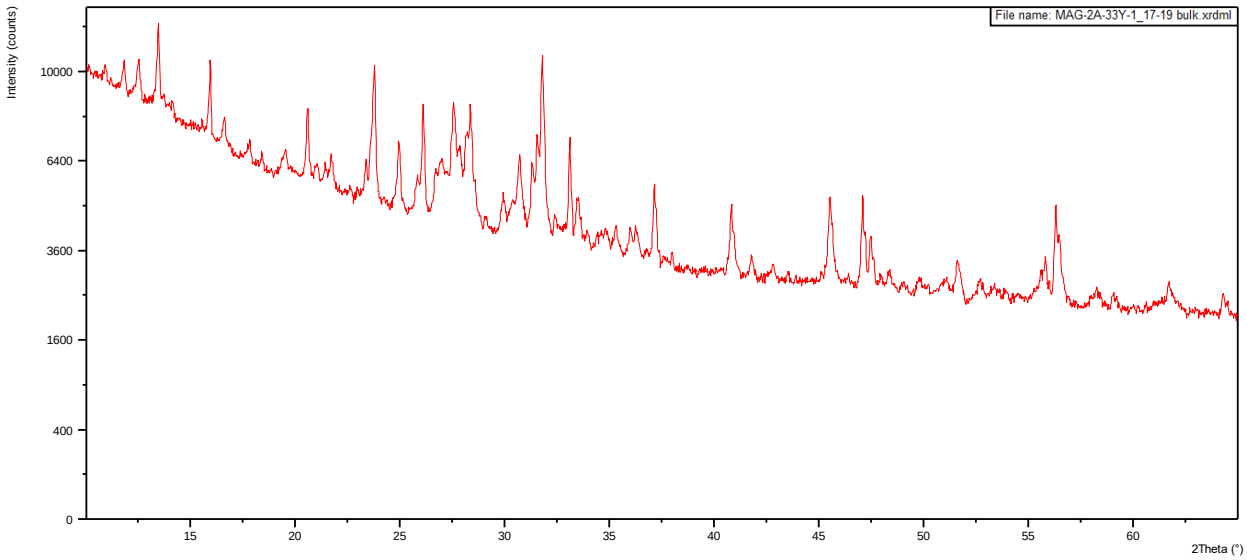
File name: MAG-2A-33Y-1_17-19 bulk.xrdml
Intensity (counts)
10000
6400
3600
1600
400
0
15
20
25
30
35
40
45
50
55
60
2Theta (°)

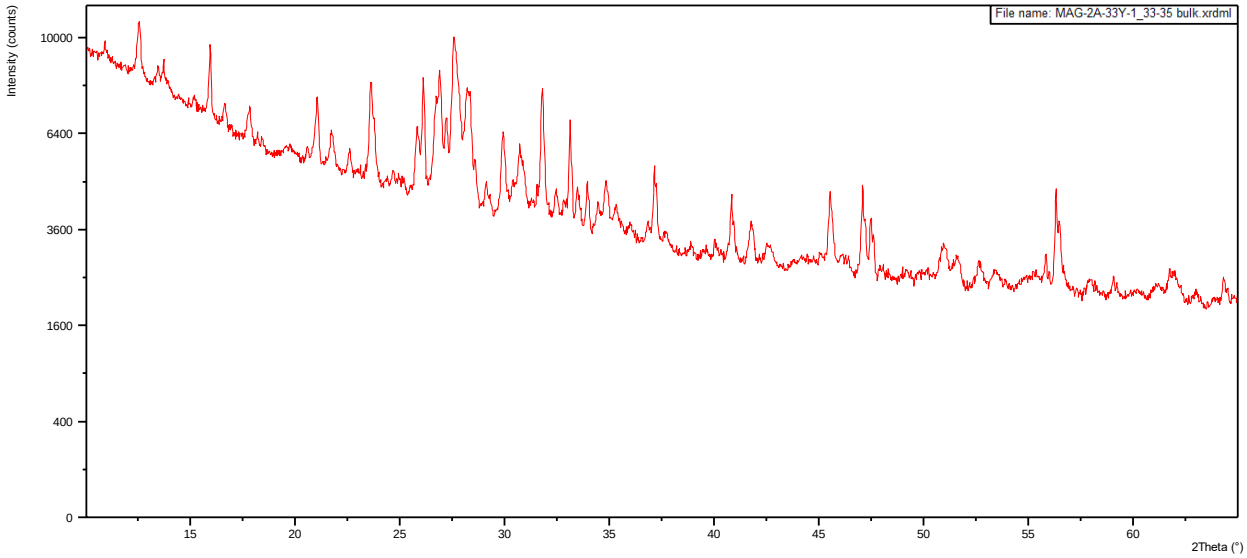
File name: MAG-2A-33Y-1_33-35 bulk.xrdml
Intensity (counts)
10000
6400
3600
1600
400
0
15
20
25
30
35
40
45
50
55
60
2Theta (°)

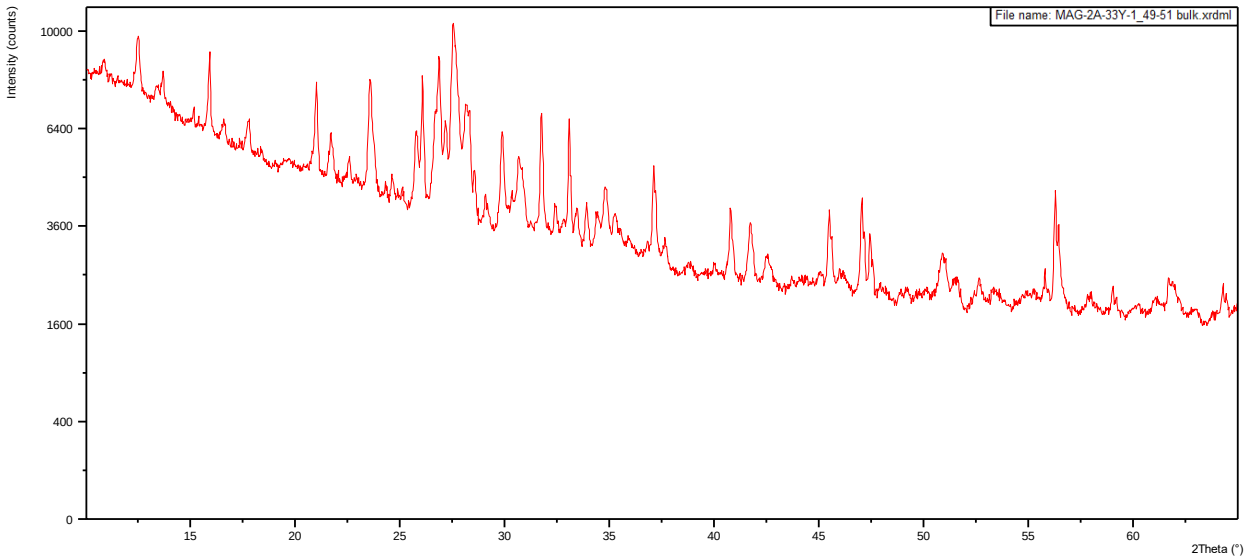
File name: MAG-2A-33Y-1_49-51 bulk.xrdml
Intensity (counts)
10000
6400
3600
1600
400
0
15
20
25
30
35
40
45
50
55
60
2Theta (°)

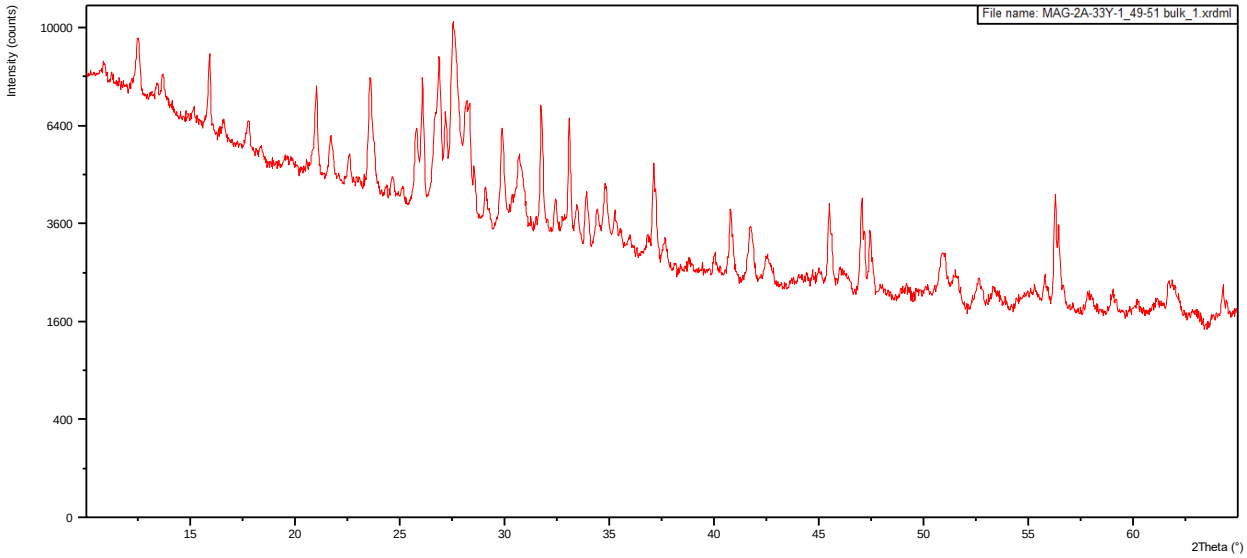
File name: MAG-2A-33Y-1_49-51 bulk_1.xrdml
Intensity (counts)
10000
6400
3600
1600
400
0
15
20
25
30
35
40
45
50
55
60
2Theta (°)

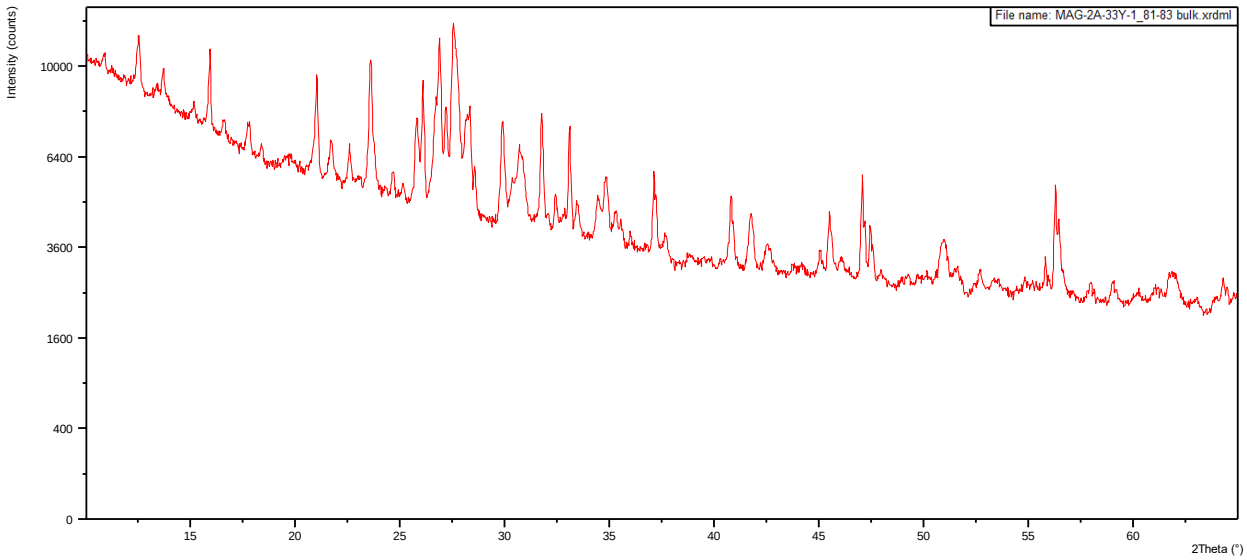
File name: MAG-2A-33Y-1_81-83 bulk.xrdml
Intensity (counts)
10000
6400
3600
1600
400
0
15
20
25
30
35
40
45
50
55
60
2Theta (°)

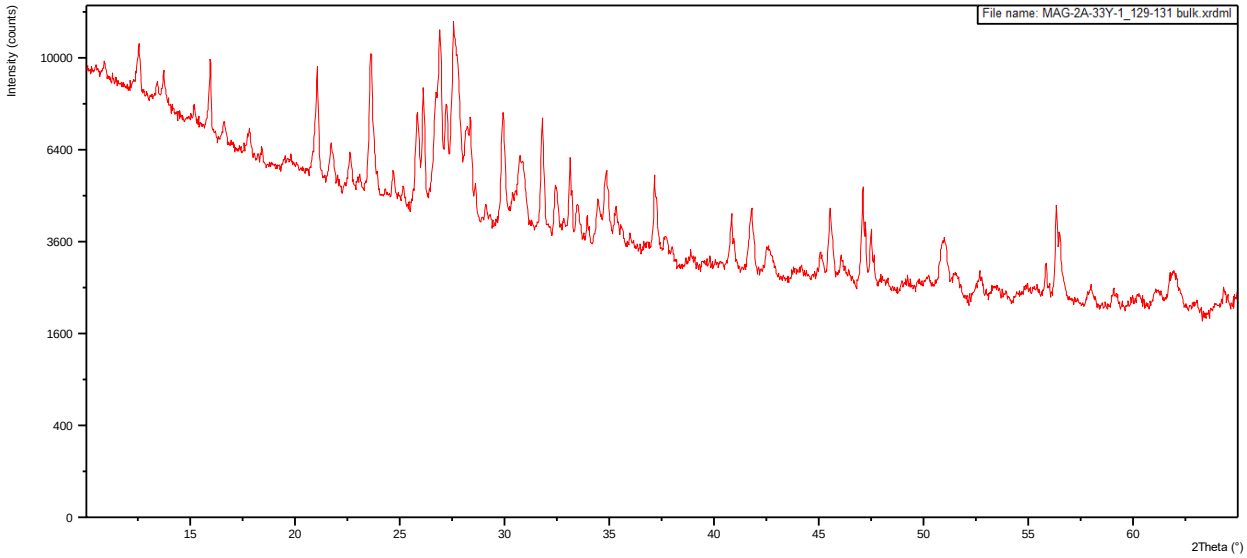
File name: MAG-2A-33Y-1_129-131 bulk.xrdml
Intensity (counts)
10000
6400
3600
1600
400
0
15
20
25
30
35
40
45
50
55
60
2Theta (°)

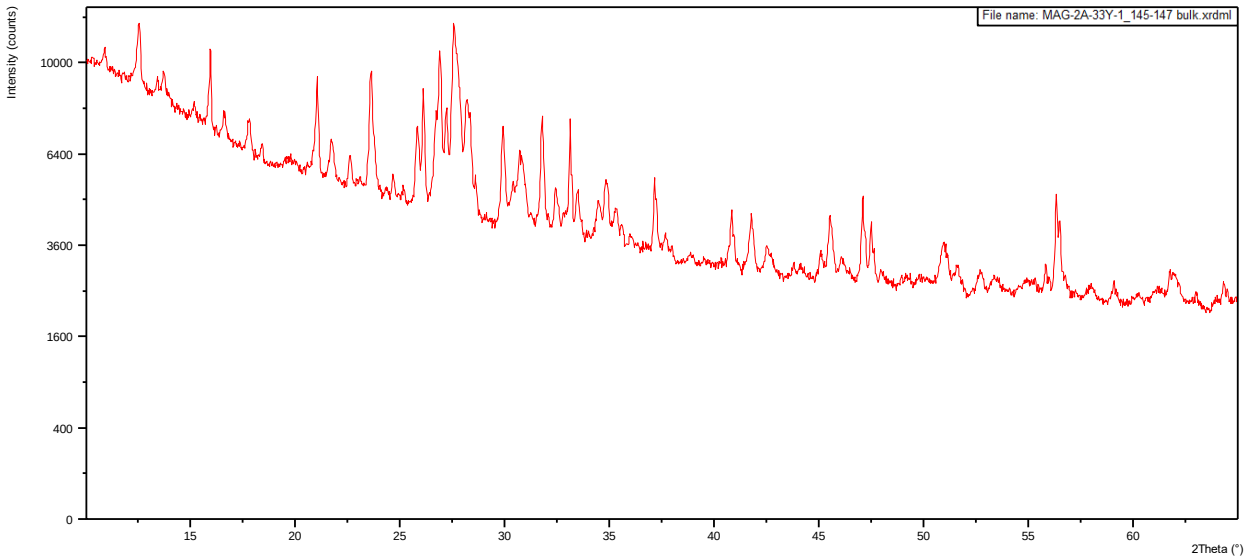
File name: MAG-2A-33Y-1_145-147 bulk.xrdml
Intensity (counts)
10000
6400
3600
1600
400
0
15
20
25
30
35
40
45
50
55
60
2Theta (°)

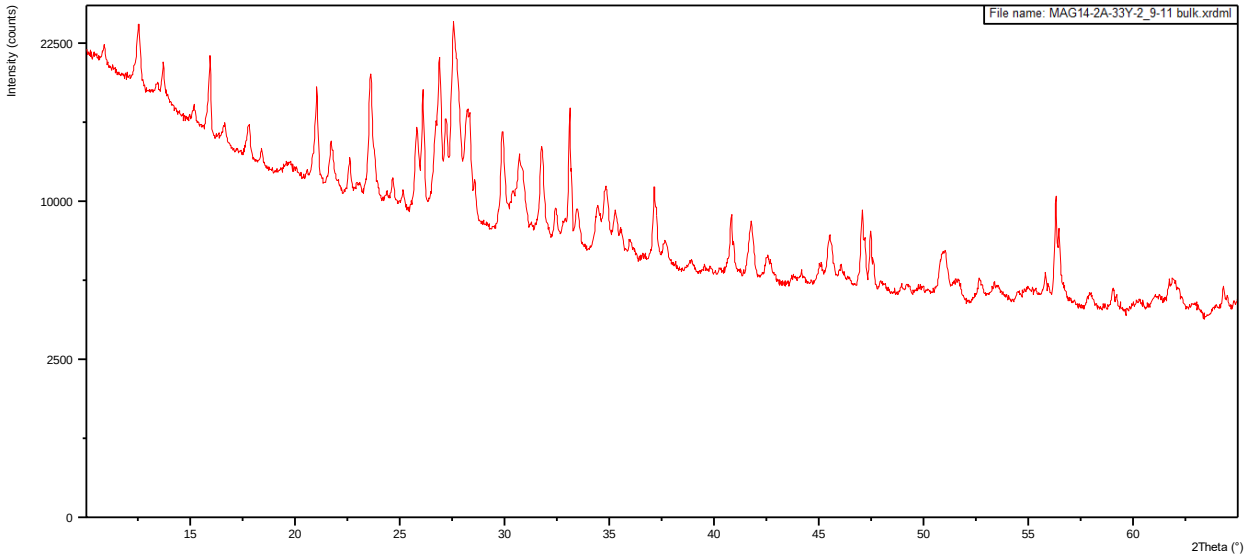
File name: MAG14-2A-33Y-2_9-11 bulk.xrdml
Intensity (counts)
22500
10000
2500
0
15
20
25
30
35
40
45
50
55
60
2Theta (°)

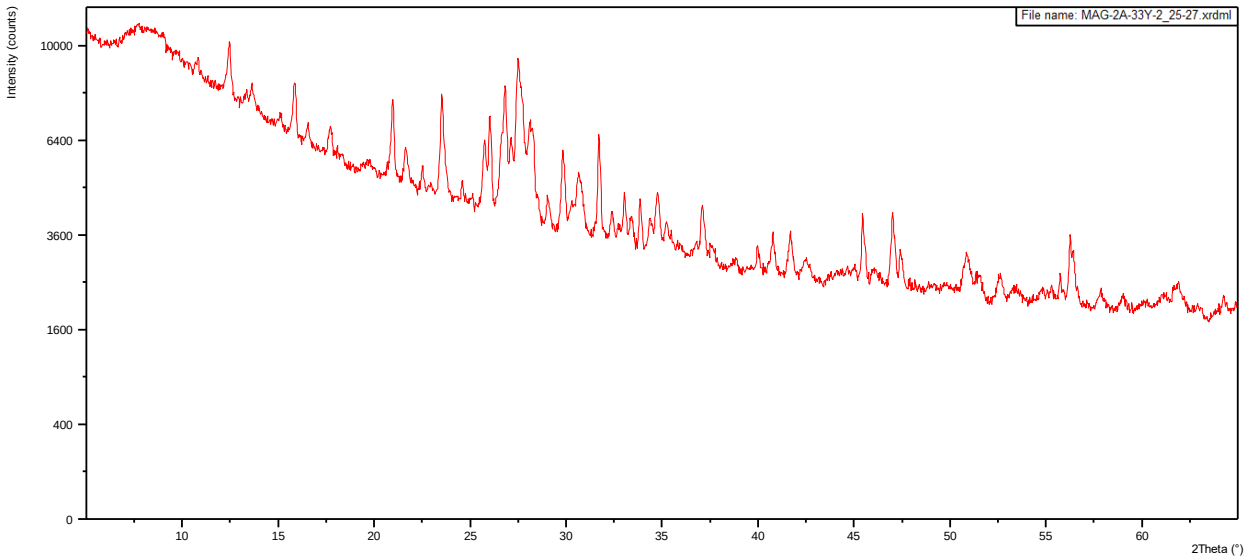
File name: MAG-2A-33Y-2_25-27.xrdml
Intensity (counts)
10000
6400
3600
1600
400
0
10
15
20
25
30
35
40
45
50
55
60
2Theta (°)

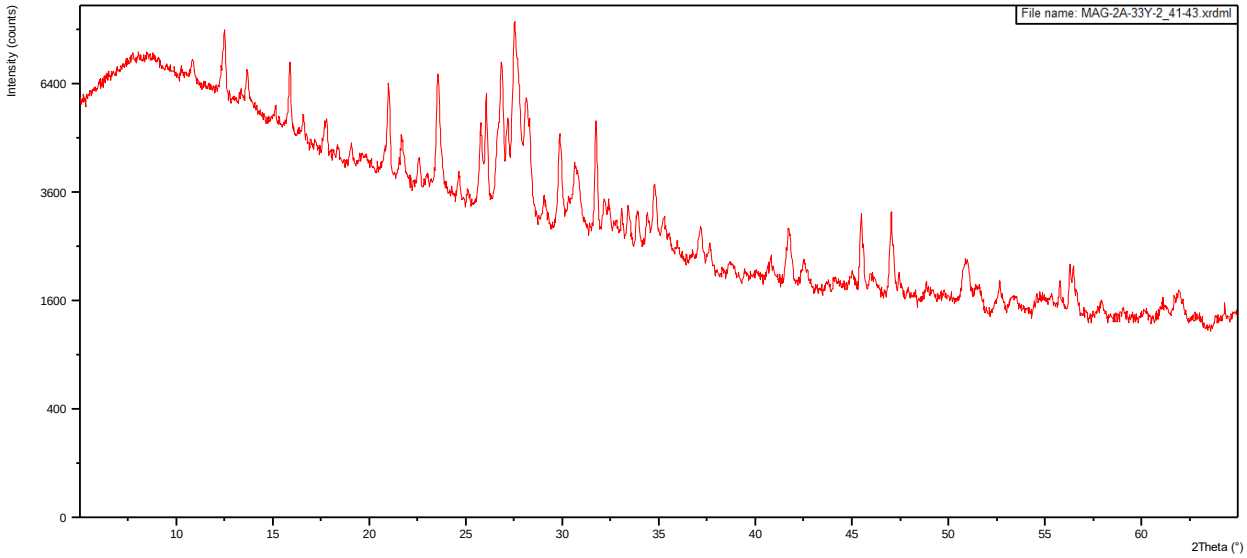
File name: MAG-2A-33Y-2_41-43.xrdml
Intensity (counts)
6400
3600
1600
400
0
10
15
20
25
30
35
40
45
50
55
60
2Theta (°)

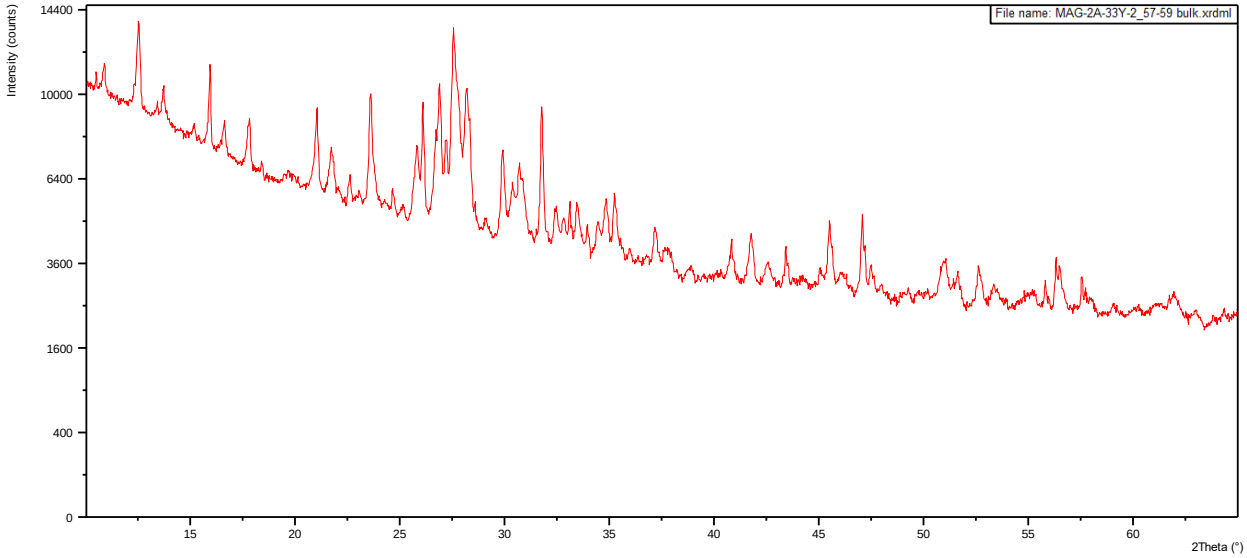
File name: MAG-2A-33Y-2_57-59 bulk.xrdml
Intensity (counts)
14400
10000
6400
3600
1600
400
0
15
20
25
30
35
40
45
50
55
60
2Theta (°)

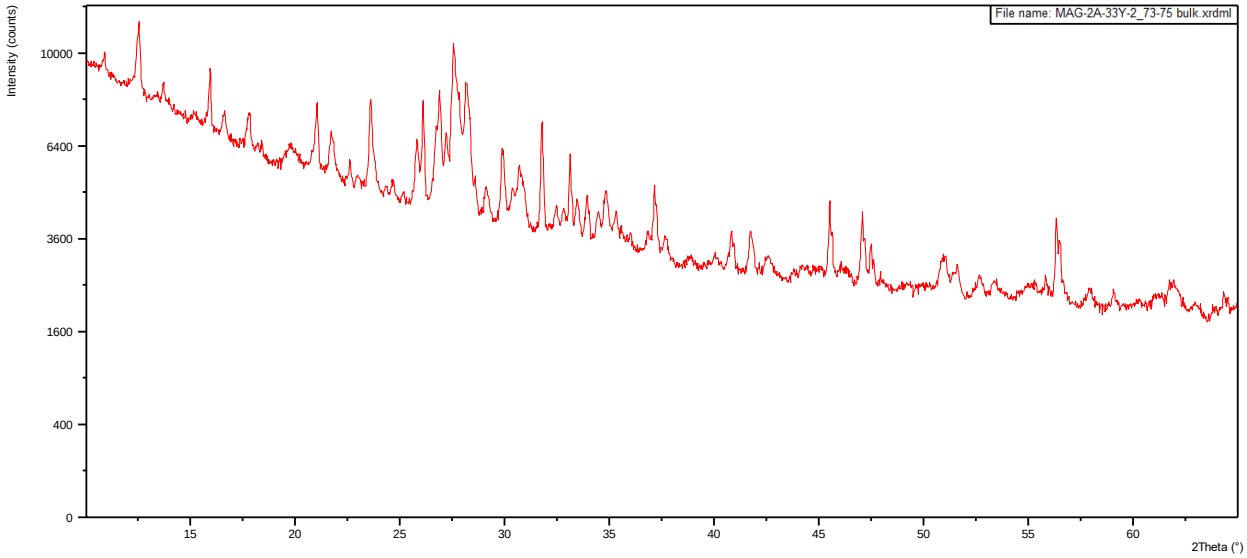
File name: MAG-2A-33Y-2_73-75 bulk.xrdml
Intensity (counts)
10000
6400
3600
1600
400
0
15
20
25
30
35
40
45
50
55
60
2Theta (°)

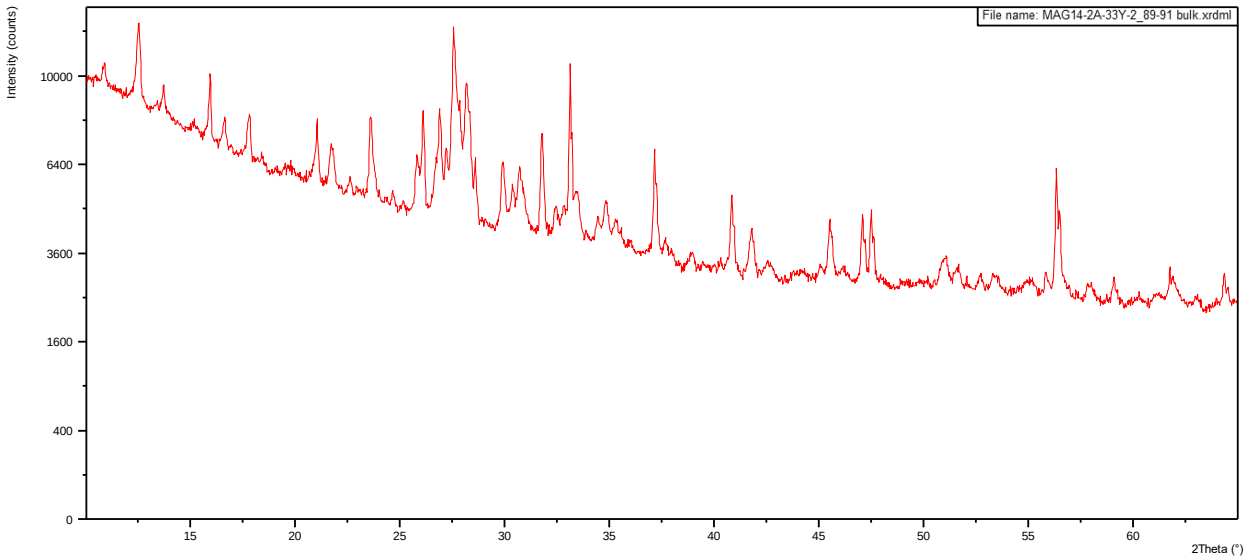
File name: MAG14-2A-33Y-2_89-91 bulk.xrdml
Intensity (counts)
10000
6400
3600
1600
400
0
15
20
25
30
35
40
45
50
55
60
2Theta (°)

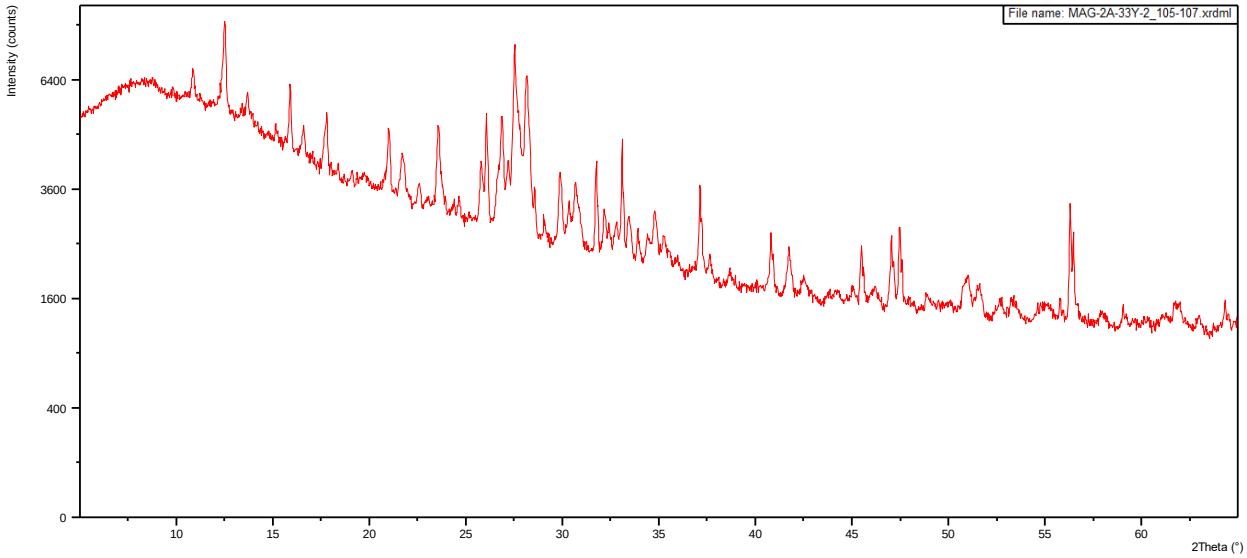
File name: MAG-2A-33Y-2_105-107.xrdml
Intensity (counts)
6400
3600
1600
400
0
10
15
20
25
30
35
40
45
50
55
60
2Theta (°)

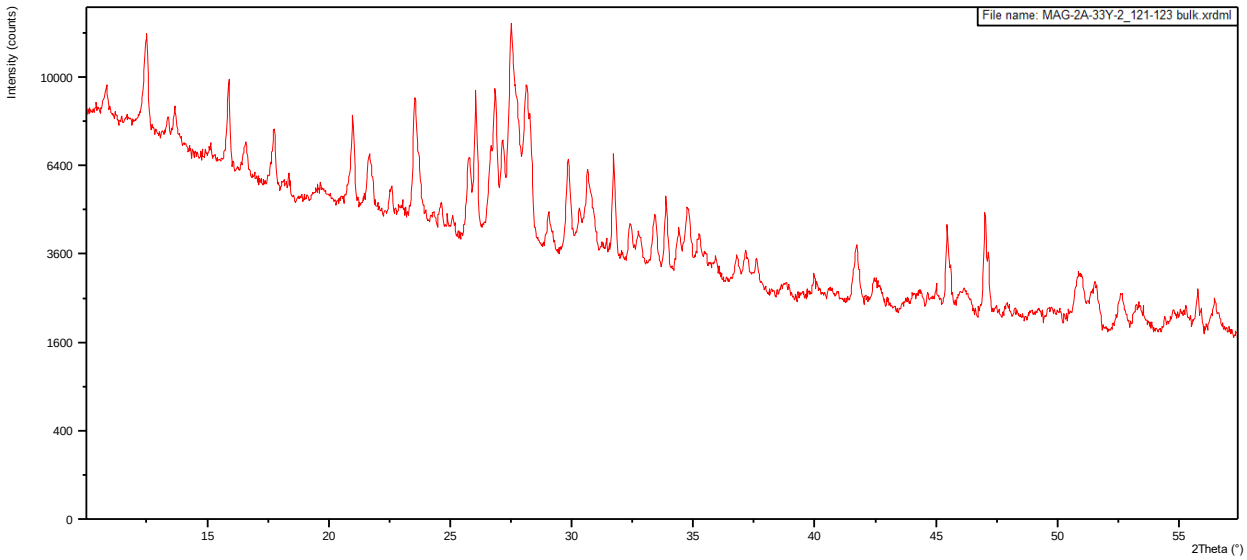
File name: MAG-2A-33Y-2_121-123 bulk.xrdml
Intensity (counts)
10000
6400
3600
1600
400
0
15
20
25
30
35
40
45
50
55
2Theta (°)

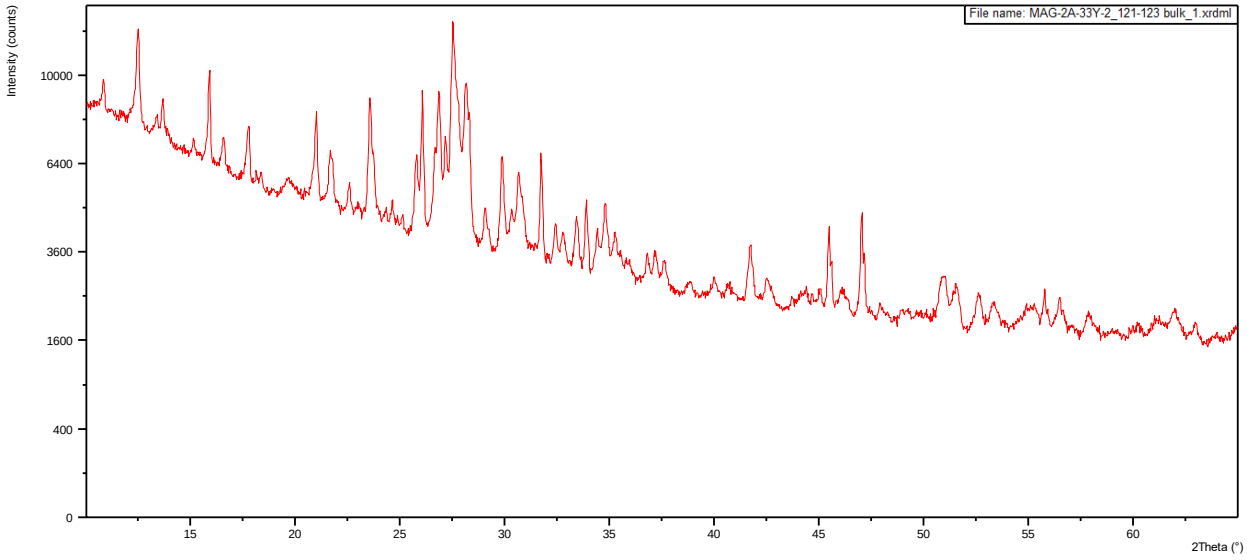
File name: MAG-2A-33Y-2_121-123 bulk_1.xrdml
Intensity (counts)
10000
6400
3600
1600
400
0
15
20
25
30
35
40
45
50
55
60
2Theta (°)

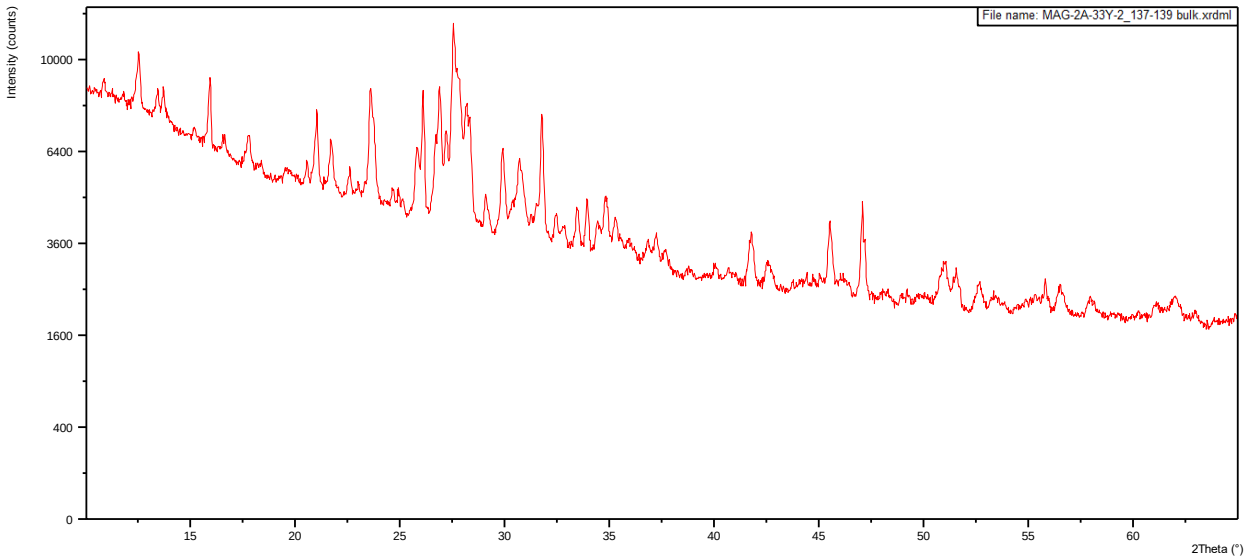
File name: MAG-2A-33Y-2_137-139 bulk.xrdml
Intensity (counts)
10000
6400
3600
1600
400
0
15
20
25
30
35
40
45
50
55
60
2Theta (°)

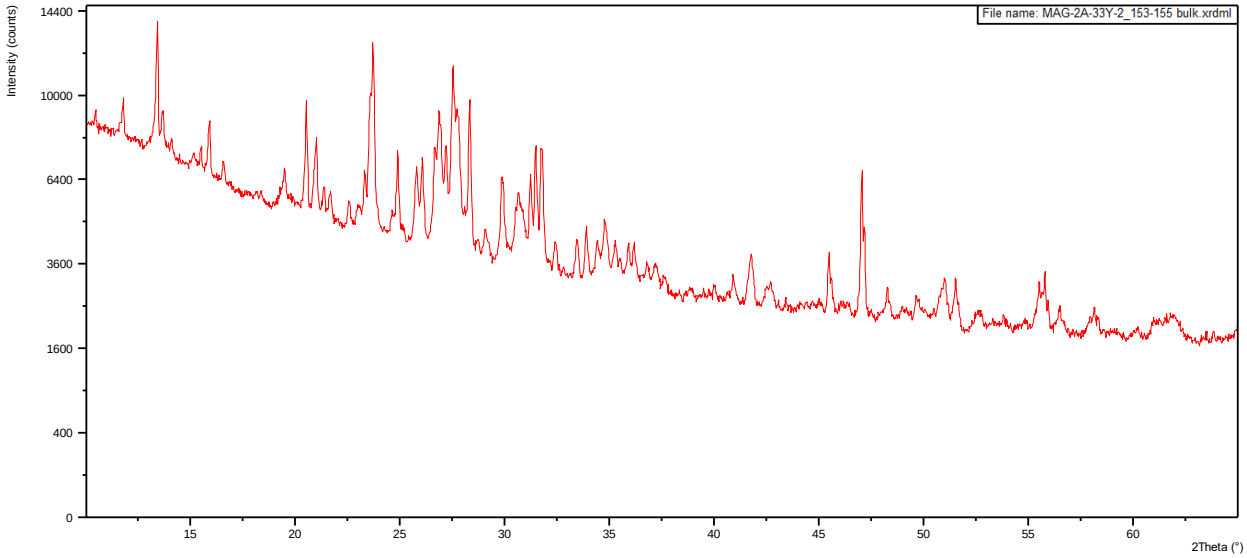
File name: MAG-2A-33Y-2_153-155 bulk.xrdml
Intensity (counts)
14400
10000
6400
3600
1600
400
0
15
20
25
30
35
40
45
50
55
60
2Theta (°)

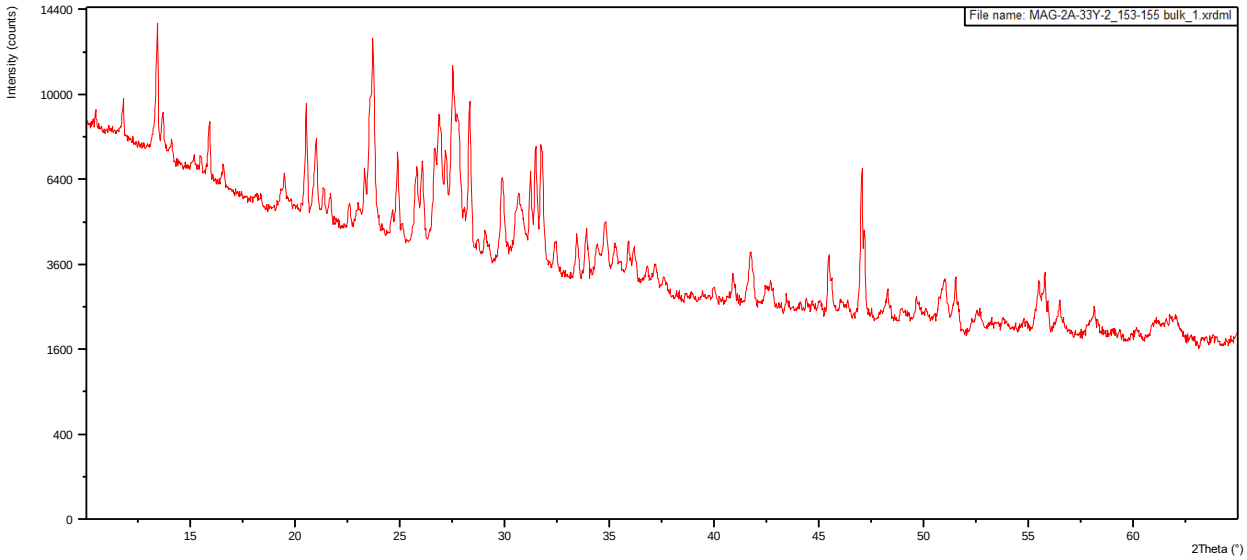
File name: MAG-2A-33Y-2_153-155 bulk_1.xrdml
Intensity (counts)
14400
10000
6400
3600
1600
400
0
15
20
25
30
35
40
45
50
55
60
2Theta (°)

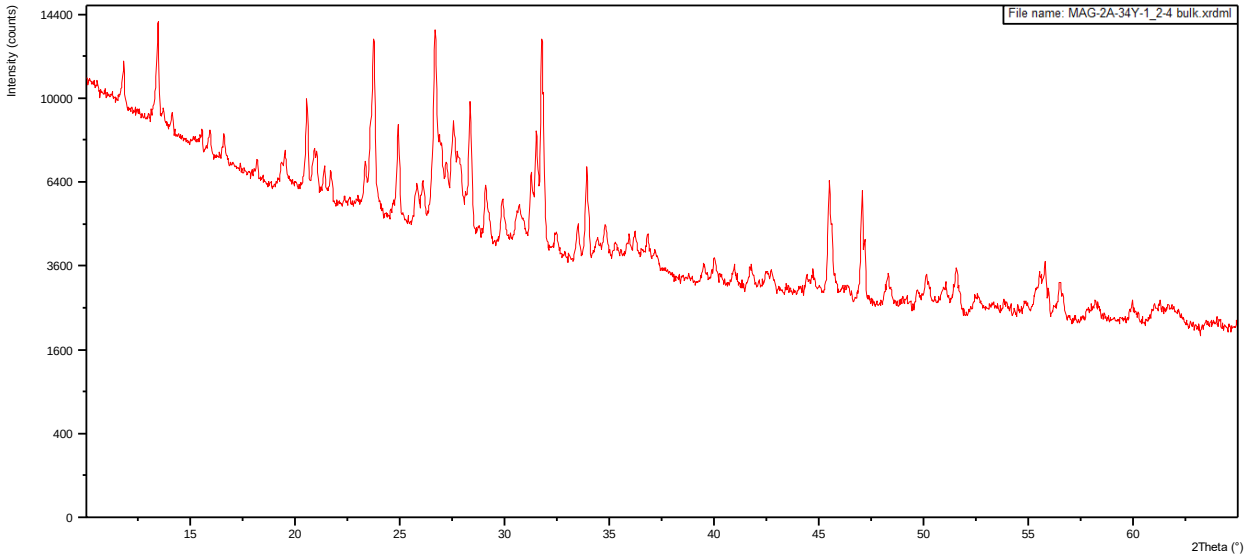
File name: MAG-2A-34Y-1_2-4 bulk.xrdml
Intensity (counts)
14400
10000
6400
3600
1600
400
0
15
20
25
30
35
40
45
50
55
60
2Theta (°)

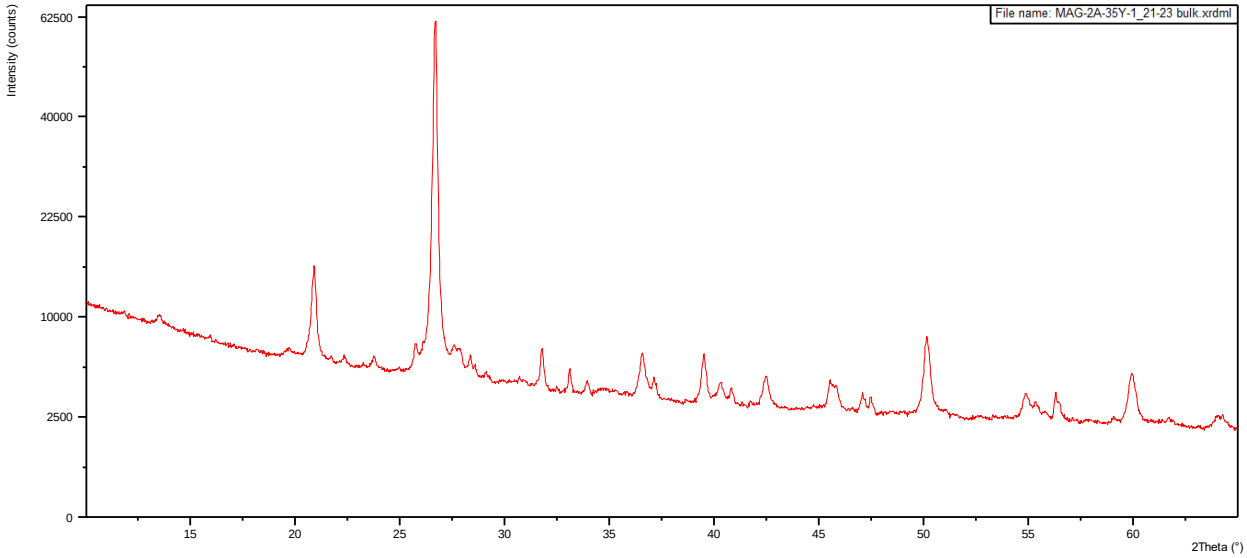
File name: MAG-2A-35Y-1_21-23 bulk.xrdml
Intensity (counts)
62500
40000
22500
10000
2500
0
15
20
25
30
35
40
45
50
55
60
2Theta (°)

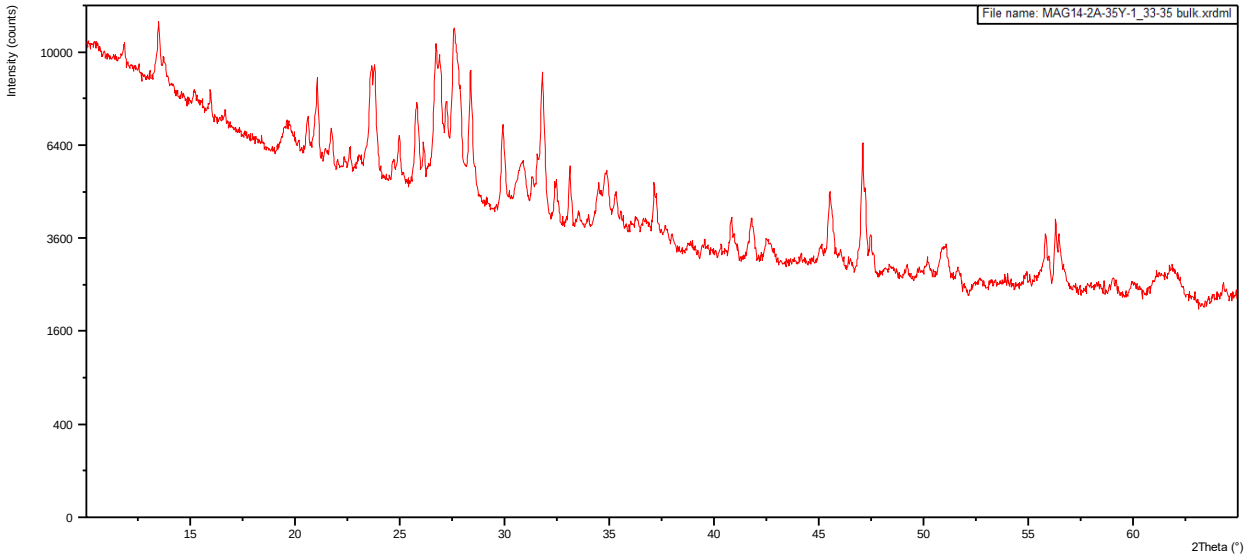
File name: MAG14-2A-35Y-1_33-35 bulk.xrdml
Intensity (counts)
10000
6400
3600
1600
400
0
15
20
25
30
35
40
45
50
55
60
2Theta (°)

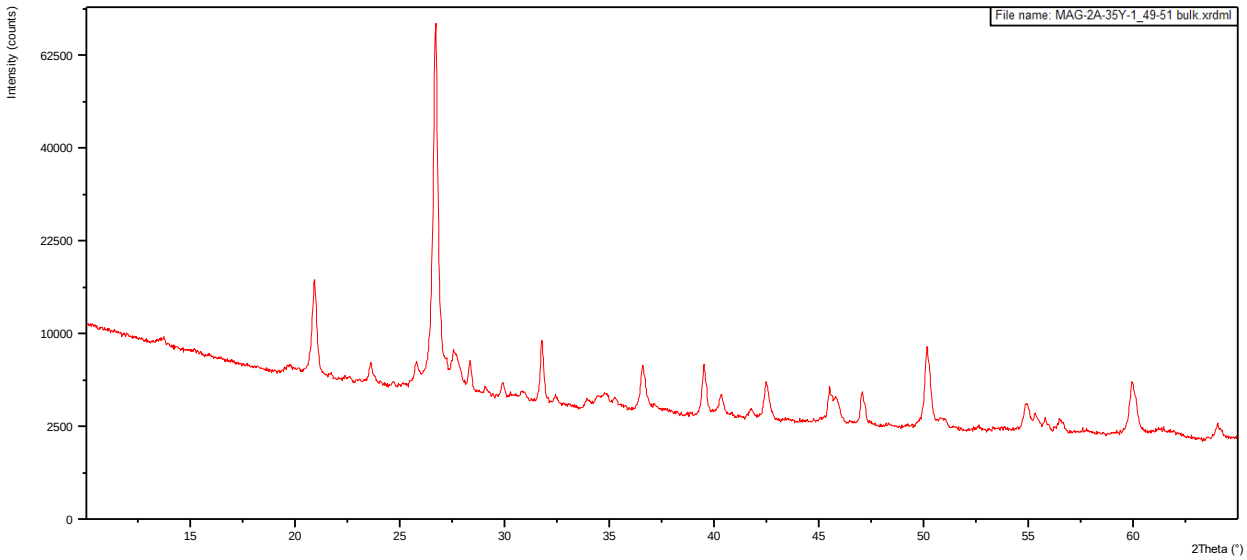
File name: MAG-2A-35Y-1_49-51 bulk.xrdml
Intensity (counts)
62500
40000
22500
10000
2500
0
15
20
25
30
35
40
45
50
55
60
2Theta (°)

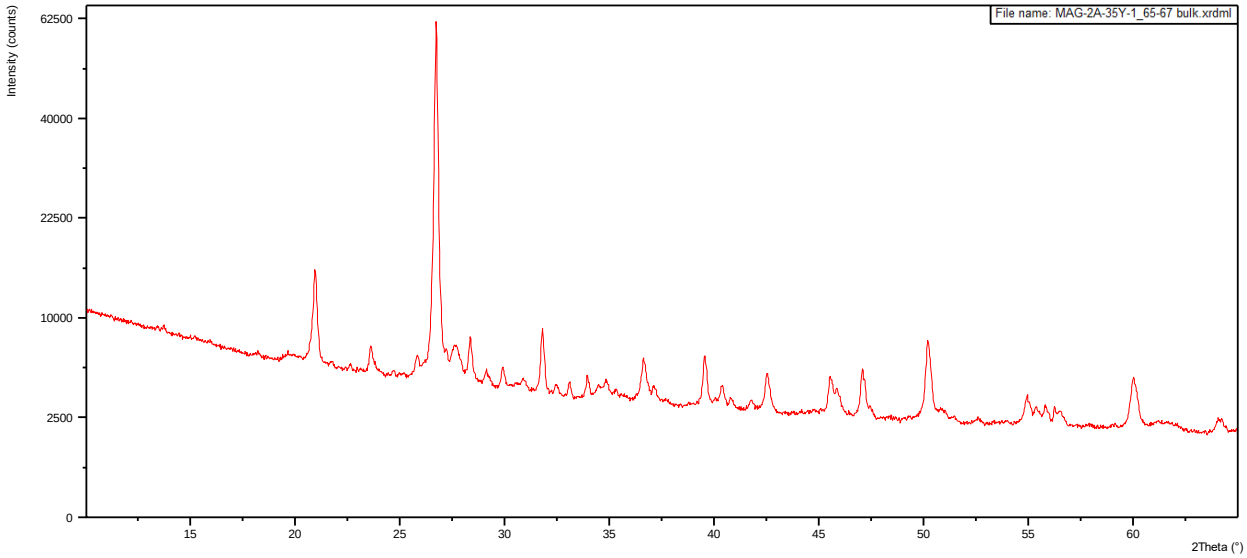
File name: MAG-2A-35Y-1_65-67 bulk.xrdml
Intensity (counts)
62500
40000
22500
10000
2500
0
15
20
25
30
35
40
45
50
55
60
2Theta (°)

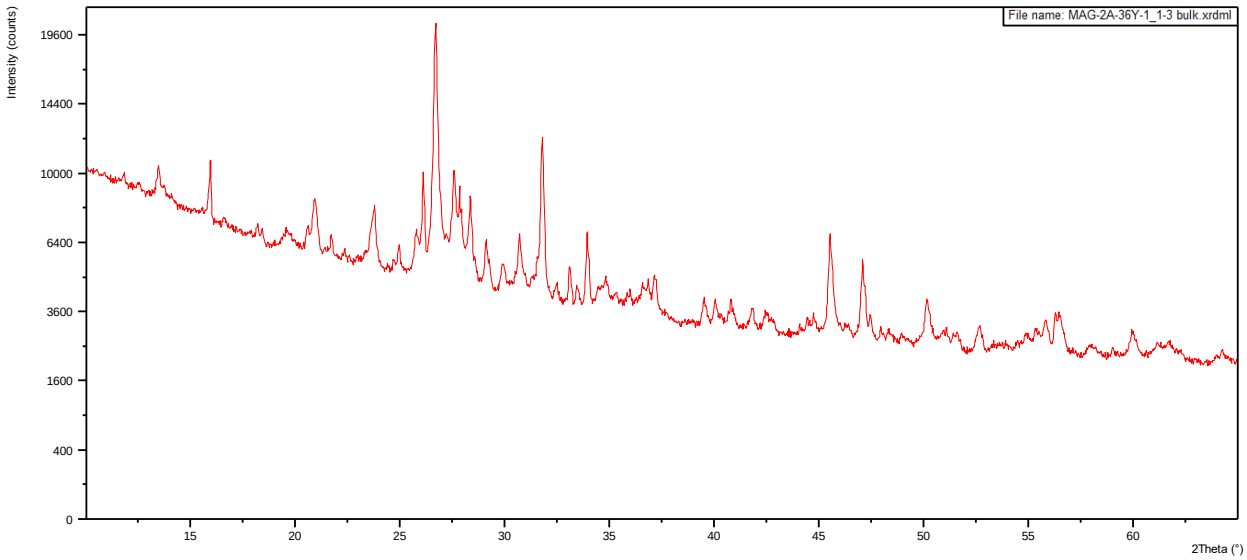
File name: MAG-2A-36Y-1_1-3 bulk.xrdml
Intensity (counts)
19600
14400
10000
6400
3600
1600
400
0
15
20
25
30
35
40
45
50
55
60
2Theta (°)

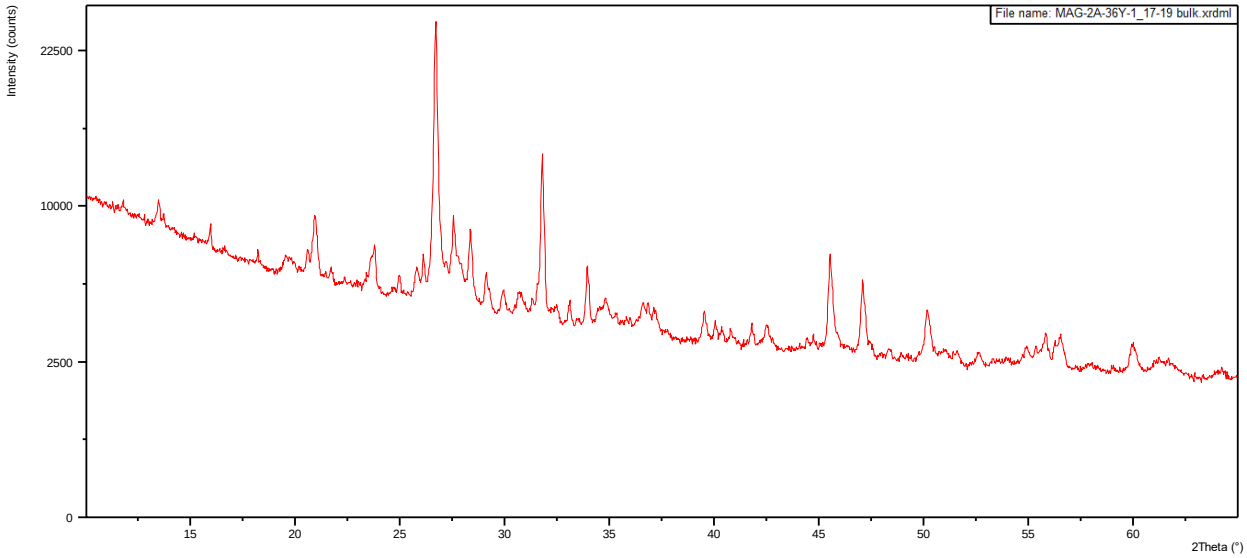
File name: MAG-2A-36Y-1_17-19 bulk.xrdml
Intensity (counts)
22500
10000
2500
0
15
20
25
30
35
40
45
50
55
60
2Theta (°)

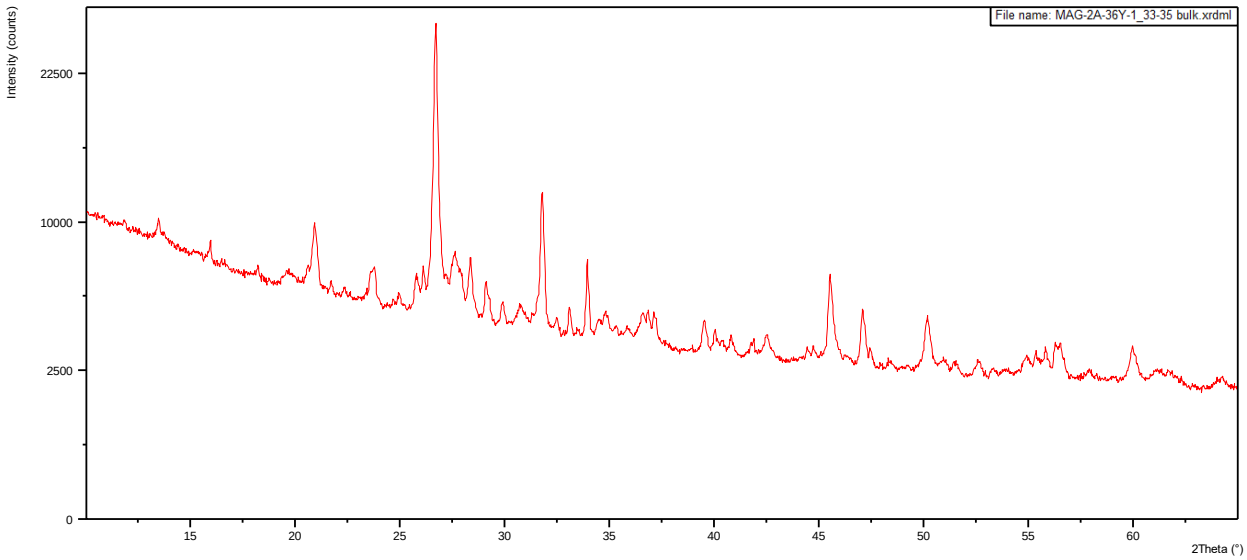
File name: MAG-2A-36Y-1_33-35 bulk.xrdml
Intensity (counts)
22500
10000
2500
0
15
20
25
30
35
40
45
50
55
60
2Theta (°)

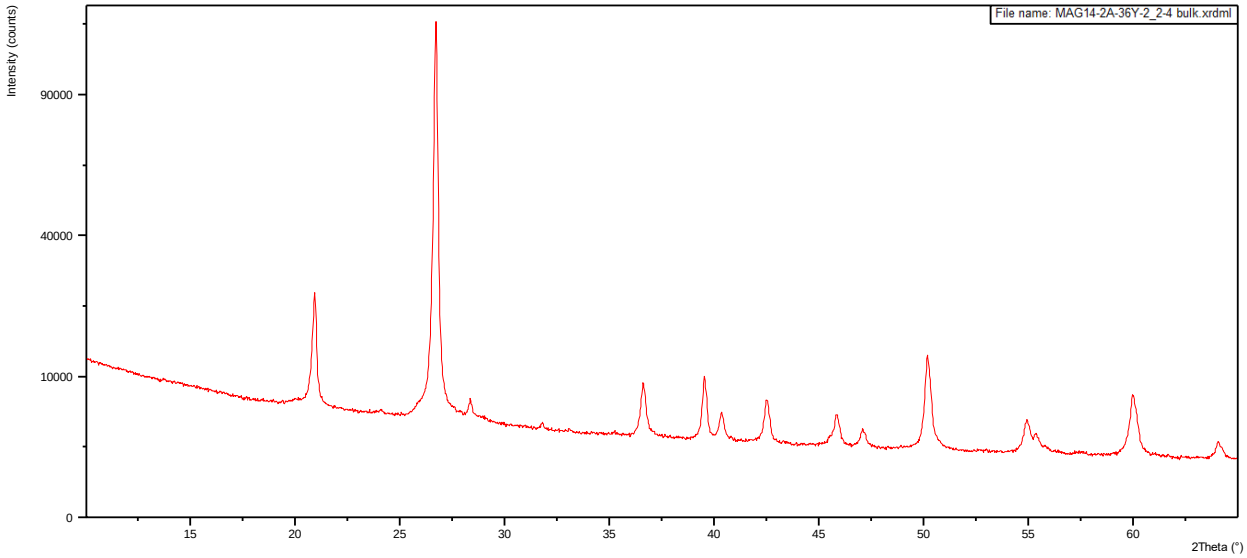
File name: MAG14-2A-36Y-2_2-4 bulk.xrdml
Intensity (counts)
90000
40000
10000
0
15
20
25
30
35
40
45
50
55
60
2Theta (°)

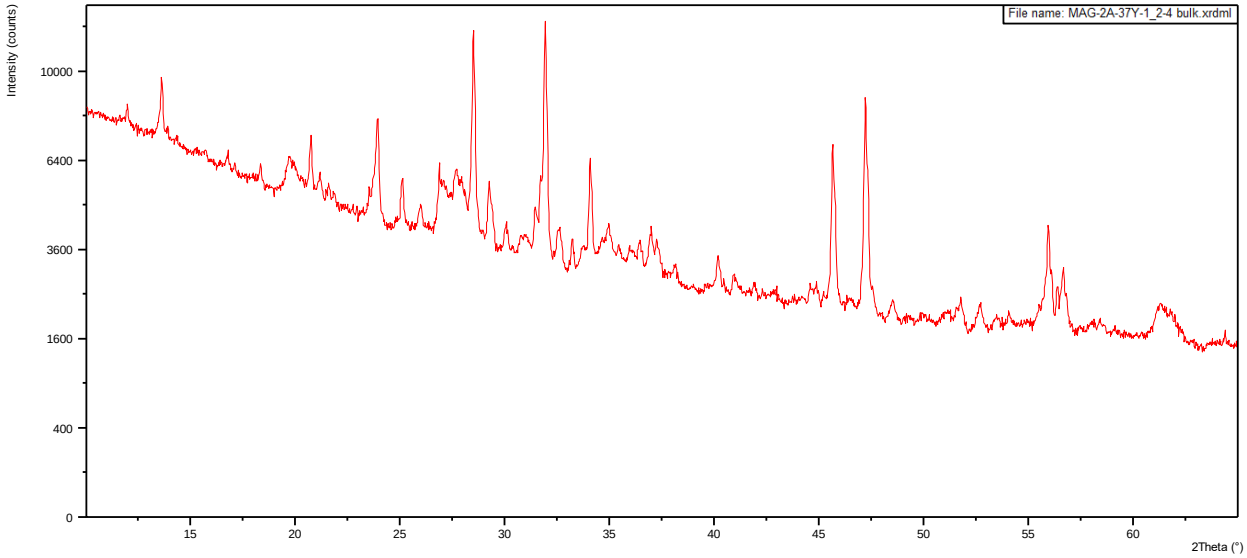
File name: MAG-2A-37Y-1_2-4 bulk.xrdml
Intensity (counts)
10000
6400
3600
1600
400
0
15
20
25
30
35
40
45
50
55
60
2Theta (°)

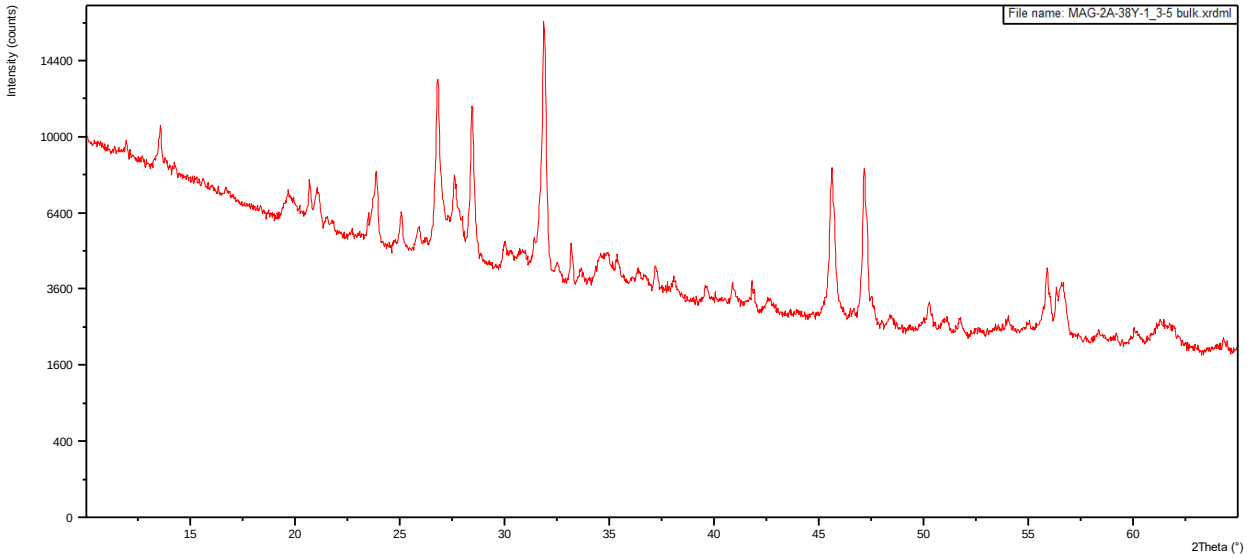
File name: MAG-2A-38Y-1_3-5 bulk.xrdml
Intensity (counts)
14400
10000
6400
3600
1600
400
0
15
20
25
30
35
40
45
50
55
60
2Theta (°)

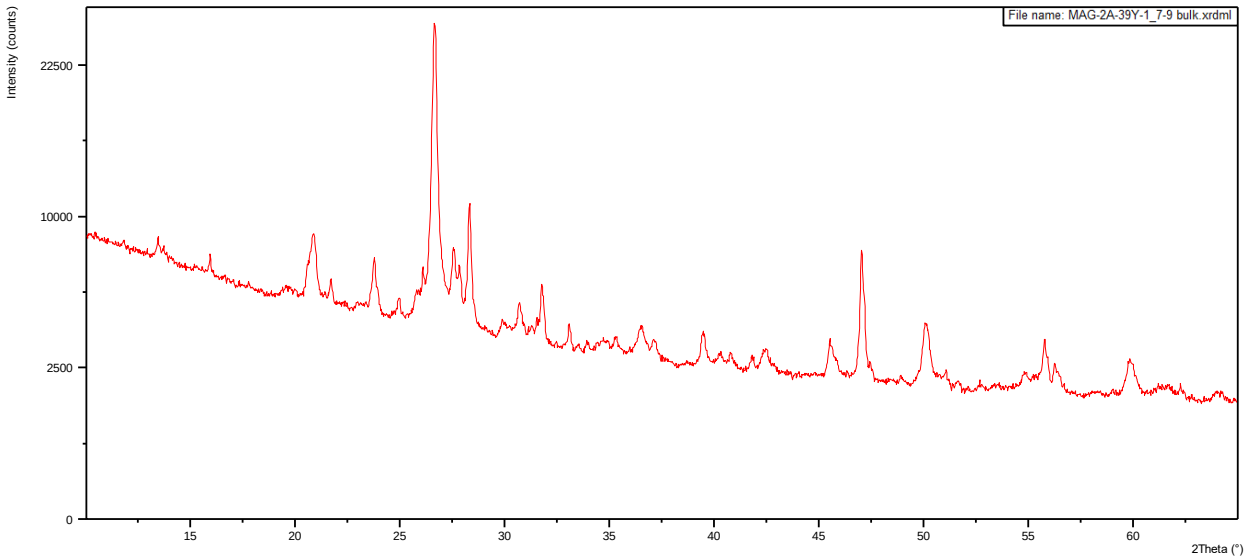
File name: MAG-2A-39Y-1_7-9 bulk.xrdml
Intensity (counts)
22500
10000
2500
0
15
20
25
30
35
40
45
50
55
60
2Theta (°)

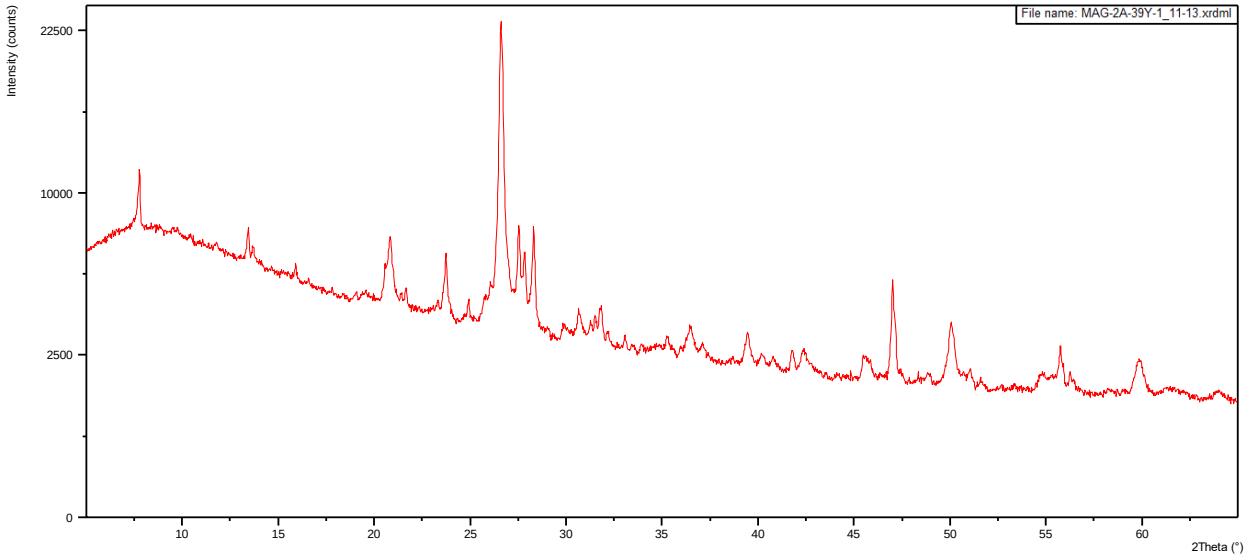
File name: MAG-2A-39Y-1_11-13.xrdml
Intensity (counts)
22500
10000
2500
0
10
15
20
25
30
35
40
45
50
55
60
2Theta (°)

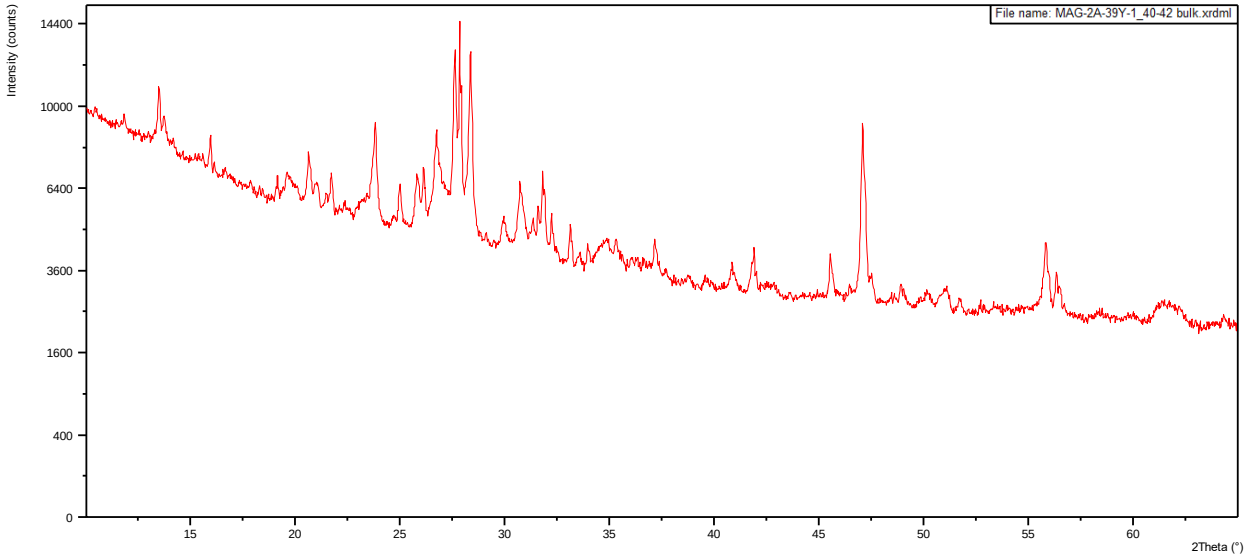
File name: MAG-2A-39Y-1_40-42 bulk.xrdml
Intensity (counts)
14400
10000
6400
3600
1600
400
0
15
20
25
30
35
40
45
50
55
60
2Theta (°)

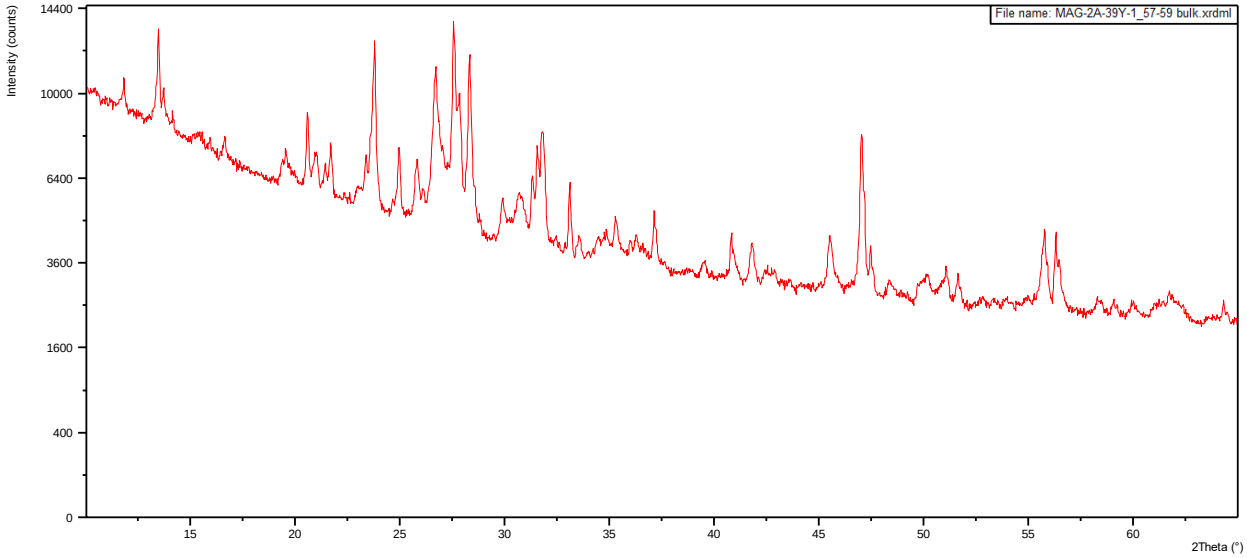
File name: MAG-2A-39Y-1_57-59 bulk.xrdml
Intensity (counts)
14400
10000
6400
3600
1600
400
0
15
20
25
30
35
40
45
50
55
60
2Theta (°)

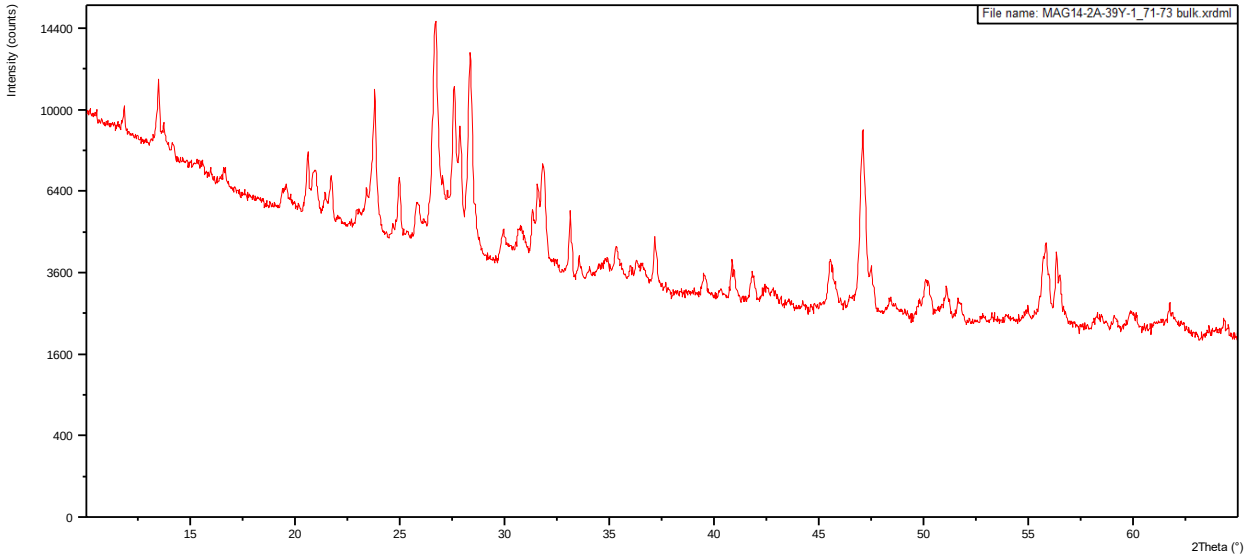
File name: MAG14-2A-39Y-1_71-73 bulk.xrdml
Intensity (counts)
14400
10000
6400
3600
1600
400
0
15
20
25
30
35
40
45
50
55
60
2Theta (°)

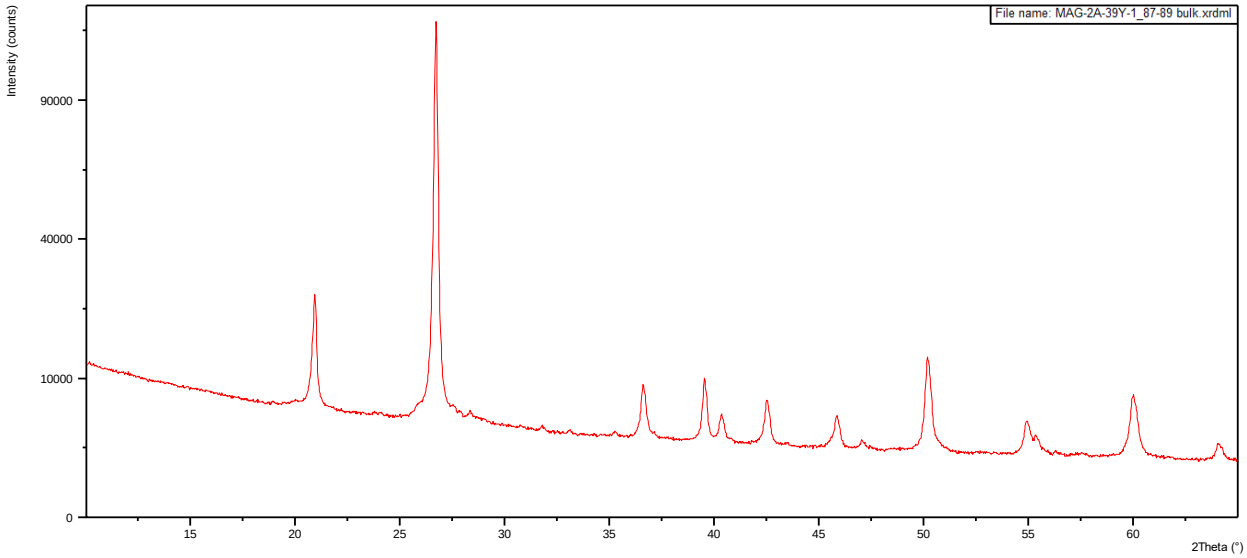
File name: MAG-2A-39Y-1_87-89 bulk.xrdml
Intensity (counts)
90000
40000
10000
0
15
20
25
30
35
40
45
50
55
60
2Theta (°)

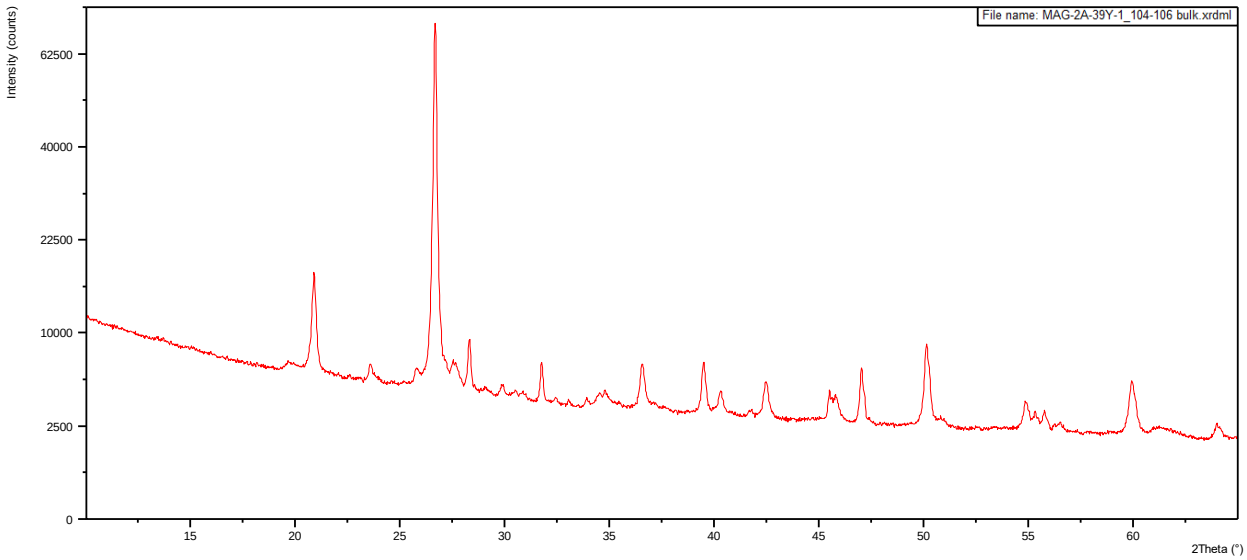
File name: MAG-2A-39Y-1_104-106 bulk.xrdml
Intensity (counts)
62500
40000
22500
10000
2500
0
15
20
25
30
35
40
45
50
55
60
2Theta (°)

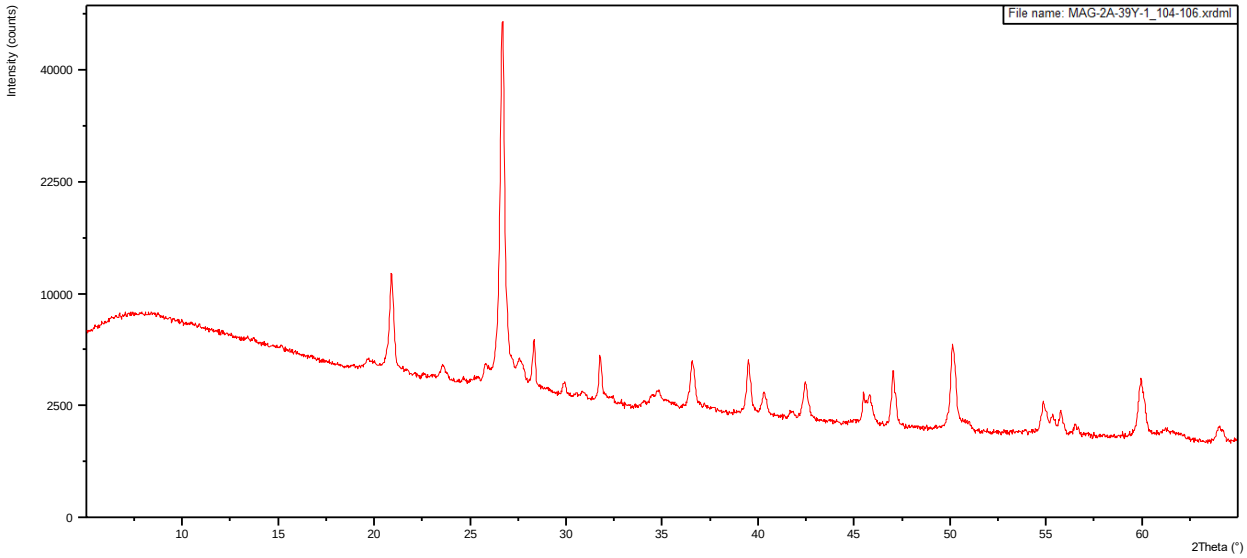
File name: MAG-2A-39Y-1_104-106.xrdml
Intensity (counts)
40000
22500
10000
2500
0
10
15
20
25
30
35
40
45
50
55
60
2Theta (°)

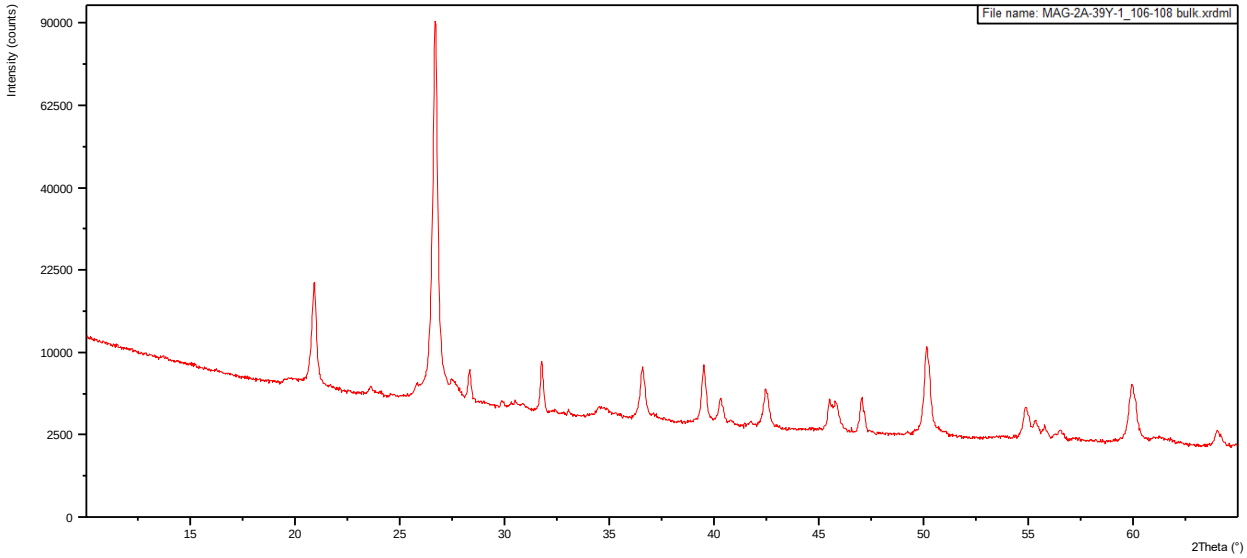
File name: MAG-2A-39Y-1_106-108 bulk.xrdml
Intensity (counts)
90000
62500
40000
22500
10000
2500
0
15
20
25
30
35
40
45
50
55
60
2Theta (°)

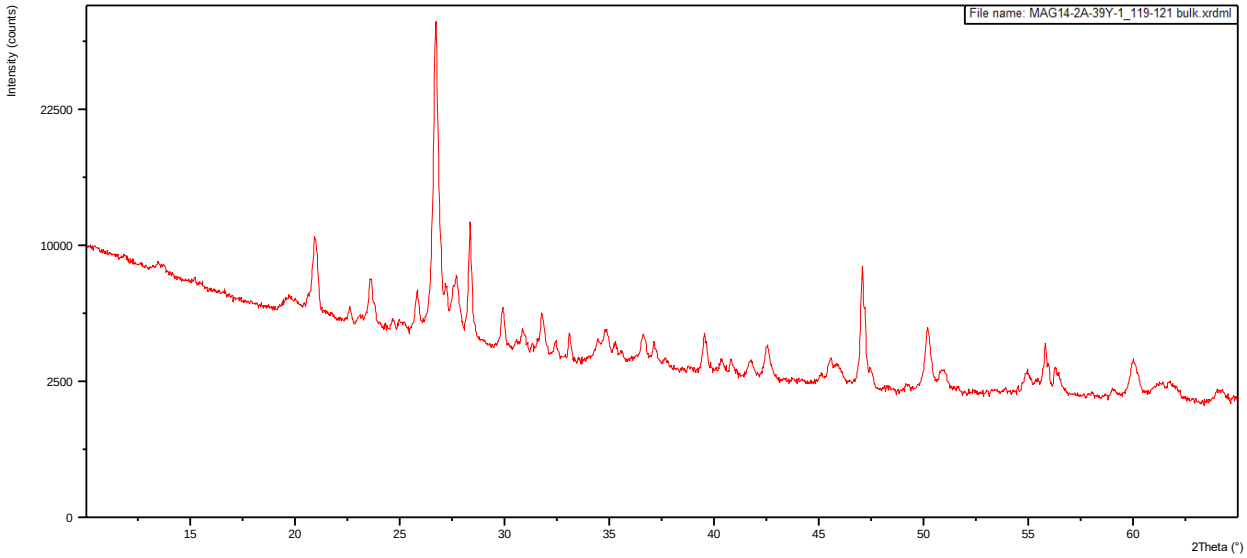
File name: MAG14-2A-39Y-1_119-121 bulk.xrdml
Intensity (counts)
22500
10000
2500
0
15
20
25
30
35
40
45
50
55
60
2Theta (°)

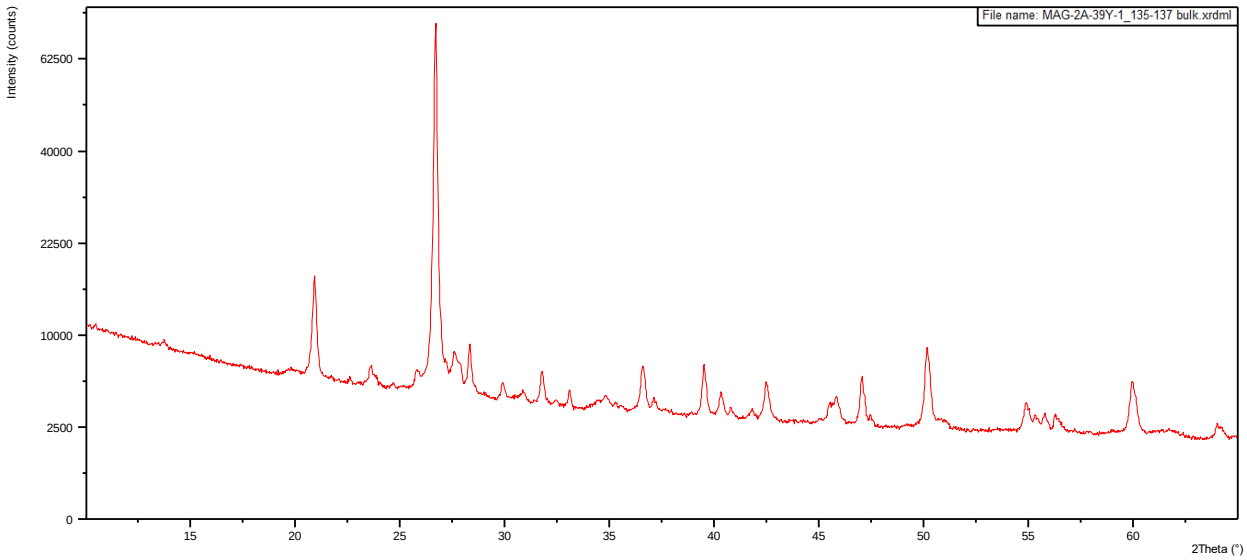
File name: MAG-2A-39Y-1_135-137 bulk.xrdml
Intensity (counts)
62500
40000
22500
10000
2500
0
15
20
25
30
35
40
45
50
55
60
2Theta (°)

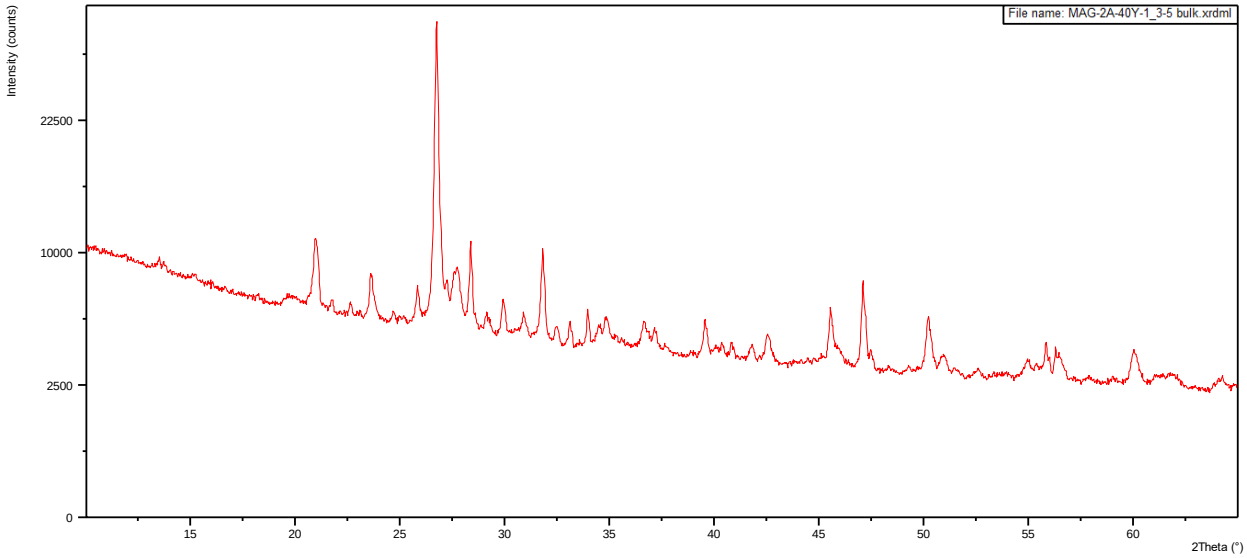
File name: MAG-2A-40Y-1_3-5 bulk.xrdml
Intensity (counts)
22500
10000
2500
0
15
20
25
30
35
40
45
50
55
60
2Theta (°)

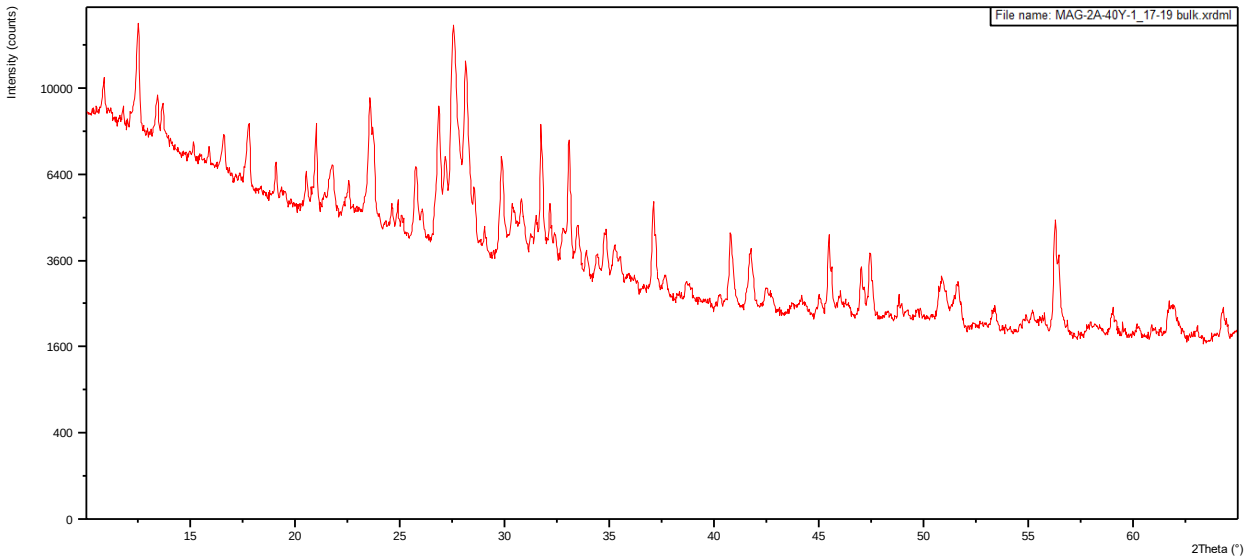
File name: MAG-2A-40Y-1_17-19 bulk.xrdml
Intensity (counts)
10000
6400
3600
1600
400
0
15
20
25
30
35
40
45
50
55
60
2Theta (°)

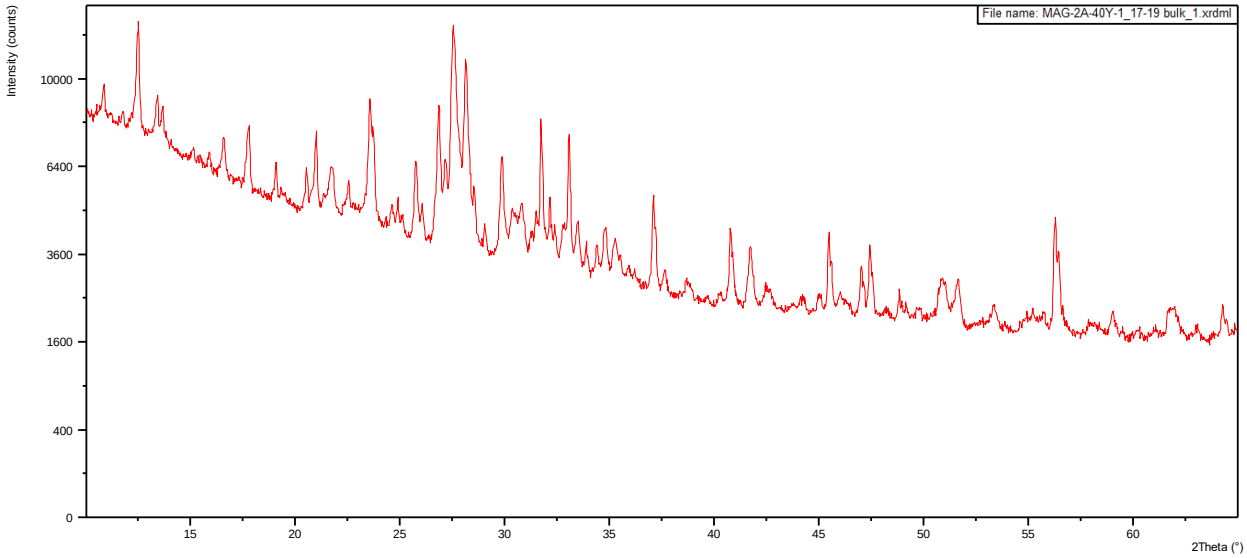
File name: MAG-2A-40Y-1_17-19 bulk_1.xrdml
Intensity (counts)
10000
6400
3600
1600
400
0
15
20
25
30
35
40
45
50
55
60
2Theta (°)

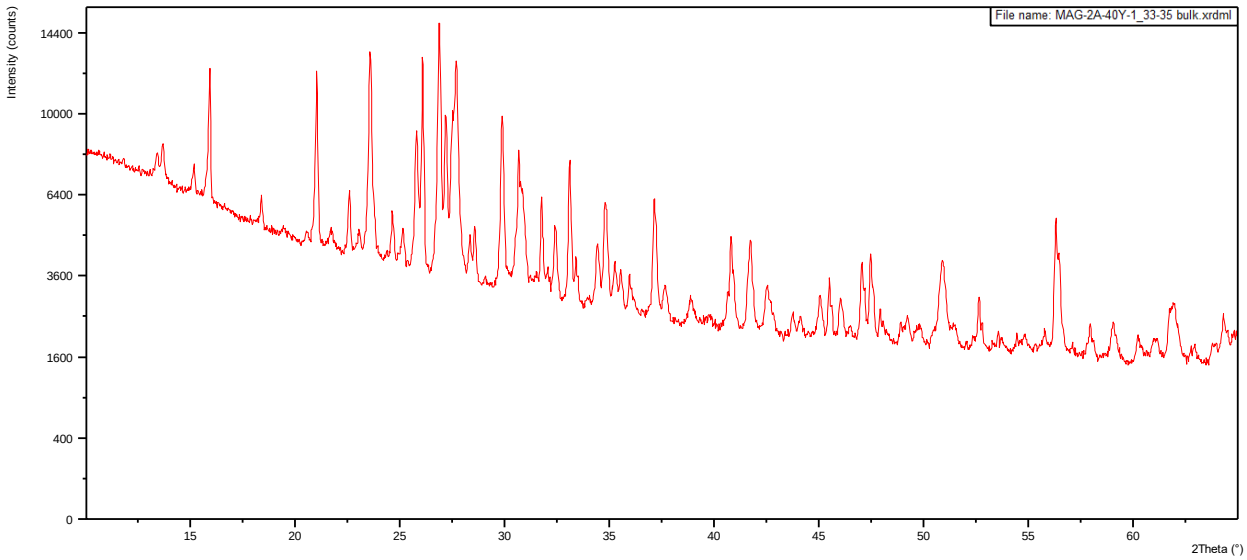
File name: MAG-2A-40Y-1_33-35 bulk.xrdml
Intensity (counts)
14400
10000
6400
3600
1600
400
0
15
20
25
30
35
40
45
50
55
60
2Theta (°)

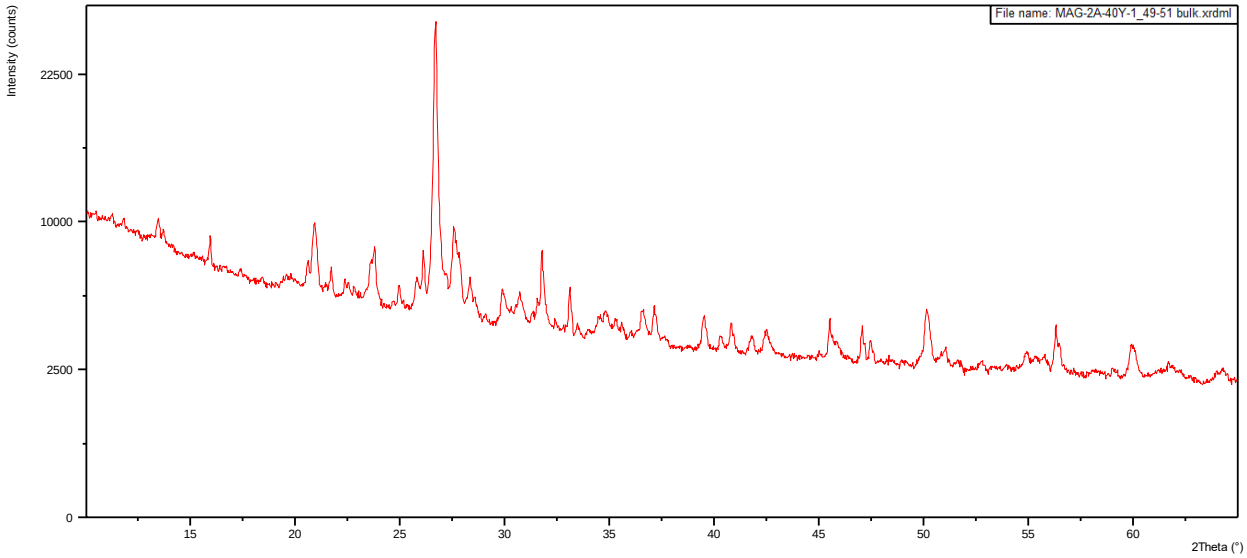
File name: MAG-2A-40Y-1_49-51 bulk.xrdml
Intensity (counts)
22500
10000
2500
0
15
20
25
30
35
40
45
50
55
60
2Theta (°)

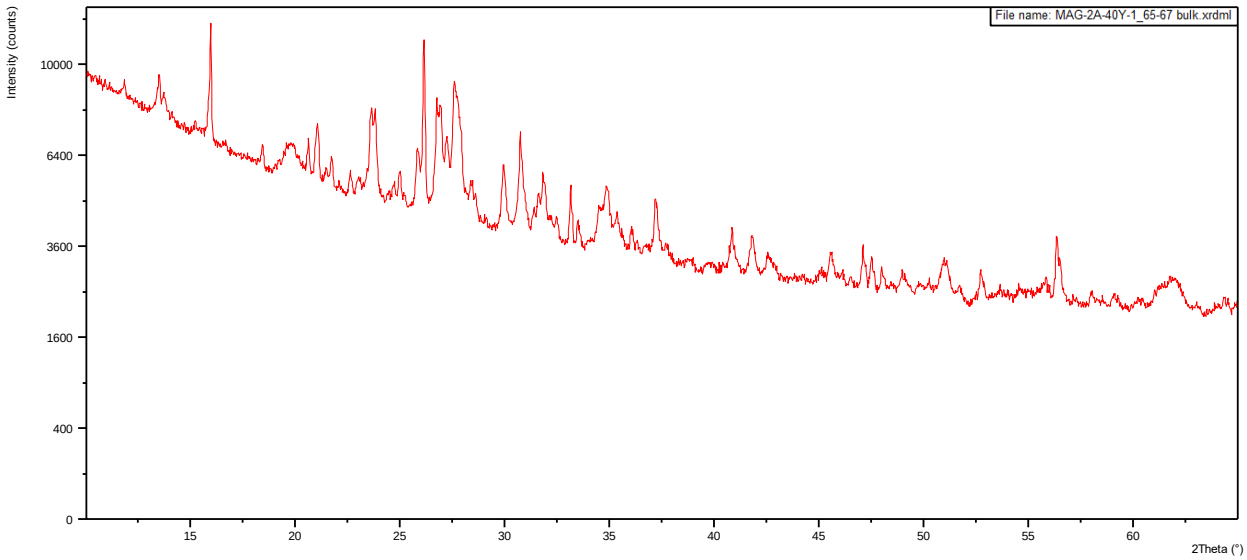
File name: MAG-2A-40Y-1_65-67 bulk.xrdml
Intensity (counts)
10000
6400
3600
1600
400
0
15
20
25
30
35
40
45
50
55
60
2Theta (°)

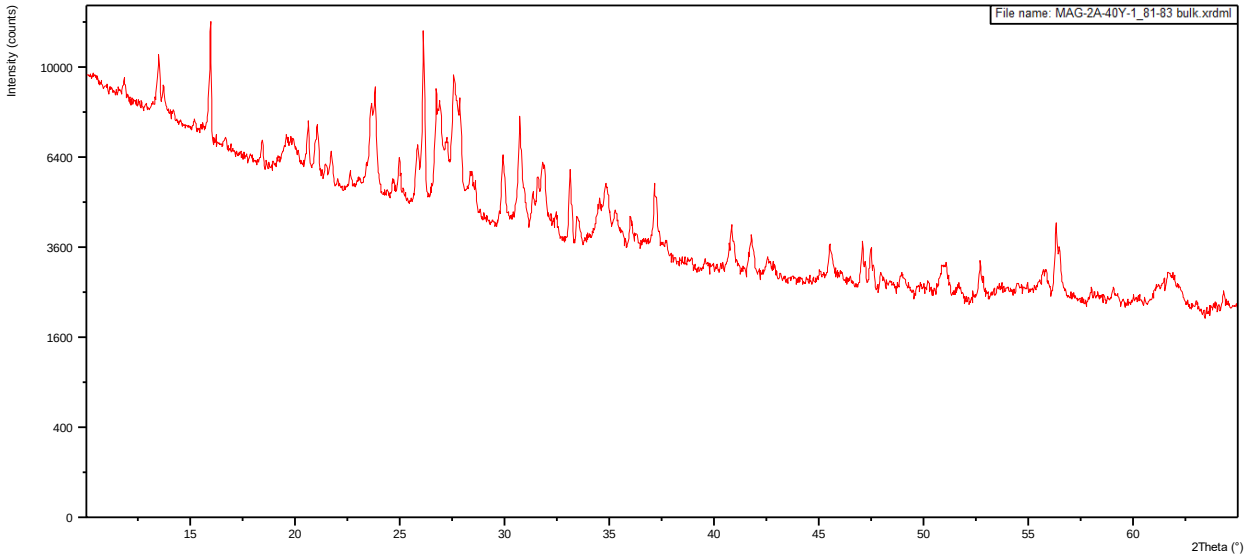
File name: MAG-2A-40Y-1_81-83 bulk.xrdml
Intensity (counts)
10000
6400
3600
1600
400
0
15
20
25
30
35
40
45
50
55
60
2Theta (°)

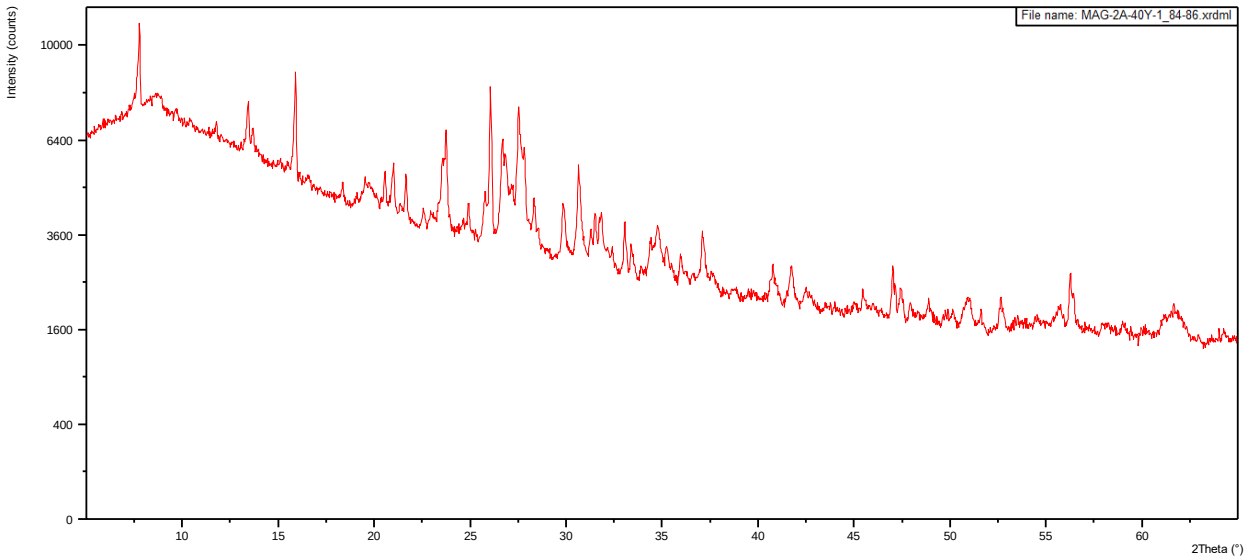
File name: MAG-2A-40Y-1_84-86.xrdml
Intensity (counts)
10000
6400
3600
1600
400
0
10
15
20
25
30
35
40
45
50
55
60
2Theta (°)

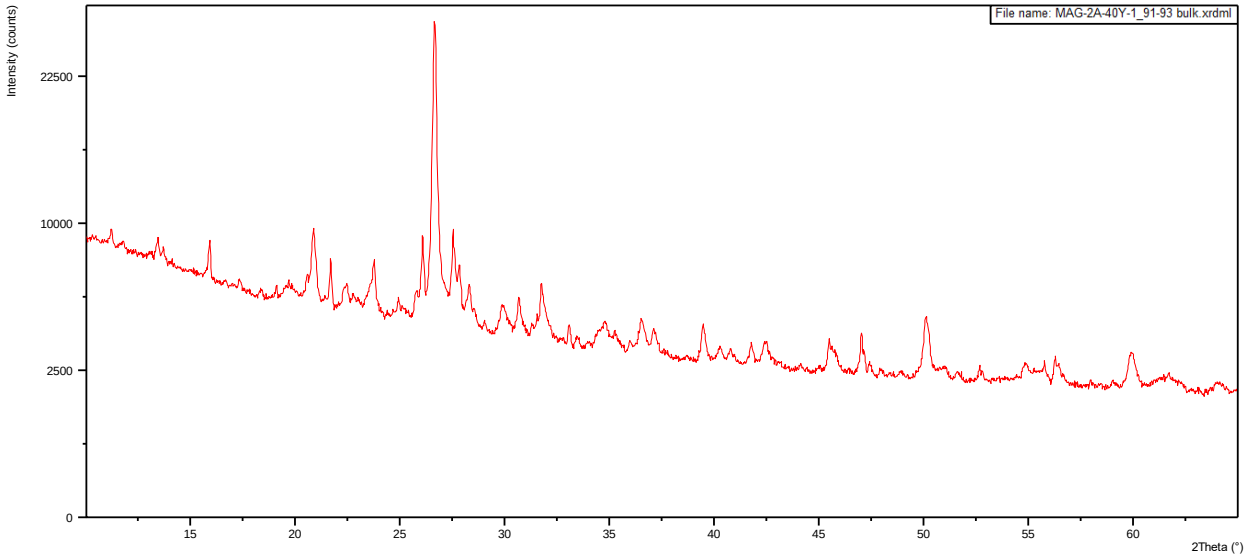
File name: MAG-2A-40Y-1_91-93 bulk.xrdml
Intensity (counts)
22500
10000
2500
0
15
20
25
30
35
40
45
50
55
60
2Theta (°)

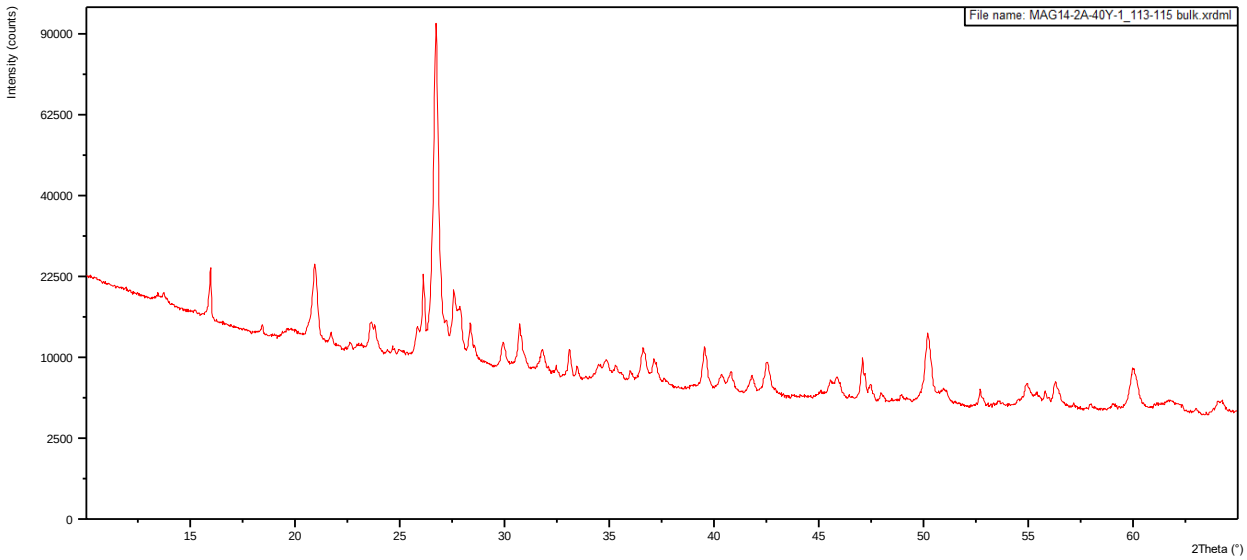
File name: MAG14-2A-40Y-1_113-115 bulk.xrdml
Intensity (counts)
90000
62500
40000
22500
10000
2500
0
15
20
25
30
35
40
45
50
55
60
2Theta (°)

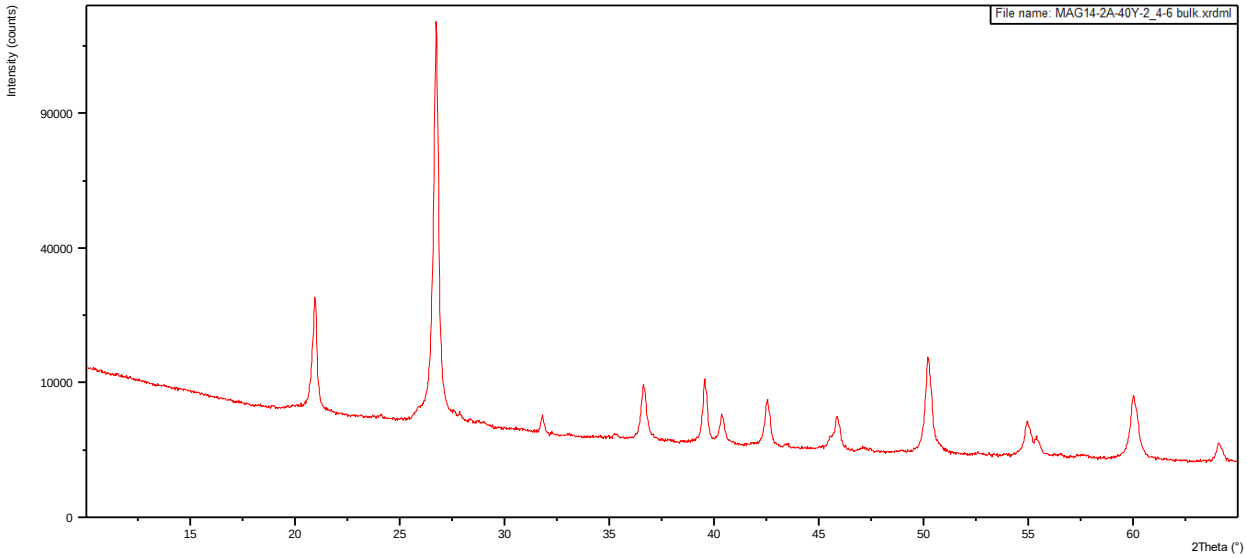
File name: MAG14-2A-40Y-2_4-6 bulk.xrdml
Intensity (counts)
90000
40000
10000
0
15
20
25
30
35
40
45
50
55
60
2Theta (°)

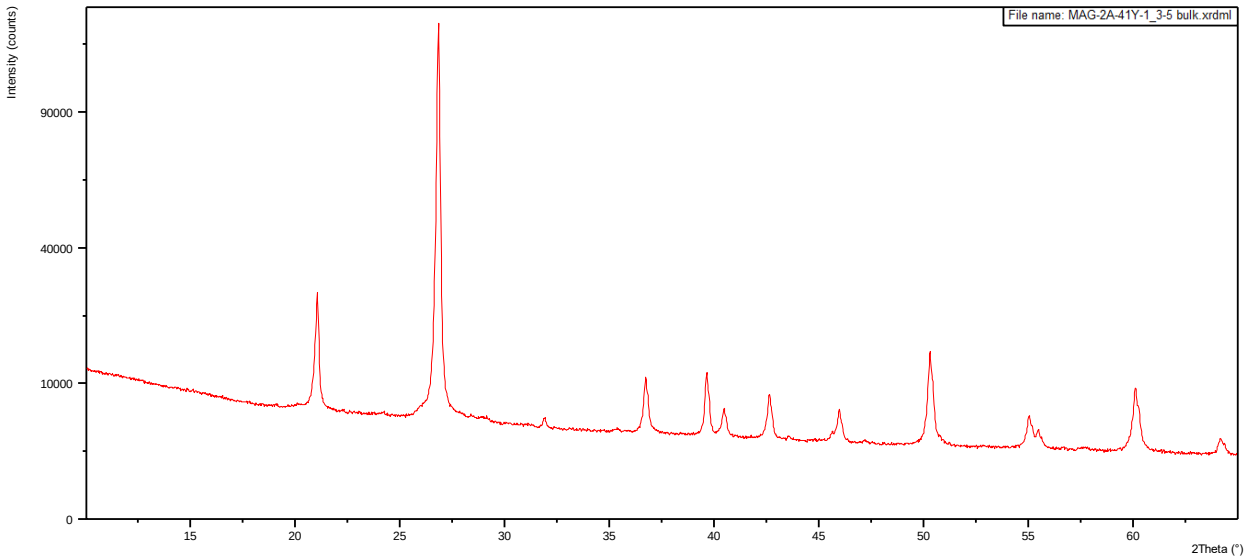
File name: MAG-2A-41Y-1_3-5 bulk.xrdml
Intensity (counts)
90000
40000
10000
0
15
20
25
30
35
40
45
50
55
60
2Theta (°)

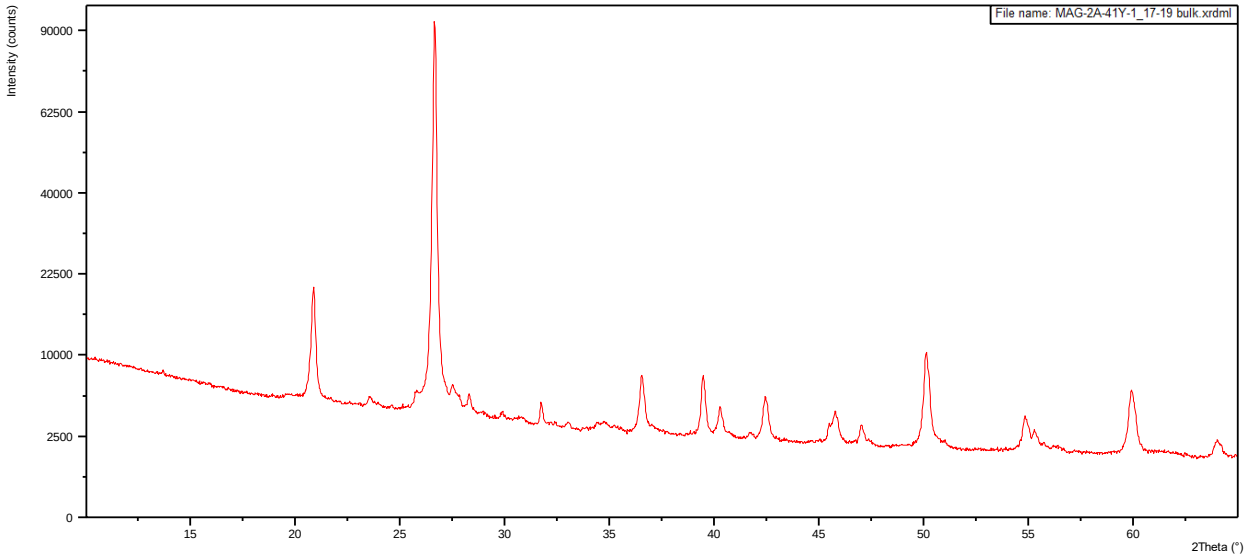
File name: MAG-2A-41Y-1_17-19 bulk.xrdml
Intensity (counts)
90000
62500
40000
22500
10000
2500
0
15
20
25
30
35
40
45
50
55
60
2Theta (°)

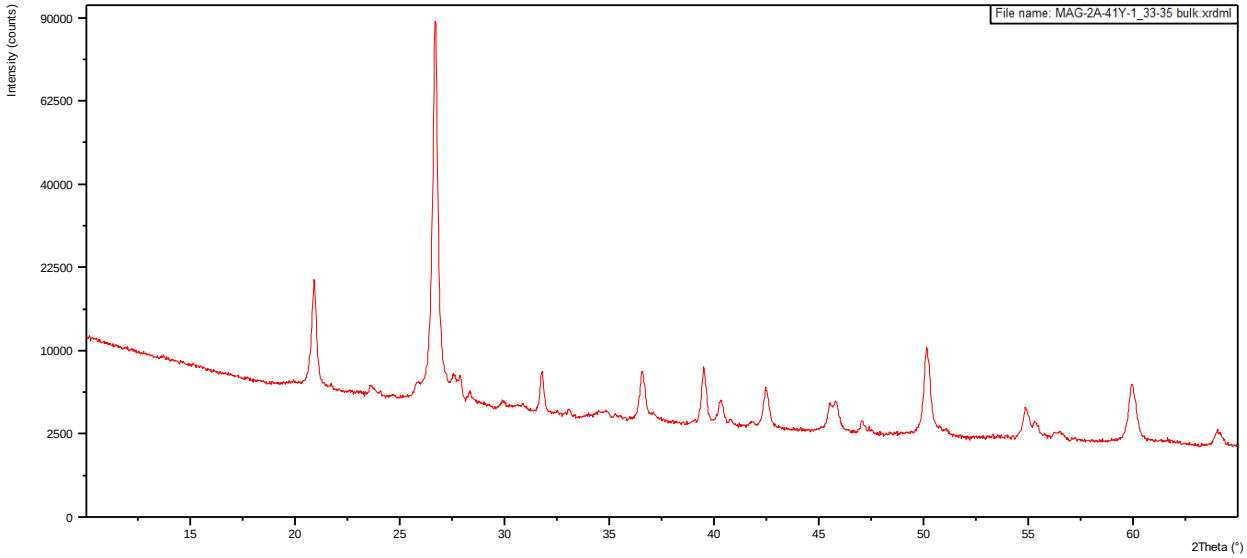
File name: MAG-2A-41Y-1_33-35 bulk.xrdml
Intensity (counts)
90000
62500
40000
22500
10000
2500
0
15
20
25
30
35
40
45
50
55
60
2Theta (°)

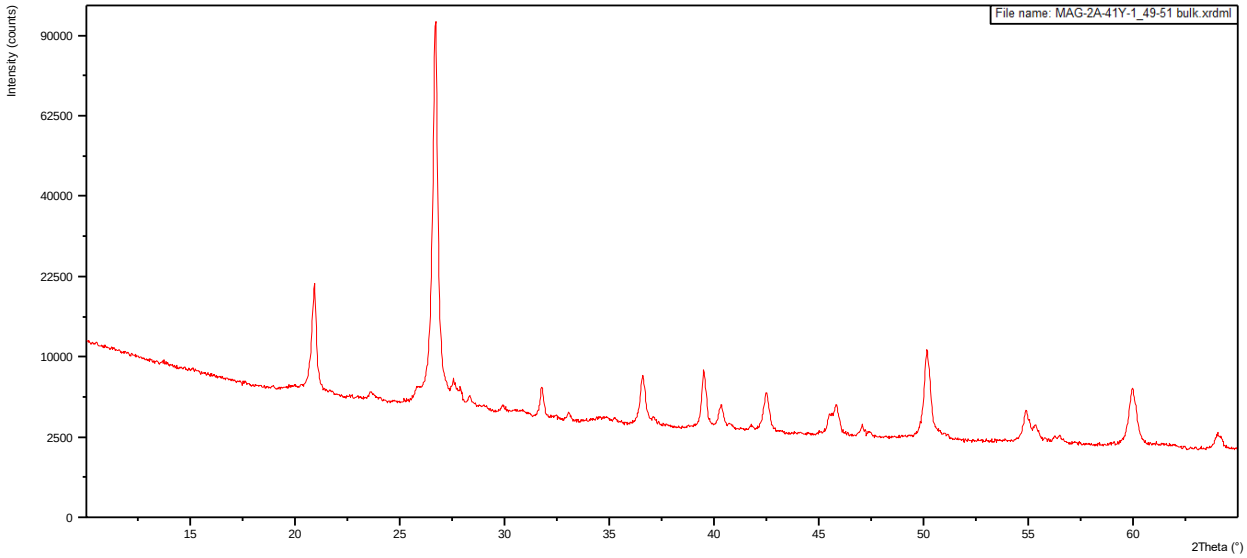
File name: MAG-2A-41Y-1_49-51 bulk.xrdml
Intensity (counts)
90000
62500
40000
22500
10000
2500
0
15
20
25
30
35
40
45
50
55
60
2Theta (°)

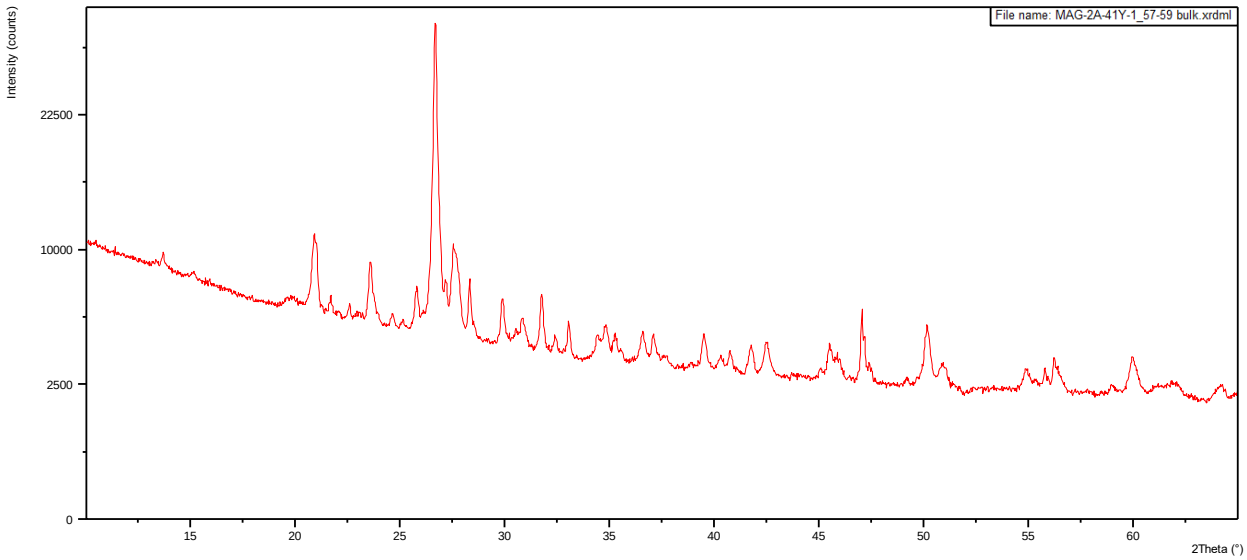
File name: MAG-2A-41Y-1_57-59 bulk.xrdml
Intensity (counts)
22500
10000
2500
0
15
20
25
30
35
40
45
50
55
60
2Theta (°)

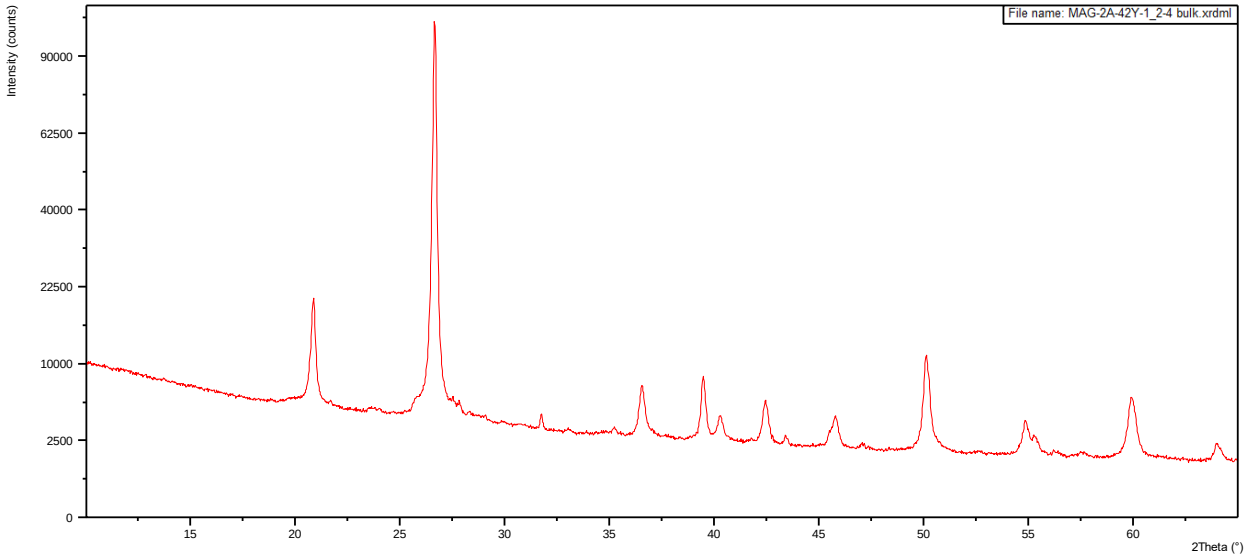
File name: MAG-2A-42Y-1_2-4 bulk.xrdml
Intensity (counts)
90000
62500
40000
22500
10000
2500
0
15
20
25
30
35
40
45
50
55
60
2Theta (°)

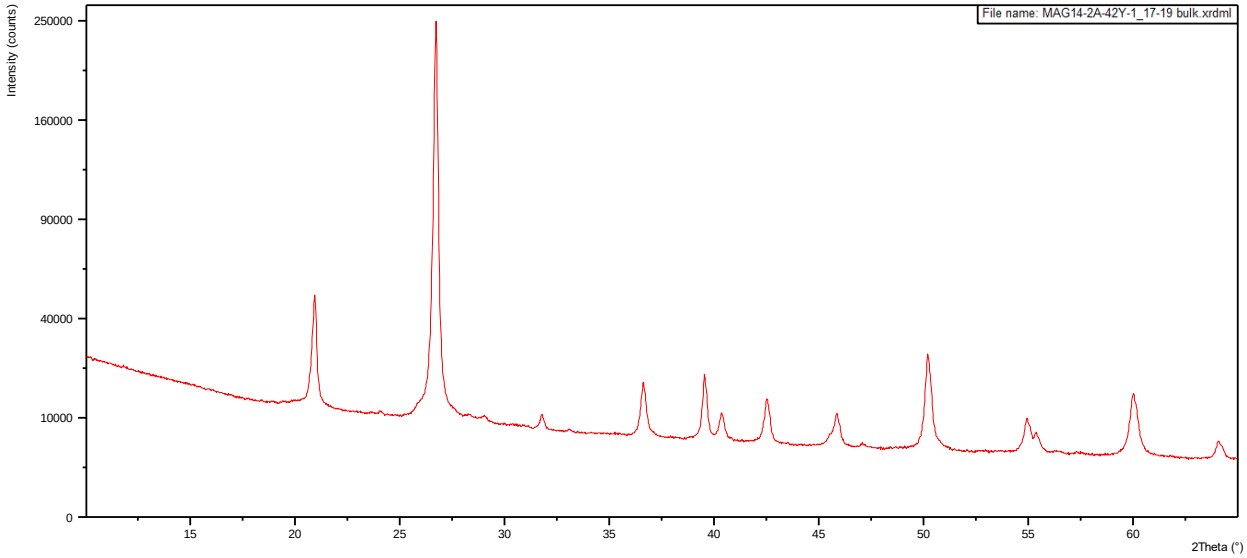
File name: MAG14-2A-42Y-1_17-19 bulk.xrdml
Intensity (counts)
250000
160000
90000
40000
10000
0
15
20
25
30
35
40
45
50
55
60
2Theta (°)

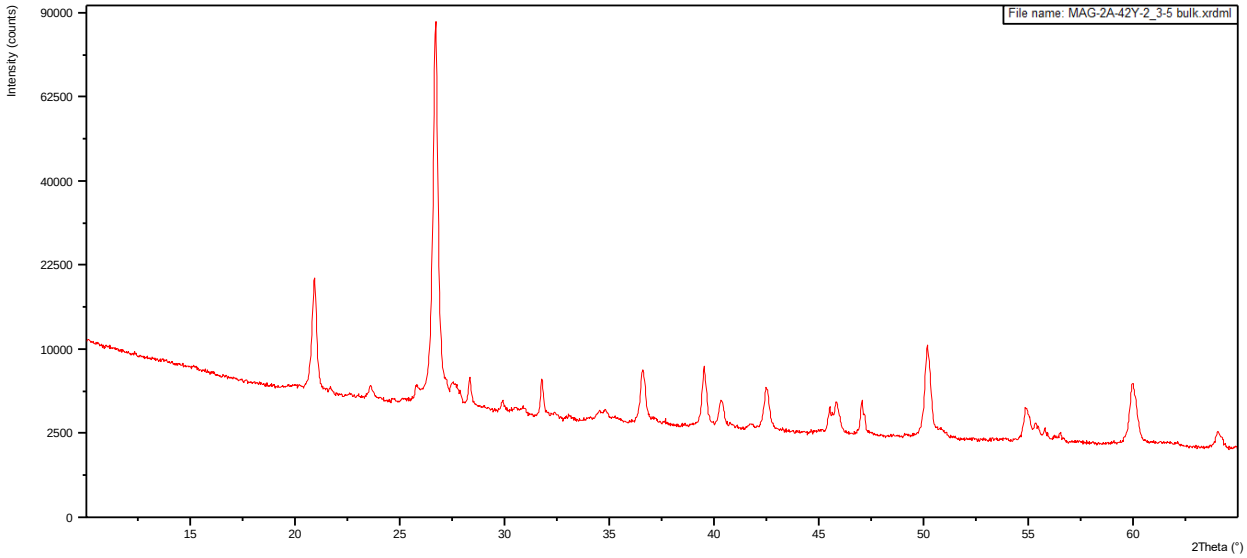
File name: MAG-2A-42Y-2_3-5 bulk.xrdml
Intensity (counts)
90000
62500
40000
22500
10000
2500
0
15
20
25
30
35
40
45
50
55
60
2Theta (°)

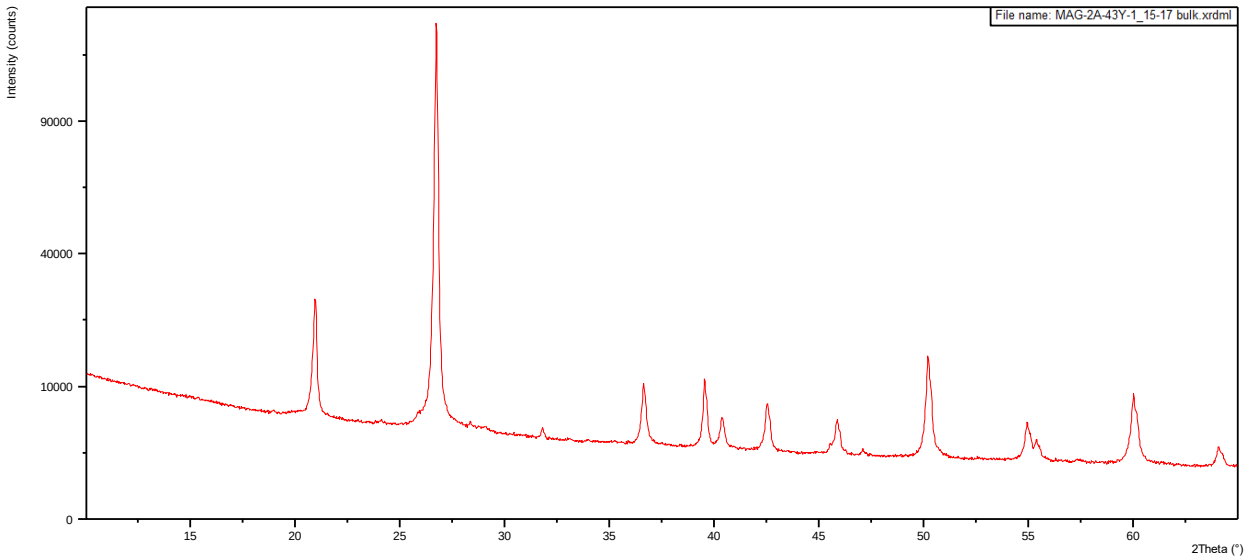
File name: MAG-2A-43Y-1_15-17 bulk.xrdml
Intensity (counts)
90000
40000
10000
0
15
20
25
30
35
40
45
50
55
60
2Theta (°)

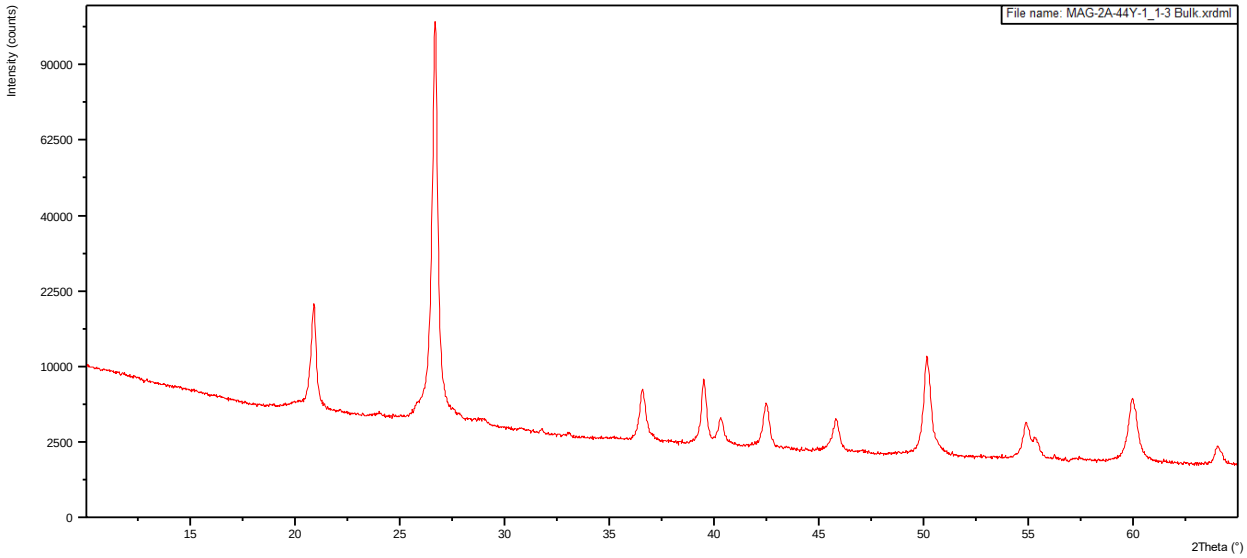
File name: MAG-2A-44Y-1_1-3 Bulk.xrdml
Intensity (counts)
90000
62500
40000
22500
10000
2500
0
15
20
25
30
35
40
45
50
55
60
2Theta (°)

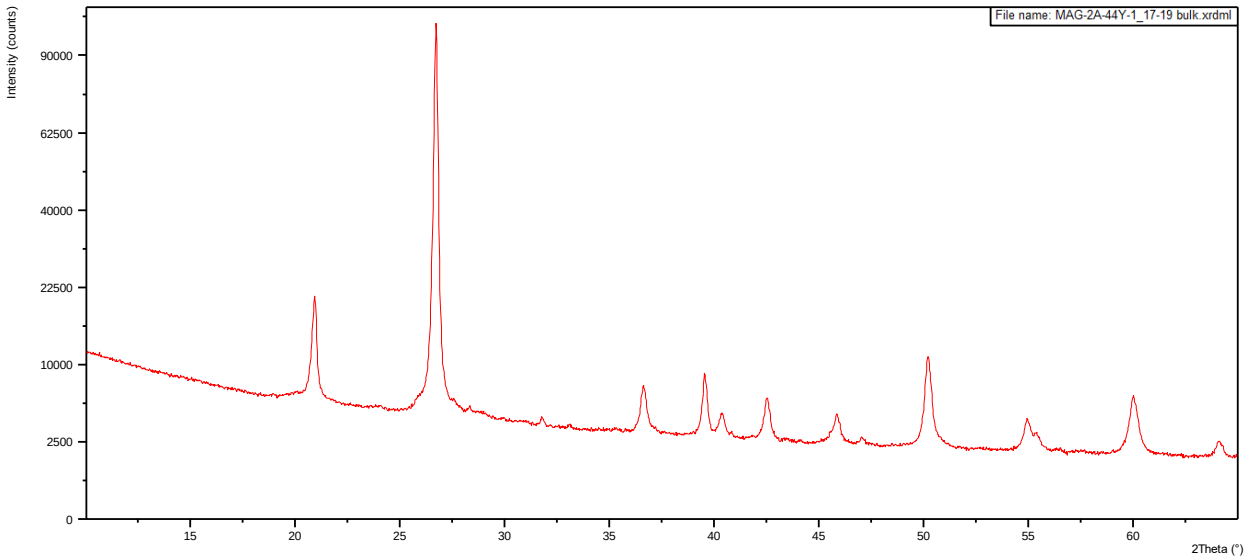
File name: MAG-2A-44Y-1_17-19 bulk.xrdml
Intensity (counts)
90000
62500
40000
22500
10000
2500
0
15
20
25
30
35
40
45
50
55
60
2Theta (°)

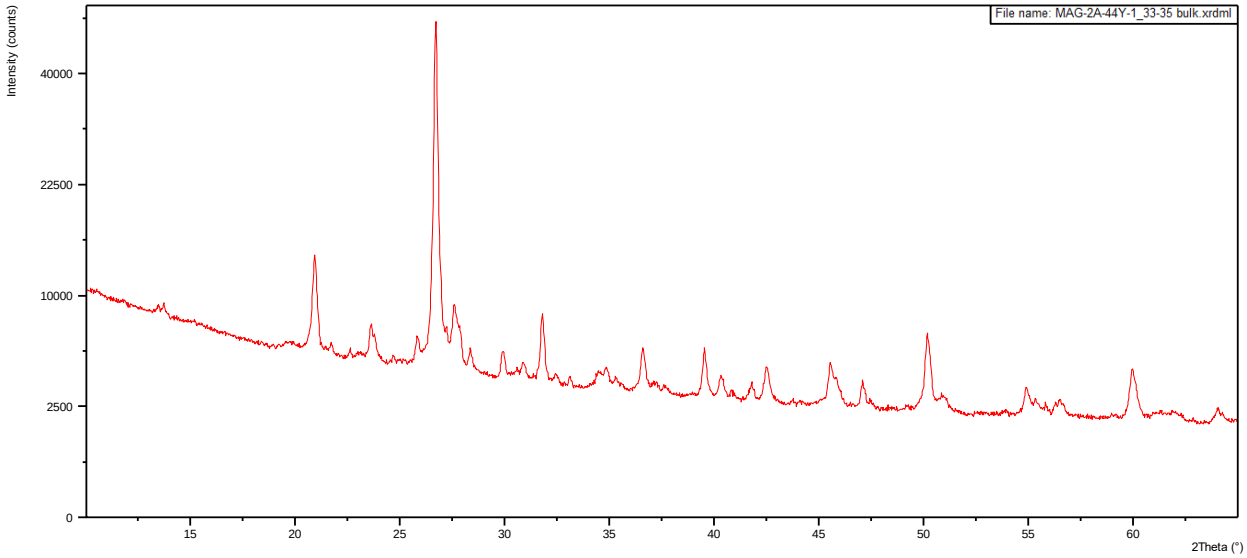
File name: MAG-2A-44Y-1_33-35 bulk.xrdml
Intensity (counts)
40000
22500
10000
2500
0
15
20
25
30
35
40
45
50
55
60
2Theta (°)

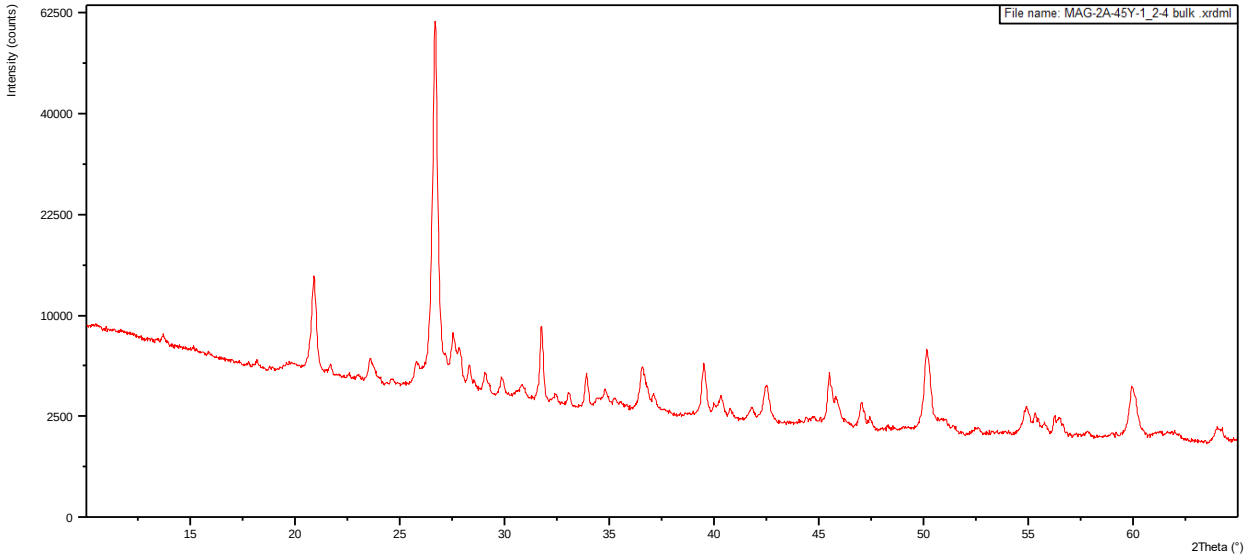
File name: MAG-2A-45Y-1_2-4 bulk .xrdml
Intensity (counts)
62500
40000
22500
10000
2500
0
15
20
25
30
35
40
45
50
55
60
2Theta (°)

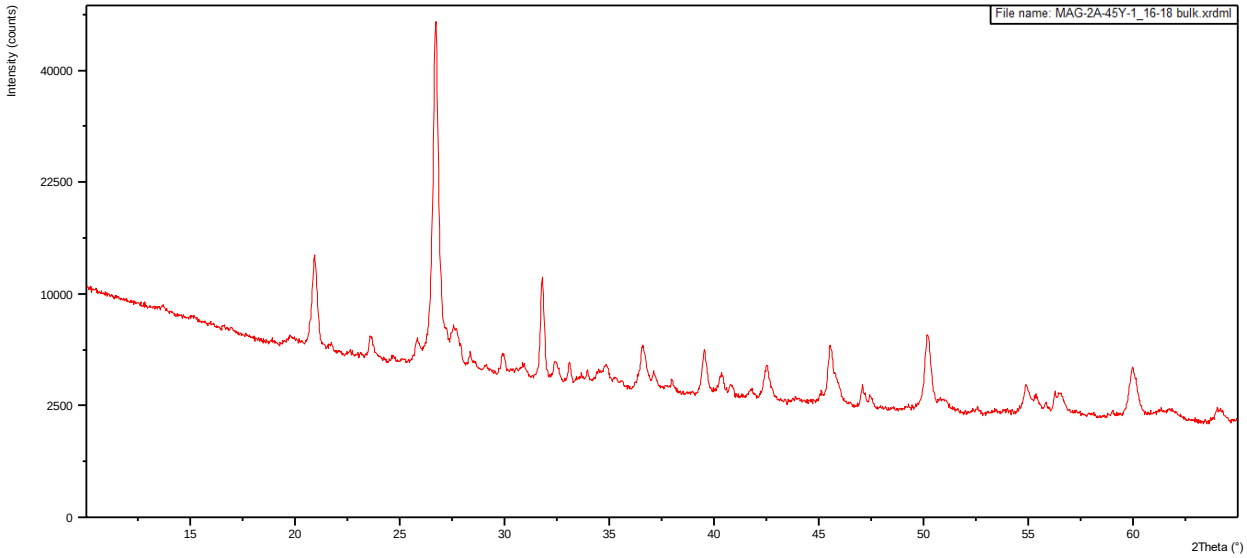
File name: MAG-2A-45Y-1_16-18 bulk.xrdml
Intensity (counts)
40000
22500
10000
2500
0
15
20
25
30
35
40
45
50
55
60
2Theta (°)

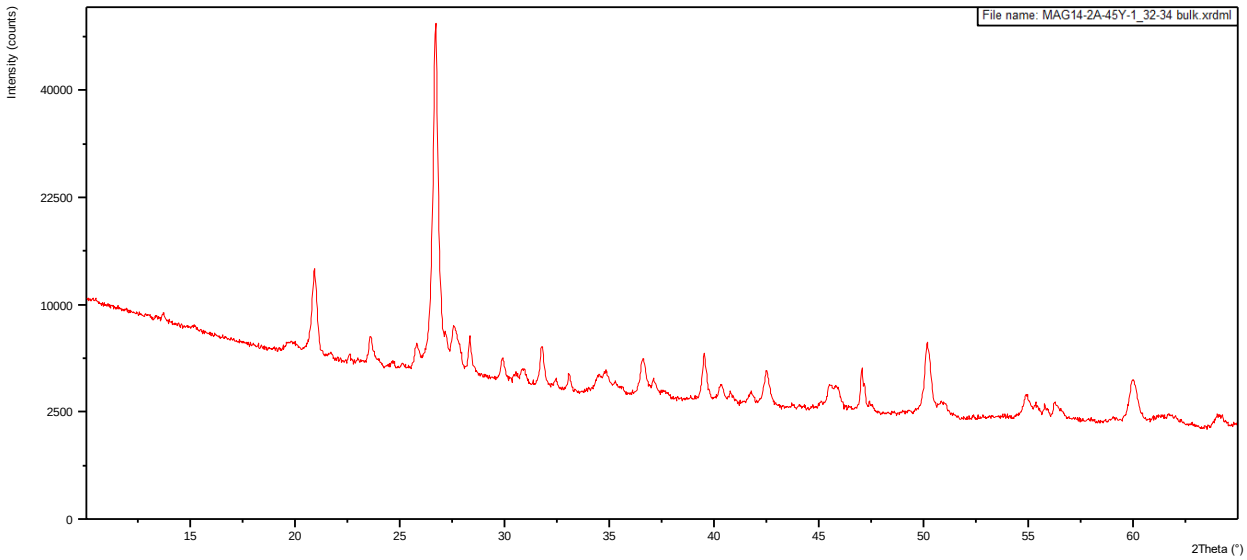
File name: MAG14-2A-45Y-1_32-34 bulk.xrdml
Intensity (counts)
40000
22500
10000
2500
0
15
20
25
30
35
40
45
50
55
60
2Theta (°)

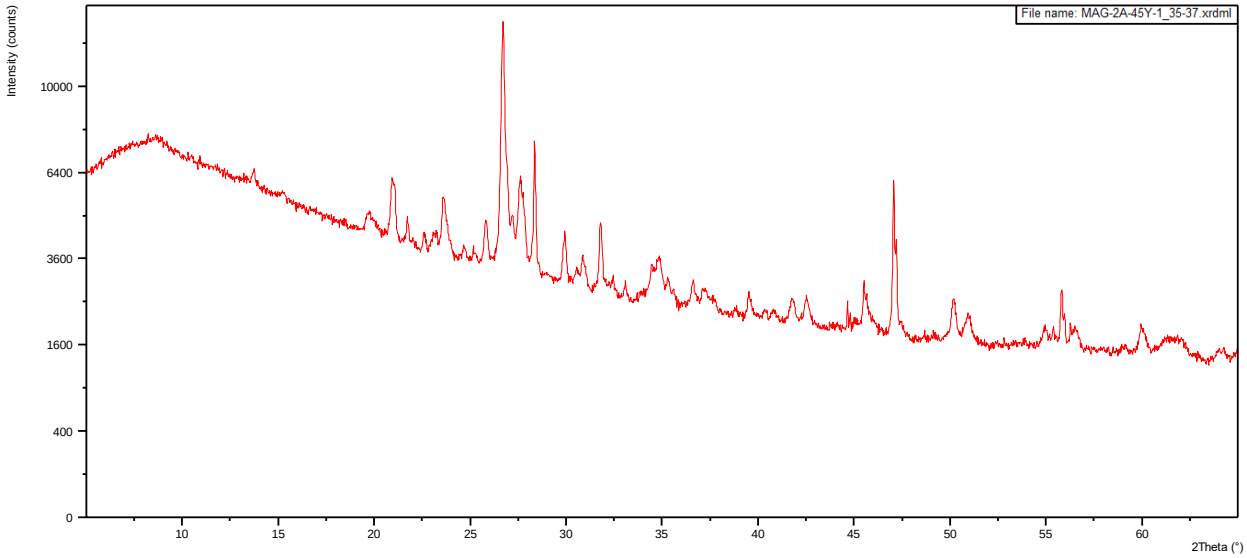
File name: MAG-2A-45Y-1_35-37.xrdml
Intensity (counts)
10000
6400
3600
1600
400
0
10
15
20
25
30
35
40
45
50
55
60
2Theta (°)

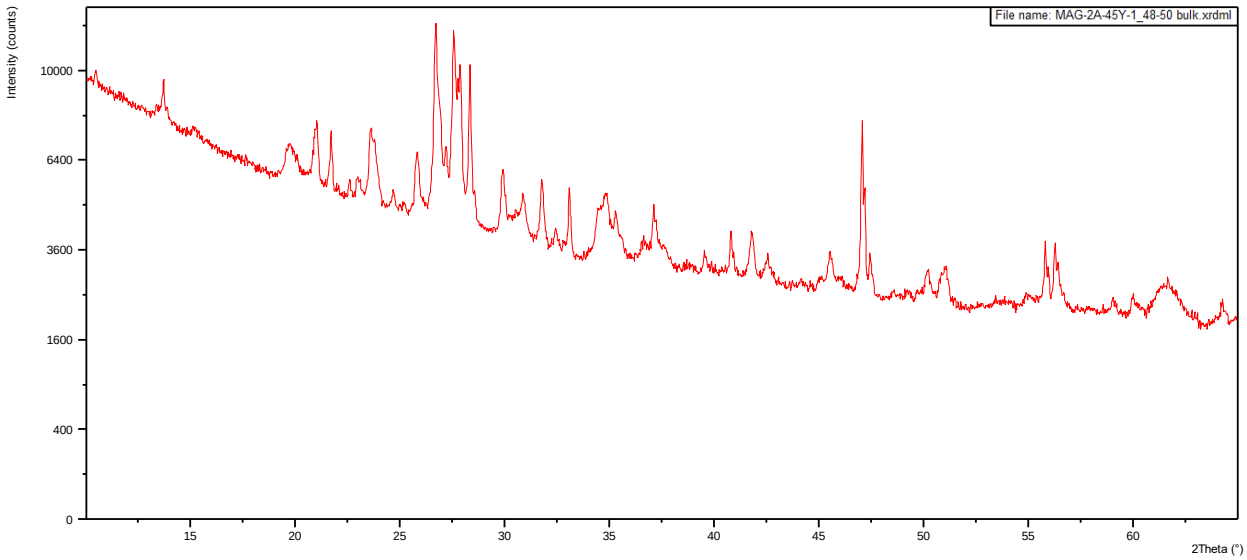
File name: MAG-2A-45Y-1_48-50 bulk.xrdml
Intensity (counts)
10000
6400
3600
1600
400
0
15
20
25
30
35
40
45
50
55
60
2Theta (°)

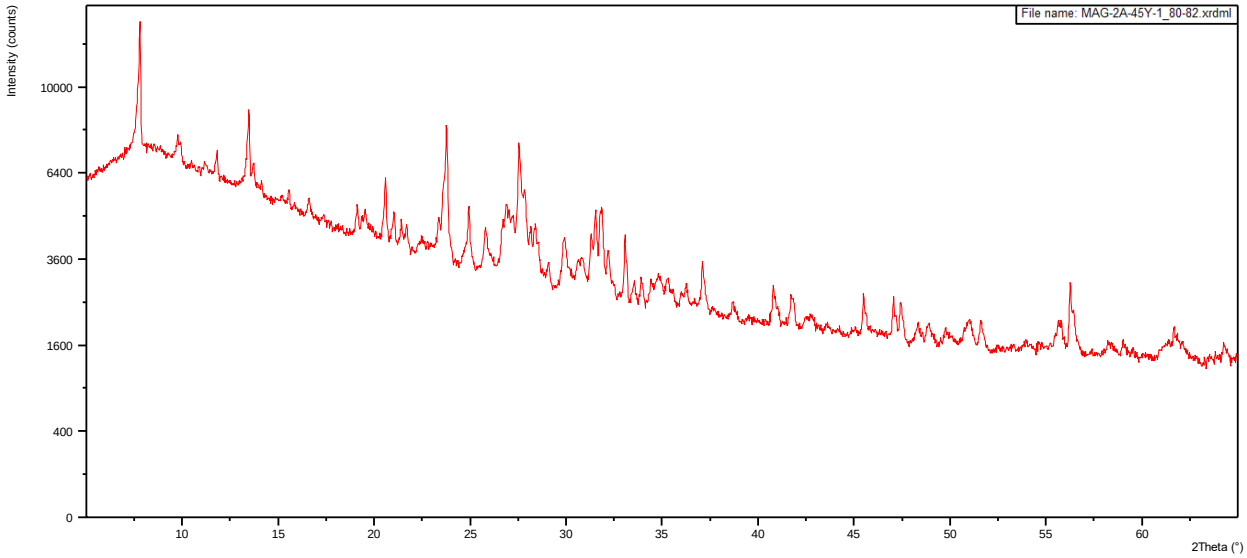
File name: MAG-2A-45Y-1_80-82.xrdml
Intensity (counts)
10000
6400
3600
1600
400
0
10
15
20
25
30
35
40
45
50
55
60
2Theta (°)

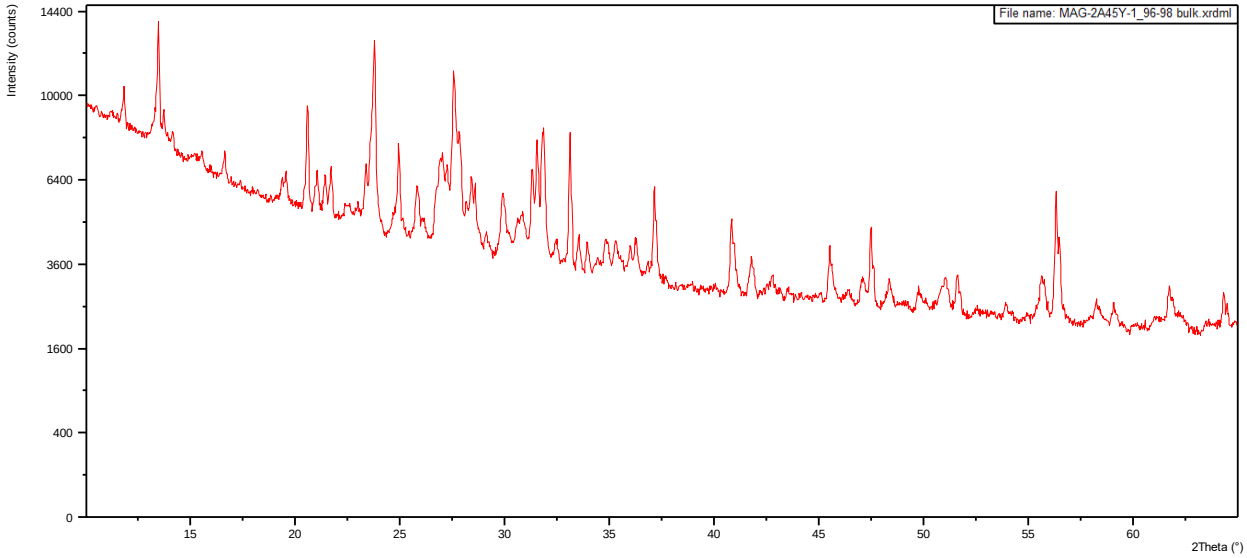
File name: MAG-2A45Y-1_96-98 bulk.xrdml
Intensity (counts)
14400
10000
6400
3600
1600
400
0
15
20
25
30
35
40
45
50
55
60
2Theta (°)

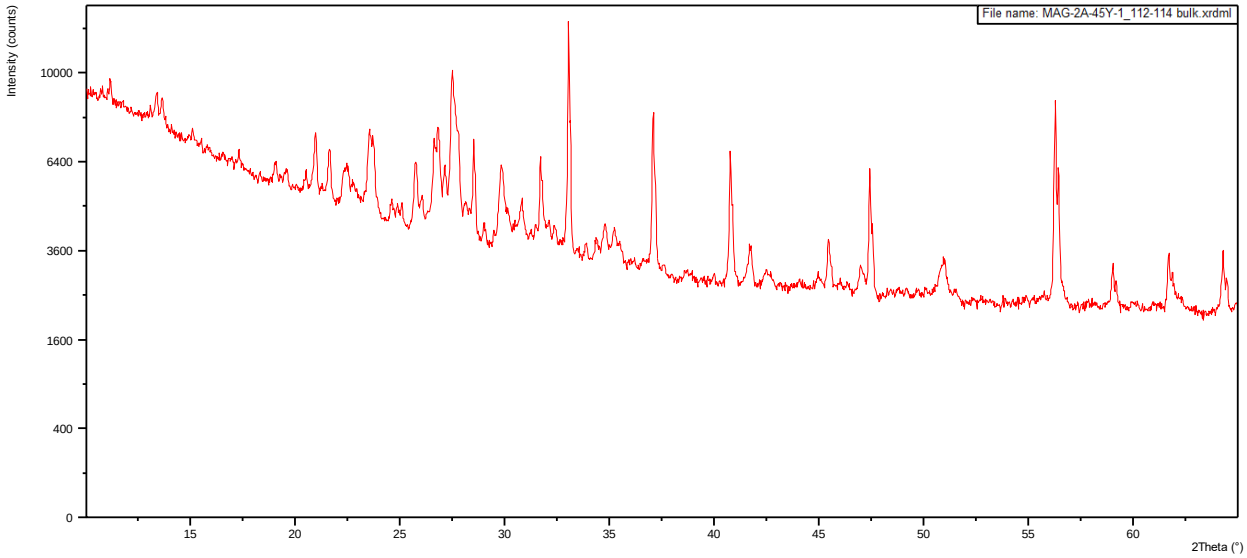
File name: MAG-2A-45Y-1_112-114 bulk.xrdml
Intensity (counts)
10000
6400
3600
1600
400
0
15
20
25
30
35
40
45
50
55
60
2Theta (°)

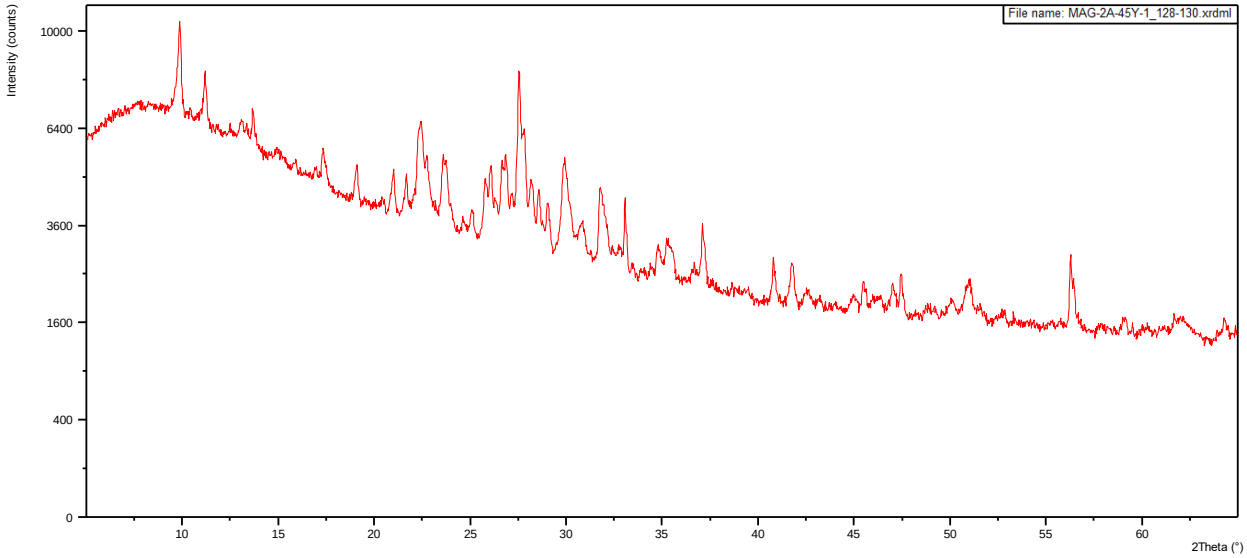
File name: MAG-2A-45Y-1_128-130.xrdml
Intensity (counts)
10000
6400
3600
1600
400
0
10
15
20
25
30
35
40
45
50
55
60
2Theta (°)

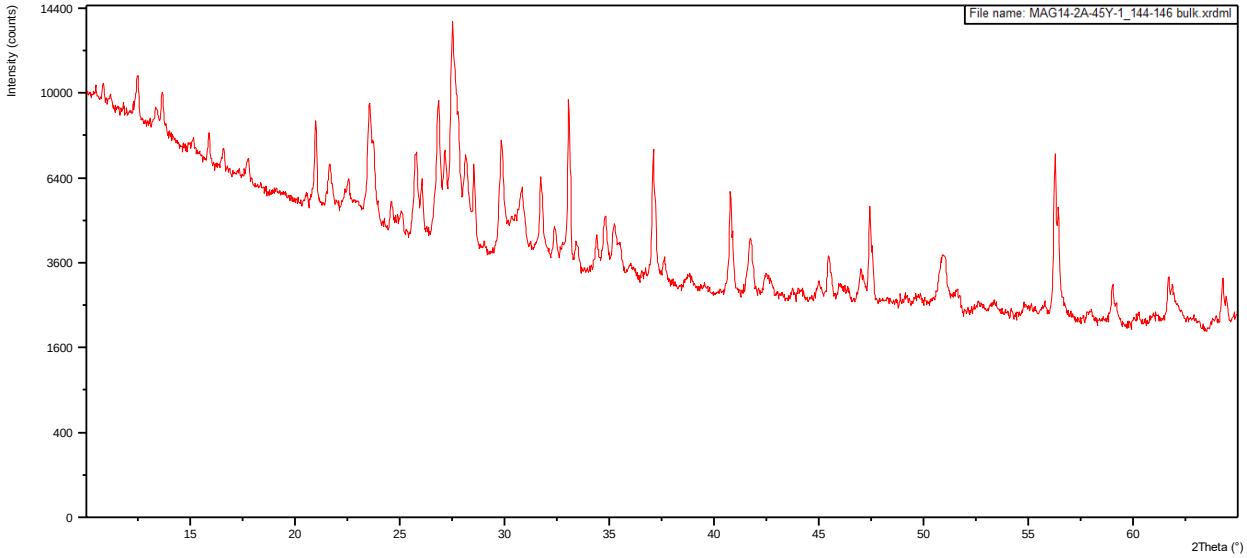
File name: MAG14-2A-45Y-1_144-146 bulk.xrdml
Intensity (counts)
14400
10000
6400
3600
1600
400
0
15
20
25
30
35
40
45
50
55
60
2Theta (°)

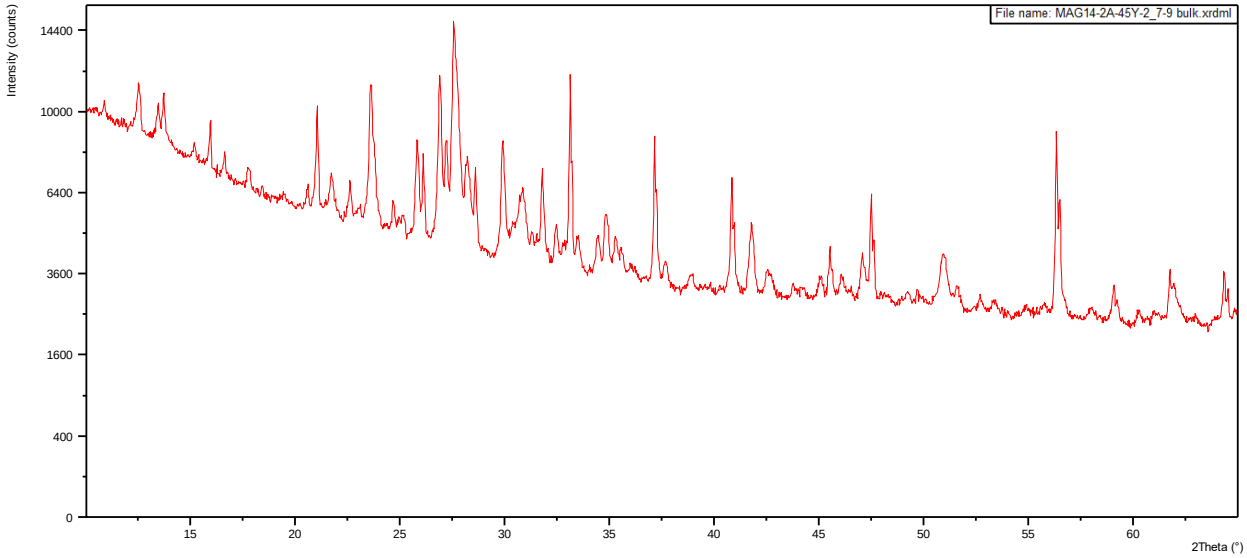
File name: MAG14-2A-45Y-2_7-9 bulk.xrdml
Intensity (counts)
14400
10000
6400
3600
1600
400
0
15
20
25
30
35
40
45
50
55
60
2Theta (°)

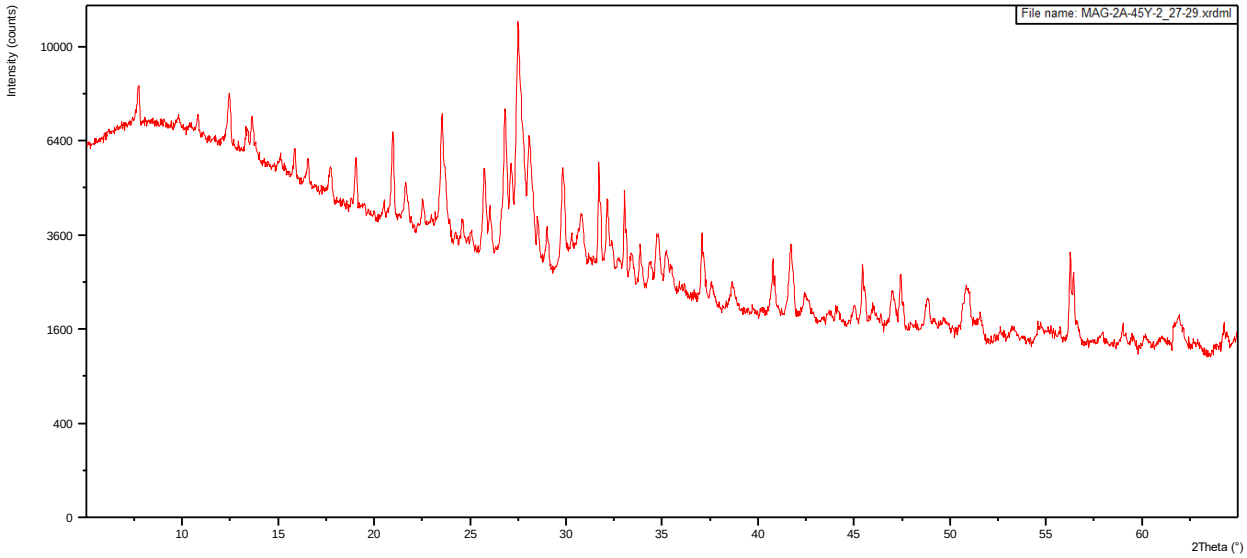
File name: MAG-2A-45Y-2_27-29.xrdml
Intensity (counts)
10000
6400
3600
1600
400
0
10
15
20
25
30
35
40
45
50
55
60
2Theta (°)

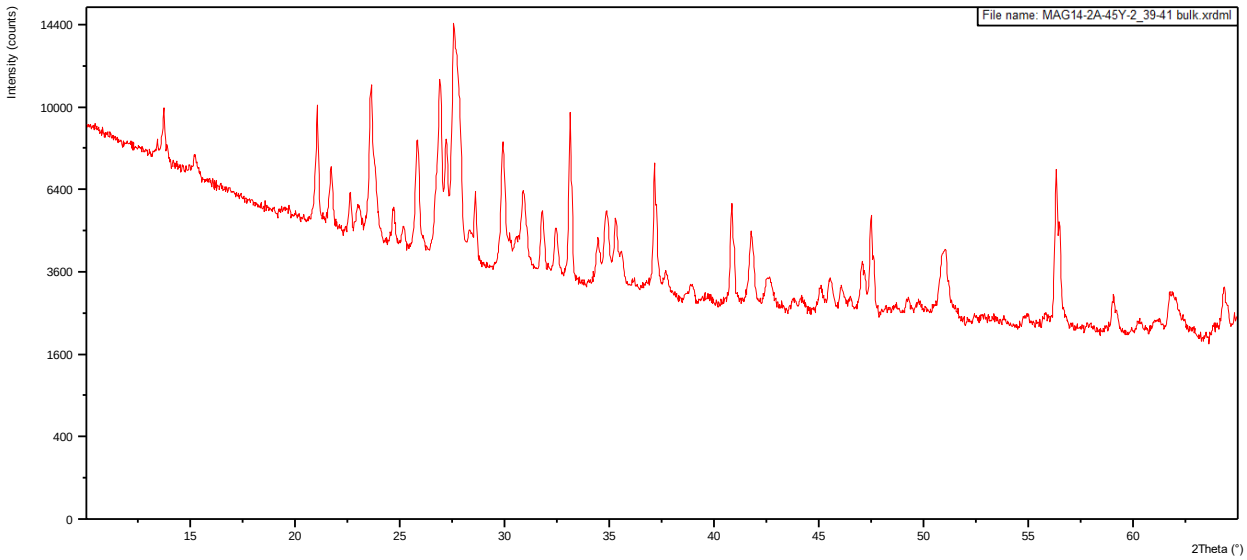
File name: MAG14-2A-45Y-2_39-41 bulk.xrdml
Intensity (counts)
14400
10000
6400
3600
1600
400
0
15
20
25
30
35
40
45
50
55
60
2Theta (°)

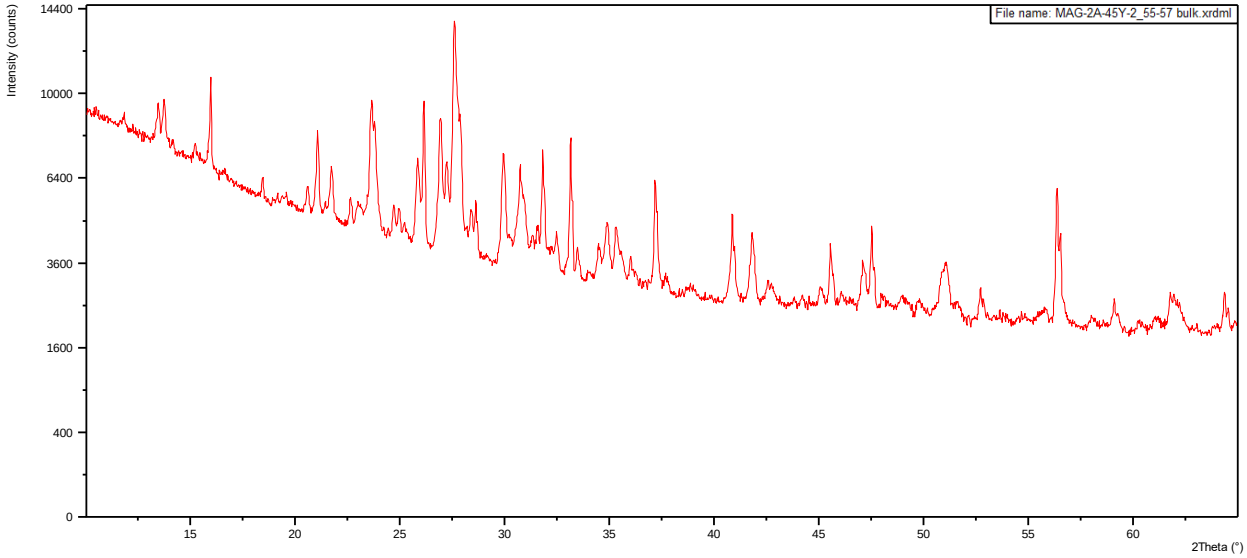
File name: MAG-2A-45Y-2_55-57 bulk.xrdml
Intensity (counts)
14400
10000
6400
3600
1600
400
0
15
20
25
30
35
40
45
50
55
60
2Theta (°)

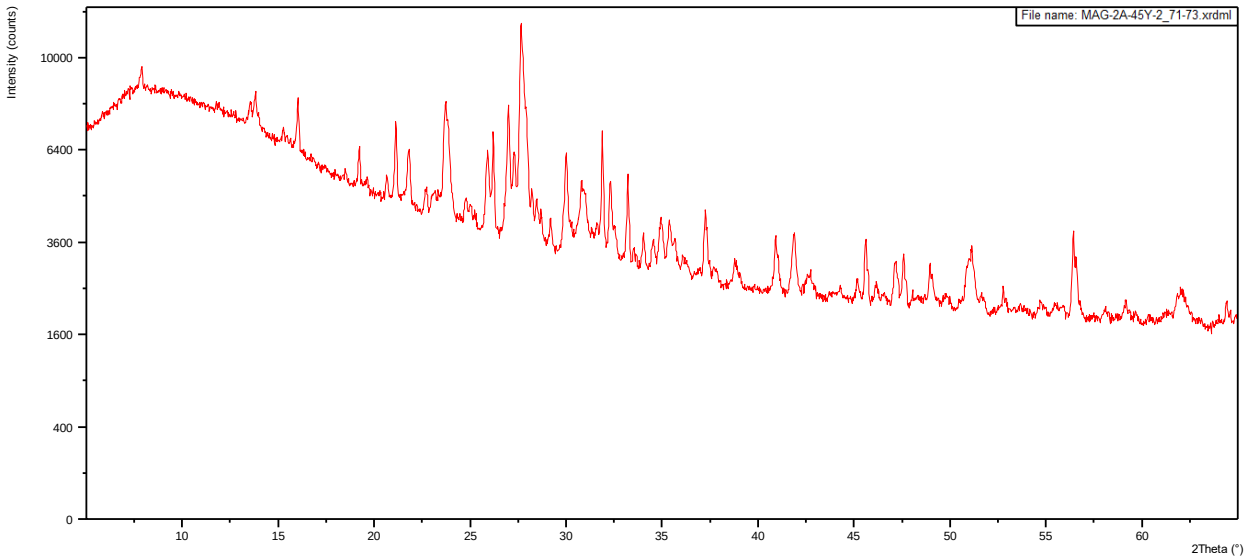
File name: MAG-2A-45Y-2_71-73.xrdml
Intensity (counts)
0
400
1600
3600
6400
10000
10
15
20
25
30
35
40
45
50
55
60
2Theta (°)

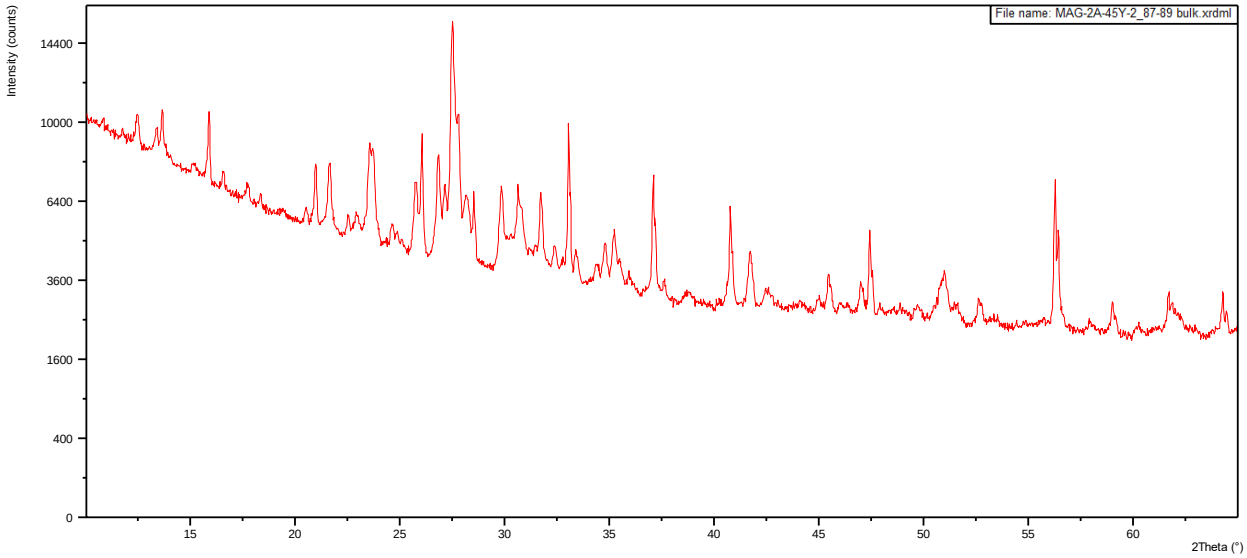
File name: MAG-2A-45Y-2_87-89 bulk.xrdml
Intensity (counts)
0
400
1600
3600
6400
10000
14400
15
20
25
30
35
40
45
50
55
60
2Theta (°)

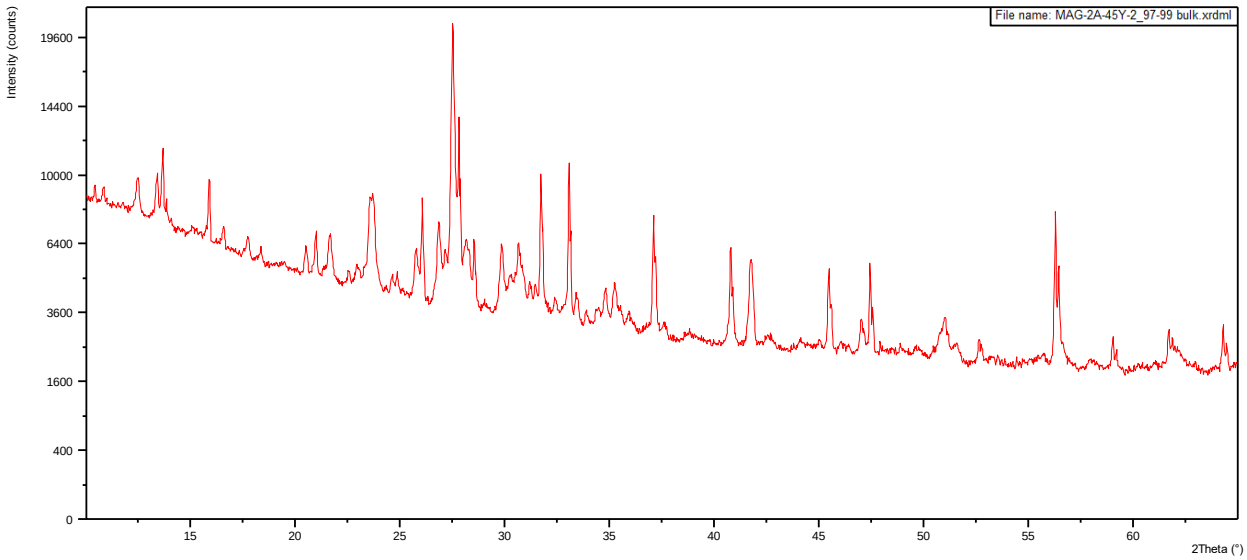
File name: MAG-2A-45Y-2_97-99 bulk.xrdml
Intensity (counts)
19600
14400
10000
6400
3600
1600
400
0
15
20
25
30
35
40
45
50
55
60
2Theta (°)

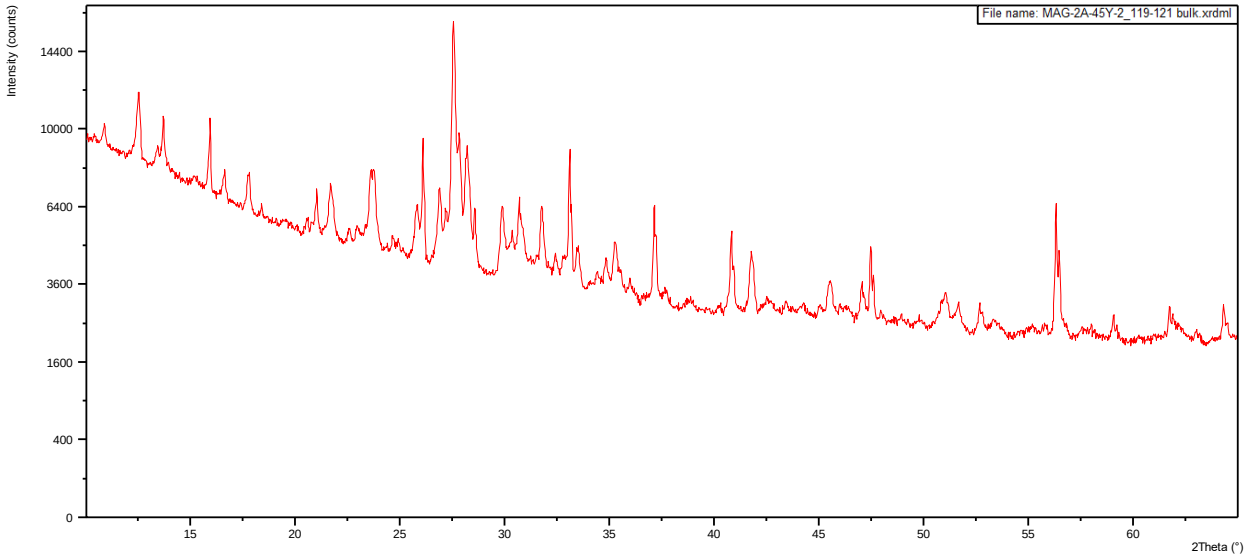
File name: MAG-2A-45Y-2_119-121 bulk.xrdml
Intensity (counts)
14400
10000
6400
3600
1600
400
0
15
20
25
30
35
40
45
50
55
60
2Theta (°)

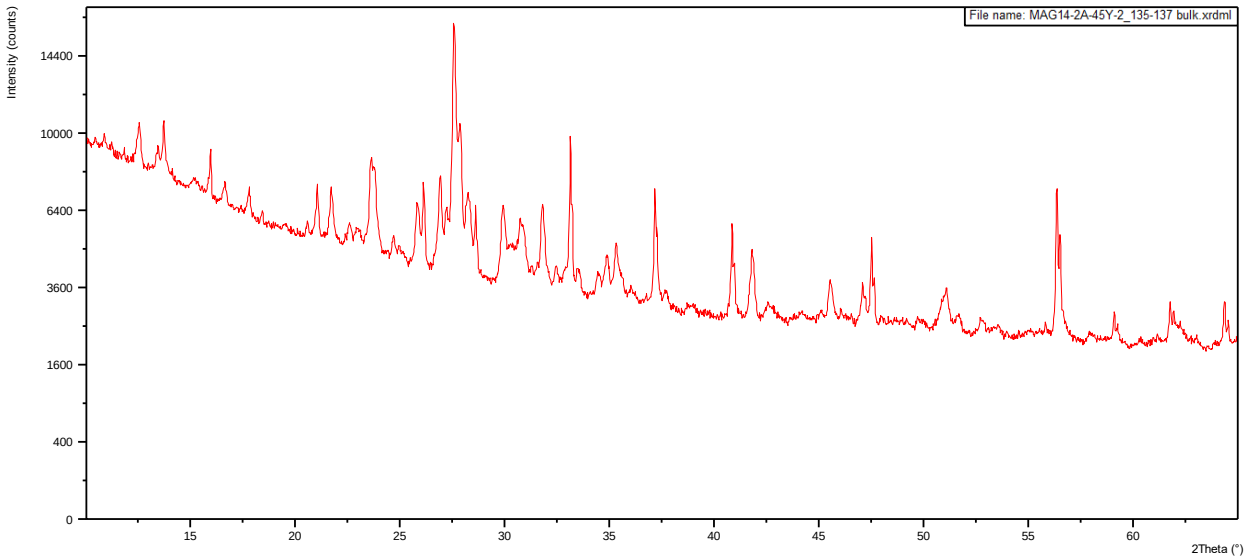
File name: MAG14-2A-45Y-2_135-137 bulk.xrdml
Intensity (counts)
14400
10000
6400
3600
1600
400
0
15
20
25
30
35
40
45
50
55
60
2Theta (°)

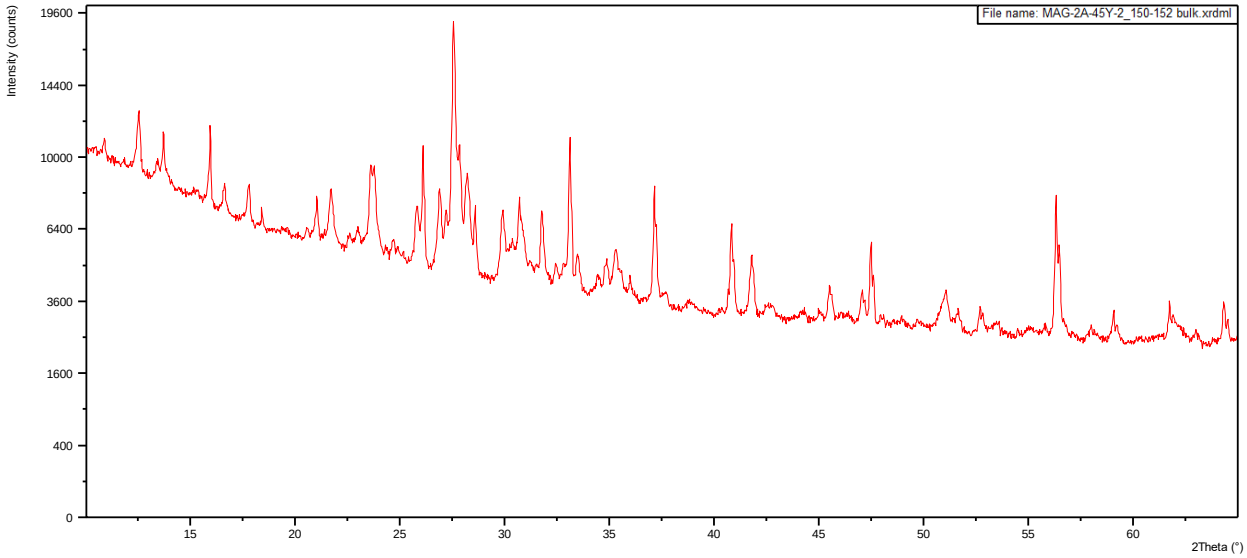
File name: MAG-2A-45Y-2_150-152 bulk.xrdml
Intensity (counts)
19600
14400
10000
6400
3600
1600
400
0
15
20
25
30
35
40
45
50
55
60
2Theta (°)

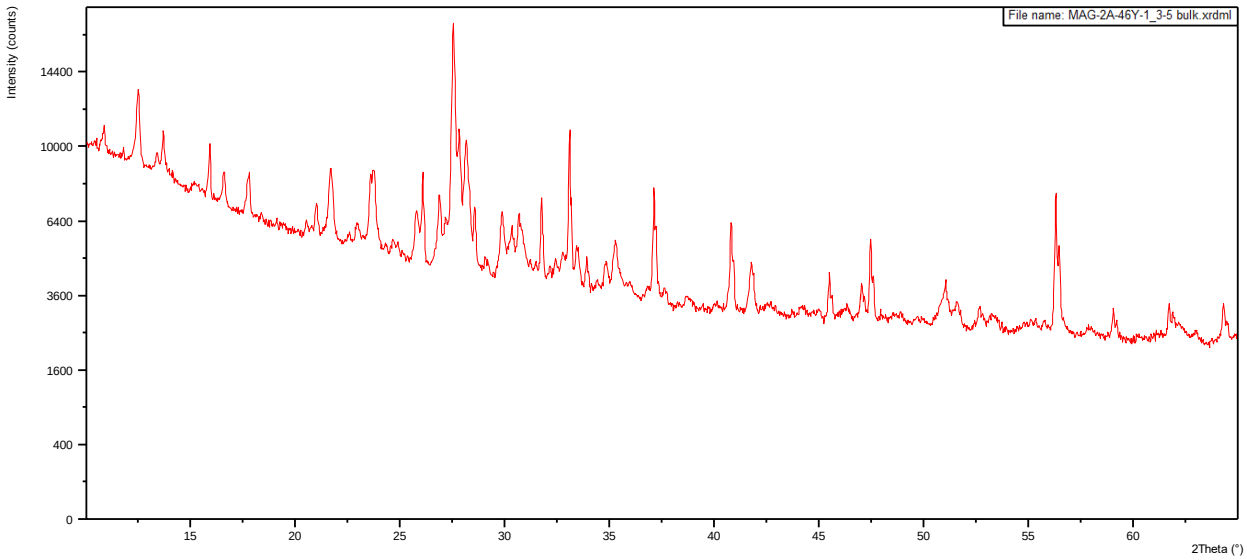
File name: MAG-2A-46Y-1_3-5 bulk.xrdml
Intensity (counts)
14400
10000
6400
3600
1600
400
0
15
20
25
30
35
40
45
50
55
60
2Theta (°)

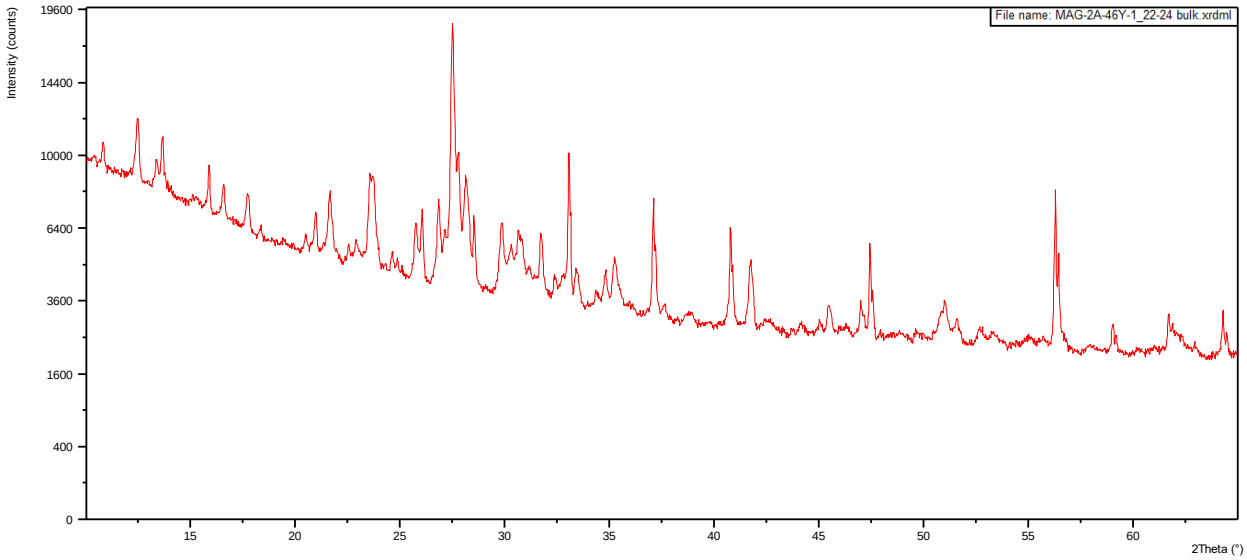
File name: MAG-2A-46Y-1_22-24 bulk.xrdml
Intensity (counts)
19600
14400
10000
6400
3600
1600
400
0
15
20
25
30
35
40
45
50
55
60
2Theta (°)

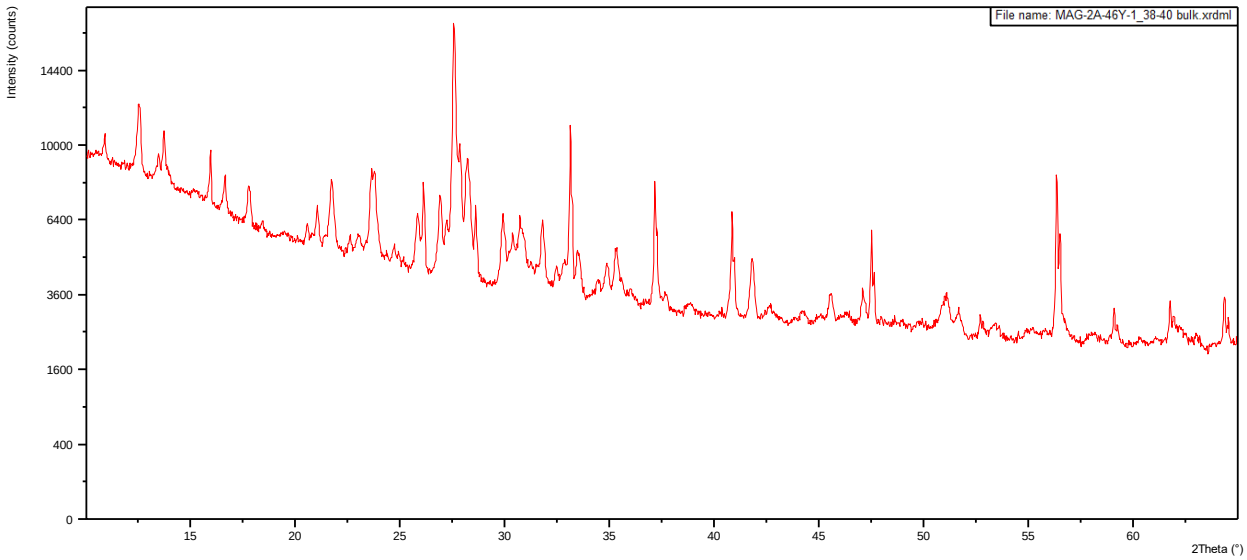
File name: MAG-2A-46Y-1_38-40 bulk.xrdml
Intensity (counts)
14400
10000
6400
3600
1600
400
0
15
20
25
30
35
40
45
50
55
60
2Theta (°)

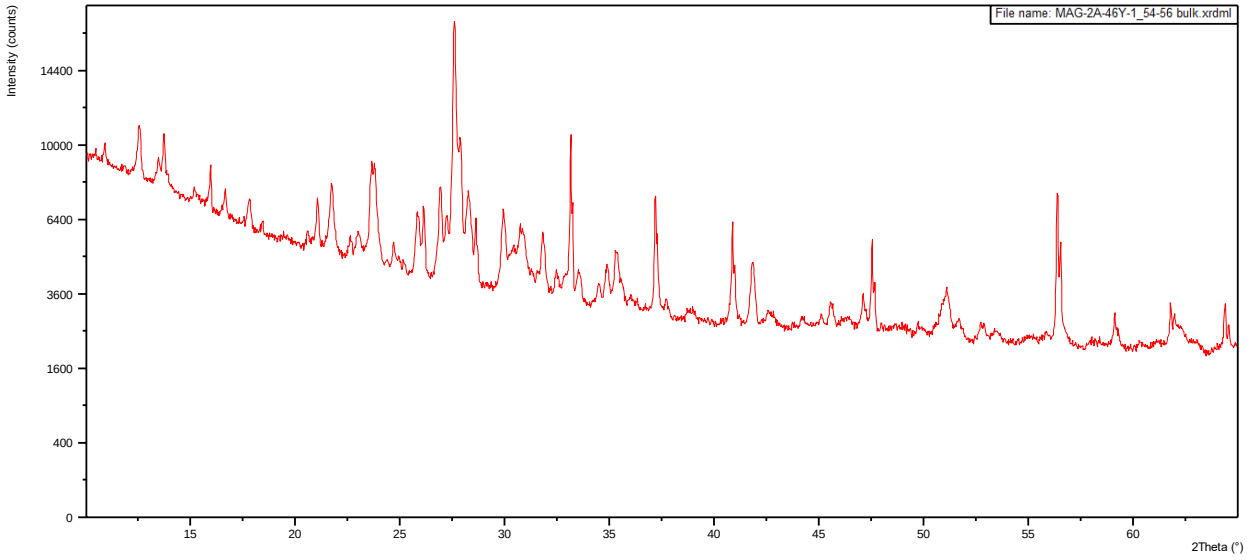
File name: MAG-2A-46Y-1_54-56 bulk.xrdml
Intensity (counts)
14400
10000
6400
3600
1600
400
0
15
20
25
30
35
40
45
50
55
60
2Theta (°)

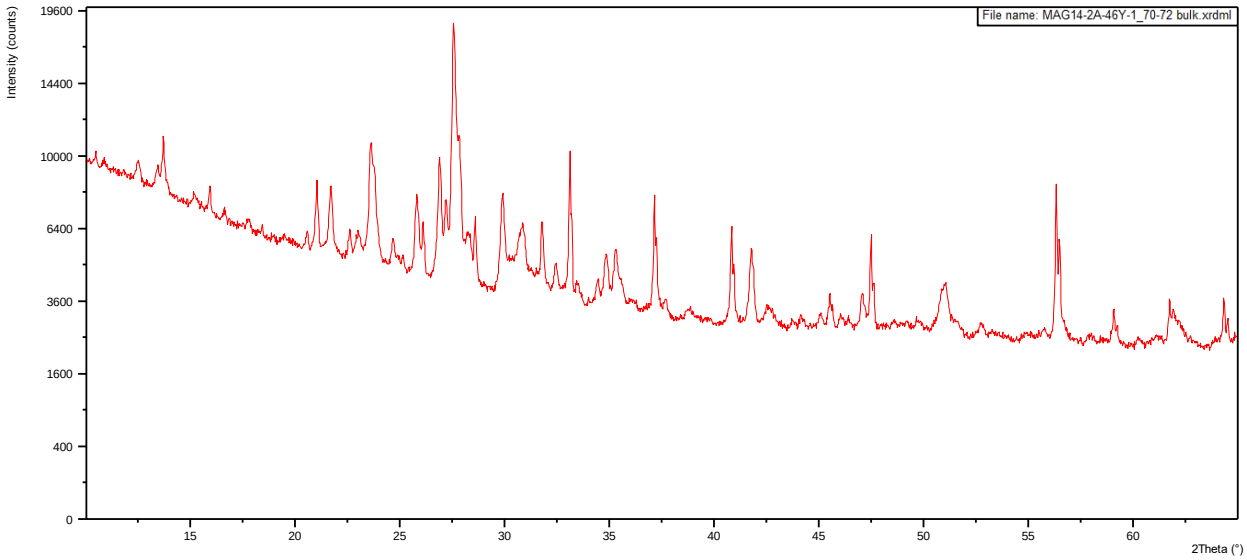
File name: MAG14-2A-46Y-1_70-72 bulk.xrdml
Intensity (counts)
19600
14400
10000
6400
3600
1600
400
0
15
20
25
30
35
40
45
50
55
60
2Theta (°)

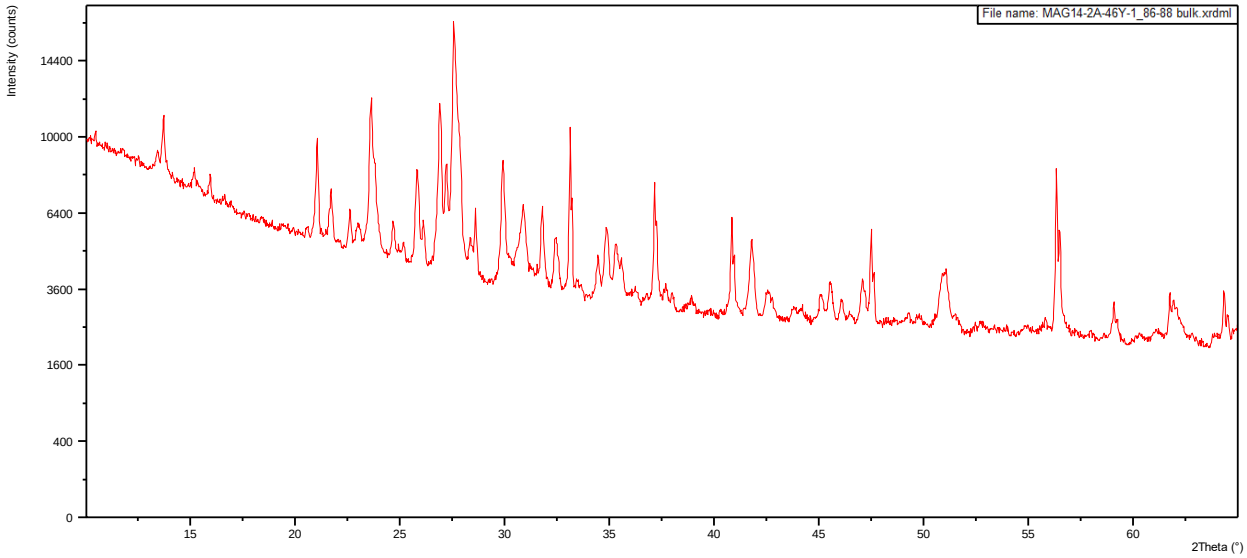
File name: MAG14-2A-46Y-1_86-88 bulk.xrdml
Intensity (counts)
14400
10000
6400
3600
1600
400
0
15
20
25
30
35
40
45
50
55
60
2Theta (°)

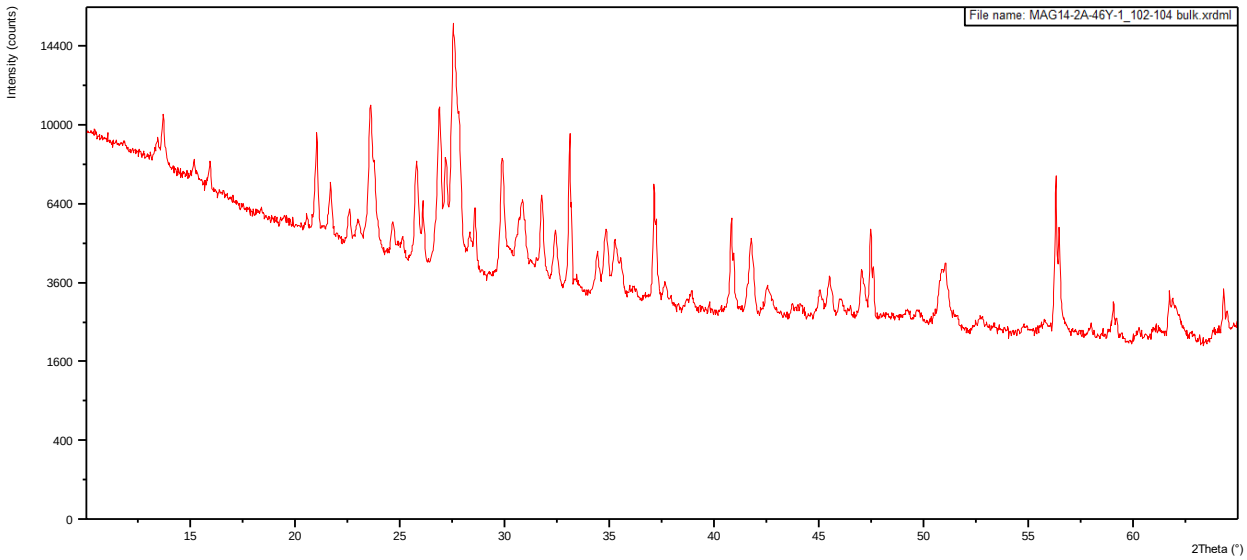
File name: MAG14-2A-46Y-1_102-104 bulk.xrdml
Intensity (counts)
14400
10000
6400
3600
1600
400
0
15
20
25
30
35
40
45
50
55
60
2Theta (°)

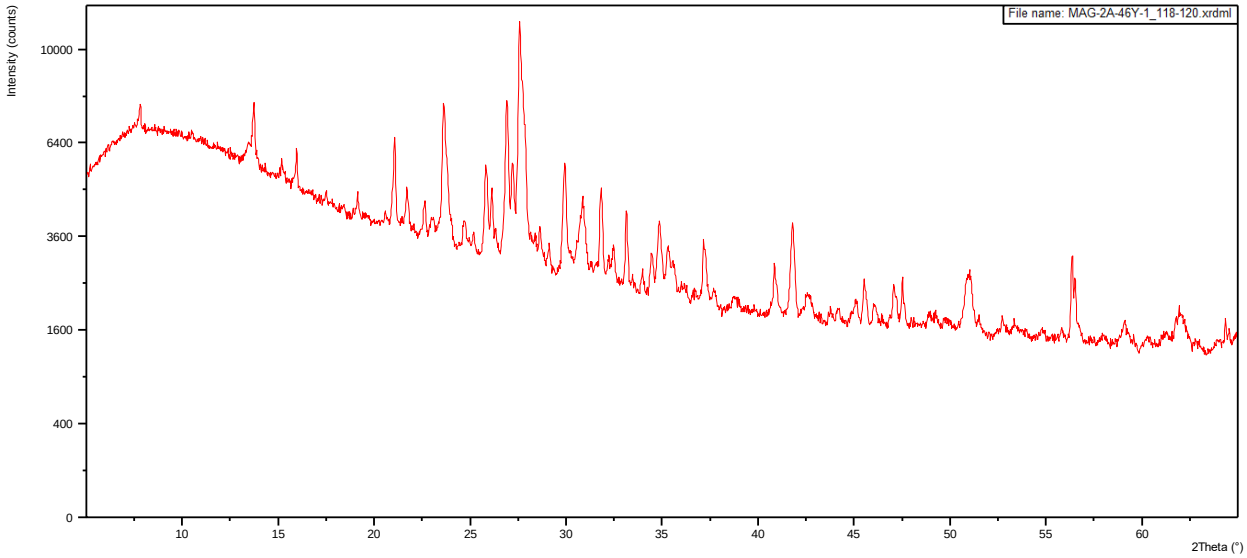
File name: MAG-2A-46Y-1_118-120.xrdml
Intensity (counts)
10000
6400
3600
1600
400
0
10
15
20
25
30
35
40
45
50
55
60
2Theta (°)

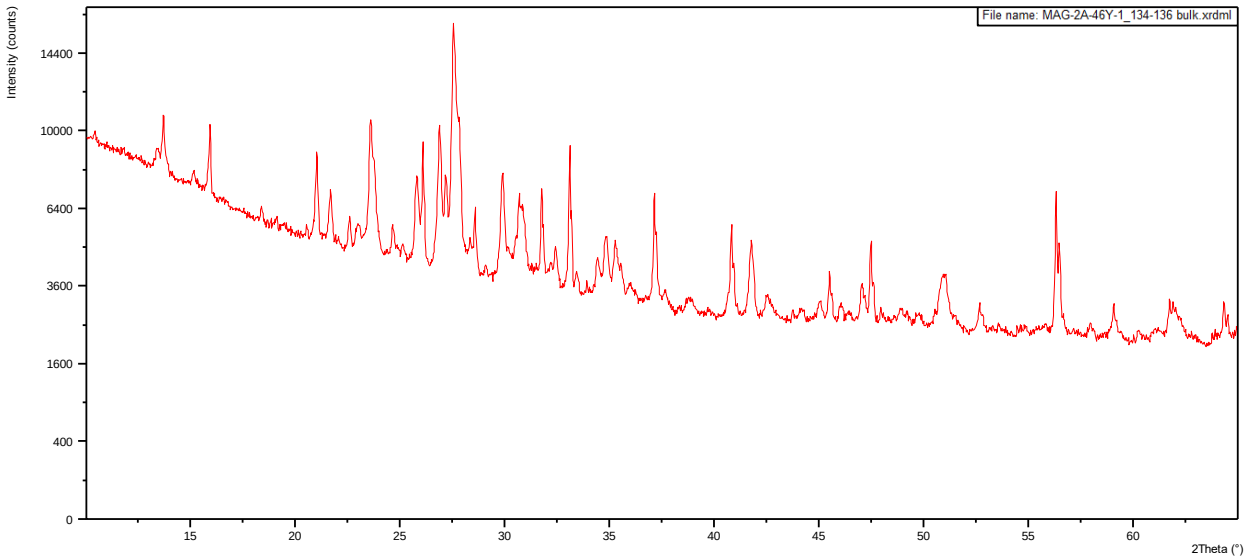
File name: MAG-2A-46Y-1_134-136 bulk.xrdml
Intensity (counts)
14400
10000
6400
3600
1600
400
0
15
20
25
30
35
40
45
50
55
60
2Theta (°)

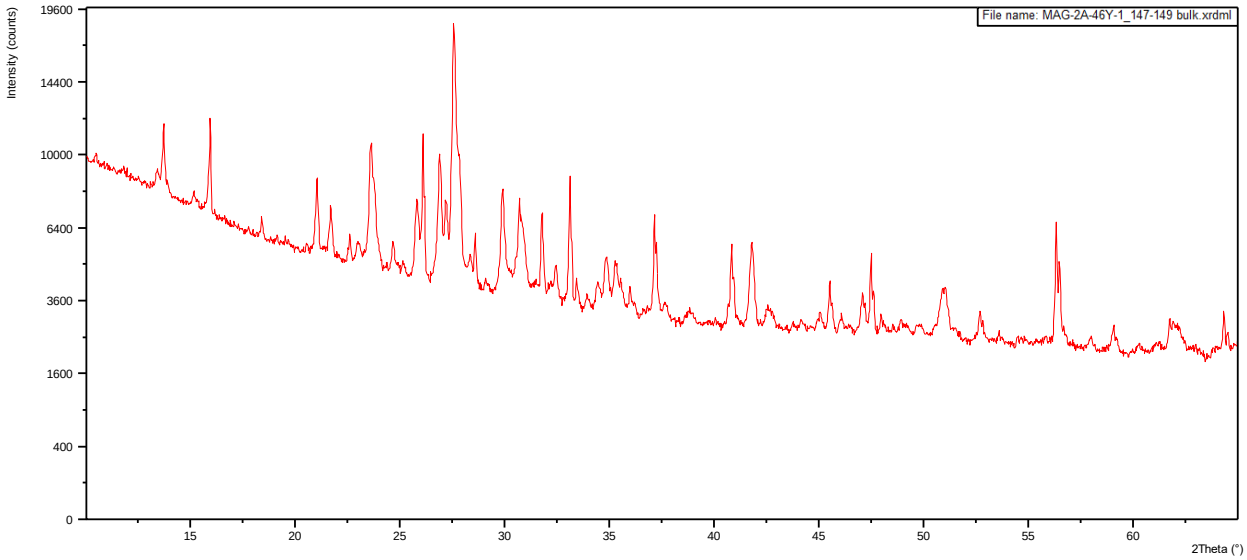
File name: MAG-2A-46Y-1_147-149 bulk.xrdml
Intensity (counts)
19600
14400
10000
6400
3600
1600
400
0
15
20
25
30
35
40
45
50
55
60
2Theta (°)

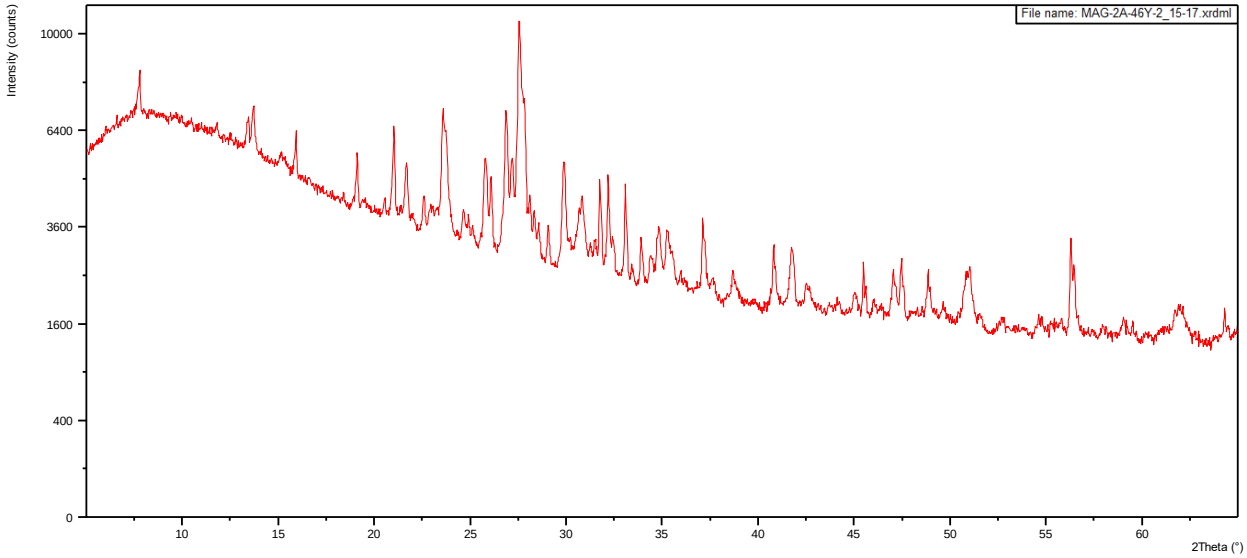
File name: MAG-2A-46Y-2_15-17.xrdml
Intensity (counts)
10000
6400
3600
1600
400
0
10
15
20
25
30
35
40
45
50
55
60
2Theta (°)

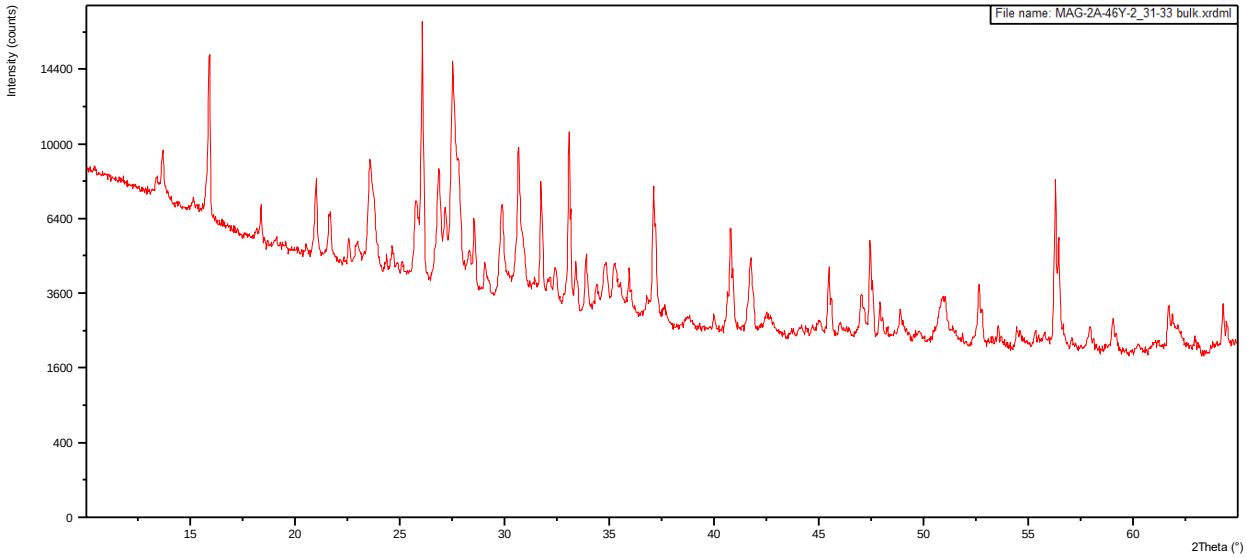
File name: MAG-2A-46Y-2_31-33 bulk.xrdml
Intensity (counts)
14400
10000
6400
3600
1600
400
0
15
20
25
30
35
40
45
50
55
60
2Theta (°)

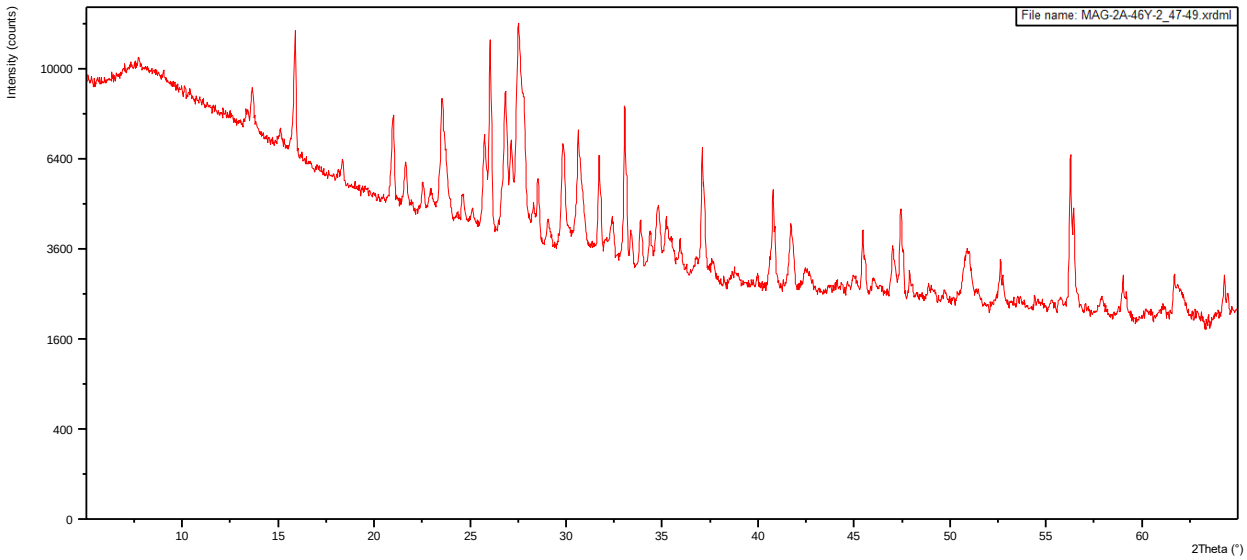
File name: MAG-2A-46Y-2_47-49.xrdml
Intensity (counts)
10000
6400
3600
1600
400
0
10
15
20
25
30
35
40
45
50
55
60
2Theta (°)

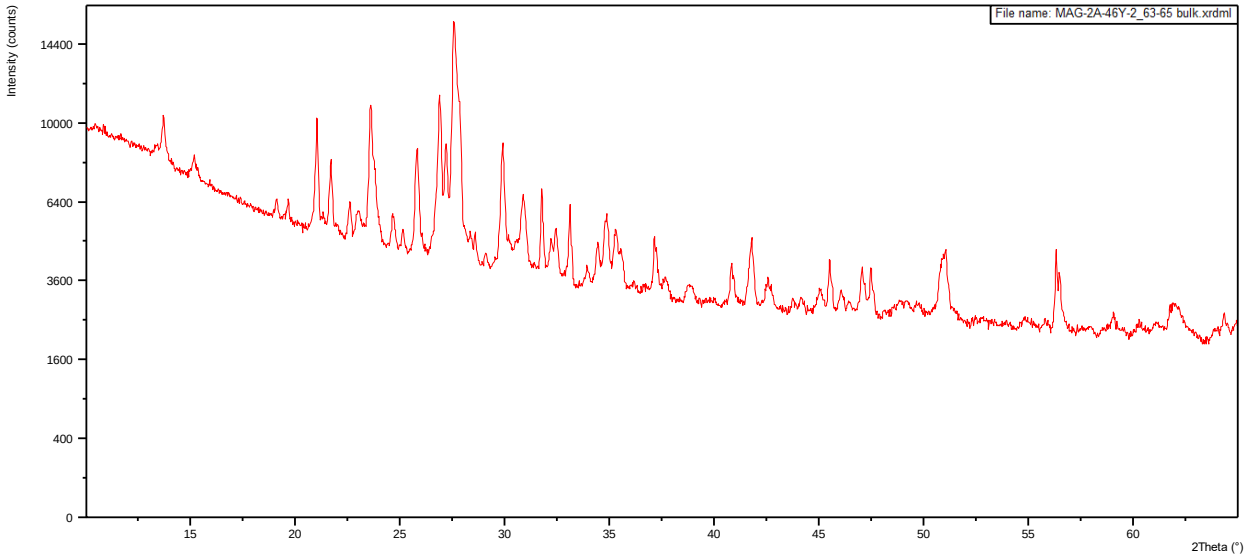
File name: MAG-2A-46Y-2_63-65 bulk.xrdml
Intensity (counts)
14400
10000
6400
3600
1600
400
0
15
20
25
30
35
40
45
50
55
60
2Theta (°)

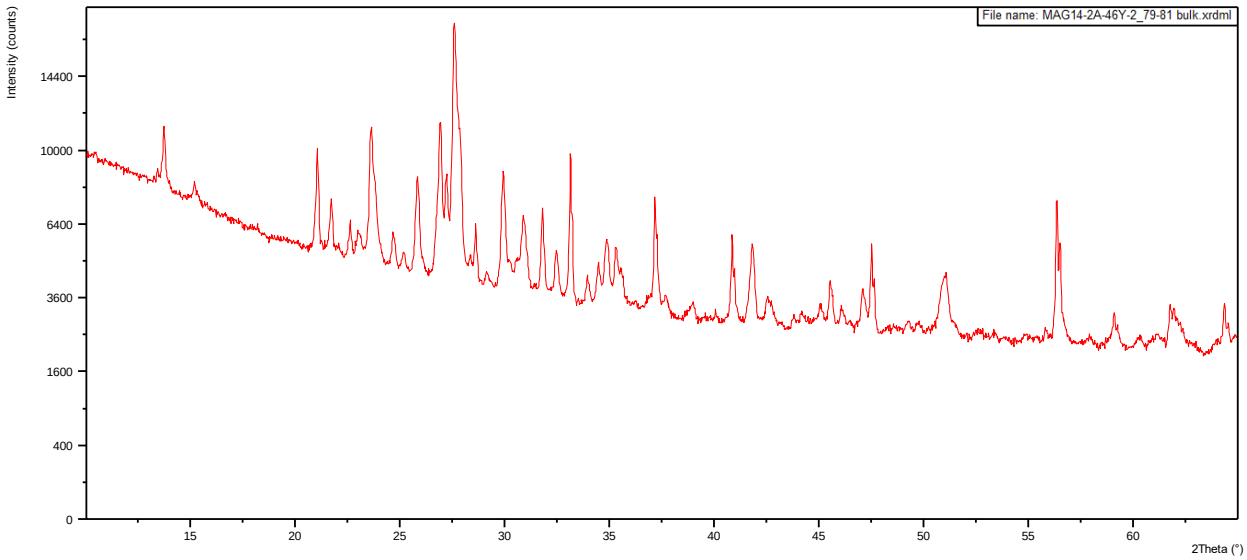
File name: MAG14-2A-46Y-2_79-81 bulk.xrdml
Intensity (counts)
14400
10000
6400
3600
1600
400
0
15
20
25
30
35
40
45
50
55
60
2Theta (°)

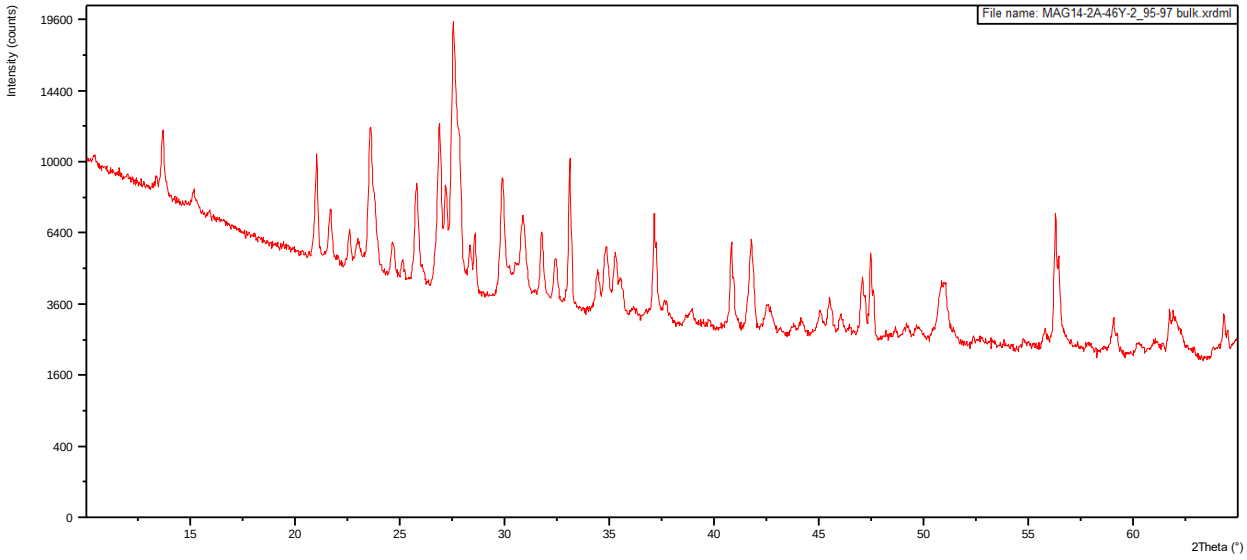
File name: MAG14-2A-46Y-2_95-97 bulk.xrdml
Intensity (counts)
19600
14400
10000
6400
3600
1600
400
0
15
20
25
30
35
40
45
50
55
60
2Theta (°)

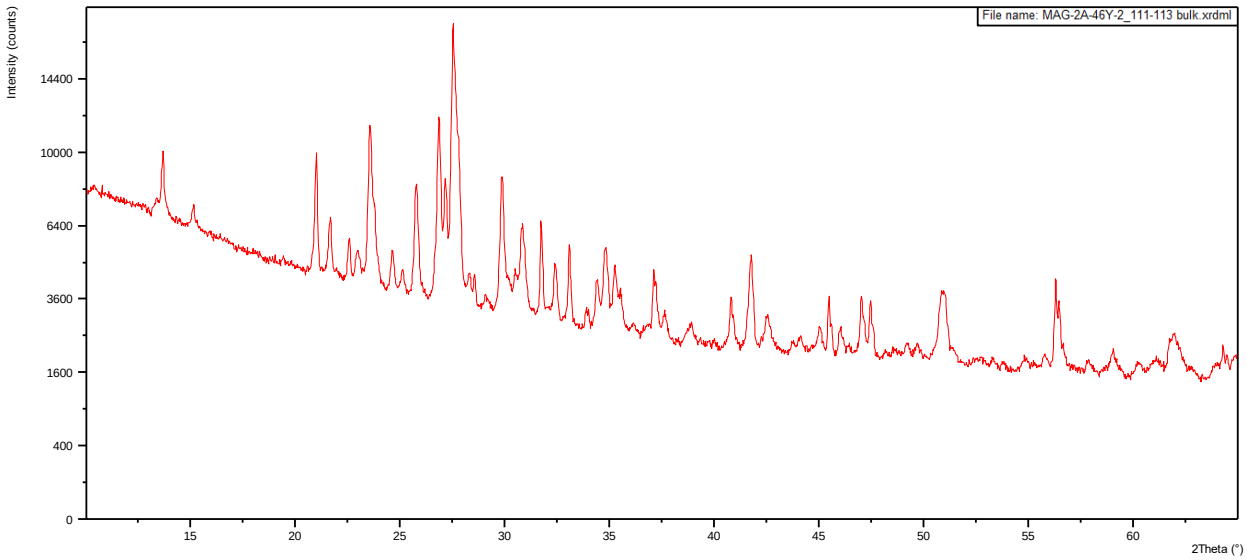
File name: MAG-2A-46Y-2_111-113 bulk.xrdml
Intensity (counts)
14400
10000
6400
3600
1600
400
0
15
20
25
30
35
40
45
50
55
60
2Theta (°)

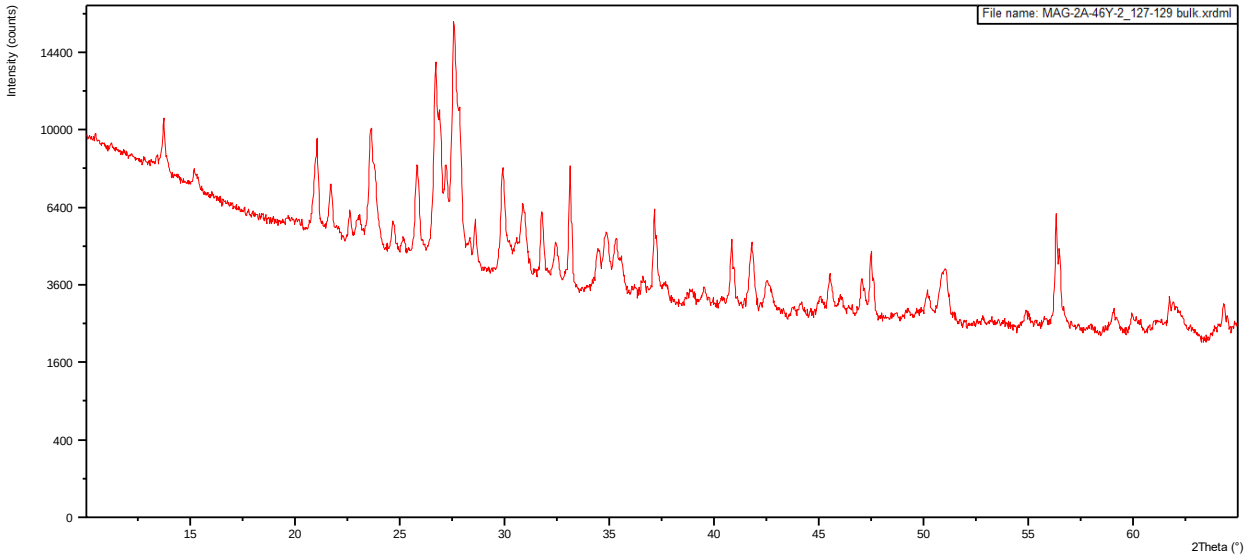
File name: MAG-2A-46Y-2_127-129 bulk.xrdml
Intensity (counts)
14400
10000
6400
3600
1600
400
0
15
20
25
30
35
40
45
50
55
60
2Theta (°)

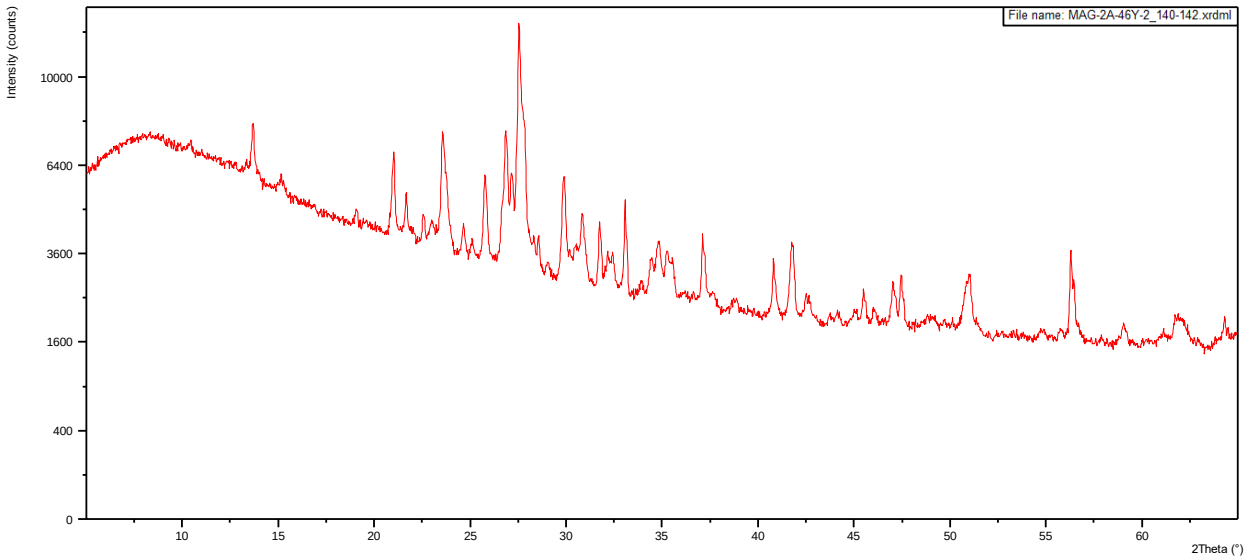
File name: MAG-2A-46Y-2_140-142.xrdml
Intensity (counts)
0
400
1600
3600
6400
10000
10
15
20
25
30
35
40
45
50
55
60
2Theta (°)

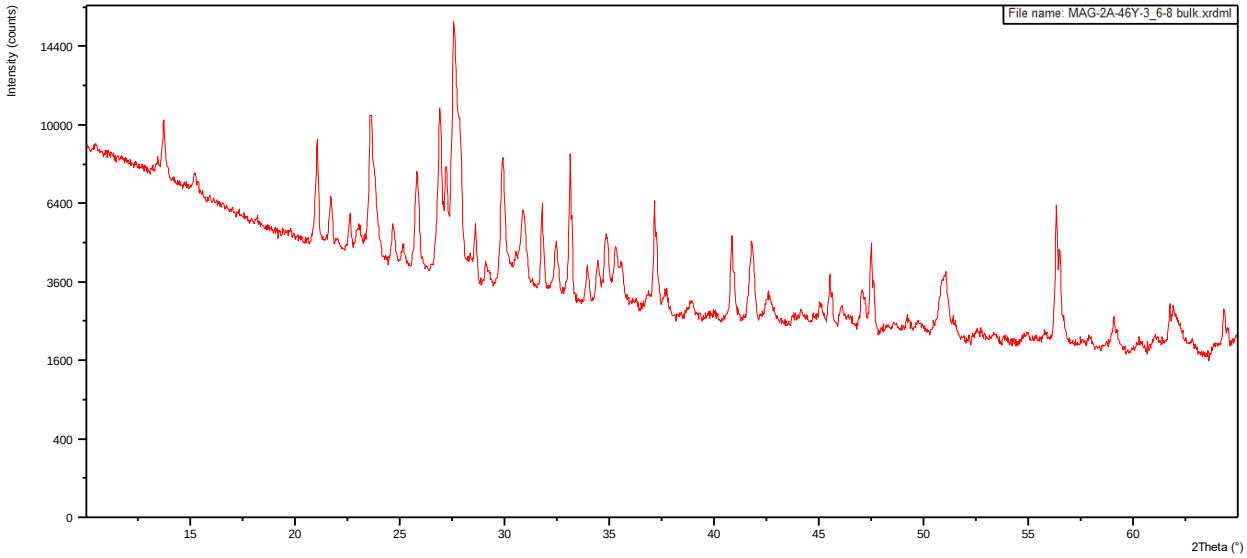
File name: MAG-2A-46Y-3_6-8 bulk.xrdml
Intensity (counts)
0
400
1600
3600
6400
10000
14400
15
20
25
30
35
40
45
50
55
60
2Theta (°)

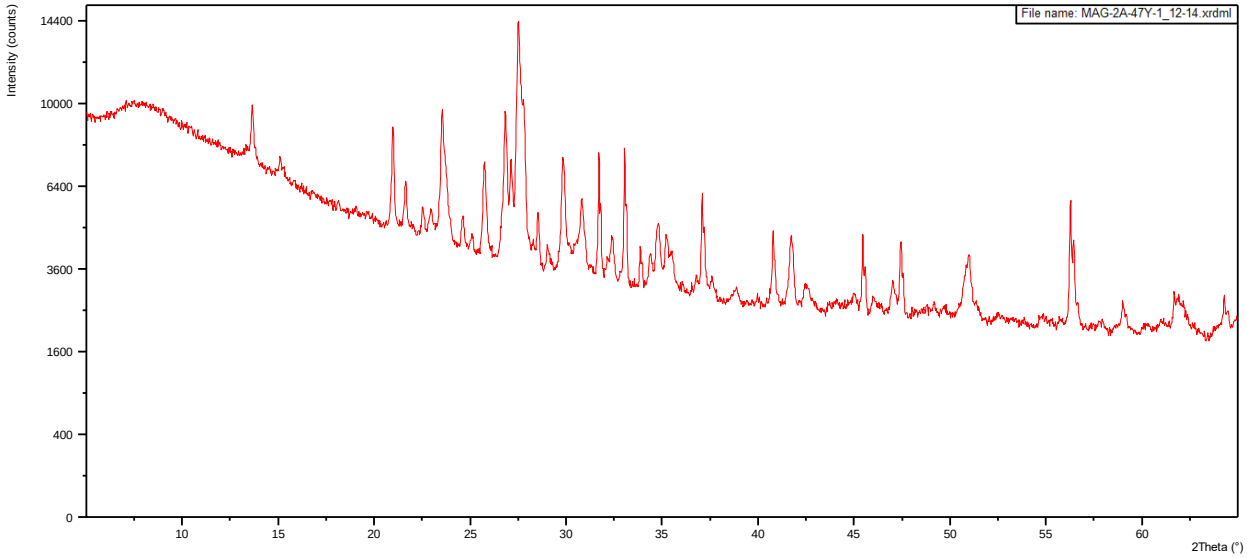
File name: MAG-2A-47Y-1_12-14.xrdml
Intensity (counts)
14400
10000
6400
3600
1600
400
0
10
15
20
25
30
35
40
45
50
55
60
2Theta (°)

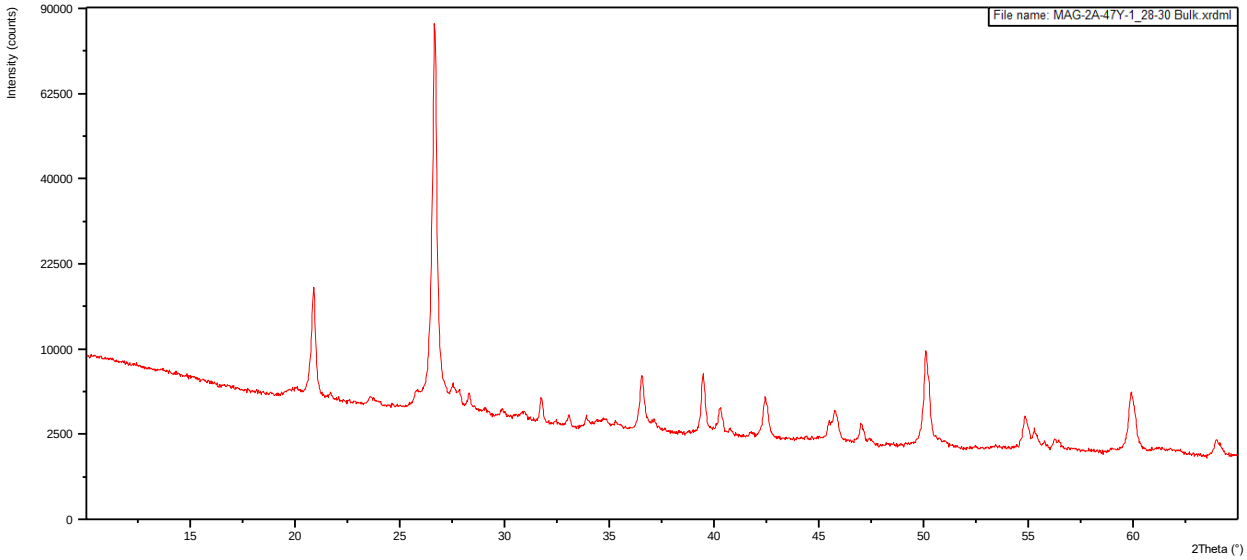
File name: MAG-2A-47Y-1_28-30 Bulk.xrdml
Intensity (counts)
90000
62500
40000
22500
10000
2500
0
15
20
25
30
35
40
45
50
55
60
2Theta (°)

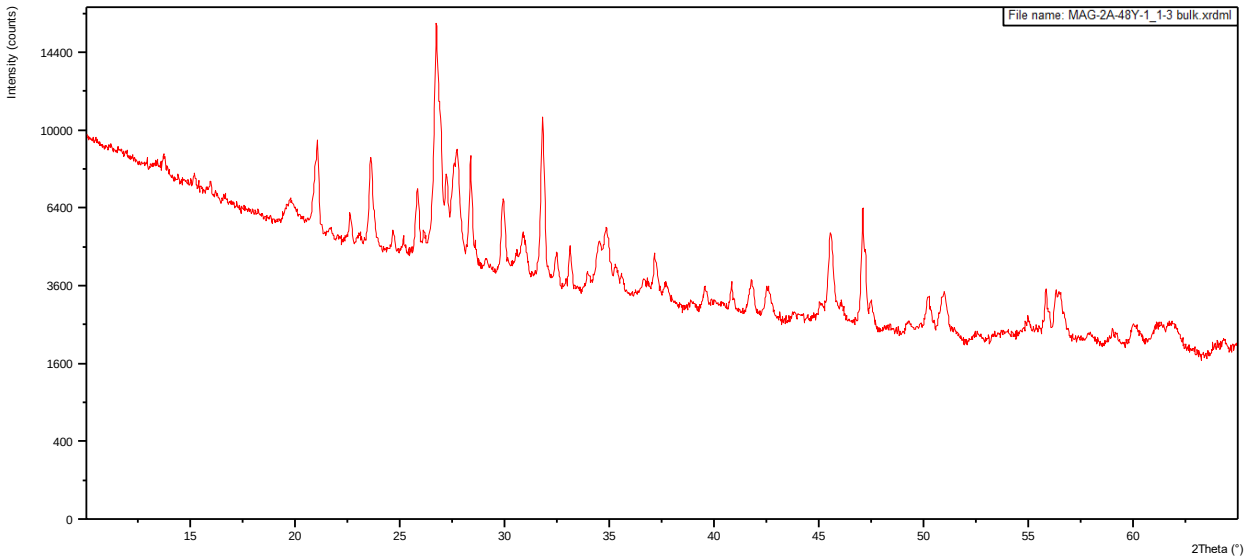
File name: MAG-2A-48Y-1_1-3 bulk.xrdml
Intensity (counts)
14400
10000
6400
3600
1600
400
0
15
20
25
30
35
40
45
50
55
60
2Theta (°)

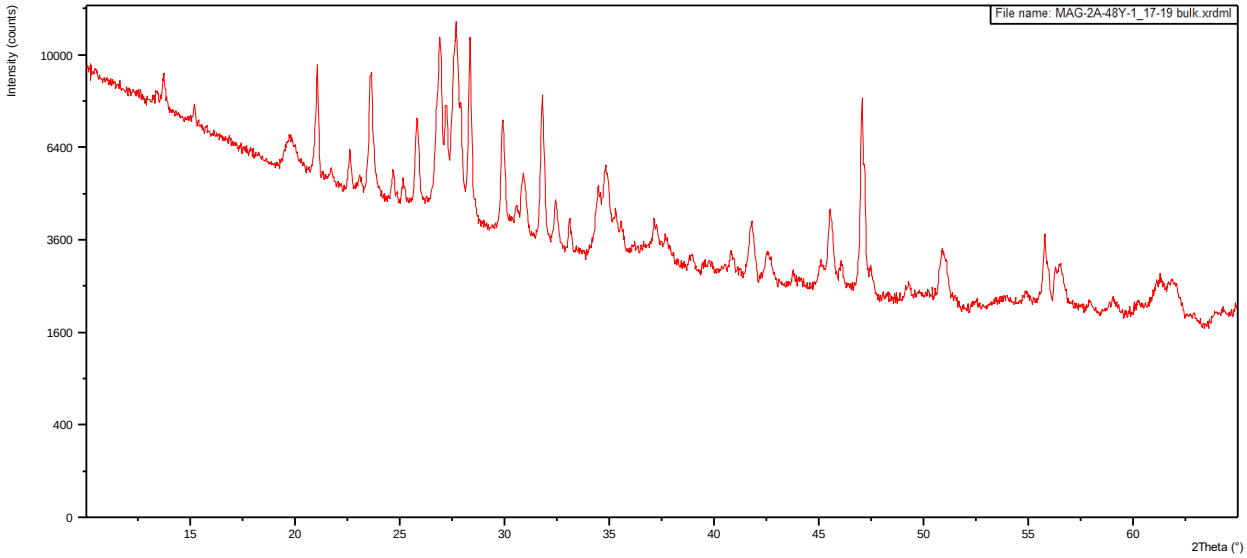
File name: MAG-2A-48Y-1_17-19 bulk.xrdml
Intensity (counts)
10000
6400
3600
1600
400
0
15
20
25
30
35
40
45
50
55
60
2Theta (°)

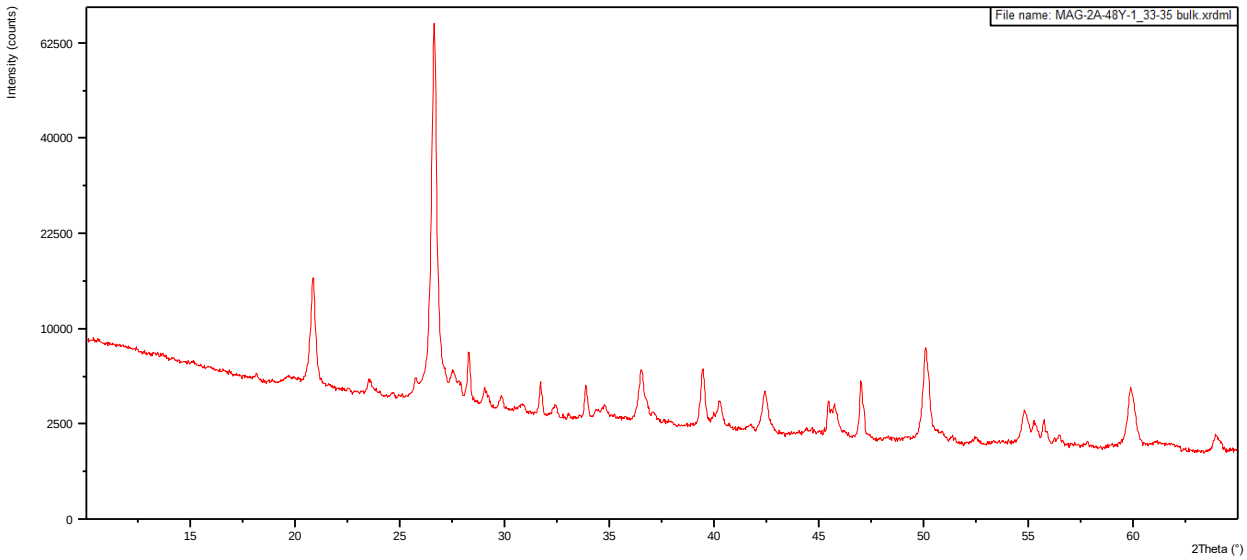
File name: MAG-2A-48Y-1_33-35 bulk.xrdml
Intensity (counts)
62500
40000
22500
10000
2500
0
15
20
25
30
35
40
45
50
55
60
2Theta (°)

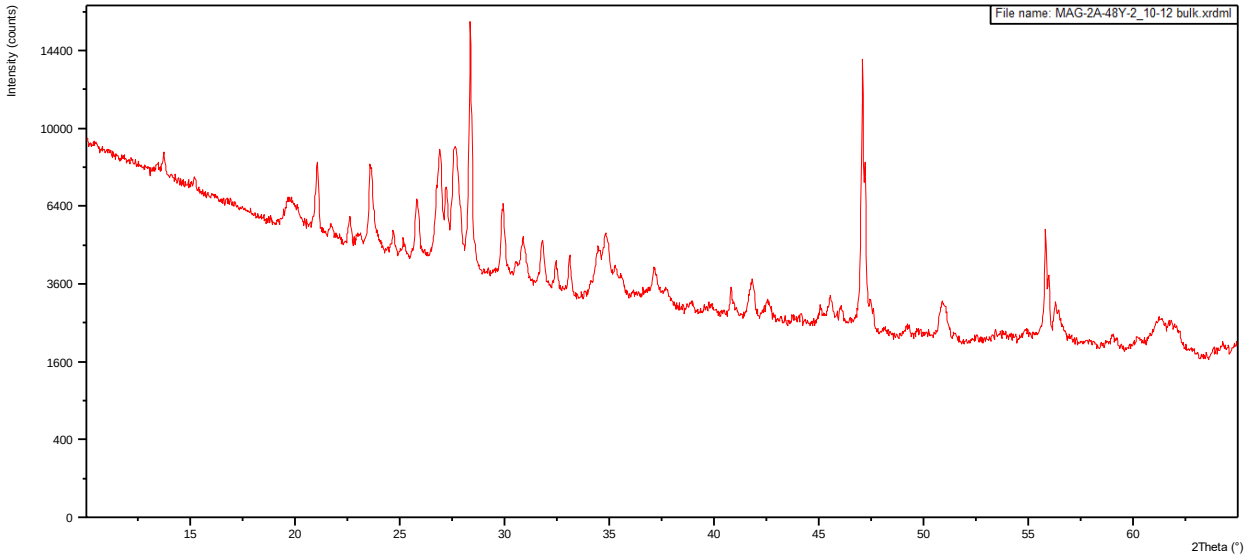
File name: MAG-2A-48Y-2_10-12 bulk.xrdml
Intensity (counts)
14400
10000
6400
3600
1600
400
0
15
20
25
30
35
40
45
50
55
60
2Theta (°)

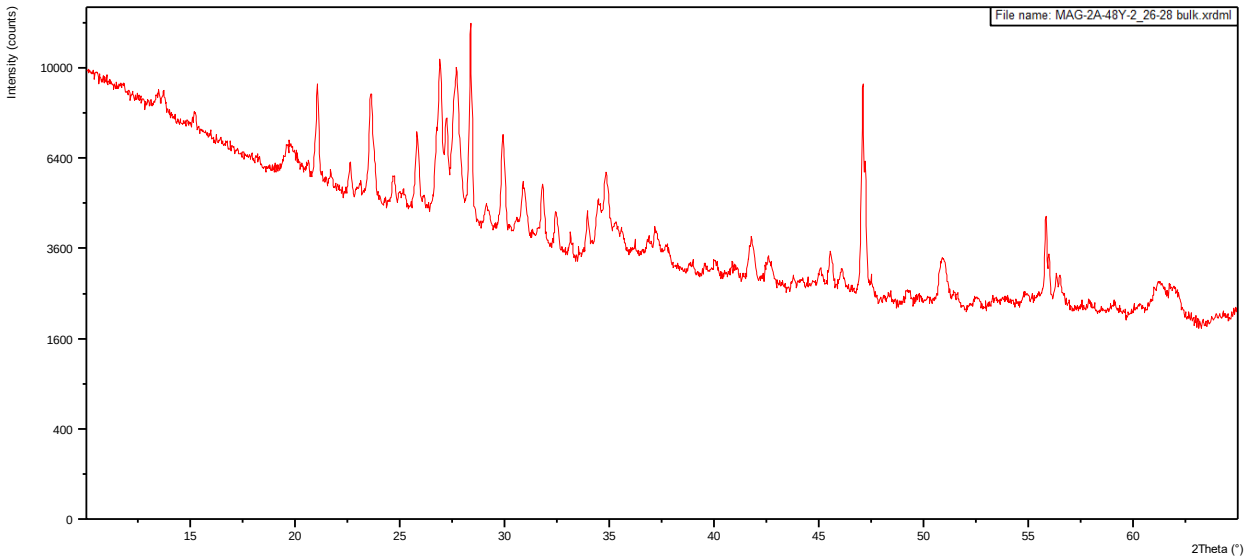
File name: MAG-2A-48Y-2_26-28 bulk.xrdml
Intensity (counts)
10000
6400
3600
1600
400
0
15
20
25
30
35
40
45
50
55
60
2Theta (°)

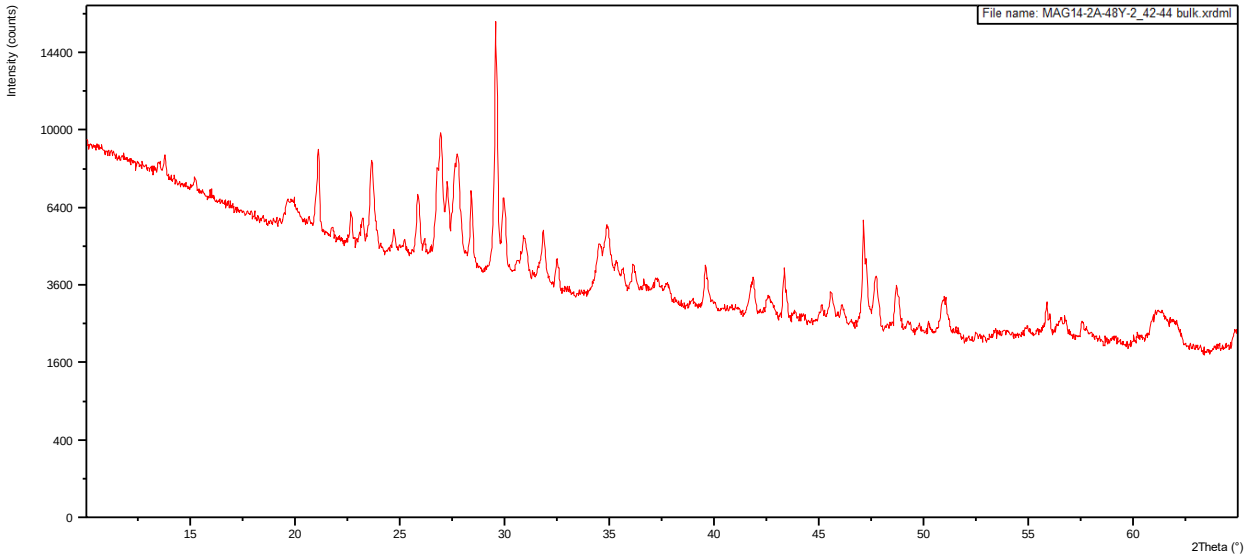
File name: MAG14-2A-48Y-2_42-44 bulk.xrdml
Intensity (counts)
14400
10000
6400
3600
1600
400
0
15
20
25
30
35
40
45
50
55
60
2Theta (°)

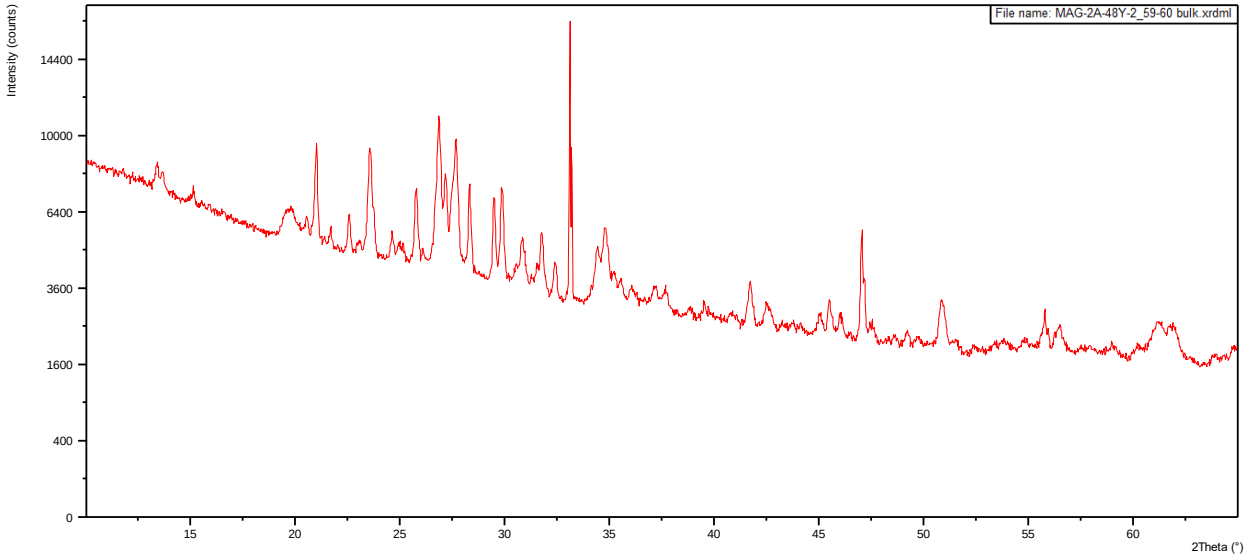
File name: MAG-2A-48Y-2_59-60 bulk.xrdml
Intensity (counts)
14400
10000
6400
3600
1600
400
0
15
20
25
30
35
40
45
50
55
60
2Theta (°)

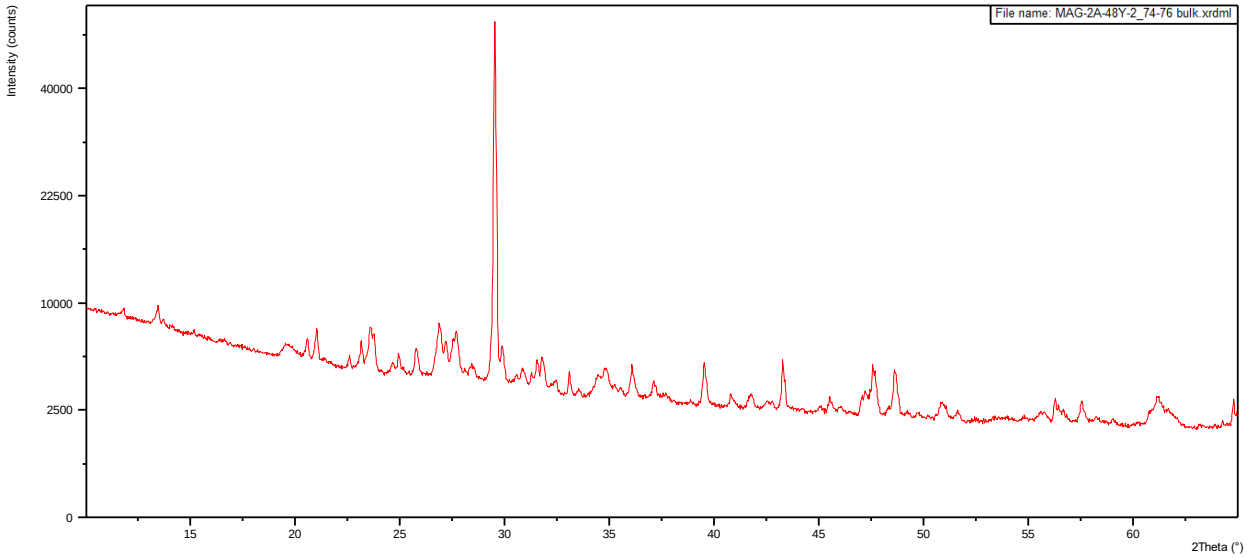
File name: MAG-2A-48Y-2_74-76 bulk.xrdml
Intensity (counts)
40000
22500
10000
2500
0
15
20
25
30
35
40
45
50
55
60
2Theta (°)

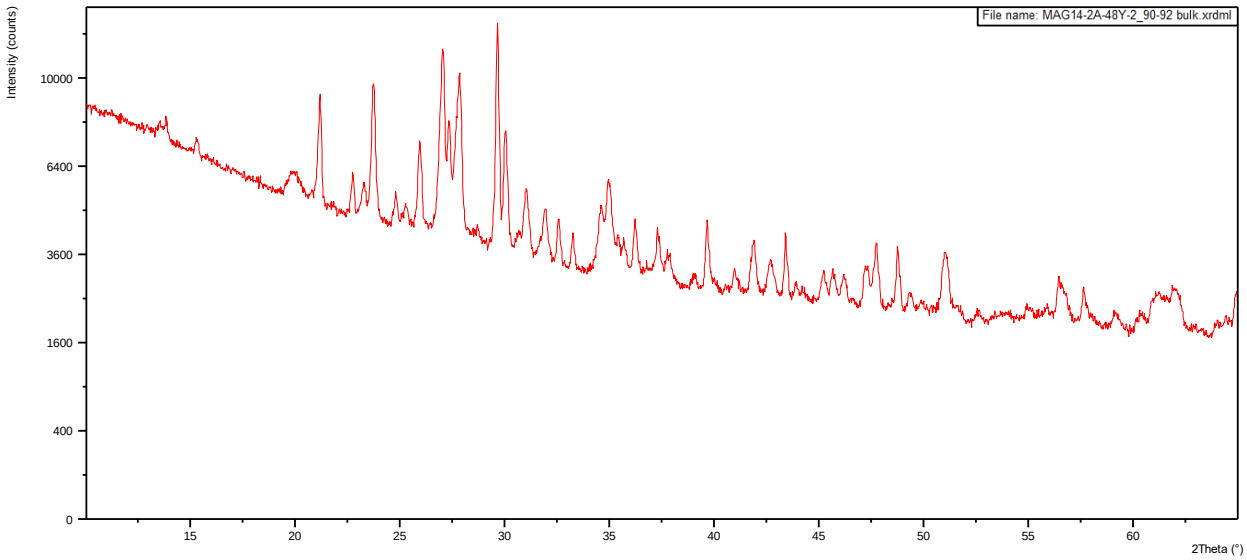
File name: MAG14-2A-48Y-2_90-92 bulk.xrdml
Intensity (counts)
10000
6400
3600
1600
400
0
15
20
25
30
35
40
45
50
55
60
2Theta (°)

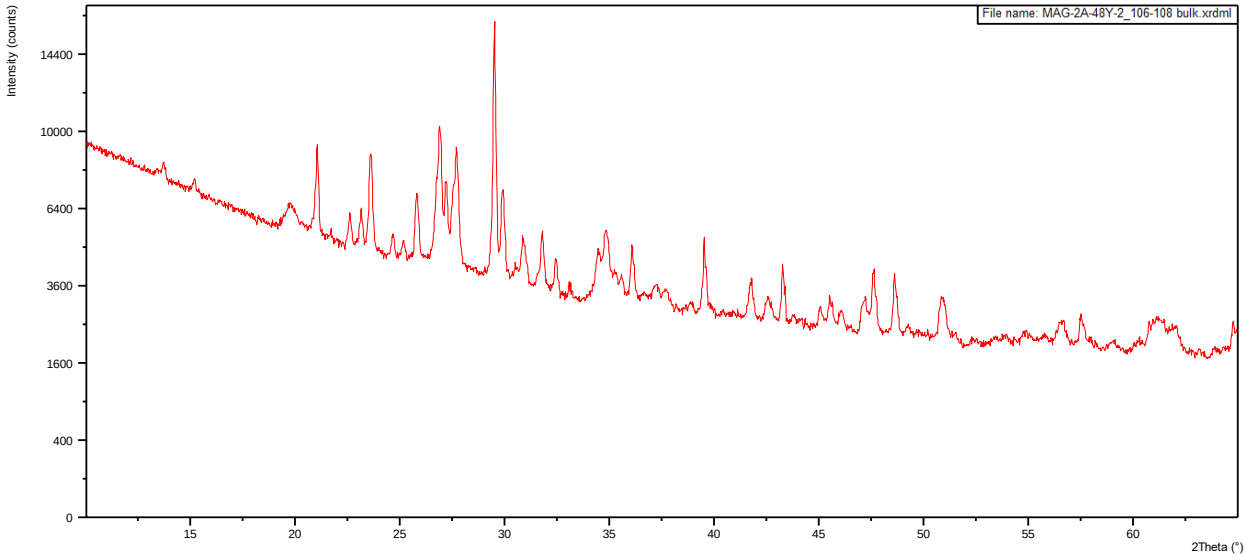
File name: MAG-2A-48Y-2_106-108 bulk.xrdml
Intensity (counts)
14400
10000
6400
3600
1600
400
0
15
20
25
30
35
40
45
50
55
60
2Theta (°)

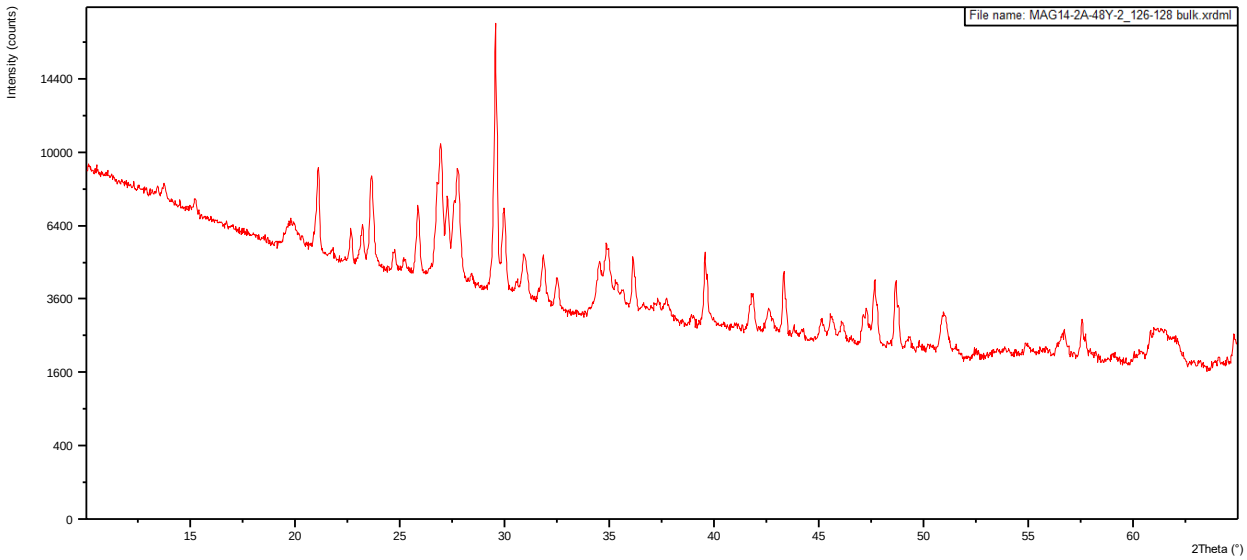
File name: MAG14-2A-48Y-2_126-128 bulk.xrdml
Intensity (counts)
14400
10000
6400
3600
1600
400
0
15
20
25
30
35
40
45
50
55
60
2Theta (°)

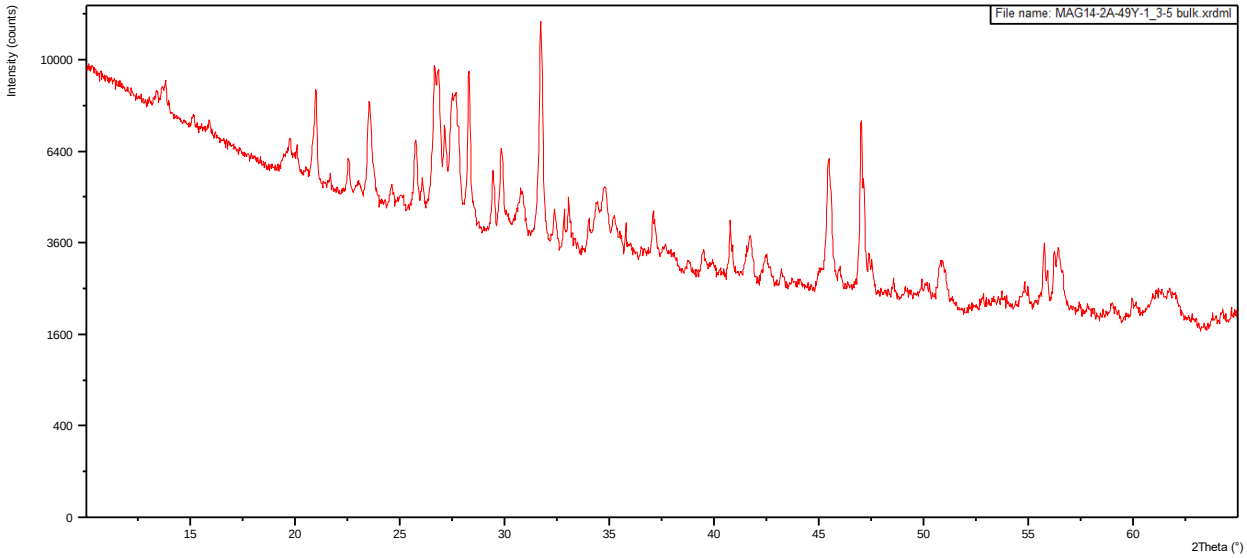
File name: MAG14-2A-49Y-1_3-5 bulk.xrdml
Intensity (counts)
10000
6400
3600
1600
400
0
15
20
25
30
35
40
45
50
55
60
2Theta (°)

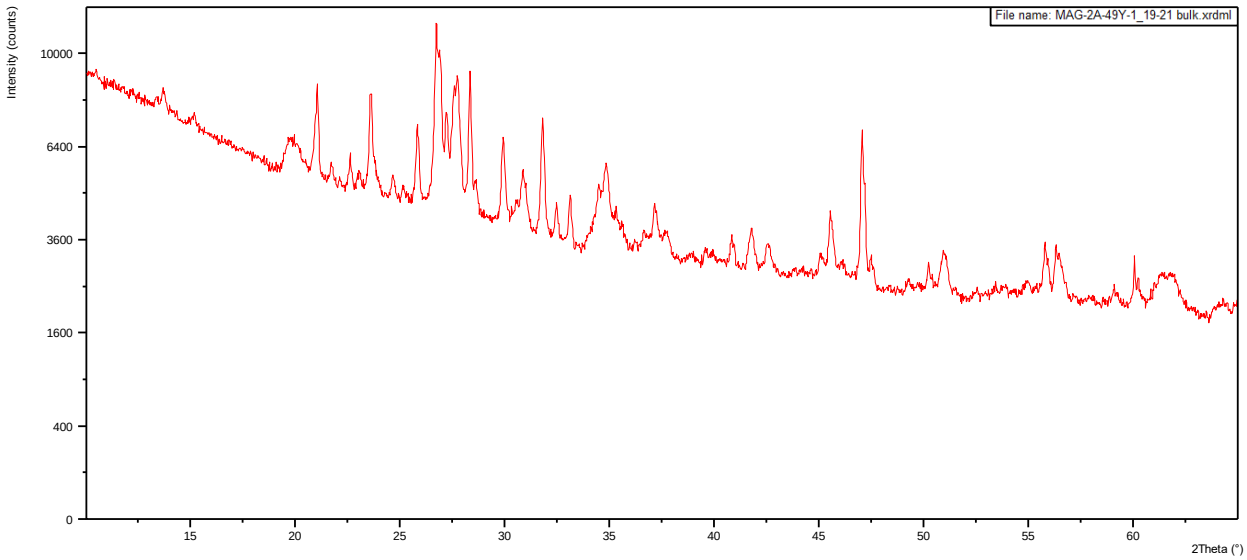
File name: MAG-2A-49Y-1_19-21 bulk.xrdml
Intensity (counts)
10000
6400
3600
1600
400
0
15
20
25
30
35
40
45
50
55
60
2Theta (°)

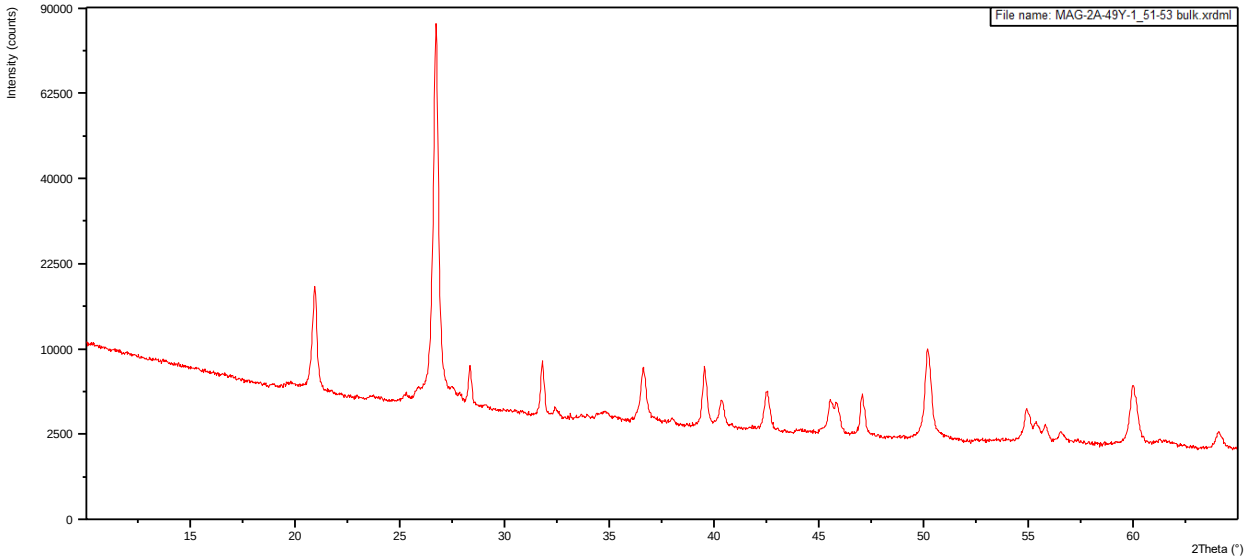
File name: MAG-2A-49Y-1_51-53 bulk.xrdml
Intensity (counts)
90000
62500
40000
22500
10000
2500
0
15
20
25
30
35
40
45
50
55
60
2Theta (°)

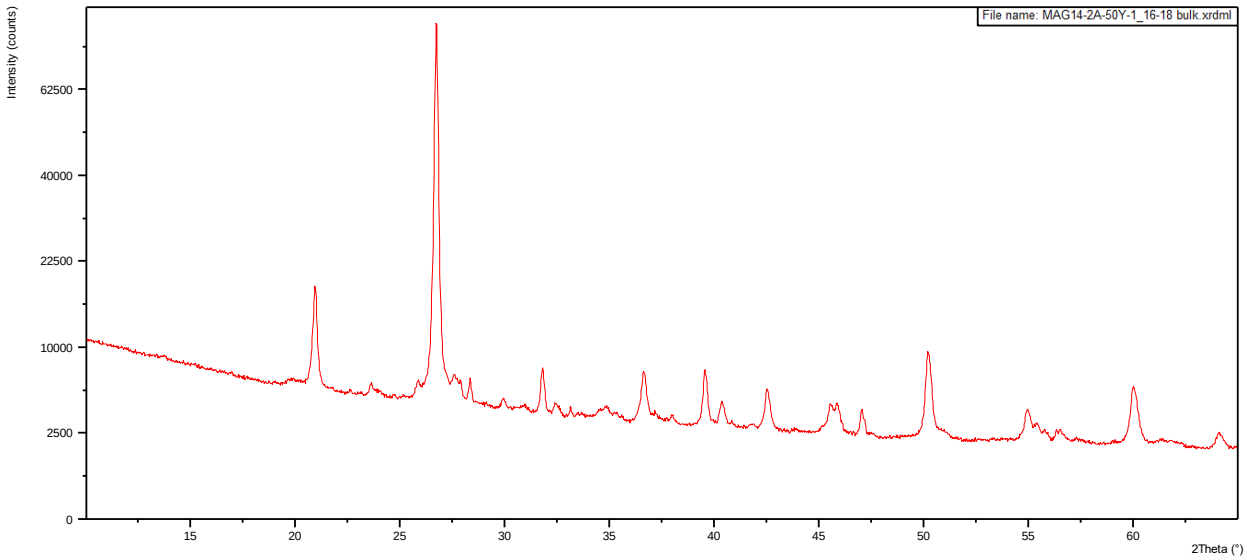
File name: MAG14-2A-50Y-1_16-18 bulk.xrdml
Intensity (counts)
62500
40000
22500
10000
2500
0
15
20
25
30
35
40
45
50
55
60
2Theta (°)

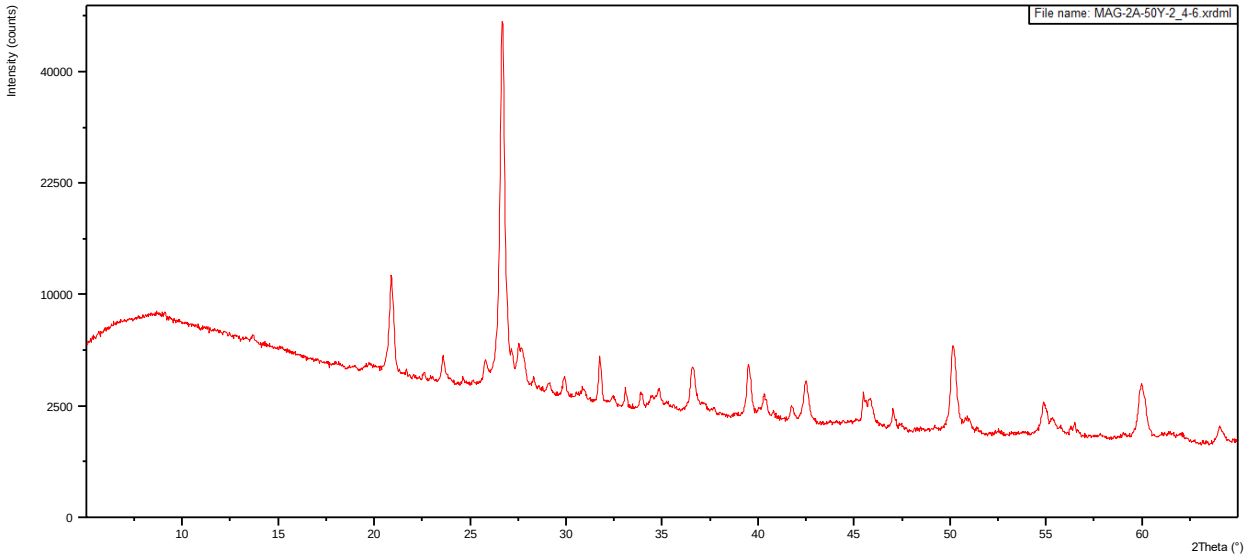
File name: MAG-2A-50Y-2_4-6.xrdml
Intensity (counts)
40000
22500
10000
2500
0
10
15
20
25
30
35
40
45
50
55
60
2Theta (°)

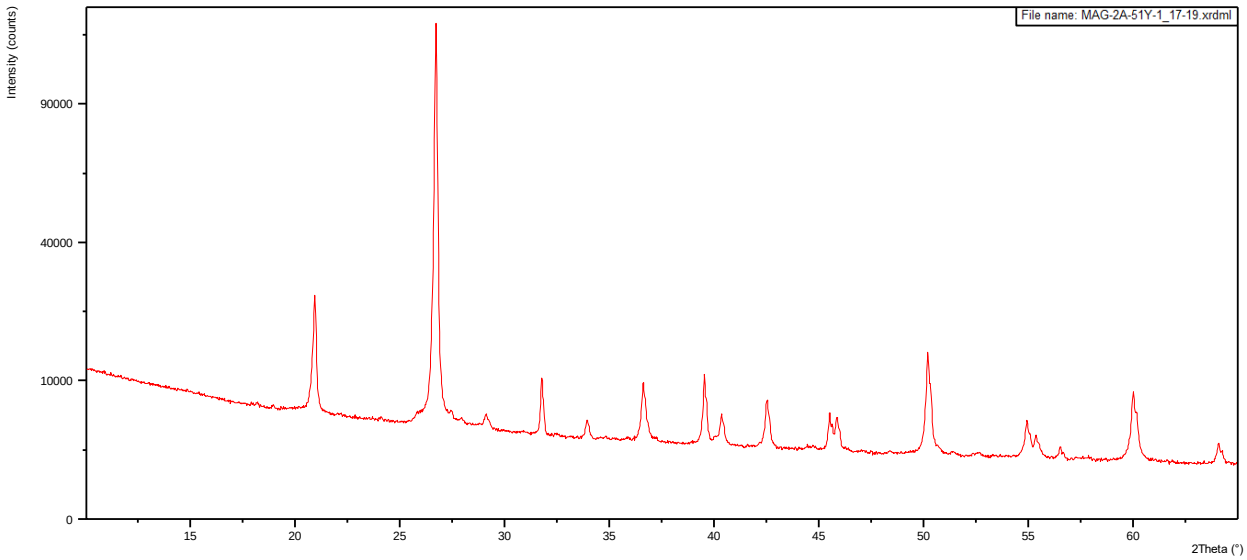
File name: MAG-2A-51Y-1_17-19.xrdml
Intensity (counts)
90000
40000
10000
0
15
20
25
30
35
40
45
50
55
60
2Theta (°)

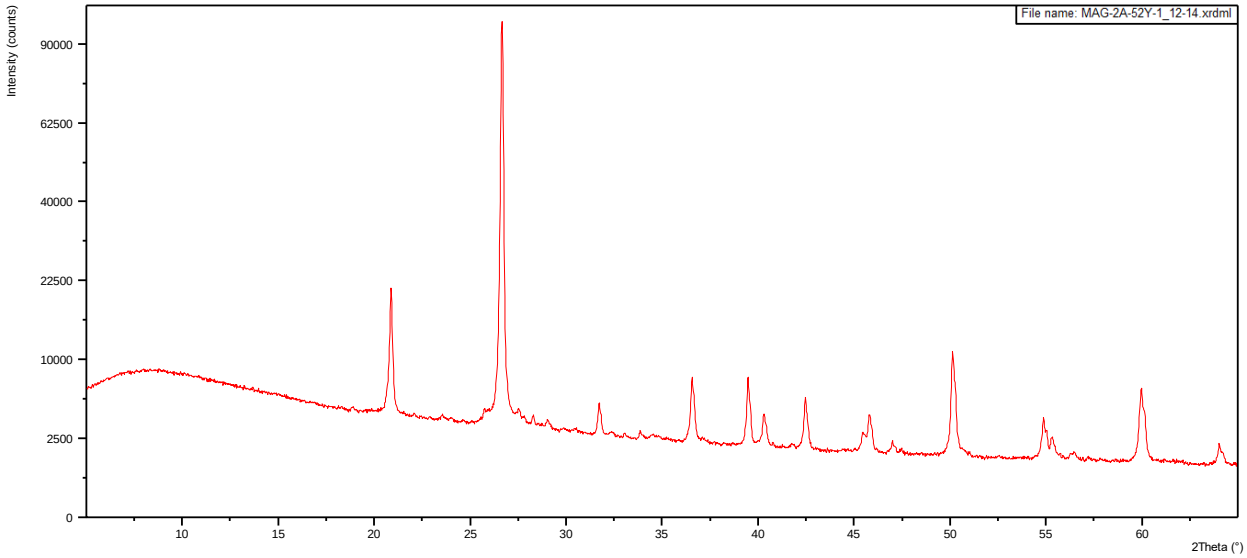
File name: MAG-2A-52Y-1_12-14.xrdml
Intensity (counts)
90000
62500
40000
22500
10000
2500
0
10
15
20
25
30
35
40
45
50
55
60
2Theta (°)

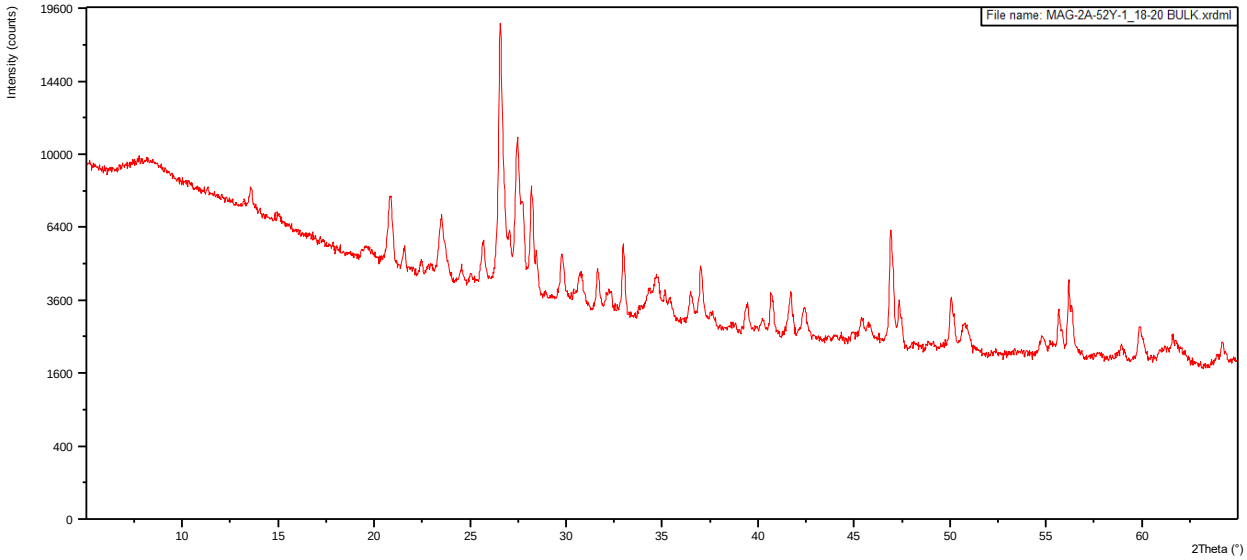
File name: MAG-2A-52Y-1_18-20 BULK.xrdml
Intensity (counts)
19600
14400
10000
6400
3600
1600
400
0
10
15
20
25
30
35
40
45
50
55
60
2Theta (°)

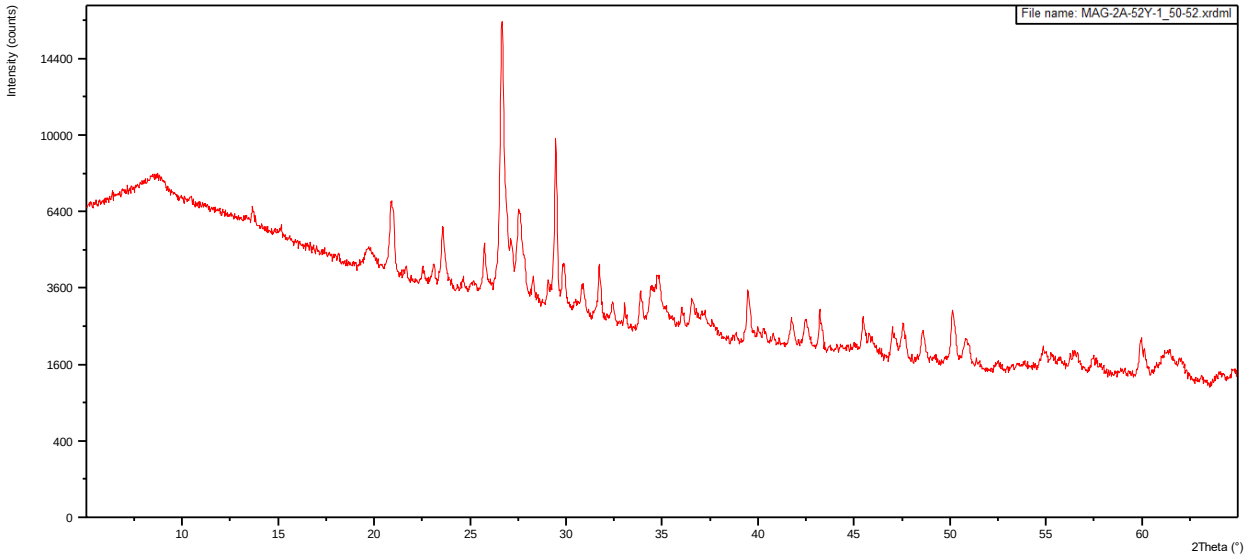
File name: MAG-2A-52Y-1_50-52.xrdml
Intensity (counts)
14400
10000
6400
3600
1600
400
0
10
15
20
25
30
35
40
45
50
55
60
2Theta (°)

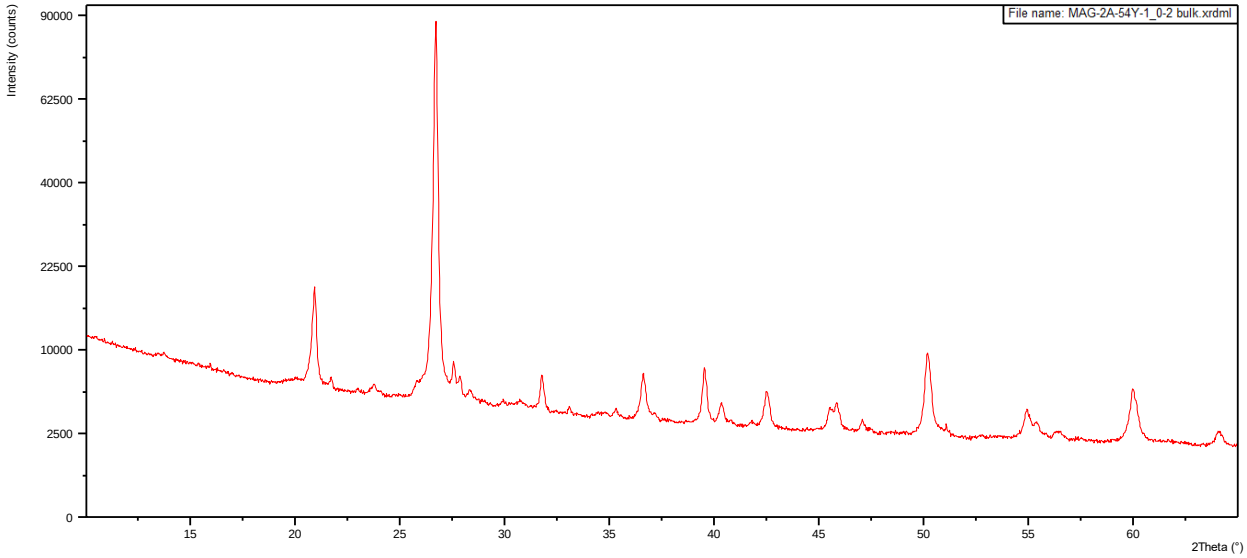
File name: MAG-2A-54Y-1_0-2 bulk.xrdml
Intensity (counts)
90000
62500
40000
22500
10000
2500
0
15
20
25
30
35
40
45
50
55
60
2Theta (°)

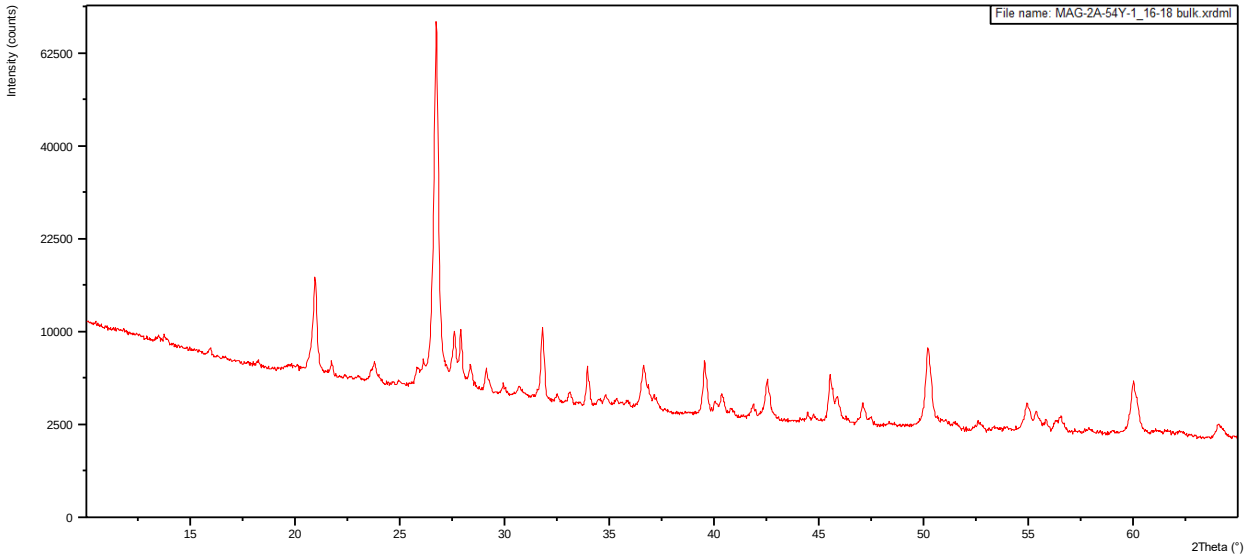
File name: MAG-2A-54Y-1_16-18 bulk.xrdml
Intensity (counts)
62500
40000
22500
10000
2500
0
15
20
25
30
35
40
45
50
55
60
2Theta (°)

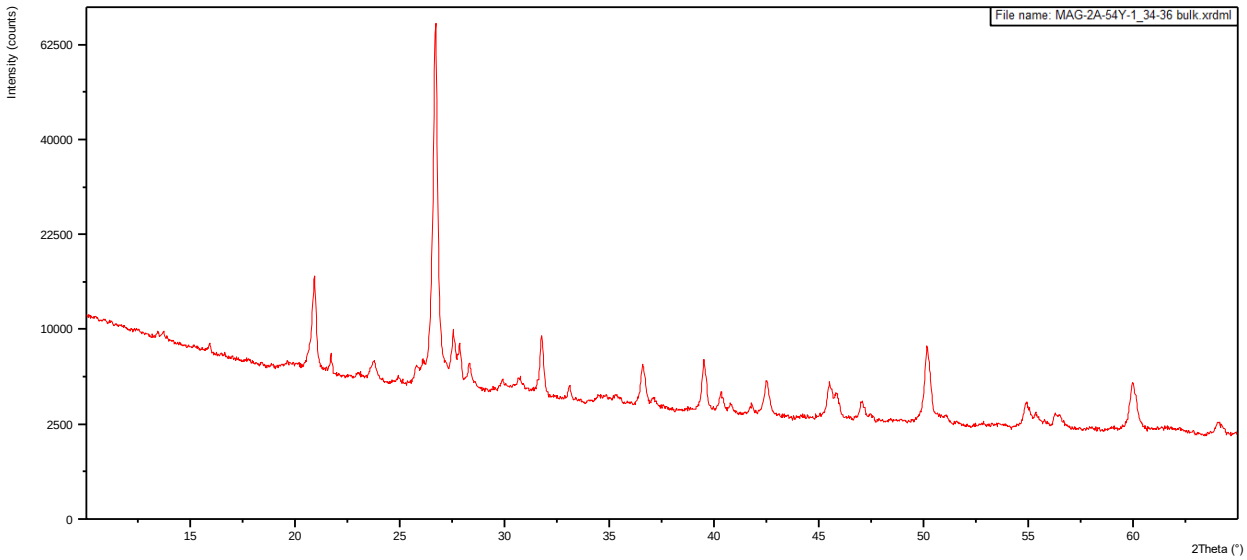
File name: MAG-2A-54Y-1_34-36 bulk.xrdml
Intensity (counts)
62500
40000
22500
10000
2500
0
15
20
25
30
35
40
45
50
55
60
2Theta (°)

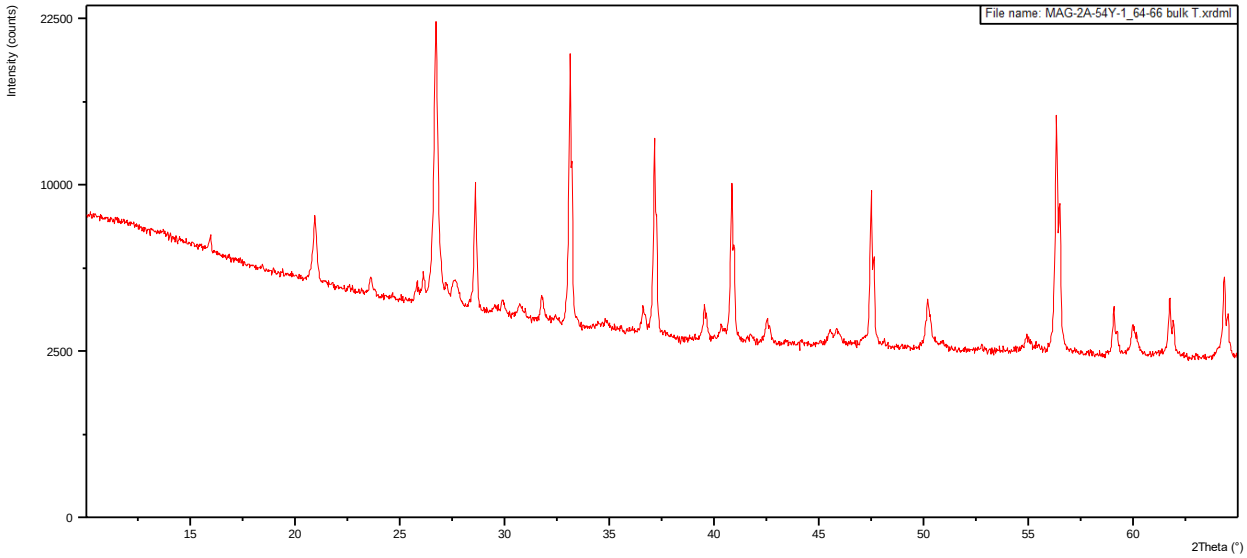
File name: MAG-2A-54Y-1_64-66 bulk T.xrdml
Intensity (counts)
22500
10000
2500
0
15
20
25
30
35
40
45
50
55
60
2Theta (°)

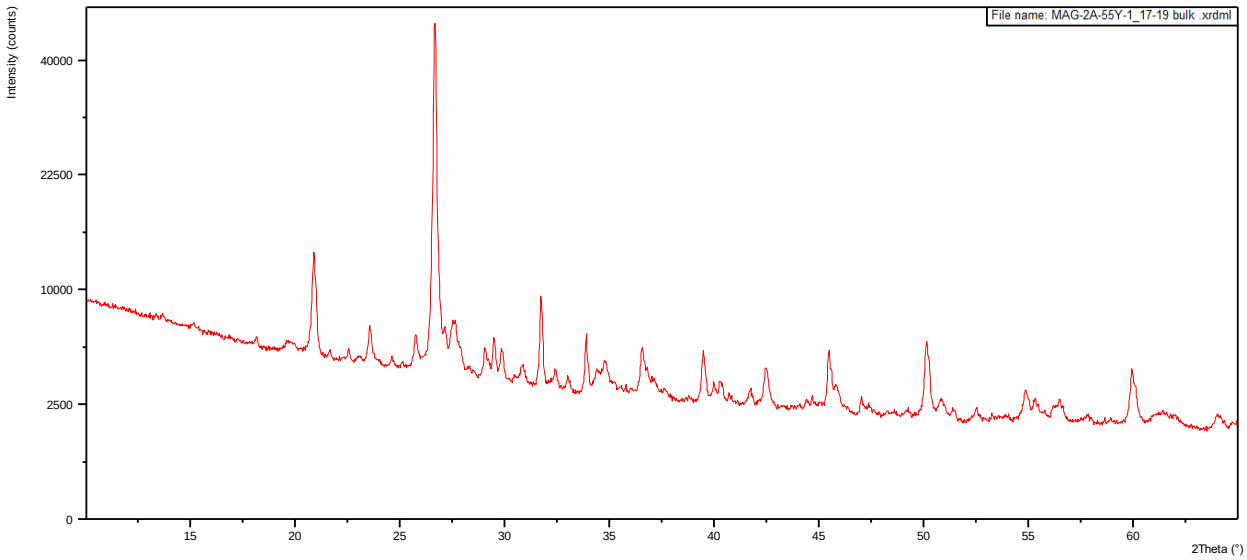
File name: MAG-2A-55Y-1_17-19 bulk .xrdml
Intensity (counts)
40000
22500
10000
2500
0
15
20
25
30
35
40
45
50
55
60
2Theta (°)

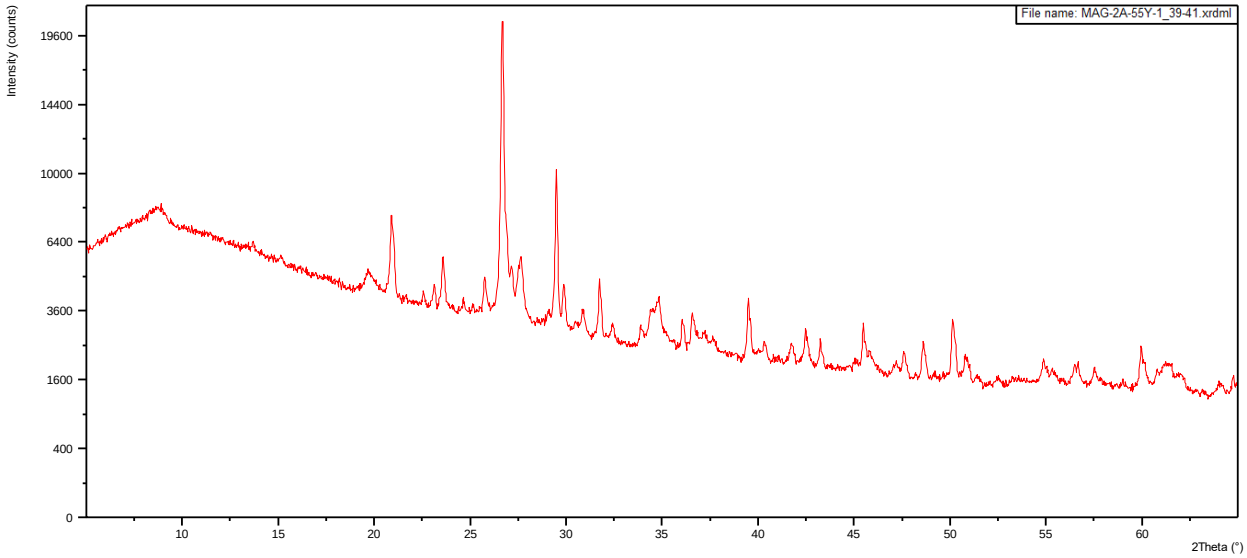
File name: MAG-2A-55Y-1_39-41.xrdml
Intensity (counts)
19600
14400
10000
6400
3600
1600
400
0
10
15
20
25
30
35
40
45
50
55
60
2Theta (°)

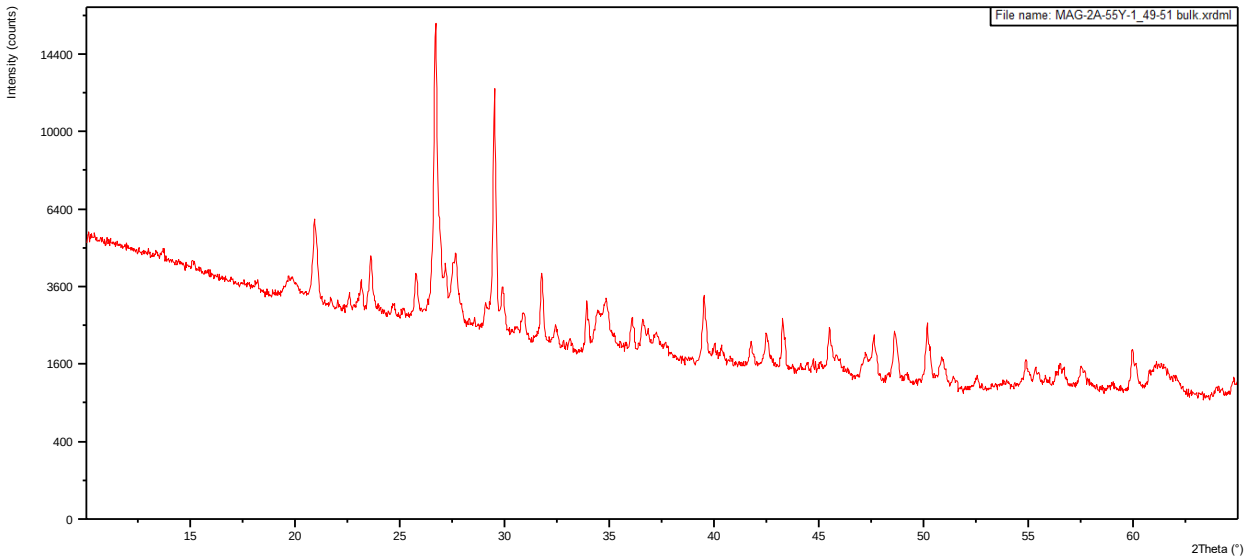
File name: MAG-2A-55Y-1_49-51 bulk.xrdml
Intensity (counts)
14400
10000
6400
3600
1600
400
0
15
20
25
30
35
40
45
50
55
60
2Theta (°)

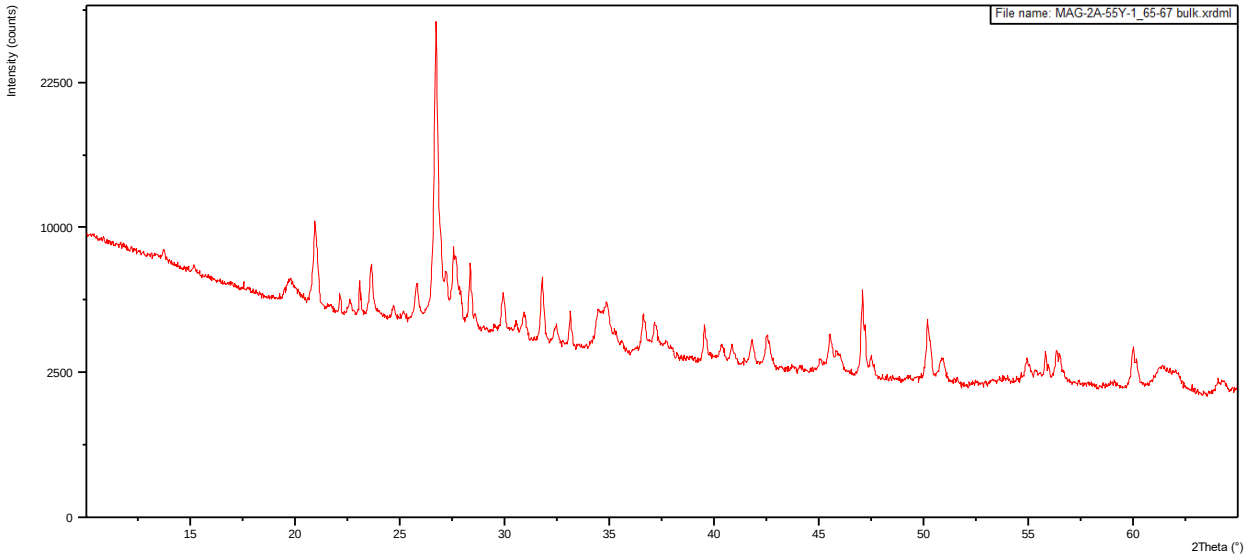
File name: MAG-2A-55Y-1_65-67 bulk.xrdml
Intensity (counts)
22500
10000
2500
0
15
20
25
30
35
40
45
50
55
60
2Theta (°)

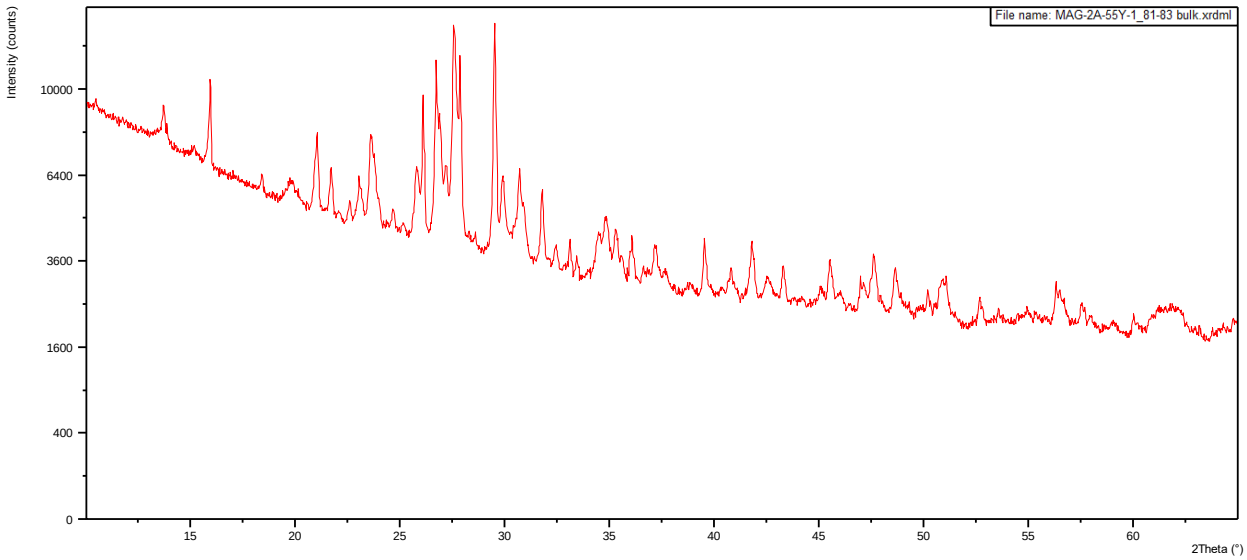
File name: MAG-2A-55Y-1_81-83 bulk.xrdml
Intensity (counts)
10000
6400
3600
1600
400
0
15
20
25
30
35
40
45
50
55
60
2Theta (°)

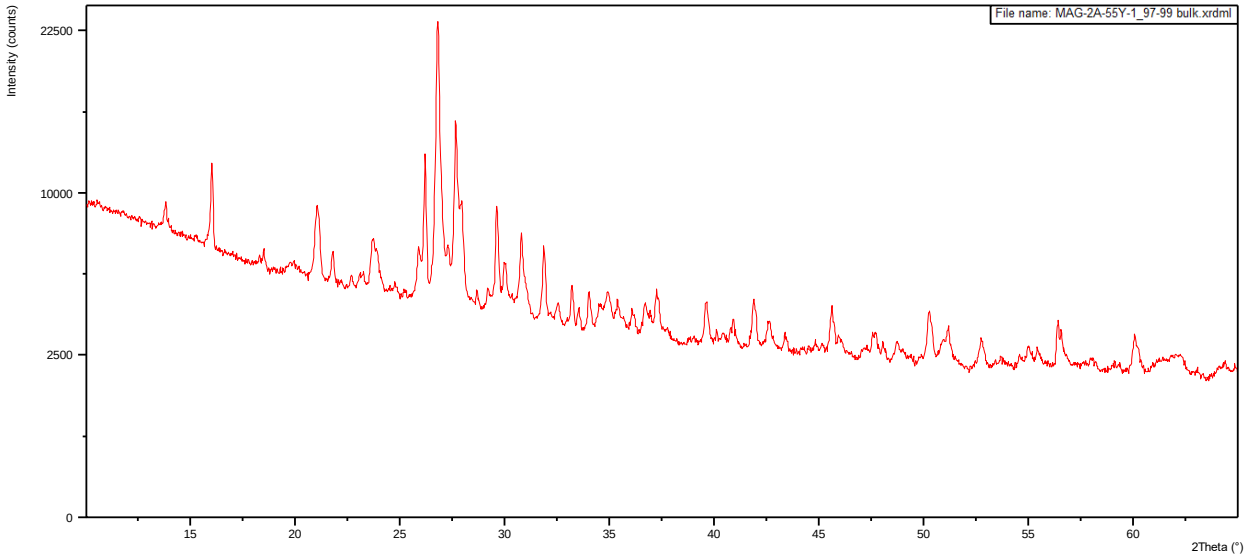
File name: MAG-2A-55Y-1_97-99 bulk.xrdml
Intensity (counts)
22500
10000
2500
0
15
20
25
30
35
40
45
50
55
60
2Theta (°)

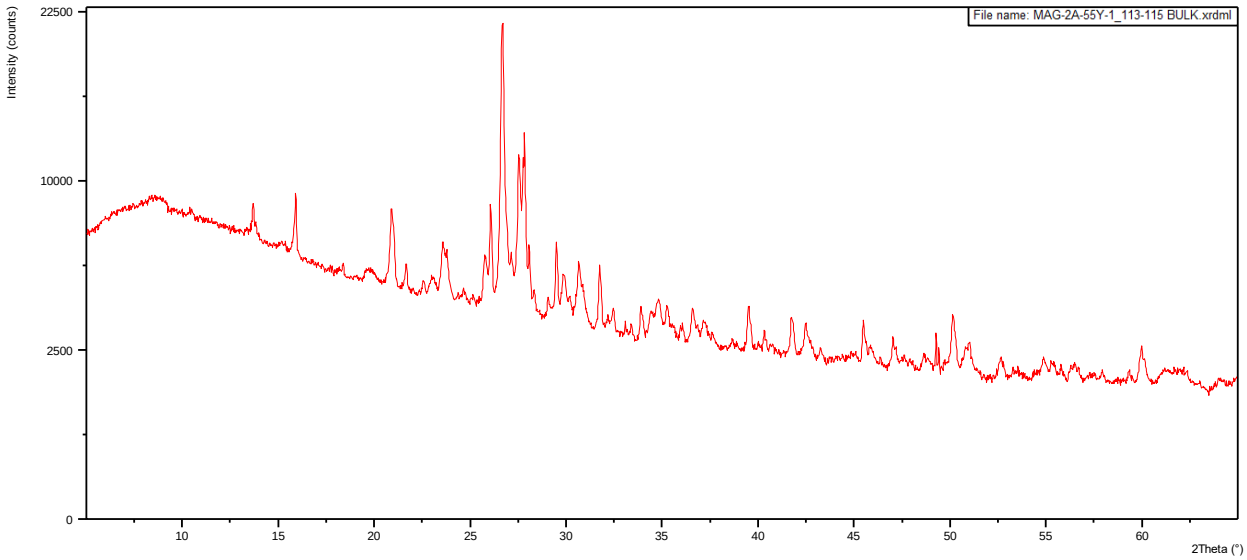
File name: MAG-2A-55Y-1_113-115 BULK.xrdml
Intensity (counts)
22500
10000
2500
0
10
15
20
25
30
35
40
45
50
55
60
2Theta (°)

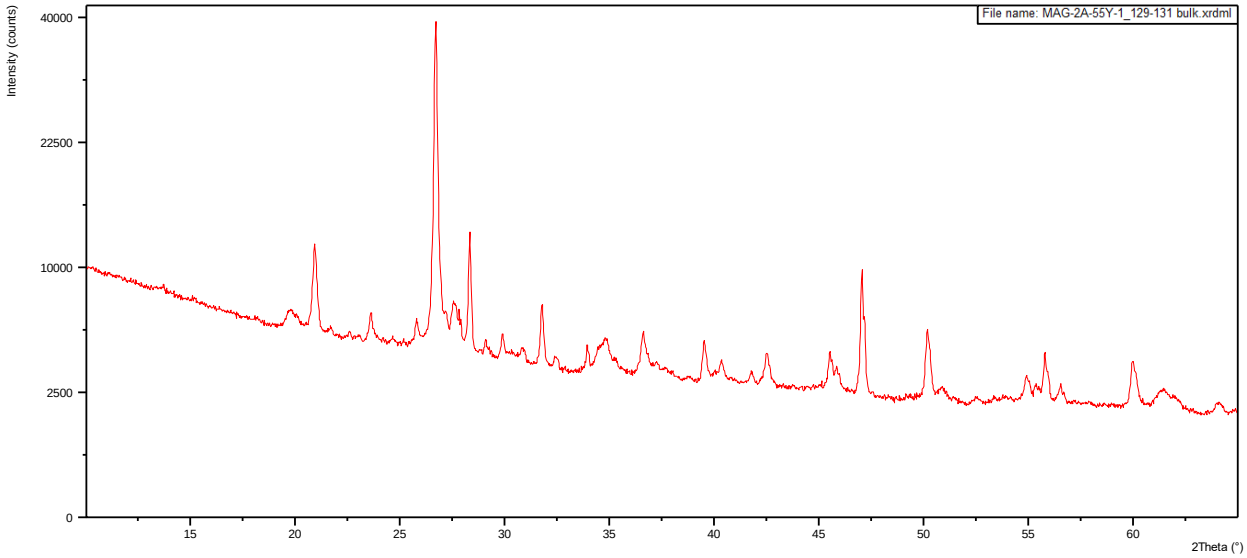
File name: MAG-2A-55Y-1_129-131 bulk.xrdml
Intensity (counts)
40000
22500
10000
2500
0
15
20
25
30
35
40
45
50
55
60
2Theta (°)

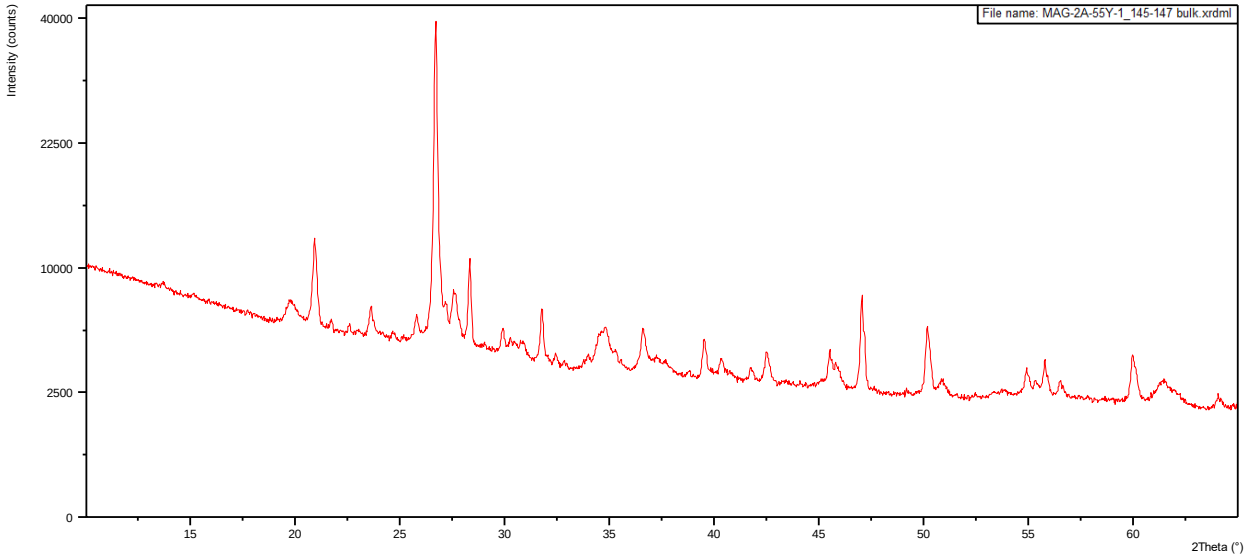
File name: MAG-2A-55Y-1_145-147 bulk.xrdml
Intensity (counts)
40000
22500
10000
2500
0
15
20
25
30
35
40
45
50
55
60
2Theta (°)

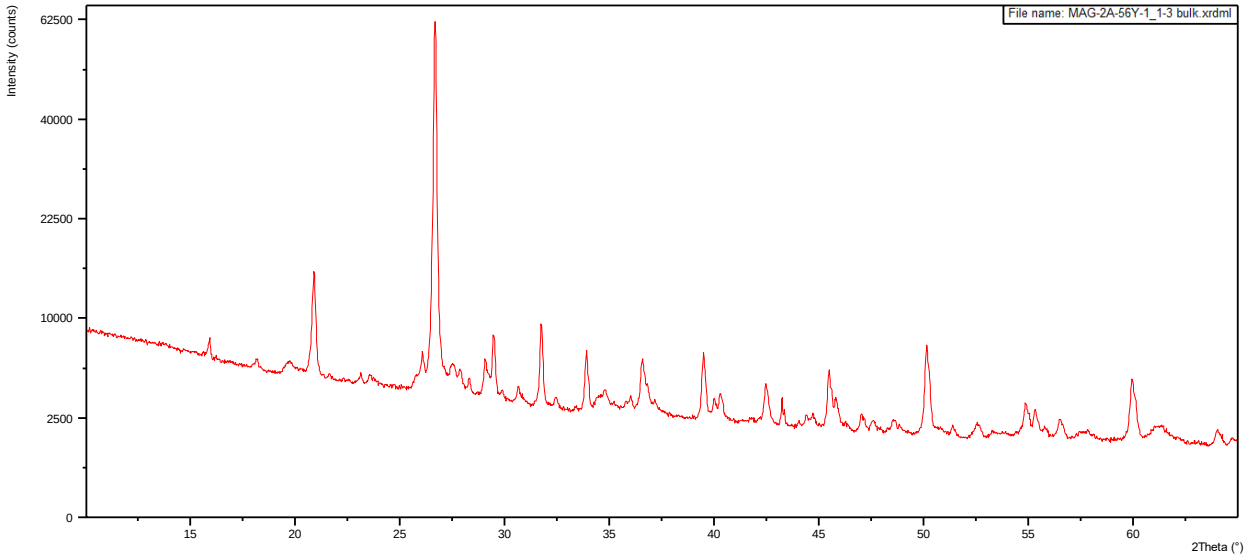
File name: MAG-2A-56Y-1_1-3 bulk.xrdml
Intensity (counts)
62500
40000
22500
10000
2500
0
15
20
25
30
35
40
45
50
55
60
2Theta (°)

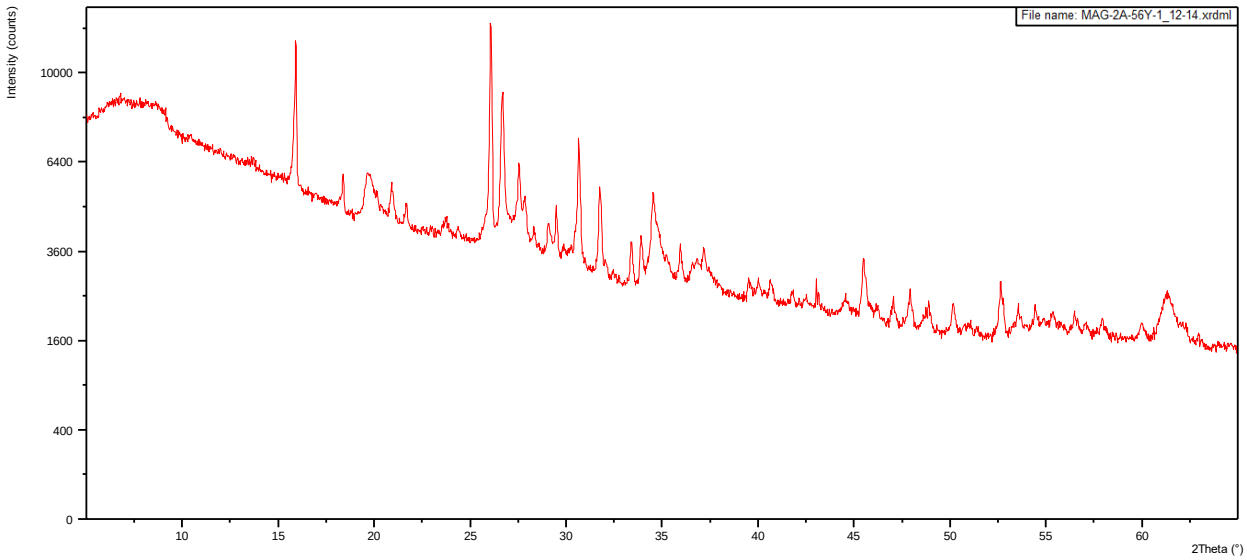
File name: MAG-2A-56Y-1_12-14.xrdml
Intensity (counts)
10000
6400
3600
1600
400
0
10
15
20
25
30
35
40
45
50
55
60
2Theta (°)

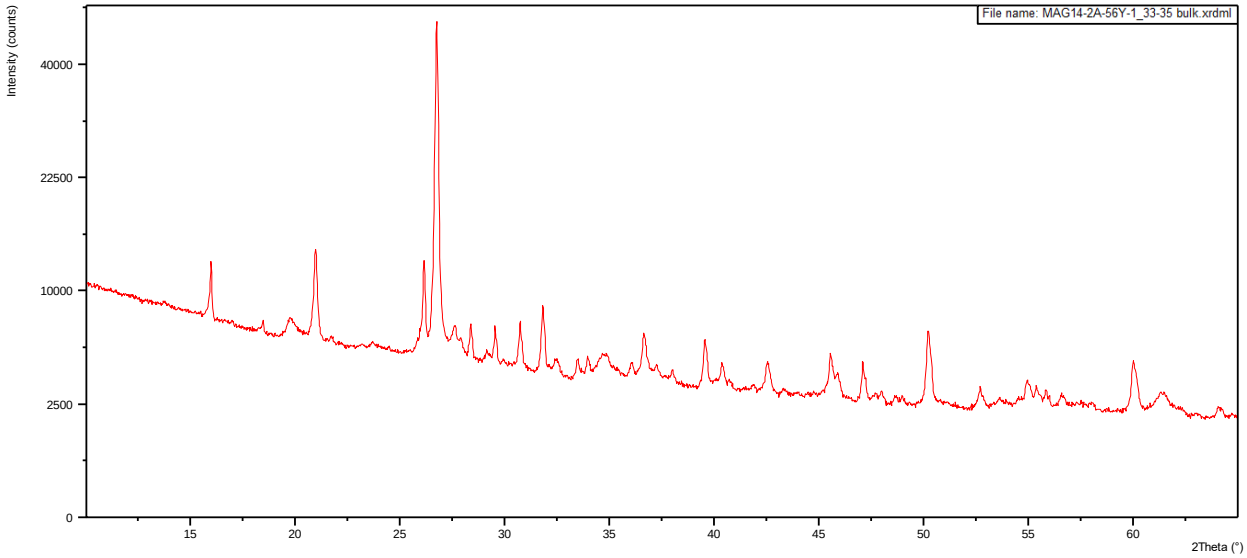
File name: MAG14-2A-56Y-1_33-35 bulk.xrdml
Intensity (counts)
40000
22500
10000
2500
0
15
20
25
30
35
40
45
50
55
60
2Theta (°)

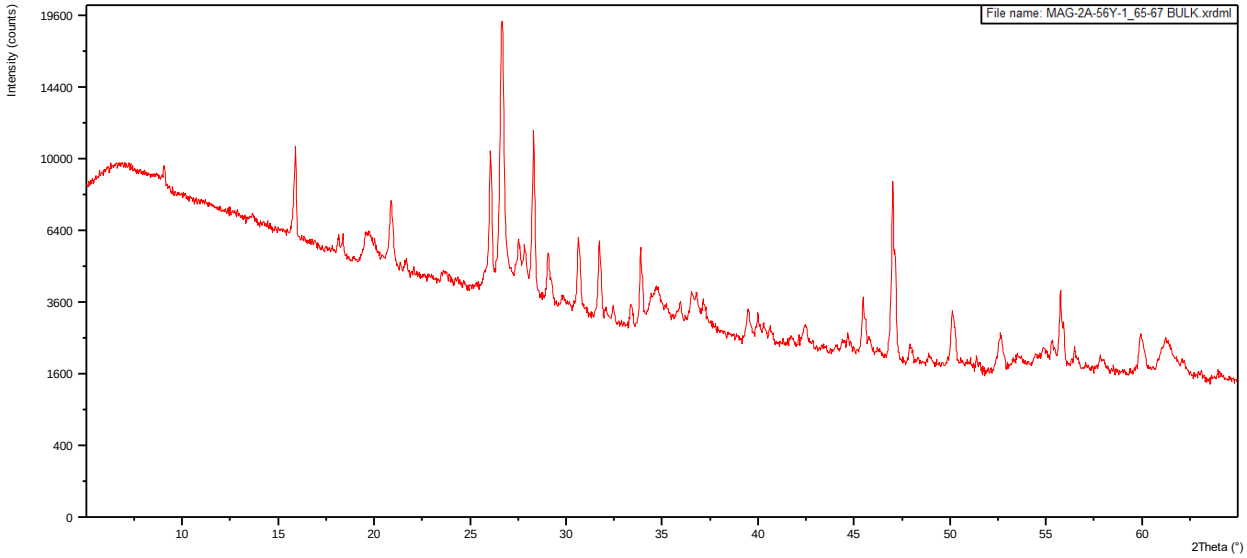
File name: MAG-2A-56Y-1_65-67 BULK.xrdml
Intensity (counts)
19600
14400
10000
6400
3600
1600
400
0
10
15
20
25
30
35
40
45
50
55
60
2Theta (°)

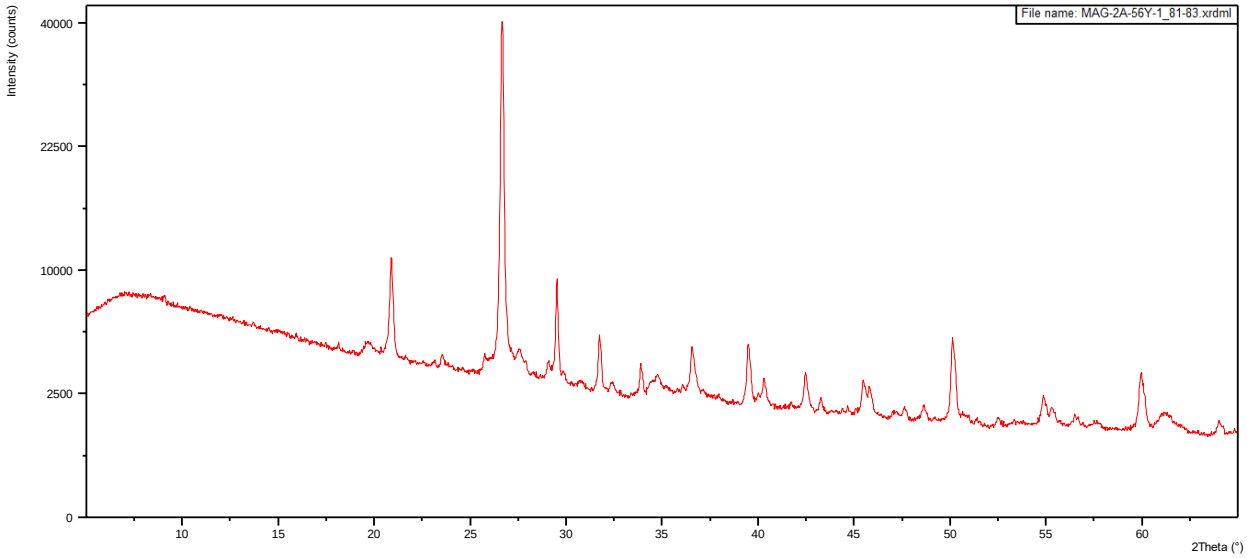
File name: MAG-2A-56Y-1_81-83.xrdml
Intensity (counts)
40000
22500
10000
2500
0
10
15
20
25
30
35
40
45
50
55
60
2Theta (°)

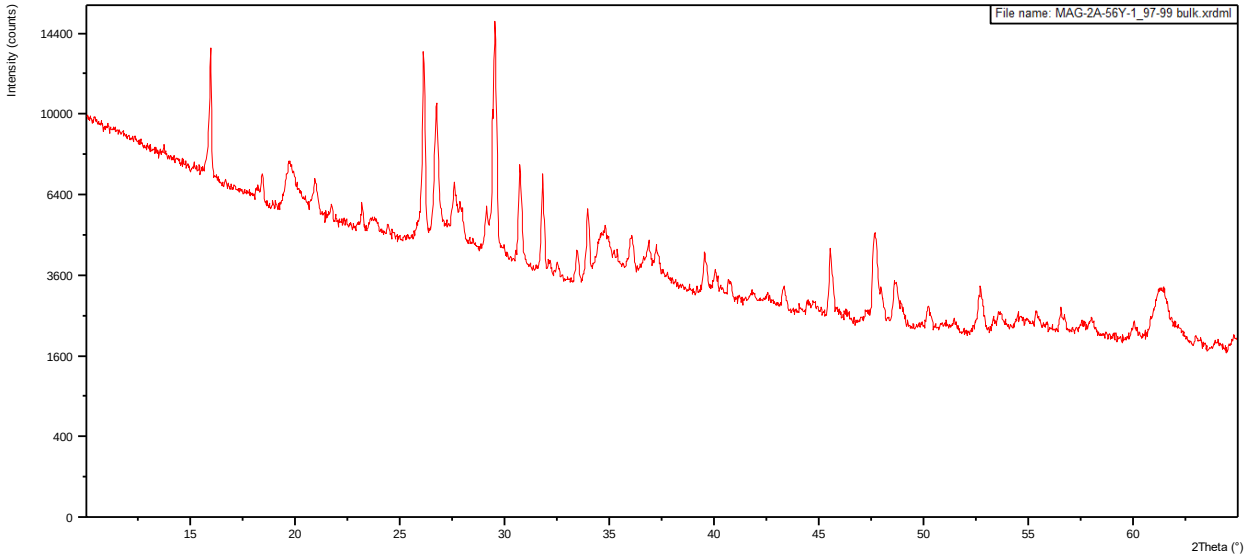
File name: MAG-2A-56Y-1_97-99 bulk.xrdml
Intensity (counts)
14400
10000
6400
3600
1600
400
0
15
20
25
30
35
40
45
50
55
60
2Theta (°)

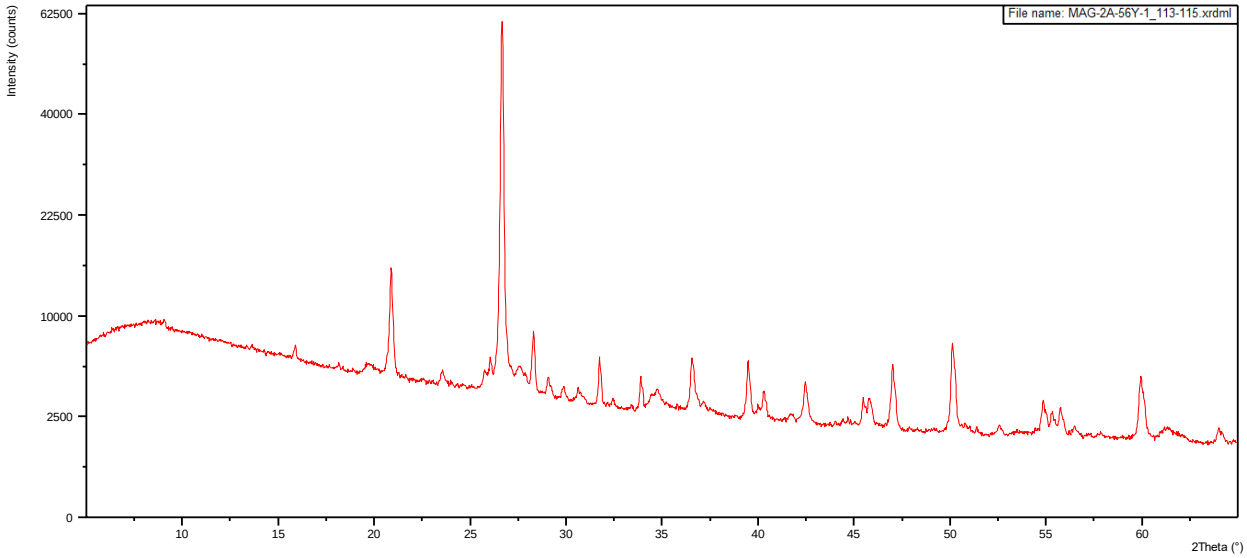
File name: MAG-2A-56Y-1_113-115.xrdml
Intensity (counts)
62500
40000
22500
10000
2500
0
10
15
20
25
30
35
40
45
50
55
60
2Theta (°)

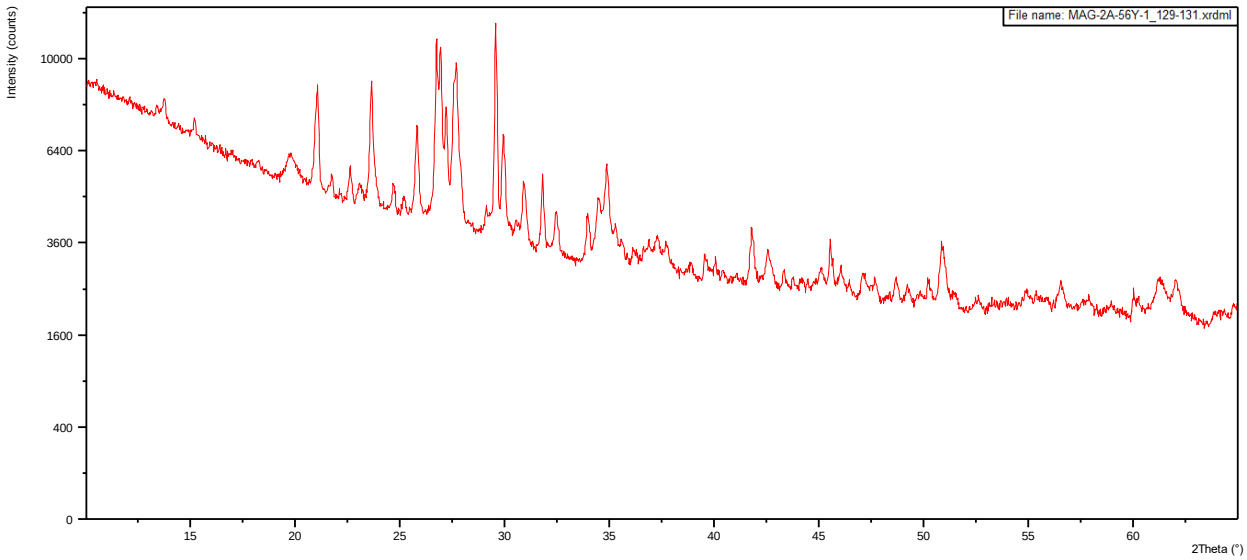
File name: MAG-2A-56Y-1_129-131.xrdml
Intensity (counts)
10000
6400
3600
1600
400
0
15
20
25
30
35
40
45
50
55
60
2Theta (°)

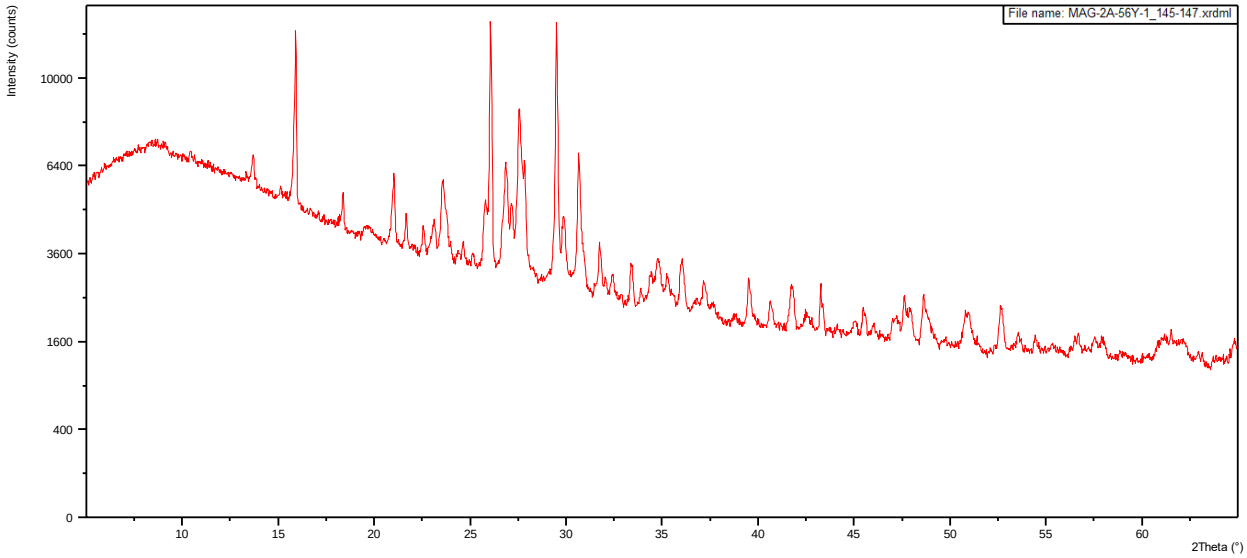
File name: MAG-2A-56Y-1_145-147.xrdml
Intensity (counts)
10000
6400
3600
1600
400
0
10
15
20
25
30
35
40
45
50
55
60
2Theta (°)

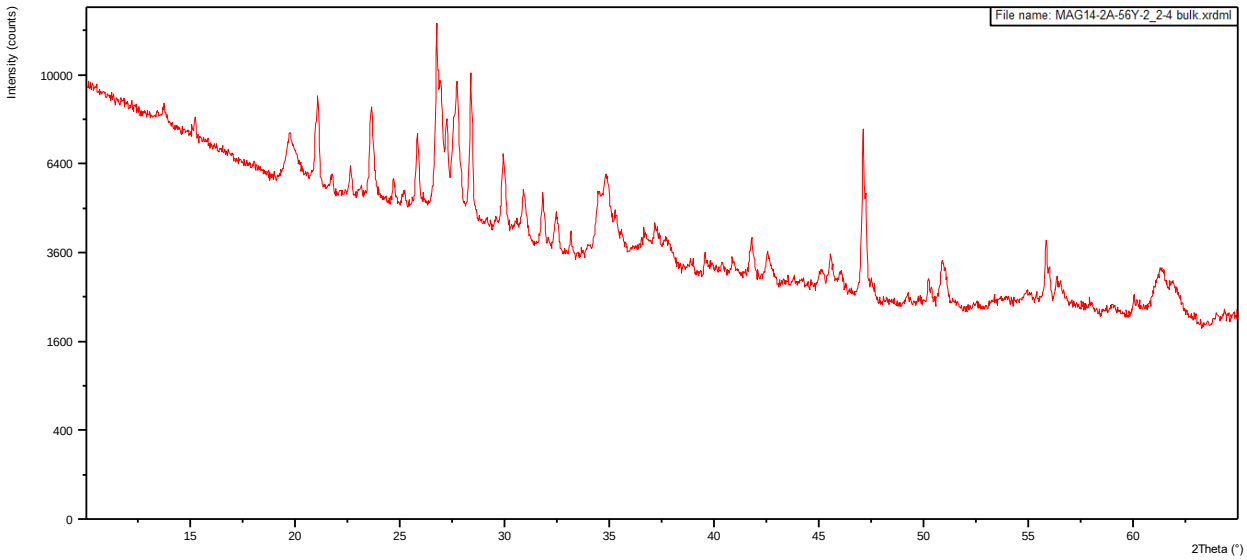
File name: MAG14-2A-56Y-2_2-4 bulk.xrdml
Intensity (counts)
10000
6400
3600
1600
400
0
15
20
25
30
35
40
45
50
55
60
2Theta (°)

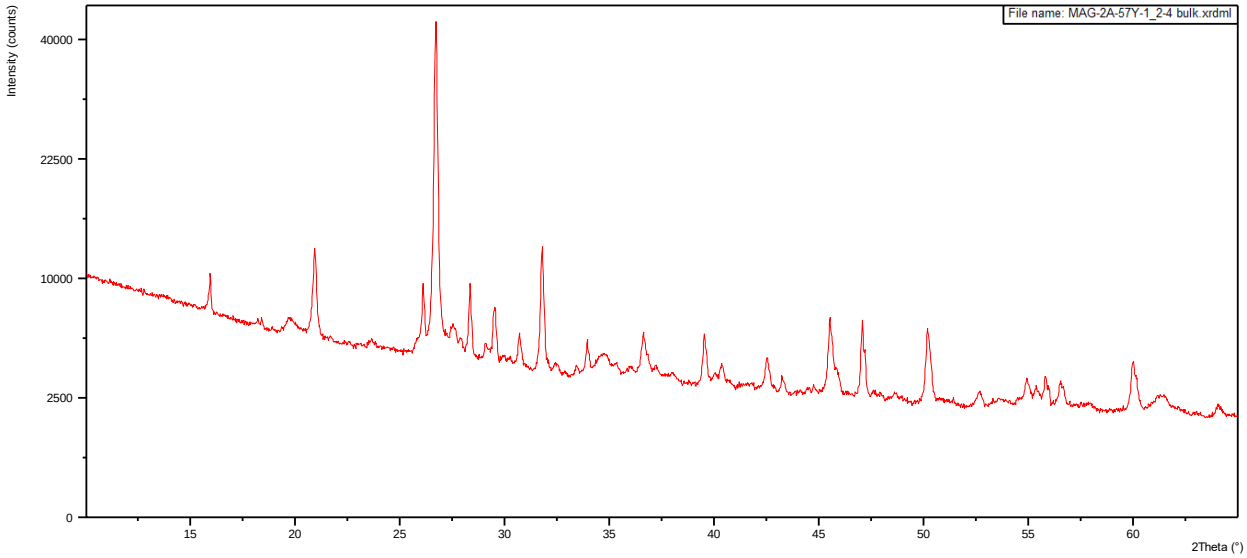
File name: MAG-2A-57Y-1_2-4 bulk.xrdml
Intensity (counts)
40000
22500
10000
2500
0
15
20
25
30
35
40
45
50
55
60
2Theta (°)

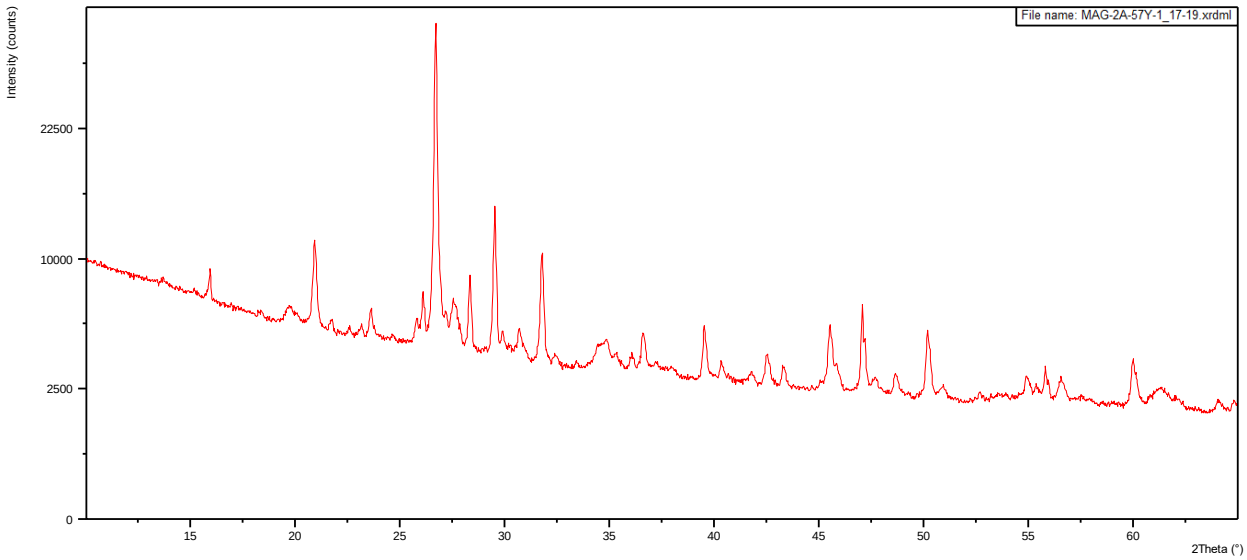
File name: MAG-2A-57Y-1_17-19.xrdml
Intensity (counts)
22500
10000
2500
0
15
20
25
30
35
40
45
50
55
60
2Theta (°)

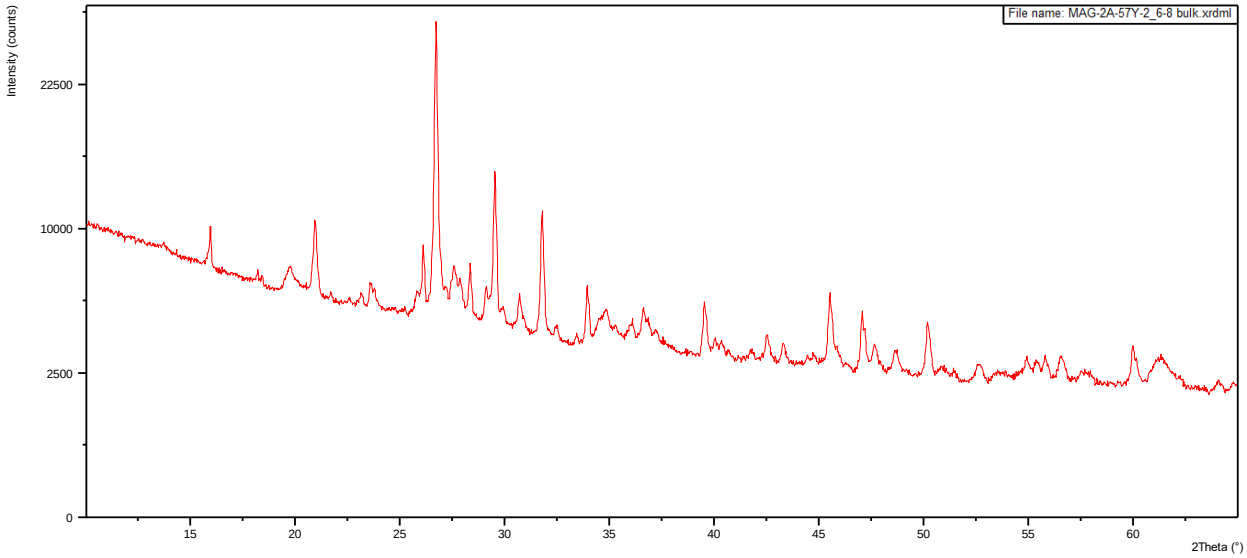
File name: MAG-2A-57Y-2_6-8 bulk.xrdml
Intensity (counts)
22500
10000
2500
0
15
20
25
30
35
40
45
50
55
60
2Theta (°)

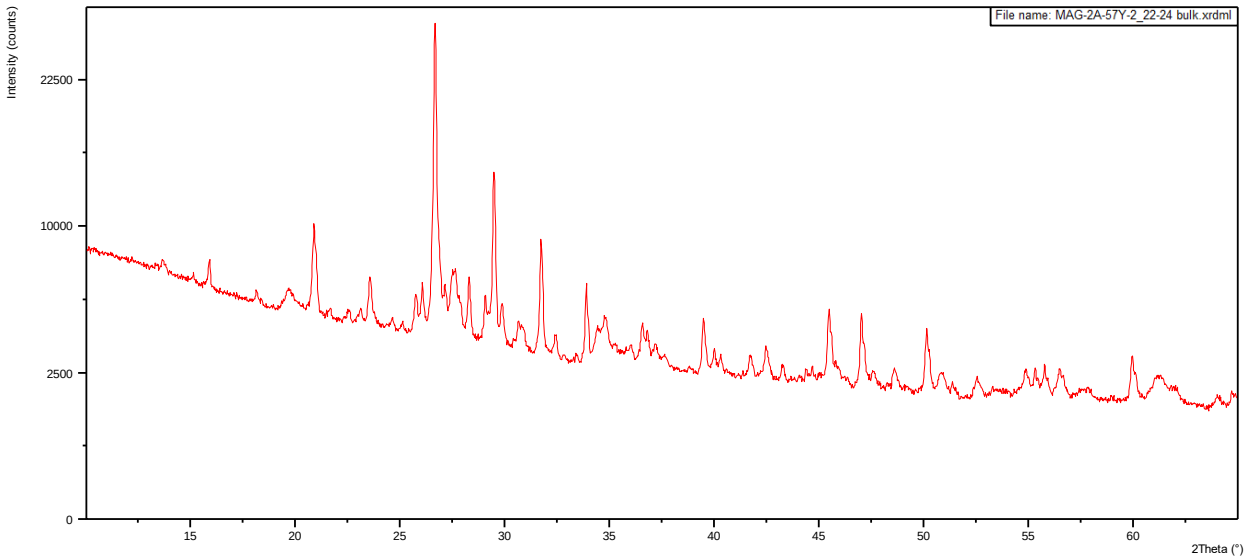
File name: MAG-2A-57Y-2_22-24 bulk.xrdml
Intensity (counts)
22500
10000
2500
0
15
20
25
30
35
40
45
50
55
60
2Theta (°)

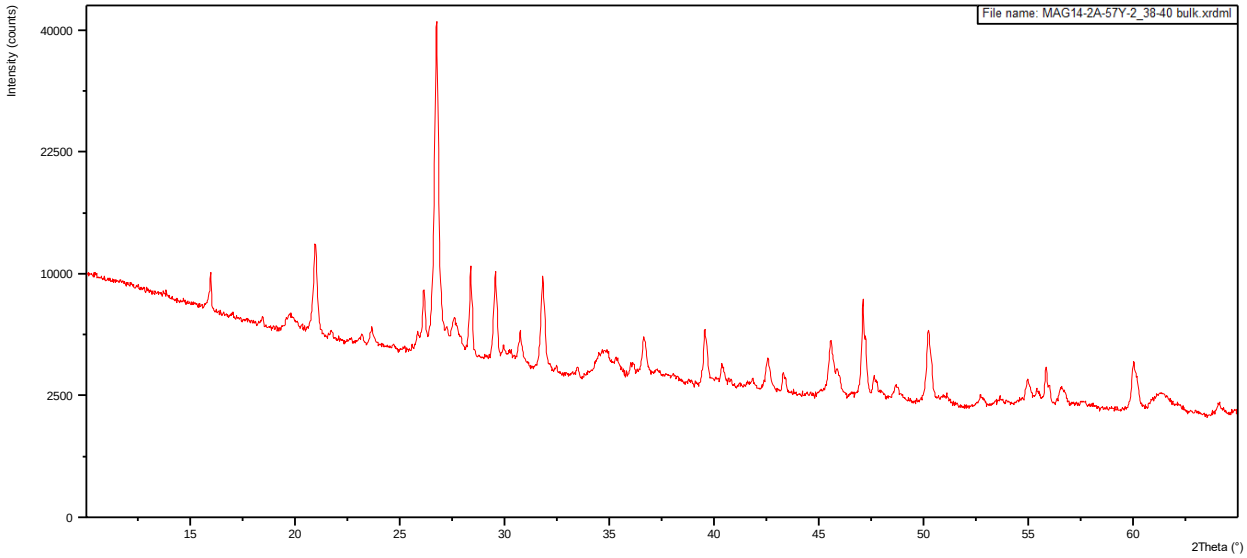
File name: MAG14-2A-57Y-2_38-40 bulk.xrdml
Intensity (counts)
40000
22500
10000
2500
0
15
20
25
30
35
40
45
50
55
60
2Theta (°)

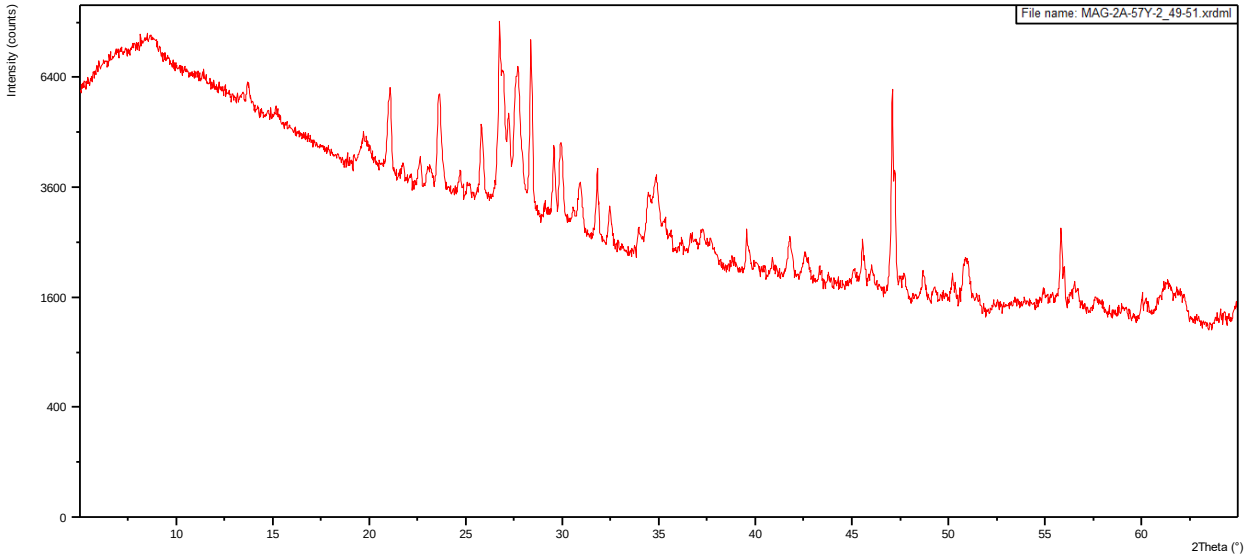
File name: MAG-2A-57Y-2_49-51.xrdml
Intensity (counts)
6400
3600
1600
400
0
10
15
20
25
30
35
40
45
50
55
60
2Theta (°)

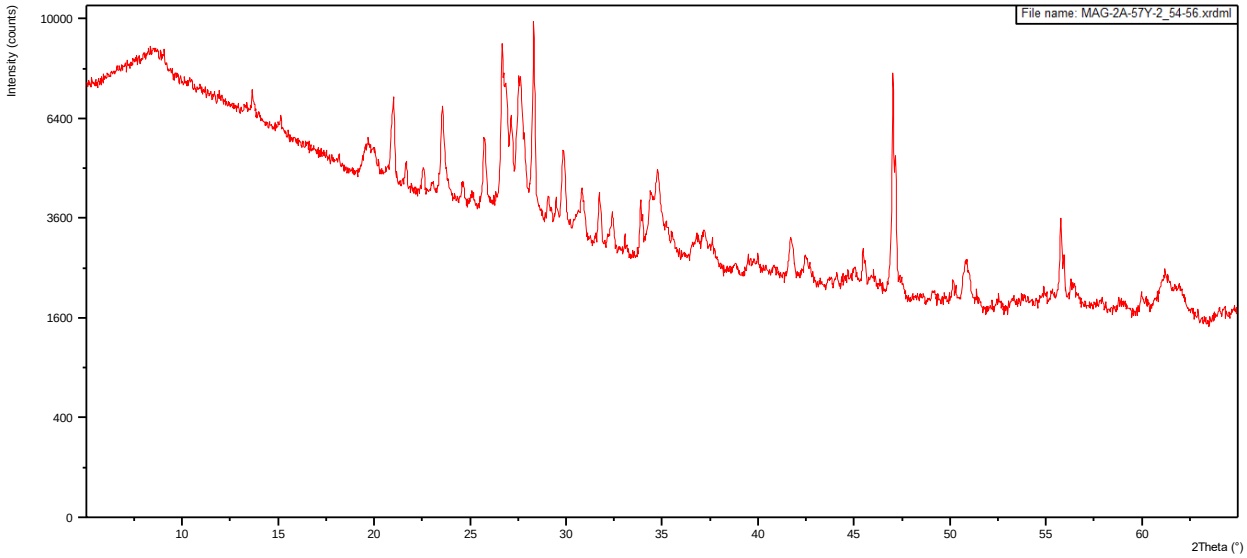
File name: MAG-2A-57Y-2_54-56.xrdml
Intensity (counts)
10000
6400
3600
1600
400
0
10
15
20
25
30
35
40
45
50
55
60
2Theta (°)

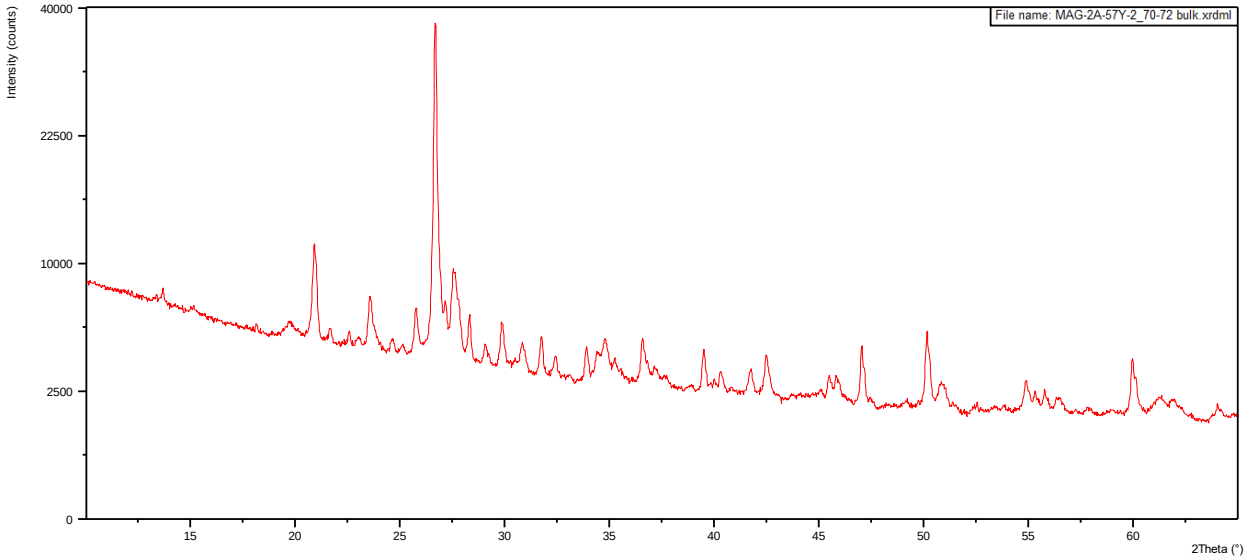
File name: MAG-2A-57Y-2_70-72 bulk.xrdml
Intensity (counts)
40000
22500
10000
2500
0
15
20
25
30
35
40
45
50
55
60
2Theta (°)

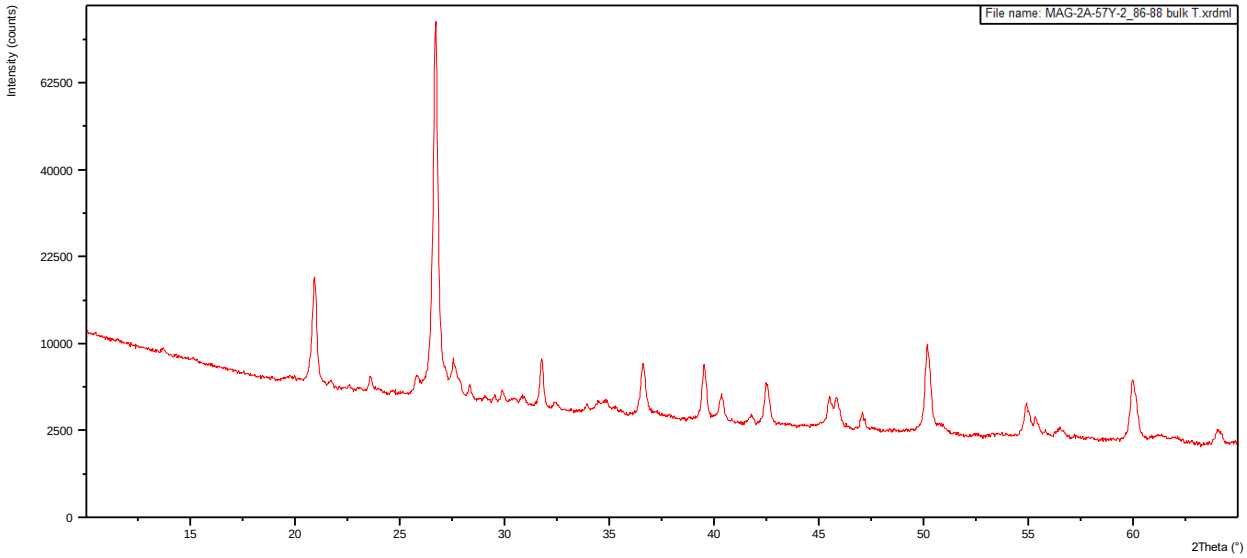
File name: MAG-2A-57Y-2_86-88 bulk T.xrdml
Intensity (counts)
62500
40000
22500
10000
2500
0
15
20
25
30
35
40
45
50
55
60
2Theta (°)

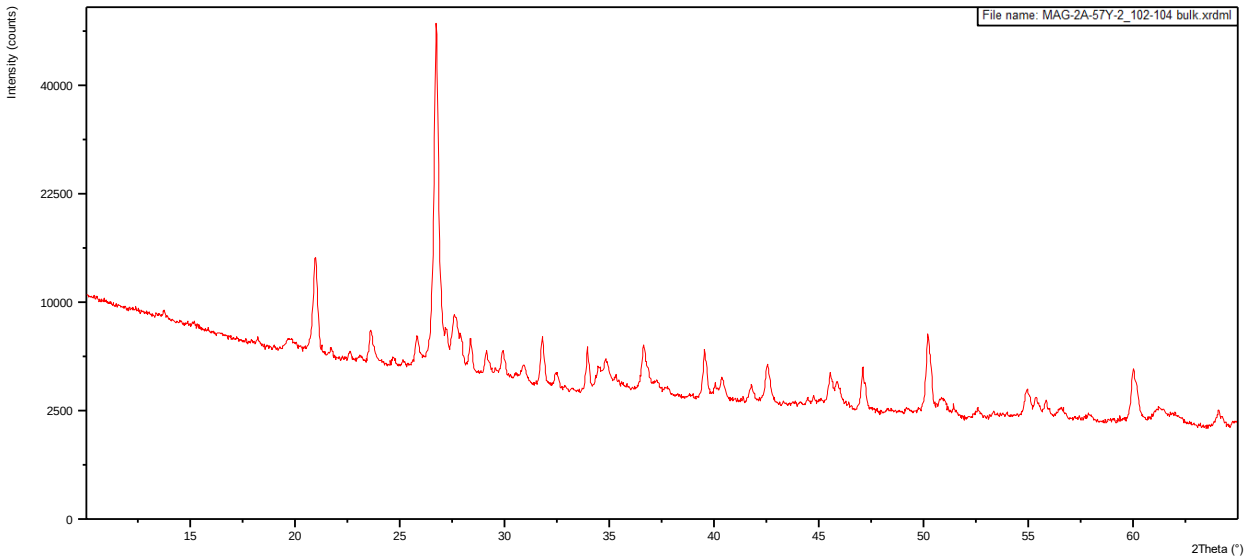
File name: MAG-2A-57Y-2_102-104 bulk.xrdml
Intensity (counts)
40000
22500
10000
2500
0
15
20
25
30
35
40
45
50
55
60
2Theta (°)

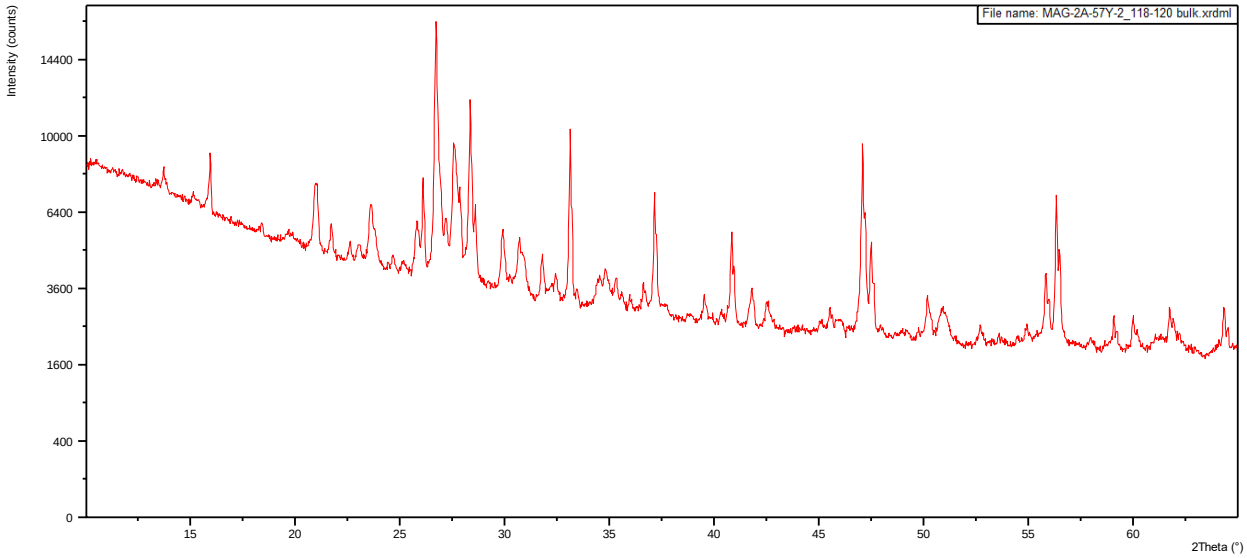
File name: MAG-2A-57Y-2_118-120 bulk.xrdml
Intensity (counts)
14400
10000
6400
3600
1600
400
0
15
20
25
30
35
40
45
50
55
60
2Theta (°)

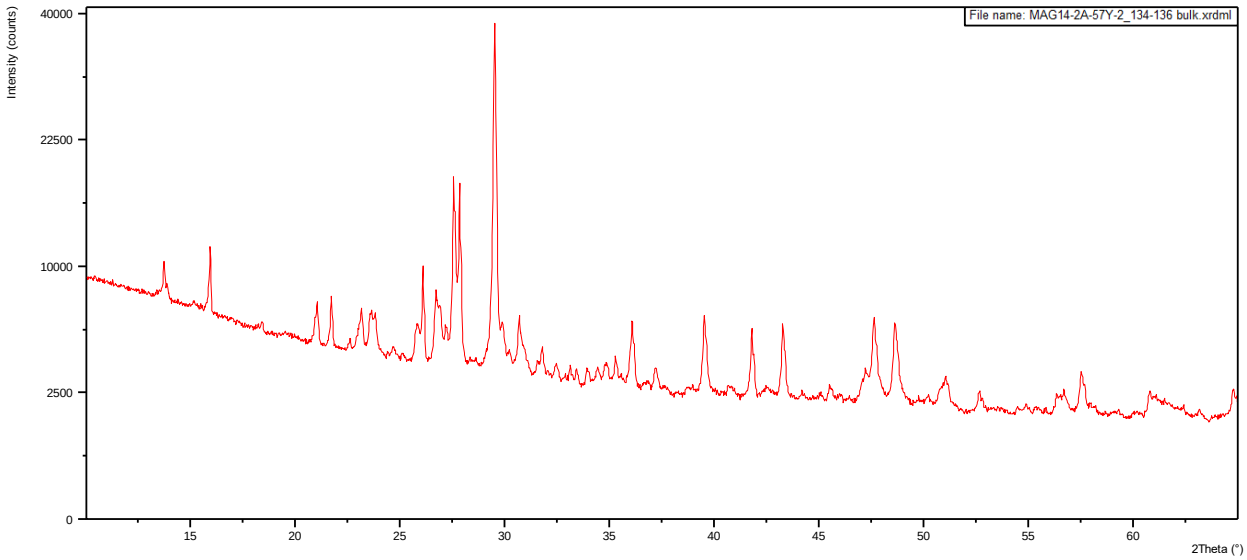
File name: MAG14-2A-57Y-2_134-136 bulk.xrdml
Intensity (counts)
40000
22500
10000
2500
0
15
20
25
30
35
40
45
50
55
60
2Theta (°)

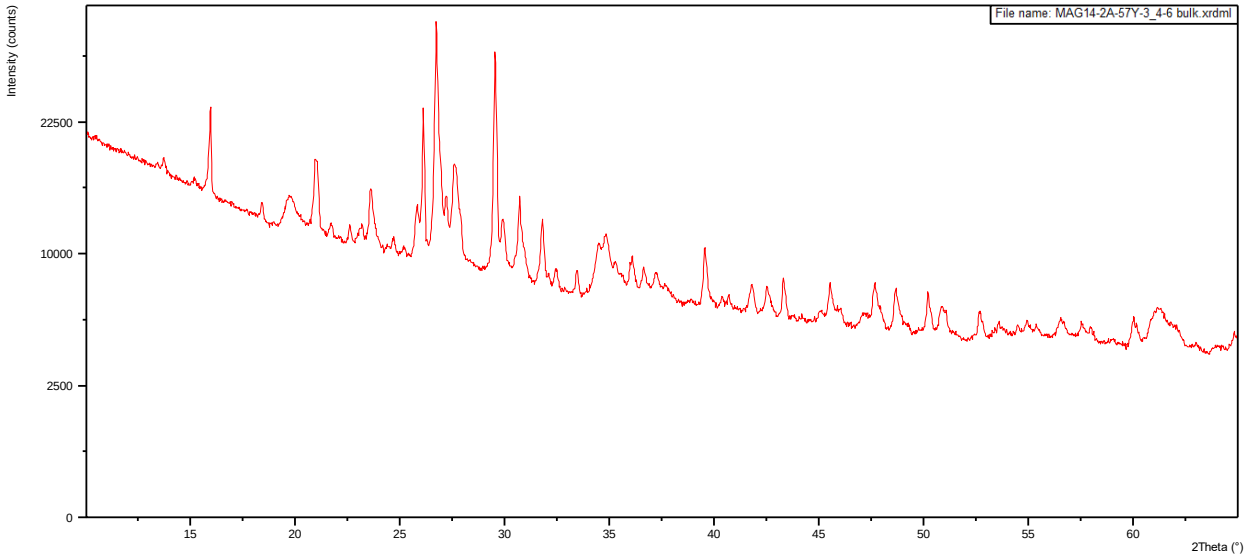
File name: MAG14-2A-57Y-3_4-6 bulk.xrdml
Intensity (counts)
22500
10000
2500
0
15
20
25
30
35
40
45
50
55
60
2Theta (°)

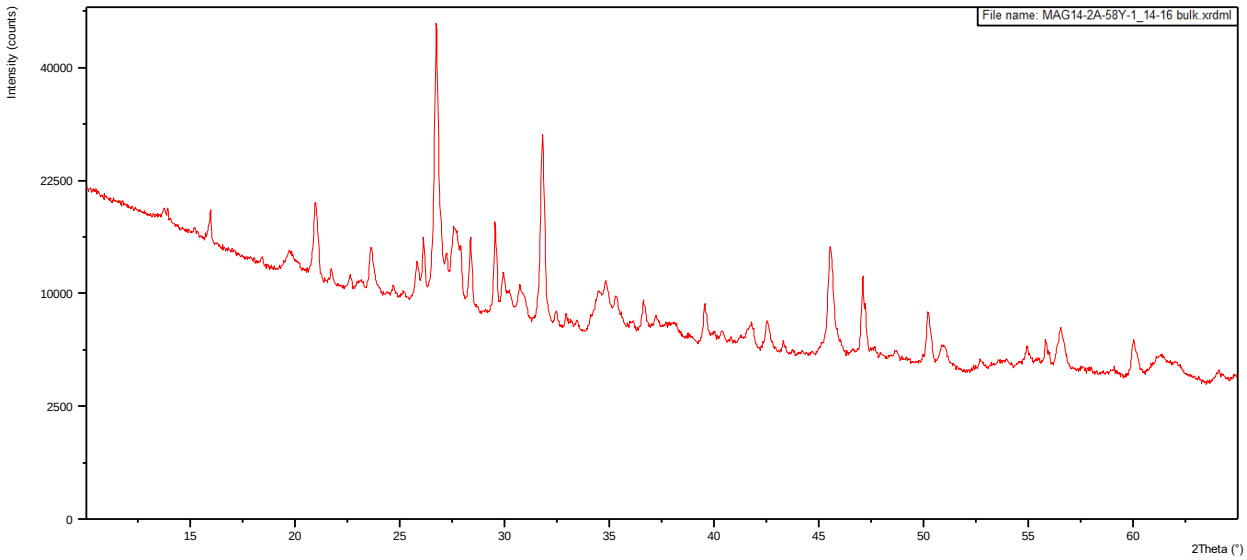
File name: MAG14-2A-58Y-1_14-16 bulk.xrdml
Intensity (counts)
40000
22500
10000
2500
0
15
20
25
30
35
40
45
50
55
60
2Theta (°)

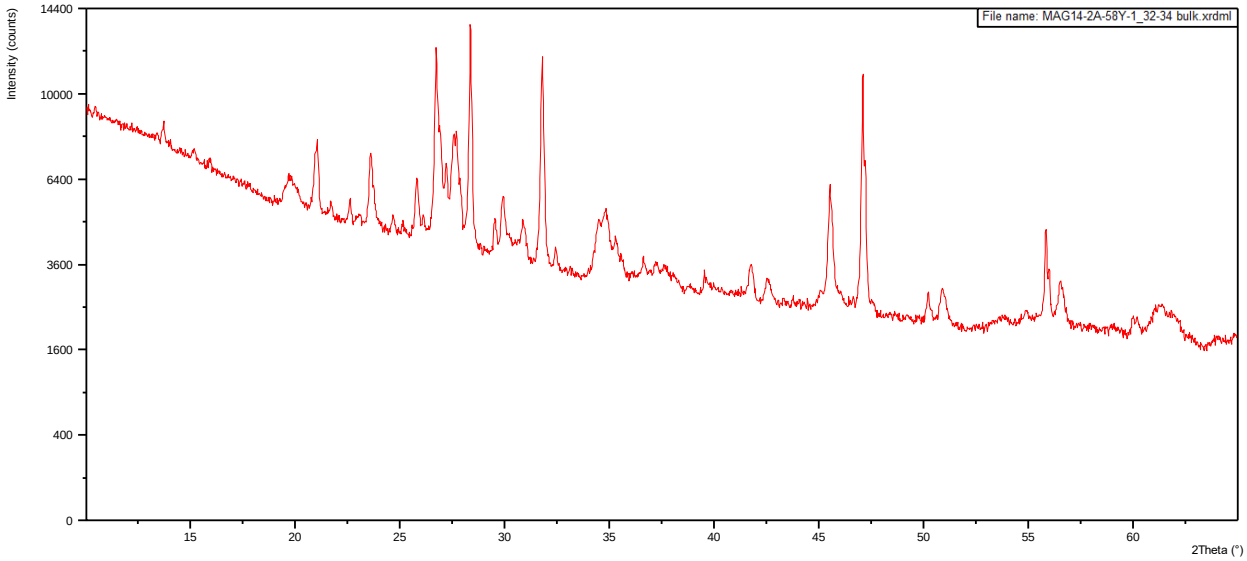
File name: MAG14-2A-58Y-1_32-34 bulk.xrdml
Intensity (counts)
14400
10000
6400
3600
1600
400
0
15
20
25
30
35
40
45
50
55
60
2Theta (°)

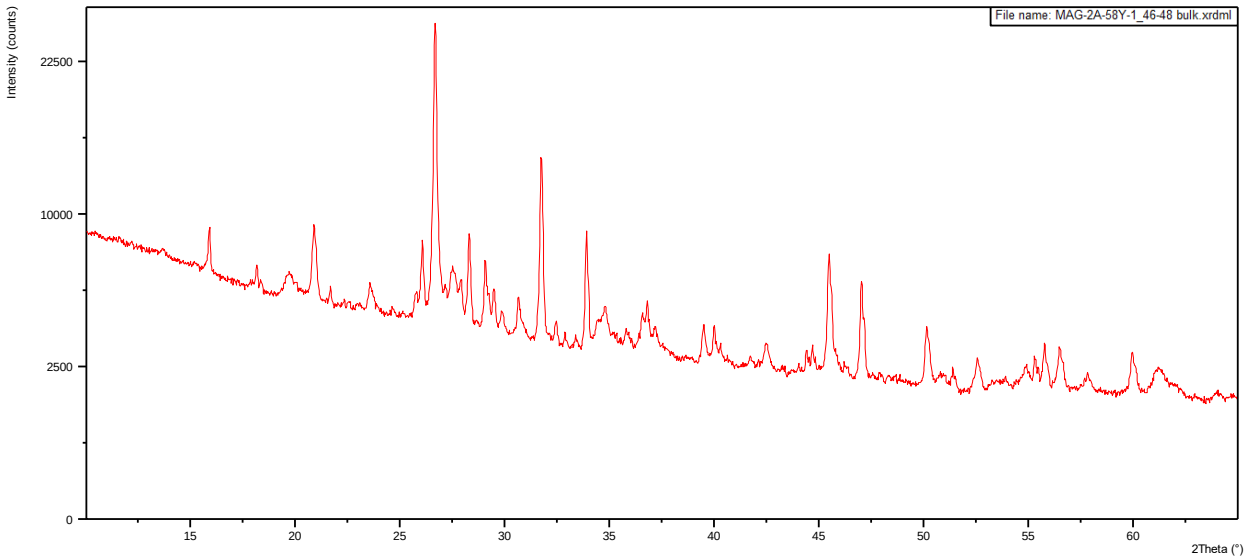
File name: MAG-2A-58Y-1_46-48 bulk.xrdml
Intensity (counts)
22500
10000
2500
0
15
20
25
30
35
40
45
50
55
60
2Theta (°)

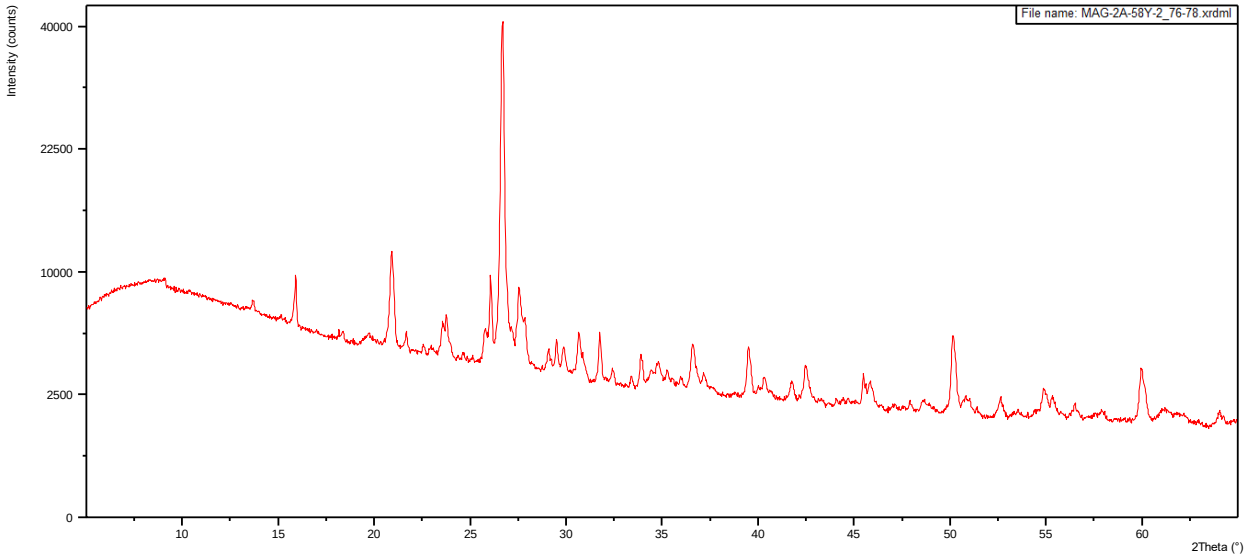
File name: MAG-2A-58Y-2_76-78.xrdml
Intensity (counts)
40000
22500
10000
2500
0
10
15
20
25
30
35
40
45
50
55
60
2Theta (°)

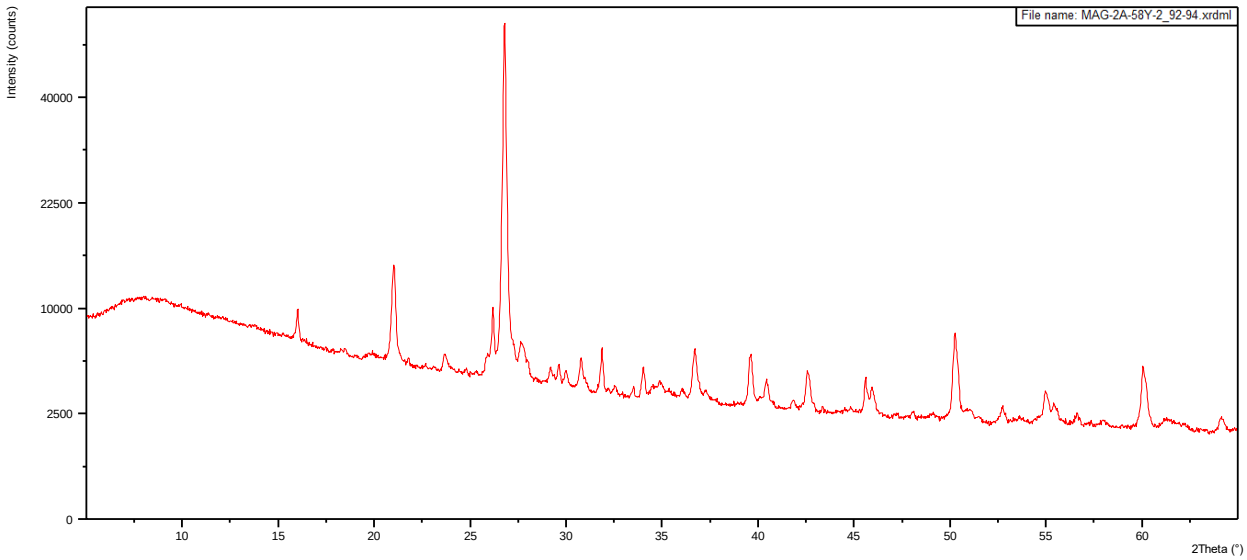
File name: MAG-2A-58Y-2_92-94.xrdml
Intensity (counts)
40000
22500
10000
2500
0
10
15
20
25
30
35
40
45
50
55
60
2Theta (°)

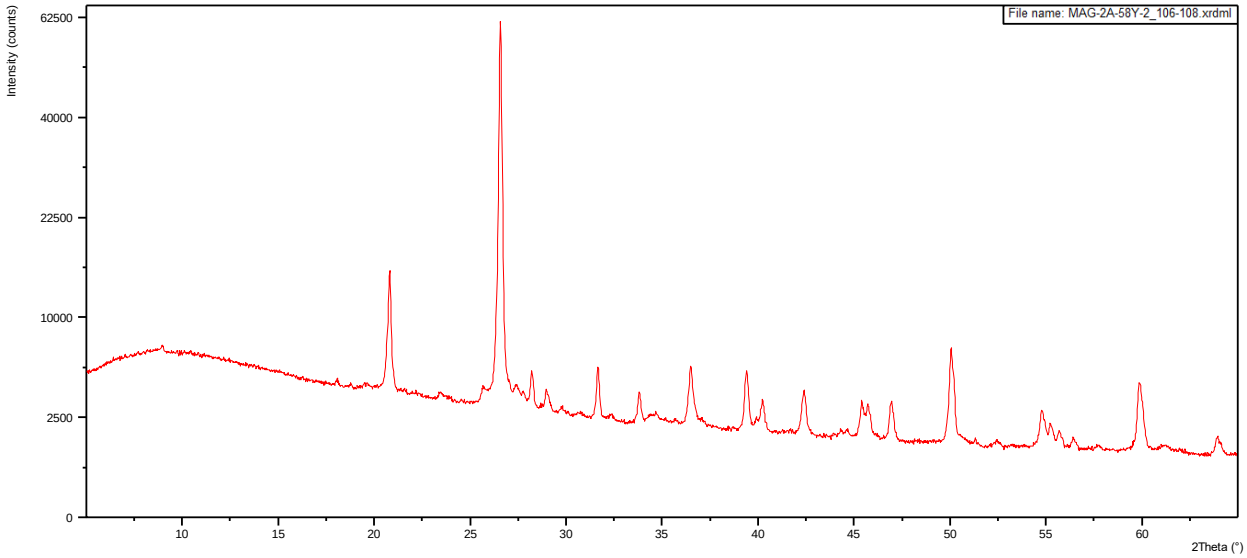
File name: MAG-2A-58Y-2_106-108.xrdml
Intensity (counts)
62500
40000
22500
10000
2500
0
10
15
20
25
30
35
40
45
50
55
60
2Theta (°)

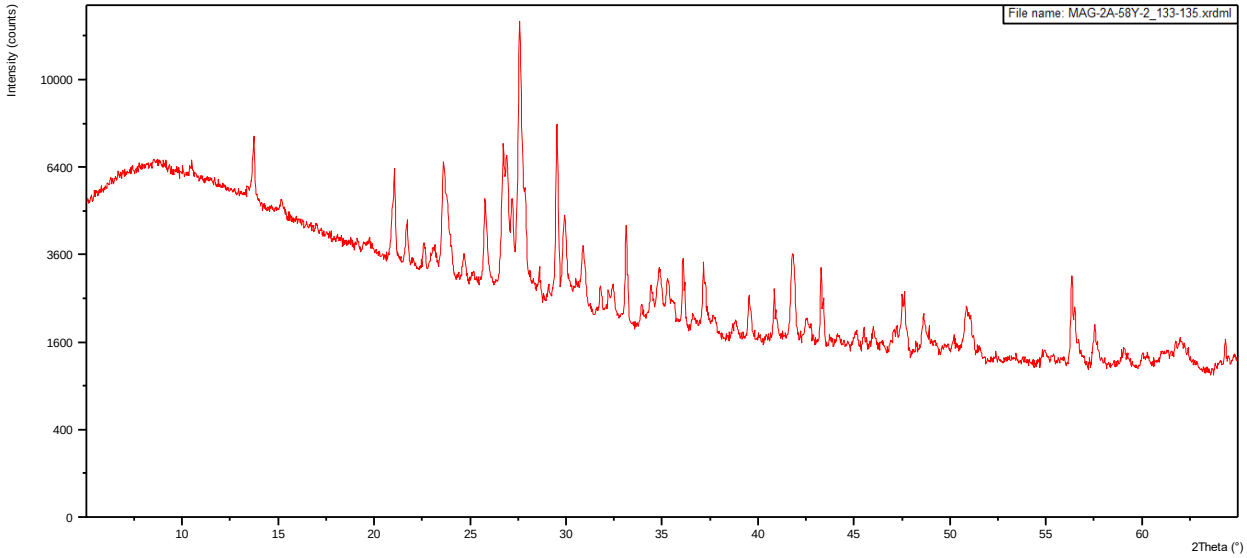
File name: MAG-2A-58Y-2_133-135.xrdml
Intensity (counts)
10000
6400
3600
1600
400
0
10
15
20
25
30
35
40
45
50
55
60
2Theta (°)

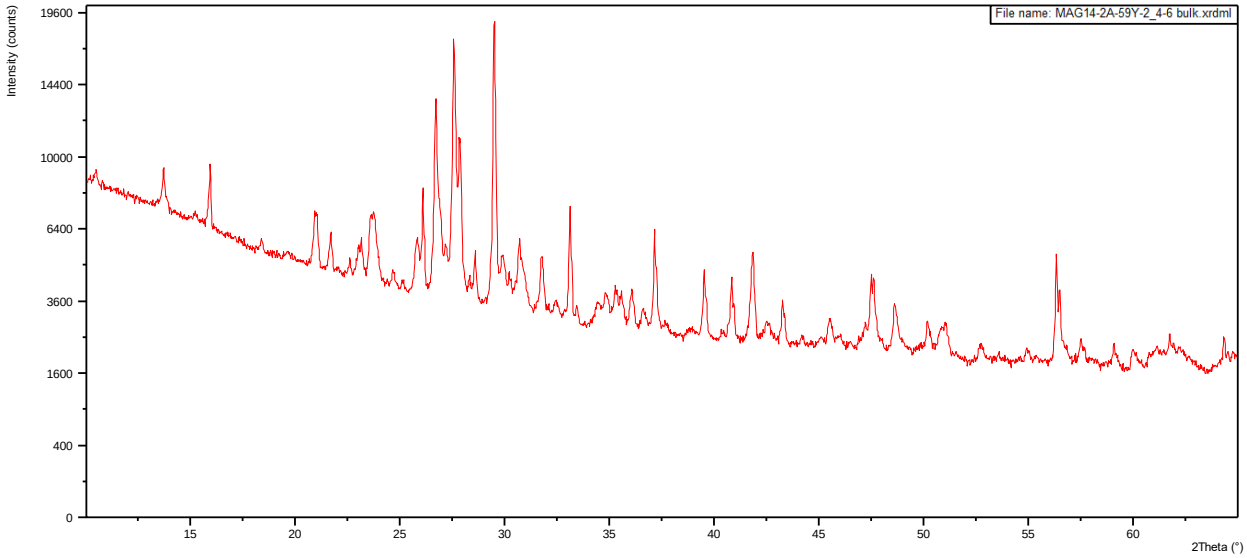
File name: MAG14-2A-59Y-2_4-6 bulk.xrdml
Intensity (counts)
19600
14400
10000
6400
3600
1600
400
0
15
20
25
30
35
40
45
50
55
60
2Theta (°)

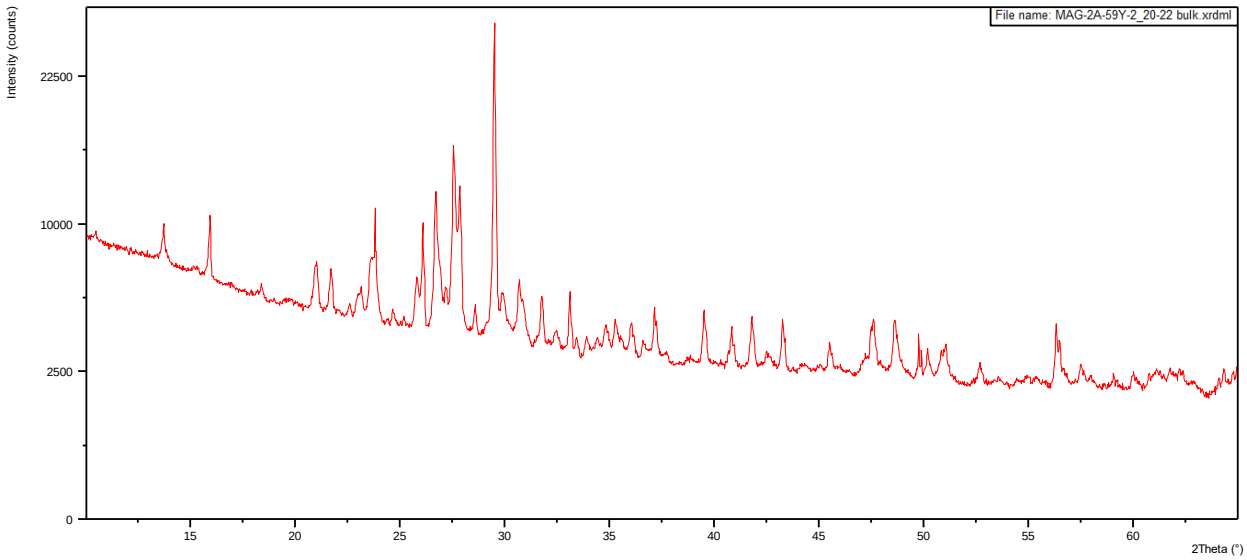
File name: MAG-2A-59Y-2_20-22 bulk.xrdml
Intensity (counts)
22500
10000
2500
0
15
20
25
30
35
40
45
50
55
60
2Theta (°)

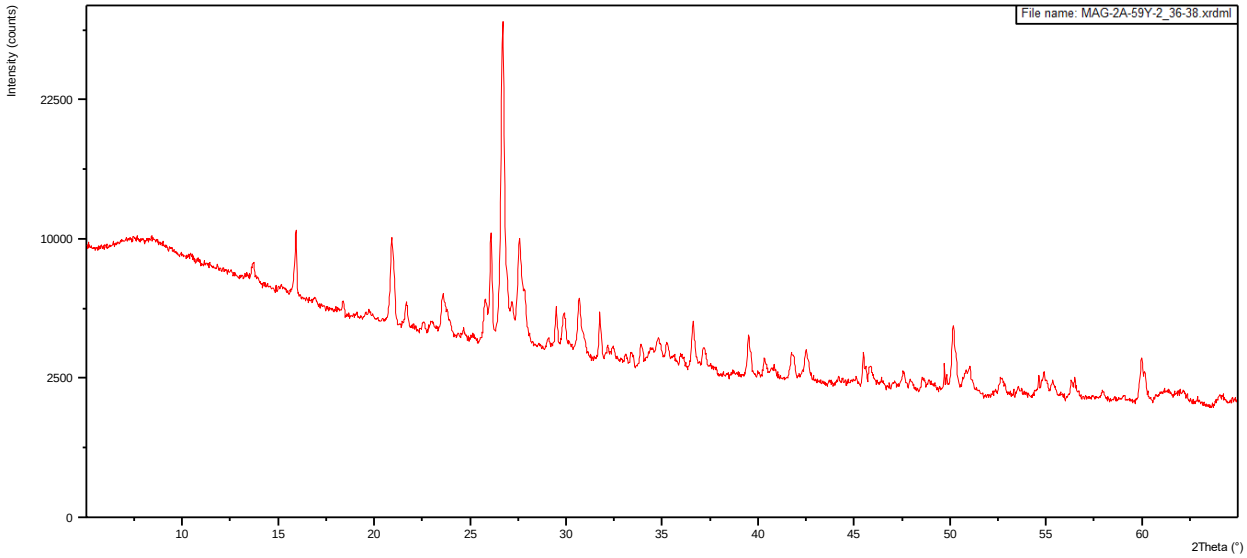
File name: MAG-2A-59Y-2_36-38.xrdml
Intensity (counts)
22500
10000
2500
0
10
15
20
25
30
35
40
45
50
55
60
2Theta (°)

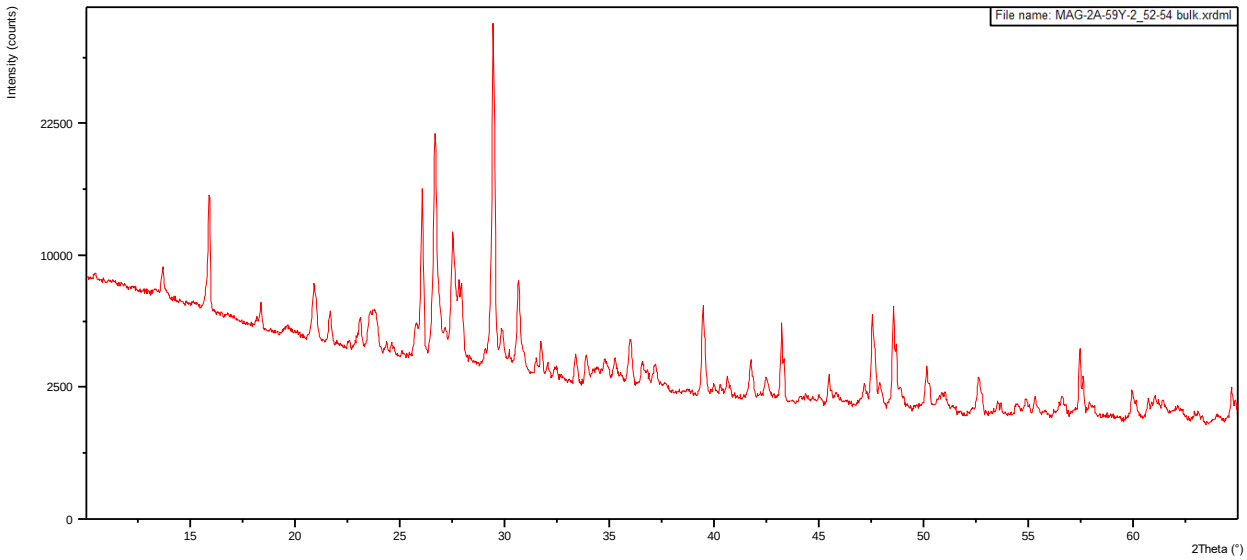
File name: MAG-2A-59Y-2_52-54 bulk.xrdml
Intensity (counts)
22500
10000
2500
0
15
20
25
30
35
40
45
50
55
60
2Theta (°)

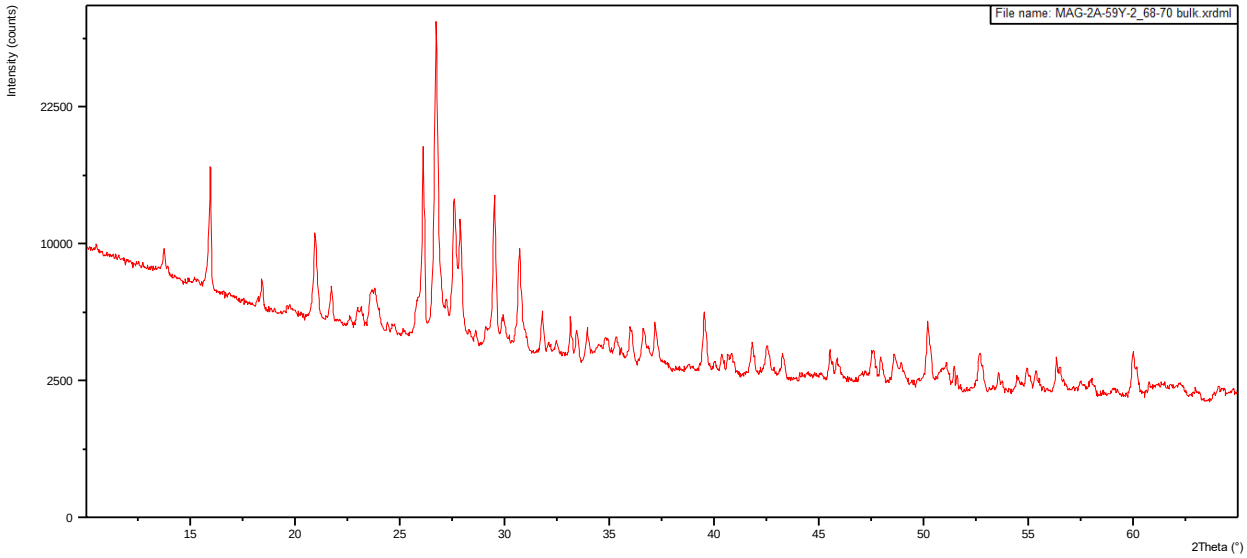
File name: MAG-2A-59Y-2_68-70 bulk.xrdml
Intensity (counts)
22500
10000
2500
0
15
20
25
30
35
40
45
50
55
60
2Theta (°)

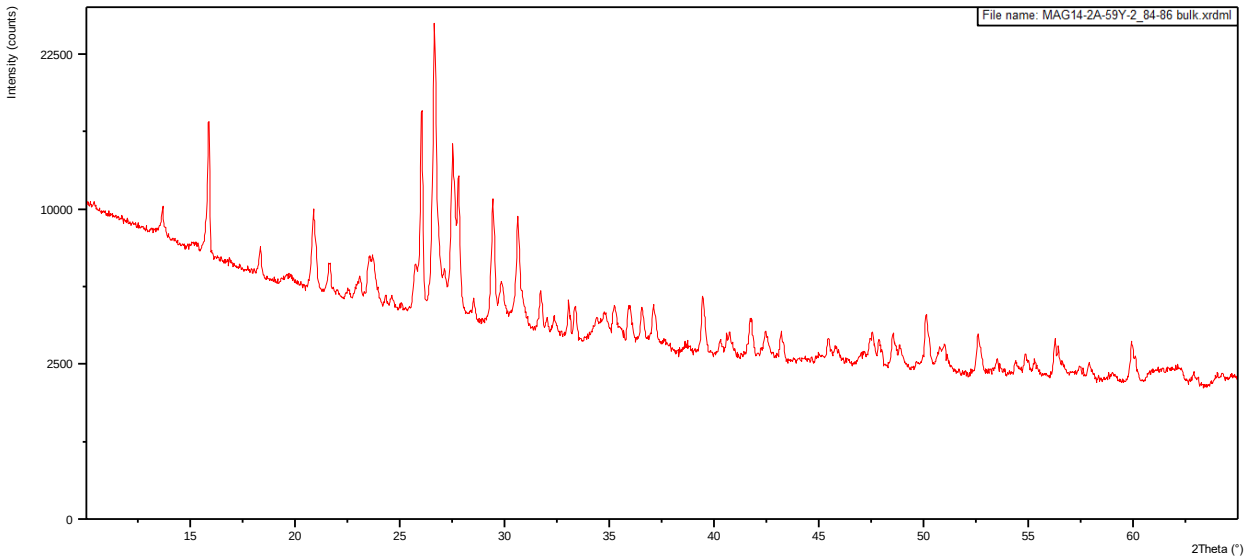
File name: MAG14-2A-59Y-2_84-86 bulk.xrdml
Intensity (counts)
22500
10000
2500
0
15
20
25
30
35
40
45
50
55
60
2Theta (°)

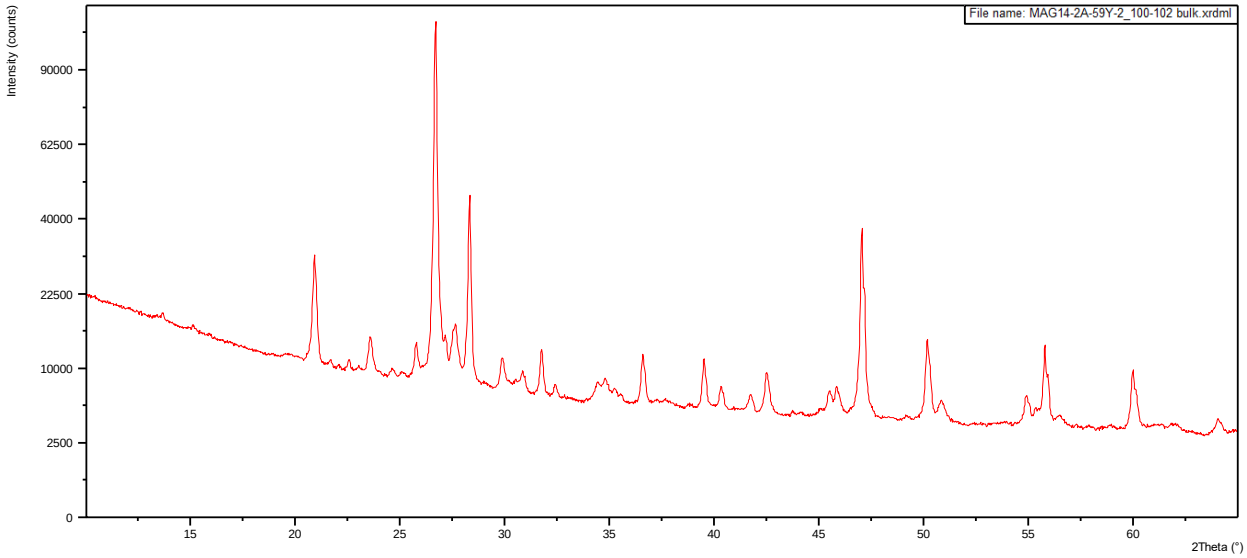
File name: MAG14-2A-59Y-2_100-102 bulk.xrdml
Intensity (counts)
90000
62500
40000
22500
10000
2500
0
15
20
25
30
35
40
45
50
55
60
2Theta (°)

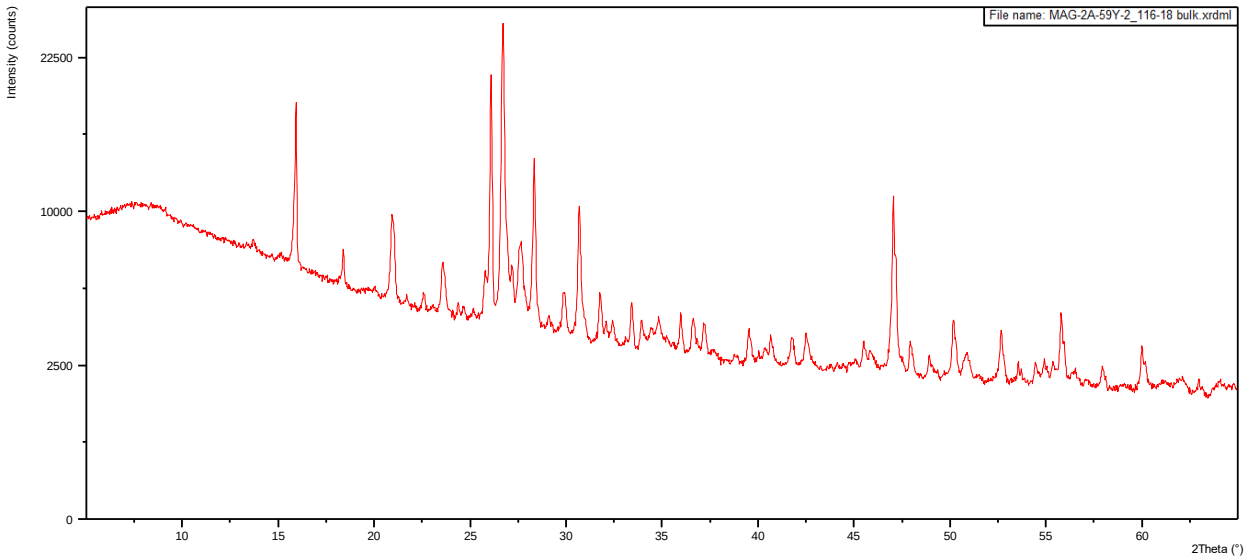
File name: MAG-2A-59Y-2_116-18 bulk.xrdml
Intensity (counts)
22500
10000
2500
0
10
15
20
25
30
35
40
45
50
55
60
2Theta (°)

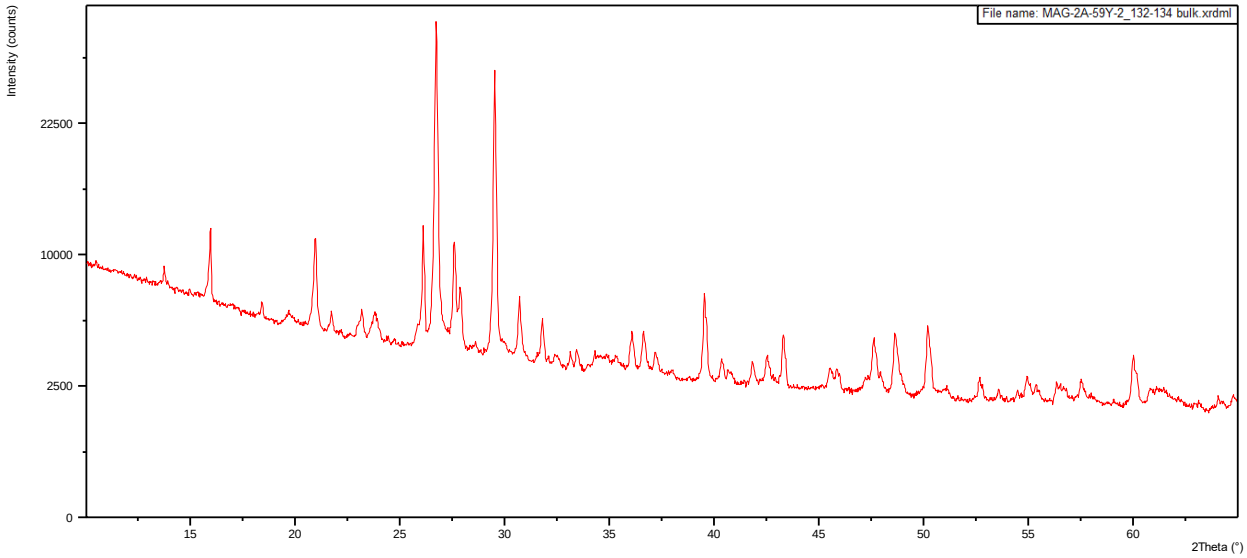
File name: MAG-2A-59Y-2_132-134 bulk.xrdml
Intensity (counts)
22500
10000
2500
0
15
20
25
30
35
40
45
50
55
60
2Theta (°)

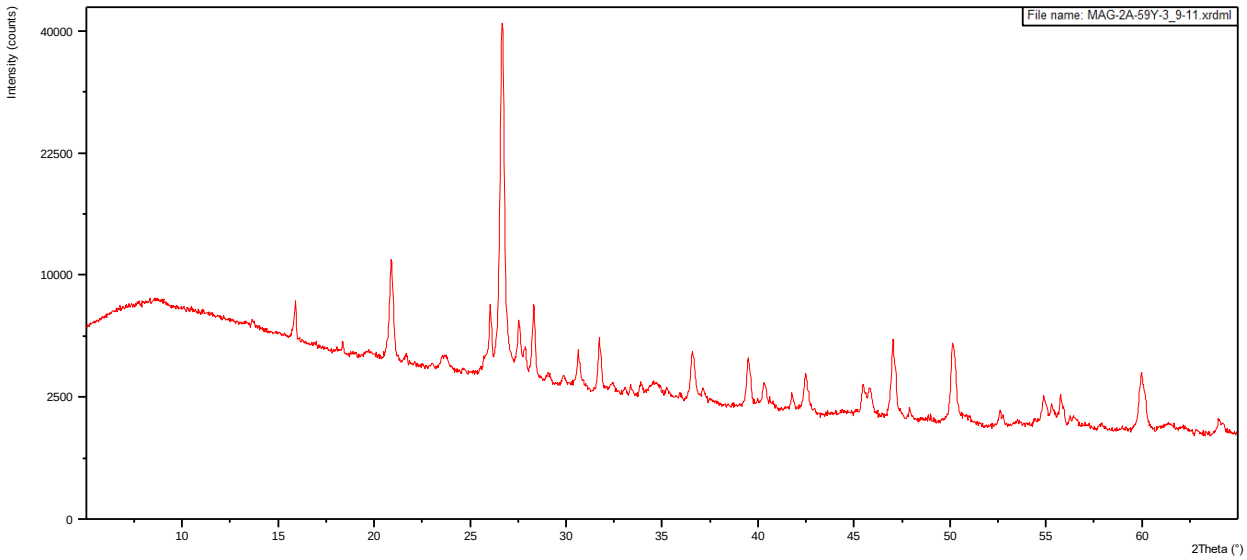
File name: MAG-2A-59Y-3_9-11.xrdml
Intensity (counts)
40000
22500
10000
2500
0
10
15
20
25
30
35
40
45
50
55
60
2Theta (°)

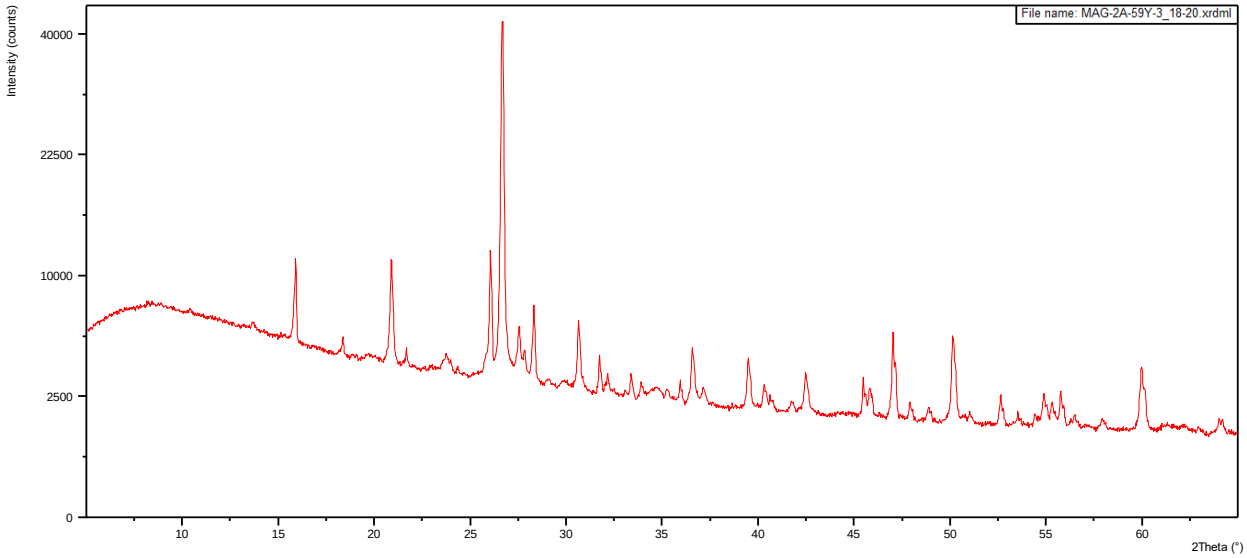
File name: MAG-2A-59Y-3_18-20.xrdml
Intensity (counts)
40000
22500
10000
2500
0
10
15
20
25
30
35
40
45
50
55
60
2Theta (°)

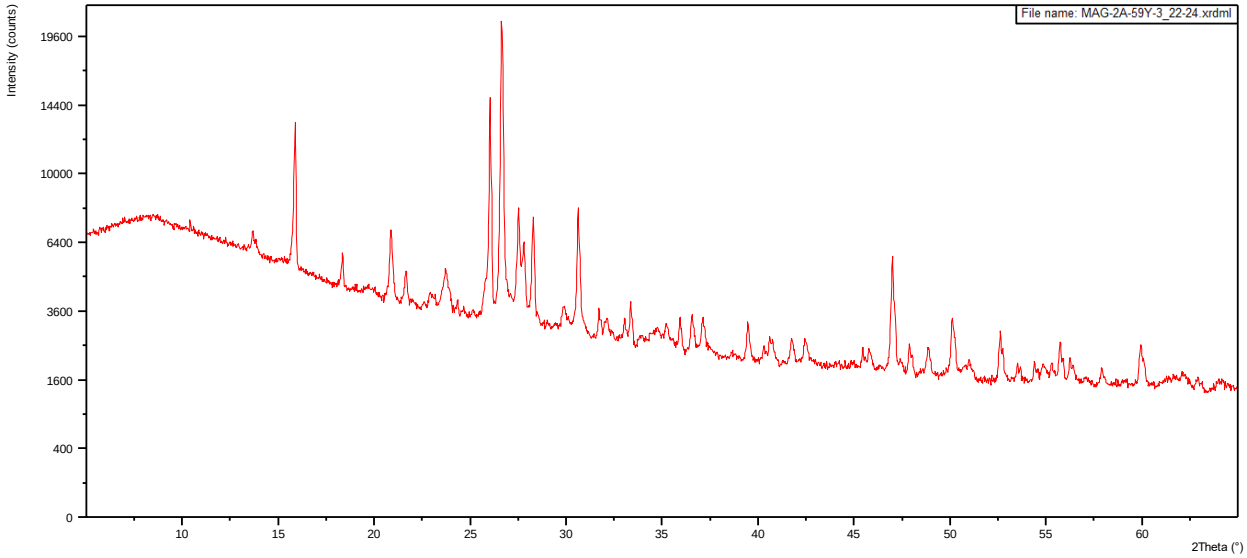
File name: MAG-2A-59Y-3_22-24.xrdml
Intensity (counts)
19600
14400
10000
6400
3600
1600
400
0
10
15
20
25
30
35
40
45
50
55
60
2Theta (°)

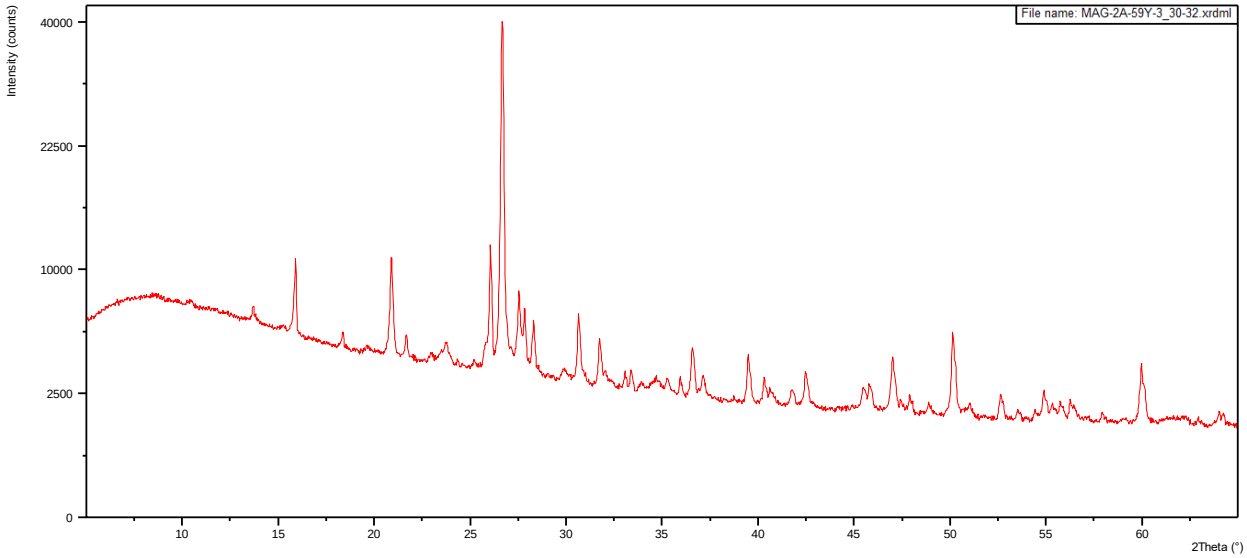
File name: MAG-2A-59Y-3_30-32.xrdml
Intensity (counts)
40000
22500
10000
2500
0
10
15
20
25
30
35
40
45
50
55
60
2Theta (°)

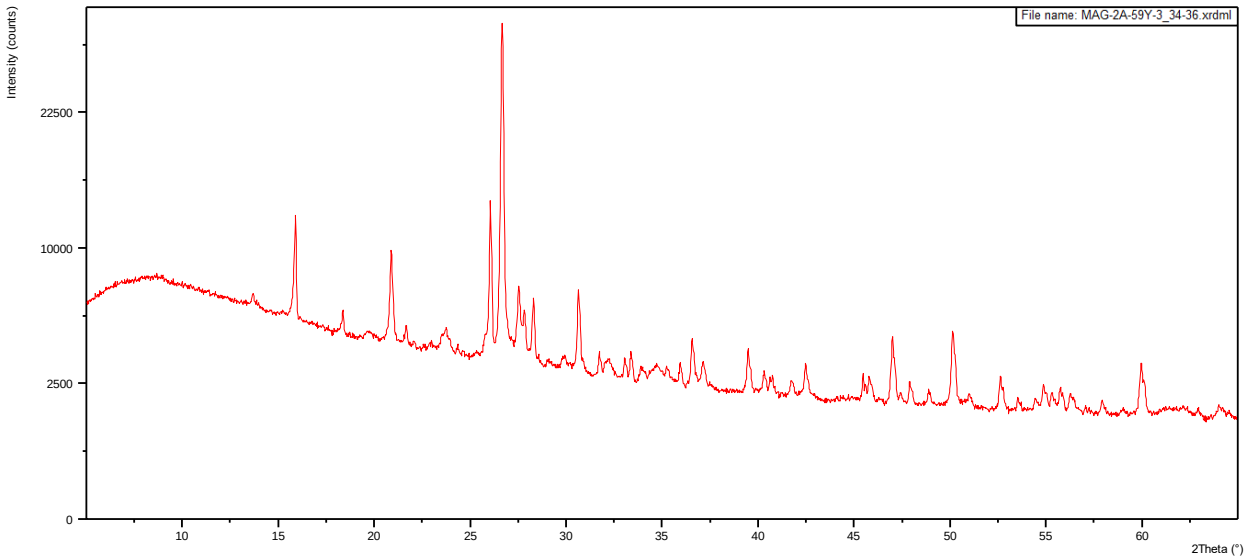
File name: MAG-2A-59Y-3_34-36.xrdml
Intensity (counts)
22500
10000
2500
0
10
15
20
25
30
35
40
45
50
55
60
2Theta (°)

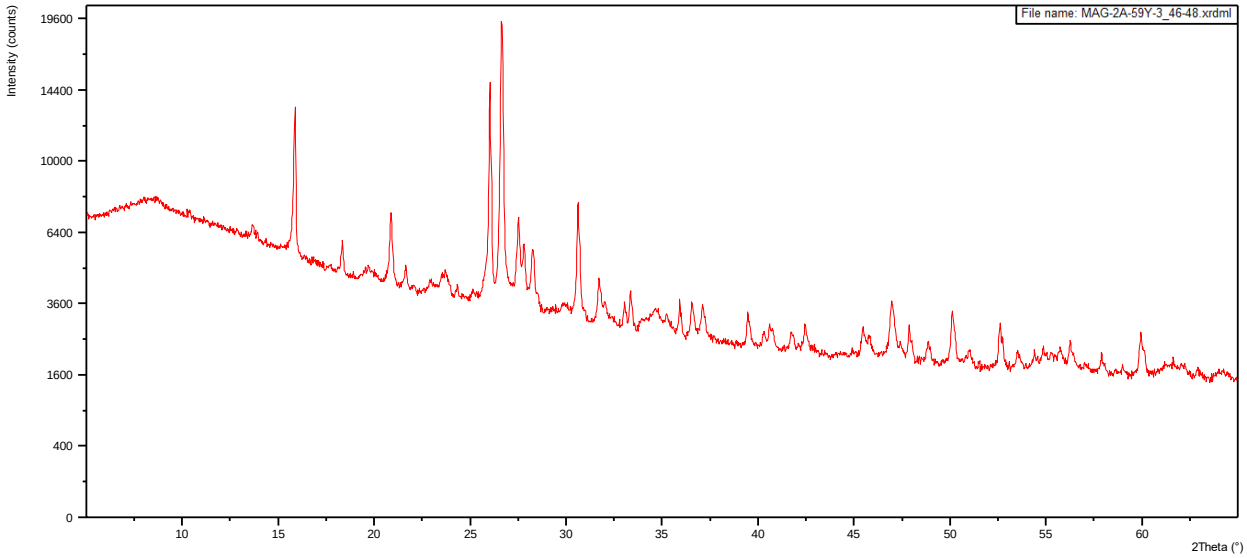
File name: MAG-2A-59Y-3_46-48.xrdml
Intensity (counts)
19600
14400
10000
6400
3600
1600
400
0
10
15
20
25
30
35
40
45
50
55
60
2Theta (°)

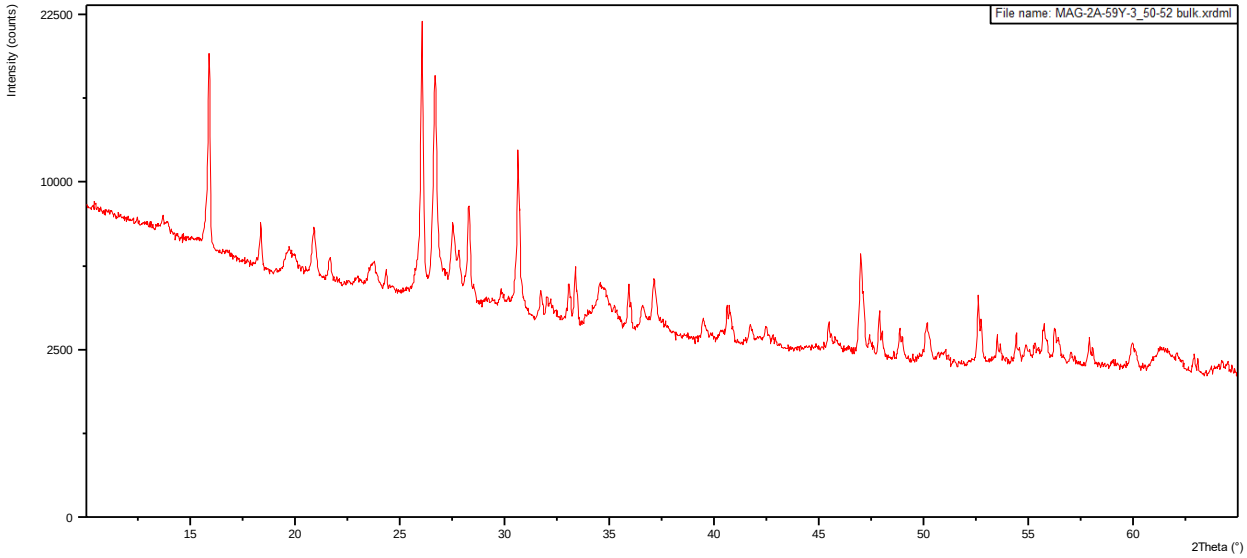
File name: MAG-2A-59Y-3_50-52 bulk.xrdml
Intensity (counts)
22500
10000
2500
0
15
20
25
30
35
40
45
50
55
60
2Theta (°)

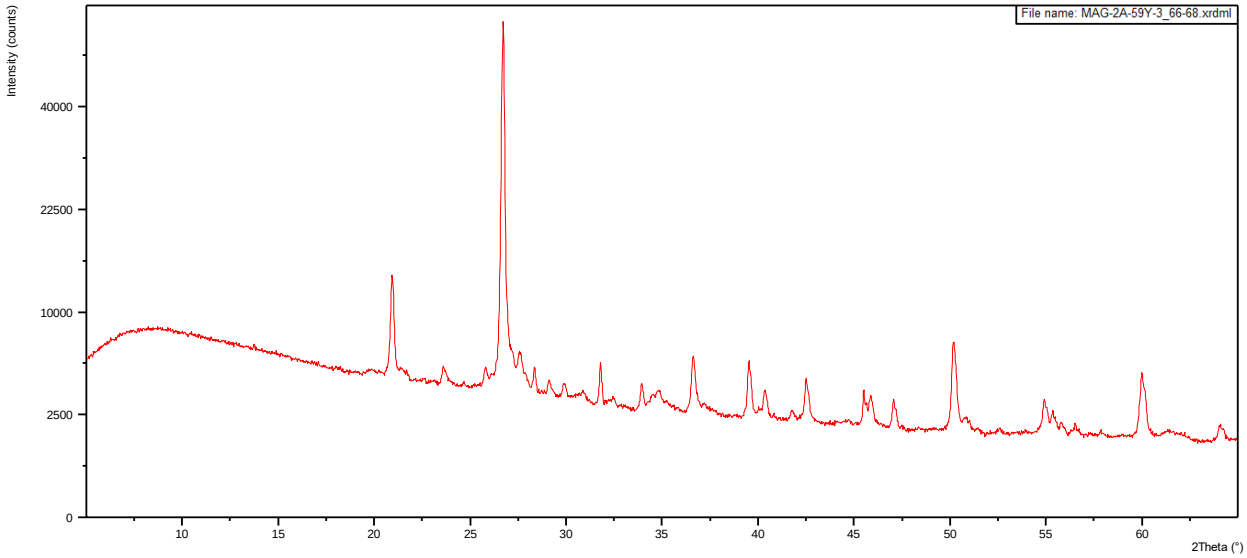
File name: MAG-2A-59Y-3_66-68.xrdml
Intensity (counts)
40000
22500
10000
2500
0
10
15
20
25
30
35
40
45
50
55
60
2Theta (°)

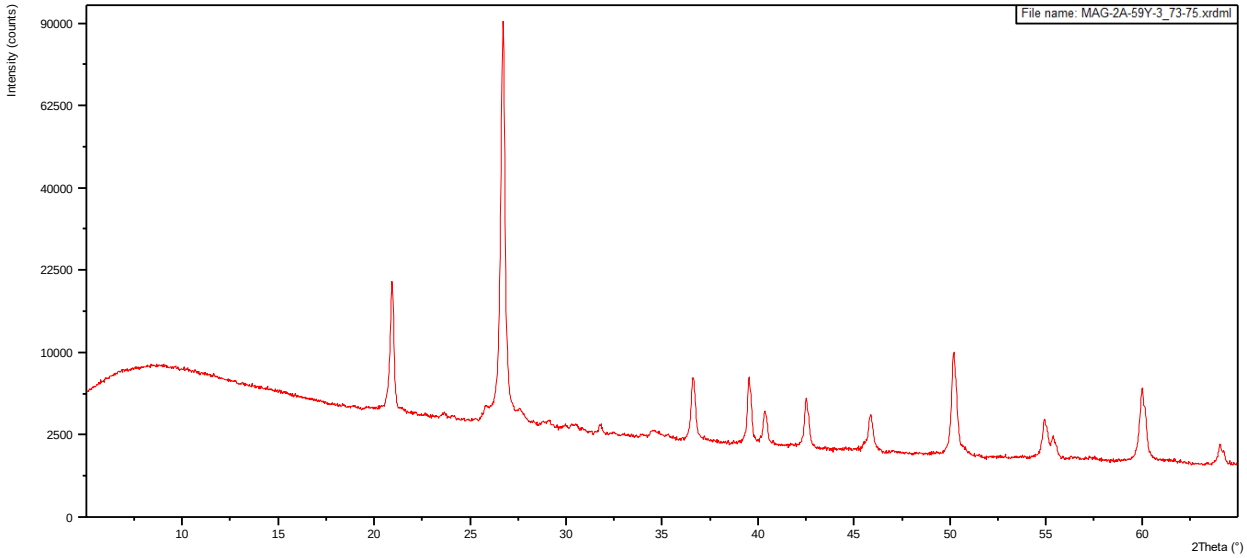
File name: MAG-2A-59Y-3_73-75.xrdml
Intensity (counts)
90000
62500
40000
22500
10000
2500
0
10
15
20
25
30
35
40
45
50
55
60
2Theta (°)

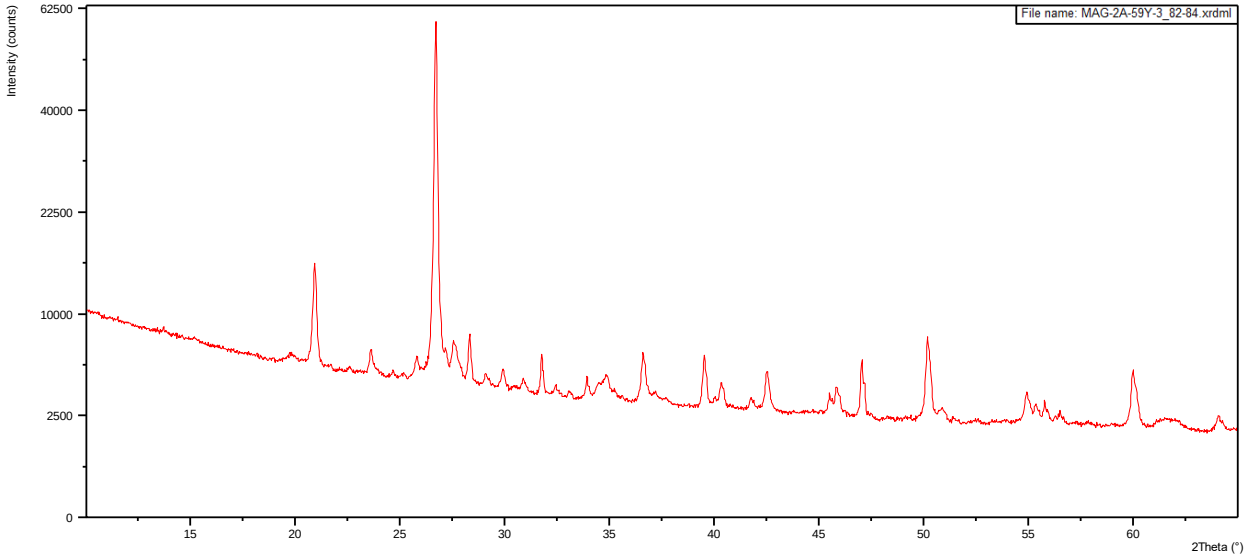
File name: MAG-2A-59Y-3_82-84.xrdml
Intensity (counts)
62500
40000
22500
10000
2500
0
15
20
25
30
35
40
45
50
55
60
2Theta (°)

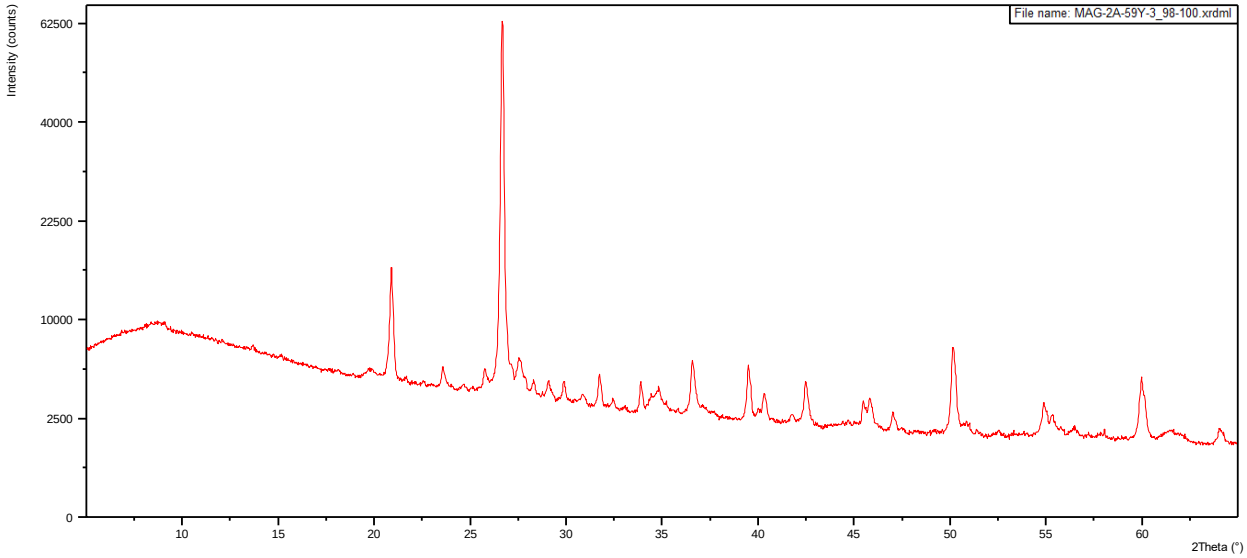
File name: MAG-2A-59Y-3_98-100.xrdml
Intensity (counts)
62500
40000
22500
10000
2500
0
10
15
20
25
30
35
40
45
50
55
60
2Theta (°)

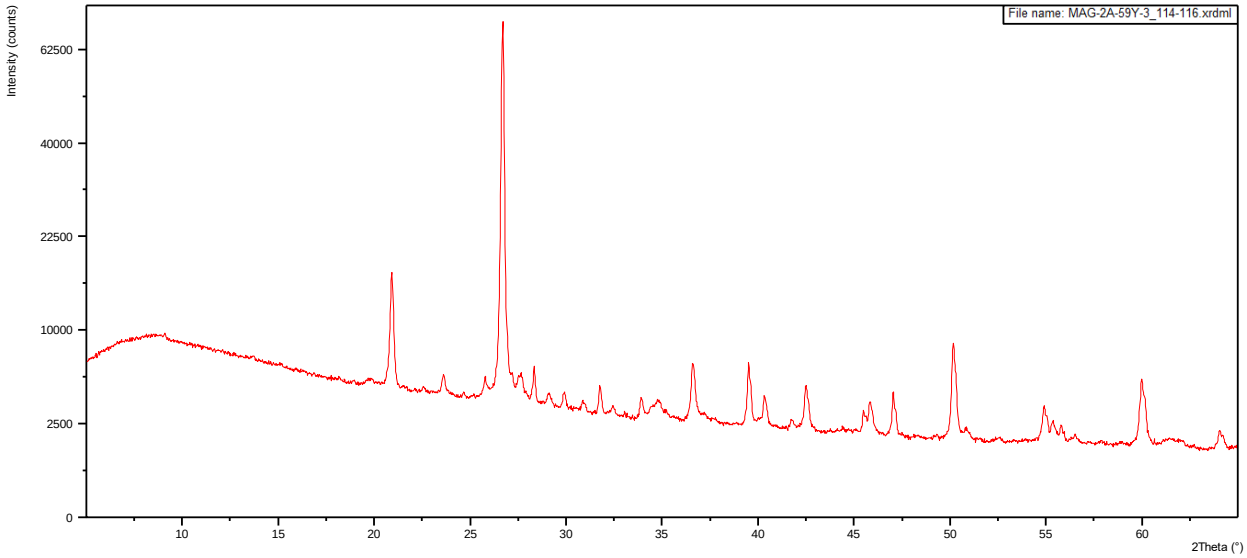
File name: MAG-2A-59Y-3_114-116.xrdml
Intensity (counts)
62500
40000
22500
10000
2500
0
10
15
20
25
30
35
40
45
50
55
60
2Theta (°)

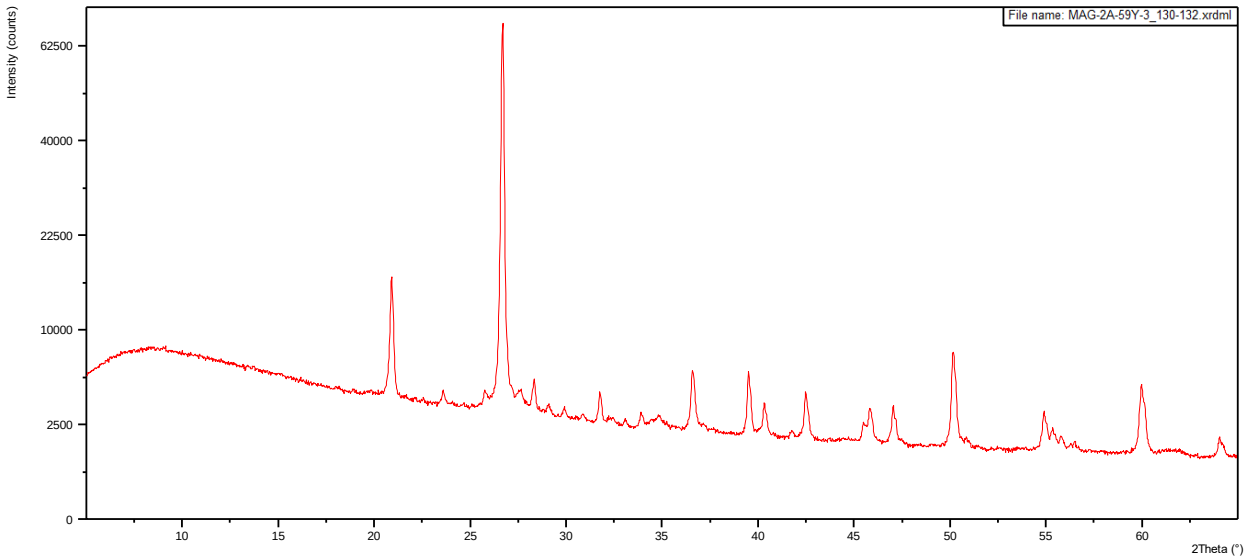
File name: MAG-2A-59Y-3_130-132.xrdml
Intensity (counts)
62500
40000
22500
10000
2500
0
10
15
20
25
30
35
40
45
50
55
60
2Theta (°)

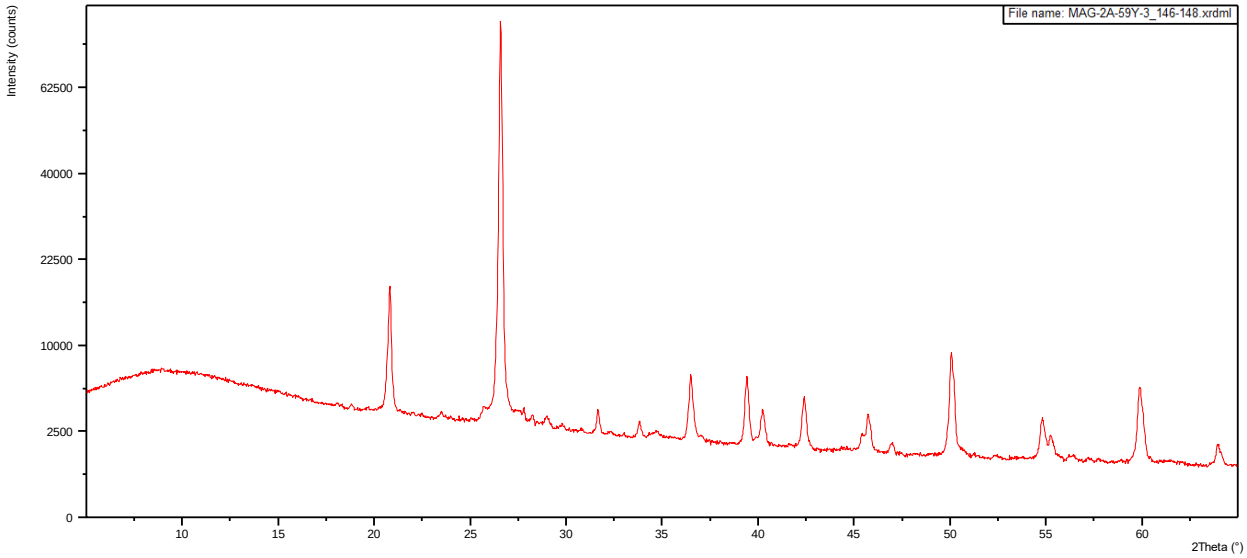
File name: MAG-2A-59Y-3_146-148.xrdml
Intensity (counts)
62500
40000
22500
10000
2500
0
10
15
20
25
30
35
40
45
50
55
60
2Theta (°)

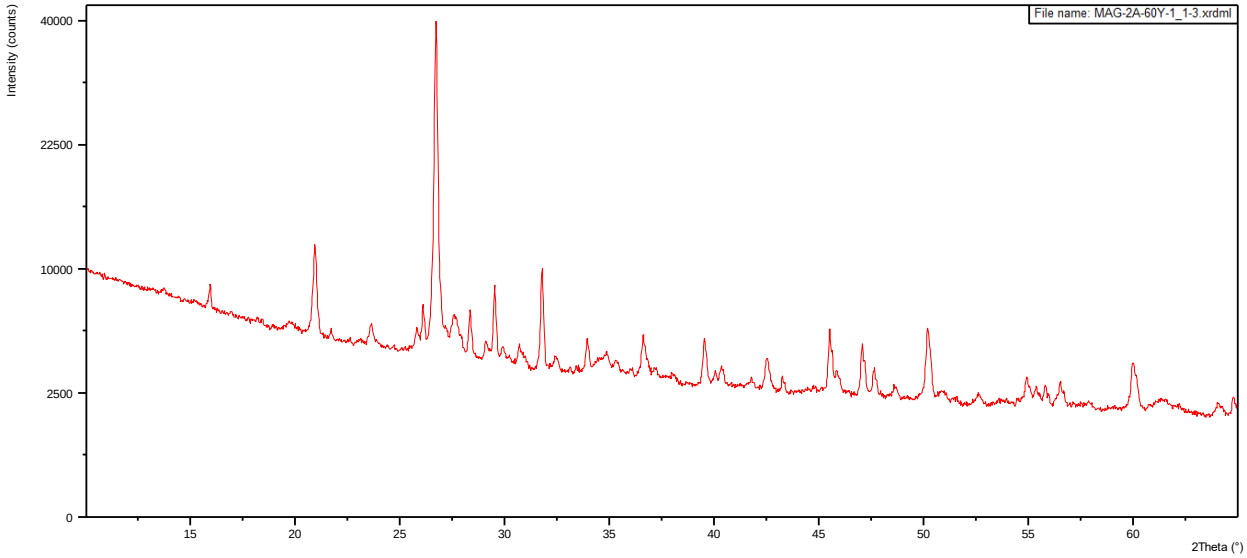
File name: MAG-2A-60Y-1_1-3.xrdml
Intensity (counts)
40000
22500
10000
2500
0
15
20
25
30
35
40
45
50
55
60
2Theta (°)

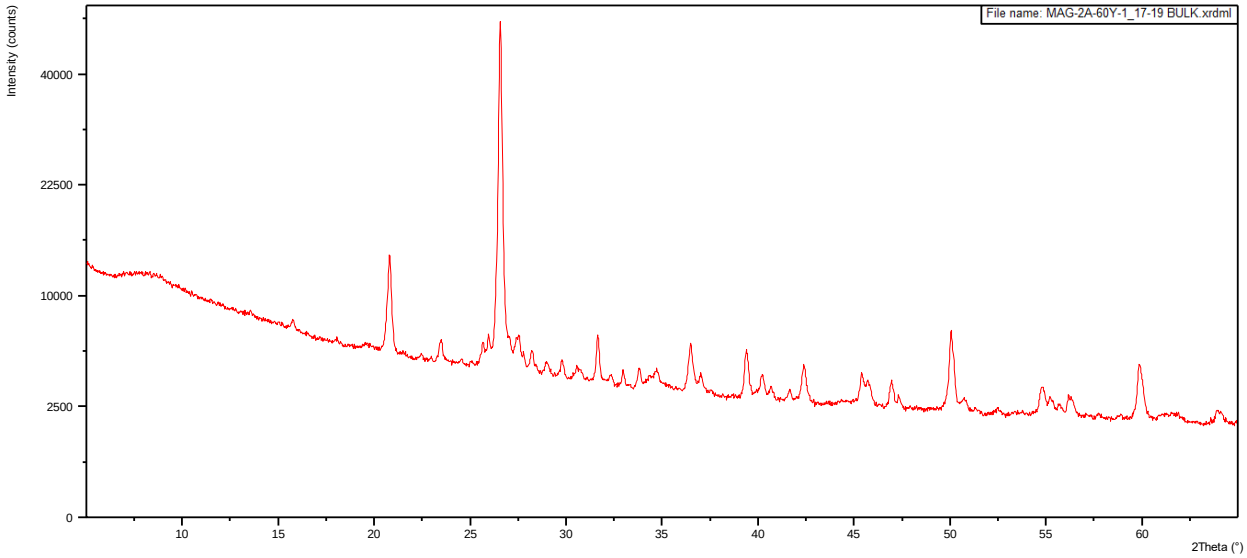
File name: MAG-2A-60Y-1_17-19 BULK.xrdml
Intensity (counts)
40000
22500
10000
2500
0
10
15
20
25
30
35
40
45
50
55
60
2Theta (°)

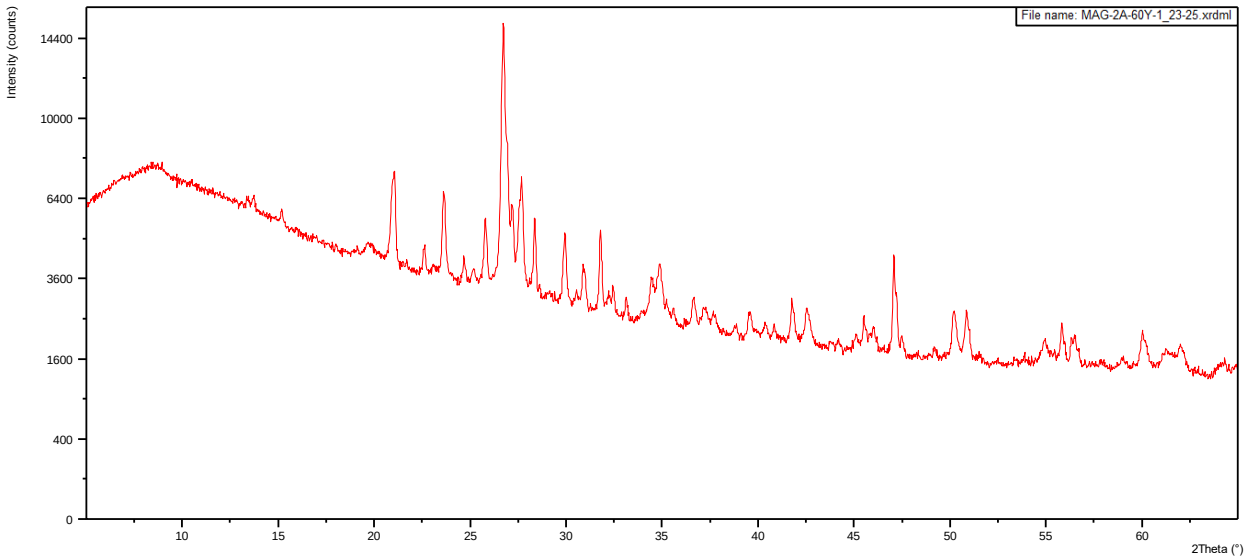
File name: MAG-2A-60Y-1_23-25.xrdml
Intensity (counts)
14400
10000
6400
3600
1600
400
0
10
15
20
25
30
35
40
45
50
55
60
2Theta (°)

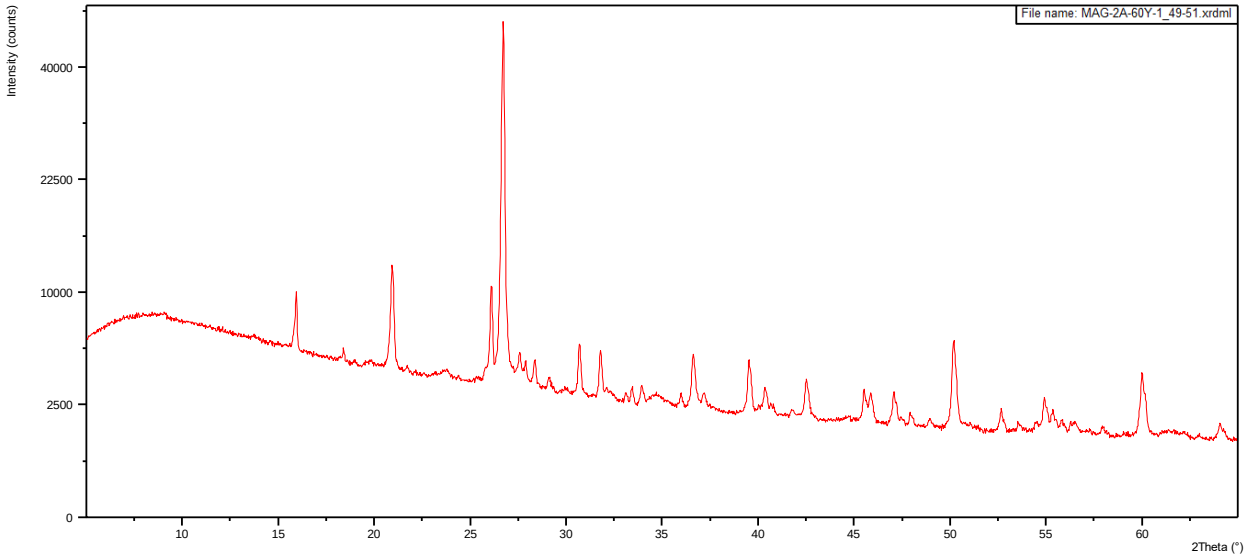
File name: MAG-2A-60Y-1_49-51.xrdml
Intensity (counts)
40000
22500
10000
2500
0
10
15
20
25
30
35
40
45
50
55
60
2Theta (°)

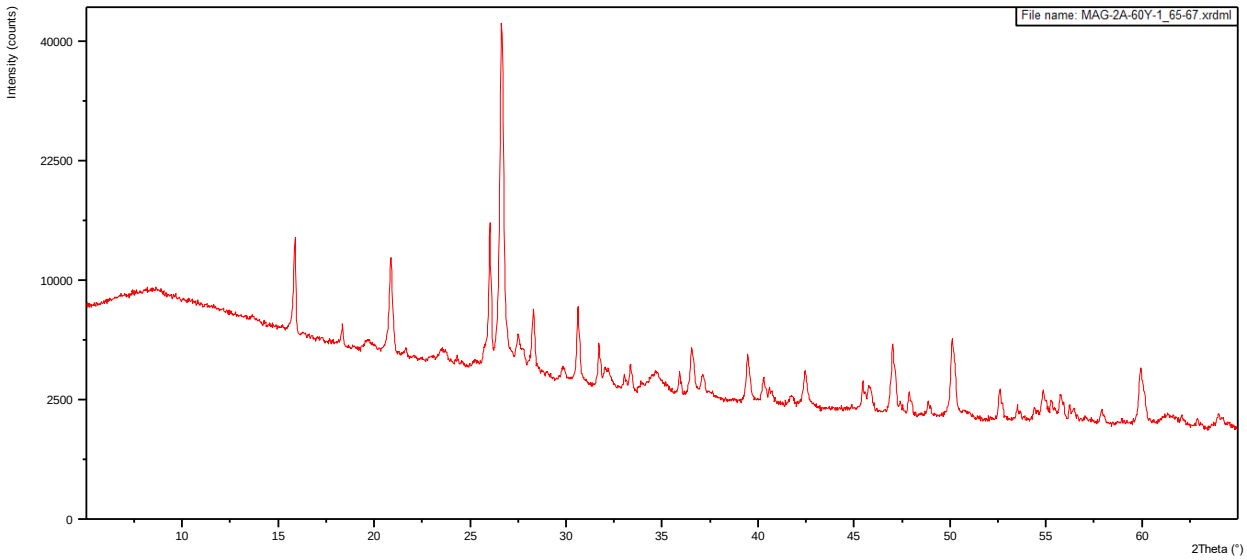
File name: MAG-2A-60Y-1_65-67.xrdml
Intensity (counts)
40000
22500
10000
2500
0
10
15
20
25
30
35
40
45
50
55
60
2Theta (°)

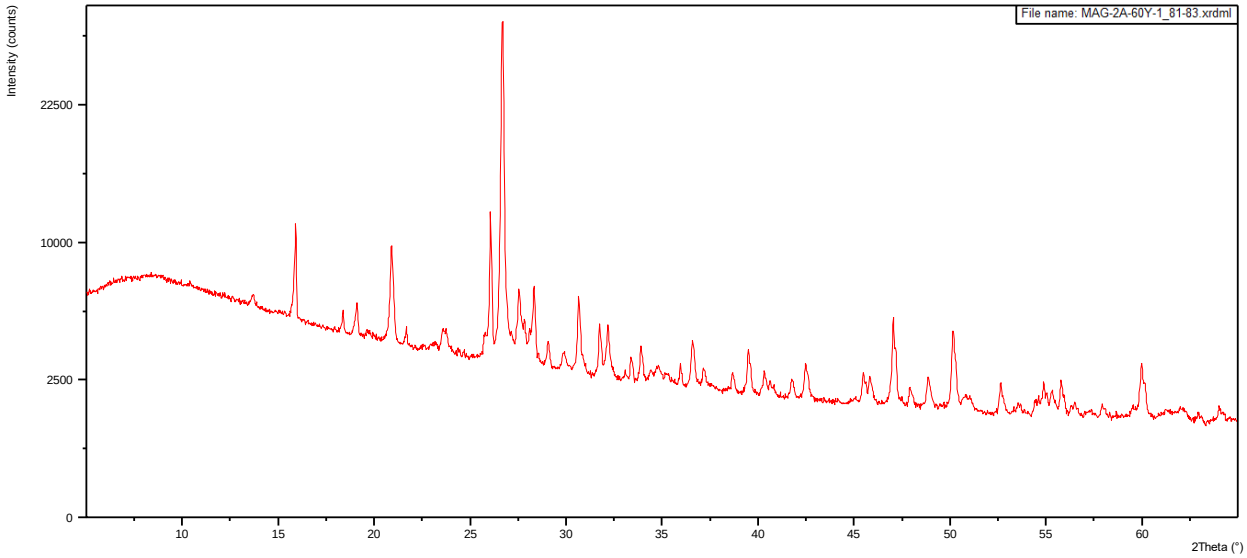
File name: MAG-2A-60Y-1_81-83.xrdml
Intensity (counts)
22500
10000
2500
0
10
15
20
25
30
35
40
45
50
55
60
2Theta (°)

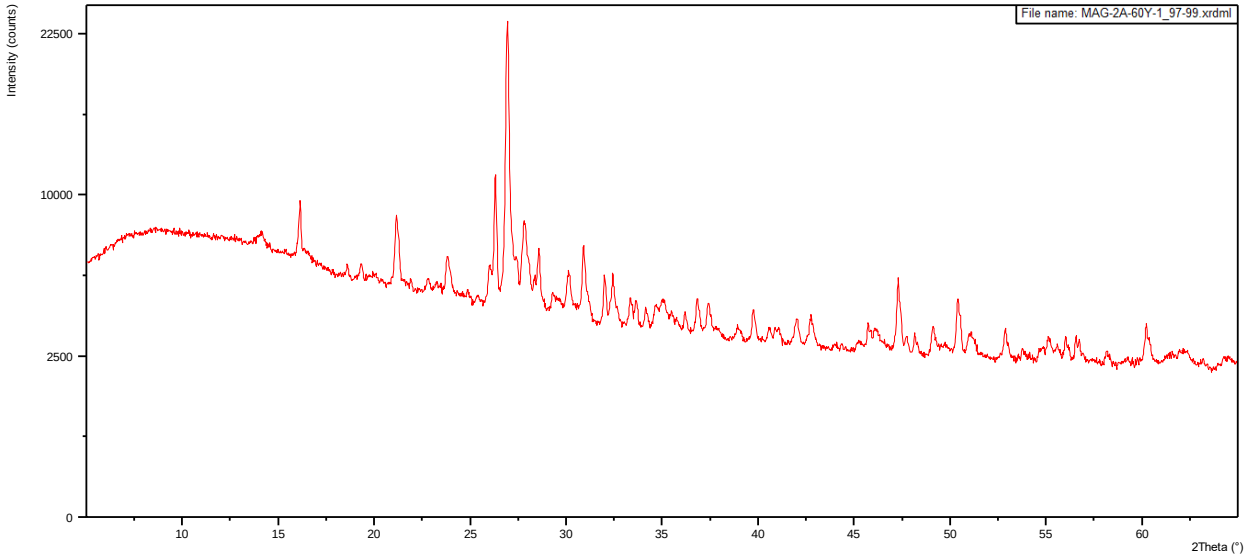
File name: MAG-2A-60Y-1_97-99.xrdml
Intensity (counts)
22500
10000
2500
0
10
15
20
25
30
35
40
45
50
55
60
2Theta (°)

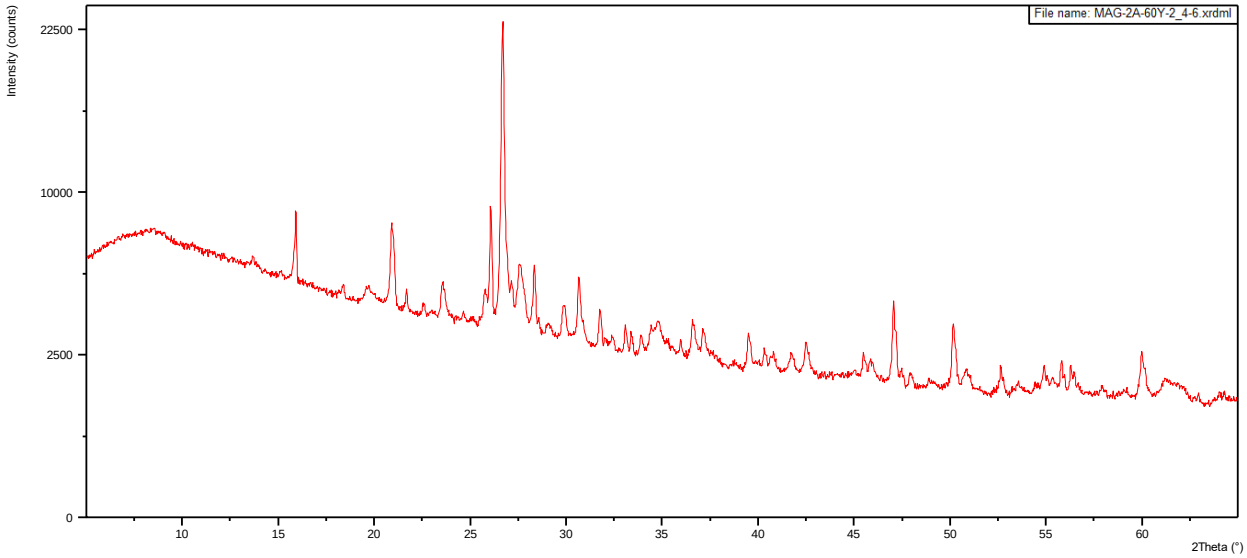
File name: MAG-2A-60Y-2_4-6.xrdml
Intensity (counts)
22500
10000
2500
0
10
15
20
25
30
35
40
45
50
55
60
2Theta (°)

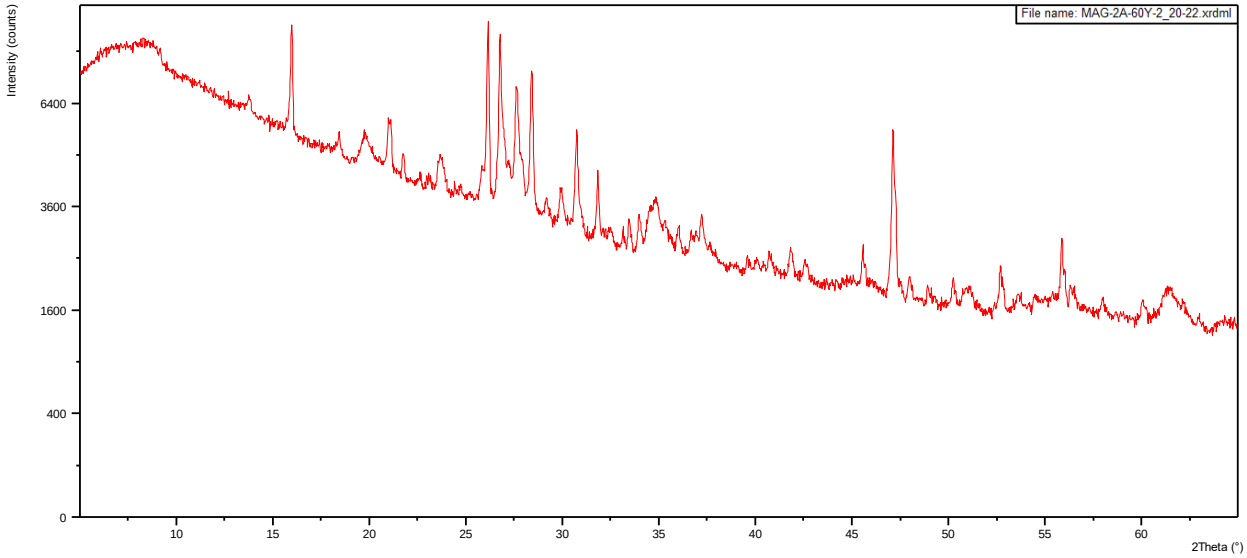
File name: MAG-2A-60Y-2_20-22.xrdml
Intensity (counts)
6400
3600
1600
400
0
10
15
20
25
30
35
40
45
50
55
60
2Theta (°)

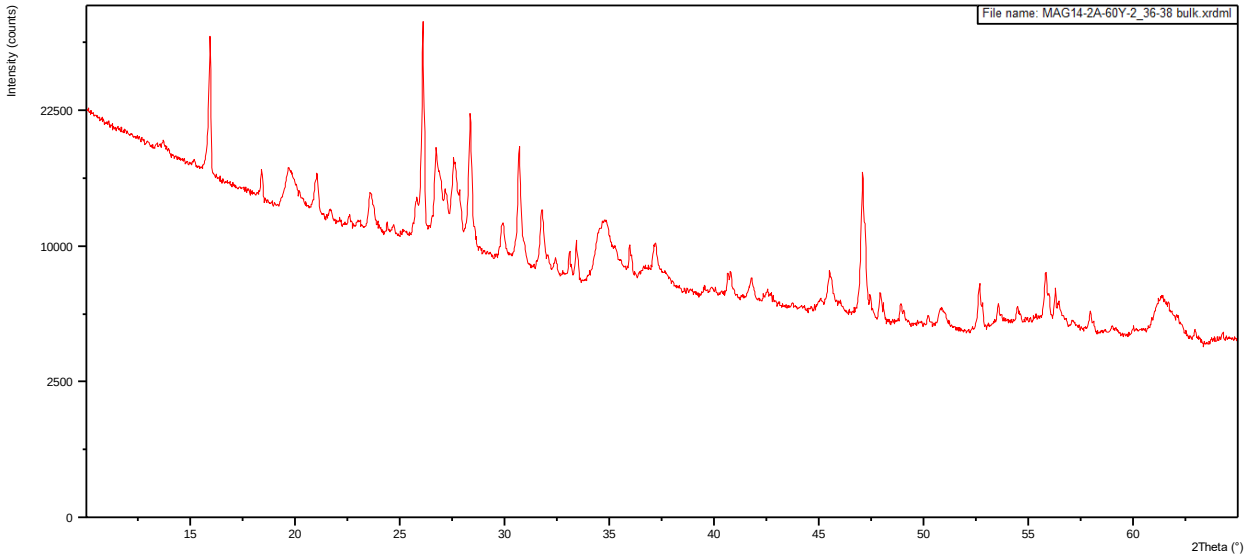
File name: MAG14-2A-60Y-2_36-38 bulk.xrdml
Intensity (counts)
22500
10000
2500
0
15
20
25
30
35
40
45
50
55
60
2Theta (°)

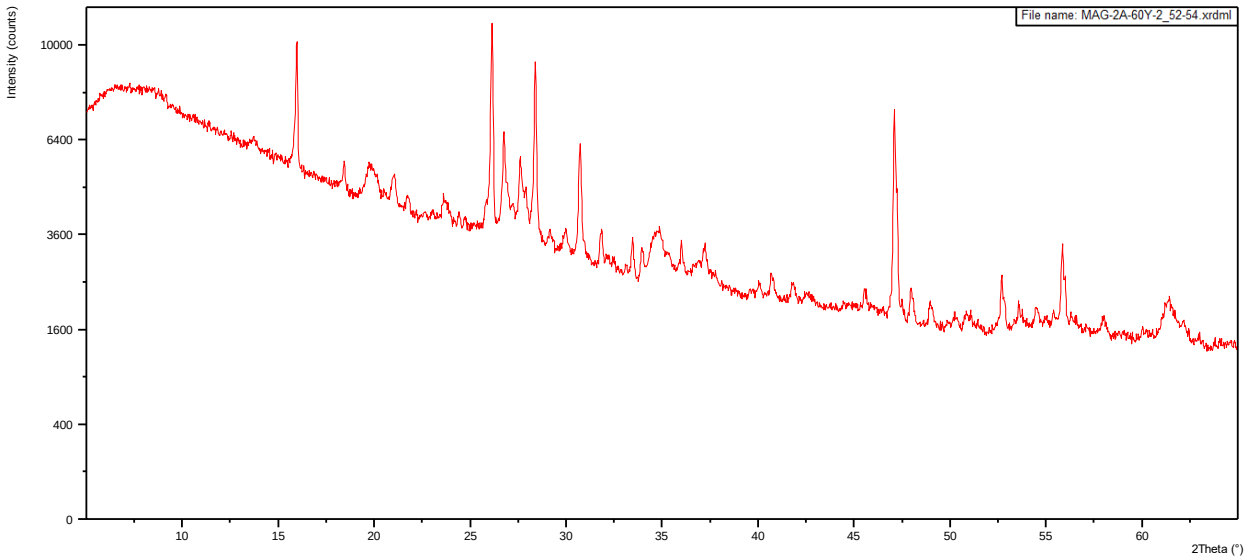
File name: MAG-2A-60Y-2_52-54.xrdml
Intensity (counts)
10000
6400
3600
1600
400
0
10
15
20
25
30
35
40
45
50
55
60
2Theta (°)

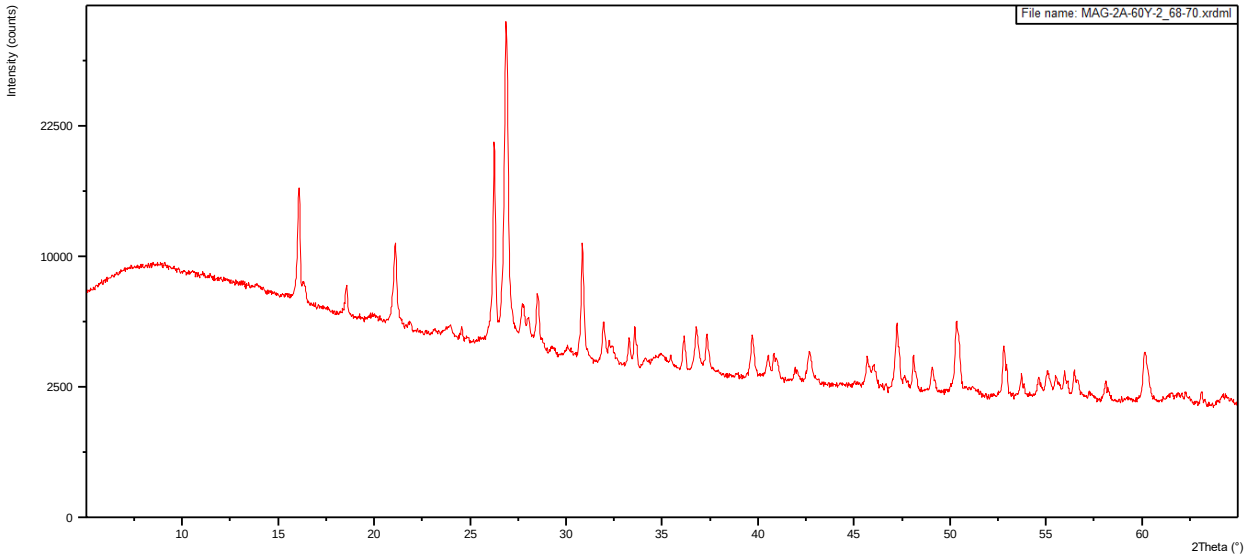
File name: MAG-2A-60Y-2_68-70.xrdml
Intensity (counts)
22500
10000
2500
0
10
15
20
25
30
35
40
45
50
55
60
2Theta (°)

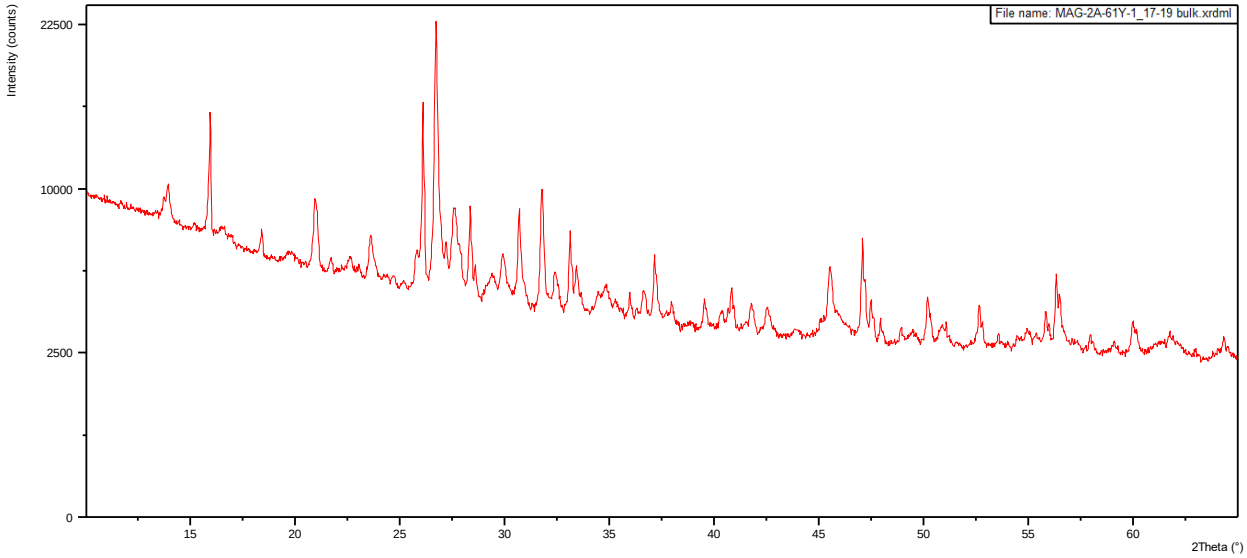
File name: MAG-2A-61Y-1_17-19 bulk.xrdml
Intensity (counts)
22500
10000
2500
0
15
20
25
30
35
40
45
50
55
60
2Theta (°)

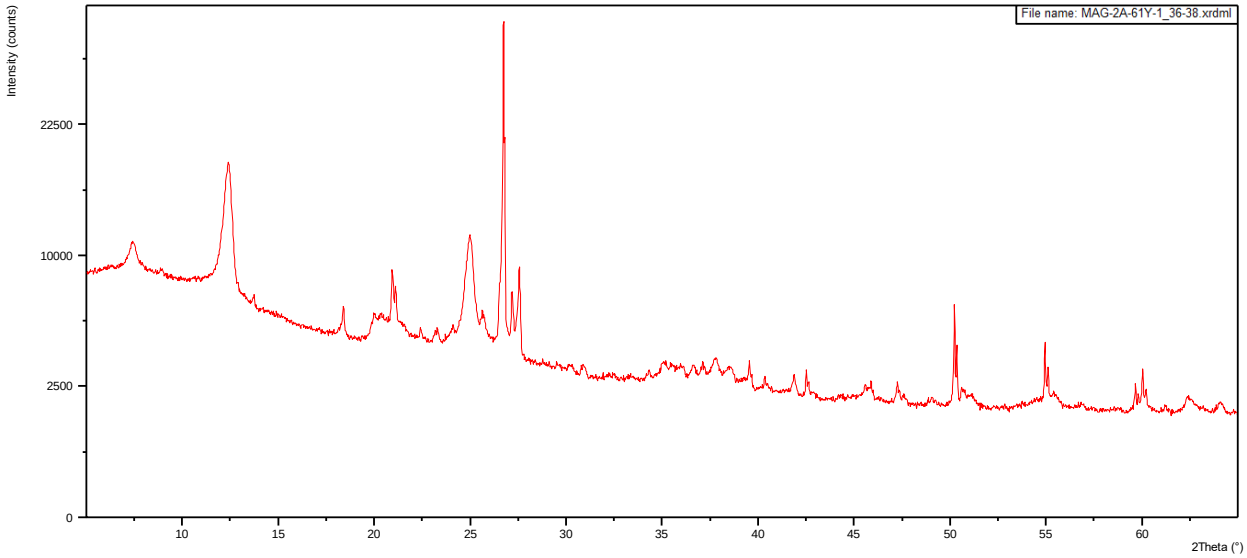
File name: MAG-2A-61Y-1_36-38.xrdml
Intensity (counts)
22500
10000
2500
0
10
15
20
25
30
35
40
45
50
55
60
2Theta (°)

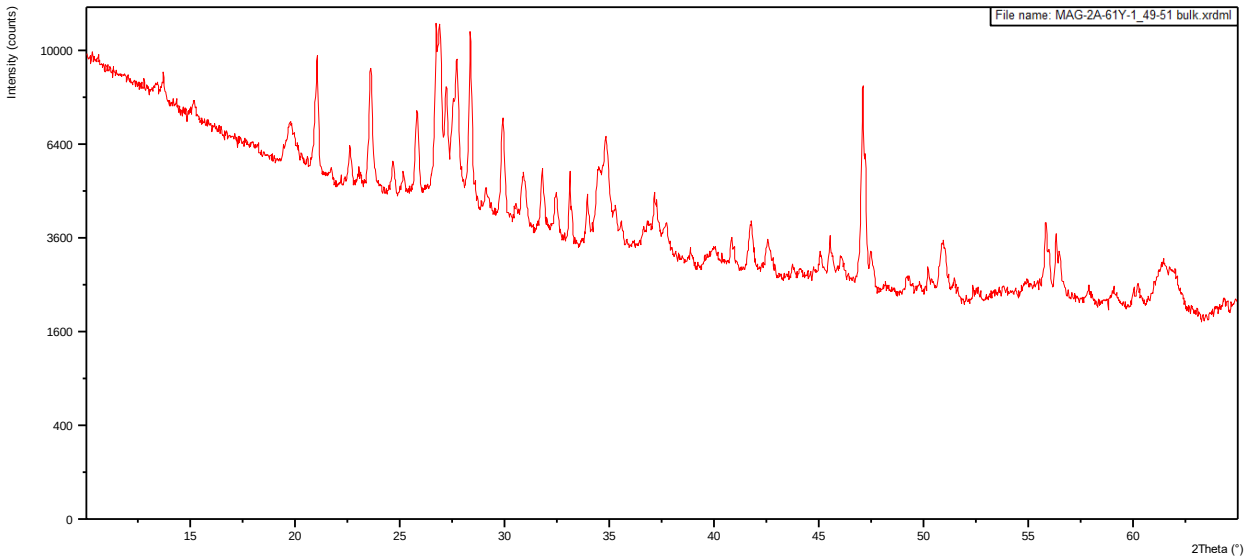
File name: MAG-2A-61Y-1_49-51 bulk.xrdml
Intensity (counts)
10000
6400
3600
1600
400
0
15
20
25
30
35
40
45
50
55
60
2Theta (°)

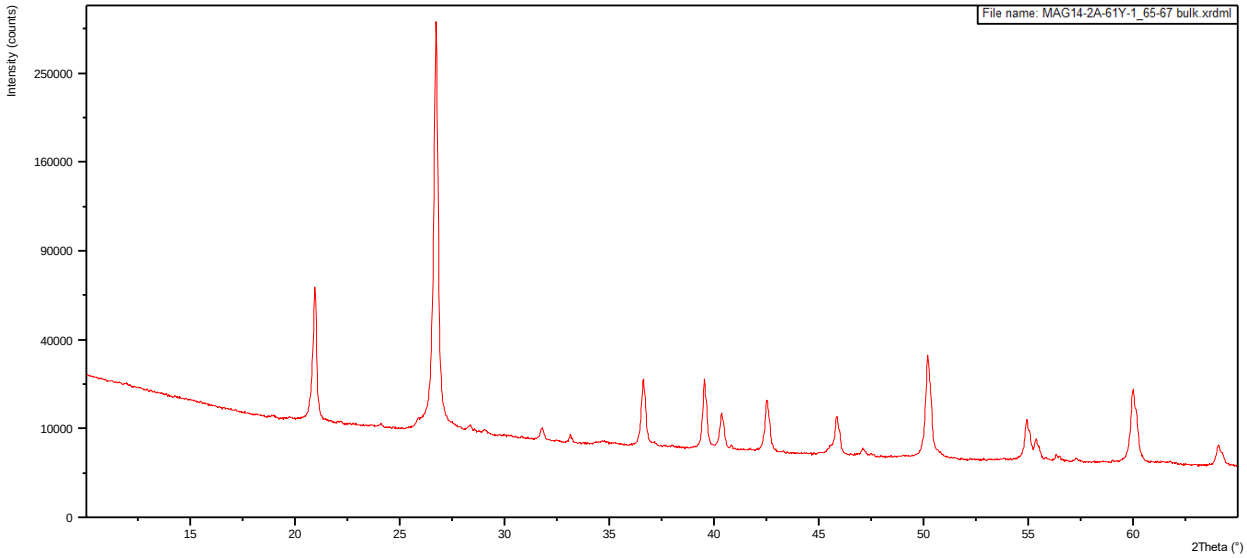
File name: MAG14-2A-61Y-1_65-67 bulk.xrdml
Intensity (counts)
250000
160000
90000
40000
10000
0
15
20
25
30
35
40
45
50
55
60
2Theta (°)

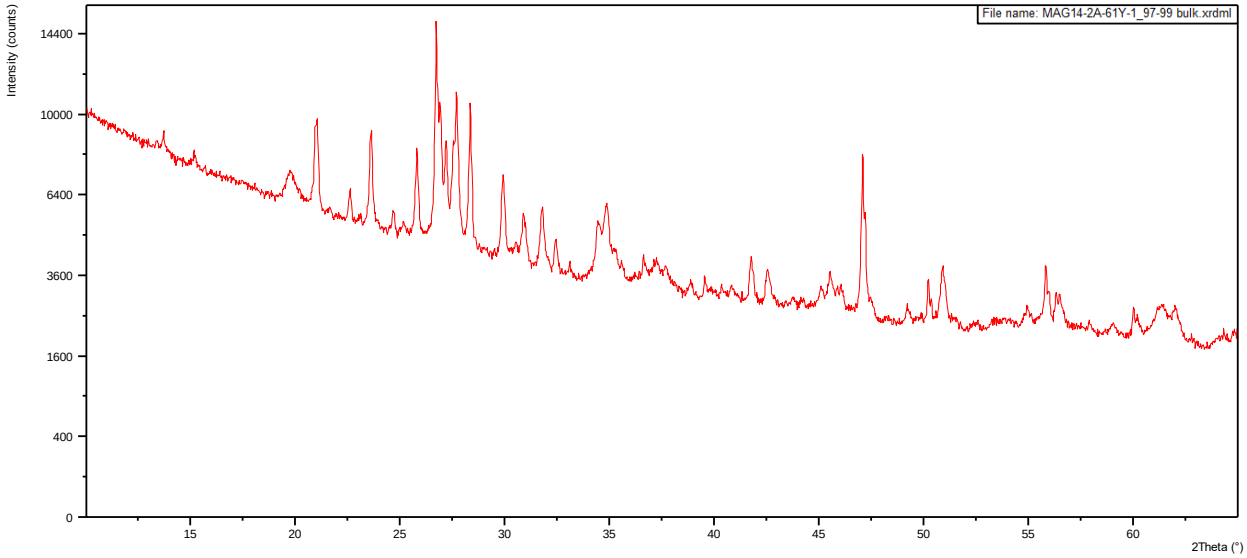
File name: MAG14-2A-61Y-1_97-99 bulk.xrdml
Intensity (counts)
14400
10000
6400
3600
1600
400
0
15
20
25
30
35
40
45
50
55
60
2Theta (°)

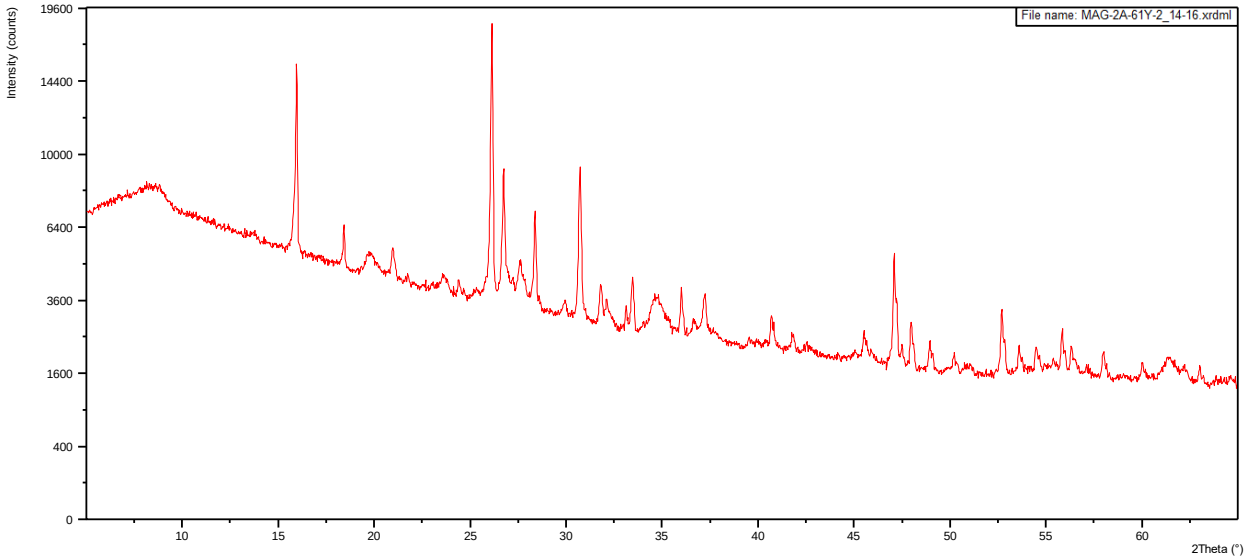
File name: MAG-2A-61Y-2_14-16.xrdml
Intensity (counts)
19600
14400
10000
6400
3600
1600
400
0
10
15
20
25
30
35
40
45
50
55
60
2Theta (°)

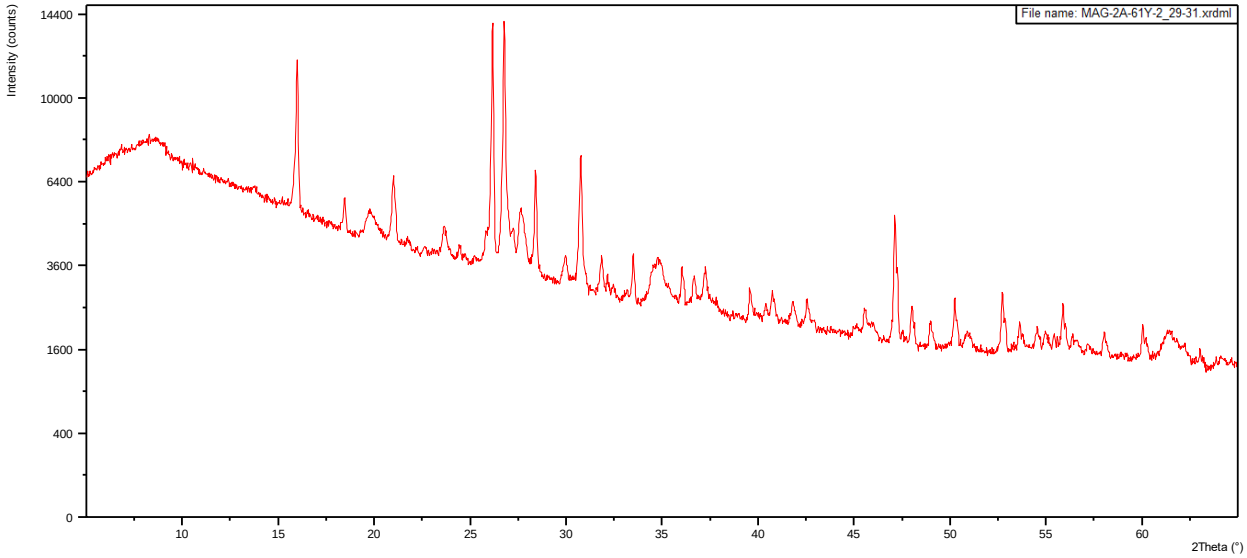
File name: MAG-2A-61Y-2_29-31.xrdml
Intensity (counts)
14400
10000
6400
3600
1600
400
0
10
15
20
25
30
35
40
45
50
55
60
2Theta (°)

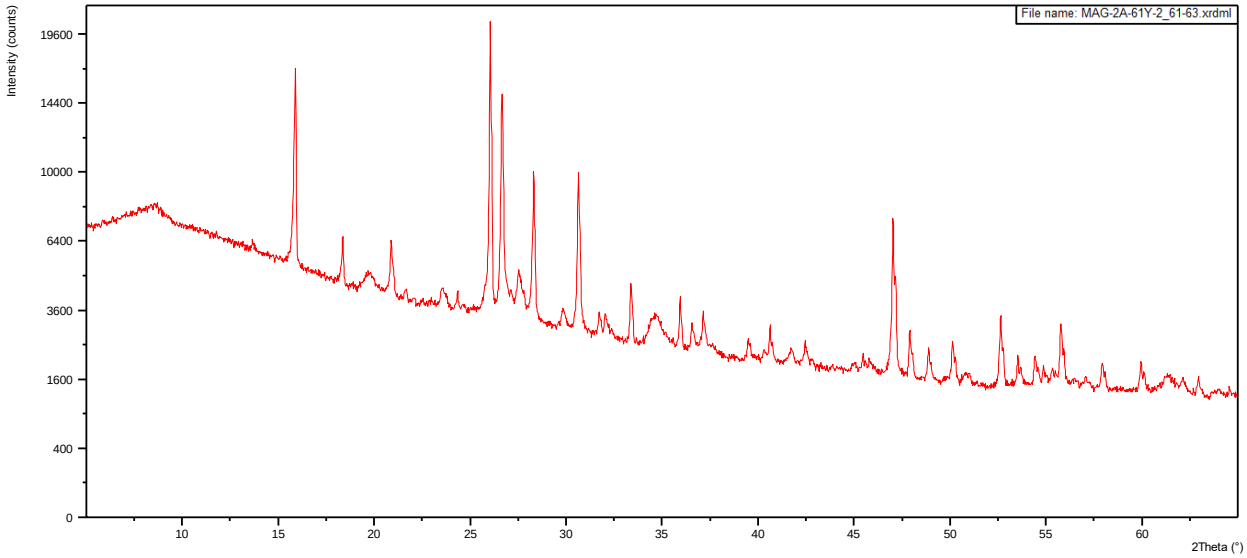
File name: MAG-2A-61Y-2_61-63.xrdml
Intensity (counts)
19600
14400
10000
6400
3600
1600
400
0
10
15
20
25
30
35
40
45
50
55
60
2Theta (°)

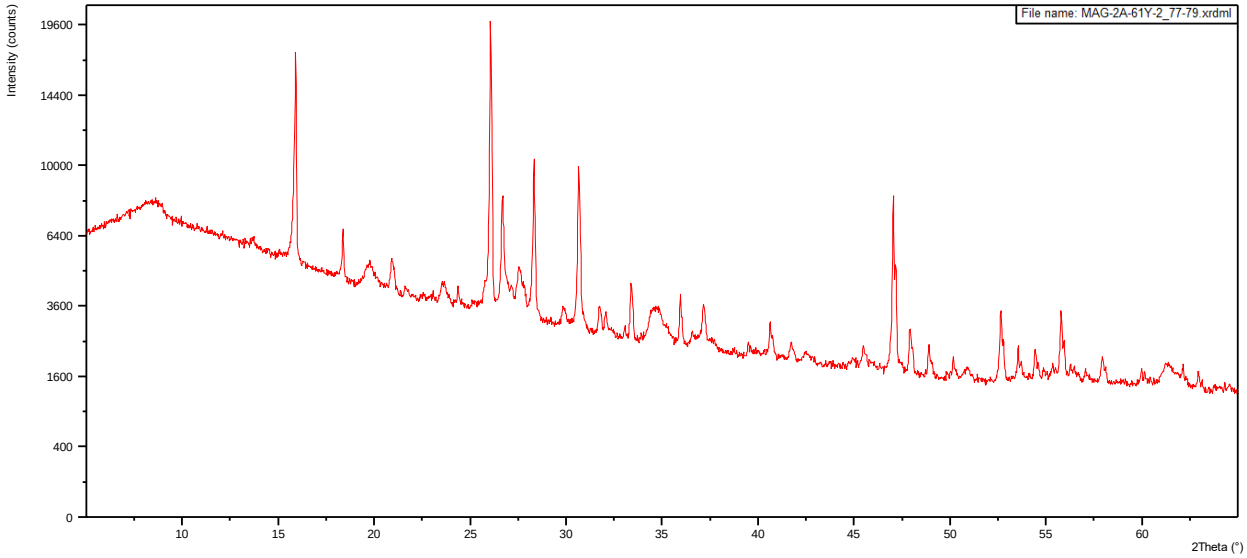
File name: MAG-2A-61Y-2_77-79.xrdml
Intensity (counts)
19600
14400
10000
6400
3600
1600
400
0
10
15
20
25
30
35
40
45
50
55
60
2Theta (°)

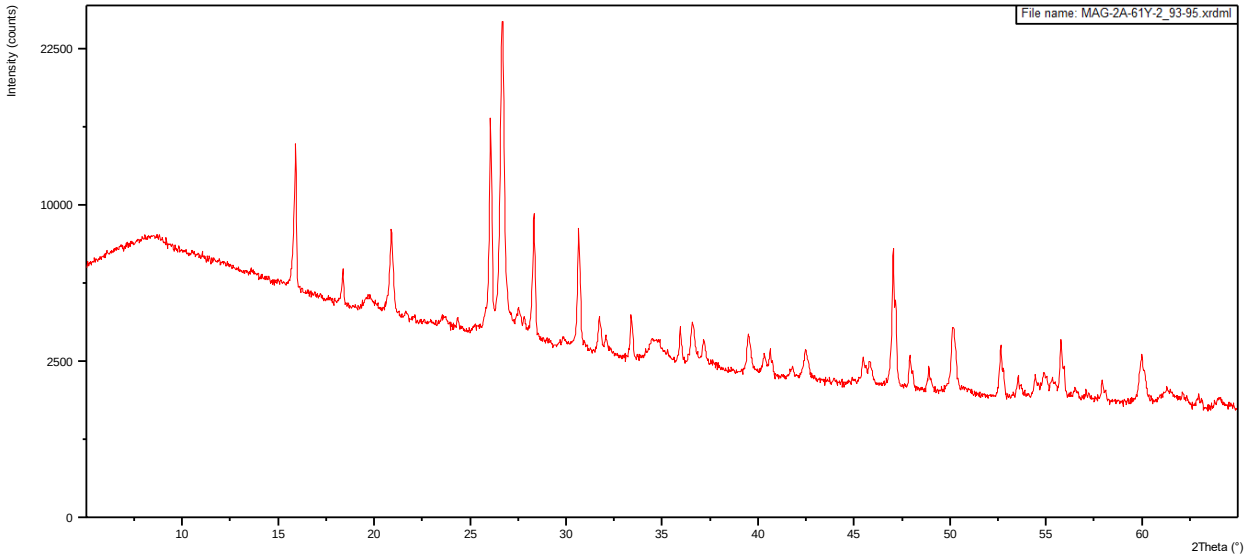
File name: MAG-2A-61Y-2_93-95.xrdml
Intensity (counts)
22500
10000
2500
0
10
15
20
25
30
35
40
45
50
55
60
2Theta (°)

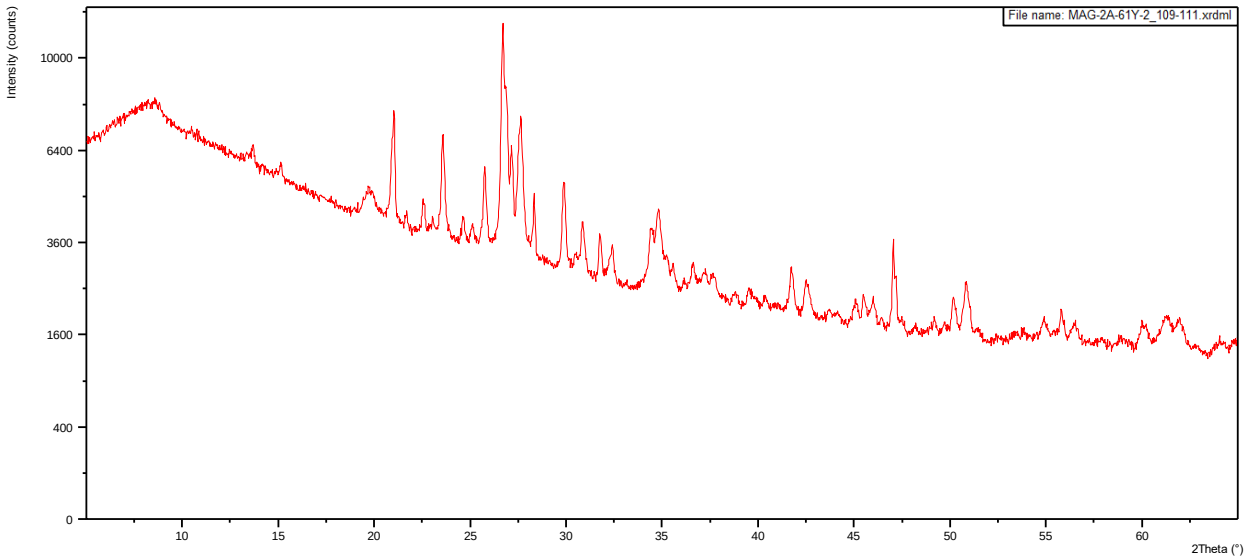
File name: MAG-2A-61Y-2_109-111.xrdml
Intensity (counts)
10000
6400
3600
1600
400
0
10
15
20
25
30
35
40
45
50
55
60
2Theta (°)

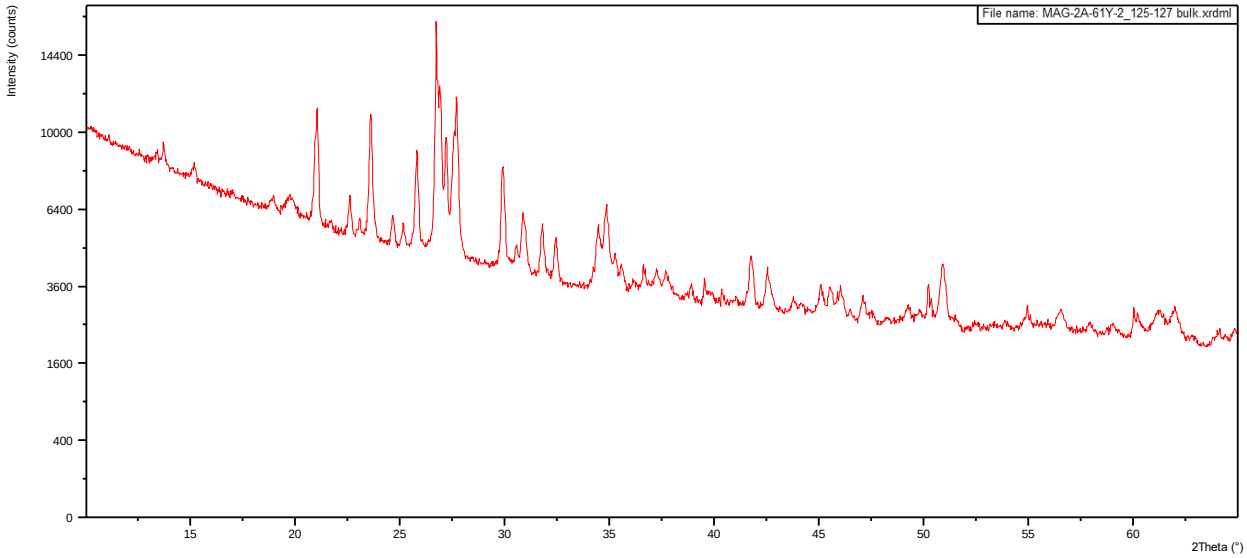
File name: MAG-2A-61Y-2_125-127 bulk.xrdml
Intensity (counts)
14400
10000
6400
3600
1600
400
0
15
20
25
30
35
40
45
50
55
60
2Theta (°)

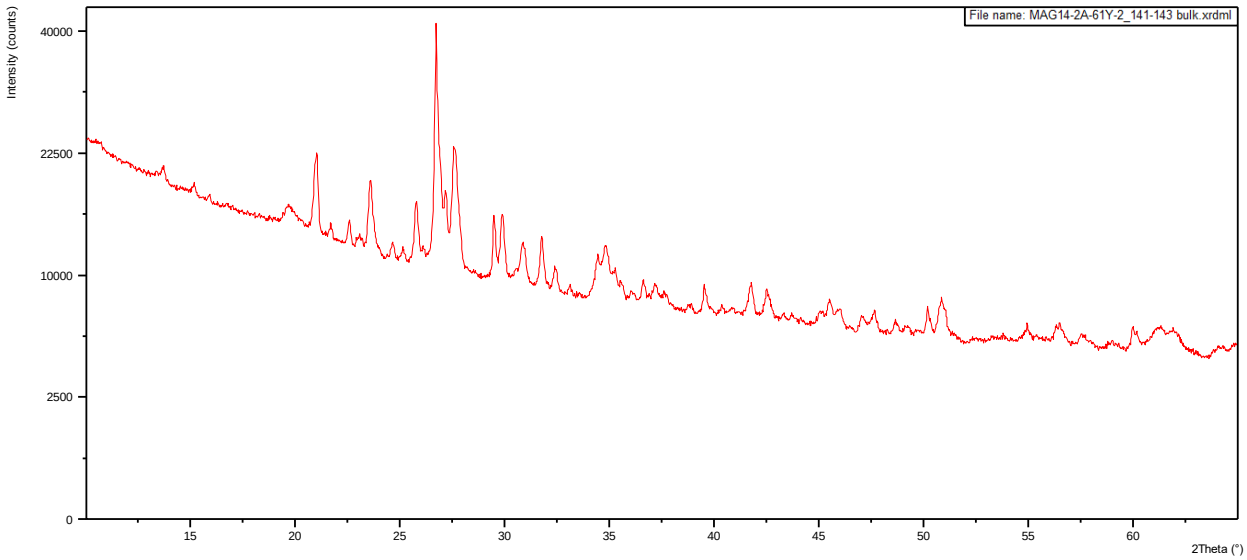
File name: MAG14-2A-61Y-2_141-143 bulk.xrdml
Intensity (counts)
40000
22500
10000
2500
0
15
20
25
30
35
40
45
50
55
60
2Theta (°)

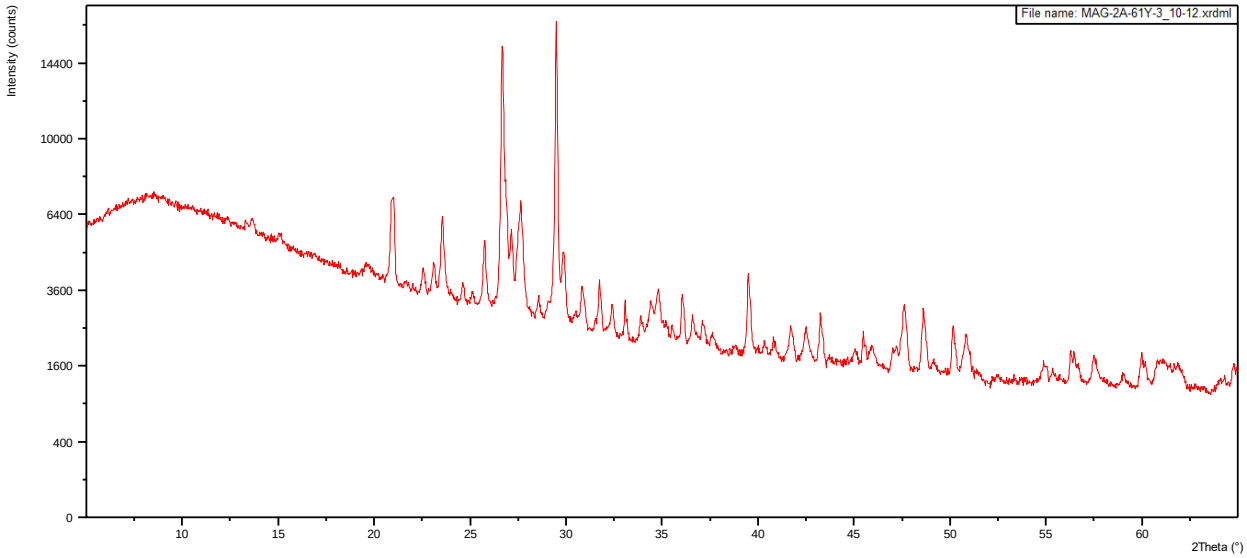
File name: MAG-2A-61Y-3_10-12.xrdml
Intensity (counts)
14400
10000
6400
3600
1600
400
0
10
15
20
25
30
35
40
45
50
55
60
2Theta (°)

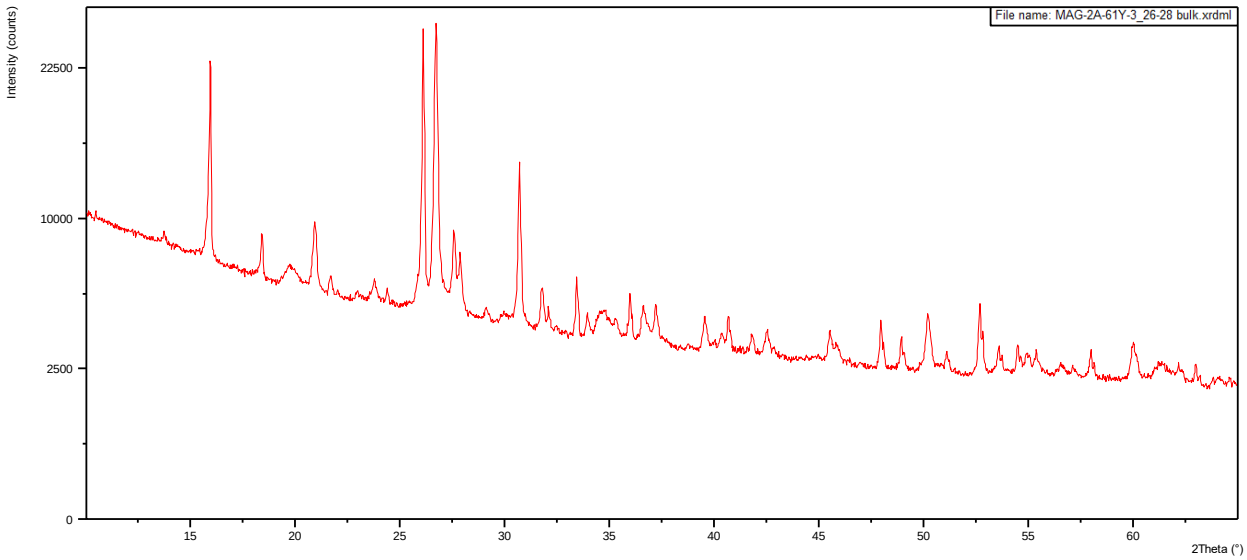
File name: MAG-2A-61Y-3_26-28 bulk.xrdml
Intensity (counts)
22500
10000
2500
0
15
20
25
30
35
40
45
50
55
60
2Theta (°)

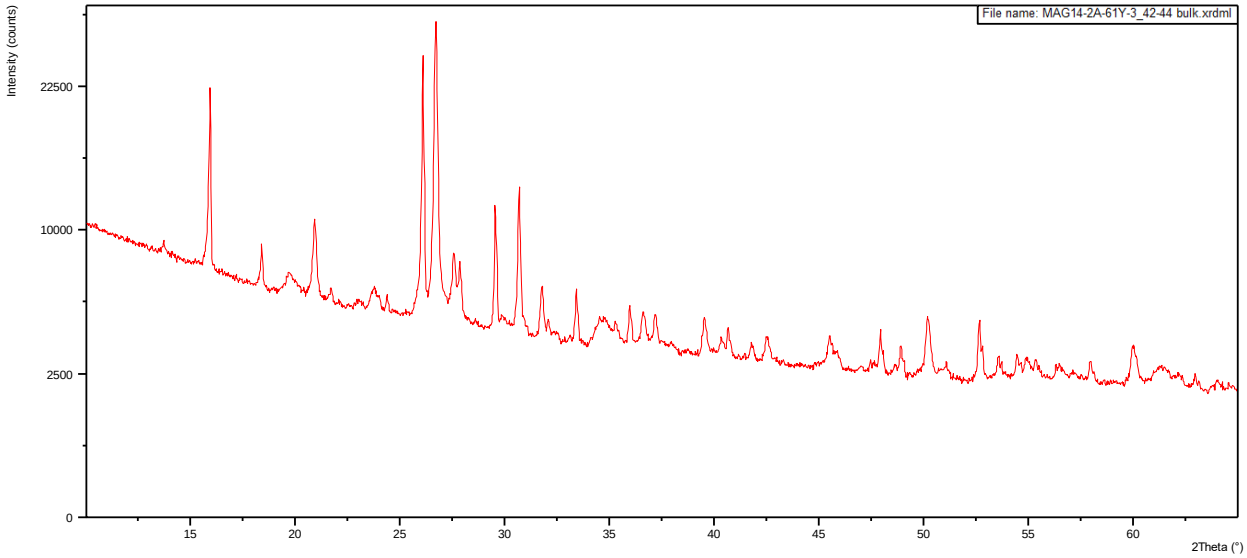
File name: MAG14-2A-61Y-3_42-44 bulk.xrdml
Intensity (counts)
22500
10000
2500
0
15
20
25
30
35
40
45
50
55
60
2Theta (°)

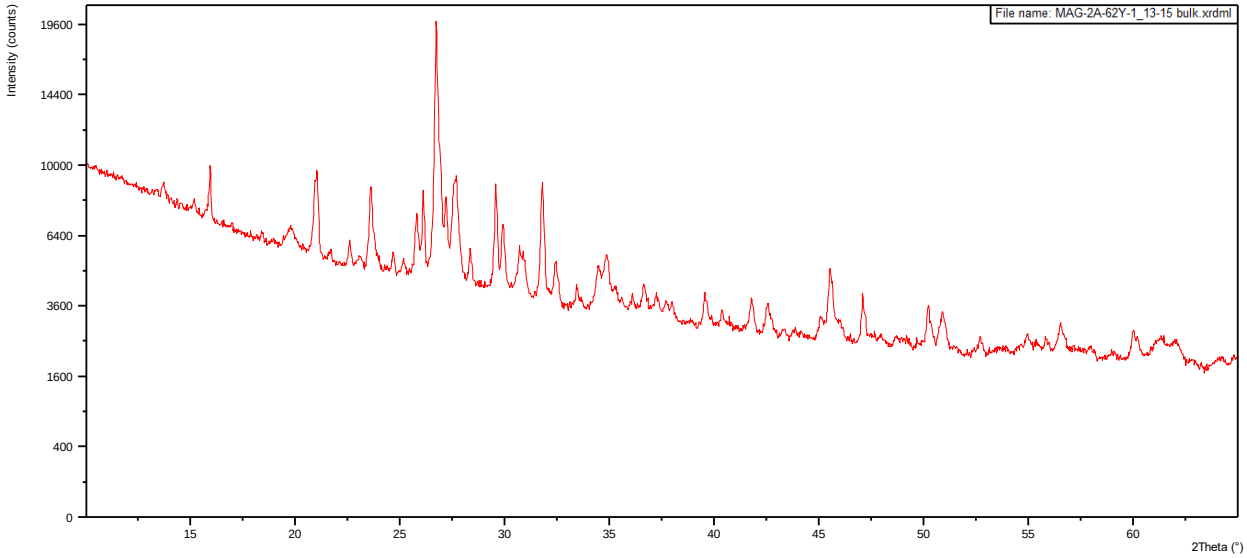
File name: MAG-2A-62Y-1_13-15 bulk.xrdml
Intensity (counts)
19600
14400
10000
6400
3600
1600
400
0
15
20
25
30
35
40
45
50
55
60
2Theta (°)

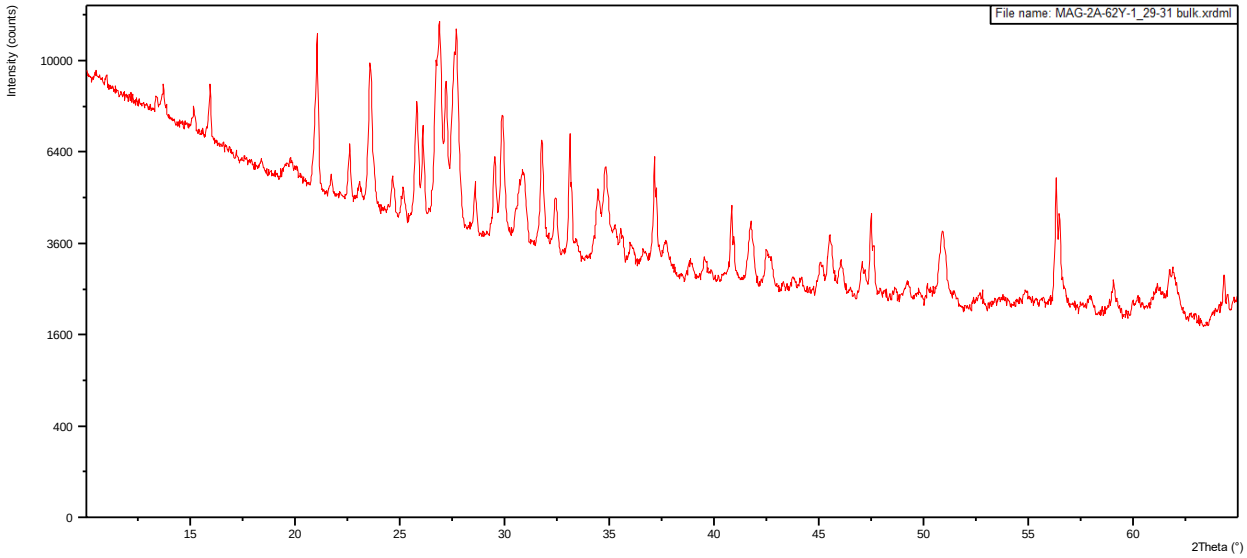
File name: MAG-2A-62Y-1_29-31 bulk.xrdml
Intensity (counts)
10000
6400
3600
1600
400
0
15
20
25
30
35
40
45
50
55
60
2Theta (°)

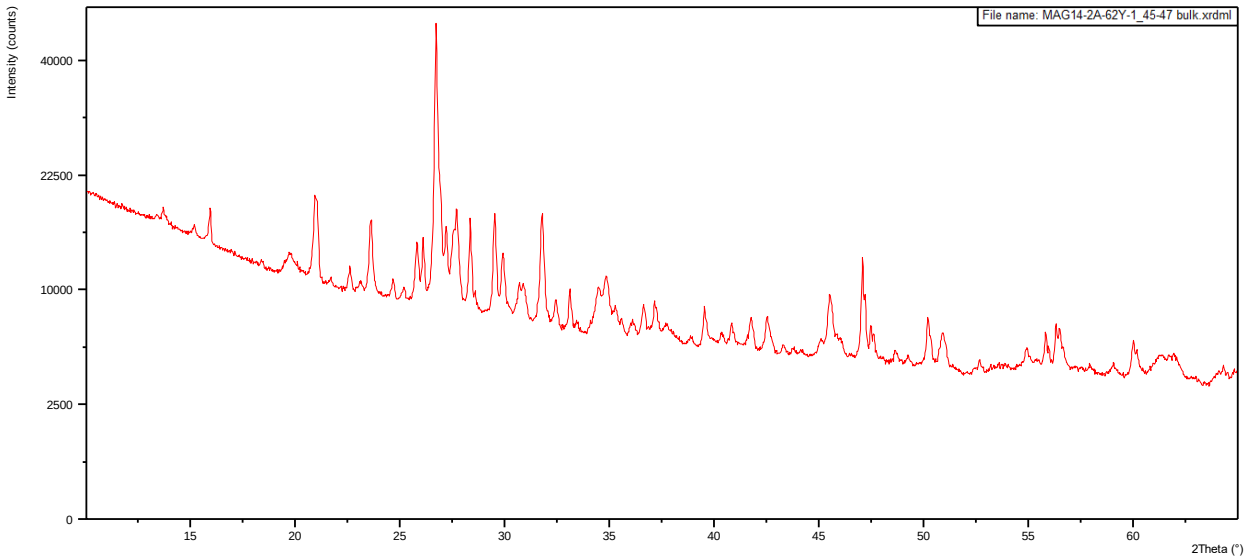
File name: MAG14-2A-62Y-1_45-47 bulk.xrdml
Intensity (counts)
40000
22500
10000
2500
0
15
20
25
30
35
40
45
50
55
60
2Theta (°)

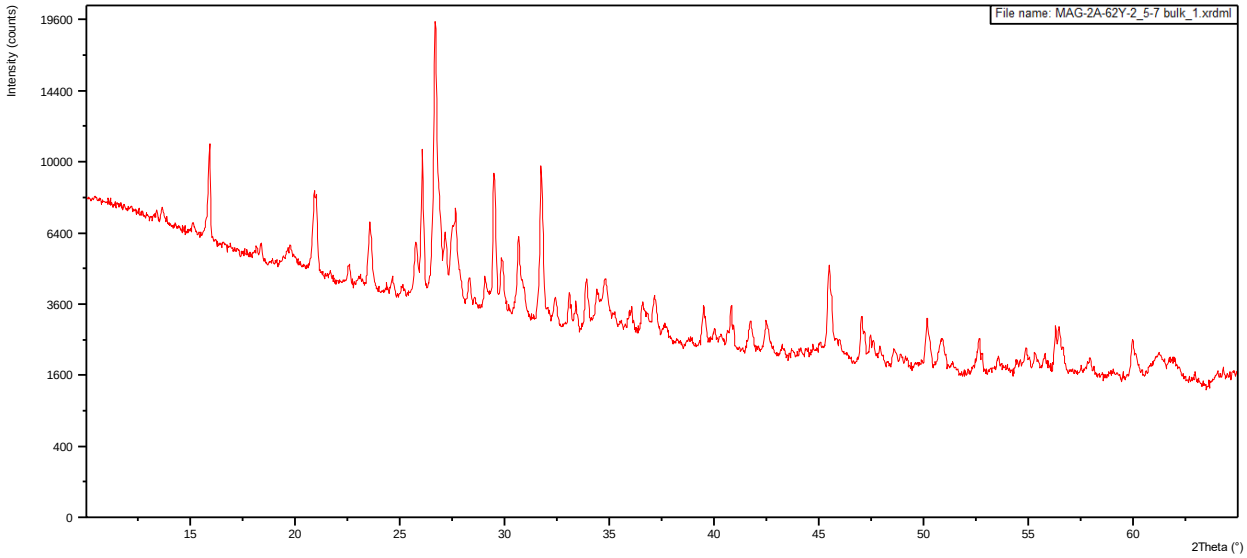
File name: MAG-2A-62Y-2_5-7 bulk_1.xrdml
Intensity (counts)
19600
14400
10000
6400
3600
1600
400
0
15
20
25
30
35
40
45
50
55
60
2Theta (°)

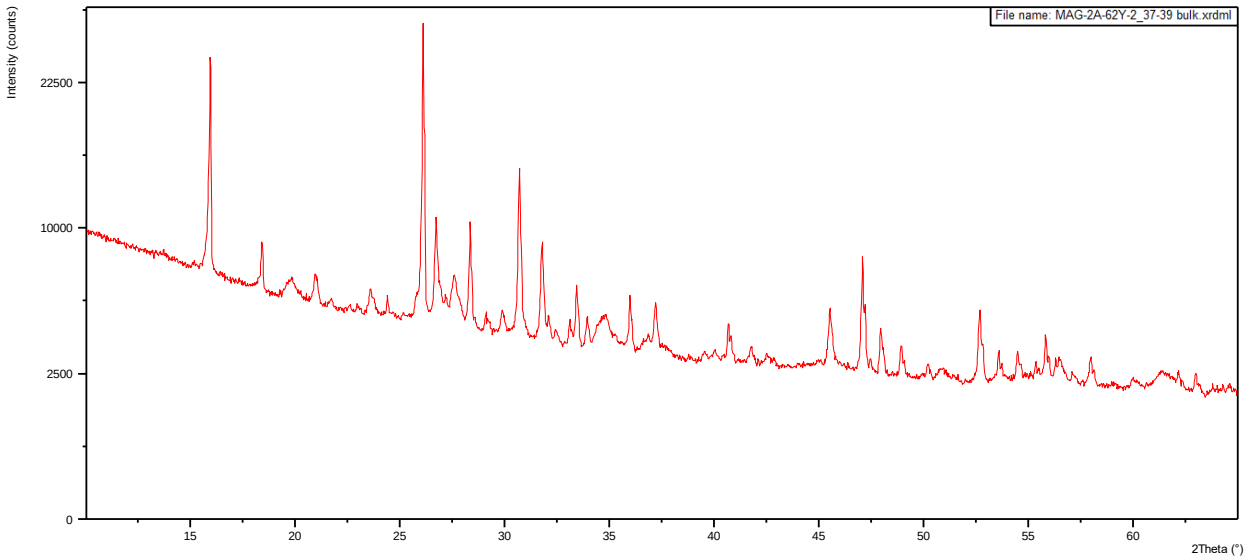
File name: MAG-2A-62Y-2_37-39 bulk.xrdml
Intensity (counts)
22500
10000
2500
0
15
20
25
30
35
40
45
50
55
60
2Theta (°)

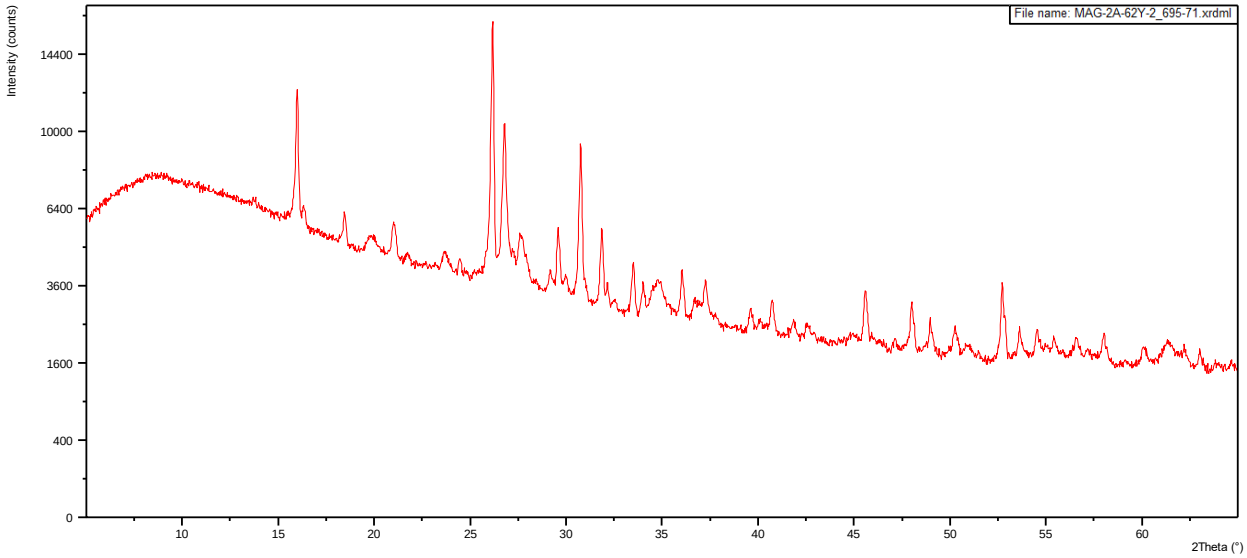
File name: MAG-2A-62Y-2_695-71.xrdml
Intensity (counts)
14400
10000
6400
3600
1600
400
0
10
15
20
25
30
35
40
45
50
55
60
2Theta (°)

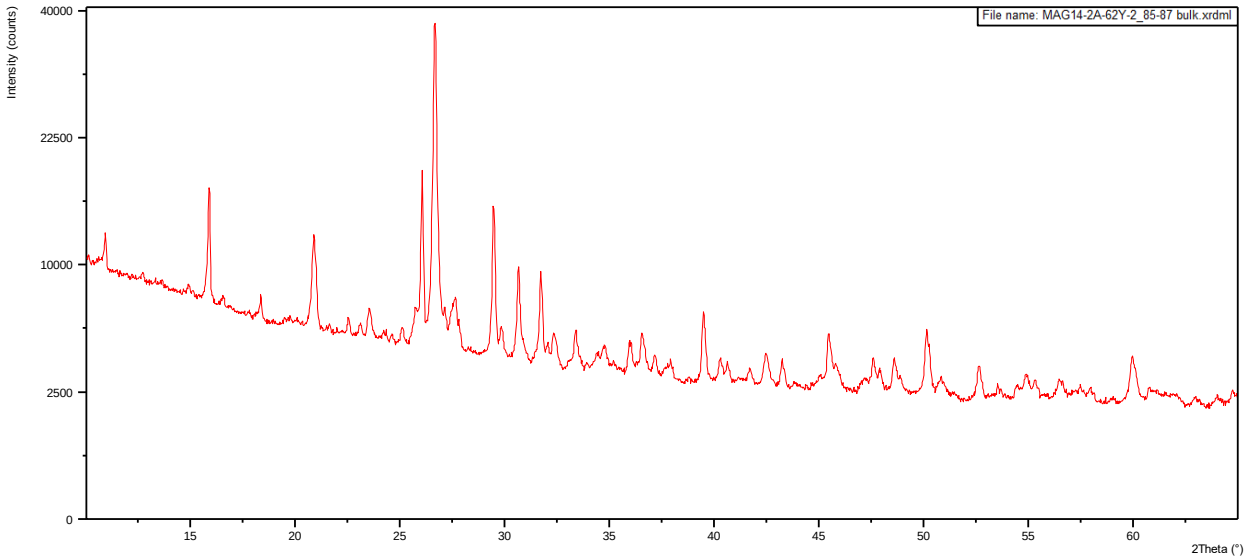
File name: MAG14-2A-62Y-2_85-87 bulk.xrdml
Intensity (counts)
40000
22500
10000
2500
0
15
20
25
30
35
40
45
50
55
60
2Theta (°)

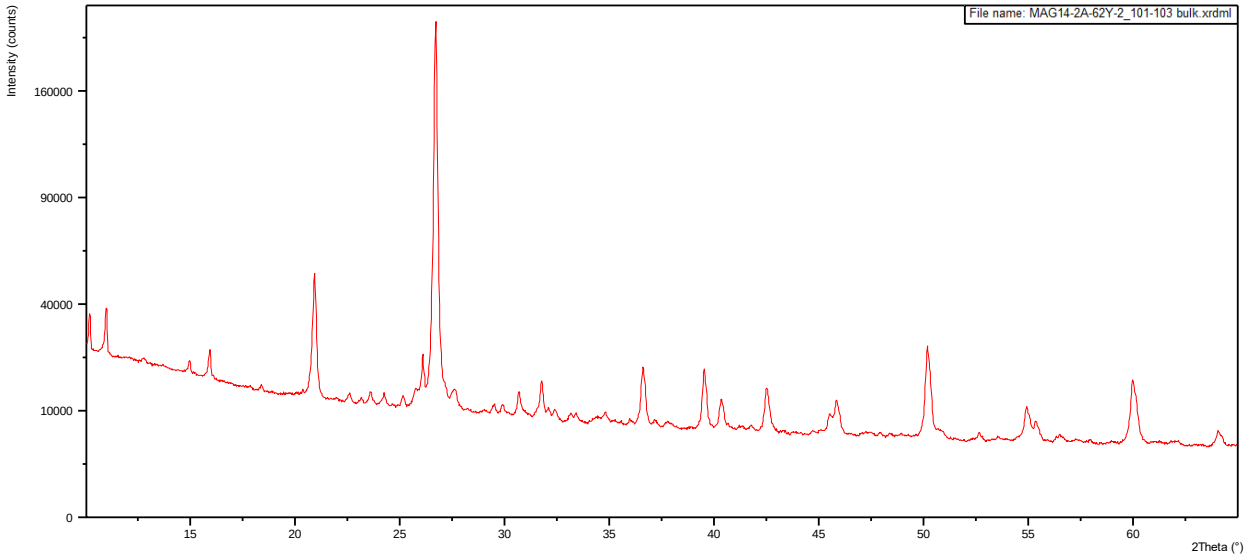
File name: MAG14-2A-62Y-2_101-103 bulk.xrdml
Intensity (counts)
160000
90000
40000
10000
0
15
20
25
30
35
40
45
50
55
60
2Theta (°)

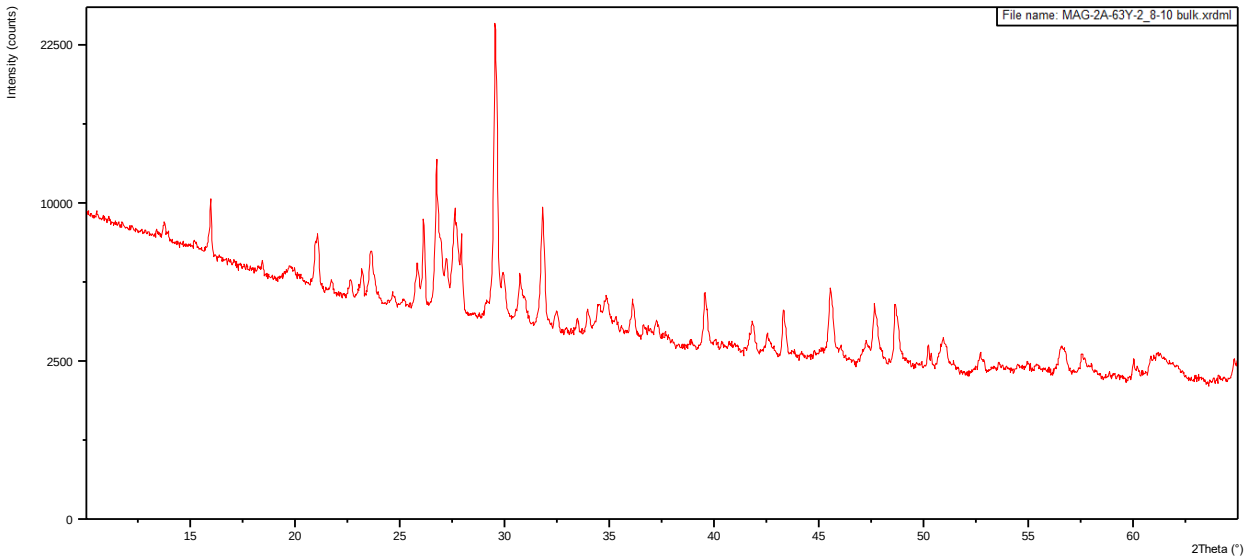
File name: MAG-2A-63Y-2_8-10 bulk.xrdml
Intensity (counts)
22500
10000
2500
0
15
20
25
30
35
40
45
50
55
60
2Theta (°)

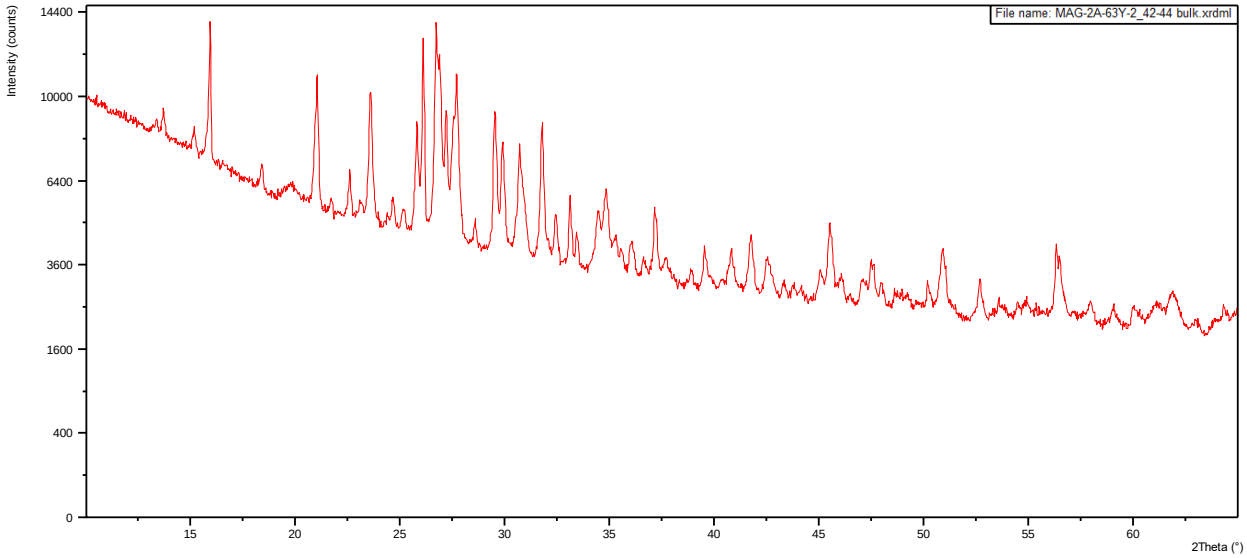
File name: MAG-2A-63Y-2_42-44 bulk.xrdml
Intensity (counts)
14400
10000
6400
3600
1600
400
0
15
20
25
30
35
40
45
50
55
60
2Theta (°)

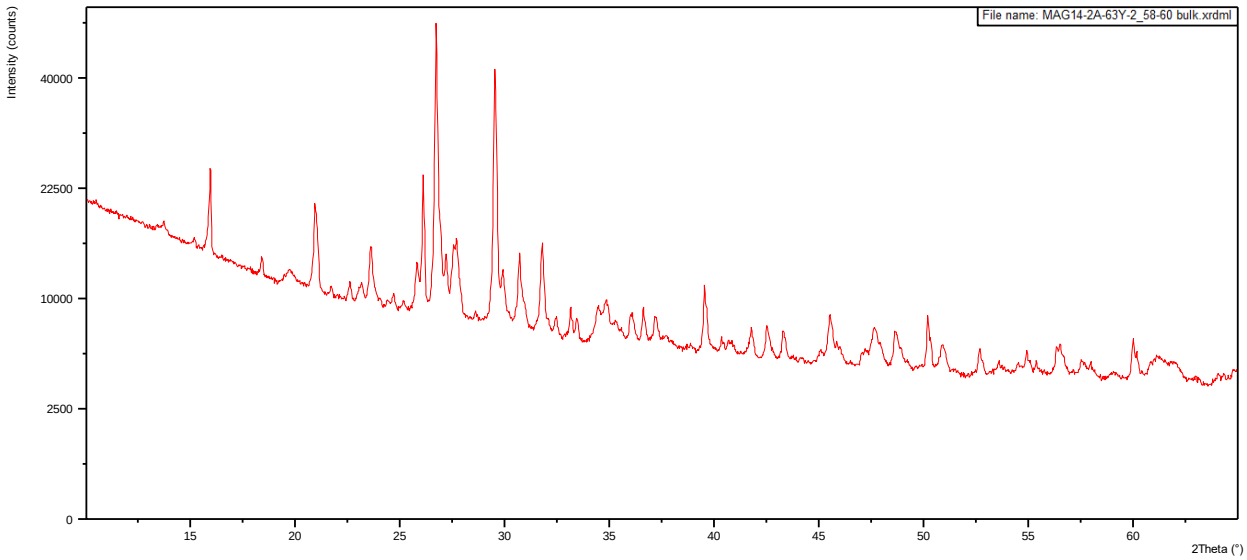
File name: MAG14-2A-63Y-2_58-60 bulk.xrdml
Intensity (counts)
40000
22500
10000
2500
0
15
20
25
30
35
40
45
50
55
60
2Theta (°)

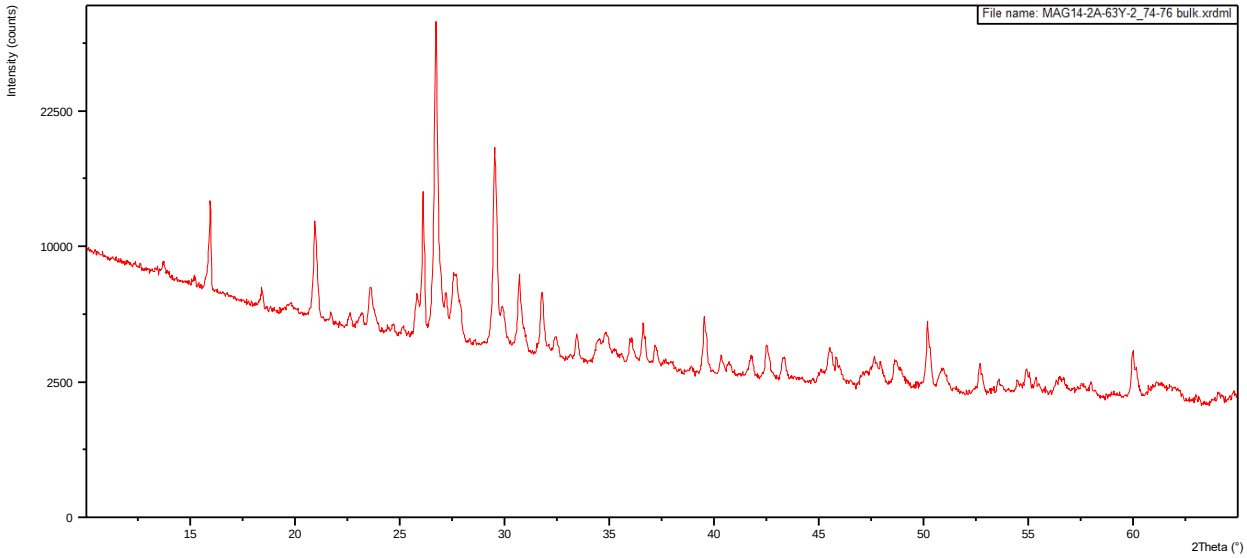
File name: MAG14-2A-63Y-2_74-76 bulk.xrdml
Intensity (counts)
22500
10000
2500
0
15
20
25
30
35
40
45
50
55
60
2Theta (°)

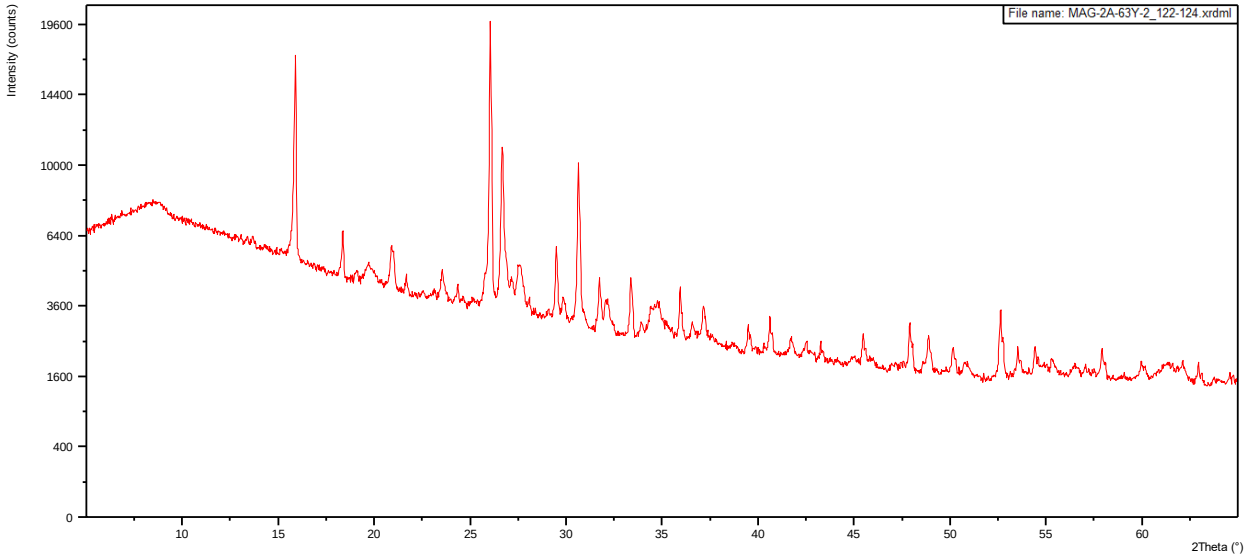
File name: MAG-2A-63Y-2_122-124.xrdml
Intensity (counts)
19600
14400
10000
6400
3600
1600
400
0
10
15
20
25
30
35
40
45
50
55
60
2Theta (°)

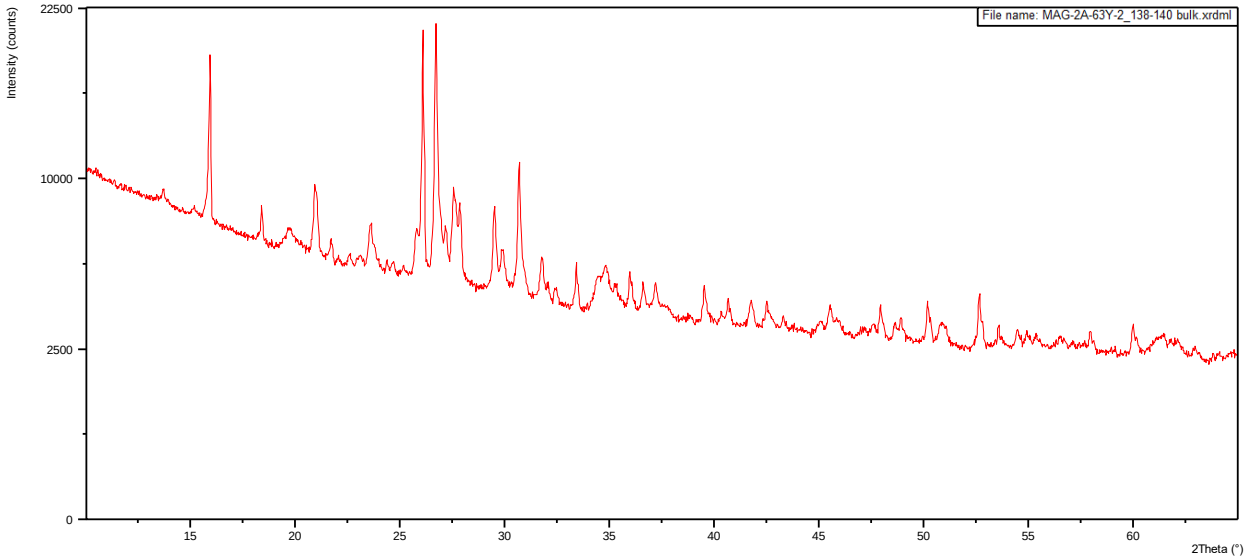
File name: MAG-2A-63Y-2_138-140 bulk.xrdml
Intensity (counts)
22500
10000
2500
0
15
20
25
30
35
40
45
50
55
60
2Theta (°)

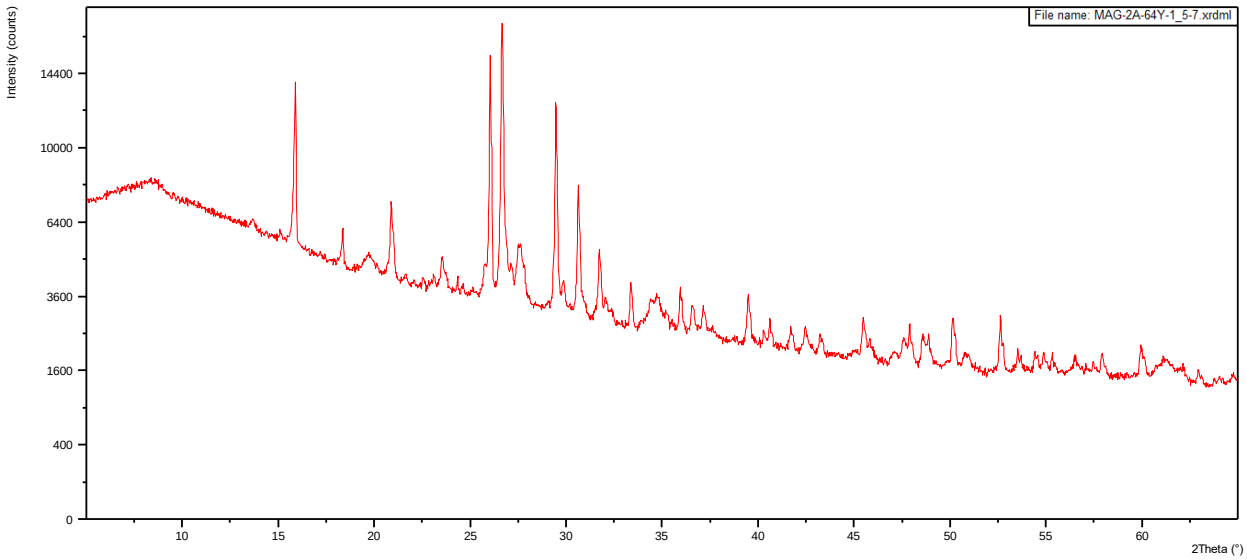
File name: MAG-2A-64Y-1_5-7.xrdml
Intensity (counts)
14400
10000
6400
3600
1600
400
0
10
15
20
25
30
35
40
45
50
55
60
2Theta (°)

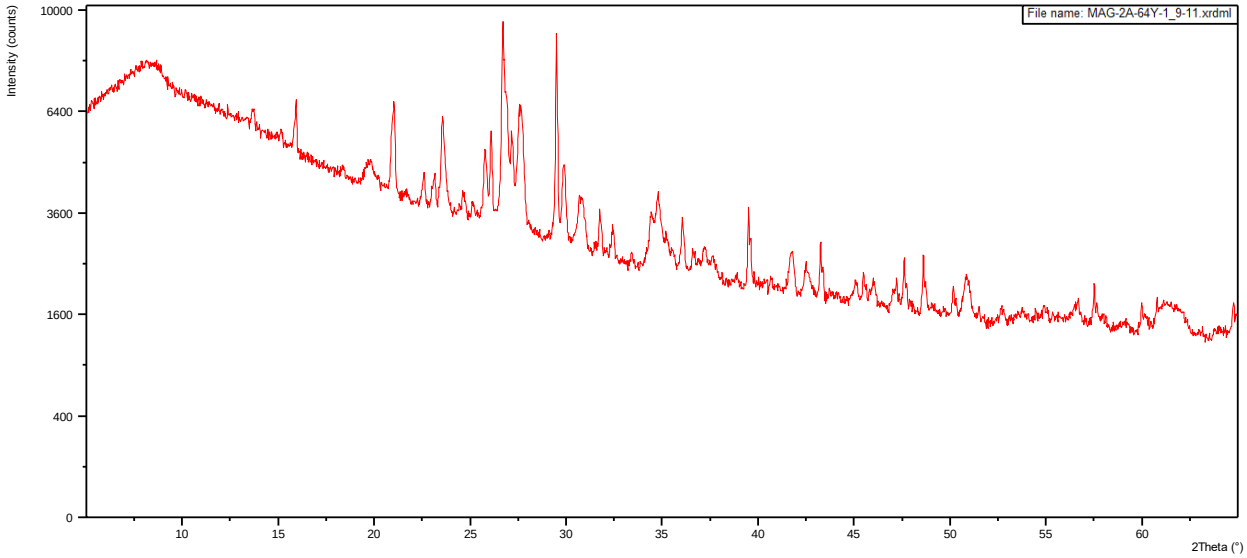
File name: MAG-2A-64Y-1_9-11.xrdml
Intensity (counts)
10000
6400
3600
1600
400
0
10
15
20
25
30
35
40
45
50
55
60
2Theta (°)

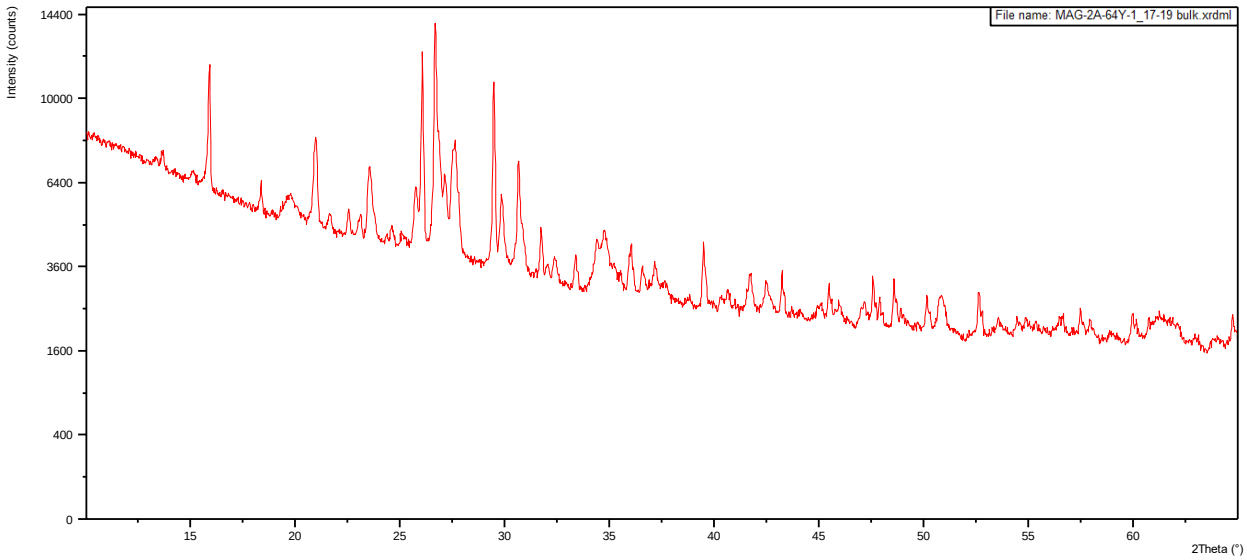
File name: MAG-2A-64Y-1_17-19 bulk.xrdml
Intensity (counts)
14400
10000
6400
3600
1600
400
0
15
20
25
30
35
40
45
50
55
60
2Theta (°)

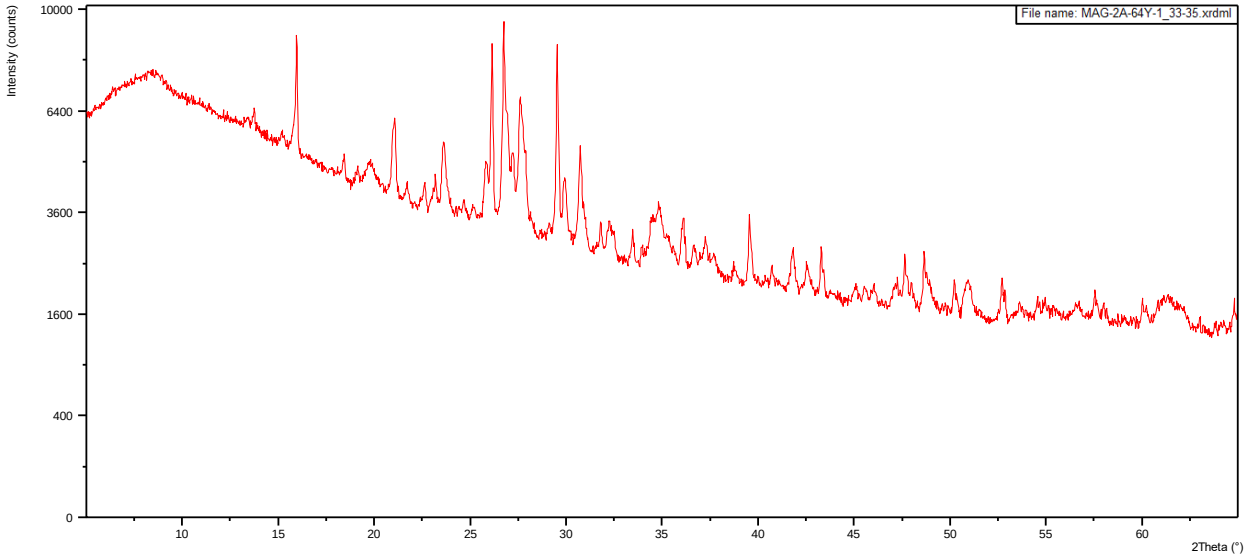
File name: MAG-2A-64Y-1_33-35.xrdml
Intensity (counts)
10000
6400
3600
1600
400
0
10
15
20
25
30
35
40
45
50
55
60
2Theta (°)

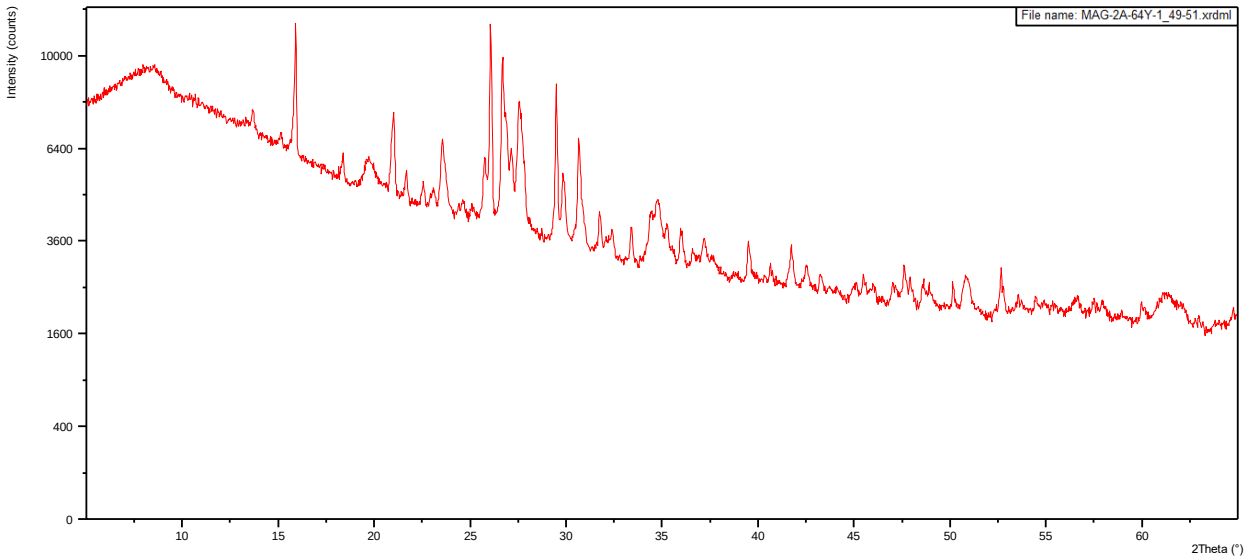
File name: MAG-2A-64Y-1_49-51.xrdml
Intensity (counts)
10000
6400
3600
1600
400
0
10
15
20
25
30
35
40
45
50
55
60
2Theta (°)

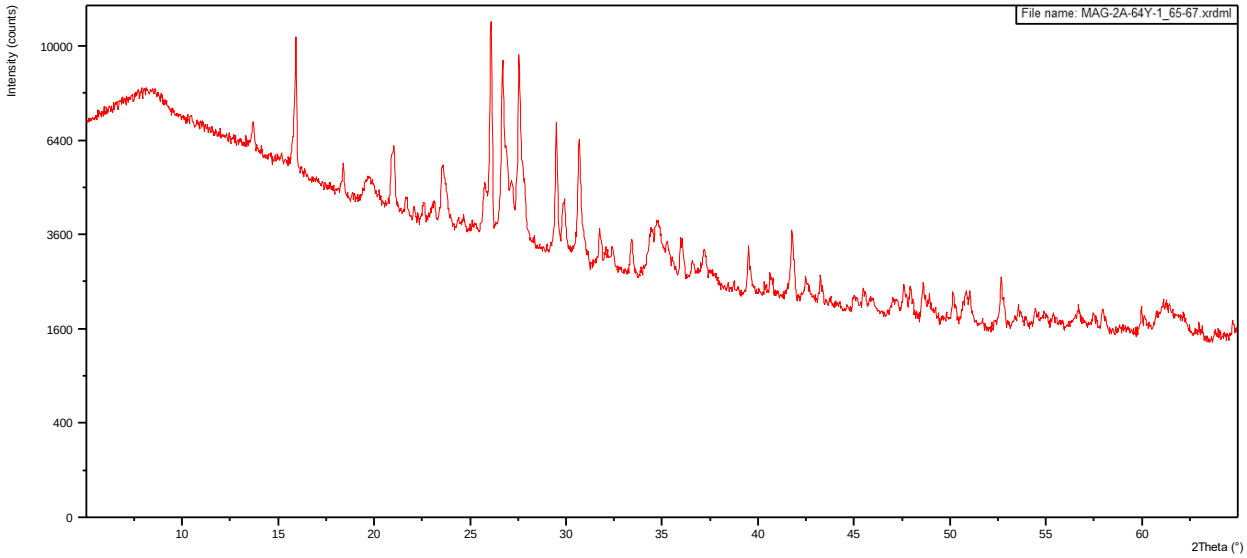
File name: MAG-2A-64Y-1_65-67.xrdml
Intensity (counts)
10000
6400
3600
1600
400
0
10
15
20
25
30
35
40
45
50
55
60
2Theta (°)

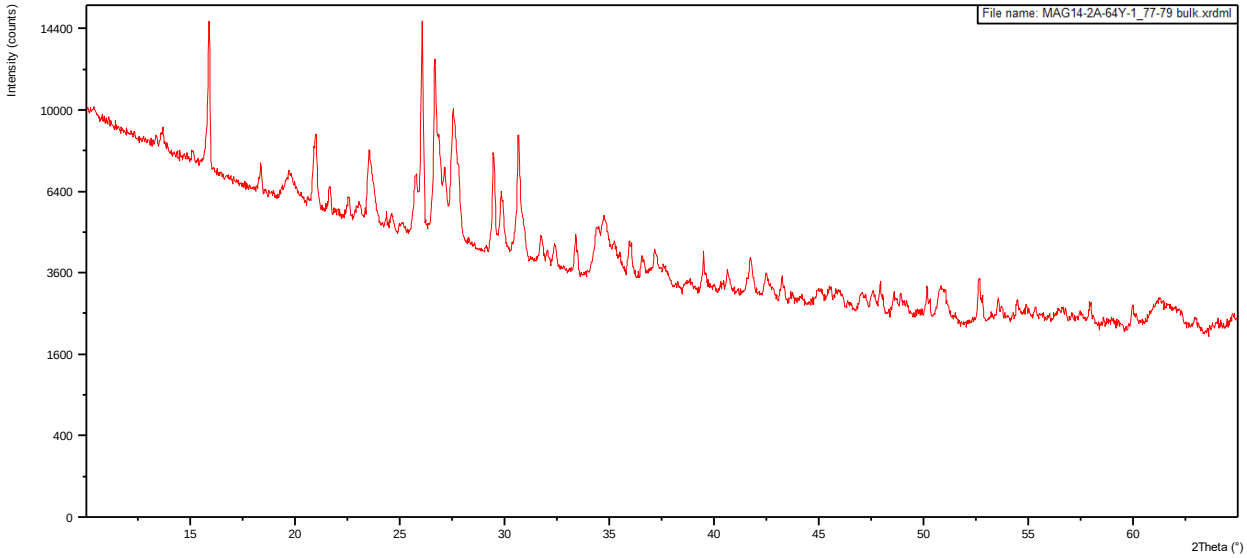
File name: MAG14-2A-64Y-1_77-79 bulk.xrdml
Intensity (counts)
14400
10000
6400
3600
1600
400
0
15
20
25
30
35
40
45
50
55
60
2Theta (°)

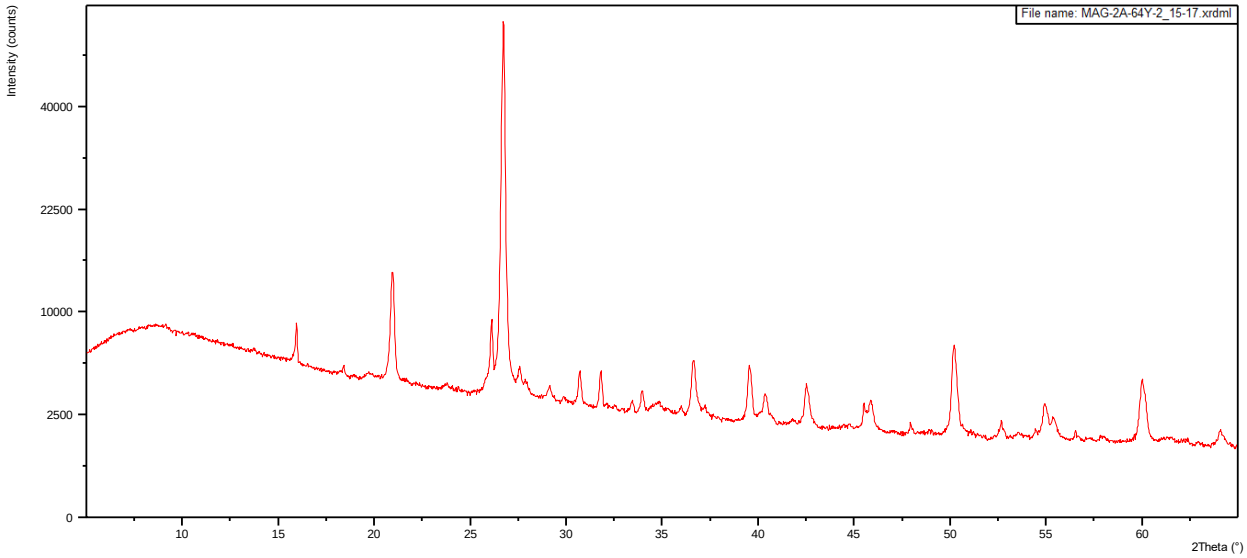
File name: MAG-2A-64Y-2_15-17.xrdml
Intensity (counts)
40000
22500
10000
2500
0
10
15
20
25
30
35
40
45
50
55
60
2Theta (°)

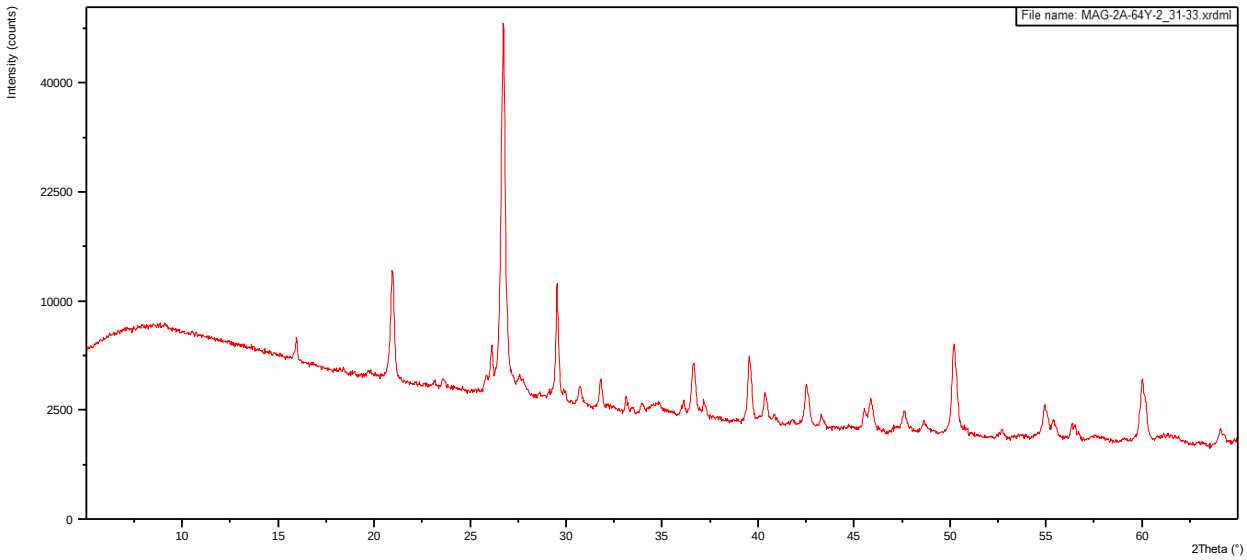
File name: MAG-2A-64Y-2_31-33.xrdml
Intensity (counts)
40000
22500
10000
2500
0
10
15
20
25
30
35
40
45
50
55
60
2Theta (°)

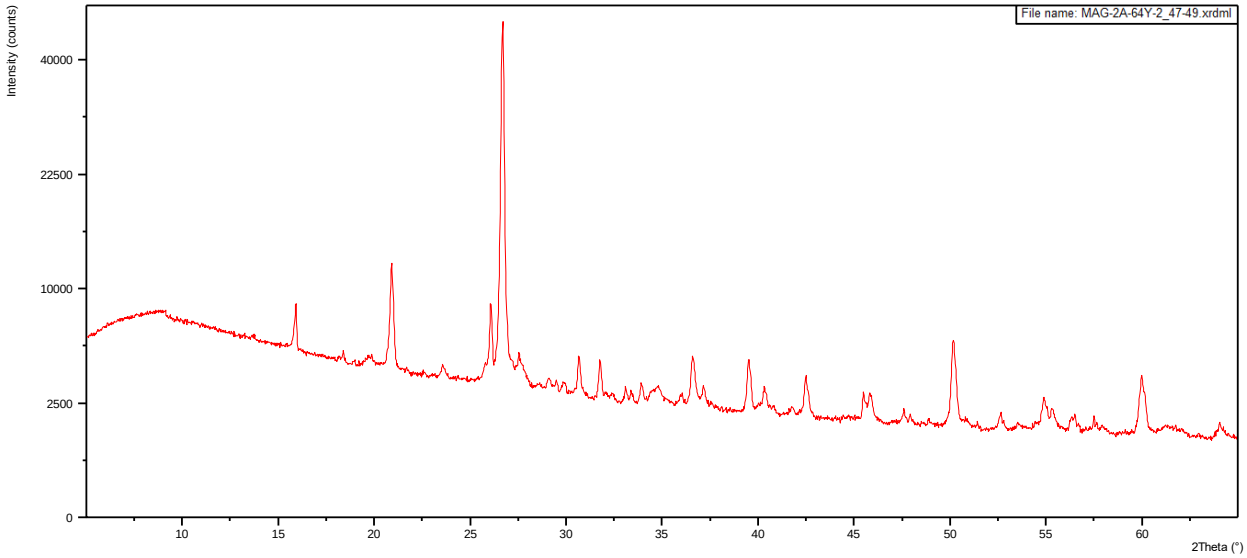
File name: MAG-2A-64Y-2_47-49.xrdml
Intensity (counts)
40000
22500
10000
2500
0
10
15
20
25
30
35
40
45
50
55
60
2Theta (°)

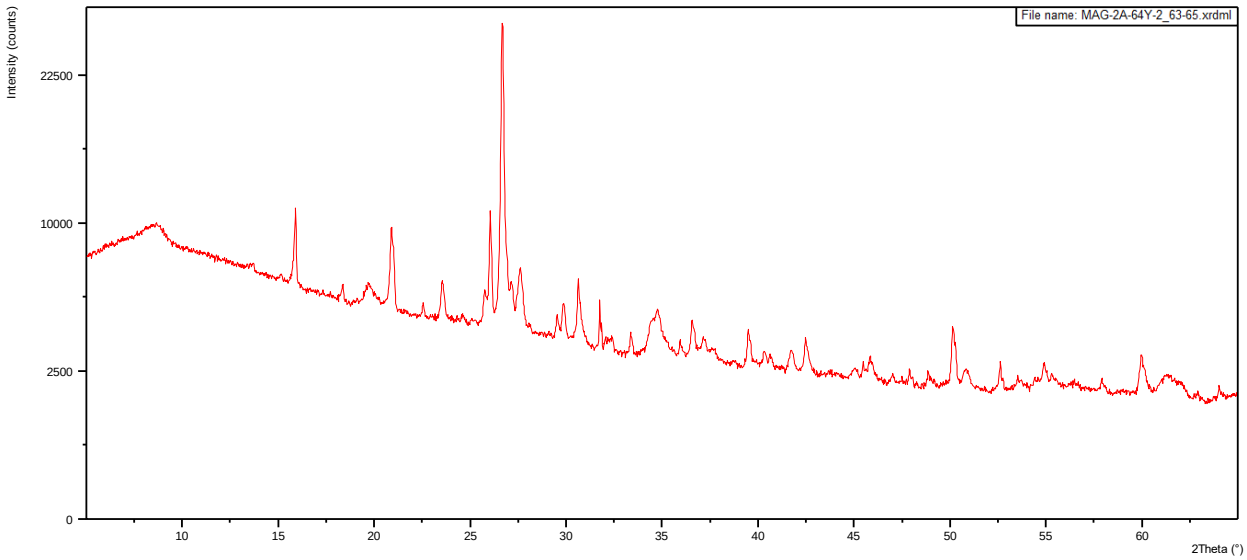
File name: MAG-2A-64Y-2_63-65.xrdml
Intensity (counts)
22500
10000
2500
0
10
15
20
25
30
35
40
45
50
55
60
2Theta (°)

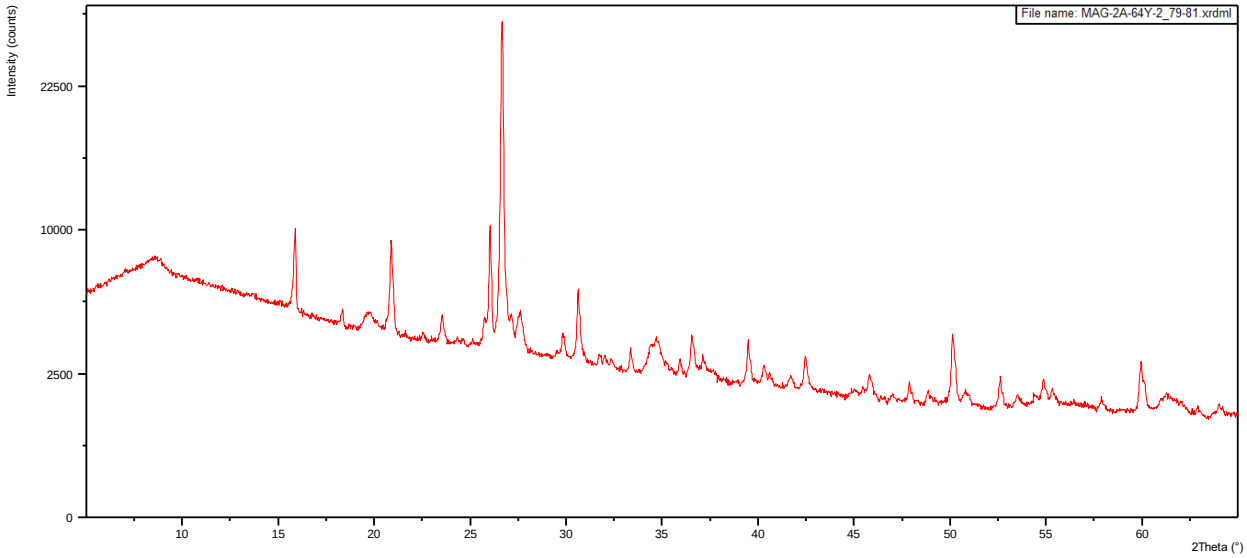
File name: MAG-2A-64Y-2_79-81.xrdml
Intensity (counts)
22500
10000
2500
0
10
15
20
25
30
35
40
45
50
55
60
2Theta (°)

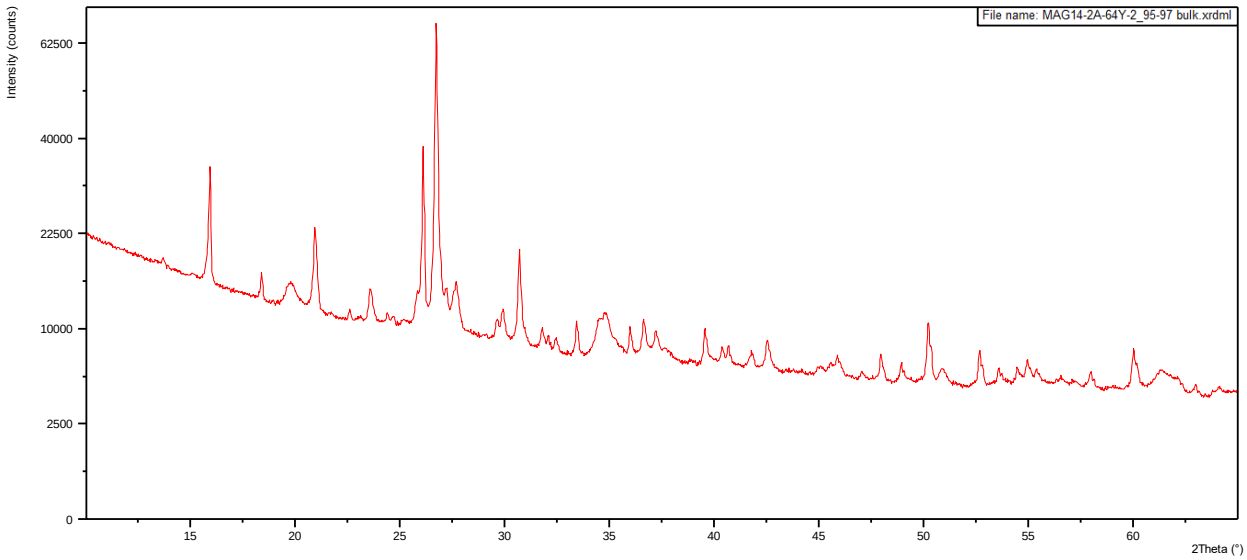
File name: MAG14-2A-64Y-2_95-97 bulk.xrdml
Intensity (counts)
62500
40000
22500
10000
2500
0
15
20
25
30
35
40
45
50
55
60
2Theta (°)

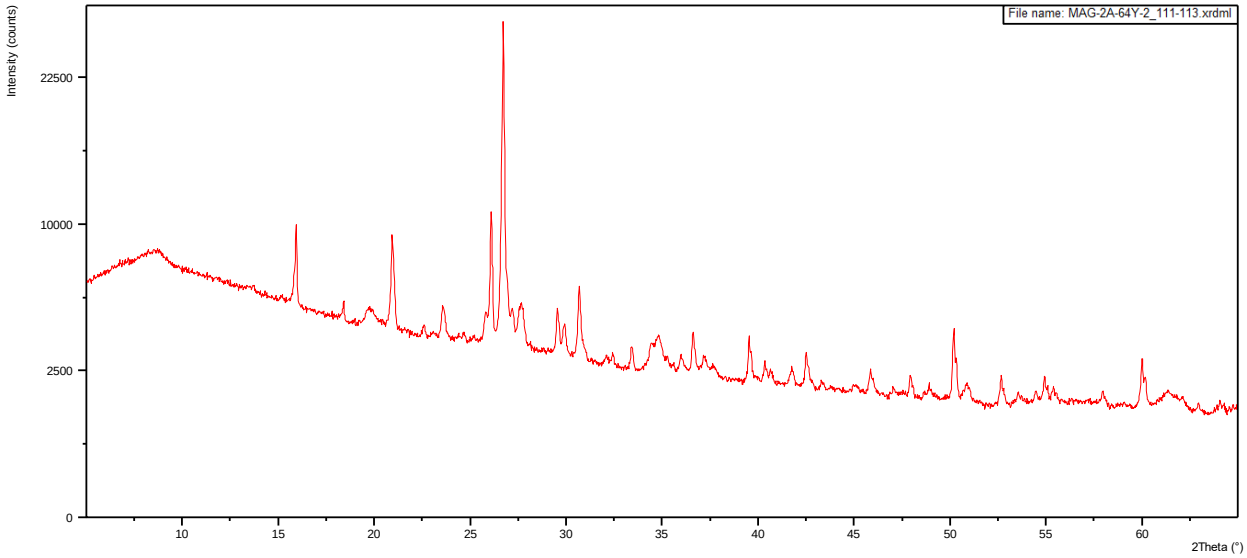
File name: MAG-2A-64Y-2_111-113.xrdml
Intensity (counts)
22500
10000
2500
0
10
15
20
25
30
35
40
45
50
55
60
2Theta (°)

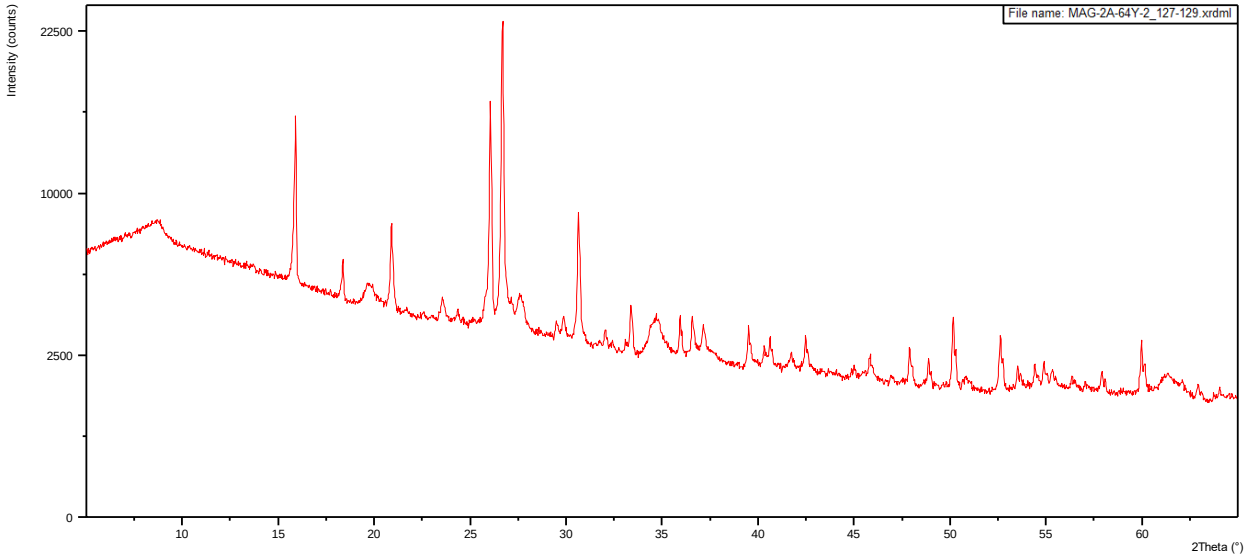
File name: MAG-2A-64Y-2_127-129.xrdml
Intensity (counts)
22500
10000
2500
0
10
15
20
25
30
35
40
45
50
55
60
2Theta (°)

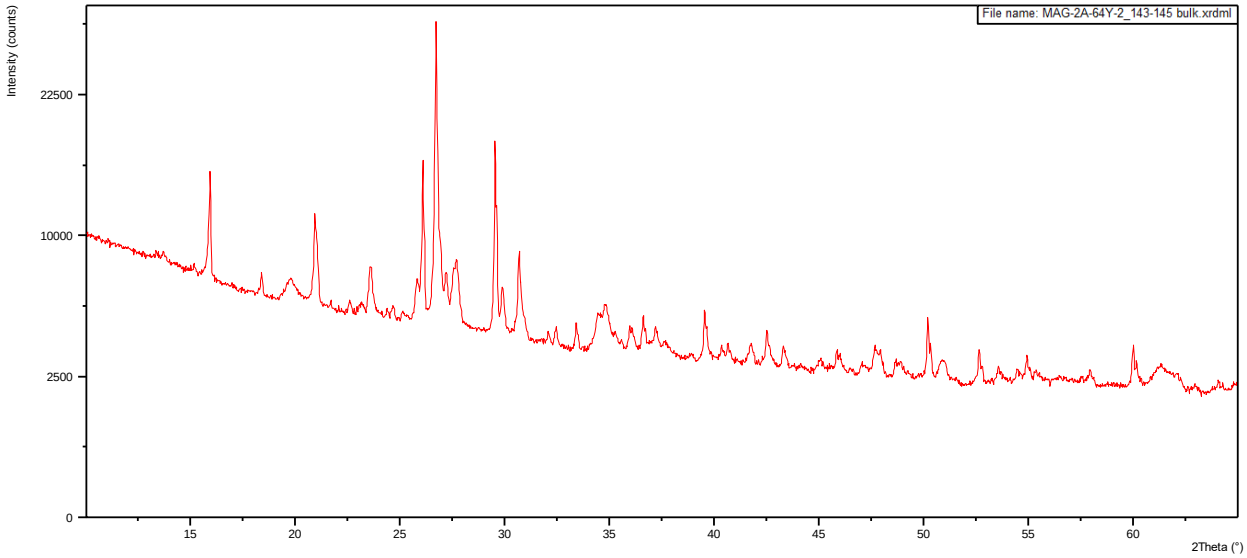
File name: MAG-2A-64Y-2_143-145 bulk.xrdml
Intensity (counts)
22500
10000
2500
0
15
20
25
30
35
40
45
50
55
60
2Theta (°)

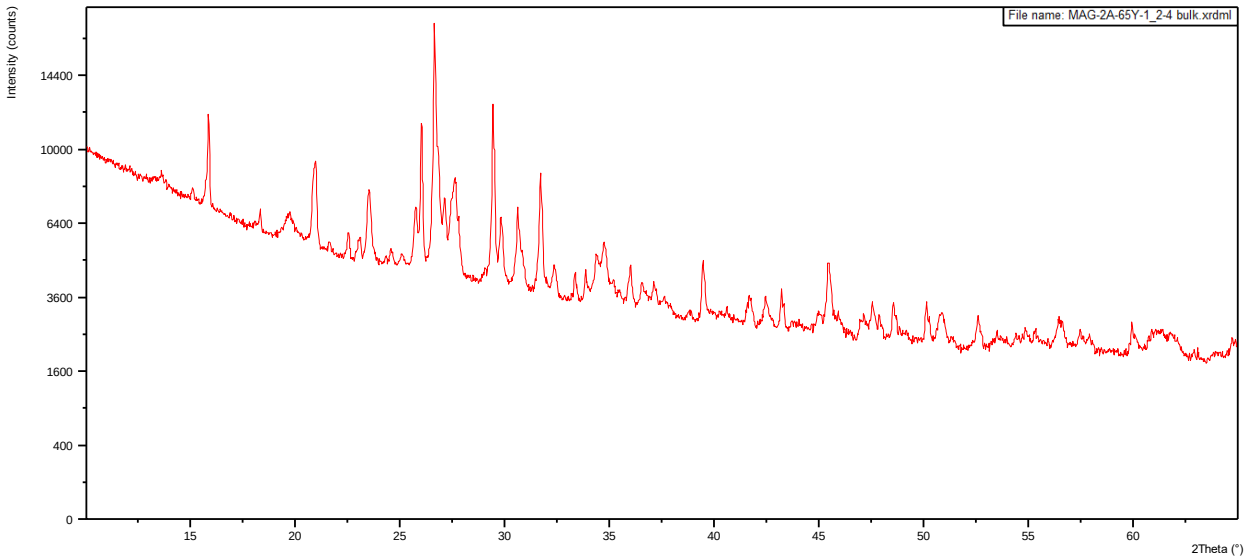
File name: MAG-2A-65Y-1_2-4 bulk.xrdml
Intensity (counts)
14400
10000
6400
3600
1600
400
0
15
20
25
30
35
40
45
50
55
60
2Theta (°)

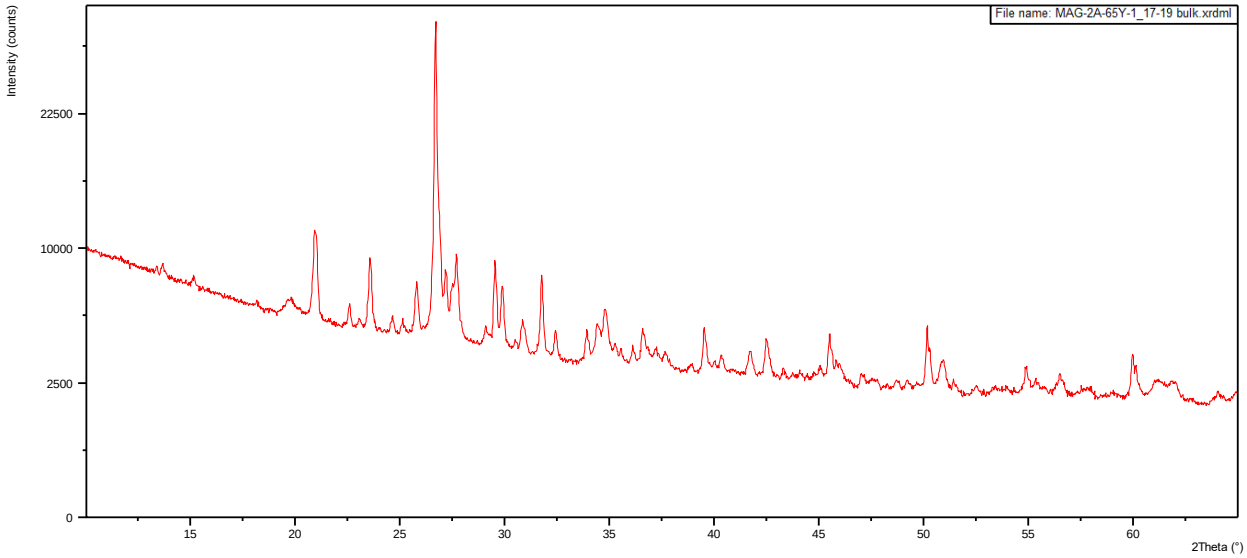
File name: MAG-2A-65Y-1_17-19 bulk.xrdml
Intensity (counts)
22500
10000
2500
0
15
20
25
30
35
40
45
50
55
60
2Theta (°)

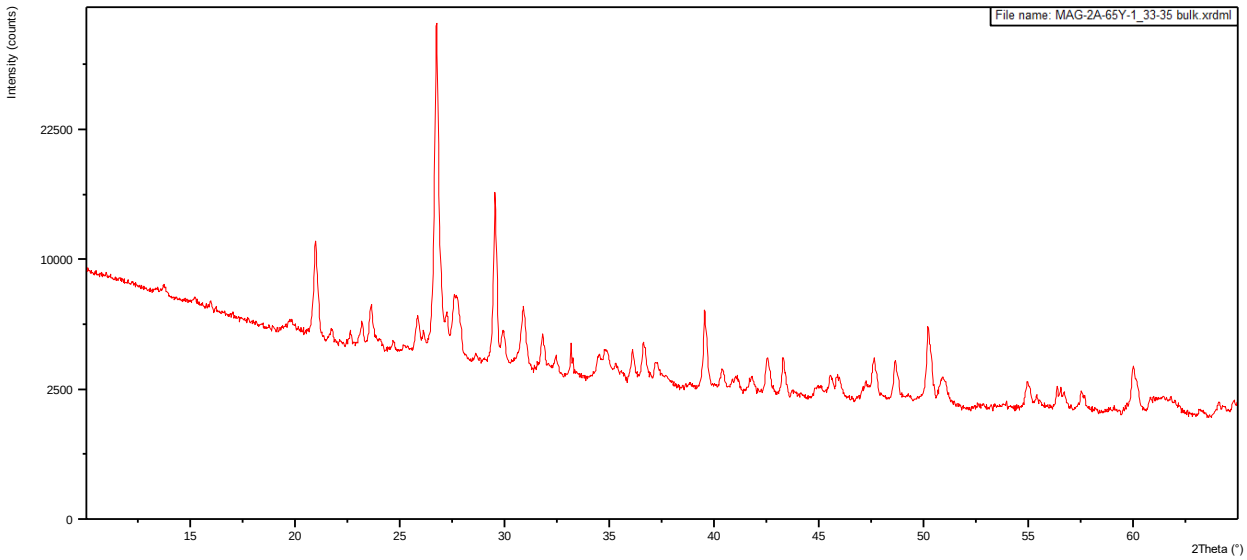
File name: MAG-2A-65Y-1_33-35 bulk.xrdml
Intensity (counts)
22500
10000
2500
0
15
20
25
30
35
40
45
50
55
60
2Theta (°)

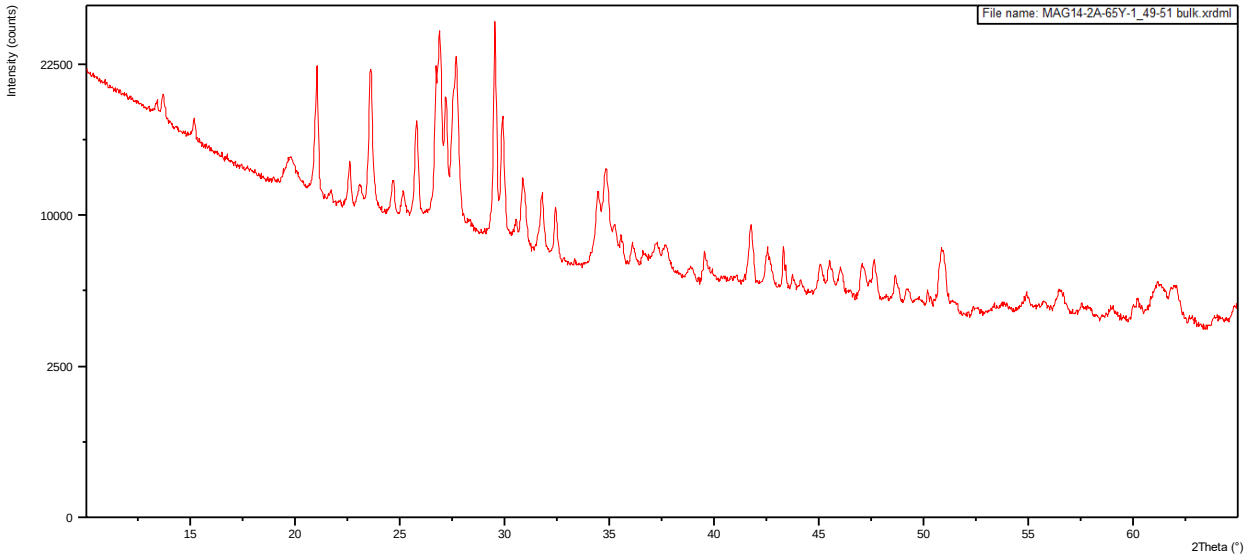
File name: MAG14-2A-65Y-1_49-51 bulk.xrdml
Intensity (counts)
22500
10000
2500
0
15
20
25
30
35
40
45
50
55
60
2Theta (°)

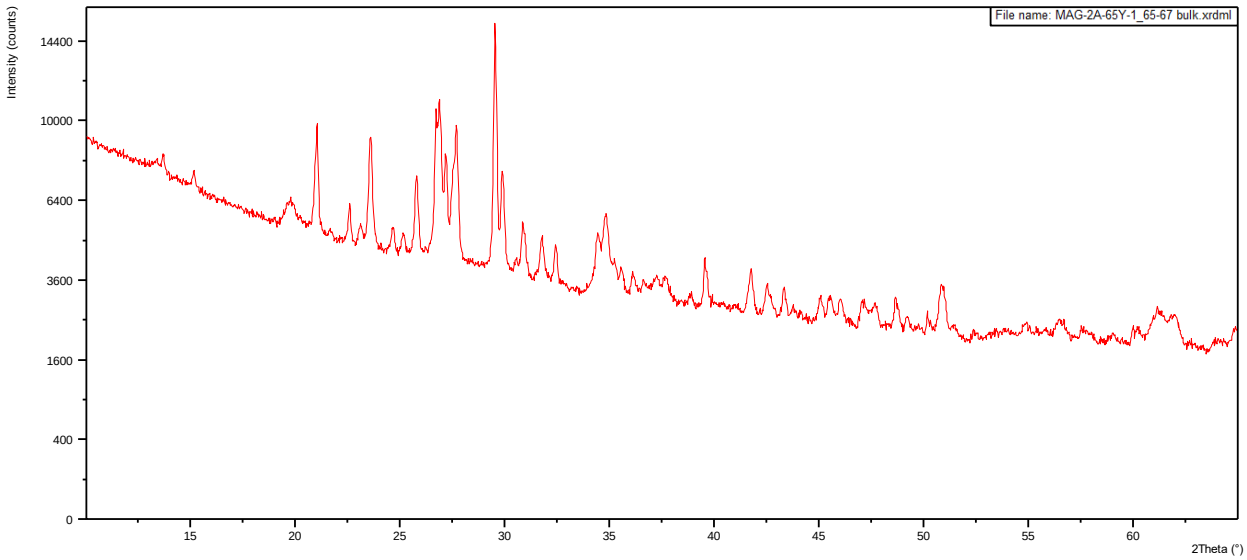
File name: MAG-2A-65Y-1_65-67 bulk.xrdml
Intensity (counts)
14400
10000
6400
3600
1600
400
0
15
20
25
30
35
40
45
50
55
60
2Theta (°)

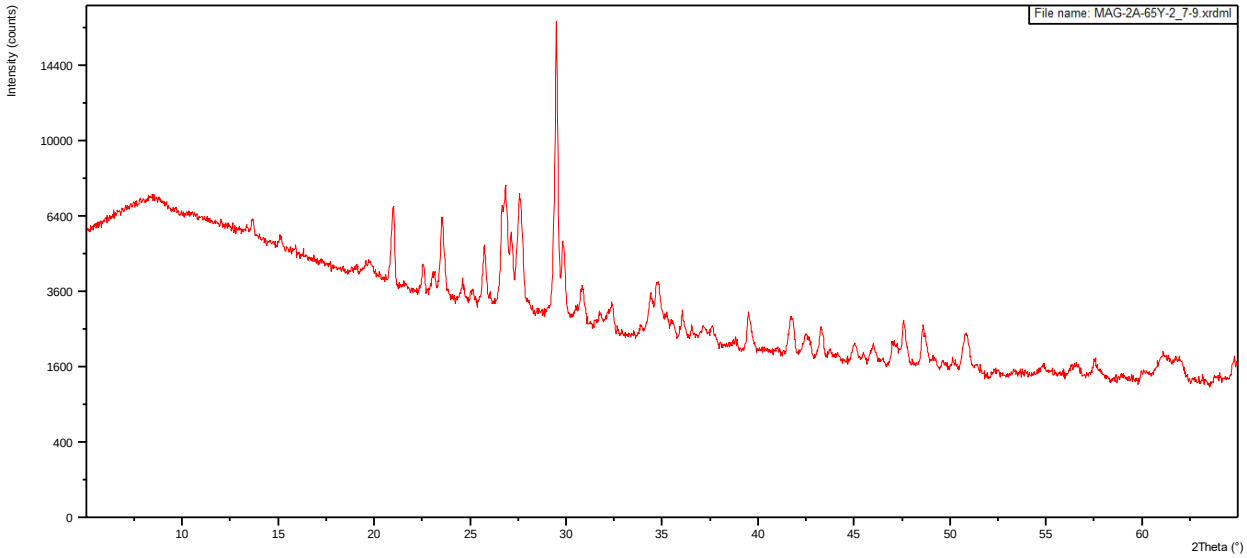
File name: MAG-2A-65Y-2_7-9.xrdml
Intensity (counts)
14400
10000
6400
3600
1600
400
0
10
15
20
25
30
35
40
45
50
55
60
2Theta (°)

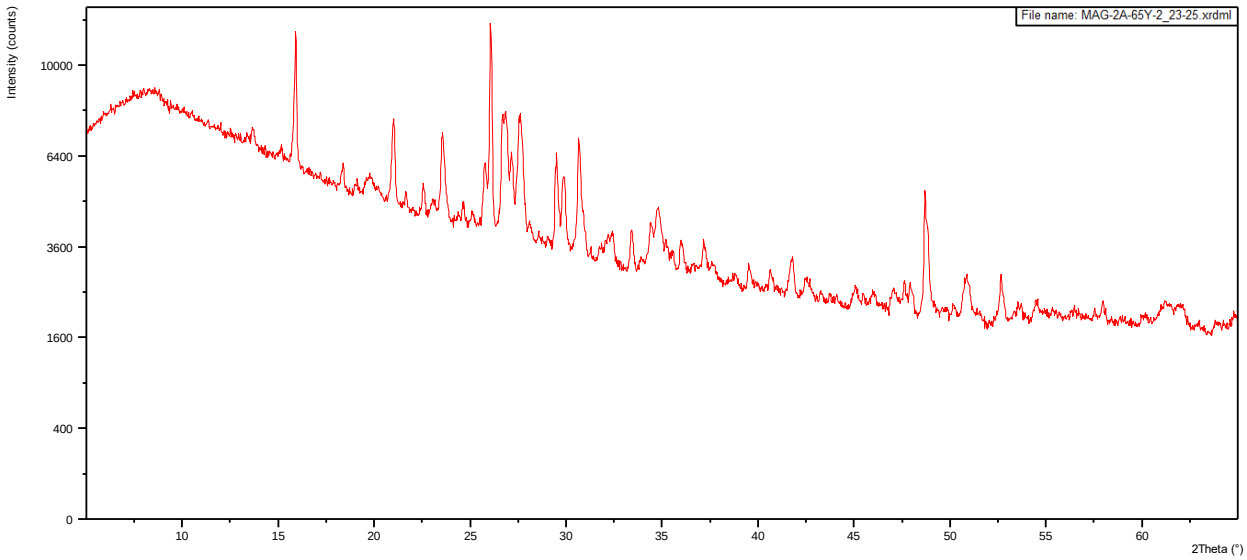
File name: MAG-2A-65Y-2_23-25.xrdml
Intensity (counts)
10000
6400
3600
1600
400
0
10
15
20
25
30
35
40
45
50
55
60
2Theta (°)

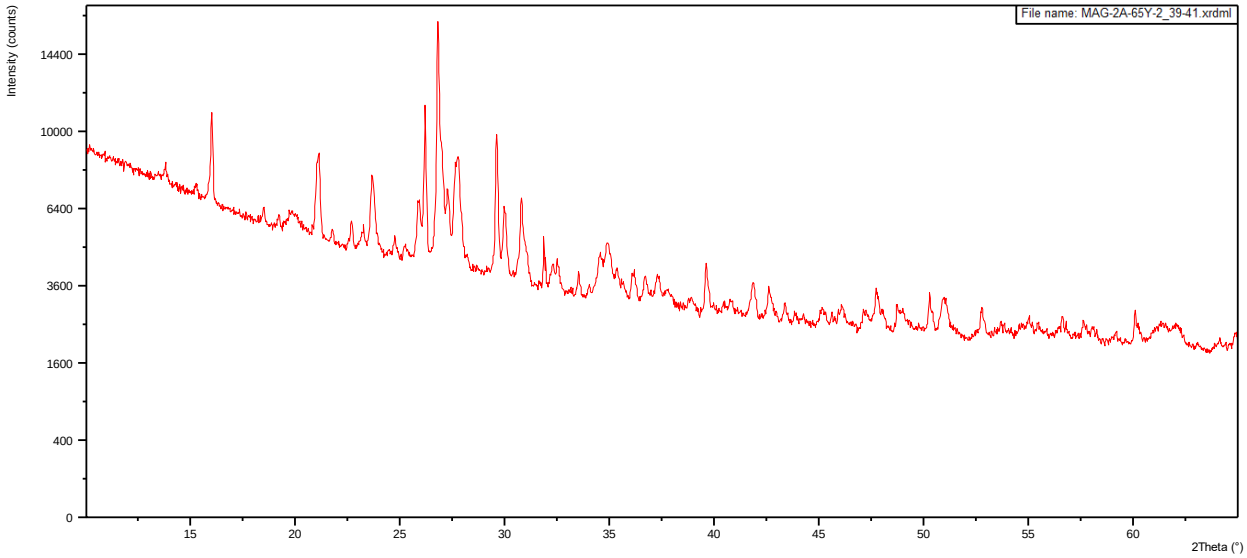
File name: MAG-2A-65Y-2_39-41.xrdml
Intensity (counts)
14400
10000
6400
3600
1600
400
0
15
20
25
30
35
40
45
50
55
60
2Theta (°)

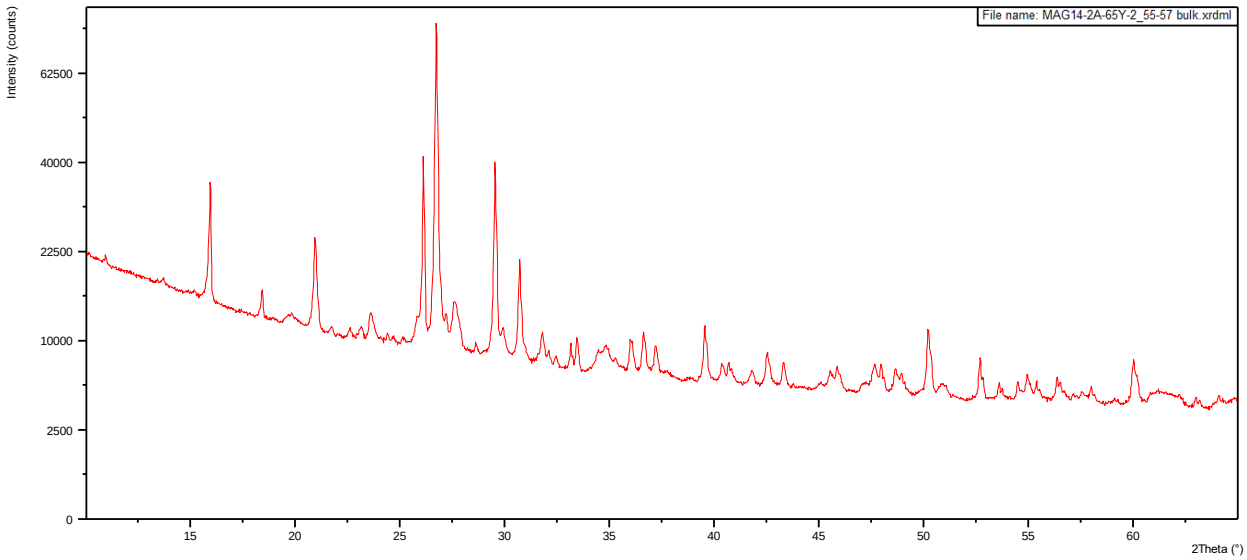
File name: MAG14-2A-65Y-2_55-57 bulk.xrdml
Intensity (counts)
62500
40000
22500
10000
2500
0
15
20
25
30
35
40
45
50
55
60
2Theta (°)

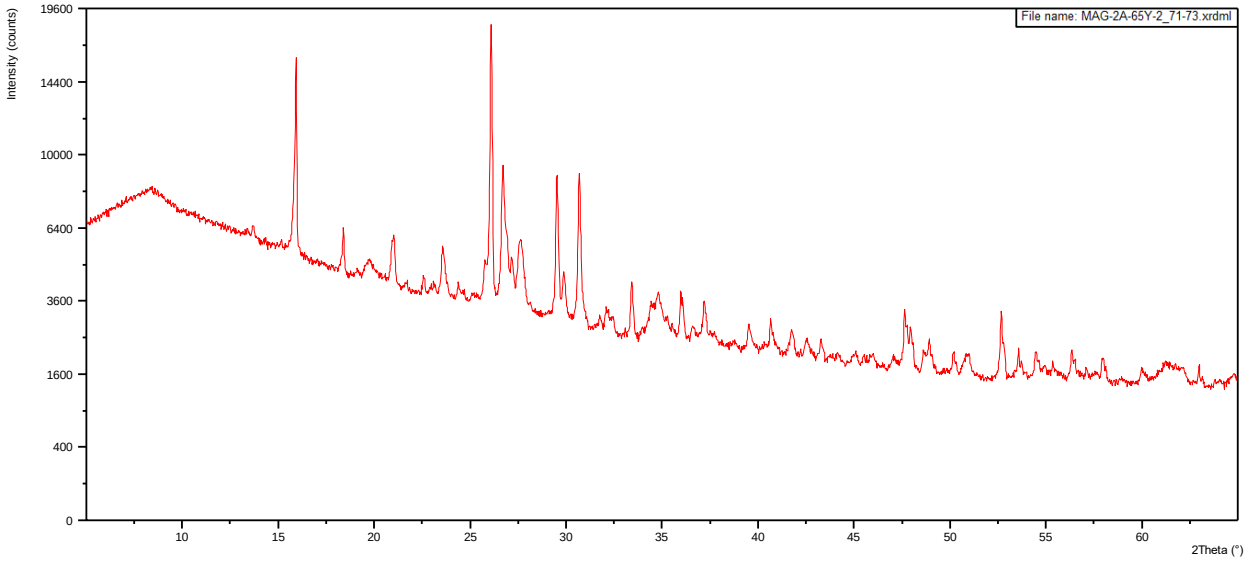
File name: MAG-2A-65Y-2_71-73.xrdml
Intensity (counts)
19600
14400
10000
6400
3600
1600
400
0
10
15
20
25
30
35
40
45
50
55
60
2Theta (°)

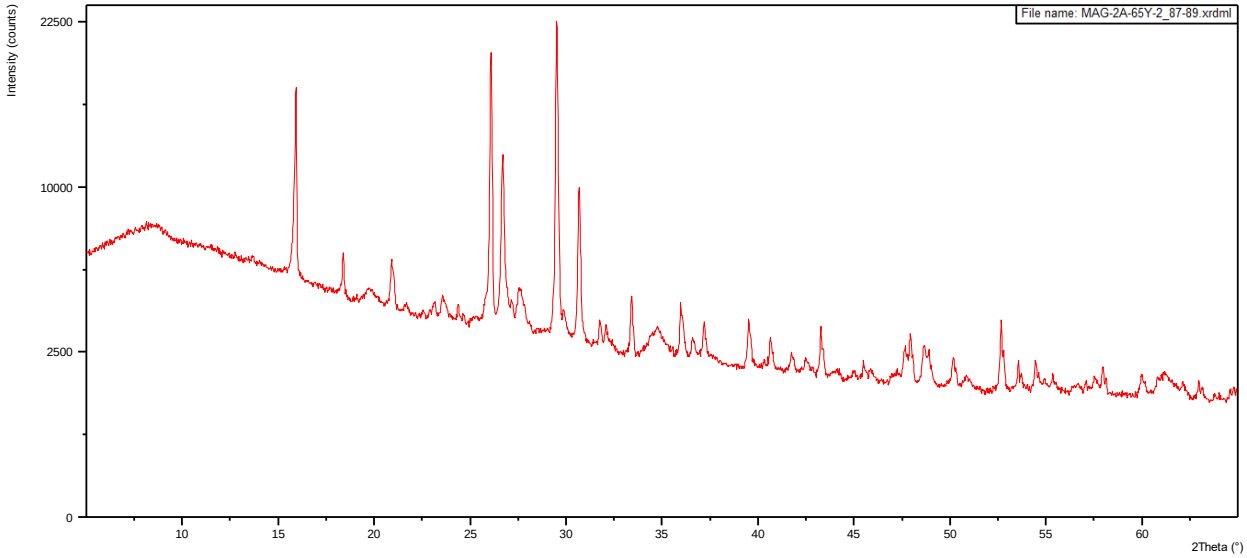
File name: MAG-2A-65Y-2_87-89.xrdml
Intensity (counts)
22500
10000
2500
0
10
15
20
25
30
35
40
45
50
55
60
2Theta (°)

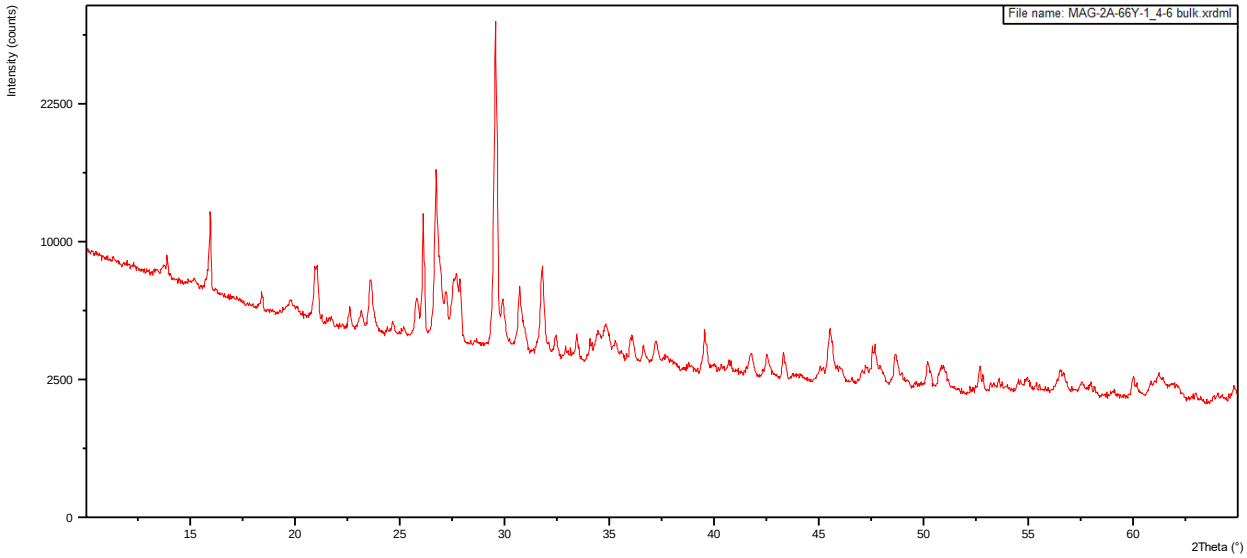
File name: MAG-2A-66Y-1_4-6 bulk.xrdml
Intensity (counts)
22500
10000
2500
0
15
20
25
30
35
40
45
50
55
60
2Theta (°)

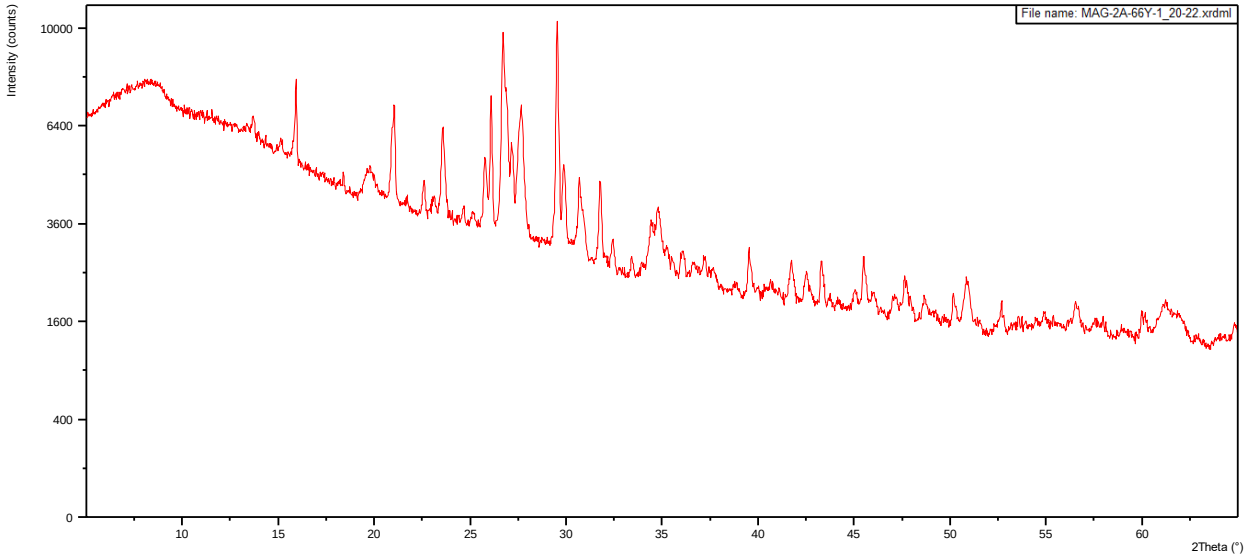
File name: MAG-2A-66Y-1_20-22.xrdml
Intensity (counts)
10000
6400
3600
1600
400
0
10
15
20
25
30
35
40
45
50
55
60
2Theta (°)

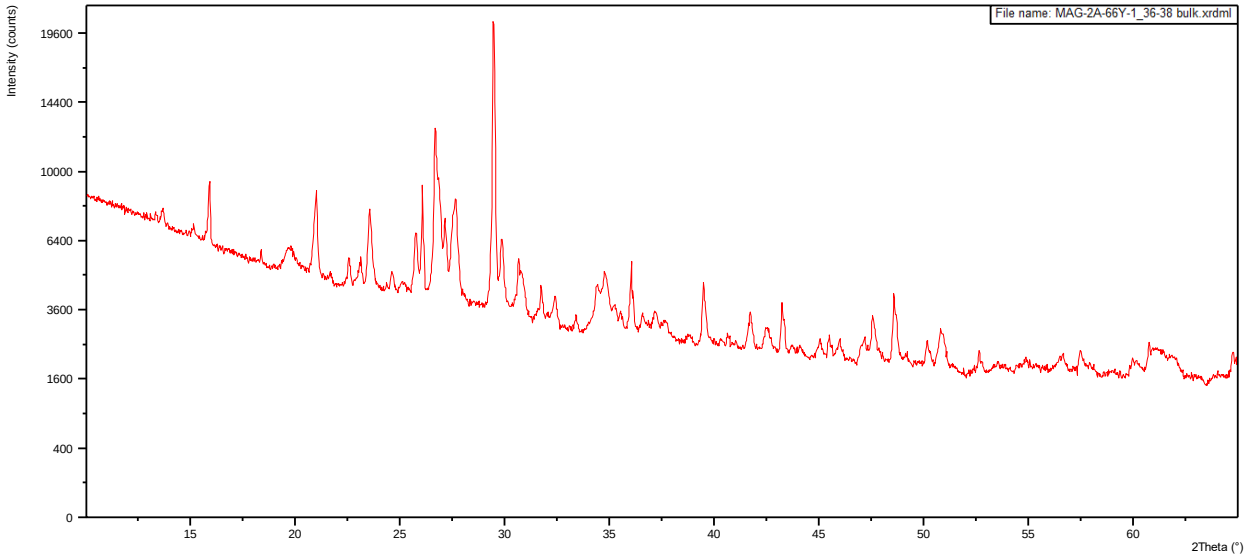
File name: MAG-2A-66Y-1_36-38 bulk.xrdml
Intensity (counts)
19600
14400
10000
6400
3600
1600
400
0
15
20
25
30
35
40
45
50
55
60
2Theta (°)

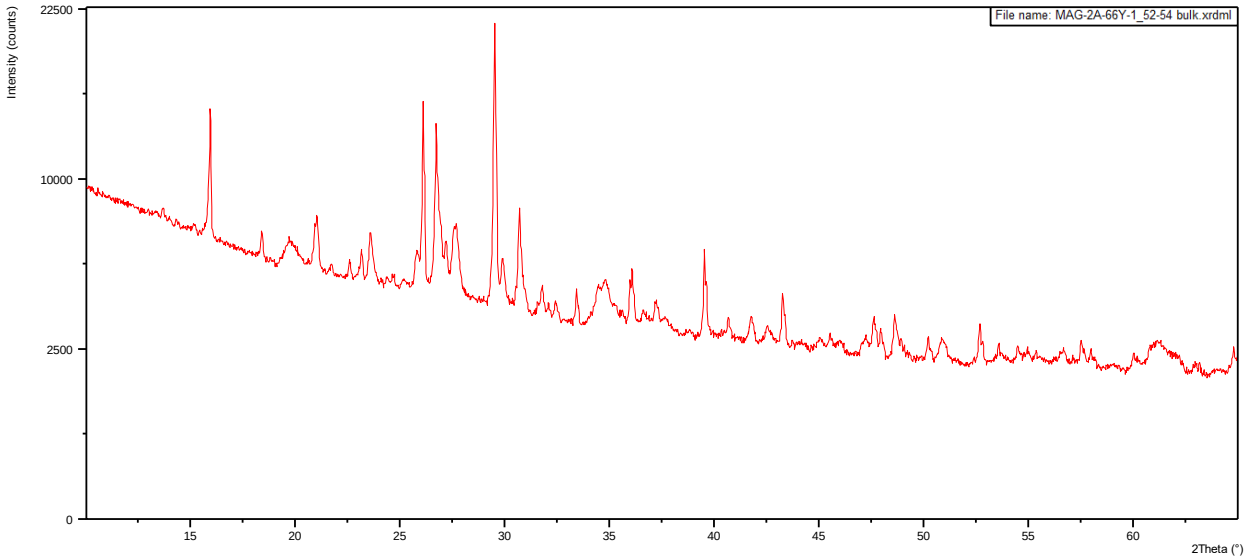
File name: MAG-2A-66Y-1_52-54 bulk.xrdml
Intensity (counts)
22500
10000
2500
0
15
20
25
30
35
40
45
50
55
60
2Theta (°)

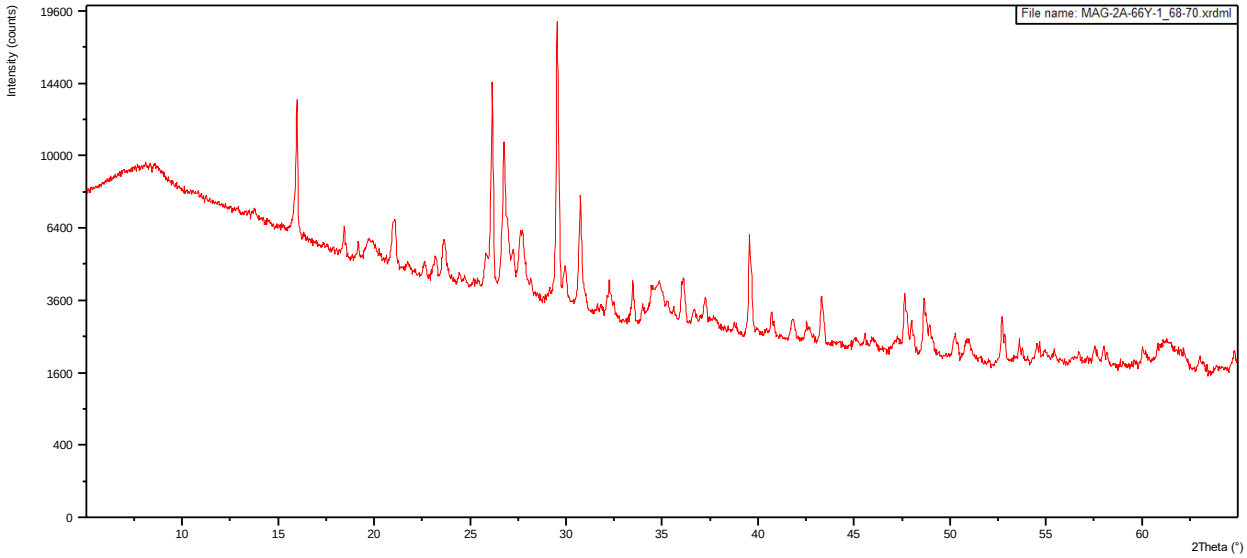
File name: MAG-2A-66Y-1_68-70.xrdml
Intensity (counts)
19600
14400
10000
6400
3600
1600
400
0
10
15
20
25
30
35
40
45
50
55
60
2Theta (°)

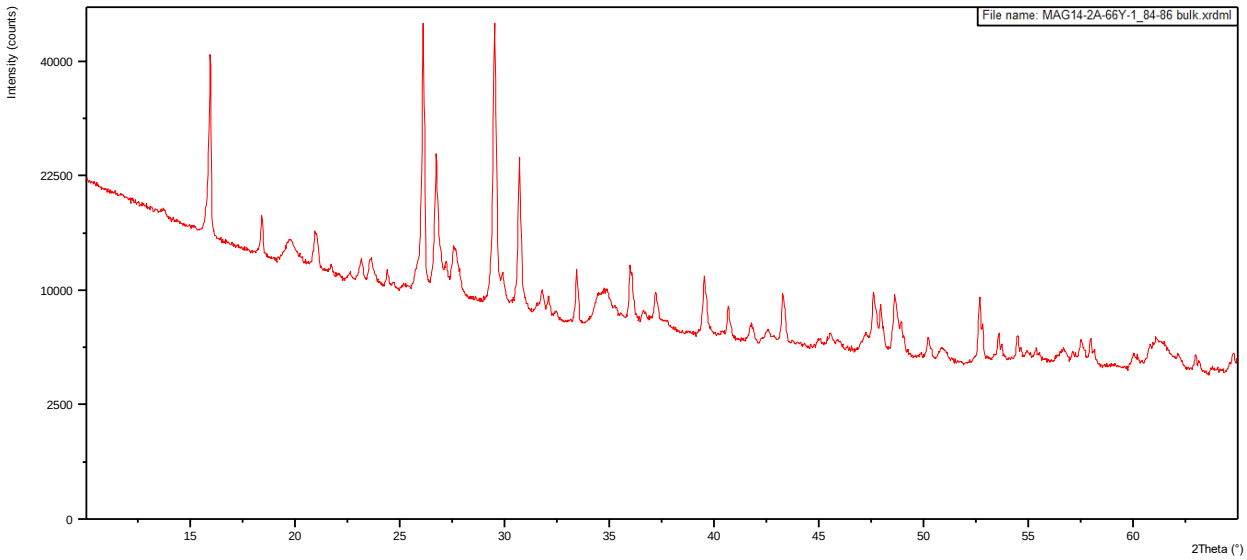
File name: MAG14-2A-66Y-1_84-86 bulk.xrdml
Intensity (counts)
40000
22500
10000
2500
0
15
20
25
30
35
40
45
50
55
60
2Theta (°)

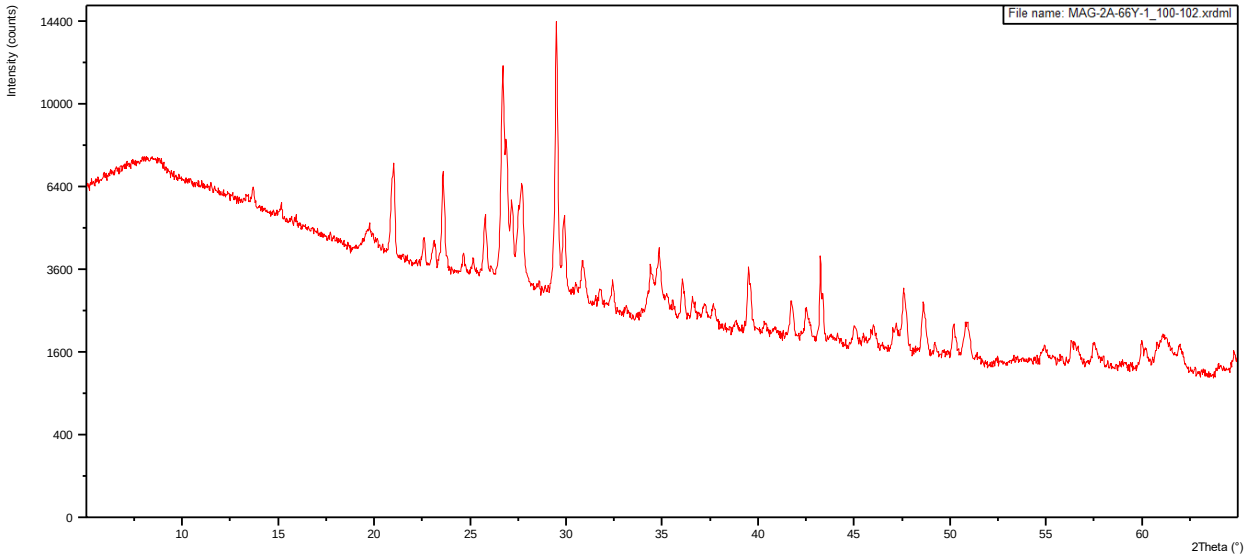
File name: MAG-2A-66Y-1_100-102.xrdml
Intensity (counts)
14400
10000
6400
3600
1600
400
0
10
15
20
25
30
35
40
45
50
55
60
2Theta (°)

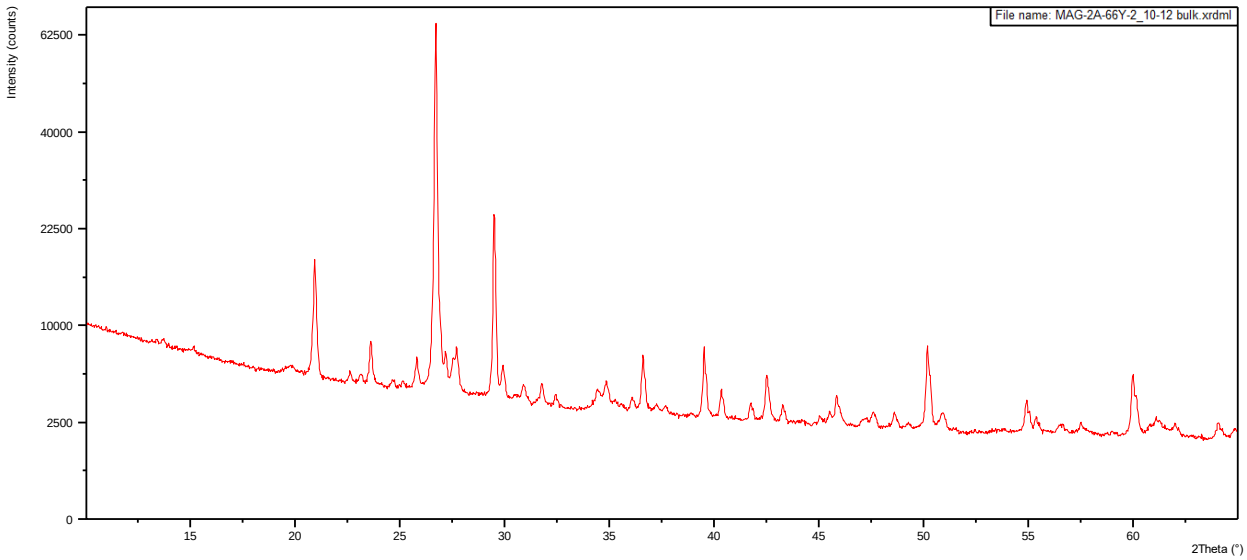
File name: MAG-2A-66Y-2_10-12 bulk.xrdml
Intensity (counts)
62500
40000
22500
10000
2500
0
15
20
25
30
35
40
45
50
55
60
2Theta (°)

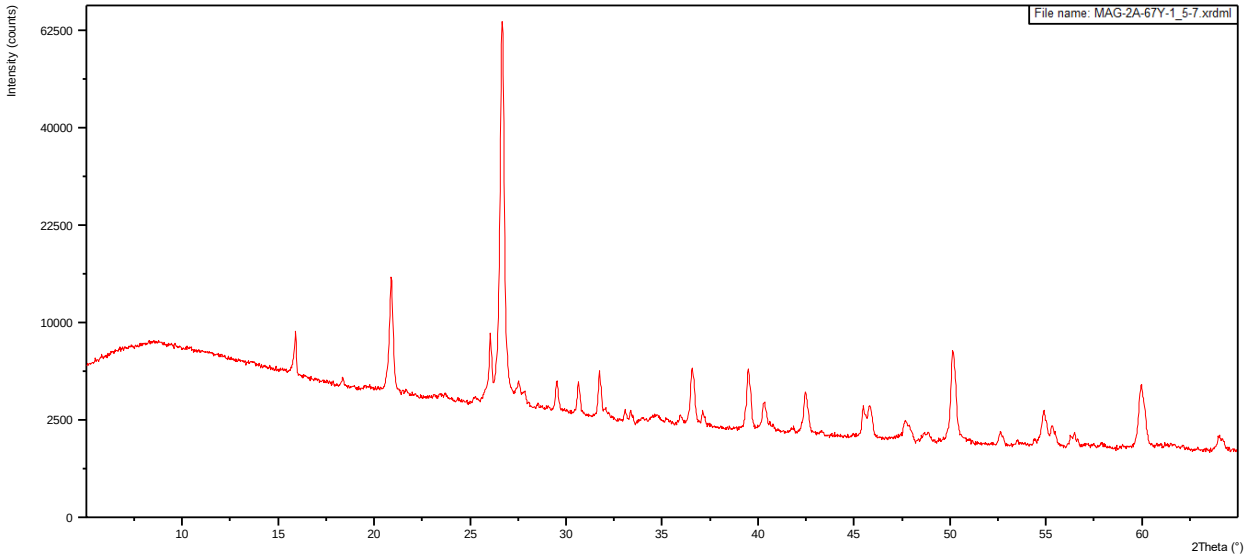
File name: MAG-2A-67Y-1_5-7.xrdml
Intensity (counts)
62500
40000
22500
10000
2500
0
10
15
20
25
30
35
40
45
50
55
60
2Theta (°)

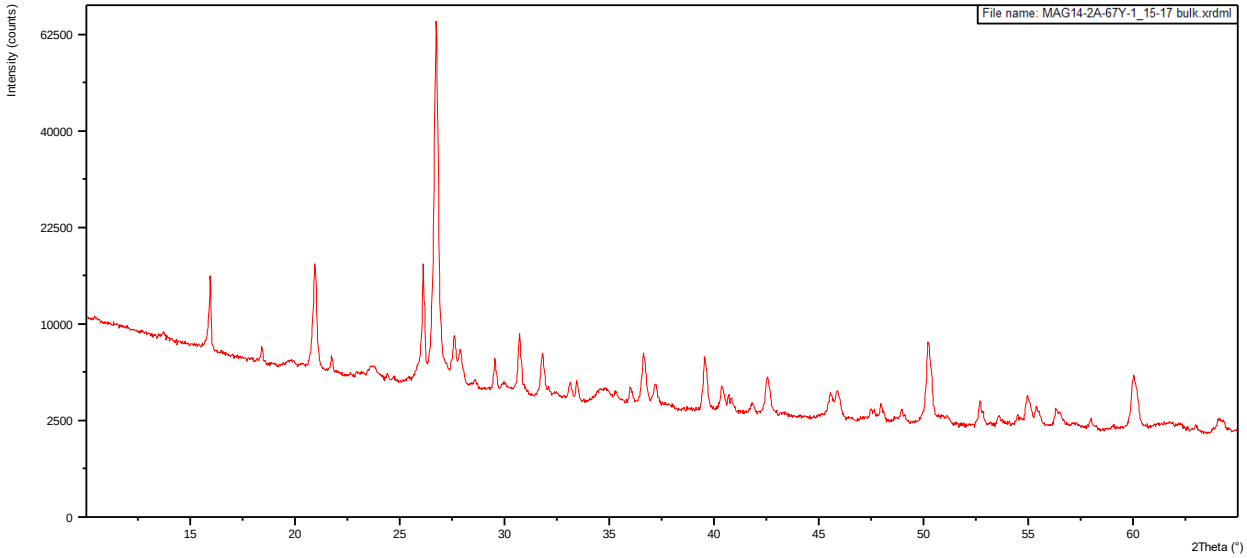
File name: MAG14-2A-67Y-1_15-17 bulk.xrdml
Intensity (counts)
62500
40000
22500
10000
2500
0
15
20
25
30
35
40
45
50
55
60
2Theta (°)

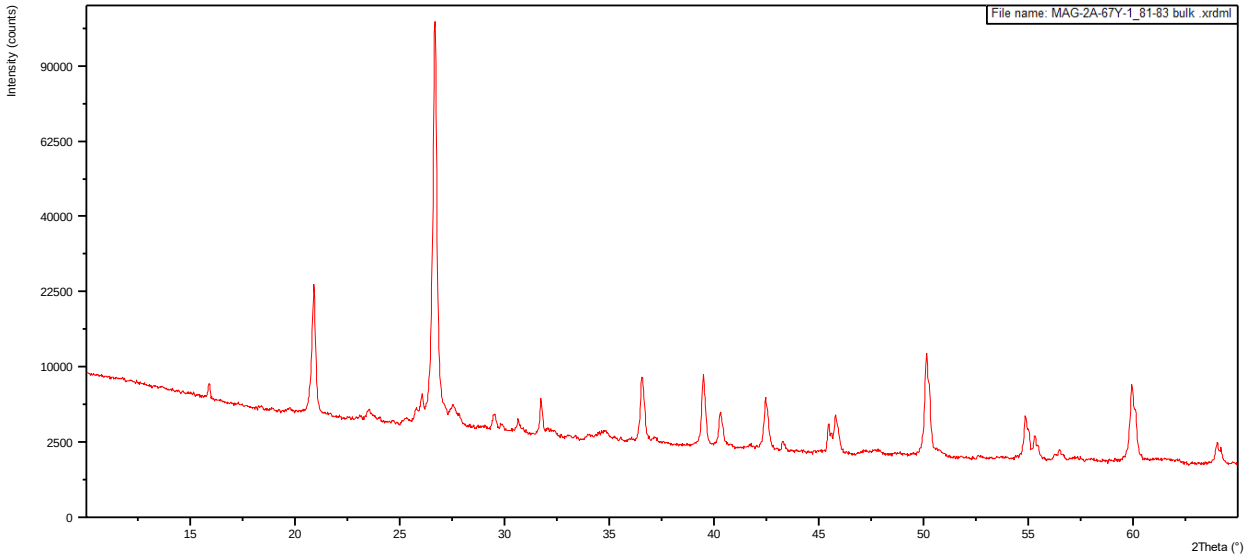
File name: MAG-2A-67Y-1_81-83 bulk .xrdml
Intensity (counts)
90000
62500
40000
22500
10000
2500
0
15
20
25
30
35
40
45
50
55
60
2Theta (°)

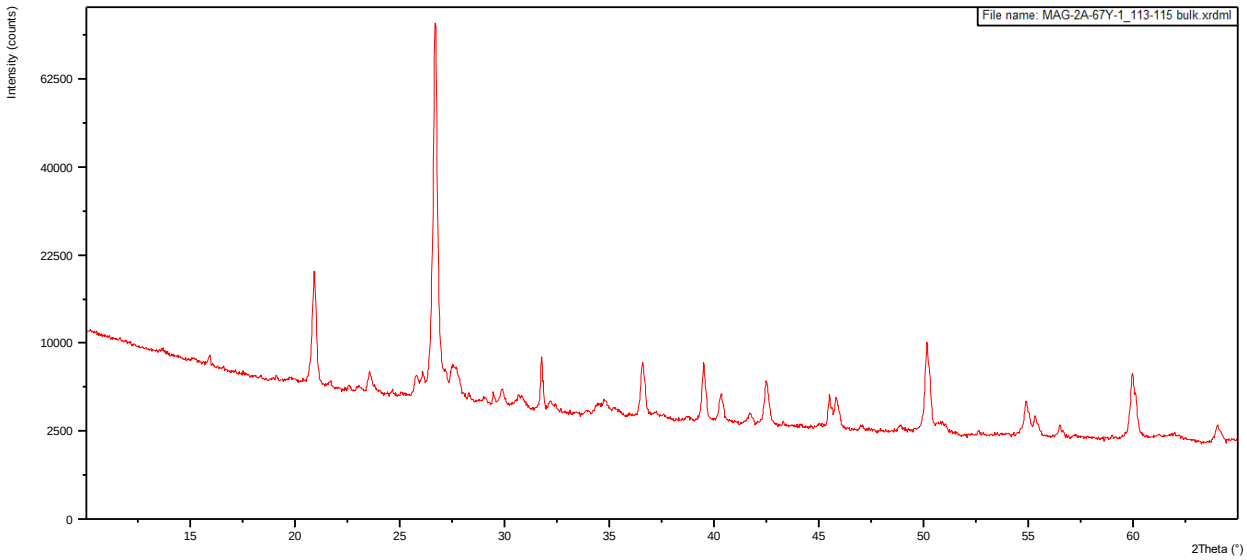
File name: MAG-2A-67Y-1_113-115 bulk.xrdml
Intensity (counts)
62500
40000
22500
10000
2500
0
15
20
25
30
35
40
45
50
55
60
2Theta (°)

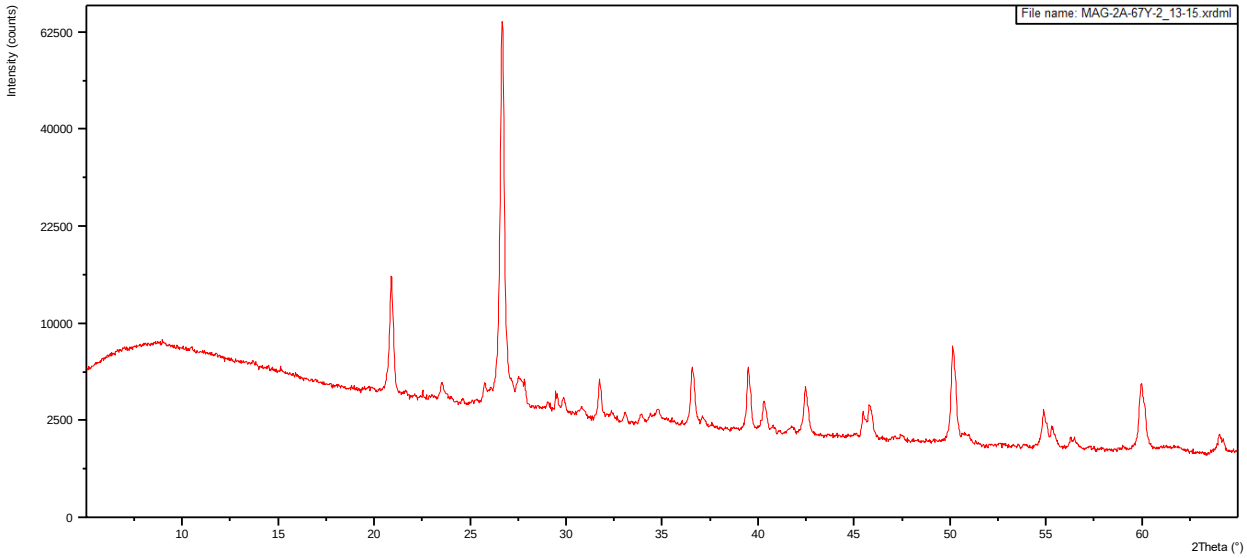
File name: MAG-2A-67Y-2_13-15.xrdml
Intensity (counts)
62500
40000
22500
10000
2500
0
10
15
20
25
30
35
40
45
50
55
60
2Theta (°)

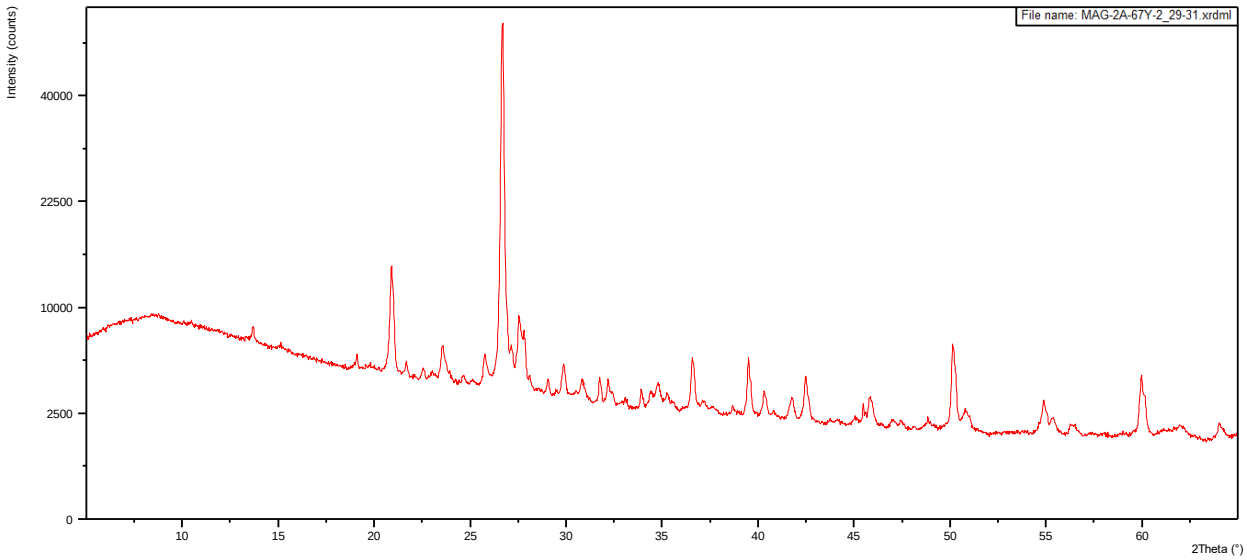
File name: MAG-2A-67Y-2_29-31.xrdml
Intensity (counts)
40000
22500
10000
2500
0
10
15
20
25
30
35
40
45
50
55
60
2Theta (°)

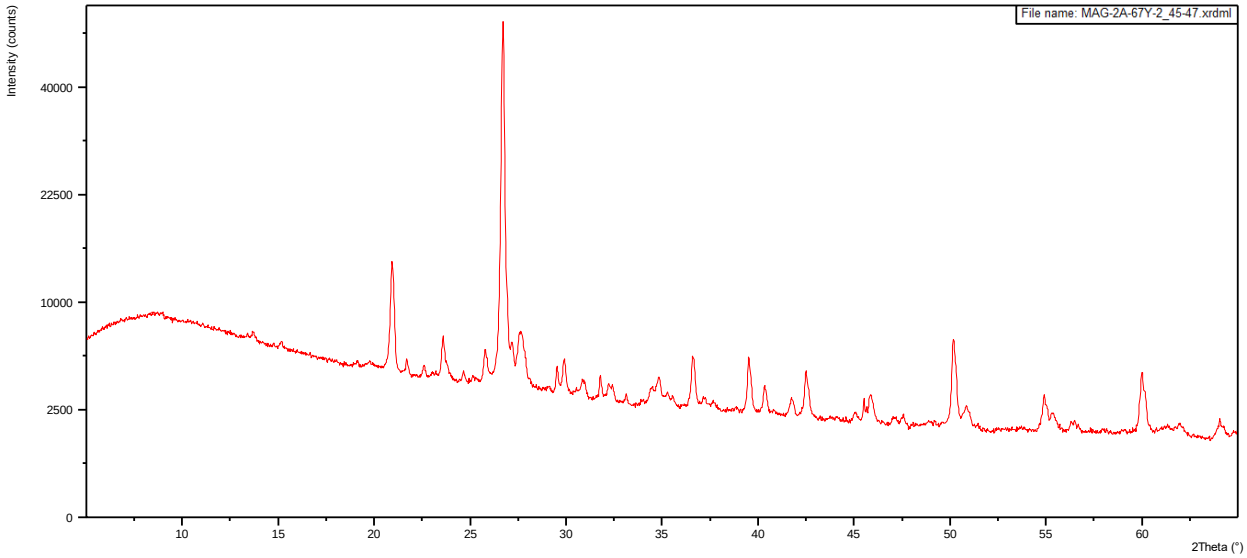
File name: MAG-2A-67Y-2_45-47.xrdml
Intensity (counts)
40000
22500
10000
2500
0
10
15
20
25
30
35
40
45
50
55
60
2Theta (°)

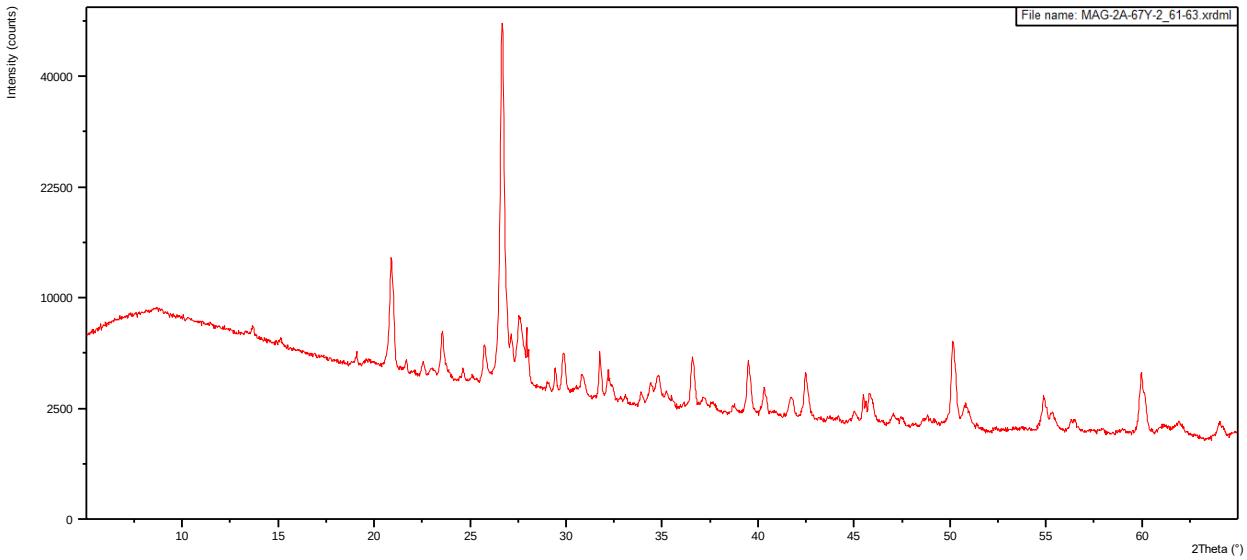
File name: MAG-2A-67Y-2_61-63.xrdml
Intensity (counts)
40000
22500
10000
2500
0
10
15
20
25
30
35
40
45
50
55
60
2Theta (°)

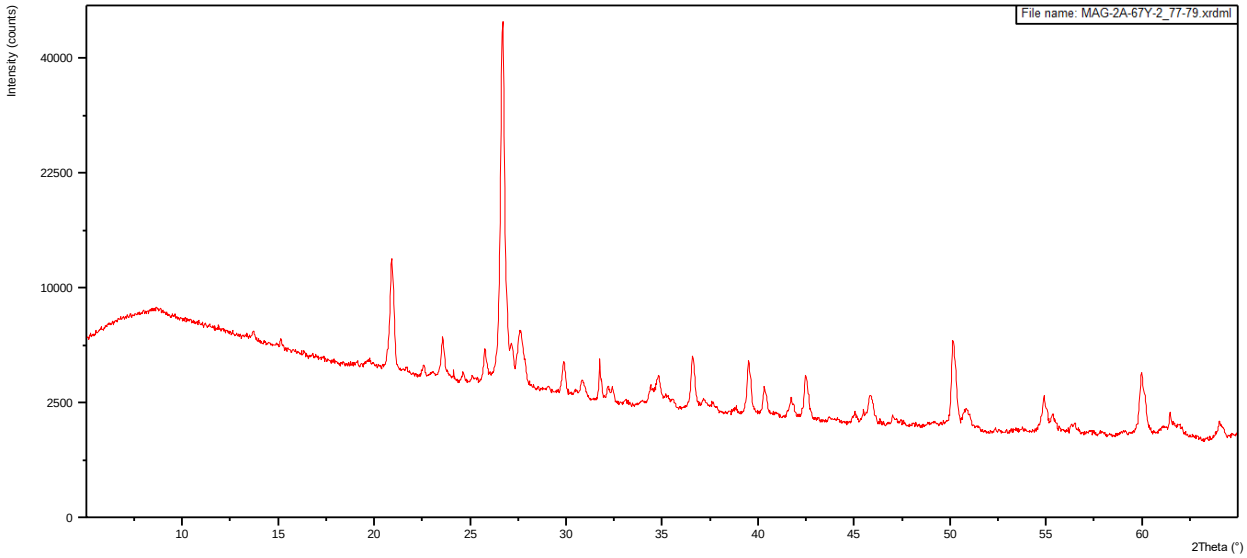
File name: MAG-2A-67Y-2_77-79.xrdml
Intensity (counts)
40000
22500
10000
2500
0
10
15
20
25
30
35
40
45
50
55
60
2Theta (°)

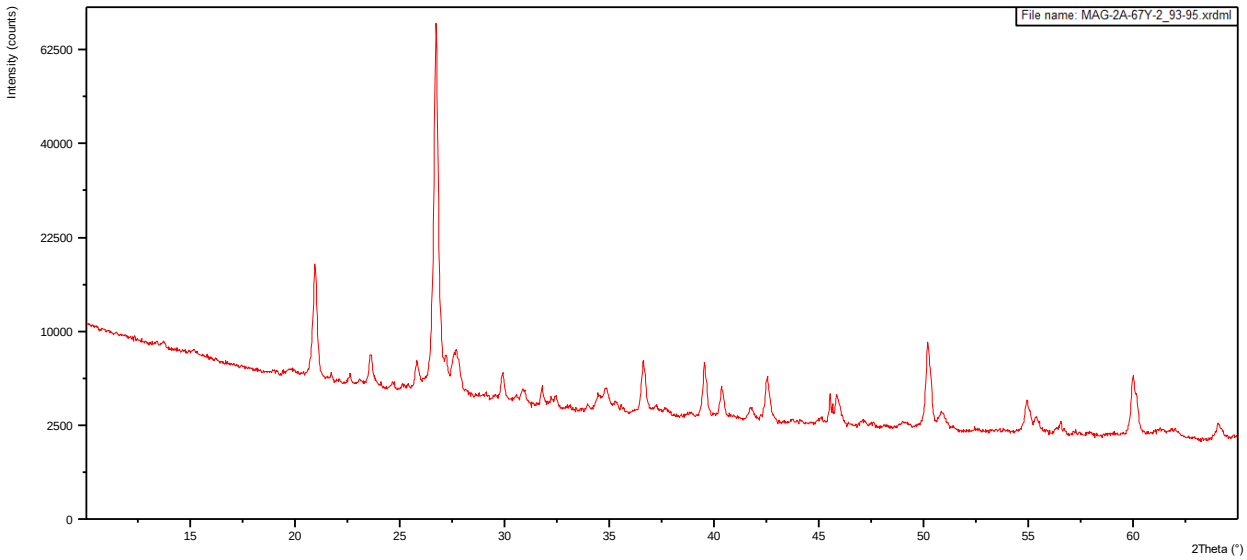
File name: MAG-2A-67Y-2_93-95.xrdml
Intensity (counts)
62500
40000
22500
10000
2500
0
15
20
25
30
35
40
45
50
55
60
2Theta (°)

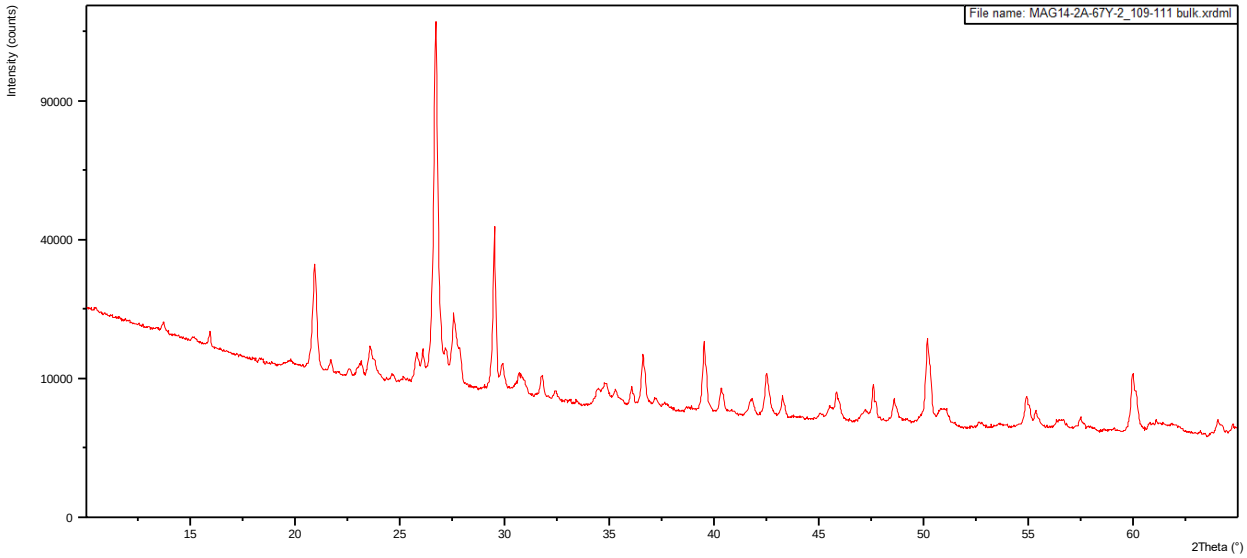
File name: MAG14-2A-67Y-2_109-111 bulk.xrdml
Intensity (counts)
90000
40000
10000
0
15
20
25
30
35
40
45
50
55
60
2Theta (°)

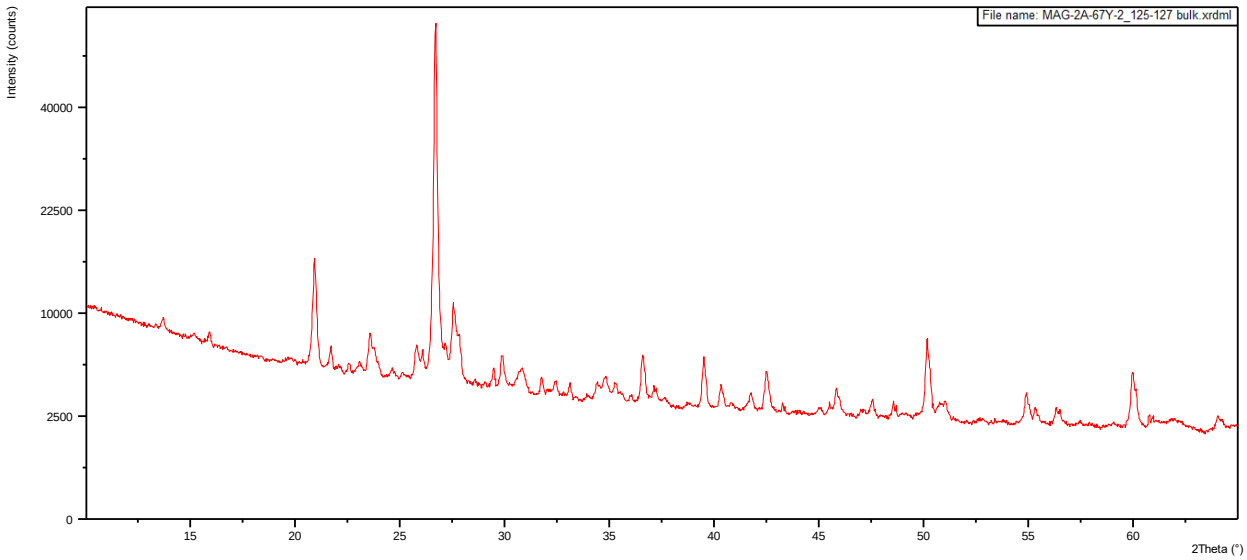
File name: MAG-2A-67Y-2_125-127 bulk.xrdml
Intensity (counts)
40000
22500
10000
2500
0
15
20
25
30
35
40
45
50
55
60
2Theta (°)

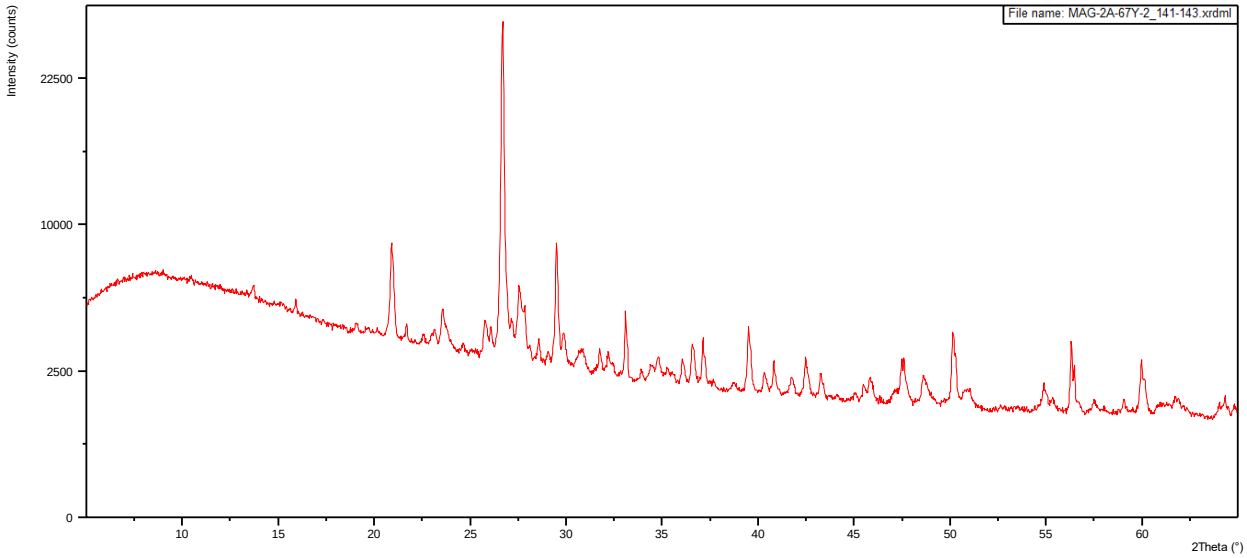
File name: MAG-2A-67Y-2_141-143.xrdml
Intensity (counts)
22500
10000
2500
0
10
15
20
25
30
35
40
45
50
55
60
2Theta (°)

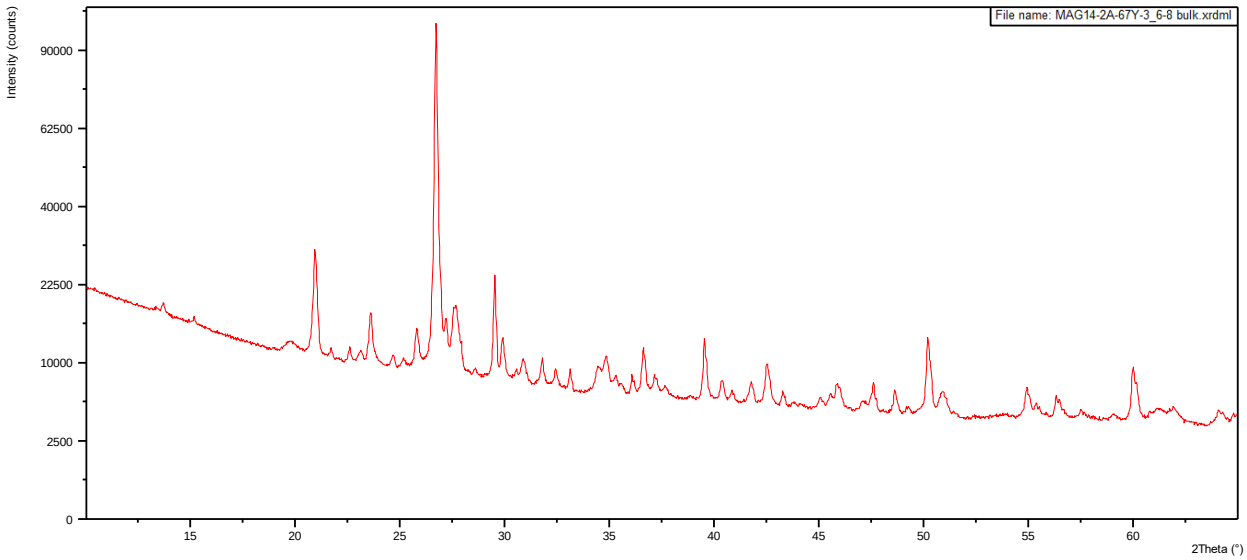
File name: MAG14-2A-67Y-3_6-8 bulk.xrdml
Intensity (counts)
90000
62500
40000
22500
10000
2500
0
15
20
25
30
35
40
45
50
55
60
2Theta (°)

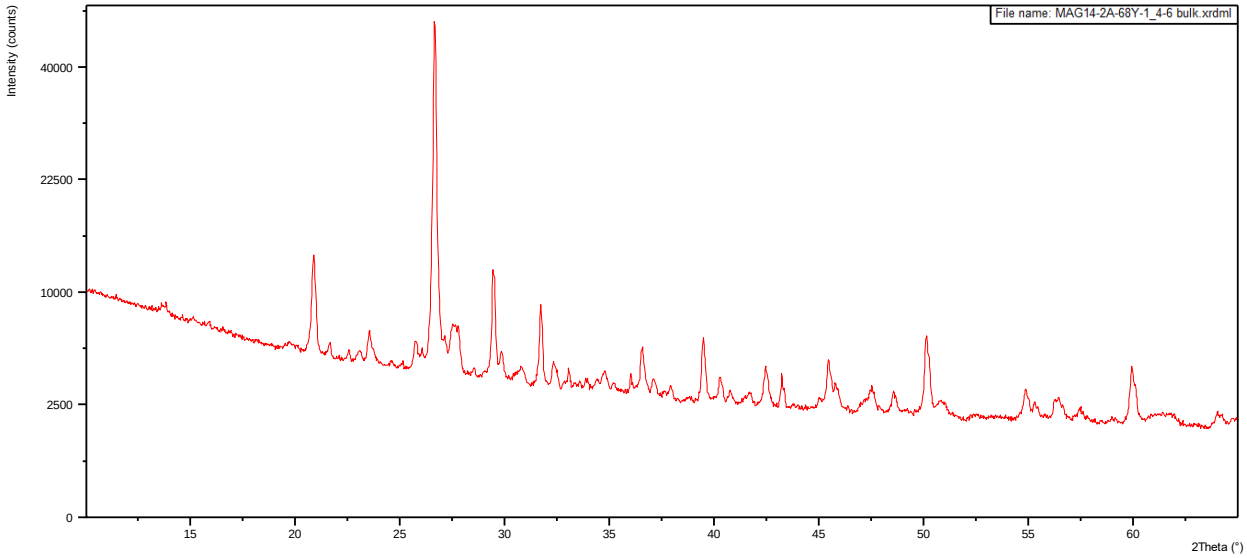
File name: MAG14-2A-68Y-1_4-6 bulk.xrdml
Intensity (counts)
40000
22500
10000
2500
0
15
20
25
30
35
40
45
50
55
60
2Theta (°)

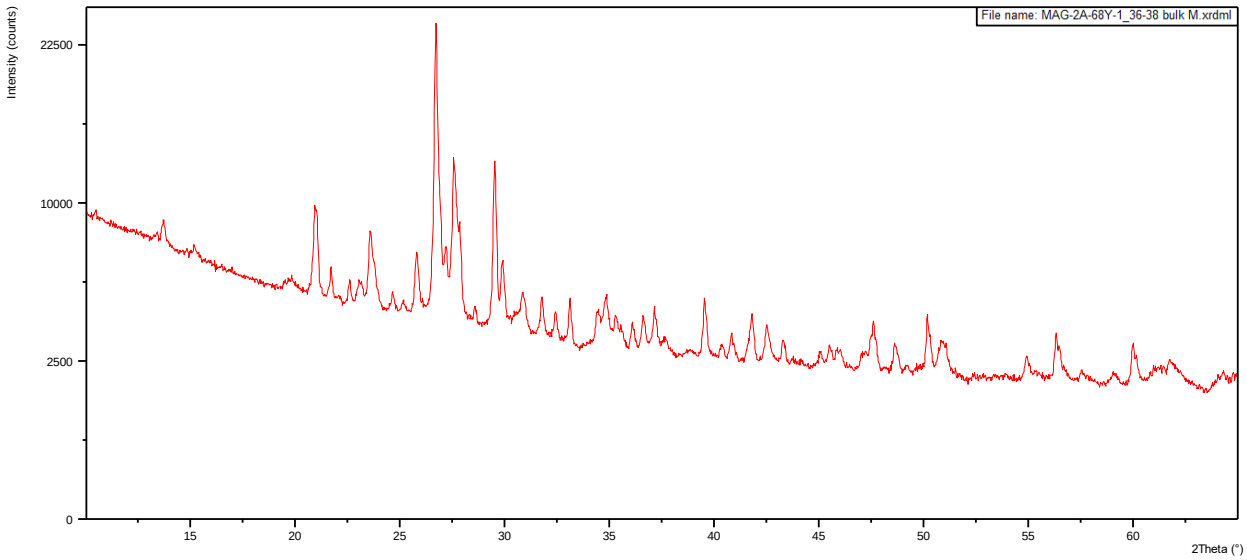
File name: MAG-2A-68Y-1_36-38 bulk M.xrdml
Intensity (counts)
22500
10000
2500
0
15
20
25
30
35
40
45
50
55
60
2Theta (°)

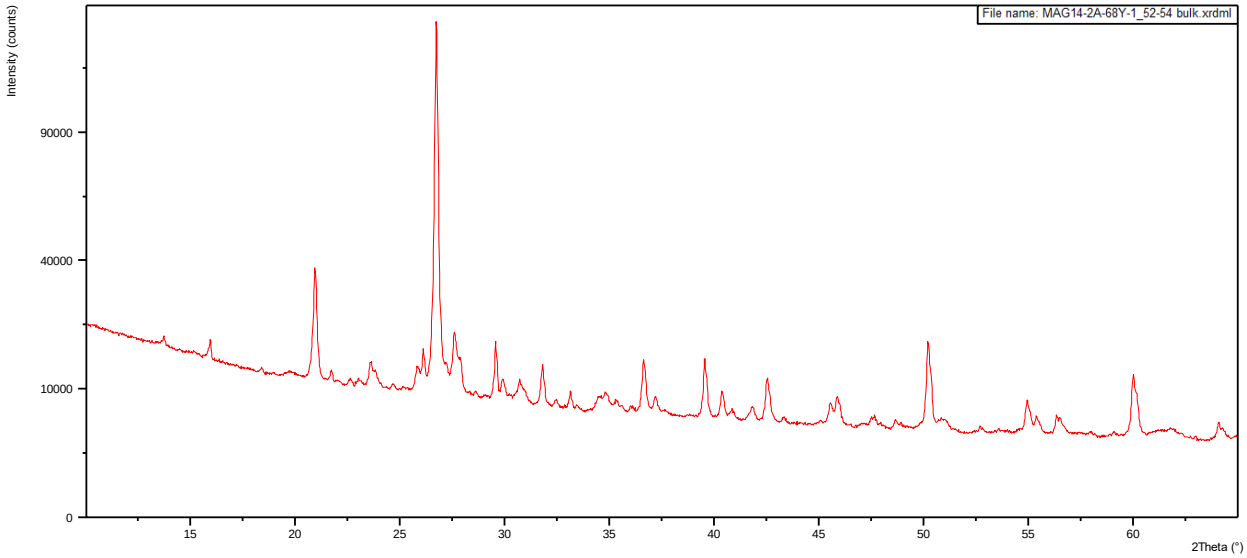
File name: MAG14-2A-68Y-1_52-54 bulk.xrdml
Intensity (counts)
90000
40000
10000
0
15
20
25
30
35
40
45
50
55
60
2Theta (°)

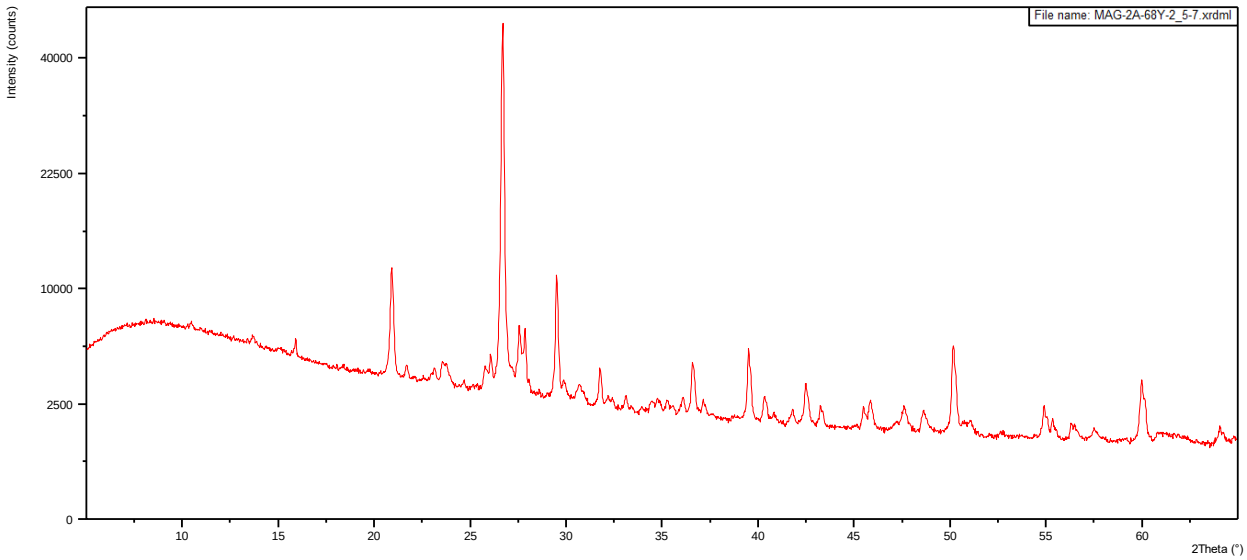
File name: MAG-2A-68Y-2_5-7.xrdml
Intensity (counts)
40000
22500
10000
2500
0
10
15
20
25
30
35
40
45
50
55
60
2Theta (°)

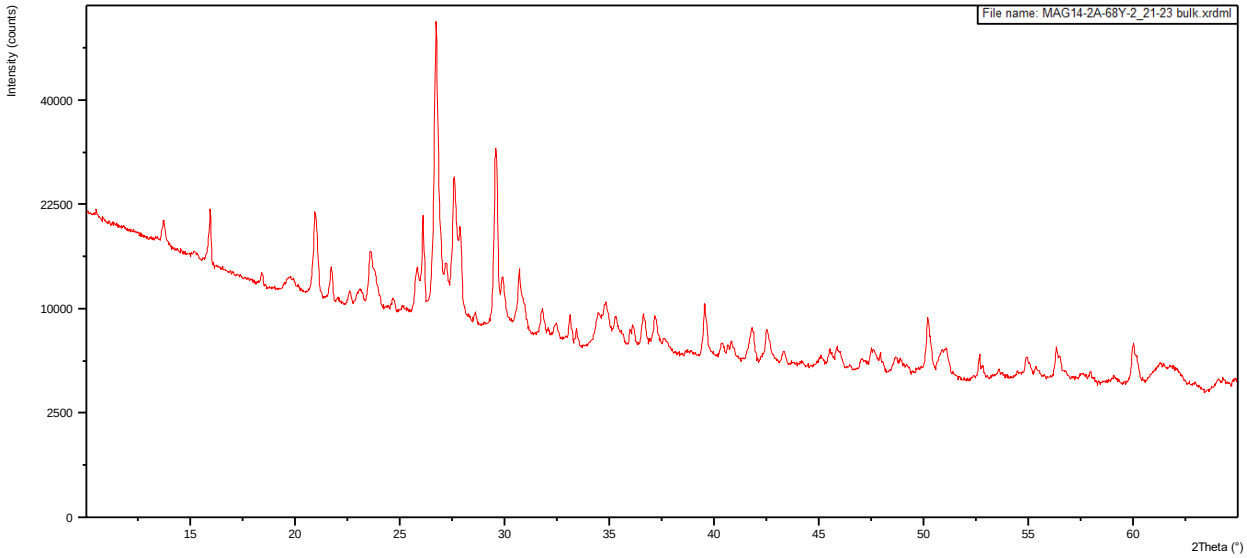
File name: MAG14-2A-68Y-2_21-23 bulk.xrdml
Intensity (counts)
40000
22500
10000
2500
0
15
20
25
30
35
40
45
50
55
60
2Theta (°)

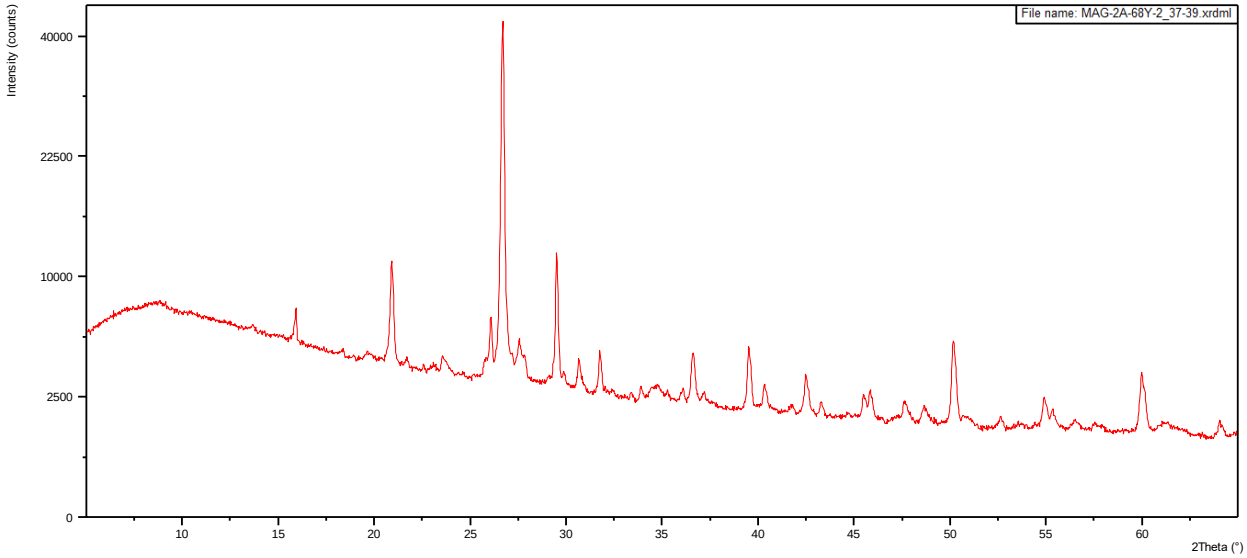
File name: MAG-2A-68Y-2_37-39.xrdml
Intensity (counts)
40000
22500
10000
2500
0
10
15
20
25
30
35
40
45
50
55
60
2Theta (°)

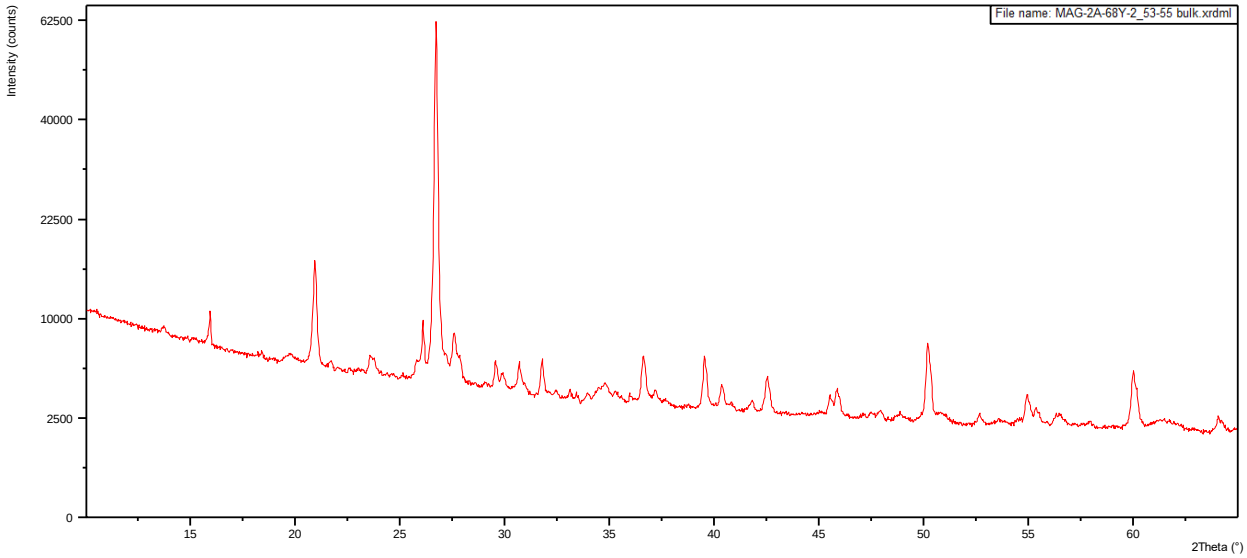
File name: MAG-2A-68Y-2_53-55 bulk.xrdml
Intensity (counts)
62500
40000
22500
10000
2500
0
15
20
25
30
35
40
45
50
55
60
2Theta (°)

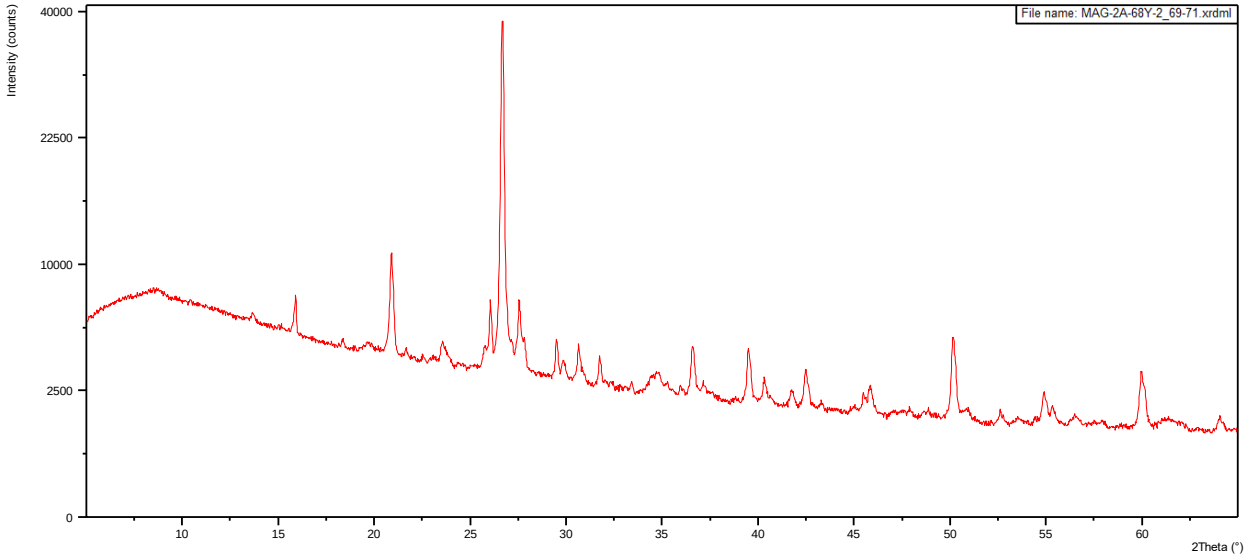
File name: MAG-2A-68Y-2_69-71.xrdml
Intensity (counts)
40000
22500
10000
2500
0
10
15
20
25
30
35
40
45
50
55
60
2Theta (°)

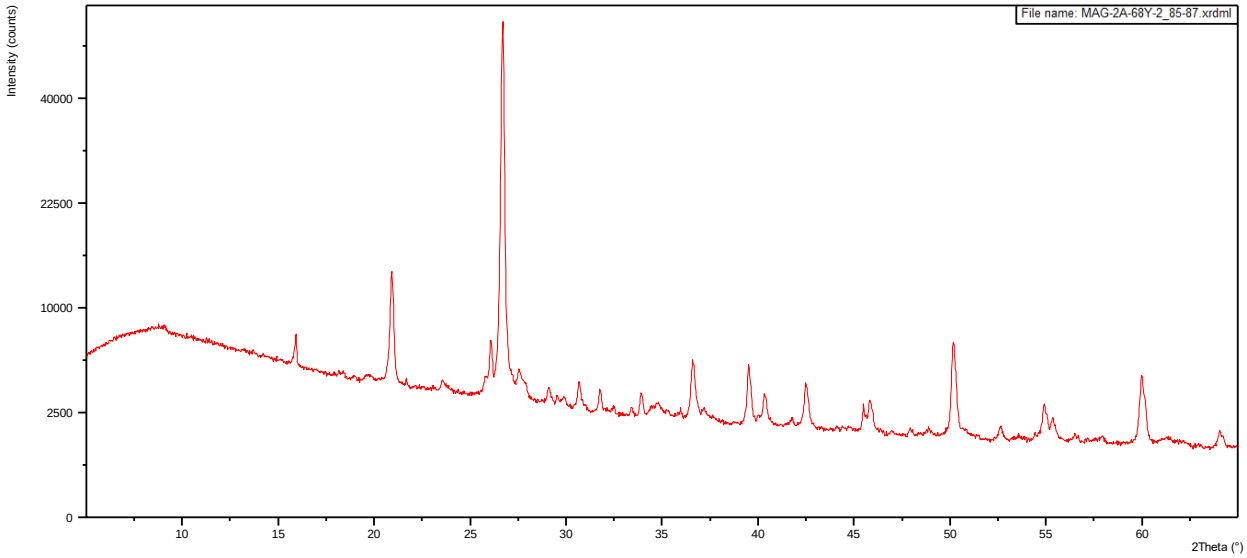
File name: MAG-2A-68Y-2_85-87.xrdml
Intensity (counts)
40000
22500
10000
2500
0
10
15
20
25
30
35
40
45
50
55
60
2Theta (°)

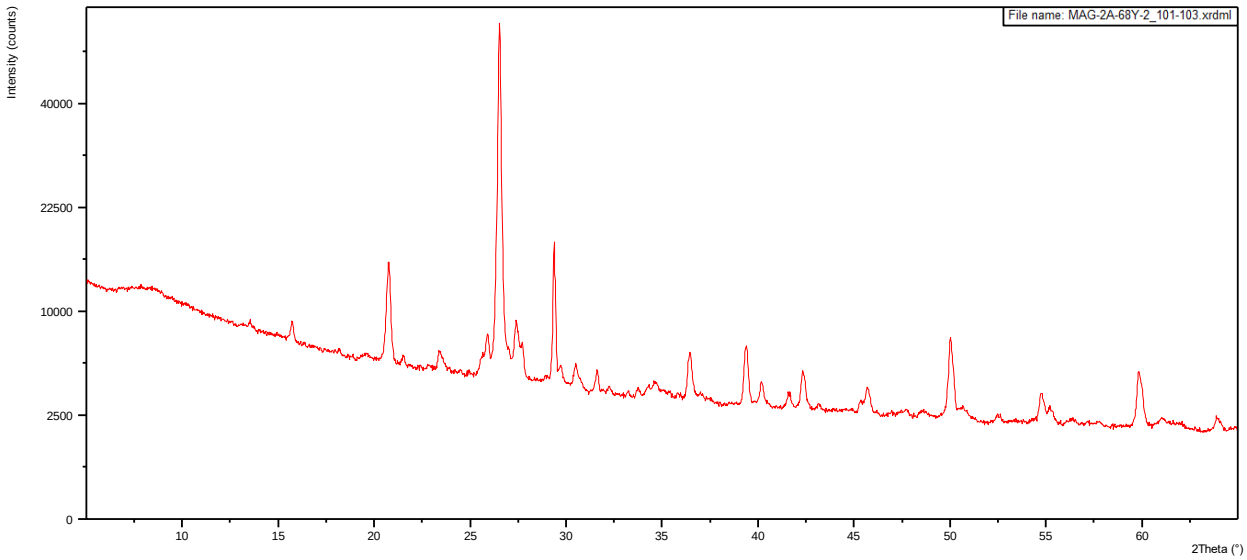
File name: MAG-2A-68Y-2_101-103.xrdml
Intensity (counts)
40000
22500
10000
2500
0
10
15
20
25
30
35
40
45
50
55
60
2Theta (°)

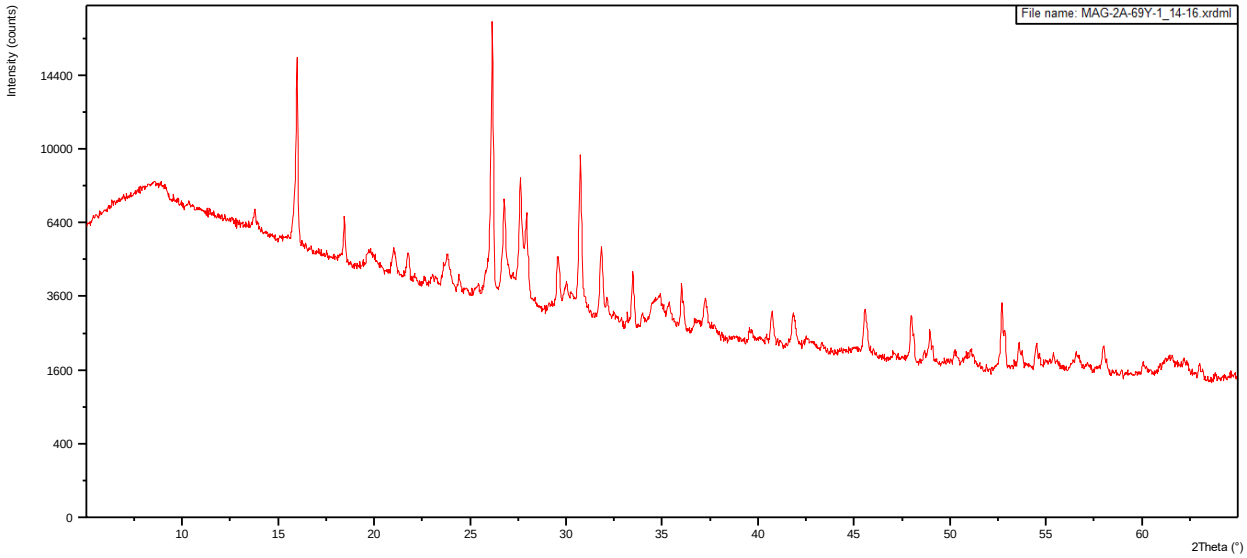
File name: MAG-2A-69Y-1_14-16.xrdml
Intensity (counts)
14400
10000
6400
3600
1600
400
0
10
15
20
25
30
35
40
45
50
55
60
2Theta (°)

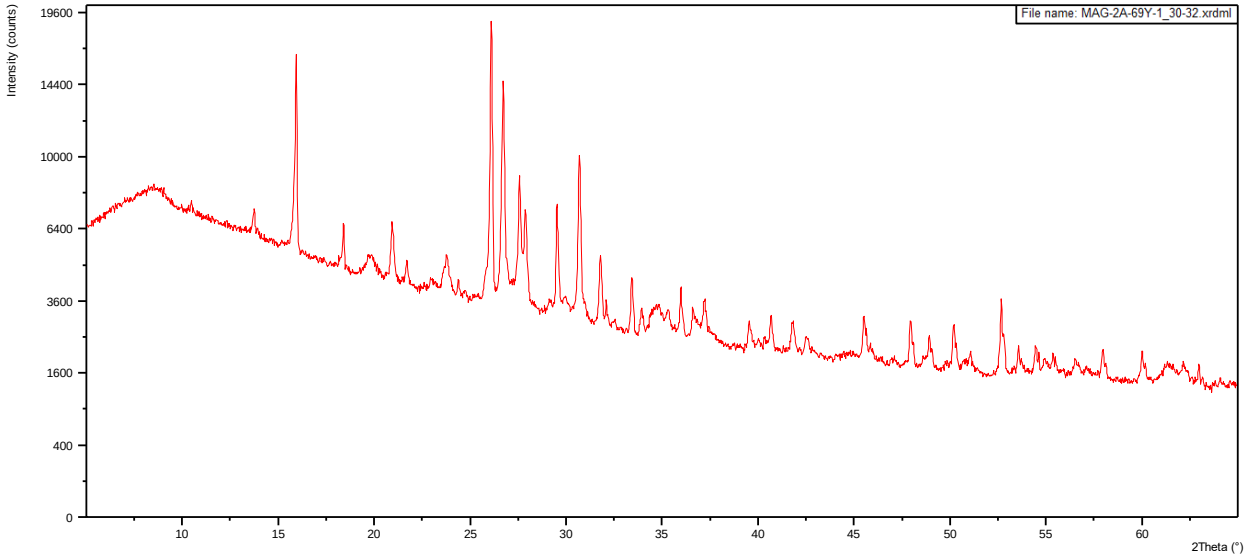
File name: MAG-2A-69Y-1_30-32.xrdml
Intensity (counts)
19600
14400
10000
6400
3600
1600
400
0
10
15
20
25
30
35
40
45
50
55
60
2Theta (°)

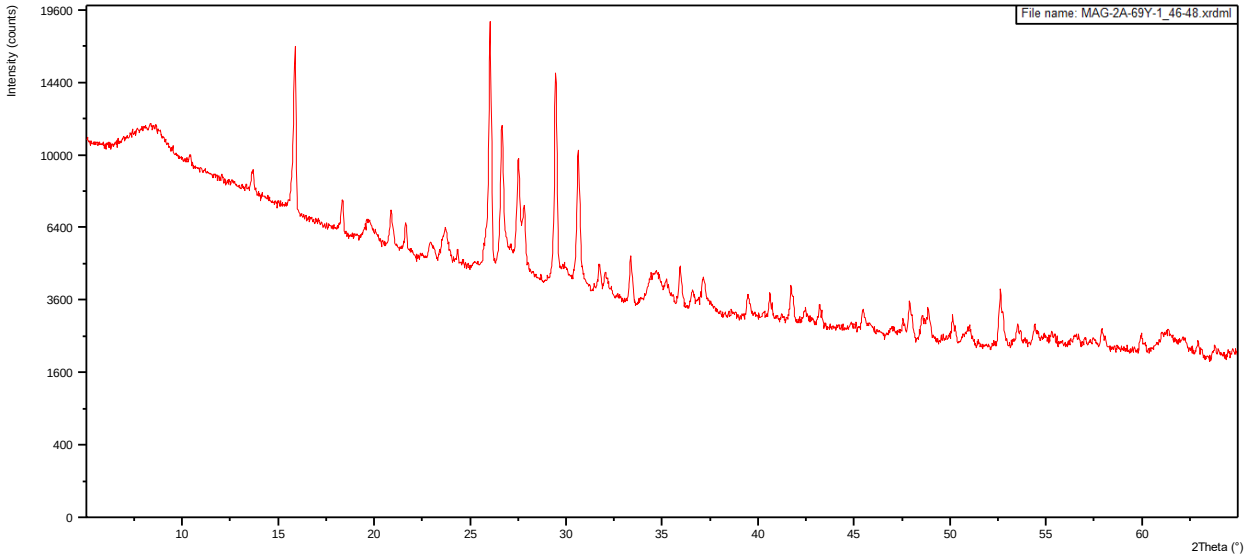
File name: MAG-2A-69Y-1_46-48.xrdml
Intensity (counts)
19600
14400
10000
6400
3600
1600
400
0
10
15
20
25
30
35
40
45
50
55
60
2Theta (°)

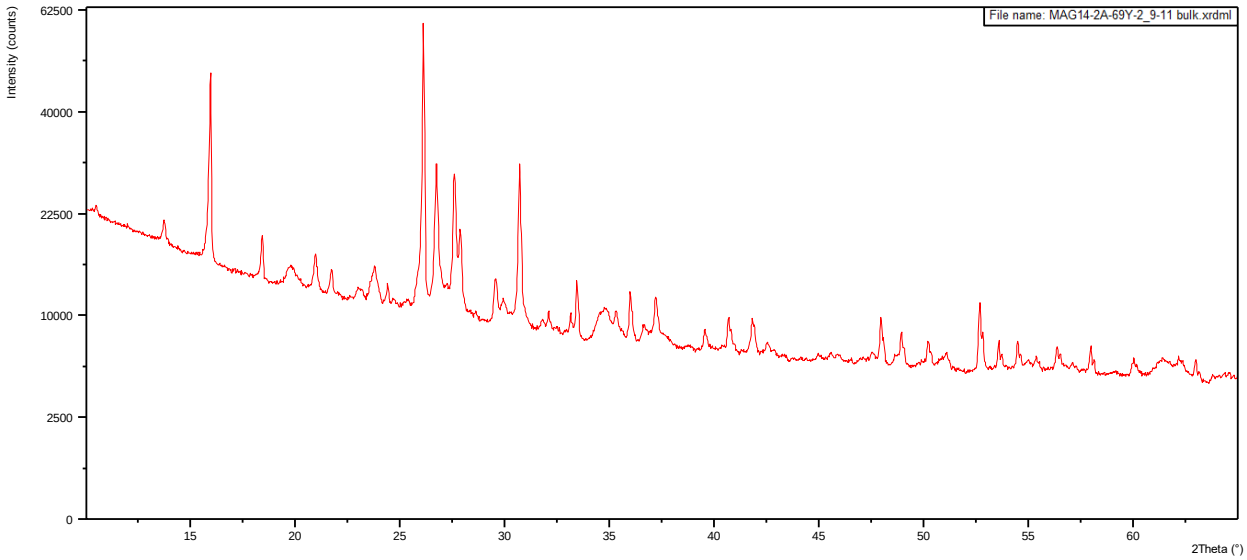
File name: MAG14-2A-69Y-2_9-11 bulk.xrdml
Intensity (counts)
62500
40000
22500
10000
2500
0
15
20
25
30
35
40
45
50
55
60
2Theta (°)

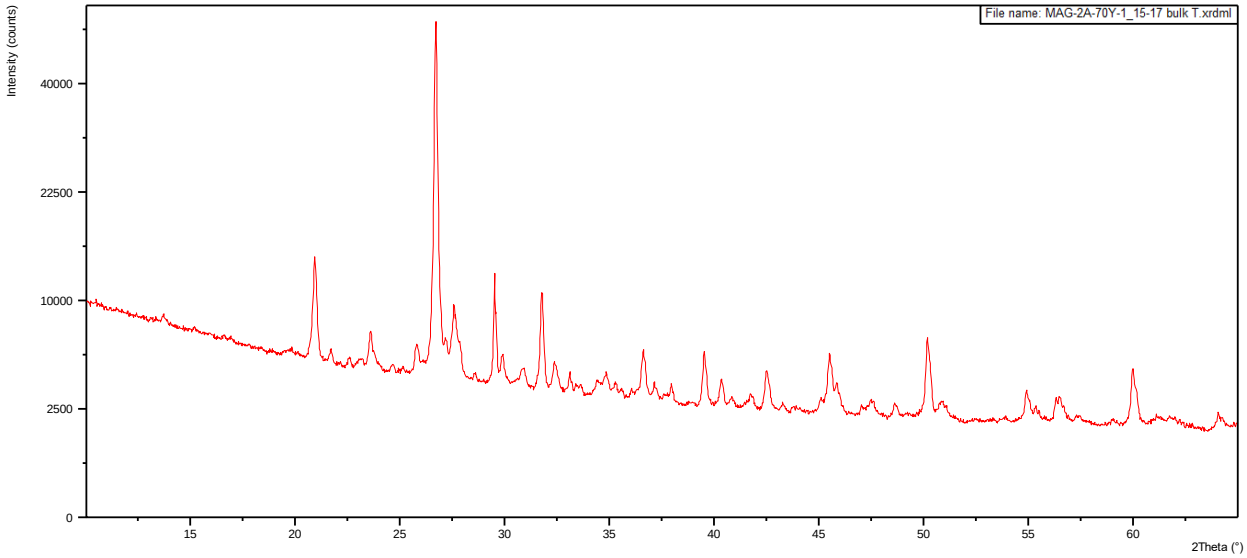
File name: MAG-2A-70Y-1_15-17 bulk T.xrdml
Intensity (counts)
40000
22500
10000
2500
0
15
20
25
30
35
40
45
50
55
60
2Theta (°)

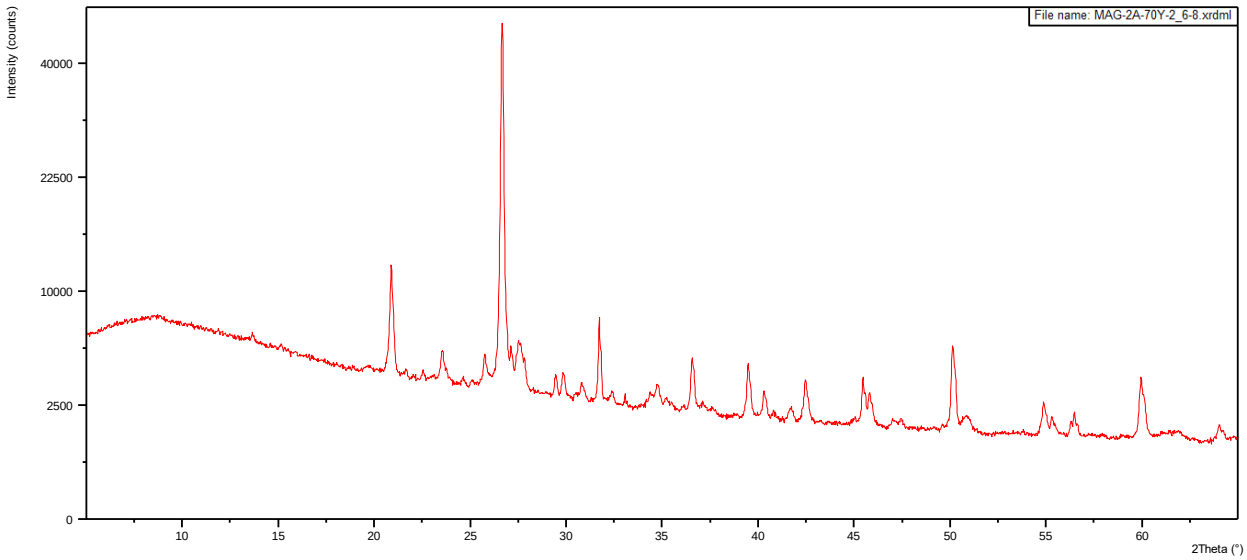
File name: MAG-2A-70Y-2_6-8.xrdml
Intensity (counts)
40000
22500
10000
2500
0
10
15
20
25
30
35
40
45
50
55
60
2Theta (°)

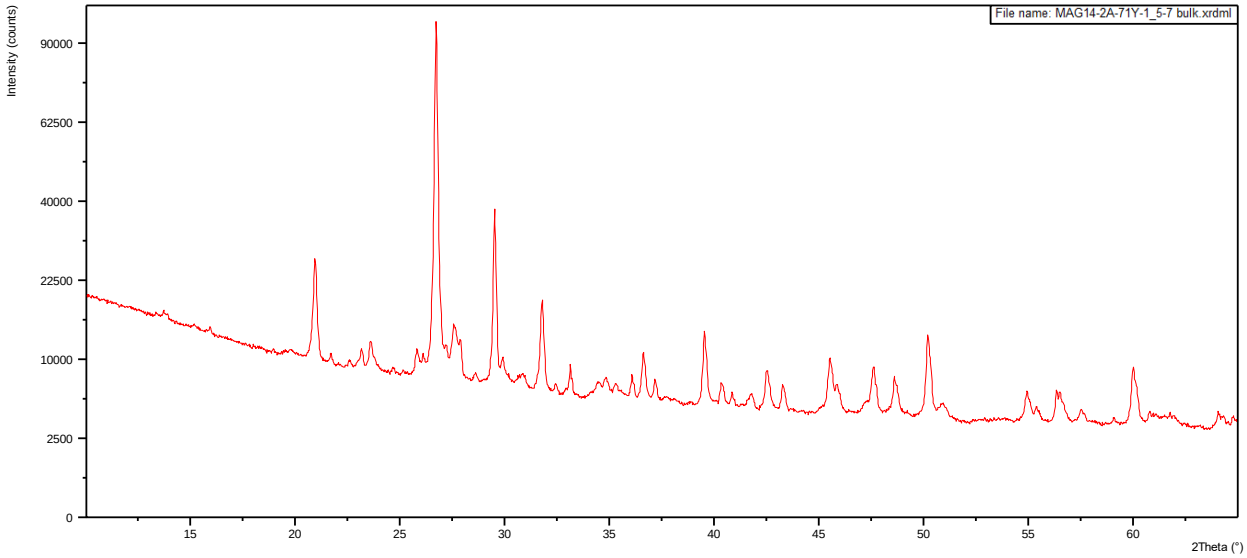
File name: MAG14-2A-71Y-1_5-7 bulk.xrdml
Intensity (counts)
90000
62500
40000
22500
10000
2500
0
15
20
25
30
35
40
45
50
55
60
2Theta (°)

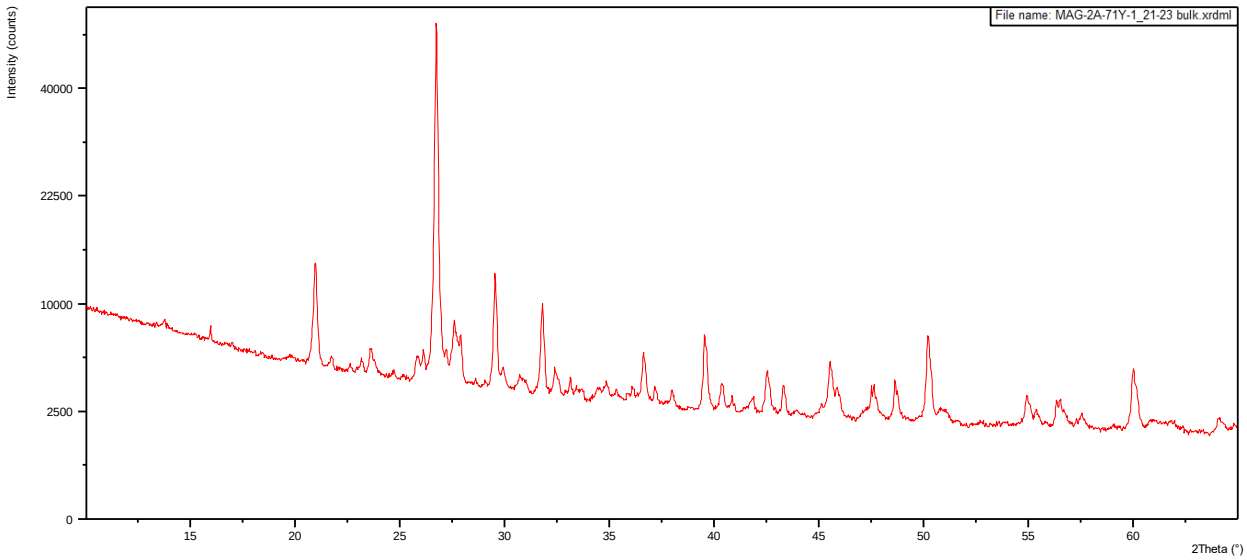
File name: MAG-2A-71Y-1_21-23 bulk.xrdml
Intensity (counts)
40000
22500
10000
2500
0
15
20
25
30
35
40
45
50
55
60
2Theta (°)

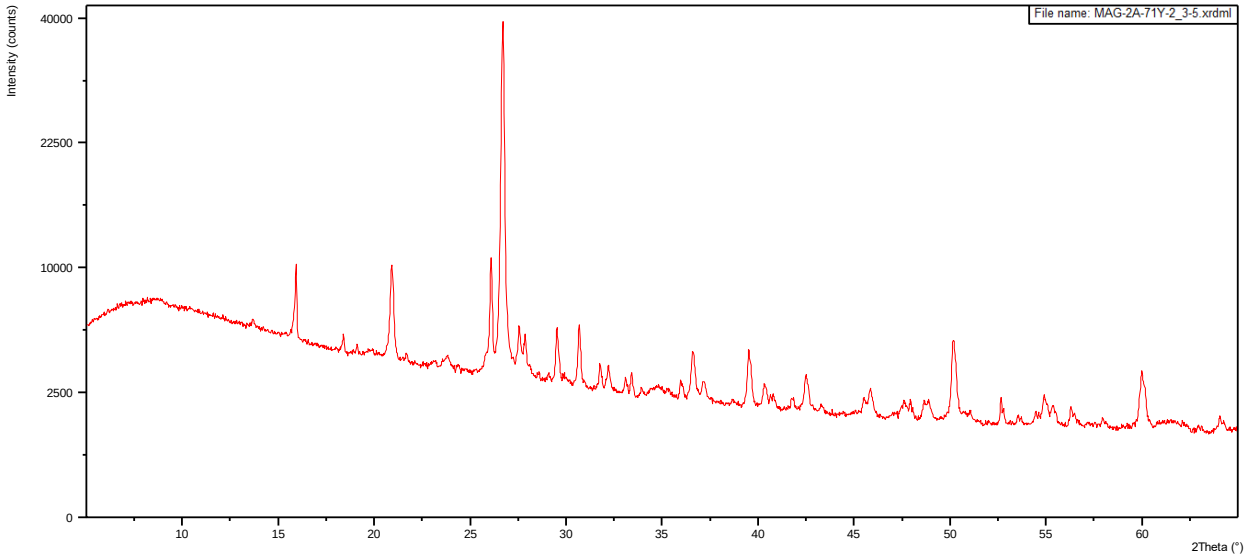
File name: MAG-2A-71Y-2_3-5.xrdml
Intensity (counts)
40000
22500
10000
2500
0
10
15
20
25
30
35
40
45
50
55
60
2Theta (°)

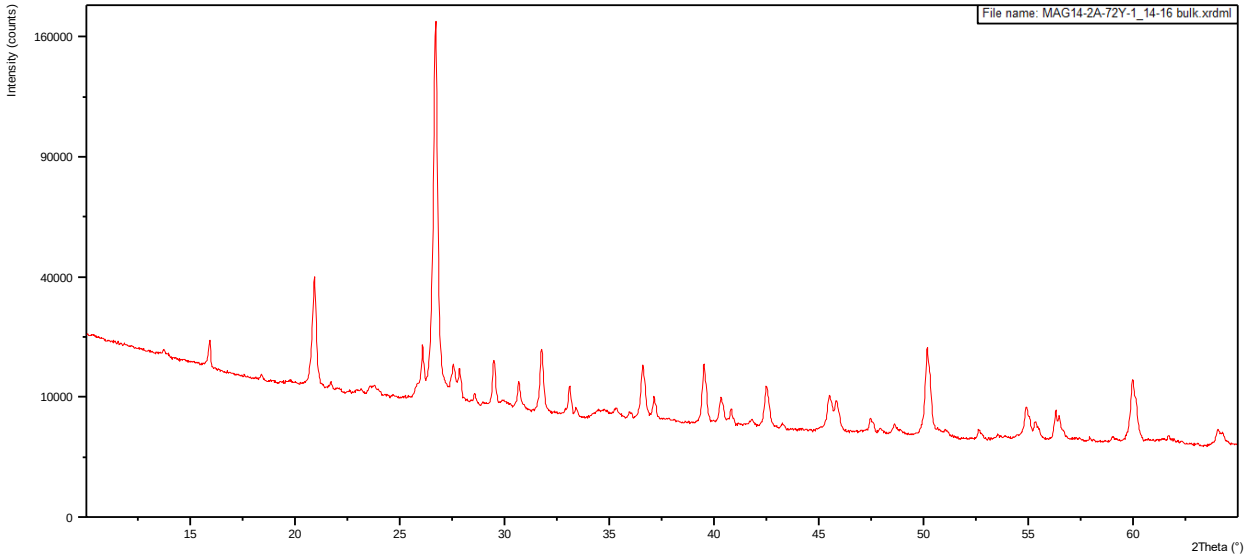
File name: MAG14-2A-72Y-1_14-16 bulk.xrdml
Intensity (counts)
160000
90000
40000
10000
0
15
20
25
30
35
40
45
50
55
60
2Theta (°)

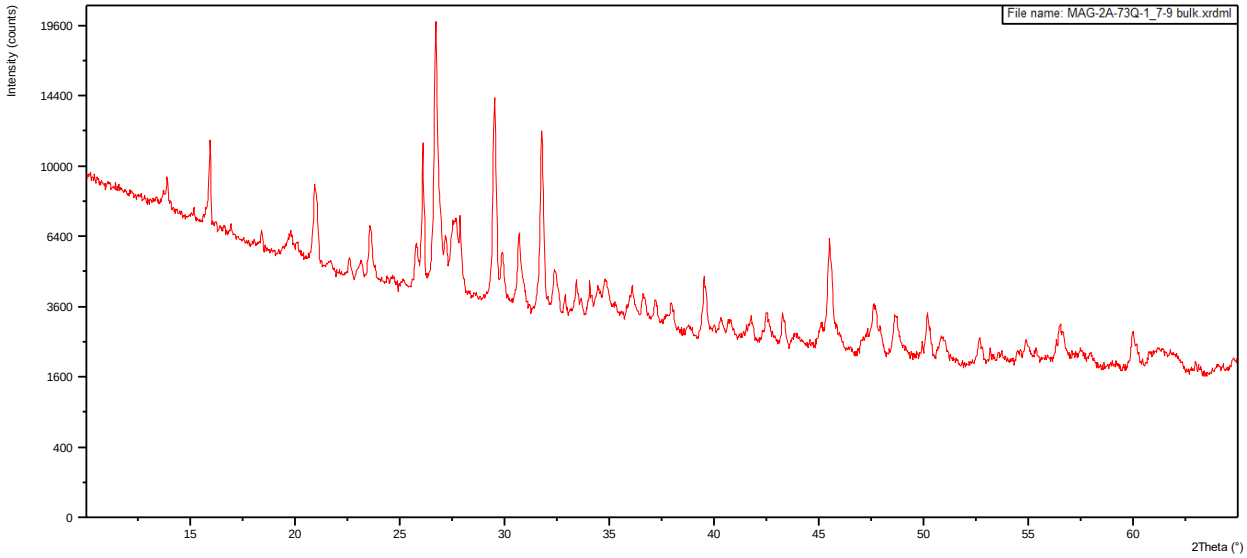
File name: MAG-2A-73Q-1_7-9 bulk.xrdml
Intensity (counts)
19600
14400
10000
6400
3600
1600
400
0
15
20
25
30
35
40
45
50
55
60
2Theta (°)

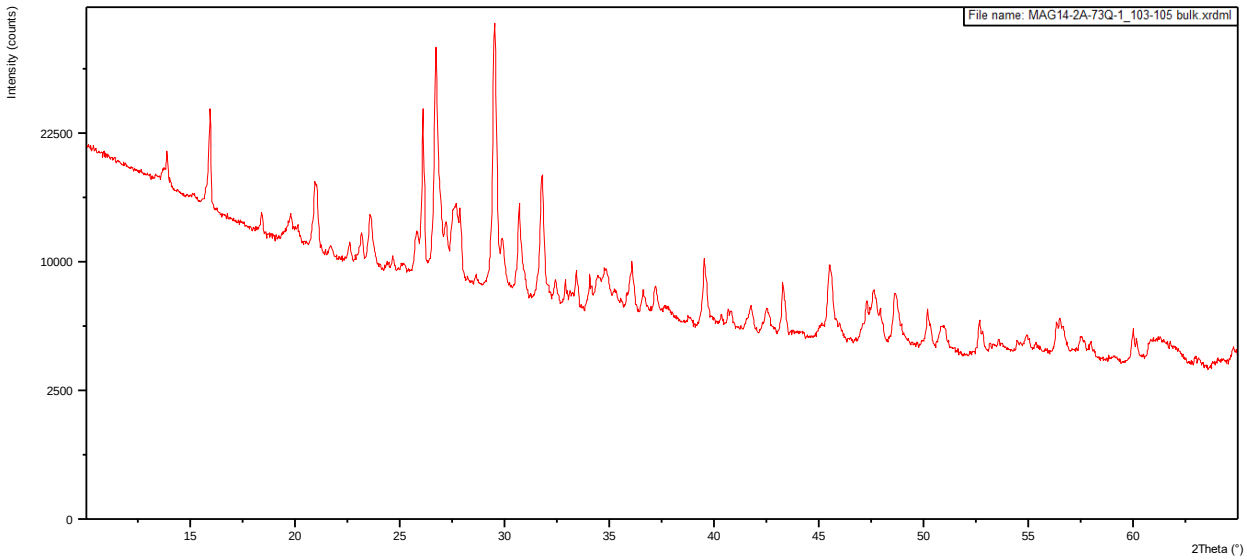
File name: MAG14-2A-73Q-1_103-105 bulk.xrdml
Intensity (counts)
22500
10000
2500
0
15
20
25
30
35
40
45
50
55
60
2Theta (°)

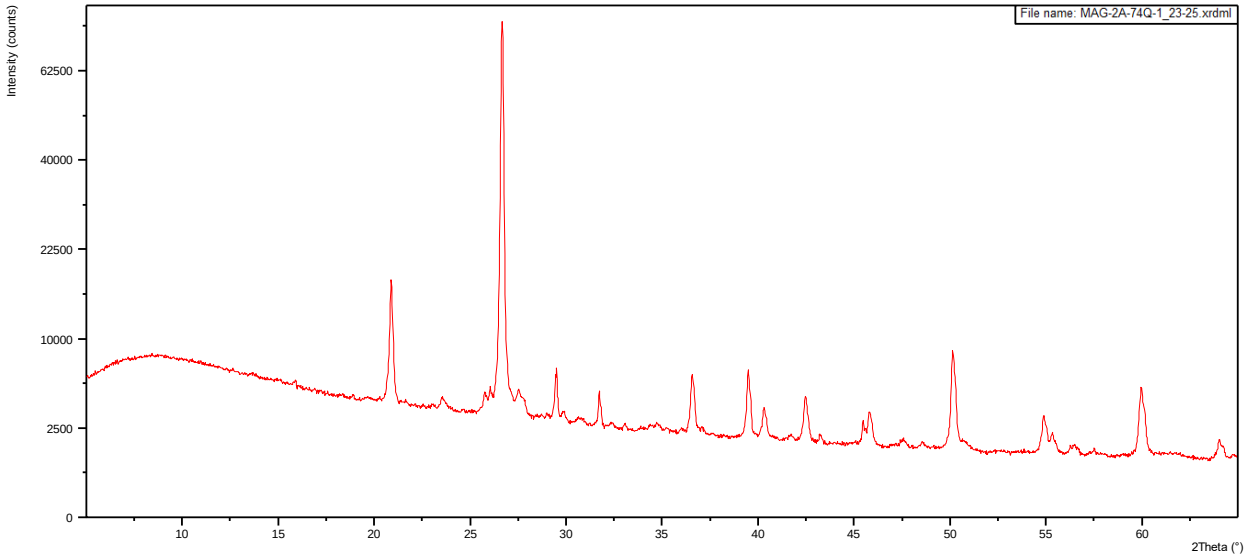
File name: MAG-2A-74Q-1_23-25.xrdml
Intensity (counts)
62500
40000
22500
10000
2500
0
10
15
20
25
30
35
40
45
50
55
60
2Theta (°)

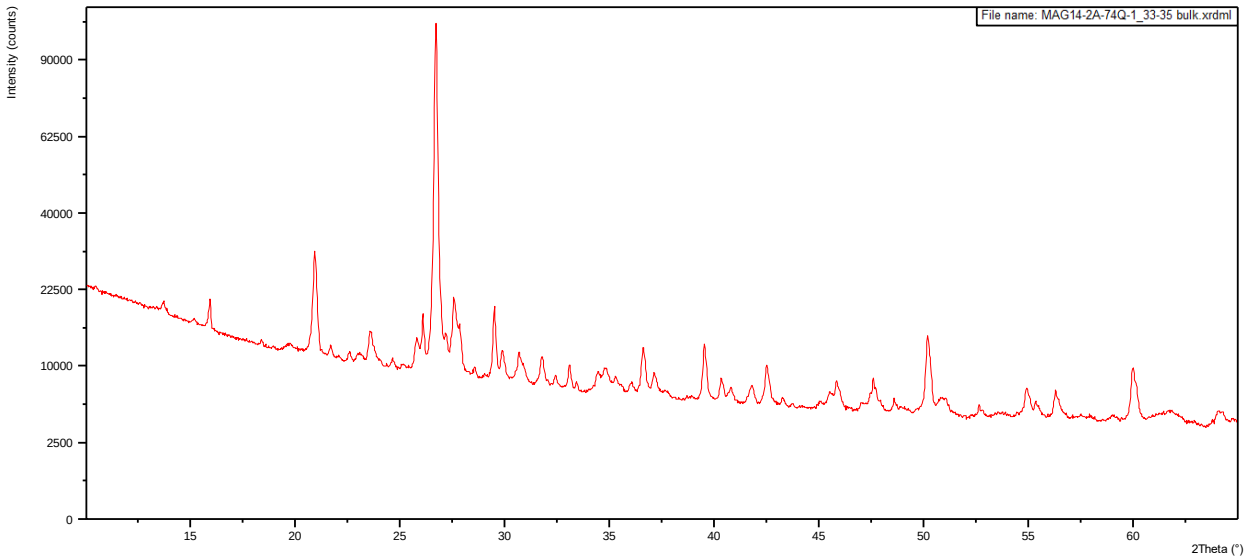
File name: MAG14-2A-74Q-1_33-35 bulk.xrdml
Intensity (counts)
90000
62500
40000
22500
10000
2500
0
15
20
25
30
35
40
45
50
55
60
2Theta (°)

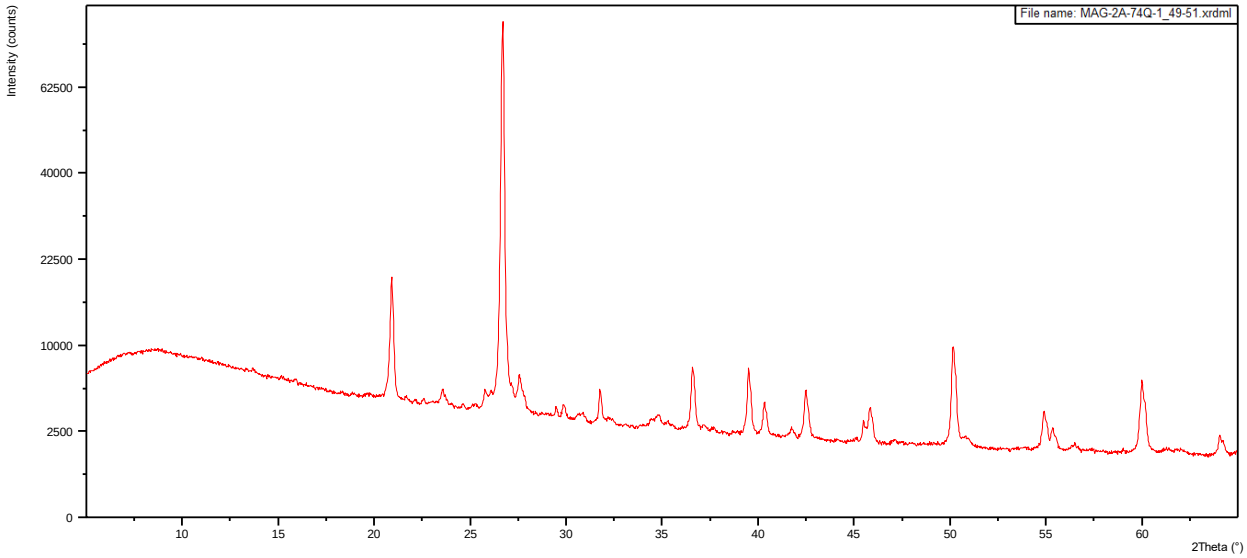
File name: MAG-2A-74Q-1_49-51.xrdml
Intensity (counts)
62500
40000
22500
10000
2500
0
10
15
20
25
30
35
40
45
50
55
60
2Theta (°)

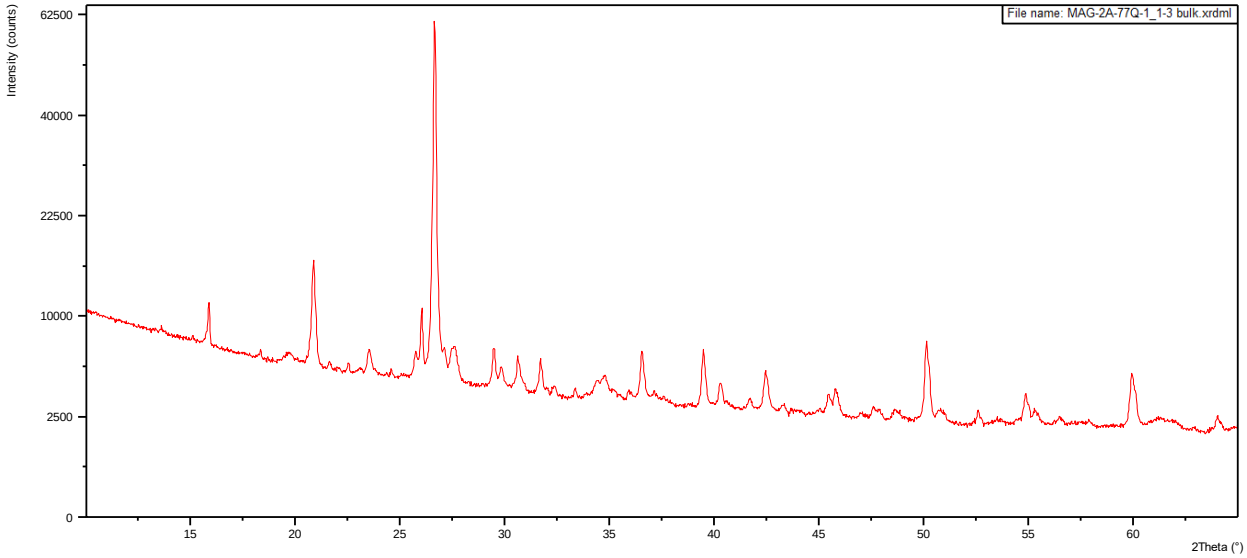
File name: MAG-2A-77Q-1_1-3 bulk.xrdml
Intensity (counts)
62500
40000
22500
10000
2500
0
15
20
25
30
35
40
45
50
55
60
2Theta (°)

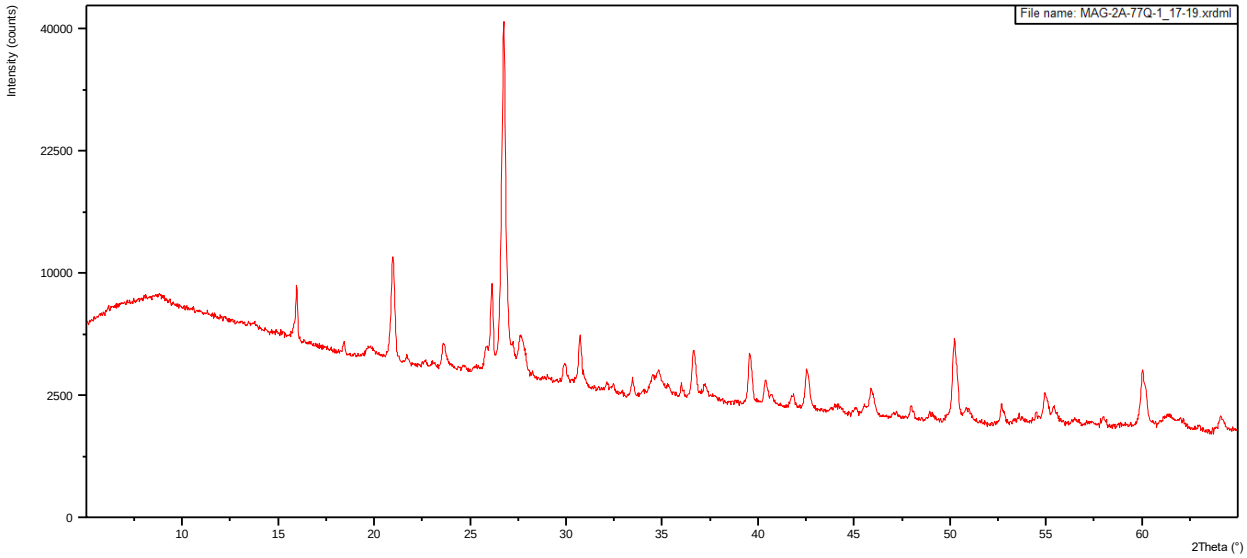
File name: MAG-2A-77Q-1_17-19.xrdml
Intensity (counts)
40000
22500
10000
2500
0
10
15
20
25
30
35
40
45
50
55
60
2Theta (°)

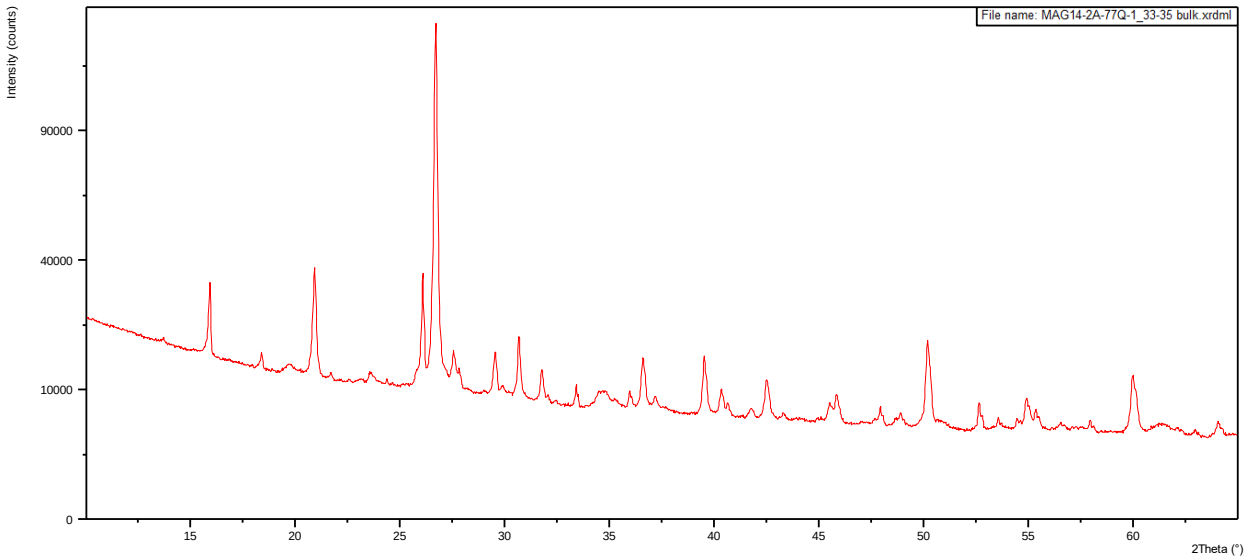
File name: MAG14-2A-77Q-1_33-35 bulk.xrdml
Intensity (counts)
90000
40000
10000
0
15
20
25
30
35
40
45
50
55
60
2Theta (°)

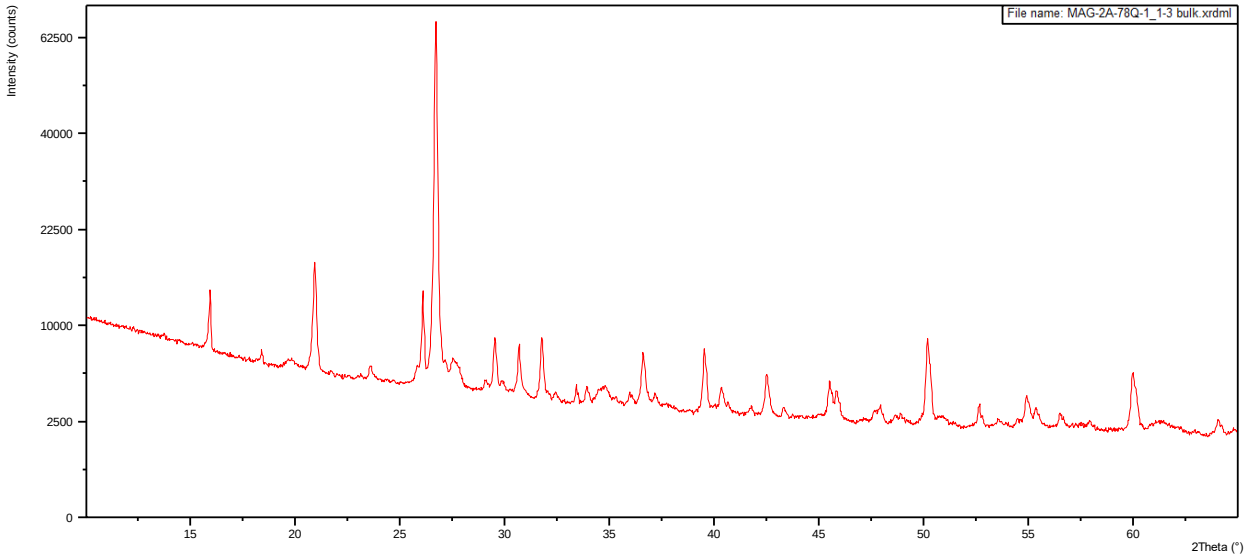
File name: MAG-2A-78Q-1_1-3 bulk.xrdml
Intensity (counts)
62500
40000
22500
10000
2500
0
15
20
25
30
35
40
45
50
55
60
2Theta (°)

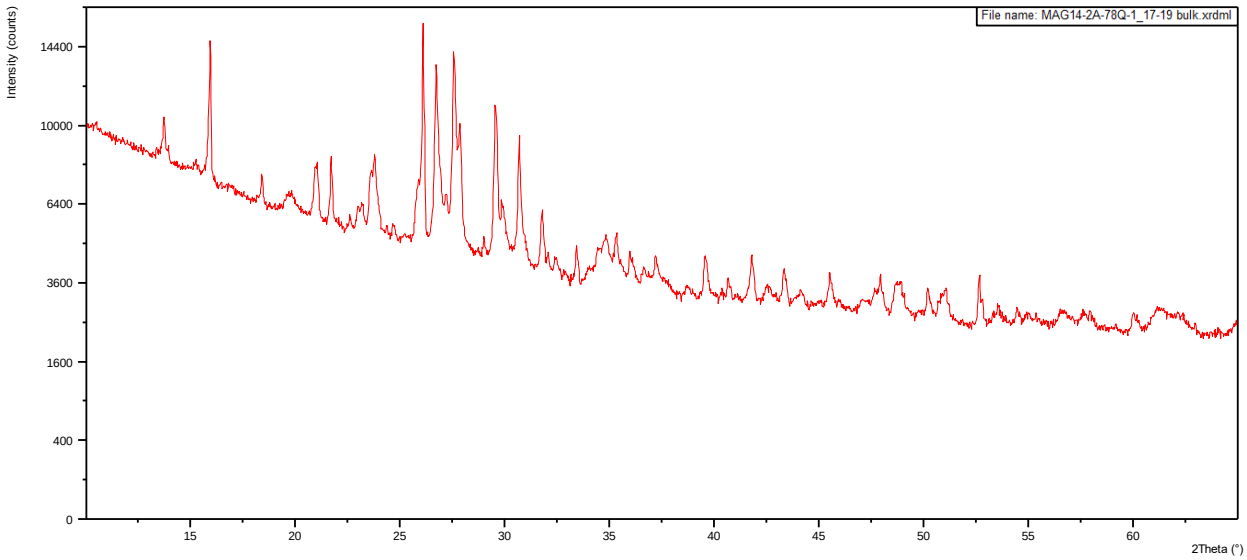
File name: MAG14-2A-78Q-1_17-19 bulk.xrdml
Intensity (counts)
14400
10000
6400
3600
1600
400
0
15
20
25
30
35
40
45
50
55
60
2Theta (°)

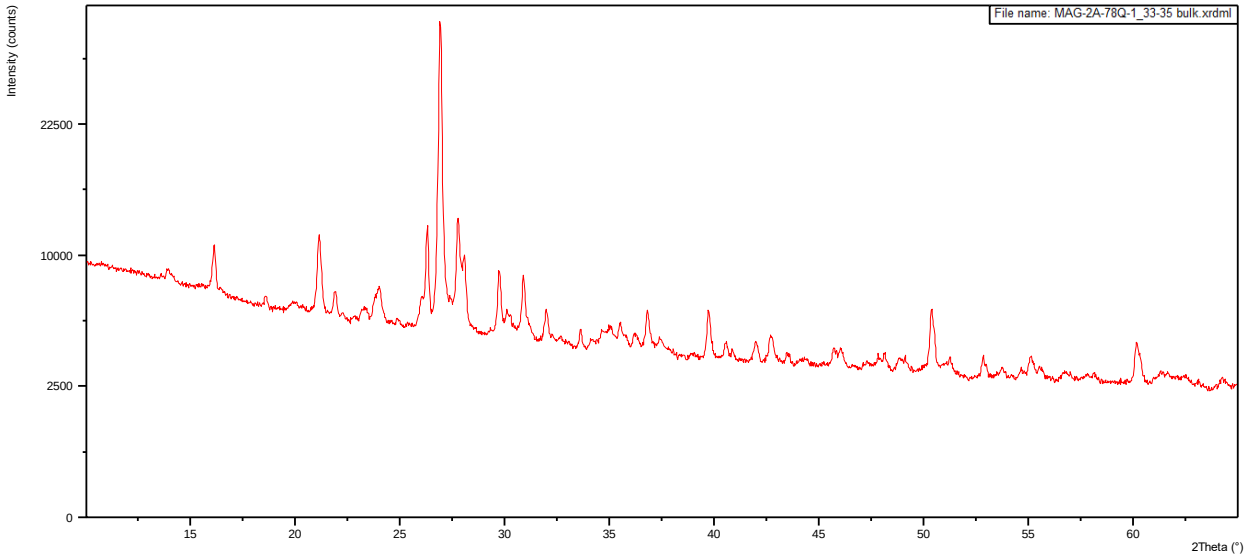
File name: MAG-2A-78Q-1_33-35 bulk.xrdml
Intensity (counts)
22500
10000
2500
0
15
20
25
30
35
40
45
50
55
60
2Theta (°)

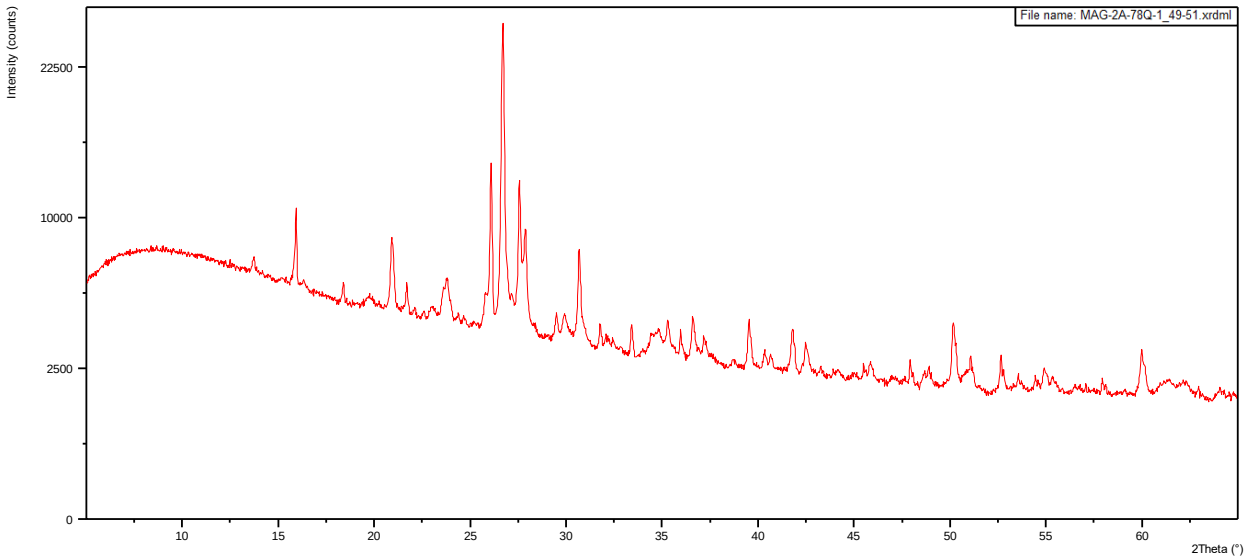
File name: MAG-2A-78Q-1_49-51.xrdml
Intensity (counts)
22500
10000
2500
0
10
15
20
25
30
35
40
45
50
55
60
2Theta (°)

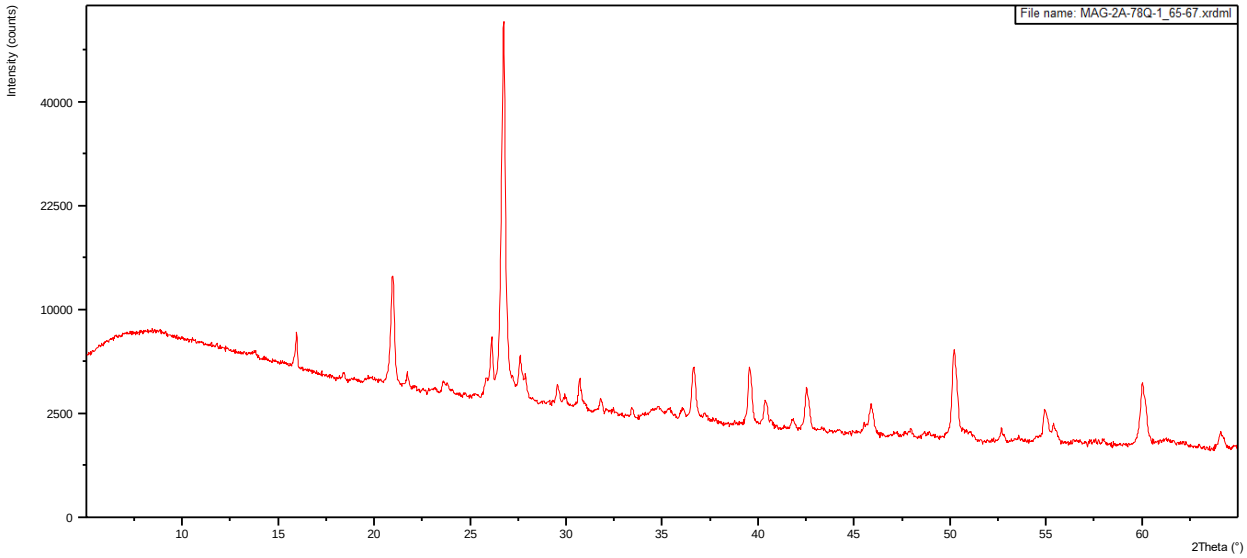
File name: MAG-2A-78Q-1_65-67.xrdml
Intensity (counts)
40000
22500
10000
2500
0
10
15
20
25
30
35
40
45
50
55
60
2Theta (°)

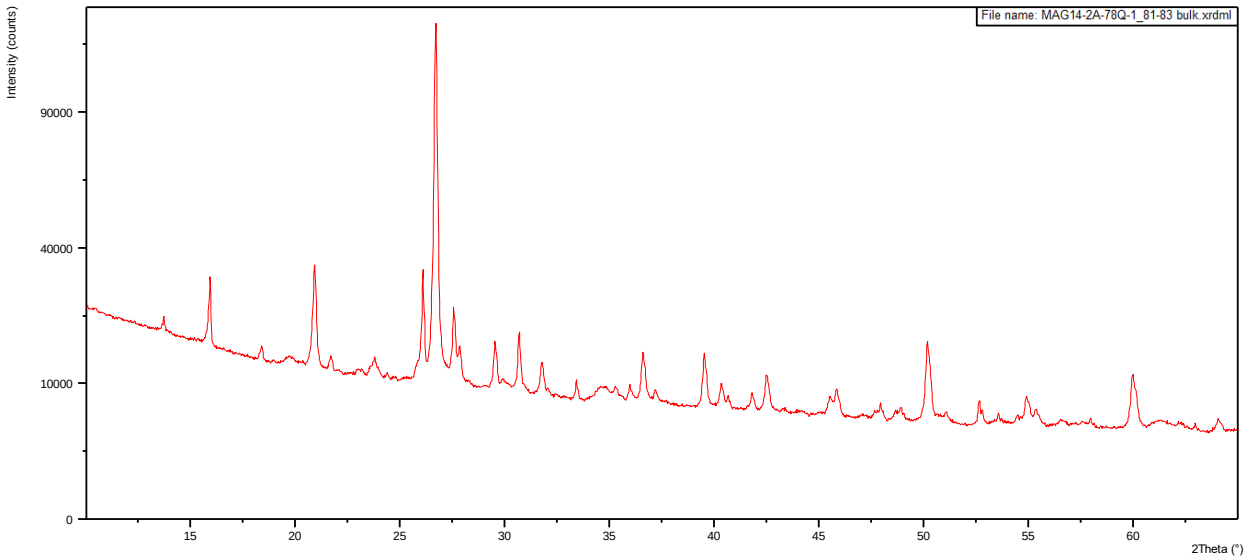
File name: MAG14-2A-78Q-1_81-83 bulk.xrdml
Intensity (counts)
90000
40000
10000
0
15
20
25
30
35
40
45
50
55
60
2Theta (°)

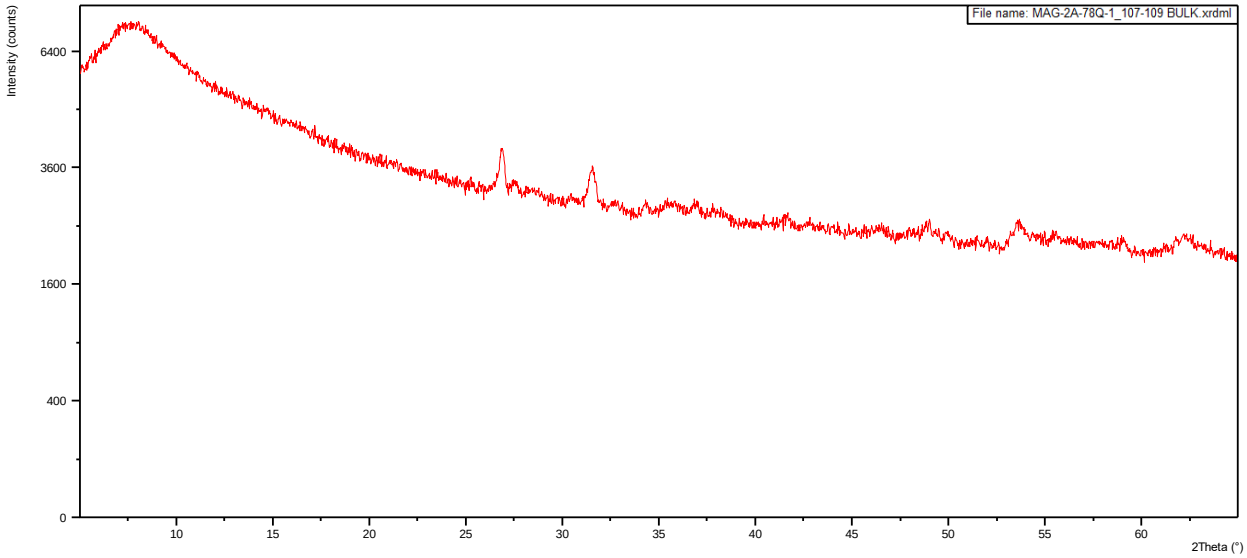
File name: MAG-2A-78Q-1_107-109 BULK.xrdml
Intensity (counts)
6400
3600
1600
400
0
10
15
20
25
30
35
40
45
50
55
60
2Theta (°)

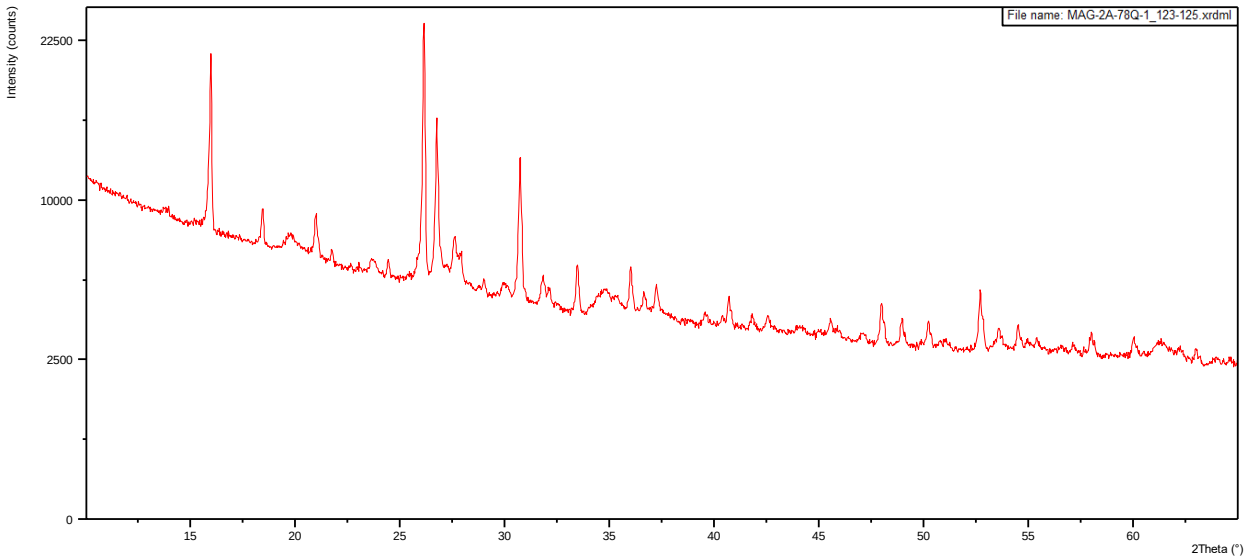
File name: MAG-2A-78Q-1_123-125.xrdml
Intensity (counts)
22500
10000
2500
0
15
20
25
30
35
40
45
50
55
60
2Theta (°)

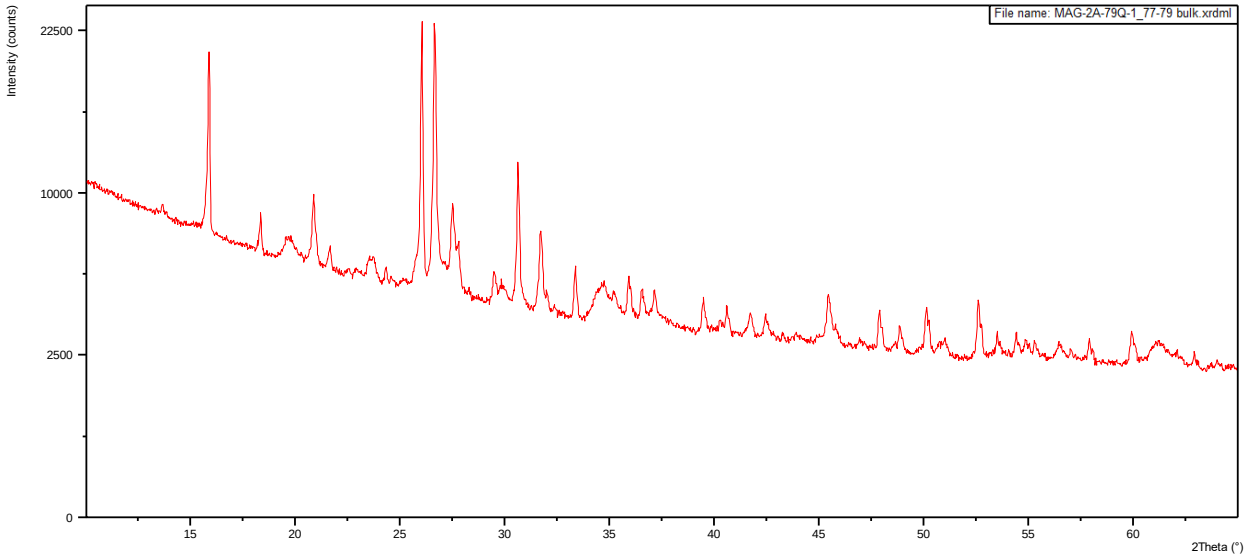
File name: MAG-2A-79Q-1_77-79 bulk.xrdml
Intensity (counts)
22500
10000
2500
0
15
20
25
30
35
40
45
50
55
60
2Theta (°)

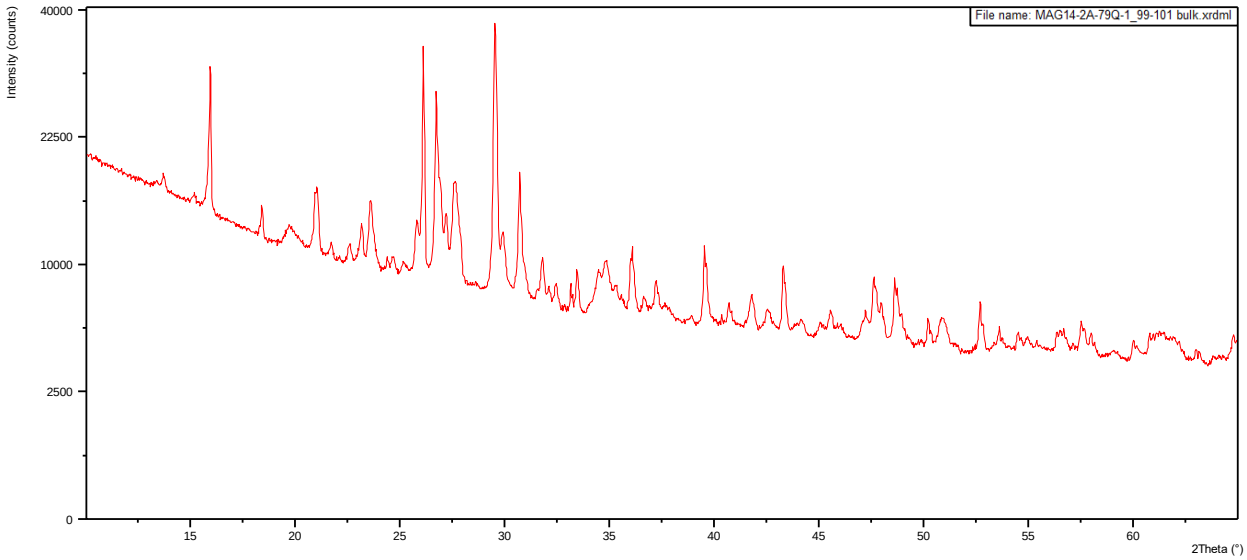
File name: MAG14-2A-79Q-1_99-101 bulk.xrdml
Intensity (counts)
40000
22500
10000
2500
0
15
20
25
30
35
40
45
50
55
60
2Theta (°)

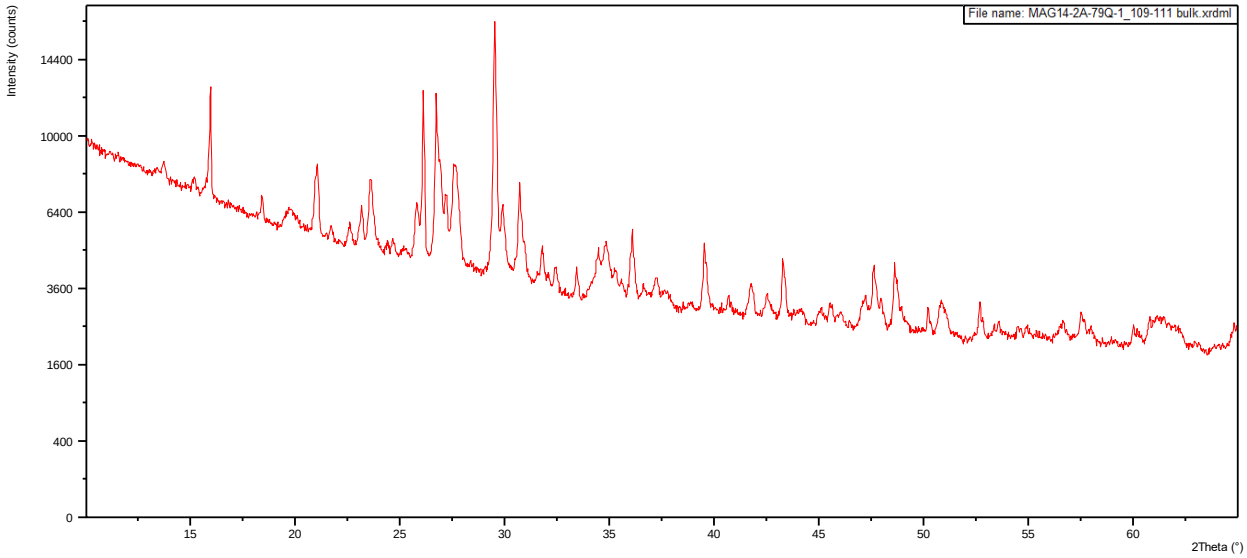
File name: MAG14-2A-79Q-1_109-111 bulk.xrdml
Intensity (counts)
14400
10000
6400
3600
1600
400
0
15
20
25
30
35
40
45
50
55
60
2Theta (°)

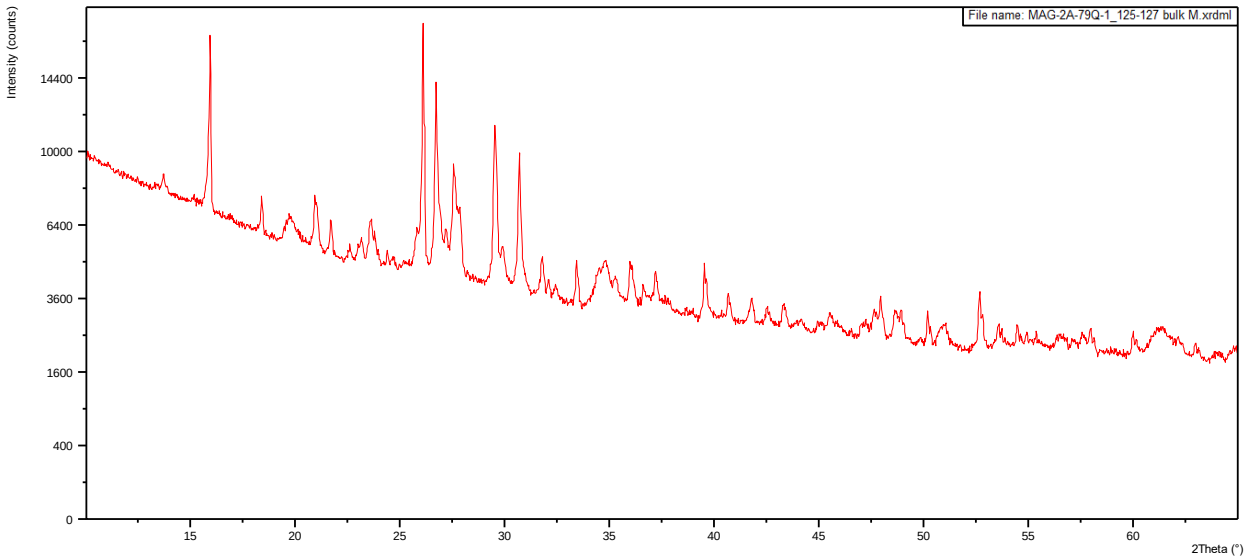
File name: MAG-2A-79Q-1_125-127 bulk M.xrdml
Intensity (counts)
14400
10000
6400
3600
1600
400
0
15
20
25
30
35
40
45
50
55
60
2Theta (°)

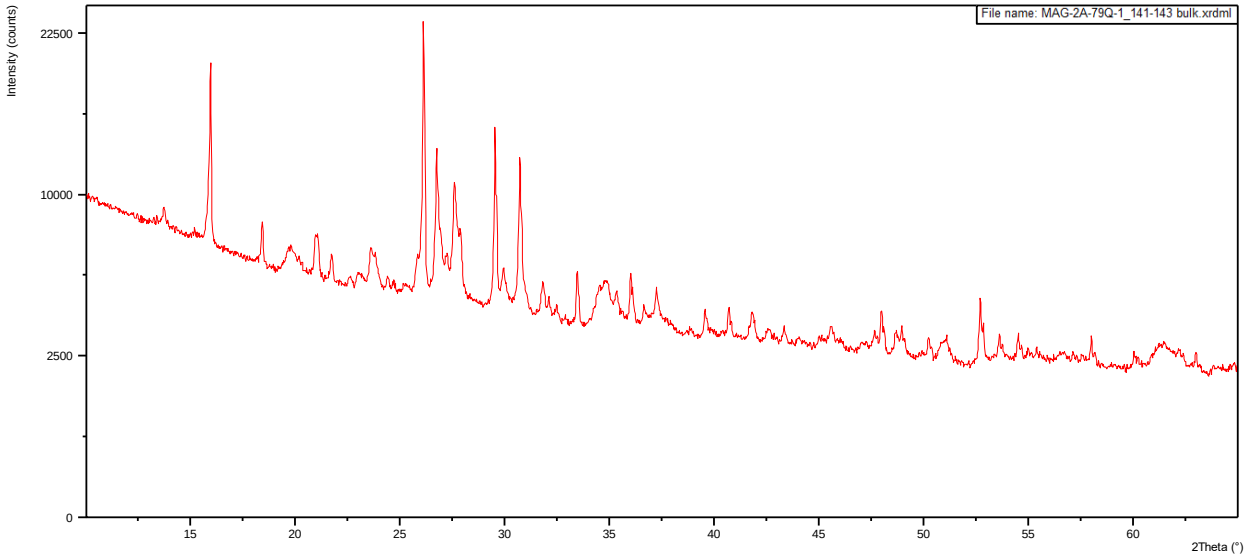
File name: MAG-2A-79Q-1_141-143 bulk.xrdml
Intensity (counts)
22500
10000
2500
0
15
20
25
30
35
40
45
50
55
60
2Theta (°)

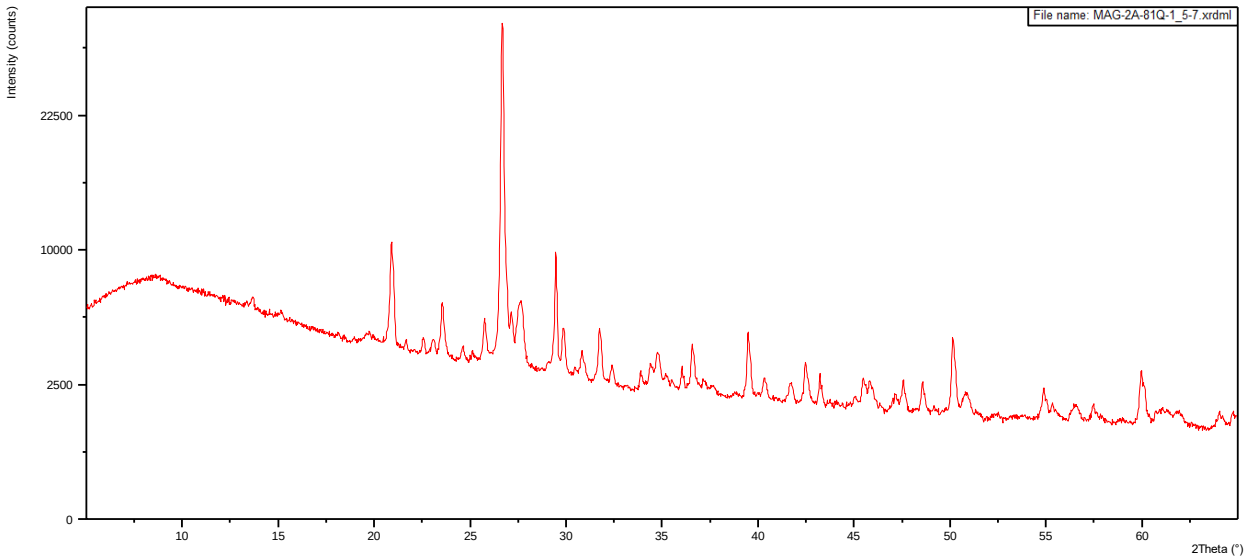
File name: MAG-2A-81Q-1_5-7.xrdml
Intensity (counts)
22500
10000
2500
0
10
15
20
25
30
35
40
45
50
55
60
2Theta (°)

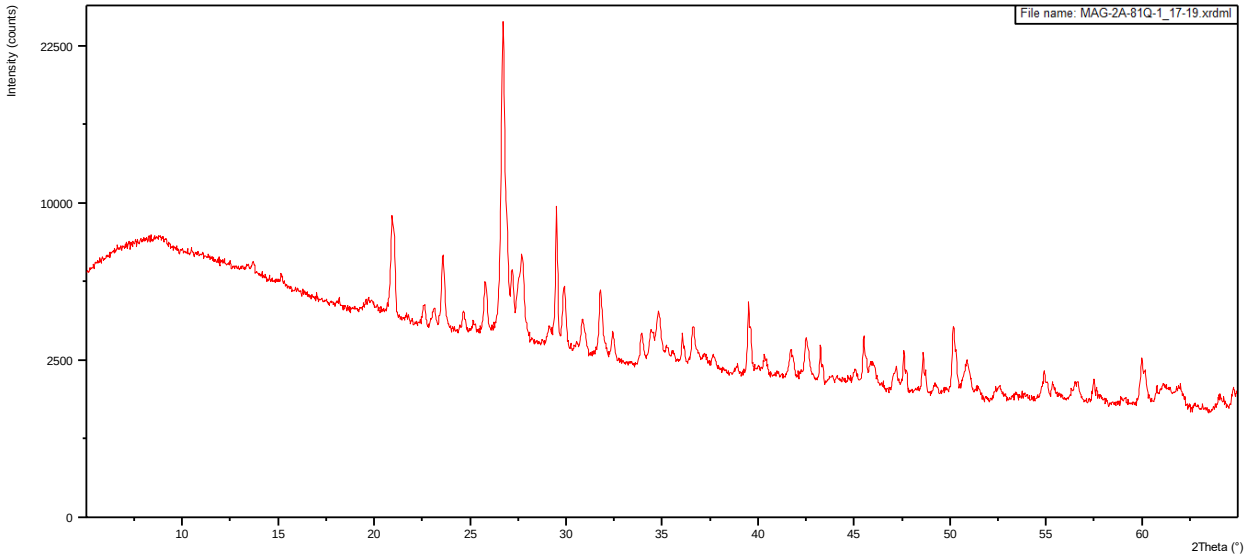
File name: MAG-2A-81Q-1_17-19.xrdml
Intensity (counts)
22500
10000
2500
0
10
15
20
25
30
35
40
45
50
55
60
2Theta (°)

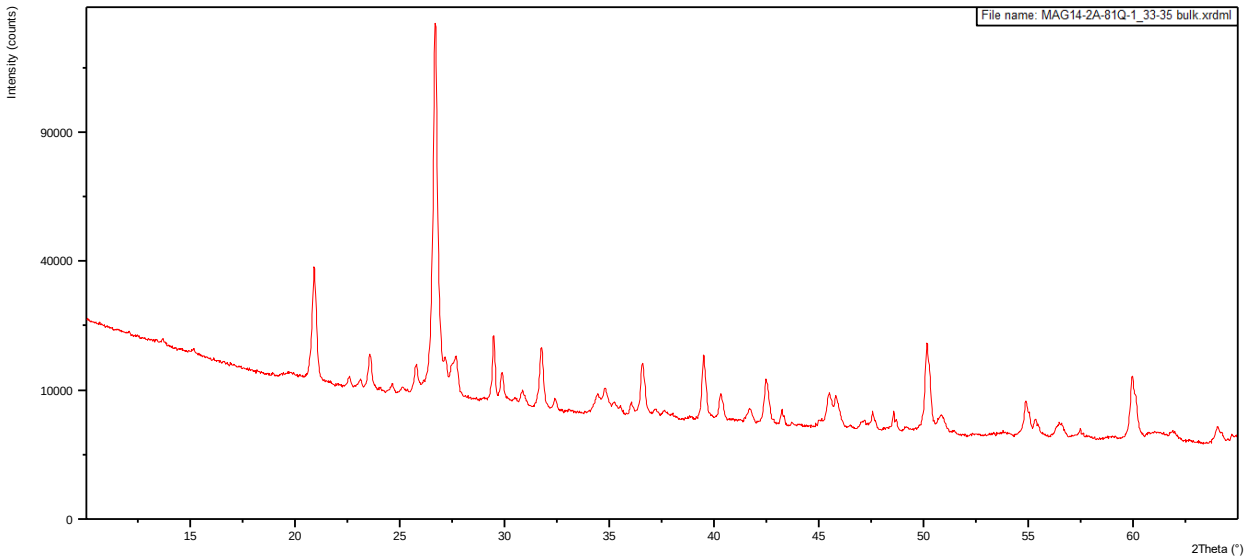
File name: MAG14-2A-81Q-1_33-35 bulk.xrdml
Intensity (counts)
90000
40000
10000
0
15
20
25
30
35
40
45
50
55
60
2Theta (°)

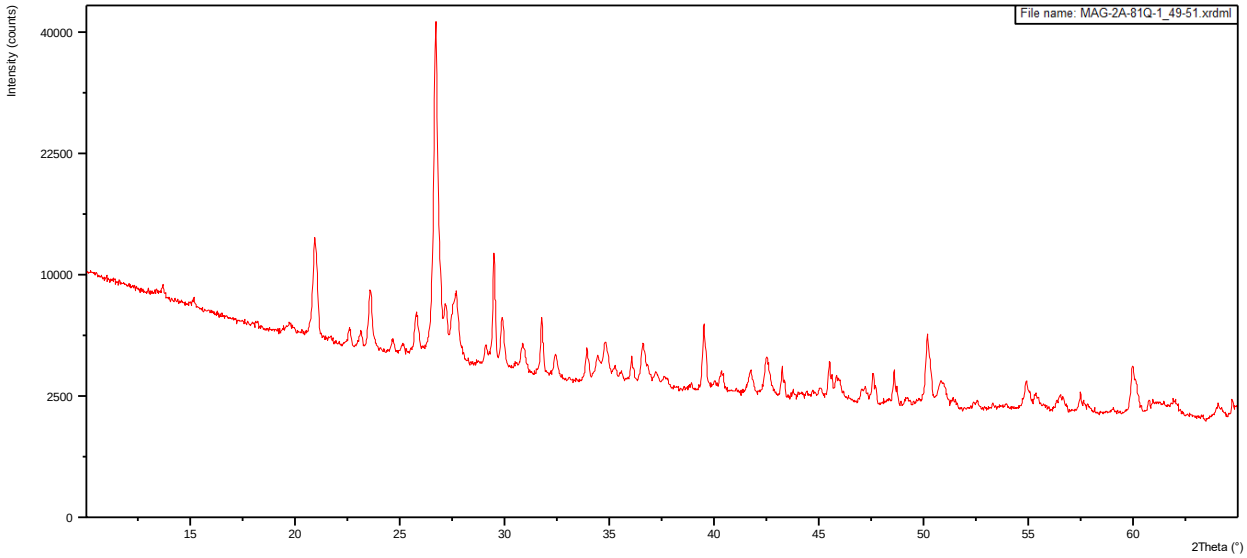
File name: MAG-2A-81Q-1_49-51.xrdml
Intensity (counts)
40000
22500
10000
2500
0
15
20
25
30
35
40
45
50
55
60
2Theta (°)

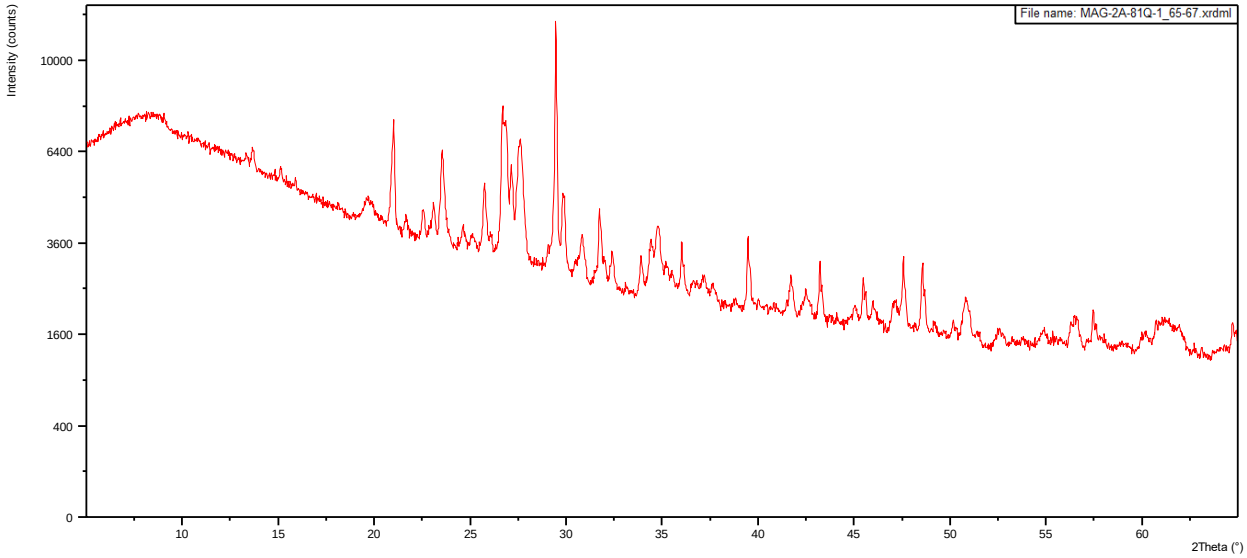
File name: MAG-2A-81Q-1_65-67.xrdml
Intensity (counts)
10000
6400
3600
1600
400
0
10
15
20
25
30
35
40
45
50
55
60
2Theta (°)

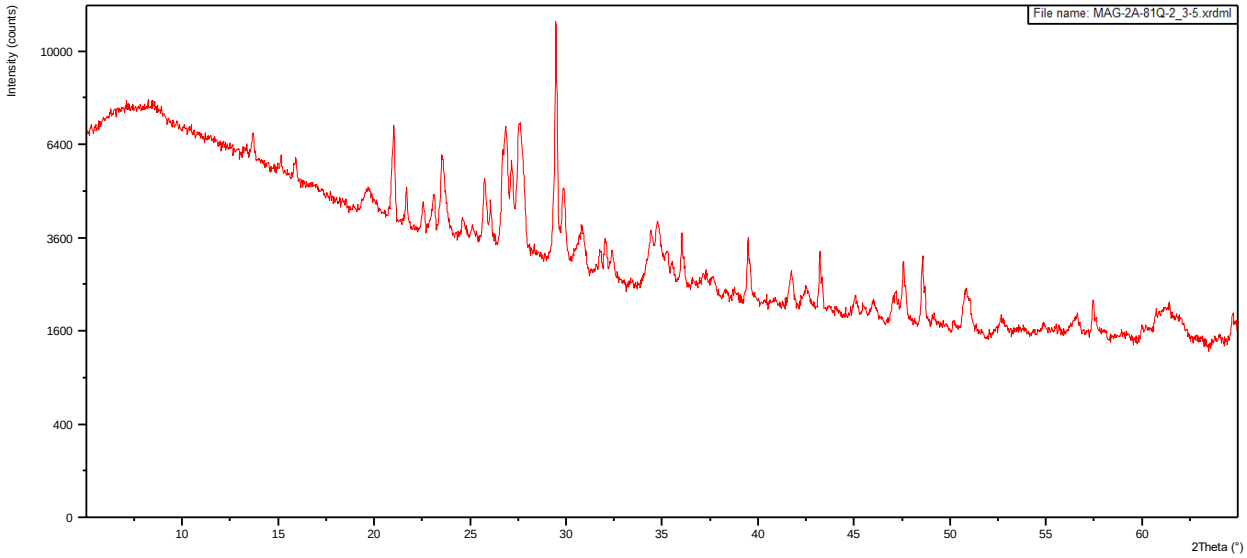
File name: MAG-2A-81Q-2_3-5.xrdml
Intensity (counts)
10000
6400
3600
1600
400
0
10
15
20
25
30
35
40
45
50
55
60
2Theta (°)

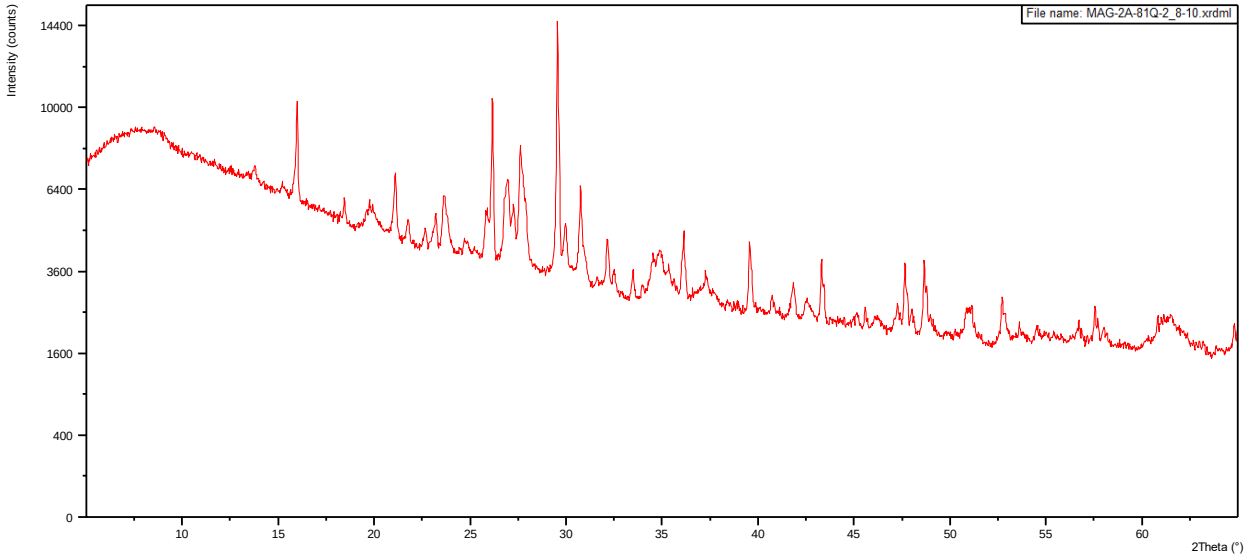
File name: MAG-2A-81Q-2_8-10.xrdml
Intensity (counts)
14400
10000
6400
3600
1600
400
0
10
15
20
25
30
35
40
45
50
55
60
2Theta (°)

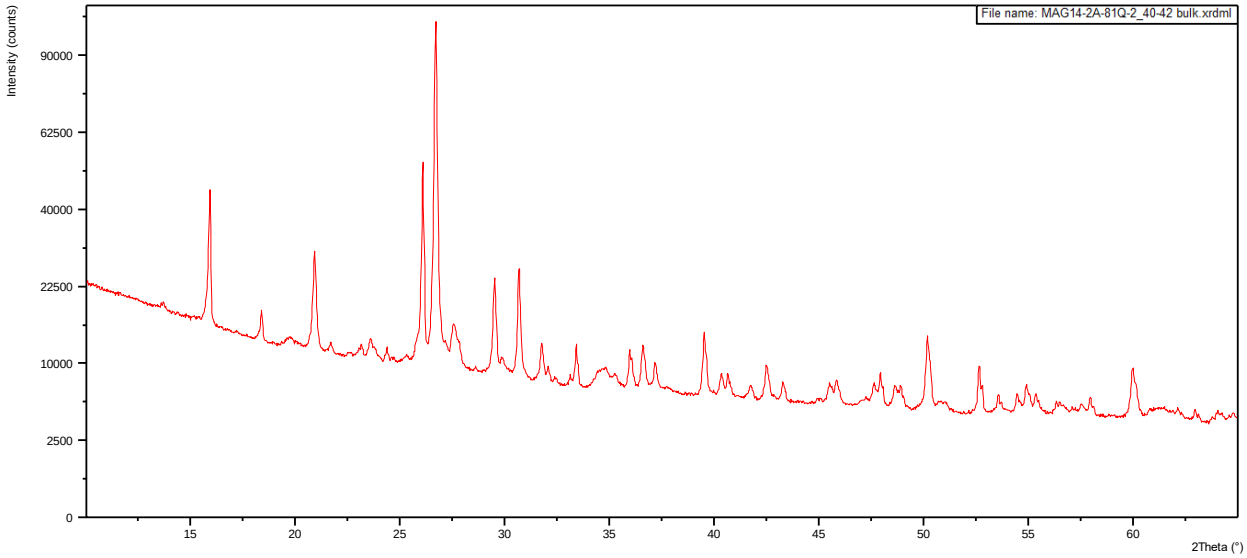
File name: MAG14-2A-81Q-2_40-42 bulk.xrdml
Intensity (counts)
90000
62500
40000
22500
10000
2500
0
15
20
25
30
35
40
45
50
55
60
2Theta (°)

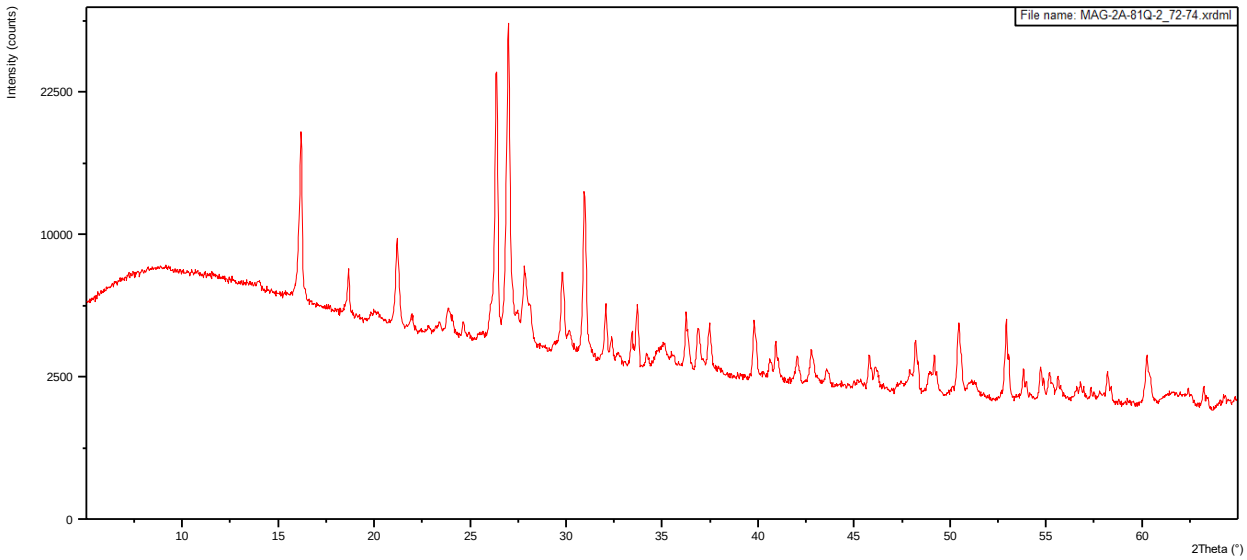
File name: MAG-2A-81Q-2_72-74.xrdml
Intensity (counts)
22500
10000
2500
0
10
15
20
25
30
35
40
45
50
55
60
2Theta (°)

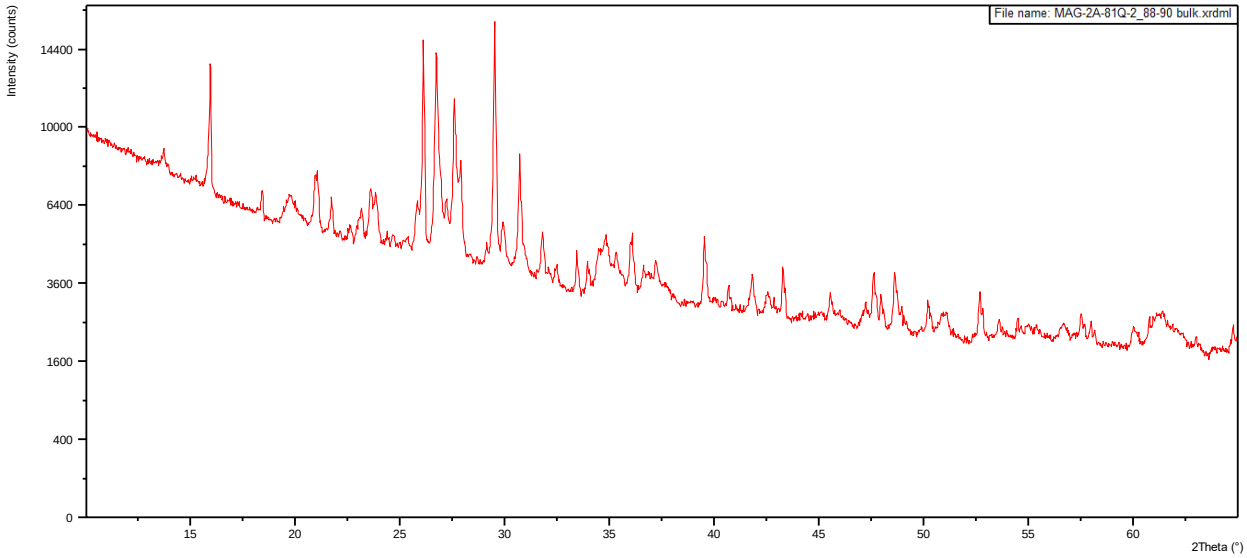
File name: MAG-2A-81Q-2_88-90 bulk.xrdml
Intensity (counts)
14400
10000
6400
3600
1600
400
0
15
20
25
30
35
40
45
50
55
60
2Theta (°)

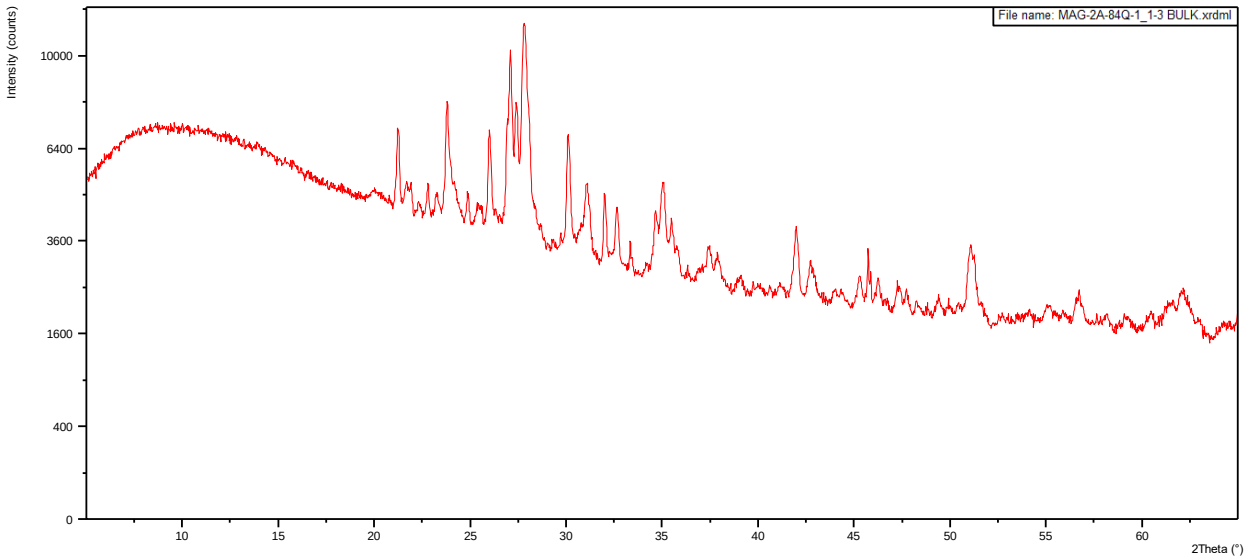
File name: MAG-2A-84Q-1_1-3 BULK.xrdml
Intensity (counts)
10000
6400
3600
1600
400
0
10
15
20
25
30
35
40
45
50
55
60
2Theta (°)

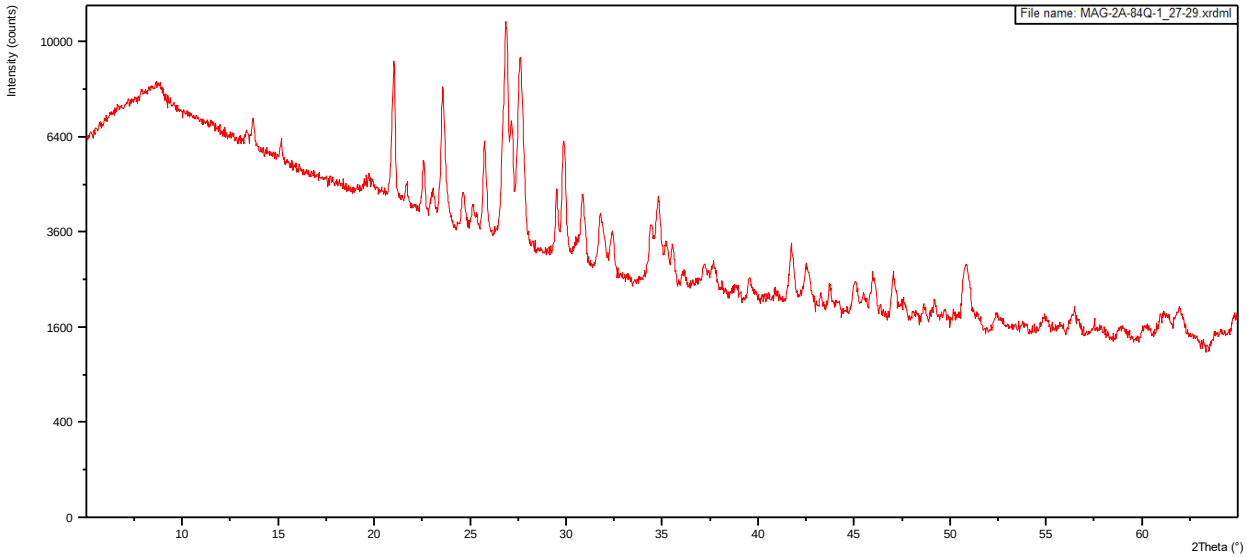
File name: MAG-2A-84Q-1_27-29.xrdml
Intensity (counts)
10000
6400
3600
1600
400
0
10
15
20
25
30
35
40
45
50
55
60
2Theta (°)

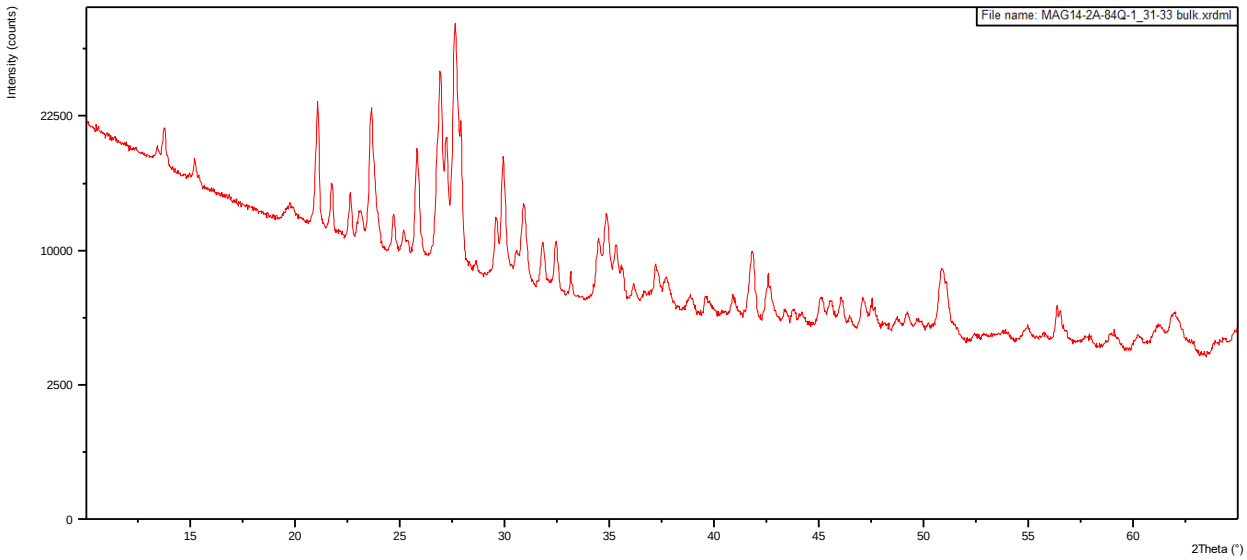
File name: MAG14-2A-84Q-1_31-33 bulk.xrdml
Intensity (counts)
0
2500
10000
22500
15
20
25
30
35
40
45
50
55
60
2Theta (°)

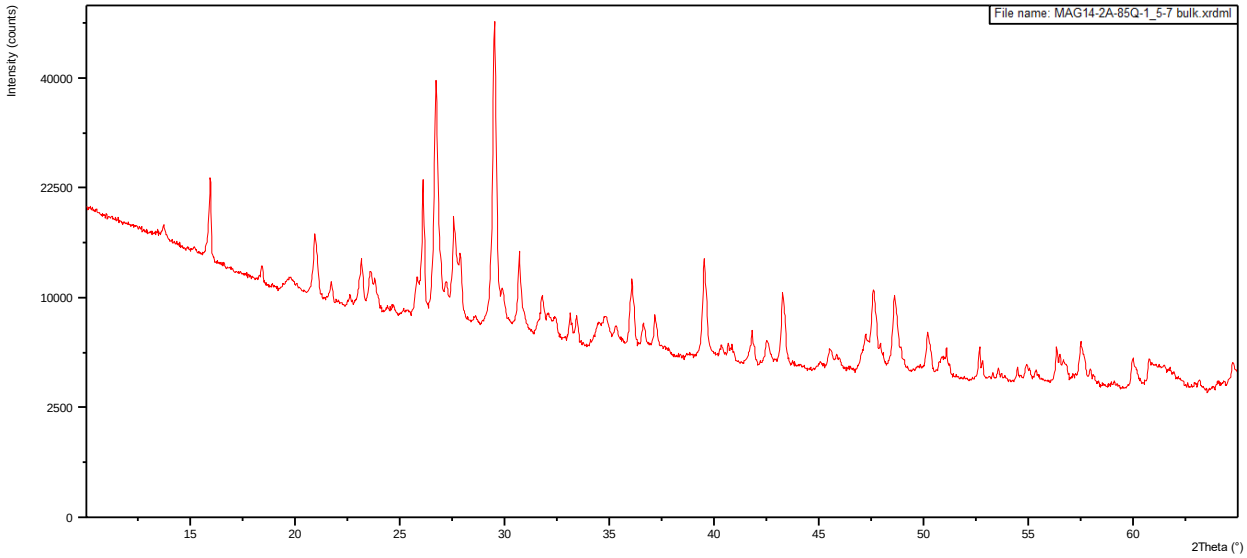
File name: MAG14-2A-85Q-1_5-7 bulk.xrdml
Intensity (counts)
0
2500
10000
22500
40000
15
20
25
30
35
40
45
50
55
60
2Theta (°)

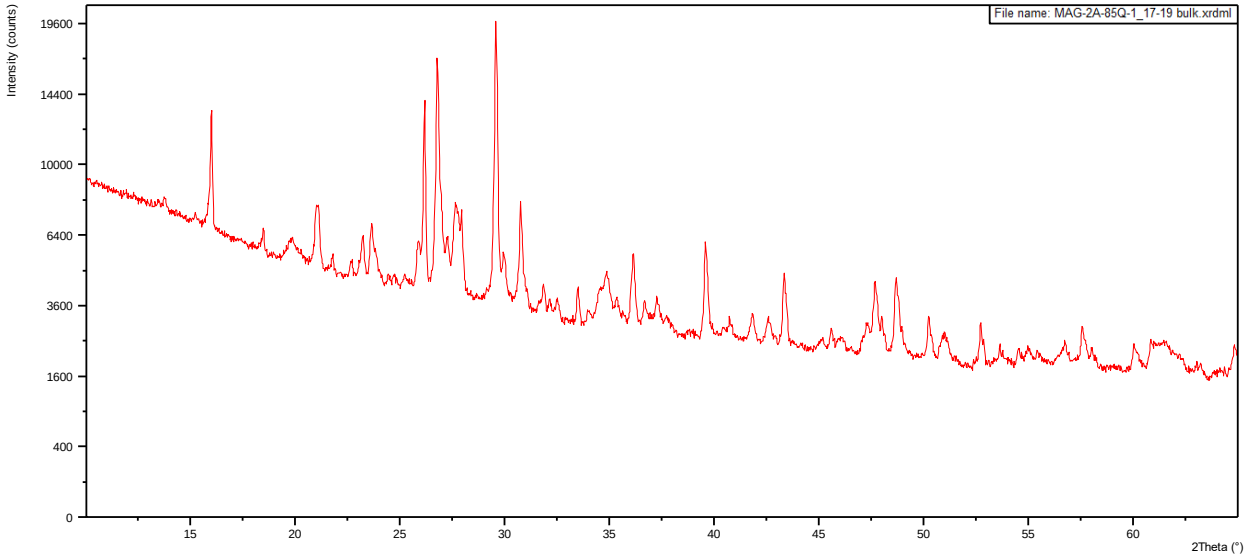
File name: MAG-2A-85Q-1_17-19 bulk.xrdml
Intensity (counts)
19600
14400
10000
6400
3600
1600
400
0
15
20
25
30
35
40
45
50
55
60
2Theta (°)

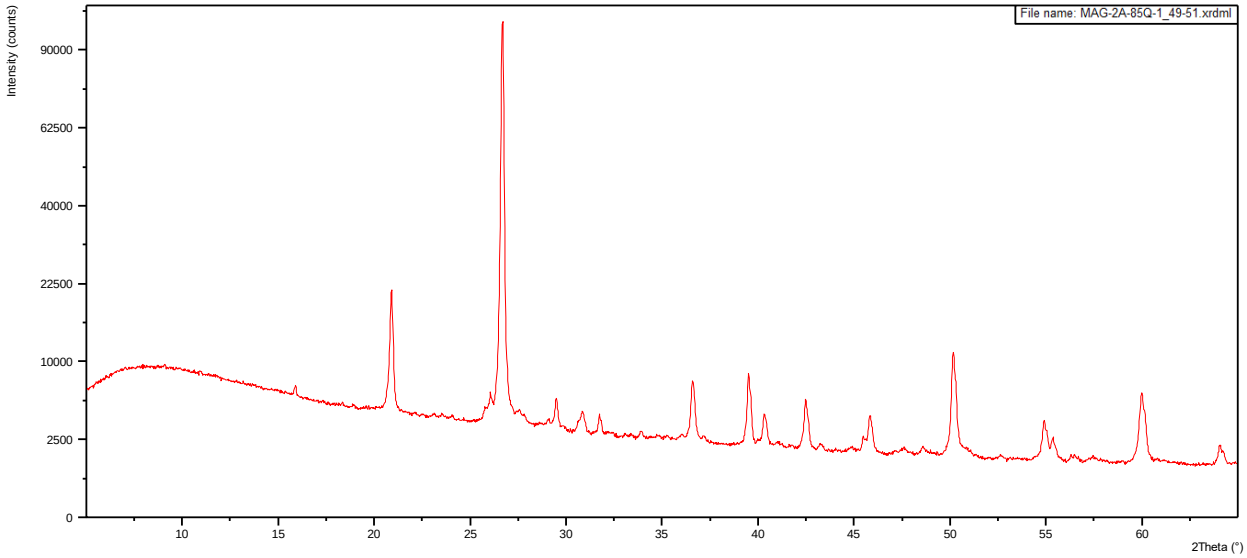
File name: MAG-2A-85Q-1_49-51.xrdml
Intensity (counts)
90000
62500
40000
22500
10000
2500
0
10
15
20
25
30
35
40
45
50
55
60
2Theta (°)

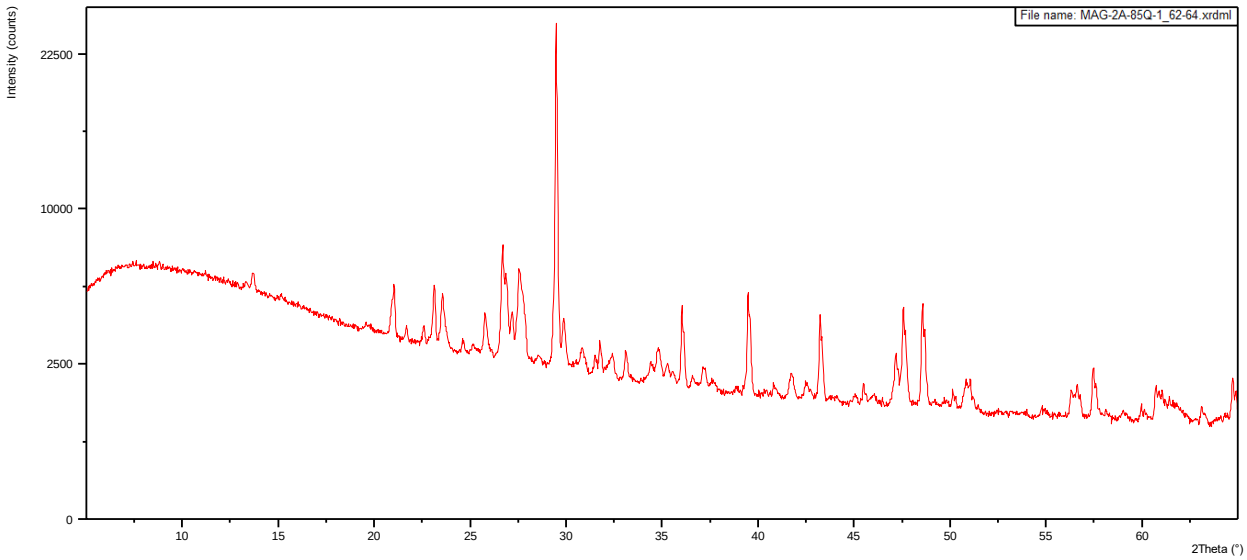
File name: MAG-2A-85Q-1_62-64.xrdml
Intensity (counts)
22500
10000
2500
0
10
15
20
25
30
35
40
45
50
55
60
2Theta (°)

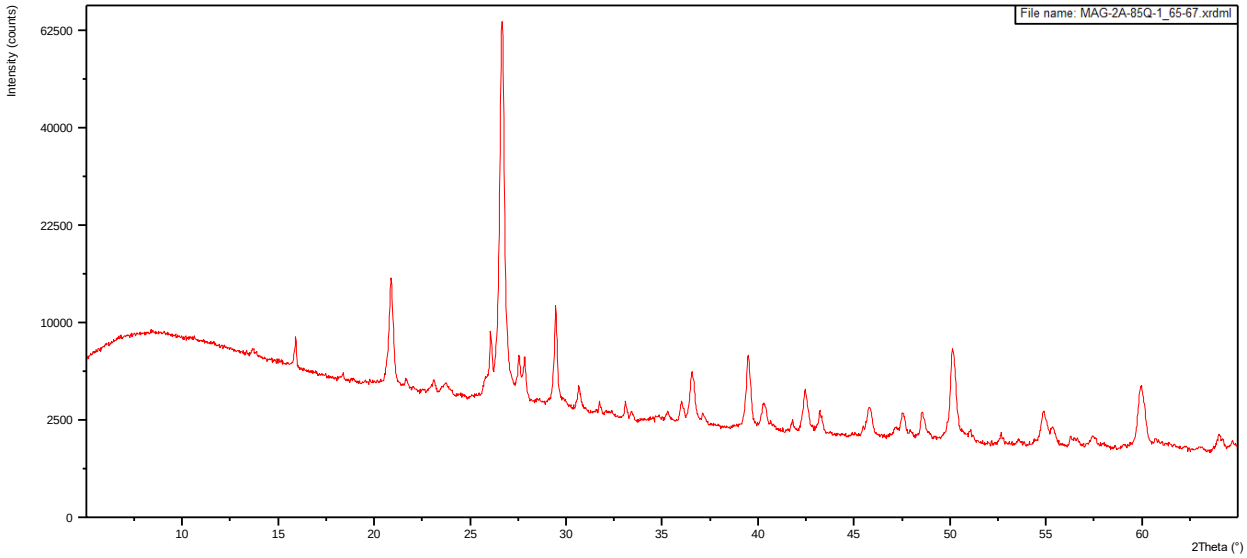
File name: MAG-2A-85Q-1_65-67.xrdml
Intensity (counts)
62500
40000
22500
10000
2500
0
10
15
20
25
30
35
40
45
50
55
60
2Theta (°)

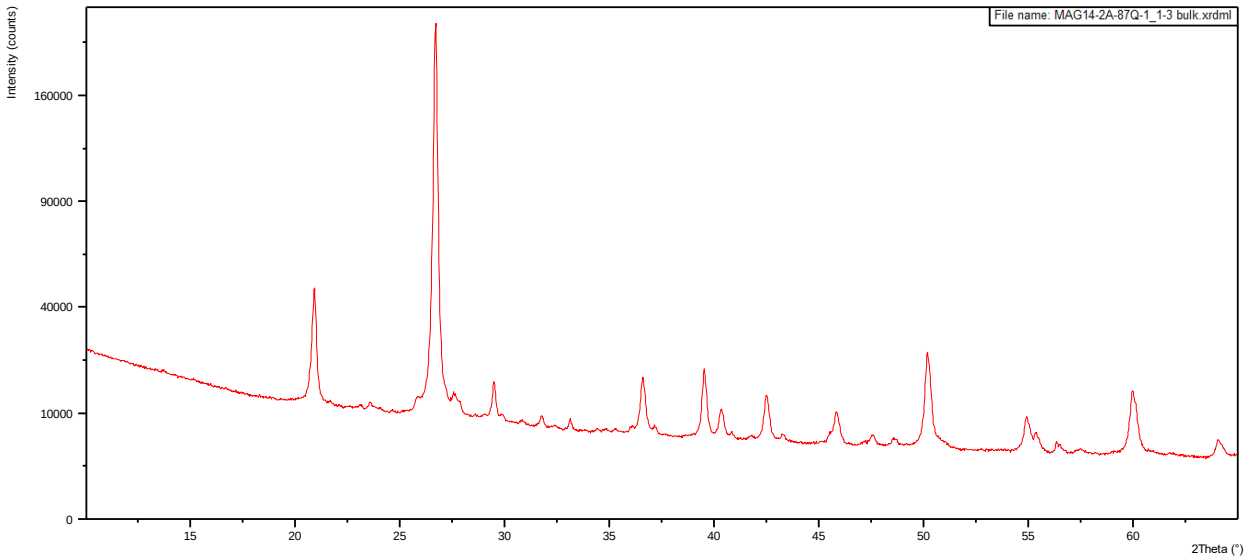
File name: MAG14-2A-87Q-1_1-3 bulk.xrdml
Intensity (counts)
160000
90000
40000
10000
0
15
20
25
30
35
40
45
50
55
60
2Theta (°)

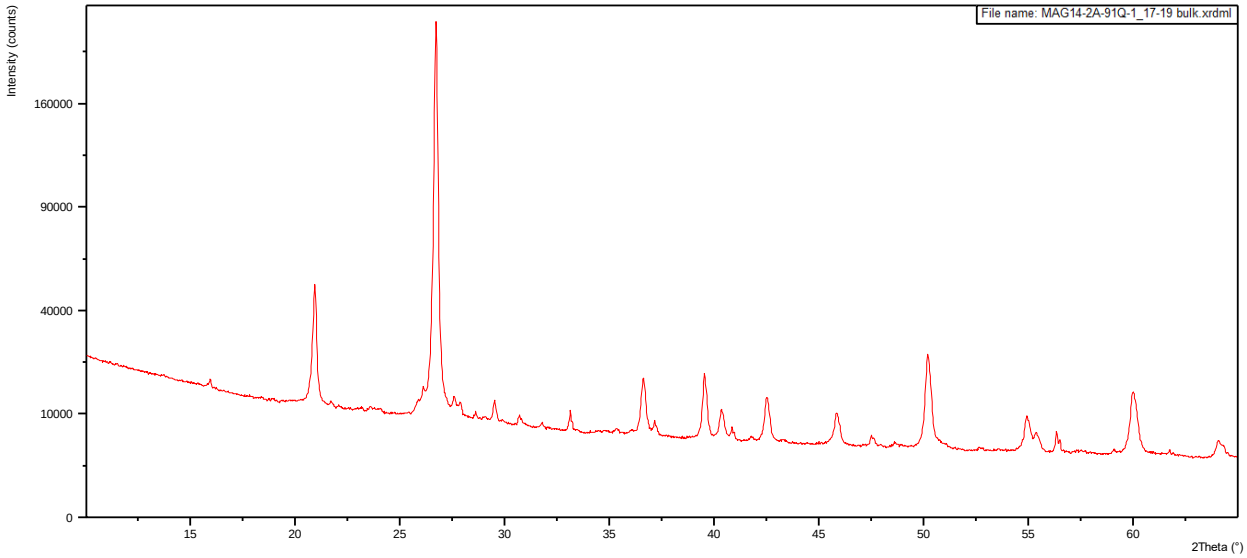
File name: MAG14-2A-91Q-1_17-19 bulk.xrdml
Intensity (counts)
160000
90000
40000
10000
0
15
20
25
30
35
40
45
50
55
60
2Theta (°)

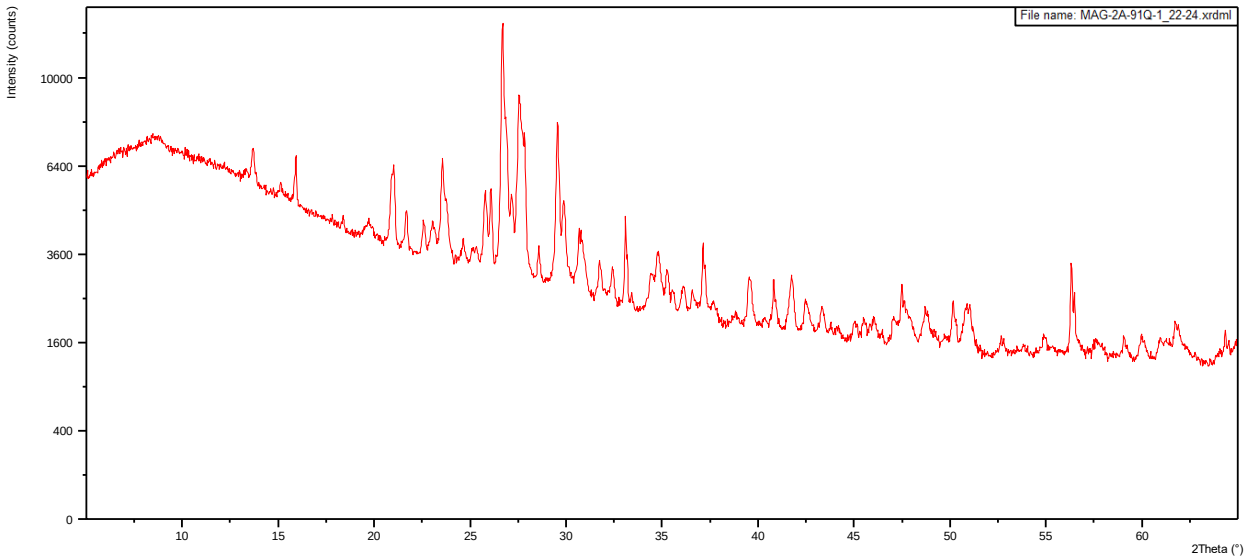
File name: MAG-2A-91Q-1_22-24.xrdml
Intensity (counts)
10000
6400
3600
1600
400
0
10
15
20
25
30
35
40
45
50
55
60
2Theta (°)

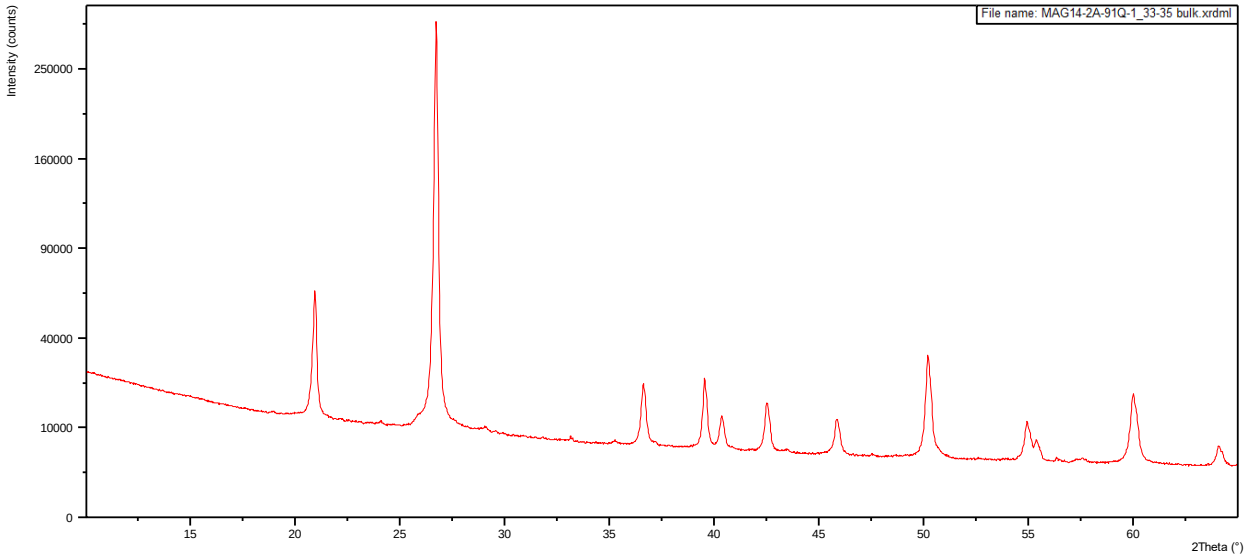
File name: MAG14-2A-91Q-1_33-35 bulk.xrdml
Intensity (counts)
250000
160000
90000
40000
10000
0
15
20
25
30
35
40
45
50
55
60
2Theta (°)

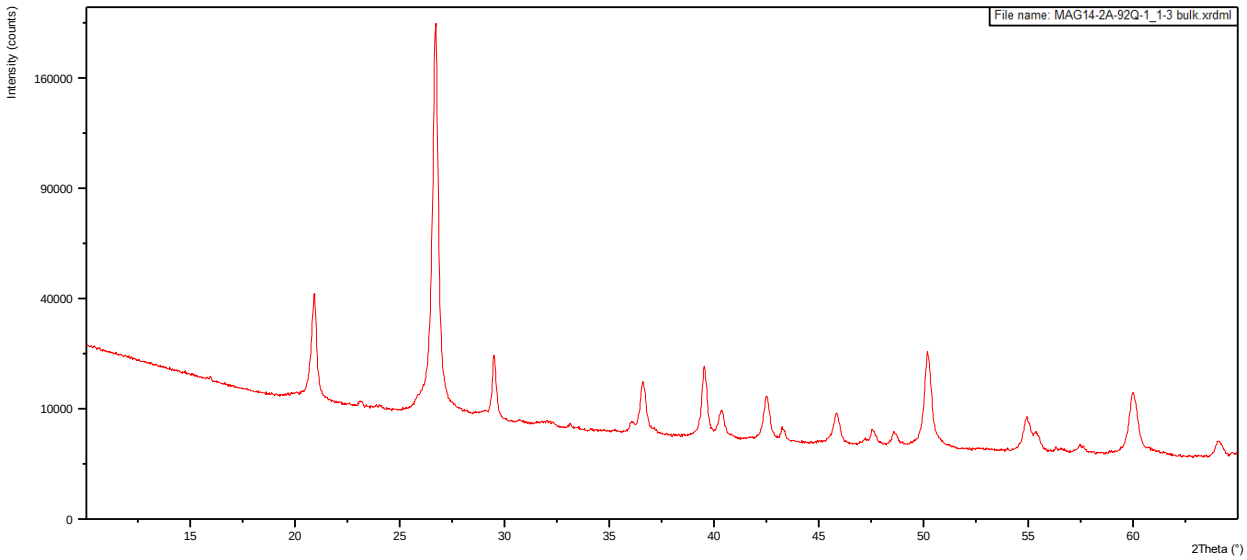
File name: MAG14-2A-92Q-1_1-3 bulk.xrdml
Intensity (counts)
160000
90000
40000
10000
0
15
20
25
30
35
40
45
50
55
60
2Theta (°)

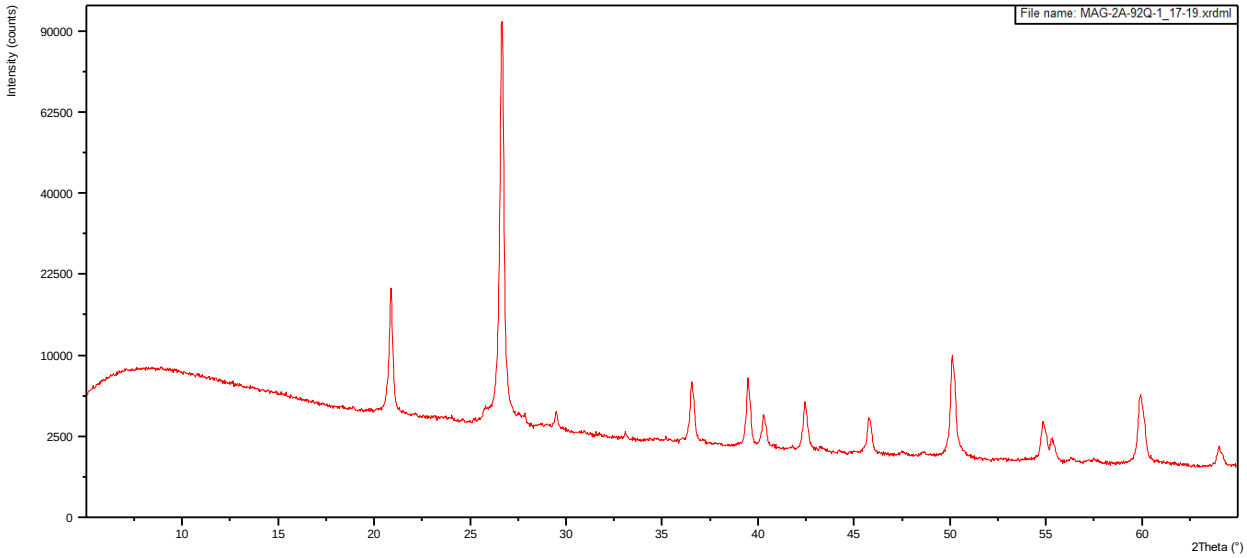
File name: MAG-2A-92Q-1_17-19.xrdml
Intensity (counts)
90000
62500
40000
22500
10000
2500
0
10
15
20
25
30
35
40
45
50
55
60
2Theta (°)

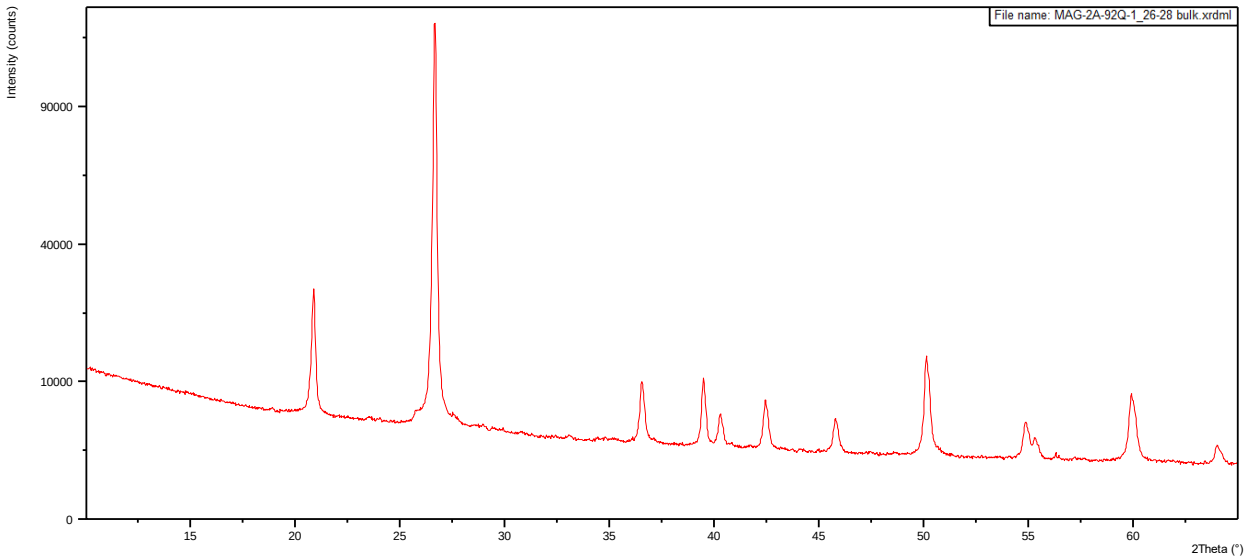
File name: MAG-2A-92Q-1_26-28 bulk.xrdml
Intensity (counts)
90000
40000
10000
0
15
20
25
30
35
40
45
50
55
60
2Theta (°)

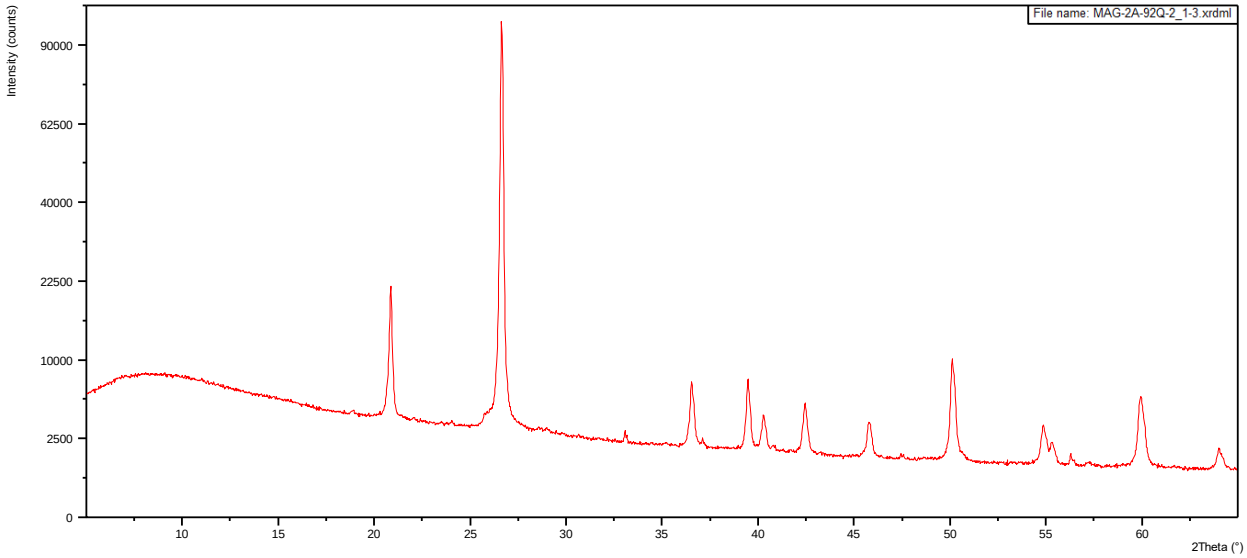
File name: MAG-2A-92Q-2_1-3.xrdml
Intensity (counts)
90000
62500
40000
22500
10000
2500
0
10
15
20
25
30
35
40
45
50
55
60
2Theta (°)

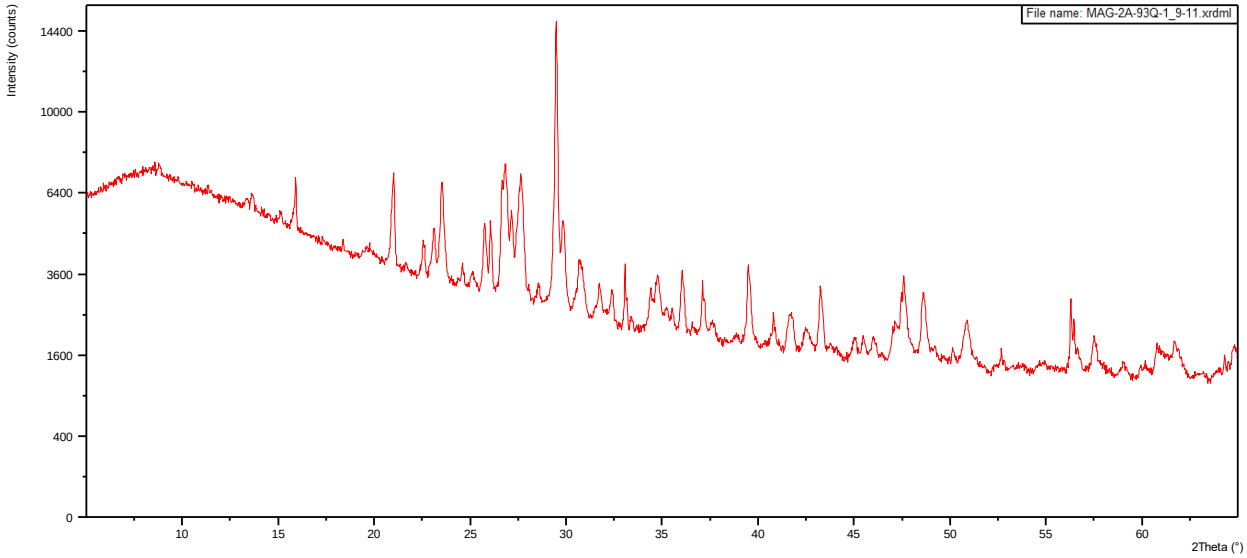
File name: MAG-2A-93Q-1_9-11.xrdml
Intensity (counts)
14400
10000
6400
3600
1600
400
0
10
15
20
25
30
35
40
45
50
55
60
2Theta (°)

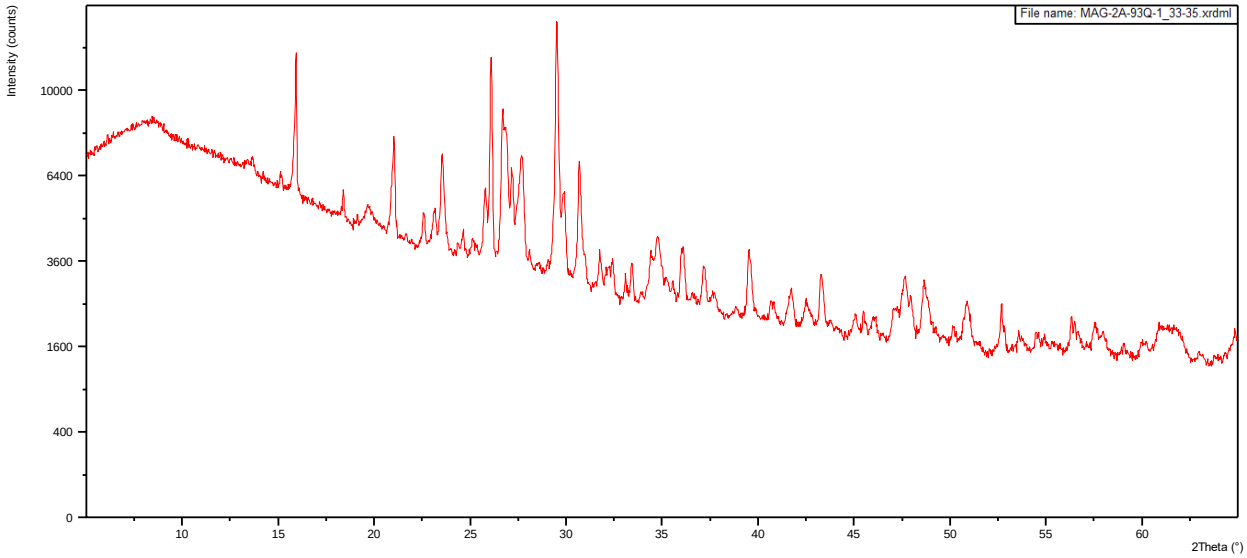
File name: MAG-2A-93Q-1_33-35.xrdml
Intensity (counts)
10000
6400
3600
1600
400
0
10
15
20
25
30
35
40
45
50
55
60
2Theta (°)

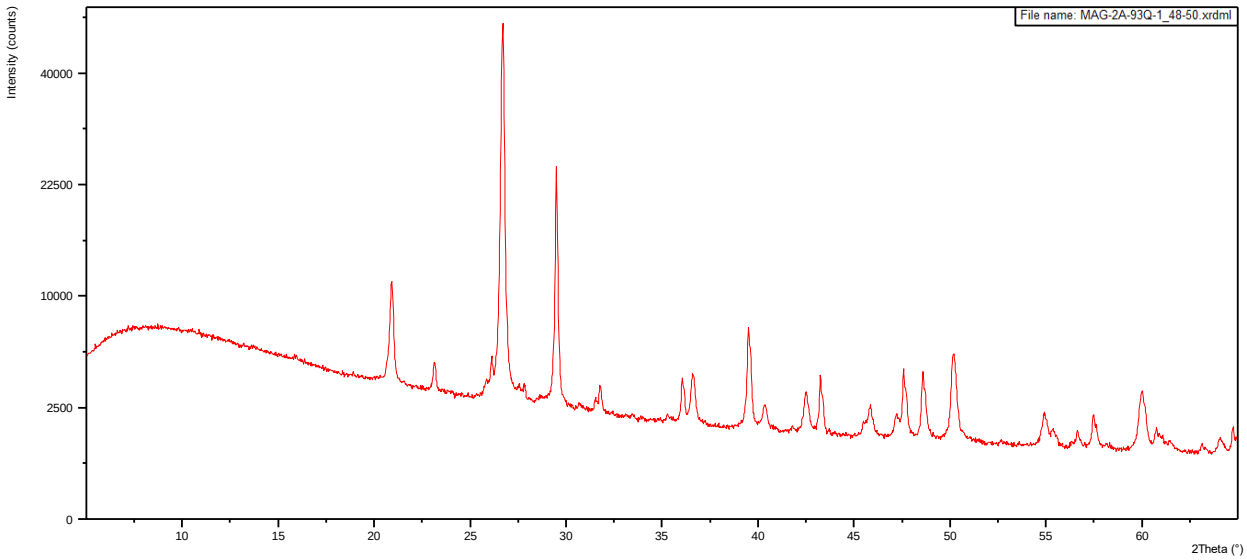
File name: MAG-2A-93Q-1_48-50.xrdml
Intensity (counts)
40000
22500
10000
2500
0
10
15
20
25
30
35
40
45
50
55
60
2Theta (°)

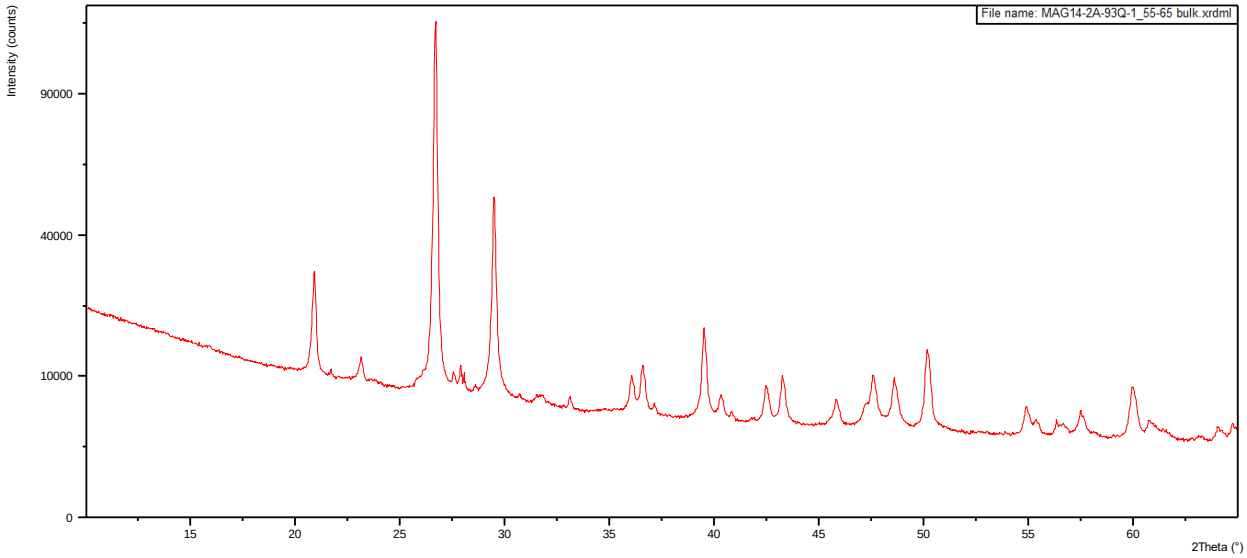
File name: MAG14-2A-93Q-1_55-65 bulk.xrdml
Intensity (counts)
90000
40000
10000
0
15
20
25
30
35
40
45
50
55
60
2Theta (°)

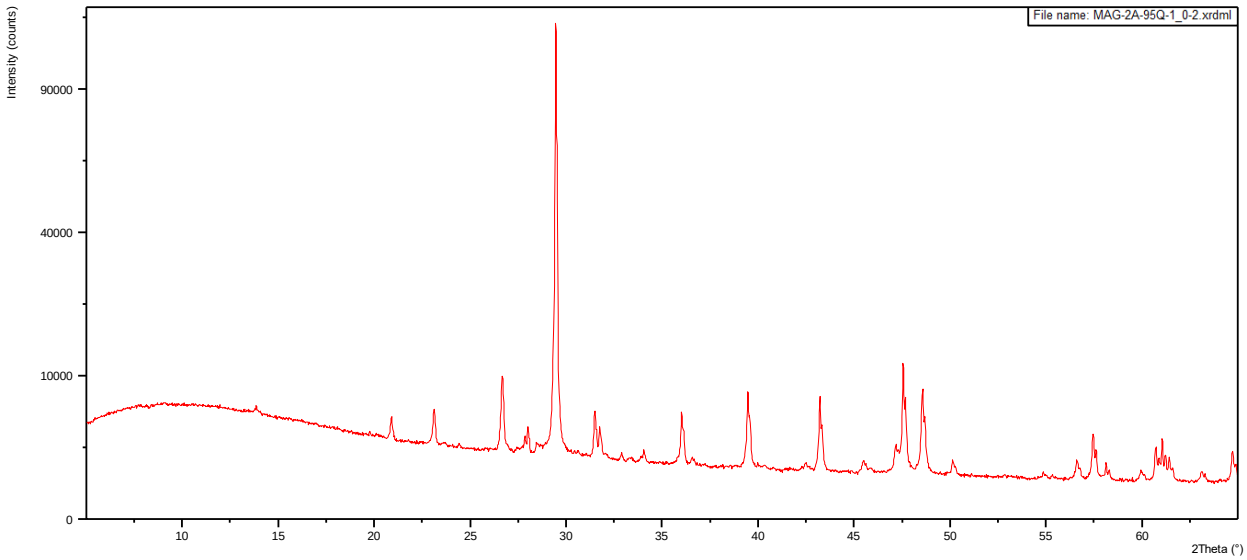
File name: MAG-2A-95Q-1_0-2.xrdml
Intensity (counts)
90000
40000
10000
0
10
15
20
25
30
35
40
45
50
55
60
2Theta (°)

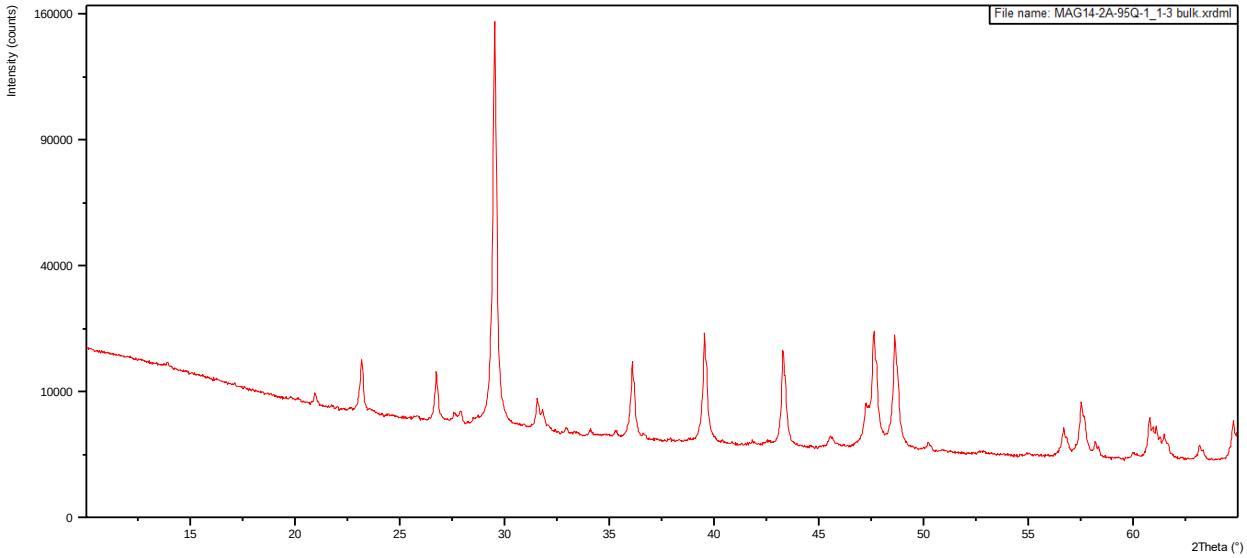
File name: MAG14-2A-95Q-1_1-3 bulk.xrdml
Intensity (counts)
160000
90000
40000
10000
0
15
20
25
30
35
40
45
50
55
60
2Theta (°)

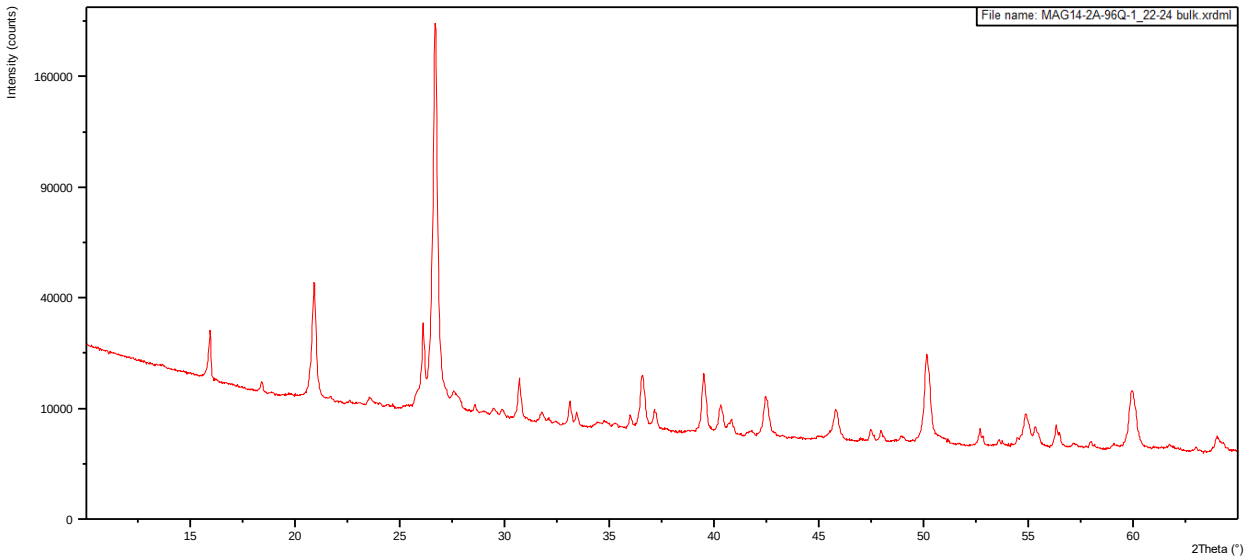
File name: MAG14-2A-96Q-1_22-24 bulk.xrdml
Intensity (counts)
160000
90000
40000
10000
0
15
20
25
30
35
40
45
50
55
60
2Theta (°)

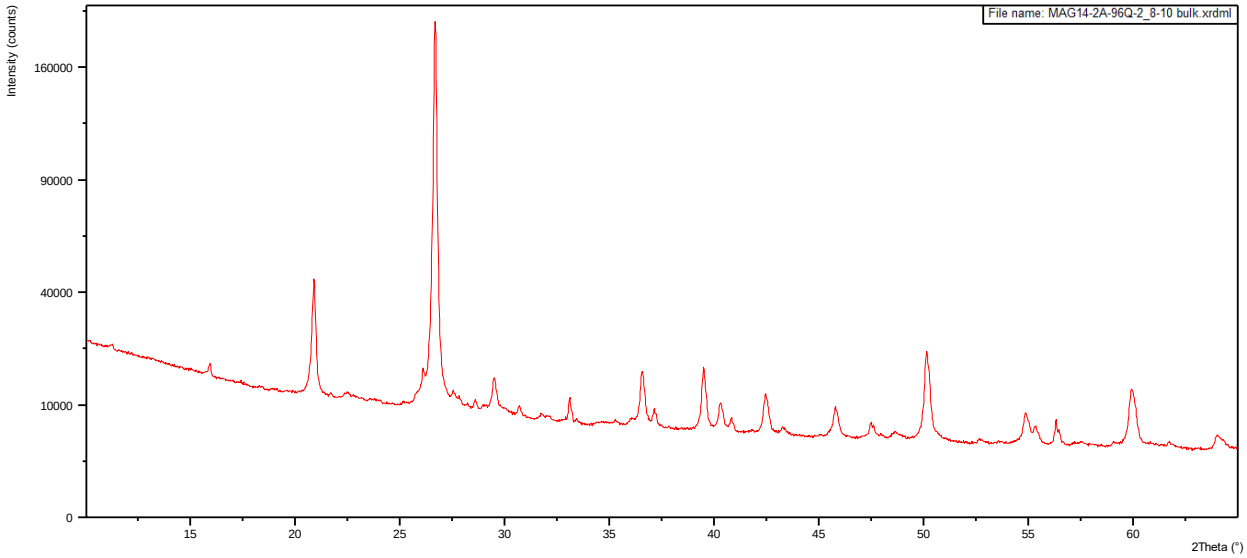
File name: MAG14-2A-96Q-2_8-10 bulk.xrdml
Intensity (counts)
160000
90000
40000
10000
0
15
20
25
30
35
40
45
50
55
60
2Theta (°)

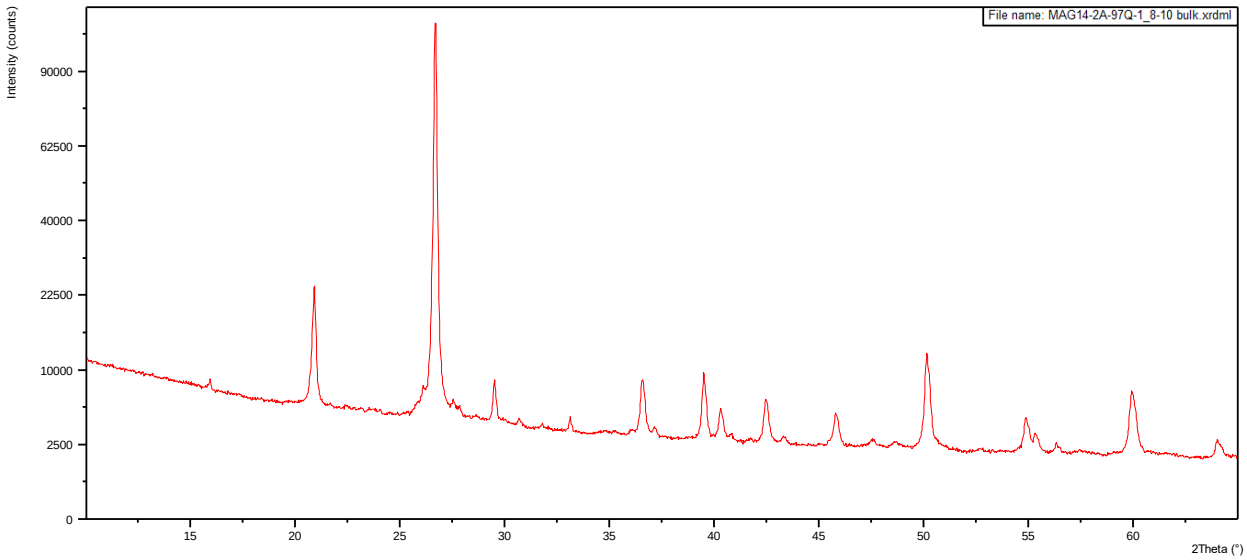
File name: MAG14-2A-97Q-1_8-10 bulk.xrdml
Intensity (counts)
90000
62500
40000
22500
10000
2500
0
15
20
25
30
35
40
45
50
55
60
2Theta (°)

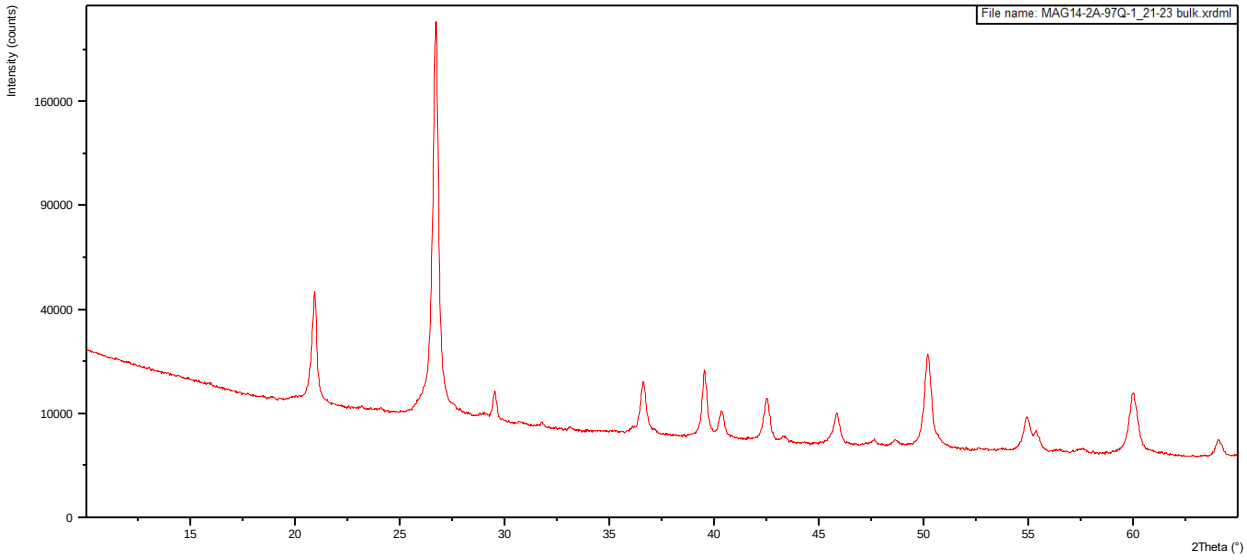
File name: MAG14-2A-97Q-1_21-23 bulk.xrdml
Intensity (counts)
160000
90000
40000
10000
0
15
20
25
30
35
40
45
50
55
60
2Theta (°)

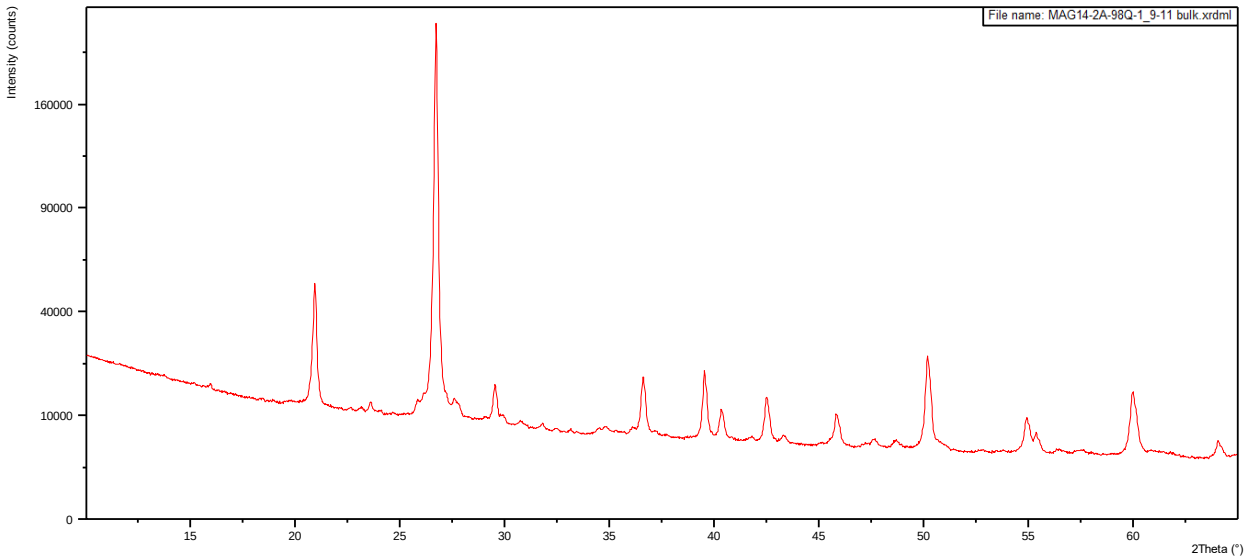
File name: MAG14-2A-98Q-1_9-11 bulk.xrdml
Intensity (counts)
160000
90000
40000
10000
0
15
20
25
30
35
40
45
50
55
60
2Theta (°)

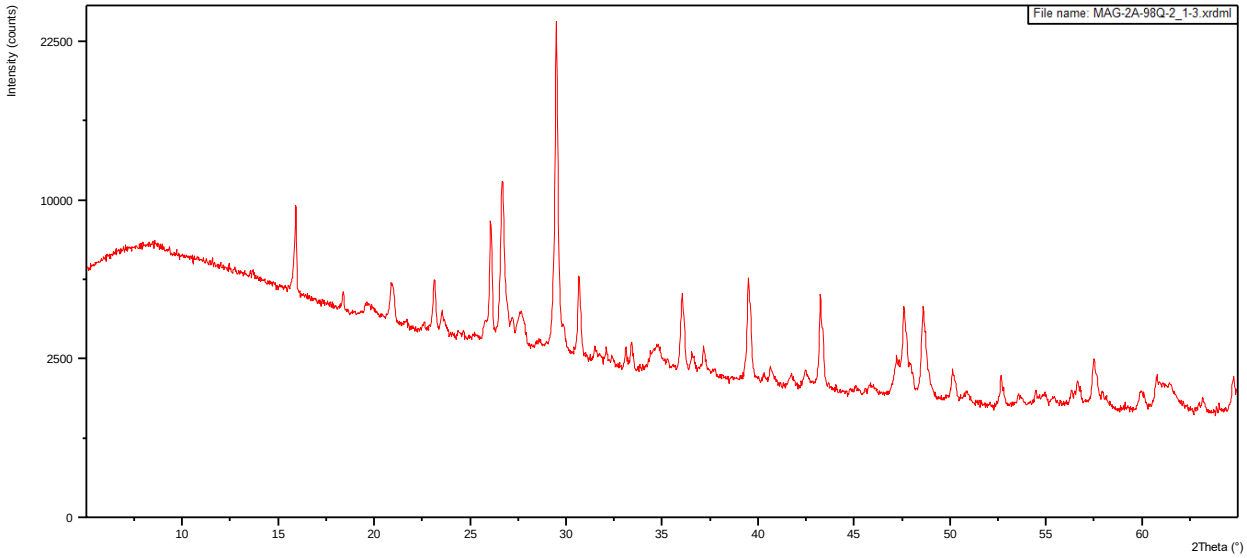
File name: MAG-2A-98Q-2_1-3.xrdml
Intensity (counts)
22500
10000
2500
0
10
15
20
25
30
35
40
45
50
55
60
2Theta (°)

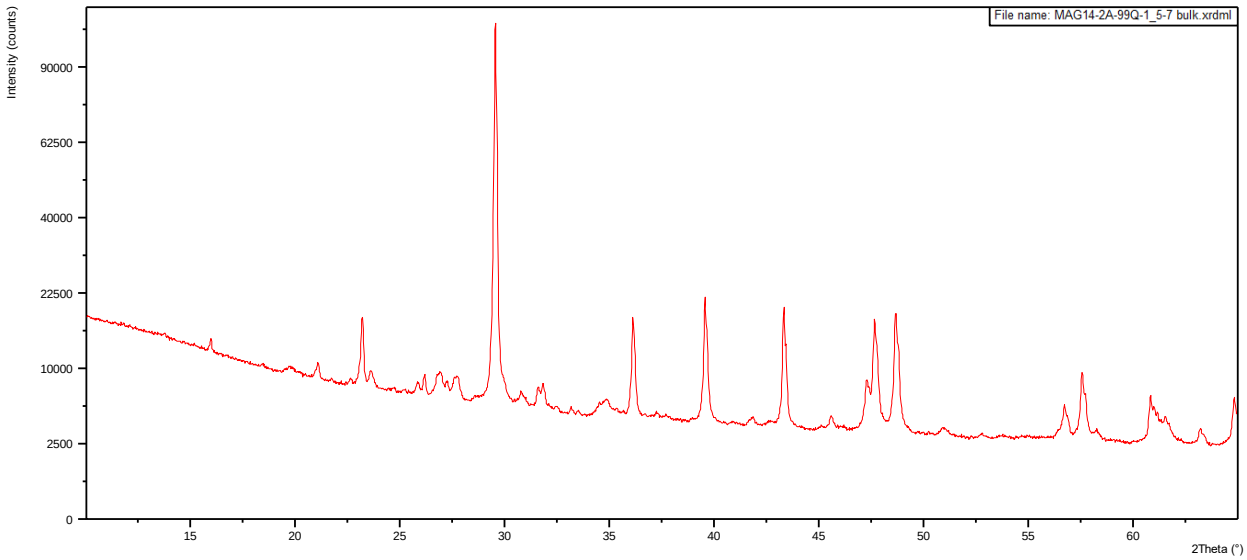
File name: MAG14-2A-99Q-1_5-7 bulk.xrdml
Intensity (counts)
90000
62500
40000
22500
10000
2500
0
15
20
25
30
35
40
45
50
55
60
2Theta (°)

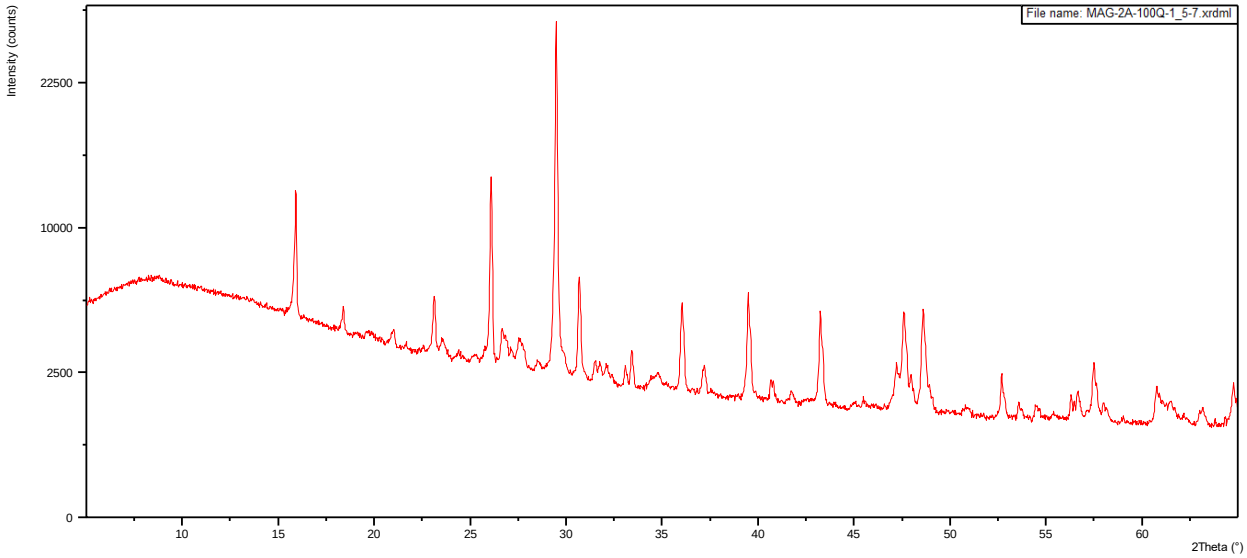
File name: MAG-2A-100Q-1_5-7.xrdml
Intensity (counts)
22500
10000
2500
0
10
15
20
25
30
35
40
45
50
55
60
2Theta (°)

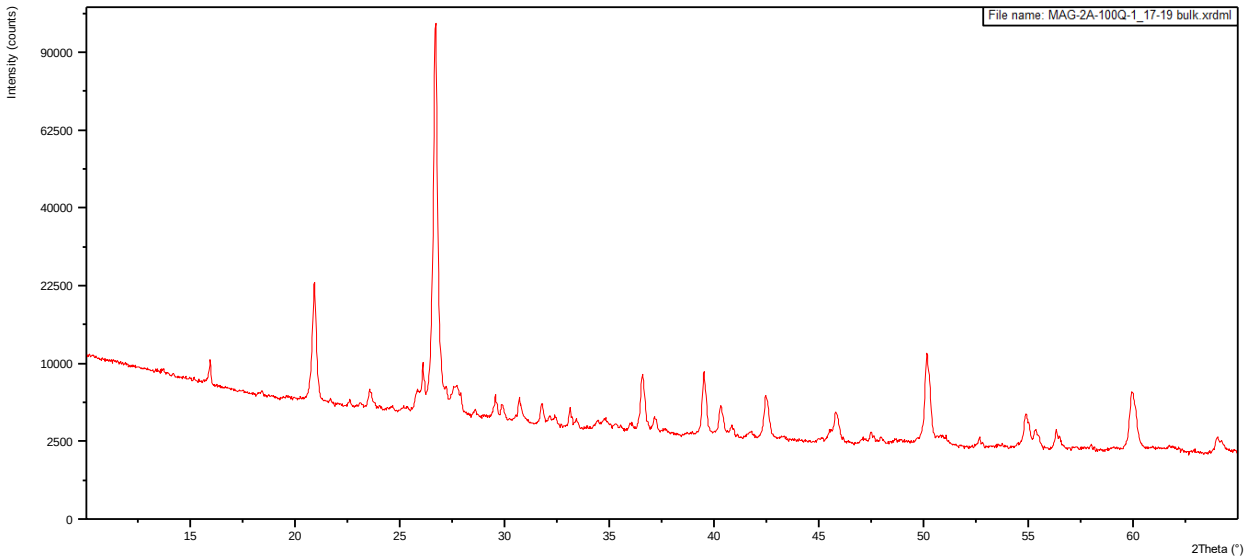
File name: MAG-2A-100Q-1_17-19 bulk.xrdml
Intensity (counts)
90000
62500
40000
22500
10000
2500
0
15
20
25
30
35
40
45
50
55
60
2Theta (°)

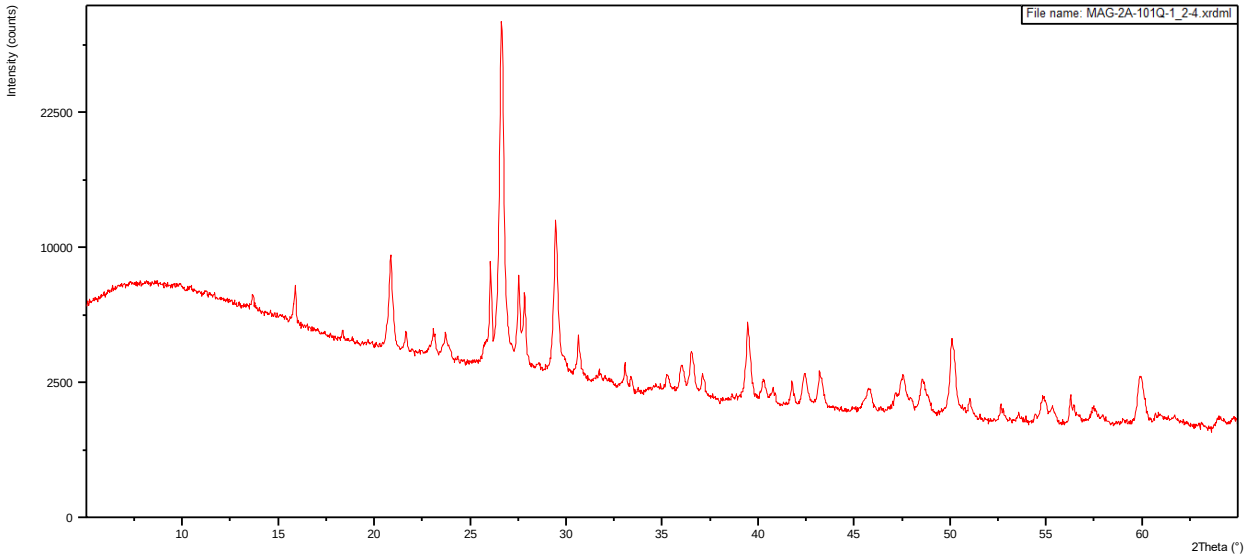
File name: MAG-2A-101Q-1_2-4.xrdml
Intensity (counts)
22500
10000
2500
0
10
15
20
25
30
35
40
45
50
55
60
2Theta (°)

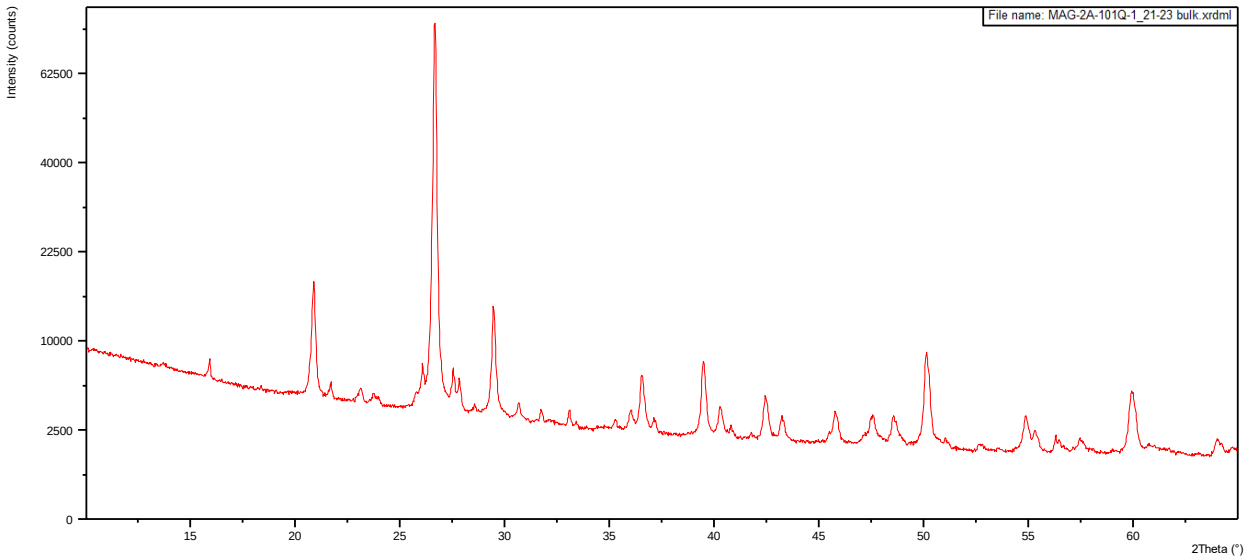
File name: MAG-2A-101Q-1_21-23 bulk.xrdml
Intensity (counts)
62500
40000
22500
10000
2500
0
15
20
25
30
35
40
45
50
55
60
2Theta (°)

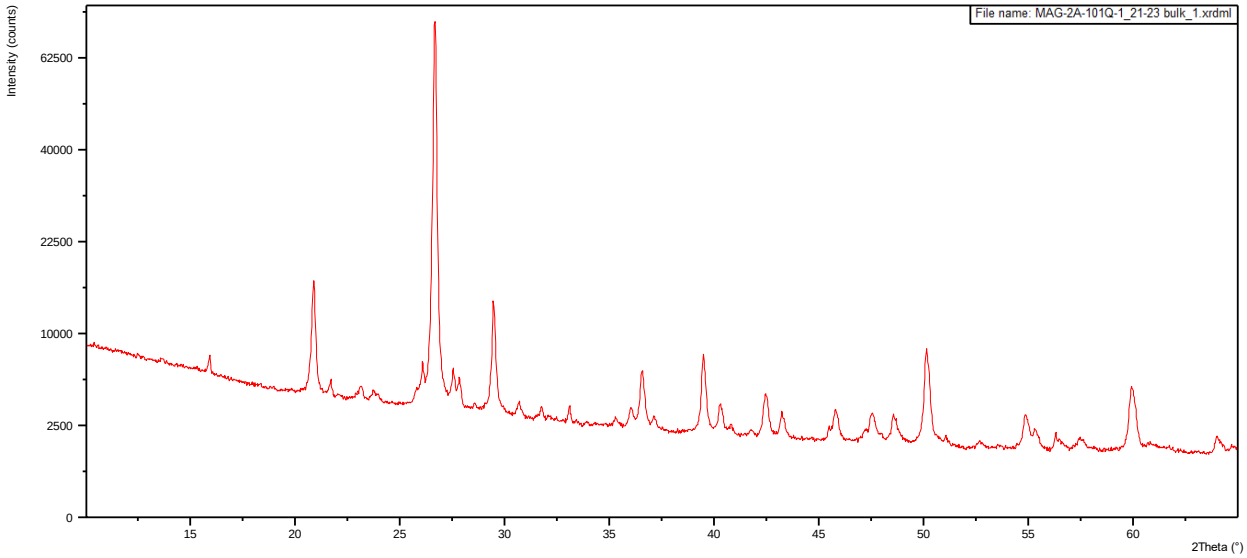
File name: MAG-2A-101Q-1_21-23 bulk_1.xrdml
Intensity (counts)
62500
40000
22500
10000
2500
0
15
20
25
30
35
40
45
50
55
60
2Theta (°)

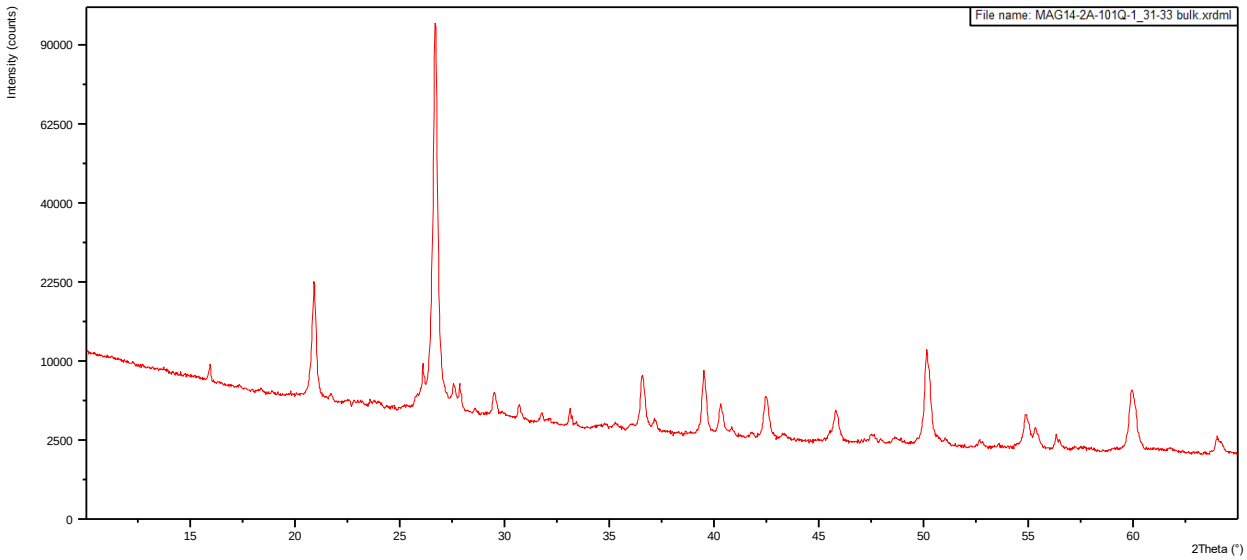
File name: MAG14-2A-101Q-1_31-33 bulk.xrdml
Intensity (counts)
90000
62500
40000
22500
10000
2500
0
15
20
25
30
35
40
45
50
55
60
2Theta (°)

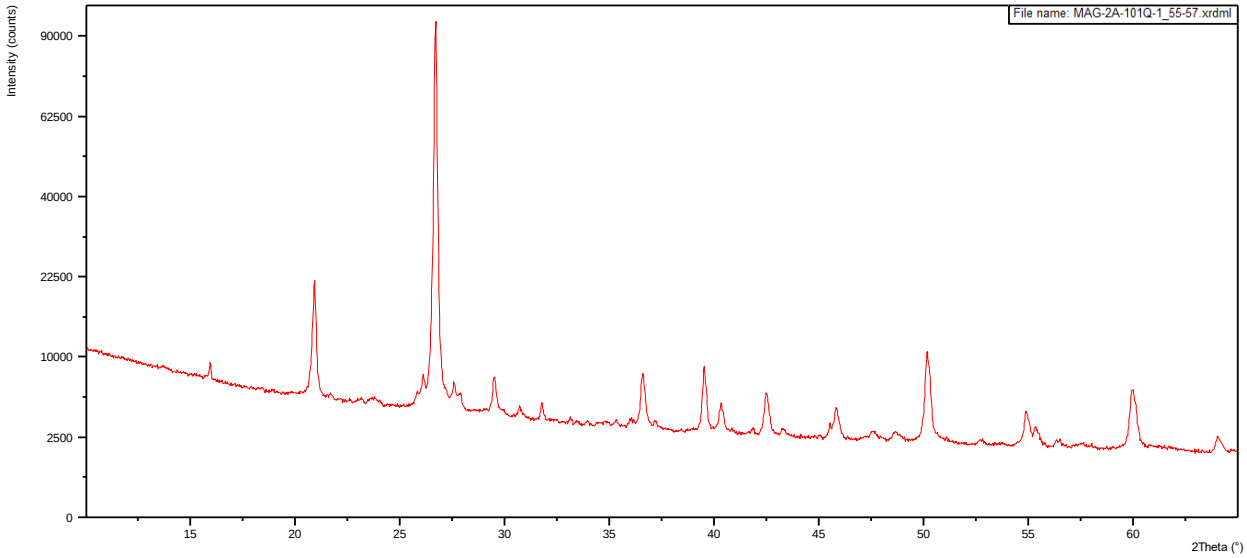
File name: MAG-2A-101Q-1_55-57.xrdml
Intensity (counts)
90000
62500
40000
22500
10000
2500
0
15
20
25
30
35
40
45
50
55
60
2Theta (°)

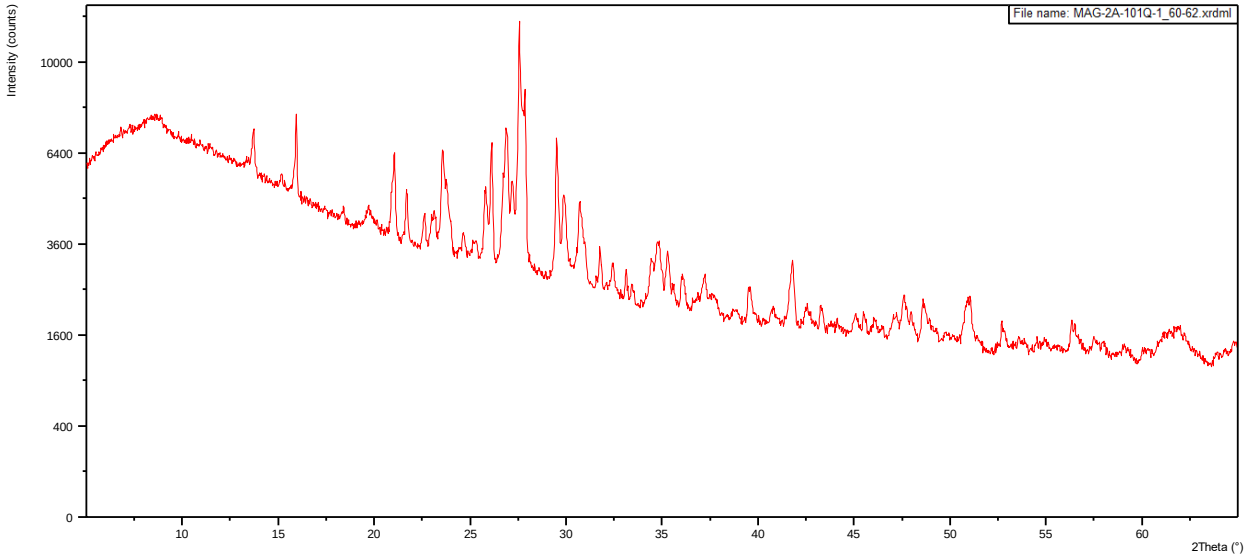
File name: MAG-2A-101Q-1_60-62.xrdml
Intensity (counts)
10000
6400
3600
1600
400
0
10
15
20
25
30
35
40
45
50
55
60
2Theta (°)

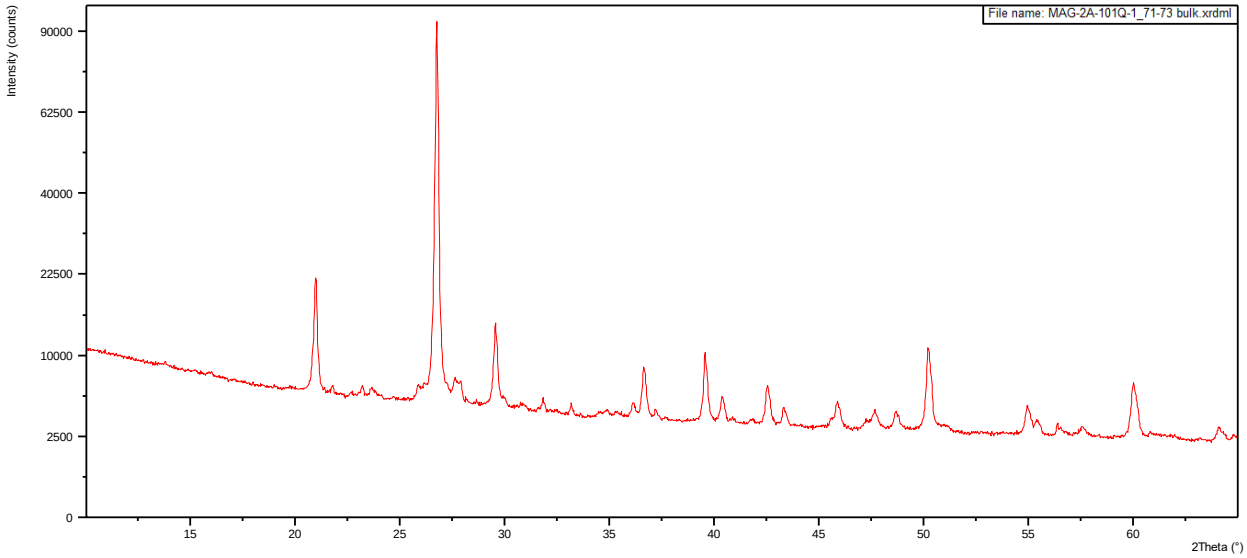
File name: MAG-2A-101Q-1_71-73 bulk.xrdml
Intensity (counts)
90000
62500
40000
22500
10000
2500
0
15
20
25
30
35
40
45
50
55
60
2Theta (°)

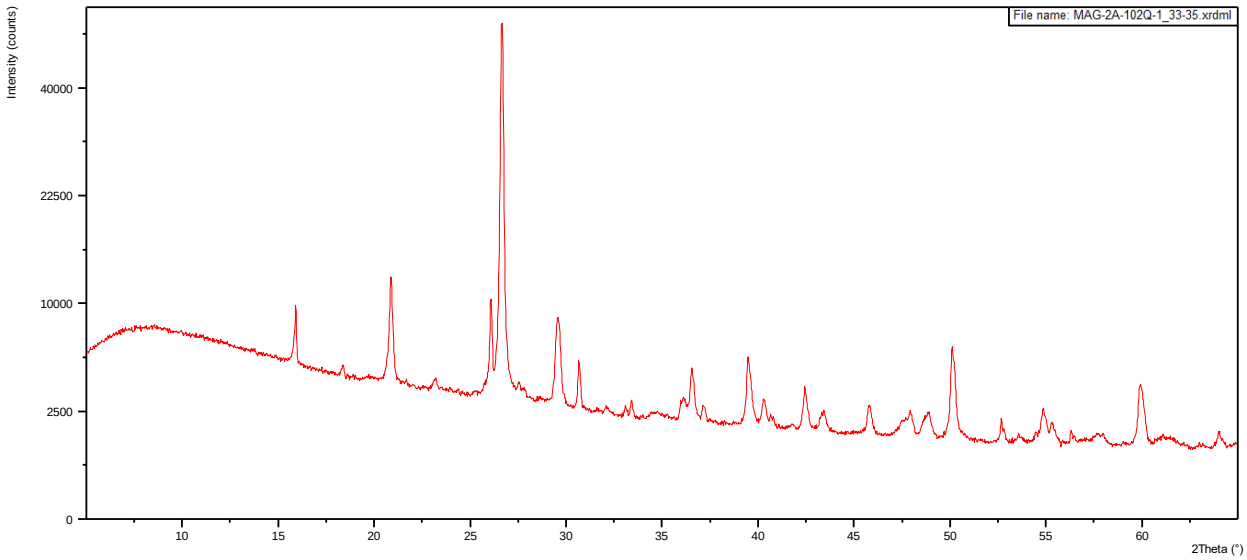
File name: MAG-2A-102Q-1_33-35.xrdml
Intensity (counts)
40000
22500
10000
2500
0
10
15
20
25
30
35
40
45
50
55
60
2Theta (°)

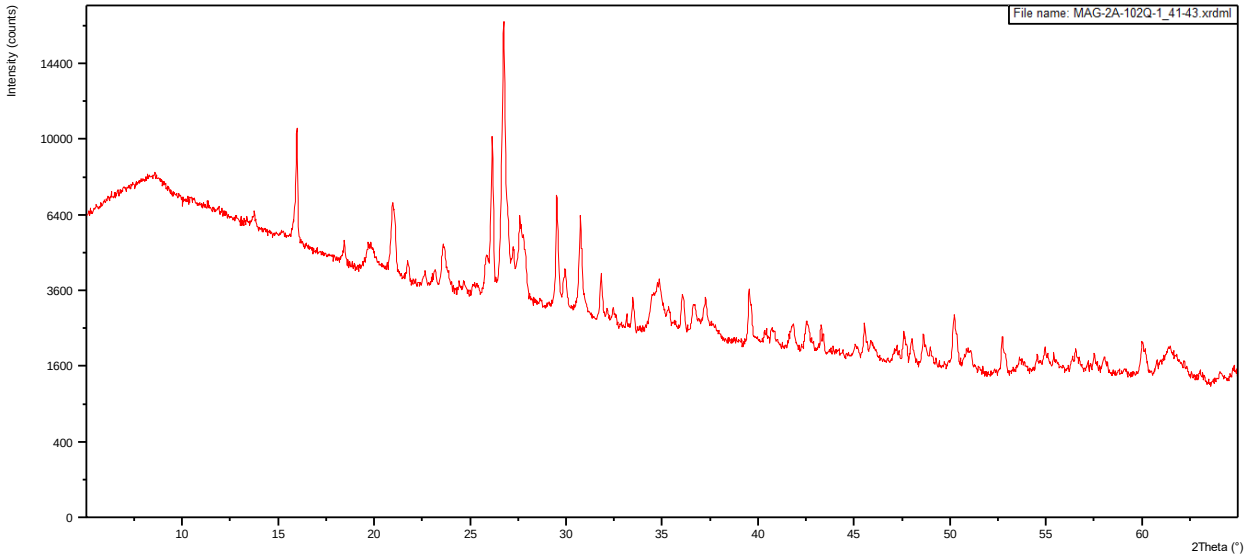
File name: MAG-2A-102Q-1_41-43.xrdml
Intensity (counts)
14400
10000
6400
3600
1600
400
0
10
15
20
25
30
35
40
45
50
55
60
2Theta (°)

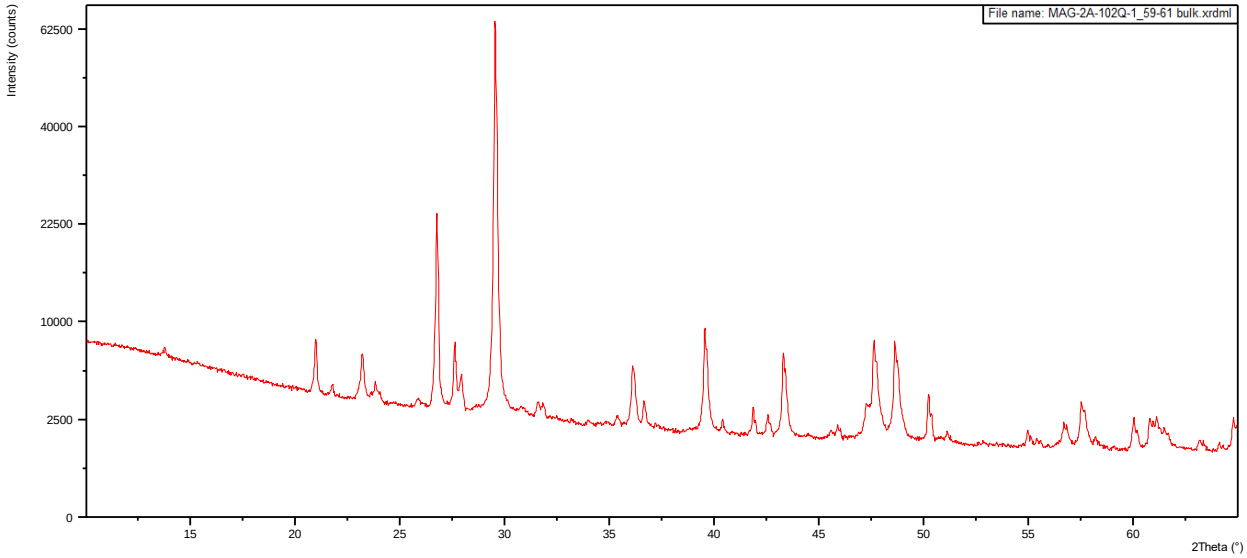

Appendix B.2: Geochemistry Matrix of Intercorrelation - HSPDP-MAG14-2A

	SiO2	Al2O3	Fe2O3	MnO	MgO	CaO	Na2O	K2O	TiO2	P2O5	LOI	S
SiO2	1	-0.003	0.015	-0.067	-0.029	-0.106	-0.84	0.031	0.032	0.035	-0.911	0.011
Al2O3	-0.003	1	0.695	0.68	0.186	0.056	-0.317	0.877	0.793	0.053	-0.378	0.283
Fe2O3	0.015	0.695	1	0.654	0.12	-0.014	-0.304	0.631	0.523	0.01	-0.326	0.835
MnO	-0.067	0.68	0.654	1	0.232	0.364	-0.315	0.644	0.581	0.062	-0.249	0.456
MgO	-0.029	0.186	0.12	0.232	1	0.289	-0.306	0.335	0.515	0.056	-0.077	-0.039
CaO	-0.106	0.056	-0.014	0.364	0.289	1	-0.276	0.109	0.15	0.219	-0.017	-0.027
Na2O	-0.84	-0.317	-0.304	-0.315	-0.306	-0.276	1	-0.375	-0.404	-0.122	0.921	-0.178
K2O	0.031	0.877	0.631	0.644	0.335	0.109	-0.375	1	0.759	0.06	-0.393	0.281
TiO2	0.032	0.793	0.523	0.581	0.515	0.15	-0.404	0.759	1	0.128	-0.333	0.104
P2O5	0.035	0.053	0.01	0.062	0.056	0.219	-0.122	0.06	0.128	1	-0.081	-0.007
LOI	-0.911	-0.378	-0.326	-0.249	-0.077	-0.017	0.921	-0.393	-0.333	-0.081	1	-0.181
S	0.011	0.283	0.835	0.456	-0.039	-0.027	-0.178	0.281	0.104	-0.007	-0.181	1

Appendix C: ODP-OLO12-1A - Olorgesailie-Koora Graben

Appendix C.1: X-ray Diffraction Patterns

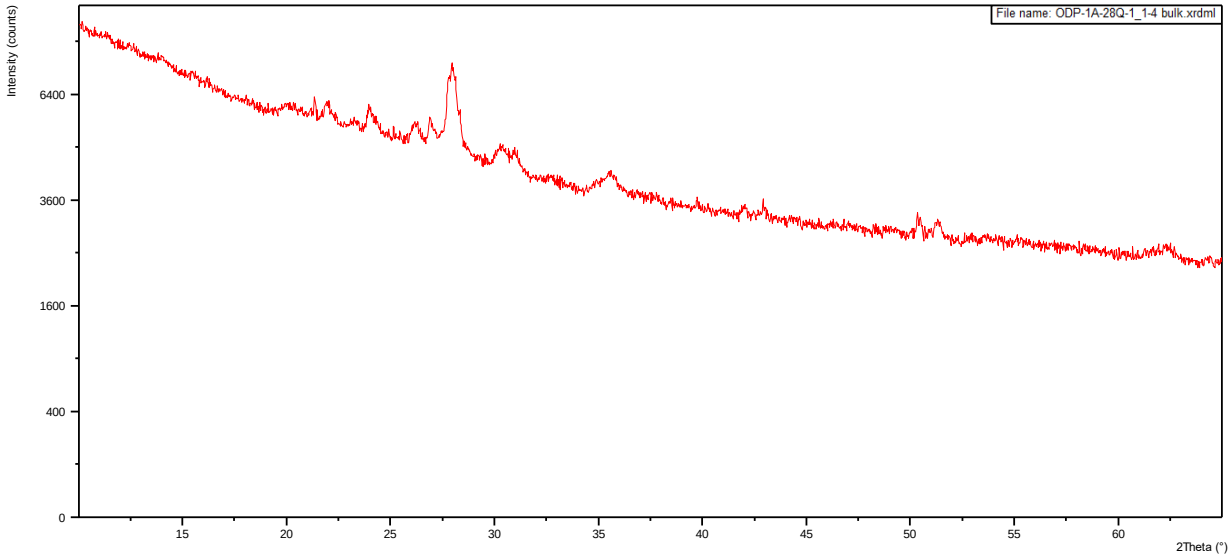

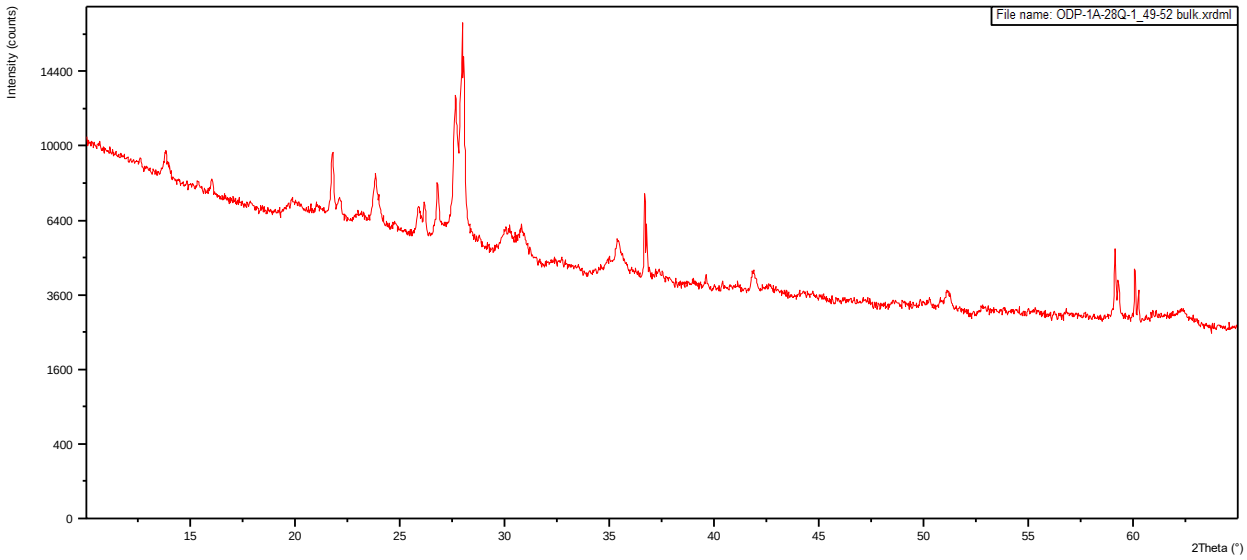

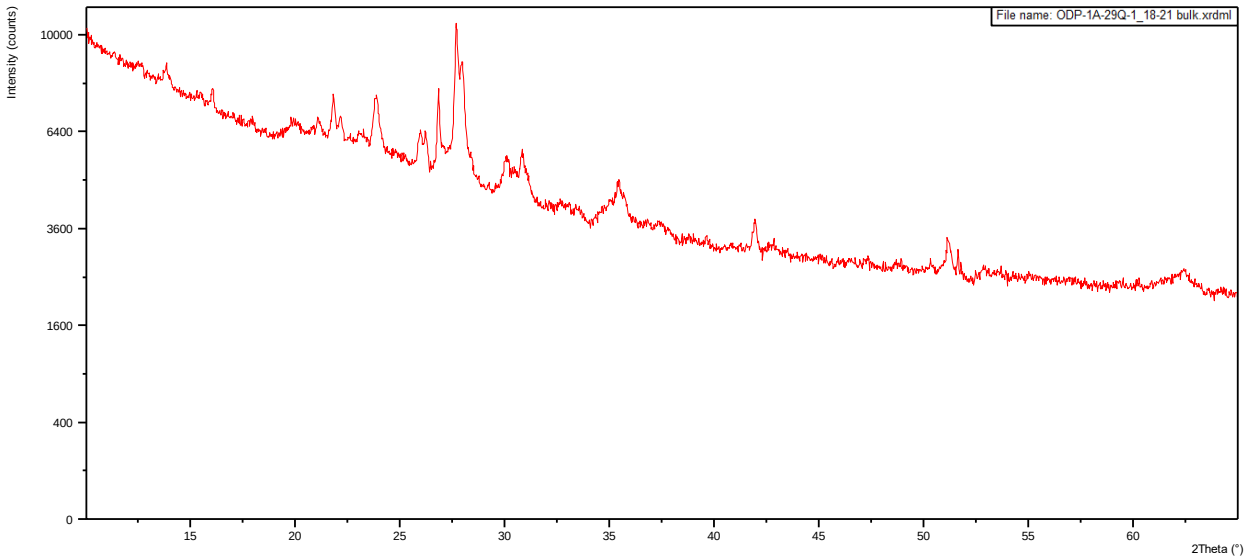
File name: ODP-1A-29Q-1_18-21 bulk.xrdml
Intensity (counts)
10000
6400
3600
1600
400
0
15
20
25
30
35
40
45
50
55
60
2Theta (°)

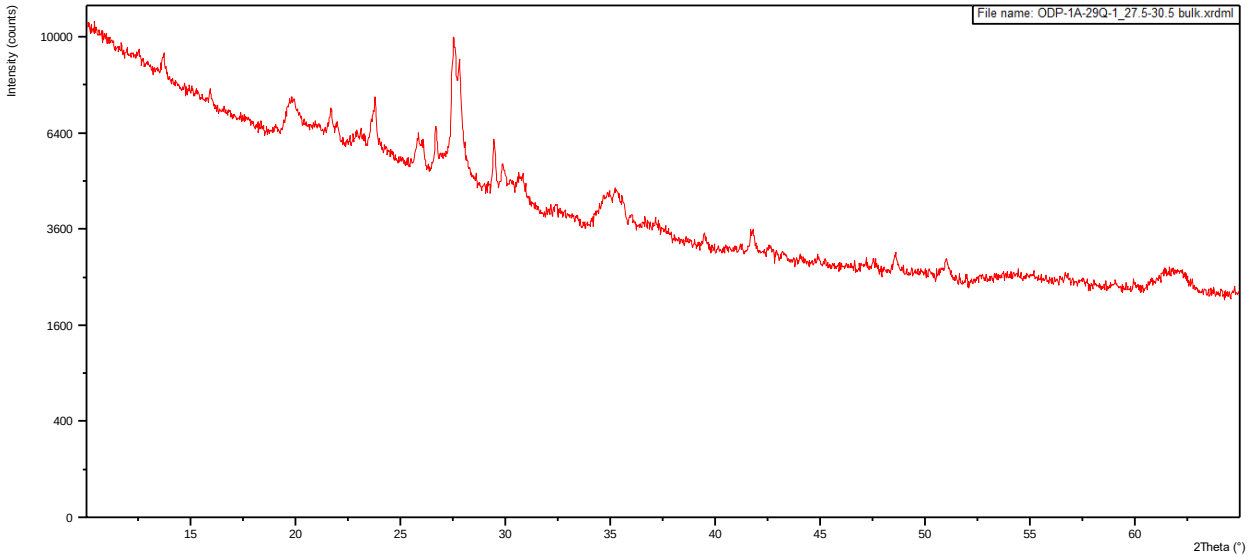
File name: ODP-1A-29Q-1_27.5-30.5 bulk.xrdml
Intensity (counts)
10000
6400
3600
1600
400
0
15
20
25
30
35
40
45
50
55
60
2Theta (°)

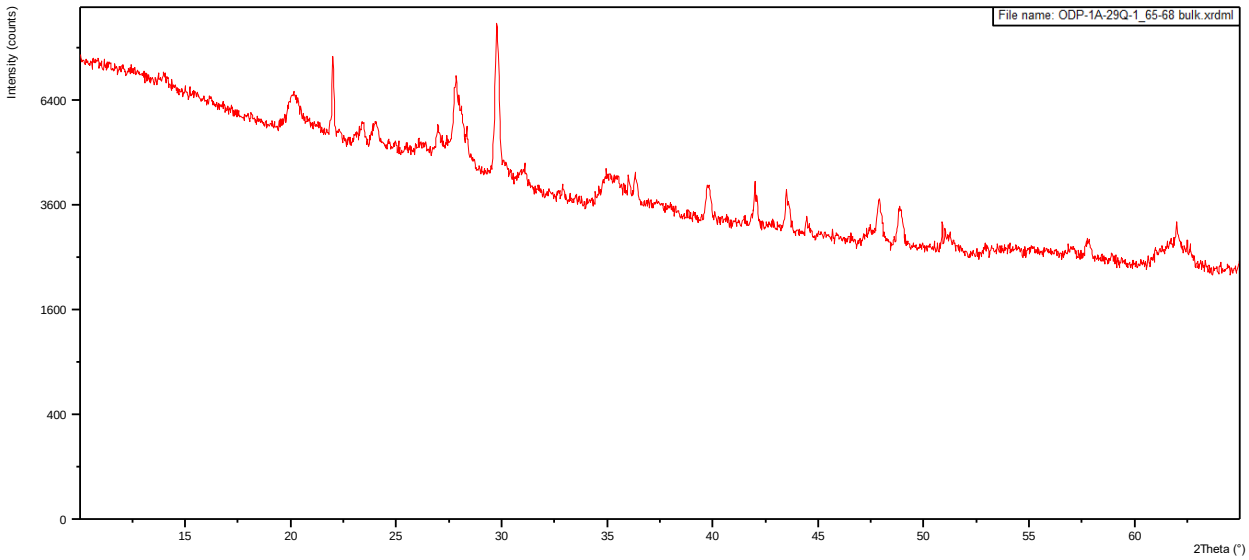
File name: ODP-1A-29Q-1_65-68 bulk.xrdml
Intensity (counts)
6400
3600
1600
400
0
15
20
25
30
35
40
45
50
55
60
2Theta (°)

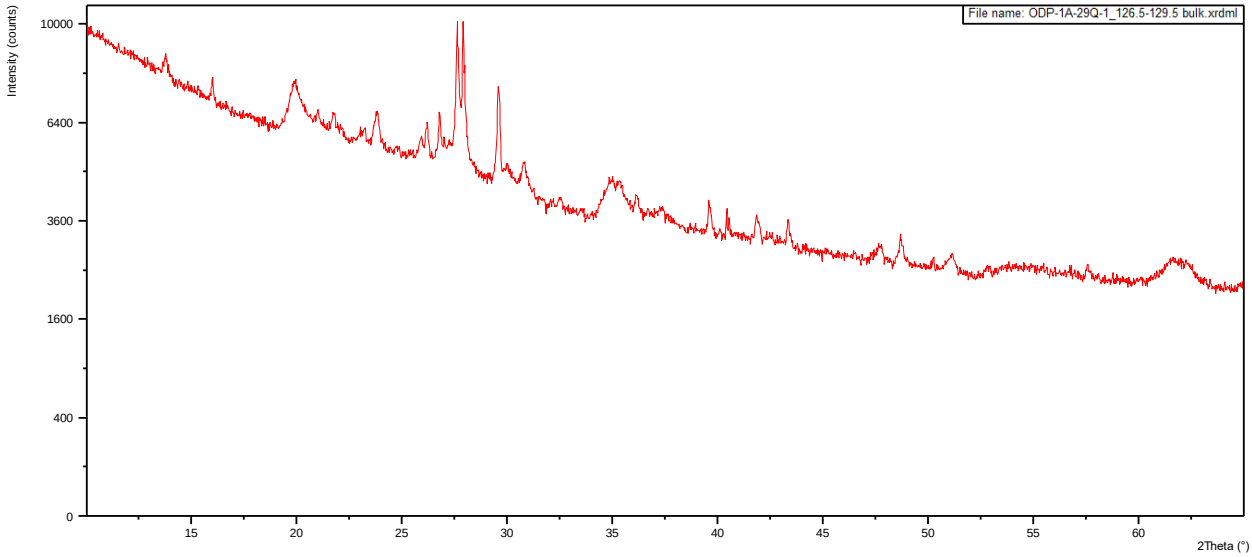
File name: ODP-1A-29Q-1_126.5-129.5 bulk.xrdml
Intensity (counts)
10000
6400
3600
1600
400
0
15
20
25
30
35
40
45
50
55
60
2Theta (°)

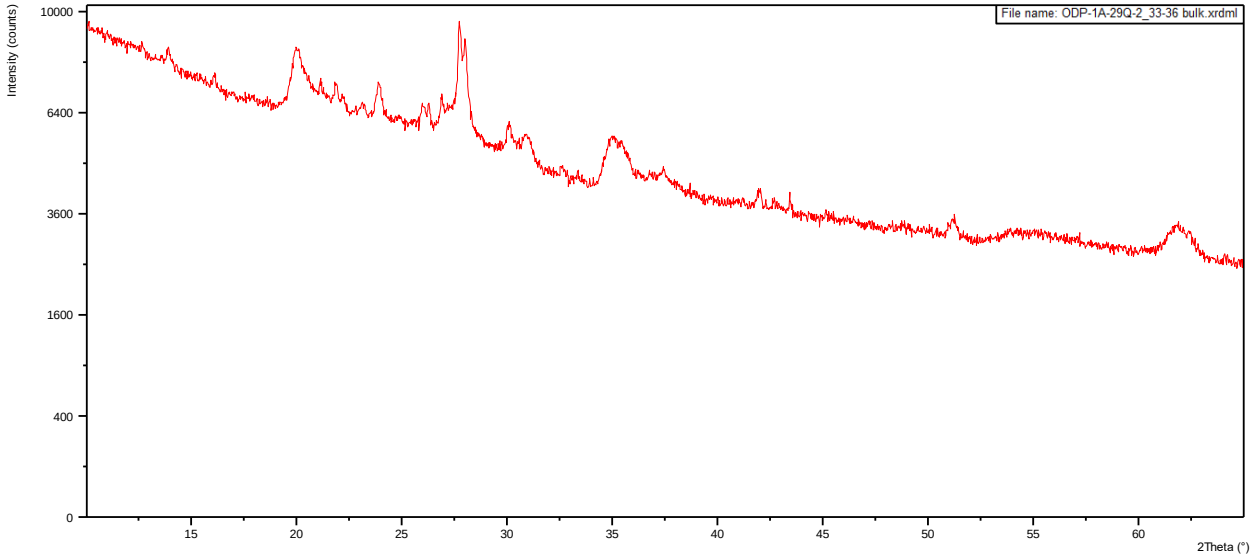
File name: ODP-1A-29Q-2_33-36 bulk.xrdml
Intensity (counts)
10000
6400
3600
1600
400
0
15
20
25
30
35
40
45
50
55
60
2Theta (°)

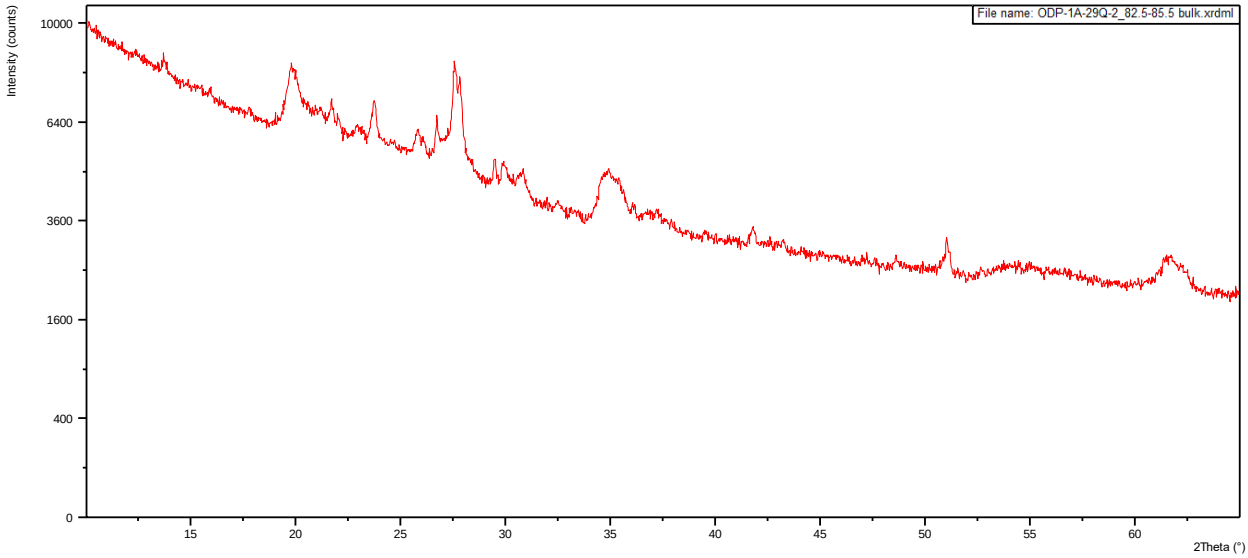
File name: ODP-1A-29Q-2_82.5-85.5 bulk.xrdml
Intensity (counts)
10000
6400
3600
1600
400
0
15
20
25
30
35
40
45
50
55
60
2Theta (°)

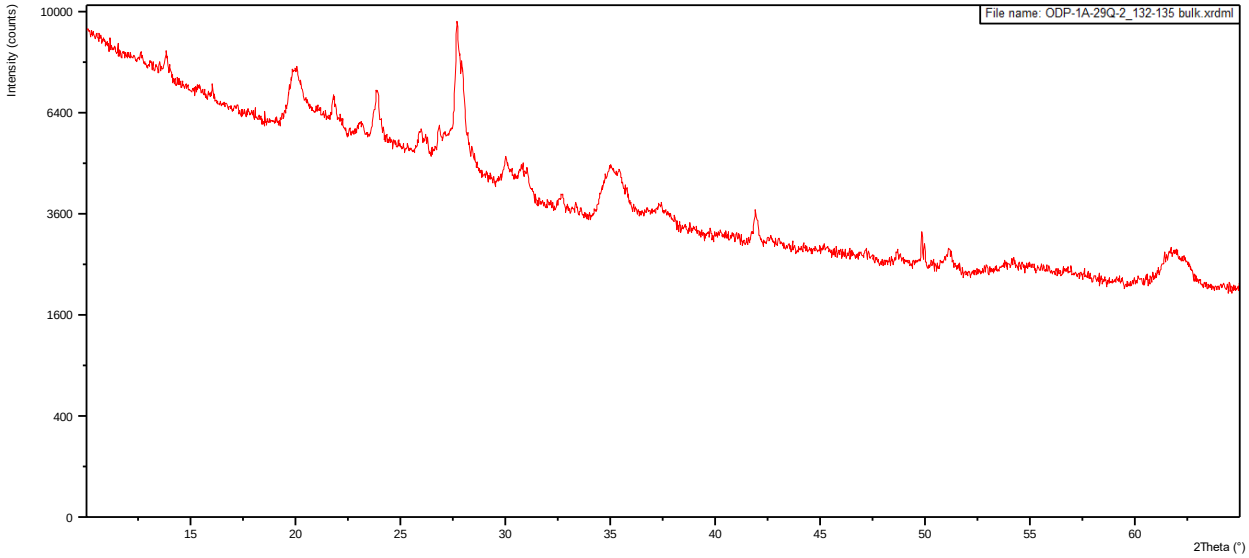
File name: ODP-1A-29Q-2_132-135 bulk.xrdml
Intensity (counts)
10000
6400
3600
1600
400
0
15
20
25
30
35
40
45
50
55
60
2Theta (°)

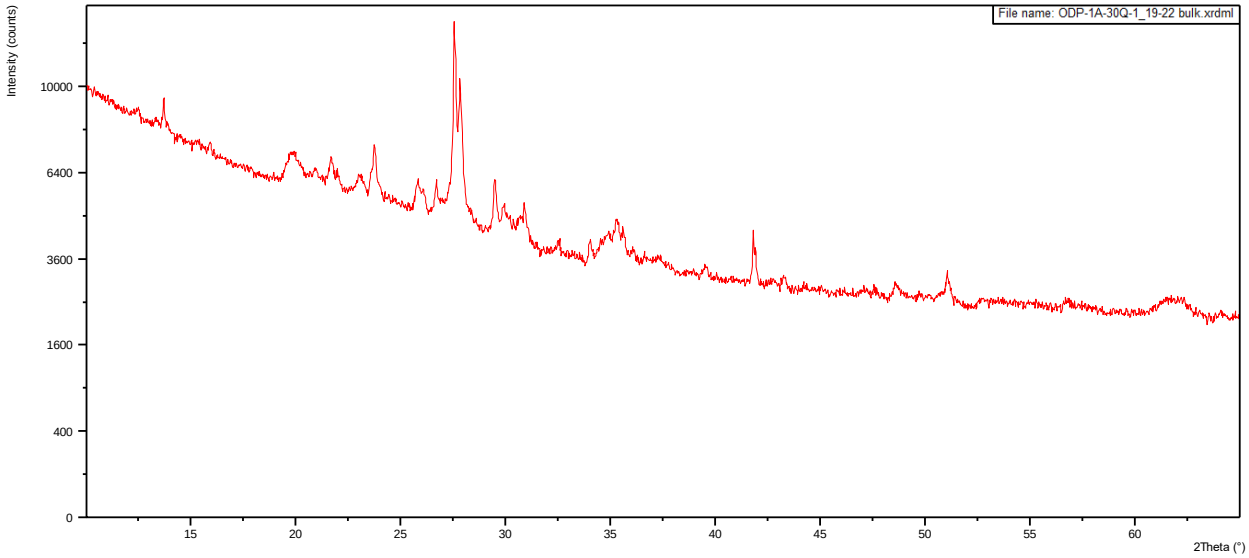
File name: ODP-1A-30Q-1_19-22 bulk.xrdml
Intensity (counts)
10000
6400
3600
1600
400
0
15
20
25
30
35
40
45
50
55
60
2Theta (°)

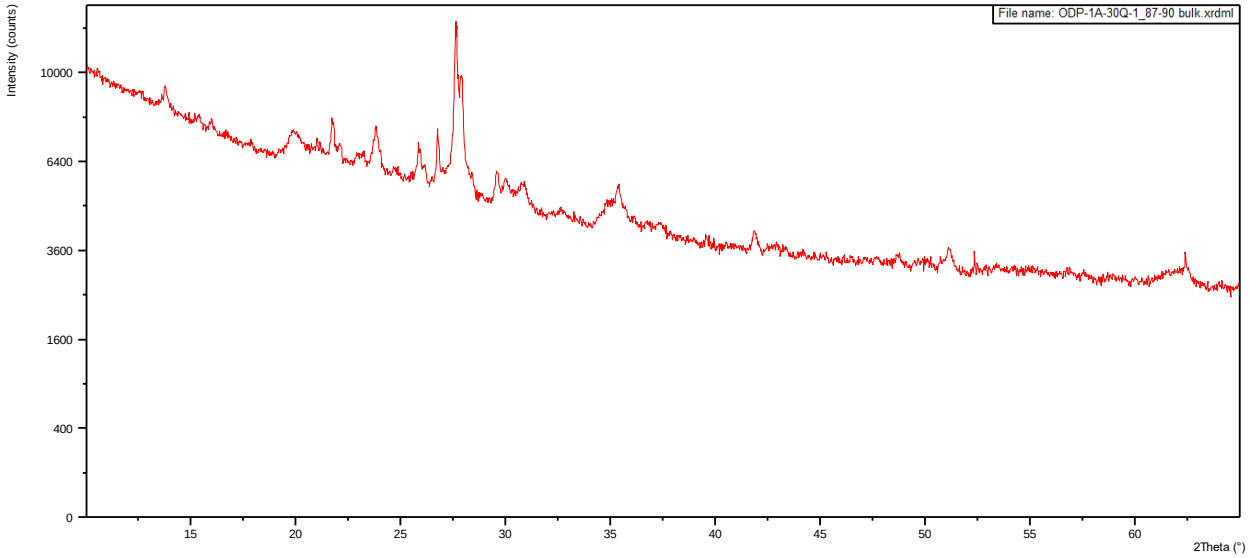
File name: ODP-1A-30Q-1_87-90 bulk.xrdml
Intensity (counts)
10000
6400
3600
1600
400
0
15
20
25
30
35
40
45
50
55
60
2Theta (°)

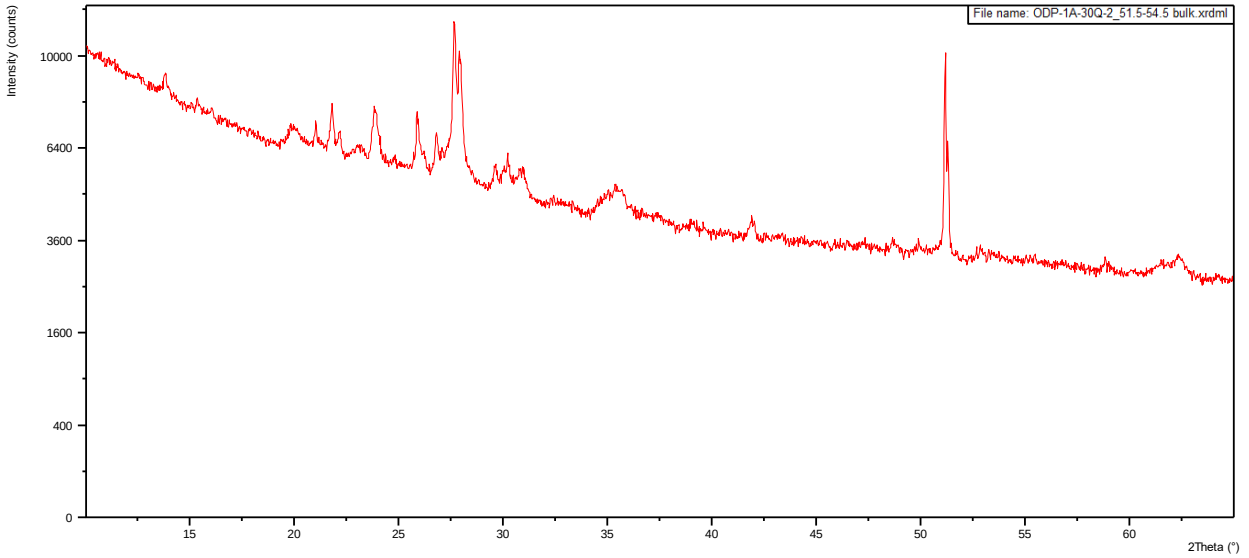
File name: ODP-1A-30Q-2_51.5-54.5 bulk.xrdml
Intensity (counts)
10000
6400
3600
1600
400
0
15
20
25
30
35
40
45
50
55
60
2Theta (°)

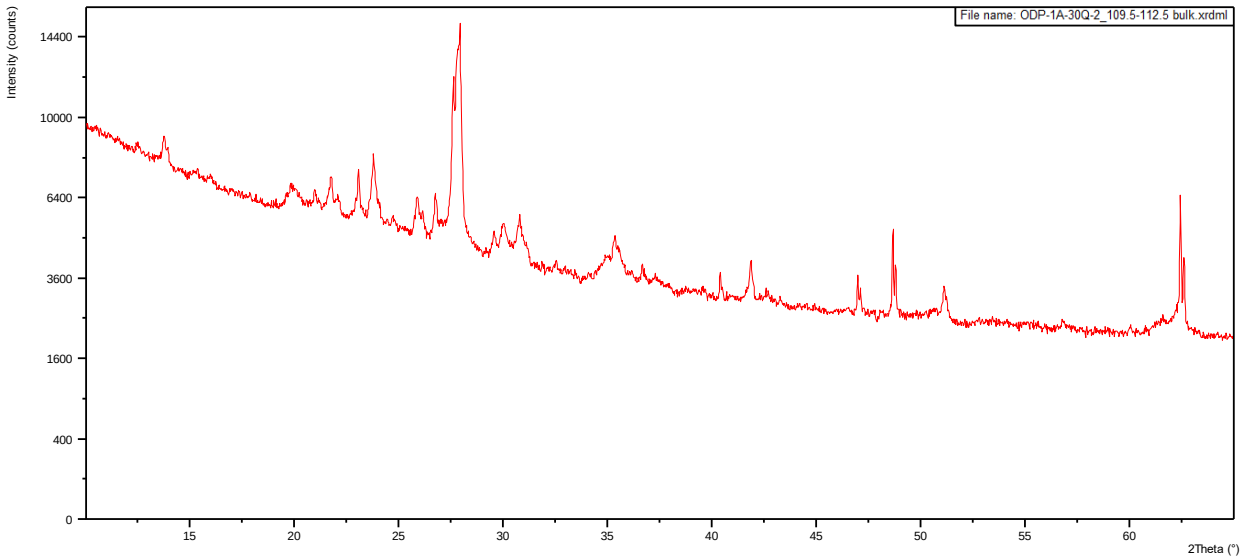
File name: ODP-1A-30Q-2_109.5-112.5 bulk.xrdml
Intensity (counts)
14400
10000
6400
3600
1600
400
0
15
20
25
30
35
40
45
50
55
60
2Theta (°)

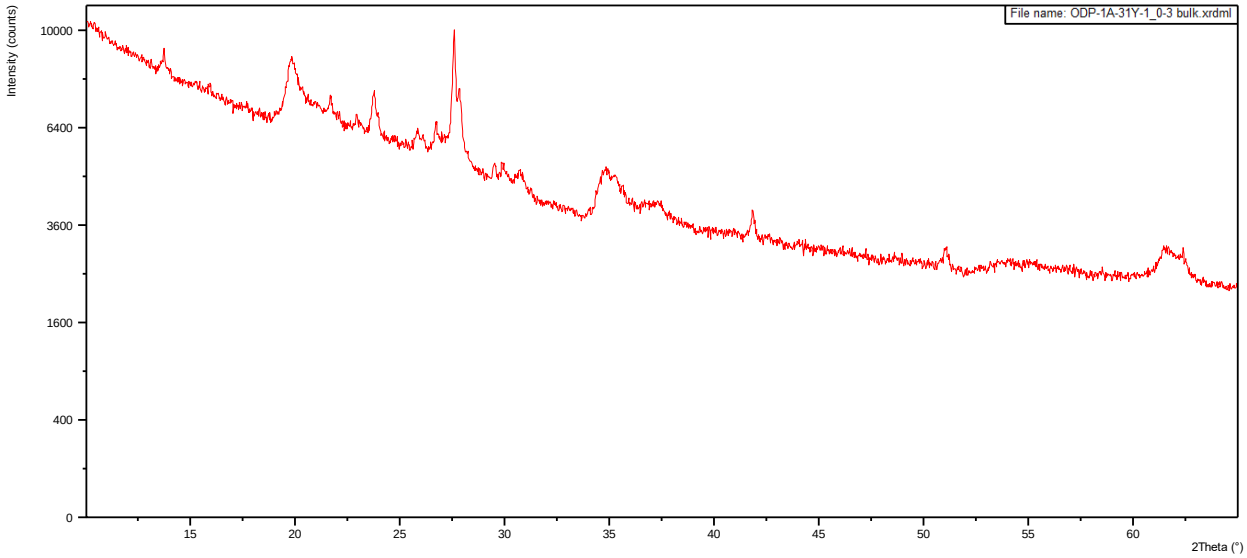
File name: ODP-1A-31Y-1_0-3 bulk.xrdml
Intensity (counts)
10000
6400
3600
1600
400
0
15
20
25
30
35
40
45
50
55
60
2Theta (°)

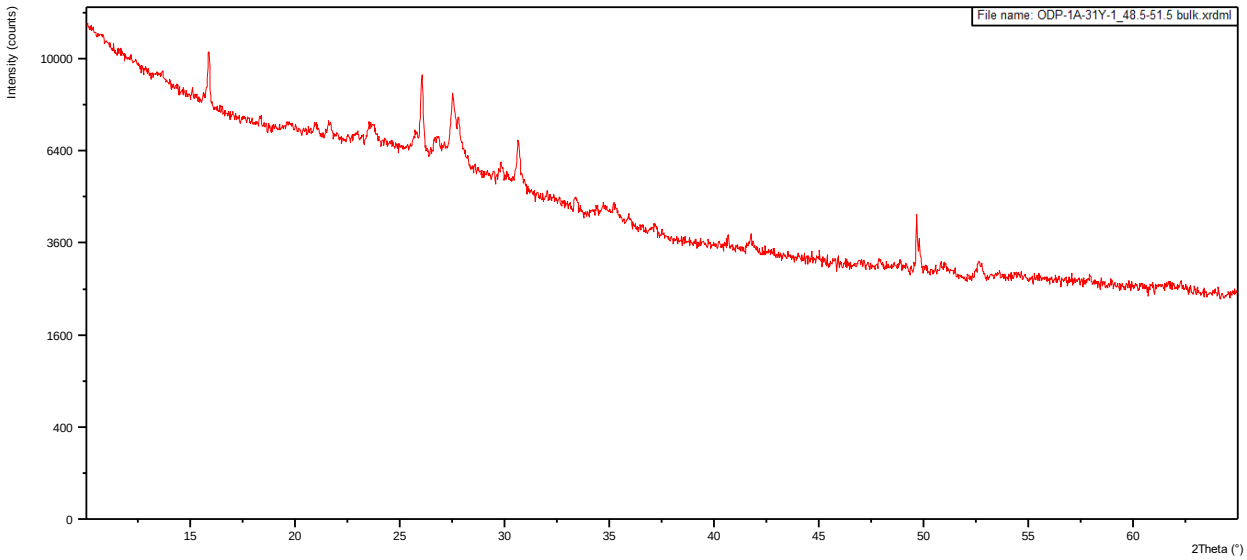
File name: ODP-1A-31Y-1_48.5-51.5 bulk.xrdml
Intensity (counts)
10000
6400
3600
1600
400
0
15
20
25
30
35
40
45
50
55
60
2Theta (°)

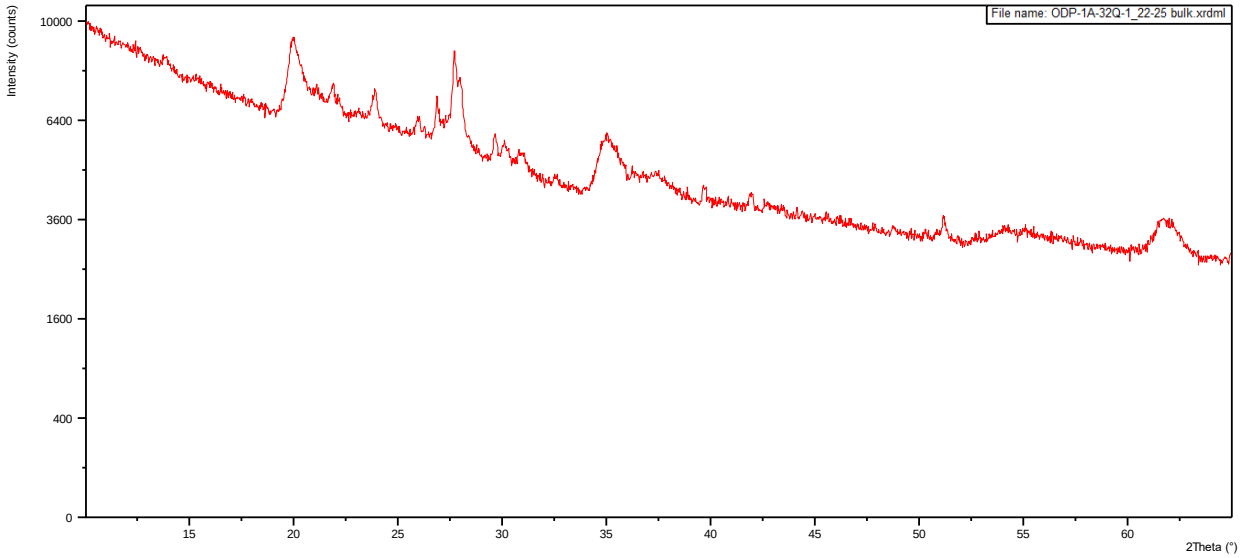
File name: ODP-1A-32Q-1_22-25 bulk.xrdml
Intensity (counts)
10000
6400
3600
1600
400
0
15
20
25
30
35
40
45
50
55
60
2Theta (°)

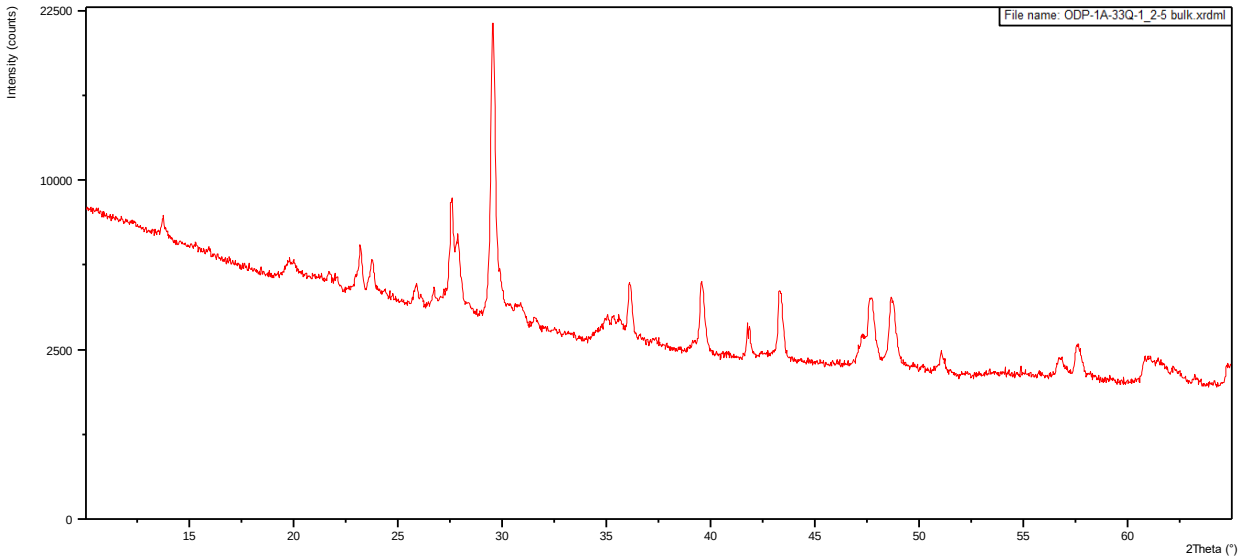
File name: ODP-1A-33Q-1_2-5 bulk.xrdml
Intensity (counts)
22500
10000
2500
0
15
20
25
30
35
40
45
50
55
60
2Theta (°)

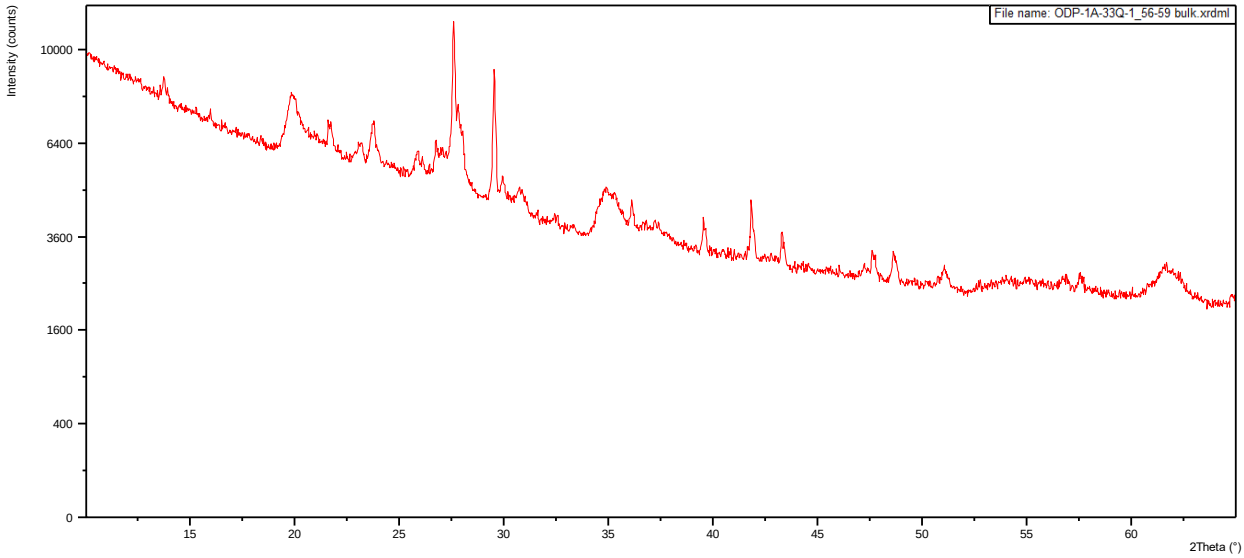
File name: ODP-1A-33Q-1_56-59 bulk.xrdml
Intensity (counts)
10000
6400
3600
1600
400
0
15
20
25
30
35
40
45
50
55
60
2Theta (°)

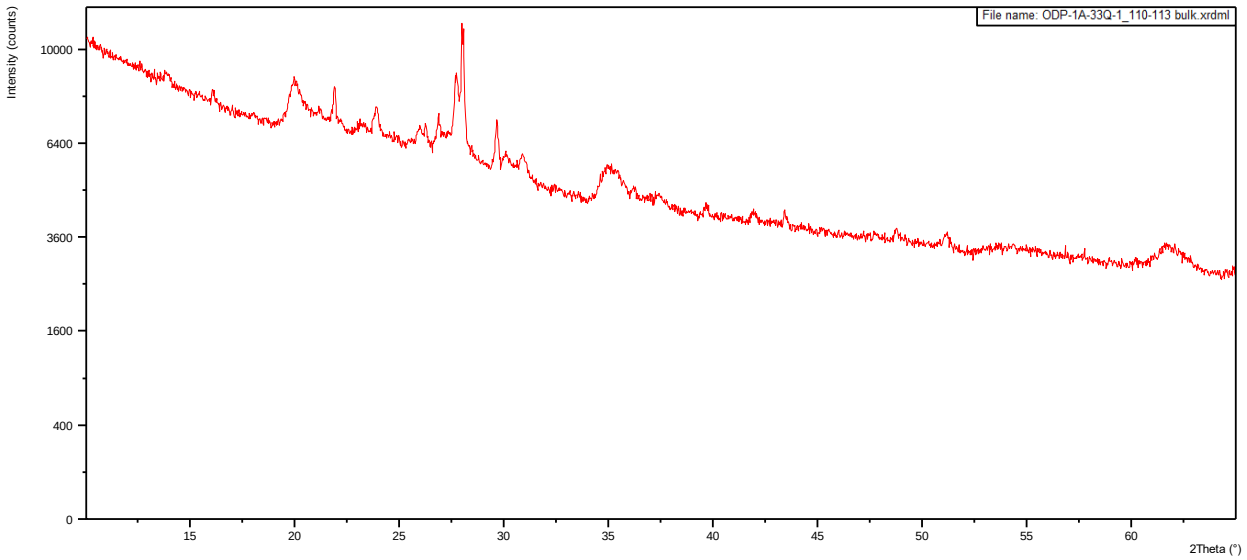
File name: ODP-1A-33Q-1_110-113 bulk.xrdml
Intensity (counts)
10000
6400
3600
1600
400
0
15
20
25
30
35
40
45
50
55
60
2Theta (°)

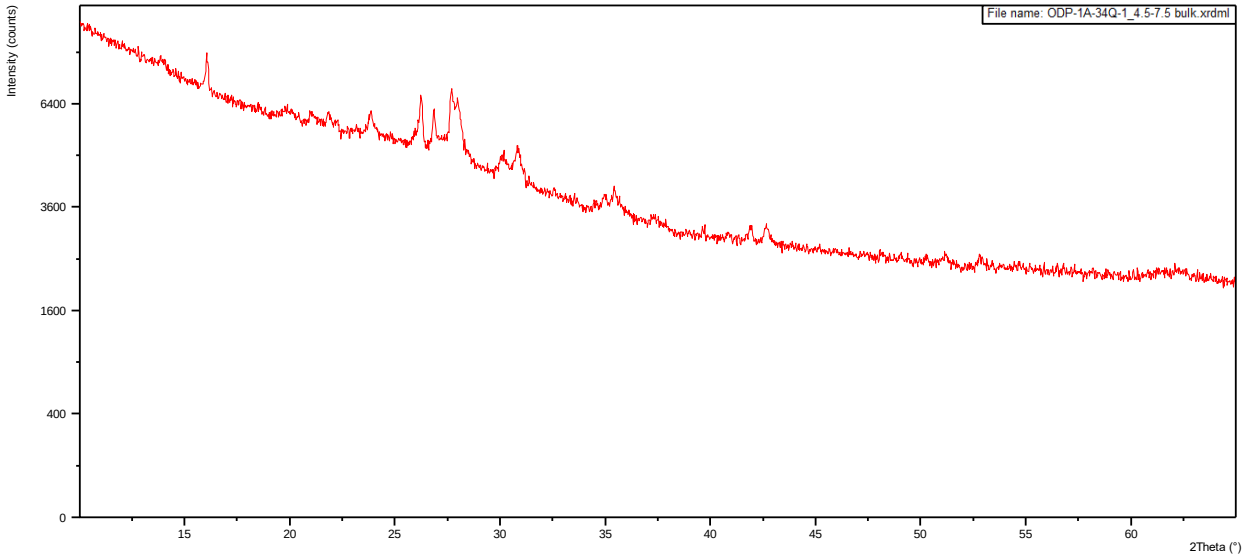
File name: ODP-1A-34Q-1_4.5-7.5 bulk.xrdml
Intensity (counts)
6400
3600
1600
400
0
15
20
25
30
35
40
45
50
55
60
2Theta (°)

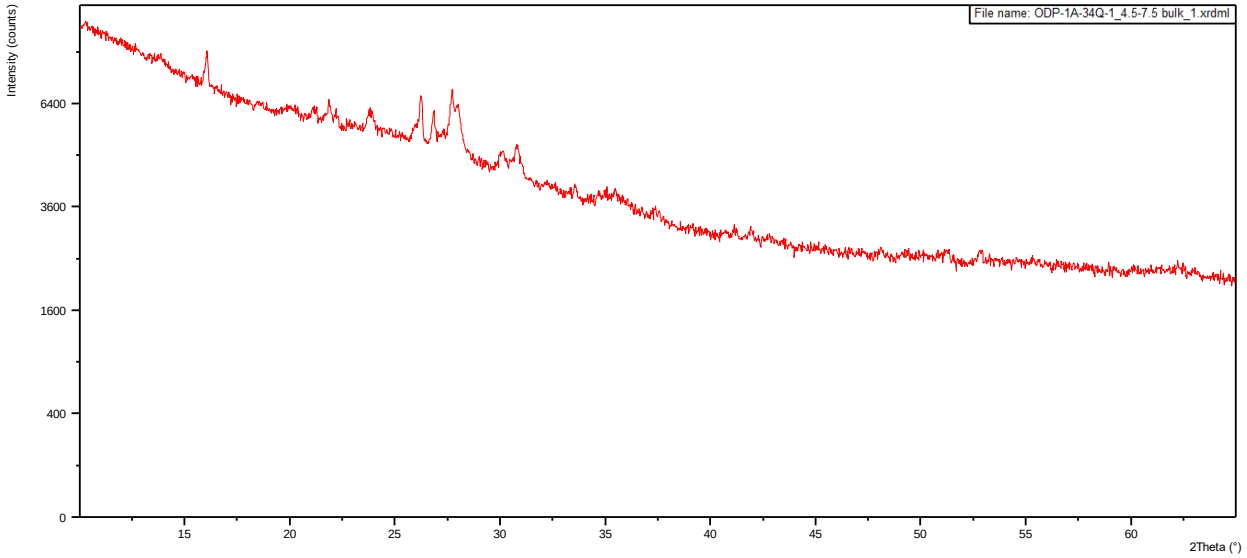
File name: ODP-1A-34Q-1_4.5-7.5 bulk_1.xrdml
Intensity (counts)
6400
3600
1600
400
0
15
20
25
30
35
40
45
50
55
60
2Theta (°)

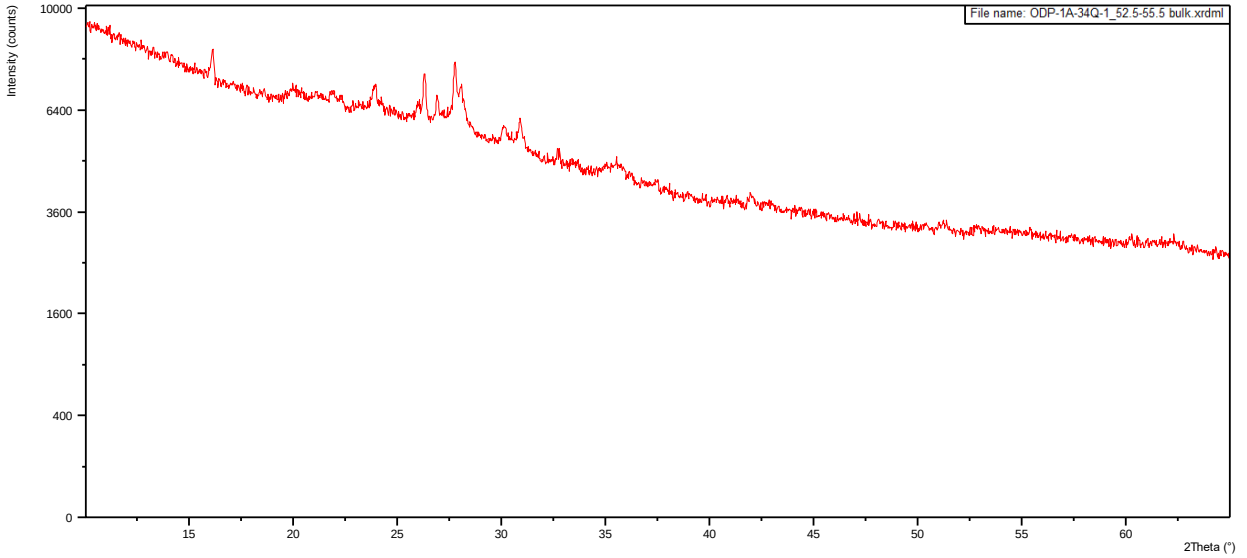
File name: ODP-1A-34Q-1_52.5-55.5 bulk.xrdml
Intensity (counts)
10000
6400
3600
1600
400
0
15
20
25
30
35
40
45
50
55
60
2Theta (°)

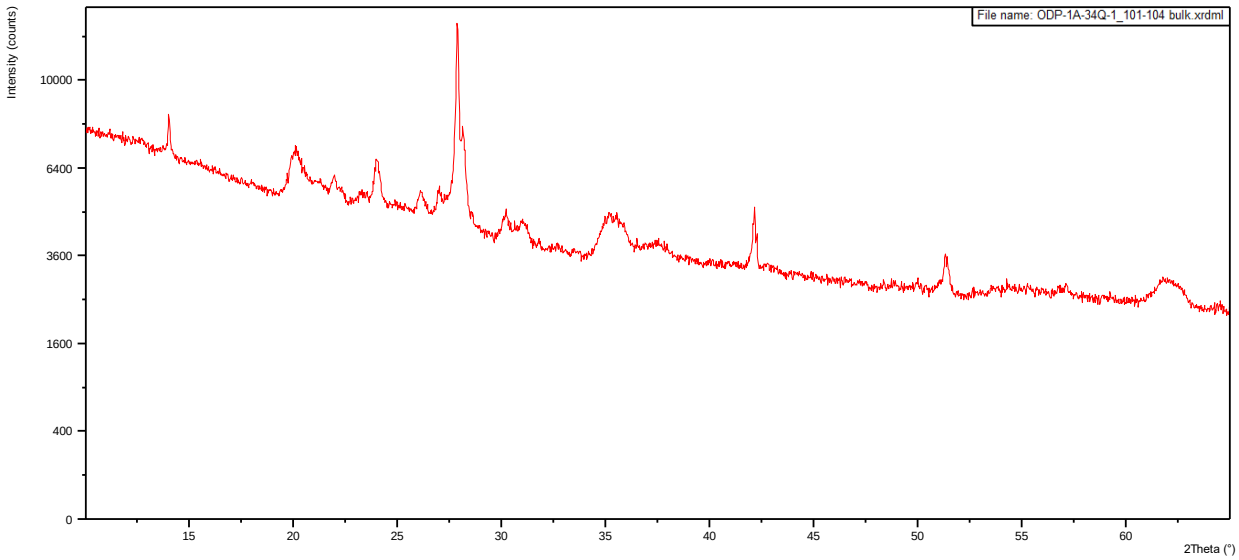
File name: ODP-1A-34Q-1_101-104 bulk.xrdml
Intensity (counts)
10000
6400
3600
1600
400
0
15
20
25
30
35
40
45
50
55
60
2Theta (°)

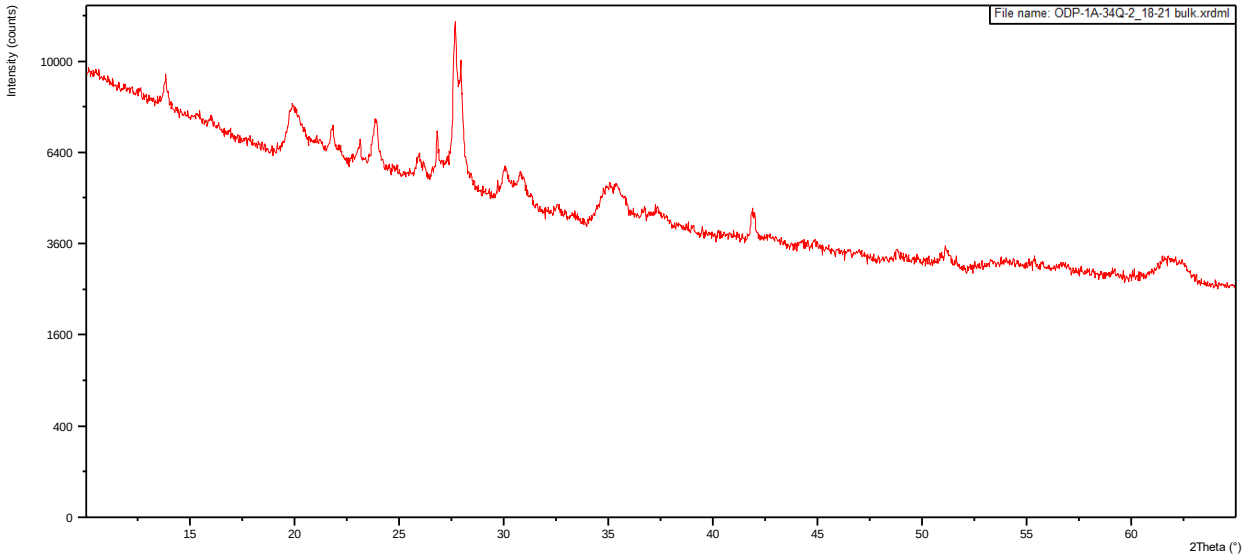
File name: ODP-1A-34Q-2_18-21 bulk.xrdml
Intensity (counts)
10000
6400
3600
1600
400
0
15
20
25
30
35
40
45
50
55
60
2Theta (°)

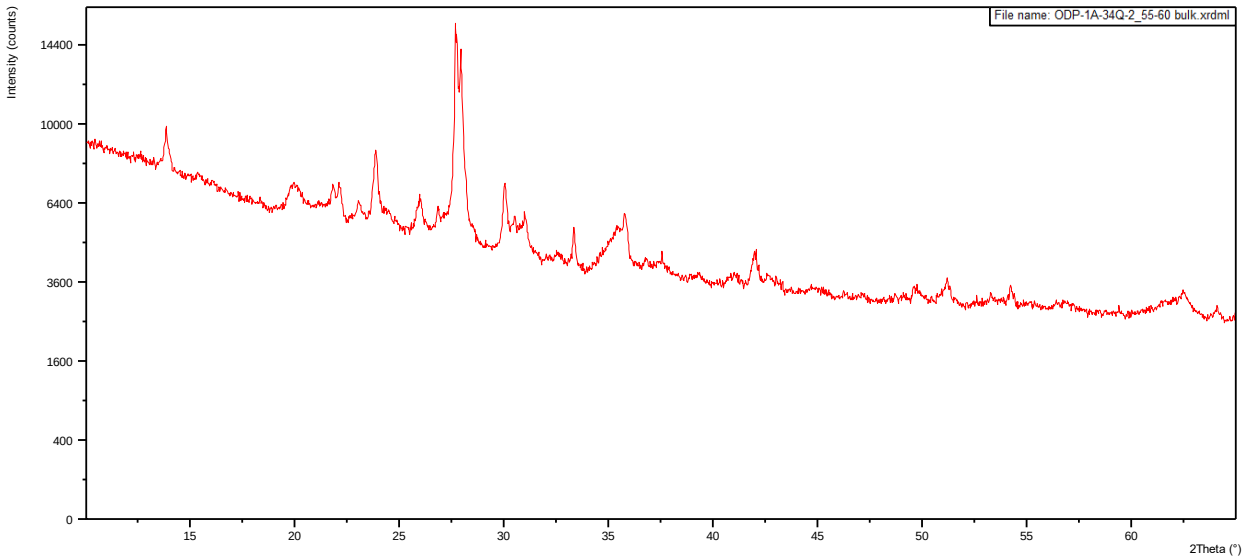
File name: ODP-1A-34Q-2_55-60 bulk.xrdml
Intensity (counts)
14400
10000
6400
3600
1600
400
0
15
20
25
30
35
40
45
50
55
60
2Theta (°)

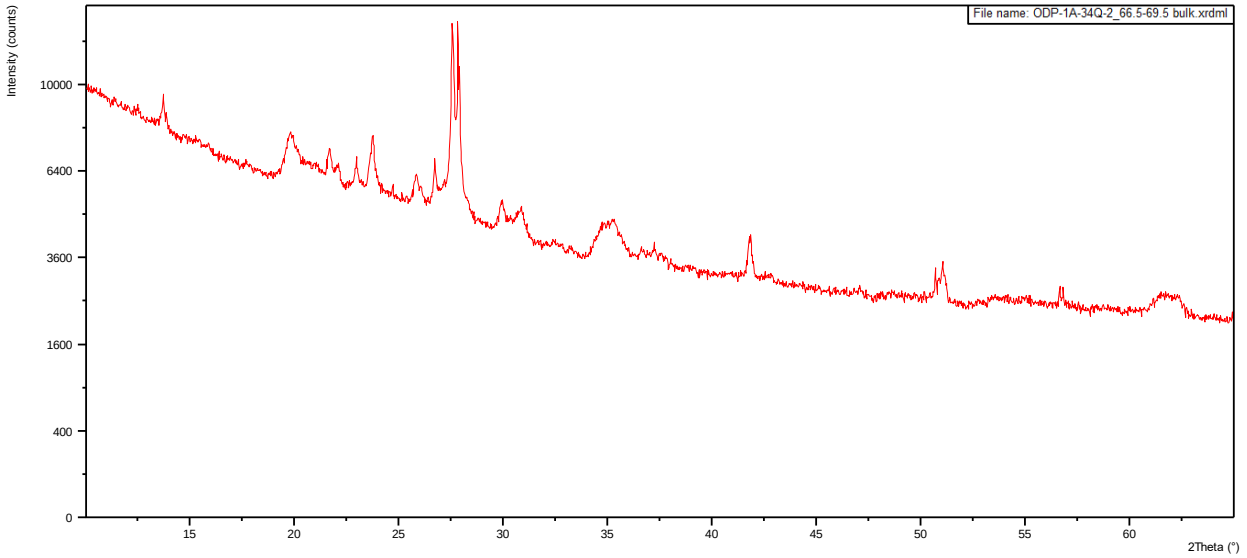
File name: ODP-1A-34Q-2_66.5-69.5 bulk.xrdml
Intensity (counts)
10000
6400
3600
1600
400
0
15
20
25
30
35
40
45
50
55
60
2Theta (°)

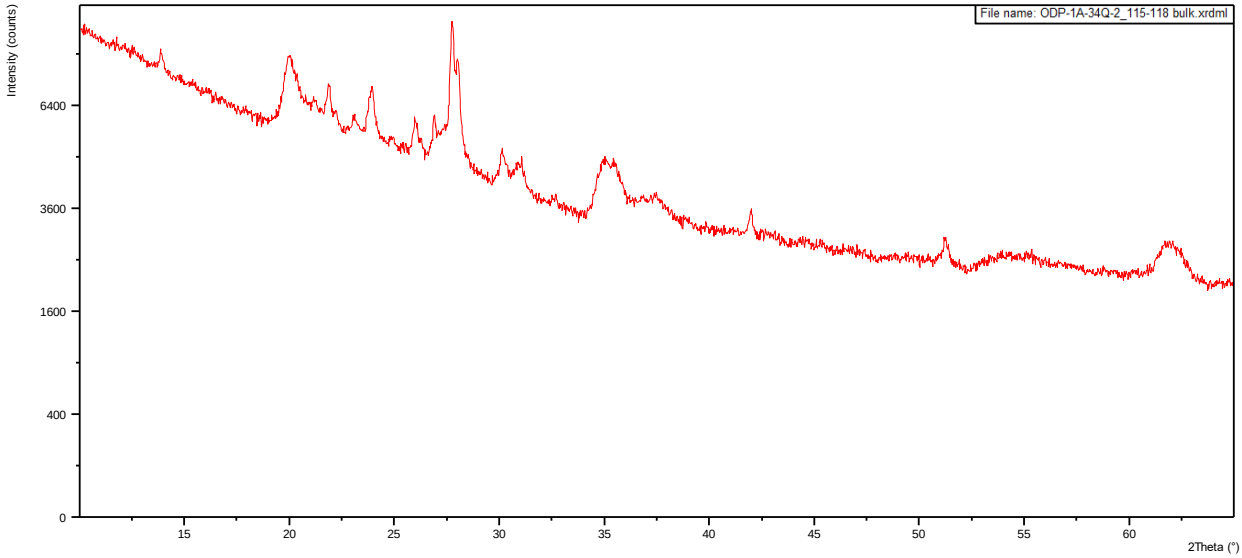
File name: ODP-1A-34Q-2_115-118 bulk.xrdml
Intensity (counts)
6400
3600
1600
400
0
15
20
25
30
35
40
45
50
55
60
2Theta (°)

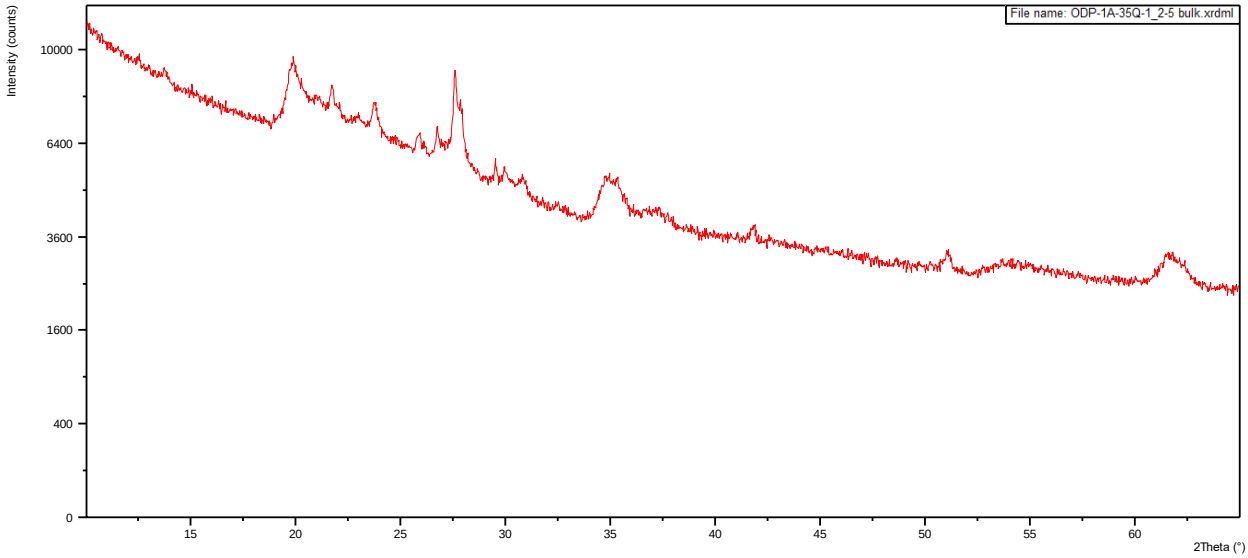
File name: ODP-1A-35Q-1_2-5 bulk.xrdml
Intensity (counts)
10000
6400
3600
1600
400
0
15
20
25
30
35
40
45
50
55
60
2Theta (°)

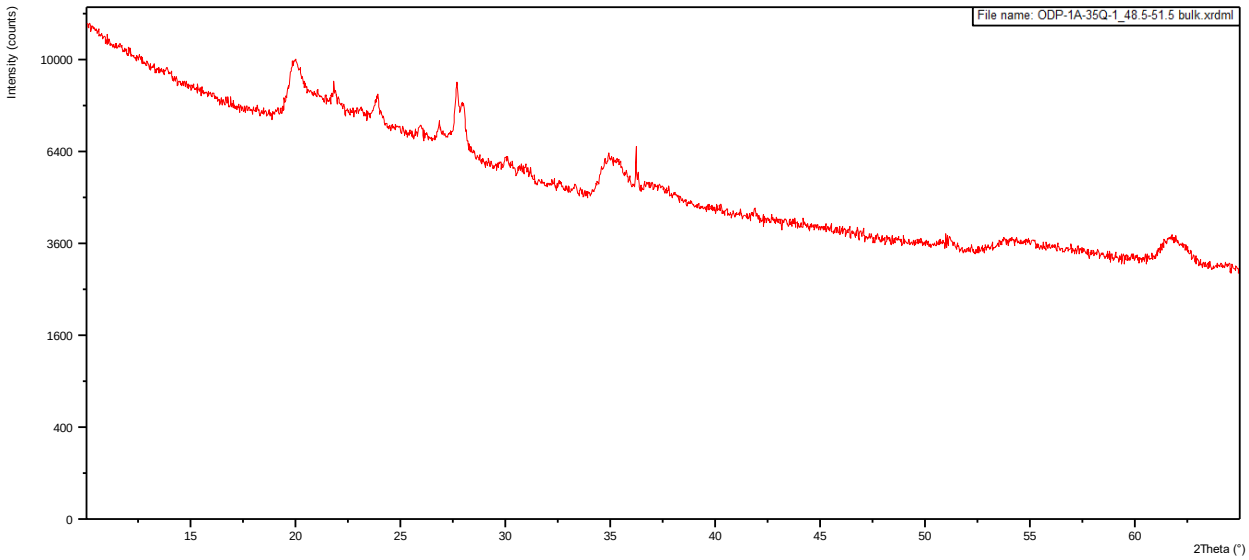
File name: ODP-1A-35Q-1_48.5-51.5 bulk.xrdml
Intensity (counts)
10000
6400
3600
1600
400
0
15
20
25
30
35
40
45
50
55
60
2Theta (°)

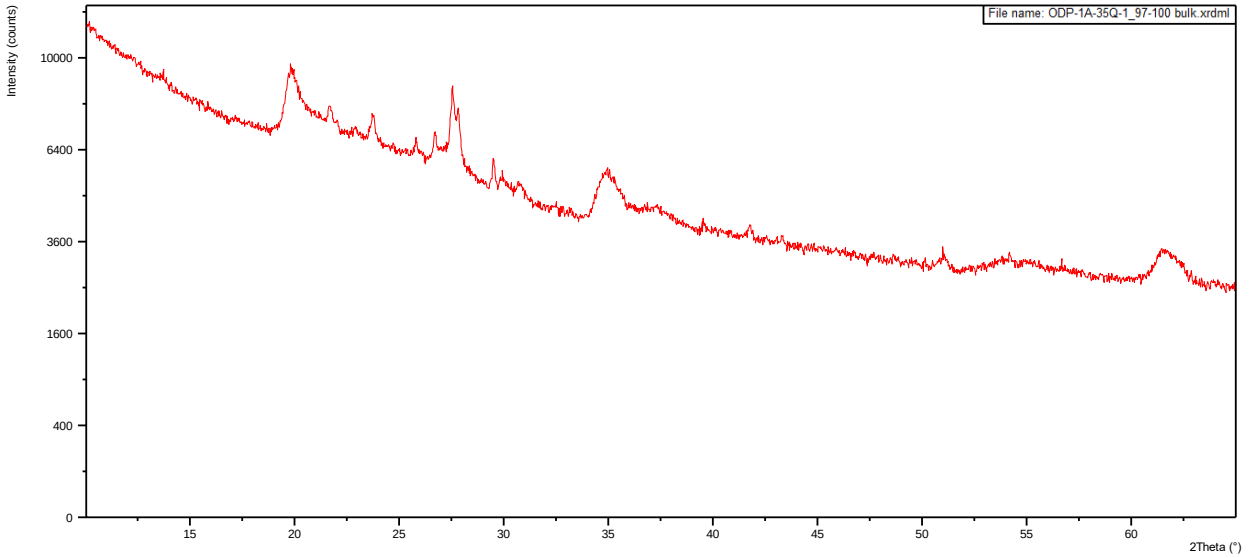
File name: ODP-1A-35Q-1_97-100 bulk.xrdml
Intensity (counts)
10000
6400
3600
1600
400
0
15
20
25
30
35
40
45
50
55
60
2Theta (°)

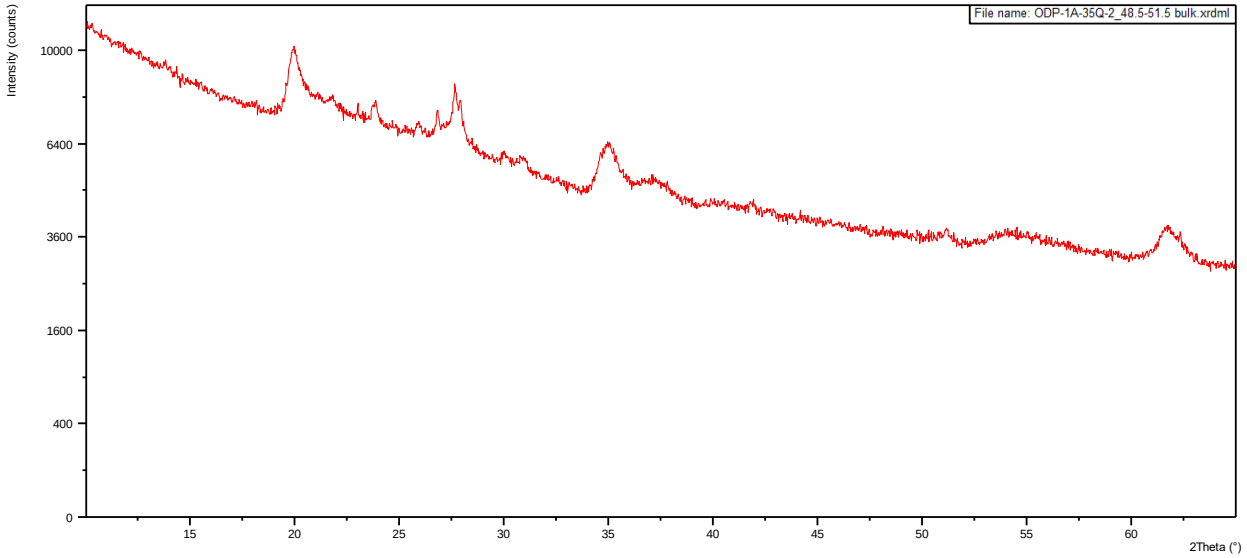
File name: ODP-1A-35Q-2_48.5-51.5 bulk.xrdml
Intensity (counts)
10000
6400
3600
1600
400
0
15
20
25
30
35
40
45
50
55
60
2Theta (°)

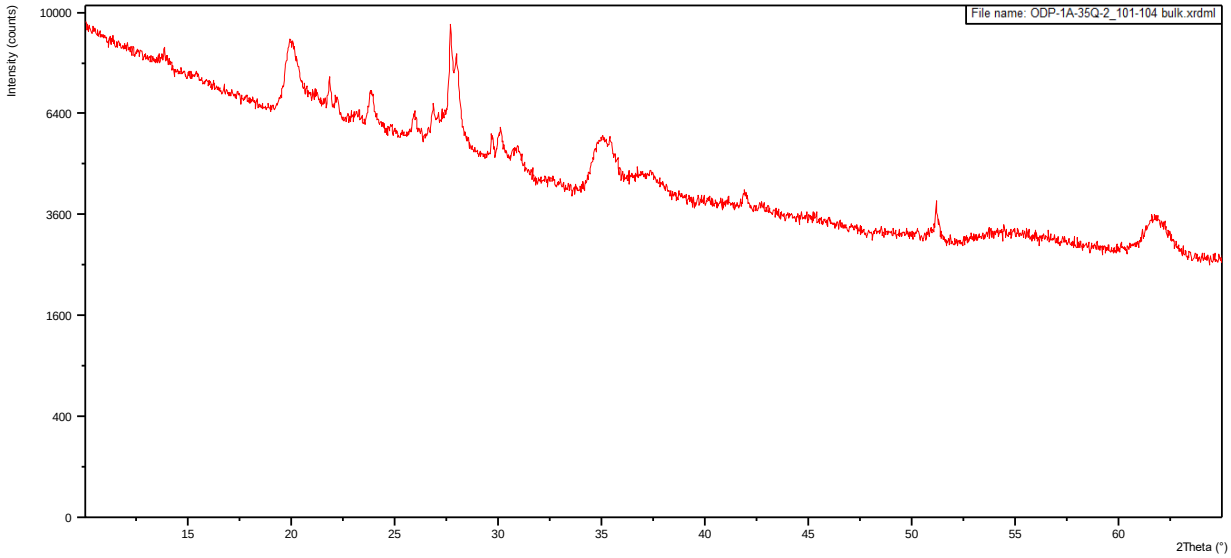
File name: ODP-1A-35Q-2_101-104 bulk.xrdml
Intensity (counts)
10000
6400
3600
1600
400
0
15
20
25
30
35
40
45
50
55
60
2Theta (°)

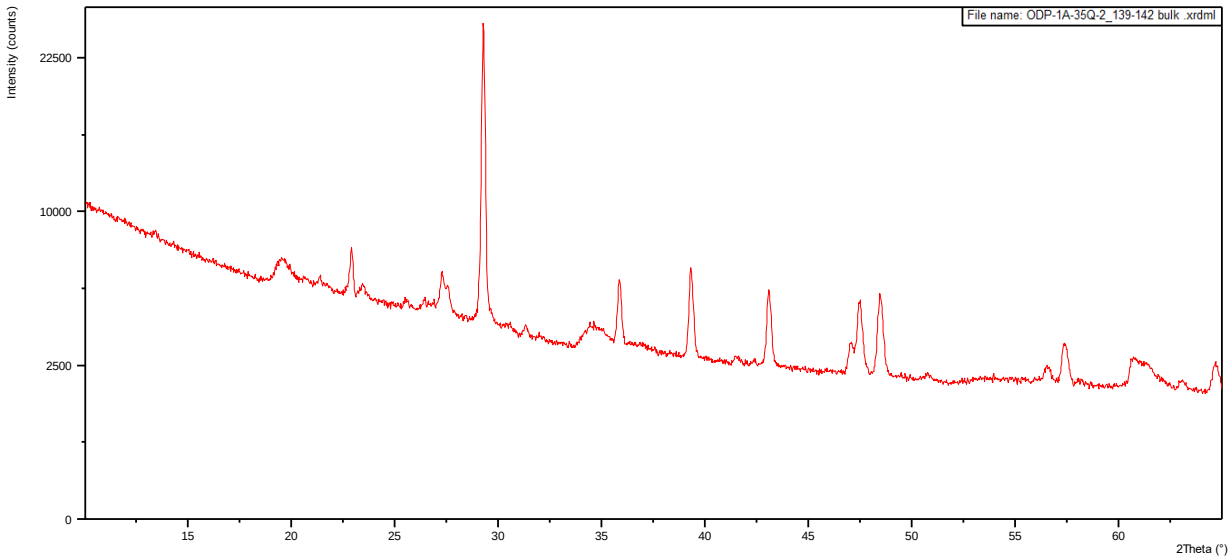
File name: ODP-1A-35Q-2_139-142 bulk .xrdml
Intensity (counts)
22500
10000
2500
0
15
20
25
30
35
40
45
50
55
60
2Theta (°)

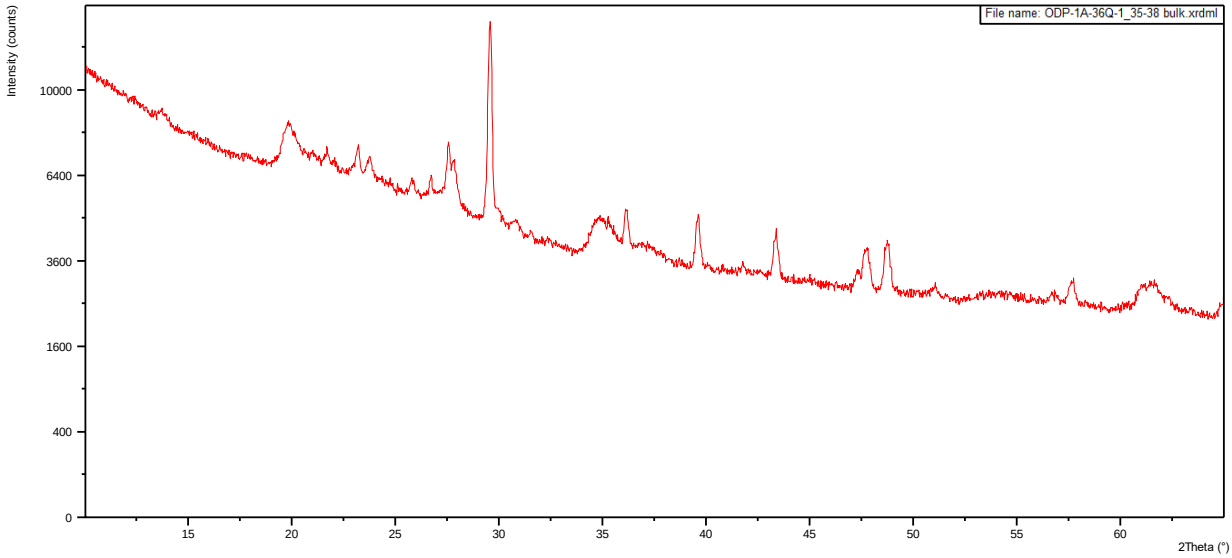
File name: ODP-1A-36Q-1_35-38 bulk.xrdml
Intensity (counts)
10000
6400
3600
1600
400
0
15
20
25
30
35
40
45
50
55
60
2Theta (°)

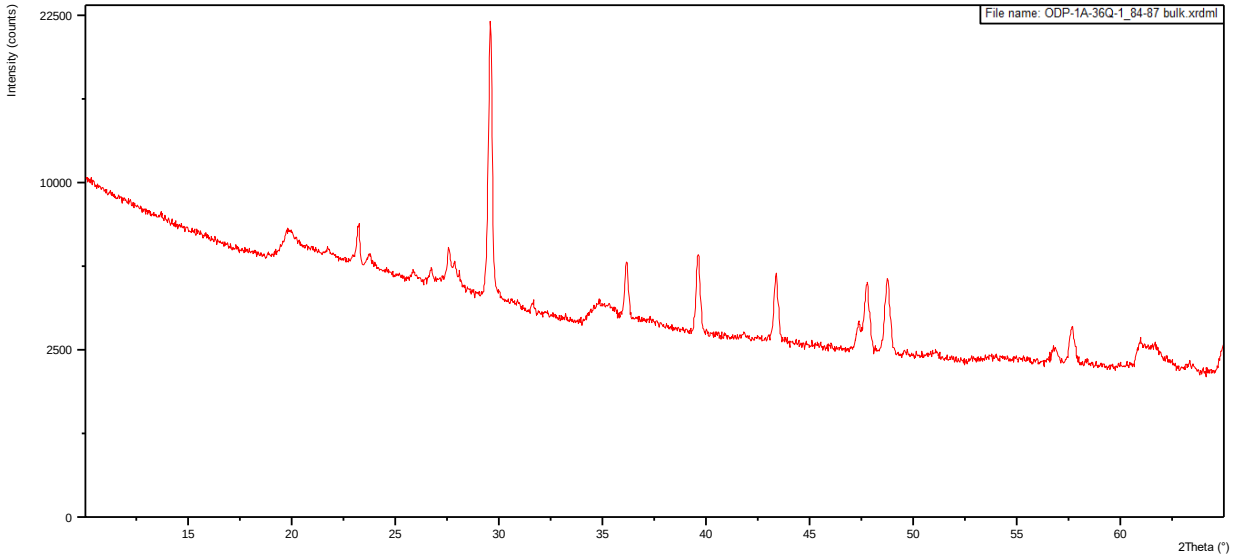
File name: ODP-1A-36Q-1_84-87 bulk.xrdml
Intensity (counts)
22500
10000
2500
0
15
20
25
30
35
40
45
50
55
60
2Theta (°)

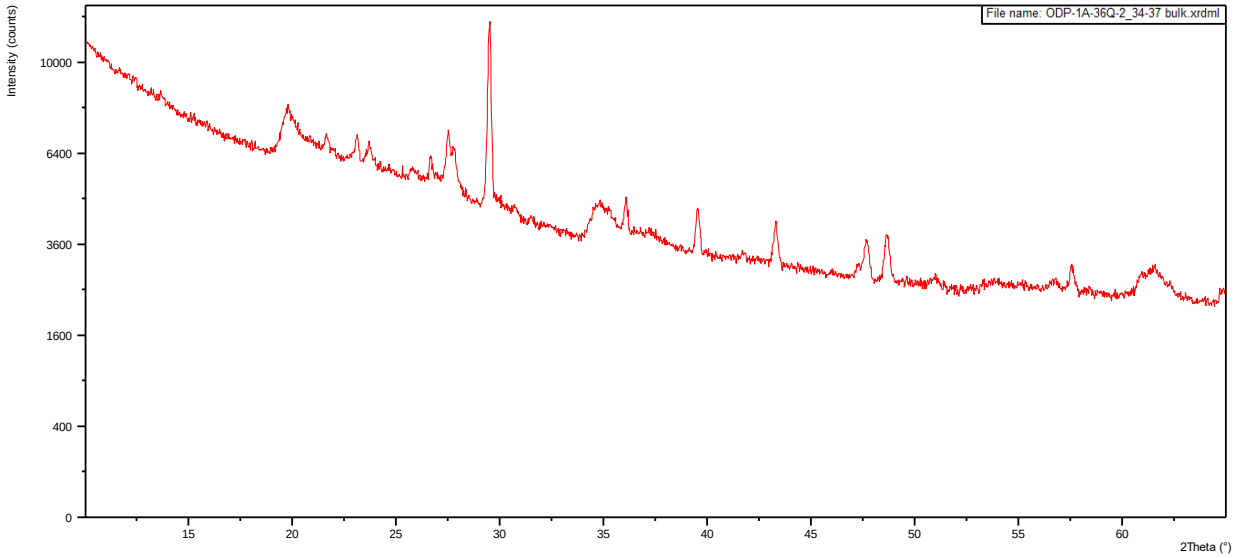
File name: ODP-1A-36Q-2_34-37 bulk.xrdml
Intensity (counts)
10000
6400
3600
1600
400
0
15
20
25
30
35
40
45
50
55
60
2Theta (°)

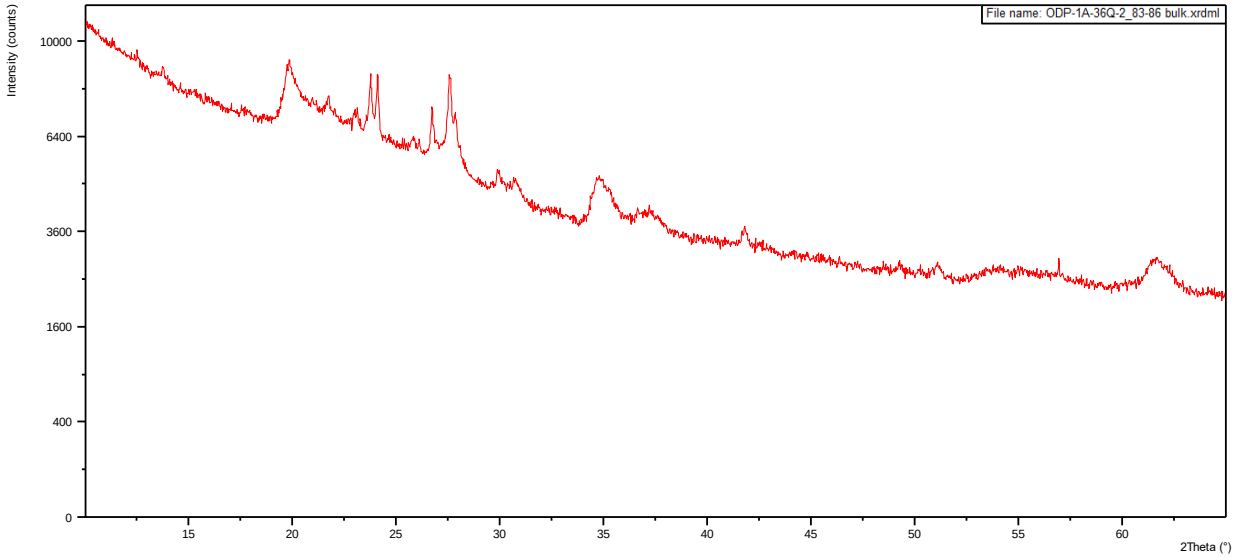
File name: ODP-1A-36Q-2_83-86 bulk.xrdml
Intensity (counts)
10000
6400
3600
1600
400
0
15
20
25
30
35
40
45
50
55
60
2Theta (°)

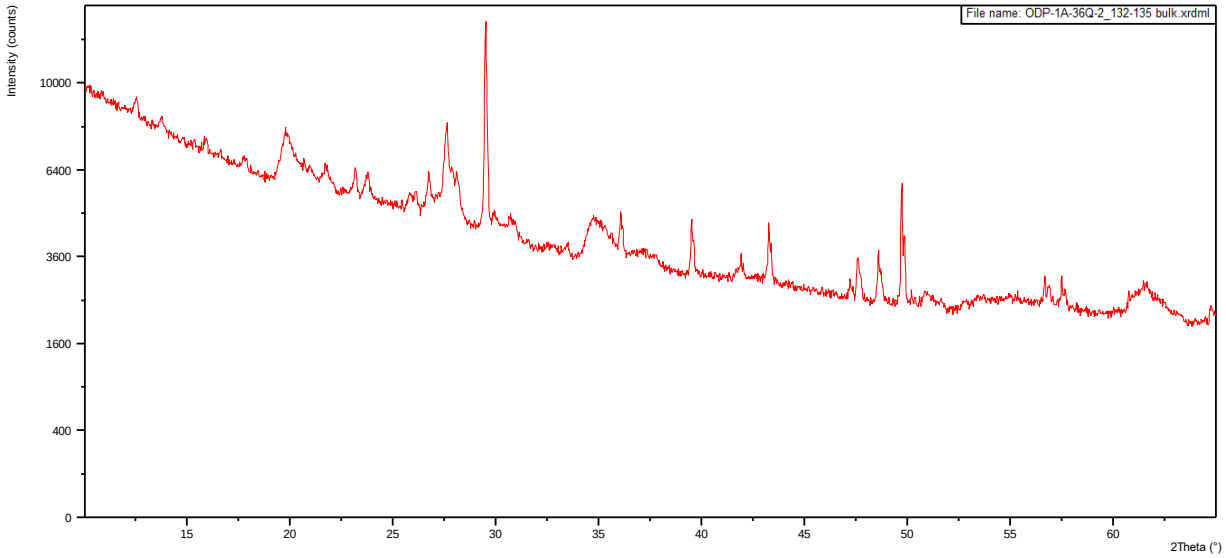
File name: ODP-1A-36Q-2_132-135 bulk.xrdml
Intensity (counts)
10000
6400
3600
1600
400
0
15
20
25
30
35
40
45
50
55
60
2Theta (°)

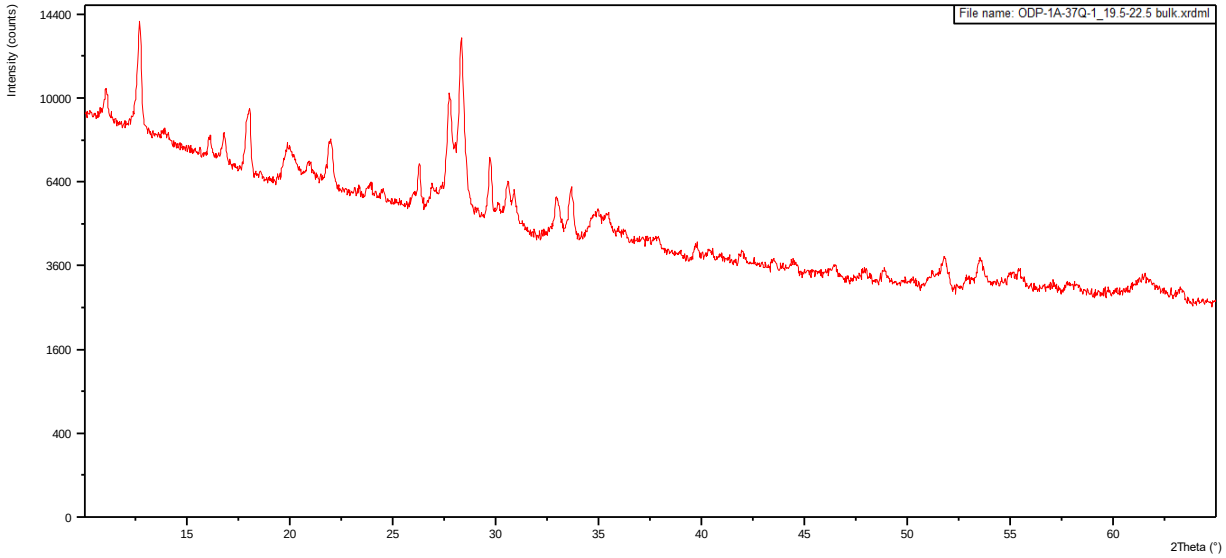
File name: ODP-1A-37Q-1_19.5-22.5 bulk.xrdml
Intensity (counts)
14400
10000
6400
3600
1600
400
0
15
20
25
30
35
40
45
50
55
60
2Theta (°)

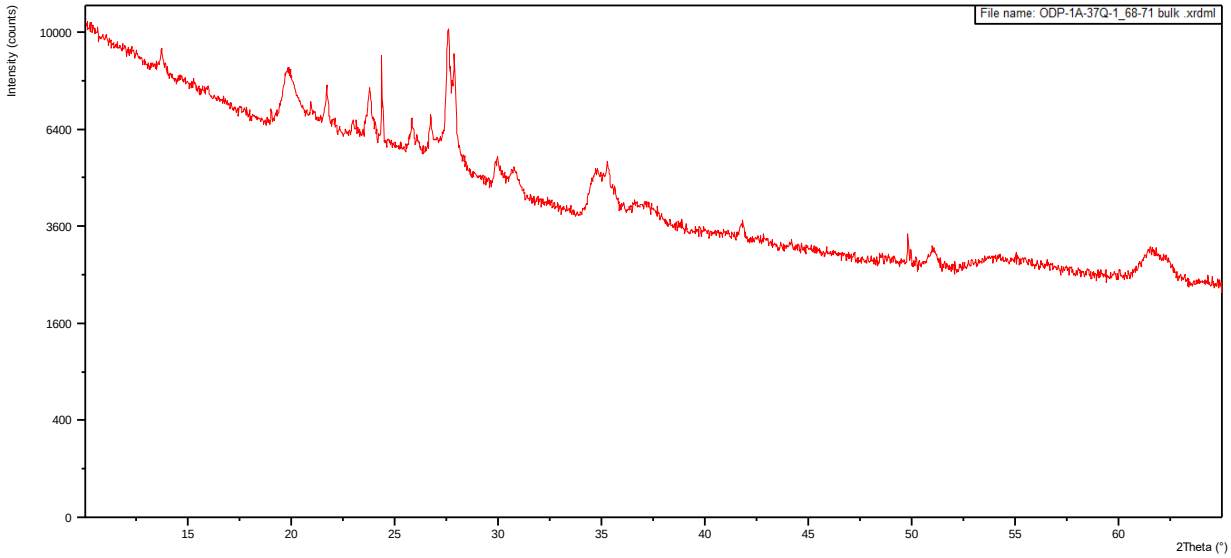
File name: ODP-1A-37Q-1_68-71 bulk .xrdml
Intensity (counts)
10000
6400
3600
1600
400
0
15
20
25
30
35
40
45
50
55
60
2Theta (°)

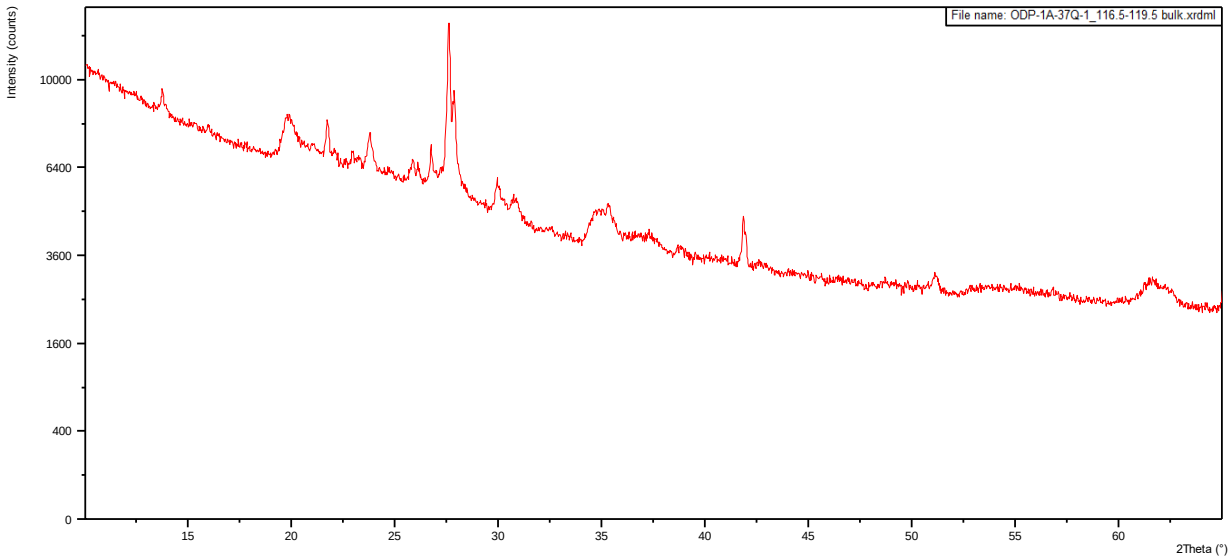
File name: ODP-1A-37Q-1_116.5-119.5 bulk.xrdml
Intensity (counts)
10000
6400
3600
1600
400
0
15
20
25
30
35
40
45
50
55
60
2Theta (°)

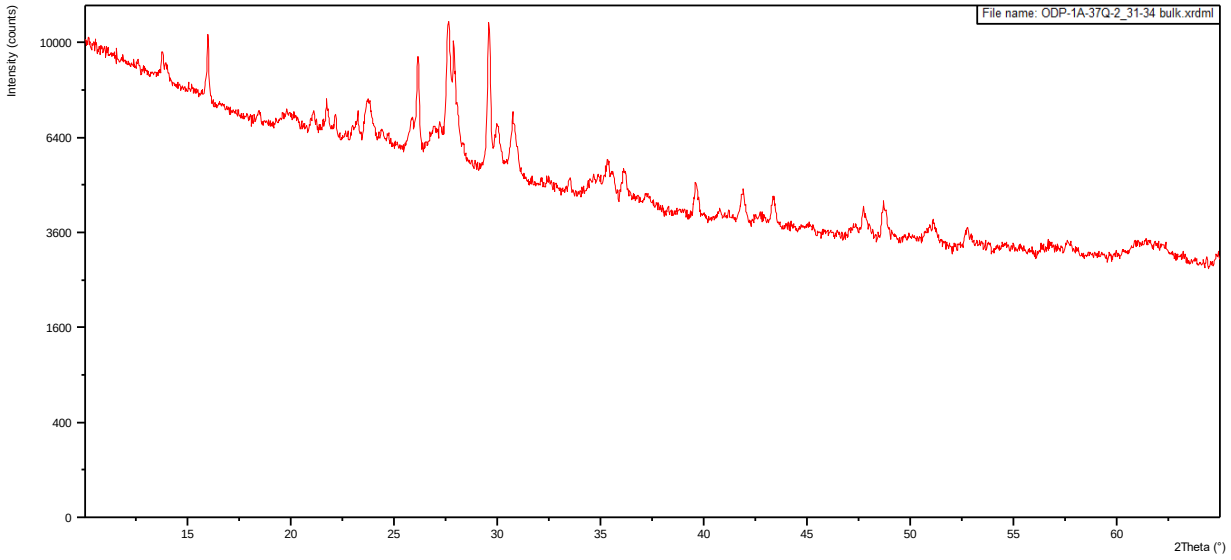
File name: ODP-1A-37Q-2_31-34 bulk.xrdml
Intensity (counts)
10000
6400
3600
1600
400
0
15
20
25
30
35
40
45
50
55
60
2Theta (°)

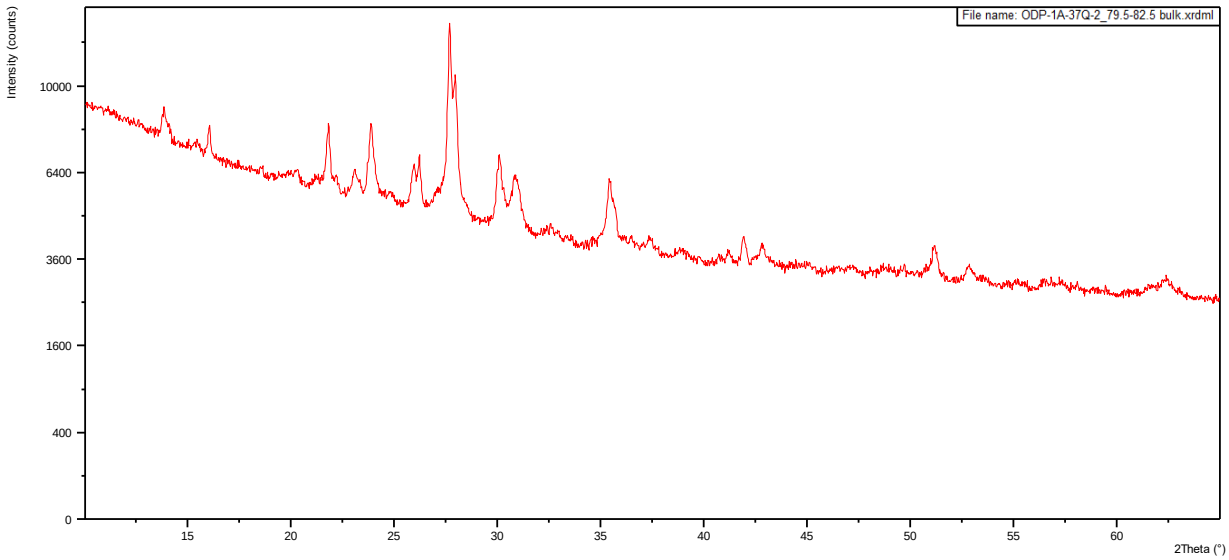
File name: ODP-1A-37Q-2_79.5-82.5 bulk.xrdml
Intensity (counts)
10000
6400
3600
1600
400
0
15
20
25
30
35
40
45
50
55
60
2Theta (°)

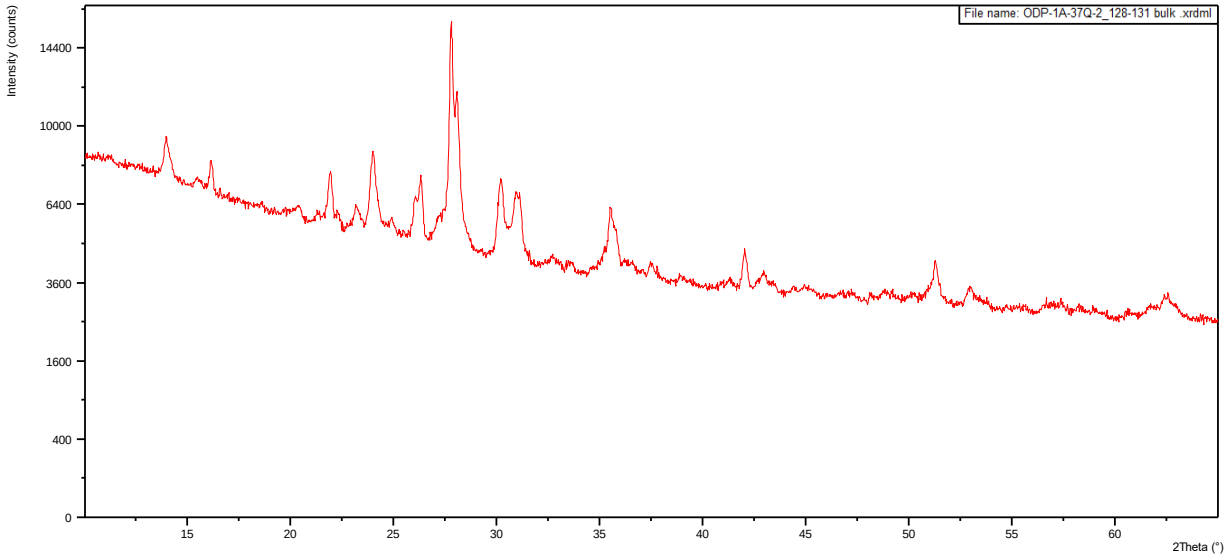
File name: ODP-1A-37Q-2_128-131 bulk .xrdml
Intensity (counts)
14400
10000
6400
3600
1600
400
0
15
20
25
30
35
40
45
50
55
60
2Theta (°)

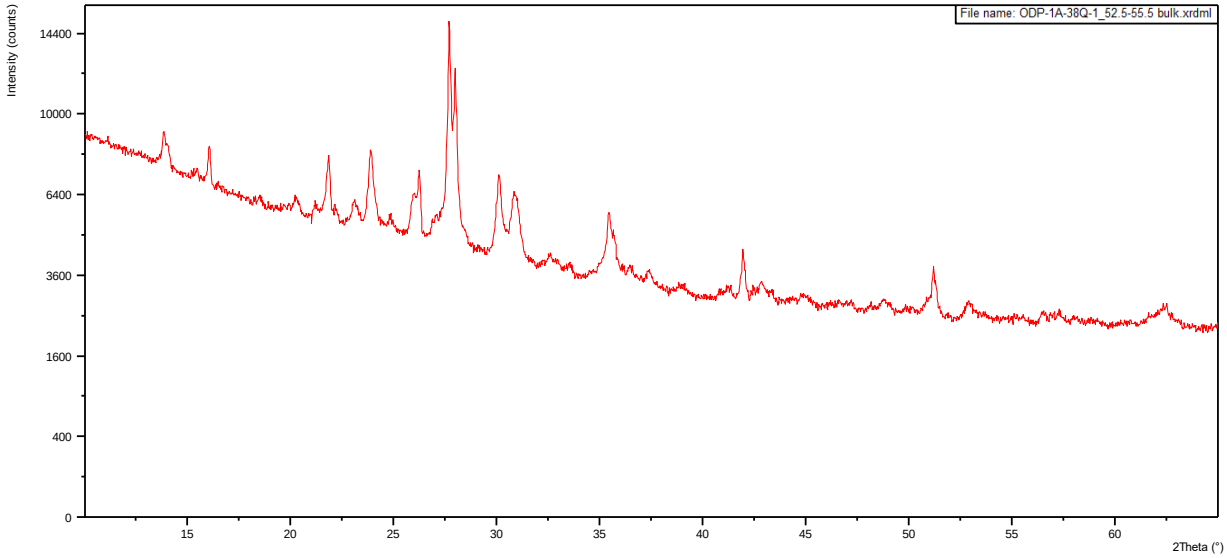
File name: ODP-1A-38Q-1_52.5-55.5 bulk.xrdml
Intensity (counts)
14400
10000
6400
3600
1600
400
0
15
20
25
30
35
40
45
50
55
60
2Theta (°)

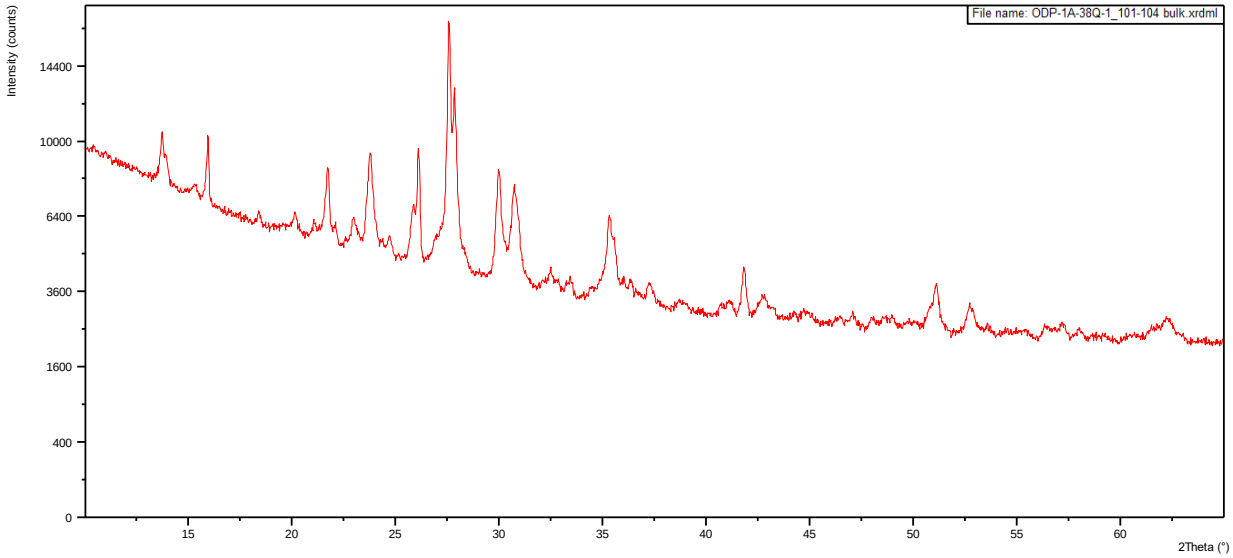
File name: ODP-1A-38Q-1_101-104 bulk.xrdml
Intensity (counts)
14400
10000
6400
3600
1600
400
0
15
20
25
30
35
40
45
50
55
60
2Theta (°)

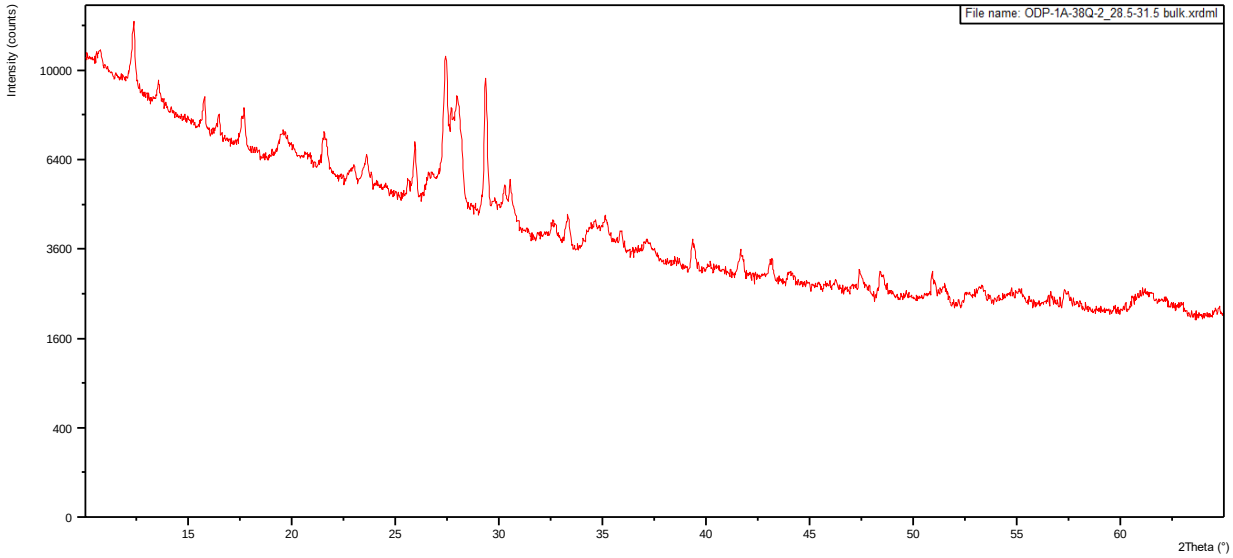
File name: ODP-1A-38Q-2_28.5-31.5 bulk.xrdml
Intensity (counts)
10000
6400
3600
1600
400
0
15
20
25
30
35
40
45
50
55
60
2Theta (°)

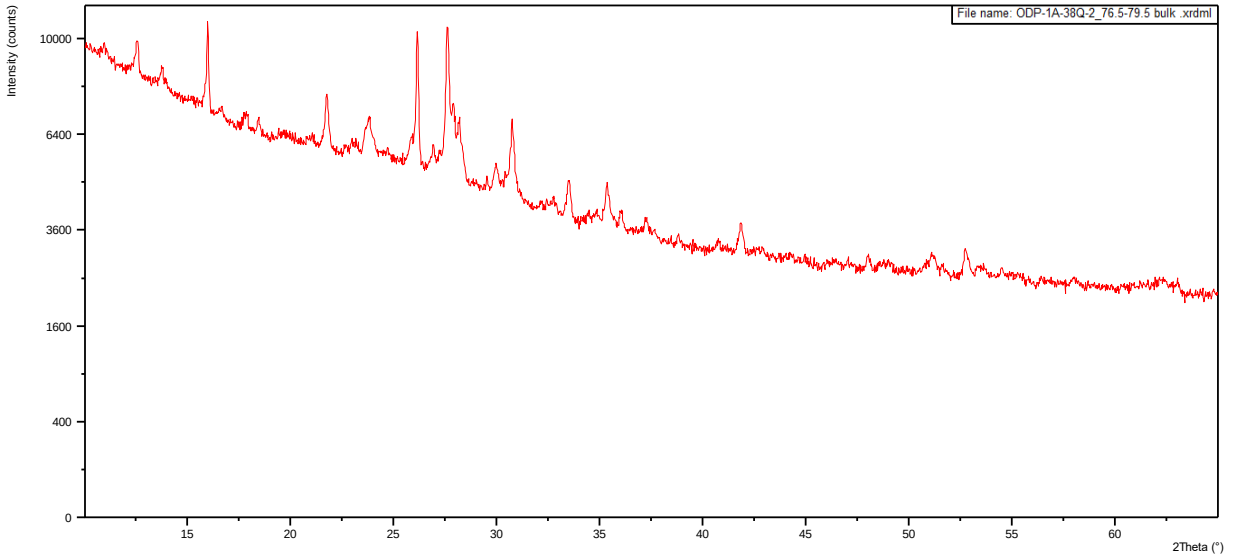
File name: ODP-1A-38Q-2_76.5-79.5 bulk .xrdml
Intensity (counts)
10000
6400
3600
1600
400
0
15
20
25
30
35
40
45
50
55
60
2Theta (°)

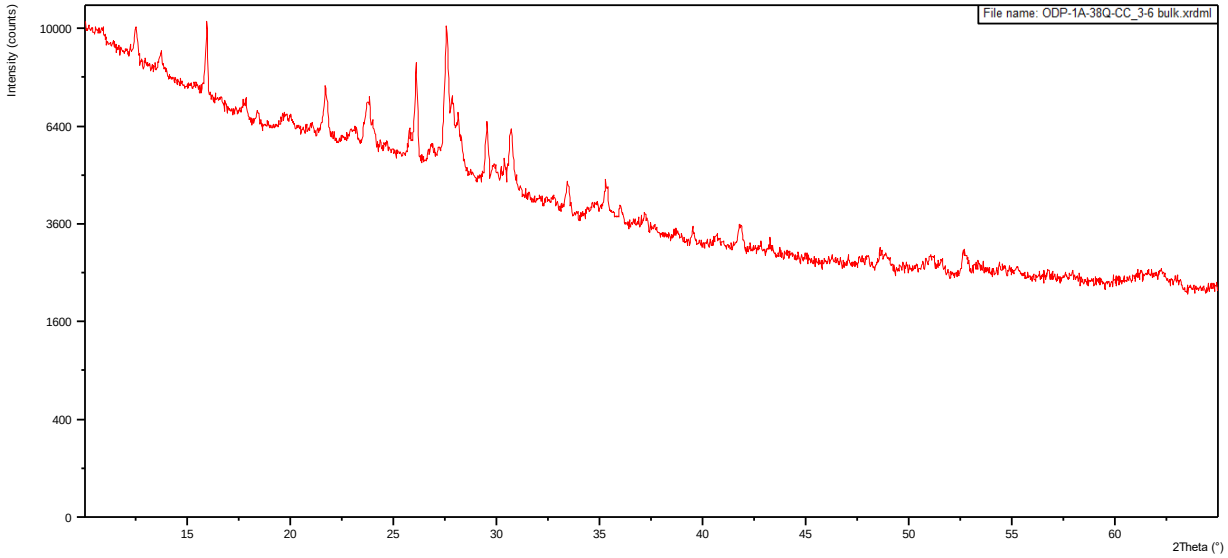
File name: ODP-1A-38Q-CC_3-6 bulk.xrdml
Intensity (counts)
10000
6400
3600
1600
400
0
15
20
25
30
35
40
45
50
55
60
2Theta (°)

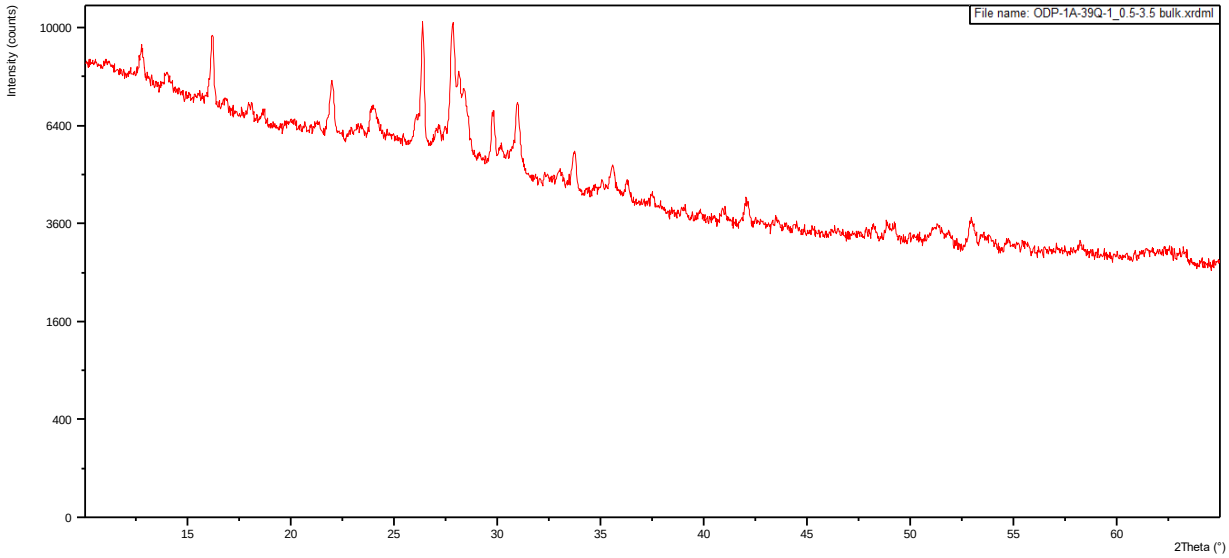
File name: ODP-1A-39Q-1_0.5-3.5 bulk.xrdml
Intensity (counts)
10000
6400
3600
1600
400
0
15
20
25
30
35
40
45
50
55
60
2Theta (°)

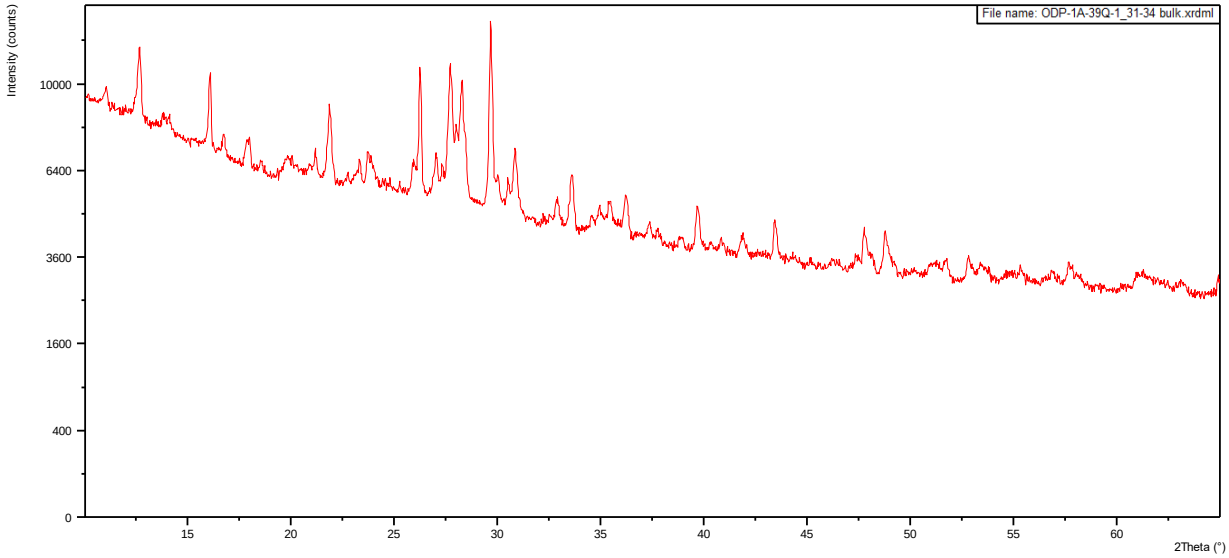
File name: ODP-1A-39Q-1_31-34 bulk.xrdml
Intensity (counts)
10000
6400
3600
1600
400
0
15
20
25
30
35
40
45
50
55
60
2Theta (°)

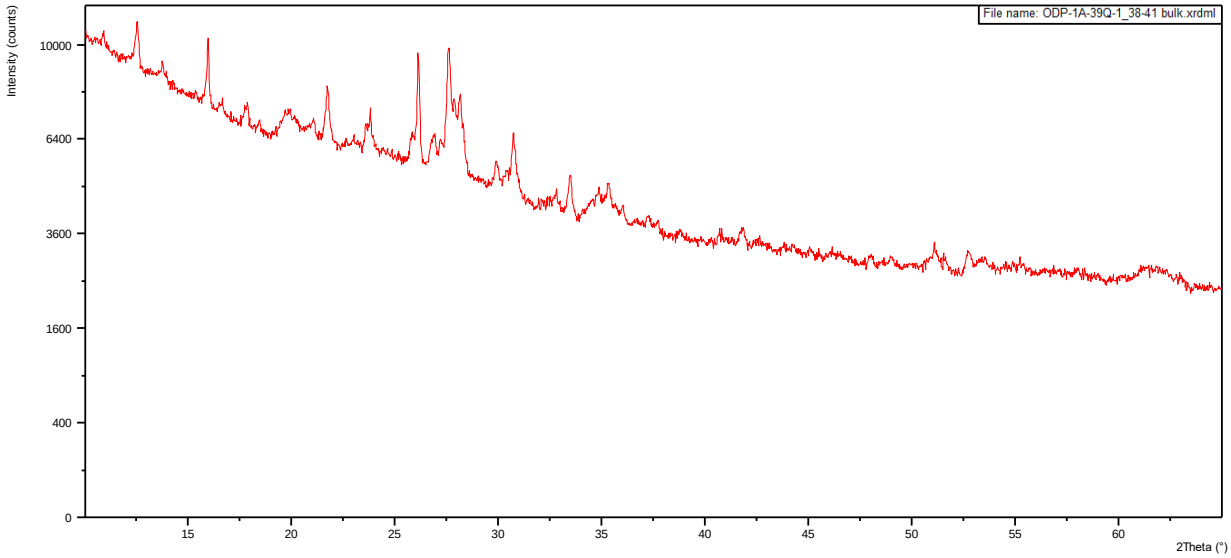
File name: ODP-1A-39Q-1_38-41 bulk.xrdml
Intensity (counts)
10000
6400
3600
1600
400
0
15
20
25
30
35
40
45
50
55
60
2Theta (°)

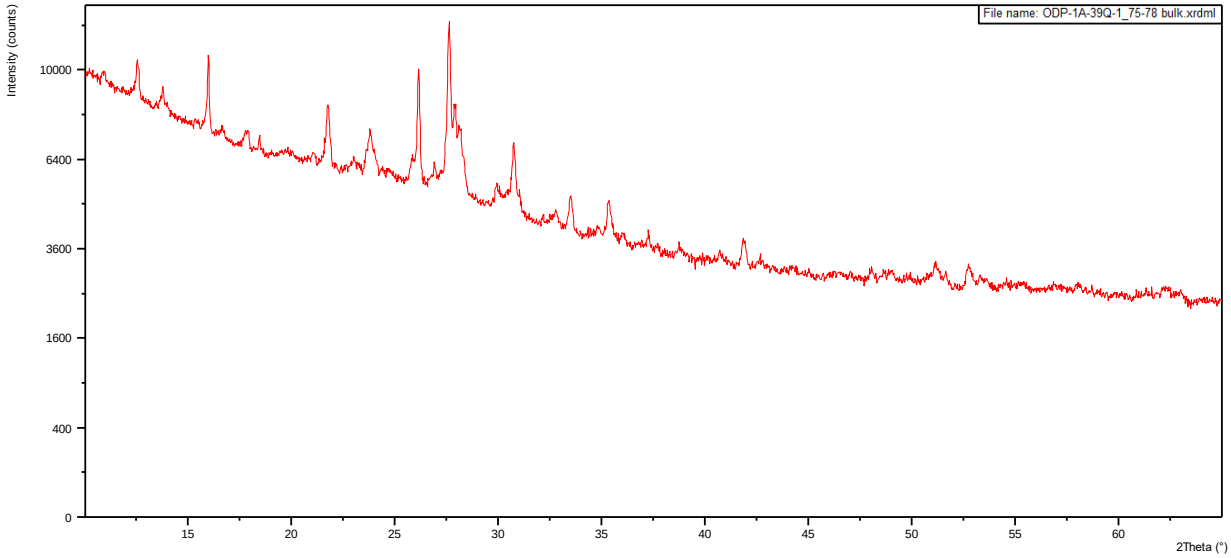
File name: ODP-1A-39Q-1_75-78 bulk.xrdml
Intensity (counts)
10000
6400
3600
1600
400
0
15
20
25
30
35
40
45
50
55
60
2Theta (°)

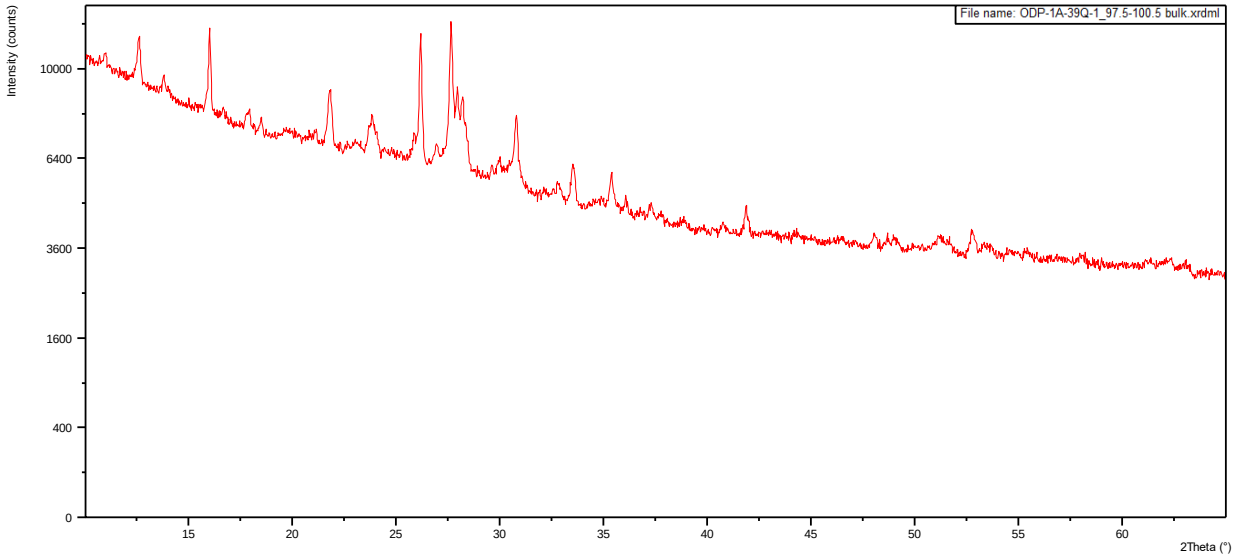
File name: ODP-1A-39Q-1_97.5-100.5 bulk.xrdml
Intensity (counts)
10000
6400
3600
1600
400
0
15
20
25
30
35
40
45
50
55
60
2Theta (°)

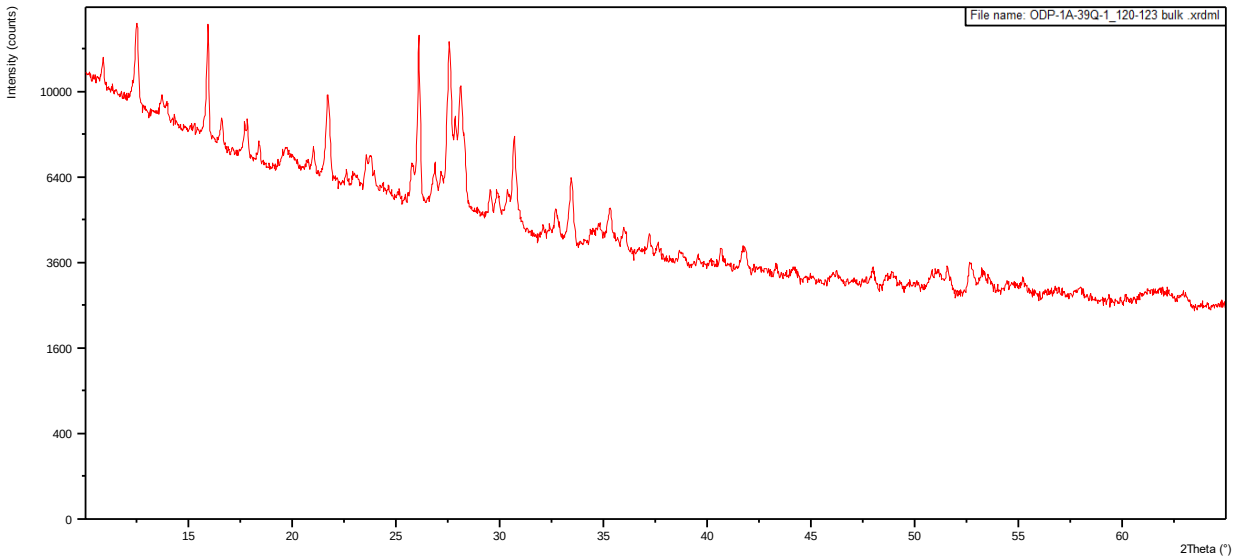
File name: ODP-1A-39Q-1_120-123 bulk .xrdml
Intensity (counts)
10000
6400
3600
1600
400
0
15
20
25
30
35
40
45
50
55
60
2Theta (°)

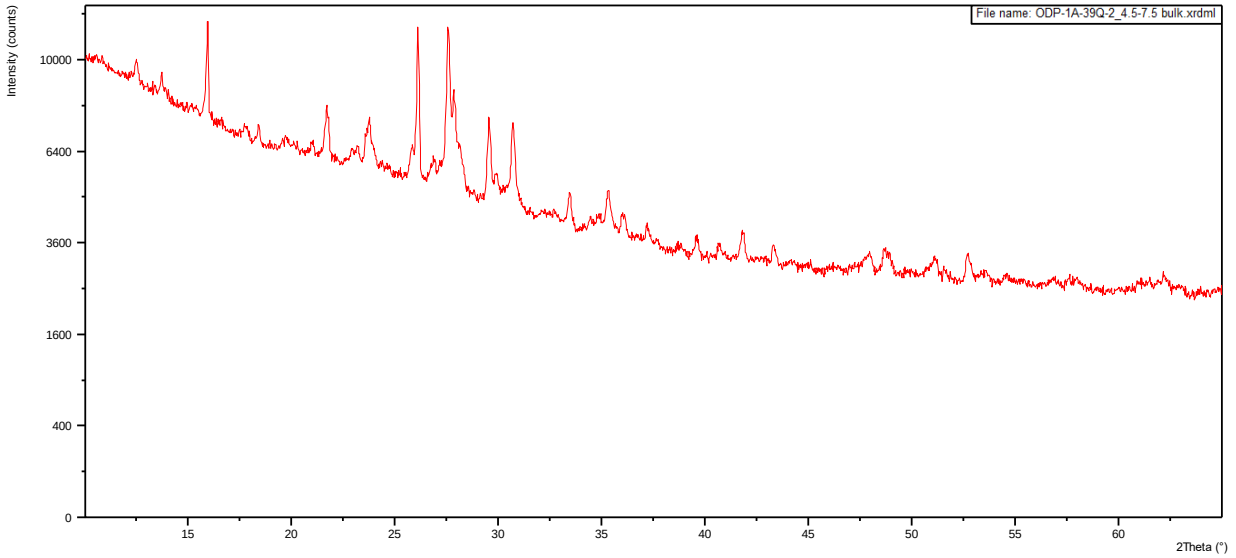
File name: ODP-1A-39Q-2_4.5-7.5 bulk.xrdml
Intensity (counts)
10000
6400
3600
1600
400
0
15
20
25
30
35
40
45
50
55
60
2Theta (°)

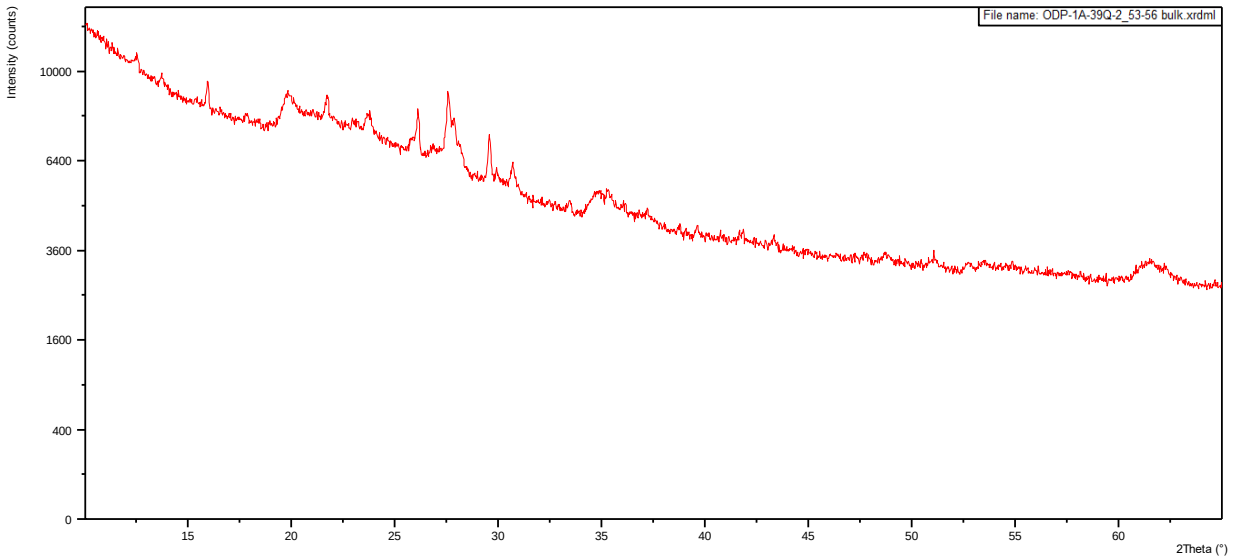
File name: ODP-1A-39Q-2_53-56 bulk.xrdml
Intensity (counts)
10000
6400
3600
1600
400
0
15
20
25
30
35
40
45
50
55
60
2Theta (°)

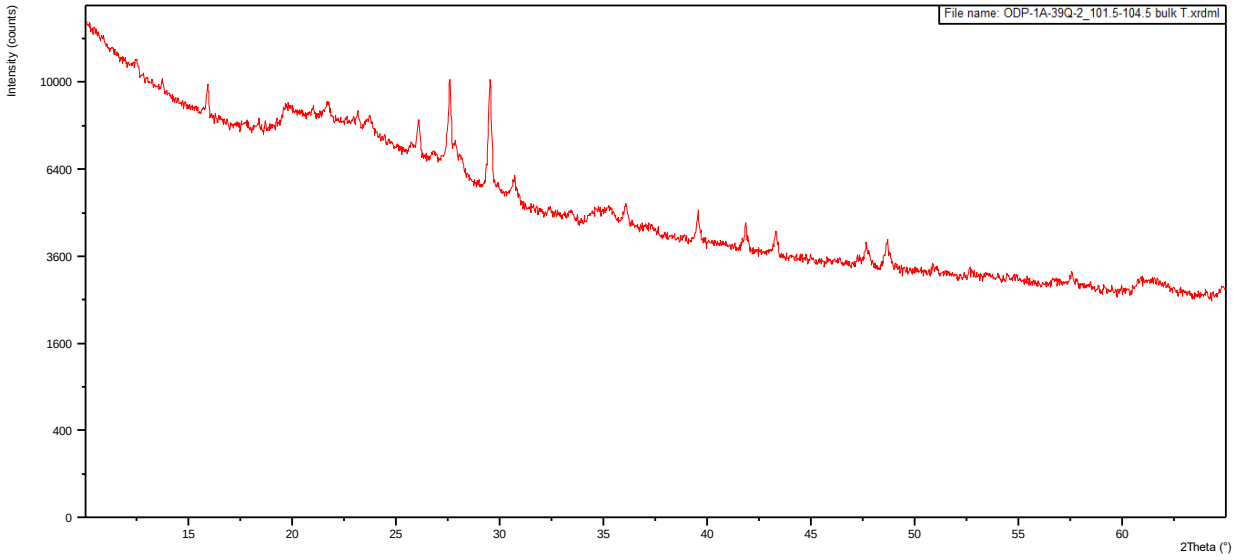
File name: ODP-1A-39Q-2_101.5-104.5 bulk T.xrdml
Intensity (counts)
10000
6400
3600
1600
400
0
15
20
25
30
35
40
45
50
55
60
2Theta (°)

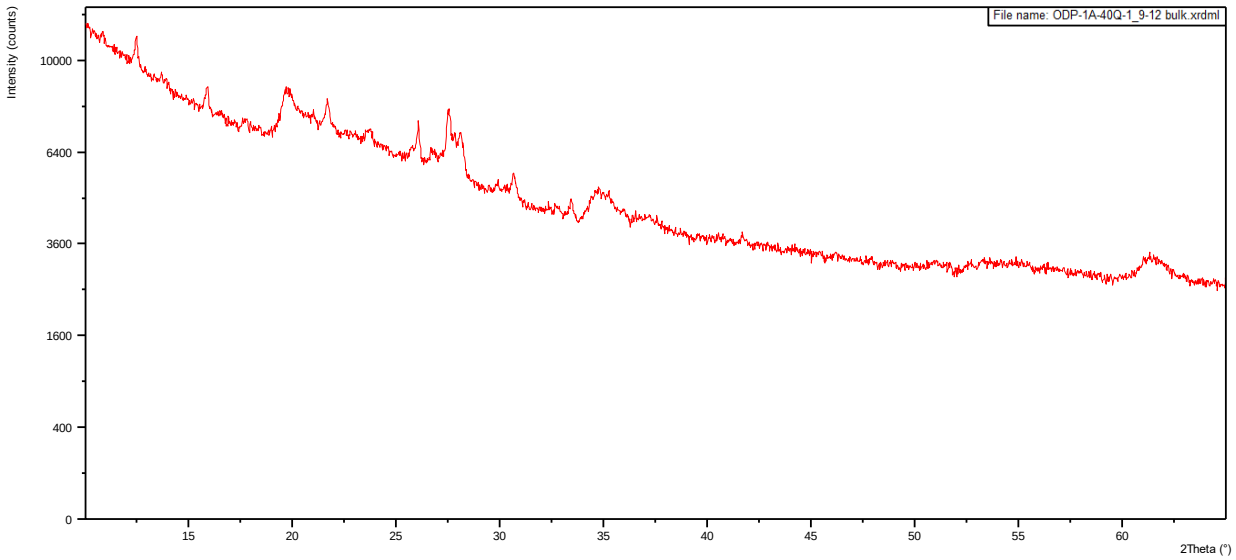
File name: ODP-1A-40Q-1_9-12 bulk.xrdml
Intensity (counts)
10000
6400
3600
1600
400
0
15
20
25
30
35
40
45
50
55
60
2Theta (°)

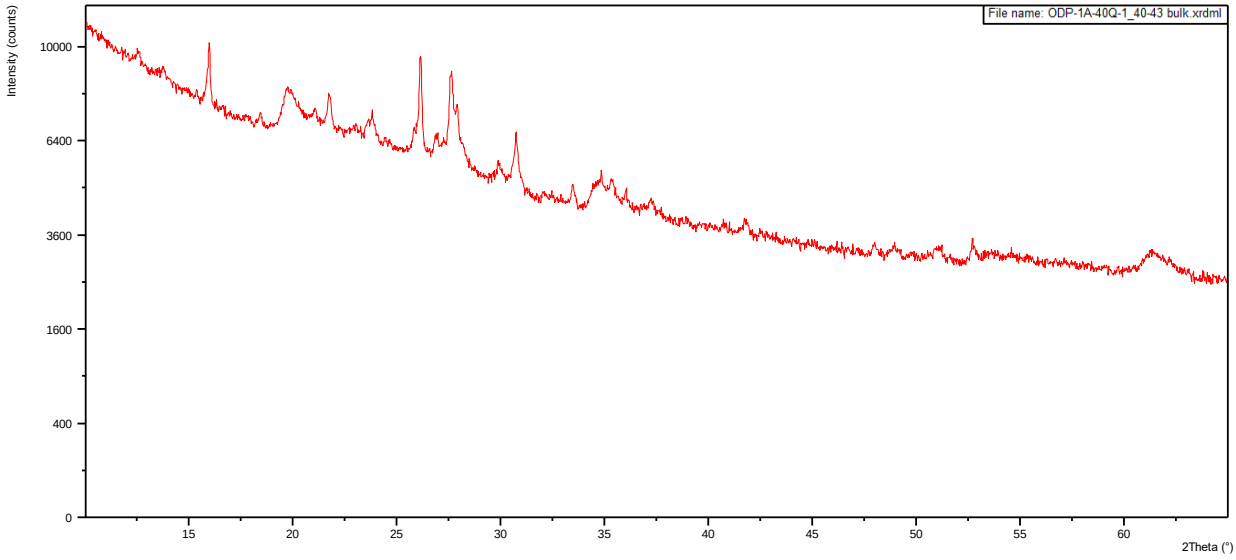
File name: ODP-1A-40Q-1_40-43 bulk.xrdml
Intensity (counts)
10000
6400
3600
1600
400
0
15
20
25
30
35
40
45
50
55
60
2Theta (°)

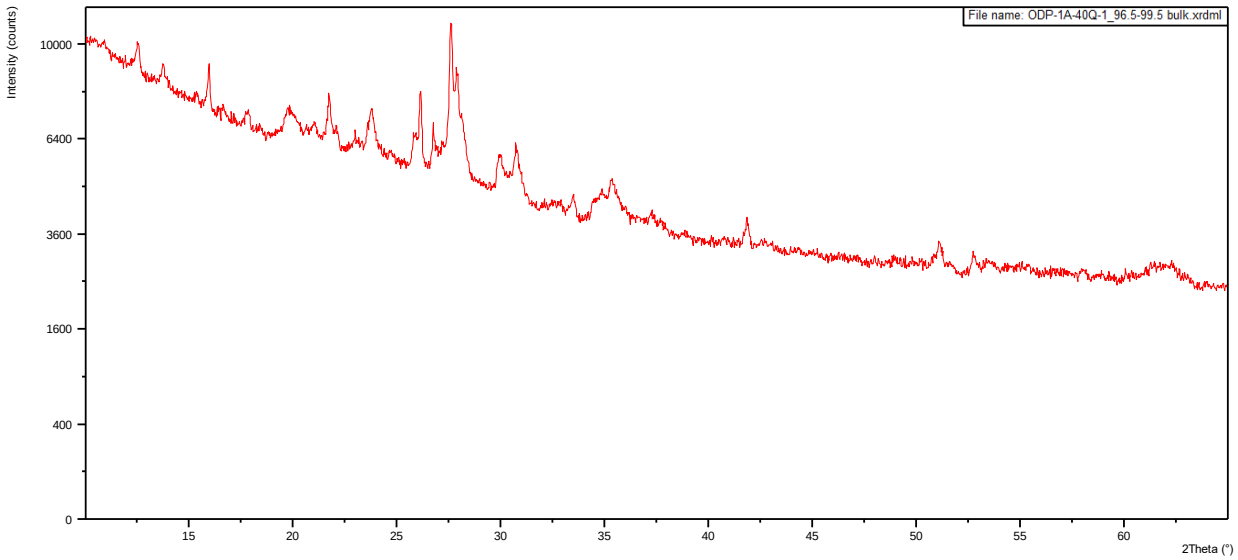
File name: ODP-1A-40Q-1_96.5-99.5 bulk.xrdml
Intensity (counts)
10000
6400
3600
1600
400
0
15
20
25
30
35
40
45
50
55
60
2Theta (°)

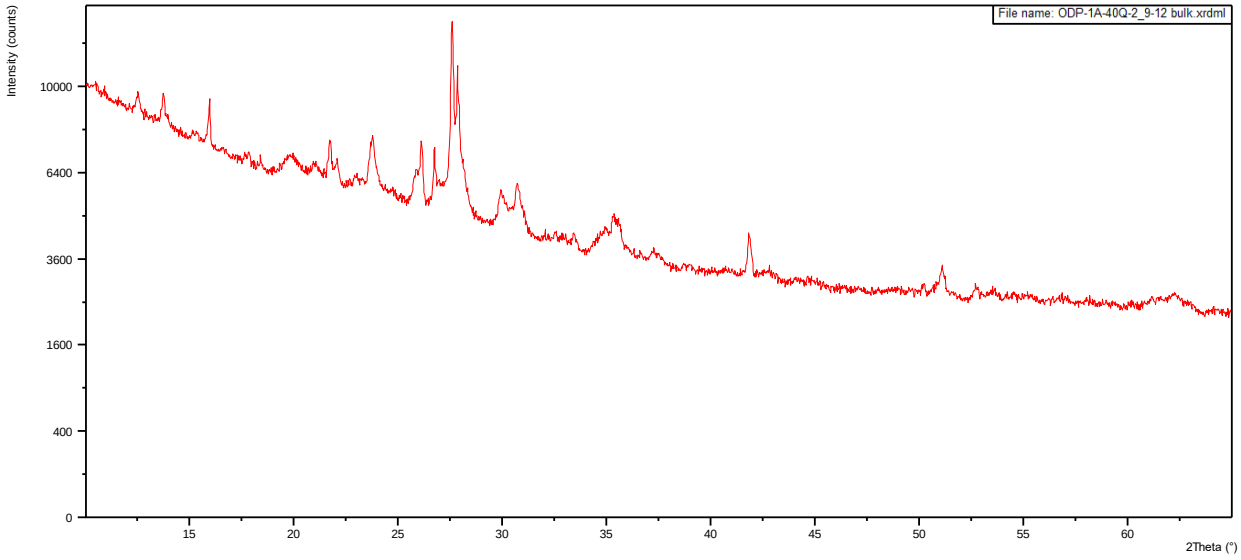
File name: ODP-1A-40Q-2_9-12 bulk.xrdml
Intensity (counts)
10000
6400
3600
1600
400
0
15
20
25
30
35
40
45
50
55
60
2Theta (°)

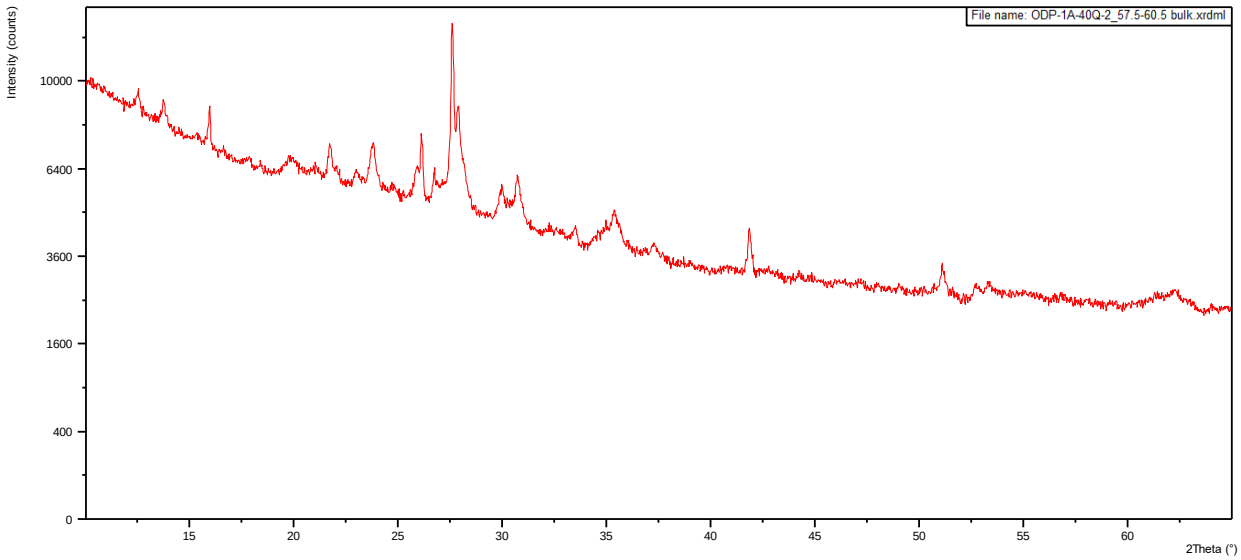
File name: ODP-1A-40Q-2_57.5-60.5 bulk.xrdml
Intensity (counts)
10000
6400
3600
1600
400
0
15
20
25
30
35
40
45
50
55
60
2Theta (°)

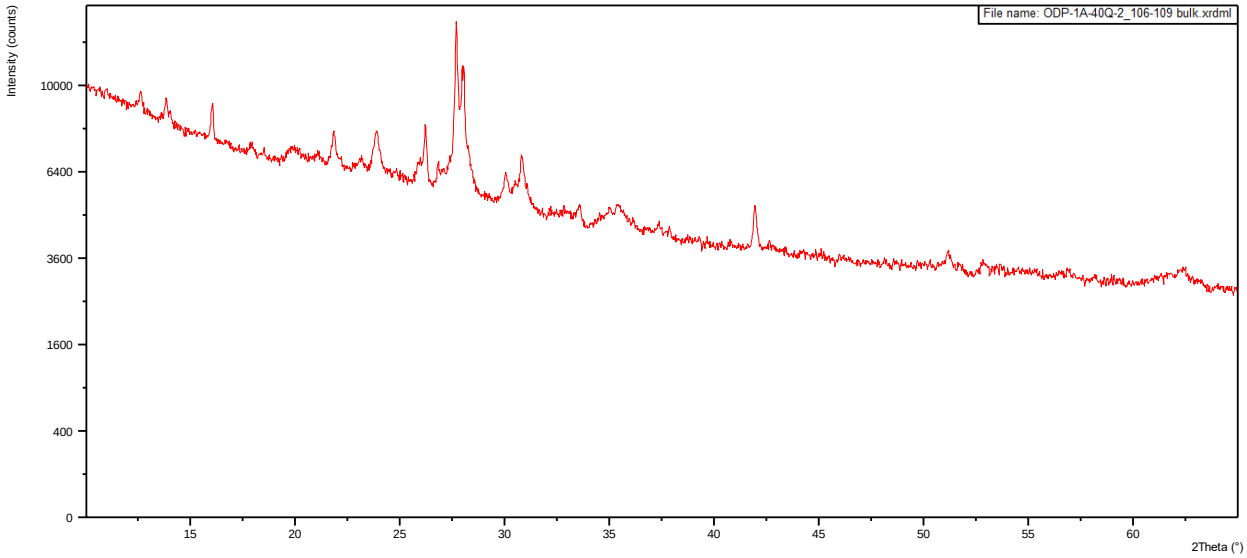
File name: ODP-1A-40Q-2_106-109 bulk.xrdml
Intensity (counts)
10000
6400
3600
1600
400
0
15
20
25
30
35
40
45
50
55
60
2Theta (°)

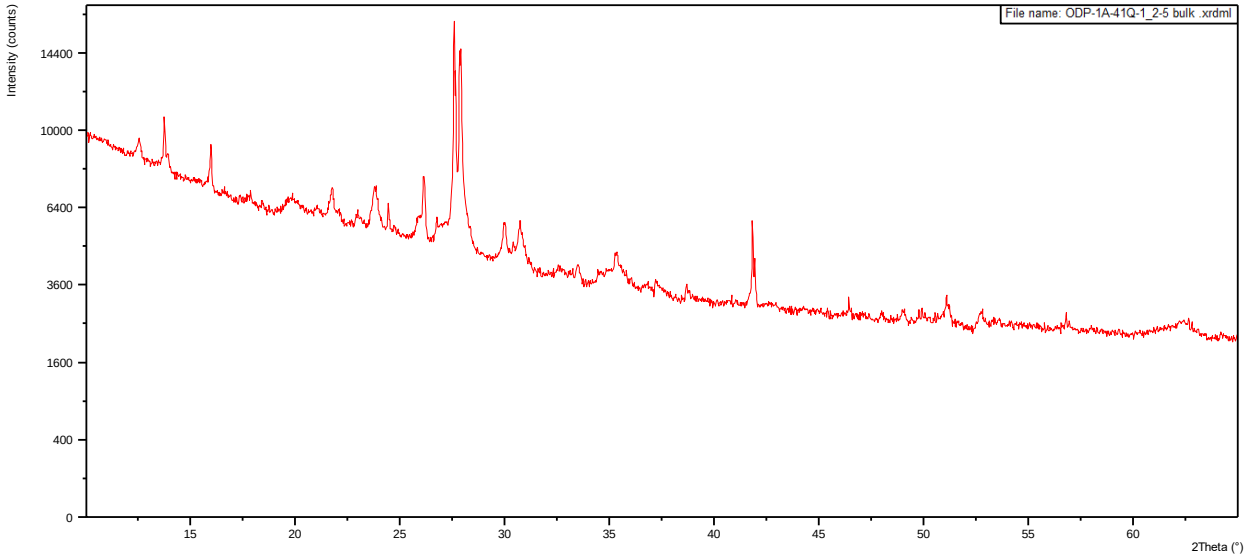
File name: ODP-1A-41Q-1_2-5 bulk .xrdml
Intensity (counts)
14400
10000
6400
3600
1600
400
0
15
20
25
30
35
40
45
50
55
60
2Theta (°)

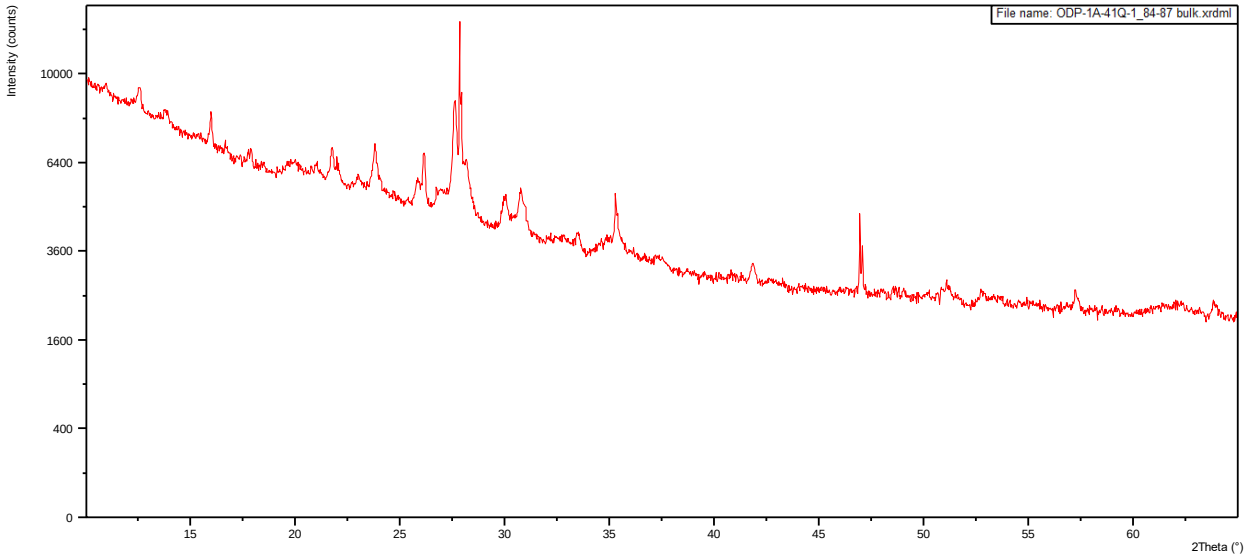
File name: ODP-1A-41Q-1_84-87 bulk.xrdml
Intensity (counts)
10000
6400
3600
1600
400
0
15
20
25
30
35
40
45
50
55
60
2Theta (°)

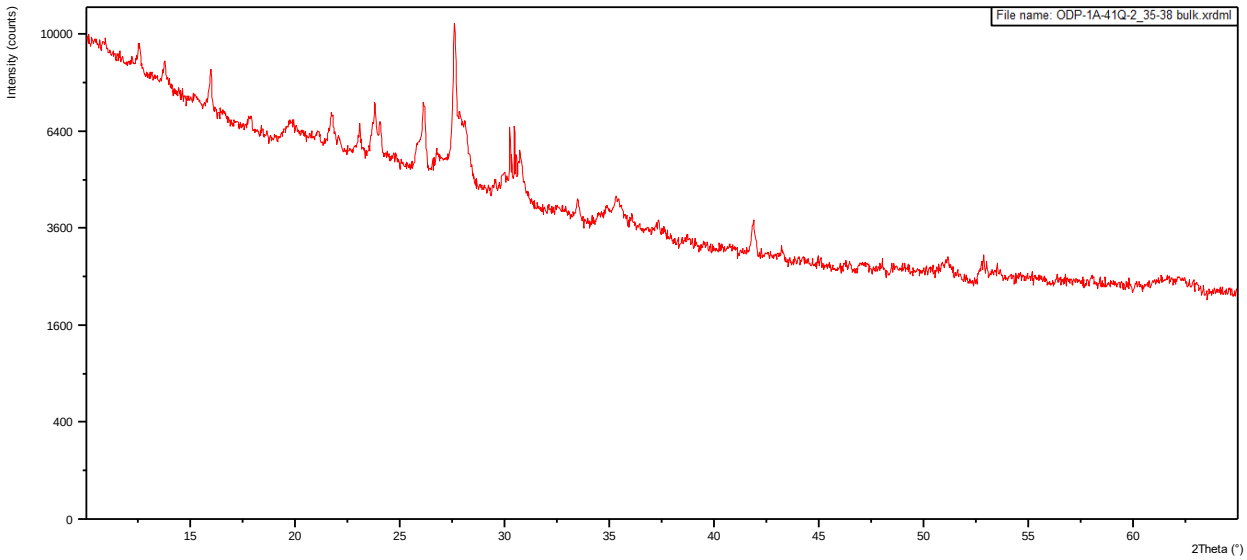
File name: ODP-1A-41Q-2_35-38 bulk.xrdml
Intensity (counts)
10000
6400
3600
1600
400
0
15
20
25
30
35
40
45
50
55
60
2Theta (°)

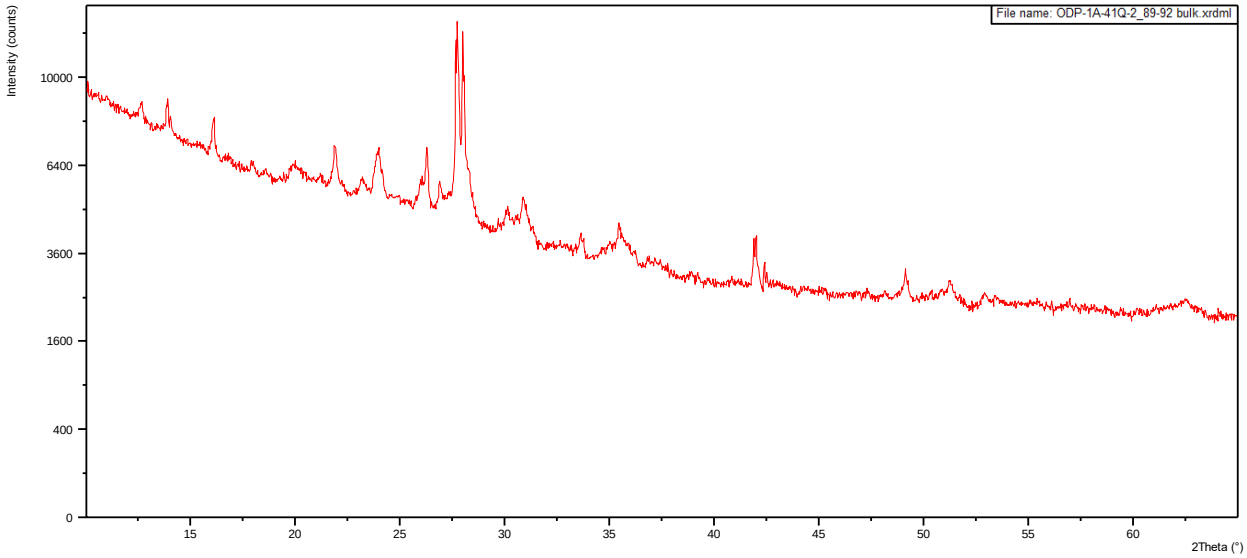
File name: ODP-1A-41Q-2_89-92 bulk.xrdml
Intensity (counts)
10000
6400
3600
1600
400
0
15
20
25
30
35
40
45
50
55
60
2Theta (°)

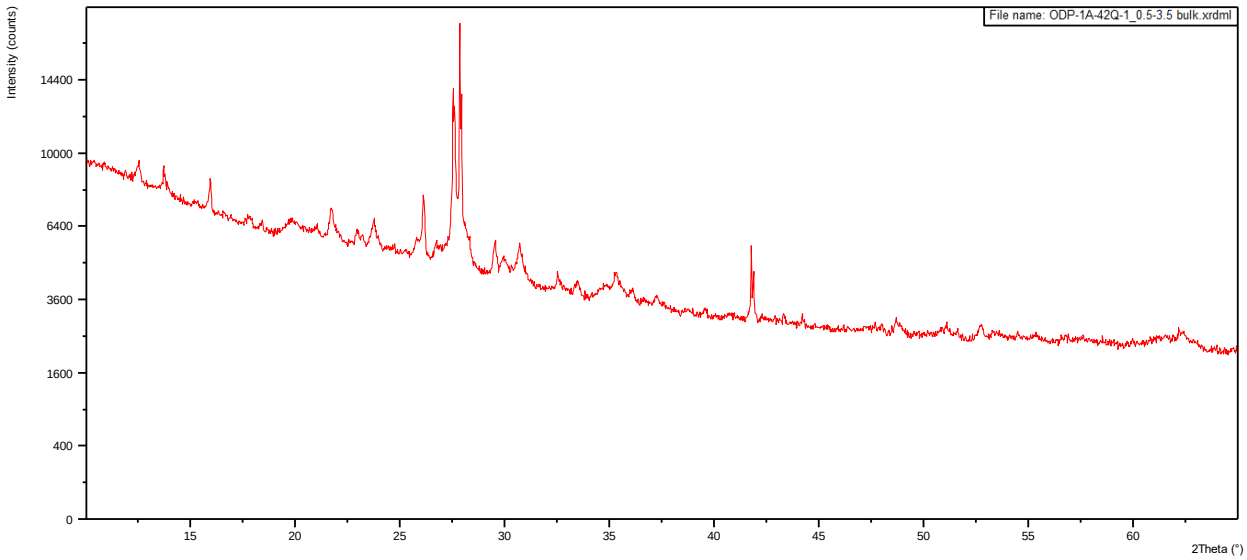
File name: ODP-1A-42Q-1_0.5-3.5 bulk.xrdml
Intensity (counts)
14400
10000
6400
3600
1600
400
0
15
20
25
30
35
40
45
50
55
60
2Theta (°)

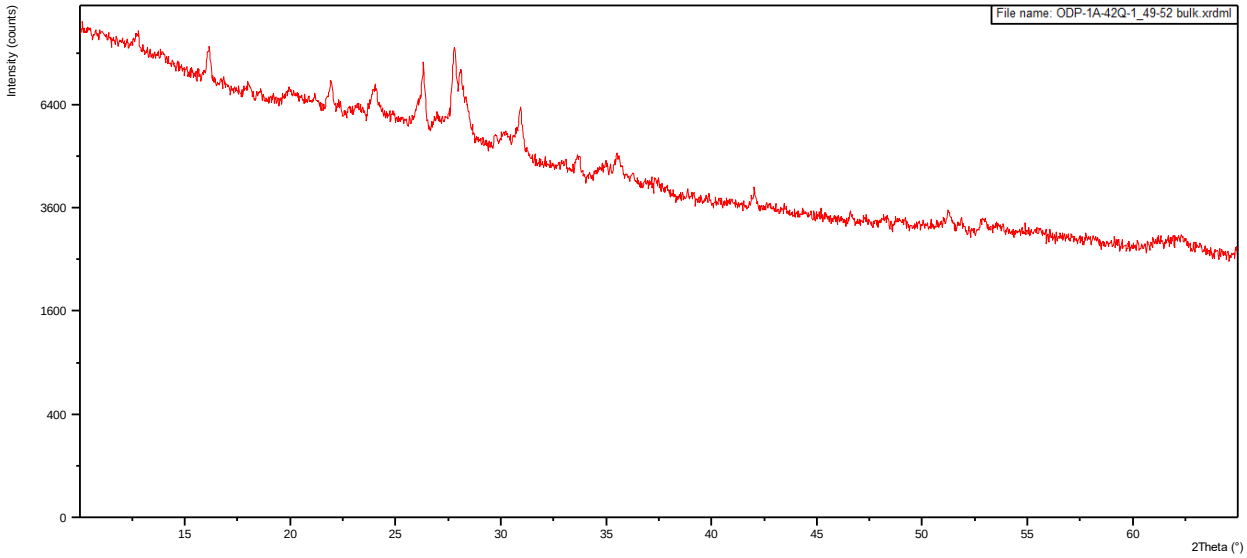
File name: ODP-1A-42Q-1_49-52 bulk.xrdml
Intensity (counts)
6400
3600
1600
400
0
15
20
25
30
35
40
45
50
55
60
2Theta (°)

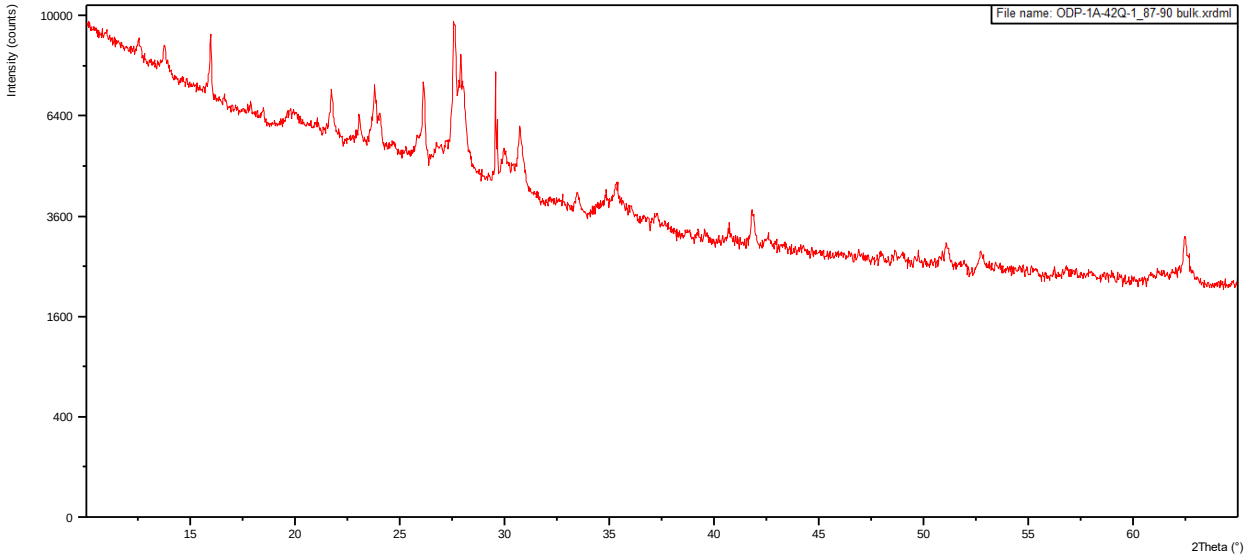
File name: ODP-1A-42Q-1_87-90 bulk.xrdml
Intensity (counts)
10000
6400
3600
1600
400
0
15
20
25
30
35
40
45
50
55
60
2Theta (°)

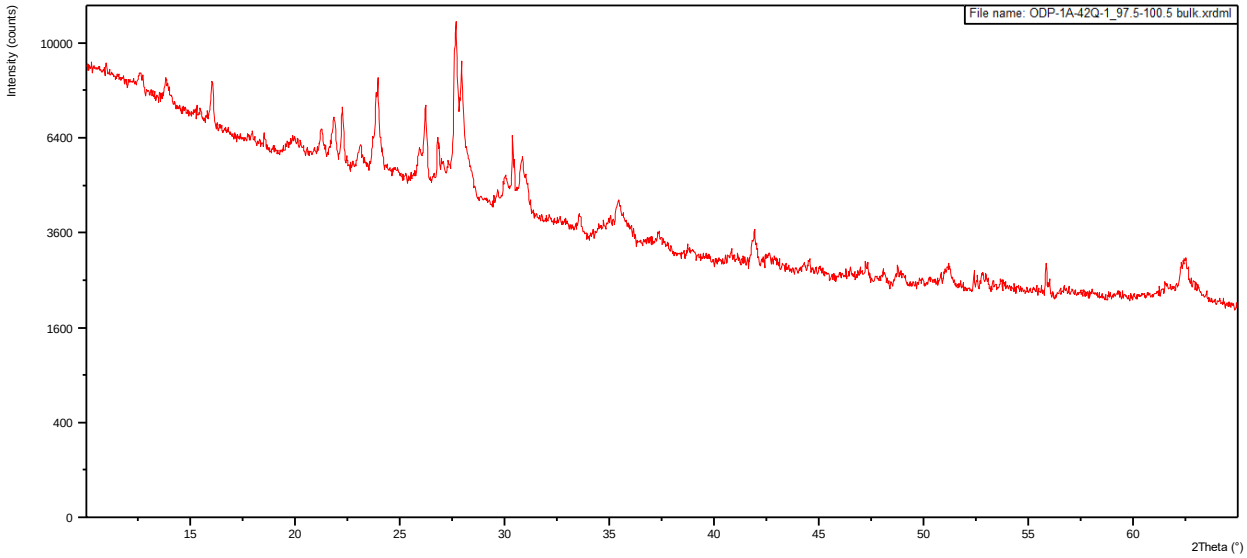
File name: ODP-1A-42Q-1_97.5-100.5 bulk.xrdml
Intensity (counts)
10000
6400
3600
1600
400
0
15
20
25
30
35
40
45
50
55
60
2Theta (°)

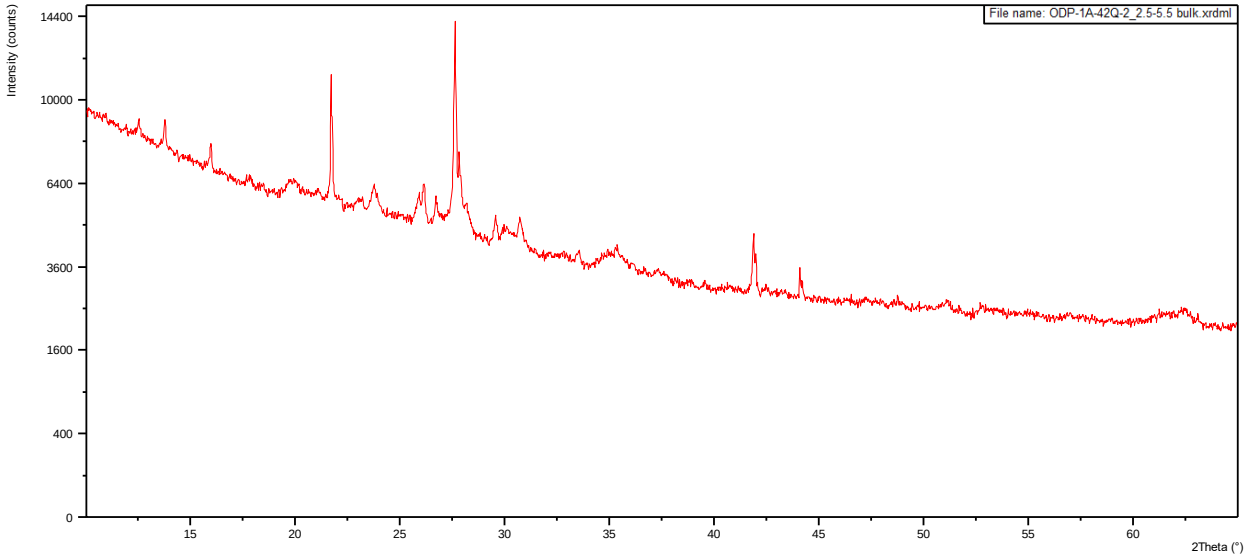
File name: ODP-1A-42Q-2_2.5-5.5 bulk.xrdml
Intensity (counts)
14400
10000
6400
3600
1600
400
0
15
20
25
30
35
40
45
50
55
60
2Theta (°)

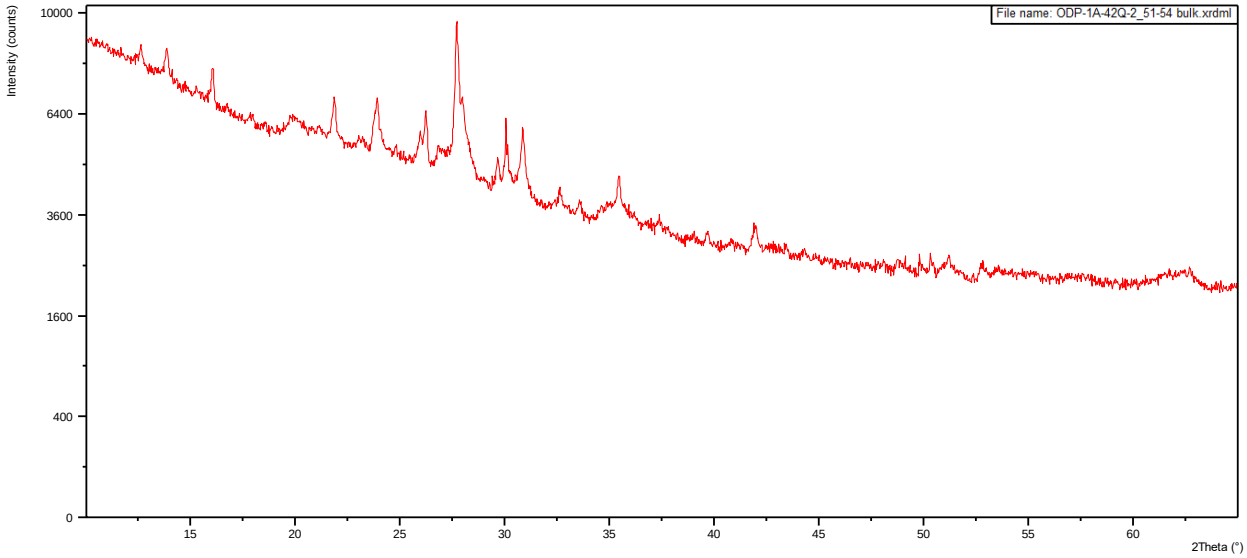
File name: ODP-1A-42Q-2_51-54 bulk.xrdml
Intensity (counts)
10000
6400
3600
1600
400
0
15
20
25
30
35
40
45
50
55
60
2Theta (°)

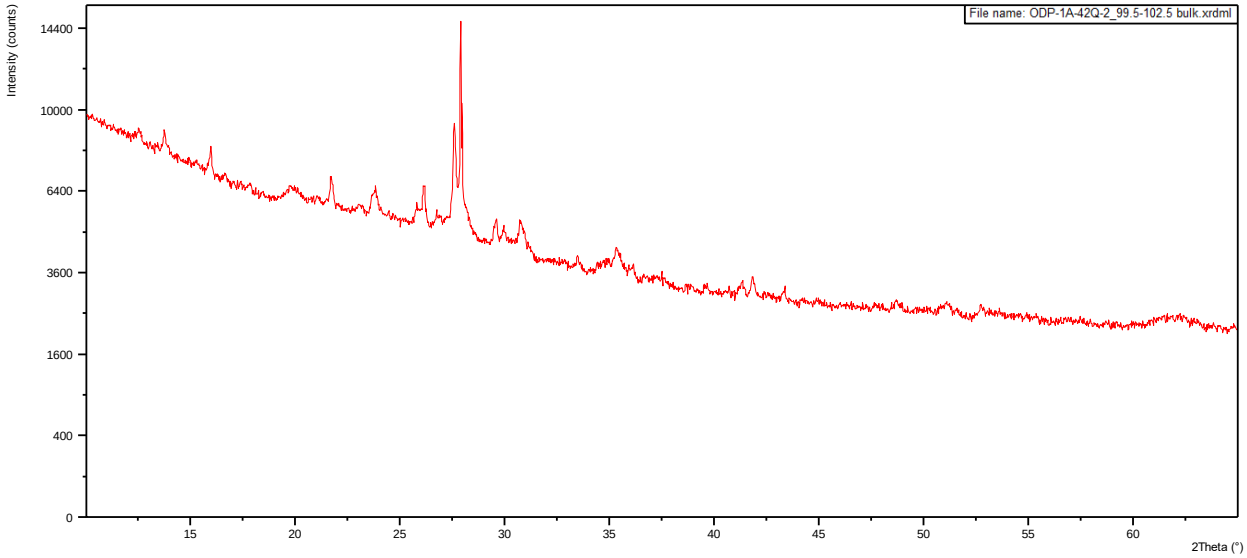
File name: ODP-1A-42Q-2_99.5-102.5 bulk.xrdml
Intensity (counts)
14400
10000
6400
3600
1600
400
0
15
20
25
30
35
40
45
50
55
60
2Theta (°)

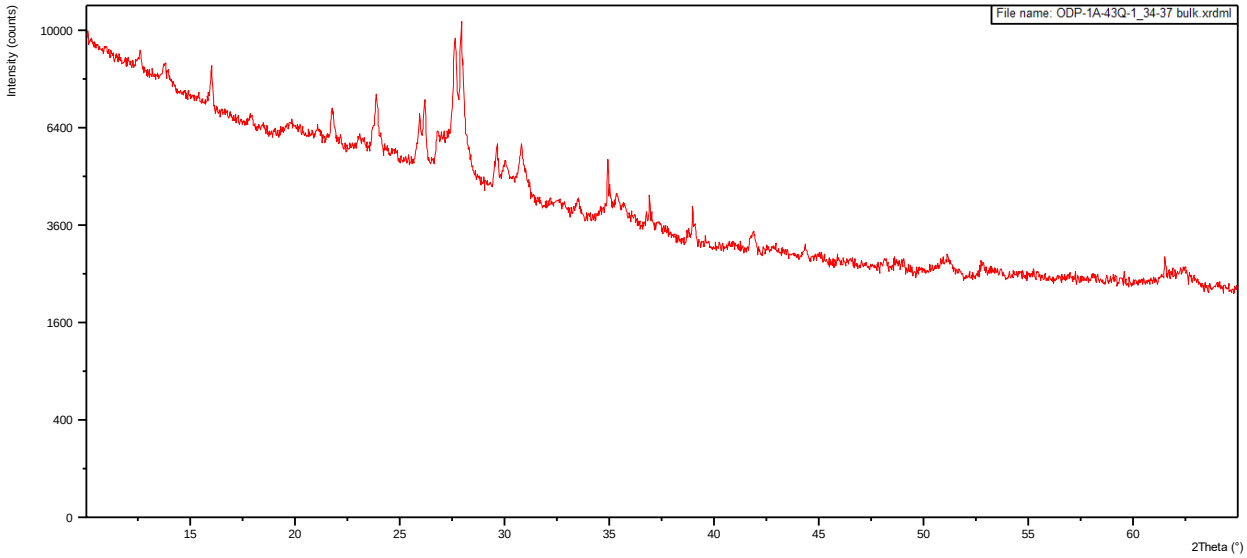
File name: ODP-1A-43Q-1_34-37 bulk.xrdml
Intensity (counts)
10000
6400
3600
1600
400
0
15
20
25
30
35
40
45
50
55
60
2Theta (°)

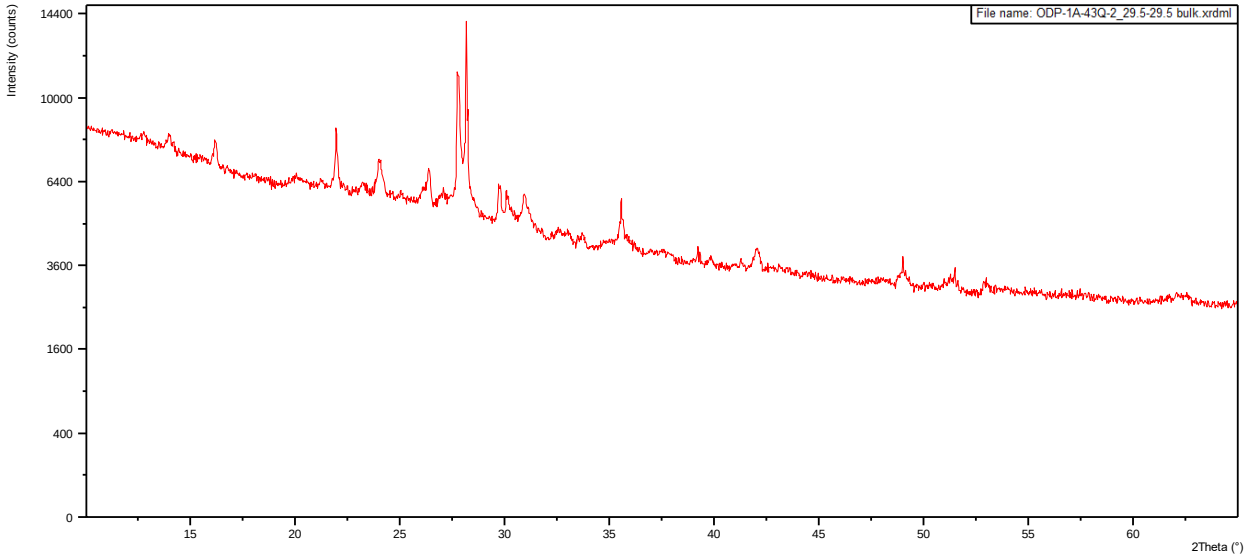
File name: ODP-1A-43Q-2_29.5-29.5 bulk.xrdml
Intensity (counts)
14400
10000
6400
3600
1600
400
0
15
20
25
30
35
40
45
50
55
60
2Theta (°)

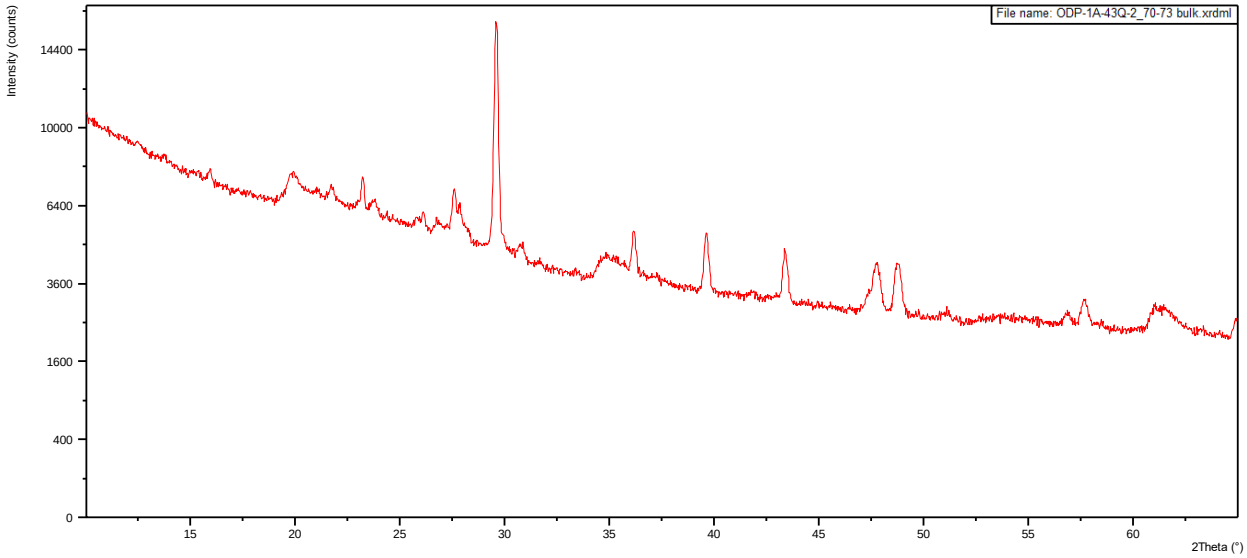
File name: ODP-1A-43Q-2_70-73 bulk.xrdml
Intensity (counts)
14400
10000
6400
3600
1600
400
0
15
20
25
30
35
40
45
50
55
60
2Theta (°)

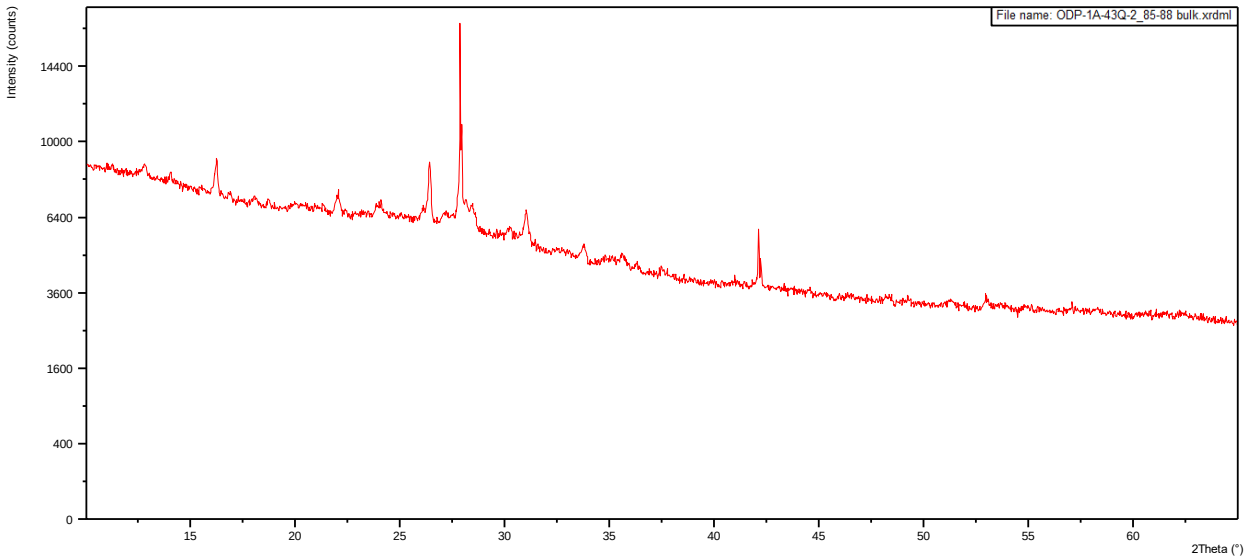
File name: ODP-1A-43Q-2_85-88 bulk.xrdml
Intensity (counts)
14400
10000
6400
3600
1600
400
0
15
20
25
30
35
40
45
50
55
60
2Theta (°)

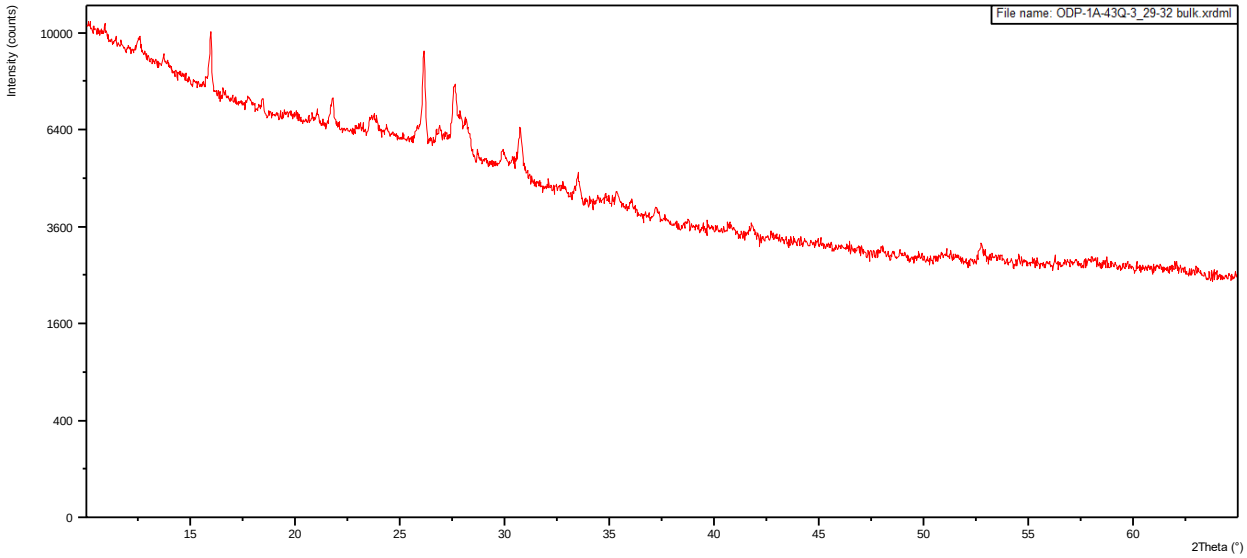
File name: ODP-1A-43Q-3_29-32 bulk.xrdml
Intensity (counts)
10000
6400
3600
1600
400
0
15
20
25
30
35
40
45
50
55
60
2Theta (°)

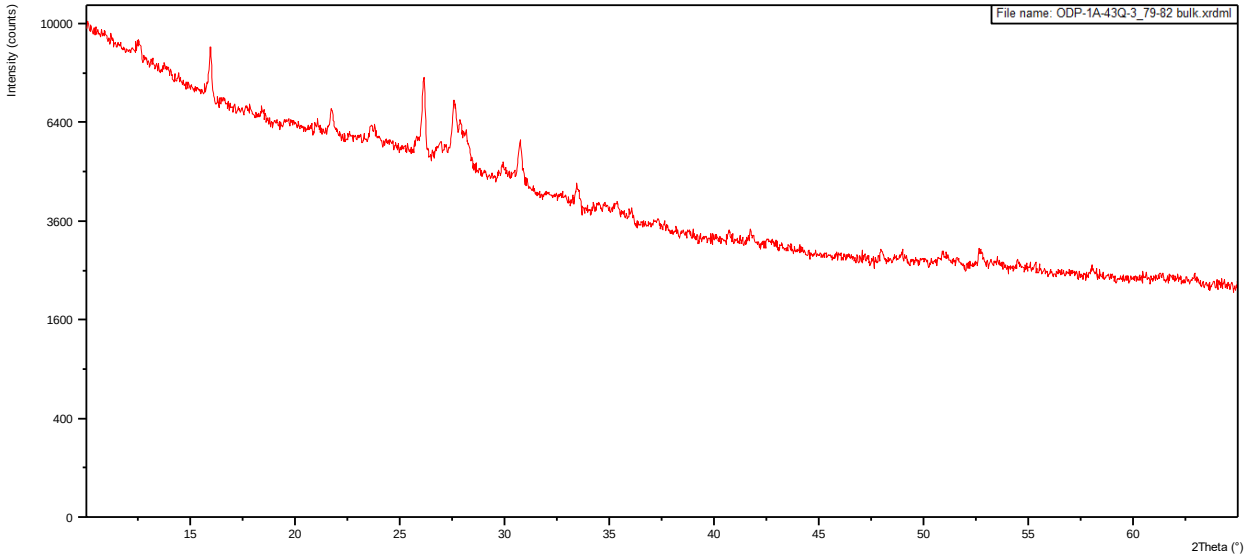
File name: ODP-1A-43Q-3_79-82 bulk.xrdml
Intensity (counts)
10000
6400
3600
1600
400
0
15
20
25
30
35
40
45
50
55
60
2Theta (°)

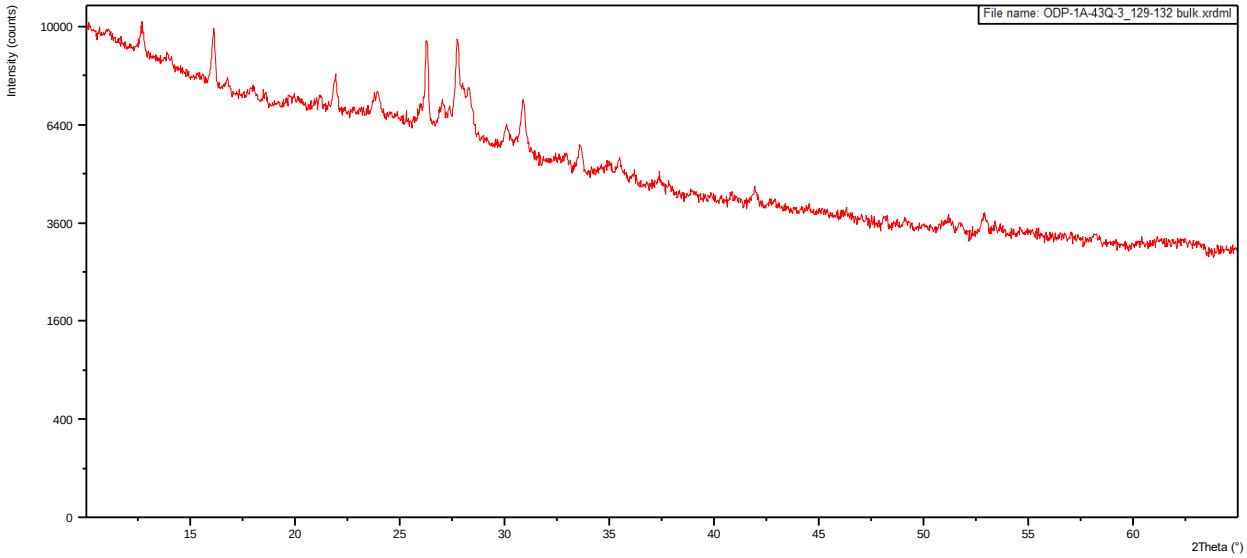
File name: ODP-1A-43Q-3_129-132 bulk.xrdml
Intensity (counts)
10000
6400
3600
1600
400
0
15
20
25
30
35
40
45
50
55
60
2Theta (°)

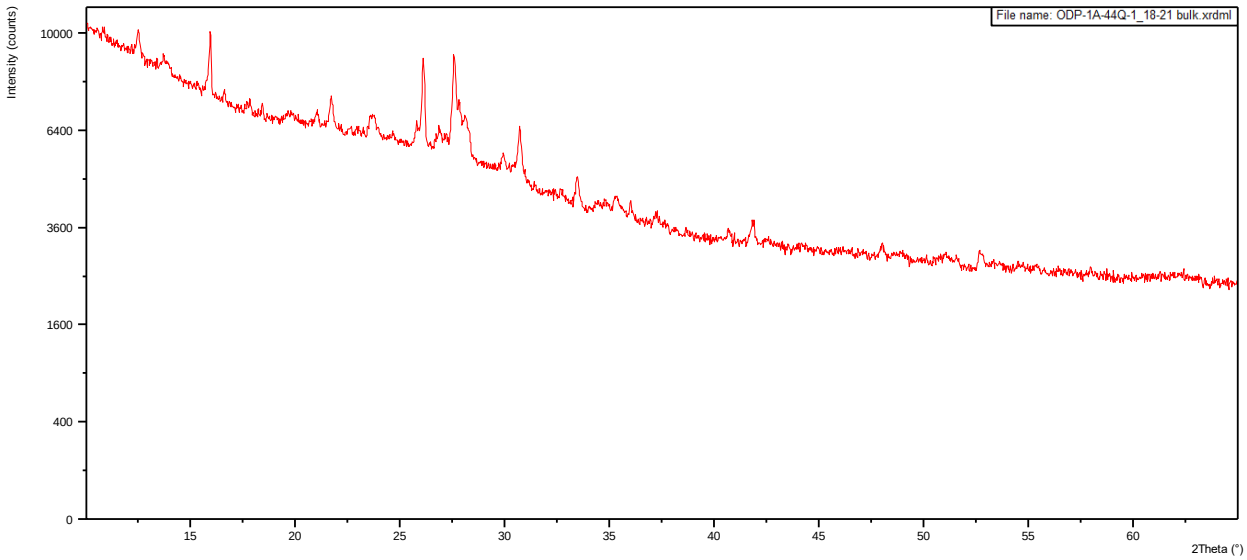
File name: ODP-1A-44Q-1_18-21 bulk.xrdml
Intensity (counts)
10000
6400
3600
1600
400
0
15
20
25
30
35
40
45
50
55
60
2Theta (°)

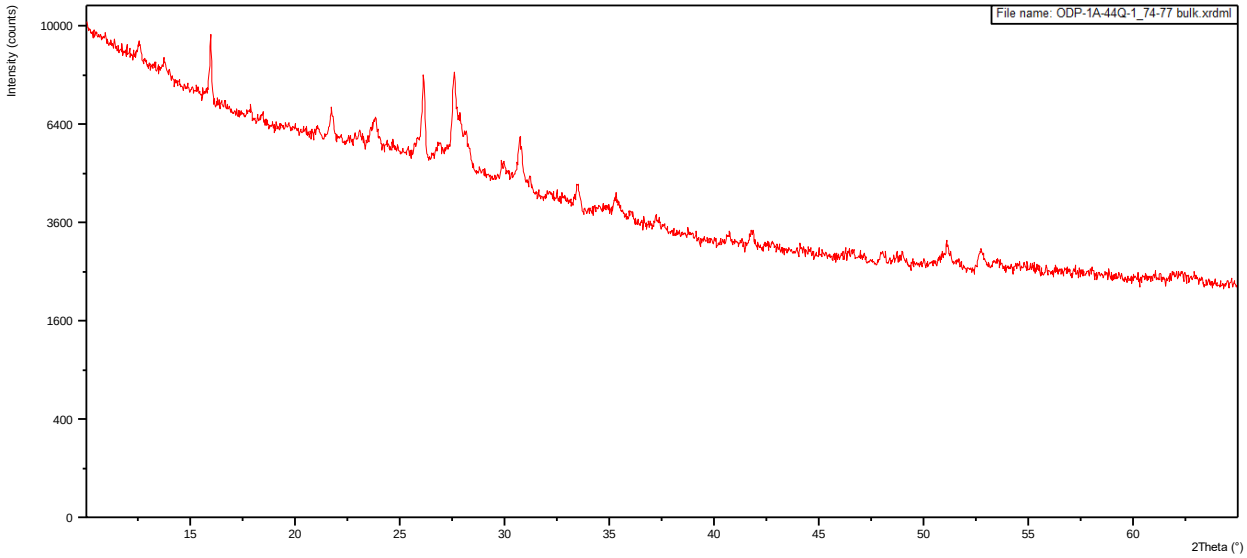
File name: ODP-1A-44Q-1_74-77 bulk.xrdml
Intensity (counts)
10000
6400
3600
1600
400
0
15
20
25
30
35
40
45
50
55
60
2Theta (°)

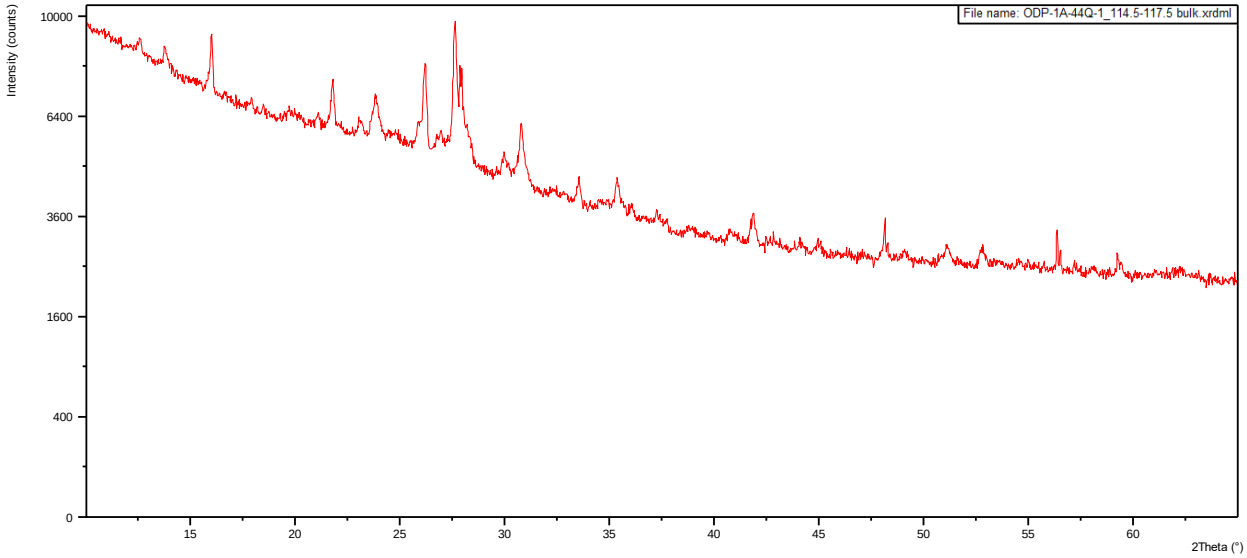
File name: ODP-1A-44Q-1_114.5-117.5 bulk.xrdml
Intensity (counts)
10000
6400
3600
1600
400
0
15
20
25
30
35
40
45
50
55
60
2Theta (°)

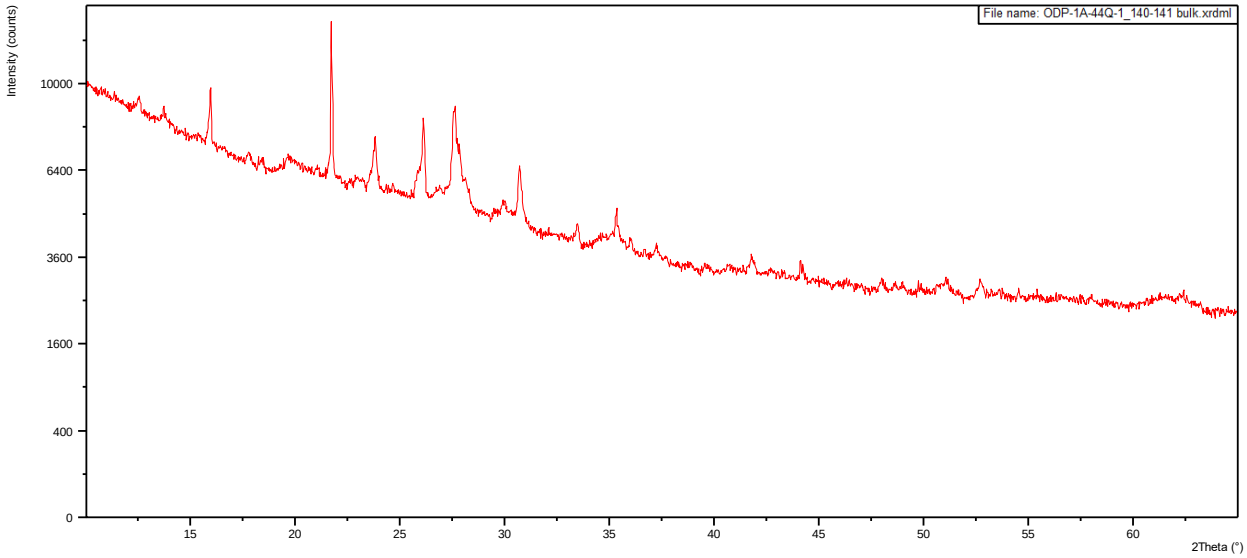
File name: ODP-1A-44Q-1_140-141 bulk.xrdml
Intensity (counts)
10000
6400
3600
1600
400
0
15
20
25
30
35
40
45
50
55
60
2Theta (°)

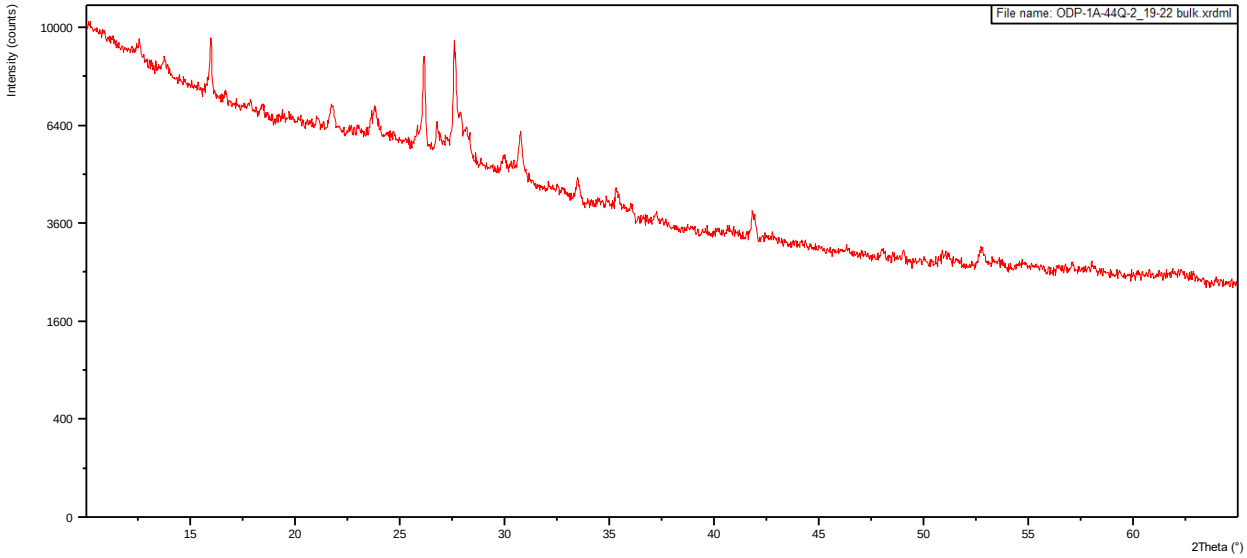
File name: ODP-1A-44Q-2_19-22 bulk.xrdml
Intensity (counts)
10000
6400
3600
1600
400
0
15
20
25
30
35
40
45
50
55
60
2Theta (°)

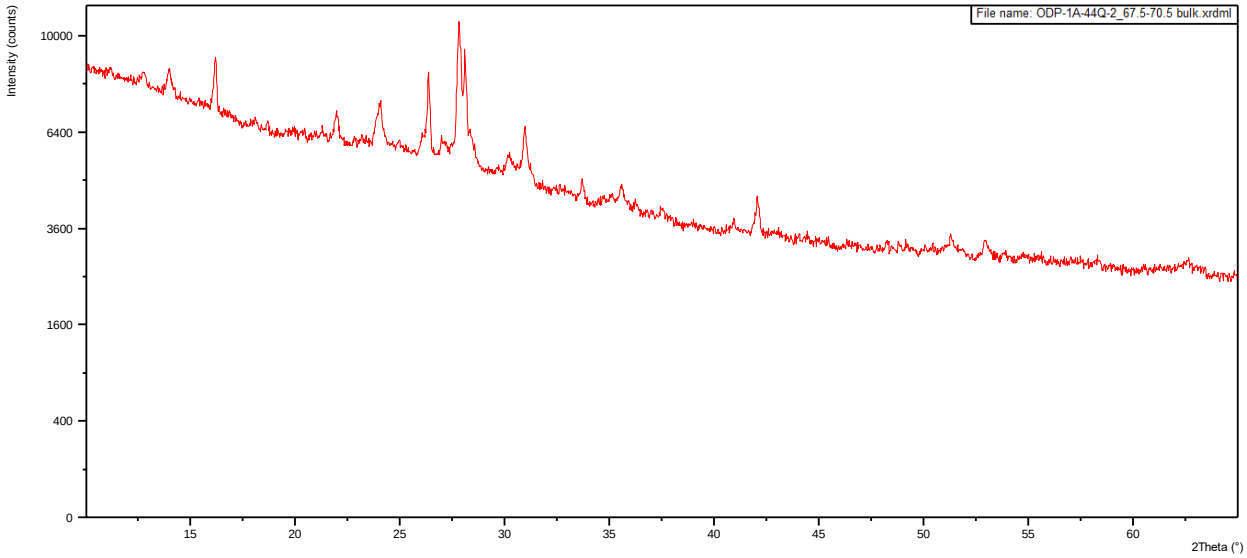
File name: ODP-1A-44Q-2_67.5-70.5 bulk.xrdml
Intensity (counts)
10000
6400
3600
1600
400
0
15
20
25
30
35
40
45
50
55
60
2Theta (°)

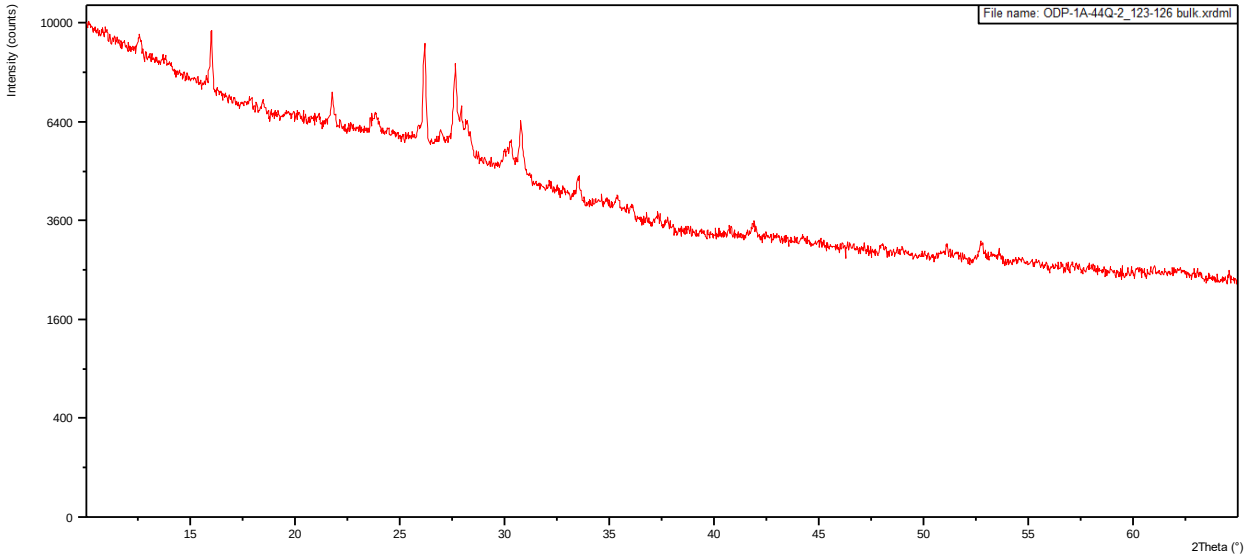
File name: ODP-1A-44Q-2_123-126 bulk.xrdml
Intensity (counts)
10000
6400
3600
1600
400
0
15
20
25
30
35
40
45
50
55
60
2Theta (°)

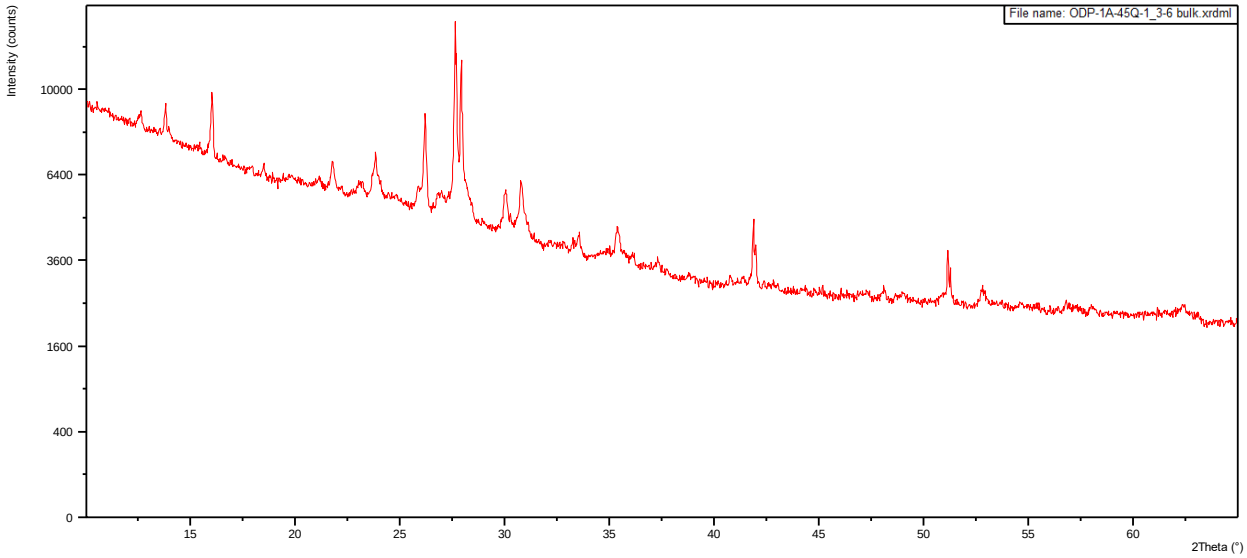
File name: ODP-1A-45Q-1_3-6 bulk.xrdml
Intensity (counts)
10000
6400
3600
1600
400
0
15
20
25
30
35
40
45
50
55
60
2Theta (°)

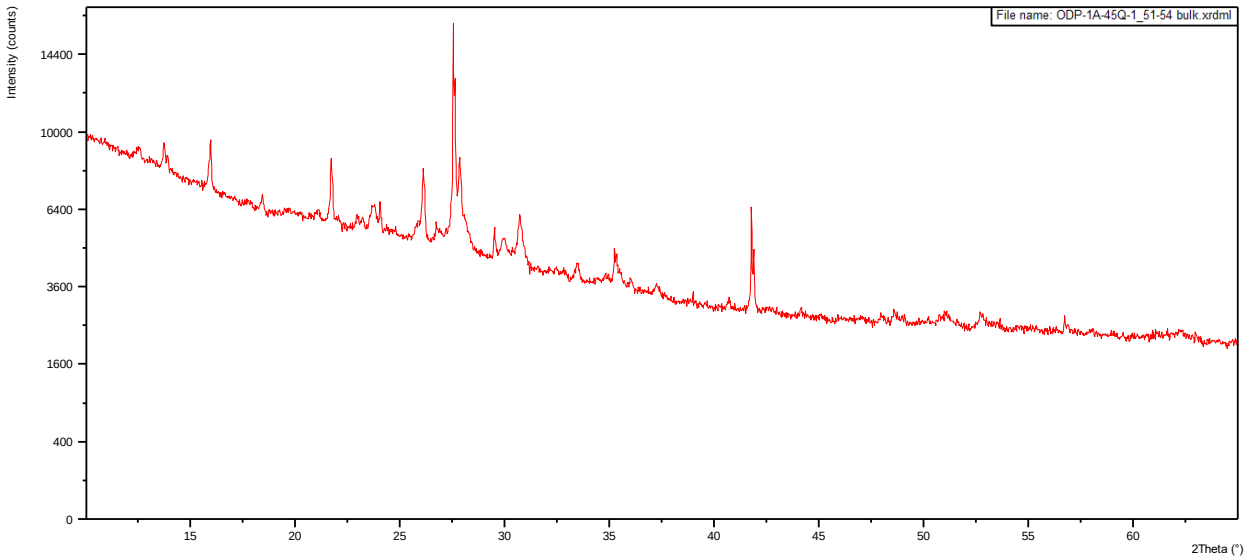
File name: ODP-1A-45Q-1_51-54 bulk.xrdml
Intensity (counts)
14400
10000
6400
3600
1600
400
0
15
20
25
30
35
40
45
50
55
60
2Theta (°)

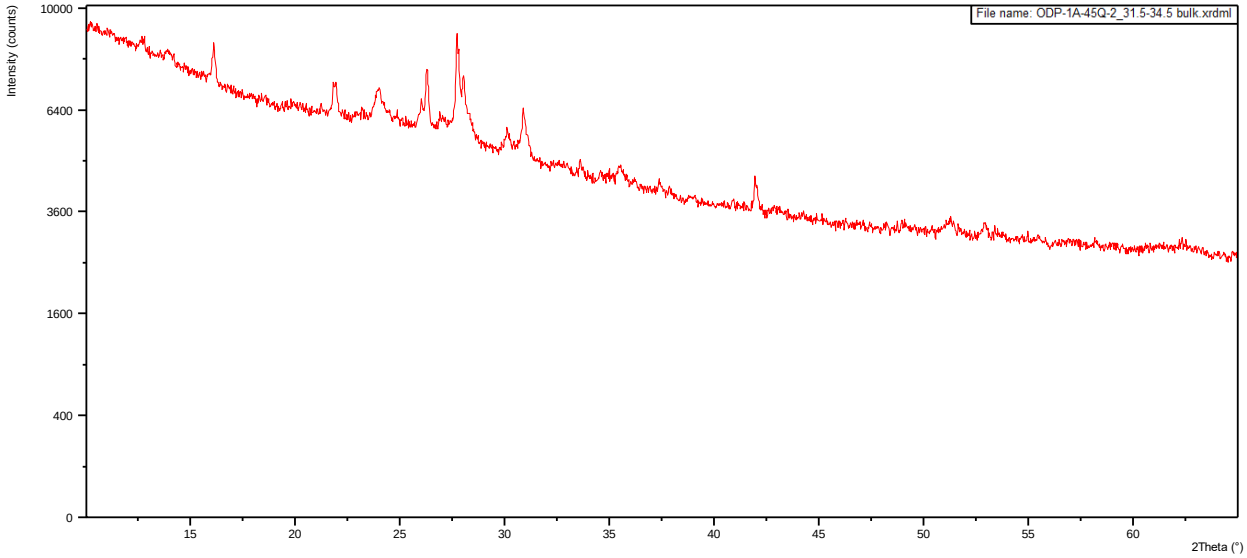
File name: ODP-1A-45Q-2_31.5-34.5 bulk.xrdml
Intensity (counts)
10000
6400
3600
1600
400
0
15
20
25
30
35
40
45
50
55
60
2Theta (°)

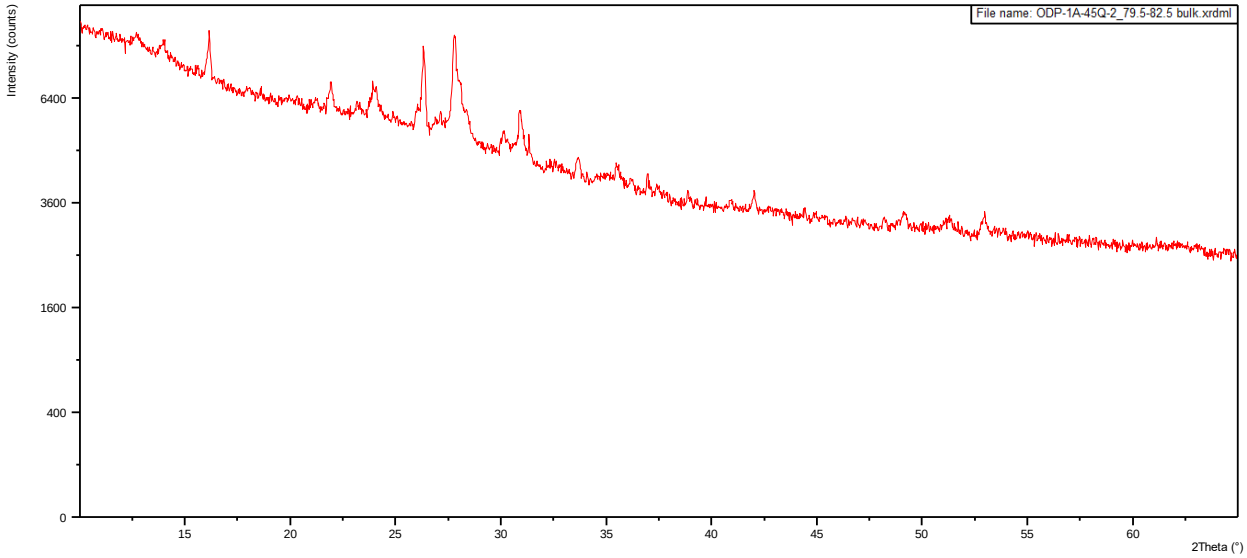
File name: ODP-1A-45Q-2_79.5-82.5 bulk.xrdml
Intensity (counts)
6400
3600
1600
400
0
15
20
25
30
35
40
45
50
55
60
2Theta (°)

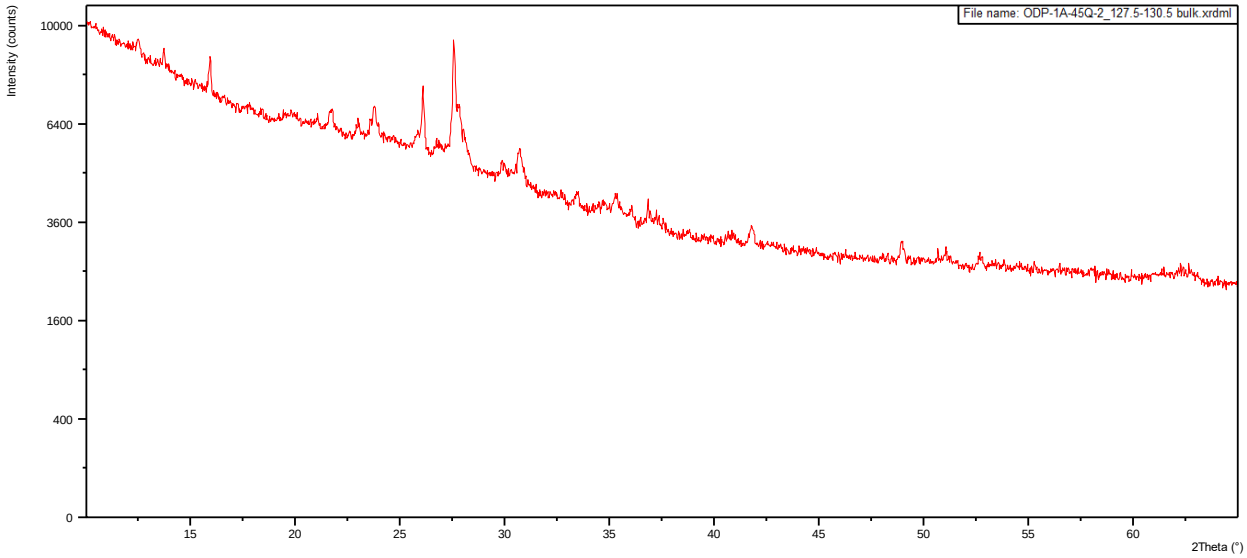
File name: ODP-1A-45Q-2_127.5-130.5 bulk.xrdml
Intensity (counts)
10000
6400
3600
1600
400
0
15
20
25
30
35
40
45
50
55
60
2Theta (°)

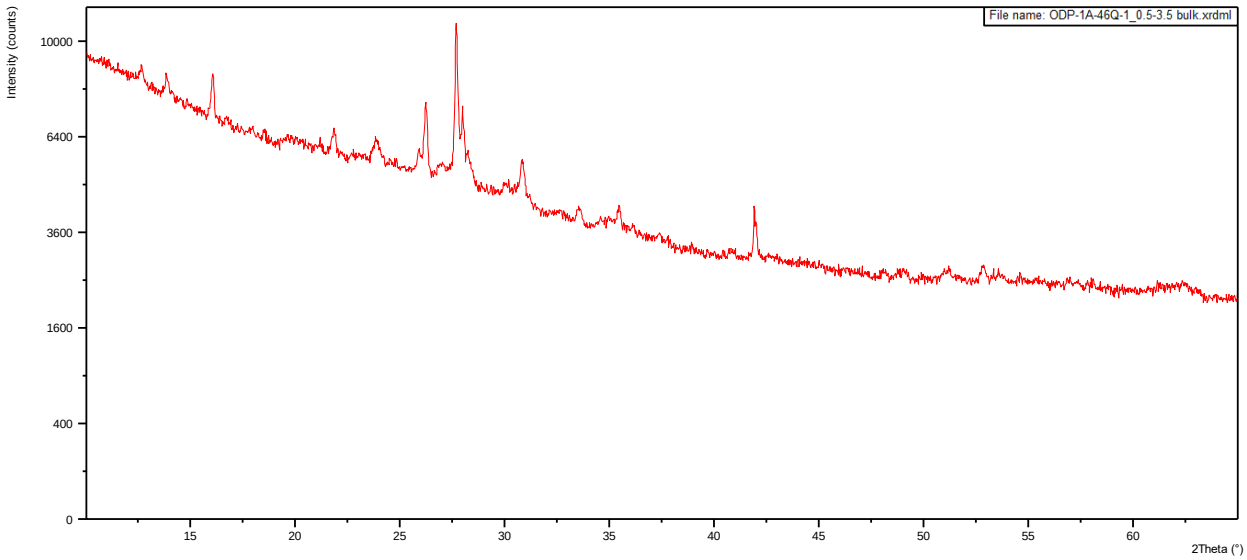
File name: ODP-1A-46Q-1_0.5-3.5 bulk.xrdml
Intensity (counts)
10000
6400
3600
1600
400
0
15
20
25
30
35
40
45
50
55
60
2Theta (°)

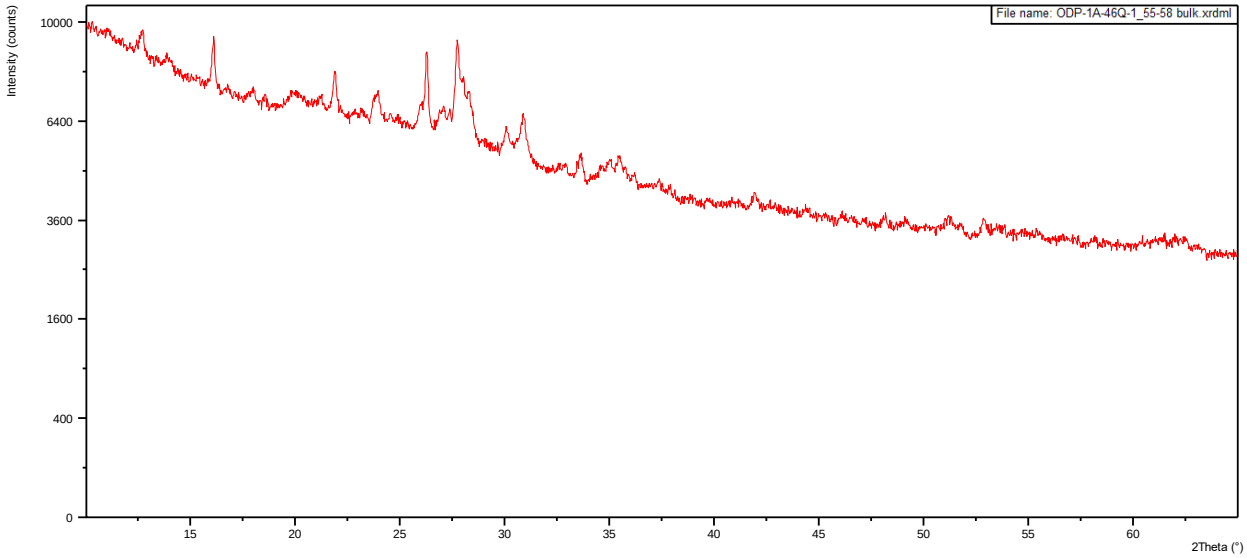
File name: ODP-1A-46Q-1_55-58 bulk.xrdml
Intensity (counts)
10000
6400
3600
1600
400
0
15
20
25
30
35
40
45
50
55
60
2Theta (°)

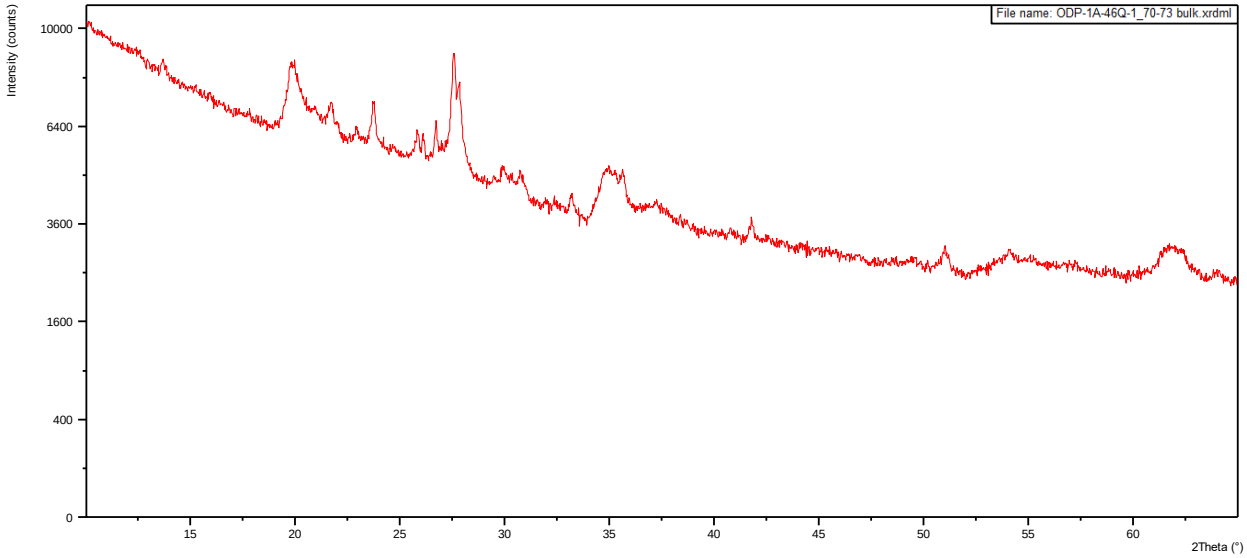
File name: ODP-1A-46Q-1_70-73 bulk.xrdml
Intensity (counts)
10000
6400
3600
1600
400
0
15
20
25
30
35
40
45
50
55
60
2Theta (°)

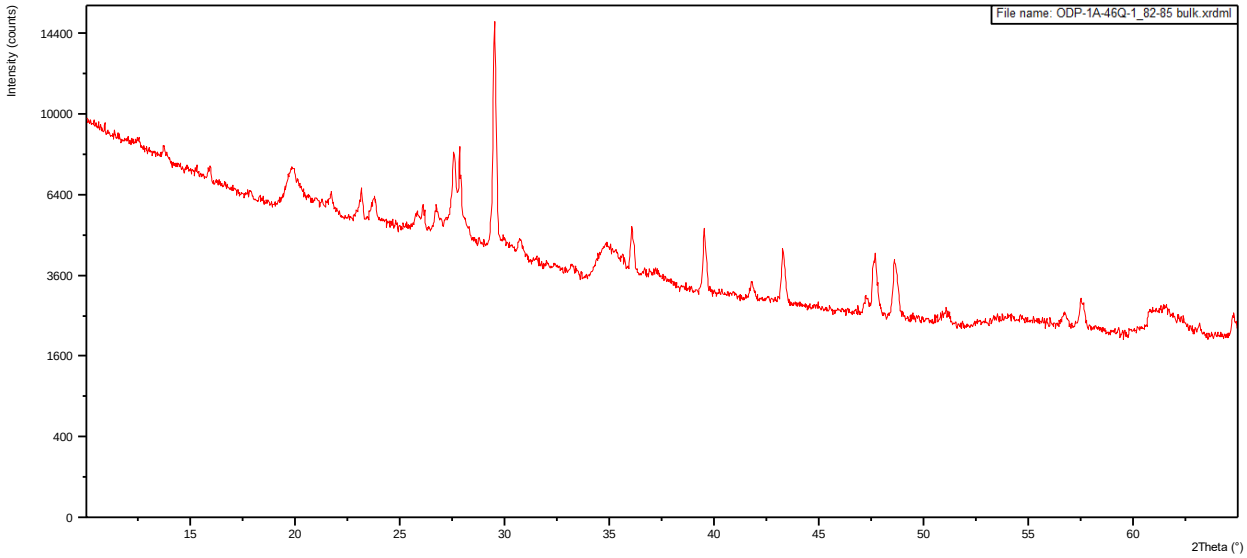
File name: ODP-1A-46Q-1_82-85 bulk.xrdml
Intensity (counts)
14400
10000
6400
3600
1600
400
0
15
20
25
30
35
40
45
50
55
60
2Theta (°)

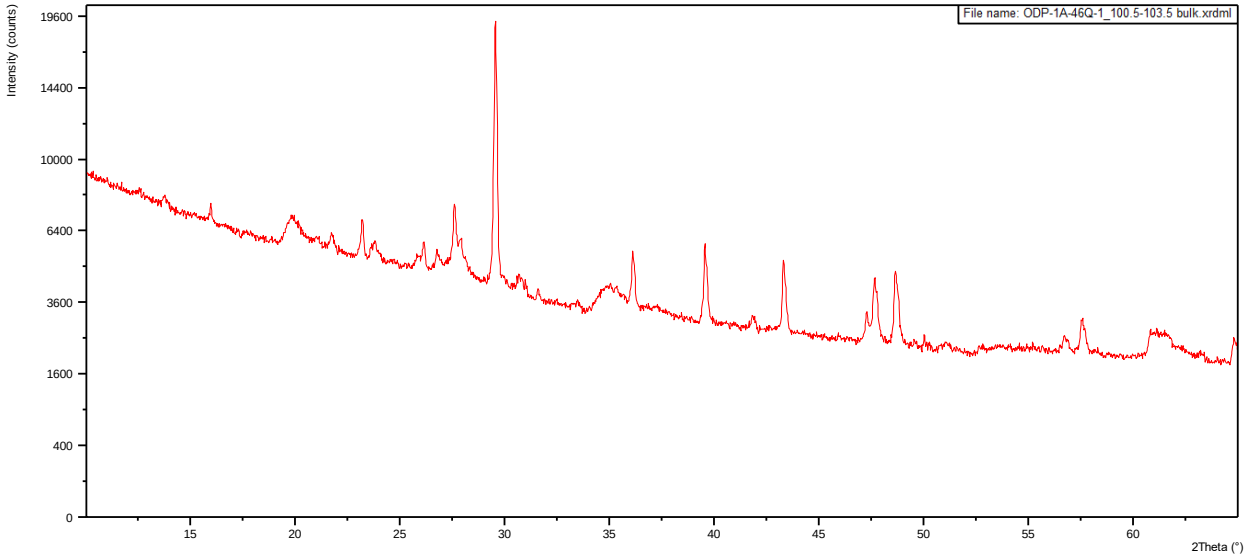
File name: ODP-1A-46Q-1_100.5-103.5 bulk.xrdml
Intensity (counts)
19600
14400
10000
6400
3600
1600
400
0
15
20
25
30
35
40
45
50
55
60
2Theta (°)

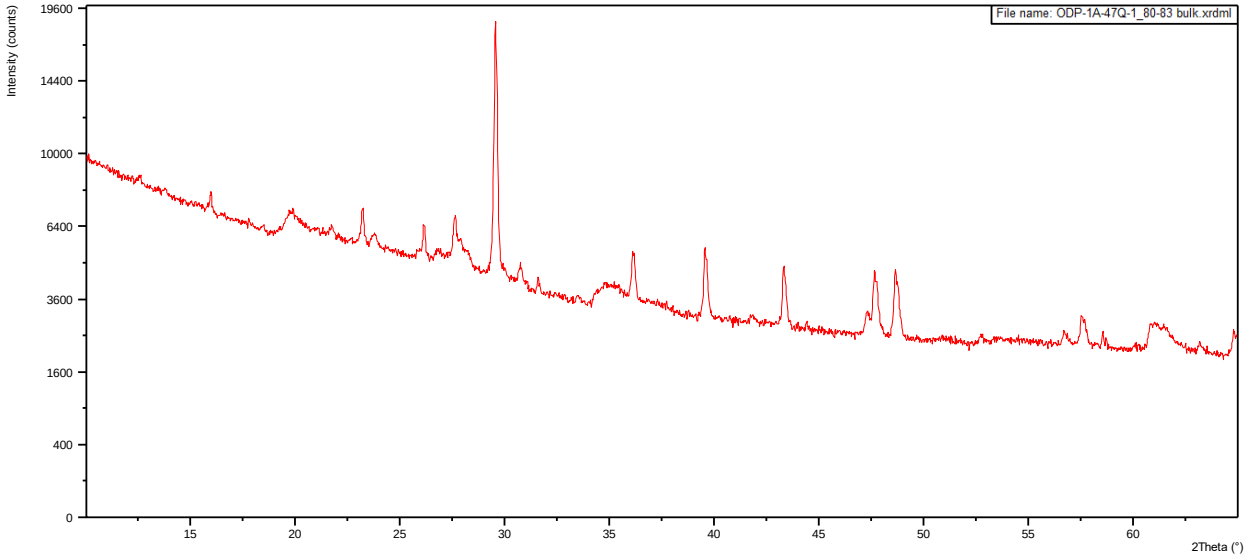
File name: ODP-1A-47Q-1_80-83 bulk.xrdml
Intensity (counts)
19600
14400
10000
6400
3600
1600
400
0
15
20
25
30
35
40
45
50
55
60
2Theta (°)

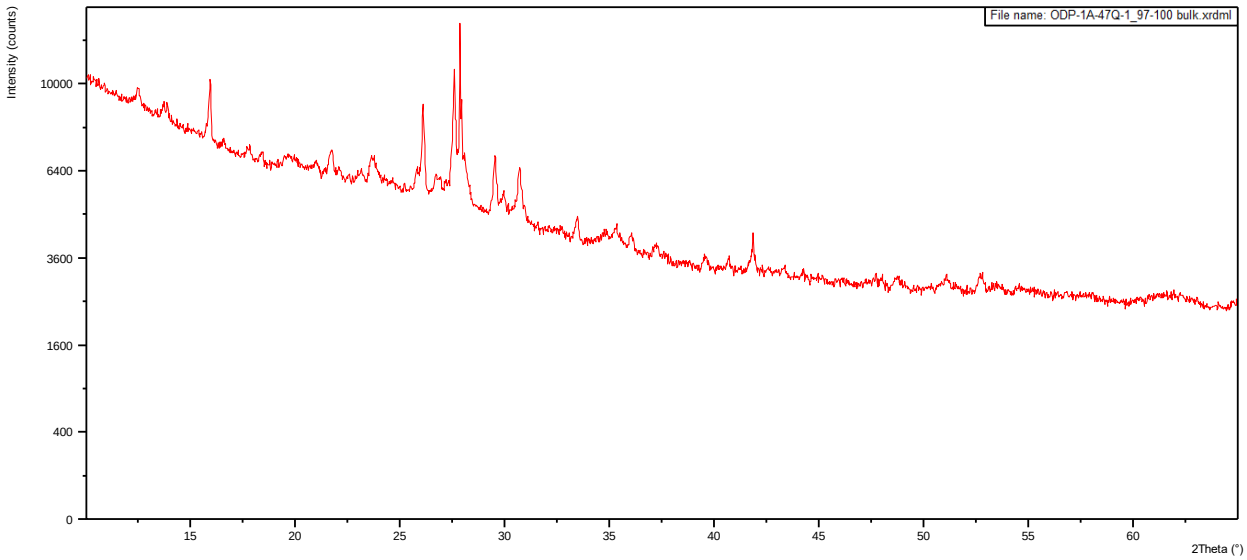
File name: ODP-1A-47Q-1_97-100 bulk.xrdml
Intensity (counts)
10000
6400
3600
1600
400
0
15
20
25
30
35
40
45
50
55
60
2Theta (°)

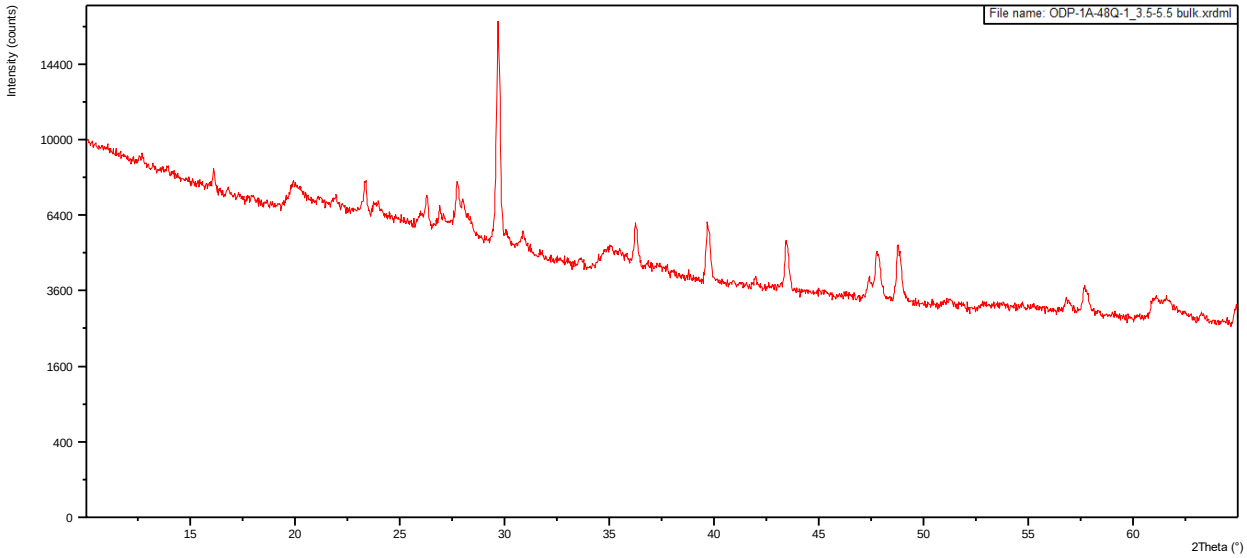
File name: ODP-1A-48Q-1_3.5-5.5 bulk.xrdml
Intensity (counts)
14400
10000
6400
3600
1600
400
0
15
20
25
30
35
40
45
50
55
60
2Theta (°)

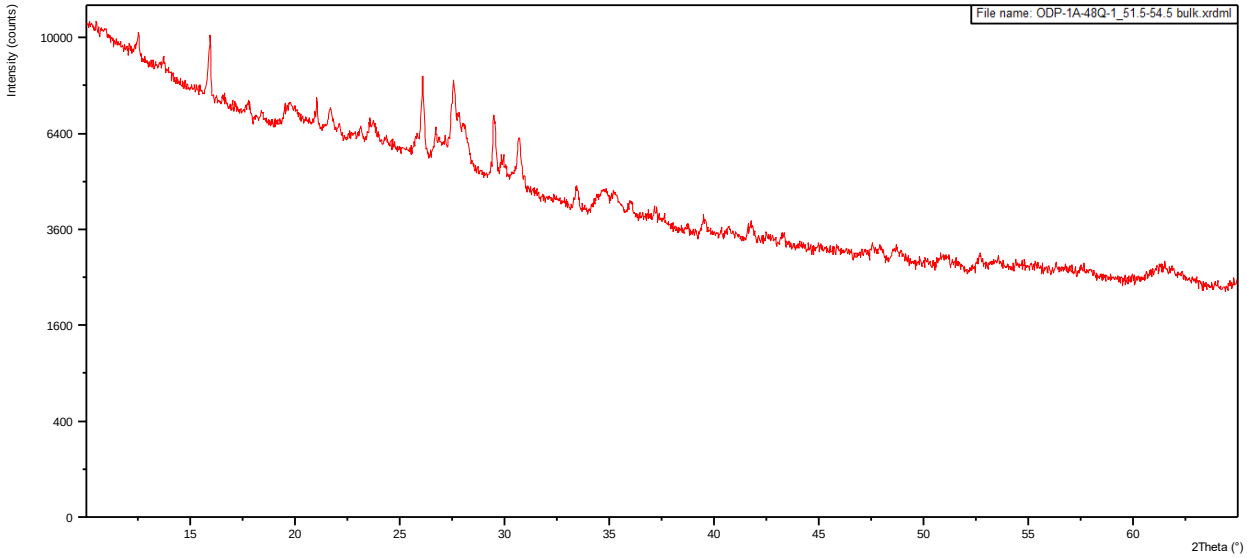
File name: ODP-1A-48Q-1_51.5-54.5 bulk.xrdml
Intensity (counts)
10000
6400
3600
1600
400
0
15
20
25
30
35
40
45
50
55
60
2Theta (°)

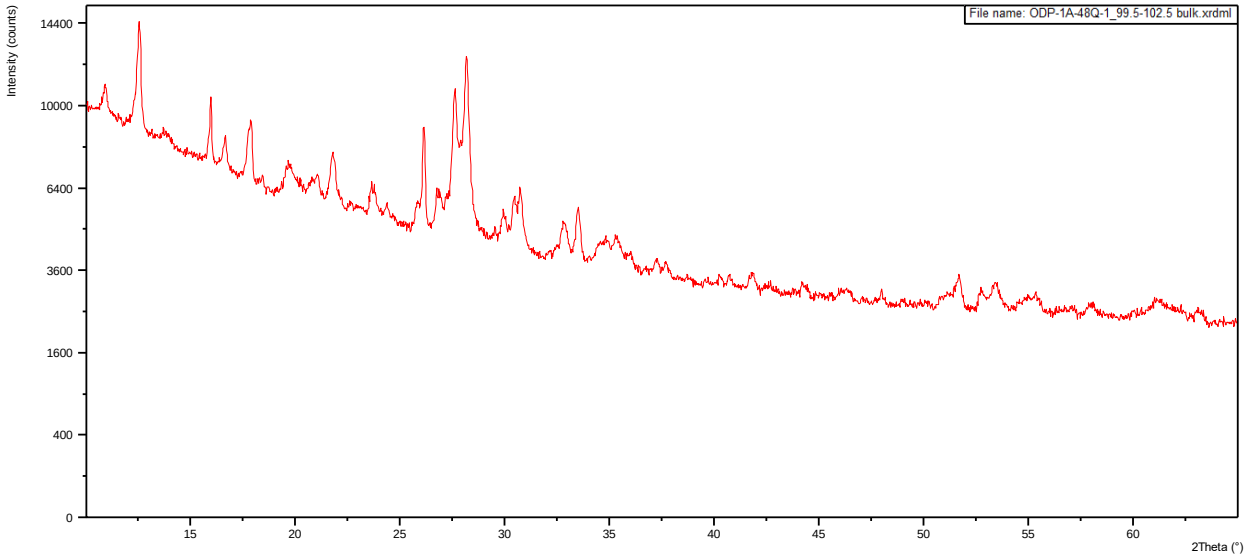
File name: ODP-1A-48Q-1_99.5-102.5 bulk.xrdml
Intensity (counts)
14400
10000
6400
3600
1600
400
0
15
20
25
30
35
40
45
50
55
60
2Theta (°)

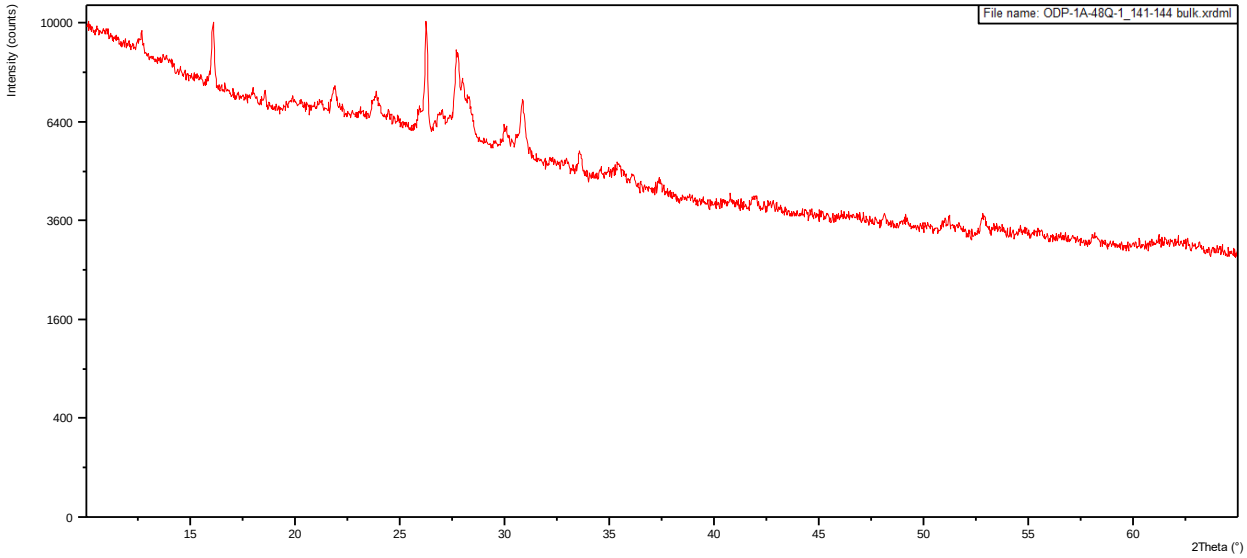
File name: ODP-1A-48Q-1_141-144 bulk.xrdml
Intensity (counts)
10000
6400
3600
1600
400
0
15
20
25
30
35
40
45
50
55
60
2Theta (°)

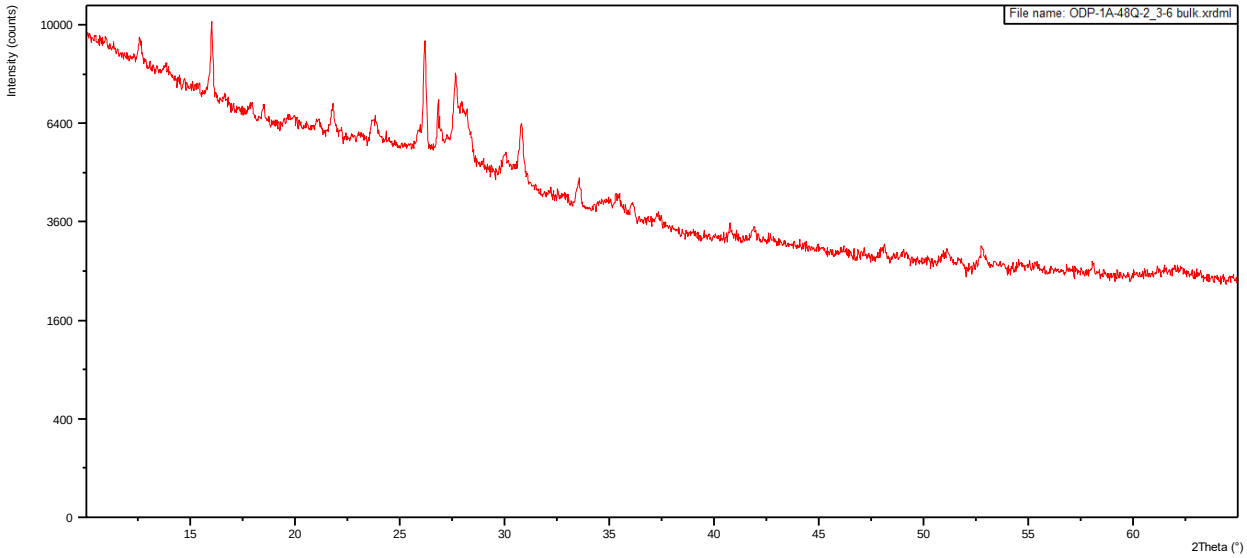
File name: ODP-1A-48Q-2_3-6 bulk.xrdml
Intensity (counts)
10000
6400
3600
1600
400
0
15
20
25
30
35
40
45
50
55
60
2Theta (°)

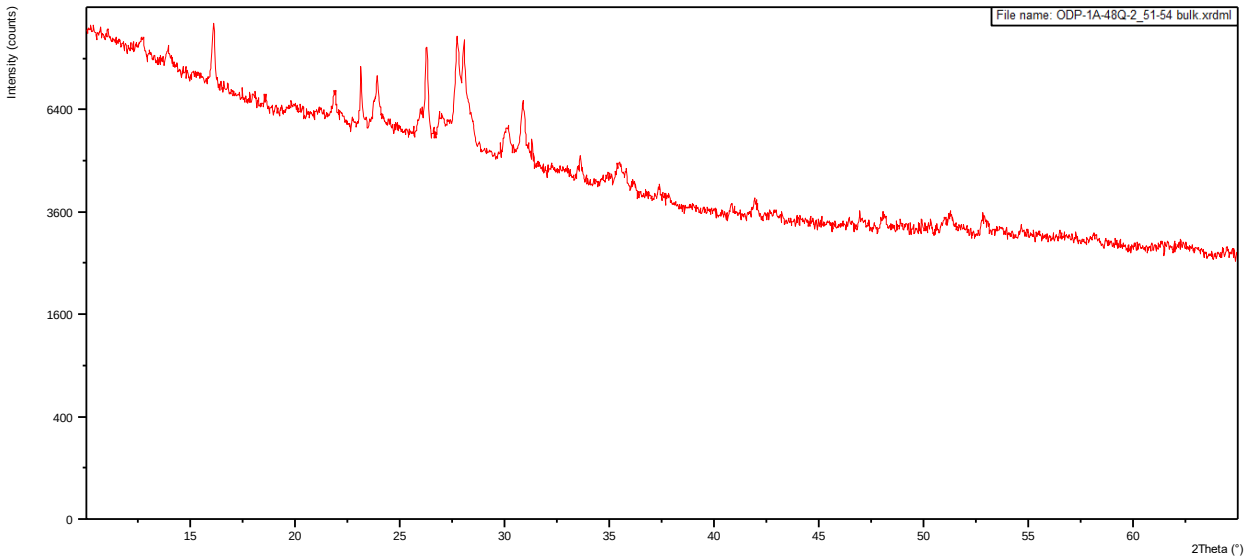
File name: ODP-1A-48Q-2_51-54 bulk.xrdml
Intensity (counts)
6400
3600
1600
400
0
15
20
25
30
35
40
45
50
55
60
2Theta (°)

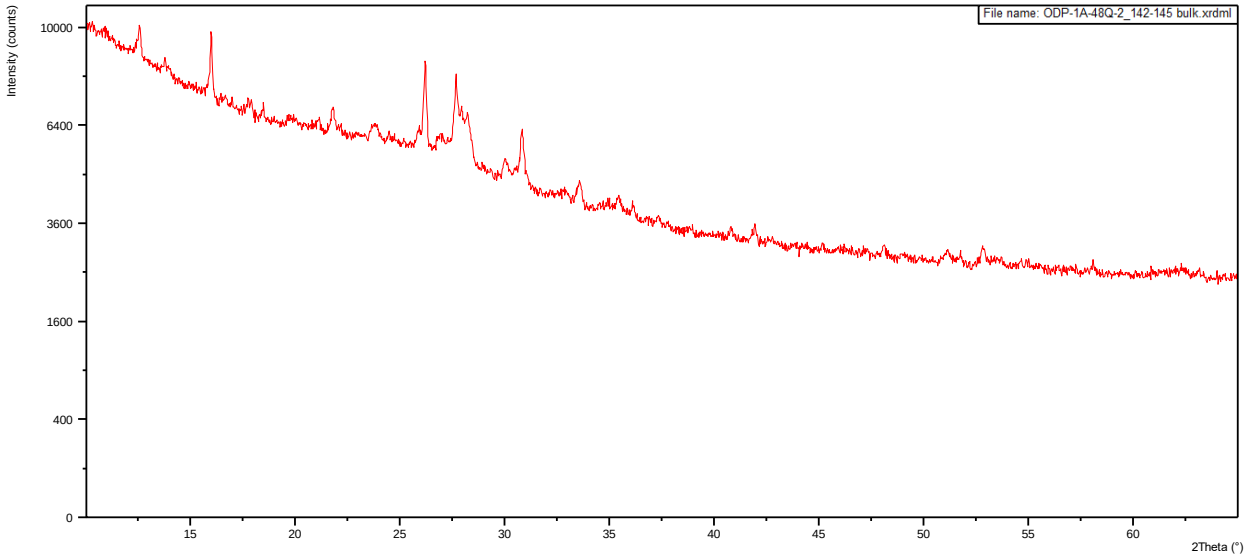
File name: ODP-1A-48Q-2_142-145 bulk.xrdml
Intensity (counts)
10000
6400
3600
1600
400
0
15
20
25
30
35
40
45
50
55
60
2Theta (°)

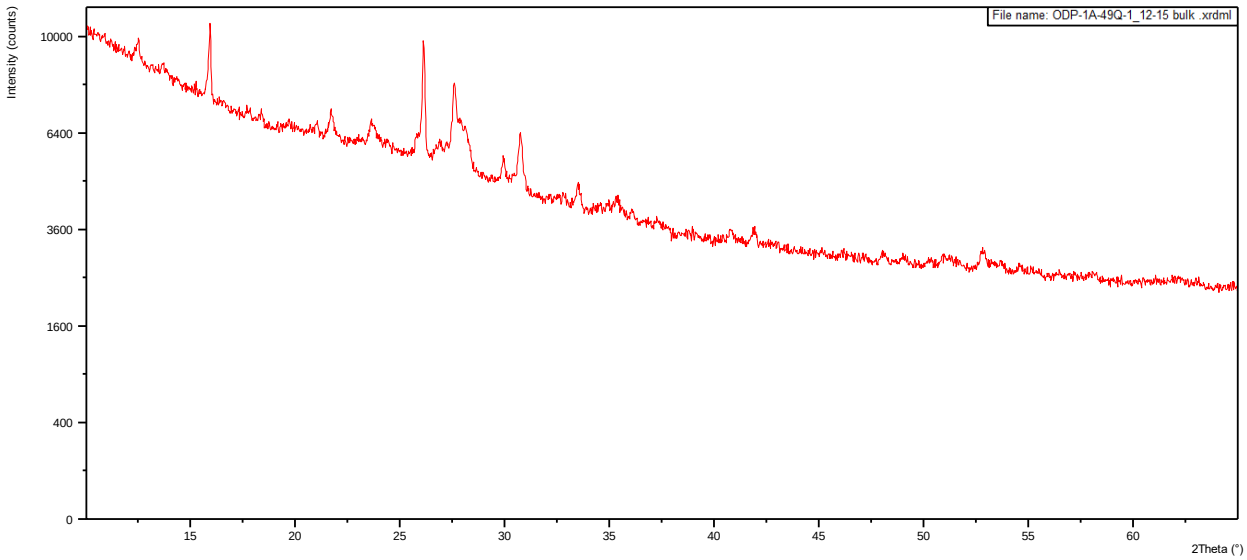
File name: ODP-1A-49Q-1_12-15 bulk .xrdml
Intensity (counts)
10000
6400
3600
1600
400
0
15
20
25
30
35
40
45
50
55
60
2Theta (°)

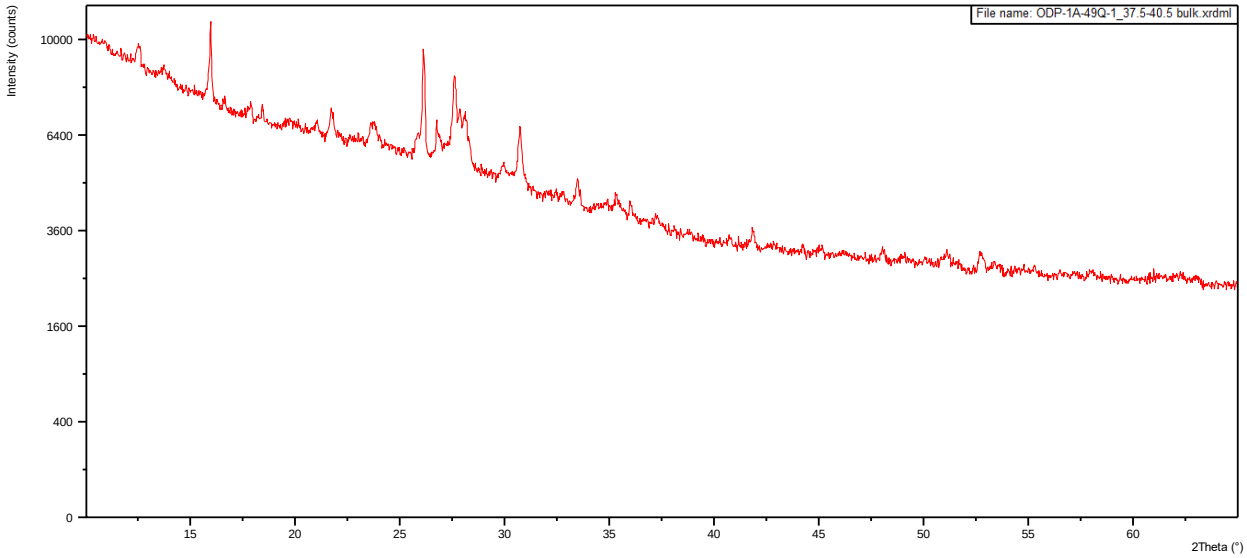
File name: ODP-1A-49Q-1_37.5-40.5 bulk.xrdml
Intensity (counts)
10000
6400
3600
1600
400
0
15
20
25
30
35
40
45
50
55
60
2Theta (°)

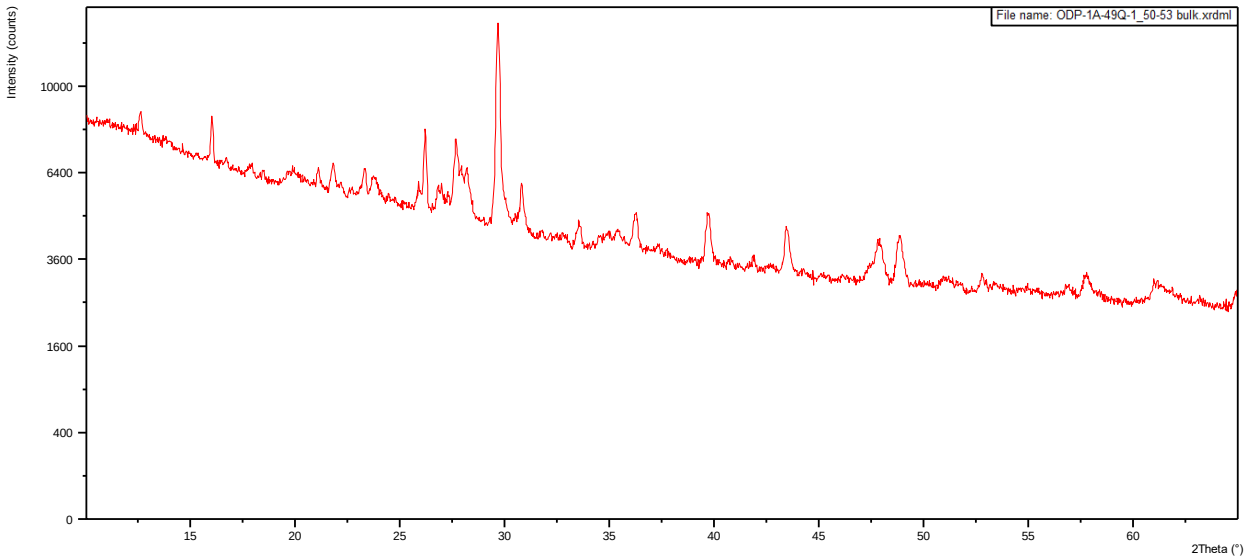
File name: ODP-1A-49Q-1_50-53 bulk.xrdml
Intensity (counts)
10000
6400
3600
1600
400
0
15
20
25
30
35
40
45
50
55
60
2Theta (°)

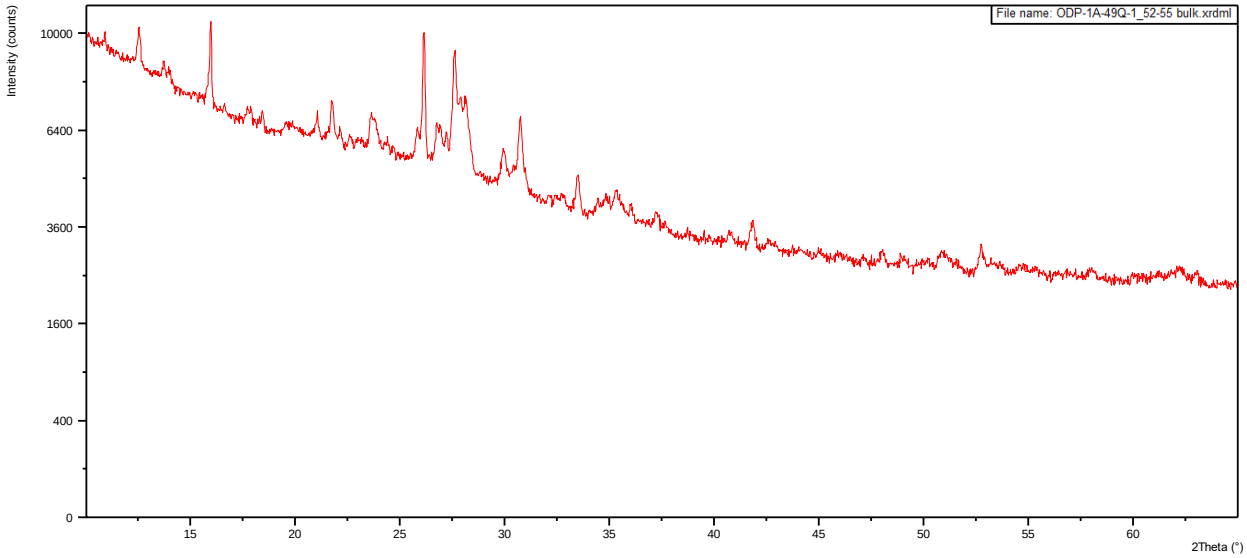
File name: ODP-1A-49Q-1_52-55 bulk.xrdml
Intensity (counts)
10000
6400
3600
1600
400
0
15
20
25
30
35
40
45
50
55
60
2Theta (°)

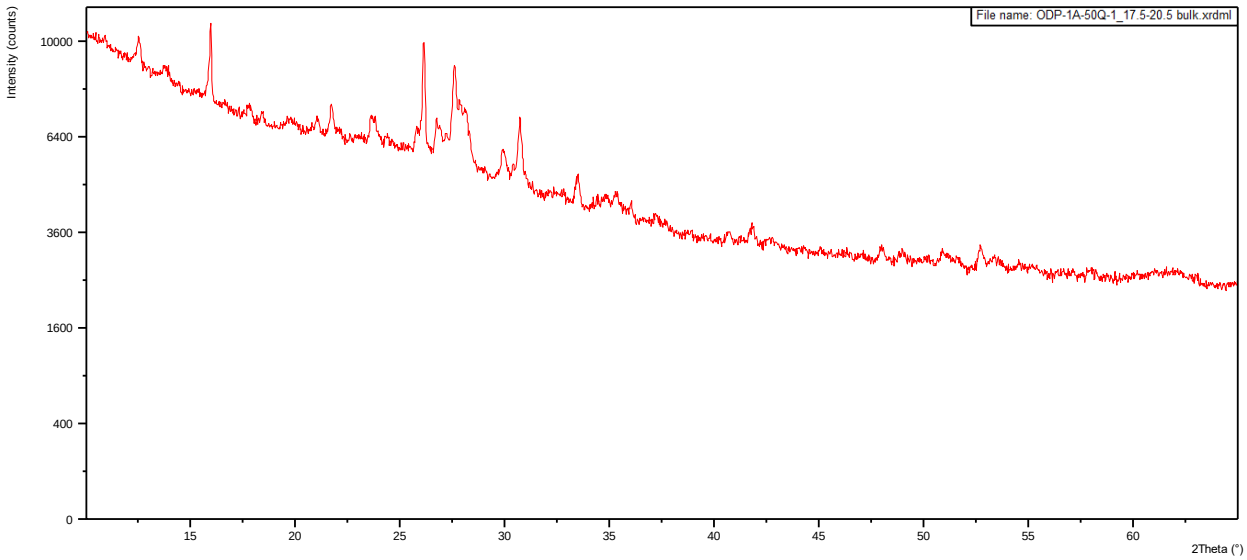
File name: ODP-1A-50Q-1_17.5-20.5 bulk.xrdml
Intensity (counts)
10000
6400
3600
1600
400
0
15
20
25
30
35
40
45
50
55
60
2Theta (°)

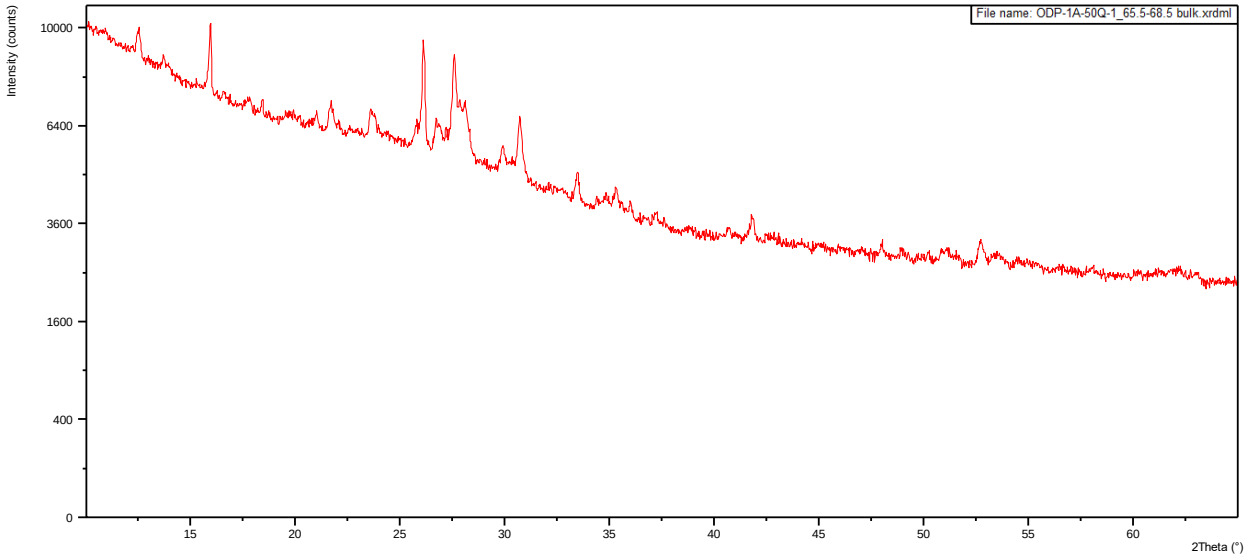
File name: ODP-1A-50Q-1_65.5-68.5 bulk.xrdml
Intensity (counts)
10000
6400
3600
1600
400
0
15
20
25
30
35
40
45
50
55
60
2Theta (°)

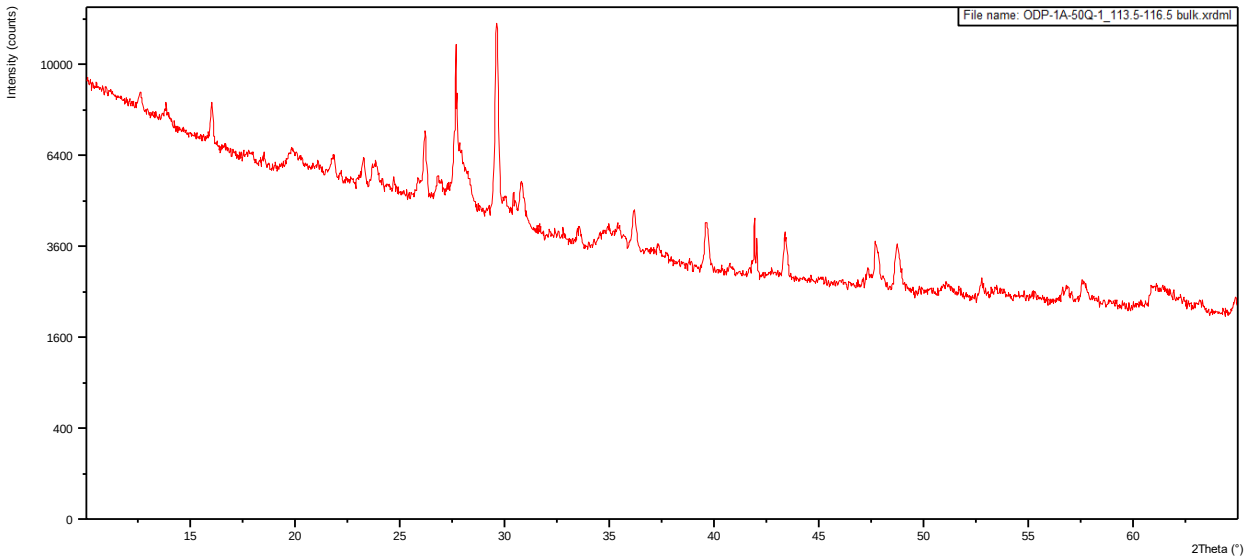
File name: ODP-1A-50Q-1_113.5-116.5 bulk.xrdml
Intensity (counts)
10000
6400
3600
1600
400
0
15
20
25
30
35
40
45
50
55
60
2Theta (°)

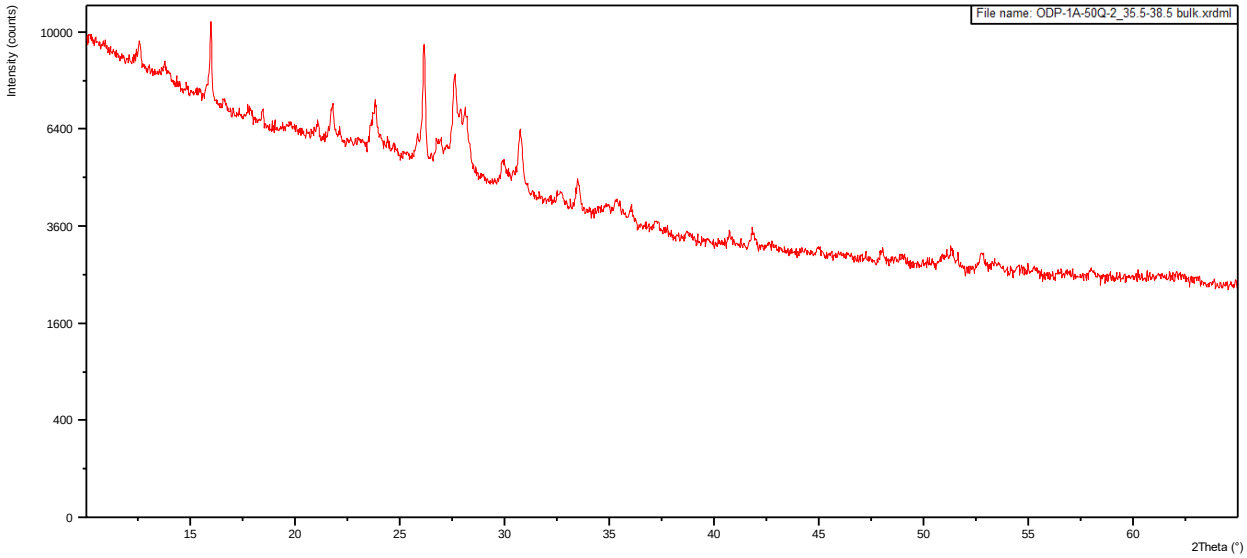
File name: ODP-1A-50Q-2_35.5-38.5 bulk.xrdml
Intensity (counts)
10000
6400
3600
1600
400
0
15
20
25
30
35
40
45
50
55
60
2Theta (°)

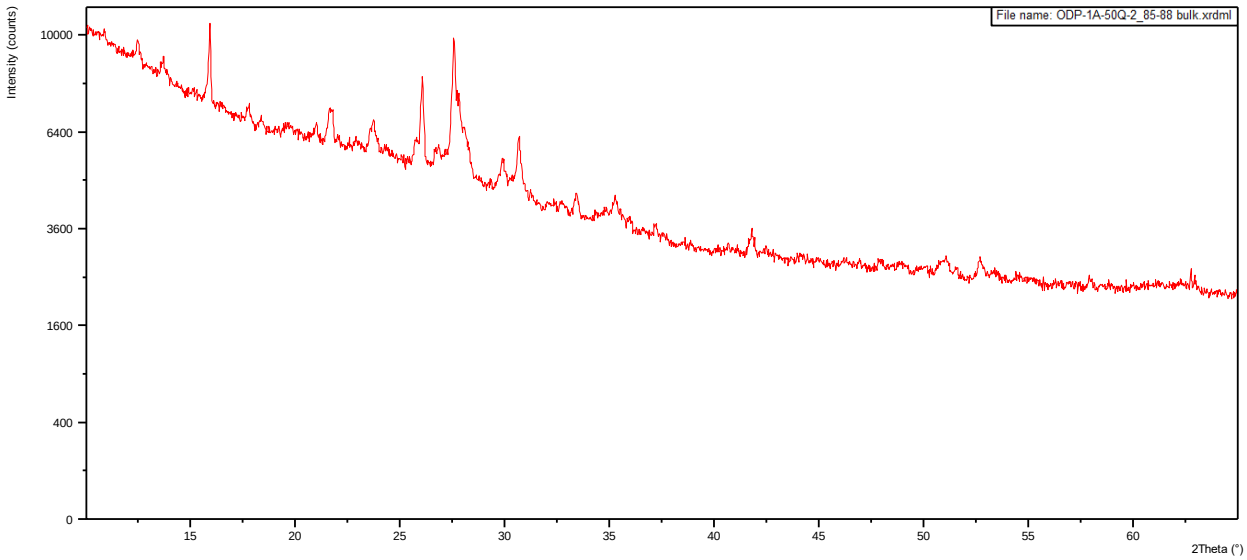
File name: ODP-1A-50Q-2_85-88 bulk.xrdml
Intensity (counts)
10000
6400
3600
1600
400
0
15
20
25
30
35
40
45
50
55
60
2Theta (°)

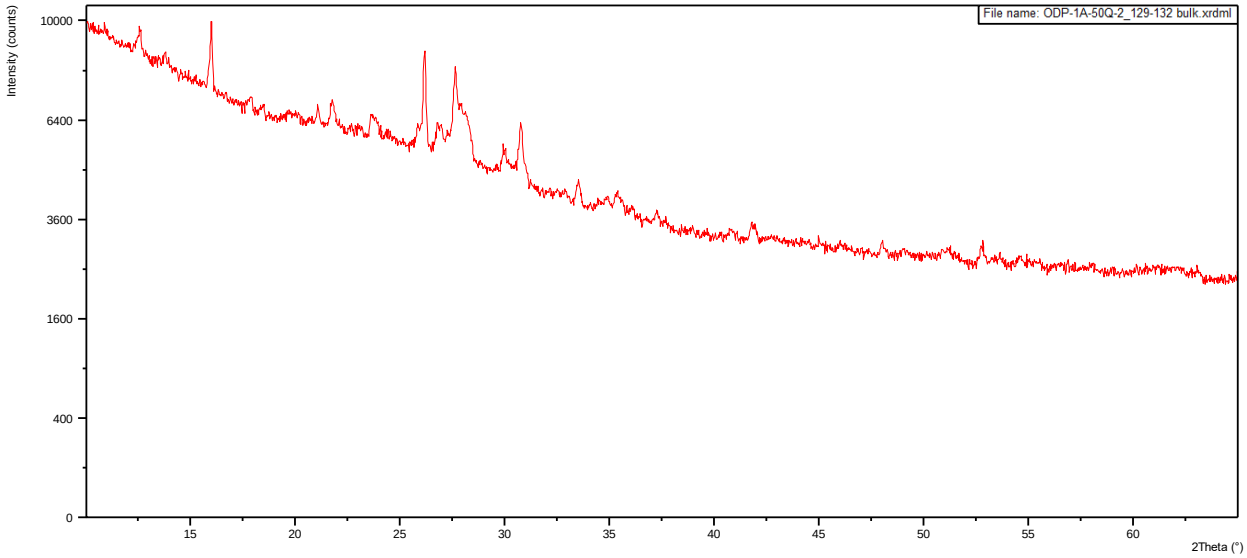
File name: ODP-1A-50Q-2_129-132 bulk.xrdml
Intensity (counts)
10000
6400
3600
1600
400
0
15
20
25
30
35
40
45
50
55
60
2Theta (°)

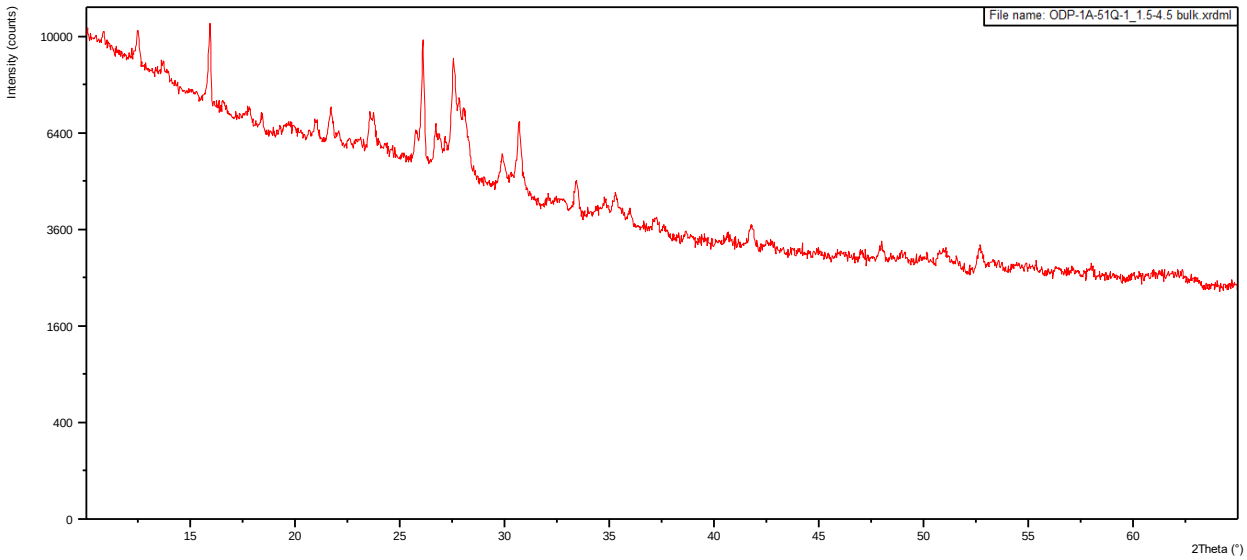
File name: ODP-1A-51Q-1_1.5-4.5 bulk.xrdml
Intensity (counts)
10000
6400
3600
1600
400
0
15
20
25
30
35
40
45
50
55
60
2Theta (°)

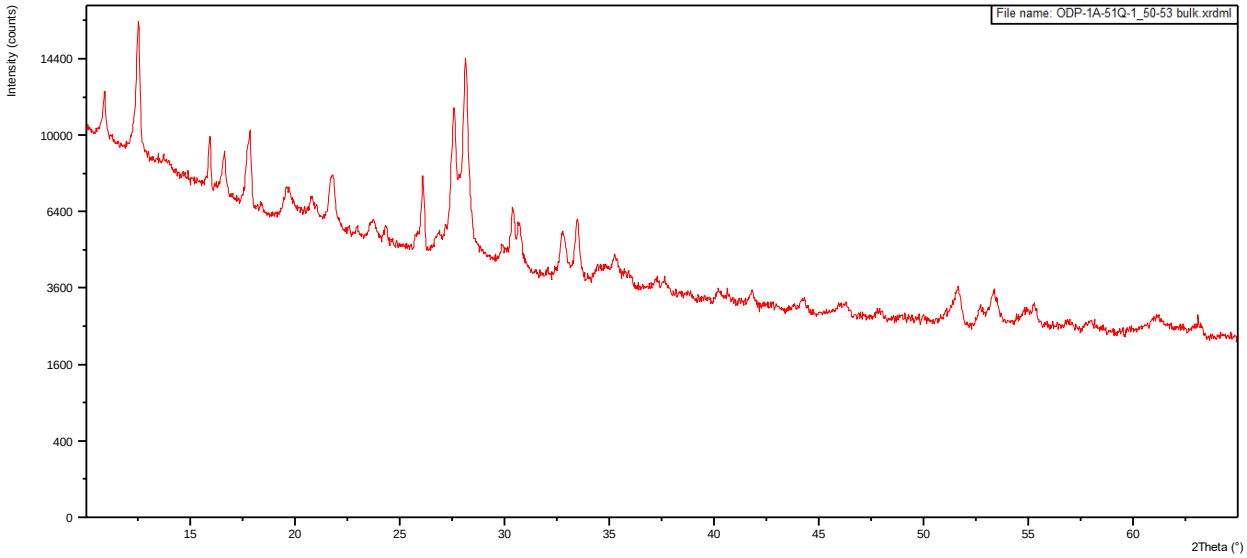
File name: ODP-1A-51Q-1_50-53 bulk.xrdml
Intensity (counts)
14400
10000
6400
3600
1600
400
0
15
20
25
30
35
40
45
50
55
60
2Theta (°)

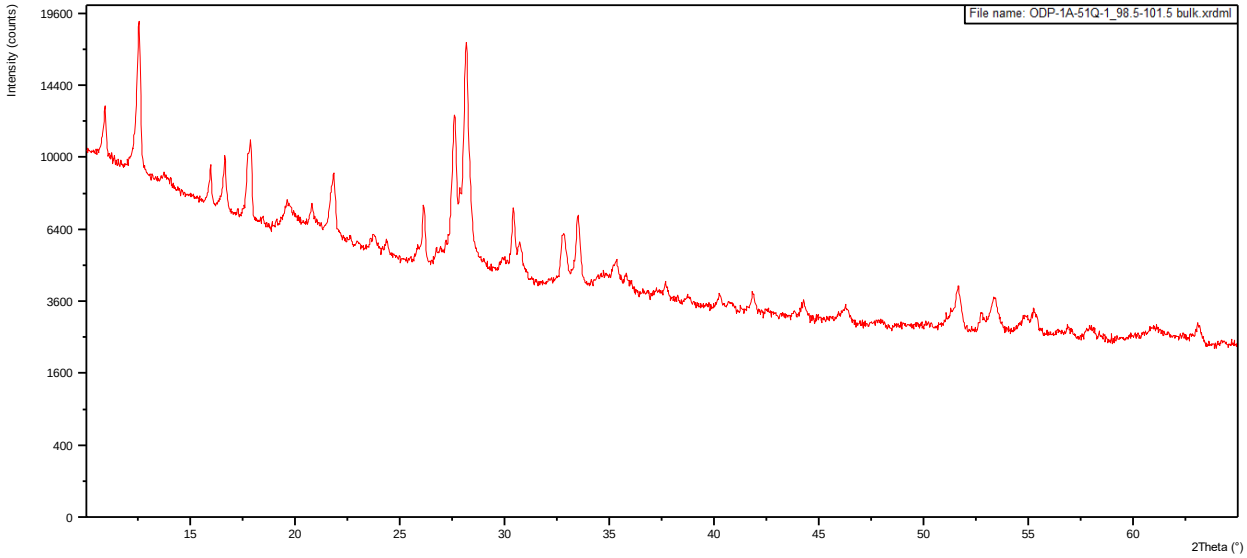
File name: ODP-1A-51Q-1_98.5-101.5 bulk.xrdml
Intensity (counts)
19600
14400
10000
6400
3600
1600
400
0
15
20
25
30
35
40
45
50
55
60
2Theta (°)

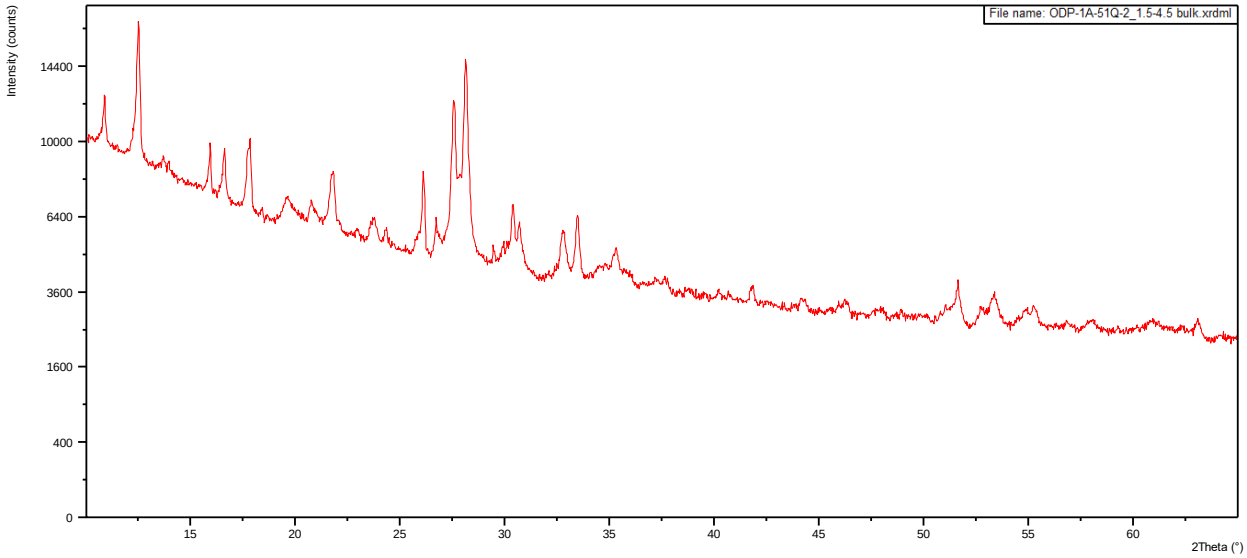
File name: ODP-1A-51Q-2_1.5-4.5 bulk.xrdml
Intensity (counts)
14400
10000
6400
3600
1600
400
0
15
20
25
30
35
40
45
50
55
60
2Theta (°)

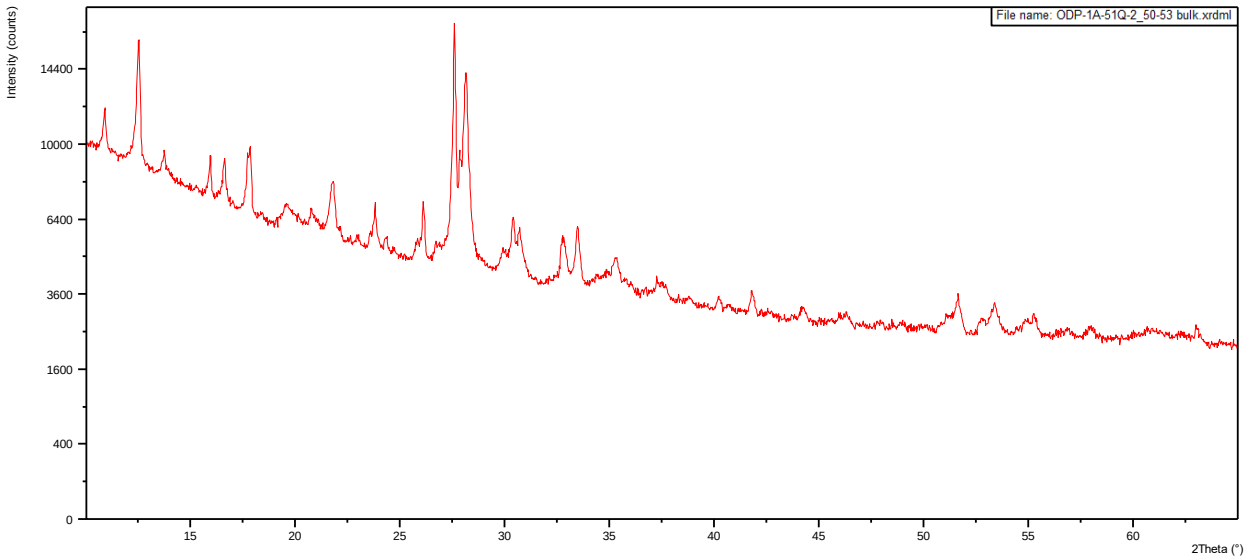
File name: ODP-1A-51Q-2_50-53 bulk.xrdml
Intensity (counts)
14400
10000
6400
3600
1600
400
0
15
20
25
30
35
40
45
50
55
60
2Theta (°)

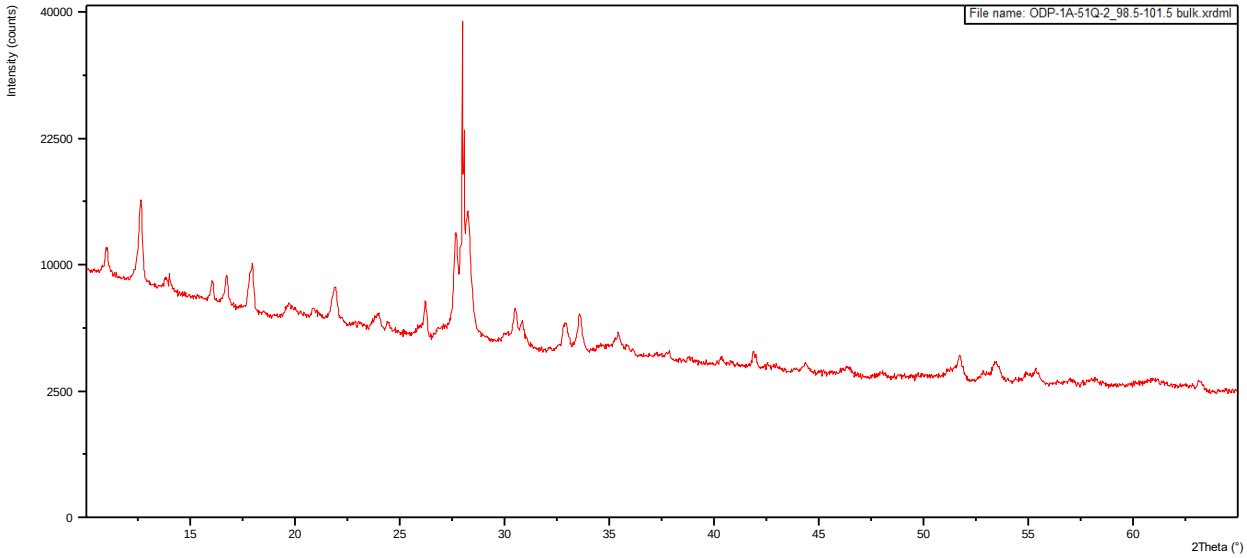
File name: ODP-1A-51Q-2_98.5-101.5 bulk.xrdml
Intensity (counts)
40000
22500
10000
2500
0
15
20
25
30
35
40
45
50
55
60
2Theta (°)

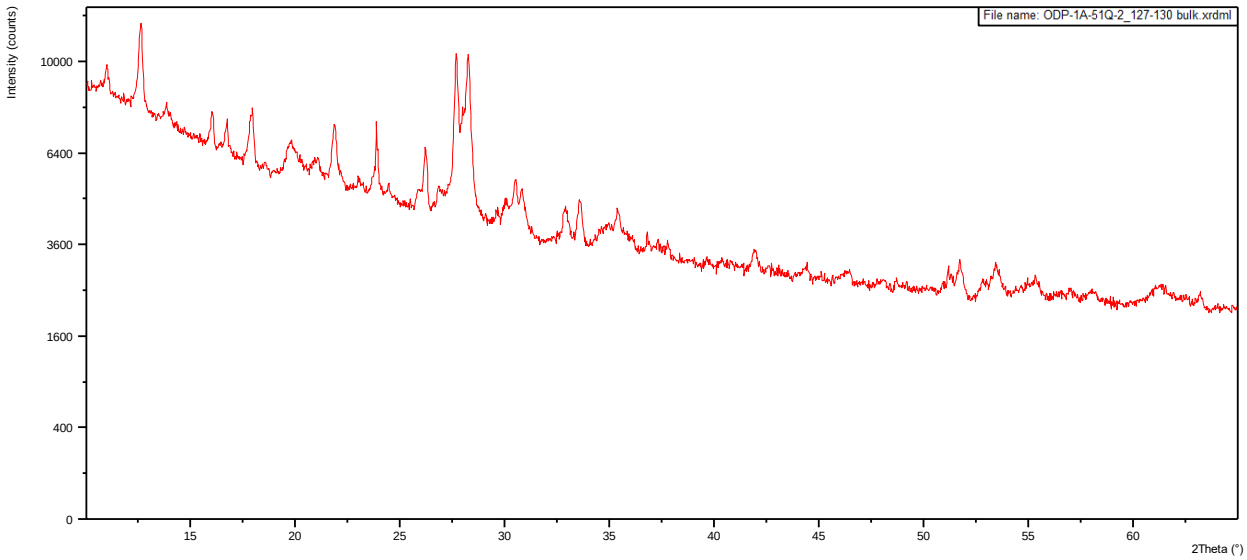
File name: ODP-1A-51Q-2_127-130 bulk.xrdml
Intensity (counts)
10000
6400
3600
1600
400
0
15
20
25
30
35
40
45
50
55
60
2Theta (°)

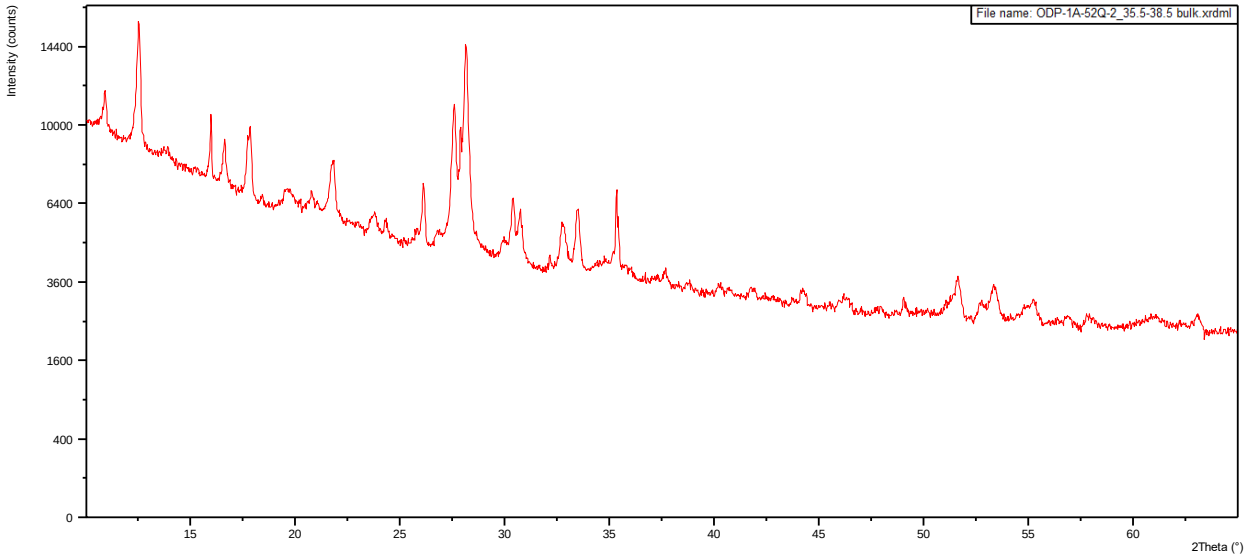
File name: ODP-1A-52Q-2_35.5-38.5 bulk.xrdml
Intensity (counts)
14400
10000
6400
3600
1600
400
0
15
20
25
30
35
40
45
50
55
60
2Theta (°)

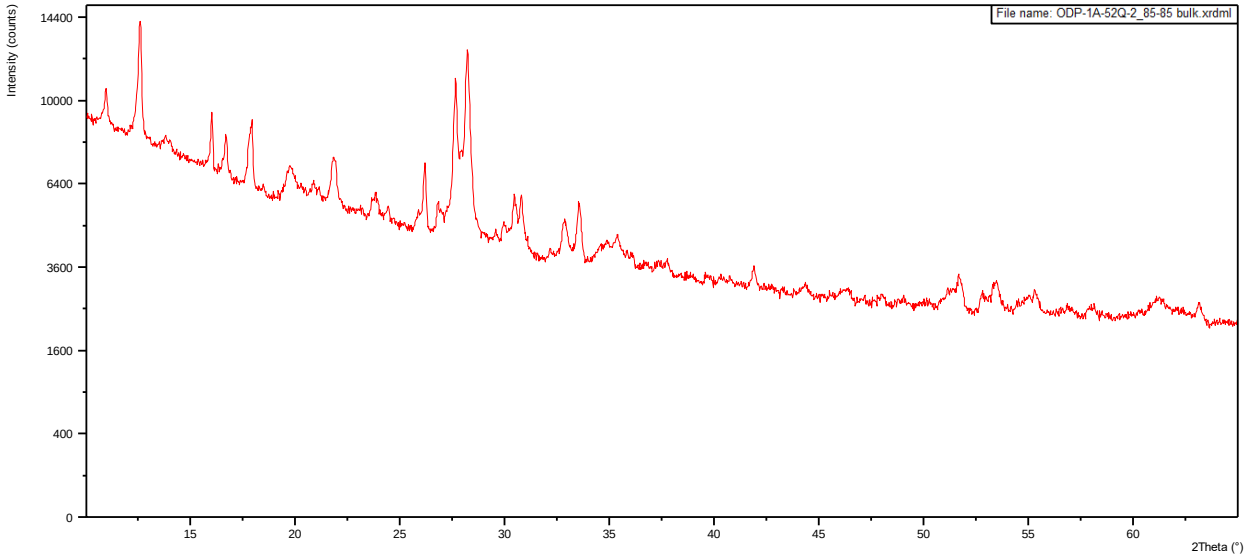
File name: ODP-1A-52Q-2_85-85 bulk.xrdml
Intensity (counts)
14400
10000
6400
3600
1600
400
0
15
20
25
30
35
40
45
50
55
60
2Theta (°)

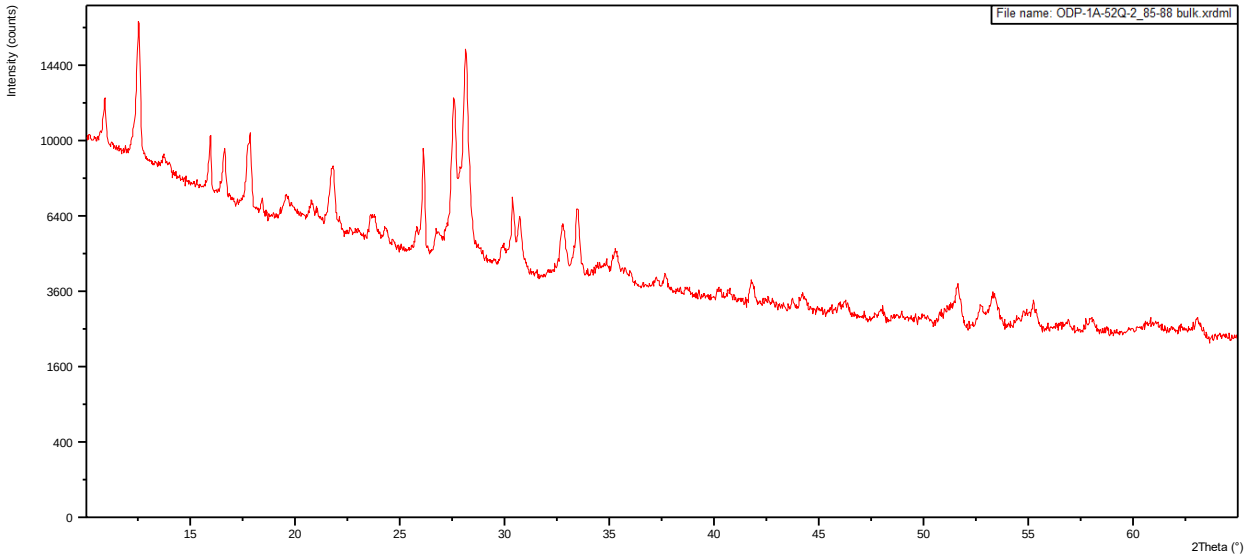
File name: ODP-1A-52Q-2_85-88 bulk.xrdml
Intensity (counts)
14400
10000
6400
3600
1600
400
0
15
20
25
30
35
40
45
50
55
60
2Theta (°)

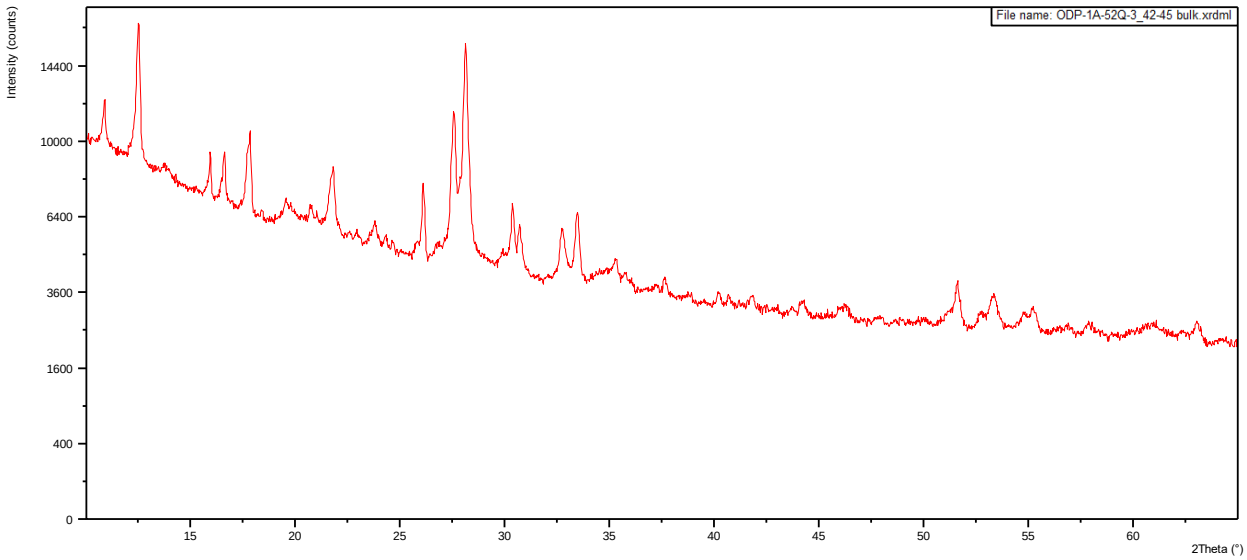
File name: ODP-1A-52Q-3_42-45 bulk.xrdml
Intensity (counts)
14400
10000
6400
3600
1600
400
0
15
20
25
30
35
40
45
50
55
60
2Theta (°)

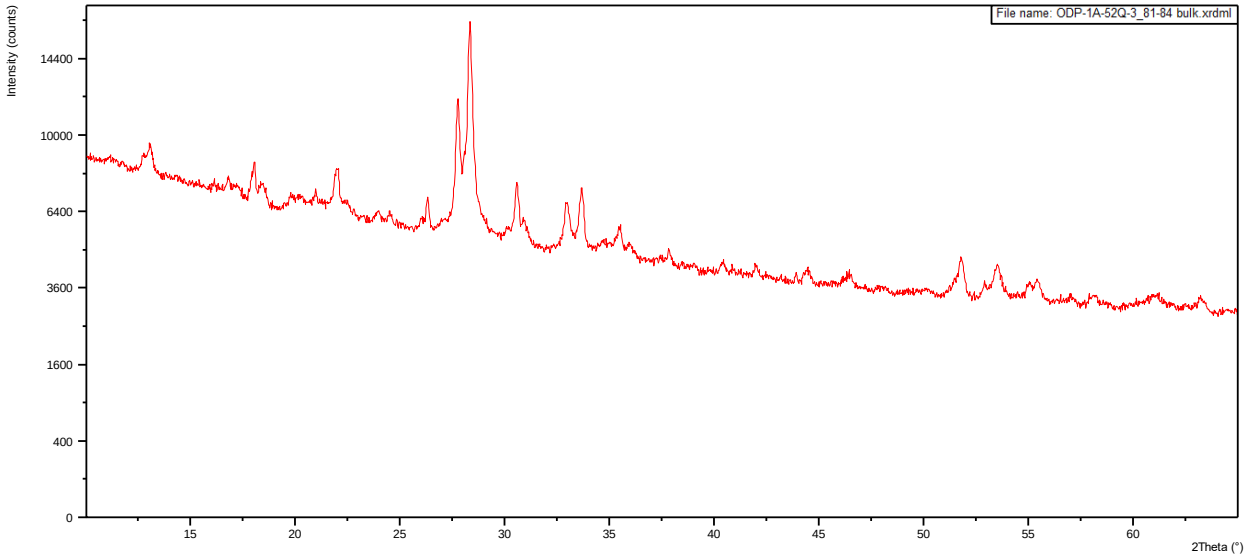
File name: ODP-1A-52Q-3_81-84 bulk.xrdml
Intensity (counts)
14400
10000
6400
3600
1600
400
0
15
20
25
30
35
40
45
50
55
60
2Theta (°)

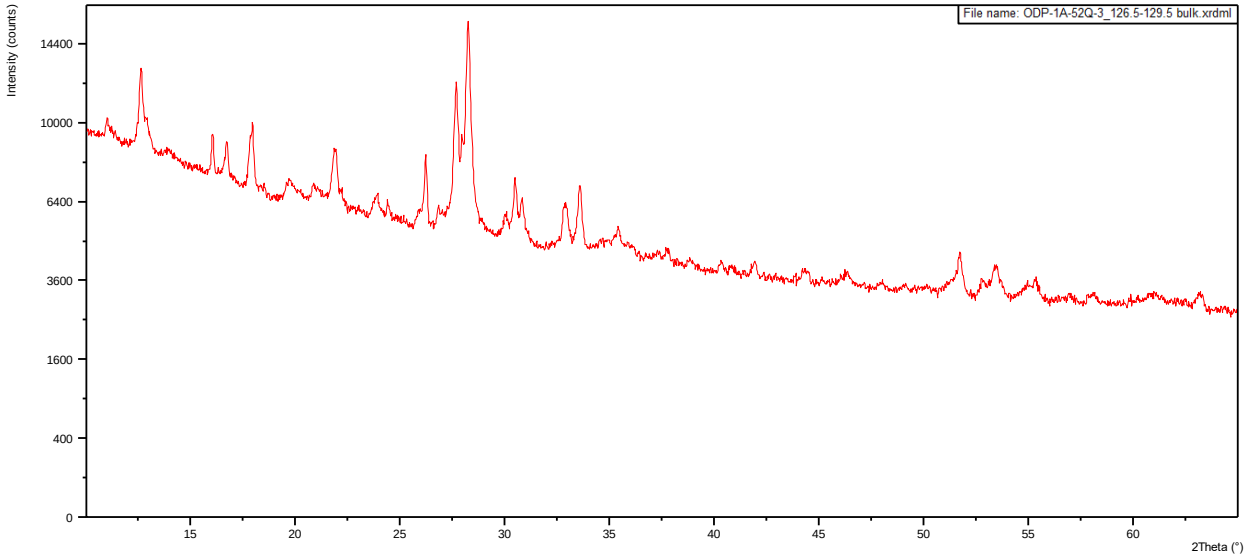
File name: ODP-1A-52Q-3_126.5-129.5 bulk.xrdml
Intensity (counts)
14400
10000
6400
3600
1600
400
0
15
20
25
30
35
40
45
50
55
60
2Theta (°)

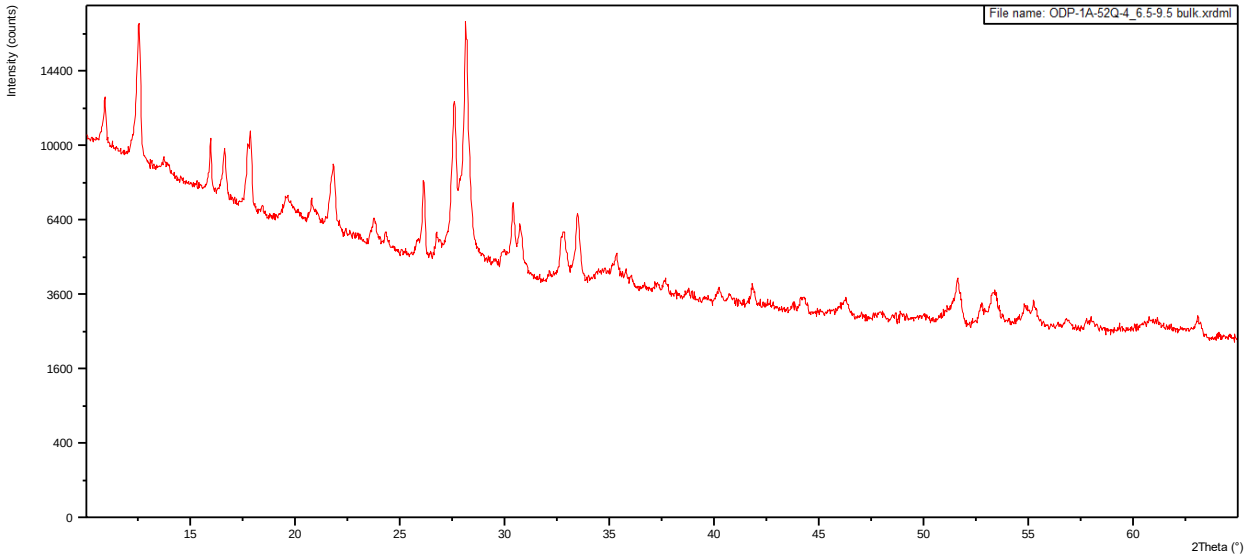
File name: ODP-1A-52Q-4_6.5-9.5 bulk.xrdml
Intensity (counts)
14400
10000
6400
3600
1600
400
0
15
20
25
30
35
40
45
50
55
60
2Theta (°)

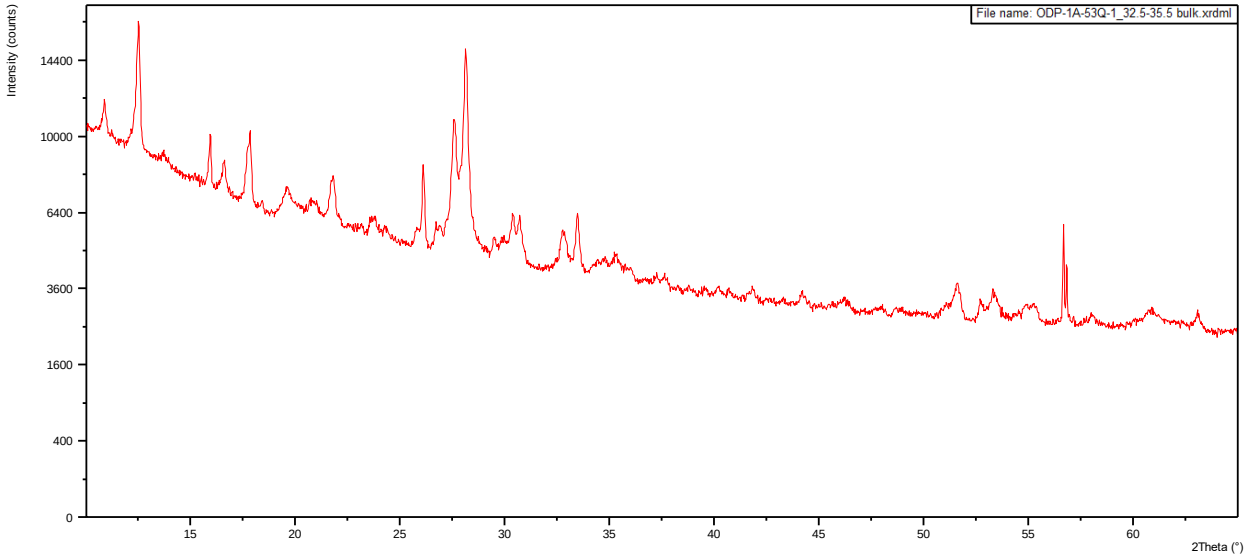
File name: ODP-1A-53Q-1_32.5-35.5 bulk.xrdml
Intensity (counts)
14400
10000
6400
3600
1600
400
0
15
20
25
30
35
40
45
50
55
60
2Theta (°)

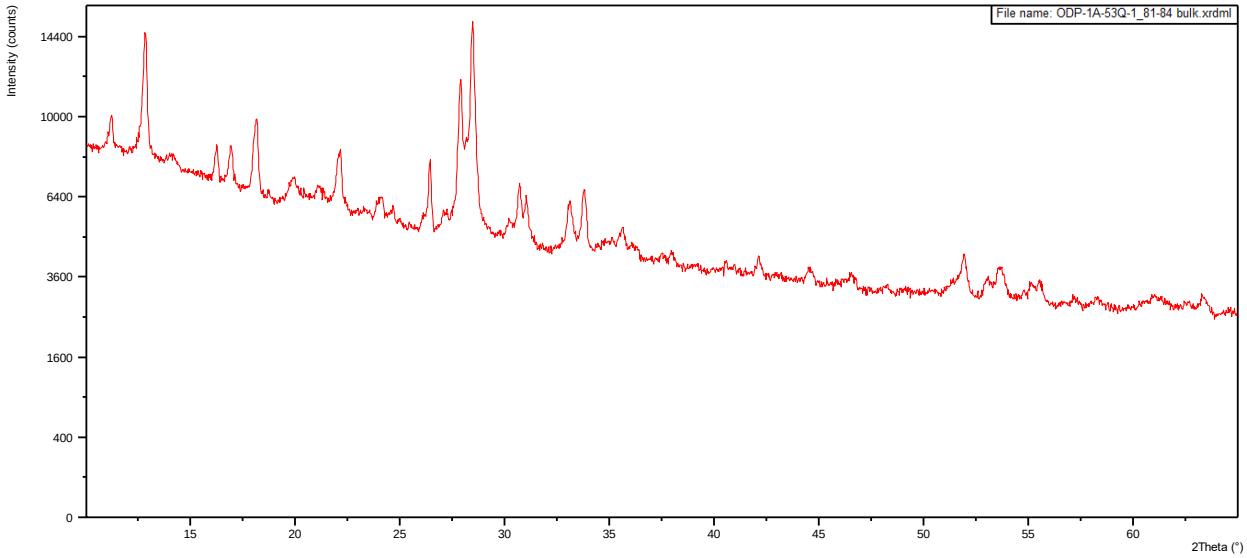
File name: ODP-1A-53Q-1_81-84 bulk.xrdml
Intensity (counts)
14400
10000
6400
3600
1600
400
0
15
20
25
30
35
40
45
50
55
60
2Theta (°)

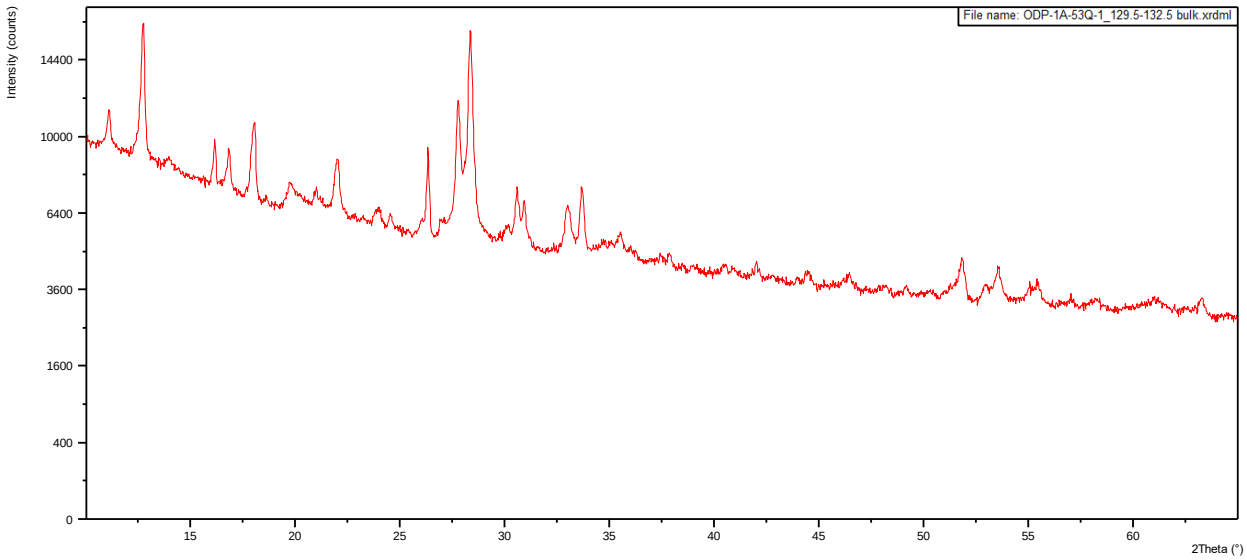
File name: ODP-1A-53Q-1_129.5-132.5 bulk.xrdml
Intensity (counts)
14400
10000
6400
3600
1600
400
0
15
20
25
30
35
40
45
50
55
60
2Theta (°)

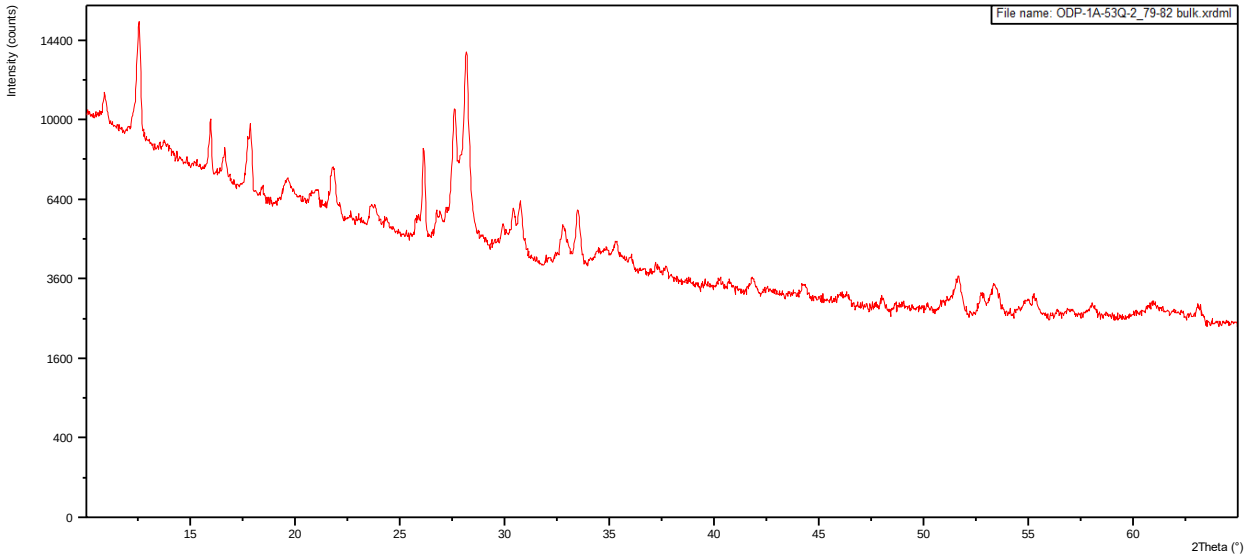
File name: ODP-1A-53Q-2_79-82 bulk.xrdml
Intensity (counts)
14400
10000
6400
3600
1600
400
0
15
20
25
30
35
40
45
50
55
60
2Theta (°)

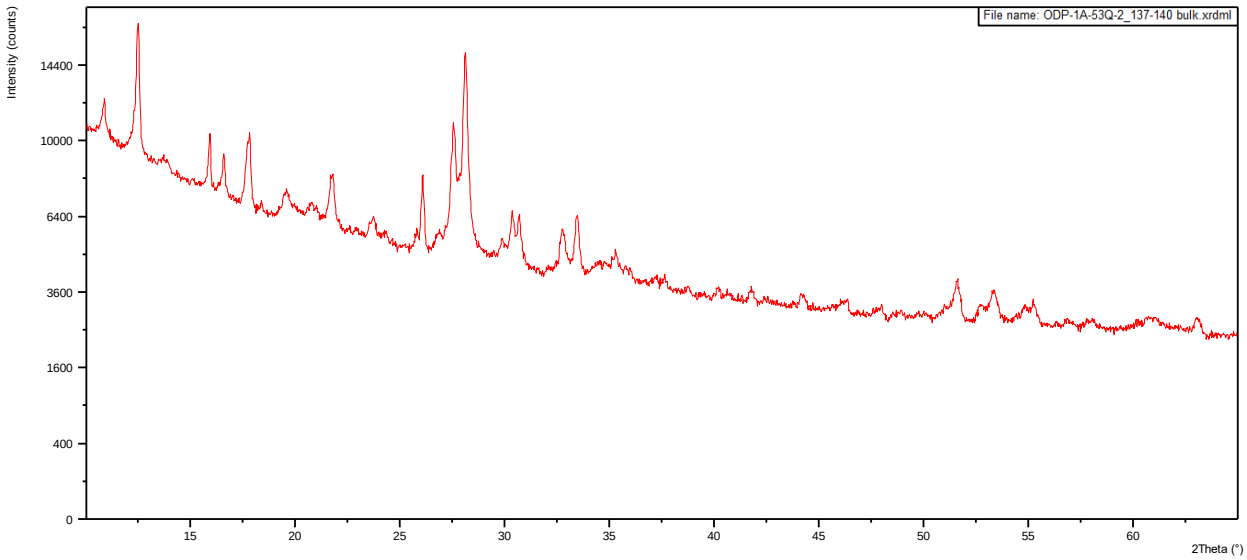
File name: ODP-1A-53Q-2_137-140 bulk.xrdml
Intensity (counts)
14400
10000
6400
3600
1600
400
0
15
20
25
30
35
40
45
50
55
60
2Theta (°)

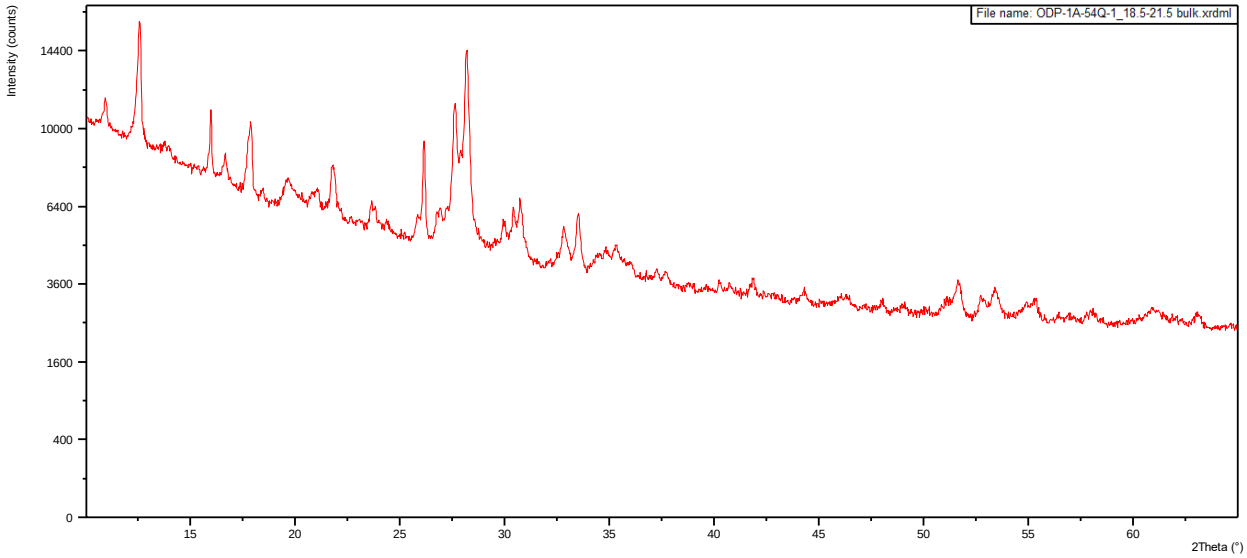
File name: ODP-1A-54Q-1_18.5-21.5 bulk.xrdml
Intensity (counts)
14400
10000
6400
3600
1600
400
0
15
20
25
30
35
40
45
50
55
60
2Theta (°)

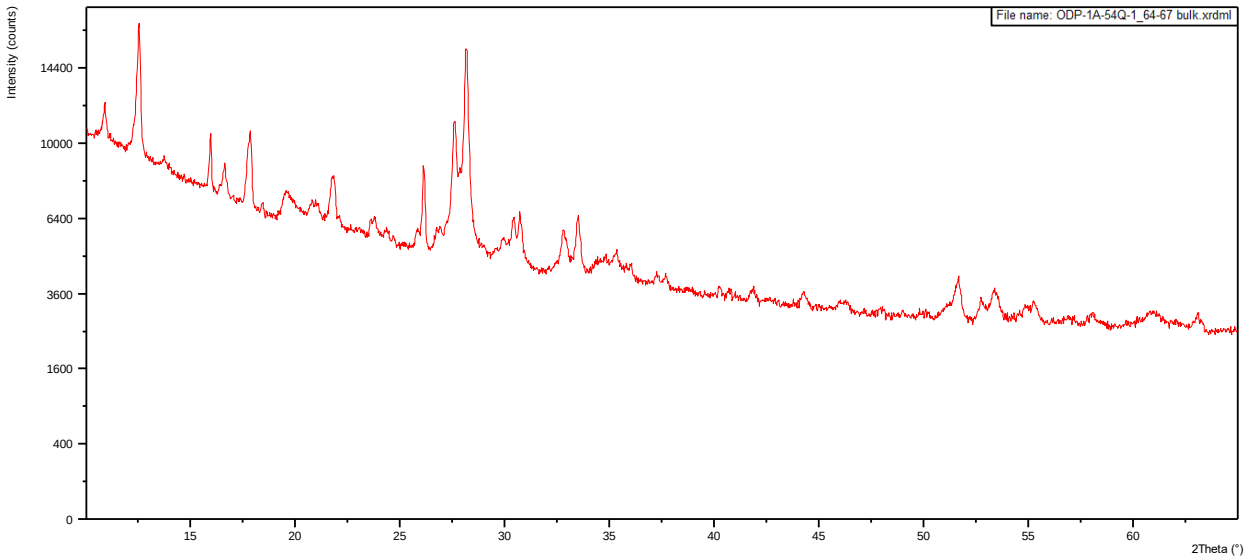
File name: ODP-1A-54Q-1_64-67 bulk.xrdml
Intensity (counts)
14400
10000
6400
3600
1600
400
0
15
20
25
30
35
40
45
50
55
60
2Theta (°)

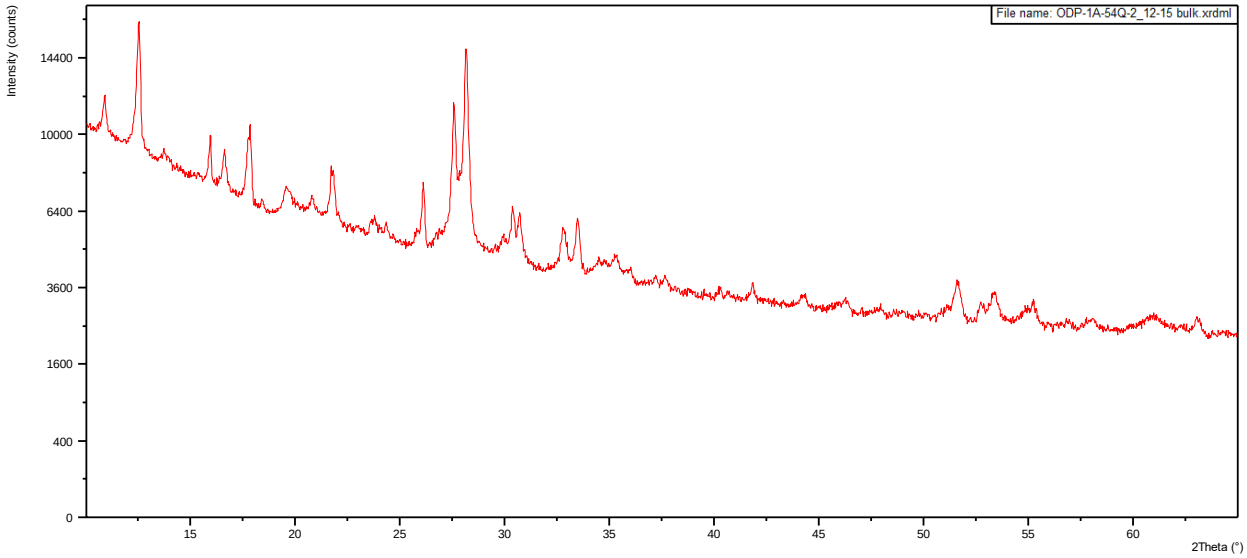
File name: ODP-1A-54Q-2_12-15 bulk.xrdml
Intensity (counts)
14400
10000
6400
3600
1600
400
0
15
20
25
30
35
40
45
50
55
60
2Theta (°)

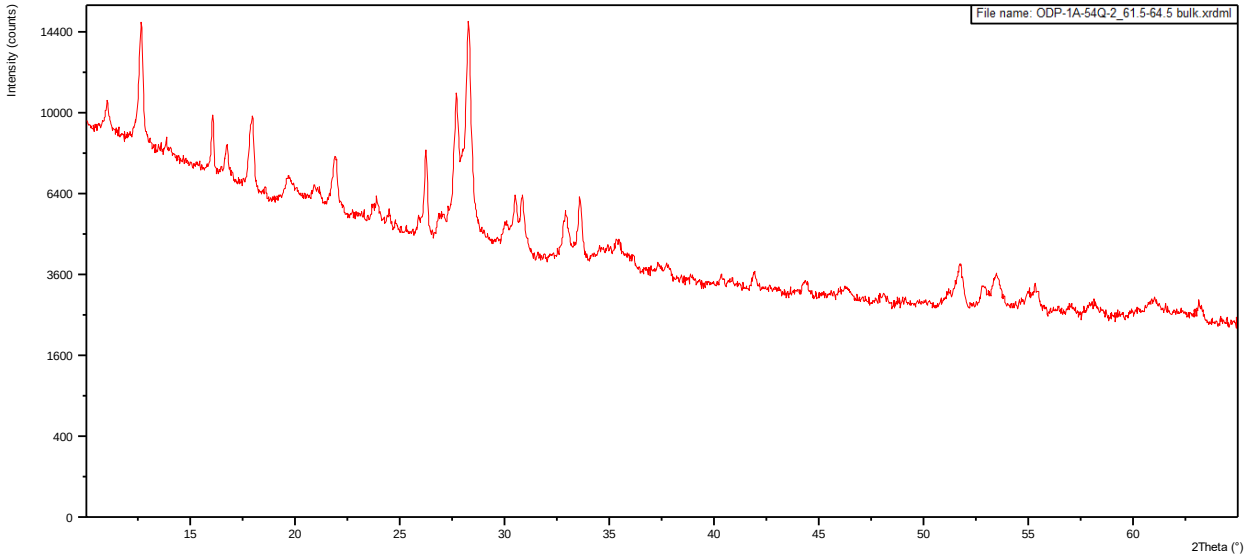
File name: ODP-1A-54Q-2_61.5-64.5 bulk.xrdml
Intensity (counts)
14400
10000
6400
3600
1600
400
0
15
20
25
30
35
40
45
50
55
60
2Theta (°)

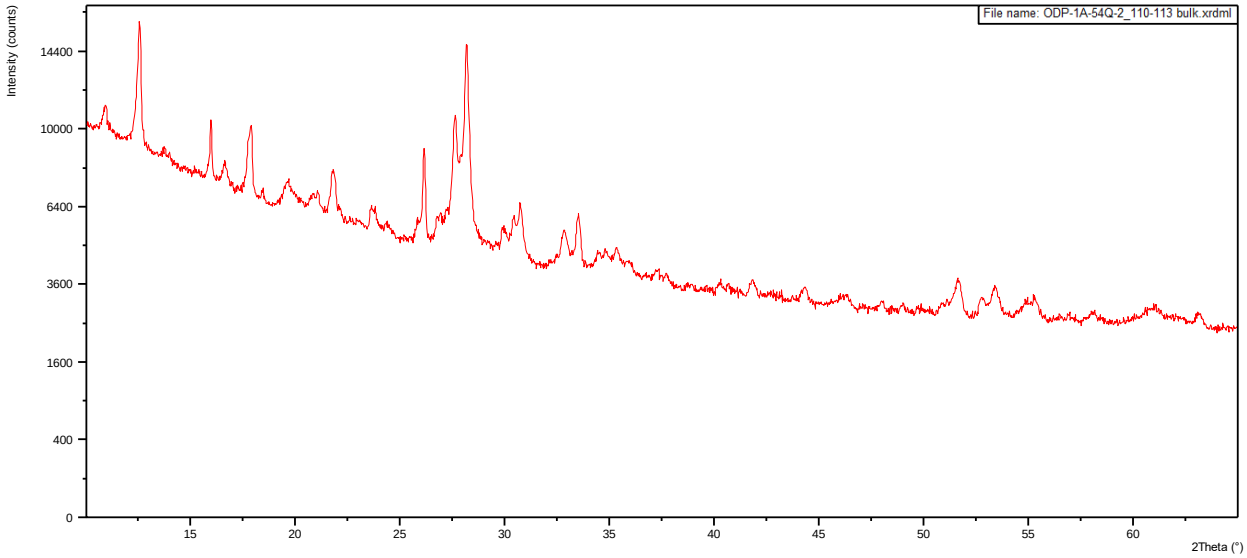
File name: ODP-1A-54Q-2_110-113 bulk.xrdml
Intensity (counts)
14400
10000
6400
3600
1600
400
0
15
20
25
30
35
40
45
50
55
60
2Theta (°)

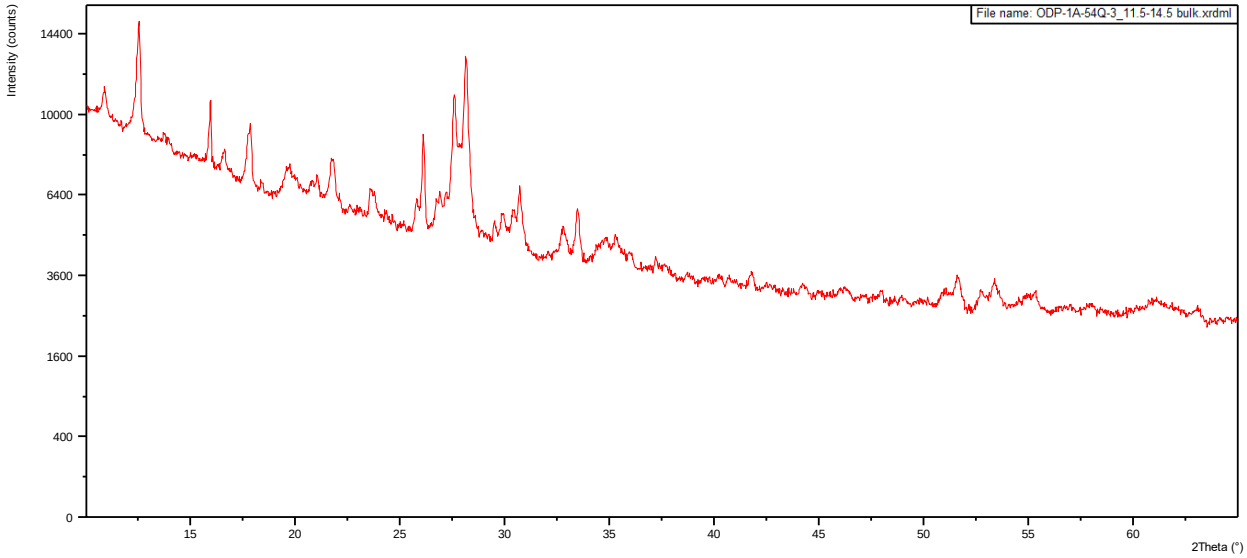
File name: ODP-1A-54Q-3_11.5-14.5 bulk.xrdml
Intensity (counts)
14400
10000
6400
3600
1600
400
0
15
20
25
30
35
40
45
50
55
60
2Theta (°)

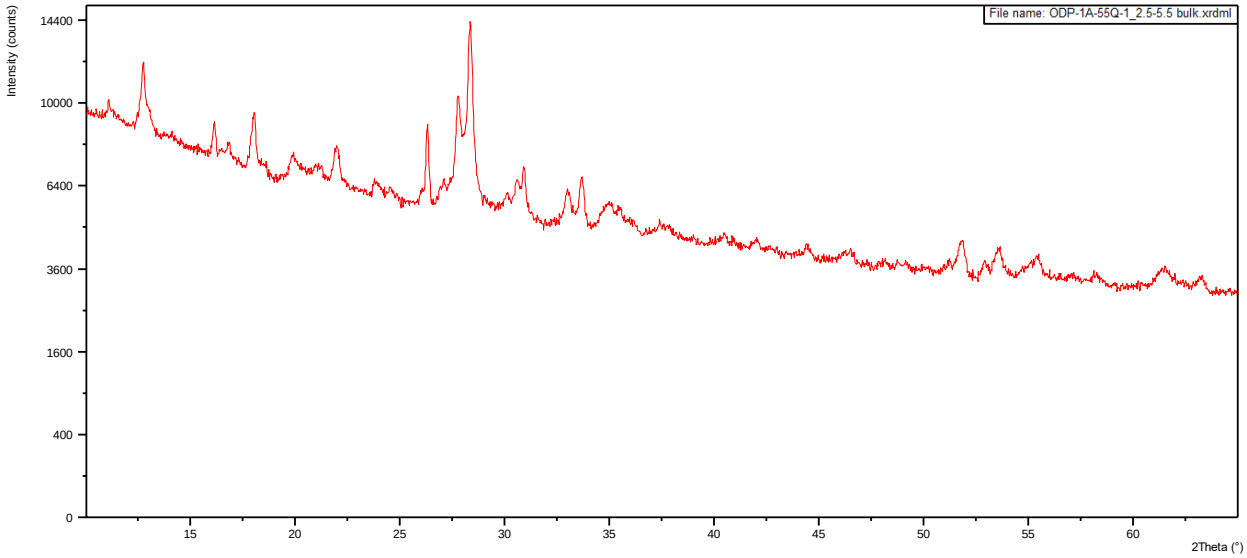
File name: ODP-1A-55Q-1_2.5-5.5 bulk.xrdml
Intensity (counts)
14400
10000
6400
3600
1600
400
0
15
20
25
30
35
40
45
50
55
60
2Theta (°)

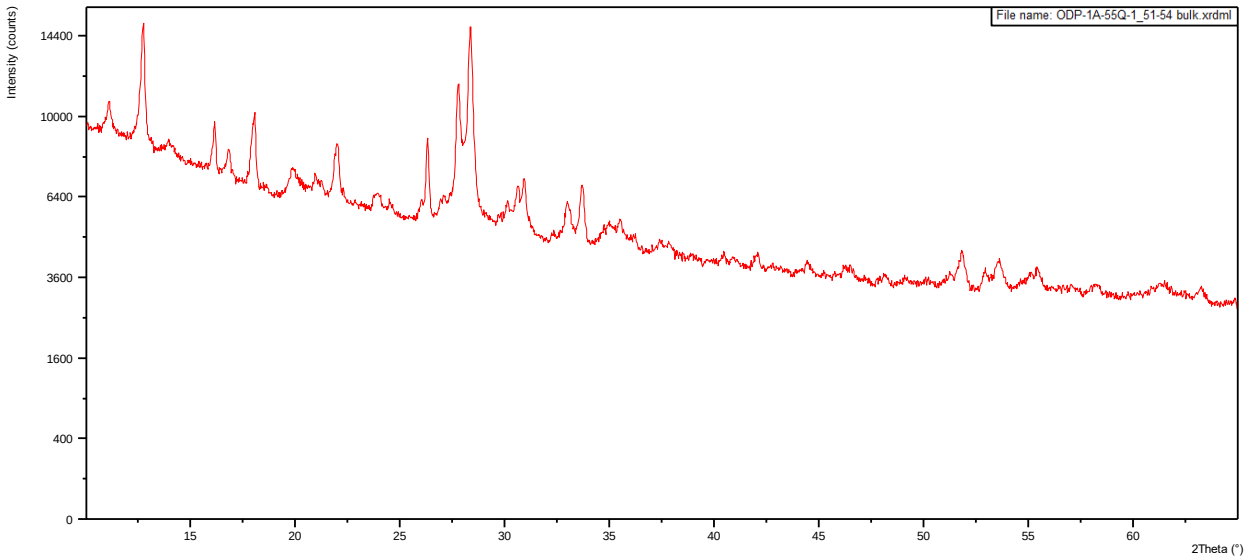
File name: ODP-1A-55Q-1_51-54 bulk.xrdml
Intensity (counts)
14400
10000
6400
3600
1600
400
0
15
20
25
30
35
40
45
50
55
60
2Theta (°)

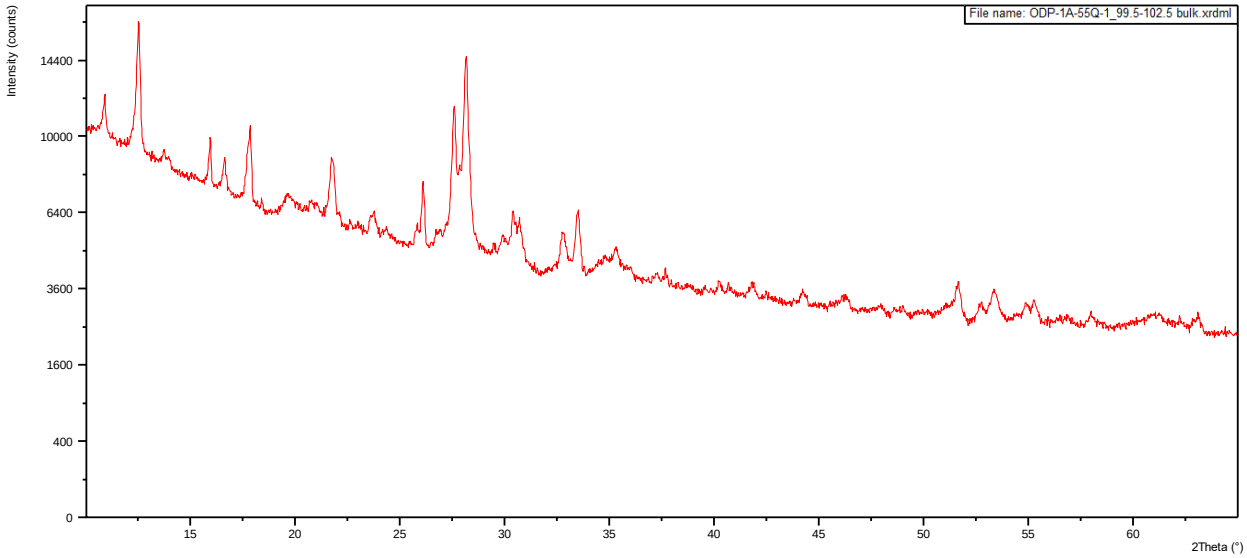
File name: ODP-1A-55Q-1_99.5-102.5 bulk.xrdml
Intensity (counts)
14400
10000
6400
3600
1600
400
0
15
20
25
30
35
40
45
50
55
60
2Theta (°)

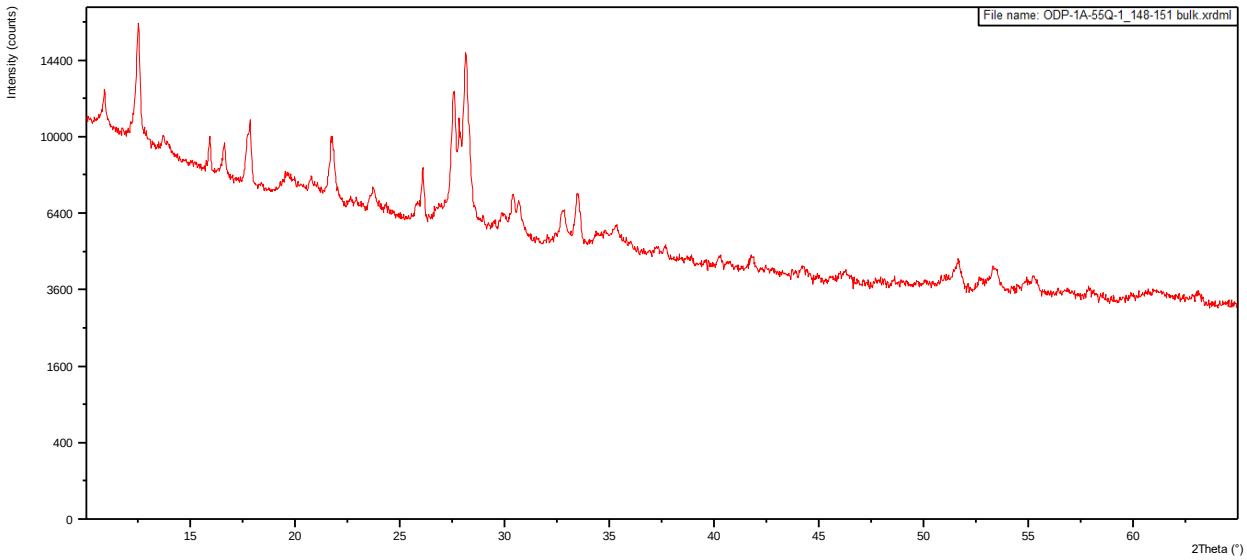
File name: ODP-1A-55Q-1_148-151 bulk.xrdml
Intensity (counts)
14400
10000
6400
3600
1600
400
0
15
20
25
30
35
40
45
50
55
60
2Theta (°)

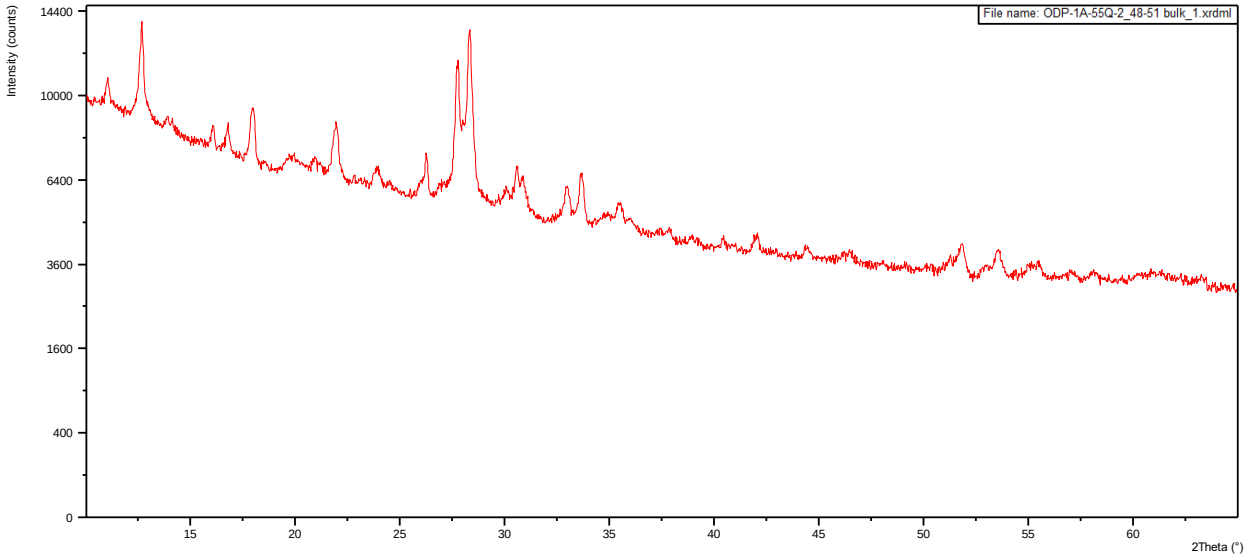
File name: ODP-1A-55Q-2_48-51 bulk_1.xrdml
Intensity (counts)
14400
10000
6400
3600
1600
400
0
15
20
25
30
35
40
45
50
55
60
2Theta (°)

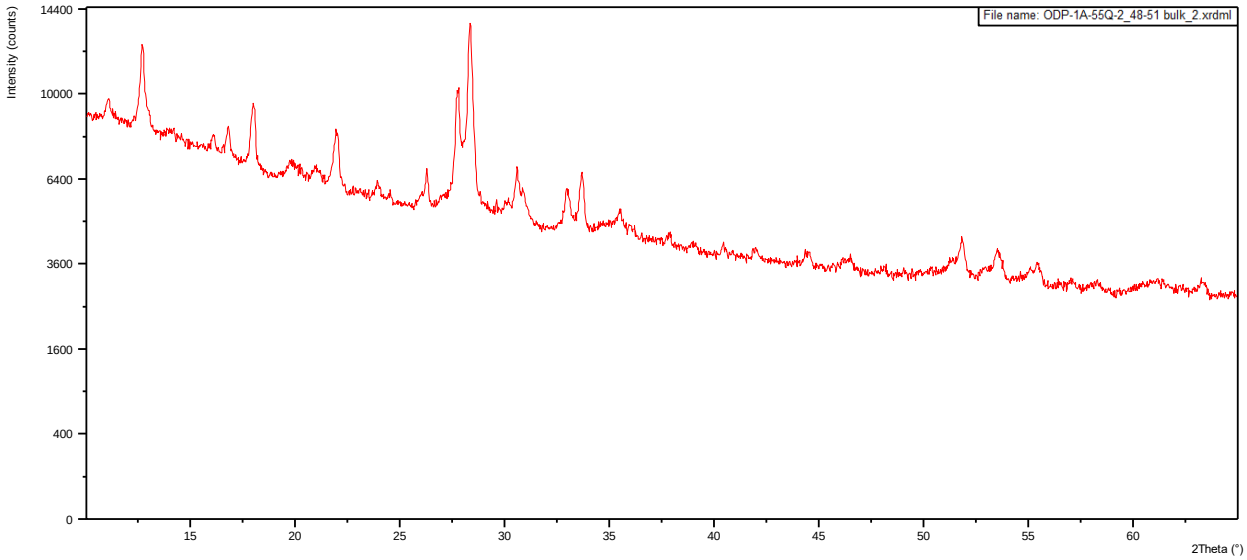
File name: ODP-1A-55Q-2_48-51 bulk_2.xrdml
Intensity (counts)
14400
10000
6400
3600
1600
400
0
15
20
25
30
35
40
45
50
55
60
2Theta (°)

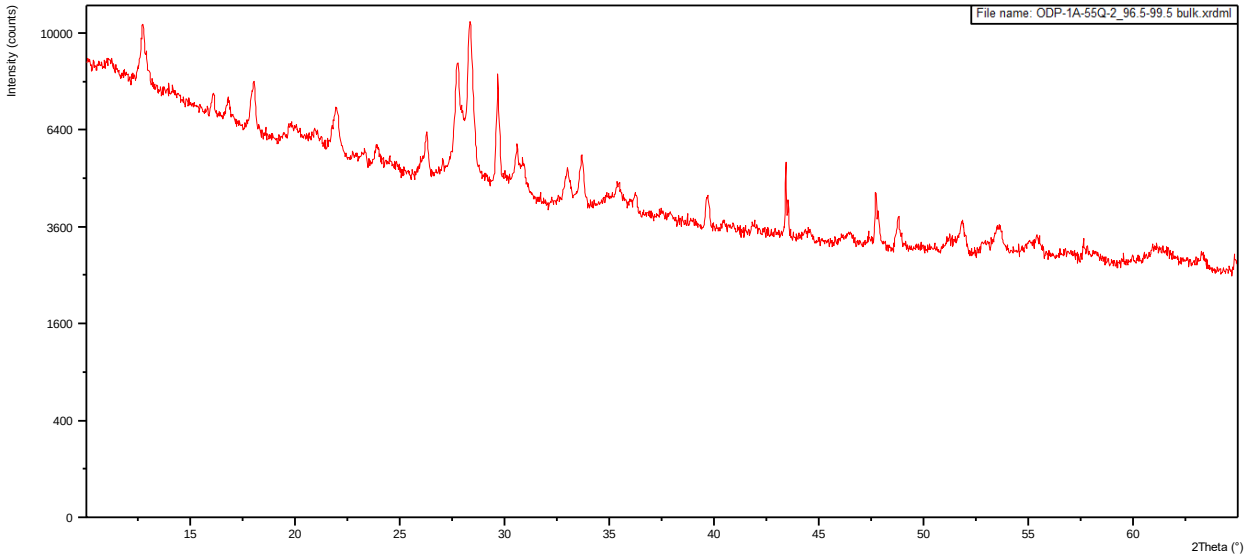
File name: ODP-1A-55Q-2_96.5-99.5 bulk.xrdml
Intensity (counts)
10000
6400
3600
1600
400
0
15
20
25
30
35
40
45
50
55
60
2Theta (°)

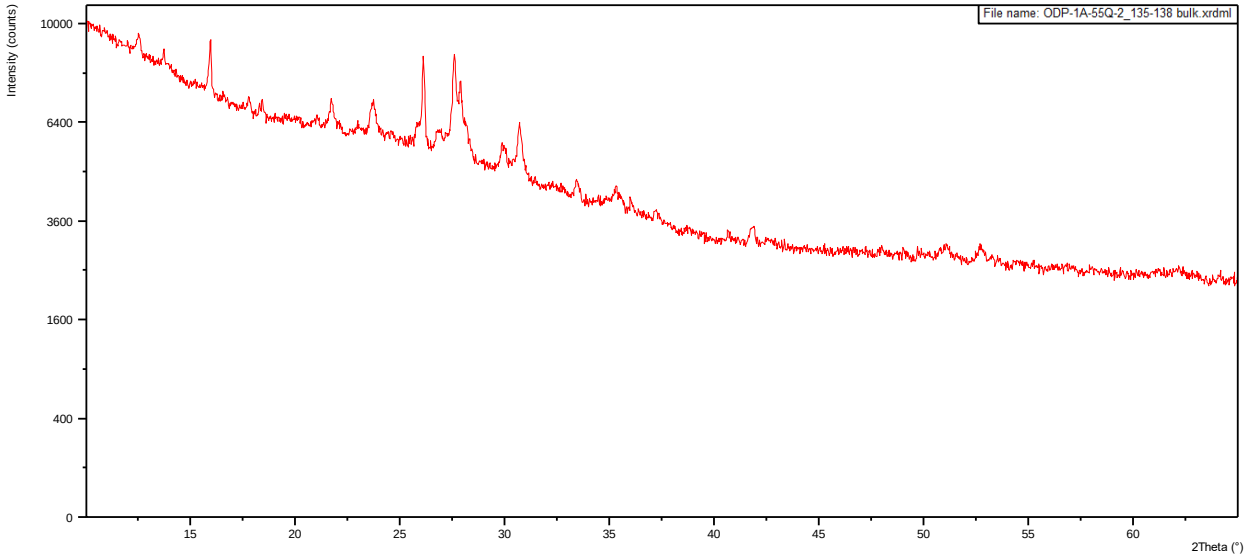
File name: ODP-1A-55Q-2_135-138 bulk.xrdml
Intensity (counts)
10000
6400
3600
1600
400
0
15
20
25
30
35
40
45
50
55
60
2Theta (°)

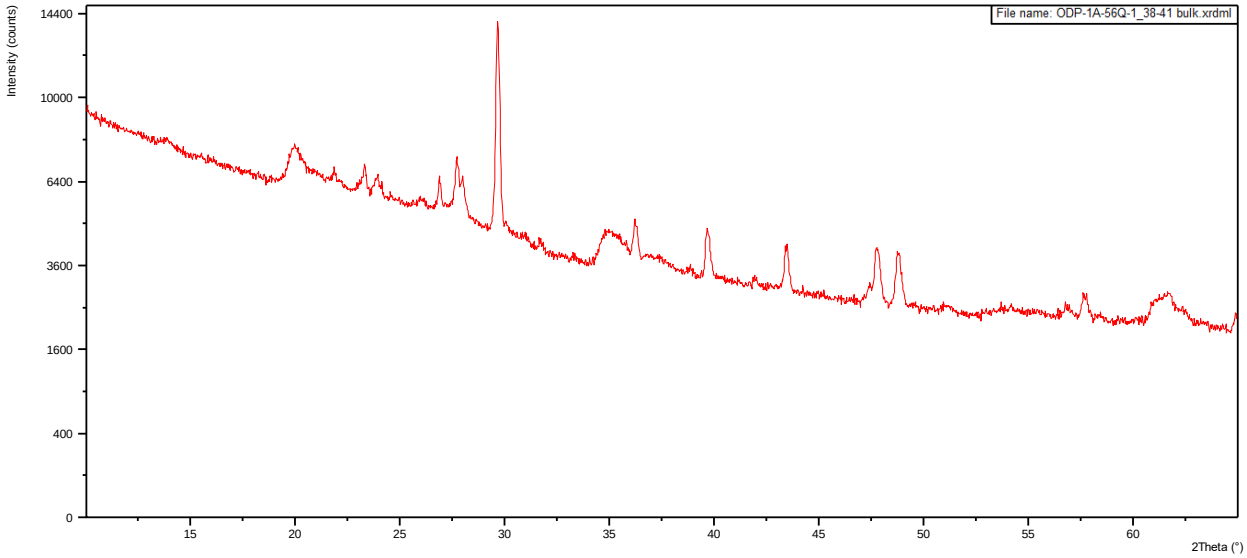
File name: ODP-1A-56Q-1_38-41 bulk.xrdml
Intensity (counts)
14400
10000
6400
3600
1600
400
0
15
20
25
30
35
40
45
50
55
60
2Theta (°)

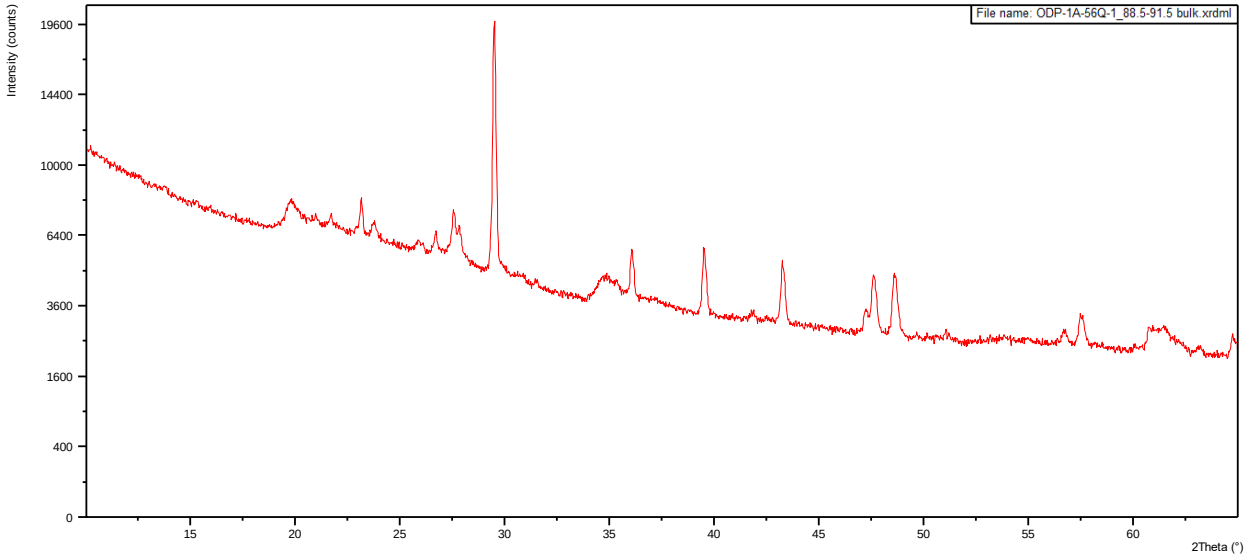
File name: ODP-1A-56Q-1_88.5-91.5 bulk.xrdml
Intensity (counts)
19600
14400
10000
6400
3600
1600
400
0
15
20
25
30
35
40
45
50
55
60
2Theta (°)

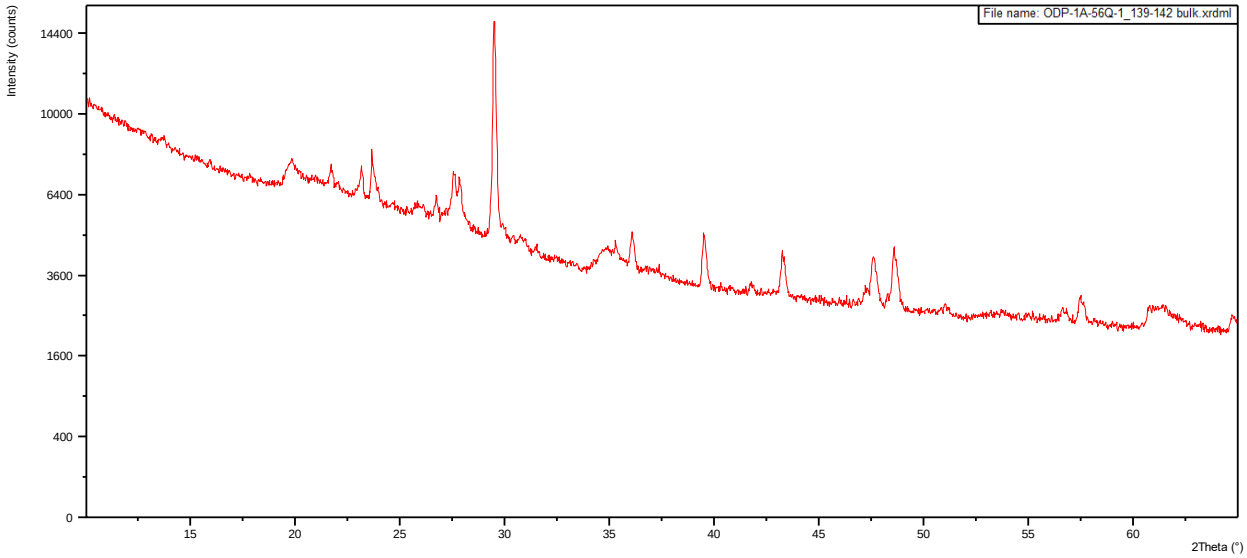
File name: ODP-1A-56Q-1_139-142 bulk.xrdml
Intensity (counts)
14400
10000
6400
3600
1600
400
0
15
20
25
30
35
40
45
50
55
60
2Theta (°)

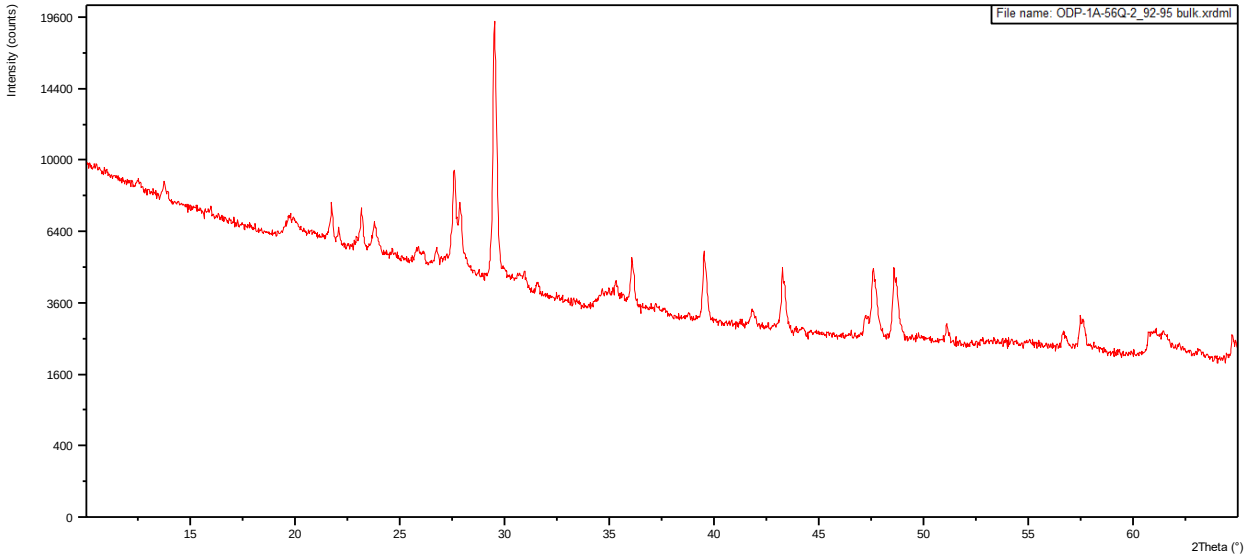
File name: ODP-1A-56Q-2_92-95 bulk.xrdml
Intensity (counts)
19600
14400
10000
6400
3600
1600
400
0
15
20
25
30
35
40
45
50
55
60
2Theta (°)

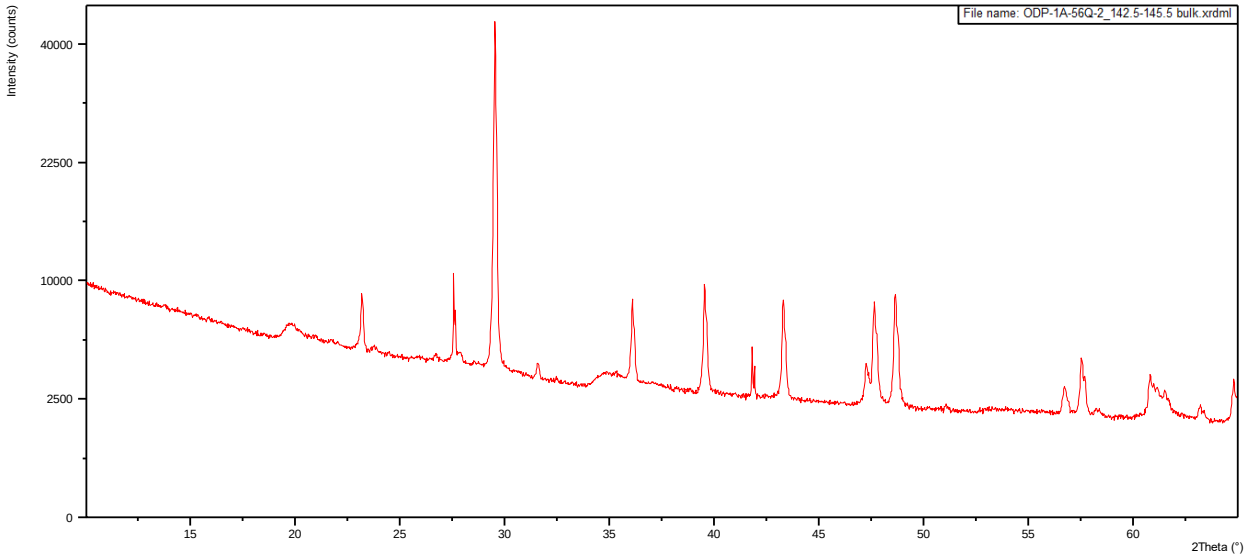
File name: ODP-1A-56Q-2_142.5-145.5 bulk.xrdml
Intensity (counts)
40000
22500
10000
2500
0
15
20
25
30
35
40
45
50
55
60
2Theta (°)

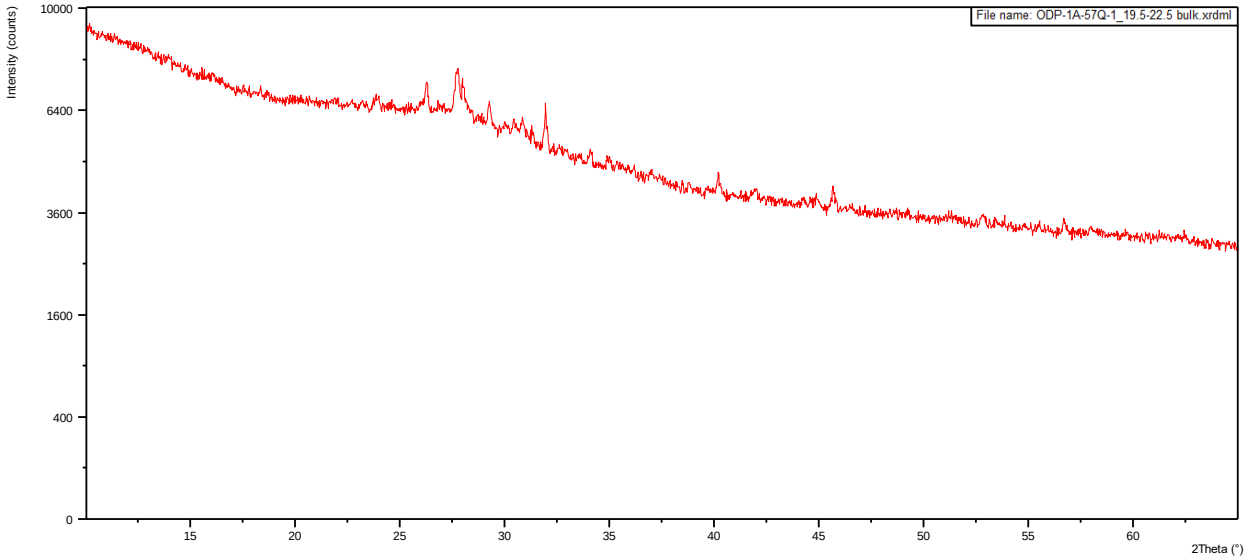
File name: ODP-1A-57Q-1_19.5-22.5 bulk.xrdml
Intensity (counts)
10000
6400
3600
1600
400
0
15
20
25
30
35
40
45
50
55
60
2Theta (°)

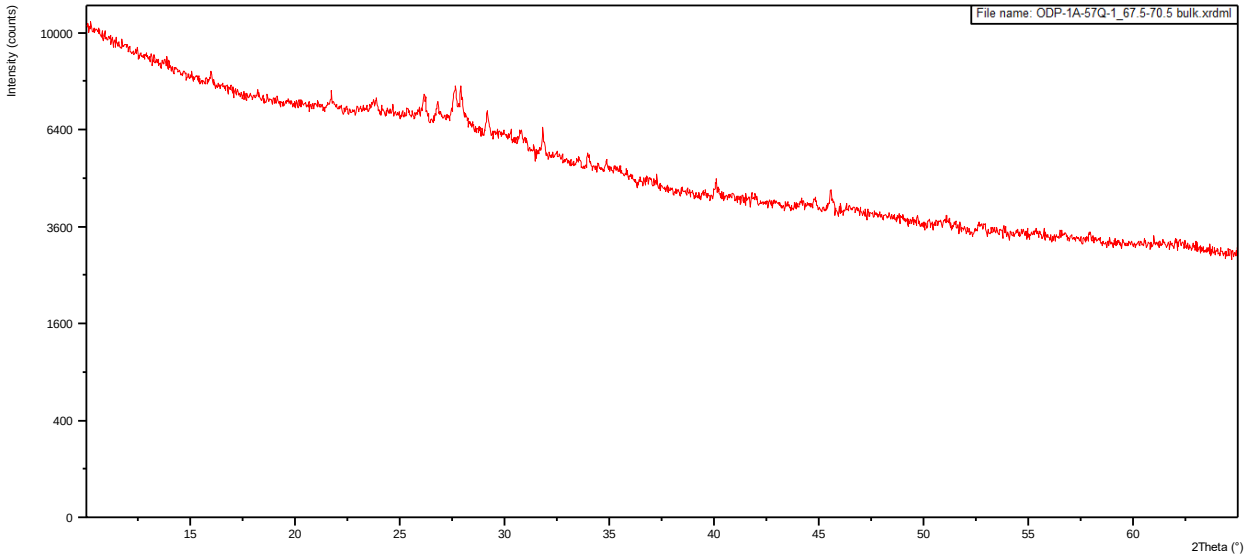
File name: ODP-1A-57Q-1_67.5-70.5 bulk.xrdml
Intensity (counts)
10000
6400
3600
1600
400
0
15
20
25
30
35
40
45
50
55
60
2Theta (°)

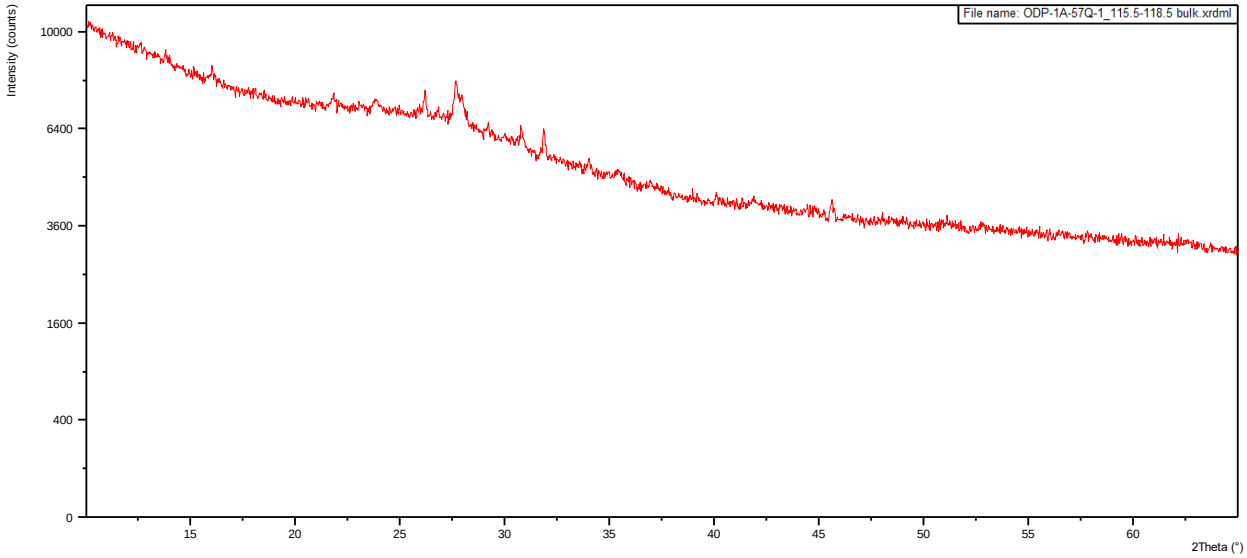
File name: ODP-1A-57Q-1_115.5-118.5 bulk.xrdml
Intensity (counts)
10000
6400
3600
1600
400
0
15
20
25
30
35
40
45
50
55
60
2Theta (°)

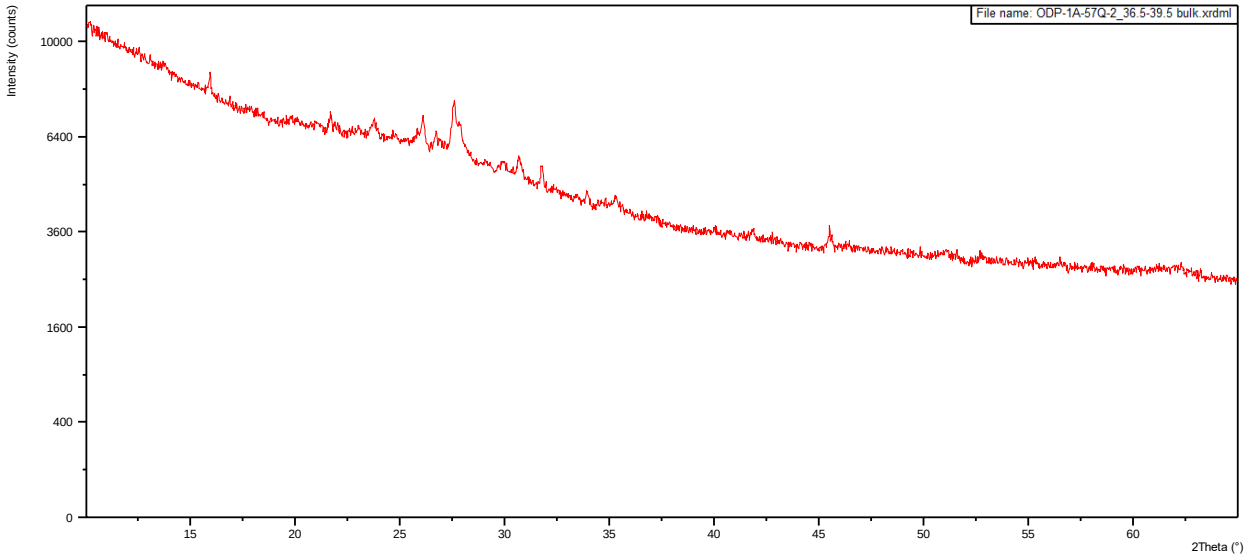
File name: ODP-1A-57Q-2_36.5-39.5 bulk.xrdml
Intensity (counts)
10000
6400
3600
1600
400
0
15
20
25
30
35
40
45
50
55
60
2Theta (°)

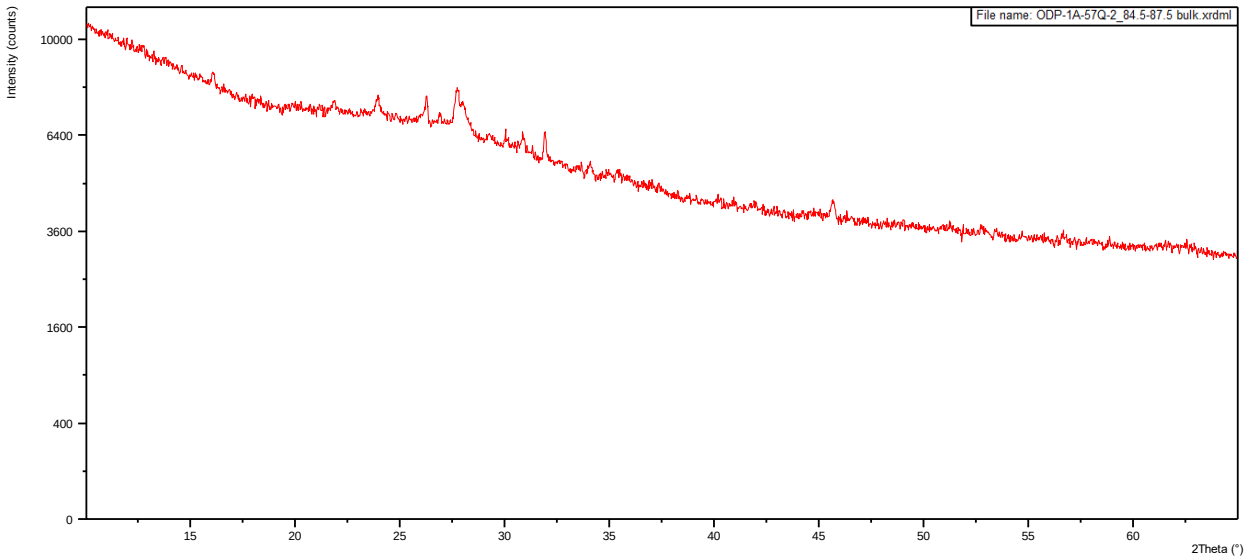
File name: ODP-1A-57Q-2_84.5-87.5 bulk.xrdml
Intensity (counts)
10000
6400
3600
1600
400
0
15
20
25
30
35
40
45
50
55
60
2Theta (°)

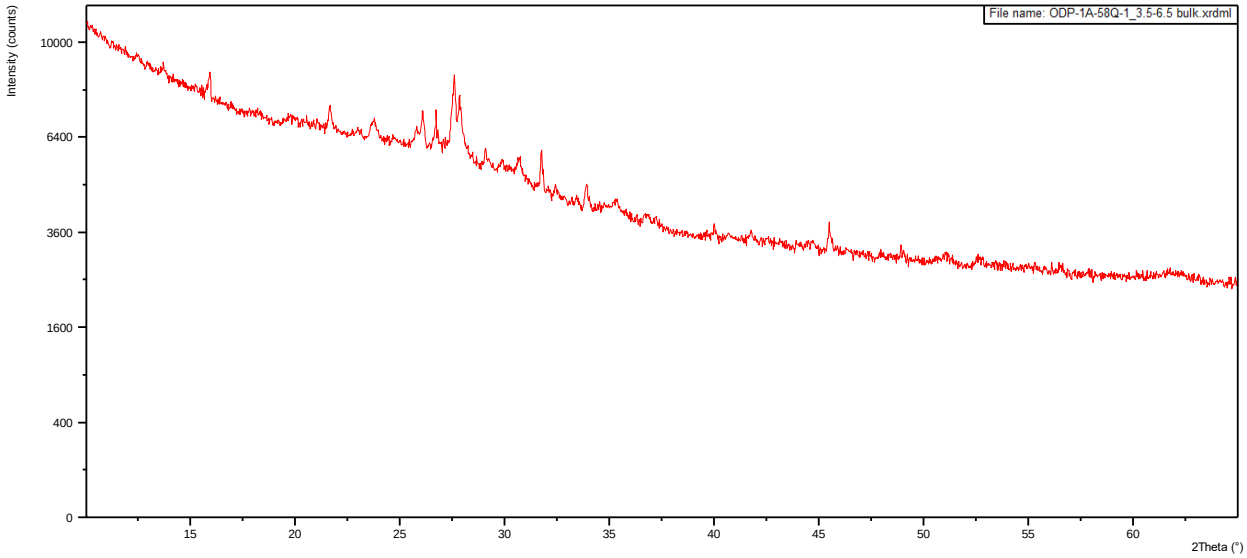
File name: ODP-1A-58Q-1_3.5-6.5 bulk.xrdml
Intensity (counts)
10000
6400
3600
1600
400
0
15
20
25
30
35
40
45
50
55
60
2Theta (°)

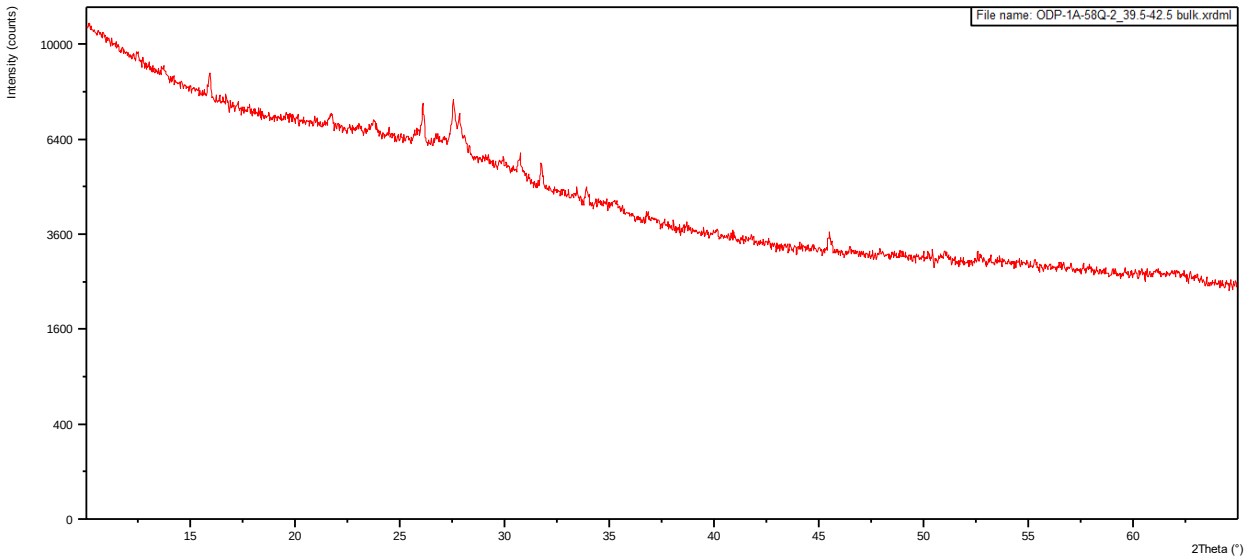
File name: ODP-1A-58Q-2_39.5-42.5 bulk.xrdml
Intensity (counts)
10000
6400
3600
1600
400
0
15
20
25
30
35
40
45
50
55
60
2Theta (°)

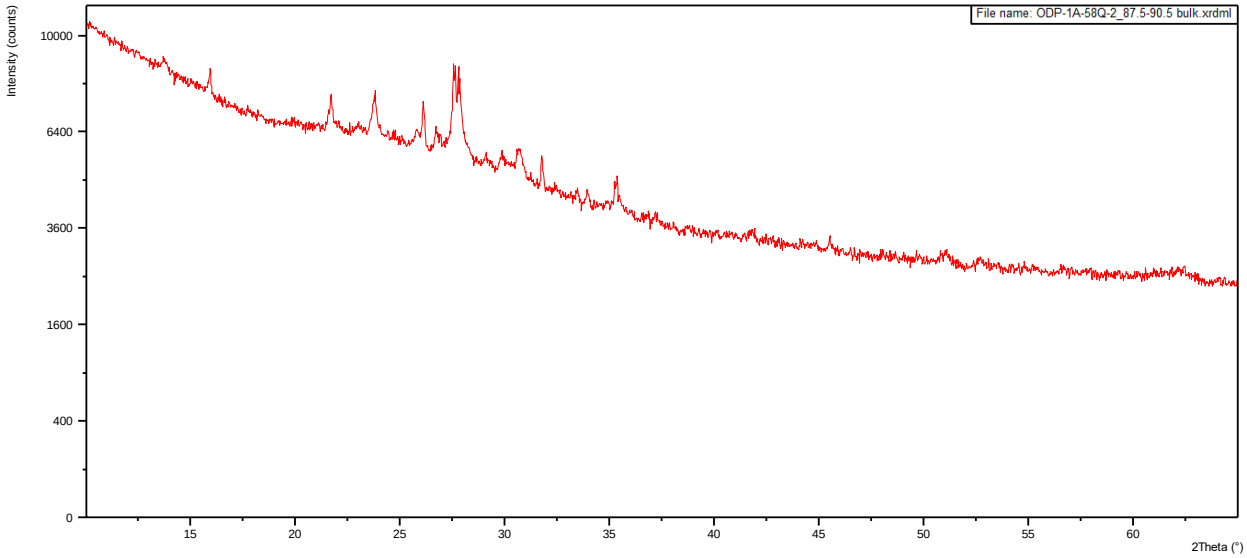
File name: ODP-1A-58Q-2_87.5-90.5 bulk.xrdml
Intensity (counts)
10000
6400
3600
1600
400
0
15
20
25
30
35
40
45
50
55
60
2Theta (°)

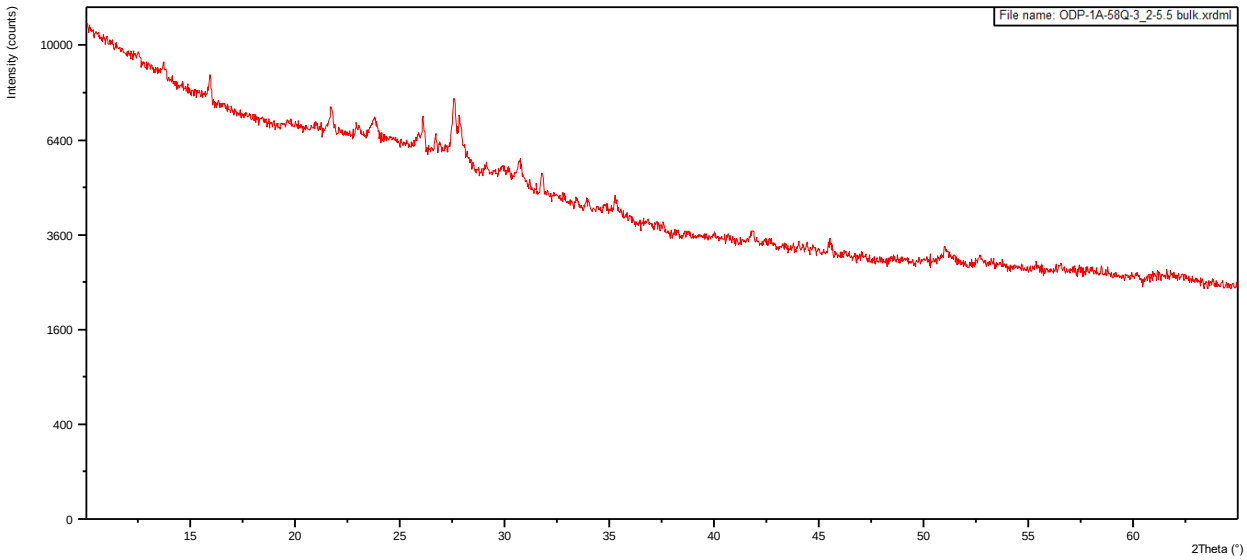
File name: ODP-1A-58Q-3_2-5.5 bulk.xrdml
Intensity (counts)
10000
6400
3600
1600
400
0
15
20
25
30
35
40
45
50
55
60
2Theta (°)

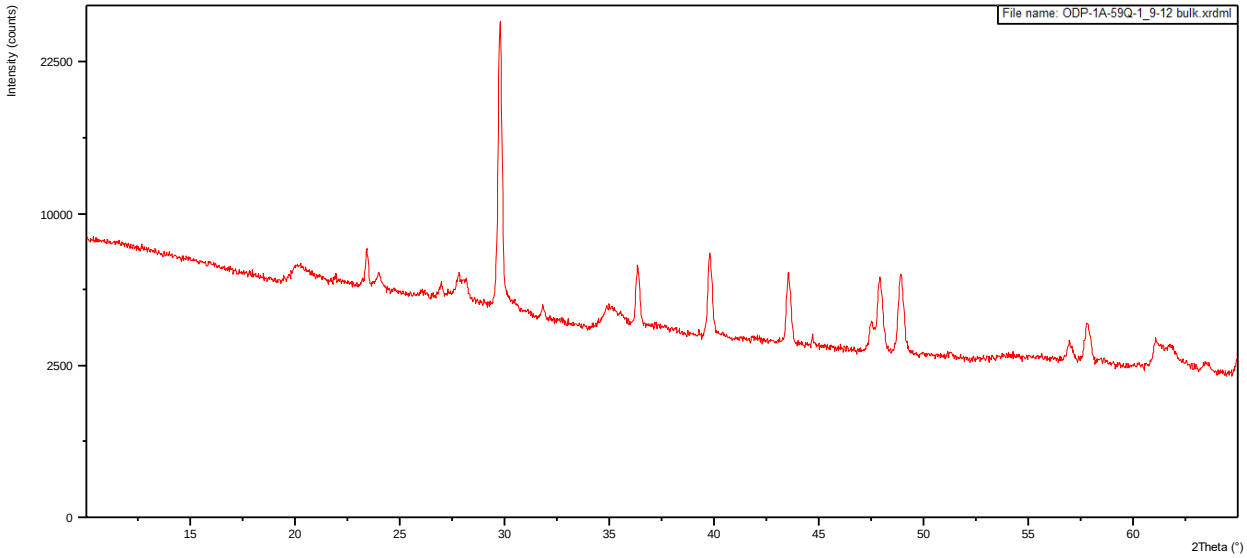
File name: ODP-1A-59Q-1_9-12 bulk.xrdml
Intensity (counts)
22500
10000
2500
0
15
20
25
30
35
40
45
50
55
60
2Theta (°)

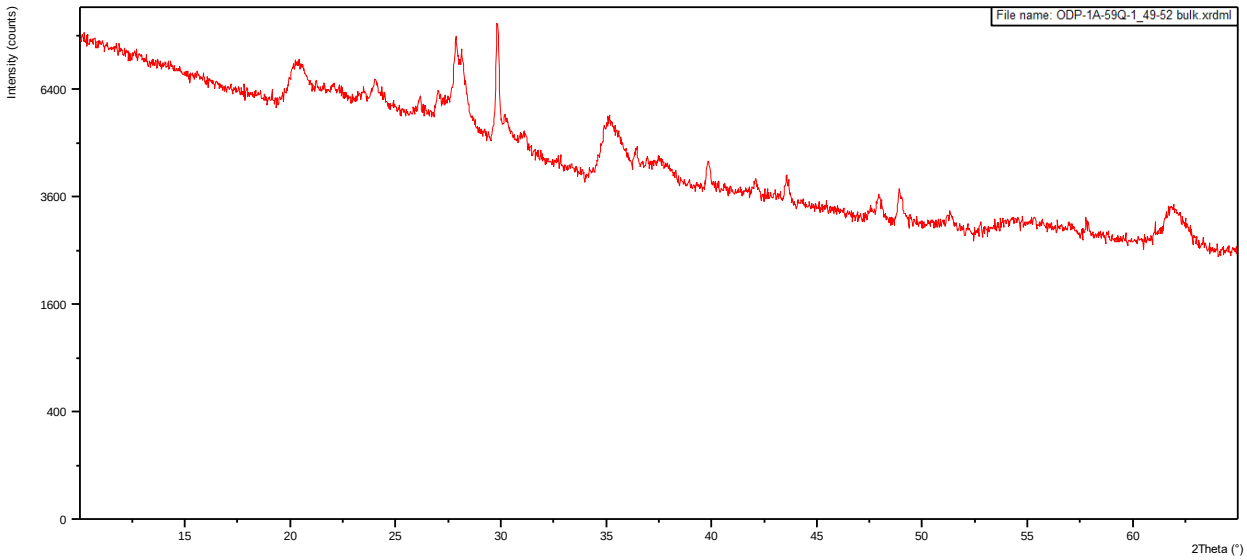
File name: ODP-1A-59Q-1_49-52 bulk.xrdml
Intensity (counts)
0
400
1600
3600
6400
15
20
25
30
35
40
45
50
55
60
2Theta (°)

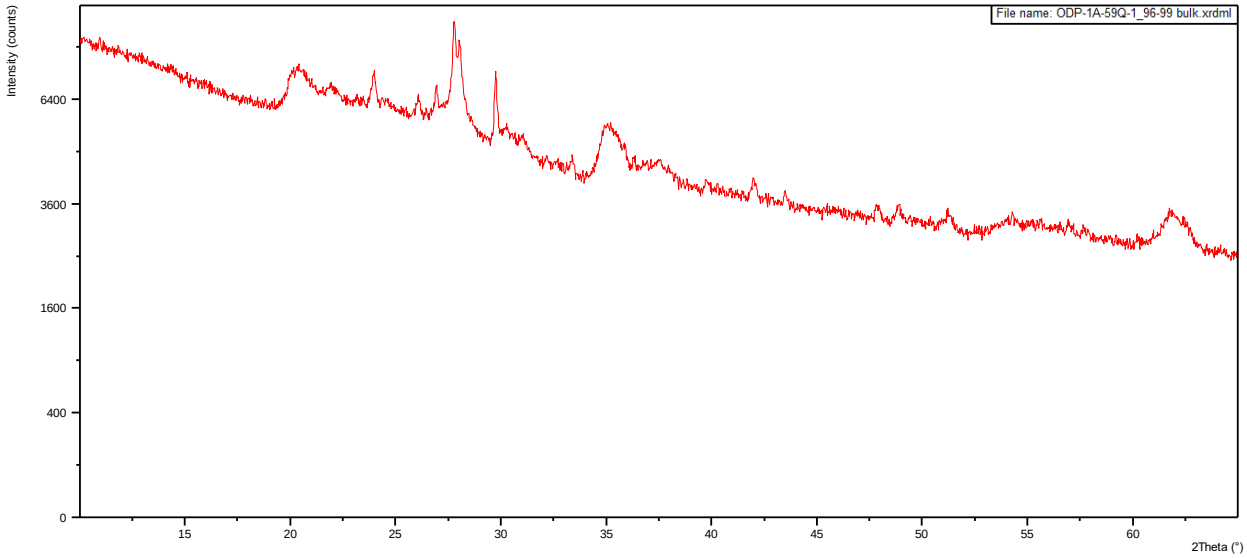
File name: ODP-1A-59Q-1_96-99 bulk.xrdml
Intensity (counts)
0
400
1600
3600
6400
15
20
25
30
35
40
45
50
55
60
2Theta (°)

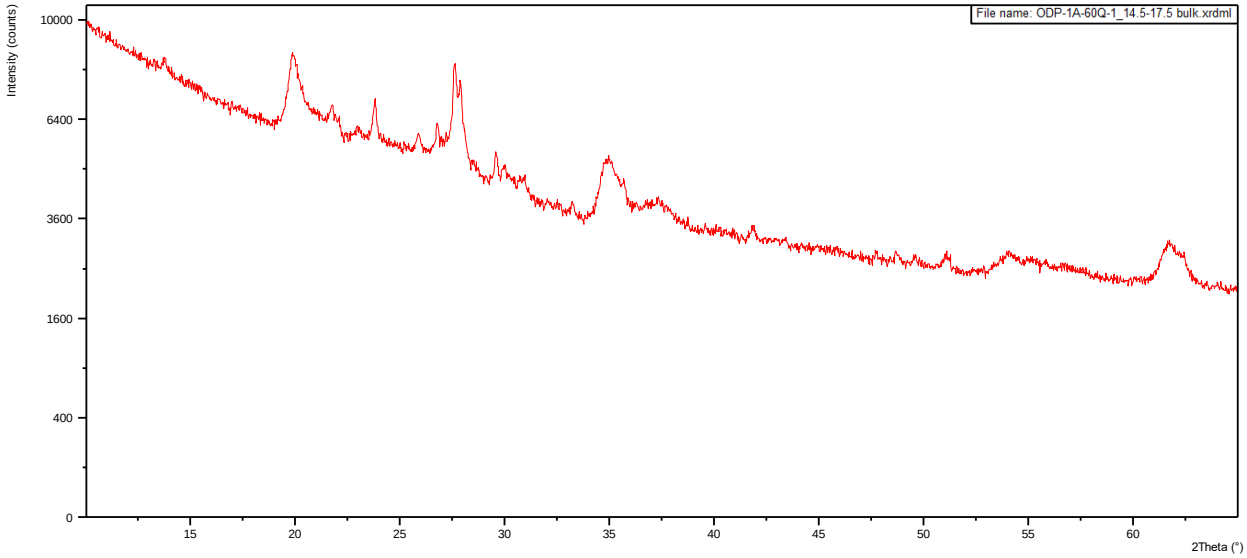
File name: ODP-1A-60Q-1_14.5-17.5 bulk.xrdml
Intensity (counts)
10000
6400
3600
1600
400
0
15
20
25
30
35
40
45
50
55
60
2Theta (°)

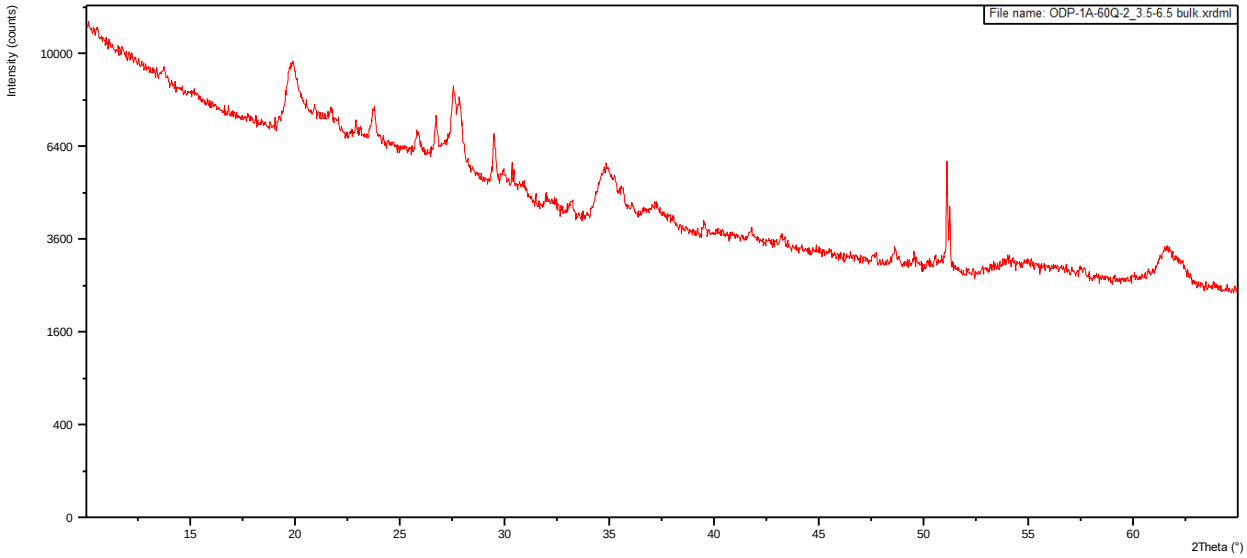
File name: ODP-1A-60Q-2_3.5-6.5 bulk.xrdml
Intensity (counts)
10000
6400
3600
1600
400
0
15
20
25
30
35
40
45
50
55
60
2Theta (°)

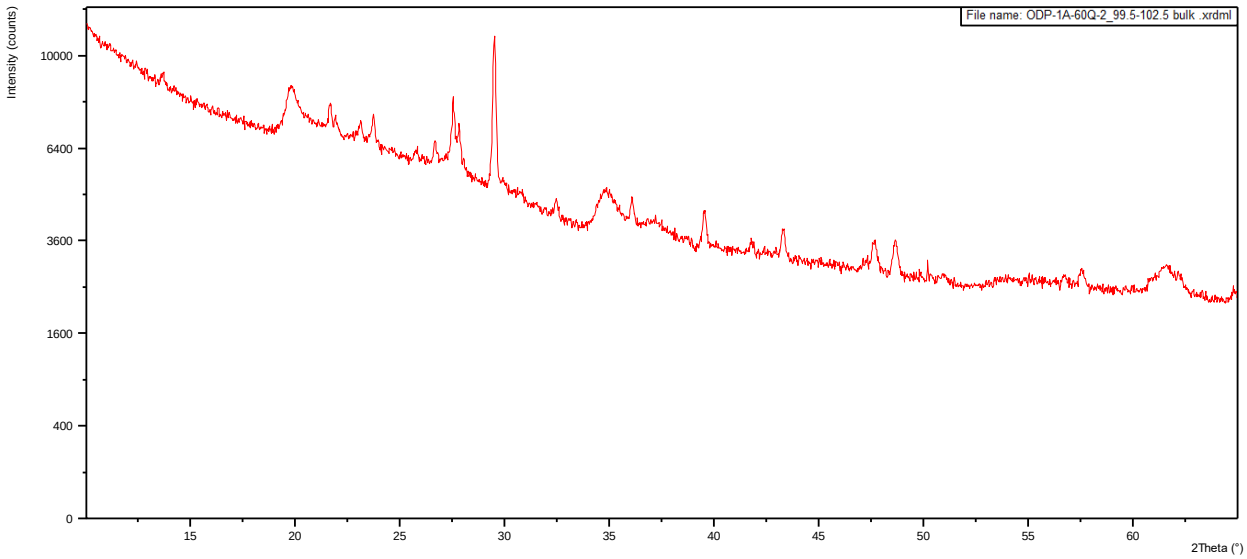
File name: ODP-1A-60Q-2_99.5-102.5 bulk .xrdml
Intensity (counts)
10000
6400
3600
1600
400
0
15
20
25
30
35
40
45
50
55
60
2Theta (°)

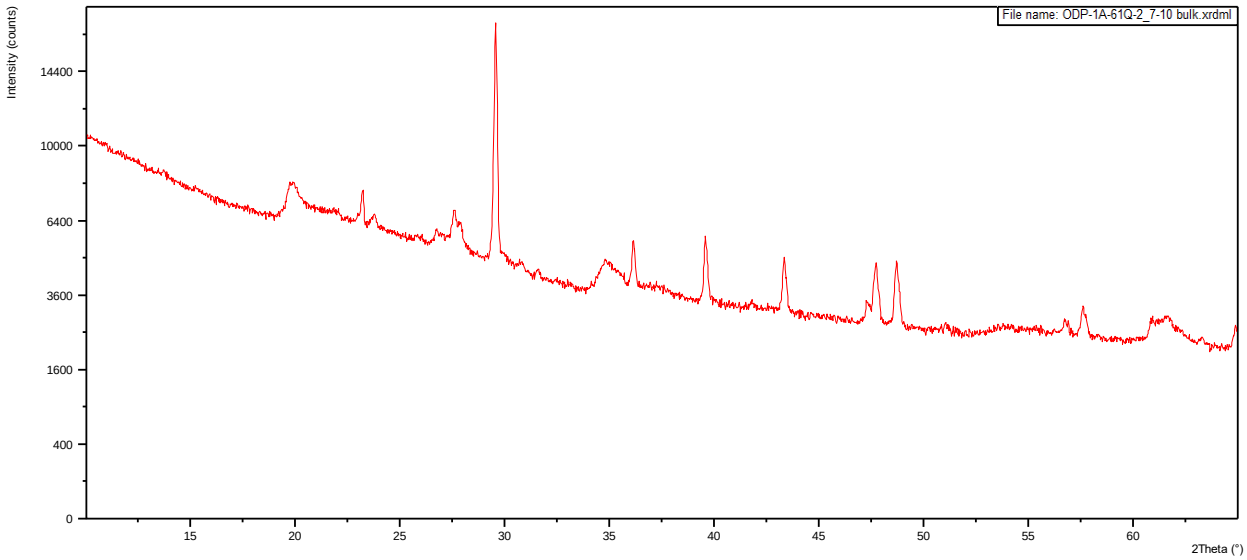
File name: ODP-1A-61Q-2_7-10 bulk.xrdml
Intensity (counts)
14400
10000
6400
3600
1600
400
0
15
20
25
30
35
40
45
50
55
60
2Theta (°)

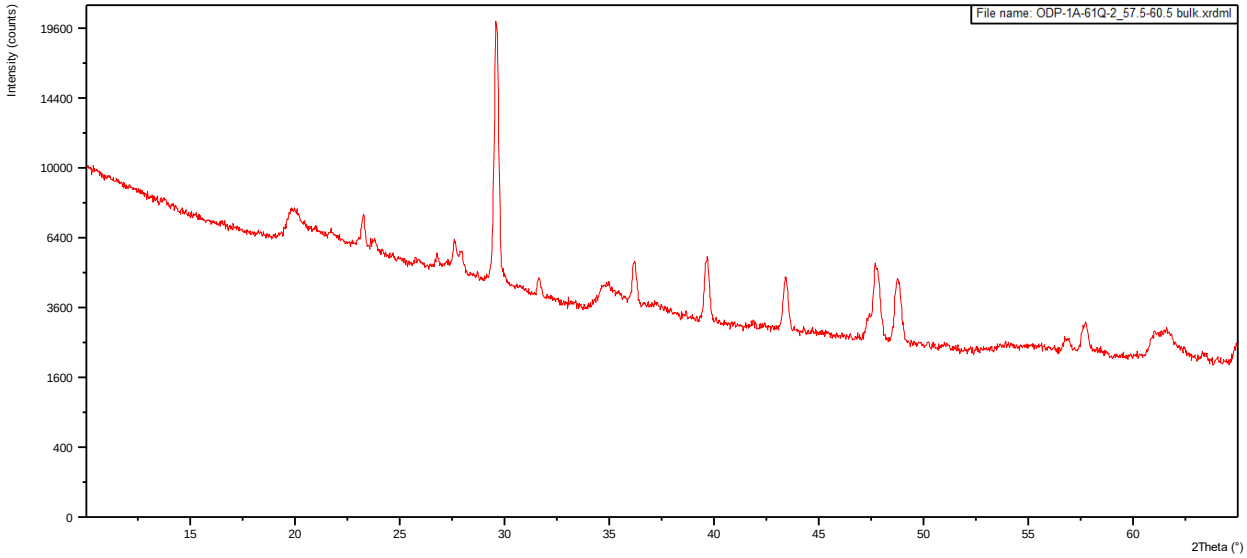
File name: ODP-1A-61Q-2_57.5-60.5 bulk.xrdml
Intensity (counts)
19600
14400
10000
6400
3600
1600
400
0
15
20
25
30
35
40
45
50
55
60
2Theta (°)

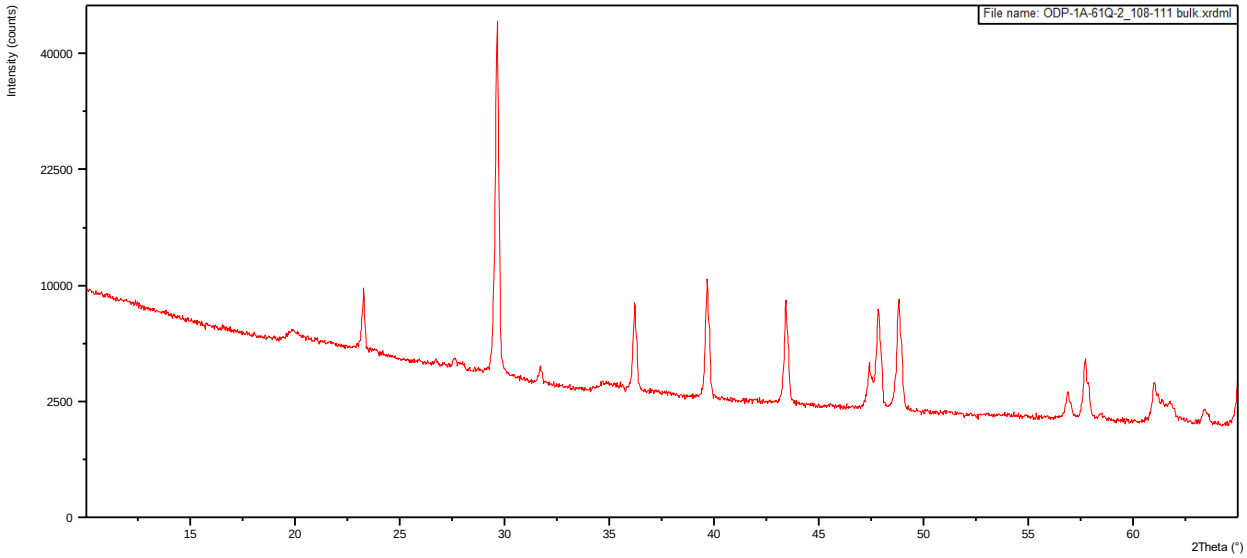
File name: ODP-1A-61Q-2_108-111 bulk.xrdml
Intensity (counts)
40000
22500
10000
2500
0
15
20
25
30
35
40
45
50
55
60
2Theta (°)

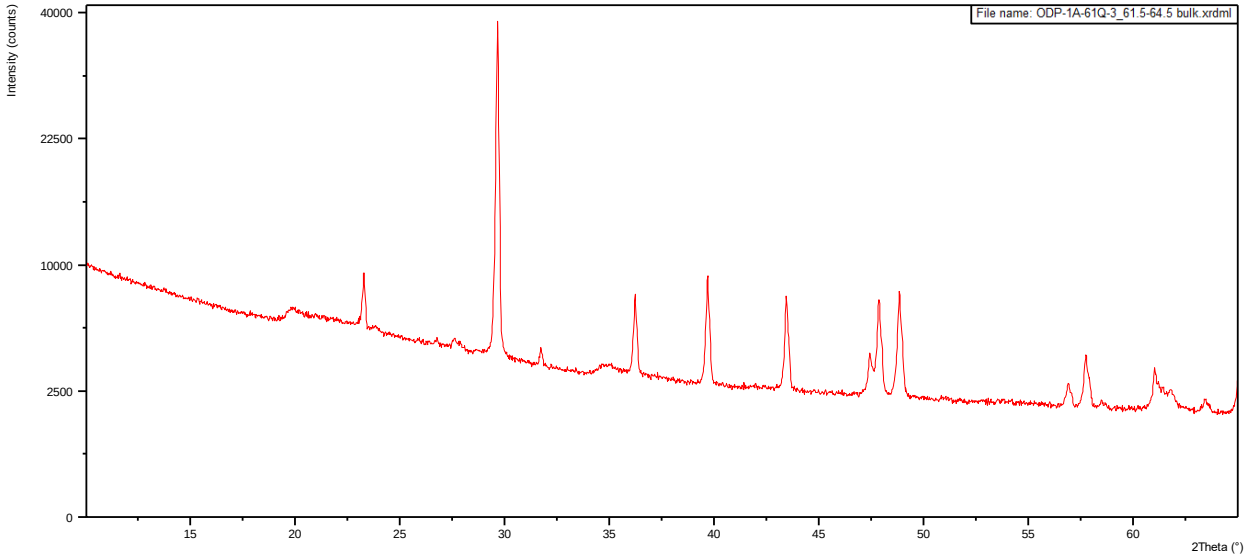
File name: ODP-1A-61Q-3_61.5-64.5 bulk.xrdml
Intensity (counts)
40000
22500
10000
2500
0
15
20
25
30
35
40
45
50
55
60
2Theta (°)

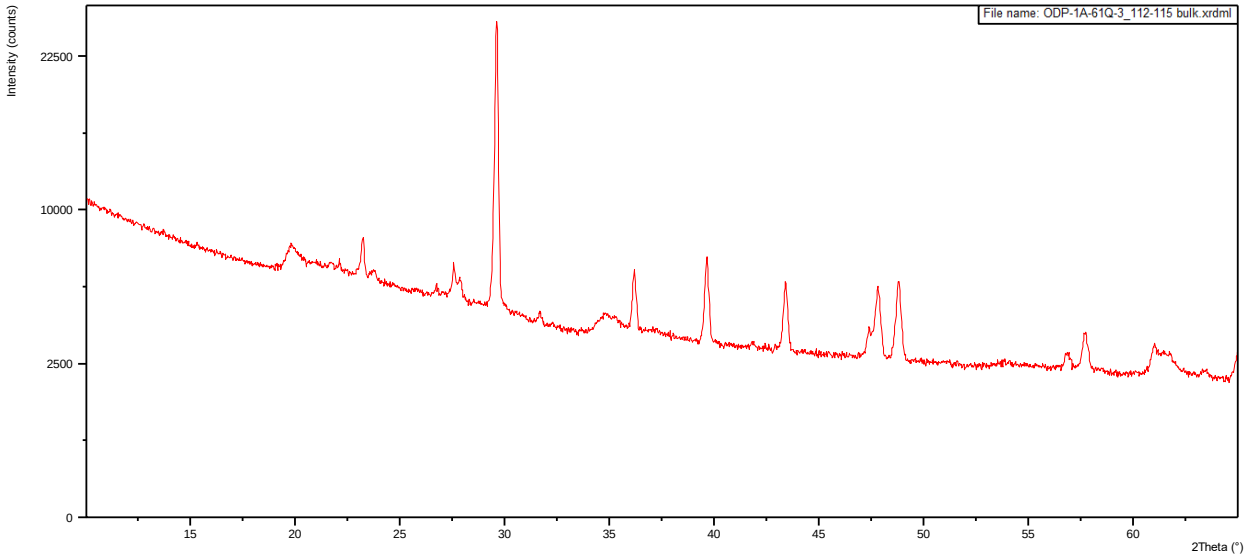
File name: ODP-1A-61Q-3_112-115 bulk.xrdml
Intensity (counts)
22500
10000
2500
0
15
20
25
30
35
40
45
50
55
60
2Theta (°)

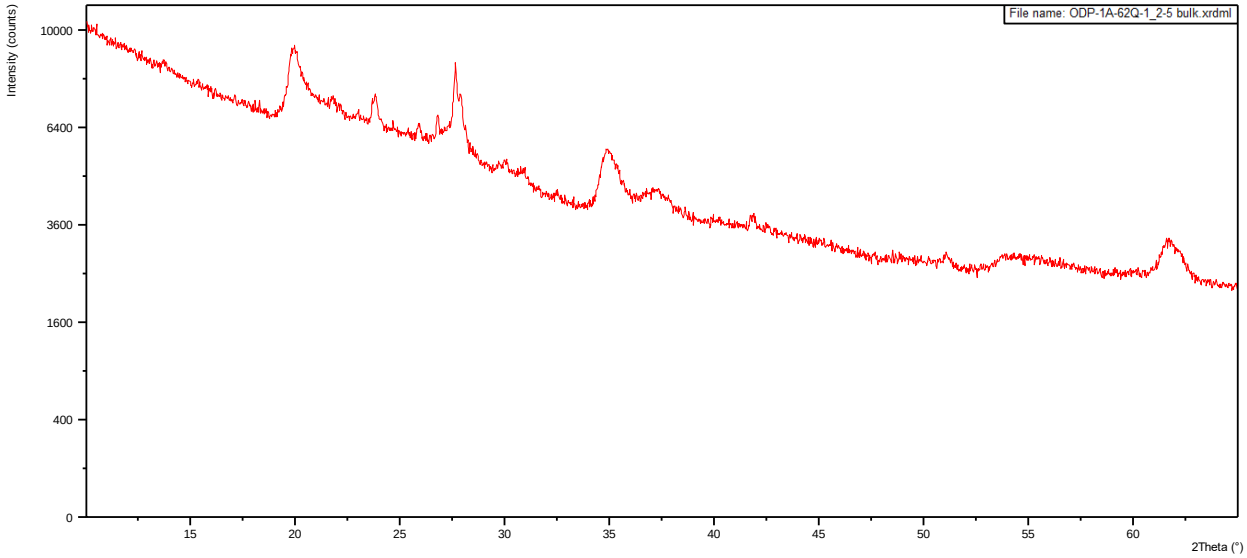
File name: ODP-1A-62Q-1_2-5 bulk.xrdml
Intensity (counts)
10000
6400
3600
1600
400
0
15
20
25
30
35
40
45
50
55
60
2Theta (°)

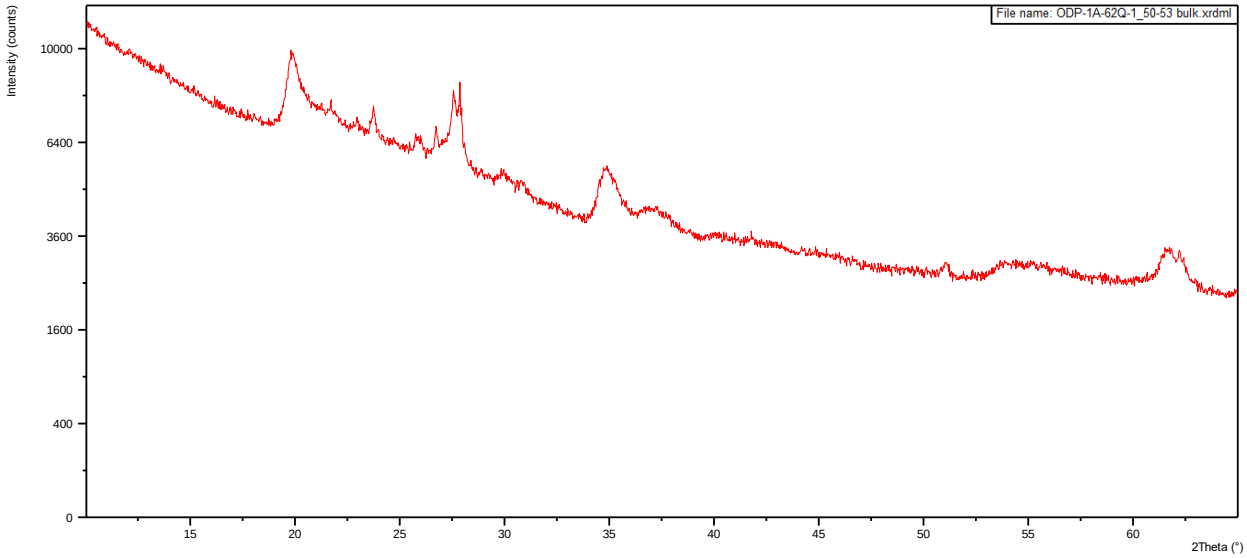
File name: ODP-1A-62Q-1_50-53 bulk.xrdml
Intensity (counts)
10000
6400
3600
1600
400
0
15
20
25
30
35
40
45
50
55
60
2Theta (°)

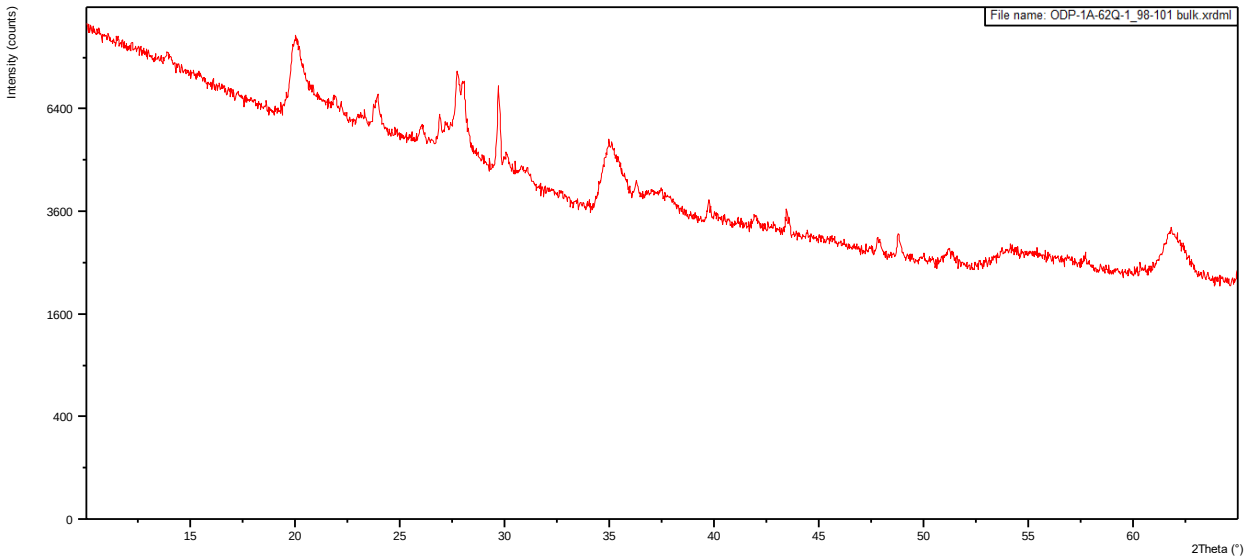
File name: ODP-1A-62Q-1_98-101 bulk.xrdml
Intensity (counts)
0
400
1600
3600
6400
15
20
25
30
35
40
45
50
55
60
2Theta (°)

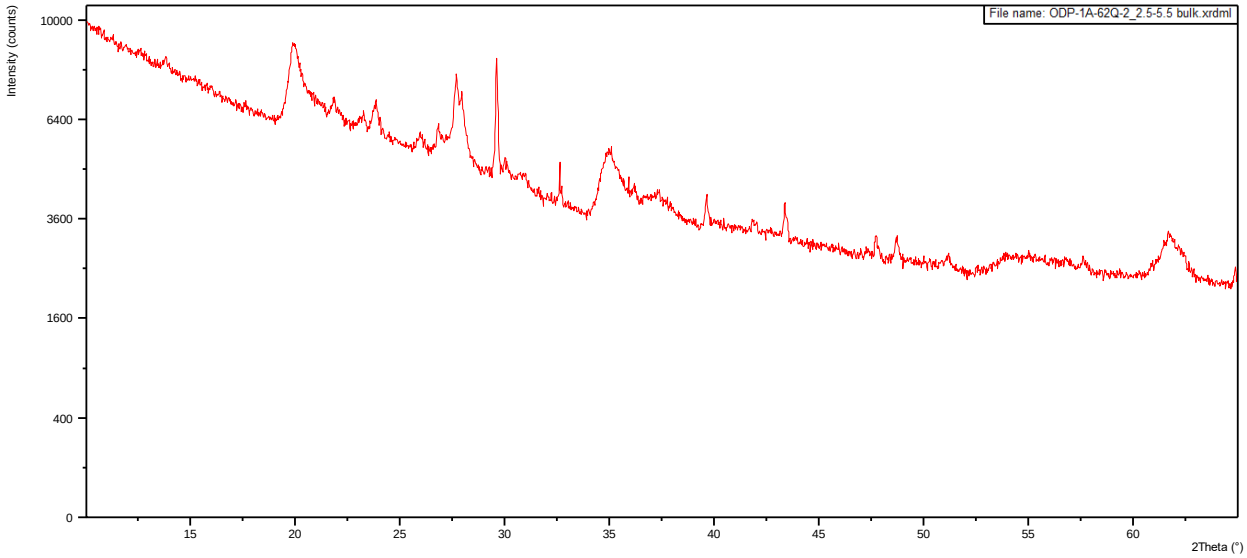
File name: ODP-1A-62Q-2_2.5-5.5 bulk.xrdml
Intensity (counts)
0
400
1600
3600
6400
10000
15
20
25
30
35
40
45
50
55
60
2Theta (°)

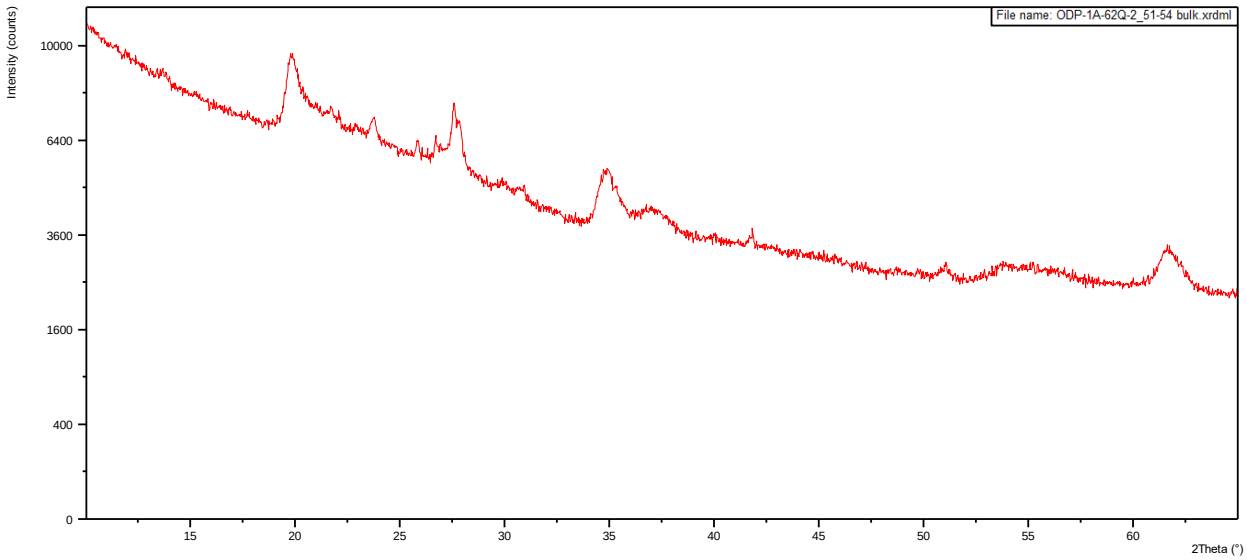
File name: ODP-1A-62Q-2_51-54 bulk.xrdml
Intensity (counts)
10000
6400
3600
1600
400
0
15
20
25
30
35
40
45
50
55
60
2Theta (°)

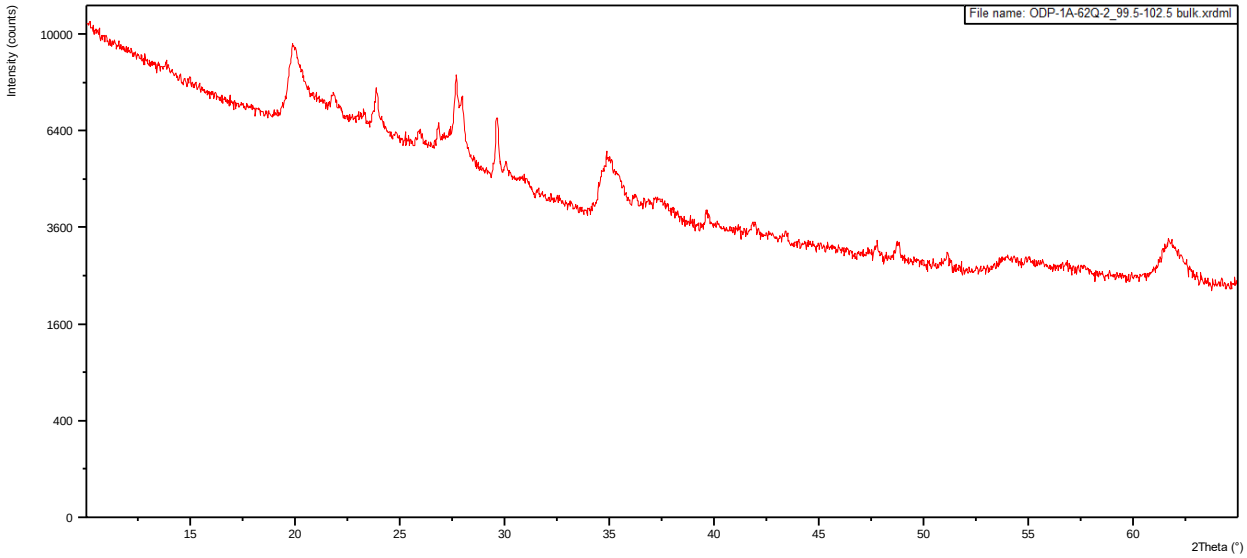
File name: ODP-1A-62Q-2_99.5-102.5 bulk.xrdml
Intensity (counts)
10000
6400
3600
1600
400
0
15
20
25
30
35
40
45
50
55
60
2Theta (°)

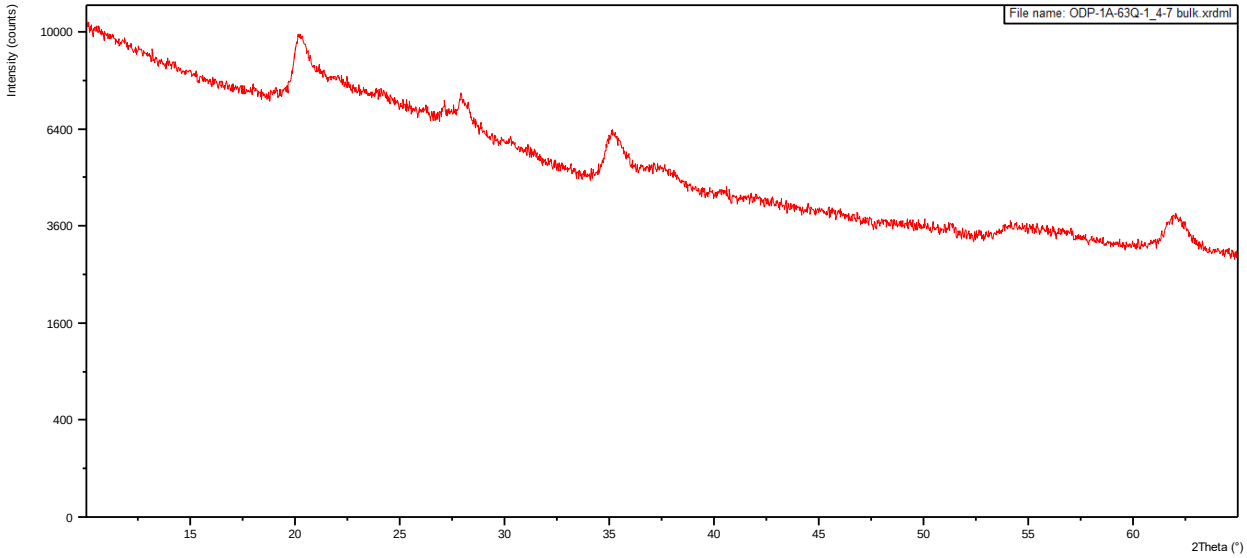
File name: ODP-1A-63Q-1_4-7 bulk.xrdml
Intensity (counts)
10000
6400
3600
1600
400
0
15
20
25
30
35
40
45
50
55
60
2Theta (°)

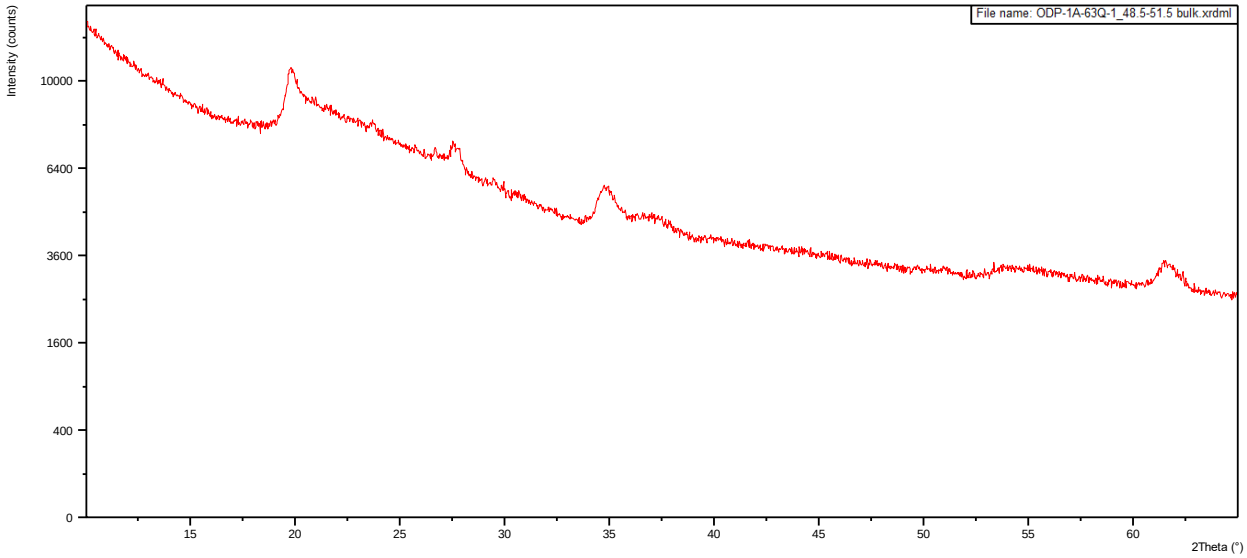
File name: ODP-1A-63Q-1_48.5-51.5 bulk.xrdml
Intensity (counts)
10000
6400
3600
1600
400
0
15
20
25
30
35
40
45
50
55
60
2Theta (°)

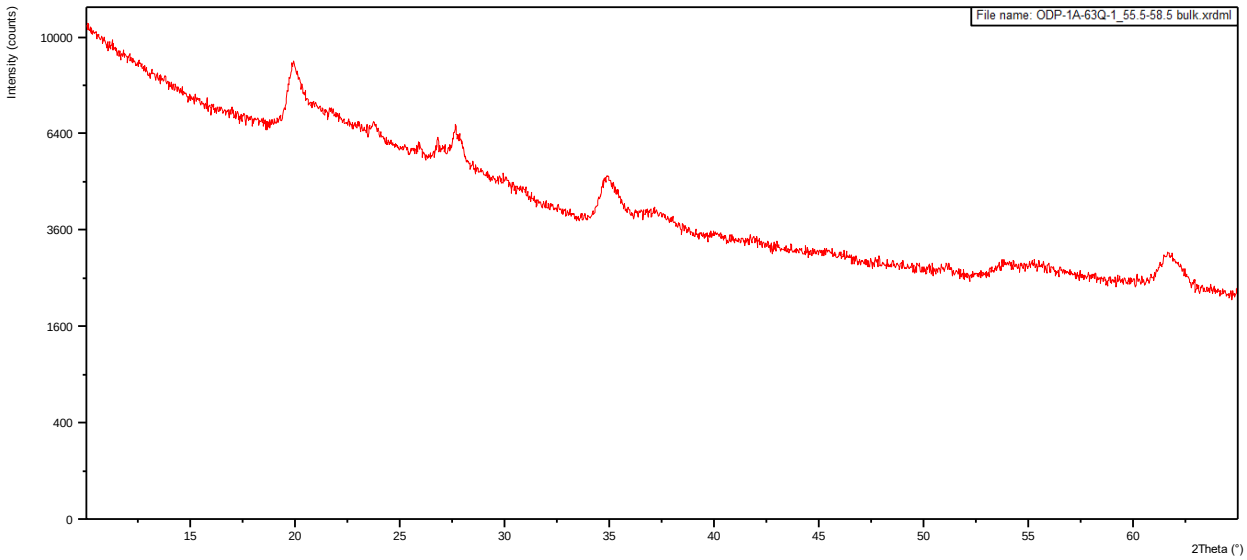
File name: ODP-1A-63Q-1_55.5-58.5 bulk.xrdml
Intensity (counts)
10000
6400
3600
1600
400
0
15
20
25
30
35
40
45
50
55
60
2Theta (°)

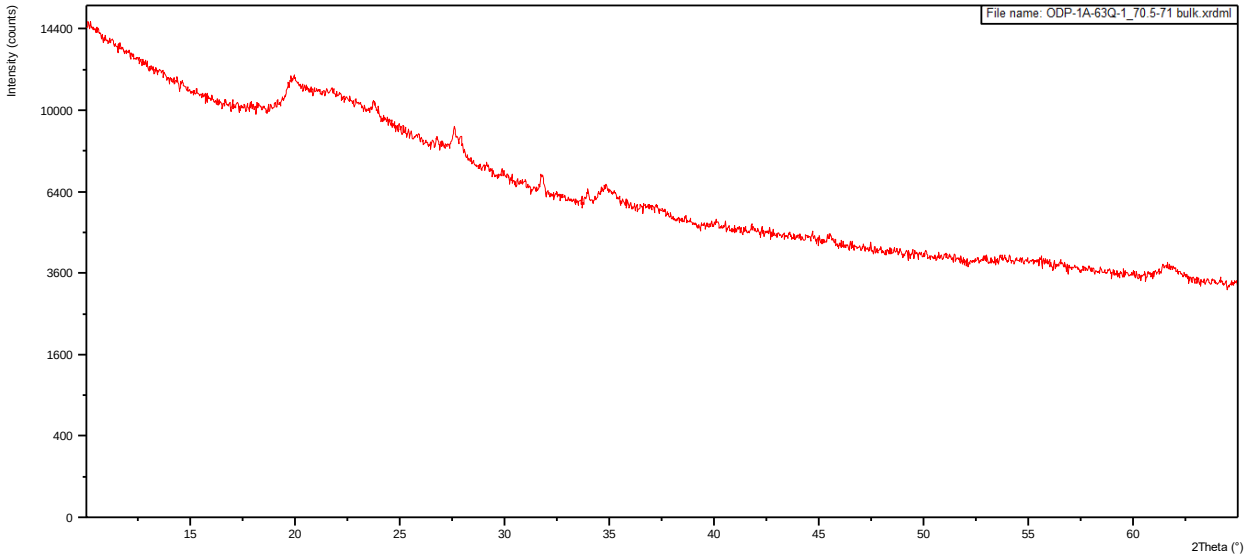
File name: ODP-1A-63Q-1_70.5-71 bulk.xrdml
Intensity (counts)
14400
10000
6400
3600
1600
400
0
15
20
25
30
35
40
45
50
55
60
2Theta (°)

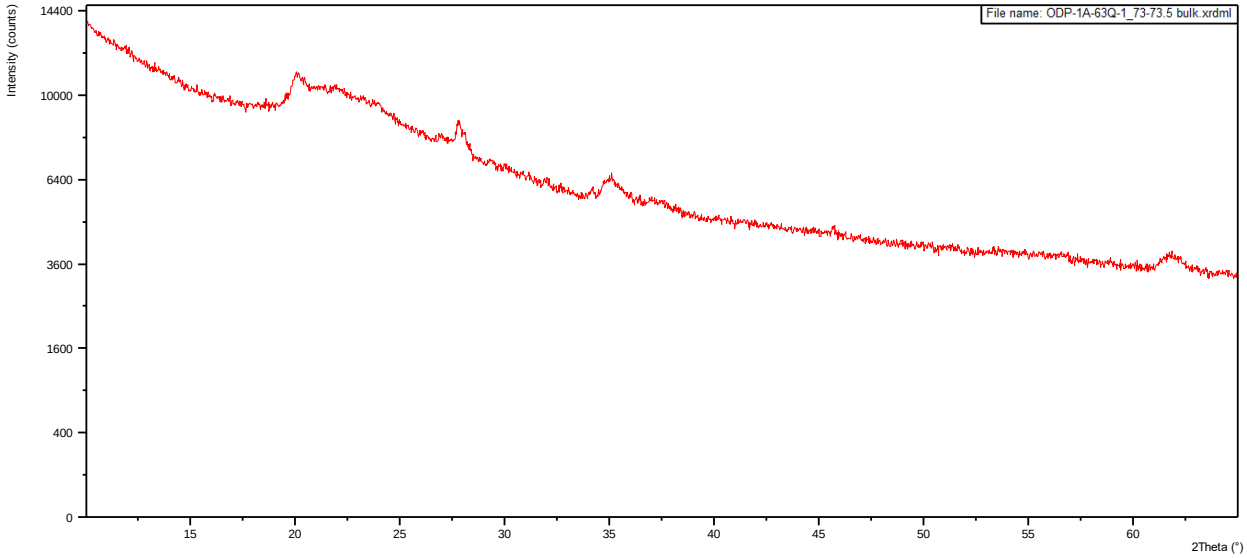
File name: ODP-1A-63Q-1_73-73.5 bulk.xrdml
Intensity (counts)
14400
10000
6400
3600
1600
400
0
15
20
25
30
35
40
45
50
55
60
2Theta (°)

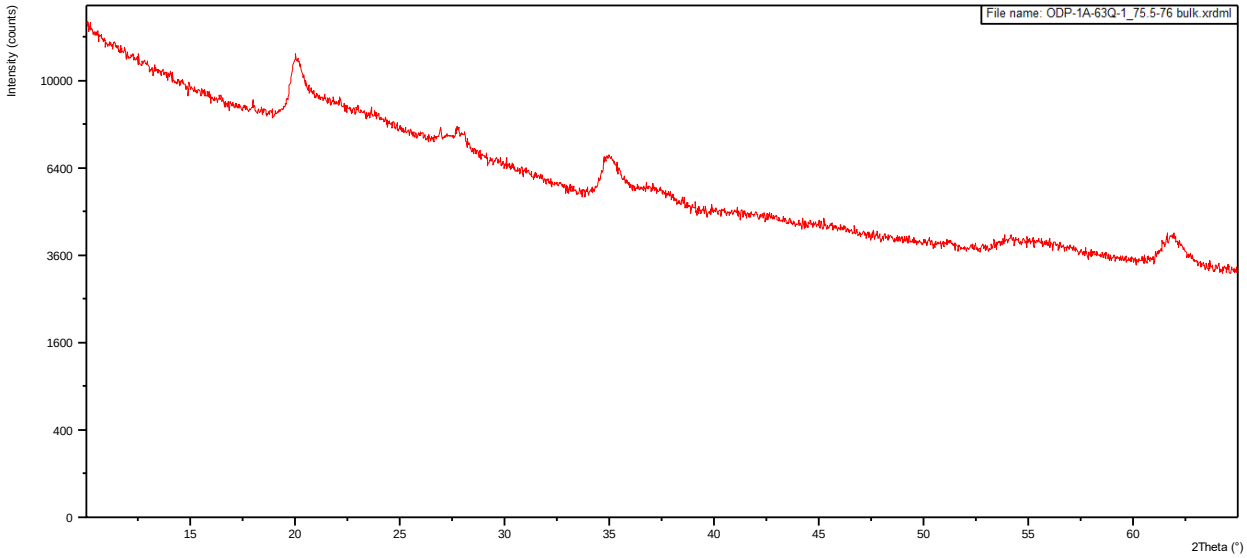
File name: ODP-1A-63Q-1_75.5-76 bulk.xrdml
Intensity (counts)
10000
6400
3600
1600
400
0
15
20
25
30
35
40
45
50
55
60
2Theta (°)

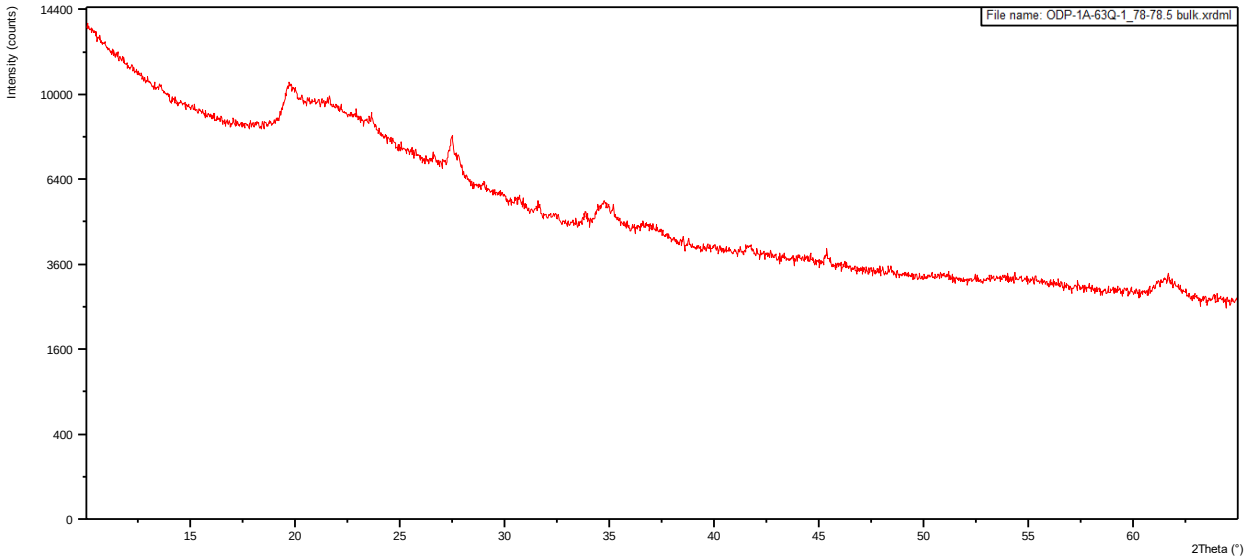
File name: ODP-1A-63Q-1_78-78.5 bulk.xrdml
Intensity (counts)
14400
10000
6400
3600
1600
400
0
15
20
25
30
35
40
45
50
55
60
2Theta (°)

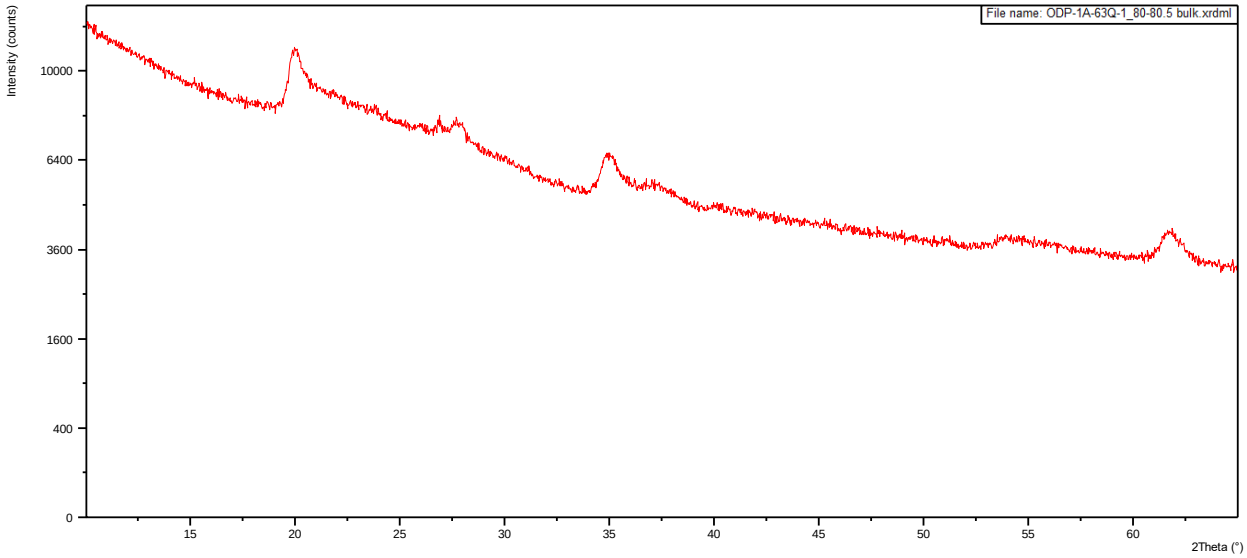
File name: ODP-1A-63Q-1_80-80.5 bulk.xrdml
Intensity (counts)
10000
6400
3600
1600
400
0
15
20
25
30
35
40
45
50
55
60
2Theta (°)

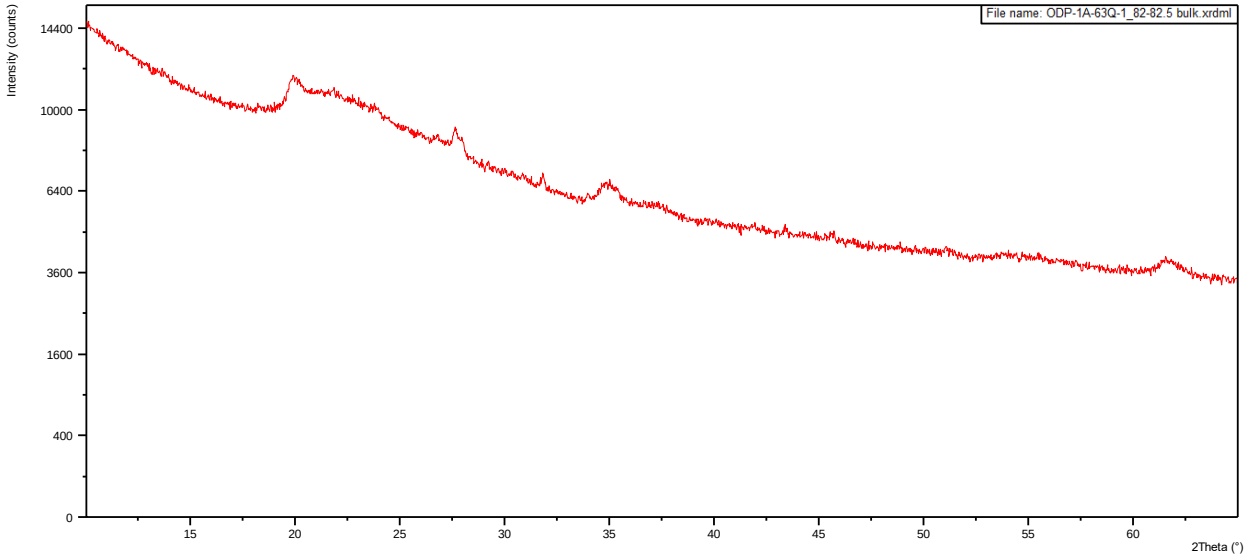
File name: ODP-1A-63Q-1_82-82.5 bulk.xrdml
Intensity (counts)
14400
10000
6400
3600
1600
400
0
15
20
25
30
35
40
45
50
55
60
2Theta (°)

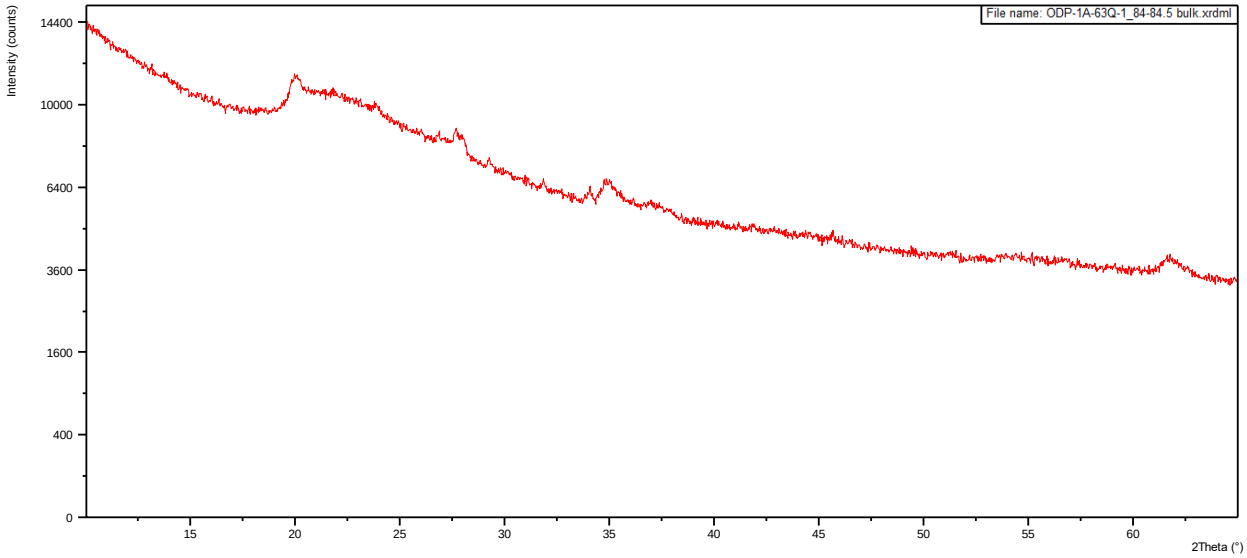
File name: ODP-1A-63Q-1_84-84.5 bulk.xrdml
Intensity (counts)
14400
10000
6400
3600
1600
400
0
15
20
25
30
35
40
45
50
55
60
2Theta (°)

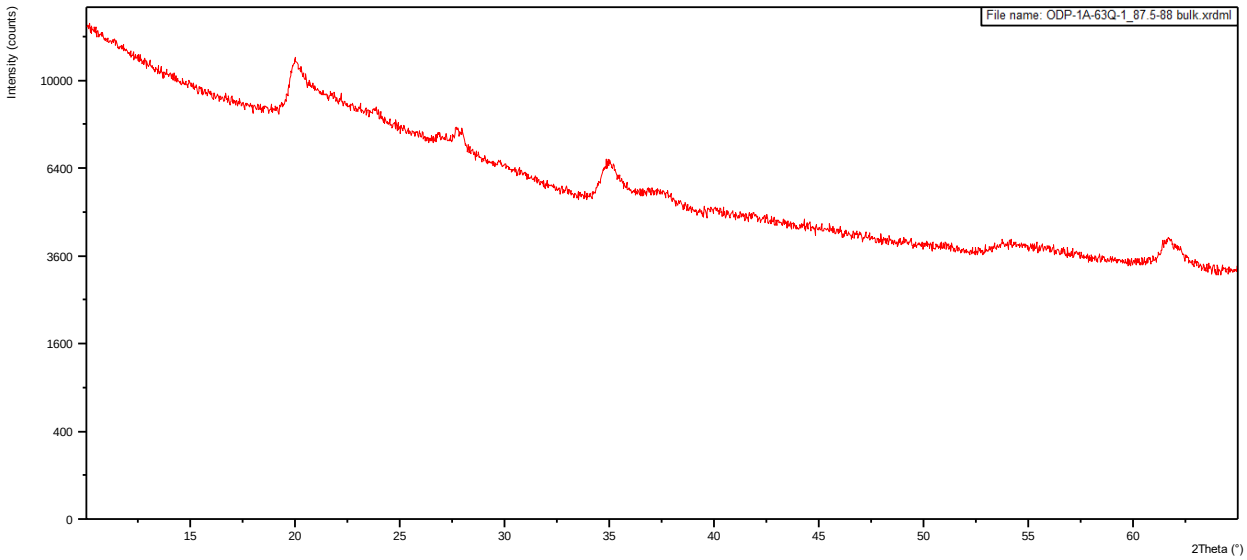
File name: ODP-1A-63Q-1_87.5-88 bulk.xrdml
Intensity (counts)
10000
6400
3600
1600
400
0
15
20
25
30
35
40
45
50
55
60
2Theta (°)

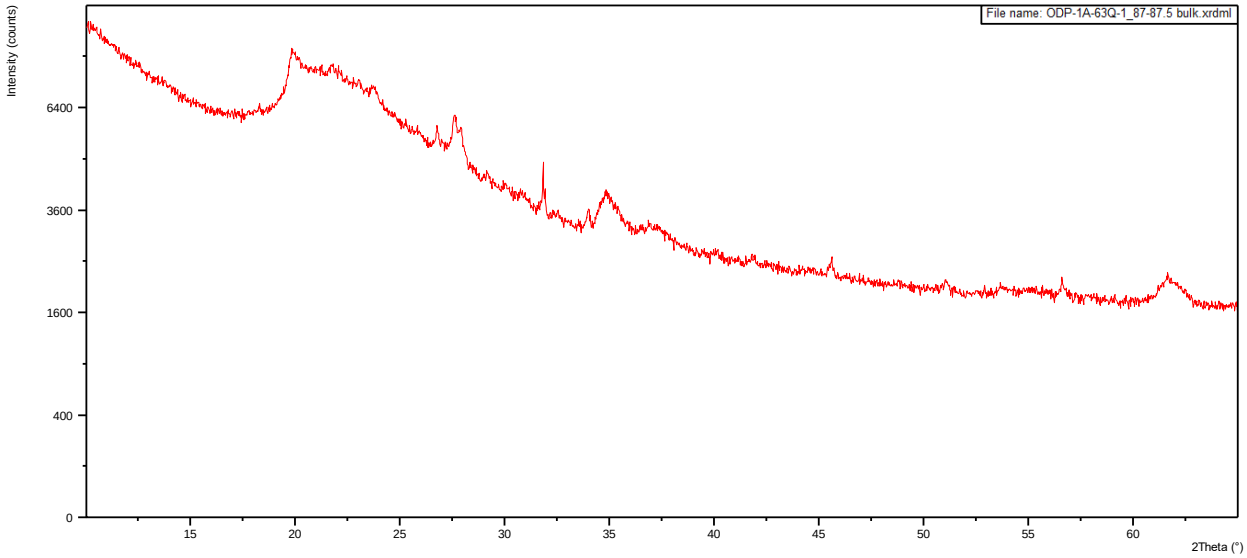
File name: ODP-1A-63Q-1_87-87.5 bulk.xrdml
Intensity (counts)
6400
3600
1600
400
0
15
20
25
30
35
40
45
50
55
60
2Theta (°)

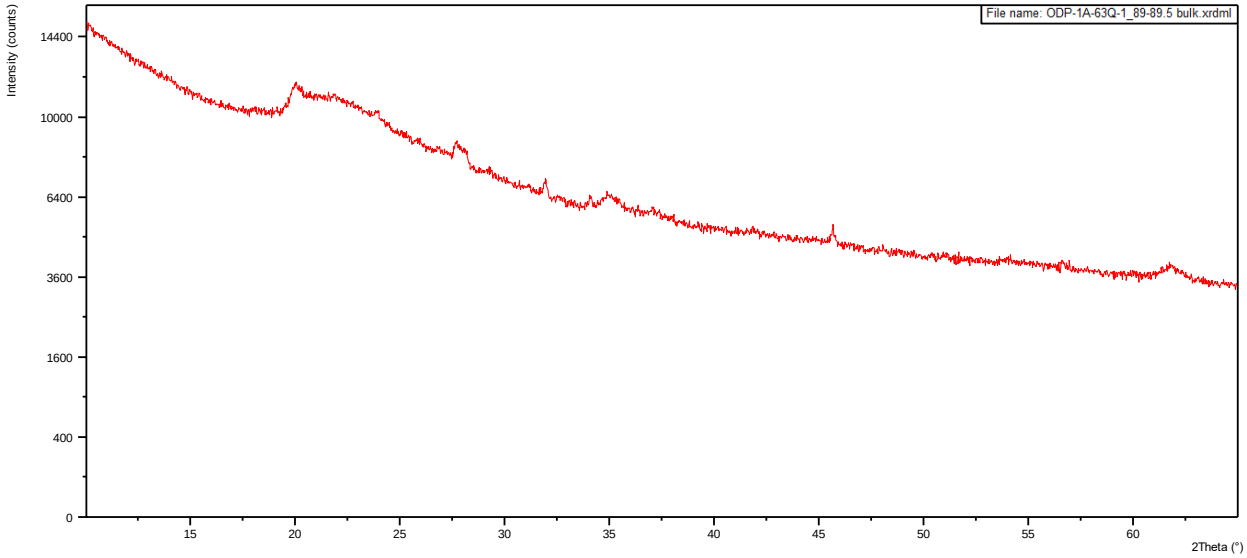
File name: ODP-1A-63Q-1_89-89.5 bulk.xrdml
Intensity (counts)
14400
10000
6400
3600
1600
400
0
15
20
25
30
35
40
45
50
55
60
2Theta (°)

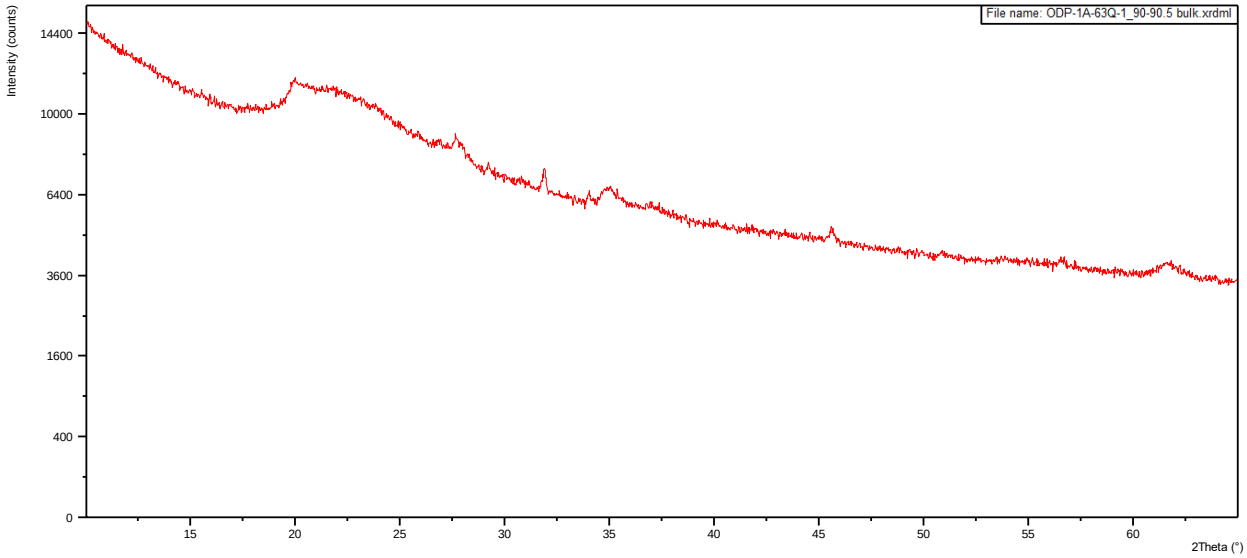
File name: ODP-1A-63Q-1_90-90.5 bulk.xrdml
Intensity (counts)
14400
10000
6400
3600
1600
400
0
15
20
25
30
35
40
45
50
55
60
2Theta (°)

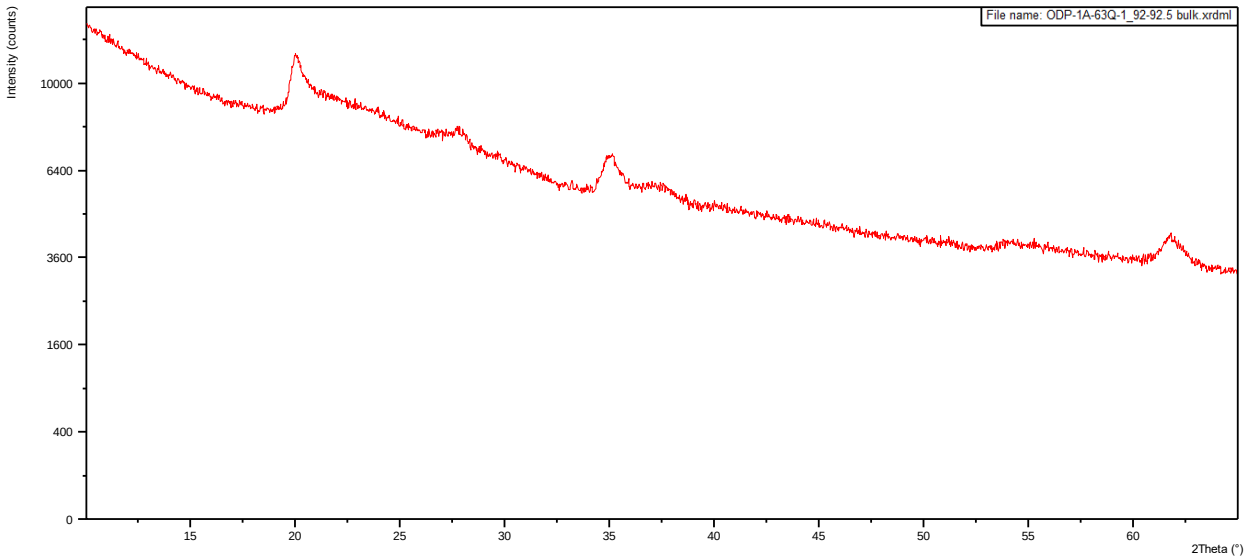
File name: ODP-1A-63Q-1_92-92.5 bulk.xrdml
Intensity (counts)
10000
6400
3600
1600
400
0
15
20
25
30
35
40
45
50
55
60
2Theta (°)

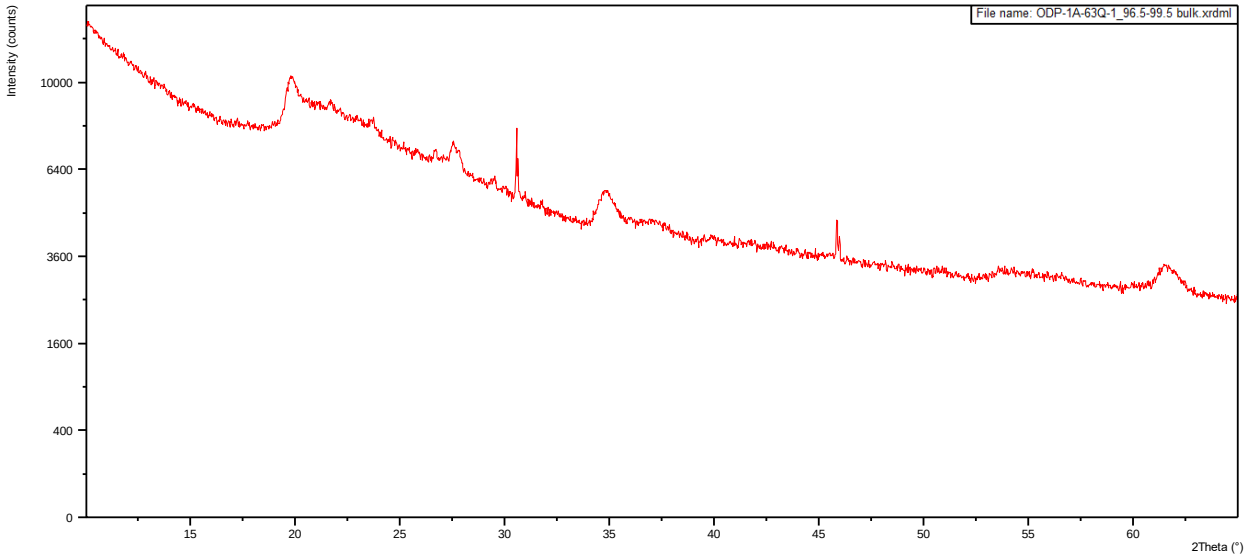
File name: ODP-1A-63Q-1_96.5-99.5 bulk.xrdml
Intensity (counts)
10000
6400
3600
1600
400
0
15
20
25
30
35
40
45
50
55
60
2Theta (°)

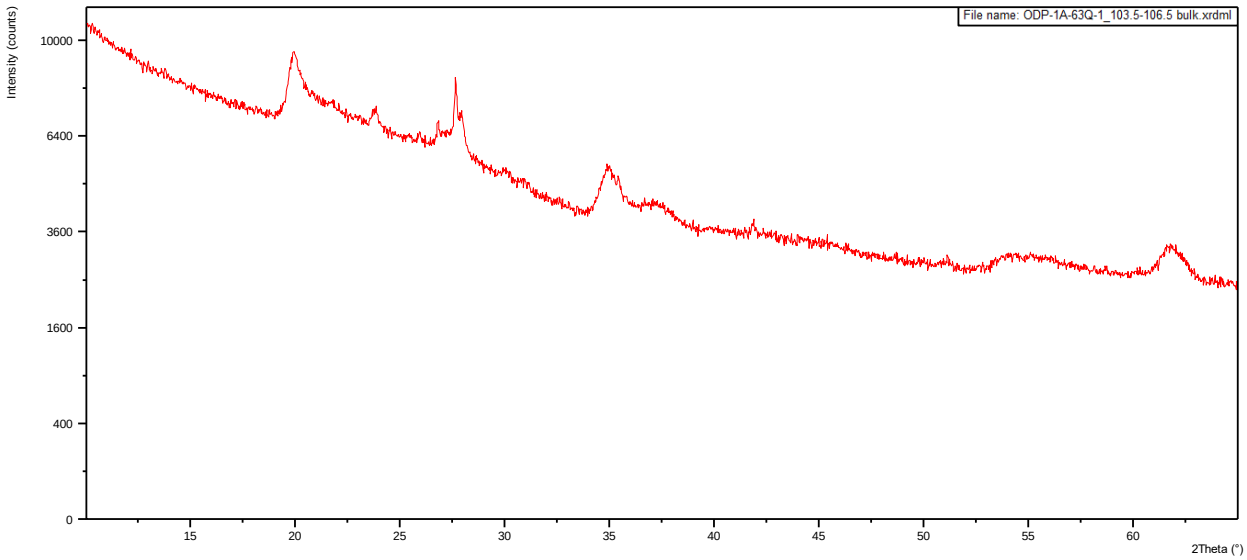
File name: ODP-1A-63Q-1_103.5-106.5 bulk.xrdml
Intensity (counts)
10000
6400
3600
1600
400
0
15
20
25
30
35
40
45
50
55
60
2Theta (°)

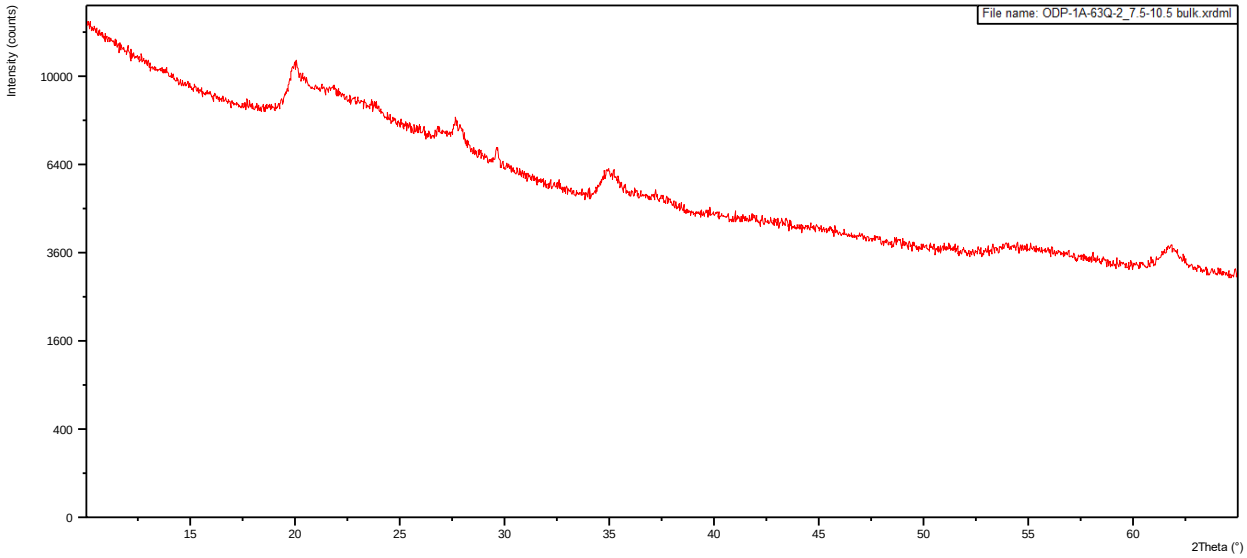
File name: ODP-1A-63Q-2_7.5-10.5 bulk.xrdml
Intensity (counts)
10000
6400
3600
1600
400
0
15
20
25
30
35
40
45
50
55
60
2Theta (°)

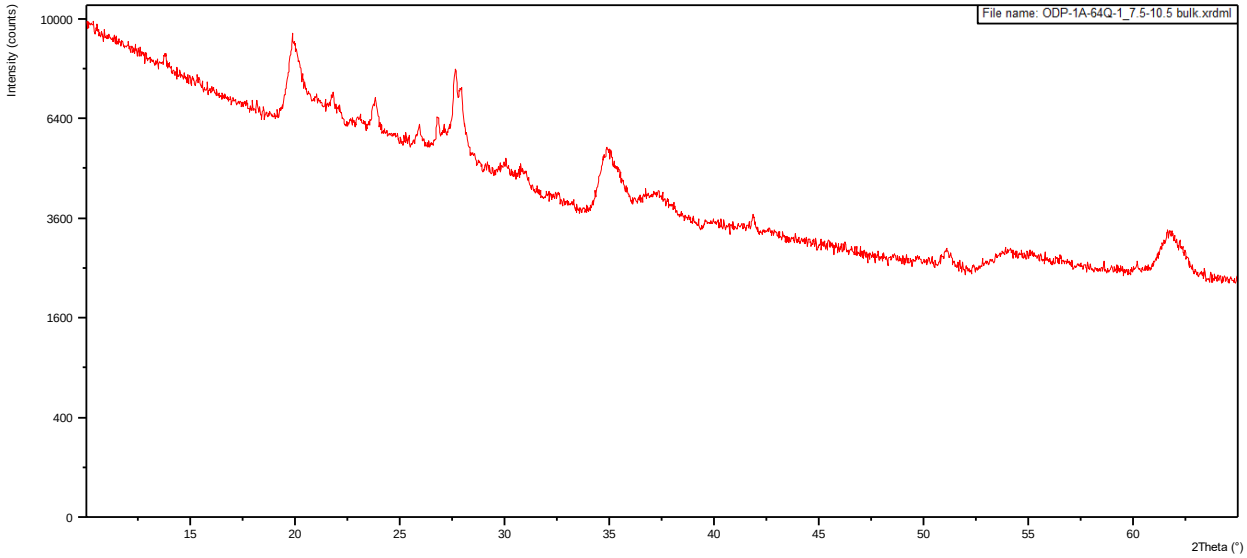
File name: ODP-1A-64Q-1_7.5-10.5 bulk.xrdml
Intensity (counts)
10000
6400
3600
1600
400
0
15
20
25
30
35
40
45
50
55
60
2Theta (°)

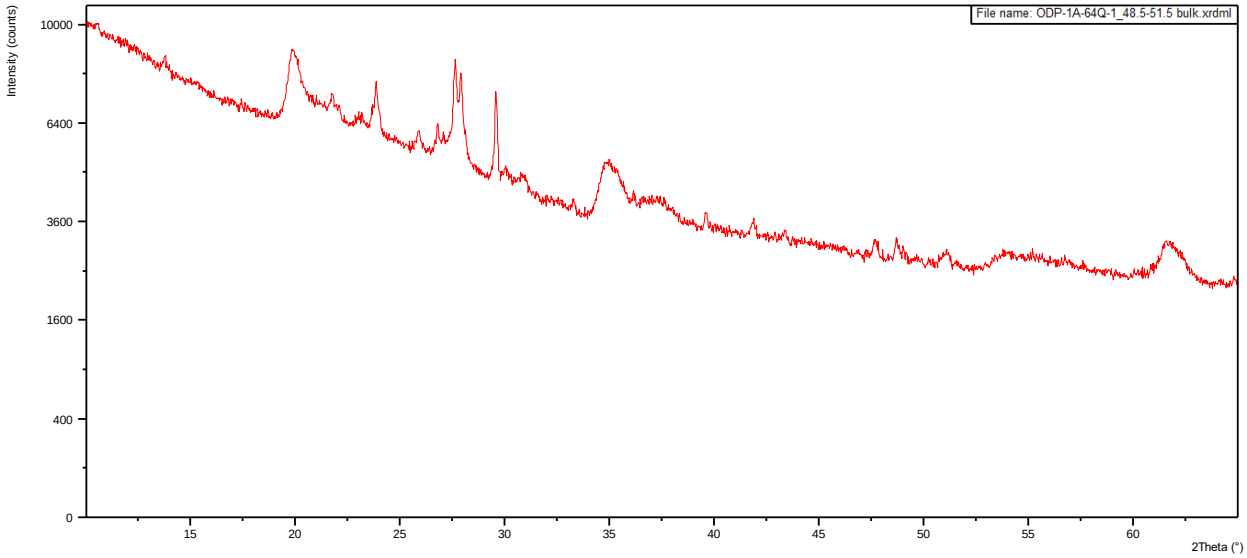
File name: ODP-1A-64Q-1_48.5-51.5 bulk.xrdml
Intensity (counts)
10000
6400
3600
1600
400
0
15
20
25
30
35
40
45
50
55
60
2Theta (°)

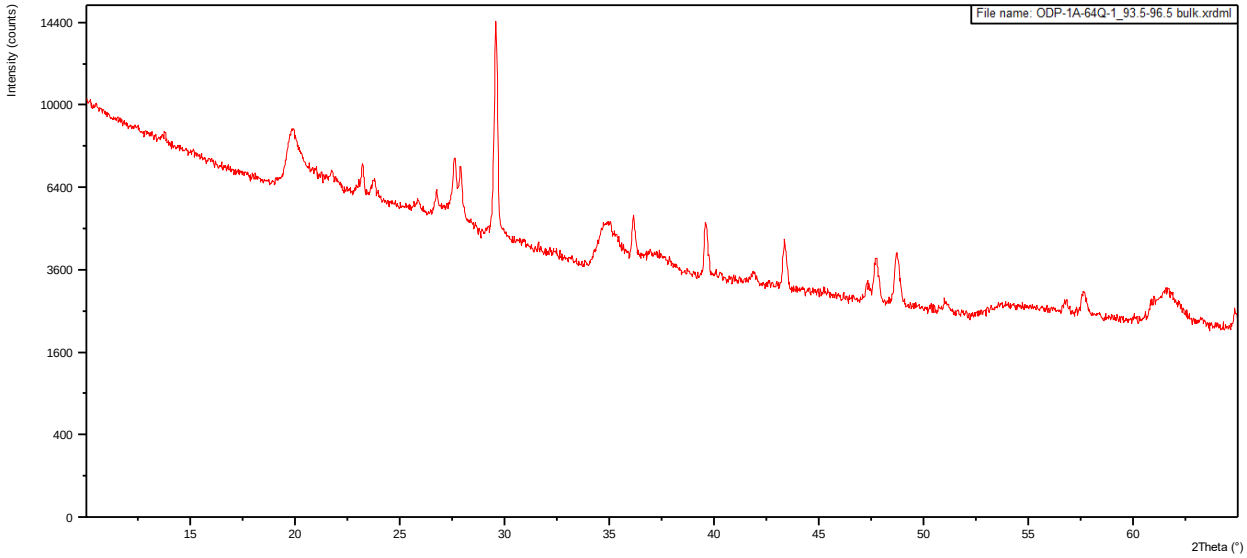
File name: ODP-1A-64Q-1_93.5-96.5 bulk.xrdml
Intensity (counts)
14400
10000
6400
3600
1600
400
0
15
20
25
30
35
40
45
50
55
60
2Theta (°)

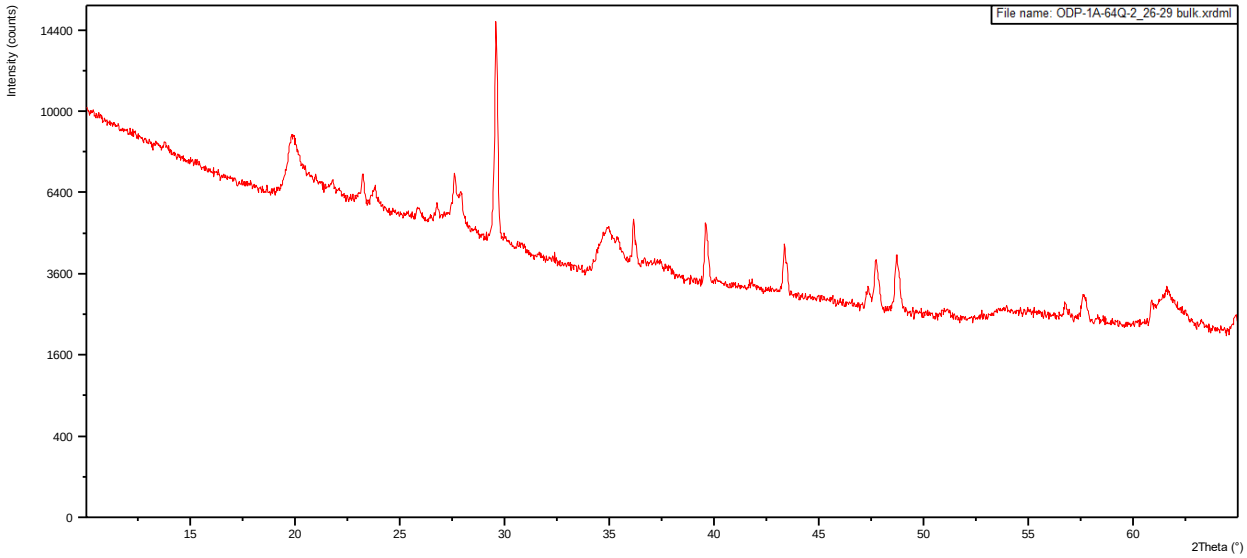
File name: ODP-1A-64Q-2_26-29 bulk.xrdml
Intensity (counts)
14400
10000
6400
3600
1600
400
0
15
20
25
30
35
40
45
50
55
60
2Theta (°)

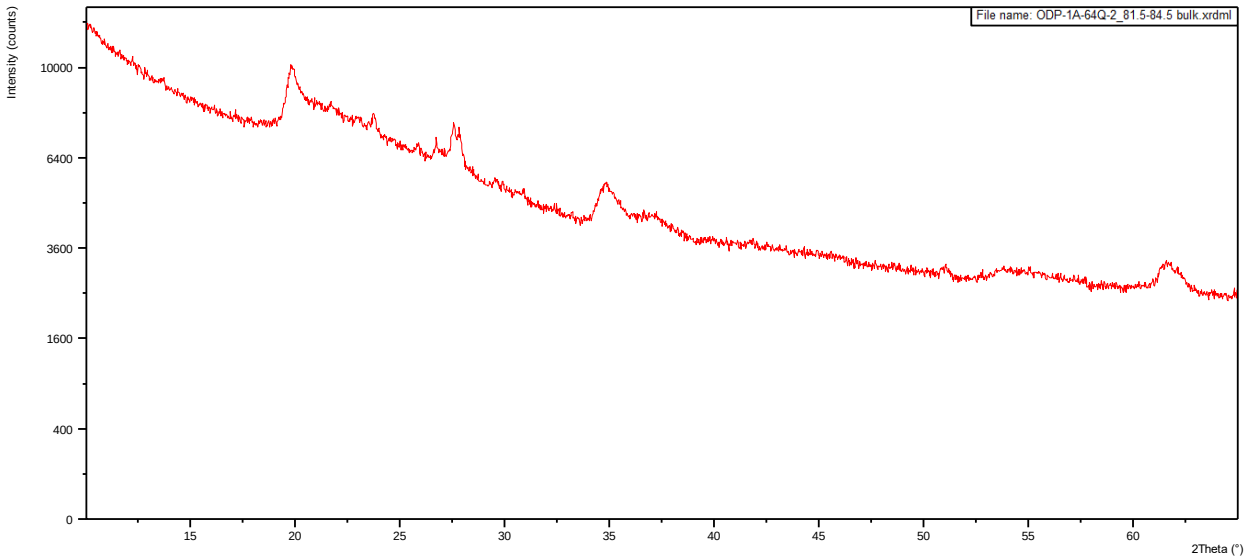
File name: ODP-1A-64Q-2_81.5-84.5 bulk.xrdml
Intensity (counts)
10000
6400
3600
1600
400
0
15
20
25
30
35
40
45
50
55
60
2Theta (°)

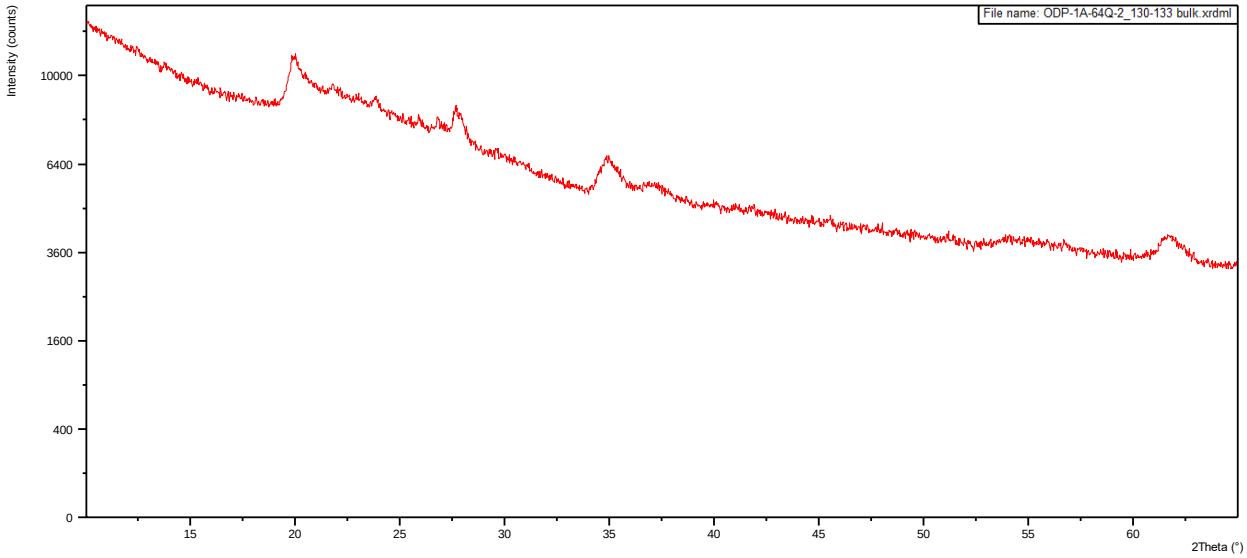
File name: ODP-1A-64Q-2_130-133 bulk.xrdml
Intensity (counts)
10000
6400
3600
1600
400
0
15
20
25
30
35
40
45
50
55
60
2Theta (°)

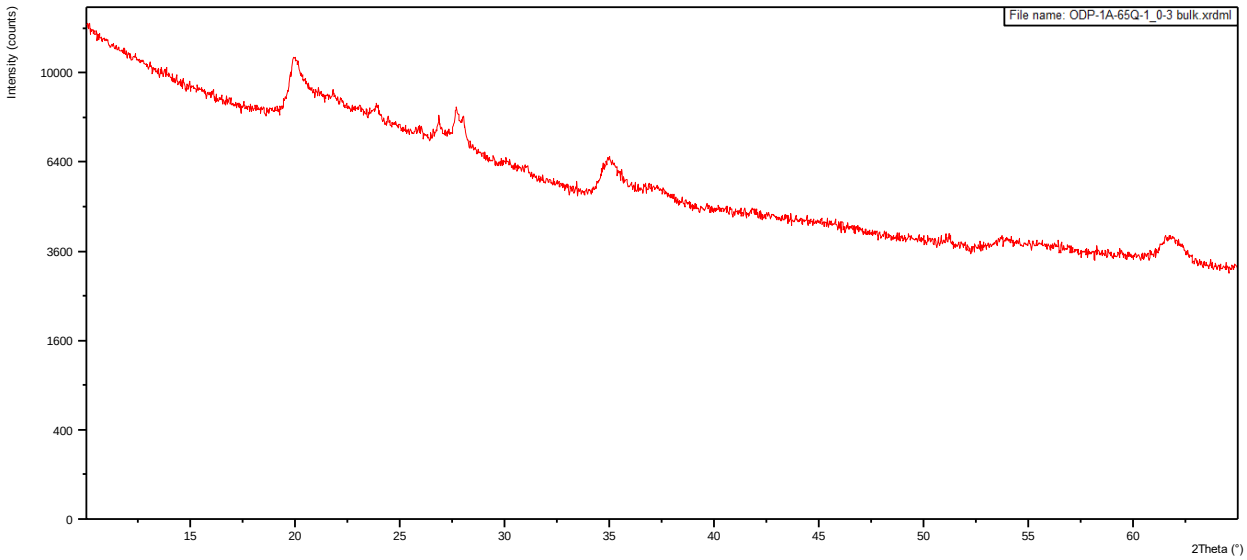
File name: ODP-1A-65Q-1_0-3 bulk.xrdml
Intensity (counts)
10000
6400
3600
1600
400
0
15
20
25
30
35
40
45
50
55
60
2Theta (°)

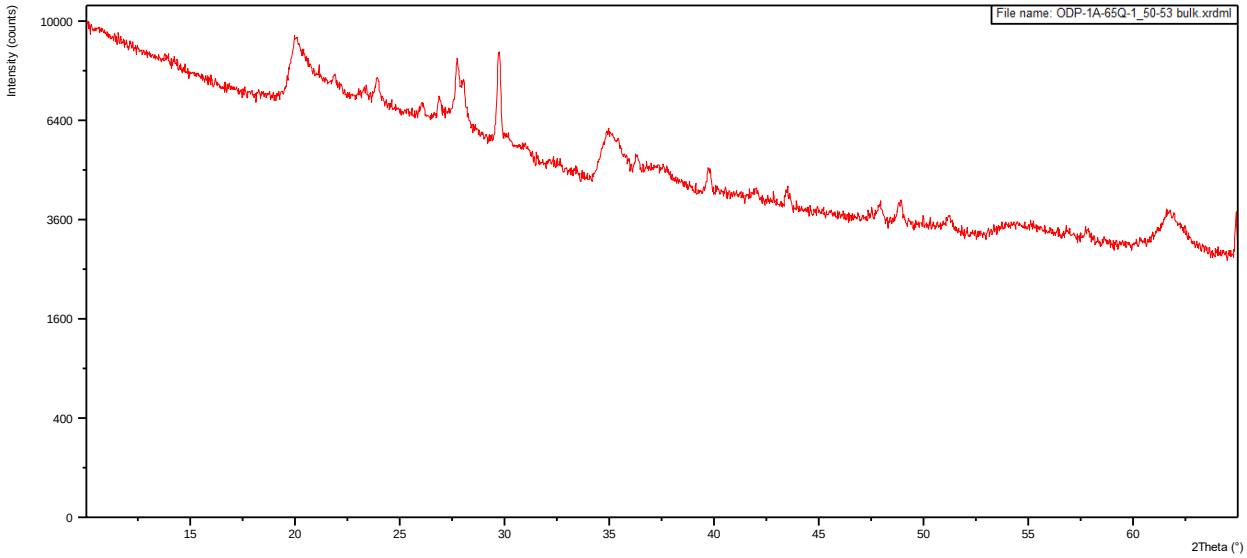
File name: ODP-1A-65Q-1_50-53 bulk.xrdml
Intensity (counts)
10000
6400
3600
1600
400
0
15
20
25
30
35
40
45
50
55
60
2Theta (°)

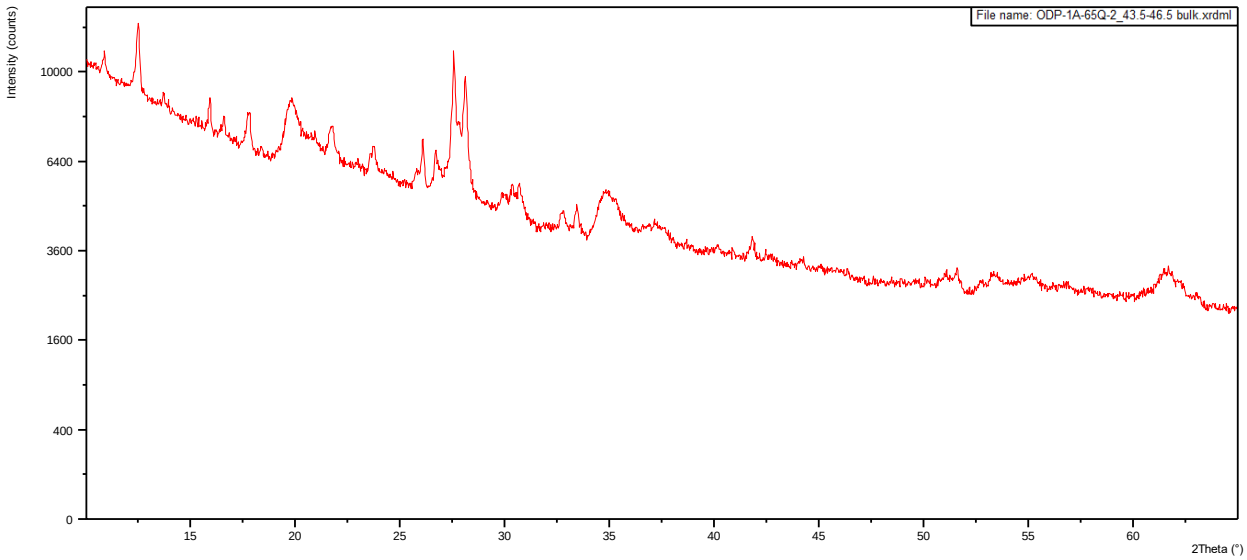
File name: ODP-1A-65Q-2_43.5-46.5 bulk.xrdml
Intensity (counts)
10000
6400
3600
1600
400
0
15
20
25
30
35
40
45
50
55
60
2Theta (°)

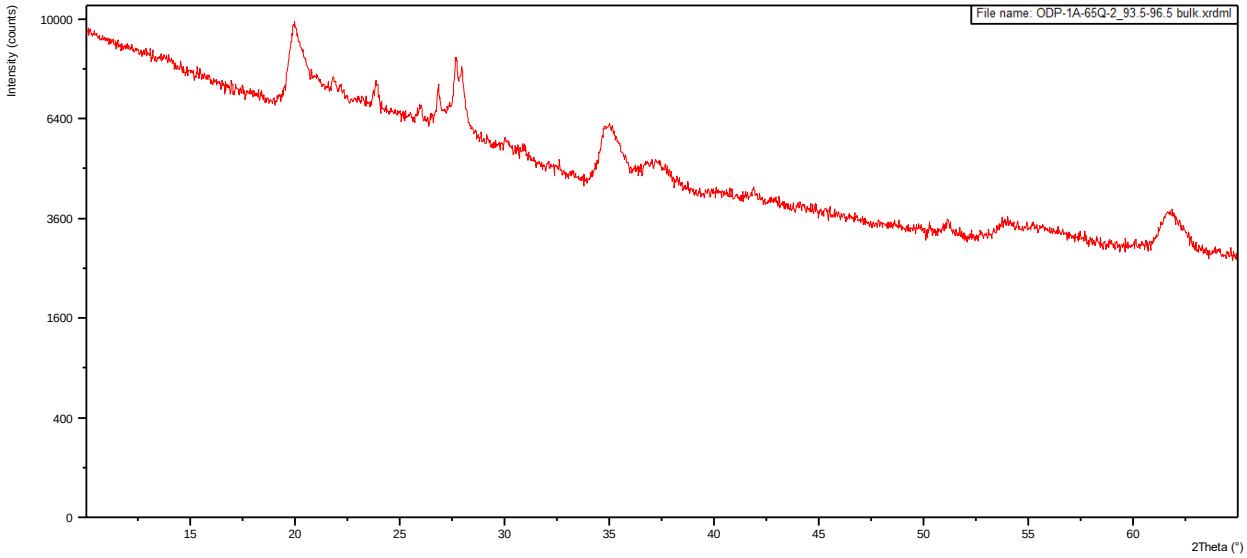
File name: ODP-1A-65Q-2_93.5-96.5 bulk.xrdml
Intensity (counts)
10000
6400
3600
1600
400
0
15
20
25
30
35
40
45
50
55
60
2Theta (°)

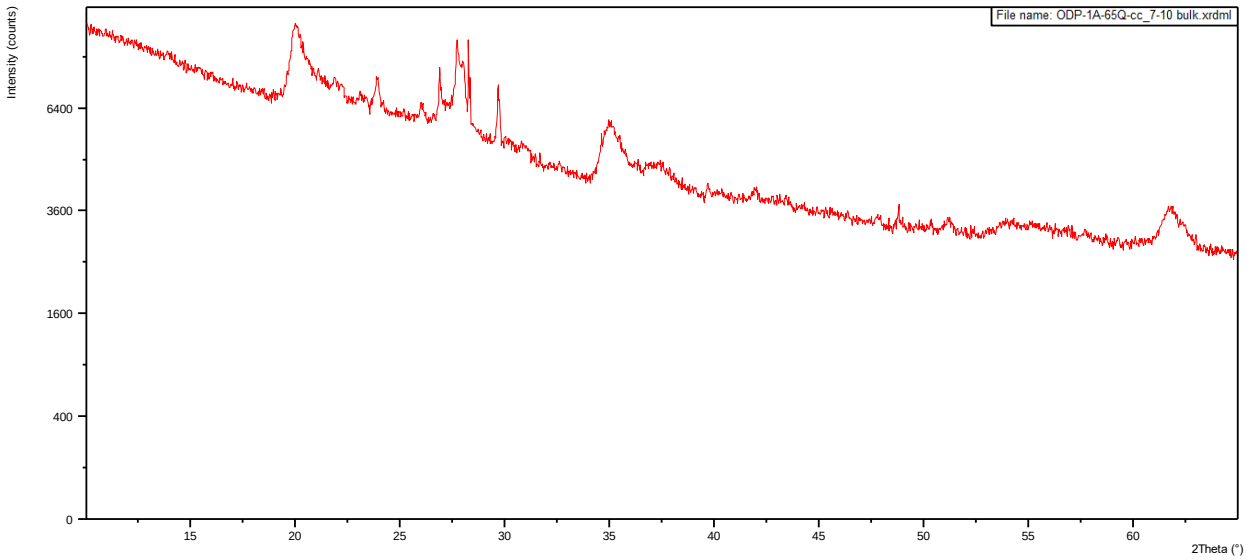
File name: ODP-1A-65Q-cc_7-10 bulk.xrdml
Intensity (counts)
6400
3600
1600
400
0
15
20
25
30
35
40
45
50
55
60
2Theta (°)

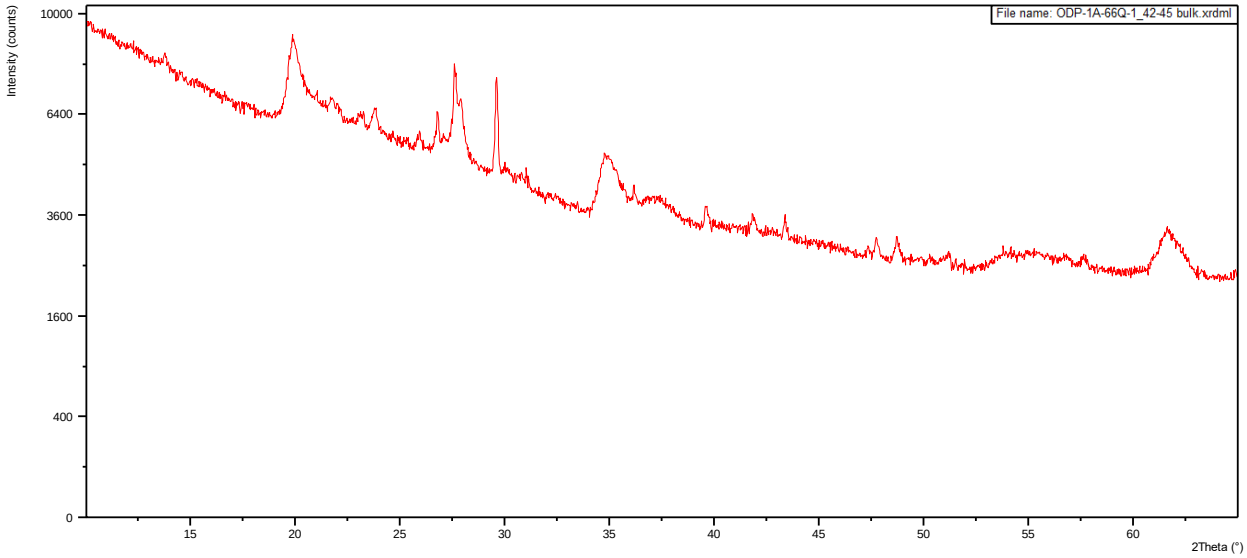
File name: ODP-1A-66Q-1_42-45 bulk.xrdml
Intensity (counts)
10000
6400
3600
1600
400
0
15
20
25
30
35
40
45
50
55
60
2Theta (°)

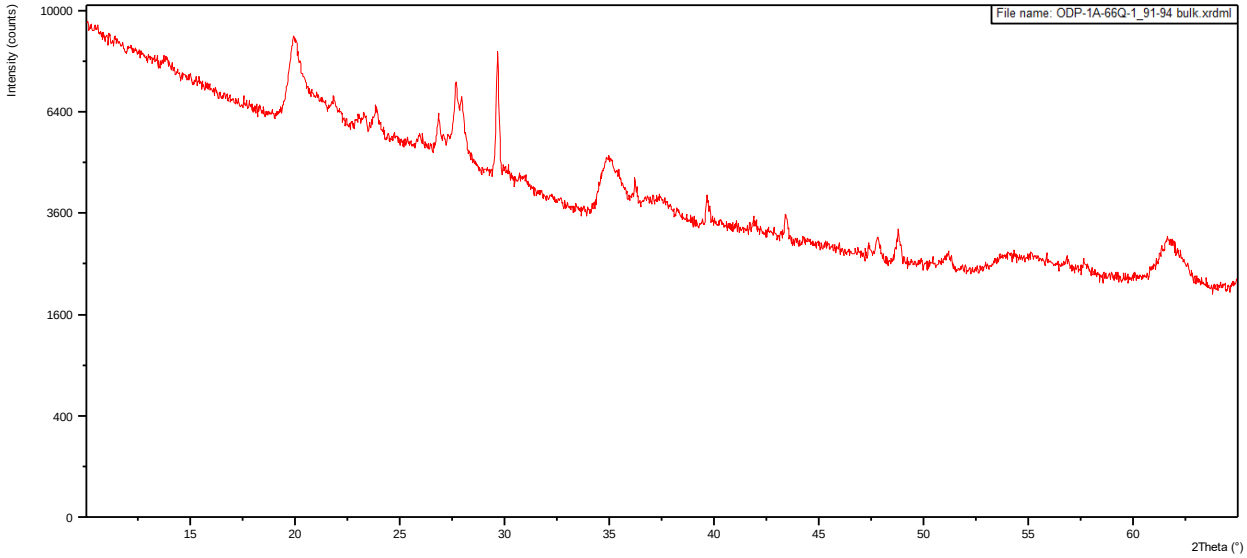
File name: ODP-1A-66Q-1_91-94 bulk.xrdml
Intensity (counts)
10000
6400
3600
1600
400
0
15
20
25
30
35
40
45
50
55
60
2Theta (°)

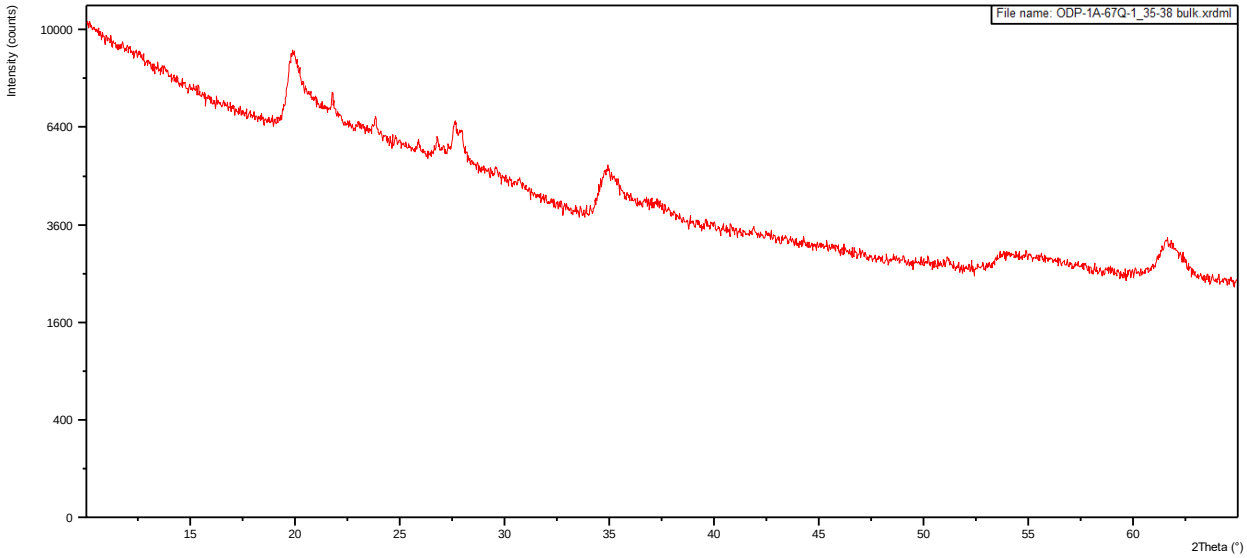
File name: ODP-1A-67Q-1_35-38 bulk.xrdml
Intensity (counts)
10000
6400
3600
1600
400
0
15
20
25
30
35
40
45
50
55
60
2Theta (°)

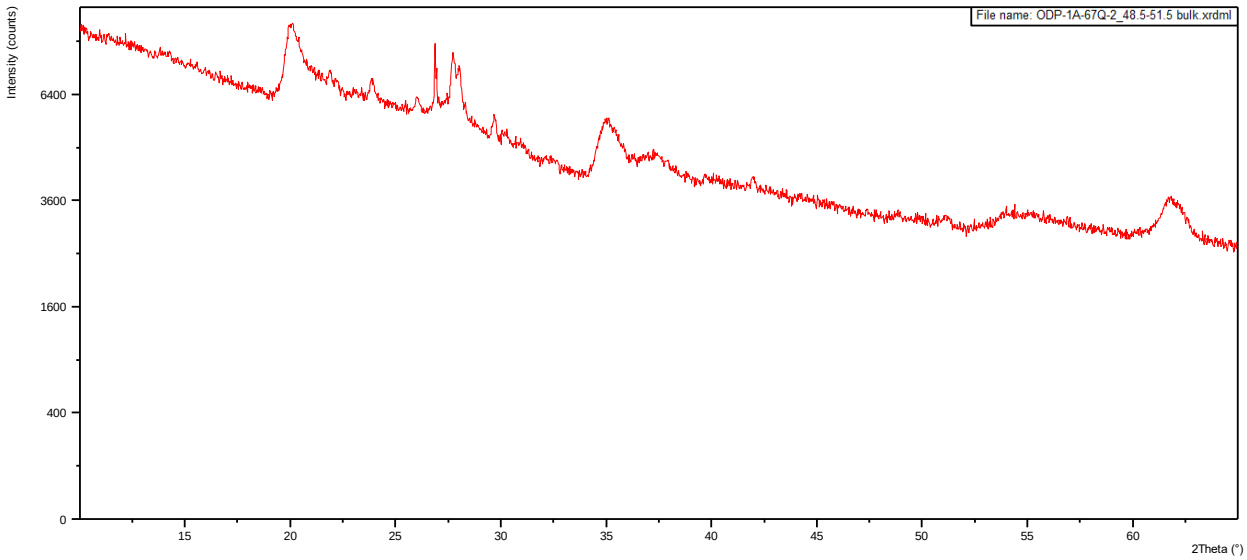
File name: ODP-1A-67Q-2_48.5-51.5 bulk.xrdml
Intensity (counts)
0
400
1600
3600
6400
15
20
25
30
35
40
45
50
55
60
2Theta (°)

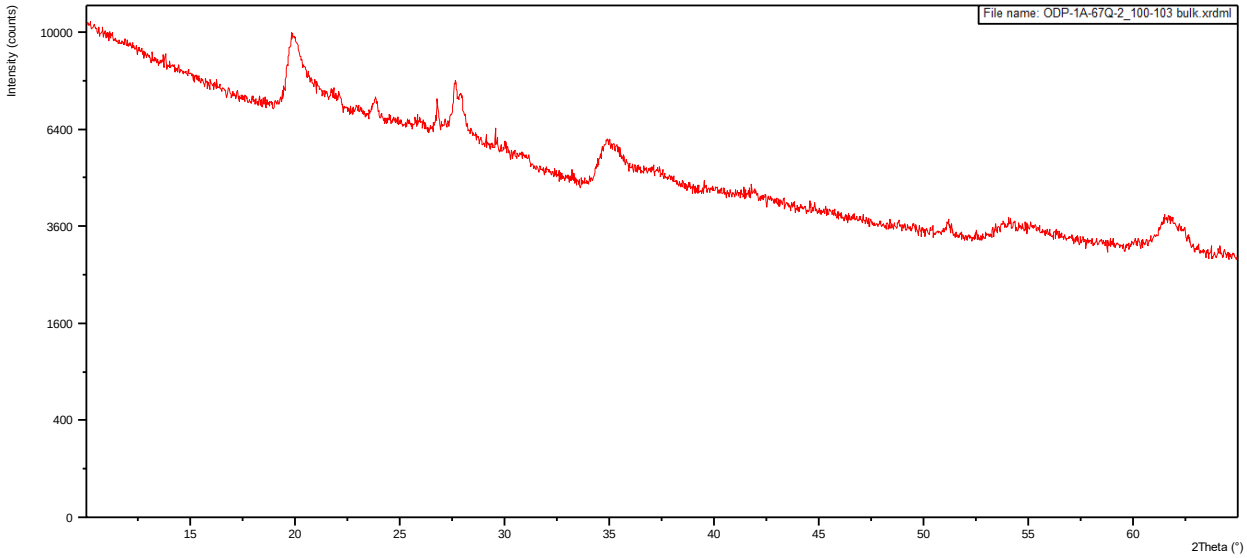
File name: ODP-1A-67Q-2_100-103 bulk.xrdml
Intensity (counts)
0
400
1600
3600
6400
10000
15
20
25
30
35
40
45
50
55
60
2Theta (°)

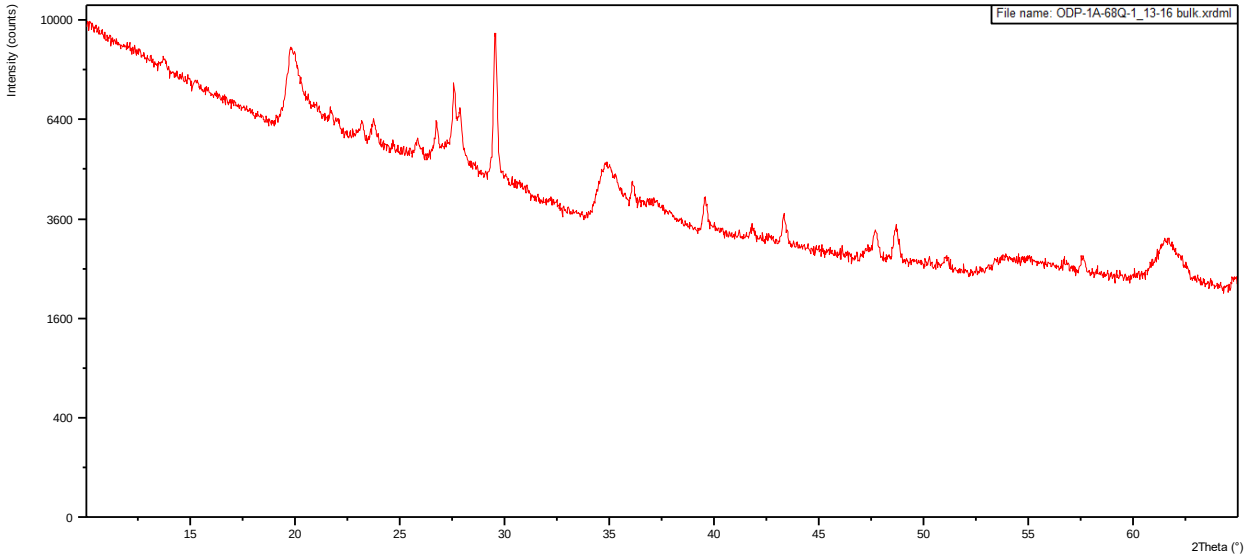
File name: ODP-1A-68Q-1_13-16 bulk.xrdml
Intensity (counts)
10000
6400
3600
1600
400
0
15
20
25
30
35
40
45
50
55
60
2Theta (°)

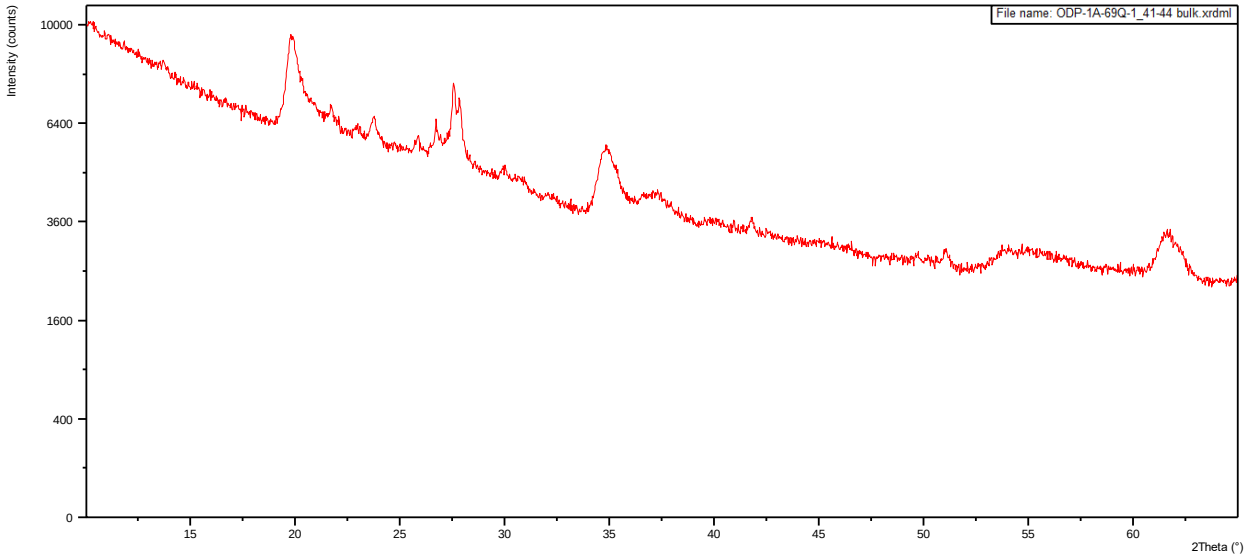
File name: ODP-1A-69Q-1_41-44 bulk.xrdml
Intensity (counts)
10000
6400
3600
1600
400
0
15
20
25
30
35
40
45
50
55
60
2Theta (°)

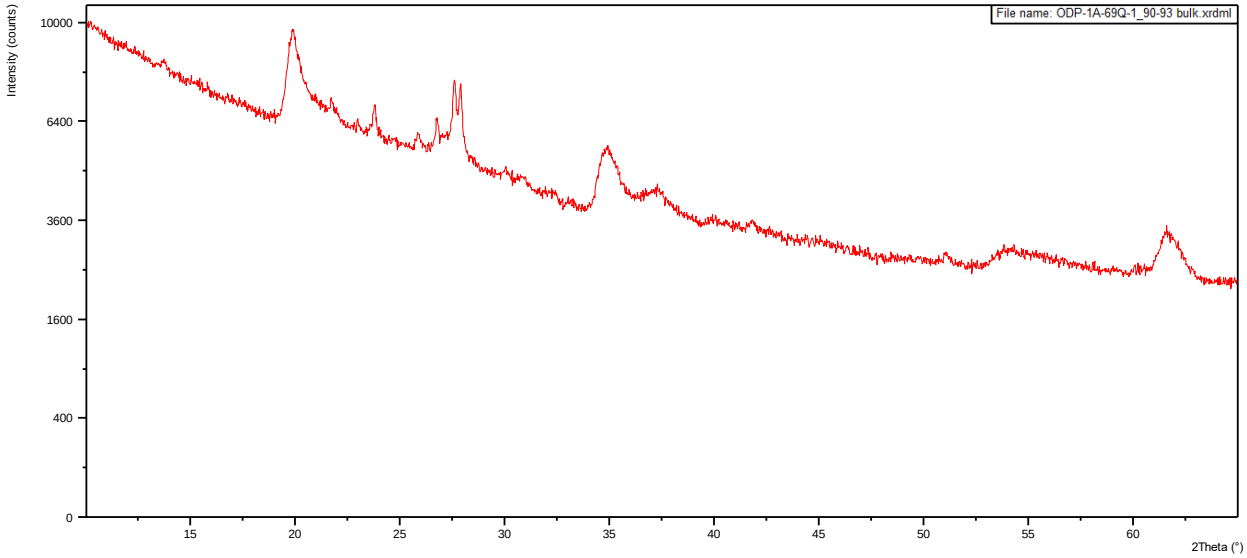
File name: ODP-1A-69Q-1_90-93 bulk.xrdml
Intensity (counts)
10000
6400
3600
1600
400
0
15
20
25
30
35
40
45
50
55
60
2Theta (°)

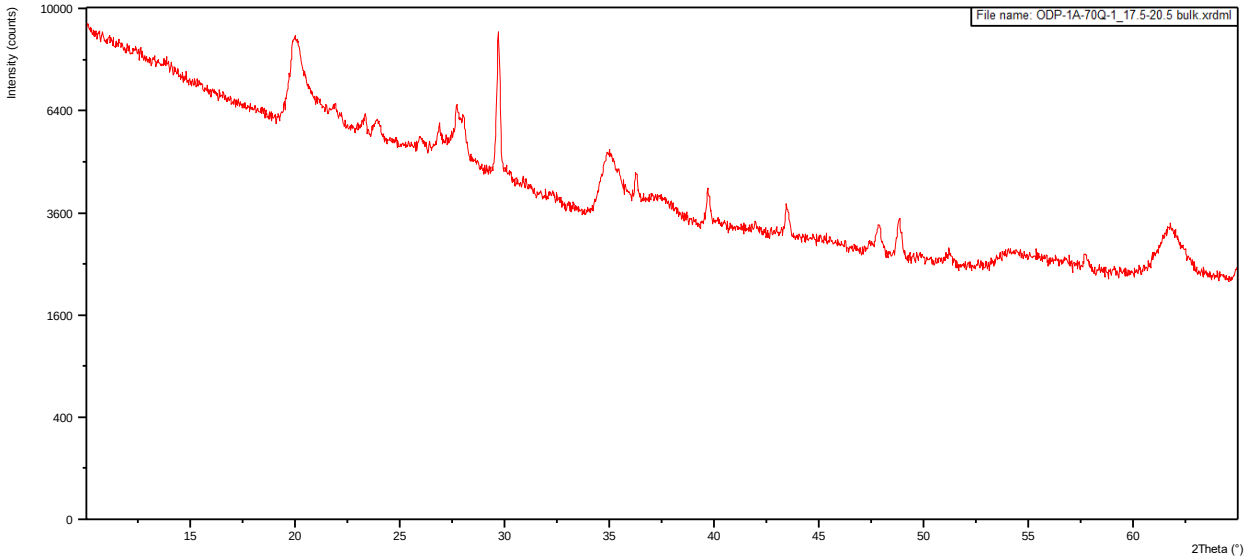
File name: ODP-1A-70Q-1_17.5-20.5 bulk.xrdml
Intensity (counts)
10000
6400
3600
1600
400
0
15
20
25
30
35
40
45
50
55
60
2Theta (°)

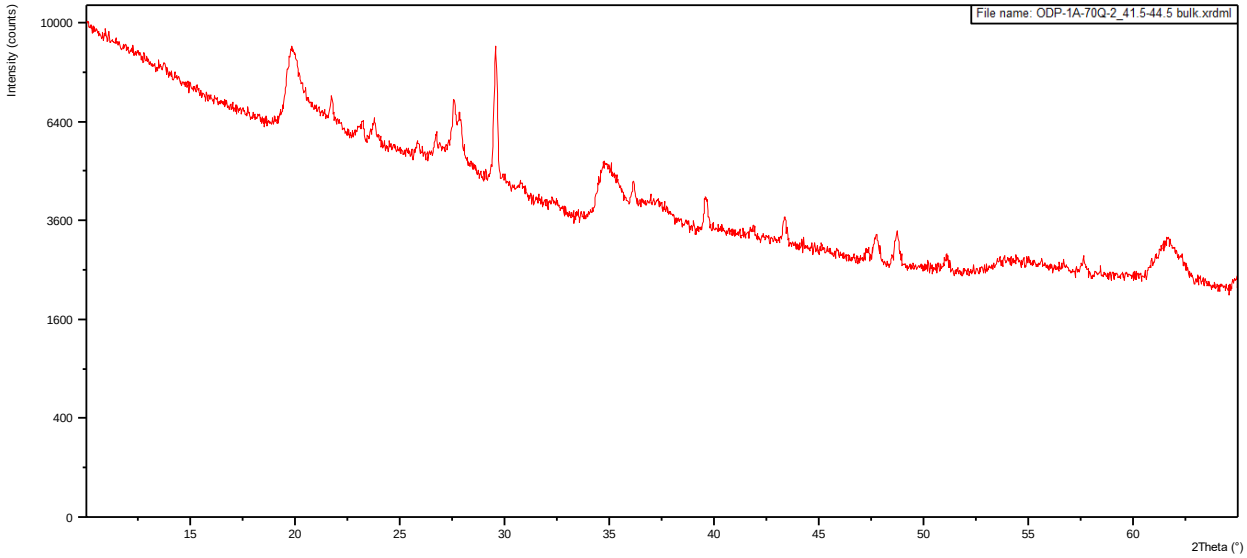
File name: ODP-1A-70Q-2_41.5-44.5 bulk.xrdml
Intensity (counts)
10000
6400
3600
1600
400
0
15
20
25
30
35
40
45
50
55
60
2Theta (°)

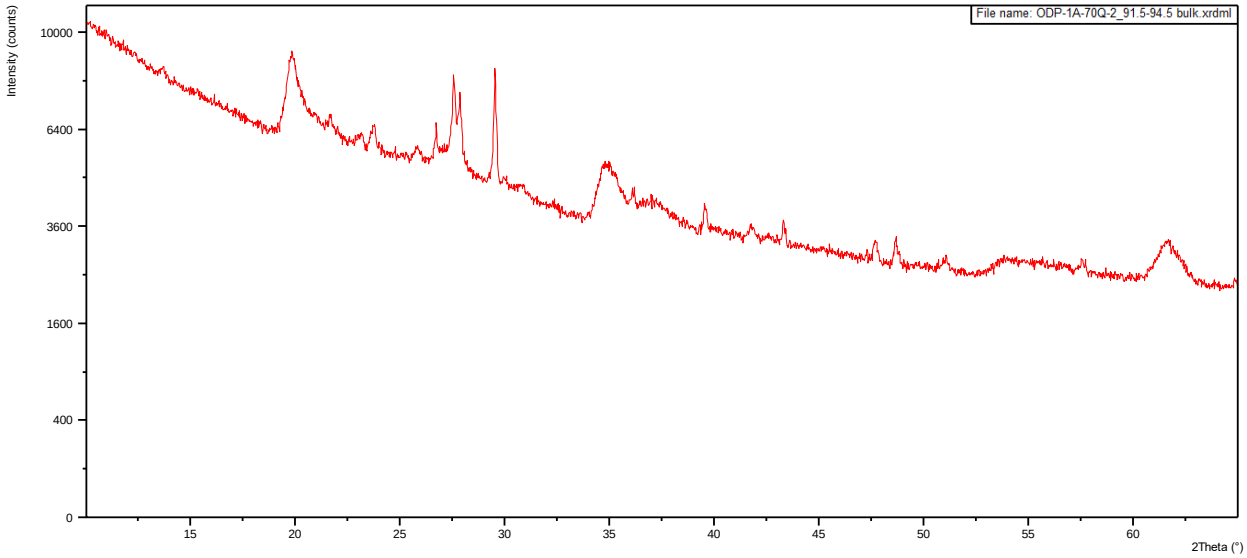
File name: ODP-1A-70Q-2_91.5-94.5 bulk.xrdml
Intensity (counts)
10000
6400
3600
1600
400
0
15
20
25
30
35
40
45
50
55
60
2Theta (°)

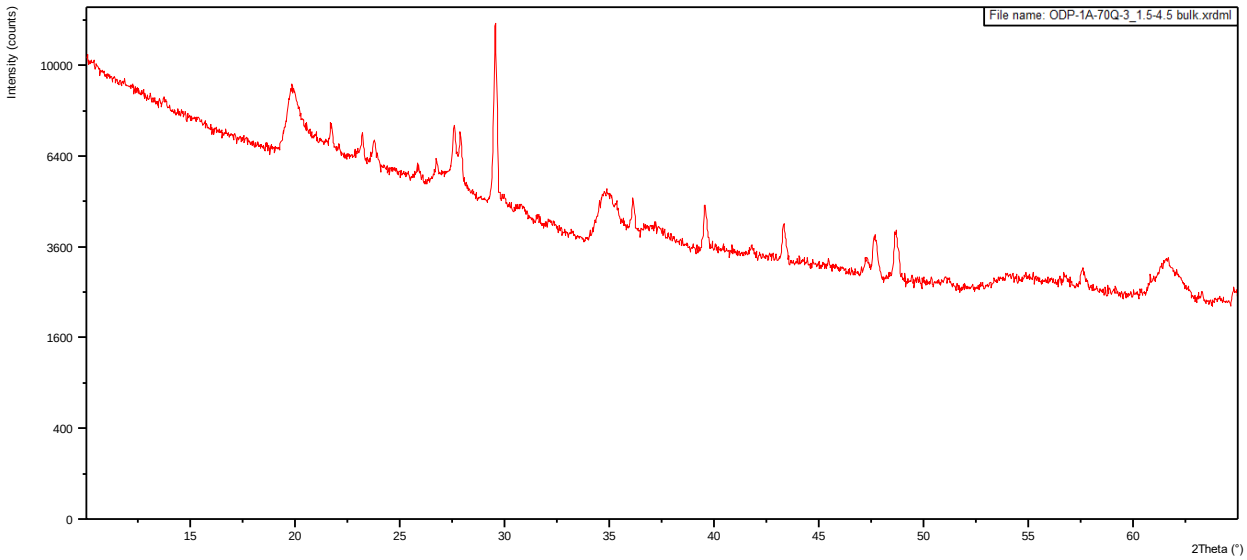
File name: ODP-1A-70Q-3_1.5-4.5 bulk.xrdml
Intensity (counts)
10000
6400
3600
1600
400
0
15
20
25
30
35
40
45
50
55
60
2Theta (°)

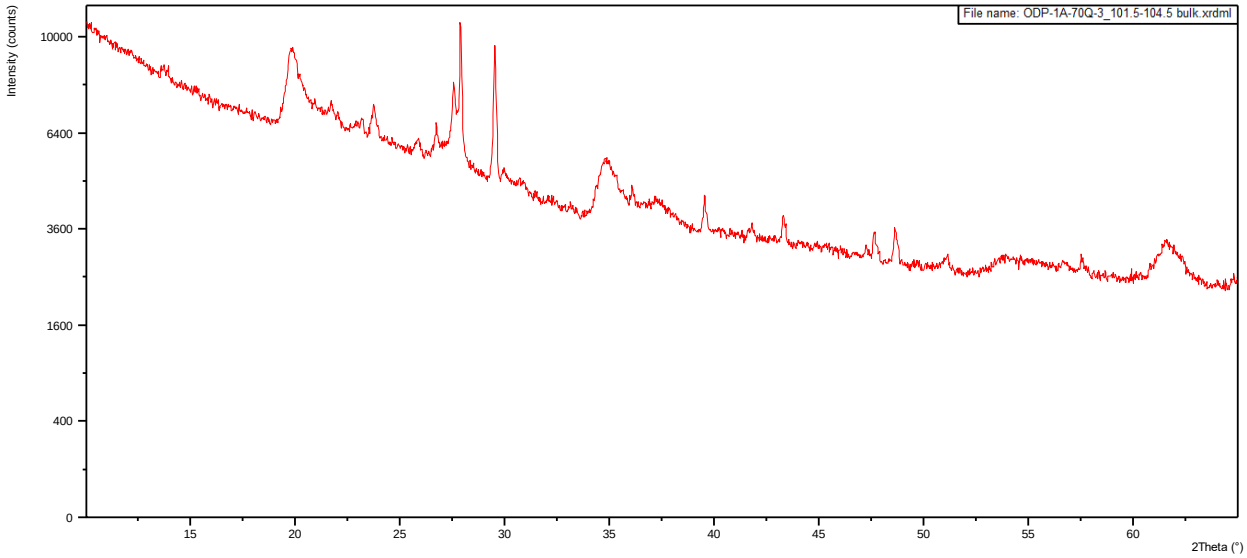
File name: ODP-1A-70Q-3_101.5-104.5 bulk.xrdml
Intensity (counts)
10000
6400
3600
1600
400
0
15
20
25
30
35
40
45
50
55
60
2Theta (°)

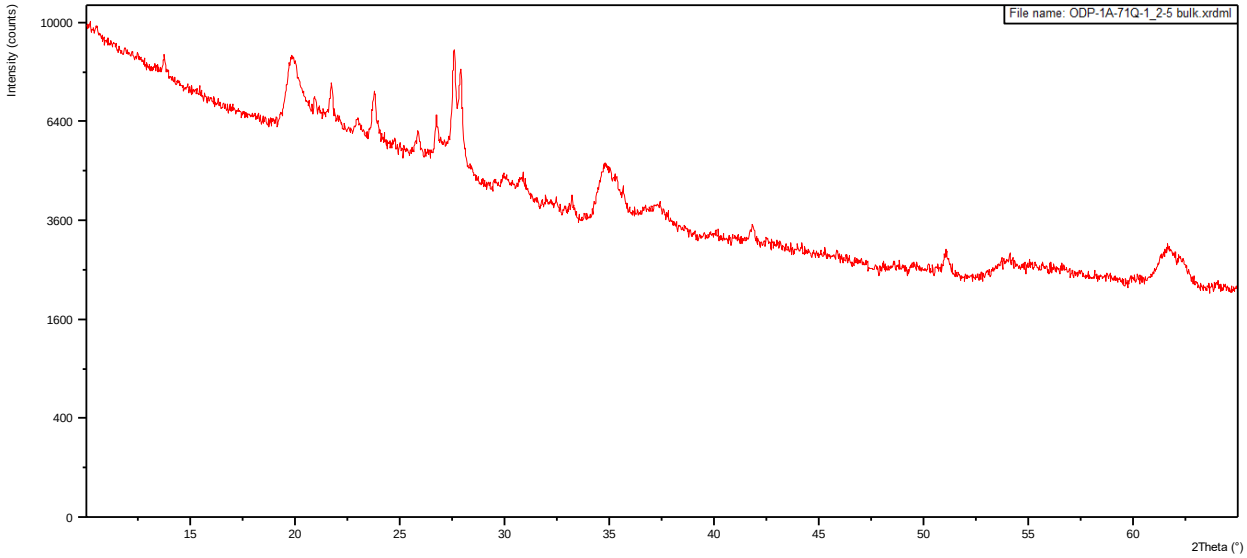
File name: ODP-1A-71Q-1_2-5 bulk.xrdml
Intensity (counts)
10000
6400
3600
1600
400
0
15
20
25
30
35
40
45
50
55
60
2Theta (°)

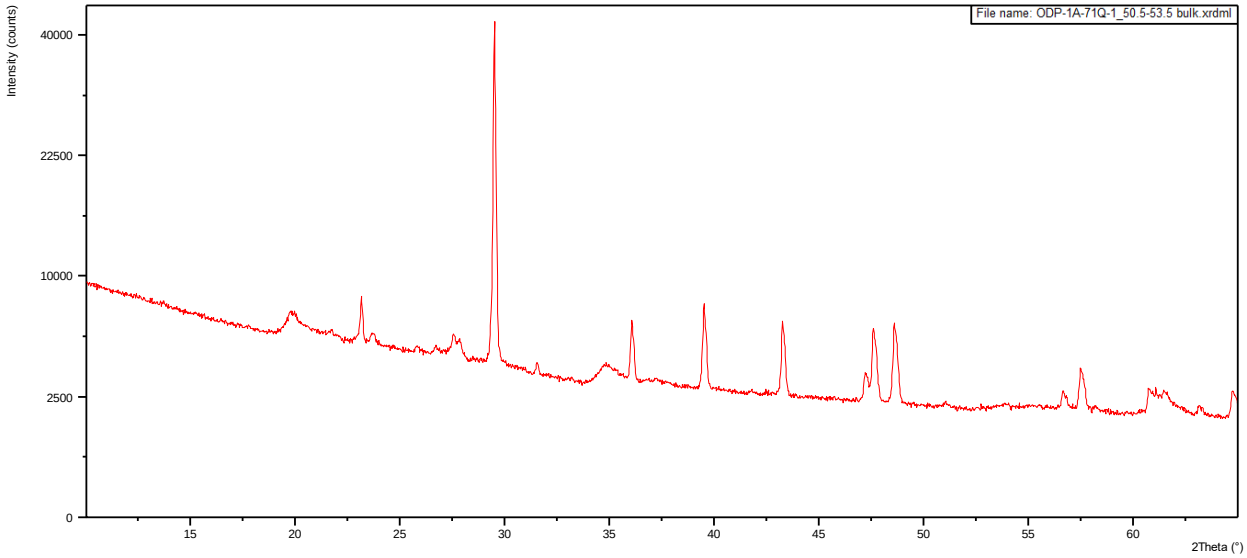
File name: ODP-1A-71Q-1_50.5-53.5 bulk.xrdml
Intensity (counts)
40000
22500
10000
2500
0
15
20
25
30
35
40
45
50
55
60
2Theta (°)

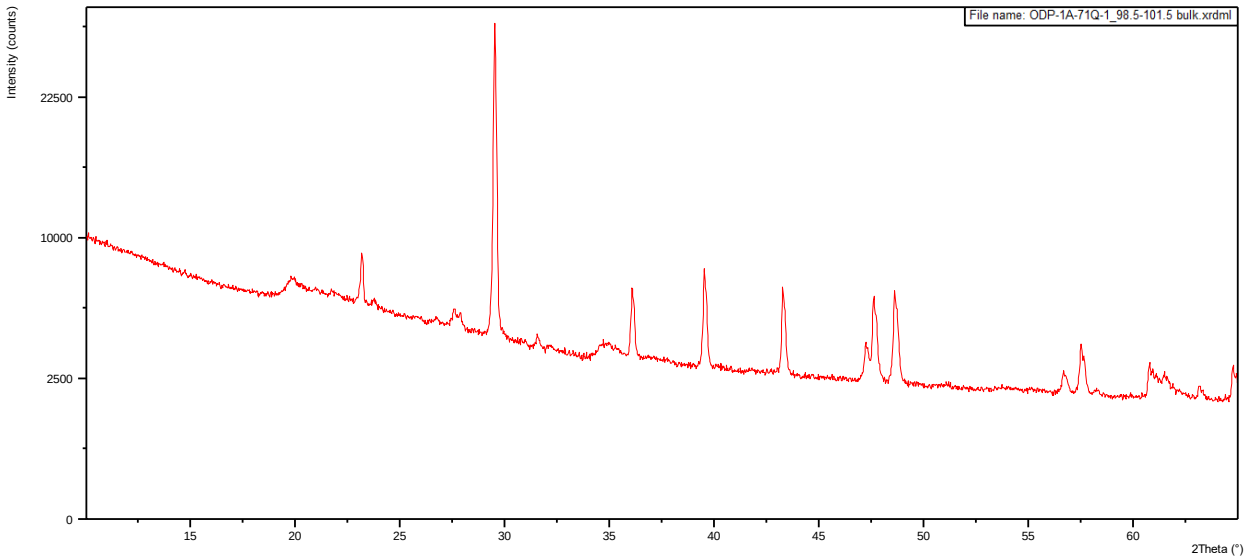
File name: ODP-1A-71Q-1_98.5-101.5 bulk.xrdml
Intensity (counts)
22500
10000
2500
0
15
20
25
30
35
40
45
50
55
60
2Theta (°)

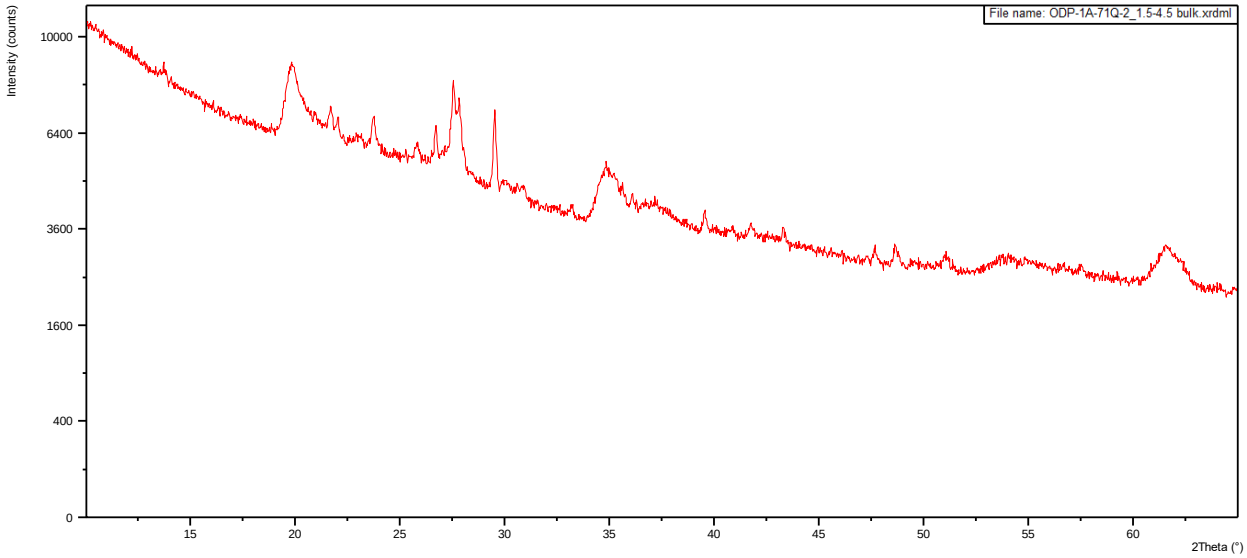
File name: ODP-1A-71Q-2_1.5-4.5 bulk.xrdml
Intensity (counts)
10000
6400
3600
1600
400
0
15
20
25
30
35
40
45
50
55
60
2Theta (°)

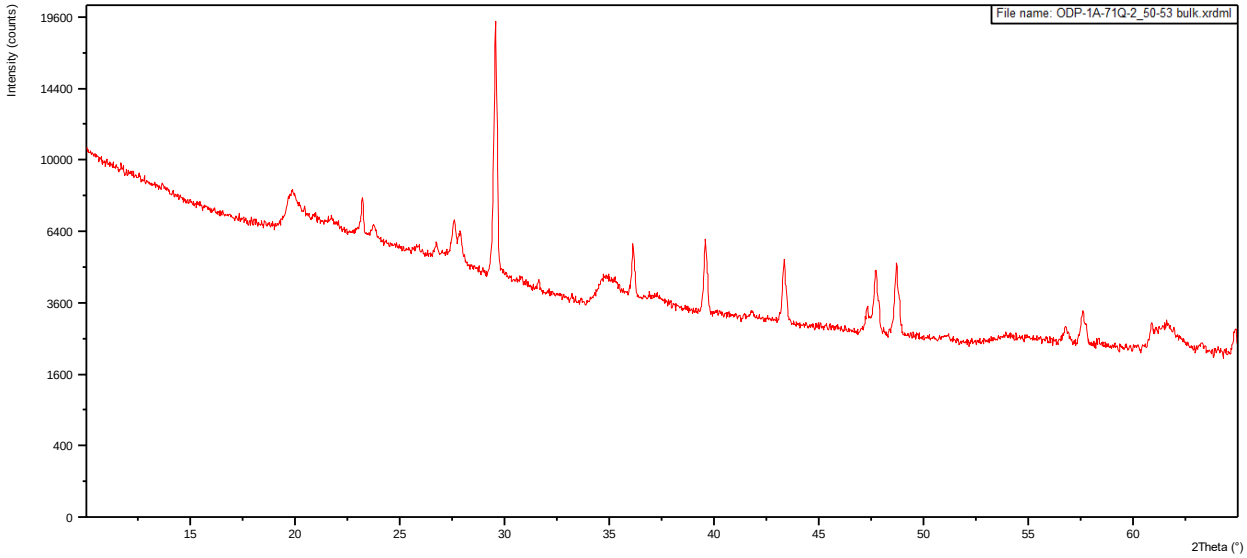
File name: ODP-1A-71Q-2_50-53 bulk.xrdml
Intensity (counts)
19600
14400
10000
6400
3600
1600
400
0
15
20
25
30
35
40
45
50
55
60
2Theta (°)

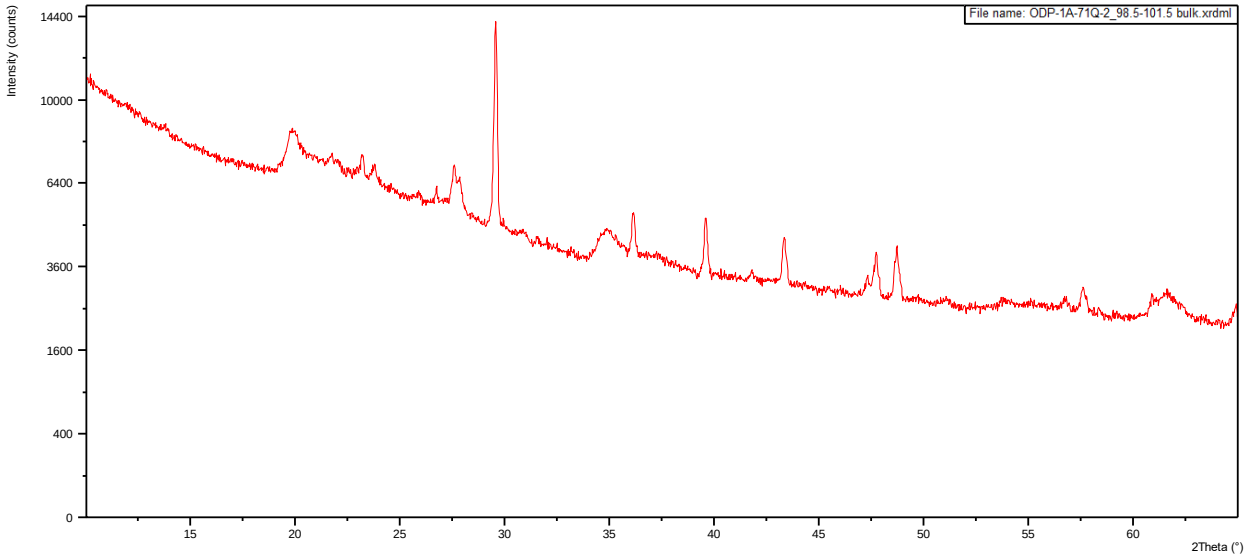
File name: ODP-1A-71Q-2_98.5-101.5 bulk.xrdml
Intensity (counts)
14400
10000
6400
3600
1600
400
0
15
20
25
30
35
40
45
50
55
60
2Theta (°)

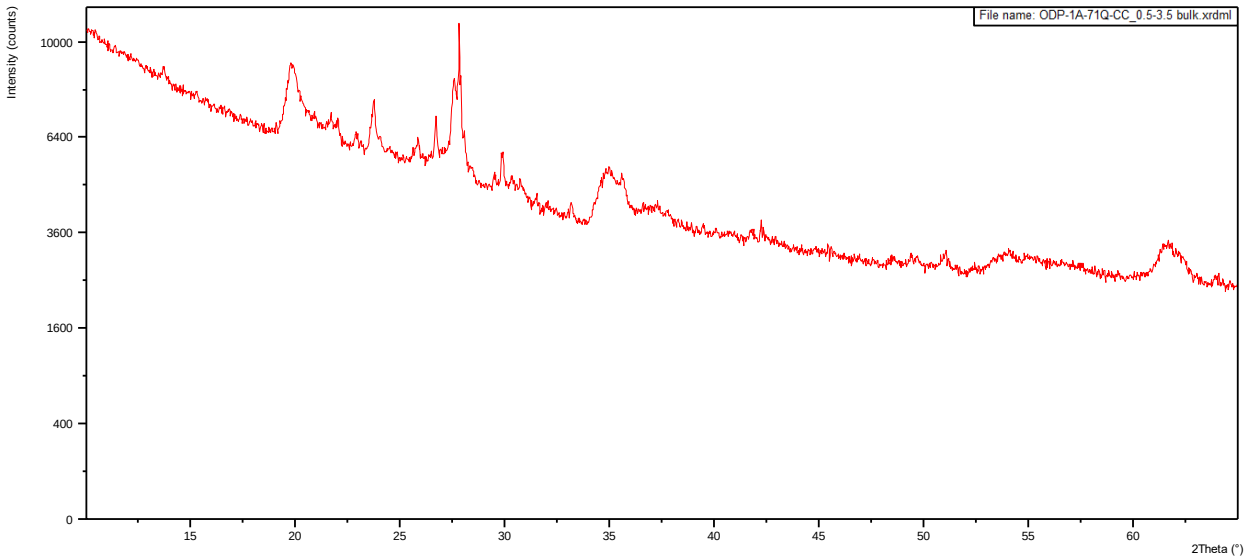
File name: ODP-1A-71Q-CC_0.5-3.5 bulk.xrdml
Intensity (counts)
10000
6400
3600
1600
400
0
15
20
25
30
35
40
45
50
55
60
2Theta (°)

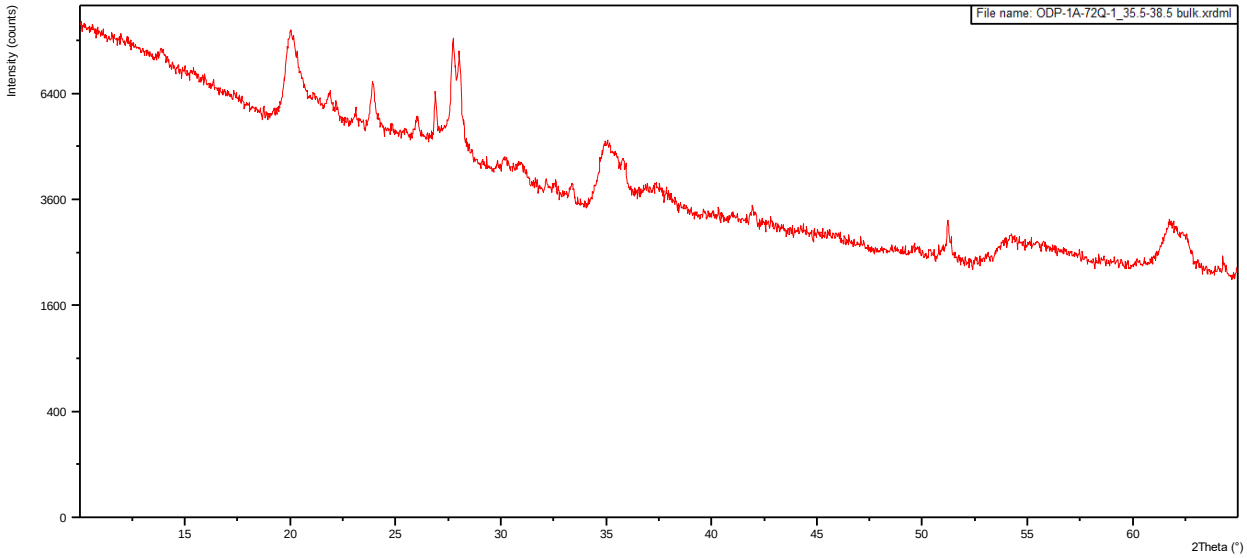
File name: ODP-1A-72Q-1_35.5-38.5 bulk.xrdml
Intensity (counts)
6400
3600
1600
400
0
15
20
25
30
35
40
45
50
55
60
2Theta (°)

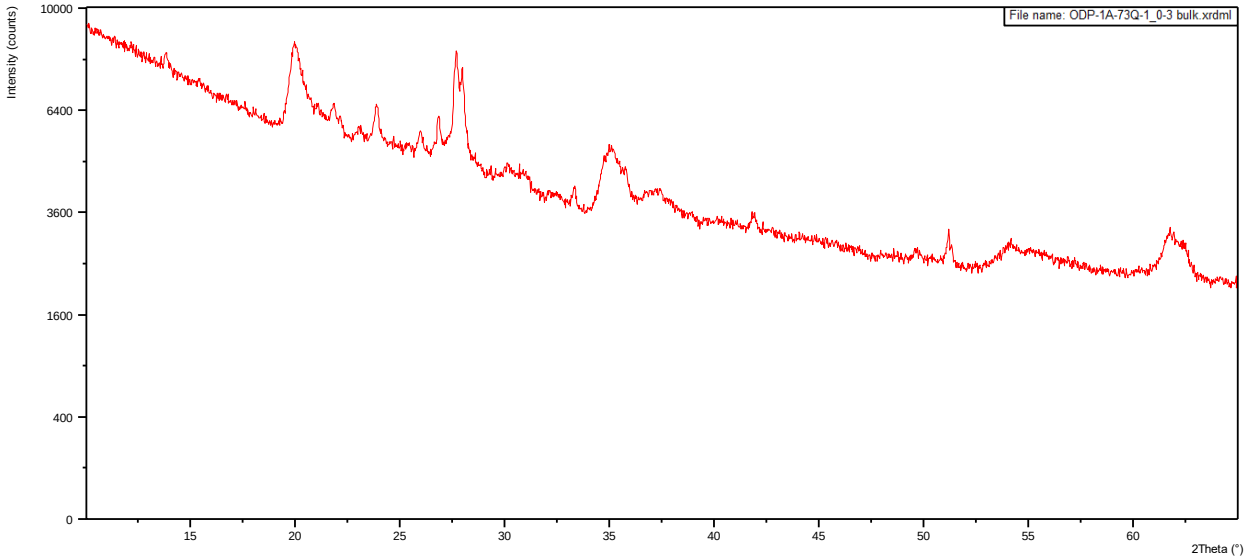
File name: ODP-1A-73Q-1_0-3 bulk.xrdml
Intensity (counts)
10000
6400
3600
1600
400
0
15
20
25
30
35
40
45
50
55
60
2Theta (°)

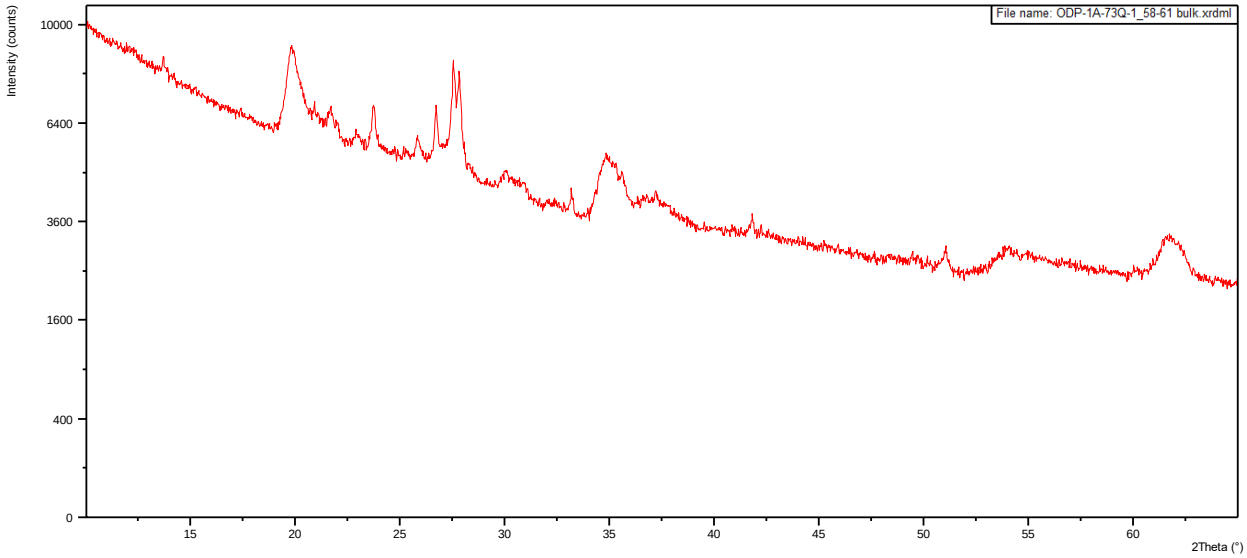
File name: ODP-1A-73Q-1_58-61 bulk.xrdml
Intensity (counts)
10000
6400
3600
1600
400
0
15
20
25
30
35
40
45
50
55
60
2Theta (°)

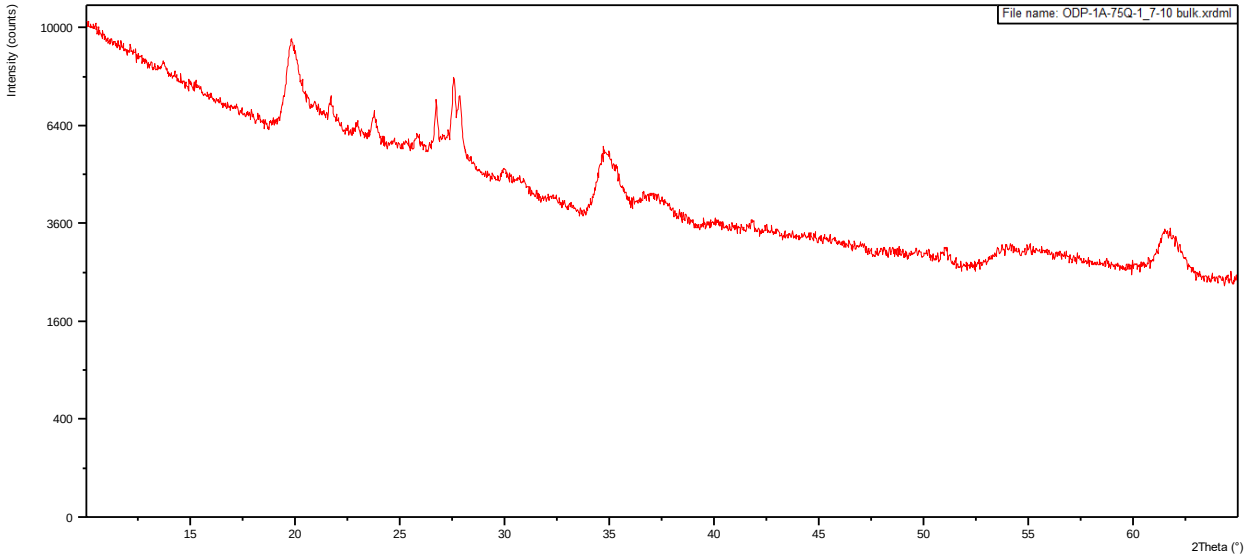
File name: ODP-1A-75Q-1_7-10 bulk.xrdml
Intensity (counts)
10000
6400
3600
1600
400
0
15
20
25
30
35
40
45
50
55
60
2Theta (°)

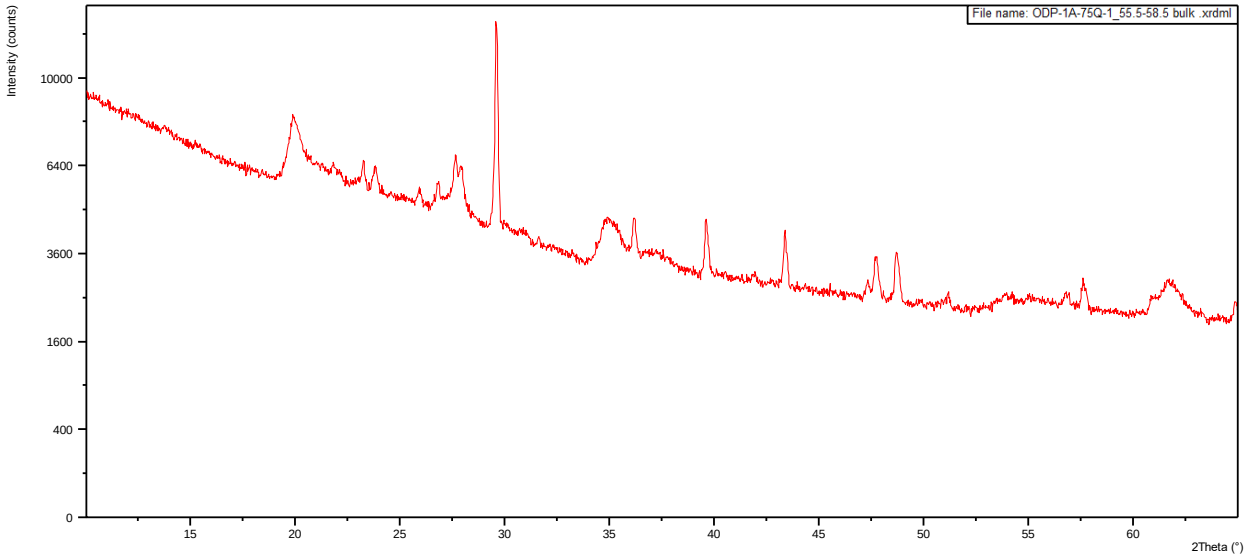
File name: ODP-1A-75Q-1_55.5-58.5 bulk .xrdml
Intensity (counts)
10000
6400
3600
1600
400
0
15
20
25
30
35
40
45
50
55
60
2Theta (°)

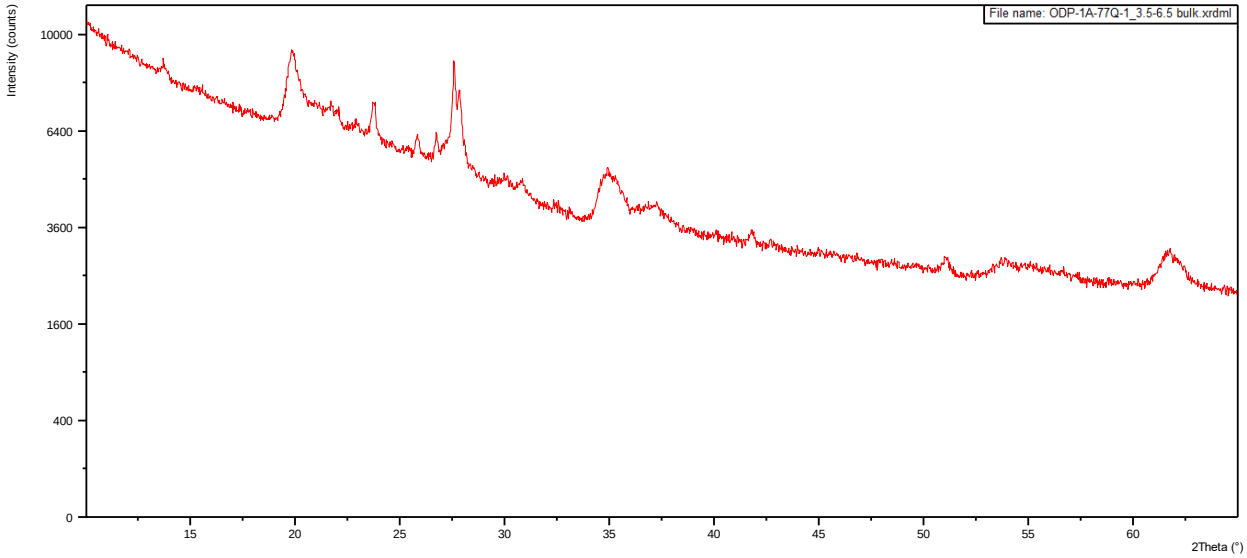
File name: ODP-1A-77Q-1_3.5-6.5 bulk.xrdml
Intensity (counts)
10000
6400
3600
1600
400
0
15
20
25
30
35
40
45
50
55
60
2Theta (°)

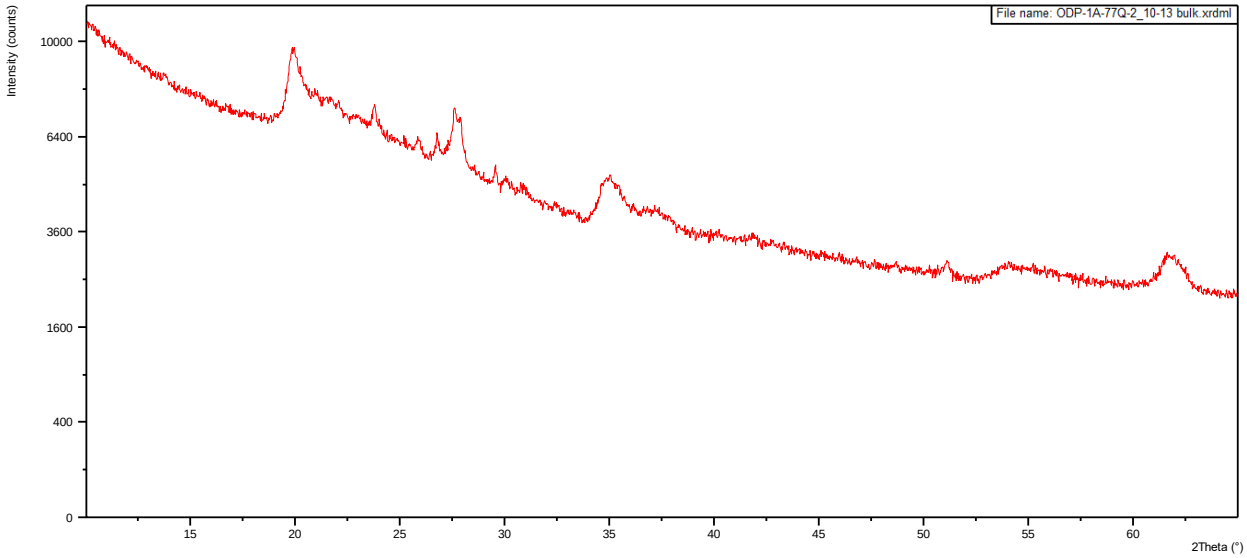
File name: ODP-1A-77Q-2_10-13 bulk.xrdml
Intensity (counts)
10000
6400
3600
1600
400
0
15
20
25
30
35
40
45
50
55
60
2Theta (°)

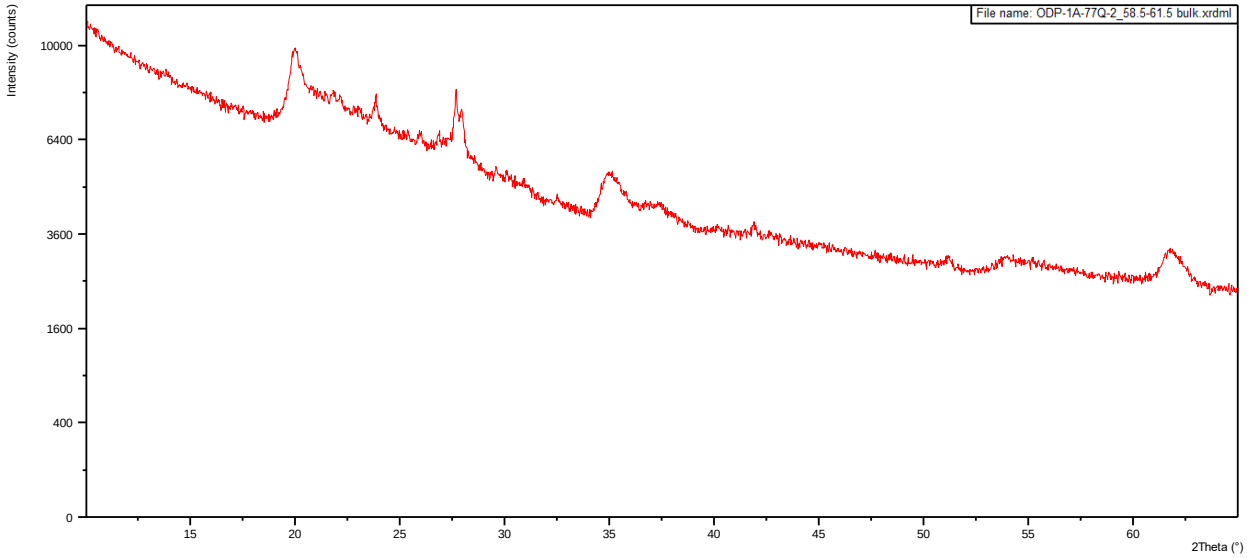
File name: ODP-1A-77Q-2_58.5-61.5 bulk.xrdml
Intensity (counts)
10000
6400
3600
1600
400
0
15
20
25
30
35
40
45
50
55
60
2Theta (°)

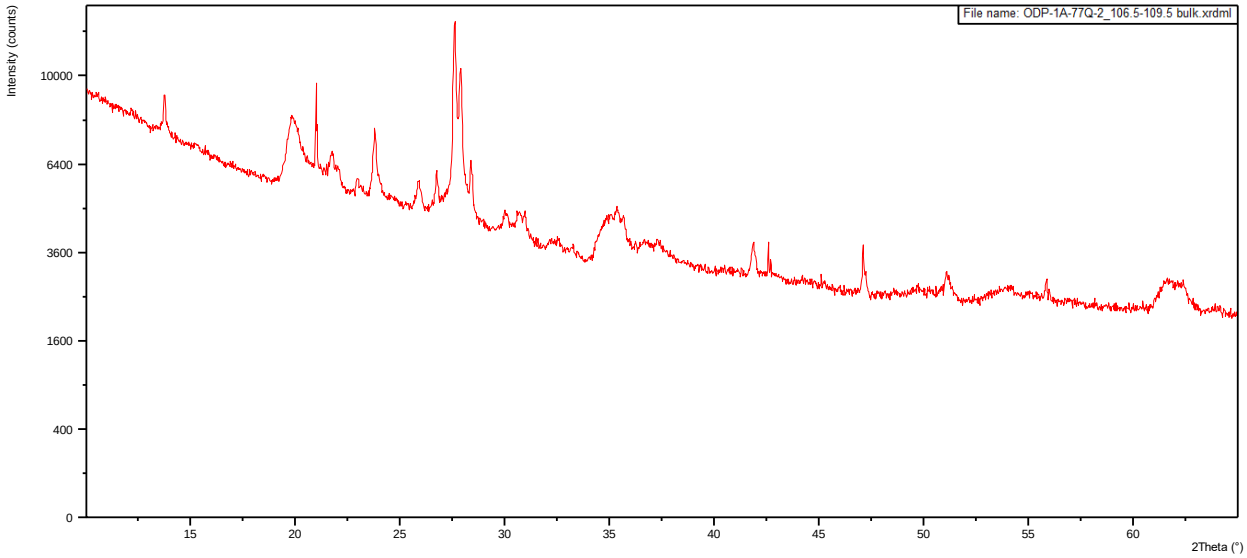
File name: ODP-1A-77Q-2_106.5-109.5 bulk.xrdml
Intensity (counts)
10000
6400
3600
1600
400
0
15
20
25
30
35
40
45
50
55
60
2Theta (°)

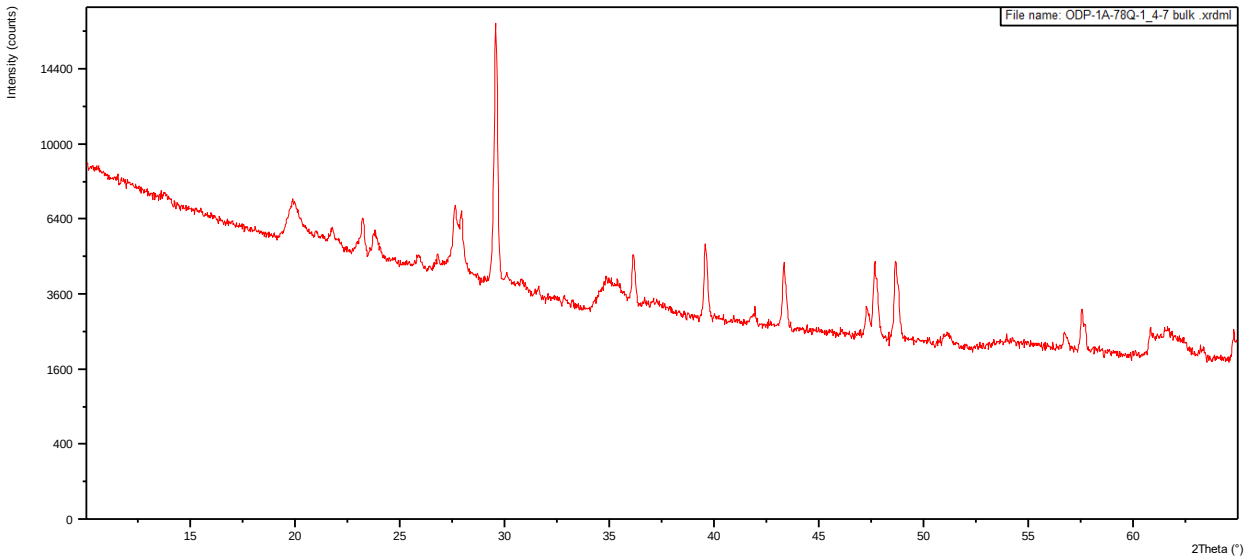
File name: ODP-1A-78Q-1_4-7 bulk .xrdml
Intensity (counts)
14400
10000
6400
3600
1600
400
0
15
20
25
30
35
40
45
50
55
60
2Theta (°)

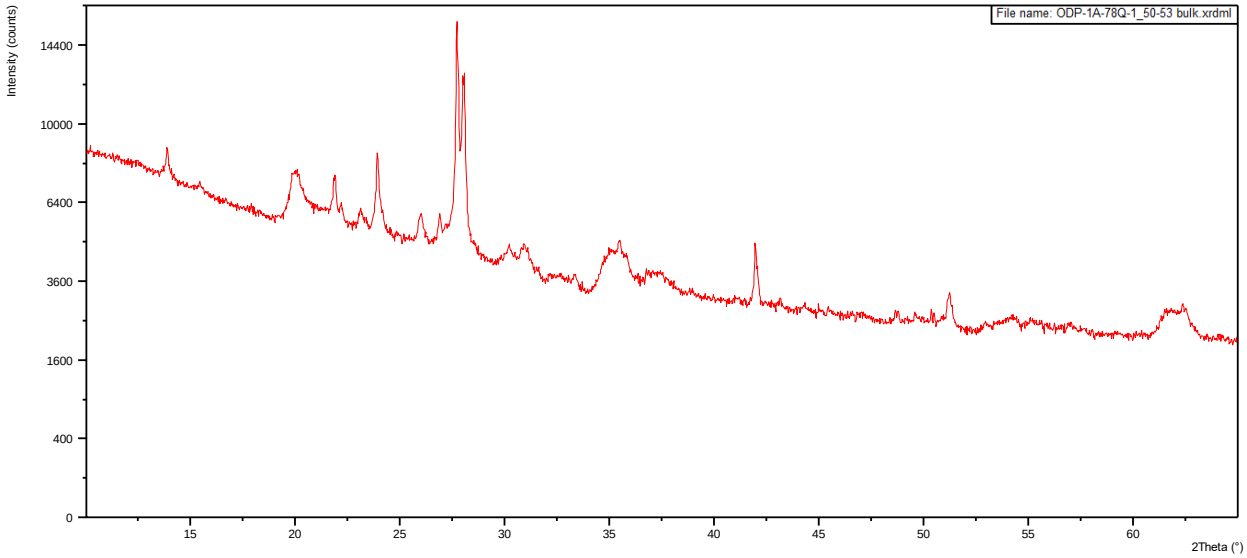
File name: ODP-1A-78Q-1_50-53 bulk.xrdml
Intensity (counts)
14400
10000
6400
3600
1600
400
0
15
20
25
30
35
40
45
50
55
60
2Theta (°)

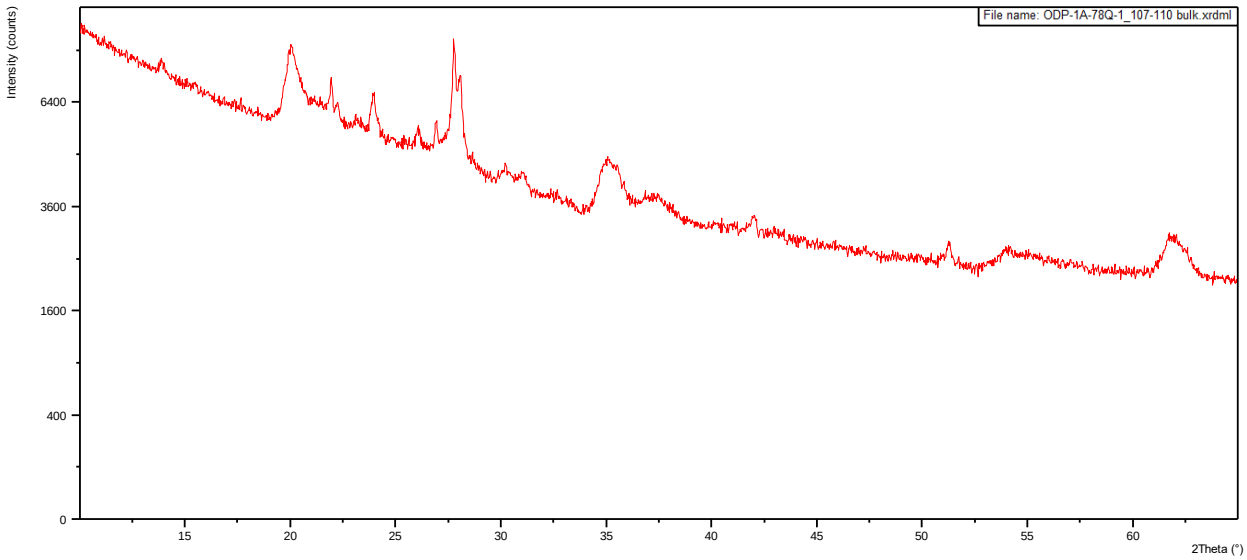
File name: ODP-1A-78Q-1_107-110 bulk.xrdml
Intensity (counts)
6400
3600
1600
400
0
15
20
25
30
35
40
45
50
55
60
2Theta (°)

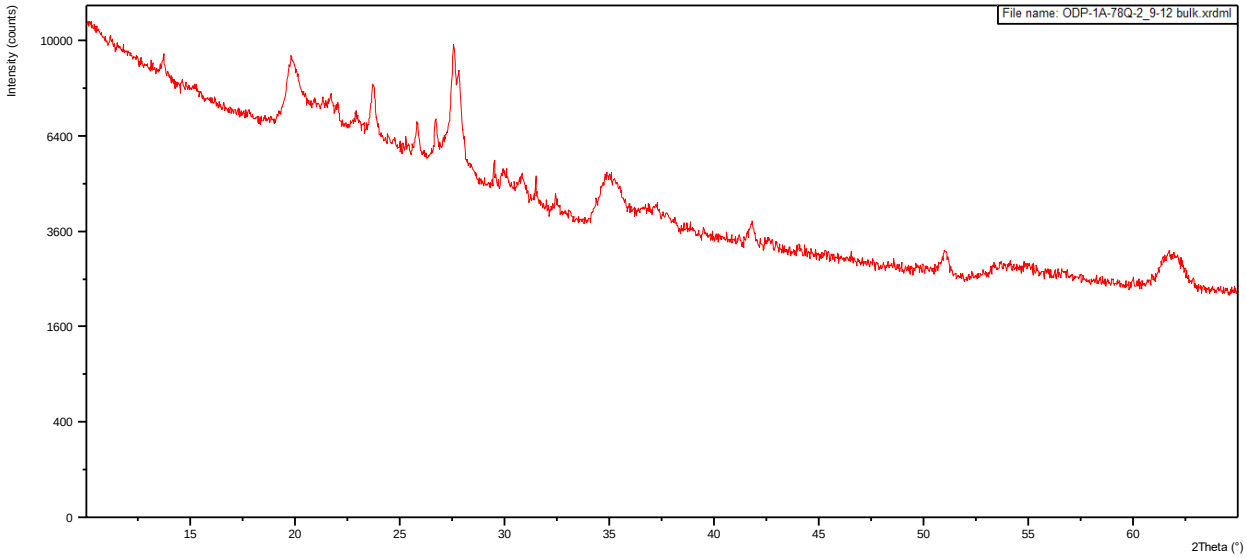
File name: ODP-1A-78Q-2_9-12 bulk.xrdml
Intensity (counts)
10000
6400
3600
1600
400
0
15
20
25
30
35
40
45
50
55
60
2Theta (°)

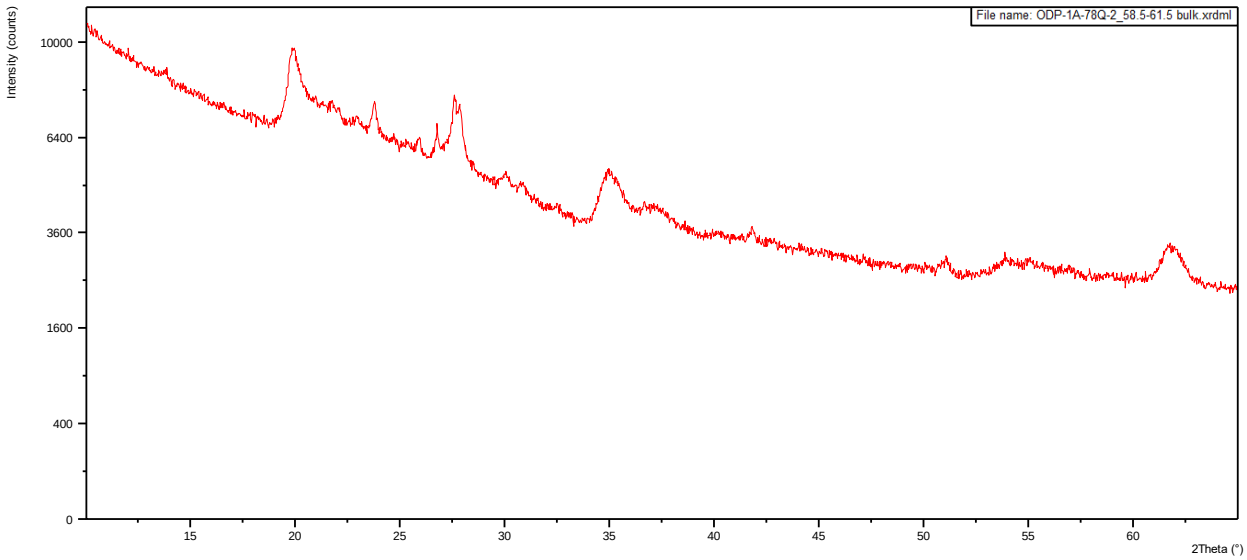
File name: ODP-1A-78Q-2_58.5-61.5 bulk.xrdml
Intensity (counts)
10000
6400
3600
1600
400
0
15
20
25
30
35
40
45
50
55
60
2Theta (°)

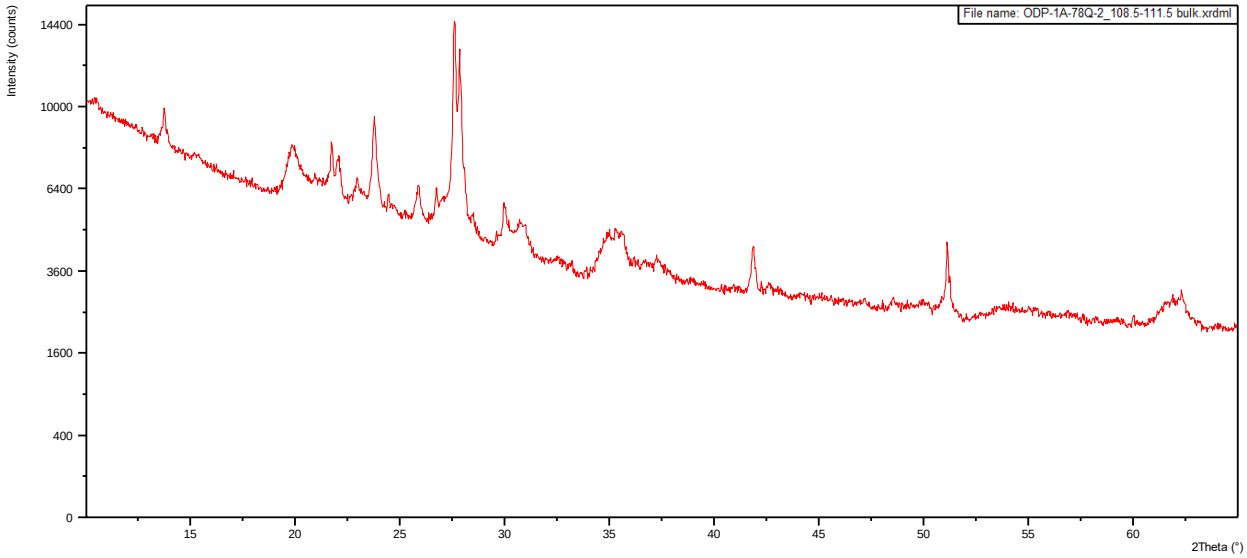
File name: ODP-1A-78Q-2_108.5-111.5 bulk.xrdml
Intensity (counts)
14400
10000
6400
3600
1600
400
0
15
20
25
30
35
40
45
50
55
60
2Theta (°)

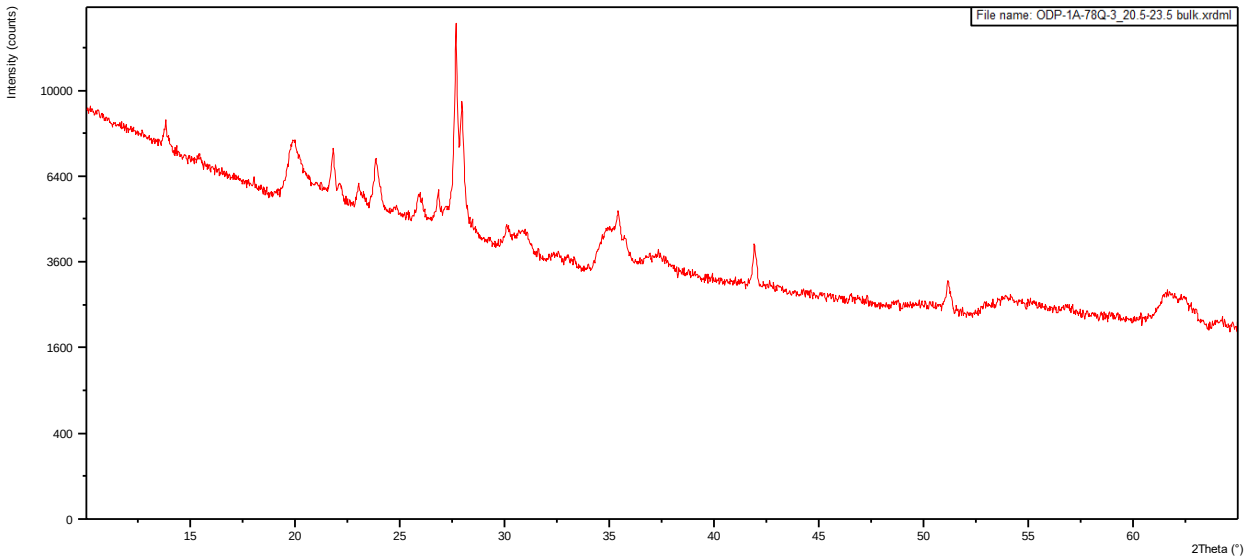
File name: ODP-1A-78Q-3_20.5-23.5 bulk.xrdml
Intensity (counts)
10000
6400
3600
1600
400
0
15
20
25
30
35
40
45
50
55
60
2Theta (°)

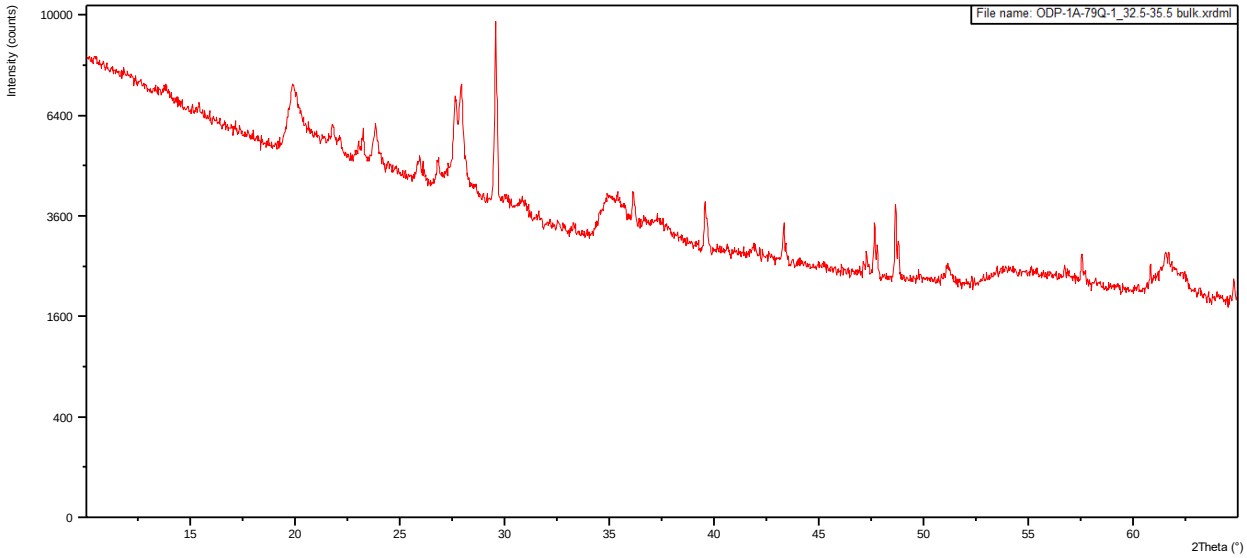
File name: ODP-1A-79Q-1_32.5-35.5 bulk.xrdml
Intensity (counts)
10000
6400
3600
1600
400
0
15
20
25
30
35
40
45
50
55
60
2Theta (°)

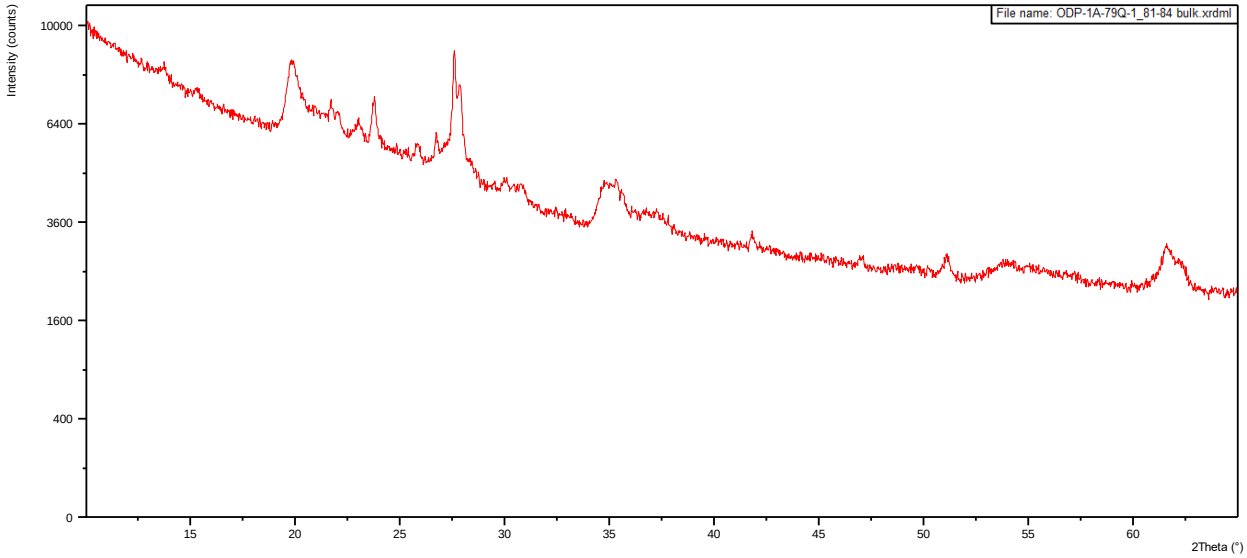
File name: ODP-1A-79Q-1_81-84 bulk.xrdml
Intensity (counts)
10000
6400
3600
1600
400
0
15
20
25
30
35
40
45
50
55
60
2Theta (°)

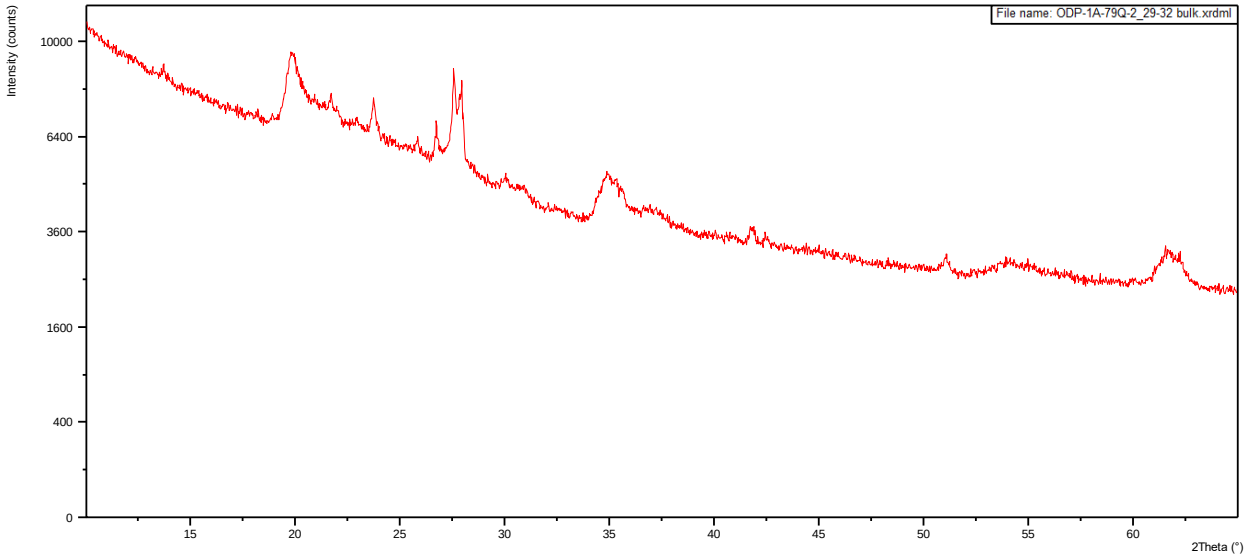
File name: ODP-1A-79Q-2_29-32 bulk.xrdml
Intensity (counts)
10000
6400
3600
1600
400
0
15
20
25
30
35
40
45
50
55
60
2Theta (°)

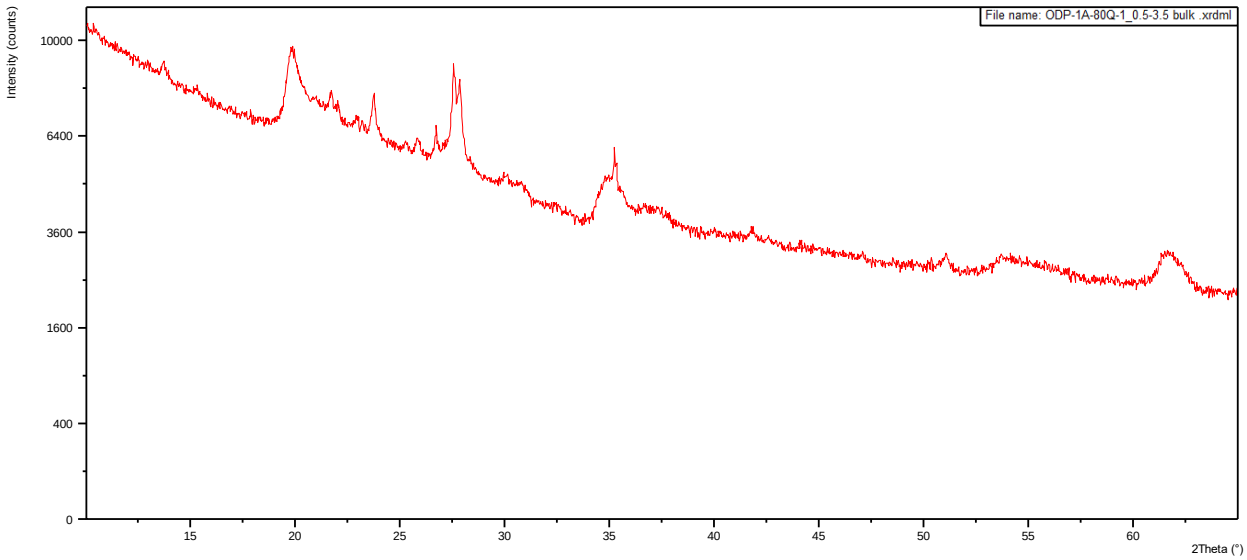
File name: ODP-1A-80Q-1_0.5-3.5 bulk .xrdml
Intensity (counts)
10000
6400
3600
1600
400
0
15
20
25
30
35
40
45
50
55
60
2Theta (°)

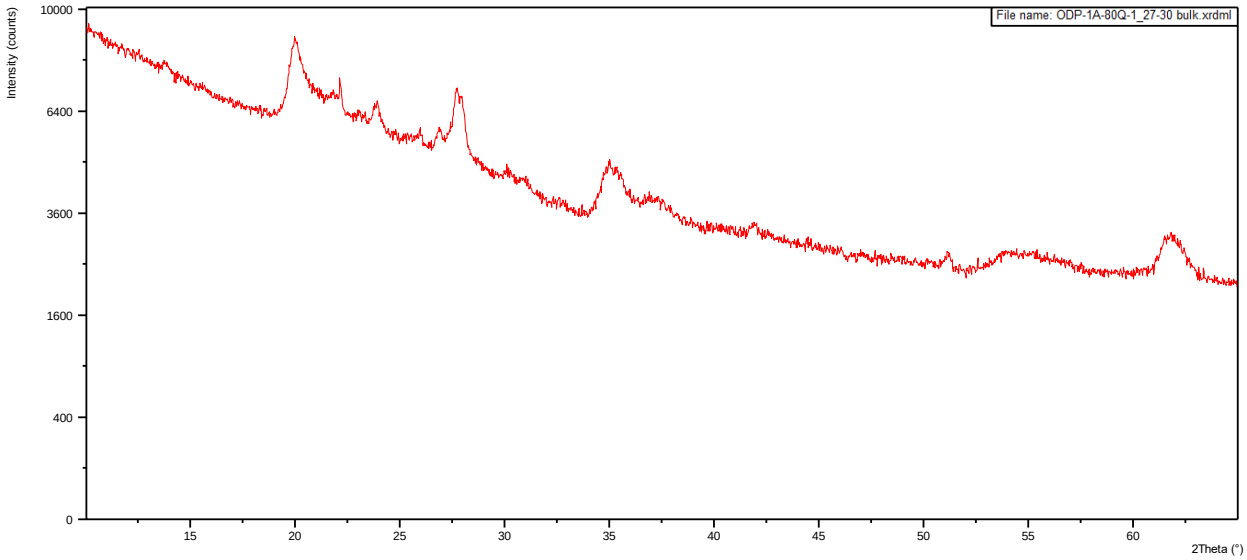
File name: ODP-1A-80Q-1_27-30 bulk.xrdml
Intensity (counts)
10000
6400
3600
1600
400
0
15
20
25
30
35
40
45
50
55
60
2Theta (°)

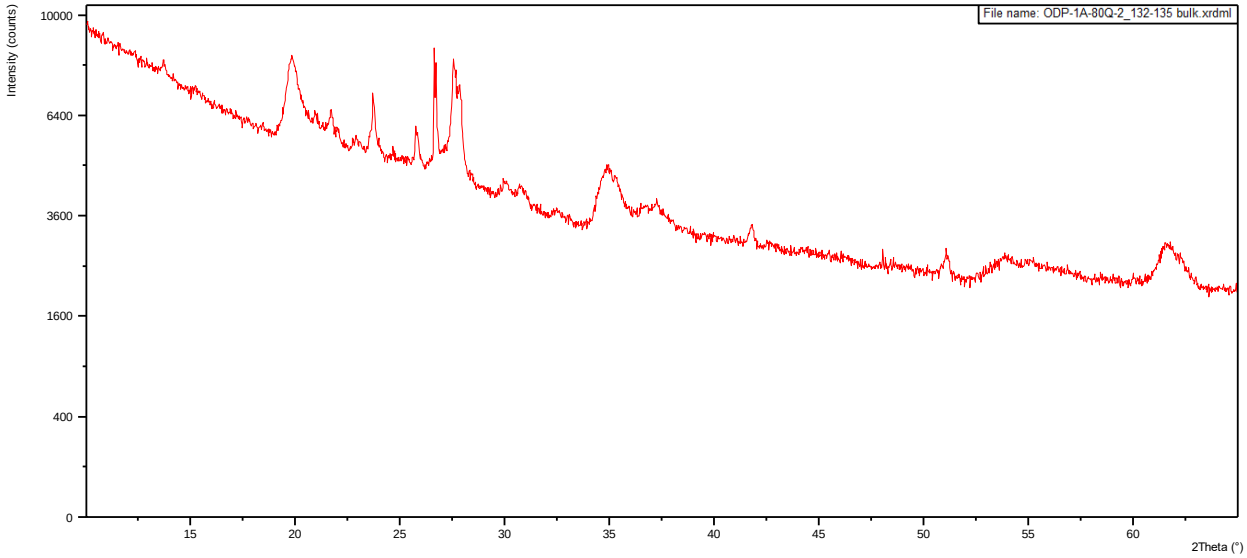
File name: ODP-1A-80Q-2_132-135 bulk.xrdml
Intensity (counts)
10000
6400
3600
1600
400
0
15
20
25
30
35
40
45
50
55
60
2Theta (°)

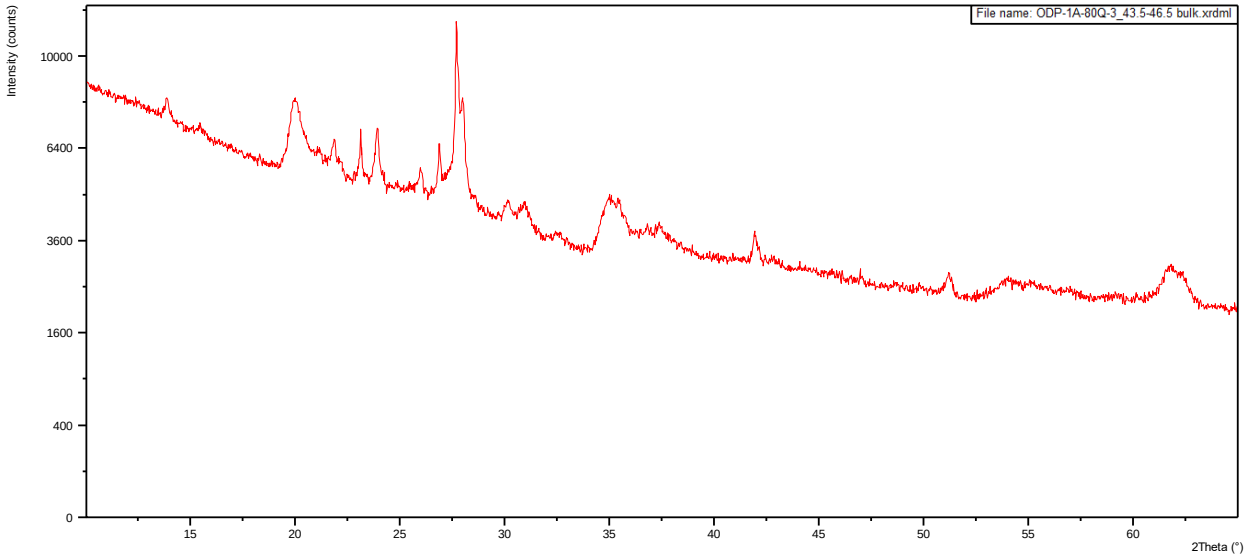
File name: ODP-1A-80Q-3_43.5-46.5 bulk.xrdml
Intensity (counts)
10000
6400
3600
1600
400
0
15
20
25
30
35
40
45
50
55
60
2Theta (°)

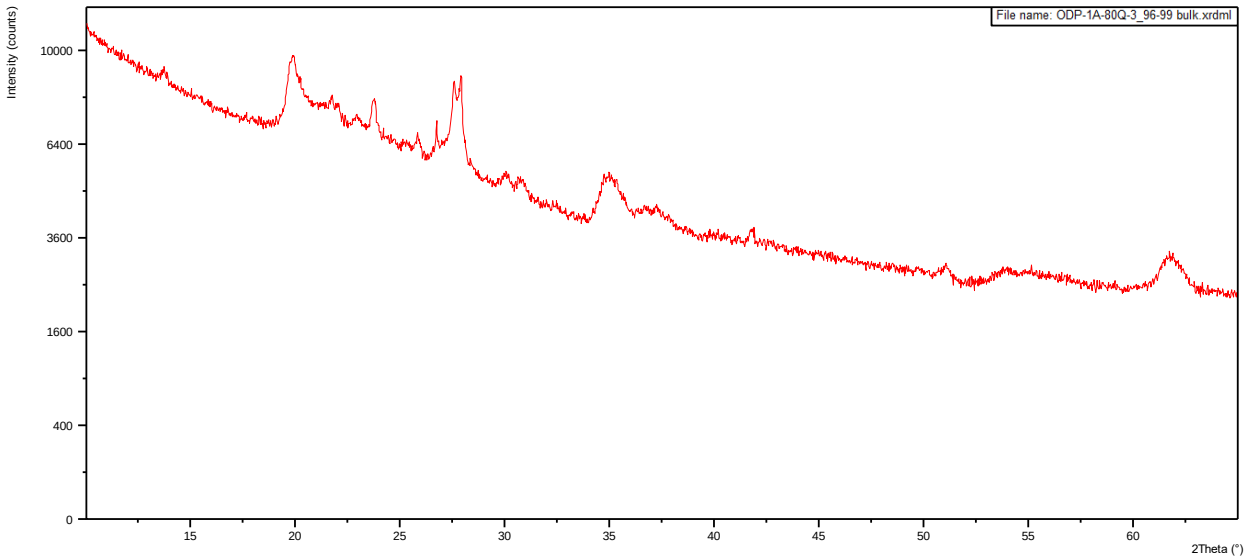
File name: ODP-1A-80Q-3_96-99 bulk.xrdml
Intensity (counts)
10000
6400
3600
1600
400
0
15
20
25
30
35
40
45
50
55
60
2Theta (°)

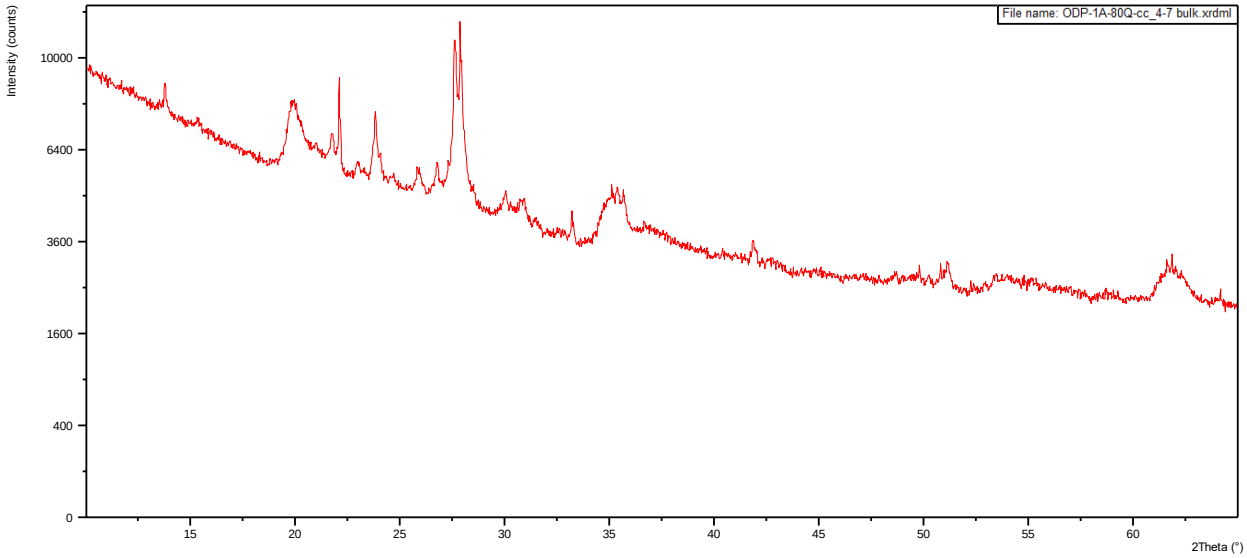
File name: ODP-1A-80Q-cc_4-7 bulk.xrdml
Intensity (counts)
10000
6400
3600
1600
400
0
15
20
25
30
35
40
45
50
55
60
2Theta (°)

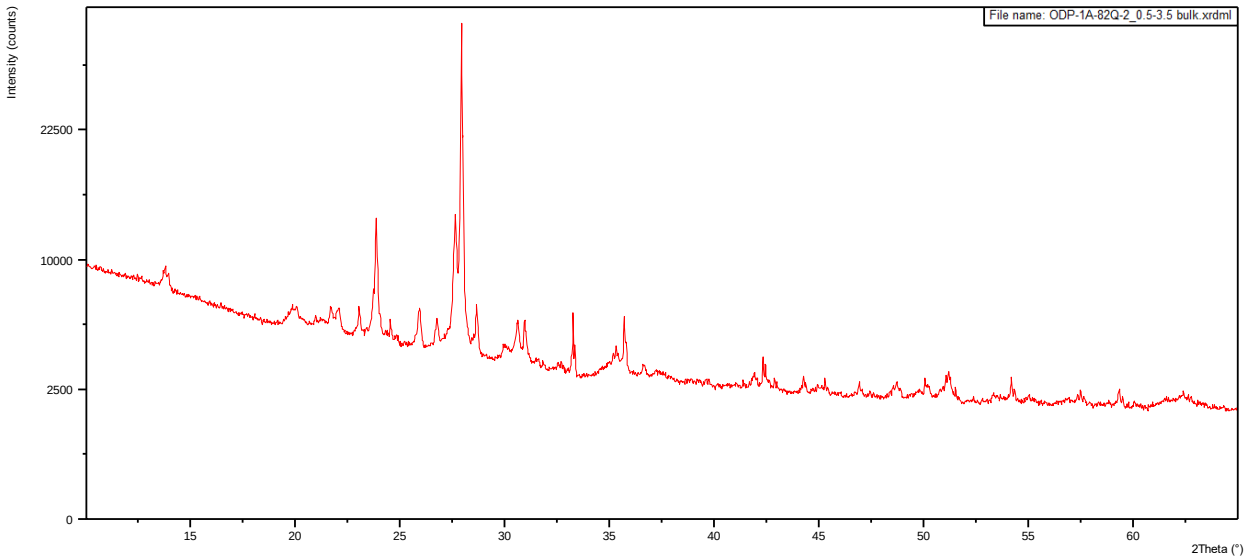
File name: ODP-1A-82Q-2_0.5-3.5 bulk.xrdml
Intensity (counts)
22500
10000
2500
0
15
20
25
30
35
40
45
50
55
60
2Theta (°)

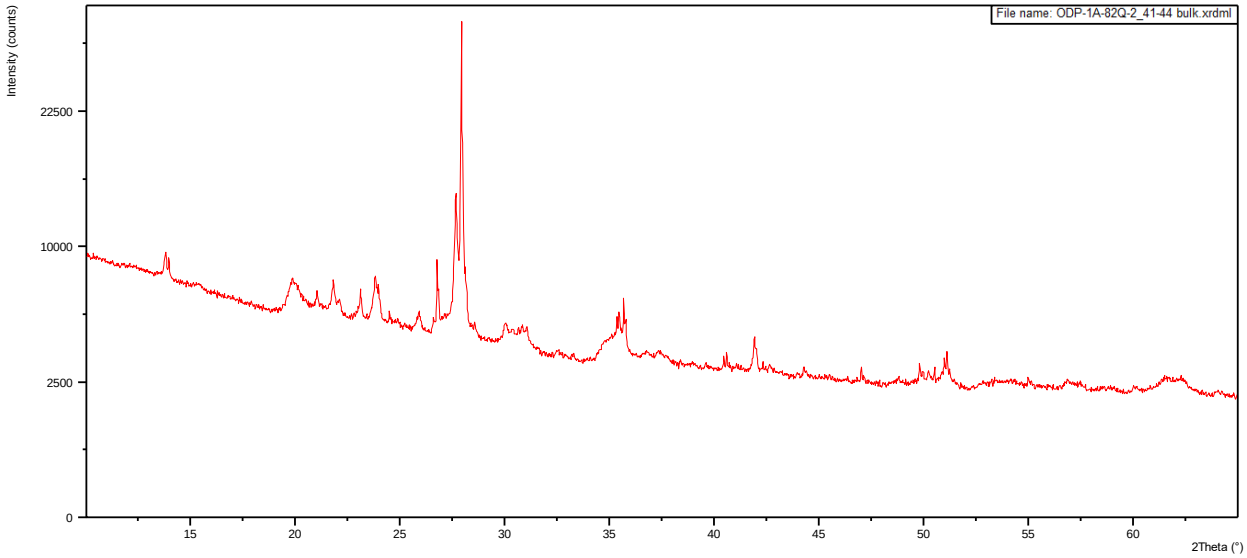
File name: ODP-1A-82Q-2_41-44 bulk.xrdml
Intensity (counts)
22500
10000
2500
0
15
20
25
30
35
40
45
50
55
60
2Theta (°)

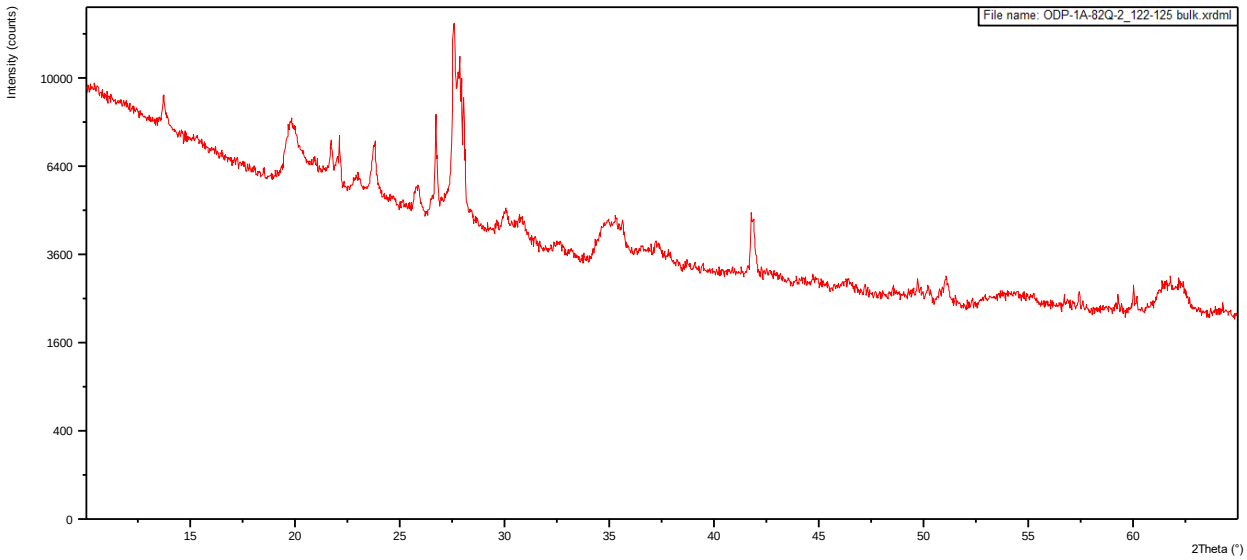
File name: ODP-1A-82Q-2_122-125 bulk.xrdml
Intensity (counts)
10000
6400
3600
1600
400
0
15
20
25
30
35
40
45
50
55
60
2Theta (°)

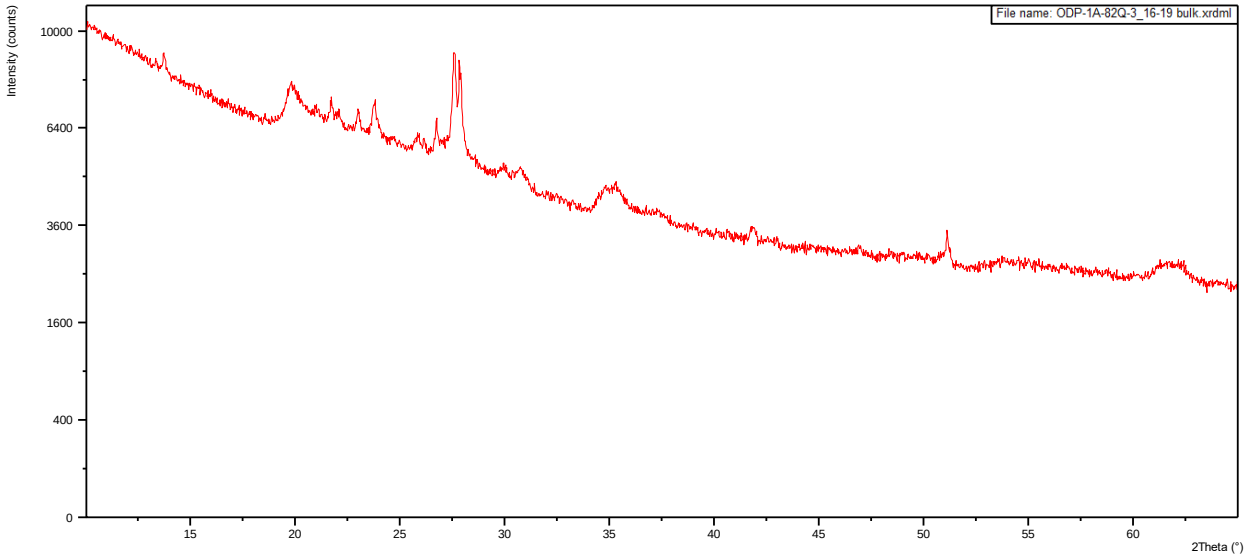
File name: ODP-1A-82Q-3_16-19 bulk.xrdml
Intensity (counts)
10000
6400
3600
1600
400
0
15
20
25
30
35
40
45
50
55
60
2Theta (°)

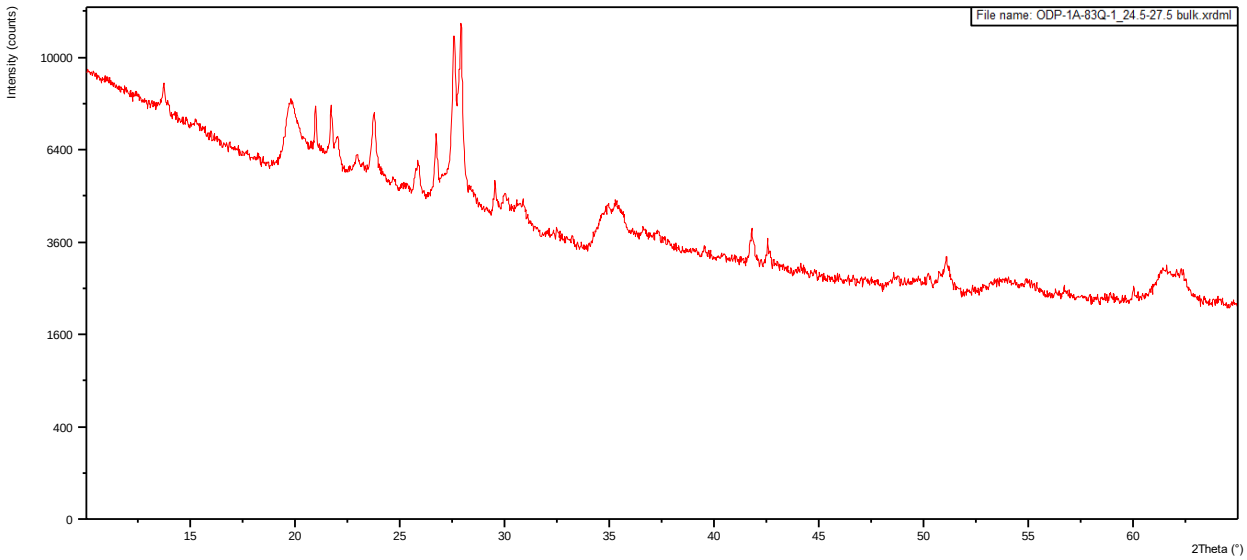
File name: ODP-1A-83Q-1_24.5-27.5 bulk.xrdml
Intensity (counts)
10000
6400
3600
1600
400
0
15
20
25
30
35
40
45
50
55
60
2Theta (°)

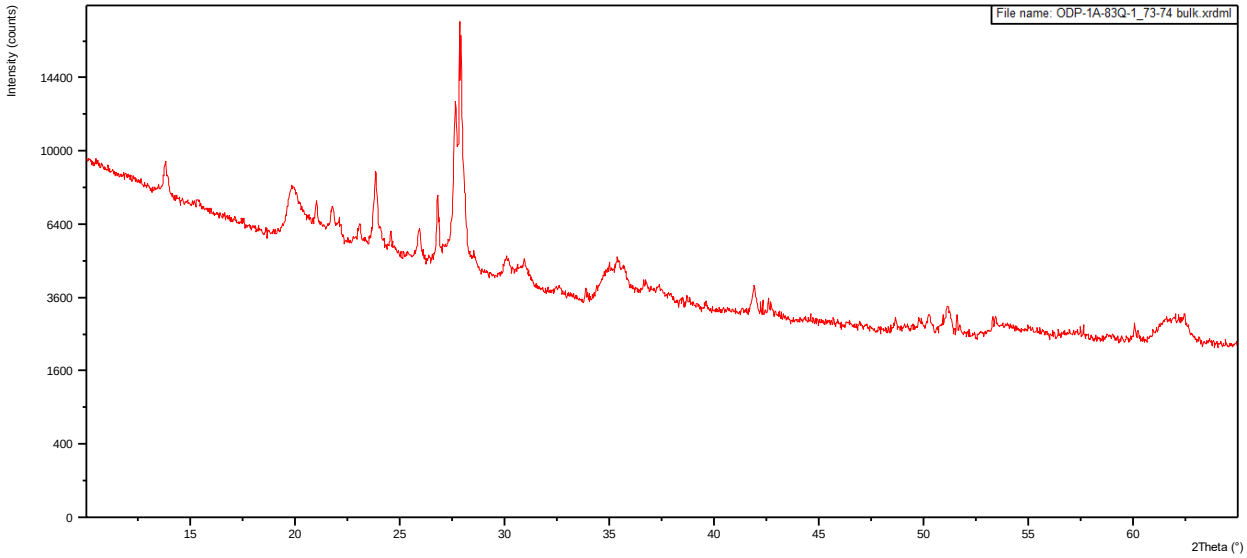
File name: ODP-1A-83Q-1_73-74 bulk.xrdml
Intensity (counts)
14400
10000
6400
3600
1600
400
0
15
20
25
30
35
40
45
50
55
60
2Theta (°)

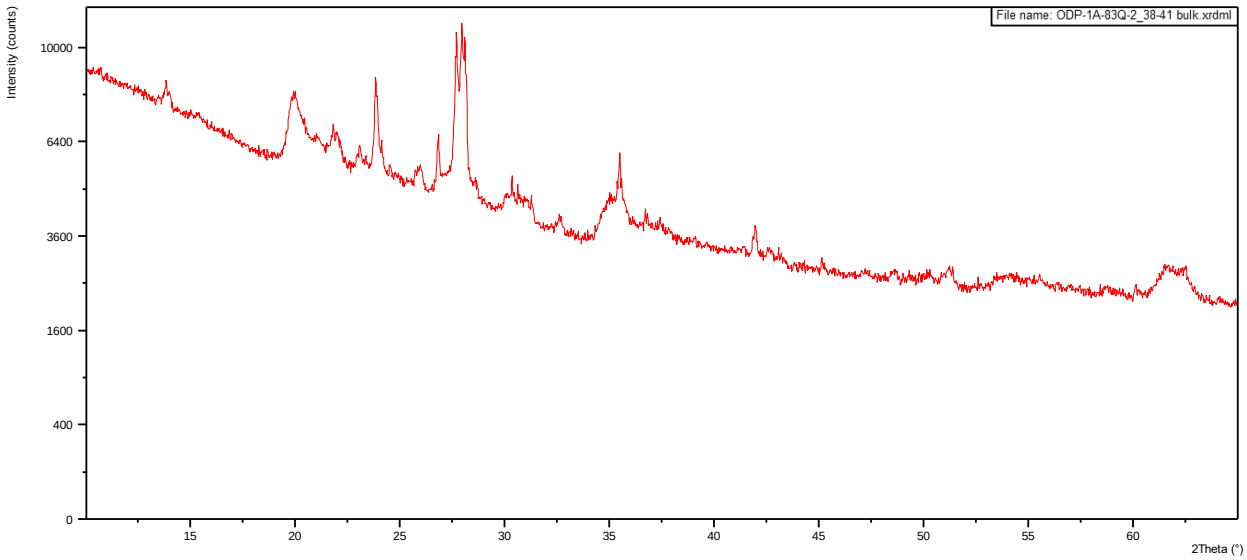
File name: ODP-1A-83Q-2_38-41 bulk.xrdml
Intensity (counts)
10000
6400
3600
1600
400
0
15
20
25
30
35
40
45
50
55
60
2Theta (°)

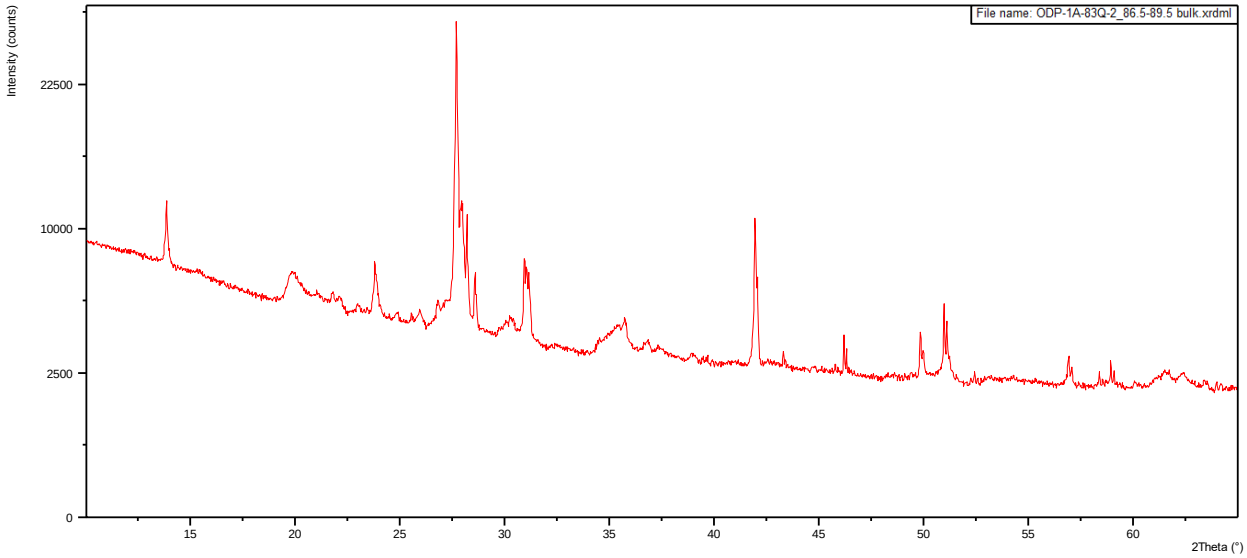
File name: ODP-1A-83Q-2_86.5-89.5 bulk.xrdml
Intensity (counts)
22500
10000
2500
0
15
20
25
30
35
40
45
50
55
60
2Theta (°)

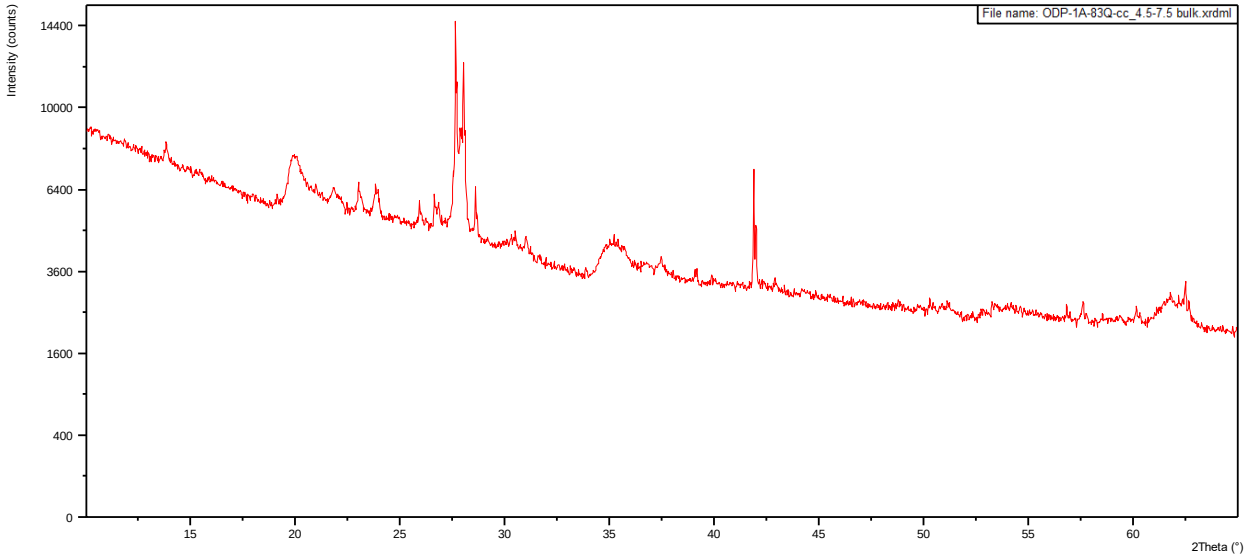
File name: ODP-1A-83Q-cc_4.5-7.5 bulk.xrdml
Intensity (counts)
14400
10000
6400
3600
1600
400
0
15
20
25
30
35
40
45
50
55
60
2Theta (°)

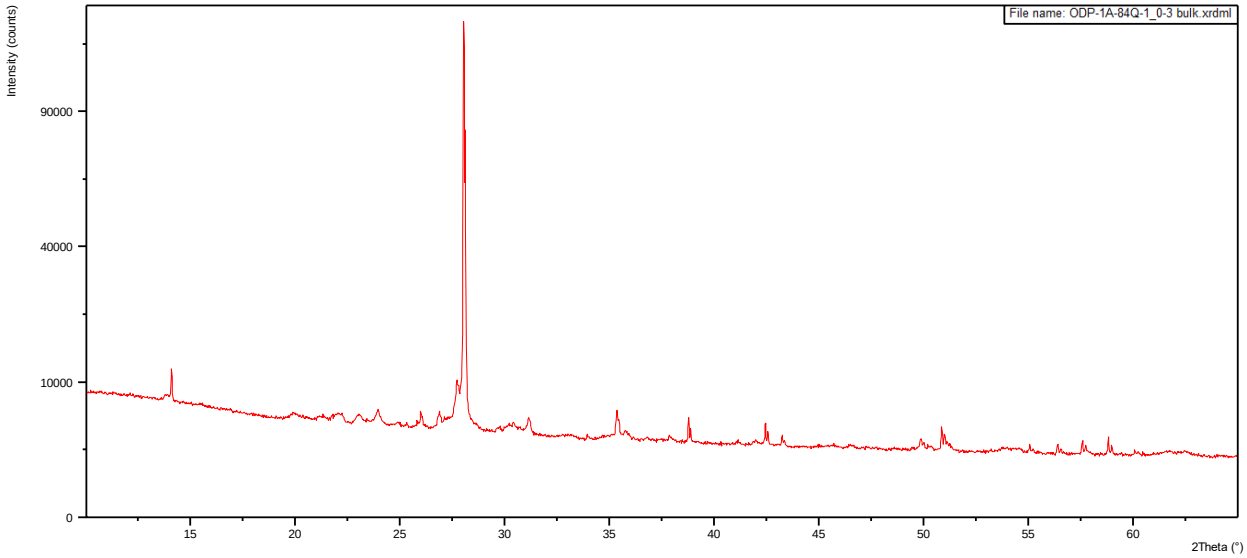
File name: ODP-1A-84Q-1_0-3 bulk.xrdml
Intensity (counts)
90000
40000
10000
0
15
20
25
30
35
40
45
50
55
60
2Theta (°)

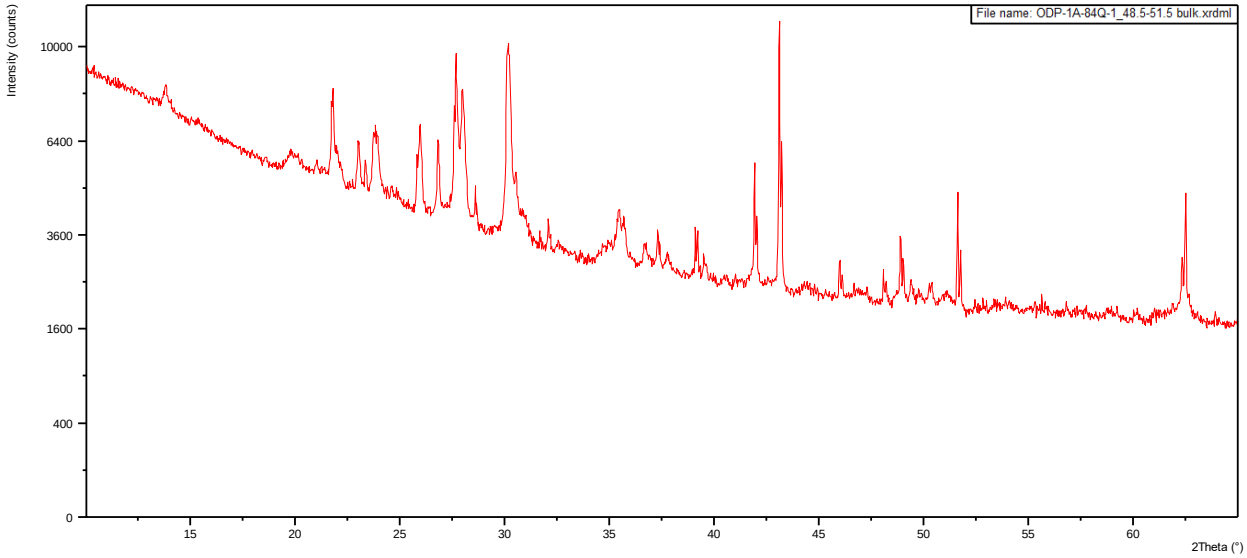
File name: ODP-1A-84Q-1_48.5-51.5 bulk.xrdml
Intensity (counts)
10000
6400
3600
1600
400
0
15
20
25
30
35
40
45
50
55
60
2Theta (°)

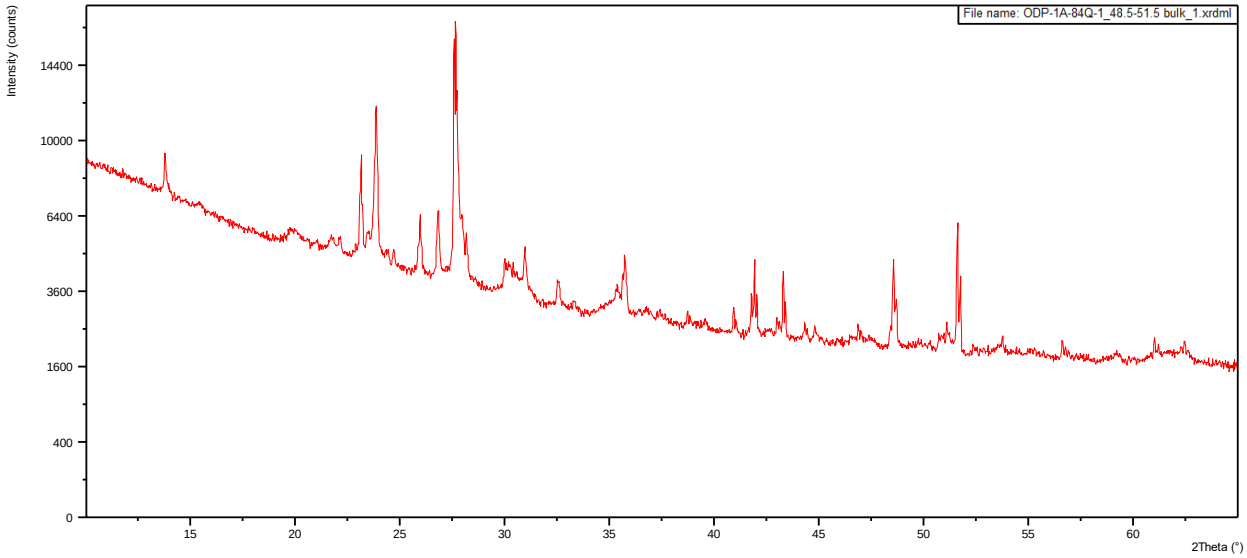
File name: ODP-1A-84Q-1_48.5-51.5 bulk_1.xrdml
Intensity (counts)
14400
10000
6400
3600
1600
400
0
15
20
25
30
35
40
45
50
55
60
2Theta (°)

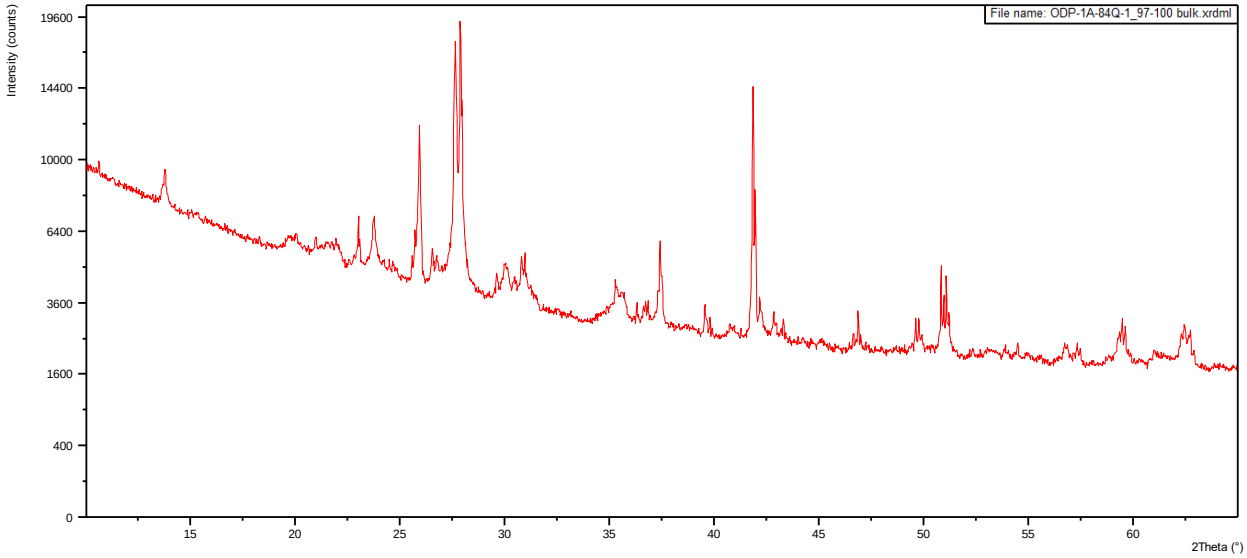
File name: ODP-1A-84Q-1_97-100 bulk.xrdml
Intensity (counts)
19600
14400
10000
6400
3600
1600
400
0
15
20
25
30
35
40
45
50
55
60
2Theta (°)

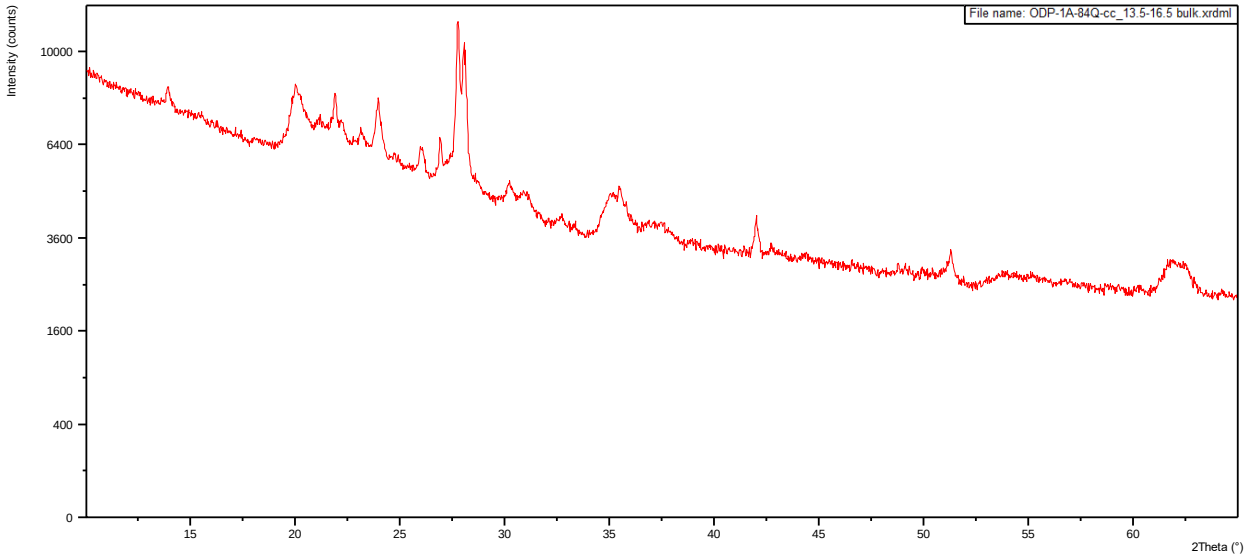
File name: ODP-1A-84Q-cc_13.5-16.5 bulk.xrdml
Intensity (counts)
10000
6400
3600
1600
400
0
15
20
25
30
35
40
45
50
55
60
2Theta (°)

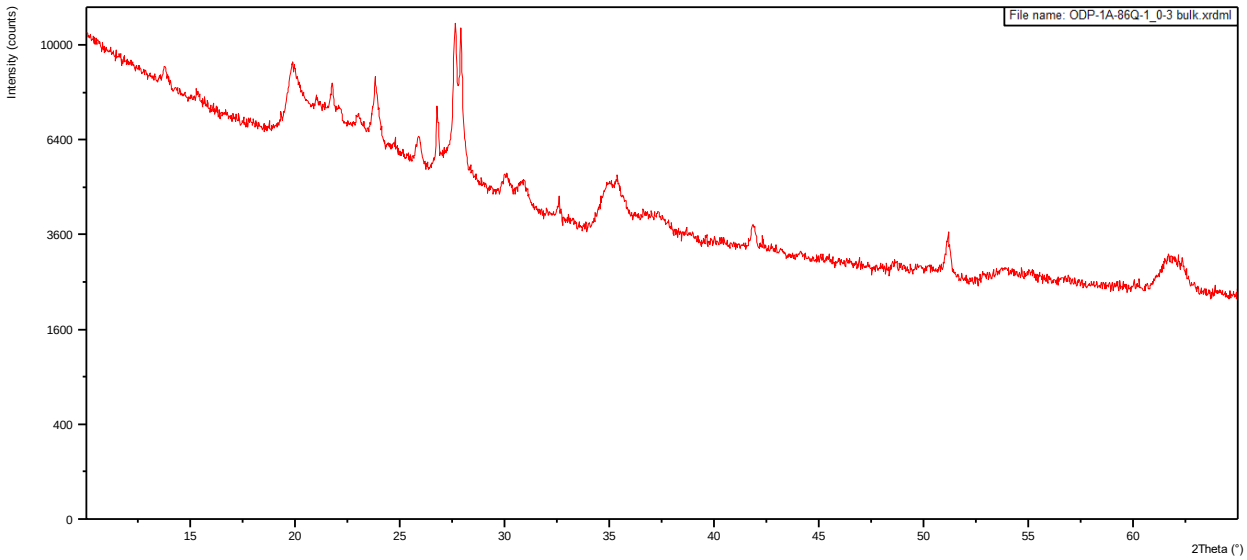
File name: ODP-1A-86Q-1_0-3 bulk.xrdml
Intensity (counts)
10000
6400
3600
1600
400
0
15
20
25
30
35
40
45
50
55
60
2Theta (°)

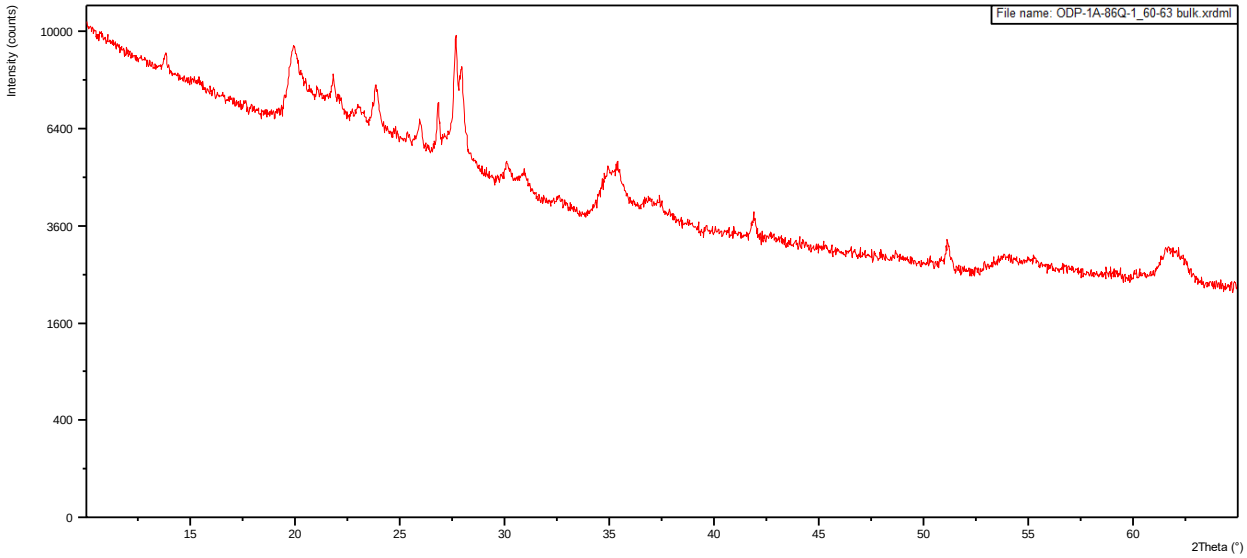
File name: ODP-1A-86Q-1_60-63 bulk.xrdml
Intensity (counts)
10000
6400
3600
1600
400
0
15
20
25
30
35
40
45
50
55
60
2Theta (°)

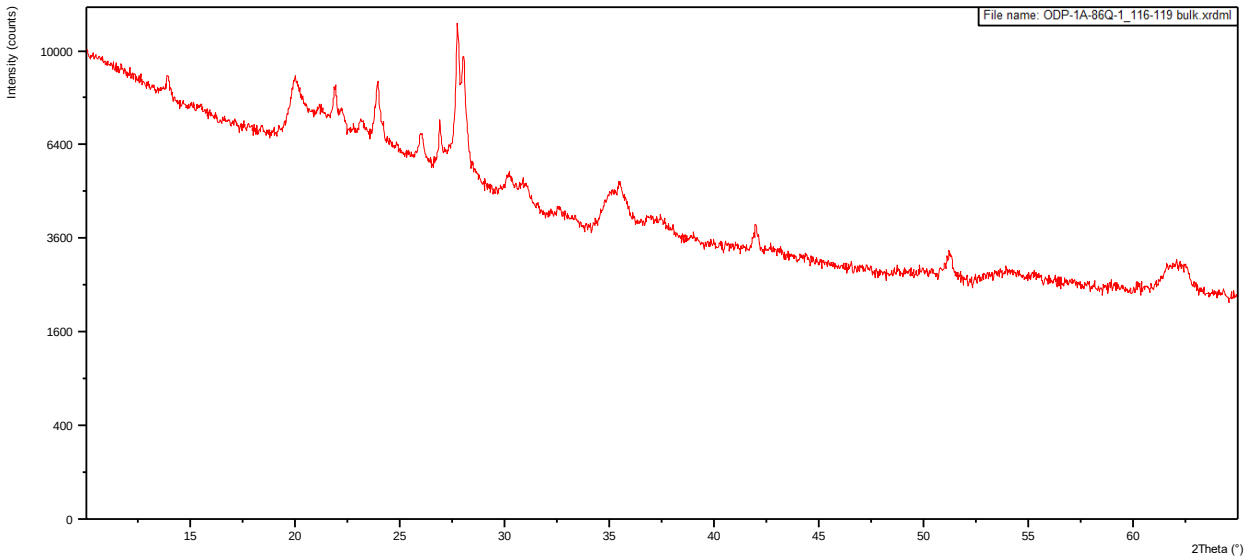
File name: ODP-1A-86Q-1_116-119 bulk.xrdml
Intensity (counts)
10000
6400
3600
1600
400
0
15
20
25
30
35
40
45
50
55
60
2Theta (°)

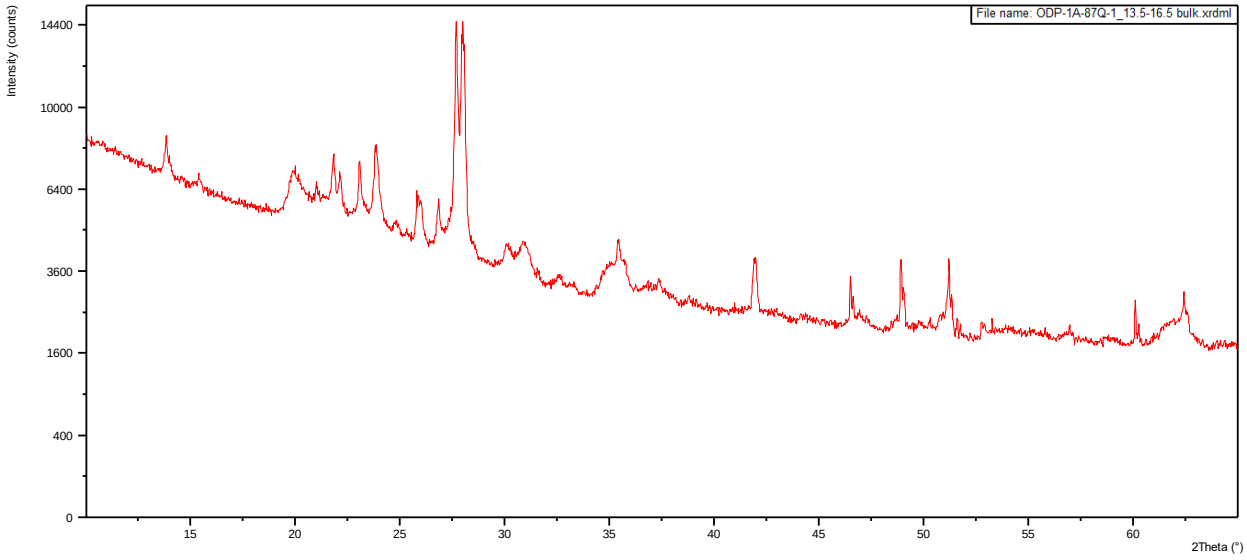
File name: ODP-1A-87Q-1_13.5-16.5 bulk.xrdml
Intensity (counts)
14400
10000
6400
3600
1600
400
0
15
20
25
30
35
40
45
50
55
60
2Theta (°)

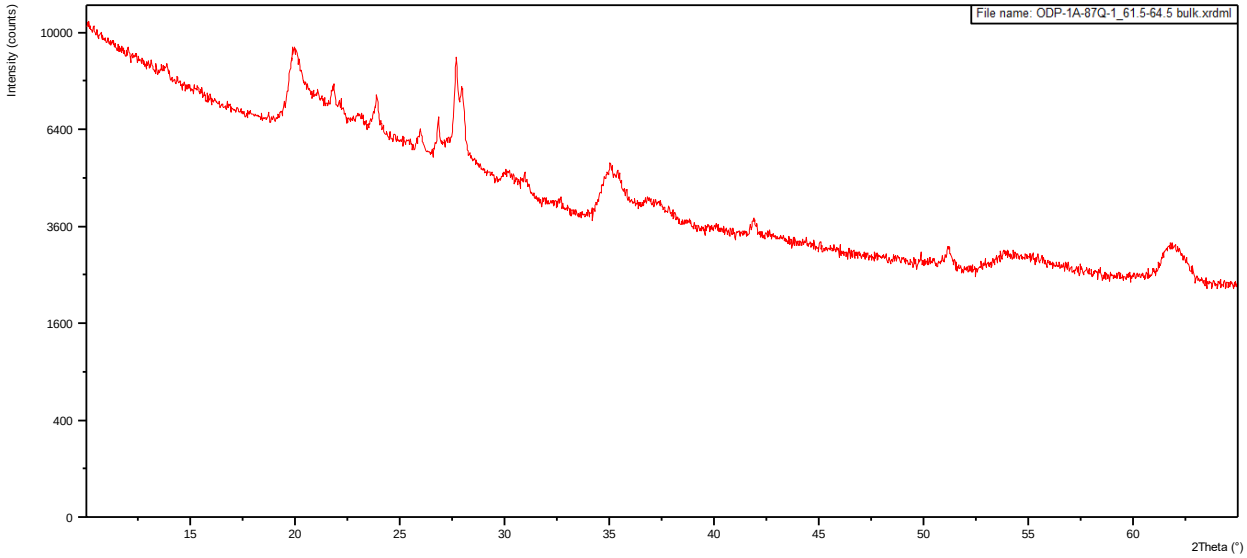

Appendix C.2: Geochemistry Matrix of Intercorrelation

	SiO2	Al2O3	Fe2O3	MnO	MgO	CaO	Na2O	K2O	TiO2	P2O5	LOI	S
SiO2	1	0.283	0.191	-0.477	-0.26	-0.765	0.087	0.086	0.172	-0.241	-0.678	0.066
Al2O3	0.283	1	0.789	0.039	-0.5	-0.703	0.555	0.678	0.43	-0.061	-0.768	0.186
Fe2O3	0.191	0.789	1	0.236	-0.57	-0.711	0.573	0.71	0.229	-0.114	-0.597	0.23
MnO	-0.477	0.039	0.236	1	-0.423	0.245	0.404	0.392	-0.376	-0.101	0.067	0.27
MgO	-0.26	-0.5	-0.57	-0.423	1	0.463	-0.73	-0.686	0.213	0.381	0.566	-0.323
CaO	-0.765	-0.703	-0.711	0.245	0.463	1	-0.403	-0.54	-0.283	0.24	0.761	-0.098
Na2O	0.087	0.555	0.573	0.404	-0.73	-0.403	1	0.875	-0.366	-0.536	-0.606	0.562
K2O	0.086	0.678	0.71	0.392	-0.686	-0.54	0.875	1	-0.237	-0.445	-0.586	0.449
TiO2	0.172	0.43	0.229	-0.376	0.213	-0.283	-0.366	-0.237	1	0.51	-0.165	-0.435
P2O5	-0.241	-0.061	-0.114	-0.101	0.381	0.24	-0.536	-0.445	0.51	1	0.292	-0.373
LOI	-0.678	-0.768	-0.597	0.067	0.566	0.761	-0.606	-0.586	-0.165	0.292	1	-0.399
S	0.066	0.186	0.23	0.27	-0.323	-0.098	0.562	0.449	-0.435	-0.373	-0.399	1

Appendix D: Southern Kenya Rift Surface and Outcrop Samples

Appendix D.1: X-ray Diffraction Patterns

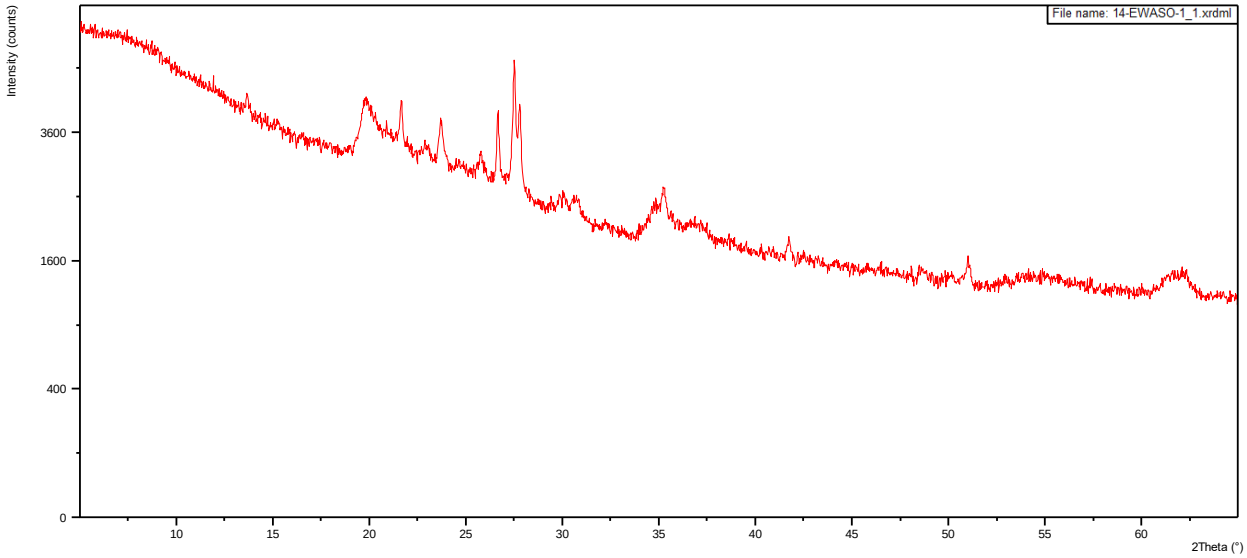

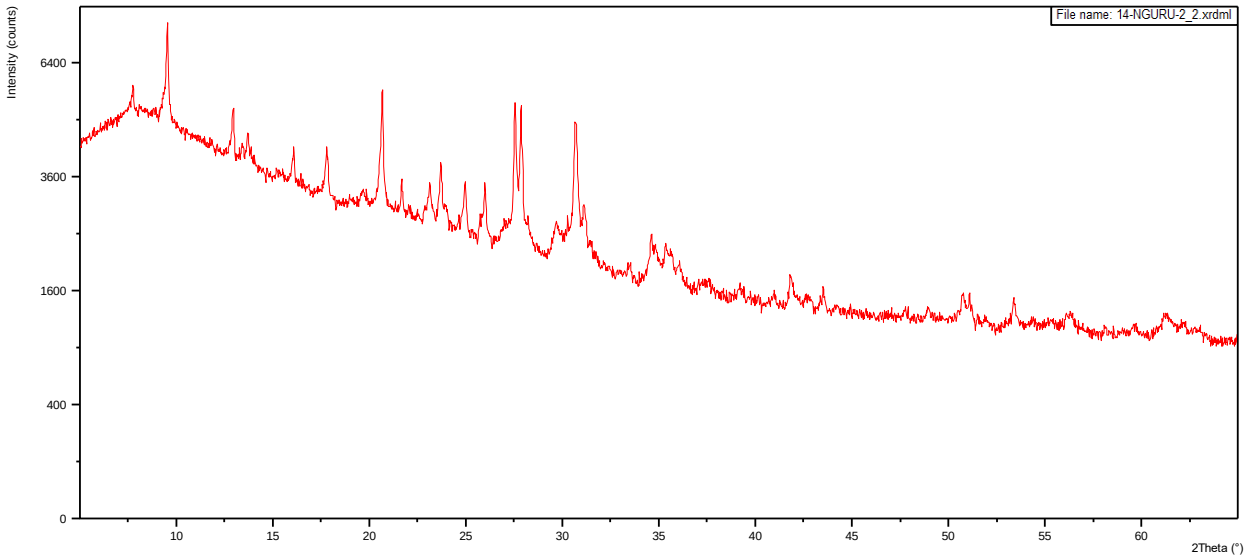

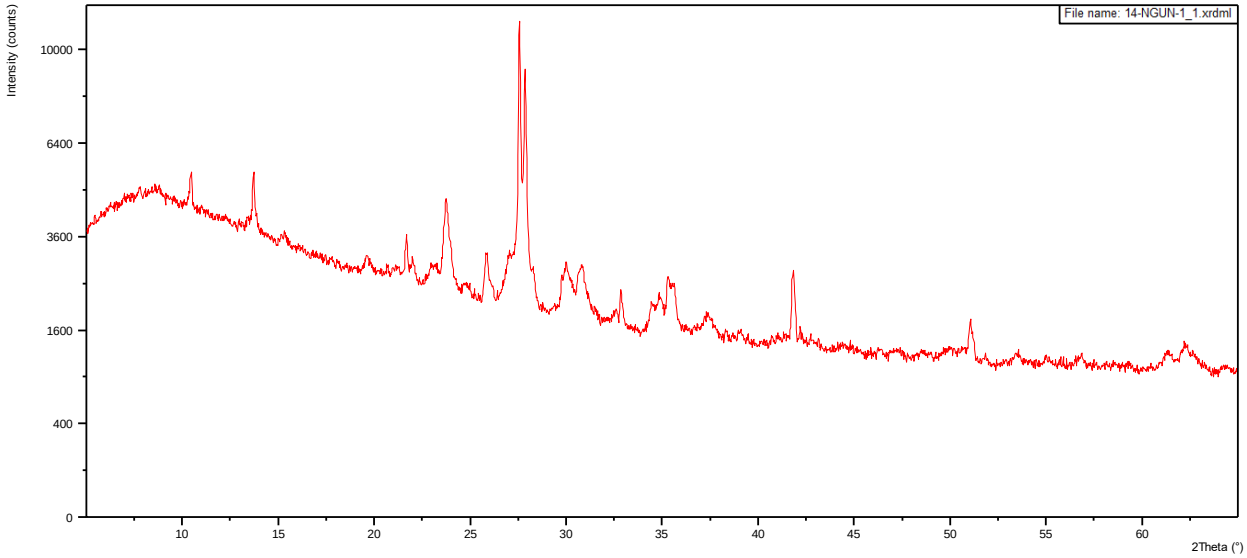
File name: 14-NGUN-1_1.xrdml
Intensity (counts)
10000
6400
3600
1600
400
0
10
15
20
25
30
35
40
45
50
55
60
2Theta (°)

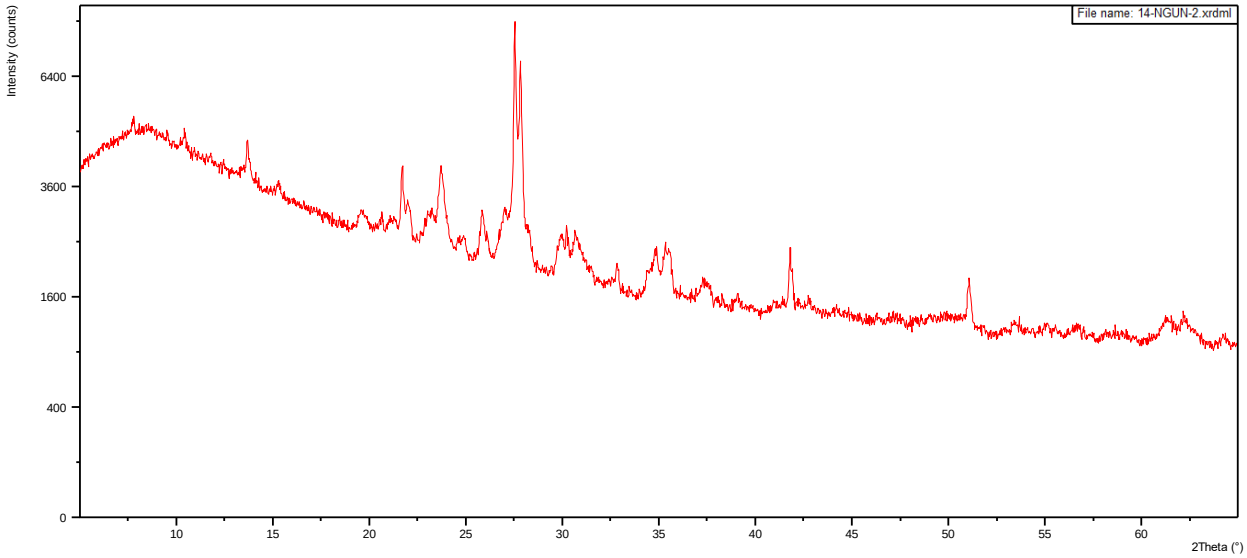
File name: 14-NGUN-2.xrdml
Intensity (counts)
6400
3600
1600
400
0
10
15
20
25
30
35
40
45
50
55
60
2Theta (°)

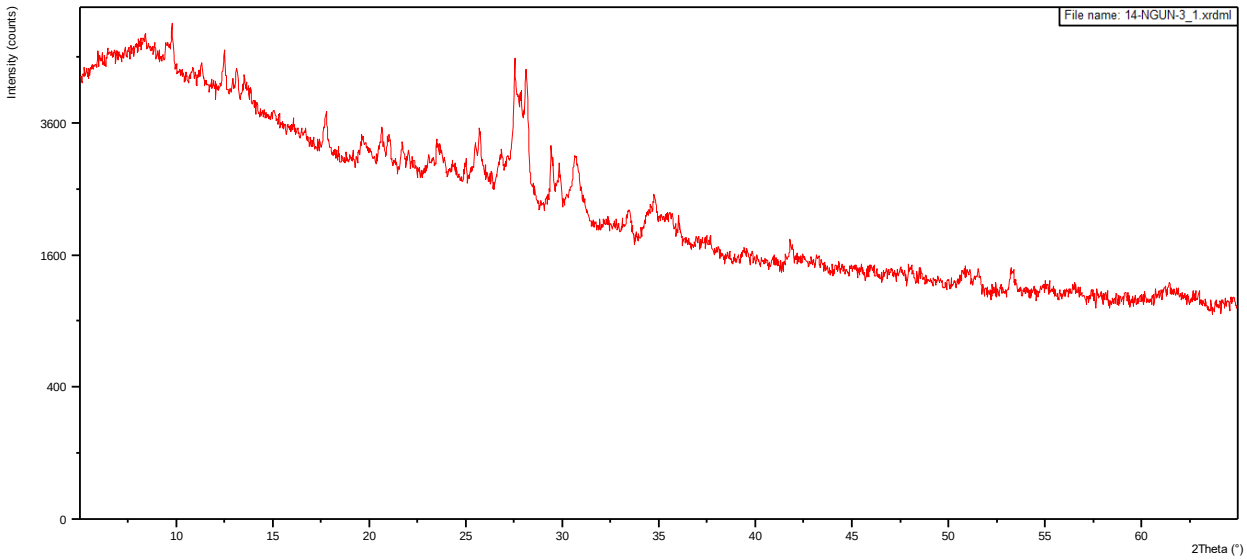
File name: 14-NGUN-3_1.xrdml
Intensity (counts)
0
400
1600
3600
10
15
20
25
30
35
40
45
50
55
60
2Theta (°)

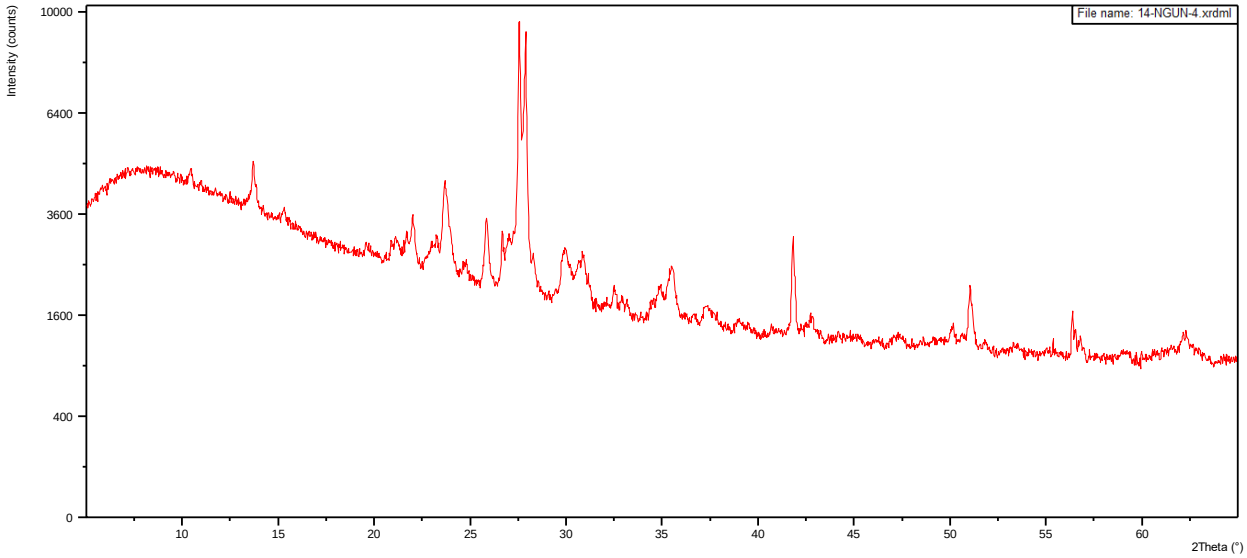
File name: 14-NGUN-4.xrdml
Intensity (counts)
0
400
1600
3600
6400
10000
10
15
20
25
30
35
40
45
50
55
60
2Theta (°)

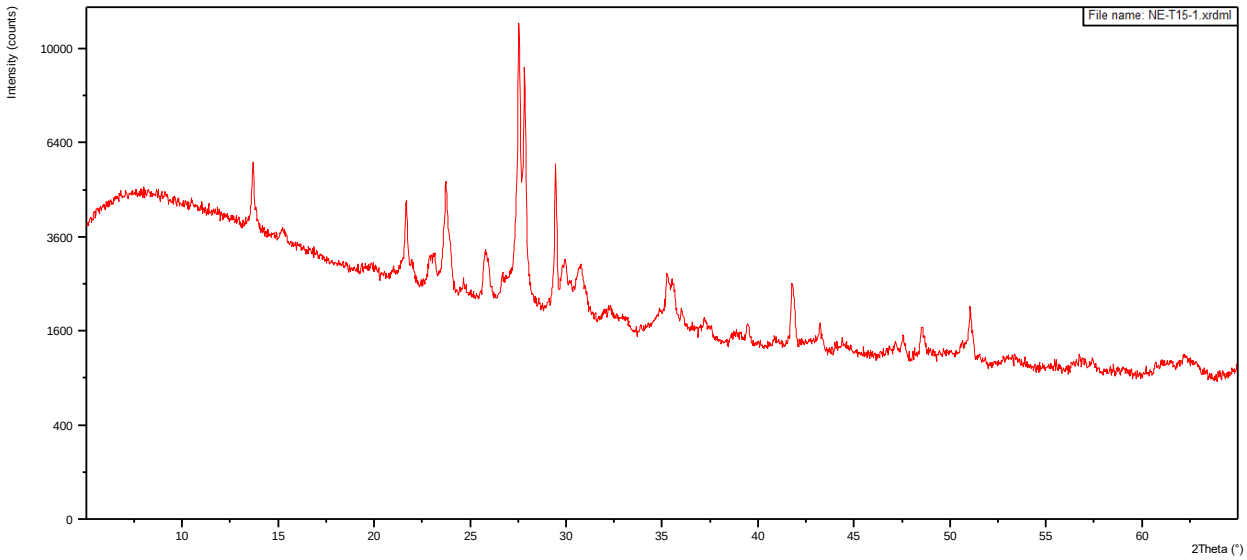
File name: NE-T15-1.xrdml
Intensity (counts)
10000
6400
3600
1600
400
0
10
15
20
25
30
35
40
45
50
55
60
2Theta (°)

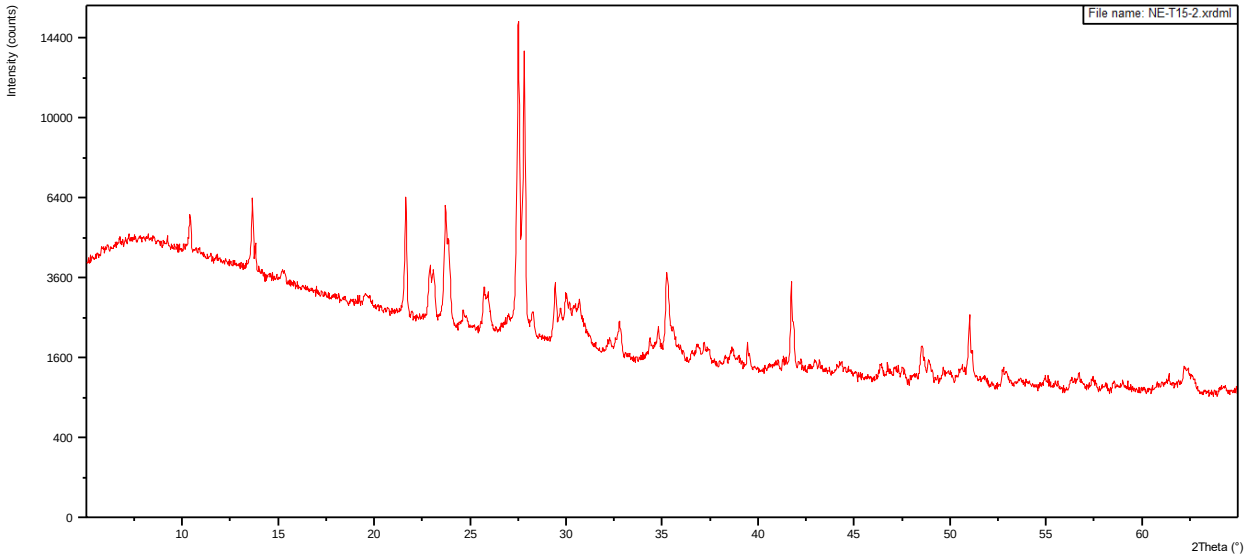
File name: NE-T15-2.xrdml
Intensity (counts)
14400
10000
6400
3600
1600
400
0
10
15
20
25
30
35
40
45
50
55
60
2Theta (°)

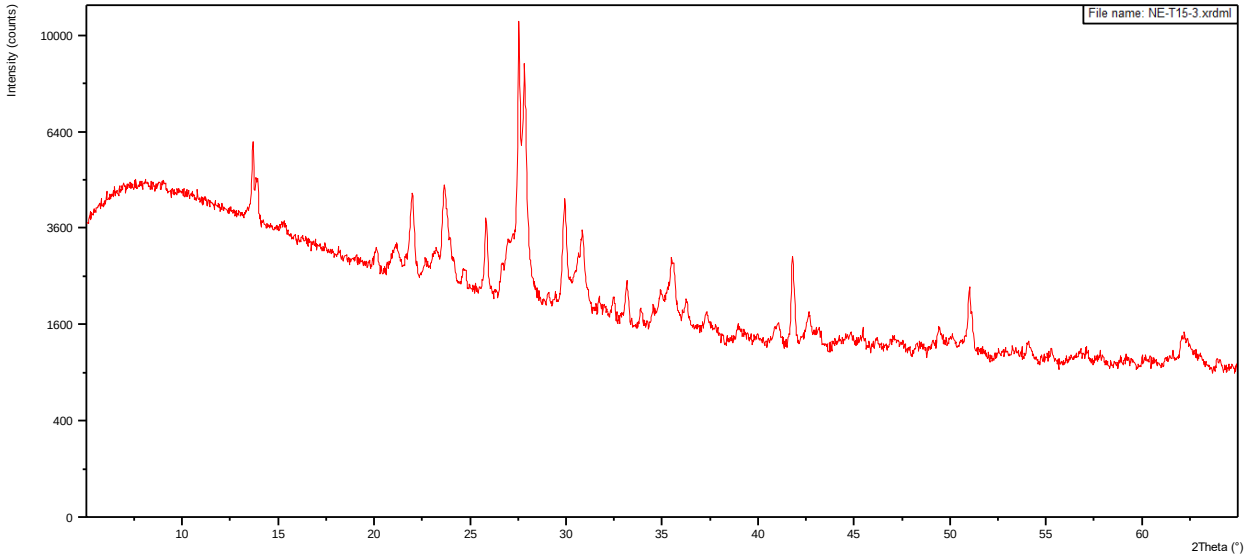
File name: NE-T15-3.xrdml
Intensity (counts)
10000
6400
3600
1600
400
0
10
15
20
25
30
35
40
45
50
55
60
2Theta (°)

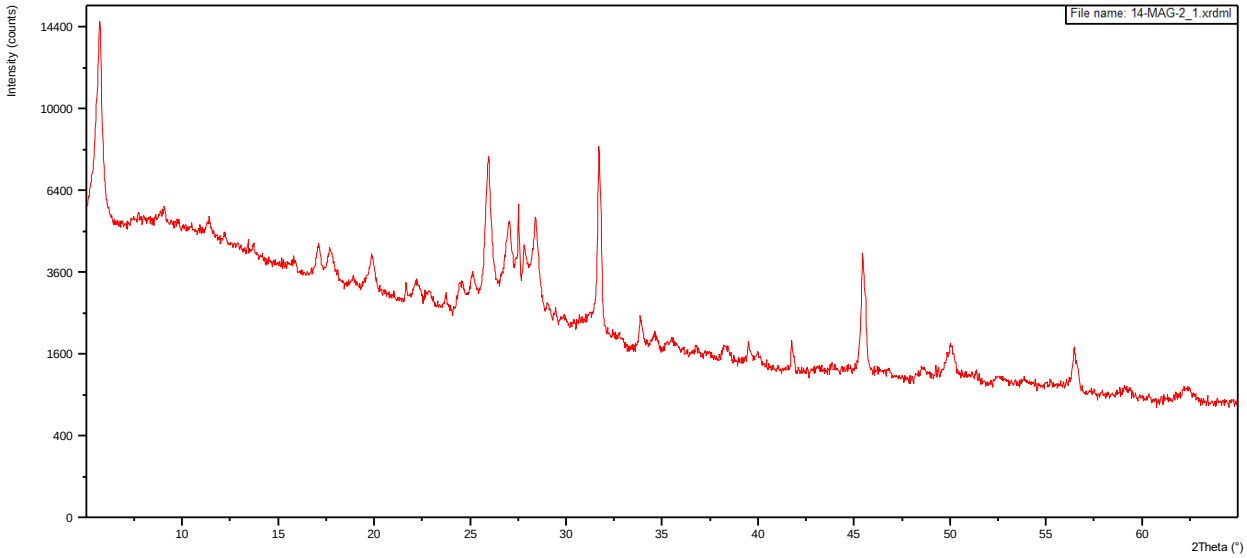
File name: 14-MAG-2_1.xrdml
Intensity (counts)
14400
10000
6400
3600
1600
400
0
10
15
20
25
30
35
40
45
50
55
60
2Theta (°)

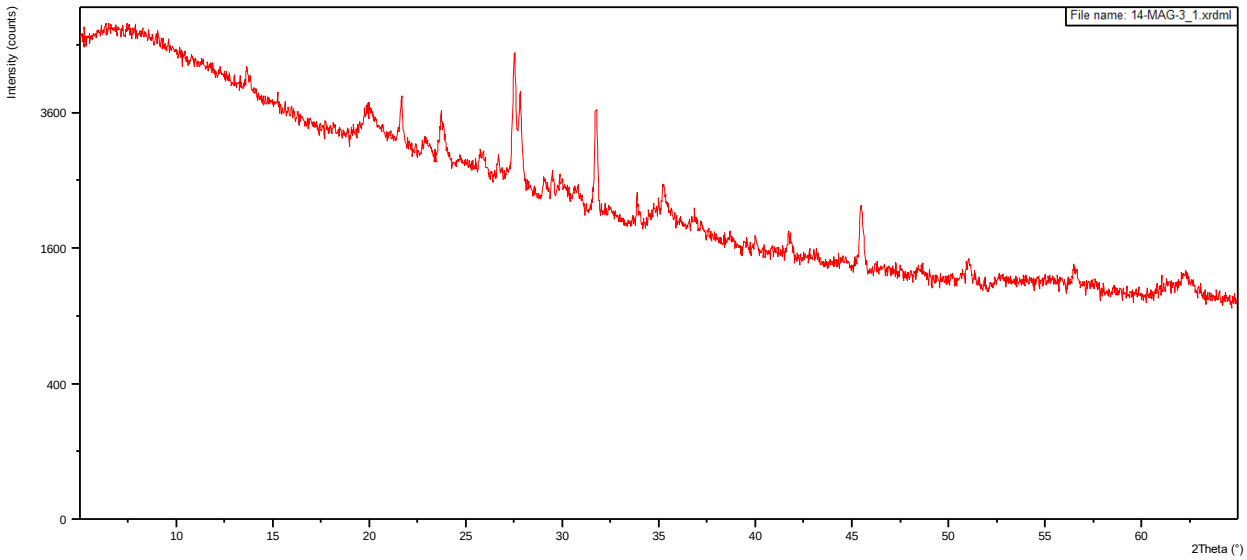
File name: 14-MAG-3_1.xrdml
Intensity (counts)
0
400
1600
3600
10
15
20
25
30
35
40
45
50
55
60
2Theta (°)

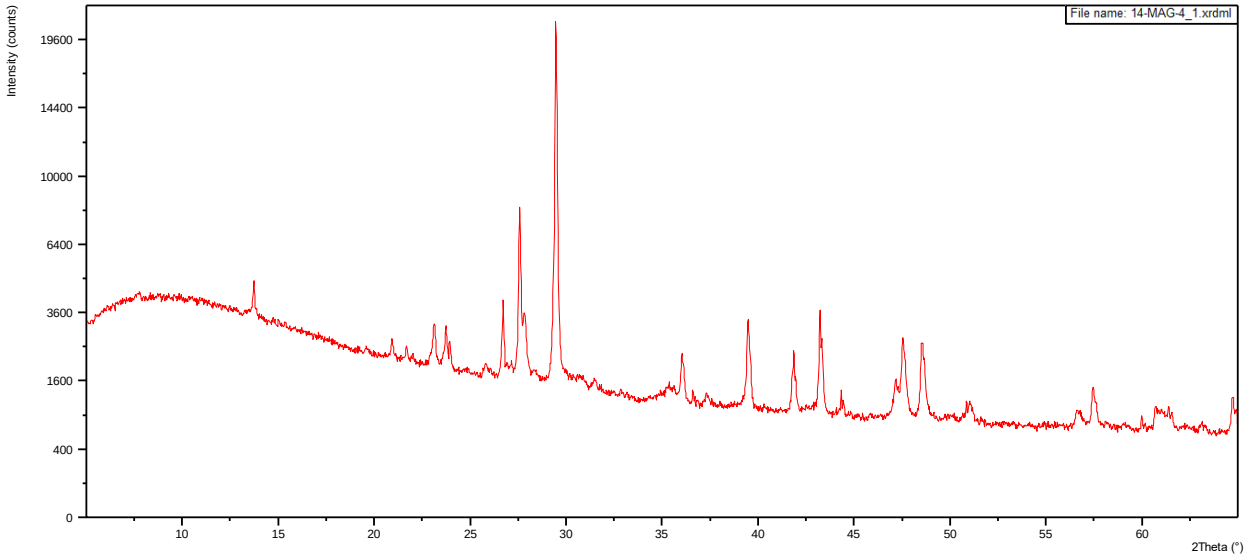
File name: 14-MAG-4_1.xrdml
Intensity (counts)
0
400
1600
3600
6400
10000
14400
19600
10
15
20
25
30
35
40
45
50
55
60
2Theta (°)

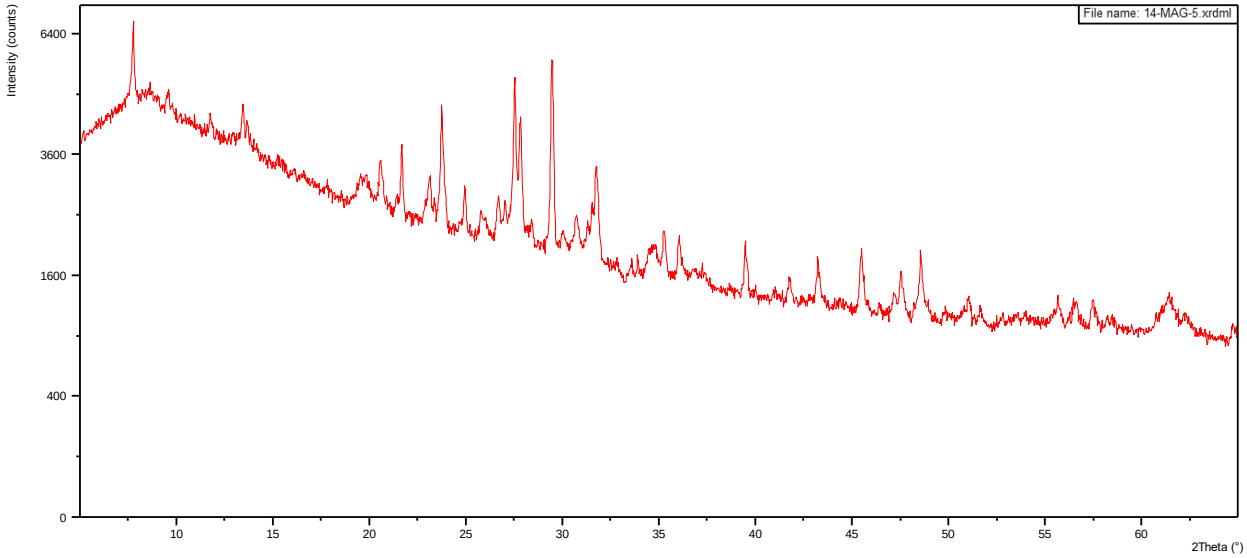
File name: 14-MAG-5.xrdml
Intensity (counts)
6400
3600
1600
400
0
10
15
20
25
30
35
40
45
50
55
60
2Theta (°)

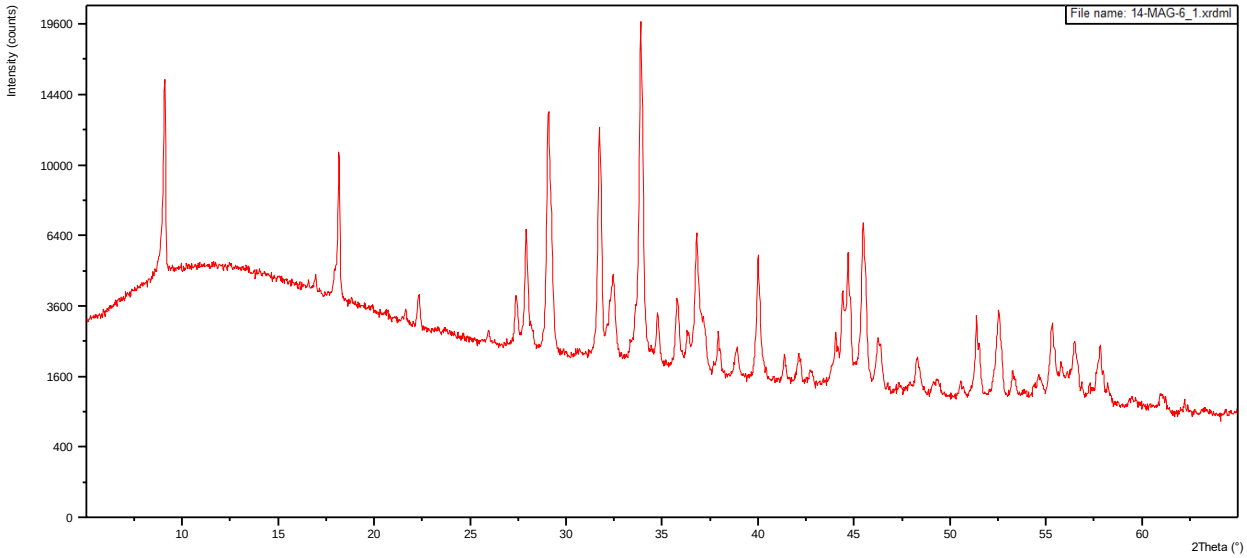
File name: 14-MAG-6_1.xrdml
Intensity (counts)
19600
14400
10000
6400
3600
1600
400
0
10
15
20
25
30
35
40
45
50
55
60
2Theta (°)

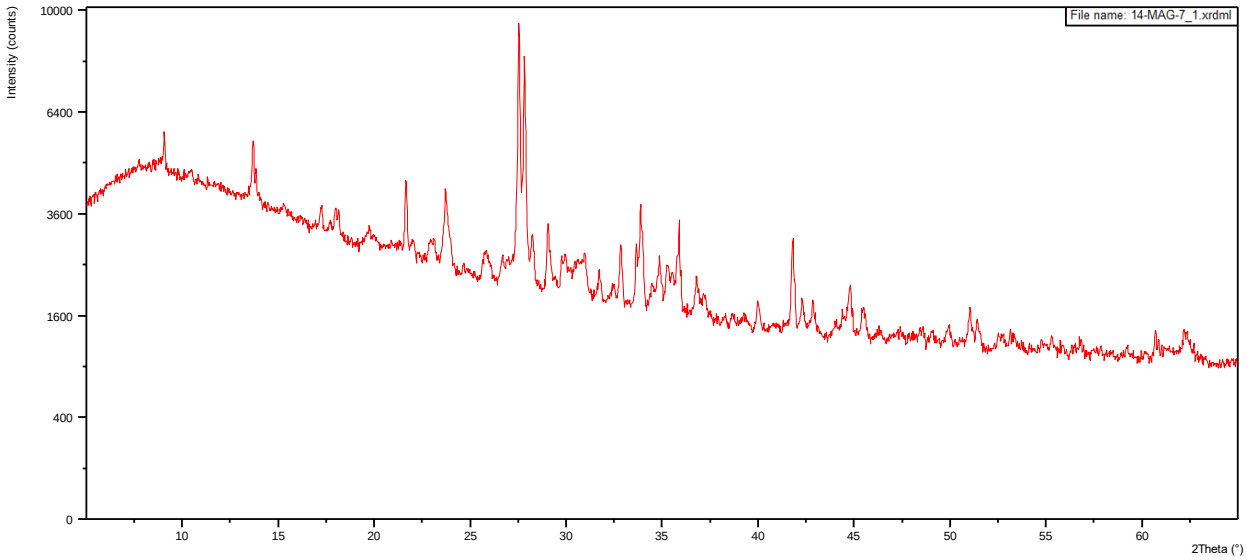
File name: 14-MAG-7_1.xrdml
Intensity (counts)
10000
6400
3600
1600
400
0
10
15
20
25
30
35
40
45
50
55
60
2Theta (°)

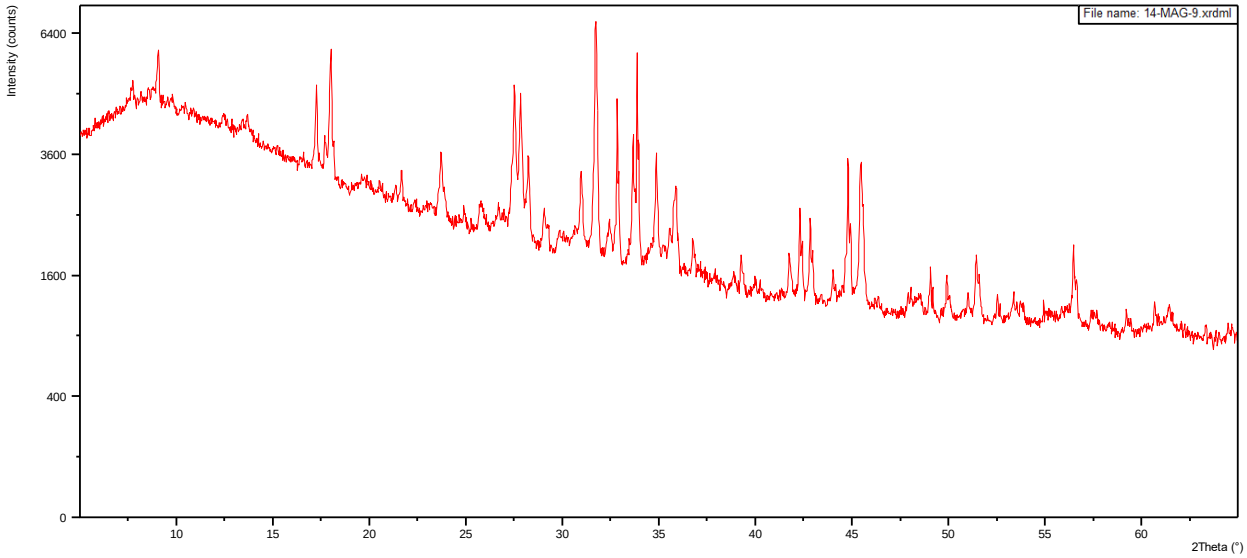
File name: 14-MAG-9.xrdml
Intensity (counts)
6400
3600
1600
400
0
10
15
20
25
30
35
40
45
50
55
60
2Theta (°)

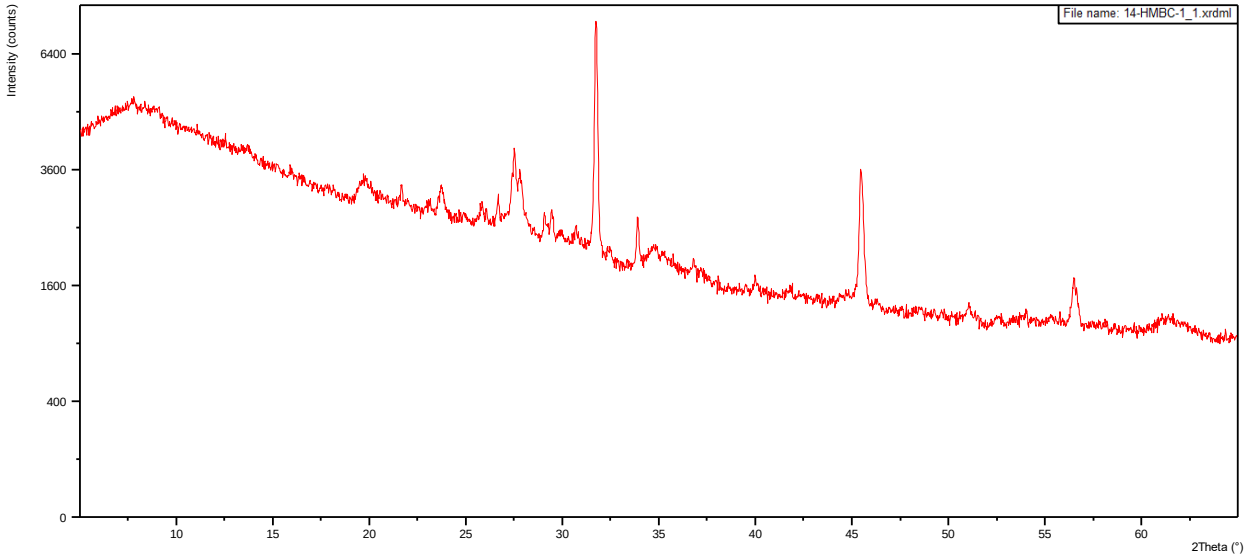
File name: 14-HMBC-1_1.xrdml
Intensity (counts)
6400
3600
1600
400
0
10
15
20
25
30
35
40
45
50
55
60
2Theta (°)

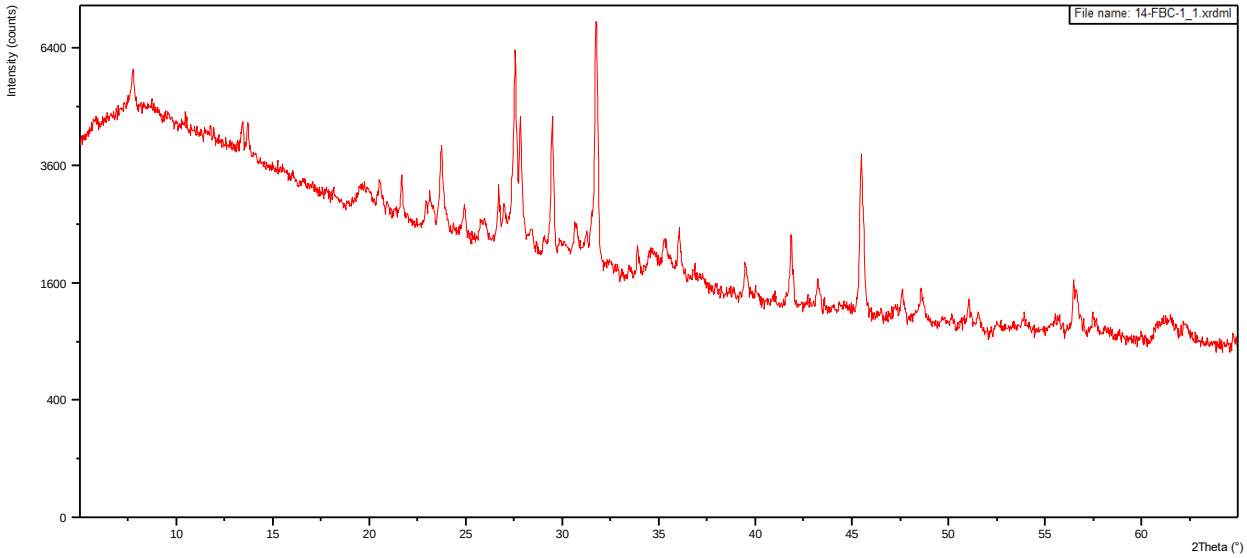
File name: 14-FBC-1_1.xrdml
Intensity (counts)
6400
3600
1600
400
0
10
15
20
25
30
35
40
45
50
55
60
2Theta (°)

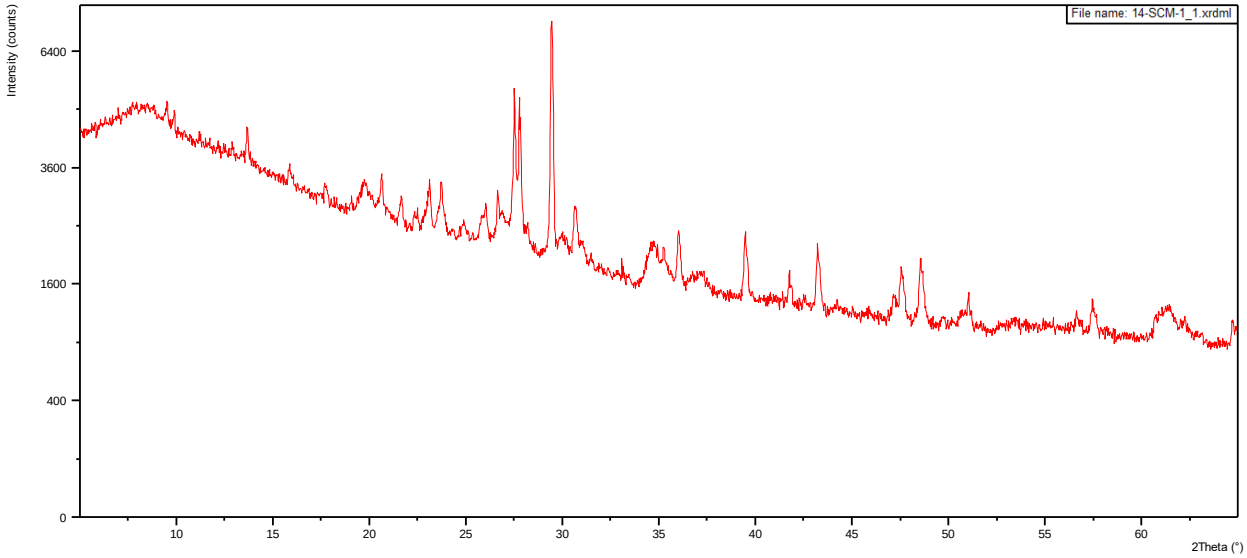
File name: 14-SCM-1_1.xrdml
Intensity (counts)
6400
3600
1600
400
0
10
15
20
25
30
35
40
45
50
55
60
2Theta (°)

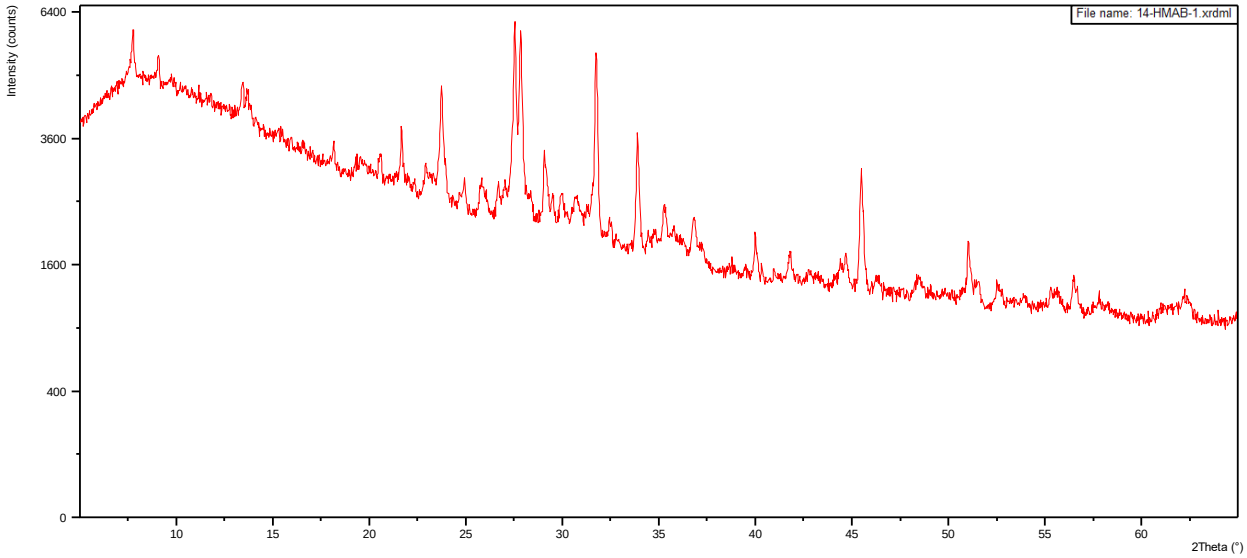
File name: 14-HMAB-1.xrdml
Intensity (counts)
6400
3600
1600
400
0
10
15
20
25
30
35
40
45
50
55
60
2Theta (°)

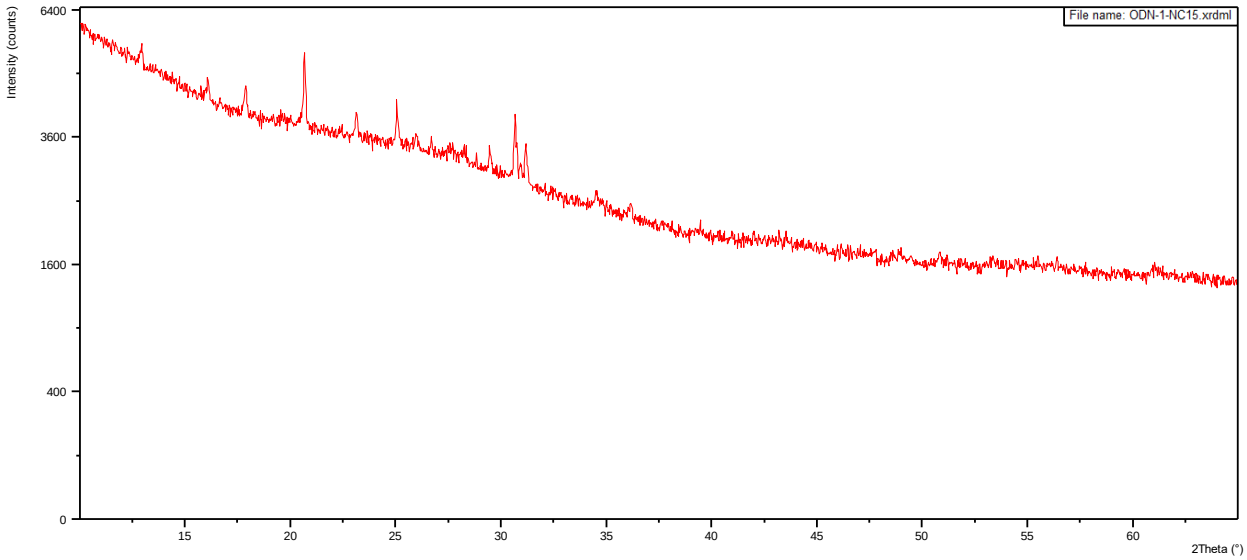
File name: ODN-1-NC15.xrdml
Intensity (counts)
6400
3600
1600
400
0
15
20
25
30
35
40
45
50
55
60
2Theta (°)

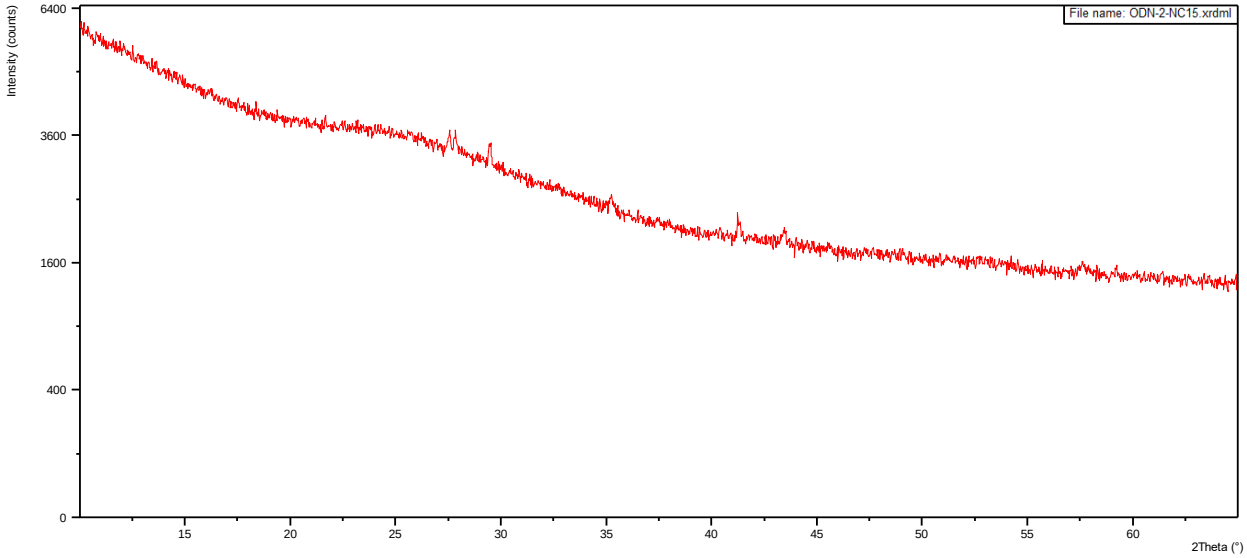
File name: ODN-2-NC15.xrdml
Intensity (counts)
6400
3600
1600
400
0
15
20
25
30
35
40
45
50
55
60
2Theta (°)

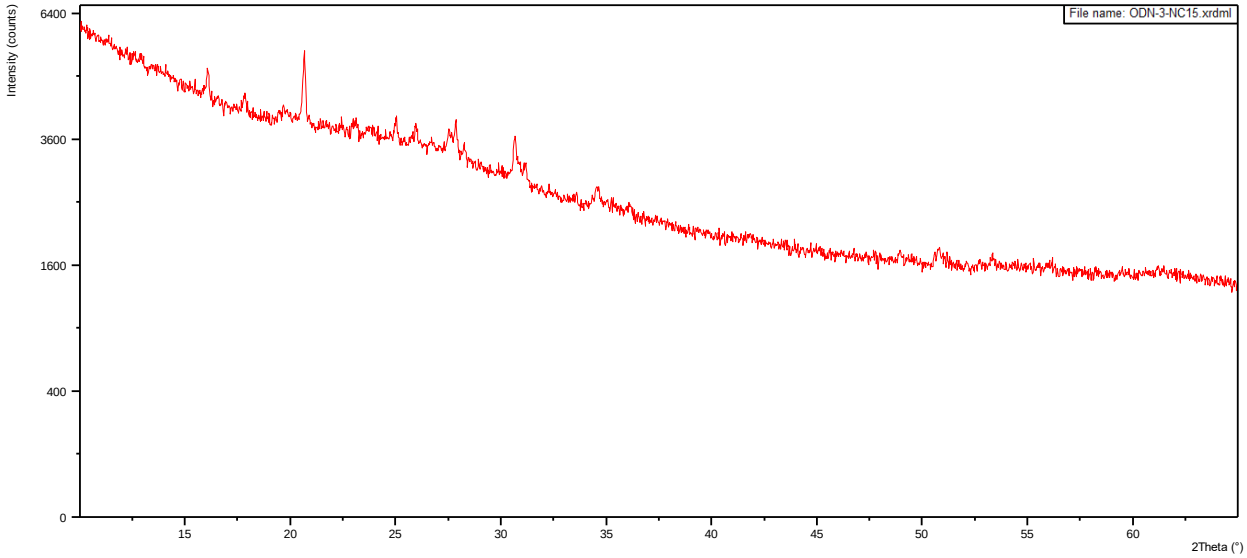
File name: ODN-3-NC15.xrdml
Intensity (counts)
6400
3600
1600
400
0
15
20
25
30
35
40
45
50
55
60
2Theta (°)

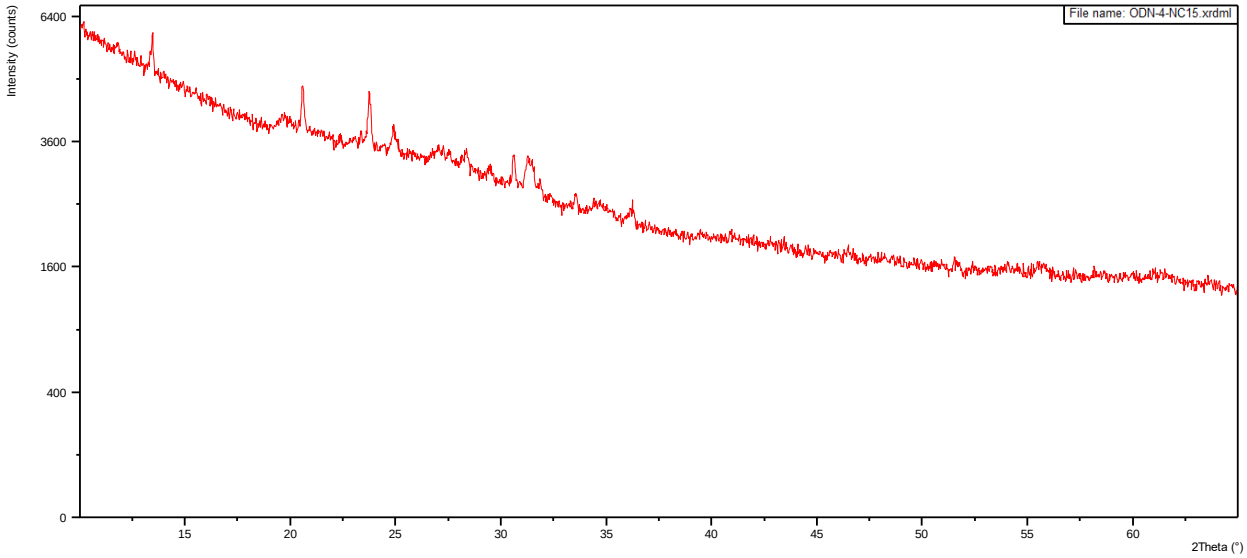
File name: ODN-4-NC15.xrdml
Intensity (counts)
6400
3600
1600
400
0
15
20
25
30
35
40
45
50
55
60
2Theta (°)

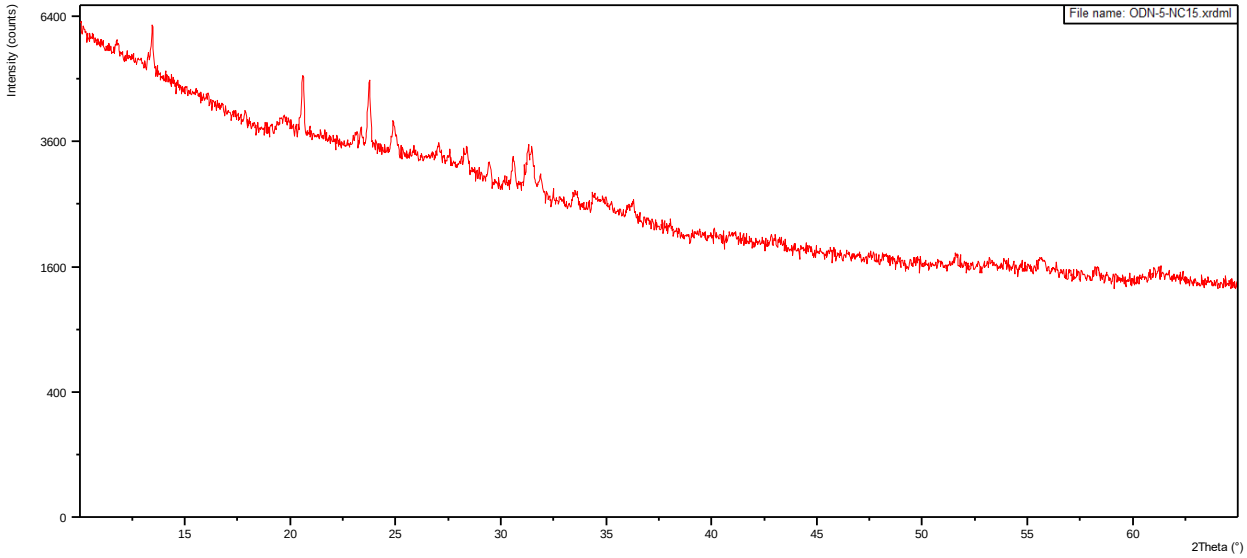
File name: ODN-5-NC15.xrdml
Intensity (counts)
6400
3600
1600
400
0
15
20
25
30
35
40
45
50
55
60
2Theta (°)

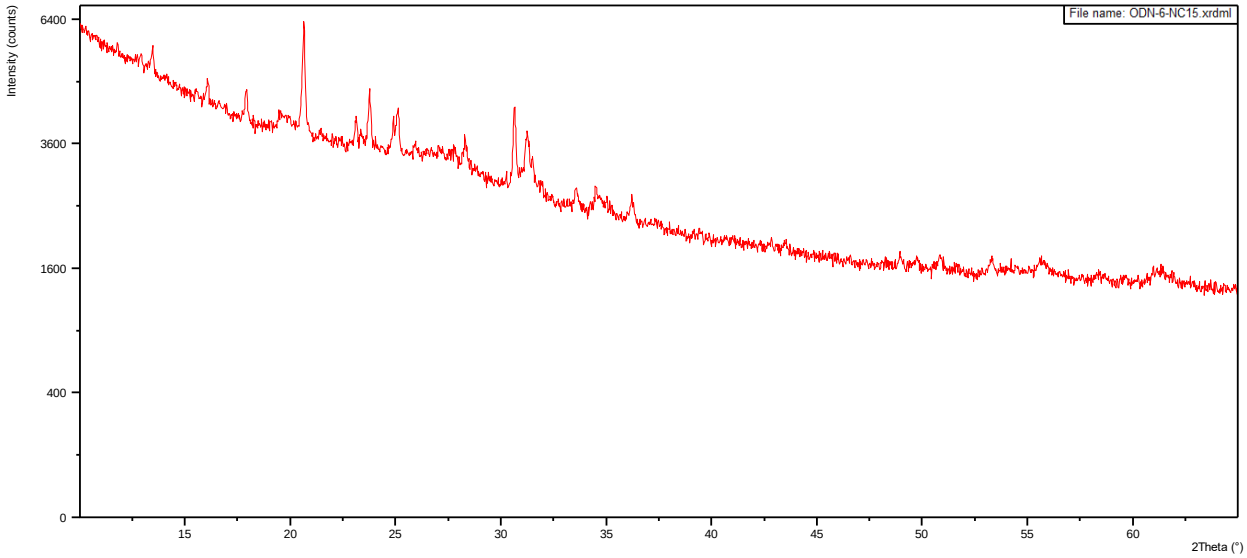
File name: ODN-6-NC15.xrdml
Intensity (counts)
6400
3600
1600
400
0
15
20
25
30
35
40
45
50
55
60
2Theta (°)

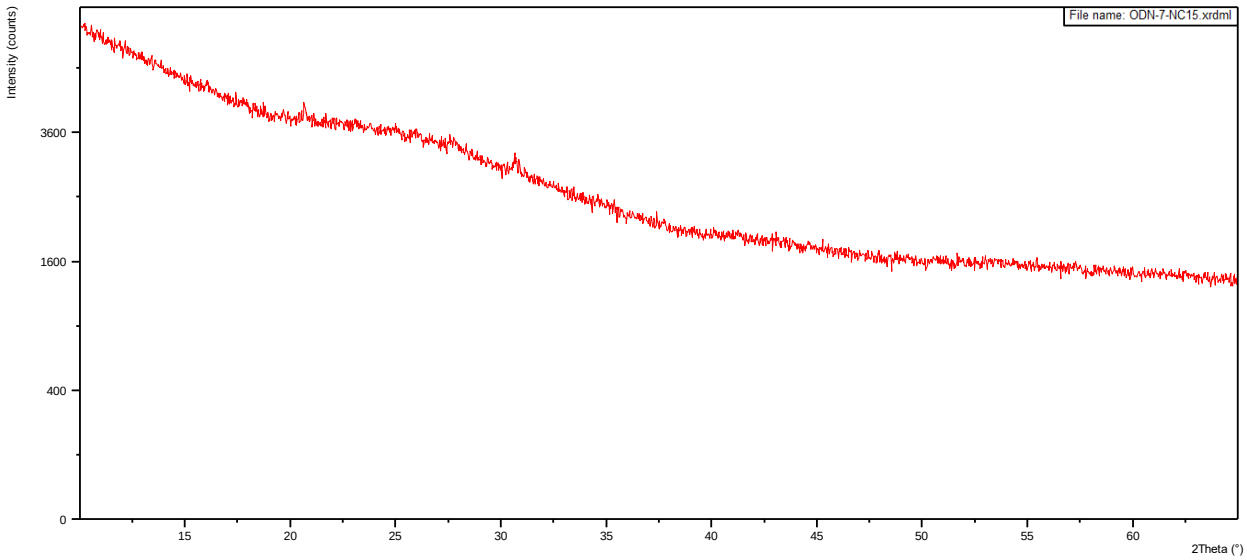
File name: ODN-7-NC15.xrdml
Intensity (counts)
3600
1600
400
0
15
20
25
30
35
40
45
50
55
60
2Theta (°)

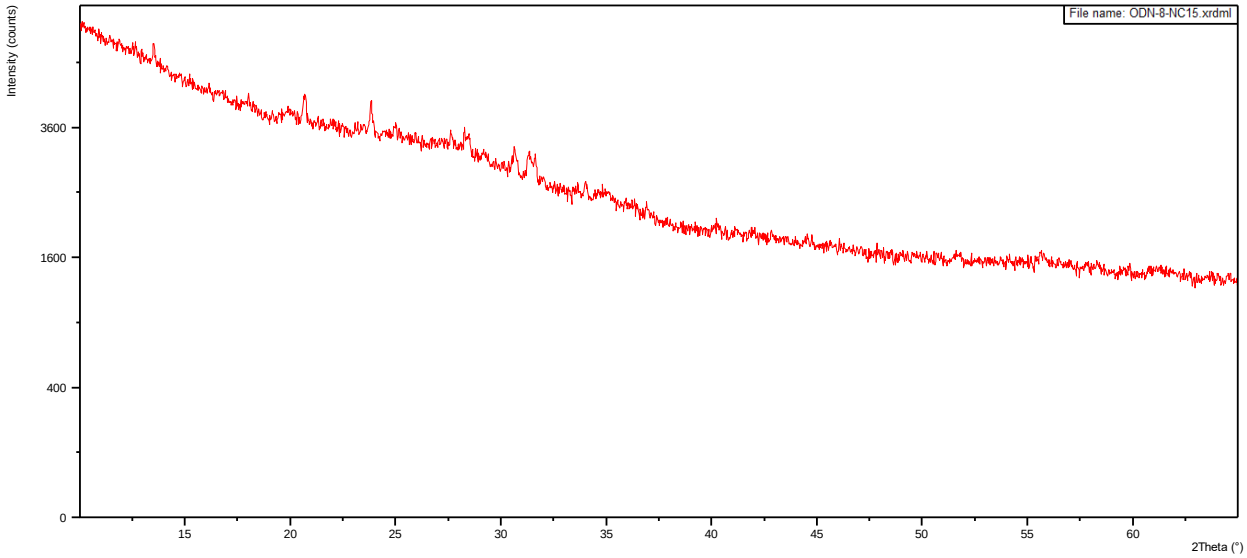
File name: ODN-8-NC15.xrdml
Intensity (counts)
3600
1600
400
0
15
20
25
30
35
40
45
50
55
60
2Theta (°)

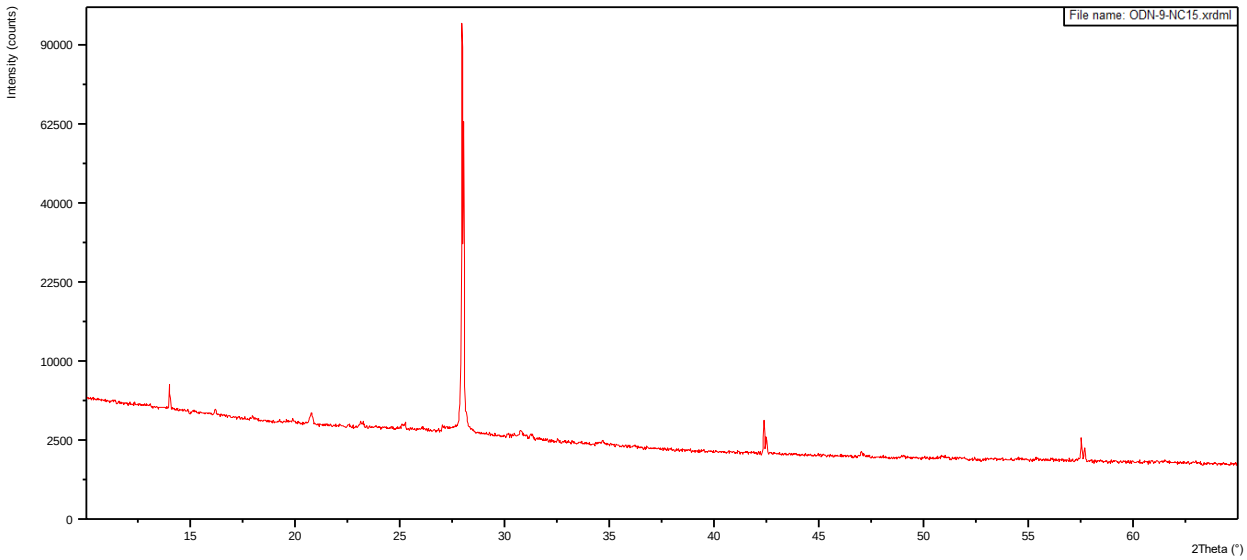
File name: ODN-9-NC15.xrdml
Intensity (counts)
90000
62500
40000
22500
10000
2500
0
15
20
25
30
35
40
45
50
55
60
2Theta (°)

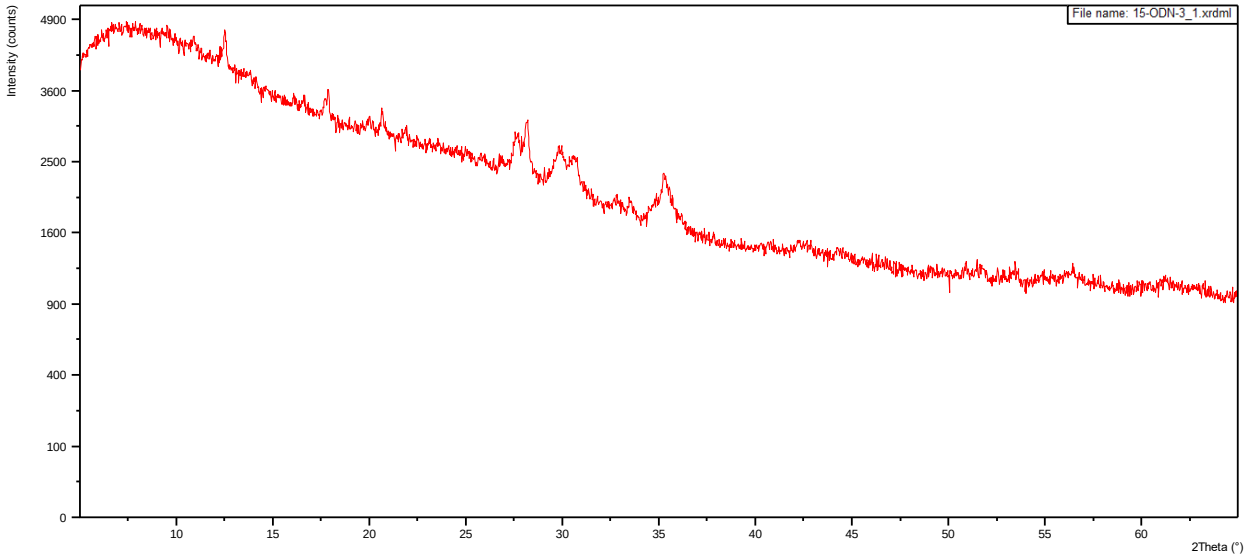
File name: 15-ODN-3_1.xrdml
Intensity (counts)
4900
3600
2500
1600
900
400
100
0
10
15
20
25
30
35
40
45
50
55
60
2Theta (°)

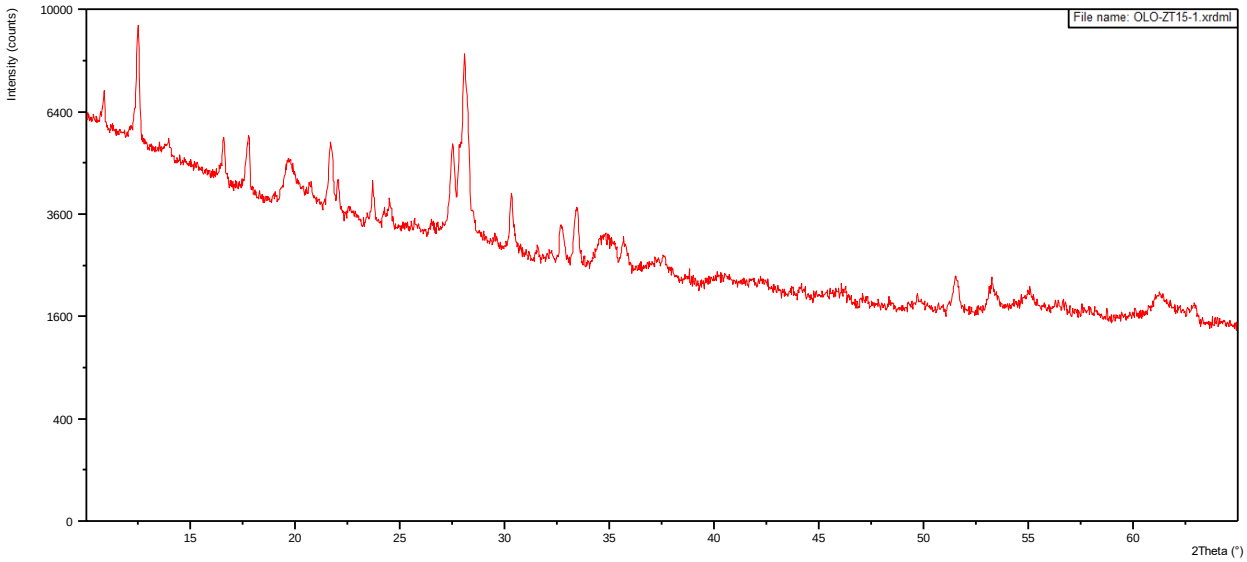
File name: OLO-ZT15-1.xrdml
Intensity (counts)
10000
6400
3600
1600
400
0
15
20
25
30
35
40
45
50
55
60
2Theta (°)

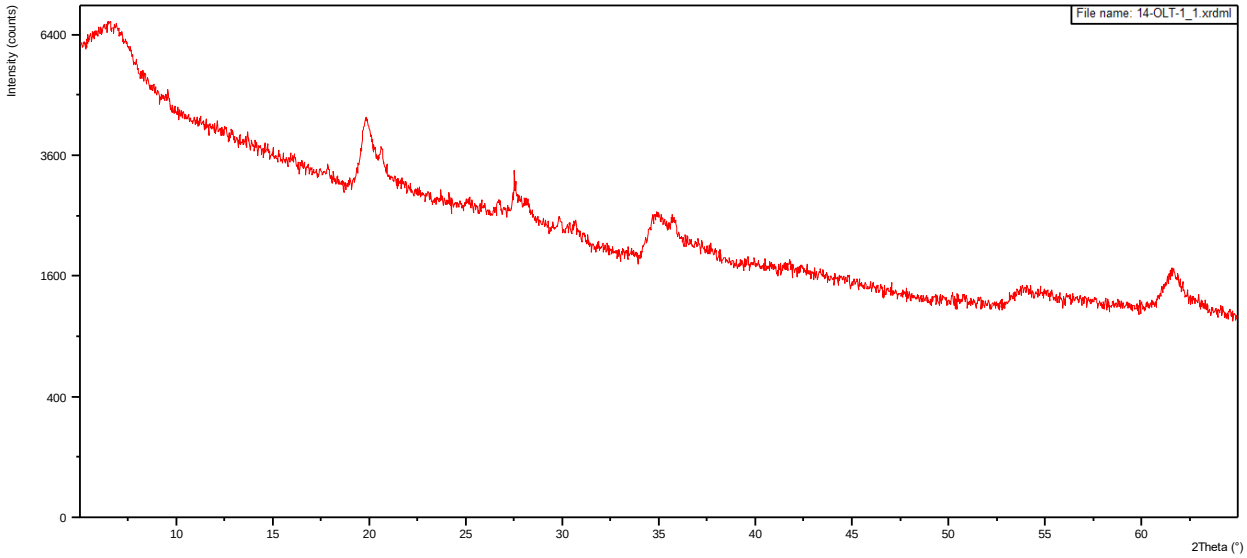
File name: 14-OLT-1_1.xrdml
Intensity (counts)
6400
3600
1600
400
0
10
15
20
25
30
35
40
45
50
55
60
2Theta (°)

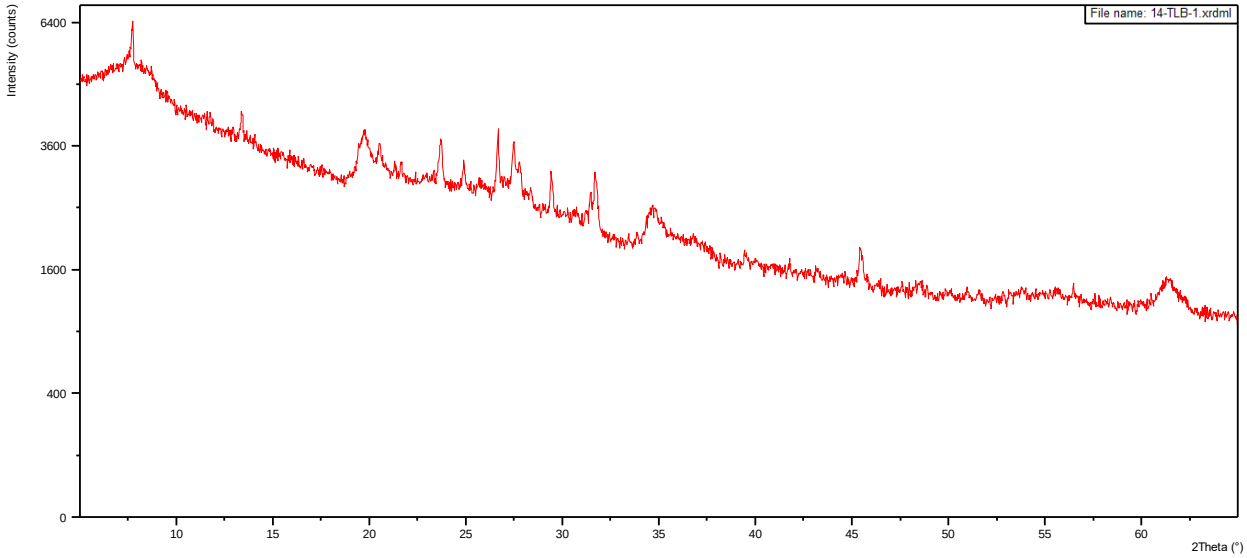
File name: 14-TLB-1.xrdml
Intensity (counts)
6400
3600
1600
400
0
10
15
20
25
30
35
40
45
50
55
60
2Theta (°)

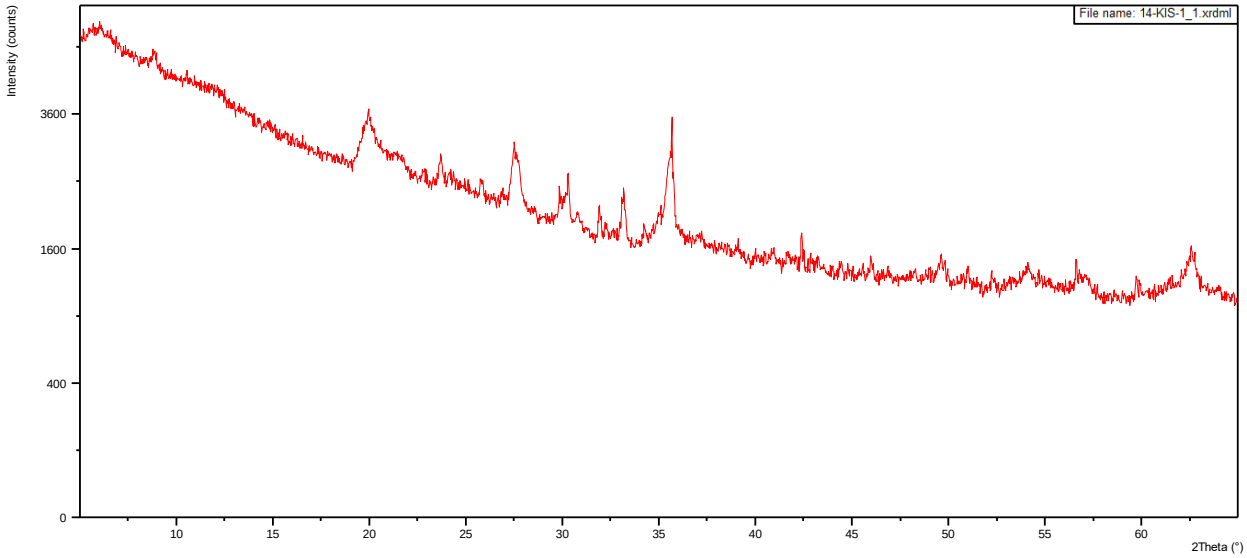
File name: 14-KIS-1_1.xrdml
Intensity (counts)
3600
1600
400
0
10
15
20
25
30
35
40
45
50
55
60
2Theta (°)

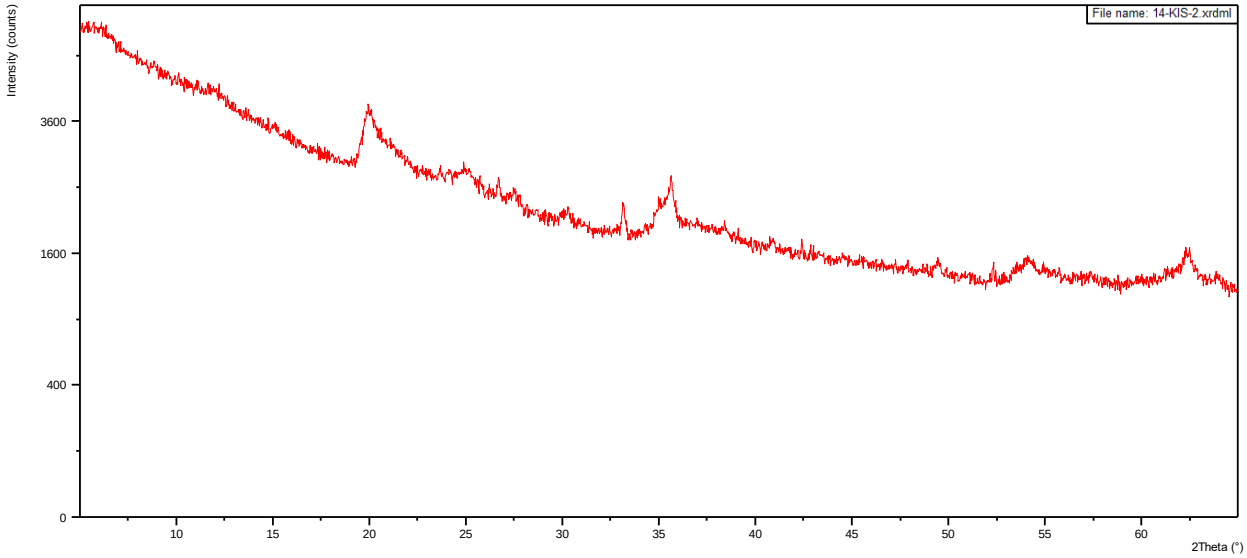
File name: 14-KIS-2.xrdml
Intensity (counts)
0
400
1600
3600
10
15
20
25
30
35
40
45
50
55
60
2Theta (°)

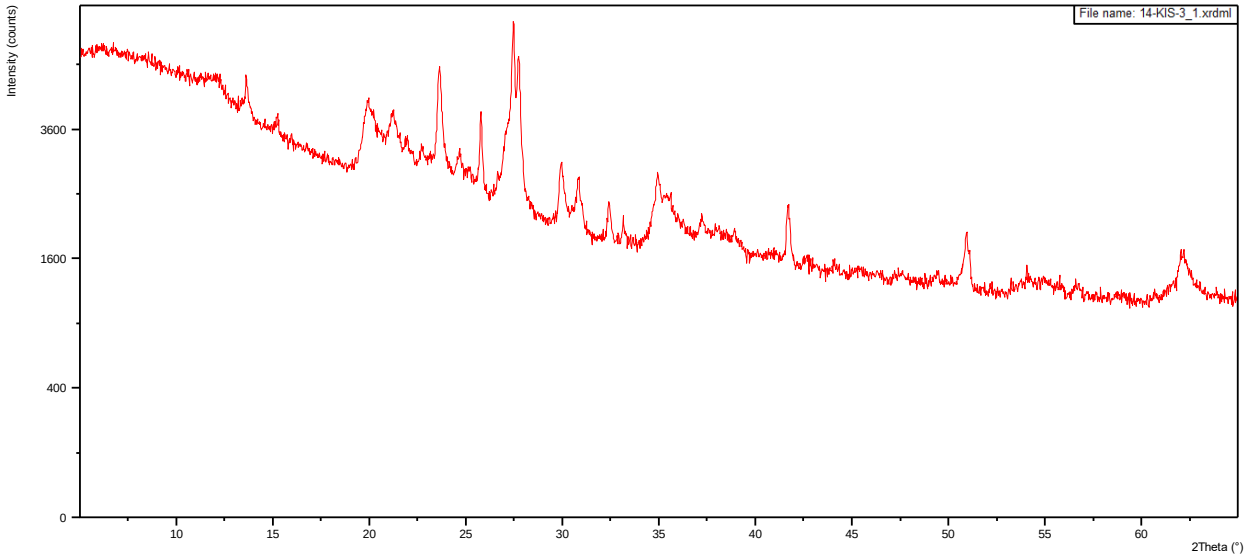
File name: 14-KIS-3_1.xrdml
Intensity (counts)
0
400
1600
3600
10
15
20
25
30
35
40
45
50
55
60
2Theta (°)

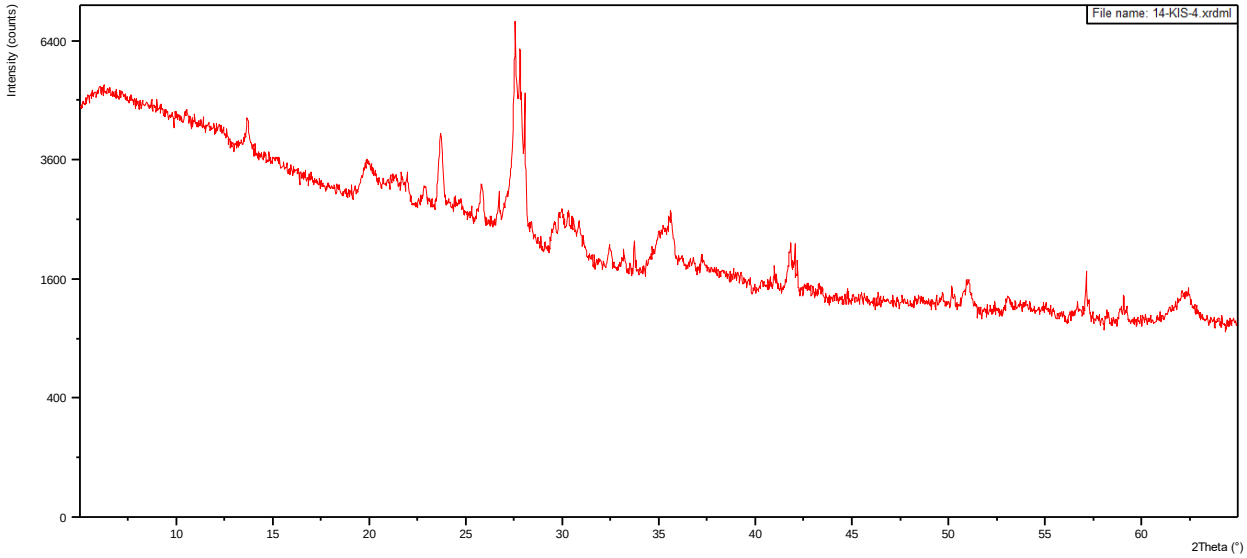
File name: 14-KIS-4.xrdml
Intensity (counts)
6400
3600
1600
400
0
10
15
20
25
30
35
40
45
50
55
60
2Theta (°)

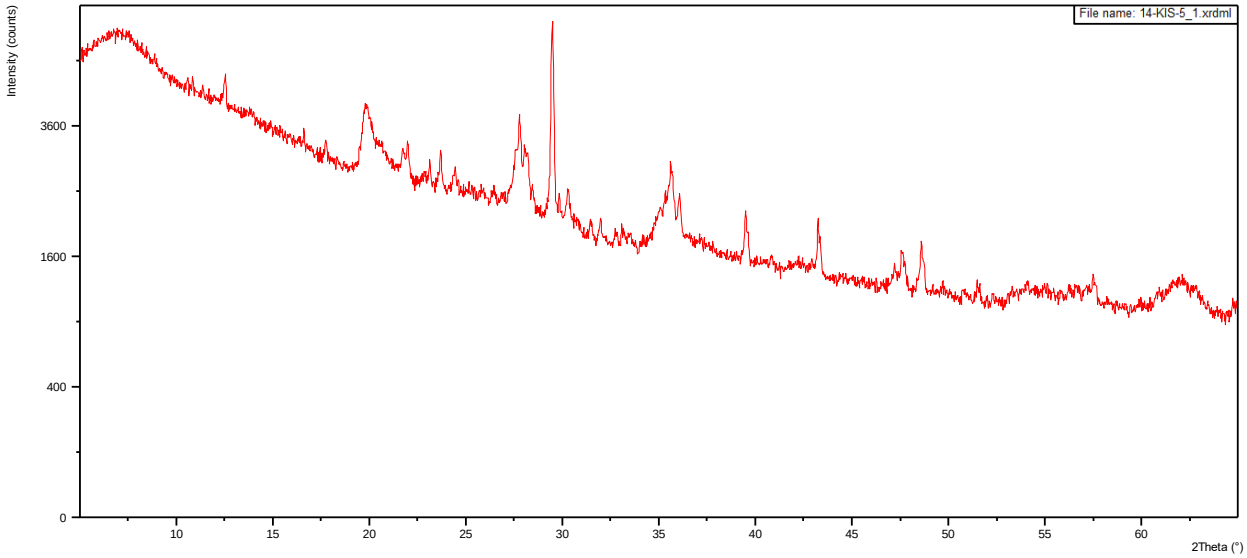
File name: 14-KIS-5_1.xrdml
Intensity (counts)
3600
1600
400
0
10
15
20
25
30
35
40
45
50
55
60
2Theta (°)

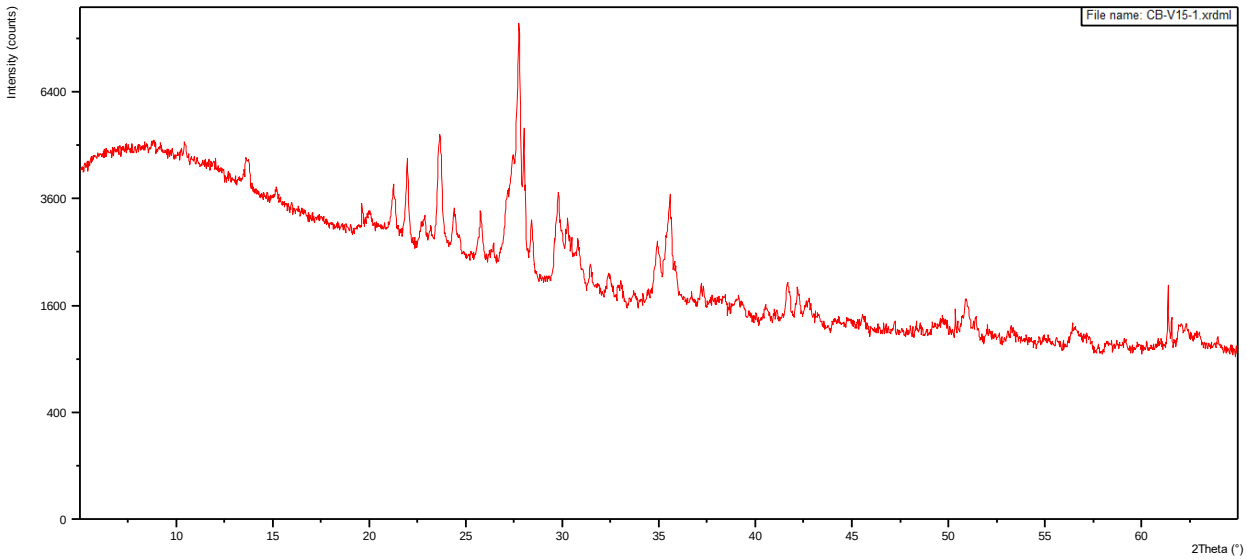
File name: CB-V15-1.xrdml
Intensity (counts)
6400
3600
1600
400
0
10
15
20
25
30
35
40
45
50
55
60
2Theta (°)

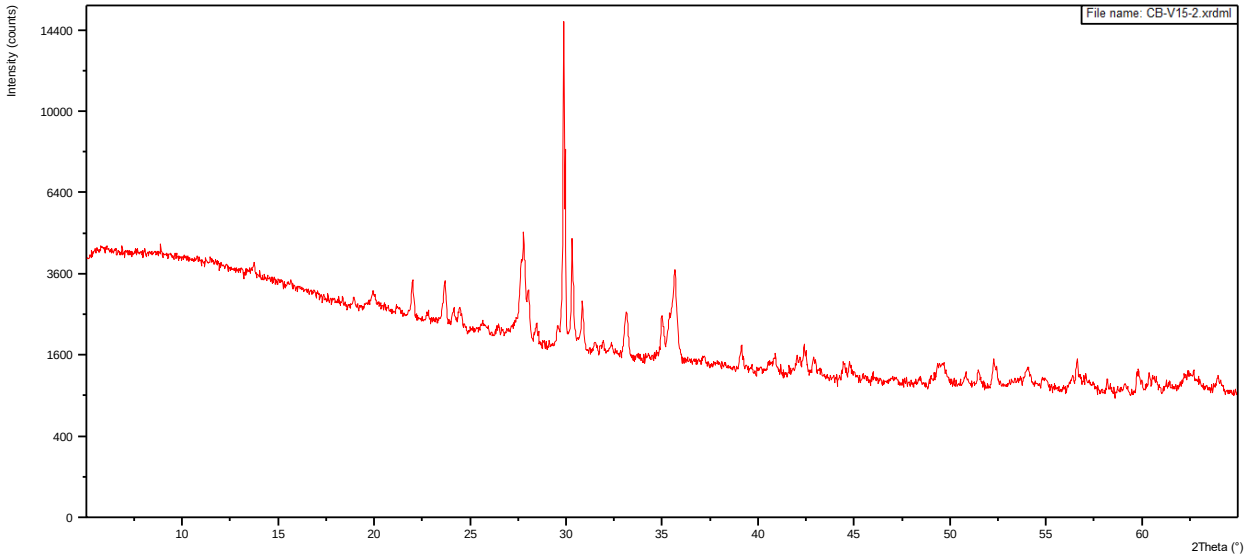
File name: CB-V15-2.xrdml
Intensity (counts)
14400
10000
6400
3600
1600
400
0
10
15
20
25
30
35
40
45
50
55
60
2Theta (°)

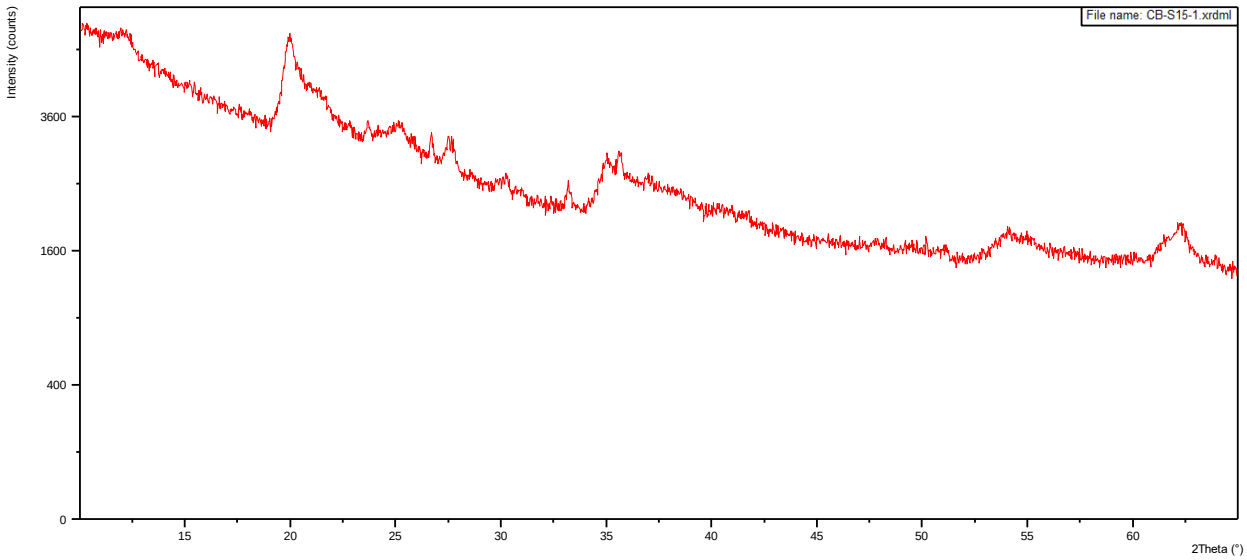
File name: CB-S15-1.xrdml
Intensity (counts)
3600
1600
400
0
15
20
25
30
35
40
45
50
55
60
2Theta (°)

Appendix D.2: SEM Images & Spectra

EDAX TEAM

Nathan Sept 25 2017

Author: Robert
Creation: 09/25/2017 1:32:08 PM

Sample Name: 14-KIS-4

Area 8

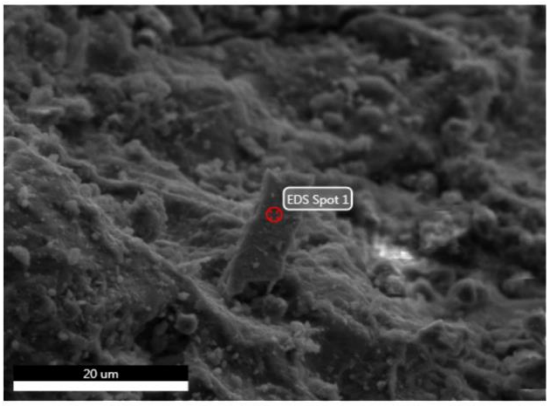

Notes:

EDAX TEAM

EDS Spot 1

kV: 15 Mag: 2219 Takeoff: 30.9 Live Time(s): 50 Amp Time(µs): 7.68 Resolution:(eV) 129.8

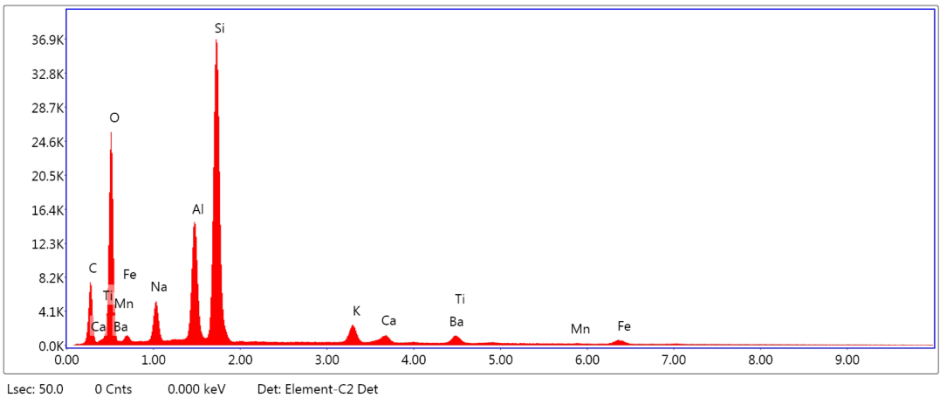

eZAF Smart Quant Results

Element	Weight %	Atomic %	Net Int.	Error %	Kratio	Z	R	A	F
C K	17.95	29.25	670.01	10.32	0.0332	1.1111	0.9497	0.1664	1.0000
O K	31.00	37.93	2905.56	8.72	0.0909	1.0591	0.9712	0.2769	1.0000
NaK	4.21	3.59	603.71	7.08	0.0204	0.9575	0.9969	0.5023	1.0055
AlK	9.51	6.90	2261.91	4.18	0.0679	0.9355	1.0110	0.7533	1.0132
SiK	25.67	17.89	6021.12	3.75	0.1914	0.9550	1.0174	0.7775	1.0042
K K	3.09	1.55	437.47	3.79	0.0262	0.8807	1.0433	0.9380	1.0262
CaK	1.61	0.78	189.26	5.28	0.0141	0.8958	1.0472	0.9520	1.0306
BaL	2.06	0.29	69.51	19.83	0.0145	0.6227	1.2199	1.0636	1.0631
TiK	1.63	0.67	152.40	6.28	0.0135	0.8098	1.0536	0.9794	1.0457
MnK	0.26	0.09	13.69	39.96	0.0021	0.7801	1.0582	0.9951	1.0688
FeK	3.02	1.06	133.30	6.92	0.0255	0.7902	1.0579	0.9986	1.0709

EDAX TEAM

Nathan Sept 25 2017

Author: Robert
Creation: 09/25/2017 1:37:41 PM

Sample Name: 14-NGUN-2

Area 1

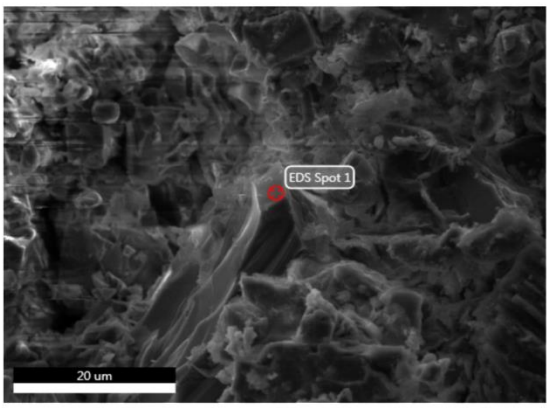

Notes:

EDAX TEAM

EDS Spot 1

kV: 15 Mag: 2058 Takeoff: 30.6 Live Time(s): 50 Amp Time(µs): 7.68 Resolution:(eV) 129.8

EDS Spot 1

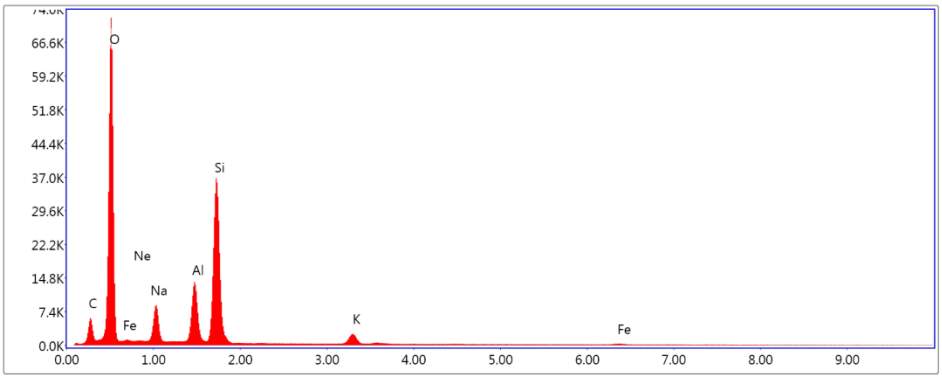

Lsec: 50.0 0 Cnts 0.000 keV Det: Element-C2 Det

eZAF Smart Quant Results

Element	Weight %	Atomic %	Net Int.	Error %	Kratio	Z	R	A	F
C K	10.03	15.36	502.82	10.25	0.0199	1.0896	0.9631	0.1823	1.0000
O K	50.70	58.31	8429.86	7.35	0.2104	1.0375	0.9836	0.3999	1.0000
NeK	0.57	0.52	115.37	11.36	0.0019	0.9877	1.0006	0.3270	1.0000
NaK	7.03	5.62	1195.76	6.94	0.0321	0.9371	1.0080	0.4854	1.0049
AlK	7.48	5.10	2120.67	4.41	0.0506	0.9151	1.0214	0.7313	1.0120
SiK	20.72	13.57	5972.95	3.75	0.1510	0.9339	1.0274	0.7777	1.0036
K K	2.58	1.21	451.83	3.42	0.0215	0.8603	1.0513	0.9509	1.0183
FeK	0.89	0.29	50.38	15.26	0.0077	0.7707	1.0630	1.0063	1.1139

EDAX TEAM

Nathan Sept 25 2017

Author: Robert
Creation: 09/25/2017 1:40:57 PM

Sample Name: 14-NGUN-2

Area 2

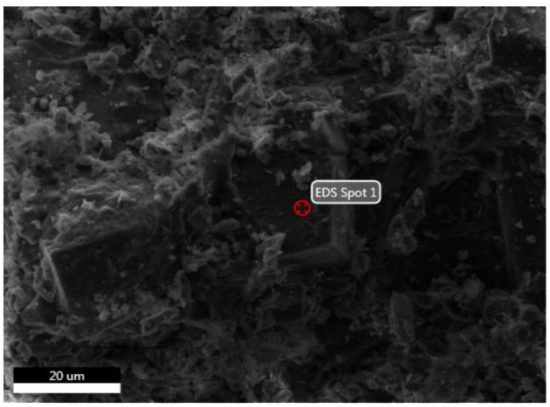

Notes:

EDAX TEAM

EDS Spot 1

kV: 15 Mag: 1357 Takeoff: 30.6 Live Time(s): 50 Amp Time(µs): 7.68 Resolution:(eV) 129.8

EDS Spot 1

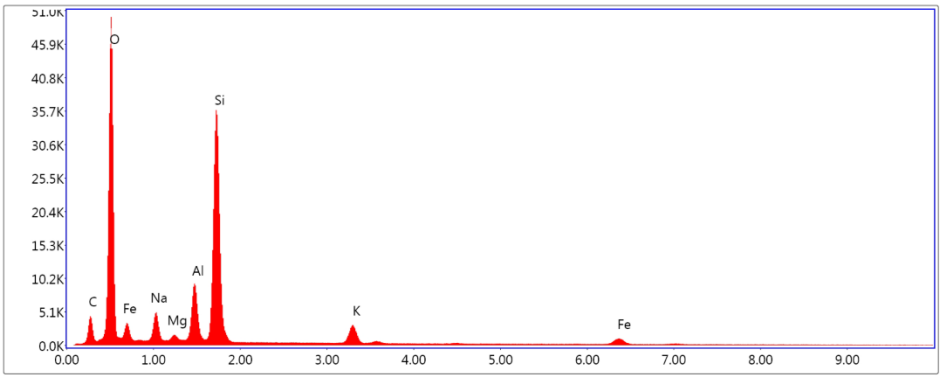

Lsec: 50.0 0 Cnts 0.000 keV Det: Element-C2 Det

eZAF Smart Quant Results

Element	Weight %	Atomic %	Net Int.	Error %	Kratio	Z	R	A	F
C K	8.72	14.17	332.44	10.81	0.0164	1.1041	0.9545	0.1707	1.0000
O K	45.86	55.92	5786.81	7.65	0.1802	1.0520	0.9757	0.3735	1.0000
NaK	4.68	3.97	619.93	7.43	0.0208	0.9507	1.0009	0.4650	1.0050
MgK	0.71	0.57	144.57	7.56	0.0041	0.9656	1.0081	0.5930	1.0093
AlK	6.07	4.39	1386.28	4.58	0.0413	0.9286	1.0148	0.7232	1.0134
SiK	24.68	17.14	5816.06	3.72	0.1835	0.9478	1.0210	0.7814	1.0040
K K	3.98	1.99	563.15	3.28	0.0334	0.8737	1.0462	0.9426	1.0204
FeK	5.31	1.85	237.34	4.88	0.0450	0.7834	1.0598	1.0040	1.0779

EDAX TEAM

Nathan Sept 25 2017

Author: Robert
Creation: 09/25/2017 1:47:36 PM

Sample Name: 15-ODN-5

Area 1

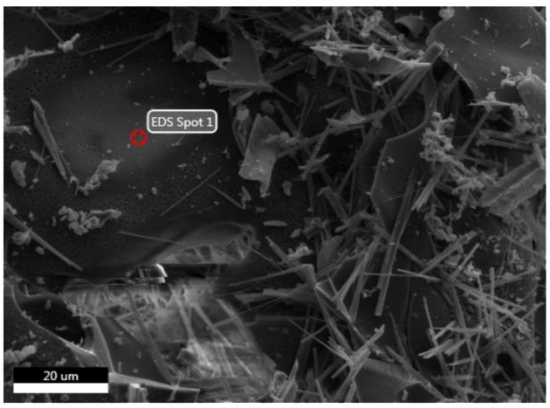

Notes:

EDAX TEAM

EDS Spot 1

kV: 15 Mag: 1204 Takeoff: 30.7 Live Time(s): 50 Amp Time(µs): 7.68 Resolution:(eV) 129.8

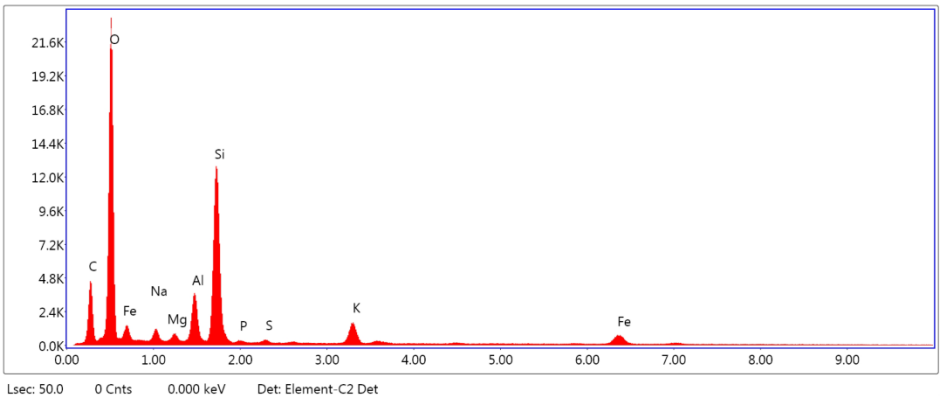

eZAF Smart Quant Results

Element	Weight %	Atomic %	Net Int.	Error %	Kratio	Z	R	A	F
C K	17.65	26.83	432.96	9.96	0.0416	1.0926	0.9578	0.2157	1.0000
O K	45.94	52.43	2696.28	8.08	0.1634	1.0409	0.9788	0.3417	1.0000
NaK	1.87	1.49	117.47	9.35	0.0077	0.9406	1.0037	0.4343	1.0041
MgK	0.61	0.46	61.70	9.64	0.0034	0.9553	1.0108	0.5853	1.0075
AlK	4.46	3.02	513.21	5.00	0.0298	0.9187	1.0174	0.7189	1.0110
SiK	17.04	11.08	2064.43	3.78	0.1269	0.9377	1.0235	0.7907	1.0049
P K	0.14	0.08	12.96	27.93	0.0010	0.8996	1.0292	0.7589	1.0080
S K	0.21	0.12	20.98	17.92	0.0017	0.9162	1.0346	0.8341	1.0119
K K	3.92	1.83	288.10	3.51	0.0334	0.8644	1.0482	0.9602	1.0252
FeK	8.16	2.67	184.13	4.83	0.0681	0.7750	1.0610	1.0064	1.0687

EDAX TEAM

Nathan Sept 25 2017

Author: Robert
Creation: 09/25/2017 1:48:42 PM

Sample Name: 15-ODN-5

Area 1

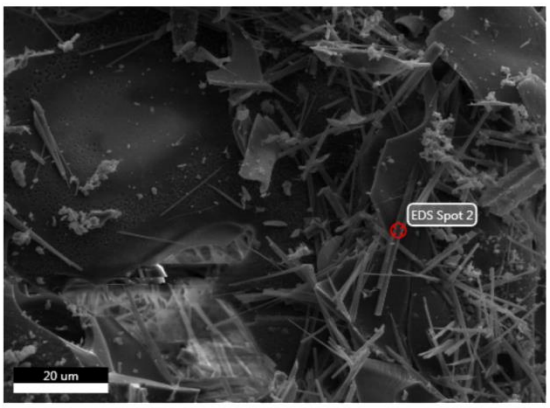

Notes:

EDAX TEAM

EDS Spot 2

kV: 15 Mag: 1204 Takeoff: 30.7 Live Time(s): 50 Amp Time(µs): 7.68 Resolution:(eV) 129.8

EDS Spot 2

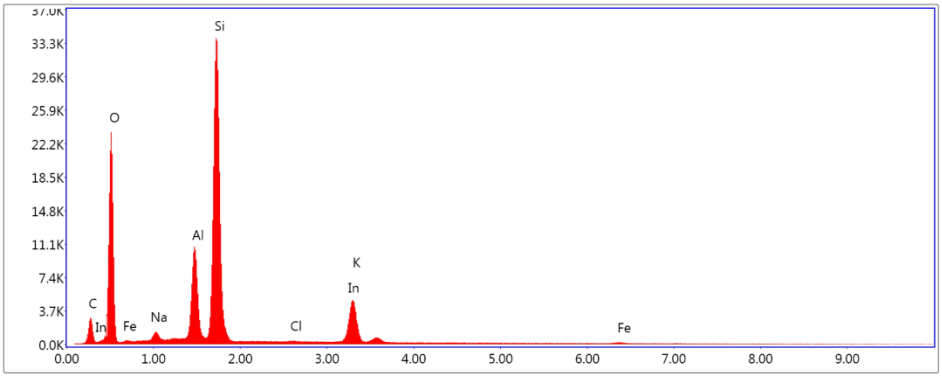

Lsec: 50.0 0 Cnts 0.000 keV Det: Element-C2 Det

eZAF Smart Quant Results

Element	Weight %	Atomic %	Net Int.	Error %	Kratio	Z	R	A	F
C K	8.19	14.02	193.61	11.32	0.0136	1.1141	0.9491	0.1490	1.0000
O K	38.20	49.10	2625.97	8.64	0.1163	1.0619	0.9707	0.2867	1.0000
NaK	0.92	0.83	94.92	9.55	0.0045	0.9600	0.9964	0.5071	1.0070
AlK	9.14	6.97	1622.92	3.90	0.0689	0.9378	1.0106	0.7895	1.0178
SiK	32.13	23.52	5541.41	3.48	0.2491	0.9573	1.0170	0.8061	1.0046
ClK	0.10	0.06	11.43	43.18	0.0007	0.8889	1.0338	0.8412	1.0187
InL	0.79	0.14	37.96	20.57	0.0057	0.6772	1.2216	1.0419	1.0254
K K	9.44	4.97	930.16	2.97	0.0787	0.8826	1.0429	0.9312	1.0141
FeK	1.09	0.40	34.52	17.94	0.0093	0.7917	1.0577	0.9980	1.0843

EDAX TEAM

Nathan Sept 25 2017

Author: Robert
Creation: 09/25/2017 1:54:03 PM

Sample Name: 15-ODN-5

Area 2

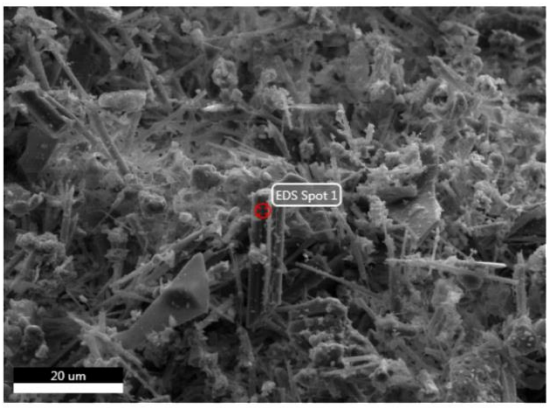

Notes:

EDAX TEAM

EDS Spot 1

kV: 15 Mag: 1392 Takeoff: 30.4 Live Time(s): 50 Amp Time(µs): 7.68 Resolution:(eV) 129.8

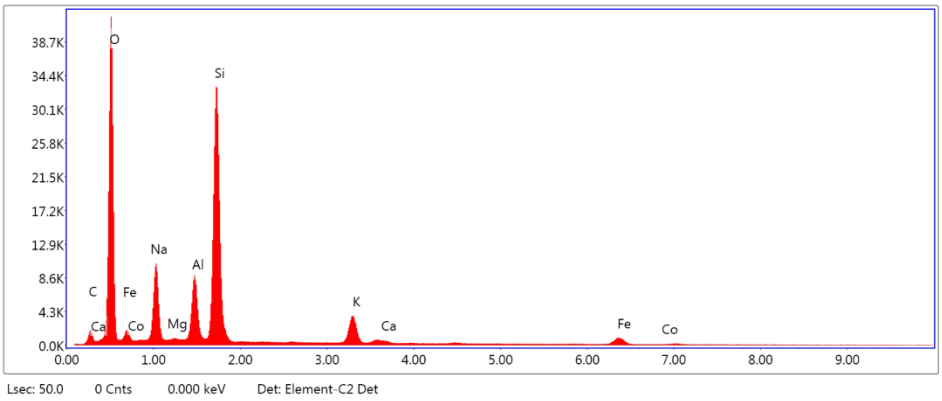

eZAF Smart Quant Results

Element	Weight %	Atomic %	Net Int.	Error %	Kratio	Z	R	A	F
C K	2.21	3.90	67.79	14.67	0.0038	1.1221	0.9481	0.1548	1.0000
O K	41.72	55.14	4780.54	7.61	0.1705	1.0696	0.9698	0.3822	1.0000
NaK	11.12	10.23	1355.28	6.96	0.0520	0.9669	0.9955	0.4813	1.0048
MgK	0.26	0.23	44.46	12.69	0.0014	0.9822	1.0029	0.5591	1.0090
AlK	6.66	5.22	1296.50	4.94	0.0442	0.9446	1.0098	0.6933	1.0130
SiK	26.56	20.00	5371.31	4.00	0.1938	0.9642	1.0162	0.7537	1.0041
K K	5.55	3.00	689.56	3.31	0.0468	0.8890	1.0423	0.9318	1.0194
CaK	0.33	0.18	34.26	13.11	0.0029	0.9042	1.0463	0.9401	1.0257
FeK	5.47	2.07	216.25	5.20	0.0469	0.7975	1.0573	1.0011	1.0742
CoK	0.12	0.04	3.89	58.82	0.0010	0.7765	1.0558	1.0027	1.0941

EDAX TEAM

Nathan Sept 25 2017

Author: Robert
Creation: 09/25/2017 1:59:16 PM

Sample Name: CB-5-1

Area 1

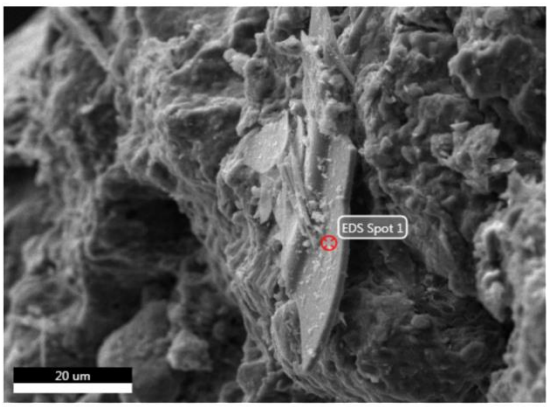

Notes:

EDAX TEAM

EDS Spot 1

kV: 15 Mag: 1506 Takeoff: 31.2 Live Time(s): 50 Amp Time(µs): 7.68 Resolution:(eV) 129.8

EDS Spot 1

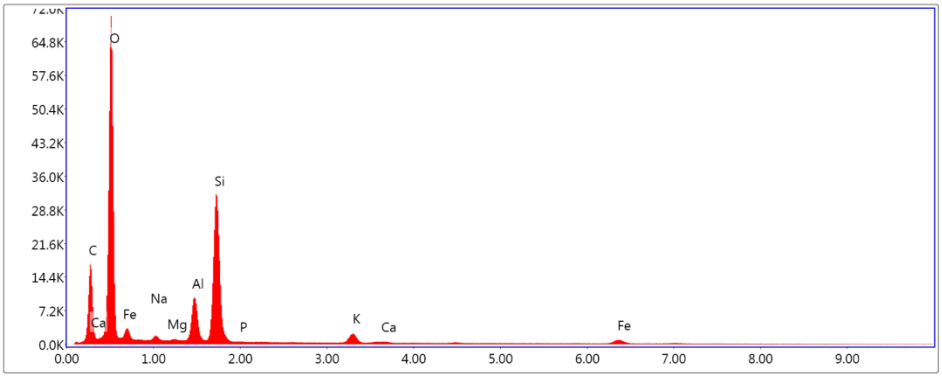

Lsec: 50.0 0 Cnts 0.000 keV Det: Element-C2 Det

eZAF Smart Quant Results

Element	Weight %	Atomic %	Net Int.	Error %	Kratio	Z	R	A	F
C K	22.79	31.89	1733.26	9.21	0.0587	1.0713	0.9687	0.2406	1.0000
O K	50.57	53.14	8267.00	7.91	0.1775	1.0197	0.9889	0.3442	1.0000
NaK	1.28	0.94	235.10	8.27	0.0055	0.9208	1.0127	0.4609	1.0043
MgK	0.28	0.20	83.86	9.00	0.0017	0.9350	1.0194	0.6182	1.0080
AlK	4.61	2.87	1524.77	4.25	0.0315	0.8990	1.0257	0.7524	1.0111
SiK	15.19	9.09	5216.03	3.38	0.1142	0.9175	1.0315	0.8159	1.0043
P K	0.09	0.05	24.66	27.21	0.0006	0.8800	1.0369	0.7879	1.0068
K K	1.89	0.81	385.61	3.75	0.0159	0.8452	1.0546	0.9713	1.0244
CaK	0.18	0.08	30.64	15.99	0.0016	0.8595	1.0580	0.9810	1.0324
FeK	3.12	0.94	198.95	5.84	0.0262	0.7570	1.0650	1.0091	1.1009

EDAX TEAM

Nathan Sept 25 2017

Author: Robert
Creation: 09/25/2017 2:04:05 PM

Sample Name: CB-5-1

Area 2

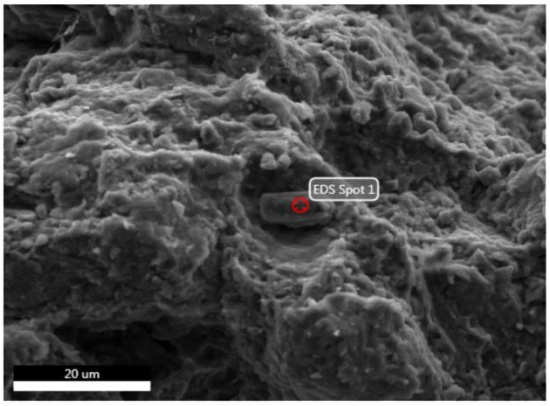

Notes:

EDAX TEAM

EDS Spot 1

kV: 15 Mag: 1740 Takeoff: 30.7 Live Time(s): 50 Amp Time(µs): 7.68 Resolution:(eV) 129.8

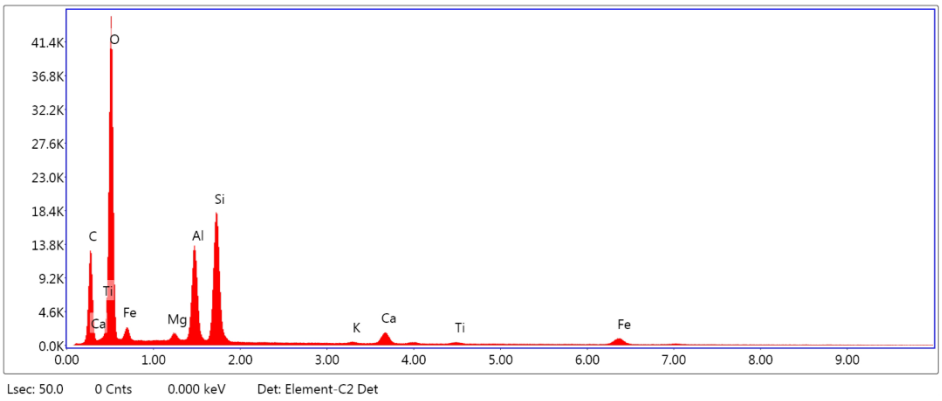

eZAF Smart Quant Results

Element	Weight %	Atomic %	Net Int.	Error %	Kratio	Z	R	A	F
C K	23.31	33.31	1265.04	9.24	0.0598	1.0780	0.9650	0.2382	1.0000
O K	46.89	50.31	5155.64	8.20	0.1538	1.0264	0.9855	0.3196	1.0000
MgK	0.83	0.59	178.66	7.20	0.0049	0.9415	1.0165	0.6161	1.0079
AlK	8.57	5.45	2041.64	4.25	0.0583	0.9053	1.0229	0.7457	1.0086
SiK	12.20	7.46	2922.42	3.81	0.0884	0.9239	1.0288	0.7812	1.0045
K K	0.20	0.09	30.48	17.26	0.0017	0.8514	1.0525	0.9695	1.0363
CaK	2.53	1.09	315.04	3.83	0.0224	0.8658	1.0560	0.9849	1.0349
TiK	0.52	0.18	50.83	15.38	0.0043	0.7825	1.0615	0.9967	1.0659
FeK	4.94	1.52	226.26	4.88	0.0412	0.7629	1.0637	1.0079	1.0832

EDAX TEAM

Nathan Sept 25 2017

Author: Robert
Creation: 09/25/2017 2:10:06 PM

Sample Name: CB-5-1

Area 3

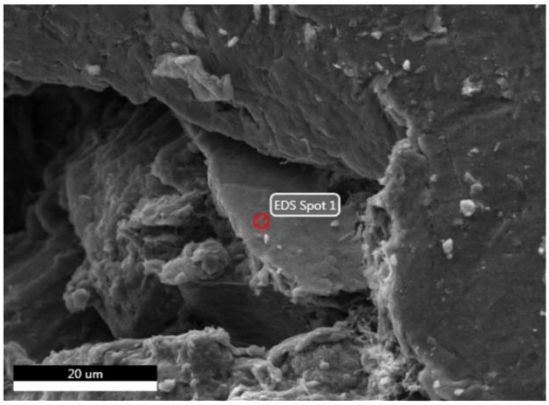

Notes:

EDAX TEAM

EDS Spot 1

kV: 15 Mag: 1824 Takeoff: 30.8 Live Time(s): 50 Amp Time(µs): 7.68 Resolution:(eV) 129.8

EDS Spot 1

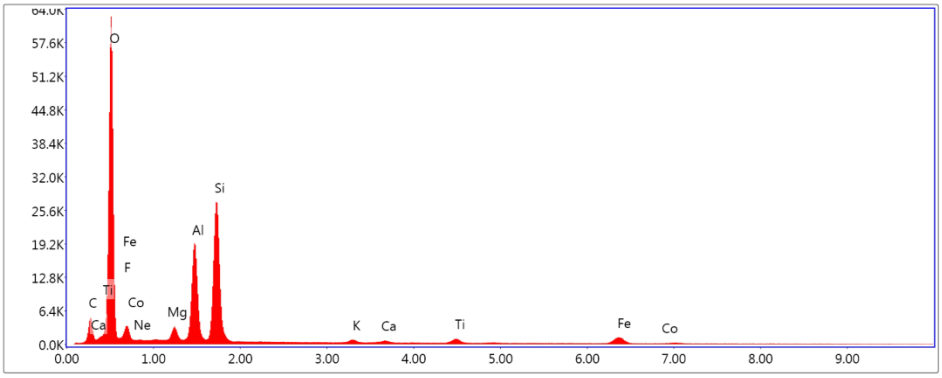

eZAF Smart Quant Results

Element	Weight %	Atomic %	Net Int.	Error %	Kratio	Z	R	A	F
C K	8.56	13.82	381.77	10.38	0.0170	1.1055	0.9547	0.1799	1.0000
O K	47.19	57.15	7103.05	7.34	0.2000	1.0533	0.9759	0.4024	1.0000
F K	2.88	2.94	249.59	11.42	0.0059	0.9772	0.9849	0.2084	1.0000
NeK	0.42	0.40	65.88	12.26	0.0012	1.0031	0.9933	0.2855	1.0000
MgK	1.73	1.38	391.51	6.43	0.0101	0.9668	1.0083	0.5968	1.0088
AlK	11.69	8.40	2925.16	4.44	0.0790	0.9298	1.0149	0.7196	1.0092
SiK	17.84	12.31	4402.16	4.17	0.1259	0.9491	1.0212	0.7403	1.0038
K K	0.60	0.30	95.74	10.80	0.0052	0.8749	1.0463	0.9468	1.0288
CaK	0.52	0.25	68.71	9.58	0.0046	0.8898	1.0501	0.9665	1.0381
TiK	1.62	0.66	172.31	5.56	0.0137	0.8043	1.0562	0.9903	1.0642
FeK	6.60	2.29	324.96	4.50	0.0559	0.7845	1.0598	1.0049	1.0737
CoK	0.33	0.11	13.11	43.59	0.0028	0.7637	1.0581	1.0056	1.0920

EDAX TEAM

Nathan Sept 25 2017

Author: Robert
Creation: 09/25/2017 2:13:40 PM

Sample Name: CB-V-1

Area 1

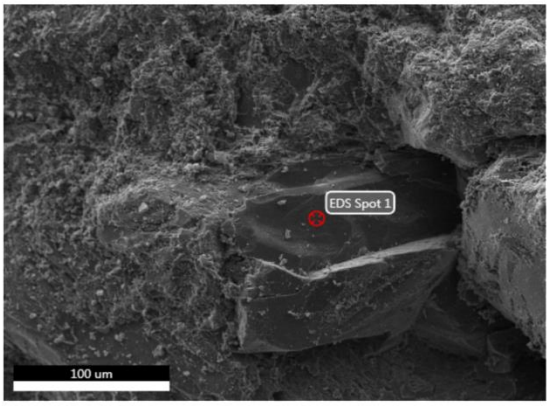

Notes:

EDAX TEAM

EDS Spot 1

kV: 15 Mag: 396 Takeoff: 30.5 Live Time(s): 50 Amp Time(µs): 7.68 Resolution:(eV) 129.8

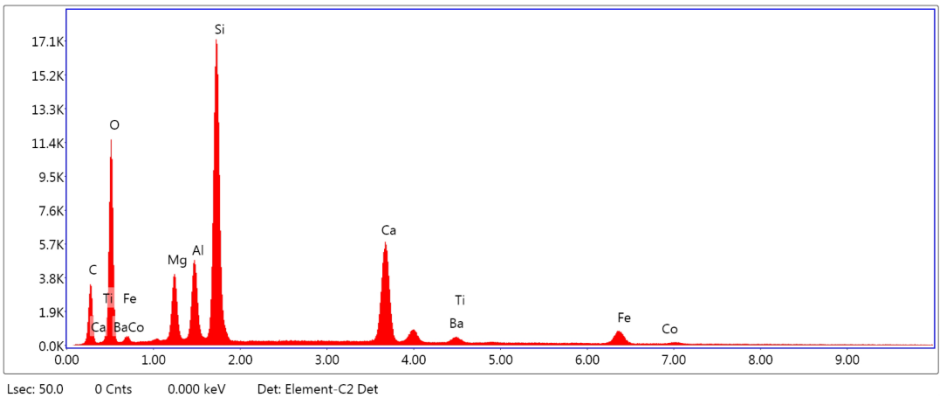

eZAF Smart Quant Results

Element	Weight %	Atomic %	Net Int.	Error %	Kratio	Z	R	A	F
C K	11.92	22.04	302.23	10.36	0.0260	1.1381	0.9318	0.1919	1.0000
O K	28.46	39.51	1277.68	9.39	0.0693	1.0860	0.9545	0.2241	1.0000
MgK	4.38	4.00	516.16	6.26	0.0256	0.9988	0.9894	0.5803	1.0075
AlK	5.41	4.46	689.68	5.27	0.0358	0.9609	0.9968	0.6798	1.0113
SiK	20.35	16.09	2750.59	4.12	0.1510	0.9812	1.0036	0.7513	1.0067
CaK	17.60	9.75	1245.06	2.54	0.1602	0.9215	1.0363	0.9644	1.0242
BaL	2.57	0.42	50.35	17.87	0.0181	0.6411	1.2092	1.0403	1.0562
TiK	0.70	0.33	38.12	14.82	0.0058	0.8335	1.0438	0.9540	1.0426
FeK	7.96	3.16	204.60	4.88	0.0675	0.8143	1.0506	0.9891	1.0525
CoK	0.65	0.25	13.47	31.80	0.0055	0.7932	1.0498	0.9930	1.0654

EDAX TEAM

Nathan Rabideaux 8 2017

Author: robert
Creation: 09/06/2017 10:19:18 AM

Sample Name: 14-KIS-1

Area 1

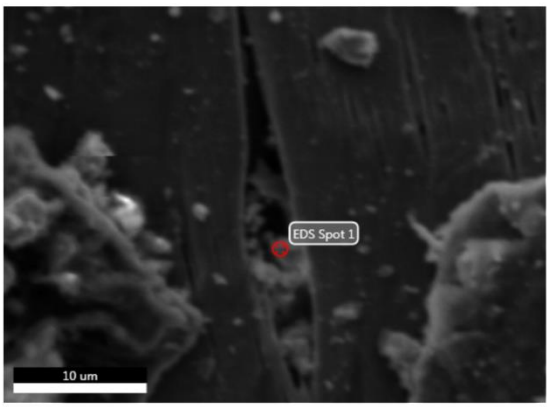

Notes:

EDAX TEAM

EDS Spot 1

kV: 15 Mag: 3382 Takeoff: 30 Live Time(s): 50 Amp Time(µs): 7.68 Resolution:(eV) 129.8

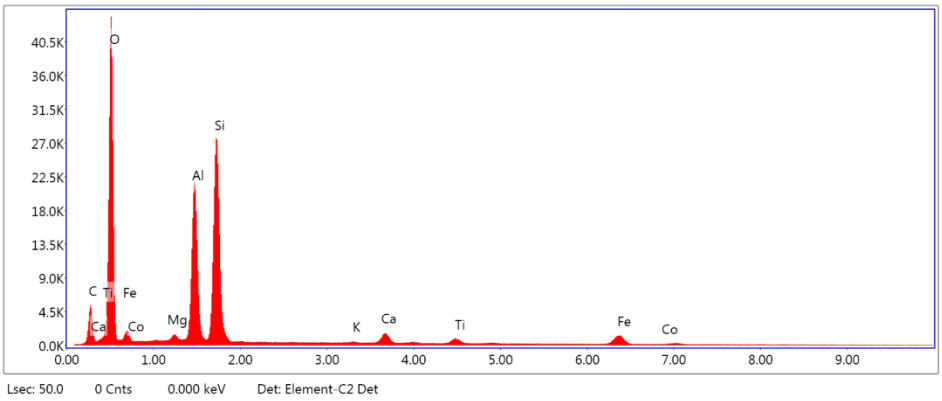

eZAF Smart Quant Results

Element	Weight %	Atomic %	Net Int.	Error %	Kratio	Z	R	A	F
C K	10.98	18.05	399.86	10.49	0.0205	1.1098	0.9512	0.1682	1.0000
O K	42.56	52.51	4786.95	8.02	0.1537	1.0577	0.9727	0.3414	1.0000
MgK	0.51	0.41	103.90	8.97	0.0030	0.9712	1.0055	0.6085	1.0100
AlK	14.05	10.28	3208.48	4.22	0.0981	0.9341	1.0123	0.7401	1.0098
SiK	20.09	14.12	4380.69	4.20	0.1418	0.9534	1.0186	0.7369	1.0039
K K	0.20	0.10	28.58	21.06	0.0017	0.8791	1.0442	0.9404	1.0323
CaK	2.34	1.15	275.68	4.16	0.0209	0.8941	1.0481	0.9629	1.0351
TiK	1.60	0.66	150.31	5.82	0.0135	0.8083	1.0544	0.9845	1.0605
FeK	7.30	2.58	318.06	4.47	0.0617	0.7885	1.0585	1.0031	1.0685
CoK	0.36	0.12	12.60	43.09	0.0030	0.7678	1.0569	1.0040	1.0856

EDAX TEAM

Nathan Rabideaux 8 2017

Author: robert
Creation: 09/06/2017 10:20:33 AM

Sample Name: 14-KIS-1

Area 1

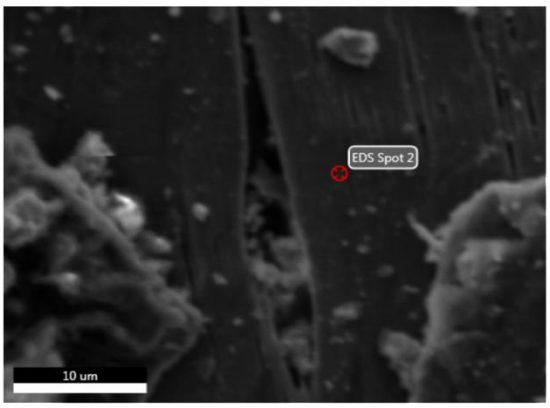

Notes:

EDAX TEAM

EDS Spot 2

kV: 15 Mag: 3382 Takeoff: 30 Live Time(s): 50 Amp Time(µs): 7.68 Resolution:(eV) 129.8

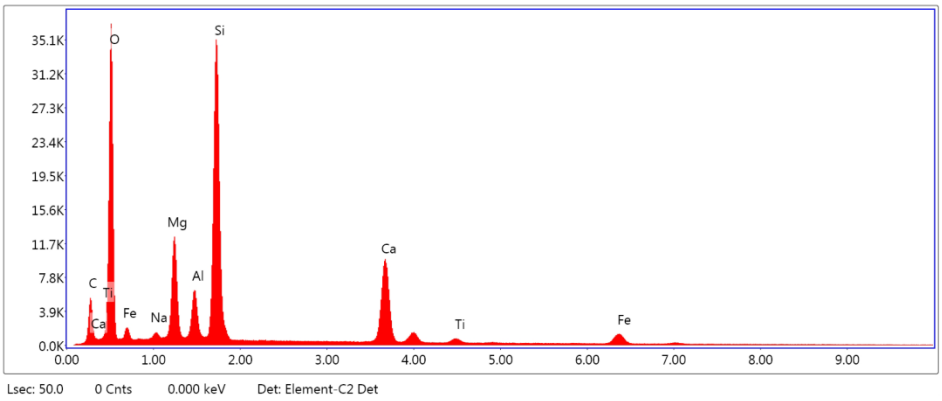

eZAF Smart Quant Results

Element	Weight %	Atomic %	Net Int.	Error %	Kratio	Z	R	A	F
C K	8.14	14.19	402.25	10.28	0.0171	1.1182	0.9440	0.1885	1.0000
O K	39.09	51.18	4033.43	8.87	0.1077	1.0661	0.9659	0.2584	1.0000
NaK	0.59	0.54	87.11	11.09	0.0025	0.9641	0.9920	0.4377	1.0052
MgK	6.96	5.99	1685.54	5.80	0.0410	0.9794	0.9996	0.5969	1.0075
AlK	3.45	2.68	875.56	5.26	0.0223	0.9421	1.0066	0.6759	1.0120
SiK	20.36	15.18	5583.11	3.93	0.1502	0.9617	1.0131	0.7627	1.0062
CaK	14.46	7.56	2050.02	2.40	0.1291	0.9023	1.0438	0.9683	1.0225
TiK	1.04	0.46	113.85	7.60	0.0085	0.8158	1.0506	0.9626	1.0413
FeK	5.91	2.22	308.41	4.58	0.0498	0.7962	1.0556	0.9954	1.0620

EDAX TEAM

Nathan Rabideaux 8 2017

Author: robert
Creation: 09/06/2017 10:25:31 AM

Sample Name: 14-KIS-1

Area 2

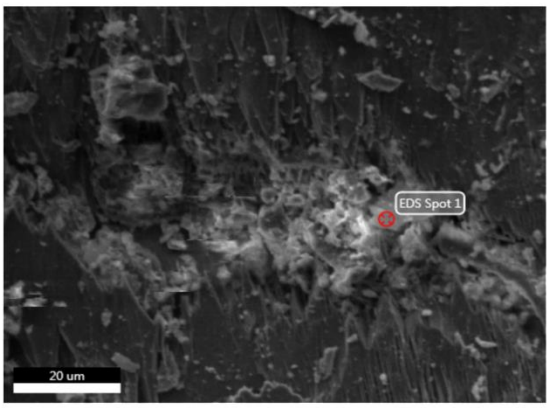

Notes:

EDAX TEAM

EDS Spot 1

kV: 15 Mag: 1359 Takeoff: 30.1 Live Time(s): 50 Amp Time(µs): 7.68 Resolution:(eV) 129.8

EDS Spot 1

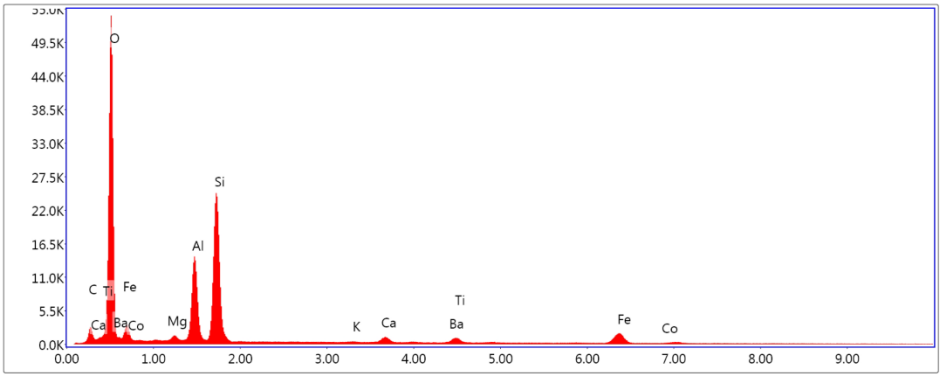

Lsec: 50.0 0 Cnts 0.000 keV Det: Element-C2 Det

eZAF Smart Quant Results

Element	Weight %	Atomic %	Net Int.	Error %	Kratio	Z	R	A	F
C K	4.80	8.33	167.15	11.60	0.0094	1.1245	0.9430	0.1741	1.0000
O K	47.50	61.92	5939.75	7.28	0.2092	1.0722	0.9650	0.4109	1.0000
MgK	0.67	0.57	114.98	8.68	0.0037	0.9853	0.9988	0.5574	1.0081
AlK	10.66	8.24	2099.89	4.79	0.0705	0.9477	1.0058	0.6914	1.0094
SiK	19.90	14.78	3949.31	4.32	0.1403	0.9675	1.0124	0.7257	1.0042
K K	0.13	0.07	17.39	31.29	0.0012	0.8926	1.0391	0.9376	1.0344
CaK	1.67	0.87	182.72	6.05	0.0152	0.9080	1.0433	0.9608	1.0414
BaL	1.56	0.24	49.33	25.31	0.0115	0.6313	1.2160	1.0705	1.0907
TiK	1.53	0.66	133.43	9.44	0.0132	0.8210	1.0501	0.9846	1.0696
FeK	11.13	4.16	442.82	3.87	0.0944	0.8014	1.0553	1.0011	1.0567
CoK	0.46	0.16	14.50	42.90	0.0038	0.7804	1.0540	1.0020	1.0709

EDAX TEAM

Nathan Rabideaux 8 2017

Author: robert
Creation: 09/06/2017 10:26:49 AM

Sample Name: 14-KIS-1

Area 2

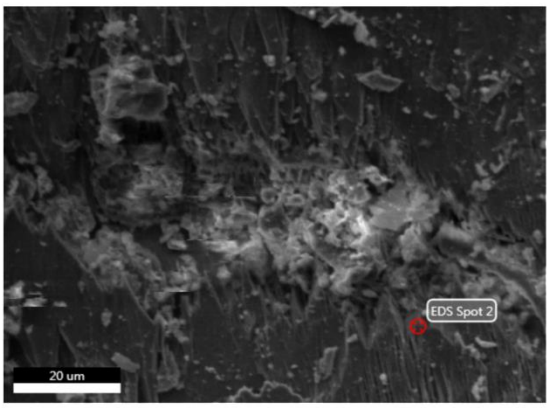

Notes:

EDAX TEAM

EDS Spot 2

kV: 15 Mag: 1359 Takeoff: 30.1 Live Time(s): 50 Amp Time(µs): 7.68 Resolution:(eV) 129.8

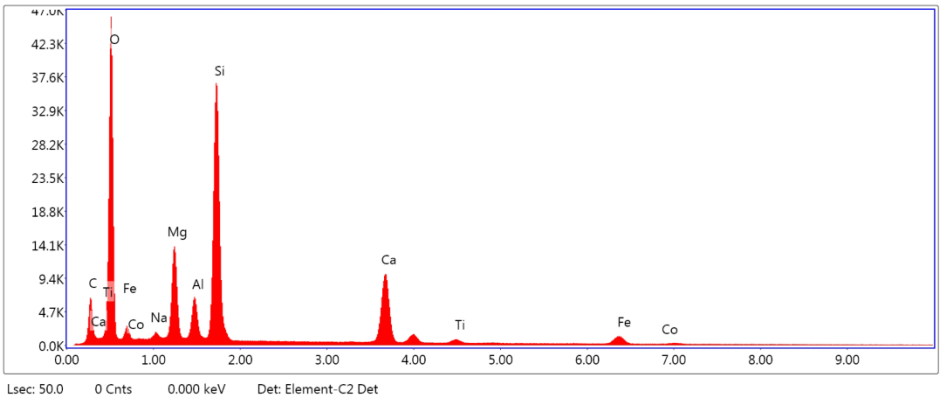

eZAF Smart Quant Results

Element	Weight %	Atomic %	Net Int.	Error %	Kratio	Z	R	A	F
C K	9.07	15.38	522.25	10.12	0.0197	1.1121	0.9472	0.1951	1.0000
O K	41.49	52.80	5046.13	8.72	0.1192	1.0601	0.9689	0.2710	1.0000
NaK	0.87	0.77	144.72	9.14	0.0037	0.9585	0.9948	0.4388	1.0051
MgK	7.00	5.86	1903.02	5.73	0.0409	0.9737	1.0022	0.5964	1.0072
AlK	3.23	2.44	919.48	5.26	0.0207	0.9365	1.0091	0.6755	1.0115
SiK	19.05	13.81	5874.23	3.91	0.1399	0.9560	1.0156	0.7641	1.0060
CaK	12.98	6.60	2072.33	2.40	0.1156	0.8967	1.0458	0.9709	1.0229
TiK	0.95	0.40	116.80	7.78	0.0077	0.8107	1.0523	0.9672	1.0421
FeK	5.02	1.83	295.42	4.69	0.0422	0.7911	1.0569	0.9972	1.0662
CoK	0.34	0.12	15.98	39.29	0.0028	0.7703	1.0555	0.9997	1.0829

EDAX TEAM

Nathan Rabideaux 8 2017

Author: robert
Creation: 09/06/2017 10:33:25 AM

Sample Name: 14-KIS-1

Area 3

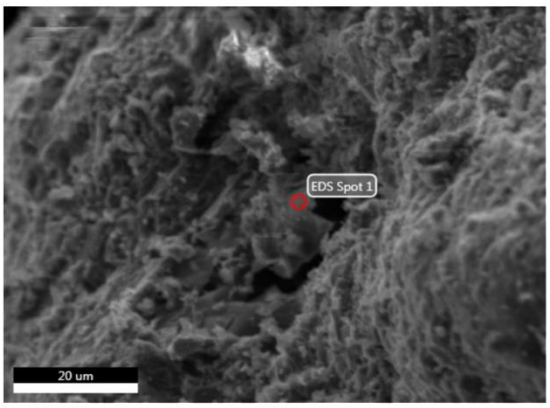

Notes:

EDAX TEAM

EDS Spot 1

kV: 15 Mag: 1580 Takeoff: 29.8 Live Time(s): 50 Amp Time(µs): 7.68 Resolution:(eV) 129.8

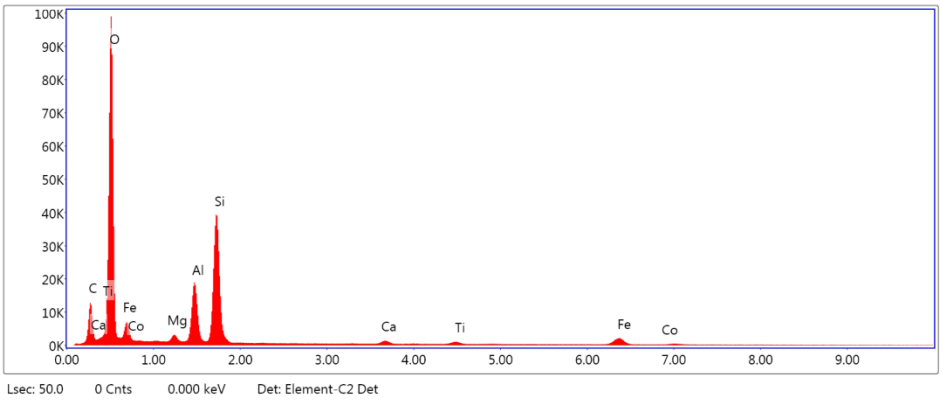

eZAF Smart Quant Results

Element	Weight %	Atomic %	Net Int.	Error %	Kratio	Z	R	A	F
C K	14.22	21.51	1065.15	9.67	0.0319	1.0901	0.9597	0.2059	1.0000
O K	51.95	59.02	11113.86	7.48	0.2079	1.0383	0.9806	0.3855	1.0000
MgK	1.10	0.82	363.49	6.56	0.0062	0.9527	1.0123	0.5860	1.0078
AlK	7.41	4.99	2767.87	4.50	0.0492	0.9162	1.0189	0.7171	1.0097
SiK	16.33	10.57	6259.91	3.85	0.1177	0.9351	1.0249	0.7676	1.0040
CaK	0.87	0.40	176.58	7.91	0.0078	0.8765	1.0530	0.9766	1.0402
TiK	0.93	0.35	150.31	7.74	0.0079	0.7922	1.0588	0.9957	1.0736
FeK	6.94	2.26	515.21	4.00	0.0581	0.7726	1.0617	1.0076	1.0750
CoK	0.25	0.08	15.13	47.04	0.0021	0.7521	1.0598	1.0074	1.0940

EDAX TEAM

Nathan Rabideaux 8 2017

Author: robert
Creation: 09/06/2017 10:34:53 AM

Sample Name: 14-KIS-1

Area 3

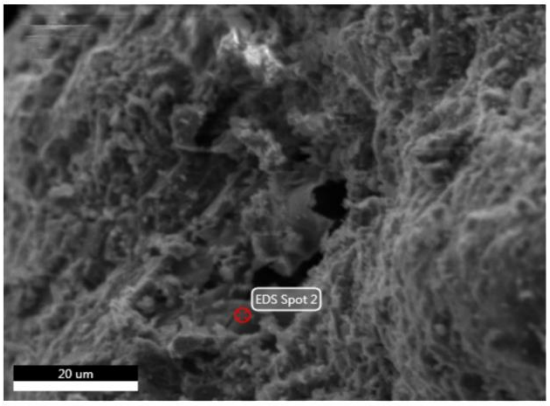

Notes:

EDAX TEAM

EDS Spot 2

kV: 15 Mag: 1580 Takeoff: 29.8 Live Time(s): 50 Amp Time(µs): 7.68 Resolution:(eV) 129.8

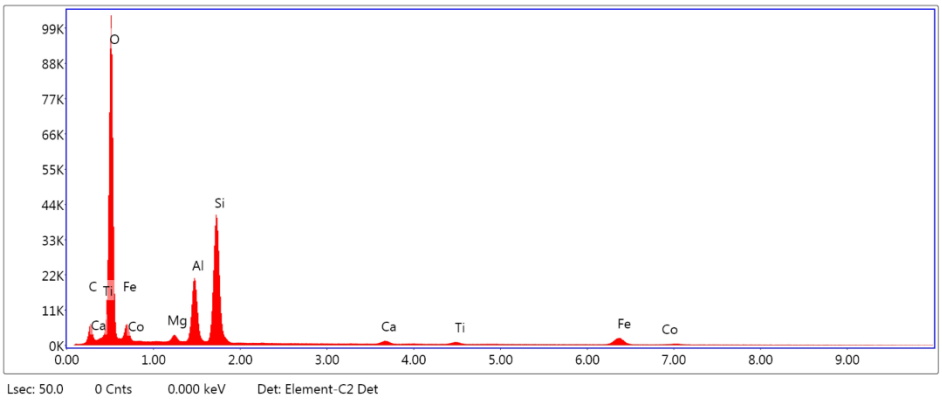

eZAF Smart Quant Results

Element	Weight %	Atomic %	Net Int.	Error %	Kratio	Z	R	A	F
C K	7.97	12.76	502.40	10.22	0.0163	1.1023	0.9544	0.1855	1.0000
O K	52.72	63.39	11503.32	7.13	0.2330	1.0504	0.9756	0.4207	1.0000
MgK	1.19	0.94	363.77	6.65	0.0067	0.9642	1.0080	0.5766	1.0082
AlK	8.95	6.38	3082.55	4.59	0.0593	0.9273	1.0147	0.7072	1.0098
SiK	18.47	12.65	6460.27	4.03	0.1315	0.9465	1.0210	0.7491	1.0039
CaK	1.07	0.51	201.42	5.42	0.0096	0.8874	1.0499	0.9694	1.0395
TiK	0.99	0.40	148.89	6.64	0.0084	0.8022	1.0561	0.9910	1.0729
FeK	8.10	2.79	558.98	3.93	0.0682	0.7825	1.0597	1.0060	1.0699
CoK	0.53	0.17	29.45	28.97	0.0044	0.7618	1.0580	1.0060	1.0862

EDAX TEAM

Nathan Rabideaux 8 2017

Author: robert
Creation: 09/06/2017 10:36:18 AM

Sample Name: 14-KIS-1

Area 3

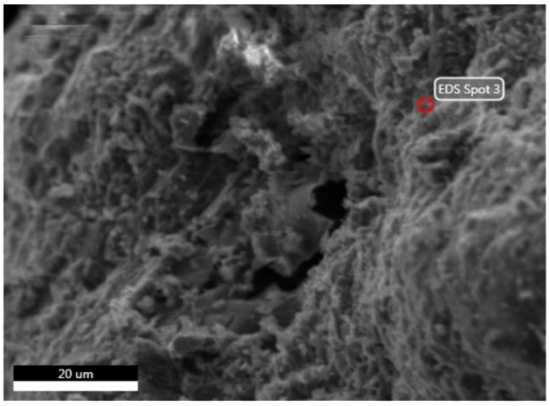

Notes:

EDS Spot 3

kV: 15 Mag: 1580 Takeoff: 29.8 Live Time(s): 50 Amp Time(µs): 7.68 Resolution:(eV) 129.8

EDS Spot 3

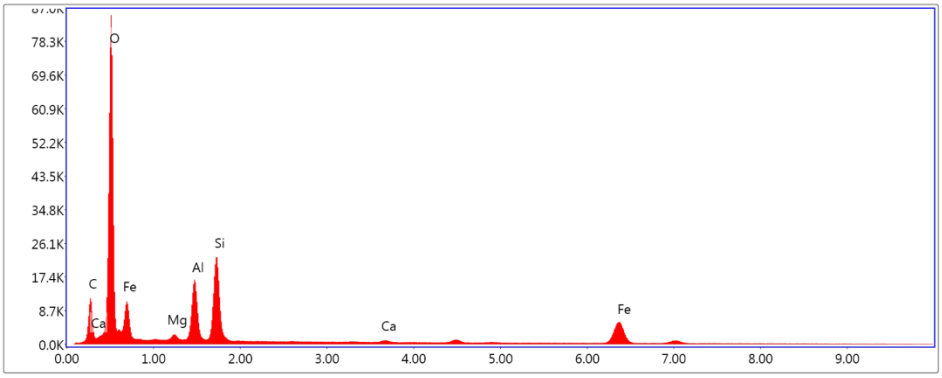

eZAF Smart Quant Results

Element	Weight %	Atomic %	Net Int.	Error %	Kratio	Z	R	A	F
C K	13.75	22.67	1013.38	9.76	0.0340	1.1182	0.9441	0.2212	1.0000
O K	44.80	55.46	9625.59	7.12	0.2017	1.0662	0.9660	0.4222	1.0000
MgK	1.00	0.81	264.64	8.02	0.0050	0.9798	0.9996	0.5121	1.0055
AlK	7.74	5.68	2393.14	5.20	0.0476	0.9425	1.0066	0.6483	1.0067
SiK	10.71	7.55	3505.59	4.47	0.0738	0.9622	1.0132	0.7128	1.0050
CaK	0.13	0.07	25.58	27.04	0.0013	0.9031	1.0439	0.9744	1.0618
FeK	21.86	7.75	1455.46	3.07	0.1837	0.7973	1.0557	1.0082	1.0453

EDAX TEAM

Nathan Rabideaux 8 2017

Author: robert
Creation: 09/06/2017 11:16:41 AM

Sample Name: 14-MAG-3

Area 1

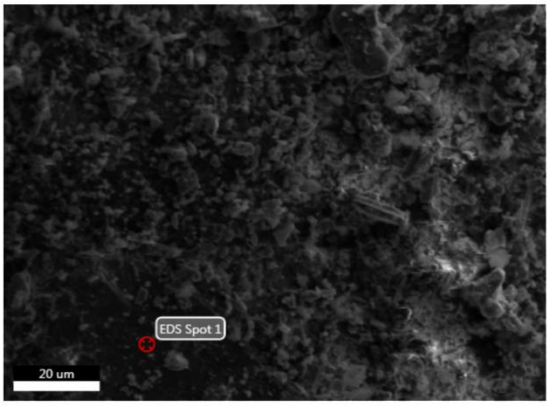

Notes:

EDS Spot 1

kV: 15	Mag: 1095	Takeoff: 29.7	Live Time(s): 50	Amp Time(µs): 7.68	Resolution:(eV) 129.8

EDS Spot 1

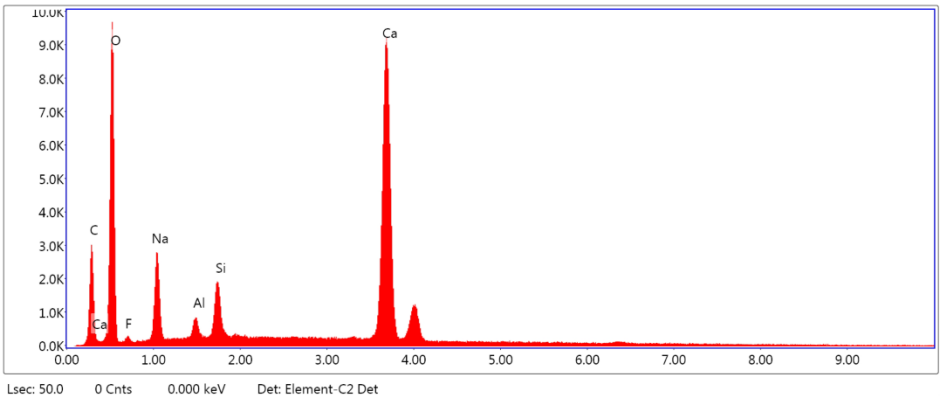

eZAF Smart Quant Results

Element	Weight %	Atomic %	Net Int.	Error %	Kratio	Z	R	A	F
C K	6.98	12.27	246.14	8.54	0.0299	1.1181	0.9409	0.3837	1.0000
O K	43.96	58.06	1066.34	9.94	0.0809	1.0662	0.9630	0.1727	1.0000
F K	0.67	0.75	15.64	19.30	0.0010	0.9896	0.9725	0.1483	1.0000
NaK	6.73	6.18	317.34	8.53	0.0258	0.9645	0.9894	0.3961	1.0032
AlK	0.72	0.57	62.98	8.82	0.0045	0.9425	1.0041	0.6594	1.0106
SiK	2.59	1.95	256.04	5.45	0.0195	0.9622	1.0107	0.7701	1.0161
CaK	38.35	20.22	1961.76	2.02	0.3500	0.9029	1.0419	0.9997	1.0113

EDAX TEAM

Nathan Rabideaux 8 2017

Author: robert
Creation: 09/06/2017 11:17:42 AM

Sample Name: 14-MAG-3

Area 1

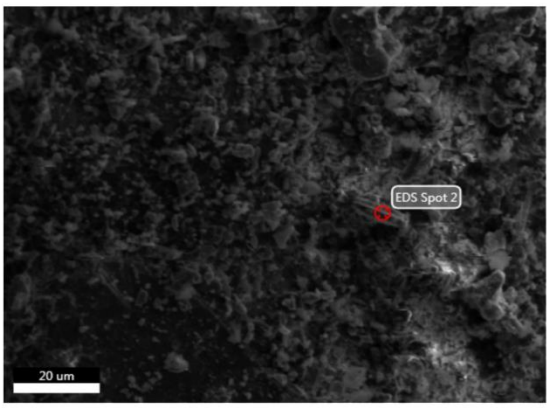

Notes:

EDAX TEAM

EDS Spot 2

kV: 15 Mag: 1095 Takeoff: 29.7 Live Time(s): 50 Amp Time(µs): 7.68 Resolution:(eV) 129.8

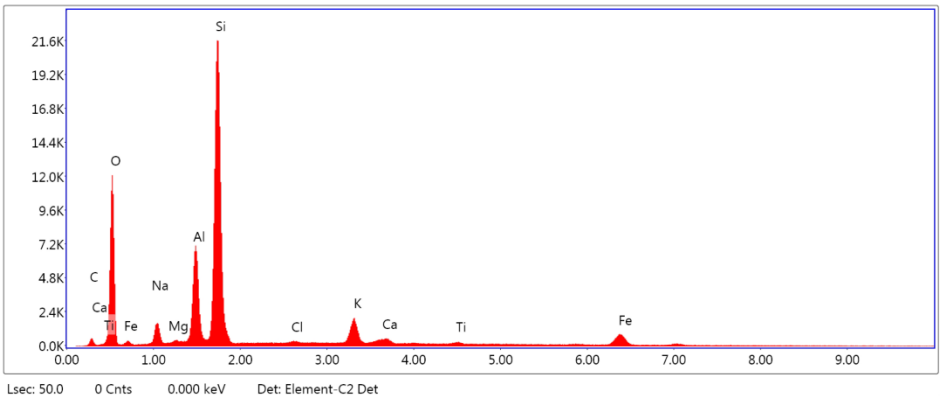

eZAF Smart Quant Results

Element	Weight %	Atomic %	Net Int.	Error %	Kratio	Z	R	A	F
C K	0.00	0.00	0.00	99.99	0.0000	1.1535	0.9311	0.1243	1.0000
O K	29.31	44.84	1223.92	8.51	0.1012	1.1006	0.9538	0.3138	1.0000
NaK	2.36	2.51	121.46	9.22	0.0107	0.9960	0.9810	0.4550	1.0060
MgK	0.00	0.00	0.01	99.99	0.0000	1.0120	0.9889	0.5971	1.0115
AlK	10.44	9.47	960.67	4.71	0.0754	0.9736	0.9962	0.7304	1.0157
SiK	37.81	32.95	3421.58	4.06	0.2843	0.9940	1.0031	0.7533	1.0041
ClK	0.08	0.06	5.31	60.18	0.0006	0.9235	1.0213	0.7989	1.0165
K K	6.02	3.77	327.82	4.29	0.0512	0.9174	1.0314	0.9055	1.0228
CaK	1.29	0.79	58.53	11.39	0.0114	0.9332	1.0359	0.9185	1.0288
TiK	0.66	0.34	24.34	24.16	0.0056	0.8439	1.0434	0.9602	1.0571
FeK	12.02	5.27	208.91	4.74	0.1040	0.8243	1.0503	0.9952	1.0549

EDAX TEAM

Nathan Rabideaux 8 2017

Author: robert
Creation: 09/06/2017 11:18:48 AM

Sample Name: 14-MAG-3

Area 1

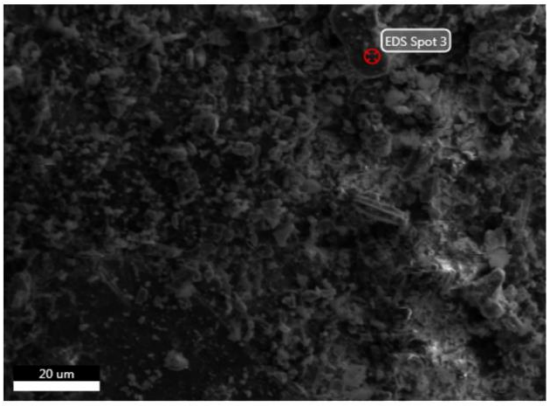

Notes:

EDAX TEAM

EDS Spot 3

kV: 15 Mag: 1095 Takeoff: 29.7 Live Time(s): 50 Amp Time(µs): 7.68 Resolution:(eV) 129.8

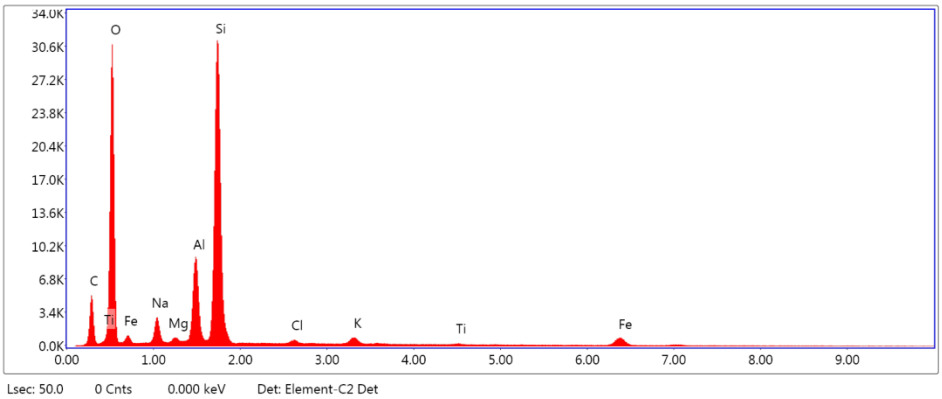

eZAF Smart Quant Results

Element	Weight %	Atomic %	Net Int.	Error %	Kratio	Z	R	A	F
C K	14.93	23.76	397.59	10.60	0.0261	1.1010	0.9551	0.1586	1.0000
O K	39.28	46.92	3349.20	8.15	0.1371	1.0490	0.9763	0.3327	1.0000
NaK	2.84	2.36	292.40	7.81	0.0128	0.9480	1.0014	0.4726	1.0055
MgK	0.18	0.14	29.61	17.24	0.0011	0.9628	1.0086	0.6139	1.0105
AlK	7.25	5.13	1308.90	4.38	0.0509	0.9260	1.0153	0.7469	1.0146
SiK	27.34	18.60	4978.36	3.66	0.2048	0.9451	1.0215	0.7894	1.0035
ClK	0.42	0.23	53.51	9.82	0.0032	0.8775	1.0378	0.8511	1.0127
K K	1.30	0.64	140.55	5.66	0.0109	0.8712	1.0466	0.9365	1.0227
TiK	0.31	0.12	22.96	25.18	0.0026	0.8009	1.0565	0.9859	1.0623
FeK	6.13	2.10	210.00	4.82	0.0518	0.7812	1.0600	1.0048	1.0756

EDAX TEAM

Nathan Rabideaux 8 2017

Author: robert
Creation: 09/06/2017 11:24:54 AM

Sample Name: 14-MAG-3

Area 2

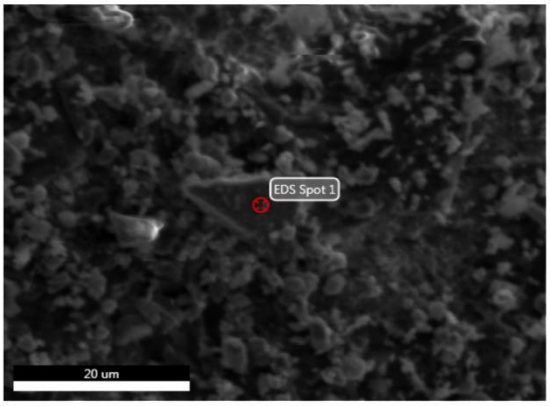

Notes:

EDAX TEAM

EDS Spot 1

kV: 15 Mag: 2237 Takeoff: 29.8 Live Time(s): 50 Amp Time(µs): 7.68 Resolution:(eV) 129.8

EDS Spot 1

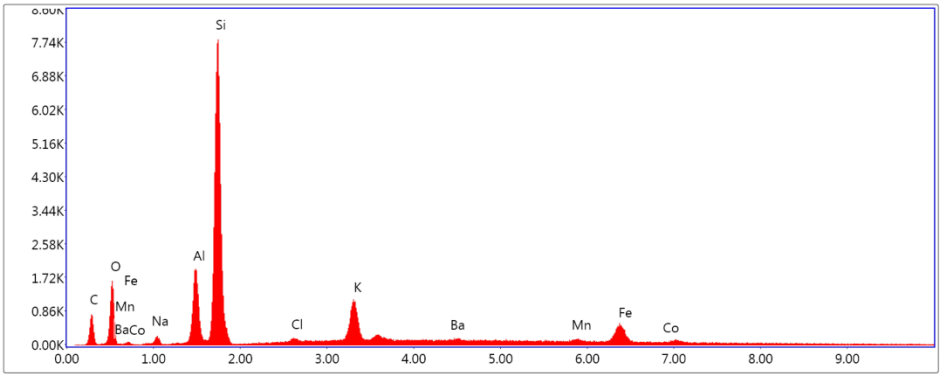

Lsec: 50.0 0 Cnts 0.000 keV Det: Element-C2 Det

eZAF Smart Quant Results

Element	Weight %	Atomic %	Net Int.	Error %	Kratio	Z	R	A	F
C K	9.23	21.25	46.84	13.91	0.0156	1.1993	0.9052	0.1411	1.0000
O K	10.45	18.06	148.52	10.45	0.0310	1.1459	0.9291	0.2585	1.0000
NaK	0.10	0.13	1.89	69.36	0.0004	1.0387	0.9580	0.3861	1.0043
AlK	7.17	7.35	246.58	6.10	0.0488	1.0163	0.9744	0.6618	1.0126
SiK	33.53	33.01	1206.97	4.61	0.2530	1.0380	0.9819	0.7229	1.0053
ClK	0.25	0.19	6.47	59.60	0.0019	0.9656	1.0020	0.7992	1.0213
K K	10.07	7.12	227.43	4.26	0.0896	0.9600	1.0135	0.9033	1.0259
BaL	5.23	1.05	28.97	12.82	0.0398	0.6804	1.1916	1.0404	1.0738
MnK	3.26	1.64	28.21	16.86	0.0290	0.8539	1.0369	0.9800	1.0629
FeK	18.86	9.33	133.45	5.84	0.1676	0.8658	1.0383	0.9857	1.0418
CoK	1.84	0.86	10.39	36.97	0.0161	0.8439	1.0387	0.9865	1.0511

EDAX TEAM

Nathan Rabideaux 8 2017

Author: robert
Creation: 09/06/2017 11:25:51 AM

Sample Name: 14-MAG-3

Area 2

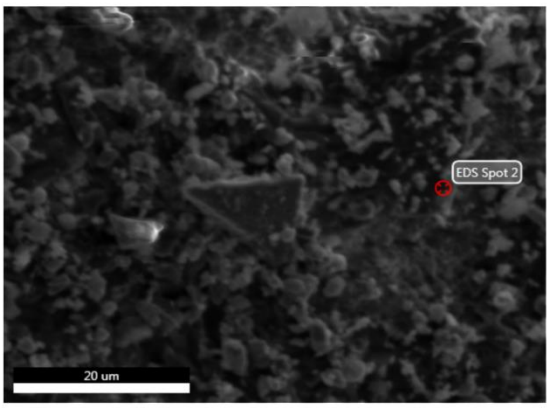

Notes:

EDAX TEAM

EDS Spot 2

kV: 15 Mag: 2237 Takeoff: 29.8 Live Time(s): 50 Amp Time(µs): 7.68 Resolution:(eV) 129.8

EDS Spot 2

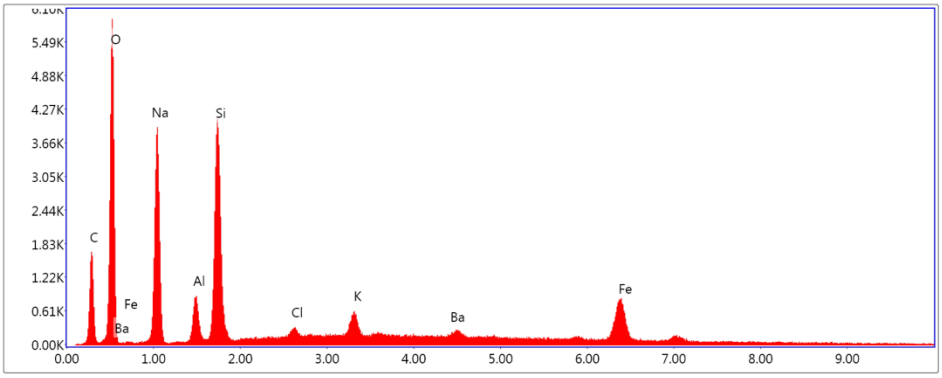

eZAF Smart Quant Results

Element	Weight %	Atomic %	Net Int.	Error %	Kratio	Z	R	A	F
C K	11.90	23.26	117.15	11.58	0.0280	1.1720	0.9206	0.2006	1.0000
O K	21.53	31.59	595.36	8.27	0.0888	1.1191	0.9438	0.3687	1.0000
NaK	19.43	19.84	469.68	8.25	0.0750	1.0137	0.9717	0.3802	1.0022
AlK	1.91	1.66	74.27	9.04	0.0105	0.9914	0.9875	0.5524	1.0068
SiK	13.23	11.06	596.86	5.58	0.0896	1.0125	0.9946	0.6652	1.0052
ClK	0.41	0.27	15.33	21.85	0.0033	0.9415	1.0136	0.8481	1.0198
K K	2.85	1.71	91.38	6.34	0.0258	0.9357	1.0243	0.9322	1.0348
BaL	5.89	1.01	45.95	13.14	0.0452	0.6628	1.2020	1.0667	1.0848
FeK	22.85	9.61	221.74	4.40	0.1994	0.8426	1.0456	0.9950	1.0410

EDAX TEAM

Nathan Rabideaux 8 2017

Author: robert
Creation: 09/06/2017 11:33:43 AM

Sample Name: 14-MAG-3

Area 3

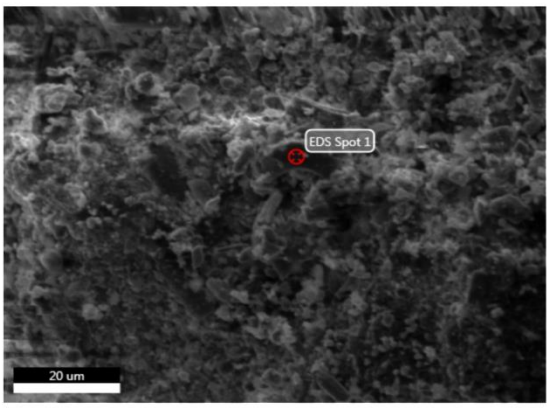

Notes:

EDAX TEAM

EDS Spot 1

kV: 15 Mag: 1354 Takeoff: 29.6 Live Time(s): 50 Amp Time(µs): 7.68 Resolution:(eV) 129.8

EDS Spot 1

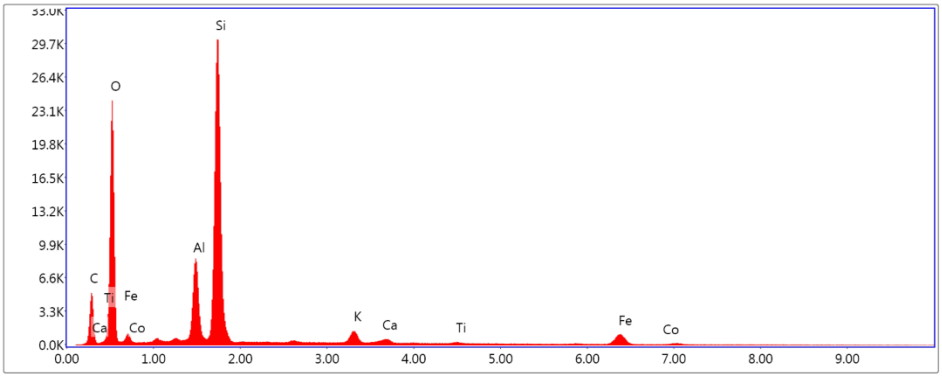

Lsec: 50.0 0 Cnts 0.000 keV Det: Element-C2 Det

eZAF Smart Quant Results

Element	Weight %	Atomic %	Net Int.	Error %	Kratio	Z	R	A	F
C K	16.31	26.57	418.19	10.53	0.0293	1.1077	0.9502	0.1622	1.0000
O K	35.80	43.78	2597.67	8.51	0.1134	1.0558	0.9717	0.3001	1.0000
AlK	7.20	5.22	1234.20	4.38	0.0511	0.9325	1.0115	0.7499	1.0147
SiK	27.86	19.41	4812.66	3.64	0.2109	0.9519	1.0178	0.7918	1.0040
K K	2.40	1.20	246.54	4.47	0.0203	0.8778	1.0436	0.9367	1.0261
CaK	0.99	0.49	85.29	8.82	0.0087	0.8928	1.0475	0.9532	1.0329
TiK	0.51	0.21	35.66	18.89	0.0043	0.8071	1.0539	0.9817	1.0646
FeK	8.58	3.01	275.17	4.50	0.0722	0.7875	1.0581	1.0031	1.0651
CoK	0.33	0.11	8.49	57.34	0.0028	0.7668	1.0566	1.0039	1.0816

EDAX TEAM

Nathan Rabideaux 8 2017

Author: robert
Creation: 09/06/2017 11:35:02 AM

Sample Name: 14-MAG-3

Area 3

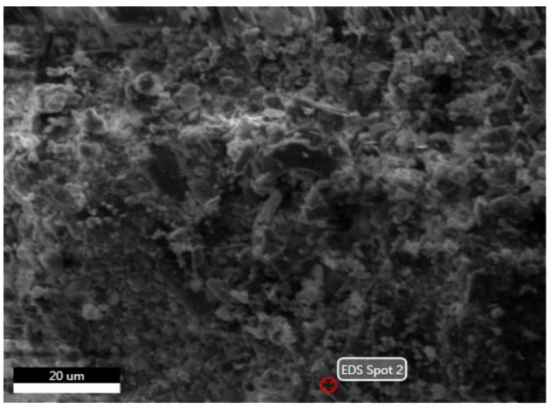

Notes:

EDAX TEAM

EDS Spot 2

kV: 15 Mag: 1354 Takeoff: 29.6 Live Time(s): 50 Amp Time(µs): 7.68 Resolution:(eV) 129.8

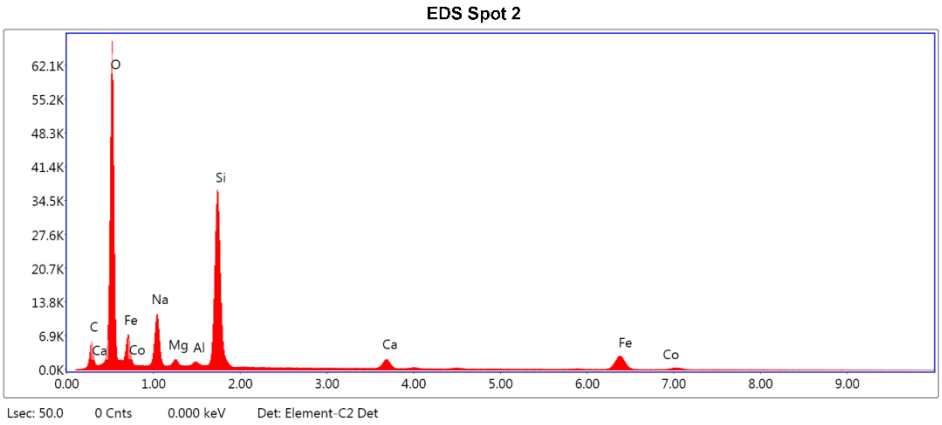

eZAF Smart Quant Results

Element	Weight %	Atomic %	Net Int.	Error %	Kratio	Z	R	A	F
C K	8.10	13.67	418.38	10.30	0.0169	1.1175	0.9471	0.1868	1.0000
O K	43.17	54.72	7498.59	7.26	0.1889	1.0653	0.9689	0.4106	1.0000
NaK	10.51	9.27	1547.15	7.64	0.0417	0.9633	0.9947	0.4101	1.0033
MgK	1.11	0.93	241.02	8.18	0.0055	0.9785	1.0021	0.5025	1.0060
AlK	0.68	0.51	172.69	7.81	0.0041	0.9412	1.0091	0.6353	1.0107
SiK	20.46	14.77	5850.83	4.05	0.1478	0.9608	1.0155	0.7488	1.0043
CaK	2.35	1.19	360.50	4.48	0.0213	0.9013	1.0457	0.9663	1.0412
FeK	13.34	4.84	744.39	3.49	0.1127	0.7952	1.0569	1.0051	1.0568
CoK	0.28	0.10	12.36	56.59	0.0023	0.7743	1.0555	1.0050	1.0716

EDAX TEAM

Nathan Rabideaux 8 2017

Author: robert
Creation: 09/06/2017 11:36:11 AM

Sample Name: 14-MAG-3

Area 3

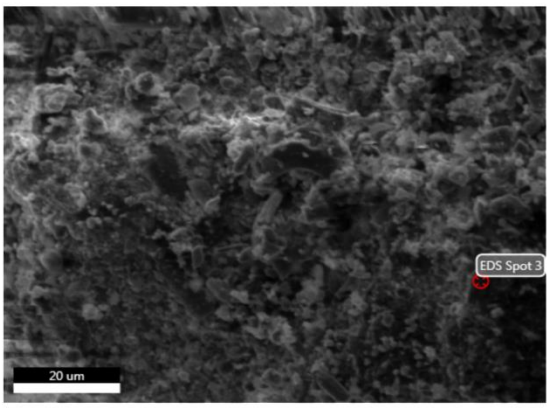

Notes:

EDAX TEAM

EDS Spot 3

kV: 15 Mag: 1354 Takeoff: 29.6 Live Time(s): 50 Amp Time(µs): 7.68 Resolution:(eV) 129.8

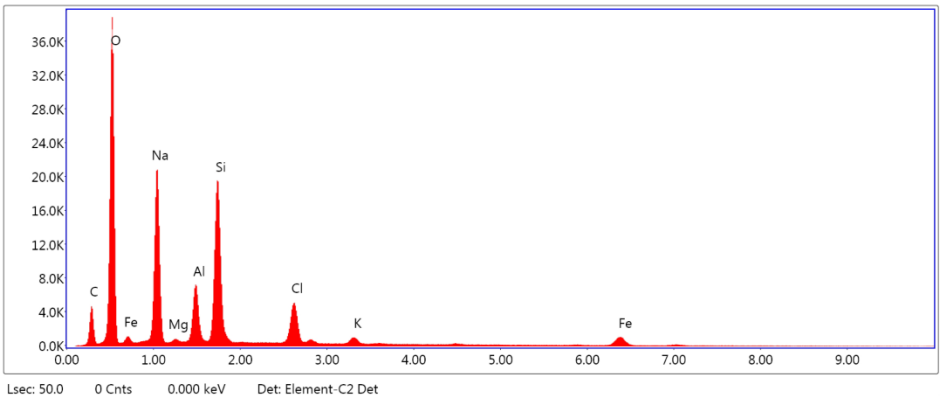

eZAF Smart Quant Results

Element	Weight %	Atomic %	Net Int.	Error %	Kratio	Z	R	A	F
C K	10.07	16.72	325.02	11.01	0.0173	1.1161	0.9530	0.1540	1.0000
O K	36.01	44.90	4225.31	7.78	0.1402	1.0635	0.9743	0.3661	1.0000
NaK	20.47	17.76	2748.53	6.62	0.0975	0.9612	0.9997	0.4940	1.0033
MgK	0.23	0.19	37.89	13.54	0.0011	0.9763	1.0069	0.5049	1.0062
AlK	5.32	3.93	1025.11	5.54	0.0323	0.9390	1.0136	0.6408	1.0088
SiK	14.78	10.50	3084.02	4.41	0.1027	0.9584	1.0199	0.7211	1.0053
ClK	5.58	3.14	914.88	3.36	0.0438	0.8898	1.0363	0.8711	1.0121
K K	1.16	0.59	155.67	5.71	0.0097	0.8835	1.0453	0.9307	1.0219
FeK	6.38	2.28	273.66	4.56	0.0546	0.7923	1.0592	1.0044	1.0748

EDAX TEAM

Nathan Rabideaux 8 2017

Author: robert
Creation: 09/06/2017 10:45:44 AM

Sample Name: 14-NGIN-3

Area 1

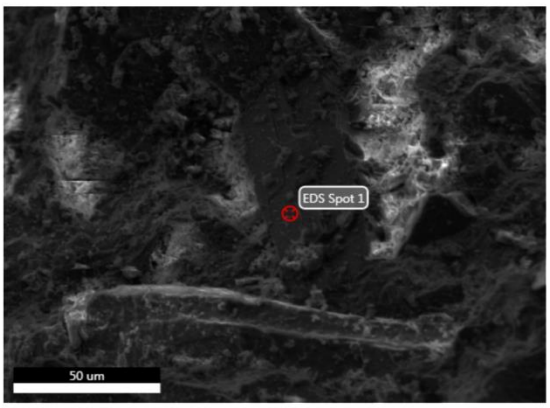

Notes:

EDAX TEAM

EDS Spot 1

kV: 15 Mag: 746 Takeoff: 30.4 Live Time(s): 50 Amp Time(µs): 7.68 Resolution:(eV) 129.8

EDS Spot 1

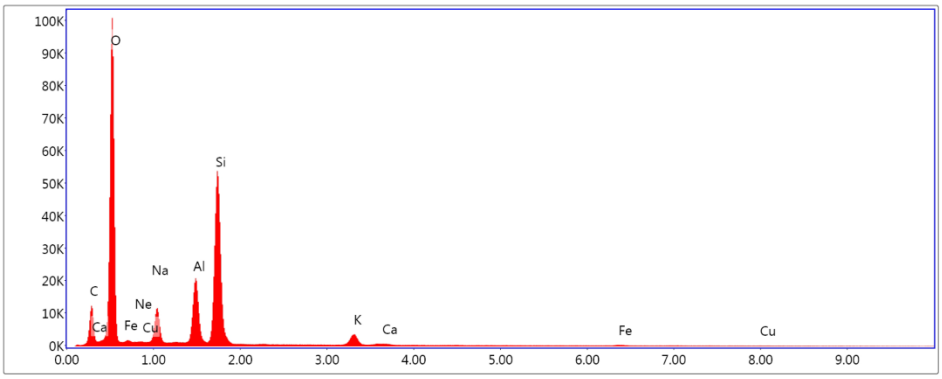

Lsec: 50.0 0 Cnts 0.000 keV Det: Element-C2 Det

eZAF Smart Quant Results

Element	Weight %	Atomic %	Net Int.	Error %	Kratio	Z	R	A	F
C K	13.66	20.46	1066.07	9.86	0.0283	1.0851	0.9645	0.1907	1.0000
O K	49.44	55.57	11381.87	7.62	0.1897	1.0332	0.9850	0.3714	1.0000
NeK	0.42	0.37	125.09	11.45	0.0013	0.9835	1.0018	0.3263	1.0000
NaK	5.93	4.64	1501.62	6.92	0.0269	0.9331	1.0093	0.4839	1.0049
AlK	7.26	4.84	3104.08	4.29	0.0494	0.9111	1.0225	0.7382	1.0119
SiK	19.64	12.58	8530.42	3.66	0.1438	0.9298	1.0285	0.7843	1.0037
K K	2.48	1.14	652.68	3.28	0.0207	0.8566	1.0522	0.9546	1.0193
CaK	0.24	0.11	53.35	10.83	0.0021	0.8711	1.0557	0.9668	1.0248
FeK	0.68	0.22	58.13	18.16	0.0059	0.7674	1.0635	1.0067	1.1194
CuK	0.25	0.07	10.94	57.17	0.0022	0.7260	1.0531	1.0072	1.2245

EDAX TEAM

Nathan Rabideaux 8 2017

Author: robert
Creation: 09/06/2017 10:47:05 AM

Sample Name: 14-NGIN-3

Area 1

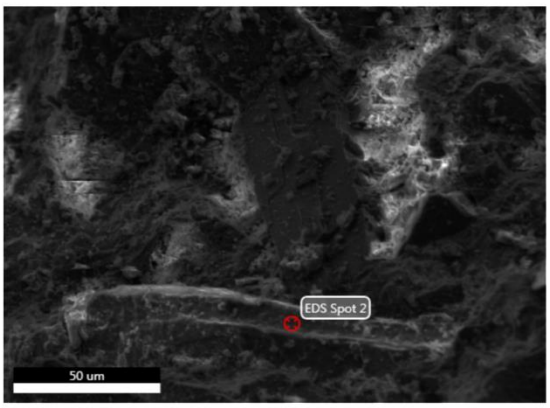

Notes:

EDAX TEAM

EDS Spot 2

kV: 15 Mag: 746 Takeoff: 30.4 Live Time(s): 50 Amp Time(µs): 7.68 Resolution:(eV) 129.8

EDS Spot 2

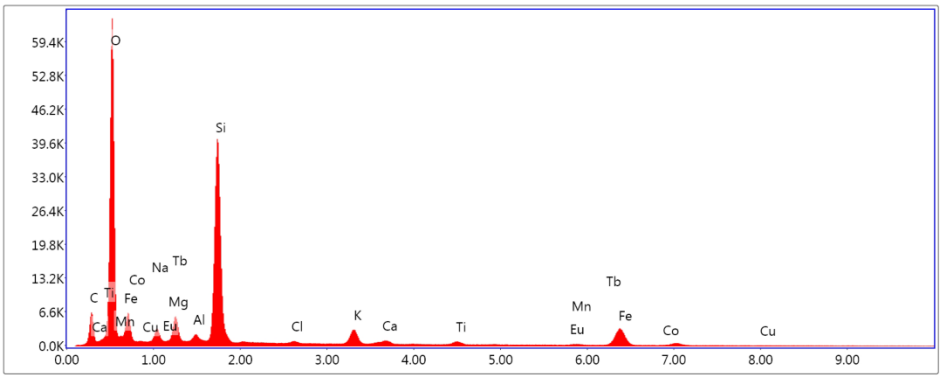

Lsec: 50.0 0 Cnts 0.000 keV Det: Element-C2 Det

eZAF Smart Quant Results

Element	Weight %	Atomic %	Net Int.	Error %	Kratio	Z	R	A	F
C K	8.59	15.22	504.70	10.15	0.0188	1.1353	0.9343	0.1931	1.0000
O K	41.85	55.64	7053.16	7.72	0.1655	1.0832	0.9568	0.3651	1.0000
NaK	2.25	2.08	356.00	8.37	0.0090	0.9804	0.9837	0.4060	1.0033
MgK	2.25	1.97	564.07	7.01	0.0121	0.9962	0.9915	0.5348	1.0057
AlK	0.80	0.63	220.26	7.33	0.0049	0.9584	0.9988	0.6343	1.0100
SiK	20.94	15.86	6423.02	4.12	0.1524	0.9786	1.0056	0.7401	1.0050
ClK	0.36	0.22	83.00	9.66	0.0028	0.9095	1.0235	0.8528	1.0192
K K	2.98	1.62	583.24	3.72	0.0260	0.9036	1.0335	0.9356	1.0332
CaK	0.87	0.46	142.28	7.25	0.0079	0.9192	1.0379	0.9503	1.0440
TiK	1.10	0.49	147.18	6.97	0.0097	0.8314	1.0452	0.9795	1.0854
EuL	1.19	0.17	39.86	31.30	0.0090	0.6175	1.1850	1.0561	1.1605
MnK	0.24	0.09	18.17	32.33	0.0021	0.8016	1.0514	0.9981	1.1100
TbL	3.07	0.41	86.49	18.36	0.0208	0.5976	1.1714	1.0516	1.0756
FeK	13.12	5.00	791.92	3.43	0.1128	0.8123	1.0516	1.0011	1.0579
CoK	0.17	0.06	8.03	57.90	0.0014	0.7912	1.0507	1.0013	1.0586
CuK	0.22	0.07	6.47	57.27	0.0018	0.7702	1.0451	0.9949	1.0880

EDAX TEAM

Nathan Rabideaux 8 2017

Author: robert
Creation: 09/06/2017 10:48:26 AM

Sample Name: 14-NGIN-3

Area 1

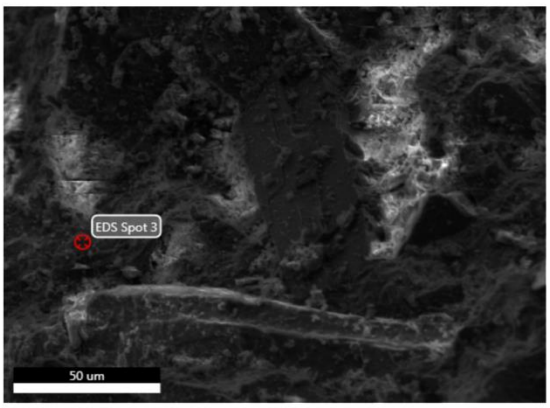

Notes:

EDS Spot 3

kV: 15 Mag: 746 Takeoff: 30.4 Live Time(s): 50 Amp Time(µs): 7.68 Resolution:(eV) 129.8

EDS Spot 3

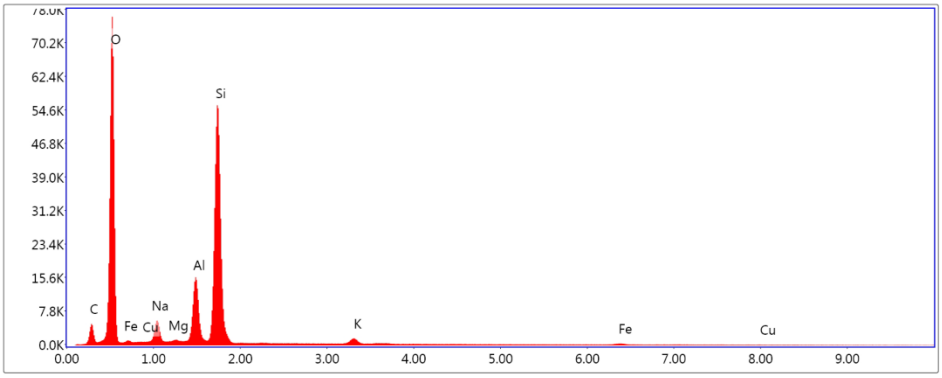

eZAF Smart Quant Results

Element	Weight %	Atomic %	Net Int.	Error %	Kratio	Z	R	A	F
C K	7.30	11.62	315.91	11.02	0.0123	1.0960	0.9592	0.1538	1.0000
O K	49.14	58.70	8414.62	7.34	0.2061	1.0439	0.9801	0.4018	1.0000
NaK	3.73	3.10	660.87	7.16	0.0174	0.9431	1.0049	0.4921	1.0061
MgK	0.19	0.15	52.71	11.91	0.0012	0.9577	1.0119	0.6257	1.0117
AlK	7.58	5.37	2296.47	4.16	0.0537	0.9210	1.0185	0.7574	1.0160
SiK	29.28	19.92	8866.49	3.53	0.2196	0.9399	1.0246	0.7955	1.0030
K K	1.37	0.67	242.84	4.48	0.0113	0.8661	1.0491	0.9363	1.0180
FeK	1.19	0.41	69.24	14.27	0.0103	0.7761	1.0616	1.0049	1.1088
CuK	0.21	0.06	6.32	58.02	0.0019	0.7345	1.0518	1.0063	1.2073

EDAX TEAM

Nathan Rabideaux 8 2017

Author: robert
Creation: 09/06/2017 10:56:36 AM

Sample Name: 14-NGIN-3

Area 2

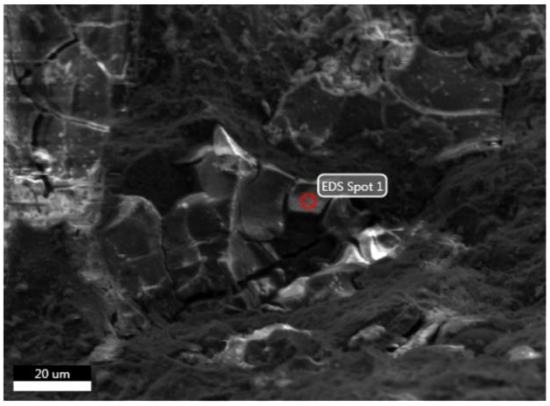

Notes:

EDAX TEAM

EDS Spot 1

kV: 15 Mag: 987 Takeoff: 30.3 Live Time(s): 50 Amp Time(µs): 7.68 Resolution:(eV) 129.8

EDS Spot 1

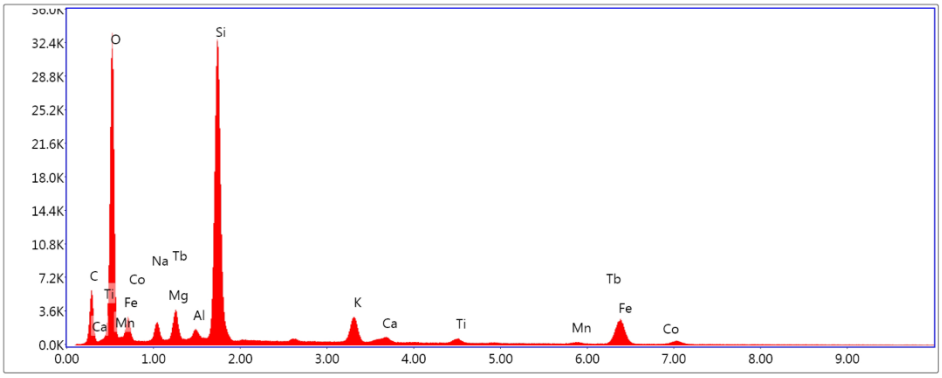

Lsec: 50.0 0 Cnts 0.000 keV Det: Element-C2 Det

eZAF Smart Quant Results

Element	Weight %	Atomic %	Net Int.	Error %	Kratio	Z	R	A	F
C K	11.37	20.54	453.94	10.27	0.0241	1.1400	0.9322	0.1856	1.0000
O K	34.44	46.70	3655.58	8.21	0.1217	1.0878	0.9548	0.3249	1.0000
NaK	2.06	1.94	229.94	8.91	0.0082	0.9847	0.9819	0.4048	1.0035
MgK	2.29	2.04	411.81	6.97	0.0125	1.0006	0.9897	0.5428	1.0062
AlK	0.76	0.61	150.73	7.46	0.0048	0.9627	0.9970	0.6444	1.0110
SiK	23.39	18.07	5147.05	4.06	0.1732	0.9830	1.0039	0.7497	1.0050
K K	4.00	2.22	553.67	3.44	0.0351	0.9076	1.0321	0.9341	1.0329
CaK	0.92	0.50	106.74	9.88	0.0084	0.9234	1.0365	0.9460	1.0438
TiK	1.18	0.54	111.77	7.31	0.0105	0.8352	1.0440	0.9769	1.0853
MnK	0.87	0.34	46.34	14.41	0.0077	0.8053	1.0504	0.9968	1.1011
TbL	3.05	0.42	60.61	21.25	0.0207	0.6004	1.1705	1.0504	1.0731
FeK	15.24	5.92	649.97	3.41	0.1314	0.8161	1.0507	1.0002	1.0558
CoK	0.41	0.15	13.72	37.75	0.0034	0.7949	1.0499	1.0001	1.0562

EDAX TEAM

Nathan Rabideaux 8 2017

Author: robert
Creation: 09/06/2017 10:58:04 AM

Sample Name: 14-NGIN-3

Area 2

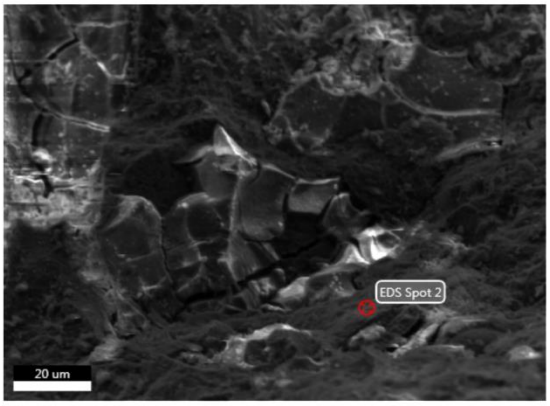

Notes:

EDAX TEAM

EDS Spot 2

kV: 15 Mag: 987 Takeoff: 30.3 Live Time(s): 50 Amp Time(µs): 7.68 Resolution:(eV) 129.8

EDS Spot 2

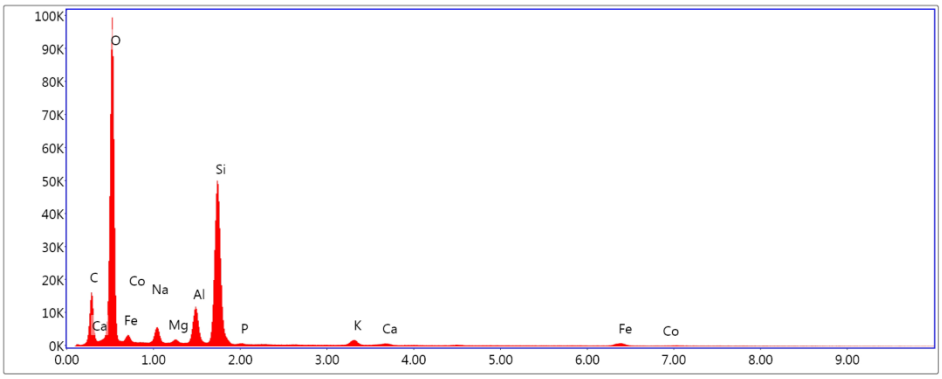

Lsec: 50.0 0 Cnts 0.000 keV Det: Element-C2 Det

eZAF Smart Quant Results

Element	Weight %	Atomic %	Net Int.	Error %	Kratio	Z	R	A	F
C K	18.08	26.08	1522.33	9.61	0.0412	1.0770	0.9667	0.2117	1.0000
O K	51.22	55.46	11320.20	7.67	0.1926	1.0254	0.9870	0.3668	1.0000
NaK	3.27	2.46	769.39	7.27	0.0141	0.9259	1.0111	0.4625	1.0045
MgK	0.55	0.39	203.20	7.25	0.0032	0.9403	1.0179	0.6038	1.0084
AlK	4.14	2.66	1718.92	4.40	0.0279	0.9041	1.0242	0.7368	1.0124
SiK	18.42	11.36	8006.08	3.43	0.1377	0.9226	1.0301	0.8071	1.0038
P K	0.18	0.10	59.36	16.27	0.0012	0.8850	1.0355	0.7606	1.0060
K K	1.12	0.50	290.60	4.55	0.0094	0.8500	1.0535	0.9624	1.0238
CaK	0.37	0.16	80.79	6.97	0.0033	0.8643	1.0569	0.9768	1.0304
FeK	2.49	0.77	204.88	6.15	0.0212	0.7614	1.0643	1.0085	1.1056
CoK	0.14	0.04	9.58	56.52	0.0012	0.7411	1.0621	1.0087	1.1328

EDAX TEAM

Nathan Rabideaux 8 2017

Author: robert
Creation: 09/06/2017 11:04:21 AM

Sample Name: 14-NGIN-3

Area 3

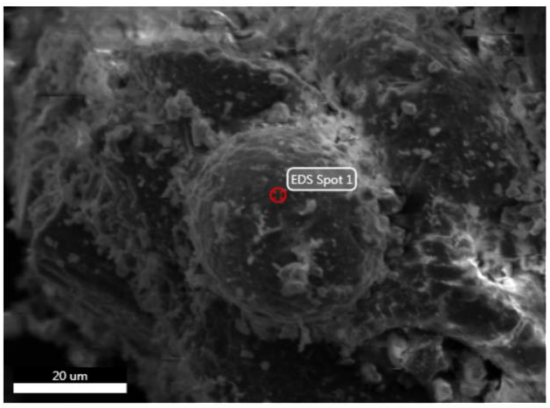

Notes:

EDAX TEAM

EDS Spot 1

kV: 15 Mag: 1436 Takeoff: 30.3 Live Time(s): 50 Amp Time(µs): 7.68 Resolution:(eV) 129.8

EDS Spot 1

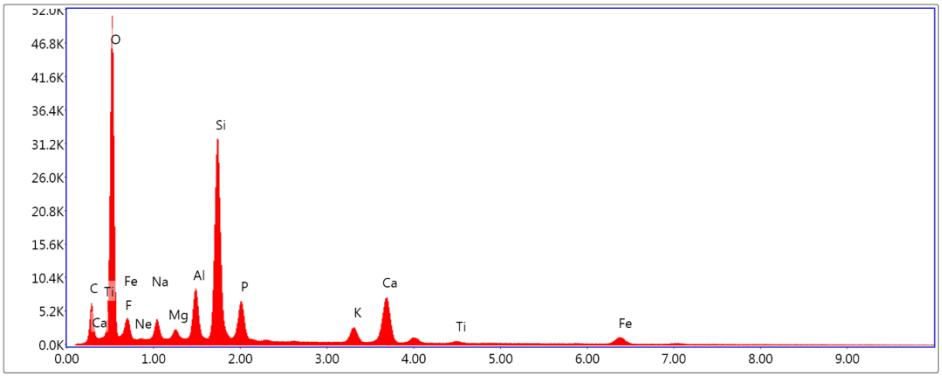

eZAF Smart Quant Results

Element	Weight %	Atomic %	Net Int.	Error %	Kratio	Z	R	A	F
C K	8.31	13.89	477.42	10.18	0.0178	1.1119	0.9500	0.1923	1.0000
O K	42.73	53.60	5666.18	8.49	0.1325	1.0597	0.9715	0.2925	1.0000
F K	4.02	4.25	397.52	10.79	0.0078	0.9833	0.9808	0.1962	1.0000
NeK	0.29	0.29	54.81	15.08	0.0008	1.0094	0.9893	0.2808	1.0000
NaK	2.67	2.33	436.62	8.07	0.0110	0.9580	0.9971	0.4276	1.0042
MgK	0.83	0.69	219.19	7.54	0.0047	0.9731	1.0045	0.5724	1.0077
AlK	4.02	2.99	1202.52	4.87	0.0268	0.9359	1.0113	0.7051	1.0119
SiK	15.91	11.36	5072.81	3.75	0.1198	0.9553	1.0177	0.7828	1.0077
P K	4.47	2.89	1104.27	4.35	0.0314	0.9165	1.0236	0.7597	1.0091
K K	2.30	1.18	452.64	3.85	0.0201	0.8808	1.0435	0.9504	1.0430
CaK	9.33	4.67	1488.19	2.66	0.0824	0.8959	1.0474	0.9639	1.0225
TiK	0.47	0.20	58.53	14.96	0.0038	0.8099	1.0538	0.9706	1.0432
FeK	4.65	1.67	276.77	5.13	0.0393	0.7901	1.0580	0.9988	1.0693

EDAX TEAM

Nathan Rabideaux 8 2017

Author: robert
Creation: 09/06/2017 11:05:33 AM

Sample Name: 14-NGIN-3

Area 3

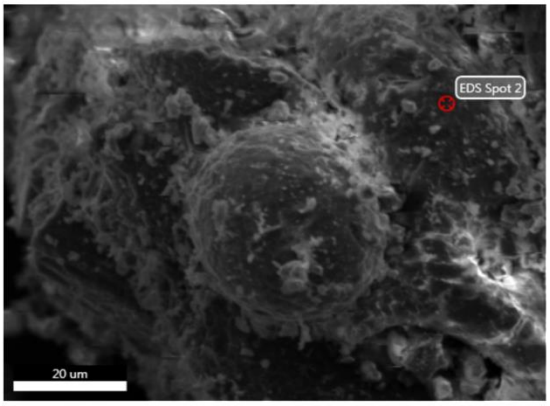

Notes:

EDAX TEAM

EDS Spot 2

kV: 15 Mag: 1436 Takeoff: 30.3 Live Time(s): 50 Amp Time(µs): 7.68 Resolution:(eV) 129.8

EDS Spot 2

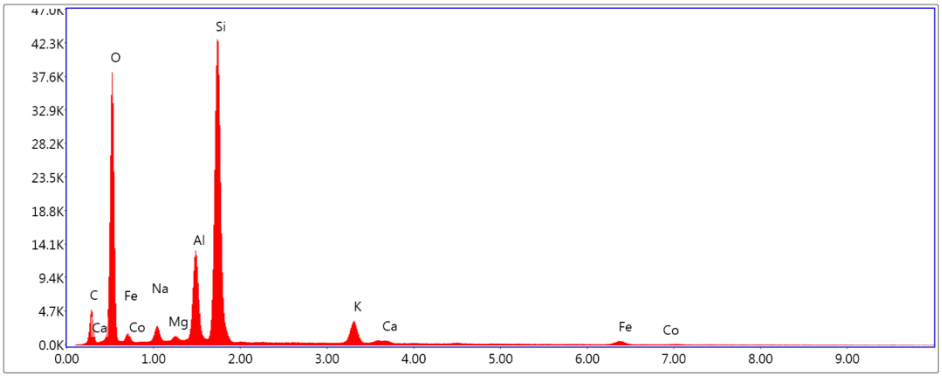

Lsec: 50.0 0 Cnts 0.000 keV Det: Element-C2 Det

eZAF Smart Quant Results

Element	Weight %	Atomic %	Net Int.	Error %	Kratio	Z	R	A	F
C K	11.31	18.39	368.92	10.67	0.0192	1.1028	0.9547	0.1540	1.0000
O K	40.63	49.58	4180.35	8.24	0.1368	1.0508	0.9759	0.3204	1.0000
NaK	1.89	1.60	254.26	7.96	0.0089	0.9496	1.0011	0.4958	1.0064
MgK	0.32	0.26	68.23	10.19	0.0020	0.9644	1.0083	0.6440	1.0122
AlK	8.29	6.00	1932.19	4.04	0.0603	0.9275	1.0150	0.7718	1.0164
SiK	29.84	20.74	6859.85	3.51	0.2268	0.9467	1.0212	0.8000	1.0038
K K	4.49	2.24	600.11	3.32	0.0373	0.8726	1.0463	0.9353	1.0181
CaK	0.46	0.22	51.16	9.96	0.0040	0.8874	1.0501	0.9460	1.0231
FeK	2.68	0.94	114.90	9.46	0.0228	0.7823	1.0599	1.0023	1.0871
CoK	0.09	0.03	3.05	59.20	0.0007	0.7616	1.0581	1.0038	1.1106

EDAX TEAM

Nathan Rabideaux 8 2017

Author: robert
Creation: 09/06/2017 9:18:48 AM

Sample Name: 14-OLT-1

Area 1

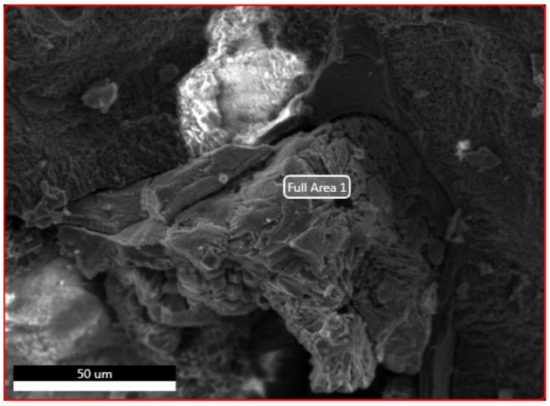

Notes:

EDAX TEAM

Full Area 1

kV: 15 Mag: 824 Takeoff: 28.7 Live Time(s): 50 Amp Time(µs): 7.68 Resolution:(eV) 129.8

Full Area 1

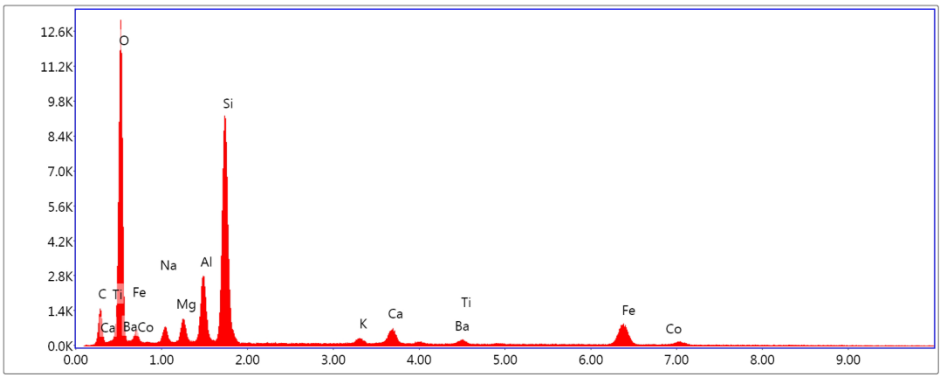

Lsec: 50.0 0 Cnts 0.000 keV Det: Element-C2 Det

eZAF Smart Quant Results

Element	Weight %	Atomic %	Net Int.	Error %	Kratio	Z	R	A	F
C K	9.28	16.69	120.69	11.29	0.0188	1.1365	0.9355	0.1779	1.0000
O K	36.75	49.62	1437.20	8.15	0.1379	1.0842	0.9580	0.3461	1.0000
NaK	2.35	2.21	86.19	10.15	0.0088	0.9812	0.9848	0.3786	1.0038
MgK	2.22	1.97	133.51	8.05	0.0115	0.9969	0.9926	0.5177	1.0066
AlK	6.05	4.85	416.77	5.90	0.0376	0.9591	0.9998	0.6413	1.0095
SiK	20.01	15.39	1478.76	4.59	0.1410	0.9792	1.0066	0.7161	1.0047
K K	0.93	0.51	45.65	11.73	0.0082	0.9039	1.0343	0.9342	1.0379
CaK	3.16	1.70	129.92	5.46	0.0289	0.9195	1.0387	0.9559	1.0411
BaL	1.80	0.28	21.65	35.76	0.0135	0.6396	1.2115	1.0686	1.0970
TiK	0.52	0.23	17.22	20.59	0.0045	0.8317	1.0459	0.9785	1.0781
FeK	15.72	6.08	235.36	4.11	0.1340	0.8123	1.0522	0.9997	1.0497
CoK	1.21	0.44	14.48	28.00	0.0102	0.7912	1.0512	1.0005	1.0607

EDAX TEAM

Nathan Rabideaux 8 2017

Author: robert
Creation: 09/06/2017 9:23:35 AM

Sample Name: 14-OLT-1

Area 2

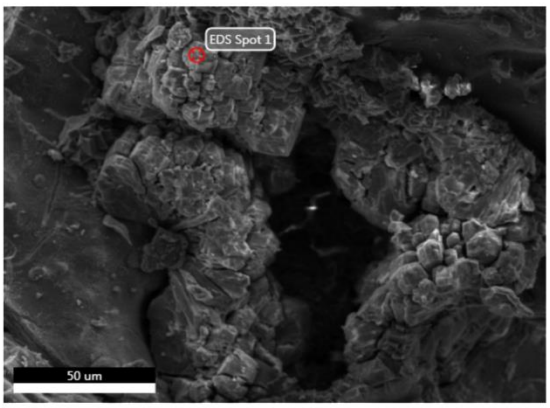

Notes:

EDAX TEAM

EDS Spot 1

kV: 15	Mag: 721	Takeoff: 28.9	Live Time(s): 50	Amp Time(µs): 7.68	Resolution:(eV) 129.8

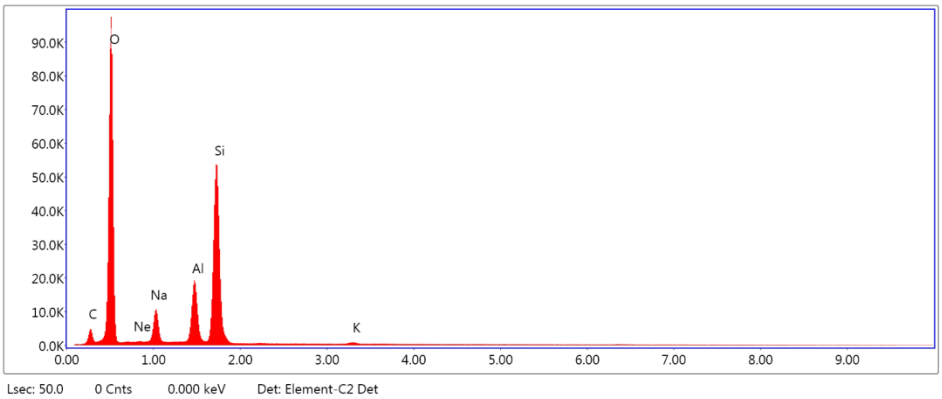

eZAF Smart Quant Results

Element	Weight %	Atomic %	Net Int.	Error %	Kratio	Z	R	A	F
C K	5.86	9.18	284.84	11.04	0.0100	1.0925	0.9624	0.1565	1.0000
O K	52.19	61.40	10870.54	6.98	0.2364	1.0403	0.9830	0.4355	1.0000
NeK	0.54	0.51	126.46	11.20	0.0018	0.9903	1.0000	0.3257	1.0000
NaK	6.76	5.54	1338.25	6.94	0.0309	0.9396	1.0075	0.4844	1.0056
AlK	8.44	5.89	2807.66	4.37	0.0575	0.9175	1.0209	0.7322	1.0138
SiK	25.79	17.29	8604.44	3.79	0.1863	0.9363	1.0269	0.7694	1.0028
K K	0.42	0.20	84.99	9.40	0.0035	0.8625	1.0509	0.9374	1.0179

EDAX TEAM

Nathan Rabideaux 8 2017

Author: robert
Creation: 09/06/2017 9:24:46 AM

Sample Name: 14-OLT-1

Area 2

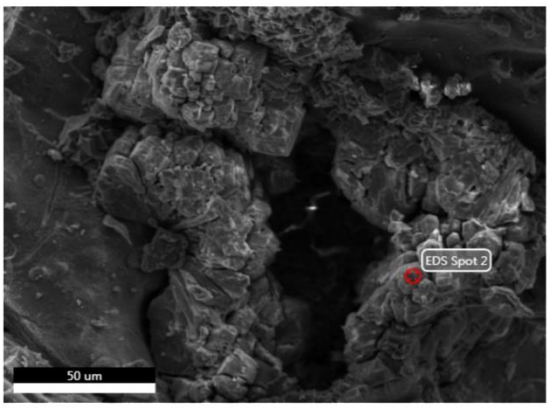

Notes:

EDAX TEAM

EDS Spot 2

kV: 15 Mag: 721 Takeoff: 28.9 Live Time(s): 50 Amp Time(µs): 7.68 Resolution:(eV) 129.8

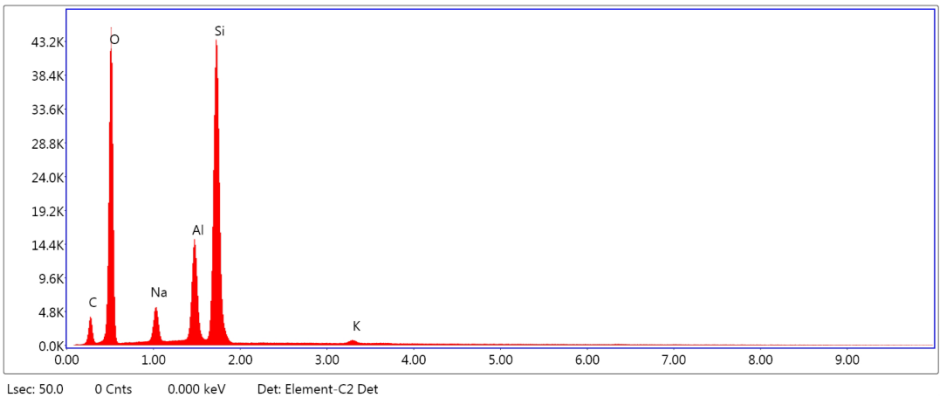

eZAF Smart Quant Results

Element	Weight %	Atomic %	Net Int.	Error %	Kratio	Z	R	A	F
C K	9.66	15.33	276.47	11.20	0.0150	1.0957	0.9600	0.1421	1.0000
O K	43.95	52.35	4959.20	7.79	0.1668	1.0435	0.9809	0.3638	1.0000
NaK	4.72	3.92	645.38	6.82	0.0231	0.9426	1.0055	0.5150	1.0068
AlK	9.71	6.86	2208.85	4.04	0.0700	0.9205	1.0191	0.7696	1.0166
SiK	31.22	21.19	6899.60	3.64	0.2311	0.9395	1.0252	0.7857	1.0027
K K	0.72	0.35	94.32	7.30	0.0059	0.8656	1.0495	0.9285	1.0166

EDAX TEAM

Nathan Rabideaux 8 2017

Author: robert
Creation: 09/06/2017 9:28:42 AM

Sample Name: 14-OLT-1

Area 3

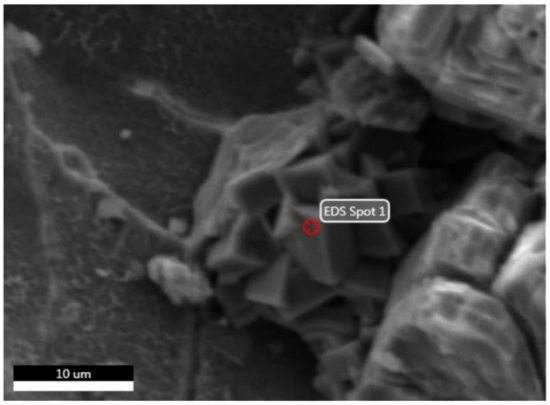

Notes:

EDAX TEAM

EDS Spot 1

kV: 15 Mag: 3046 Takeoff: 29 Live Time(s): 50 Amp Time(µs): 7.68 Resolution:(eV) 129.8

EDS Spot 1

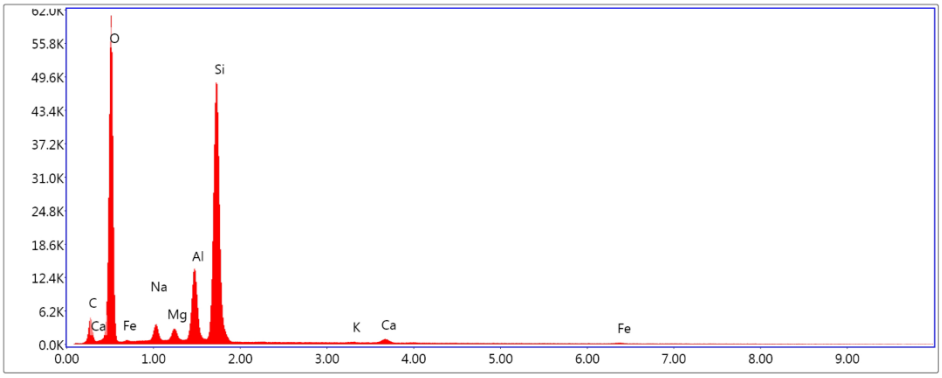

Lsec: 50.0 0 Cnts 0.000 keV Det: Element-C2 Det

eZAF Smart Quant Results

Element	Weight %	Atomic %	Net Int.	Error %	Kratio	Z	R	A	F
C K	9.46	14.80	349.46	10.99	0.0157	1.0919	0.9608	0.1523	1.0000
O K	48.14	56.56	6730.70	7.62	0.1877	1.0399	0.9816	0.3749	1.0000
NaK	2.50	2.05	389.93	7.52	0.0116	0.9393	1.0062	0.4893	1.0066
MgK	1.30	1.01	316.63	6.17	0.0080	0.9539	1.0132	0.6341	1.0120
AlK	7.68	5.35	2058.86	4.20	0.0541	0.9173	1.0197	0.7557	1.0162
SiK	29.08	19.46	7779.67	3.57	0.2163	0.9361	1.0257	0.7921	1.0029
K K	0.13	0.06	20.73	27.67	0.0011	0.8625	1.0500	0.9351	1.0207
CaK	1.05	0.49	139.93	6.75	0.0091	0.8771	1.0536	0.9594	1.0234
FeK	0.65	0.22	33.81	20.23	0.0056	0.7728	1.0621	1.0053	1.1127

EDAX TEAM

Nathan Rabideaux 8 2017

Author: robert
Creation: 09/06/2017 9:31:53 AM

Sample Name: 14-OLT-1

Area 4

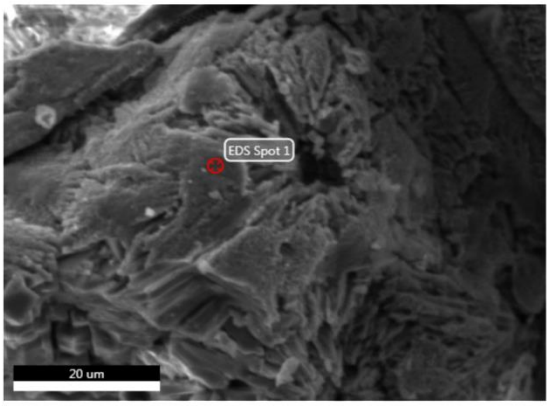

Notes:

EDAX TEAM

EDS Spot 1

kV: 15 Mag: 1860 Takeoff: 28.8 Live Time(s): 50 Amp Time(µs): 7.68 Resolution:(eV) 129.8

EDS Spot 1

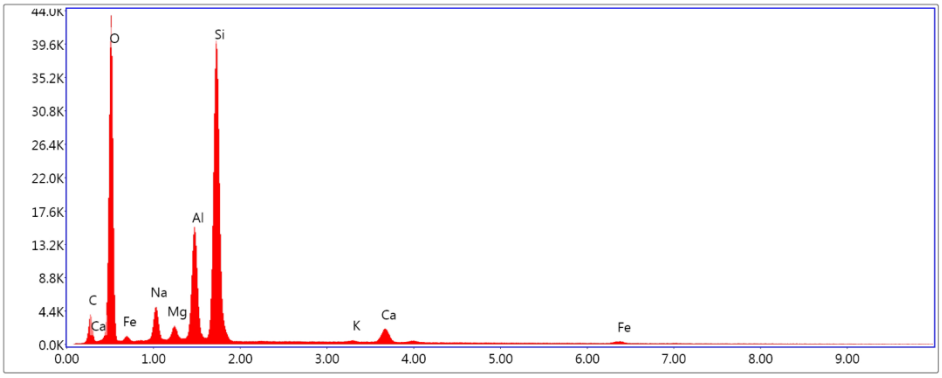

Lsec: 50.0 0 Cnts 0.000 keV Det: Element-C2 Det

eZAF Smart Quant Results

Element	Weight %	Atomic %	Net Int.	Error %	Kratio	Z	R	A	F
C K	8.20	13.39	250.99	11.20	0.0133	1.1026	0.9559	0.1473	1.0000
O K	43.07	52.81	4714.31	8.02	0.1544	1.0504	0.9770	0.3414	1.0000
NaK	4.10	3.50	553.84	7.22	0.0193	0.9492	1.0021	0.4922	1.0063
MgK	1.15	0.92	235.62	7.03	0.0069	0.9640	1.0093	0.6220	1.0116
AlK	9.99	7.27	2274.18	4.27	0.0701	0.9270	1.0159	0.7454	1.0144
SiK	28.34	19.80	6332.55	3.85	0.2062	0.9462	1.0221	0.7665	1.0033
K K	0.29	0.15	40.17	16.54	0.0025	0.8720	1.0471	0.9300	1.0258
CaK	3.28	1.61	373.47	3.88	0.0284	0.8868	1.0508	0.9551	1.0222
FeK	1.58	0.55	69.65	10.52	0.0135	0.7816	1.0603	1.0028	1.0954

EDAX TEAM

Nathan Rabideaux 8 2017

Author: robert
Creation: 09/06/2017 9:35:25 AM

Sample Name: 14-OLT-1

Area 5

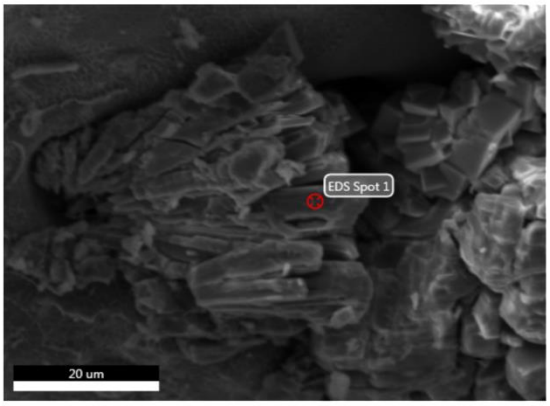

Notes:

EDAX TEAM

EDS Spot 1

kV: 15	Mag: 1849	Takeoff: 29	Live Time(s): 50	Amp Time(µs): 7.68	Resolution:(eV) 129.8

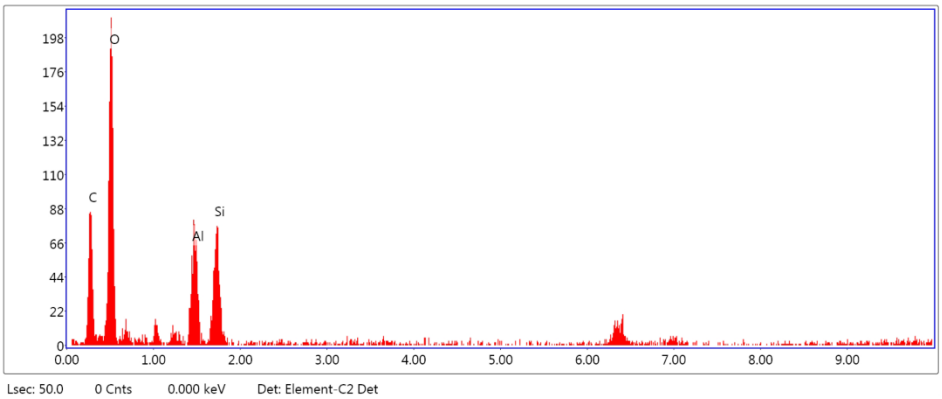

eZAF Smart Quant Results

Element	Weight %	Atomic %	Net Int.	Error %	Kratio	Z	R	A	F
C K	31.98	41.59	9.15	14.46	0.0880	1.0547	0.9776	0.2609	1.0000
O K	48.41	47.28	24.62	11.75	0.1467	1.0033	0.9970	0.3020	1.0000
AlK	9.66	5.59	11.99	8.86	0.0673	0.8838	1.0323	0.7830	1.0079
SiK	9.96	5.54	12.10	9.19	0.0719	0.9018	1.0378	0.7978	1.0036

EDAX TEAM

Nathan Rabideaux 8 2017

Author: robert
Creation: 09/06/2017 9:44:04 AM

Sample Name: 14-OLT-1

Area 7

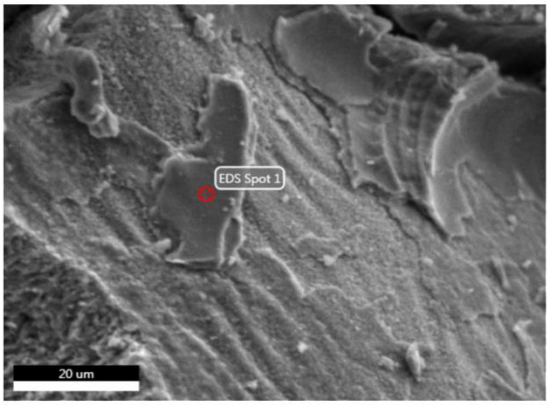

Notes:

EDAX TEAM

EDS Spot 1

kV: 15 Mag: 1597 Takeoff: 28.9 Live Time(s): 50 Amp Time(µs): 7.68 Resolution:(eV) 129.8

EDS Spot 1

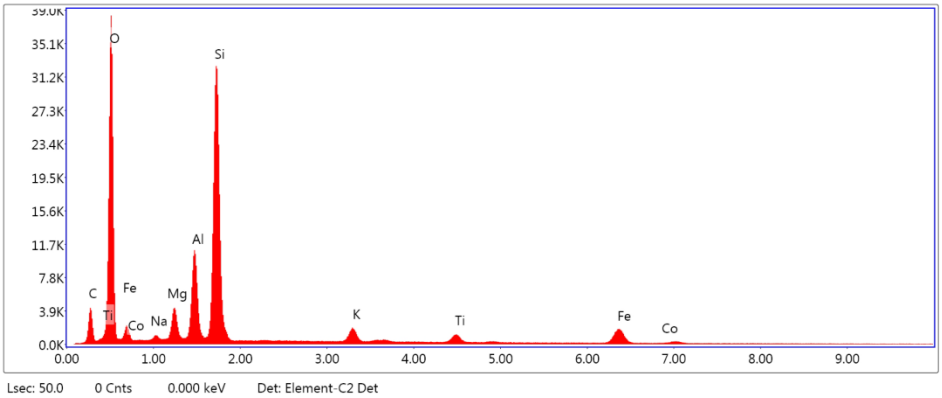

eZAF Smart Quant Results

Element	Weight %	Atomic %	Net Int.	Error %	Kratio	Z	R	A	F
C K	9.00	15.54	293.88	10.98	0.0163	1.1217	0.9447	0.1612	1.0000
O K	39.62	51.34	4182.88	8.07	0.1432	1.0695	0.9666	0.3380	1.0000
NaK	0.39	0.35	43.04	15.13	0.0016	0.9672	0.9926	0.4165	1.0049
MgK	2.71	2.31	501.18	6.57	0.0155	0.9825	1.0001	0.5762	1.0085
AlK	7.65	5.88	1569.98	4.89	0.0506	0.9451	1.0071	0.6921	1.0117
SiK	24.50	18.09	5189.03	4.10	0.1769	0.9648	1.0136	0.7451	1.0042
K K	2.34	1.24	312.43	4.01	0.0200	0.8899	1.0402	0.9325	1.0284
TiK	2.30	1.00	209.07	4.93	0.0198	0.8184	1.0510	0.9822	1.0678
FeK	11.06	4.10	460.04	3.80	0.0937	0.7988	1.0559	1.0019	1.0586
CoK	0.44	0.16	14.79	34.38	0.0037	0.7778	1.0546	1.0028	1.0732

EDAX TEAM

Nathan Rabideaux 8 2017

Author: robert
Creation: 09/06/2017 9:45:11 AM

Sample Name: 14-OLT-1

Area 7

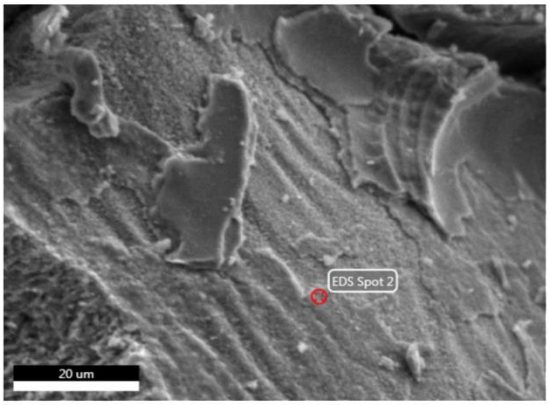

Notes:

EDAX TEAM

EDS Spot 2

kV: 15 Mag: 1597 Takeoff: 28.9 Live Time(s): 50 Amp Time(µs): 7.68 Resolution:(eV) 129.8

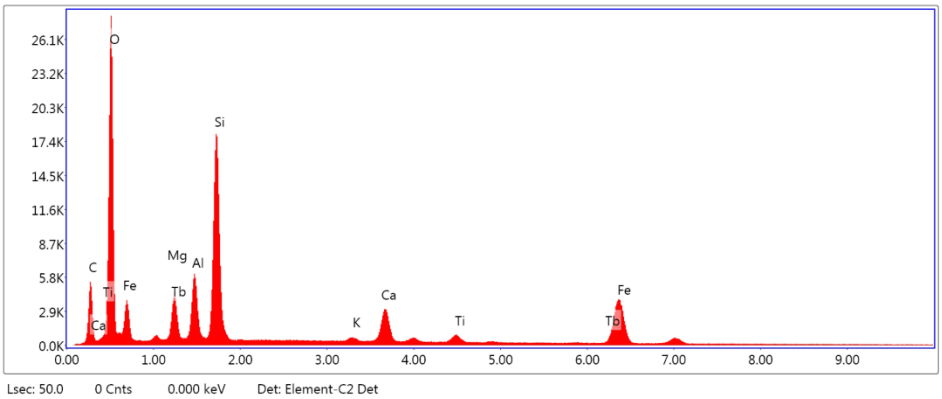

eZAF Smart Quant Results

Element	Weight %	Atomic %	Net Int.	Error %	Kratio	Z	R	A	F
C K	10.54	20.50	433.38	10.10	0.0250	1.1653	0.9178	0.2038	1.0000
O K	31.72	46.33	3066.15	8.38	0.1095	1.1129	0.9412	0.3101	1.0000
MgK	2.35	2.26	373.12	7.55	0.0120	1.0248	0.9775	0.4960	1.0048
AlK	4.60	3.98	799.99	6.17	0.0269	0.9862	0.9852	0.5884	1.0073
SiK	14.67	12.21	2818.72	4.91	0.1002	1.0073	0.9924	0.6741	1.0056
K K	0.52	0.31	70.74	12.69	0.0047	0.9311	1.0225	0.9297	1.0491
CaK	5.29	3.08	605.16	3.38	0.0502	0.9475	1.0273	0.9533	1.0504
TiK	1.69	0.83	157.17	5.71	0.0155	0.8574	1.0356	0.9718	1.0980
TbL	5.41	0.80	103.55	12.73	0.0372	0.6175	1.1643	1.0497	1.0601
FeK	23.21	9.71	960.75	3.13	0.2040	0.8388	1.0443	0.9980	1.0499

EDAX TEAM

Nathan Rabideaux 8 2017

Author: robert
Creation: 09/06/2017 9:55:02 AM

Sample Name: 14-OLT-1

Area 8

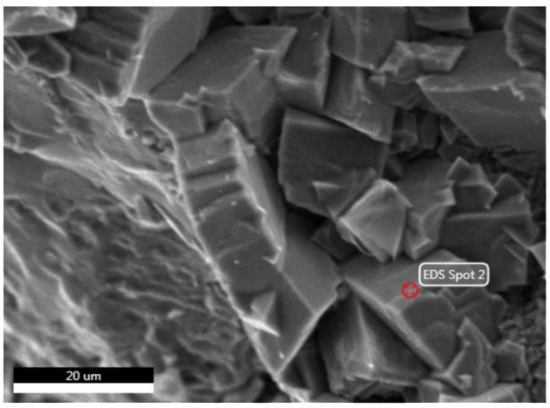

Notes:

EDAX TEAM

EDS Spot 2

kV: 15 Mag: 1781 Takeoff: 30.2 Live Time(s): 50 Amp Time(µs): 7.68 Resolution:(eV) 129.8

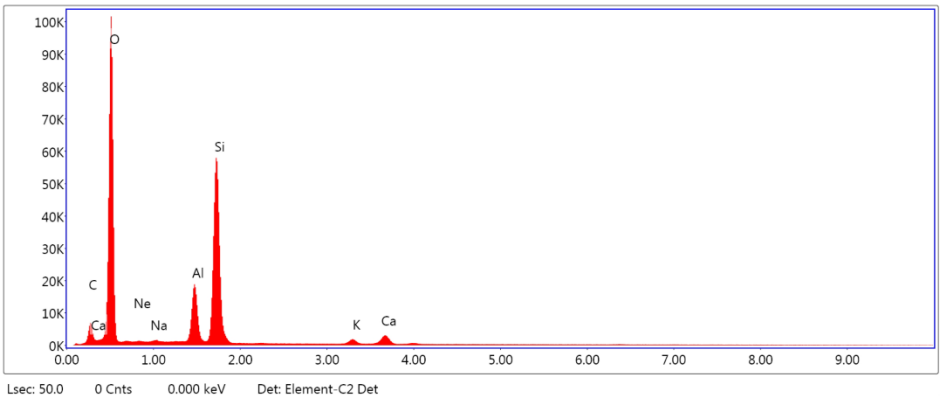

eZAF Smart Quant Results

Element	Weight %	Atomic %	Net Int.	Error %	Kratio	Z	R	A	F
C K	7.42	11.46	455.43	10.39	0.0142	1.0880	0.9620	0.1758	1.0000
O K	55.49	64.36	11369.32	7.47	0.2223	1.0361	0.9827	0.3867	1.0000
NeK	0.80	0.74	193.74	9.89	0.0024	0.9863	0.9997	0.3081	1.0000
NaK	0.58	0.47	119.40	9.77	0.0025	0.9358	1.0072	0.4620	1.0058
AlK	7.23	4.97	2736.05	4.09	0.0510	0.9138	1.0206	0.7611	1.0149
SiK	24.31	16.06	9240.42	3.47	0.1824	0.9326	1.0266	0.8016	1.0037
K K	1.19	0.56	267.53	4.88	0.0099	0.8592	1.0507	0.9485	1.0256
CaK	2.99	1.38	557.29	3.27	0.0258	0.8737	1.0543	0.9661	1.0213

EDAX TEAM

Nathan Rabideaux 8 2017

Author: robert
Creation: 09/06/2017 9:55:02 AM

Sample Name: 14-OLT-1

Area 8

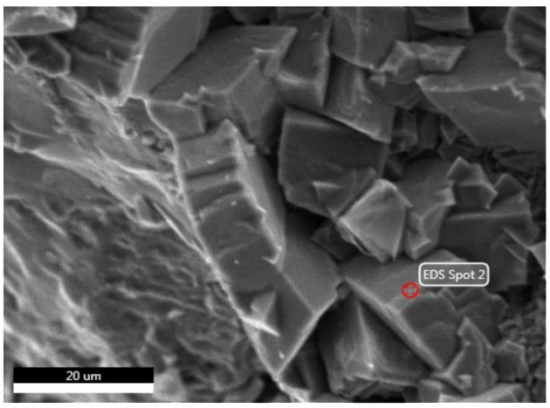

Notes:

EDAX TEAM

EDS Spot 2

kV: 15 Mag: 1781 Takeoff: 30.2 Live Time(s): 50 Amp Time(µs): 7.68 Resolution:(eV) 129.8

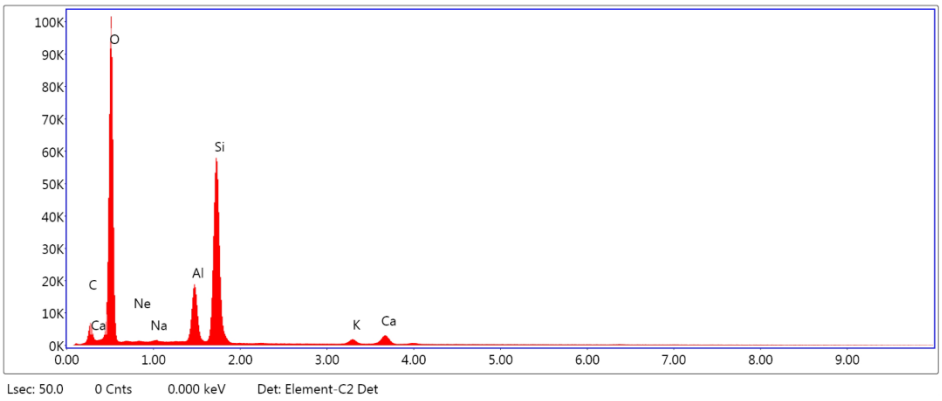

eZAF Smart Quant Results

Element	Weight %	Atomic %	Net Int.	Error %	Kratio	Z	R	A	F
C K	7.42	11.46	455.43	10.39	0.0142	1.0880	0.9620	0.1758	1.0000
O K	55.49	64.36	11369.32	7.47	0.2223	1.0361	0.9827	0.3867	1.0000
NeK	0.80	0.74	193.74	9.89	0.0024	0.9863	0.9997	0.3081	1.0000
NaK	0.58	0.47	119.40	9.77	0.0025	0.9358	1.0072	0.4620	1.0058
AlK	7.23	4.97	2736.05	4.09	0.0510	0.9138	1.0206	0.7611	1.0149
SiK	24.31	16.06	9240.42	3.47	0.1824	0.9326	1.0266	0.8016	1.0037
K K	1.19	0.56	267.53	4.88	0.0099	0.8592	1.0507	0.9485	1.0256
CaK	2.99	1.38	557.29	3.27	0.0258	0.8737	1.0543	0.9661	1.0213

EDAX TEAM

Nathan Rabideaux 8 2017

Author: robert
Creation: 09/06/2017 9:55:56 AM

Sample Name: 14-OLT-1

Area 8

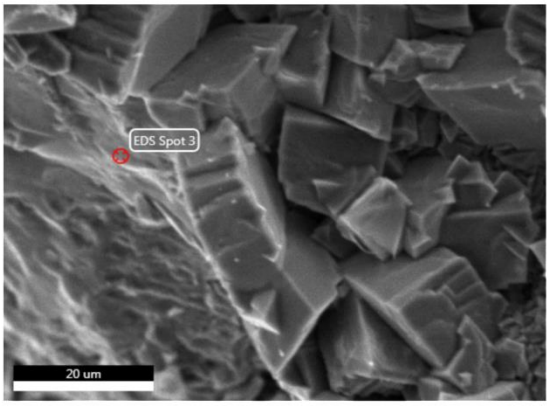

Notes:

EDAX TEAM

EDS Spot 3

kV: 15 Mag: 1781 Takeoff: 30.2 Live Time(s): 50 Amp Time(µs): 7.68 Resolution:(eV) 129.8

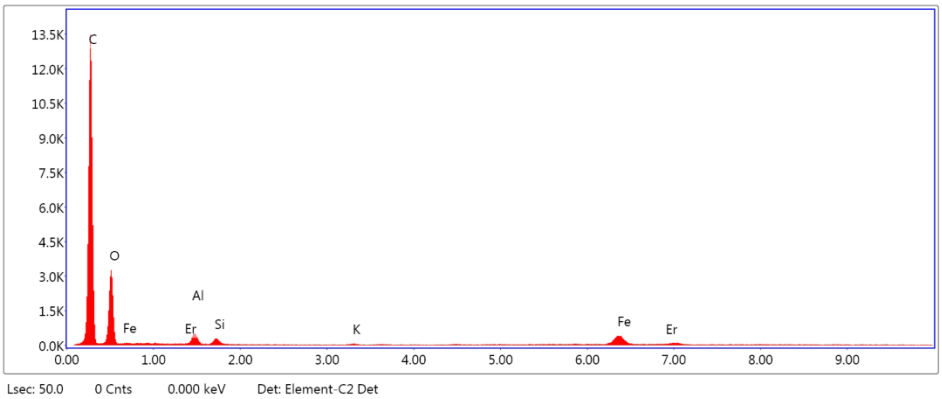

eZAF Smart Quant Results

Element	Weight %	Atomic %	Net Int.	Error %	Kratio	Z	R	A	F
C K	57.94	72.82	1403.07	6.57	0.3088	1.0652	0.9632	0.5003	1.0000
O K	23.93	22.58	371.43	9.87	0.0513	1.0147	0.9838	0.2112	1.0000
AlK	1.25	0.70	59.81	7.37	0.0079	0.8960	1.0215	0.6980	1.0043
SiK	0.68	0.36	35.46	8.16	0.0049	0.9146	1.0275	0.7931	1.0063
K K	0.16	0.06	5.40	39.43	0.0014	0.8437	1.0514	0.9915	1.0506
FeK	11.29	3.05	111.80	5.65	0.0935	0.7571	1.0630	1.0128	1.0810
ErL	4.75	0.43	16.37	31.07	0.0294	0.5348	1.1542	1.0515	1.0994

EDAX TEAM

Nathan Rabideaux 8 2017

Author: robert
Creation: 09/06/2017 10:02:23 AM

Sample Name: 15-ODN-G

Area 1

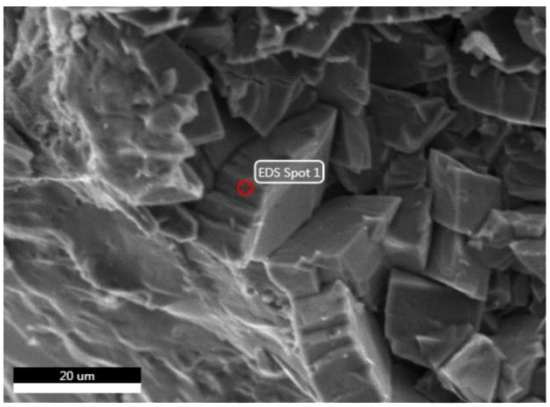

Notes:

EDAX TEAM

EDS Spot 1

kV: 15 Mag: 1619 Takeoff: 30.2 Live Time(s): 50 Amp Time(µs): 7.68 Resolution:(eV) 129.8

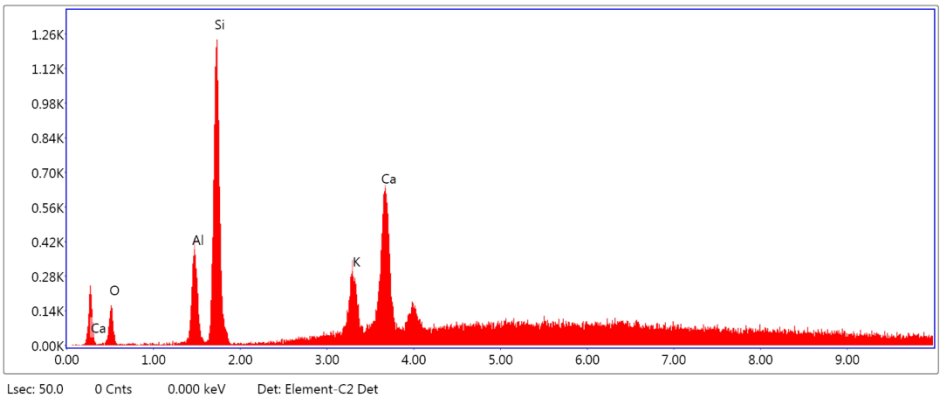

eZAF Smart Quant Results

Element	Weight %	Atomic %	Net Int.	Error %	Kratio	Z	R	A	F
O K	13.35	24.50	16.86	14.18	0.0196	1.1259	0.9362	0.1308	1.0000
AlK	8.35	9.09	58.02	6.17	0.0645	0.9973	0.9808	0.7617	1.0164
SiK	28.19	29.48	195.11	4.59	0.2295	1.0185	0.9881	0.7919	1.0095
K K	11.78	8.84	49.94	8.91	0.1105	0.9409	1.0188	0.9341	1.0674
CaK	38.34	28.09	124.17	4.79	0.3421	0.9573	1.0238	0.9229	1.0100

EDAX TEAM

Nathan Rabideaux 8 2017

Author: robert
Creation: 09/06/2017 10:03:17 AM

Sample Name: 15-ODN-G

Area 1

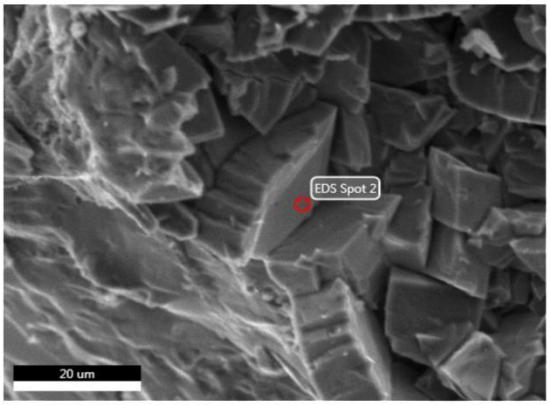

Notes:

EDAX TEAM

EDS Spot 2

kV: 15 Mag: 1619 Takeoff: 30.2 Live Time(s): 50 Amp Time(µs): 7.68 Resolution:(eV) 129.8

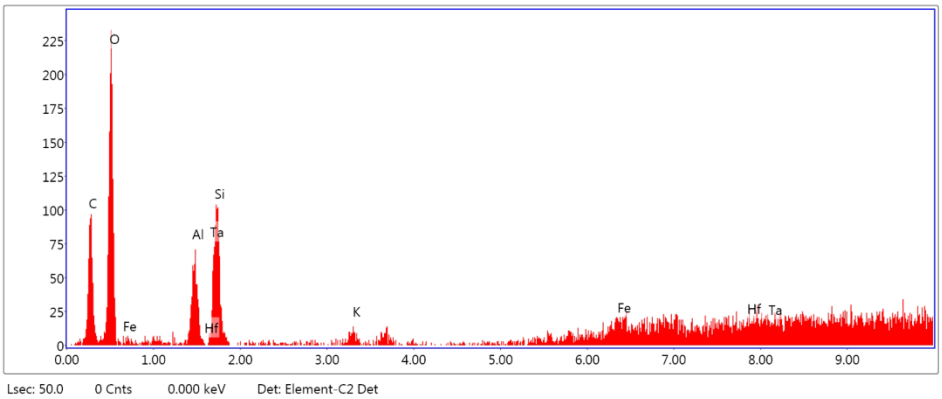

eZAF Smart Quant Results

Element	Weight %	Atomic %	Net Int.	Error %	Kratio	Z	R	A	F
C K	8.55	32.84	10.66	14.73	0.0278	1.4646	0.7753	0.2220	1.0000
O K	10.63	30.66	25.53	11.52	0.0418	1.4019	0.7990	0.2805	1.0000
AlK	1.87	3.19	9.97	10.88	0.0156	1.2517	0.8496	0.6644	1.0028
TaM	0.87	0.22	1.83	28.86	0.0065	0.8239	1.1636	0.7866	1.1668
SiK	3.95	6.50	14.54	11.73	0.0240	1.2805	0.8588	0.4728	1.0036
K K	0.71	0.84	2.13	18.82	0.0066	1.1953	0.9017	0.7578	1.0266
FeK	11.91	9.84	14.96	7.83	0.1484	1.1045	0.9565	0.9618	1.1733
HfL	61.53	15.91	16.72	6.03	0.5142	0.7652	1.0516	1.0130	1.0781

EDAX TEAM

Nathan Rabideaux 8 2017

Author: robert
Creation: 09/06/2017 10:08:31 AM

Sample Name: 15-ODN-G

Area 2

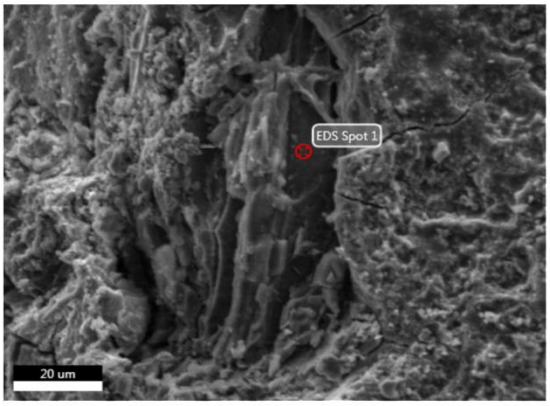

Notes:

EDAX TEAM

EDS Spot 1

kV: 15 Mag: 1128 Takeoff: 30.3 Live Time(s): 50 Amp Time(µs): 7.68 Resolution:(eV) 129.8

EDS Spot 1

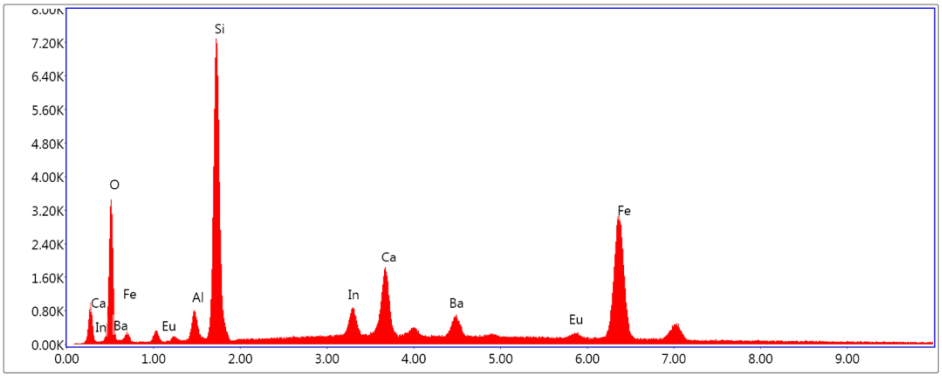

Lsec: 50.0 0 Cnts 0.000 keV Det: Element-C2 Det

eZAF Smart Quant Results

Element	Weight %	Atomic %	Net Int.	Error %	Kratio	Z	R	A	F
O K	8.25	22.75	367.79	9.02	0.0326	1.2740	0.8652	0.3107	1.0000
AlK	1.47	2.41	93.15	9.23	0.0079	1.1348	0.9151	0.4694	1.0065
SiK	15.28	24.01	1160.01	5.99	0.1040	1.1601	0.9237	0.5831	1.0063
InL	5.64	2.17	165.11	4.74	0.0494	0.8276	1.1289	1.0045	1.0540
CaK	7.10	7.81	357.33	3.78	0.0751	1.0978	0.9688	0.9231	1.0439
BaL	10.97	3.52	157.60	6.79	0.0926	0.7675	1.1405	1.0210	1.0776
EuL	6.36	1.85	61.32	15.97	0.0525	0.7473	1.1306	1.0199	1.0837
FeK	44.93	35.49	819.48	3.32	0.4411	0.9819	1.0018	0.9695	1.0314

EDAX TEAM

Nathan 10 11 2017

Author: Robert
Creation: 10/17/2017 2:02:48 PM

Sample Name: 14-MAG-2

Area 1

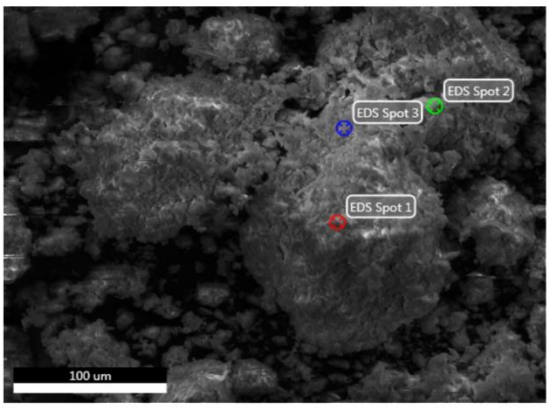

Notes:

EDAX TEAM

EDS Spot 1

kV: 15 Mag: 779 Takeoff: 30.5 Live Time(s): 50 Amp Time(µs): 0.24 Resolution:(eV) 155.9

EDS Spot 1

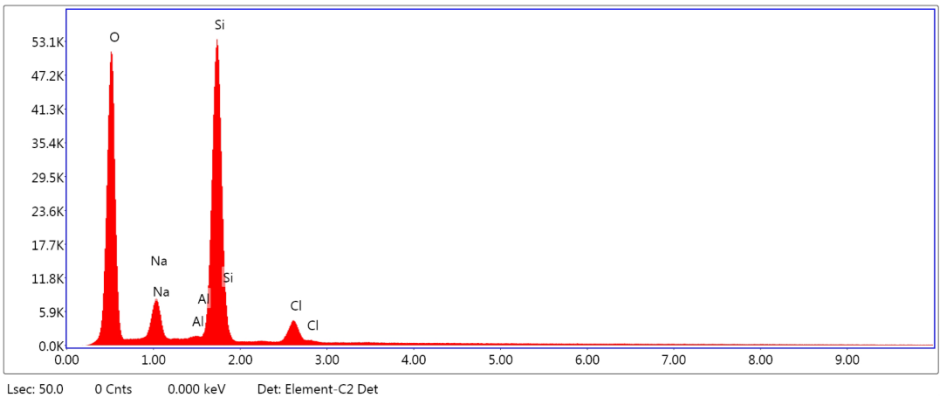

eZAF Smart Quant Results

Element	Weight %	Atomic %	Net Int.	Error %	Kratio	Z	R	A	F
O K	50.64	63.85	11048.19	6.99	0.2326	1.0528	0.9771	0.4363	1.0000
NaK	8.31	7.29	1779.72	6.69	0.0403	0.9513	1.0021	0.5068	1.0065
AlK	0.45	0.33	155.27	7.90	0.0031	0.9290	1.0160	0.7361	1.0231
SiK	36.35	26.11	13526.63	3.12	0.2885	0.9482	1.0222	0.8337	1.0036
ClK	4.25	2.42	1029.23	3.81	0.0316	0.8801	1.0383	0.8380	1.0080

EDAX TEAM

EDS Spot 2

kV: 15 Mag: 779 Takeoff: 30.5 Live Time(s): 50 Amp Time(µs): 0.24 Resolution:(eV) 155.9

EDS Spot 2

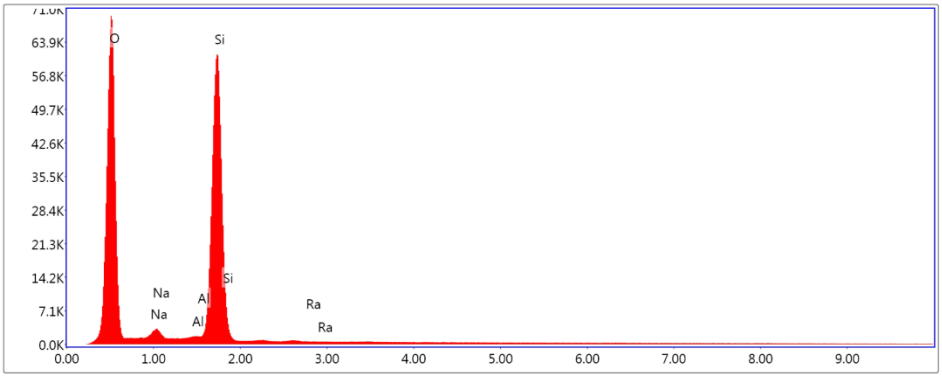

Lsec: 50.0 0 Cnts 0.000 keV Det: Element-C2 Det

eZAF Smart Quant Results

Element	Weight %	Atomic %	Net Int.	Error %	Kratio	Z	R	A	F
O K	58.23	70.73	15010.17	6.44	0.2963	1.0421	0.9803	0.4883	1.0000
NaK	2.56	2.16	547.47	7.70	0.0116	0.9414	1.0050	0.4798	1.0073
AlK	0.30	0.21	111.99	9.45	0.0021	0.9193	1.0186	0.7595	1.0261
SiK	38.87	26.89	15624.37	2.90	0.3124	0.9382	1.0247	0.8545	1.0025
RaM	0.05	0.00	6.73	29.40	0.0004	0.5619	1.4111	1.1362	1.3540

EDS Spot 3

kV: 15 Mag: 779 Takeoff: 30.5 Live Time(s): 50 Amp Time(µs): 0.24 Resolution:(eV) 155.9

EDS Spot 3

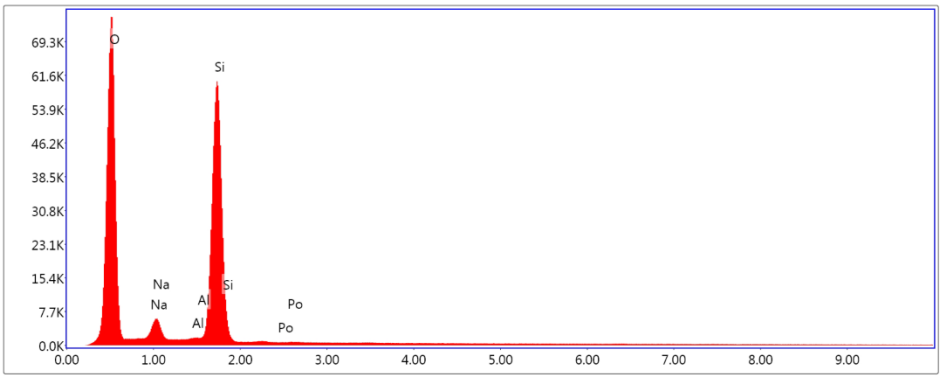

Lsec: 50.0 0 Cnts 0.000 keV Det: Element-C2 Det

eZAF Smart Quant Results

Element	Weight %	Atomic %	Net Int.	Error %	Kratio	Z	R	A	F
O K	57.84	70.05	16365.05	6.30	0.3022	1.0424	0.9809	0.5013	1.0000
NaK	5.66	4.77	1306.79	7.05	0.0260	0.9416	1.0056	0.4839	1.0065
AlK	0.33	0.23	128.54	8.71	0.0023	0.9195	1.0191	0.7399	1.0233
SiK	36.15	24.94	15244.58	3.07	0.2852	0.9384	1.0252	0.8385	1.0026
PoM	0.02	0.00	3.39	34.25	0.0002	0.5853	1.4066	1.1014	1.2628

EDAX TEAM

Nathan 10 11 2017

Author: Robert
Creation: 10/17/2017 2:08:33 PM

Sample Name: 14-MAG-2

Area 2

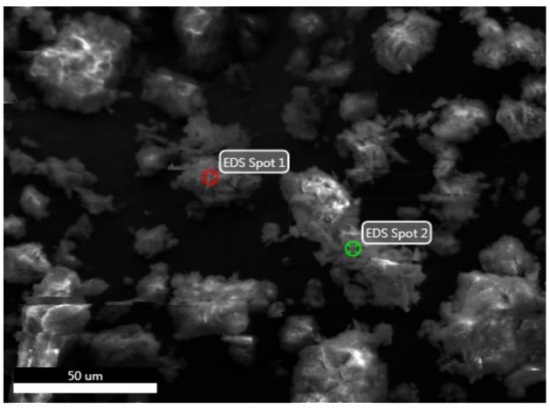

Notes:

EDAX TEAM

EDS Spot 1

kV: 15 Mag: 1456 Takeoff: 30.5 Live Time(s): 50 Amp Time(µs): 0.24 Resolution:(eV) 155.9

EDS Spot 1

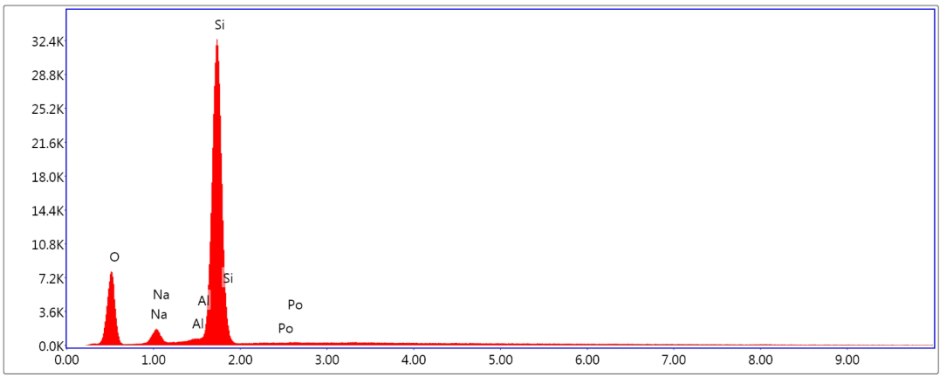

Lsec: 50.0 0 Cnts 0.000 keV Det: Element-C2 Det

eZAF Smart Quant Results

Element	Weight %	Atomic %	Net Int.	Error %	Kratio	Z	R	A	F
O K	29.14	41.77	1412.61	8.36	0.1047	1.0736	0.9657	0.3349	1.0000
NaK	1.97	1.97	146.34	8.57	0.0117	0.9707	0.9918	0.6008	1.0138
AlK	0.00	0.00	0.02	99.99	0.0000	0.9483	1.0063	0.8461	1.0507
SiK	68.89	56.26	8197.40	2.28	0.6151	0.9680	1.0129	0.9208	1.0020
PoM	0.00	0.00	0.00	70.50	0.0000	0.6040	1.3918	0.9853	1.2083

EDAX TEAM

EDS Spot 2

kV: 15 Mag: 1456 Takeoff: 30.5 Live Time(s): 50 Amp Time(µs): 0.24 Resolution:(eV) 155.9

EDS Spot 2

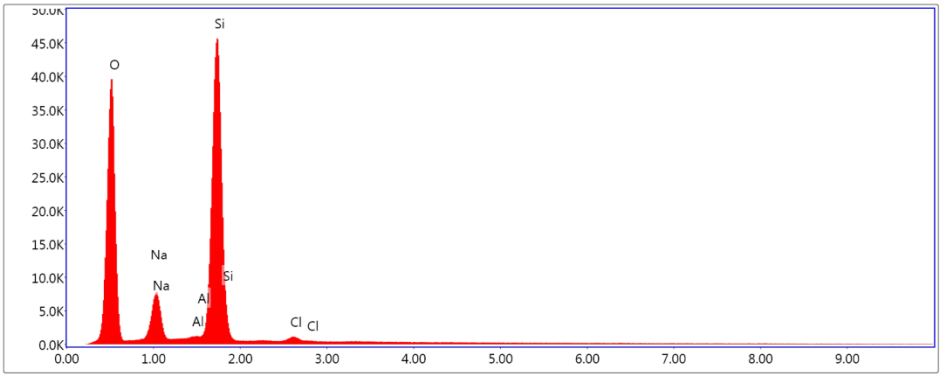

Lsec: 50.0 0 Cnts 0.000 keV Det: Element-C2 Det

eZAF Smart Quant Results

Element	Weight %	Atomic %	Net Int.	Error %	Kratio	Z	R	A	F
O K	48.50	61.44	8360.90	6.88	0.2294	1.0529	0.9770	0.4493	1.0000
NaK	9.55	8.42	1615.20	6.57	0.0477	0.9513	1.0021	0.5213	1.0070
AlK	0.25	0.19	66.43	12.31	0.0017	0.9291	1.0159	0.7368	1.0250
SiK	40.82	29.45	11673.81	3.11	0.3243	0.9482	1.0221	0.8356	1.0026
ClK	0.89	0.51	162.04	8.68	0.0065	0.8801	1.0383	0.8231	1.0082

EDAX TEAM

Nathan Oct 3 2017

Author: Robert
Creation: 10/04/2017 10:28:32 AM

Sample Name: 14-TLB-1

Area 4

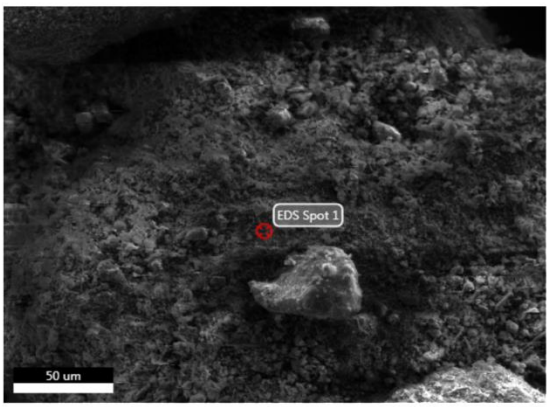

Notes:

EDAX TEAM

EDS Spot 1

kV: 15 Mag: 507 Takeoff: 30.2 Live Time(s): 50 Amp Time(µs): 7.68 Resolution:(eV) 129.8

EDS Spot 1

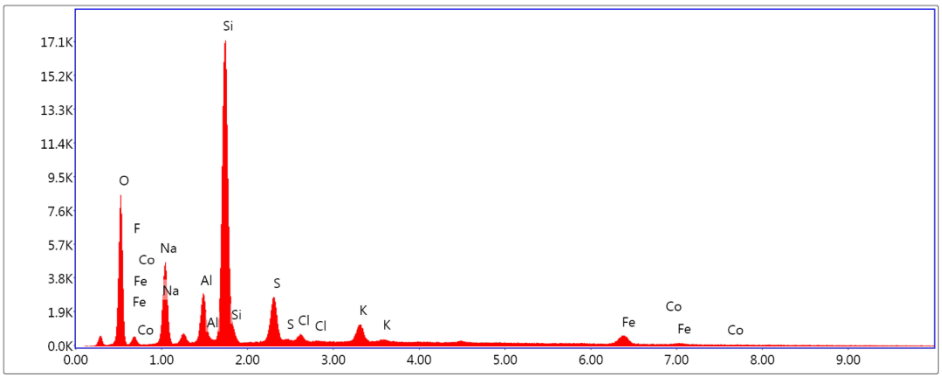

Lsec: 50.0 0 Cnts 0.000 keV Det: Element-C2 Det

eZAF Smart Quant Results

Element	Weight %	Atomic %	Net Int.	Error %	Kratio	Z	R	A	F
O K	24.08	37.43	803.82	8.69	0.0845	1.1032	0.9538	0.3183	1.0000
F K	0.00	0.00	0.02	99.99	0.0000	1.0240	0.9635	0.2894	1.0000
NaK	10.88	11.77	478.28	7.41	0.0540	0.9983	0.9809	0.4945	1.0054
AlK	4.31	3.98	299.20	5.88	0.0300	0.9758	0.9961	0.7009	1.0172
SiK	36.72	32.51	2682.41	3.90	0.2849	0.9962	1.0030	0.7744	1.0056
S K	7.83	6.07	414.35	5.45	0.0565	0.9738	1.0155	0.7344	1.0087
ClK	0.88	0.62	42.37	10.88	0.0065	0.9256	1.0212	0.7805	1.0128
K K	4.34	2.76	181.09	5.79	0.0362	0.9194	1.0314	0.8898	1.0191
FeK	10.19	4.54	139.21	6.16	0.0887	0.8260	1.0502	0.9951	1.0592
CoK	0.76	0.32	8.35	56.95	0.0066	0.8046	1.0495	0.9976	1.0731

EDAX TEAM

Nathan Oct 3 2017

Author: Robert
Creation: 10/04/2017 10:34:46 AM

Sample Name: 14-TLB-1

Area 5

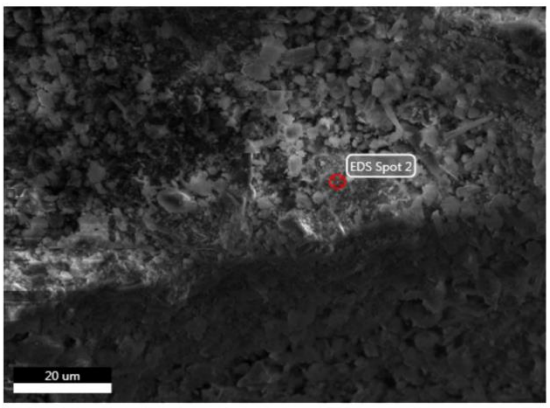

Notes:

EDAX TEAM

EDS Spot 2

kV: 15 Mag: 1244 Takeoff: 30.1 Live Time(s): 50 Amp Time(µs): 7.68 Resolution:(eV) 129.8

EDS Spot 2

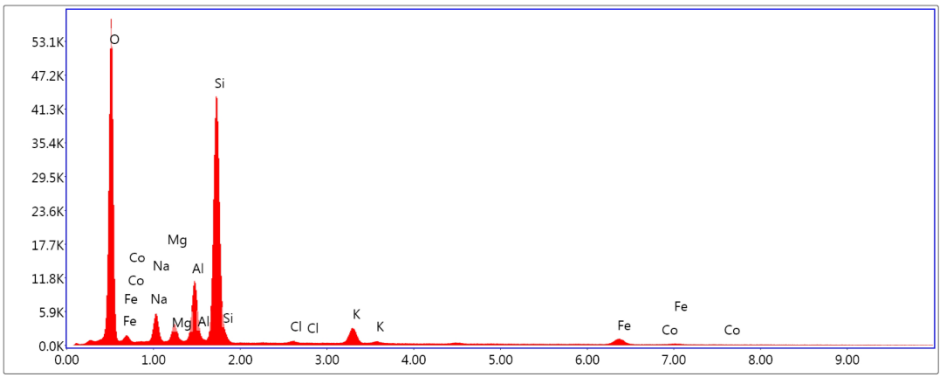

eZAF Smart Quant Results

Element	Weight %	Atomic %	Net Int.	Error %	Kratio	Z	R	A	F
O K	46.13	61.22	6660.18	7.23	0.2041	1.0679	0.9694	0.4144	1.0000
NaK	4.72	4.36	644.36	7.46	0.0212	0.9655	0.9953	0.4625	1.0056
MgK	1.91	1.67	400.06	6.53	0.0112	0.9807	1.0027	0.5891	1.0100
AlK	7.02	5.53	1630.60	4.74	0.0476	0.9432	1.0095	0.7087	1.0144
SiK	29.98	22.66	7148.56	3.88	0.2210	0.9628	1.0160	0.7629	1.0037
ClK	0.24	0.14	41.05	11.84	0.0018	0.8940	1.0328	0.8325	1.0141
K K	3.85	2.09	554.27	3.46	0.0322	0.8877	1.0421	0.9258	1.0196
FeK	5.85	2.22	270.01	4.82	0.0501	0.7963	1.0572	1.0016	1.0744
CoK	0.30	0.11	11.01	56.84	0.0025	0.7753	1.0557	1.0031	1.0933

EDAX TEAM

Nathan Oct 3 2017

Author: Robert
Creation: 10/04/2017 10:34:46 AM

Sample Name: 14-TLB-1

Area 5

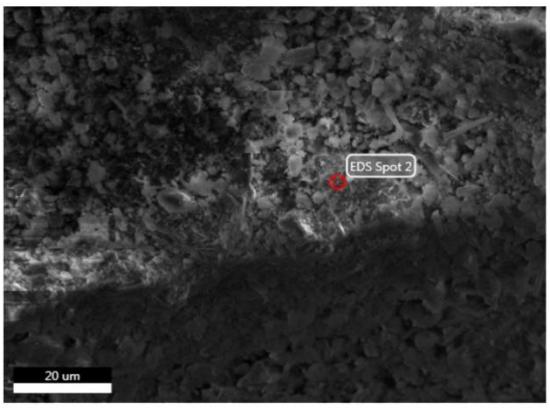

Notes:

EDAX TEAM

EDS Spot 2

kV: 15 Mag: 1244 Takeoff: 30.1 Live Time(s): 50 Amp Time(µs): 7.68 Resolution:(eV) 129.8

EDS Spot 2

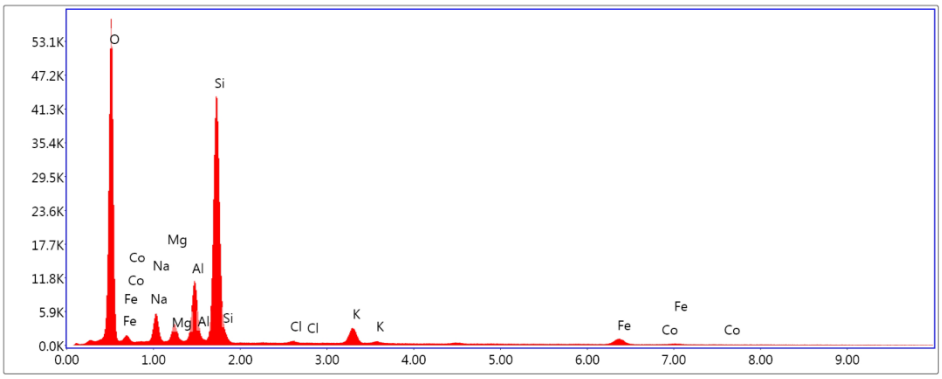

eZAF Smart Quant Results

Element	Weight %	Atomic %	Net Int.	Error %	Kratio	Z	R	A	F
O K	46.13	61.22	6660.18	7.23	0.2041	1.0679	0.9694	0.4144	1.0000
NaK	4.72	4.36	644.36	7.46	0.0212	0.9655	0.9953	0.4625	1.0056
MgK	1.91	1.67	400.06	6.53	0.0112	0.9807	1.0027	0.5891	1.0100
AlK	7.02	5.53	1630.60	4.74	0.0476	0.9432	1.0095	0.7087	1.0144
SiK	29.98	22.66	7148.56	3.88	0.2210	0.9628	1.0160	0.7629	1.0037
ClK	0.24	0.14	41.05	11.84	0.0018	0.8940	1.0328	0.8325	1.0141
K K	3.85	2.09	554.27	3.46	0.0322	0.8877	1.0421	0.9258	1.0196
FeK	5.85	2.22	270.01	4.82	0.0501	0.7963	1.0572	1.0016	1.0744
CoK	0.30	0.11	11.01	56.84	0.0025	0.7753	1.0557	1.0031	1.0933

EDAX TEAM

Nathan Oct 3 2017

Author: Robert
Creation: 10/04/2017 10:36:28 AM

Sample Name: 14-TLB-1

Area 5

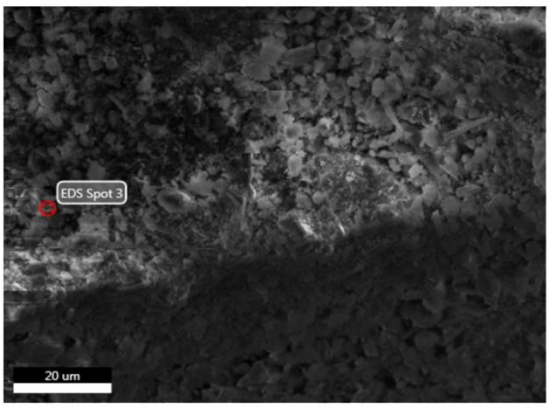

Notes:

EDAX TEAM

EDS Spot 3

kV: 15 Mag: 1244 Takeoff: 30.1 Live Time(s): 6.3 Amp Time(µs): 7.68 Resolution:(eV) 129.8

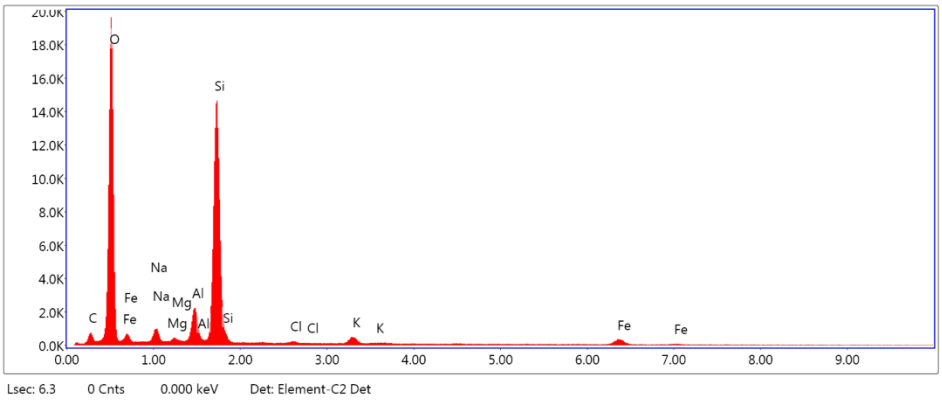

eZAF Smart Quant Results

Element	Weight %	Atomic %	Net Int.	Error %	Kratio	Z	R	A	F
C K	2.94	4.92	253.28	15.54	0.0049	1.1076	0.9525	0.1516	1.0000
O K	50.74	63.77	18924.17	7.20	0.2309	1.0554	0.9739	0.4311	1.0000
NaK	2.68	2.35	884.57	9.21	0.0116	0.9539	0.9993	0.4501	1.0056
MgK	0.38	0.31	198.18	13.20	0.0022	0.9689	1.0066	0.5939	1.0106
AlK	4.37	3.26	2591.24	5.18	0.0301	0.9318	1.0133	0.7279	1.0167
SiK	31.07	22.24	19214.43	3.66	0.2365	0.9511	1.0196	0.7975	1.0035
ClK	0.30	0.17	129.18	17.84	0.0023	0.8830	1.0361	0.8424	1.0126
K K	1.79	0.92	646.84	6.20	0.0150	0.8767	1.0450	0.9318	1.0212
FeK	5.73	2.06	659.69	6.85	0.0487	0.7861	1.0590	1.0039	1.0774

EDAX TEAM

Nathan 10 11 2017

Author: Robert
Creation: 10/17/2017 1:37:18 PM

Sample Name: 15-ODN-9

Area 1

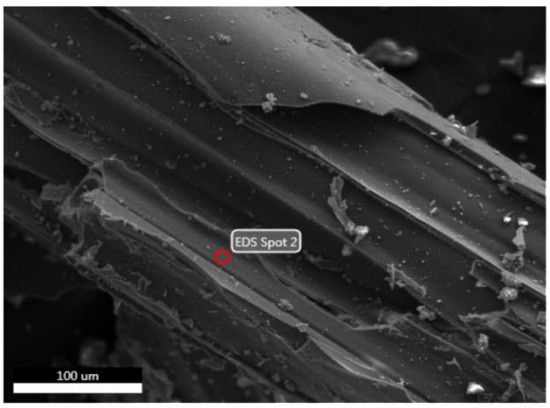

Notes:

EDAX TEAM

EDS Spot 2

kV: 15 Mag: 653 Takeoff: 30 Live Time(s): 50 Amp Time(µs): 0.24 Resolution:(eV) 155.9

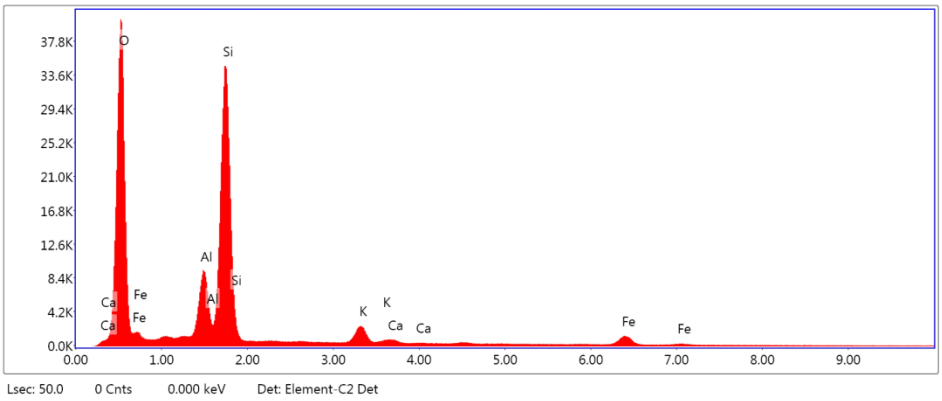

eZAF Smart Quant Results

Element	Weight %	Atomic %	Net Int.	Error %	Kratio	Z	R	A	F
O K	50.76	66.47	8567.64	7.19	0.2257	1.0642	0.9697	0.4177	1.0000
AlK	7.47	5.80	2096.74	4.45	0.0526	0.9400	1.0098	0.7371	1.0155
SiK	30.81	22.98	8737.50	3.68	0.2319	0.9595	1.0162	0.7813	1.0038
K K	3.42	1.83	574.99	3.79	0.0287	0.8847	1.0423	0.9289	1.0218
CaK	0.59	0.31	83.39	9.45	0.0052	0.8998	1.0462	0.9443	1.0283
FeK	6.95	2.61	371.48	4.41	0.0591	0.7936	1.0573	1.0019	1.0703

EDAX TEAM

Nathan 10 11 2017

Author: Robert
Creation: 10/17/2017 1:49:22 PM

Sample Name: 15-ODN-9

Area 2

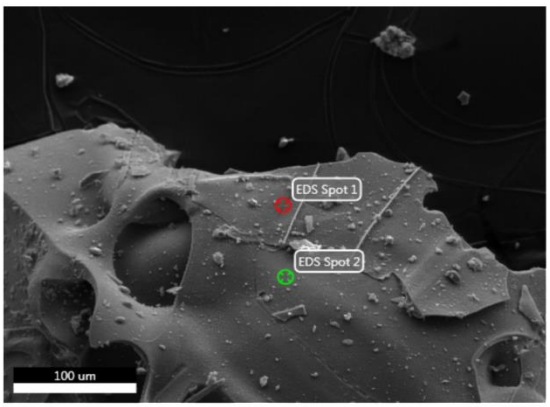

Notes:

EDAX TEAM

EDS Spot 1

kV: 15 Mag: 624 Takeoff: 30.3 Live Time(s): 50 Amp Time(µs): 0.24 Resolution:(eV) 155.9

EDS Spot 1

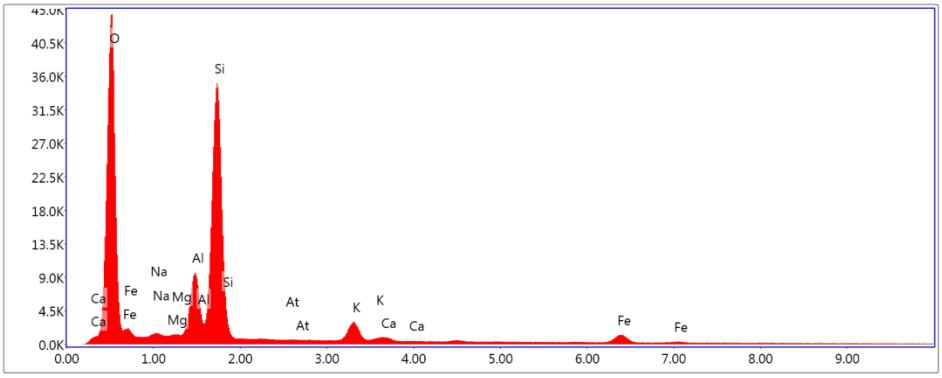

eZAF Smart Quant Results

Element	Weight %	Atomic %	Net Int.	Error %	Kratio	Z	R	A	F
O K	52.83	68.18	9368.60	7.09	0.2392	1.0607	0.9714	0.4267	1.0000
NaK	0.17	0.15	25.90	47.27	0.0007	0.9589	0.9970	0.4378	1.0056
MgK	0.00	0.00	0.02	99.99	0.0000	0.9739	1.0043	0.6008	1.0108
AlK	7.00	5.36	2016.27	4.44	0.0491	0.9367	1.0112	0.7382	1.0155
SiK	29.75	21.87	8698.37	3.65	0.2245	0.9561	1.0175	0.7860	1.0038
AtM	0.00	0.00	0.00	99.99	0.0000	0.5995	1.3986	1.1239	1.5594
K K	3.68	1.94	635.71	3.75	0.0309	0.8815	1.0434	0.9326	1.0212
CaK	0.49	0.25	70.99	9.21	0.0043	0.8965	1.0473	0.9464	1.0276
FeK	6.08	2.25	333.96	5.05	0.0517	0.7906	1.0580	1.0023	1.0734

EDAX TEAM

EDS Spot 2

kV: 15 Mag: 624 Takeoff: 30.3 Live Time(s): 50 Amp Time(µs): 0.24 Resolution:(eV) 155.9

EDS Spot 2

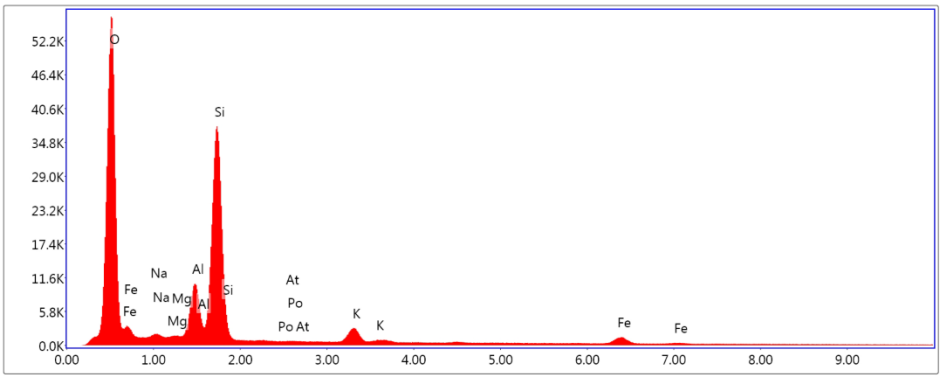

Lsec: 50.0 0 Cnts 0.000 keV Det: Element-C2 Det

eZAF Smart Quant Results

Element	Weight %	Atomic %	Net Int.	Error %	Kratio	Z	R	A	F
O K	54.84	69.67	12177.45	6.81	0.2629	1.0576	0.9732	0.4532	1.0000
NaK	1.14	1.01	206.14	9.89	0.0048	0.9559	0.9987	0.4366	1.0054
MgK	0.24	0.20	69.86	14.11	0.0014	0.9709	1.0059	0.5925	1.0102
AlK	7.07	5.33	2366.95	4.51	0.0488	0.9338	1.0127	0.7286	1.0144
SiK	27.57	19.95	9411.05	3.71	0.2054	0.9531	1.0190	0.7785	1.0038
PoM	0.00	0.00	0.18	55.30	0.0000	0.5947	1.3992	1.1125	1.4916
AtM	0.00	0.00	0.10	56.19	0.0000	0.5975	1.4004	1.1306	1.5369
K K	3.32	1.72	677.82	3.10	0.0278	0.8786	1.0446	0.9357	1.0207
FeK	5.82	2.12	377.87	4.85	0.0495	0.7879	1.0587	1.0034	1.0760

EDAX TEAM

Nathan 10 11 2017

Author: Robert
Creation: 10/17/2017 1:54:13 PM

Sample Name: 15-ODN-9

Area 3

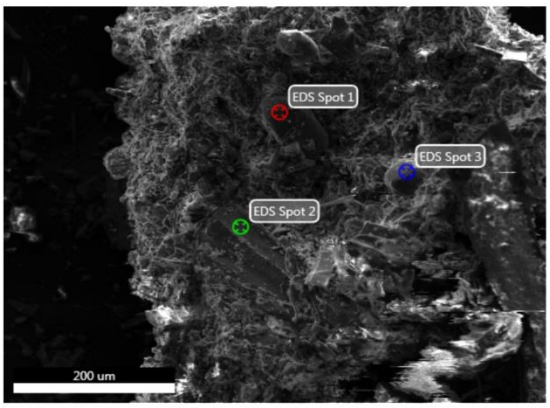

Notes:

EDAX TEAM

EDS Spot 1

kV: 15 Mag: 410 Takeoff: 30.2 Live Time(s): 50 Amp Time(µs): 0.24 Resolution:(eV) 155.9

EDS Spot 1

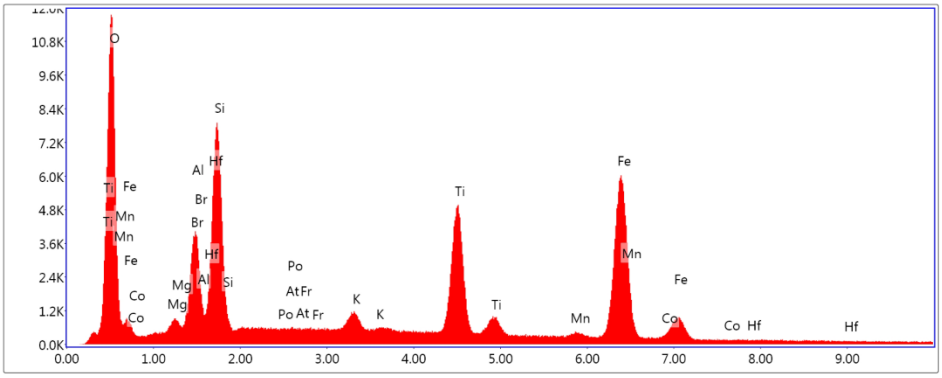

eZAF Smart Quant Results

Element	Weight %	Atomic %	Net Int.	Error %	Kratio	Z	R	A	F
O K	22.37	45.51	2269.89	8.45	0.0825	1.1908	0.9117	0.3095	1.0000
MgK	0.01	0.01	1.22	71.61	0.0000	1.0984	0.9503	0.3931	1.0039
BrL	0.00	0.00	0.01	99.99	0.0000	0.8294	1.1149	0.6856	1.0092
AlK	4.16	5.02	678.58	7.10	0.0235	1.0575	0.9587	0.5309	1.0059
SiK	8.91	10.32	1674.85	5.51	0.0614	1.0804	0.9666	0.6338	1.0066
PoM	0.00	0.00	0.00	99.99	0.0000	0.6759	1.3346	1.1129	1.9887
AtM	0.00	0.00	0.00	99.99	0.0000	0.6793	1.3366	1.1299	2.0900
FrM	0.00	0.00	0.00	99.99	0.0000	0.6521	1.3406	1.1383	2.3546
K K	0.98	0.81	139.84	10.48	0.0096	1.0003	1.0002	0.9315	1.0597
TiK	14.35	9.75	1402.74	3.04	0.1431	0.9222	1.0159	0.9825	1.1008
MnK	0.81	0.48	42.87	18.84	0.0077	0.8914	1.0269	0.9836	1.0857
FeK	47.67	27.78	1999.12	2.86	0.4399	0.9042	1.0291	0.9900	1.0309
CoK	0.47	0.26	15.76	49.37	0.0043	0.8819	1.0304	0.9888	1.0392
HfL	0.27	0.05	2.65	43.91	0.0018	0.6077	1.0914	1.0109	1.0924

EDAX TEAM

EDS Spot 2

kV: 15 Mag: 410 Takeoff: 30.2 Live Time(s): 50 Amp Time(µs): 0.24 Resolution:(eV) 155.9

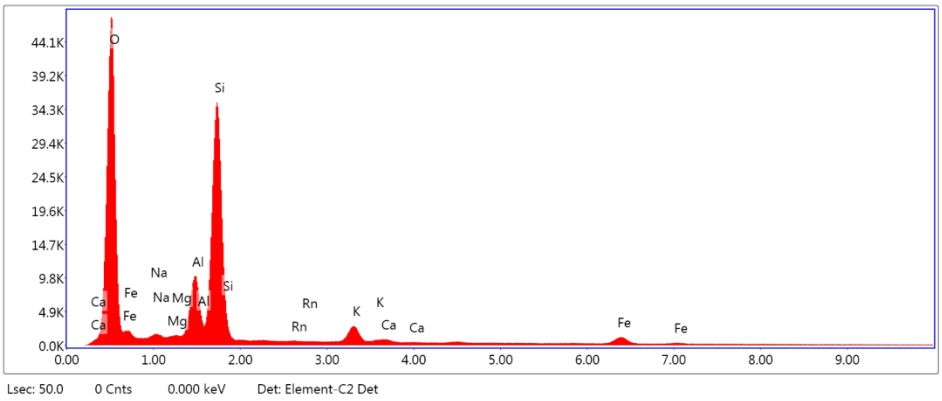

eZAF Smart Quant Results

Element	Weight %	Atomic %	Net Int.	Error %	Kratio	Z	R	A	F
O K	54.09	69.05	10081.59	6.97	0.2510	1.0581	0.9728	0.4384	1.0000
NaK	0.31	0.28	49.73	20.80	0.0013	0.9564	0.9983	0.4391	1.0057
MgK	0.00	0.00	0.13	99.99	0.0000	0.9714	1.0056	0.6014	1.0109
AlK	7.31	5.54	2160.22	4.43	0.0513	0.9342	1.0124	0.7390	1.0153
SiK	29.28	21.29	8748.08	3.66	0.2198	0.9535	1.0187	0.7842	1.0037
RnM	0.00	0.00	0.00	99.99	0.0000	0.5708	1.4013	1.1266	1.5980
K K	3.24	1.69	573.50	4.06	0.0271	0.8790	1.0443	0.9332	1.0208
CaK	0.33	0.17	48.83	14.35	0.0029	0.8940	1.0482	0.9482	1.0275
FeK	5.43	1.99	306.92	5.24	0.0463	0.7883	1.0586	1.0030	1.0768

EDS Spot 3

kV: 15 Mag: 410 Takeoff: 30.2 Live Time(s): 50 Amp Time(µs): 0.24 Resolution:(eV) 155.9

EDS Spot 3

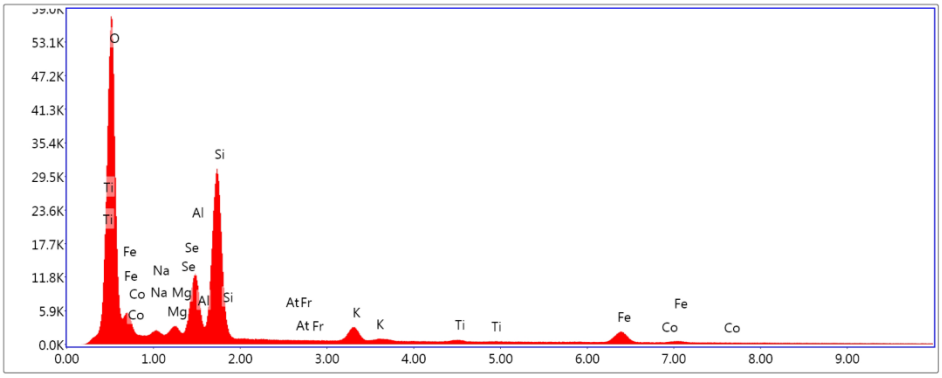

Lsec: 50.0 0 Cnts 0.000 keV Det: Element-C2 Det

eZAF Smart Quant Results

Element	Weight %	Atomic %	Net Int.	Error %	Kratio	Z	R	A	F
O K	53.22	69.22	12369.29	6.68	0.2645	1.0662	0.9692	0.4662	1.0000
NaK	1.37	1.24	236.15	10.11	0.0054	0.9640	0.9950	0.4099	1.0046
MgK	1.25	1.07	356.95	7.43	0.0070	0.9792	1.0024	0.5628	1.0084
SeL	0.02	0.01	3.85	99.99	0.0001	0.7291	1.1685	0.8339	1.0154
AlK	8.25	6.36	2667.67	4.84	0.0544	0.9418	1.0093	0.6927	1.0110
SiK	22.43	16.62	7456.58	4.10	0.1609	0.9614	1.0158	0.7433	1.0041
AtM	0.00	0.00	0.00	99.99	0.0000	0.6029	1.3965	1.1372	1.5989
FrM	0.00	0.00	0.00	99.99	0.0000	0.5785	1.3993	1.1462	1.7397
K K	2.86	1.52	600.55	3.72	0.0244	0.8865	1.0419	0.9378	1.0255
TiK	0.42	0.18	60.26	19.65	0.0036	0.8152	1.0524	0.9834	1.0715
FeK	9.89	3.68	648.35	3.94	0.0840	0.7954	1.0570	1.0036	1.0637
CoK	0.29	0.10	15.35	55.78	0.0025	0.7745	1.0556	1.0042	1.0801

EDAX TEAM

Nathan 10 11 2017

Author: Robert
Creation: 10/17/2017 11:05:49 AM

Sample Name: 15-OLD-2T

Area 1

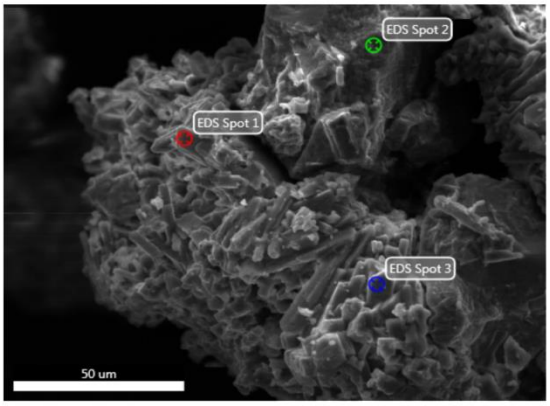

Notes:

EDAX TEAM

EDS Spot 1

kV: 15 Mag: 1733 Takeoff: 30 Live Time(s): 50 Amp Time(µs): 0.24 Resolution:(eV) 155.9

EDS Spot 1

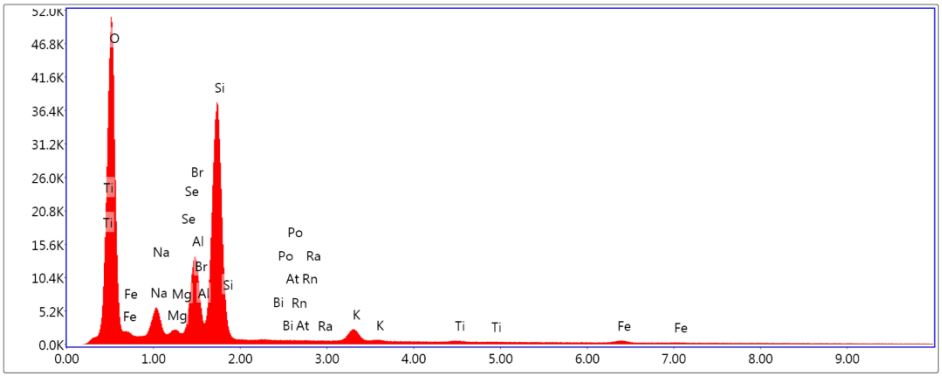

eZAF Smart Quant Results

Element	Weight %	Atomic %	Net Int.	Error %	Kratio	Z	R	A	F
O K	51.40	65.75	10838.63	7.03	0.2358	1.0603	0.9731	0.4326	1.0000
NaK	5.29	4.71	1050.38	7.22	0.0245	0.9584	0.9986	0.4809	1.0055
MgK	0.68	0.57	202.43	8.09	0.0040	0.9734	1.0058	0.6022	1.0102
SeL	0.16	0.04	29.26	25.61	0.0011	0.7248	1.1724	0.8877	1.0186
BrL	2.27	0.58	424.33	4.56	0.0159	0.7342	1.1774	0.9375	1.0163
AlK	7.50	5.69	2502.73	4.52	0.0518	0.9362	1.0126	0.7290	1.0124
SiK	28.35	20.66	9359.80	3.94	0.2052	0.9556	1.0189	0.7549	1.0031
BiM	0.00	0.00	0.24	85.53	0.0000	0.5905	1.3979	1.0739	1.3519
PoM	0.00	0.00	0.00	99.99	0.0000	0.5962	1.3991	1.0954	1.3810
AtM	0.00	0.00	0.00	99.99	0.0000	0.5991	1.4003	1.1147	1.4142
RnM	0.00	0.00	0.00	99.99	0.0000	0.5720	1.4016	1.1161	1.4674
RaM	0.00	0.00	0.00	72.51	0.0000	0.5726	1.4046	1.1356	1.5565
K K	2.43	1.27	490.17	4.63	0.0202	0.8809	1.0445	0.9273	1.0174
TiK	0.30	0.13	41.00	22.47	0.0025	0.8098	1.0547	0.9797	1.0447
FeK	1.61	0.59	106.42	11.20	0.0140	0.7899	1.0587	1.0025	1.0976

EDS Spot 2

kV: 15 Mag: 1733 Takeoff: 30 Live Time(s): 50 Amp Time(µs): 0.24 Resolution:(eV) 155.9

EDS Spot 2

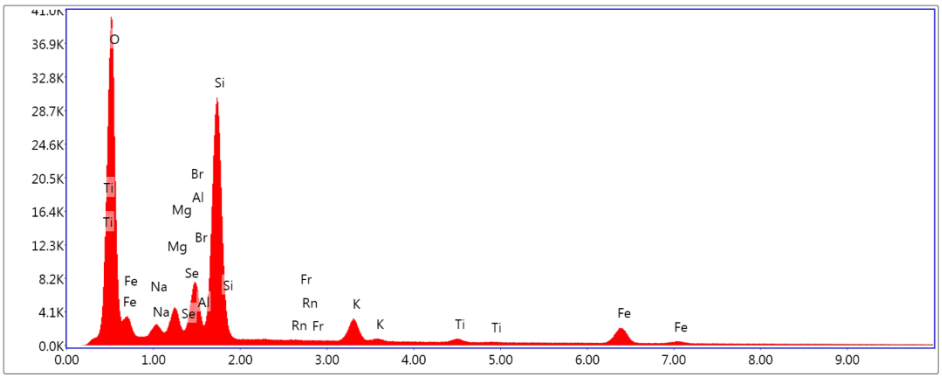

Lsec: 50.0 0 Cnts 0.000 keV Det: Element-C2 Det

eZAF Smart Quant Results

Element	Weight %	Atomic %	Net Int.	Error %	Kratio	Z	R	A	F
O K	46.87	64.40	8462.04	7.26	0.2082	1.0810	0.9613	0.4110	1.0000
NaK	2.17	2.08	336.38	9.03	0.0089	0.9779	0.9878	0.4155	1.0045
MgK	3.08	2.78	772.45	6.61	0.0173	0.9935	0.9955	0.5615	1.0075
SeL	0.13	0.04	19.61	41.45	0.0008	0.7398	1.1606	0.8132	1.0143
BrL	2.69	0.74	420.19	5.18	0.0178	0.7495	1.1659	0.8696	1.0136
AlK	3.66	2.98	1015.52	5.41	0.0238	0.9557	1.0026	0.6736	1.0108
SiK	25.64	20.07	7464.37	4.15	0.1851	0.9757	1.0093	0.7369	1.0040
RnM	0.00	0.00	0.00	81.38	0.0000	0.5845	1.3902	1.1183	1.6755
FrM	0.00	0.00	0.00	99.99	0.0000	0.5874	1.3918	1.1289	1.7414
K K	3.85	2.16	706.14	3.58	0.0329	0.9003	1.0366	0.9278	1.0240
TiK	0.80	0.37	100.36	11.87	0.0069	0.8281	1.0479	0.9769	1.0657
FeK	11.11	4.37	641.13	3.65	0.0953	0.8085	1.0536	1.0010	1.0601

EDS Spot 3

kV: 15 Mag: 1733 Takeoff: 30 Live Time(s): 50 Amp Time(µs): 0.24 Resolution:(eV) 155.9

EDS Spot 3

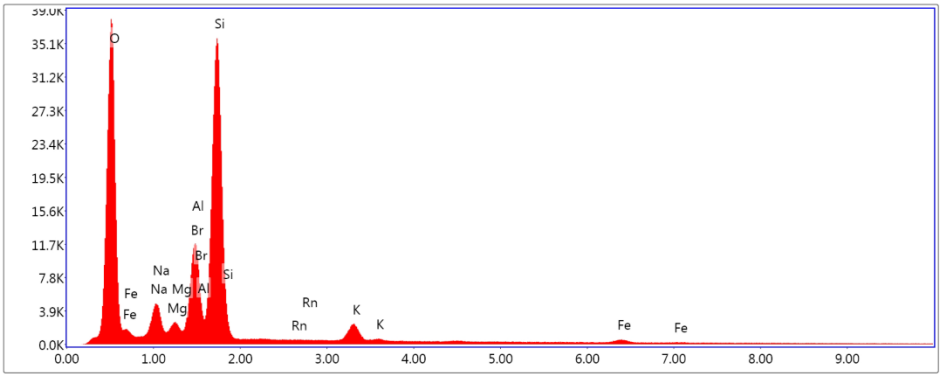

Lsec: 50.0 0 Cnts 0.000 keV Det: Element-C2 Det

eZAF Smart Quant Results

Element	Weight %	Atomic %	Net Int.	Error %	Kratio	Z	R	A	F
O K	47.09	62.58	8068.38	7.38	0.2013	1.0706	0.9675	0.3992	1.0000
NaK	5.12	4.73	912.43	7.15	0.0244	0.9681	0.9935	0.4901	1.0055
MgK	1.31	1.14	348.85	7.00	0.0079	0.9834	1.0009	0.6109	1.0099
BrL	4.87	1.30	803.69	2.79	0.0345	0.7418	1.1719	0.9407	1.0146
AlK	5.53	4.36	1628.46	4.59	0.0387	0.9459	1.0079	0.7309	1.0119
SiK	30.97	23.44	8926.29	4.01	0.2244	0.9655	1.0144	0.7480	1.0030
RnM	0.01	0.00	1.25	51.90	0.0001	0.5782	1.3962	1.0993	1.4612
K K	3.16	1.72	555.23	3.59	0.0262	0.8905	1.0408	0.9186	1.0161
FeK	1.94	0.74	112.64	10.17	0.0170	0.7990	1.0563	1.0009	1.0923

EDAX TEAM

Nathan 10 11 2017

Author: Robert
Creation: 10/17/2017 11:15:30 AM

Sample Name: 15-OLD-2T

Area 2

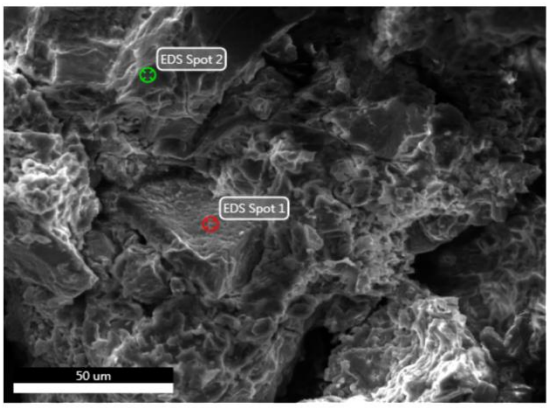

Notes:

EDS Spot 1

kV: 15 Mag: 1624 Takeoff: 30.4 Live Time(s): 50 Amp Time(µs): 0.24 Resolution:(eV) 155.9

EDS Spot 1

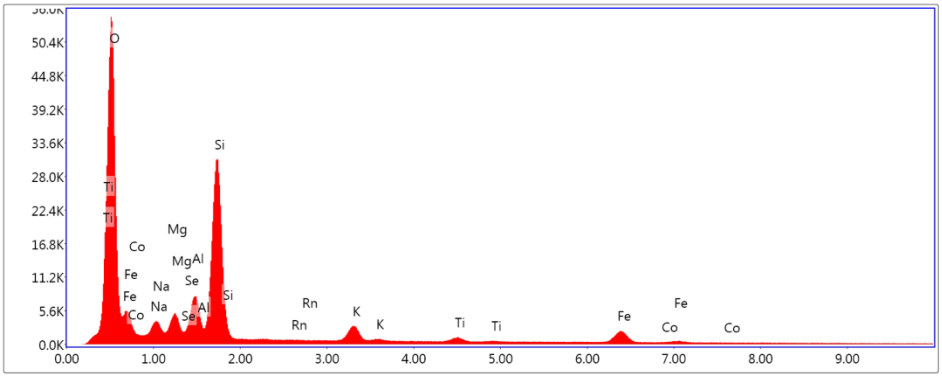

Lsec: 50.0 0 Cnts 0.000 keV Det: Element-C2 Det

eZAF Smart Quant Results

Element	Weight %	Atomic %	Net Int.	Error %	Kratio	Z	R	A	F
O K	51.53	67.48	11669.16	6.80	0.2505	1.0679	0.9686	0.4552	1.0000
NaK	3.43	3.13	599.83	8.31	0.0138	0.9656	0.9944	0.4159	1.0044
MgK	2.97	2.56	828.95	6.79	0.0162	0.9808	1.0019	0.5543	1.0076
SeL	0.01	0.00	0.99	99.99	0.0000	0.7303	1.1679	0.8047	1.0140
AlK	5.19	4.03	1618.10	5.13	0.0332	0.9434	1.0088	0.6708	1.0113
SiK	22.76	16.98	7575.60	4.06	0.1645	0.9630	1.0153	0.7472	1.0042
RnM	0.00	0.00	0.00	99.99	0.0000	0.5766	1.3973	1.1363	1.6960
K K	2.94	1.57	615.05	4.54	0.0251	0.8880	1.0415	0.9384	1.0262
TiK	1.15	0.50	163.14	10.07	0.0099	0.8166	1.0521	0.9834	1.0685
FeK	9.78	3.67	637.52	3.86	0.0831	0.7968	1.0568	1.0030	1.0630
CoK	0.24	0.09	12.73	56.17	0.0020	0.7759	1.0554	1.0037	1.0795

EDS Spot 2

kV: 15 Mag: 1624 Takeoff: 30.4 Live Time(s): 50 Amp Time(µs): 0.24 Resolution:(eV) 155.9

EDS Spot 2

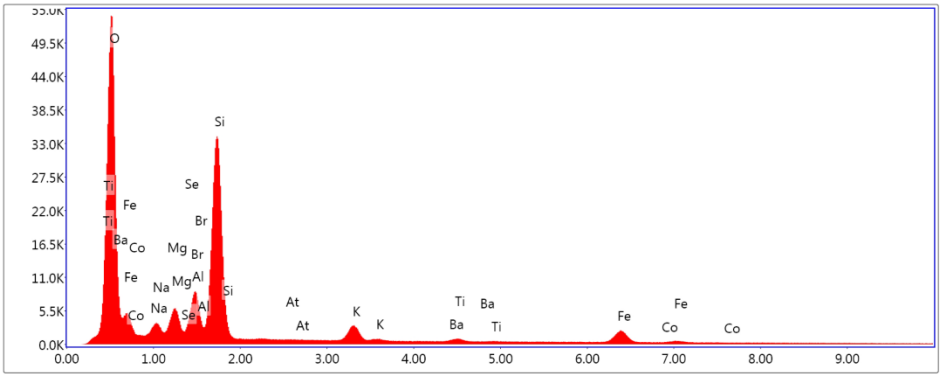

eZAF Smart Quant Results

Element	Weight %	Atomic %	Net Int.	Error %	Kratio	Z	R	A	F
O K	49.30	66.28	11712.94	7.01	0.2304	1.0765	0.9636	0.4342	1.0000
NaK	3.33	3.11	651.95	8.05	0.0138	0.9737	0.9899	0.4238	1.0043
MgK	3.66	3.24	1139.42	6.39	0.0205	0.9892	0.9975	0.5613	1.0070
SeL	0.33	0.09	59.33	14.33	0.0020	0.7367	1.1629	0.8050	1.0132
BrL	2.71	0.73	519.36	4.24	0.0176	0.7463	1.1681	0.8595	1.0127
AlK	3.18	2.54	1084.41	5.46	0.0204	0.9516	1.0045	0.6668	1.0100
SiK	23.91	18.31	8609.62	4.15	0.1713	0.9715	1.0112	0.7346	1.0038
AtM	0.08	0.01	14.85	33.52	0.0009	0.6094	1.3910	1.1221	1.5282
K K	3.21	1.77	731.45	3.24	0.0274	0.8962	1.0381	0.9309	1.0224
BaL	0.36	0.06	20.37	55.60	0.0027	0.6339	1.2151	1.0650	1.0891
TiK	0.70	0.31	107.91	11.75	0.0060	0.8243	1.0492	0.9794	1.0598
FeK	8.97	3.46	643.66	3.84	0.0769	0.8047	1.0546	1.0014	1.0634
CoK	0.26	0.10	15.16	55.89	0.0022	0.7837	1.0534	1.0025	1.0799

EDAX TEAM

Nathan 10 11 2017

Author: Robert
Creation: 10/17/2017 11:19:57 AM

Sample Name: 15-OLD-2T

Area 3

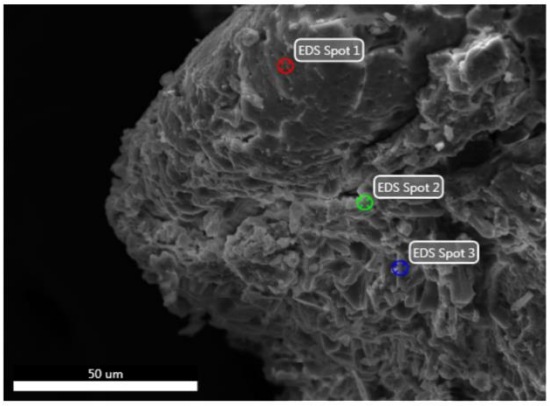

Notes:

EDAX TEAM

EDS Spot 1

kV: 15 Mag: 1868 Takeoff: 30.1 Live Time(s): 50 Amp Time(µs): 0.24 Resolution:(eV) 155.9

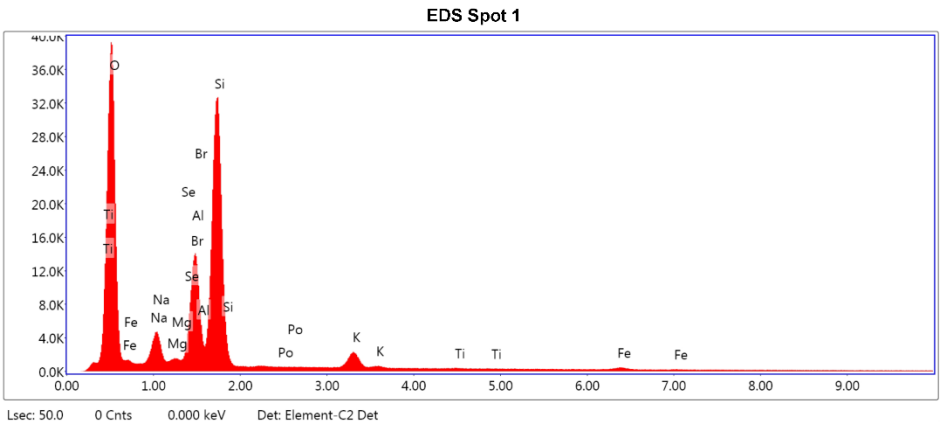

eZAF Smart Quant Results

Element	Weight %	Atomic %	Net Int.	Error %	Kratio	Z	R	A	F
O K	48.69	63.59	8404.79	7.28	0.2123	1.0658	0.9705	0.4091	1.0000
NaK	5.01	4.55	878.07	7.16	0.0238	0.9636	0.9962	0.4904	1.0056
MgK	0.33	0.29	87.68	11.49	0.0020	0.9787	1.0036	0.6124	1.0106
SeL	0.32	0.08	50.10	13.65	0.0021	0.7288	1.1698	0.9031	1.0192
BrL	3.10	0.81	507.55	3.26	0.0221	0.7382	1.1749	0.9485	1.0157
AlK	8.67	6.71	2533.74	4.34	0.0610	0.9413	1.0104	0.7385	1.0119
SiK	29.19	21.71	8242.60	4.03	0.2099	0.9609	1.0168	0.7462	1.0031
PoM	0.00	0.00	0.20	54.82	0.0000	0.5996	1.3965	1.0848	1.3857
K K	3.06	1.64	531.61	3.77	0.0255	0.8859	1.0428	0.9227	1.0164
TiK	0.19	0.08	22.47	37.90	0.0016	0.8145	1.0532	0.9764	1.0427
FeK	1.43	0.53	81.65	13.69	0.0125	0.7947	1.0576	1.0015	1.0964

EDAX TEAM

EDS Spot 2

kV: 15 Mag: 1868 Takeoff: 30.1 Live Time(s): 50 Amp Time(µs): 0.24 Resolution:(eV) 155.9

EDS Spot 2

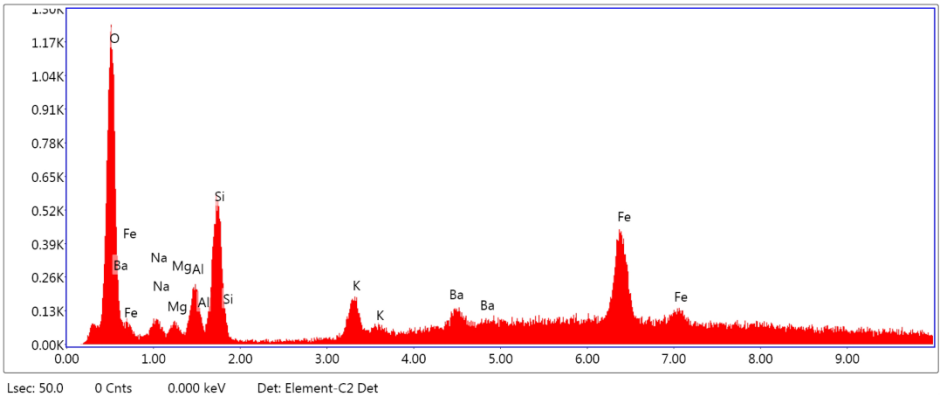

Lsec: 50.0 0 Cnts 0.000 keV Det: Element-C2 Det

eZAF Smart Quant Results

Element	Weight %	Atomic %	Net Int.	Error %	Kratio	Z	R	A	F
O K	24.60	46.68	272.89	7.53	0.1355	1.1780	0.9147	0.4677	1.0000
NaK	4.79	6.33	27.20	12.88	0.0145	1.0686	0.9444	0.2824	1.0022
MgK	2.08	2.59	19.61	12.94	0.0089	1.0866	0.9532	0.3914	1.0038
AlK	4.86	5.47	55.57	8.84	0.0263	1.0460	0.9614	0.5138	1.0057
SiK	10.74	11.60	141.57	6.66	0.0709	1.0687	0.9693	0.6146	1.0056
K K	2.96	2.30	29.83	10.85	0.0281	0.9894	1.0026	0.9209	1.0412
BaL	6.60	1.46	16.55	38.66	0.0543	0.7021	1.1809	1.0598	1.1057
FeK	43.36	23.57	132.16	5.95	0.3970	0.8943	1.0308	0.9914	1.0327

EDAX TEAM

EDS Spot 3

kV: 15 Mag: 1868 Takeoff: 30.1 Live Time(s): 50 Amp Time(µs): 0.24 Resolution:(eV) 155.9

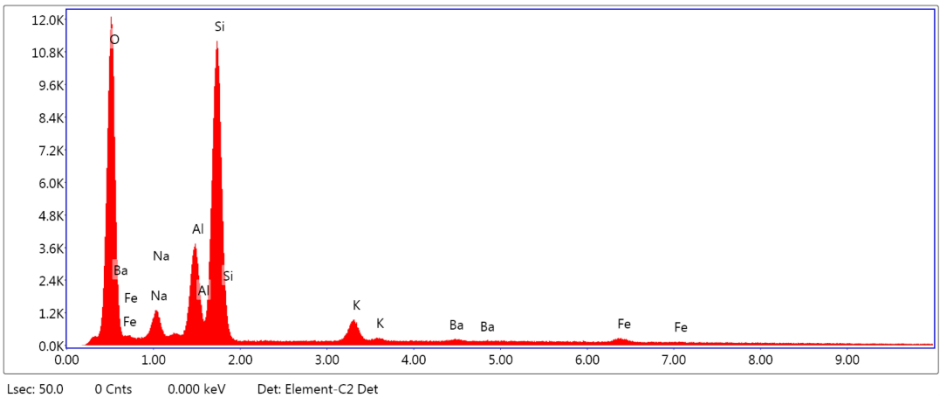

eZAF Smart Quant Results

Element	Weight %	Atomic %	Net Int.	Error %	Kratio	Z	R	A	F
O K	46.21	61.34	2577.90	7.42	0.2030	1.0699	0.9684	0.4106	1.0000
NaK	4.87	4.50	265.38	8.04	0.0224	0.9674	0.9943	0.4728	1.0057
AlK	9.69	7.63	899.77	4.71	0.0675	0.9452	1.0086	0.7266	1.0142
SiK	30.41	23.00	2806.70	4.06	0.2228	0.9648	1.0151	0.7566	1.0036
K K	3.85	2.09	215.97	4.63	0.0322	0.8897	1.0414	0.9233	1.0192
BaL	1.94	0.30	26.60	39.77	0.0138	0.6290	1.2181	1.0618	1.0672
FeK	3.02	1.15	54.49	13.28	0.0260	0.7982	1.0567	0.9988	1.0760

EDAX TEAM

Nathan 10 11 2017

Author: Robert
Creation: 10/17/2017 11:25:31 AM

Sample Name: 15-OLD-2T

Area 4

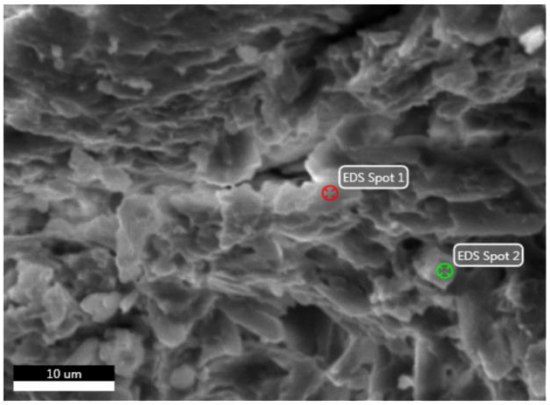

Notes:

EDAX TEAM

EDS Spot 1

kV: 15 Mag: 5135 Takeoff: 30.1 Live Time(s): 50 Amp Time(µs): 0.24 Resolution:(eV) 155.9

EDS Spot 1

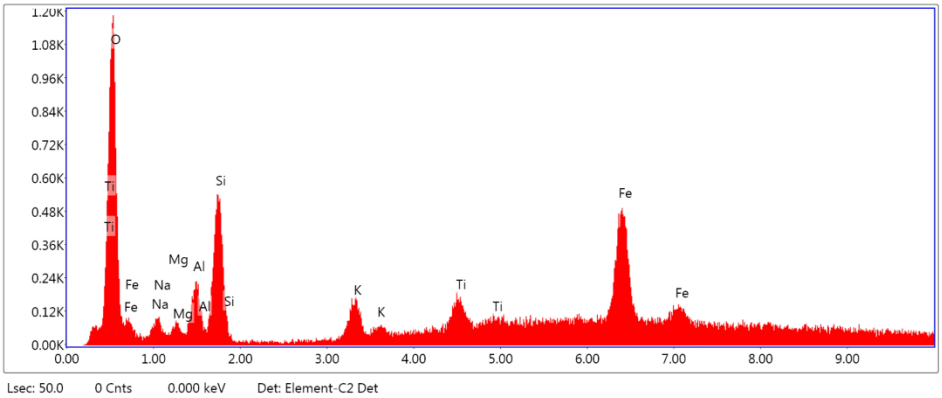

Lsec: 50.0 0 Cnts 0.000 keV Det: Element-C2 Det

eZAF Smart Quant Results

Element	Weight %	Atomic %	Net Int.	Error %	Kratio	Z	R	A	F
O K	25.34	46.99	243.43	8.34	0.1164	1.1654	0.9227	0.3943	1.0000
NaK	4.38	5.65	25.45	12.82	0.0131	1.0567	0.9519	0.2817	1.0023
MgK	1.77	2.16	17.59	13.56	0.0077	1.0743	0.9605	0.4015	1.0039
AlK	4.47	4.91	54.05	8.94	0.0246	1.0341	0.9686	0.5296	1.0060
SiK	9.73	10.28	135.65	6.57	0.0654	1.0563	0.9763	0.6323	1.0062
K K	3.22	2.44	33.89	11.31	0.0307	0.9773	1.0087	0.9308	1.0493
TiK	4.83	2.99	35.75	12.81	0.0480	0.9005	1.0234	0.9784	1.1271
FeK	46.27	24.58	145.17	5.44	0.4200	0.8821	1.0350	0.9973	1.0318

EDAX TEAM

EDS Spot 2

kV: 15 Mag: 5135 Takeoff: 30.1 Live Time(s): 50 Amp Time(µs): 0.24 Resolution:(eV) 155.9

EDS Spot 2

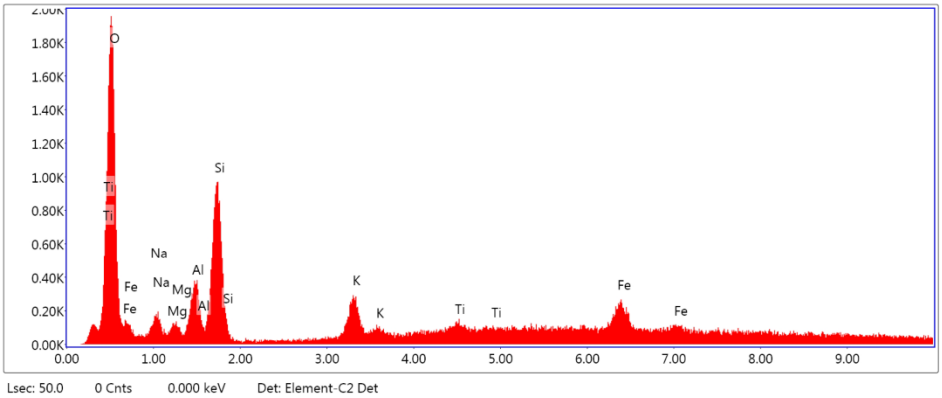

Lsec: 50.0 0 Cnts 0.000 keV Det: Element-C2 Det

eZAF Smart Quant Results

Element	Weight %	Atomic %	Net Int.	Error %	Kratio	Z	R	A	F
O K	43.01	61.76	411.73	8.07	0.1880	1.0955	0.9558	0.3991	1.0000
NaK	5.46	5.46	41.28	10.91	0.0202	0.9914	0.9828	0.3724	1.0034
MgK	2.08	1.96	25.12	12.08	0.0104	1.0073	0.9906	0.4964	1.0059
AlK	6.28	5.35	87.88	7.17	0.0382	0.9691	0.9979	0.6231	1.0083
SiK	16.00	13.09	242.58	5.42	0.1117	0.9894	1.0047	0.7016	1.0055
K K	5.95	3.49	60.80	8.33	0.0526	0.9133	1.0328	0.9399	1.0312
TiK	2.35	1.13	16.29	26.94	0.0209	0.8402	1.0446	0.9783	1.0804
FeK	18.88	7.77	58.71	10.84	0.1621	0.8207	1.0512	1.0000	1.0465

EDAX TEAM

Nathan 10 11 2017

Author: Robert
Creation: 10/17/2017 11:33:46 AM

Sample Name: 15-OLD-2T

Area 6

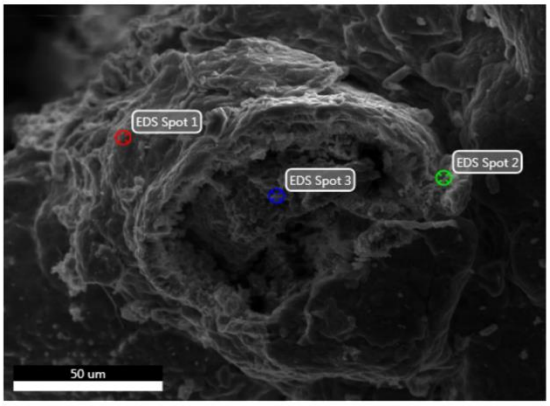

Notes:

EDAX TEAM

EDS Spot 1

kV: 15 Mag: 1514 Takeoff: 29.2 Live Time(s): 50 Amp Time(µs): 0.24 Resolution:(eV) 155.9

EDS Spot 1

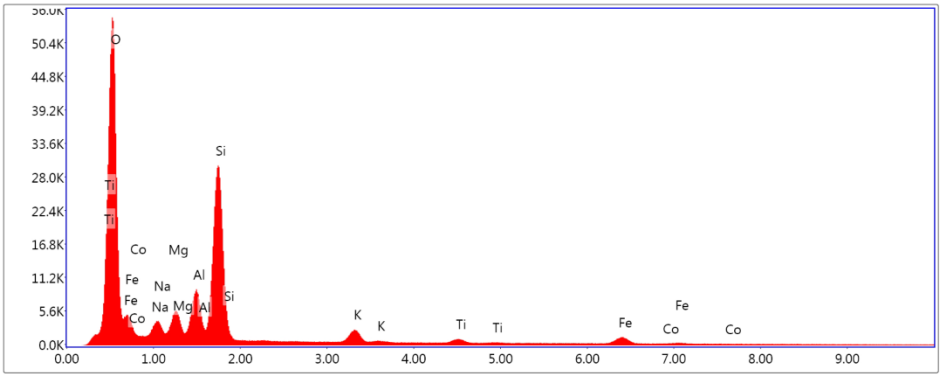

Lsec: 50.0 0 Cnts 0.000 keV Det: Element-C2 Det

eZAF Smart Quant Results

Element	Weight %	Atomic %	Net Int.	Error %	Kratio	Z	R	A	F
O K	53.14	67.65	11993.99	6.86	0.2526	1.0598	0.9733	0.4484	1.0000
NaK	4.40	3.90	819.18	7.75	0.0184	0.9579	0.9988	0.4341	1.0049
MgK	4.01	3.36	1168.72	6.34	0.0222	0.9729	1.0060	0.5657	1.0080
AlK	6.42	4.84	2052.89	5.08	0.0408	0.9357	1.0128	0.6725	1.0113
SiK	22.40	16.24	7546.02	4.12	0.1588	0.9550	1.0191	0.7394	1.0039
K K	2.66	1.39	569.90	3.59	0.0225	0.8804	1.0447	0.9372	1.0234
TiK	1.36	0.58	195.50	6.75	0.0114	0.8093	1.0548	0.9840	1.0564
FeK	5.36	1.95	363.10	4.93	0.0457	0.7895	1.0588	1.0034	1.0770
CoK	0.25	0.09	13.69	55.86	0.0021	0.7686	1.0572	1.0045	1.0967

EDAX TEAM

EDS Spot 2

kV: 15 Mag: 1514 Takeoff: 29.2 Live Time(s): 50 Amp Time(µs): 0.24 Resolution:(eV) 155.9

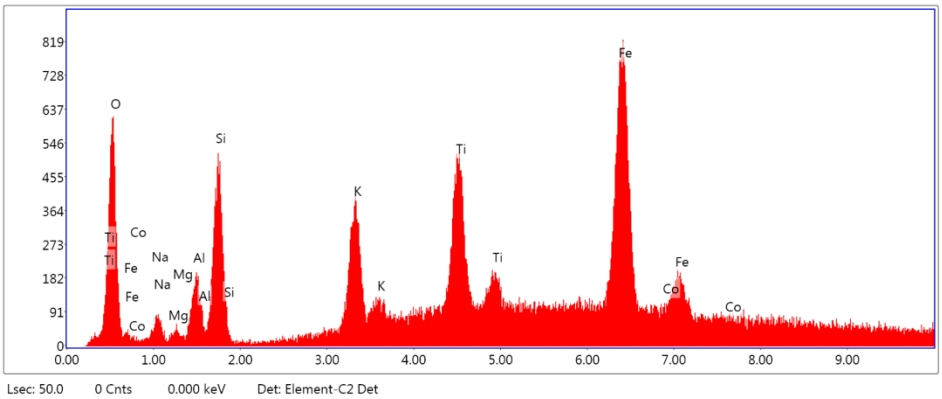

eZAF Smart Quant Results

Element	Weight %	Atomic %	Net Int.	Error %	Kratio	Z	R	A	F
O K	11.97	28.35	121.63	9.98	0.0415	1.2231	0.8982	0.2831	1.0000
NaK	2.54	4.18	18.61	14.24	0.0068	1.1102	0.9286	0.2398	1.0019
MgK	0.59	0.93	7.79	19.93	0.0024	1.1290	0.9377	0.3568	1.0034
AlK	2.66	3.74	44.03	9.57	0.0142	1.0870	0.9463	0.4874	1.0055
SiK	6.13	8.27	121.36	6.94	0.0413	1.1108	0.9544	0.6025	1.0072
K K	5.64	5.46	88.70	6.52	0.0567	1.0291	0.9895	0.9274	1.0539
TiK	12.32	9.75	133.38	5.55	0.1261	0.9493	1.0063	0.9718	1.1088
FeK	55.29	37.50	257.30	4.44	0.5242	0.9321	1.0216	0.9876	1.0299
CoK	2.86	1.84	10.58	48.11	0.0266	0.9095	1.0235	0.9866	1.0364

EDS Spot 3

kV: 15 Mag: 1514 Takeoff: 29.2 Live Time(s): 50 Amp Time(µs): 0.24 Resolution:(eV) 155.9

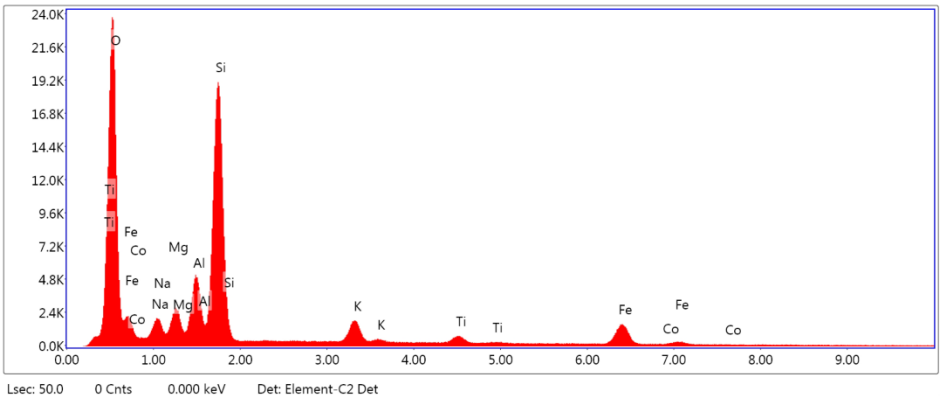

eZAF Smart Quant Results

Element	Weight %	Atomic %	Net Int.	Error %	Kratio	Z	R	A	F
O K	43.31	60.39	5130.26	7.41	0.1877	1.0838	0.9614	0.4000	1.0000
NaK	3.69	3.58	376.64	8.58	0.0147	0.9804	0.9879	0.4047	1.0045
MgK	3.27	3.00	534.91	7.06	0.0177	0.9960	0.9955	0.5399	1.0077
AlK	6.26	5.17	1147.19	5.36	0.0397	0.9581	1.0027	0.6545	1.0112
SiK	24.73	19.64	4821.96	4.30	0.1763	0.9781	1.0093	0.7259	1.0043
K K	3.61	2.06	452.90	3.55	0.0311	0.9024	1.0366	0.9276	1.0274
TiK	1.87	0.87	159.50	6.37	0.0162	0.8300	1.0479	0.9775	1.0697
FeK	12.84	5.13	502.34	3.77	0.1099	0.8103	1.0536	1.0005	1.0555
CoK	0.43	0.16	13.46	54.18	0.0036	0.7892	1.0526	1.0015	1.0696

EDAX TEAM

Nathan 10 11 2017

Author: Robert
Creation: 10/17/2017 11:39:31 AM

Sample Name: 15-OLD-2T

Area 7

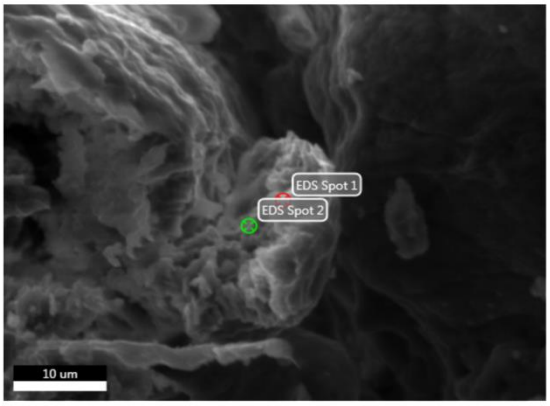

Notes:

EDAX TEAM

EDS Spot 1

kV: 15 Mag: 4731 Takeoff: 29.2 Live Time(s): 50 Amp Time(µs): 0.24 Resolution:(eV) 155.9

EDS Spot 1

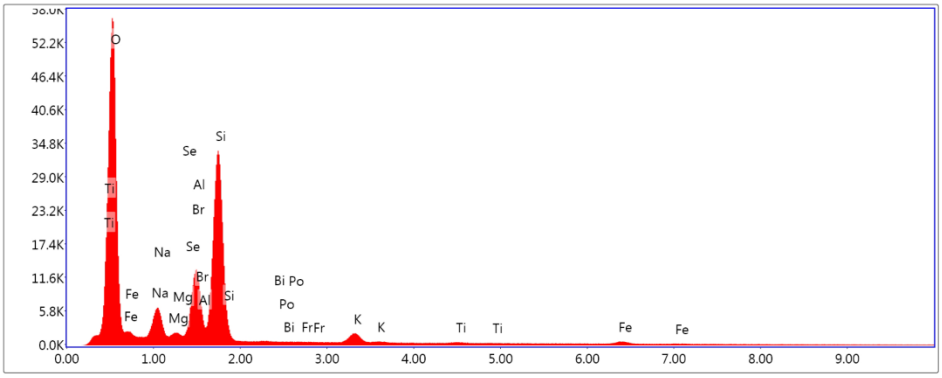

Lsec: 50.0 0 Cnts 0.000 keV Det: Element-C2 Det

eZAF Smart Quant Results

Element	Weight %	Atomic %	Net Int.	Error %	Kratio	Z	R	A	F
O K	53.88	67.65	12137.67	6.75	0.2614	1.0564	0.9754	0.4592	1.0000
NaK	6.71	5.86	1305.08	7.23	0.0300	0.9547	1.0006	0.4656	1.0051
MgK	0.64	0.53	186.47	8.92	0.0036	0.9696	1.0078	0.5777	1.0094
SeL	0.15	0.04	25.87	28.62	0.0009	0.7219	1.1746	0.8628	1.0171
BrL	1.64	0.41	302.44	5.49	0.0112	0.7313	1.1796	0.9159	1.0155
AlK	7.63	5.68	2505.97	4.71	0.0510	0.9325	1.0145	0.7084	1.0115
SiK	25.17	18.00	8303.56	4.07	0.1787	0.9517	1.0208	0.7437	1.0032
BiM	0.00	0.00	0.00	99.99	0.0000	0.5881	1.4001	1.0898	1.3542
PoM	0.00	0.00	0.00	99.99	0.0000	0.5938	1.4013	1.1109	1.3830
FrM	0.00	0.00	0.00	99.99	0.0000	0.5725	1.4051	1.1413	1.5105
K K	1.95	1.00	401.87	5.80	0.0162	0.8772	1.0460	0.9316	1.0185
TiK	0.21	0.09	29.30	29.55	0.0018	0.8064	1.0559	0.9828	1.0484
FeK	2.03	0.73	136.52	9.04	0.0176	0.7864	1.0596	1.0040	1.0984

EDAX TEAM

EDS Spot 2

kV: 15 Mag: 4731 Takeoff: 29.2 Live Time(s): 50 Amp Time(µs): 0.24 Resolution:(eV) 155.9

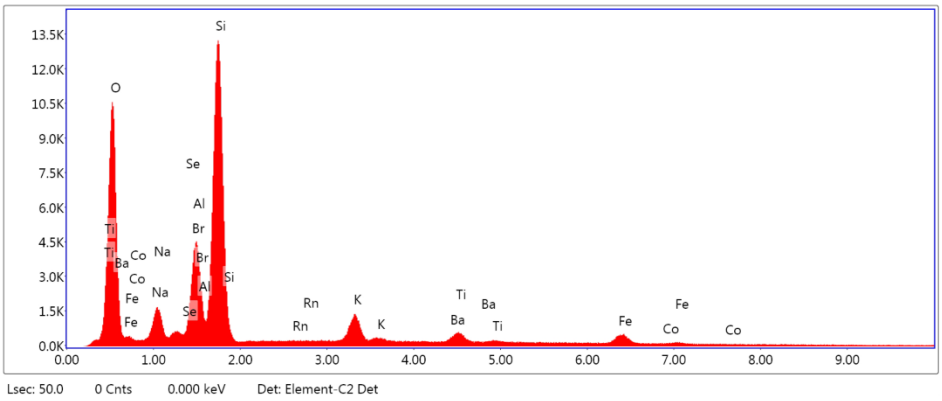

eZAF Smart Quant Results

Element	Weight %	Atomic %	Net Int.	Error %	Kratio	Z	R	A	F
O K	37.24	56.98	2216.50	8.15	0.1412	1.1162	0.9433	0.3397	1.0000
NaK	4.44	4.73	283.05	8.49	0.0192	1.0110	0.9712	0.4263	1.0041
SeL	0.20	0.06	11.77	42.66	0.0013	0.7654	1.1423	0.8213	1.0151
BrL	8.22	2.52	515.17	3.45	0.0563	0.7755	1.1478	0.8735	1.0116
AlK	2.57	2.33	286.96	6.45	0.0173	0.9888	0.9870	0.6744	1.0093
SiK	29.58	25.78	3287.68	4.63	0.2093	1.0098	0.9942	0.6980	1.0038
RnM	0.01	0.00	0.47	65.70	0.0001	0.6055	1.3722	1.0790	1.5891
K K	4.68	2.93	337.76	3.70	0.0403	0.9331	1.0240	0.9040	1.0224
BaL	4.39	0.78	77.52	15.28	0.0323	0.6609	1.2017	1.0522	1.0590
TiK	1.41	0.72	69.53	12.73	0.0123	0.8591	1.0369	0.9640	1.0486
FeK	6.56	2.88	152.02	6.43	0.0579	0.8401	1.0453	0.9902	1.0602
CoK	0.70	0.29	13.10	40.53	0.0062	0.8186	1.0451	0.9940	1.0749

Appendix D.3: Geochemistry Matrices of Intercorrelation

Appendix D.3.1: Principal Component Analysis

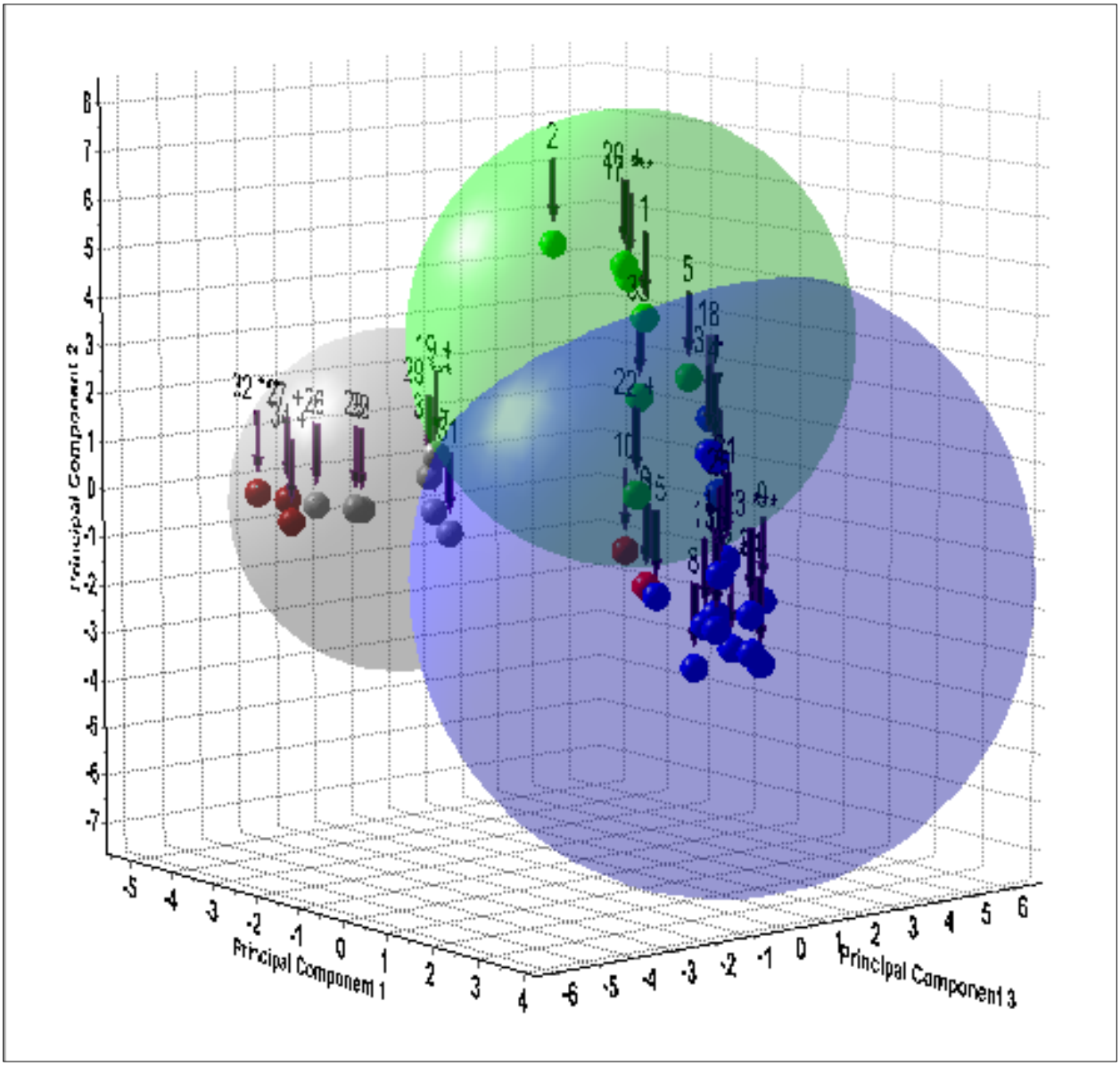

Appendix D.3.2: Southern Kenya Rift Bulk Geochemistry

	SiO2	Al2O3	Fe2O3	CaO	MgO	Na2O	K2O	TiO2	MnO	P2O5	LOI
SiO2	1	0.302	0.158	-0.388	-0.142	-0.597	0.617	-0.142	0.475	-0.061	-0.855
Al2O3	0.302	1	0.688	-0.195	0.144	-0.688	0.055	0.58	0.523	0.323	-0.58
Fe2O3	0.158	0.688	1	-0.1	0.424	-0.647	-0.02	0.874	0.528	0.608	-0.513
CaO	-0.388	-0.195	-0.1	1	0.179	-0.125	-0.253	0.06	-0.02	0.137	0.168
MgO	-0.142	0.144	0.424	0.179	1	-0.239	-0.4	0.554	-0.111	0.582	-0.092
Na2O	-0.597	-0.688	-0.647	-0.125	-0.239	1	-0.252	-0.453	-0.646	-0.28	0.769
K2O	0.617	0.055	-0.02	-0.253	-0.4	-0.252	1	-0.391	0.498	-0.292	-0.562
TiO2	-0.142	0.58	0.874	0.06	0.554	-0.453	-0.391	1	0.165	0.737	-0.234
MnO	0.475	0.523	0.528	-0.02	-0.111	-0.646	0.498	0.165	1	0.038	-0.636
P2O5	-0.061	0.323	0.608	0.137	0.582	-0.28	-0.292	0.737	0.038	1	-0.265
LOI	-0.855	-0.58	-0.513	0.168	-0.092	0.769	-0.562	-0.234	-0.636	-0.265	1

Appendix D.3.3: Geochemistry Cluster 1 – Western Region

	SiO2	Al2O3	Fe2O3	CaO	MgO	Na2O	K2O	TiO2	MnO	P2O5	LOI
SiO2	1	0.982	0.978	0.607	0.778	0.774	0.873	0.958	0.916	0.496	0.32
Al2O3	0.982	1	0.963	0.546	0.767	0.674	0.777	0.92	0.904	0.425	0.421
Fe2O3	0.978	0.963	1	0.608	0.713	0.761	0.837	0.906	0.921	0.541	0.307
CaO	0.607	0.546	0.608	1	0.474	0.498	0.589	0.517	0.725	0.424	0.193
MgO	0.778	0.767	0.713	0.474	1	0.378	0.68	0.878	0.832	0.147	0.559
Na2O	0.774	0.674	0.761	0.498	0.378	1	0.854	0.725	0.568	0.622	-0.163
K2O	0.873	0.777	0.837	0.589	0.68	0.854	1	0.911	0.759	0.469	-0.095
TiO2	0.958	0.92	0.906	0.517	0.878	0.725	0.911	1	0.88	0.408	0.284
MnO	0.916	0.904	0.921	0.725	0.832	0.568	0.759	0.88	1	0.539	0.501
P2O5	0.496	0.425	0.541	0.424	0.147	0.622	0.469	0.408	0.539	1	0.093
LOI	0.32	0.421	0.307	0.193	0.559	-0.163	-0.095	0.284	0.501	0.093	1

Appendix D.3.4: Geochemistry Cluster 2 – Southern Region

	SiO2	Al2O3	Fe2O3	CaO	MgO	Na2O	K2O	TiO2	MnO	P2O5	LOI
SiO2	1	0.426	0.409	-0.208	0.241	-0.71	0.328	0.371	0.226	0.117	-0.387
Al2O3	0.426	1	0.993	-0.032	0.4	-0.568	0.829	0.954	0.793	0.243	0.199
Fe2O3	0.409	0.993	1	-0.002	0.447	-0.578	0.83	0.955	0.822	0.292	0.257
CaO	-0.208	-0.032	-0.002	1	0.064	-0.488	0.088	0.068	0.496	0.054	0.011
MgO	0.241	0.4	0.447	0.064	1	-0.392	0.654	0.555	0.307	0.756	0.094
Na2O	-0.71	-0.568	-0.578	-0.488	-0.392	1	-0.558	-0.594	-0.701	-0.204	0.209
K2O	0.328	0.829	0.83	0.088	0.654	-0.558	1	0.914	0.598	0.279	0.088
TiO2	0.371	0.954	0.955	0.068	0.555	-0.594	0.914	1	0.791	0.37	0.222
MnO	0.226	0.793	0.822	0.496	0.307	-0.701	0.598	0.791	1	0.315	0.335
P2O5	0.117	0.243	0.292	0.054	0.756	-0.204	0.279	0.37	0.315	1	0.224
LOI	-0.387	0.199	0.257	0.011	0.094	0.209	0.088	0.222	0.335	0.224	1

Appendix D.3.5: Geochemistry Cluster 3 – Central Region

	SiO2	Al2O3	Fe2O3	CaO	MgO	Na2O	K2O	TiO2	MnO	P2O5	LOI
SiO2	1	0.398	0.233	0.355	-0.187	0.651	-0.641	-0.199	0.449	0.366	0.557
Al2O3	0.398	1	0.494	0.362	-0.081	0.367	-0.466	-0.039	-0.206	0.102	-0.337
Fe2O3	0.233	0.494	1	-0.305	0.383	0.086	-0.214	0.259	-0.145	0.359	-0.312
CaO	0.355	0.362	-0.305	1	-0.013	0.144	-0.695	-0.346	-0.019	0.084	0.132
MgO	-0.187	-0.081	0.383	-0.013	1	-0.598	0.138	0.129	-0.038	0.223	-0.16
Na2O	0.651	0.367	0.086	0.144	-0.598	1	-0.57	-0.082	0.196	0.328	0.514
K2O	-0.641	-0.466	-0.214	-0.695	0.138	-0.57	1	0.047	-0.093	-0.548	-0.299
TiO2	-0.199	-0.039	0.259	-0.346	0.129	-0.082	0.047	1	0.521	0.667	-0.154
MnO	0.449	-0.206	-0.145	-0.019	-0.038	0.196	-0.093	0.521	1	0.585	0.491
P2O5	0.366	0.102	0.359	0.084	0.223	0.328	-0.548	0.667	0.585	1	0.38
LOI	0.557	-0.337	-0.312	0.132	-0.16	0.514	-0.299	-0.154	0.491	0.38	1

Appendix D.3.6: Geochemistry Cluster 4 – Northern Region

	SiO2	Al2O3	Fe2O3	CaO	MgO	Na2O	K2O	TiO2	MnO	P2O5	LOI
SiO2	1	-0.221	-0.879	-0.309	-0.052	0.799	0.883	-0.854	-0.27	-0.53	0.221
Al2O3	-0.221	1	0.025	-0.124	-0.77	-0.513	-0.097	0.046	0.486	-0.225	-0.334
Fe2O3	-0.879	0.025	1	0.33	0.335	-0.695	-0.808	0.959	0.424	0.653	-0.008
CaO	-0.309	-0.124	0.33	1	0.425	-0.145	-0.425	0.478	-0.242	0.675	0.095
MgO	-0.052	-0.77	0.335	0.425	1	0.068	-0.288	0.26	-0.072	0.423	0.336
Na2O	0.799	-0.513	-0.695	-0.145	0.068	1	0.78	-0.624	-0.603	-0.251	0.185
K2O	0.883	-0.097	-0.808	-0.425	-0.288	0.78	1	-0.765	-0.316	-0.446	-0.016
TiO2	-0.854	0.046	0.959	0.478	0.26	-0.624	-0.765	1	0.28	0.772	-0.001
MnO	-0.27	0.486	0.424	-0.242	-0.072	-0.603	-0.316	0.28	1	-0.189	0.288
P2O5	-0.53	-0.225	0.653	0.675	0.423	-0.251	-0.446	0.772	-0.189	1	-0.062
LOI	0.221	-0.334	-0.008	0.095	0.336	0.185	-0.016	-0.001	0.288	-0.062	1